School of Civil Engineering

SUBSIDENCE PREDICTION AND MINE DESIGN FOR UNDERGROUND COAL MINING IN THE COLLIE BASIN

Ian Misich

"This thesis is presented as part of the requirements for
the award of the degree of Doctor of Philosophy
of the
Curtin University of Technology"

October 1997

DECLARATION

The program of work adopted for this thesis was derived by the author. Data collection has been completed either solely by the author, or with assistance from personnel working under the author's direction. Areas of work involving specialist outside assistance include drilling, survey, some computer analysis, some drafting, and centrifuge model construction and operation. Where other personnel have been involved, the level of their involvement has been described within the body of the thesis in the relevant sections. All data collation and analysis has been done solely by the author.

During the process of completing this thesis, nine papers were presented at international conferences. These papers were presented at the:

1) 4th International Mine Water Association Congress. Ljublana, Slovenia. September 1991.

2) 6th ANZ annual Conference on Geomechanics Christchurch, New Zealand. February 1992

3) 11th International Conference on Ground Control in Mining. Wollongong, N.S.W. July 1992.

4) Conference on Environmental Management, Geo-Water and Engineering Aspects. Wollongong, N.S.W. February 1993.

5) 12th International Conference on Ground Control in Mining. Morgantown, West Virginia. August 1993.

6) Conference on Mine Subsidence in Urban and Developed Areas. Rock Springs, Wyoming USA. September 1993.

7) International Conference on Environmental Issues and Waste Management in Energy and Mineral Production. Perth WA, August 1994.

8) 5th International Mine Water Association Congress. Nottingham U.K.. September 1994

9) 5th International Symposium on Land Subsidence - FISOLS '95. The Hague, Denmark.

An edited version of the paper from the 11th International Conference on Ground Control in Mining. Wollongong, N.S.W. July 1992 was used by the Australian Journal of Mining in the November 1992 edition (pp 35 to 39).

With the exception of papers 2 and 4, all were written personally, with some minor guidance from my supervisors. The two exceptions were co-authored. Of these nine listed papers, only three were not presented personally - papers 2, 4, and 6.

In order to investigate certain aspects of the thesis, it was necessary to source funding from the Minerals and Energy Research Institute of Western Australia (MERIWA). As required by MERIWA, it was necessary to prepare a separate report which details the work and results pertinent to the grant. The MERIWA report is currently in draft form and will be finalised early in 1998.

ACKNOWLEDGMENTS

The author wishes to thank Western Collieries Ltd (WCL) and MERIWA for their support, encouragement and funding of this project. This research project would not have been possible without the support given and faith shown by WCL management at various stages throughout the study. In this regard, the following people are graciously acknowledged: Mr Tom Ivankovich, Mr David Crawford, Mr Kevin Douglas, Mr Ron Lockhart, Mr John Janetski, Mr Gary Farmer, and Mr Geoff Blackford.

The author also owes thanks to the WCL mine surveyors who have diligently surveyed monitoring stations over a long period, and geologists who provided geological records when required. These personnel include Mr Geoff Gribble, Mr Geoff Turner, Mr Kevin Moir, Mr Cos Pineri, Mr Peter Sheddon, Mr Ray Speck, Mr Peter Ashton, Mr Mike Betlinski and Mr David Chapman. Valuable assistance was also given by Mr Garry Hammond in providing hydrological advice and records at certain times in the project, and Mrs Julia Larking for assistance with drafting the numerous centrifuge model subsidence development plots.

Reference is also made to the assistance provided by Mr Kevin Stone and Mr Josh White during the centrifuge modelling stages, and Mr Ken McNabb and Mr Lee Wardle in the Numerical modelling phase of investigation. Professor Barry Whittaker and Dr David Reddish are gratefully thanked for allowing the author to attend the Nottingham University and use of the university's FEM subsidence prediction program.

Special thanks are forwarded to my thesis committee for their support, encouragement and friendship over the years. These understanding fellows are Dr Stef Kapusniak, Mr Robert Hopkins, Professor Odwyn Jones, Mr Albert Evans, and Mr Martin Press. Special mention is given to Odwyn and Dr Hamid Nikraz for their assistance with the preparation of this manuscript, and Albert, who encouraged me to write and present a number of papers at international conferences, and for his support and good company during our study trips to overseas research institutions and mine sites.

Finally, acknowledgements are due to my family, who have tried to understand the long process and tribulations involved with completing a part-time PhD dissertation.

TABLE OF CONTENTS

LIST OF FIGURES

LIST OF TABLES

GLOSSARY OF TERMS AND SYMBOLS

A	>>	area
Aos, α	>>	angle of shear/caving angle (see diagram below)
Ap	>>	area of pillar
API	>>	American Petroleum Institute units
dA	>>	elementary area
BE	>>	boundary element
β	>>	angle of break
C	>>	cohesive strength
c	>>	convergence
Cm	>>	compaction coefficient
Cp	>>	circumference of pillar
D	>>	thickness of solid rock between mine and water
2-D	>>	two dimensional
3-D	>>	three dimensional
E	>>	elastic modulus
Emax	>>	maximum strain
ϵ	>>	strain
ς	>>	limit angle
%E	>>	percentage extraction
F	>>	flexibility
FE	>>	finite element
FOS	>>	factor of safety
FOSc	>>	factor of safety for coal pillars
FOSipc	>>	factor of safety for intra panel coal pillars
FOSips	>>	factor of safey for intra panel sandstone pillars
Fs	>>	flexural strength
G	>>	shear modulus, geometry
g	>>	acelerated gravity and weight
γ	>>	rock density
H	>>	depth, hydraulic gradient
h	>>	height above seam
Δl	>>	vertical deformation

I	>>	polar moments of inertia
K	>>	permeability, empirical strain coefficient
Kb	>>	aquifer thickness
L	>>	length
Δl	>>	change in length
Mh	>>	mining height
MPa	>>	mega pascals
N	>>	normal stress
ν	>>	poissons ratio
σ	>>	vertical stress
PL	>>	pillar load
PS	>>	pillar strength
P	>>	pore fluid pressure
ϕ	>>	coefficient of friction
π	>>	pi
Qu	>>	bearing capacity
Q	>>	force of reation
R	>>	radius of rotation, radius of critical area
r	>>	radius, position of face
r^2	>>	coefficient of determination
S	>>	subsidence
Sc	>>	storage coefficient
Sf	>>	subsidence factor
Sh	>>	subsidence at h above mine
Smax	>>	maximum subsidence
Ss	>>	subsidence at surface, shear strength
Sy	>>	Vw/Vb
T	>>	effective mining height
t	>>	time, thickness
Ts	>>	tensile strength, transmissivity
τ	>>	shear stress
UCS	>>	unconfined compressive strength
V	>>	linear velocity
v	>>	horizontal displacement

Vr	>>	volume of water released
Vb	>>	unit volume of aquifer
W	>>	width, unit weight, system loads
X	>>	distance from panel edge
x	>>	distance from centre of extraction

KEY TERMS

Caving — failure of rock involving detachment, and free-fall of failed rock.

Shearing — failure of rock involving no rotation of failed mass.

Shear dilation — The bulking/swelling of strata along the line of shear

Primary caving > The first stage of collapse of the immediate mine roof - vertical movement only.

Secondary caving> The second stage of collapse above the mine roof - vertical movement only.

Tertiary caving> The third stage of collapse above the mine roof - cantilever type translational collapse. The vertical extent is limited by the first large-scale bridging layer.

Vertical sagging > In the middle section of the panel, above the first large-scale bridging layer. Strata appears to remain intact

Translational sagging > Involves translational elastic movement towards the middle of the panel. May involve crushing of strata, but ground appears to remain intact.

Stages of Ground Movement

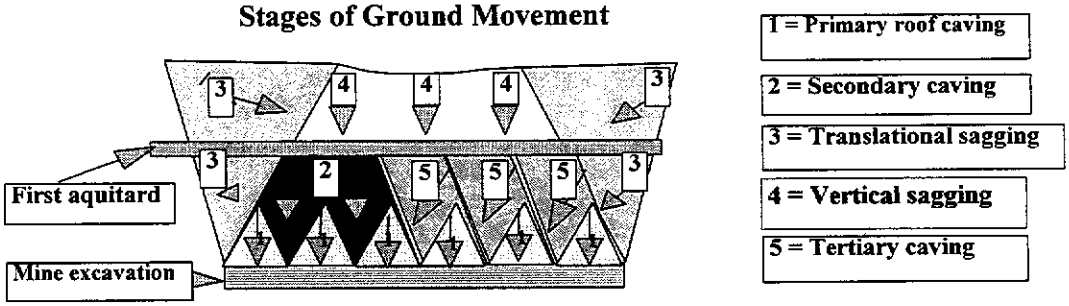

Definition of angle of shear / caving

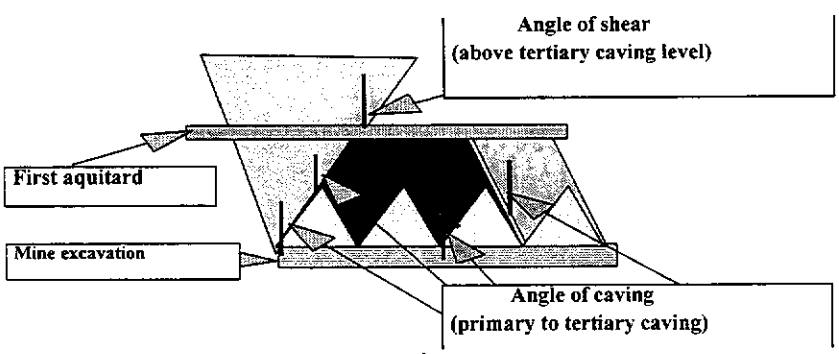

SUBSIDENCE PREDICTION AND MINE DESIGN FOR UNDERGROUND COAL MINING IN THE COLLIE BASIN

ABSTRACT

The subsidence characteristics of the Collie Basin sediments have been investigated to provide site specific design criteria for the Wongawilli method of coal extraction. As historical coal extraction (bord and pillar) methods did not generally give rise to large scale subsidence, there were very few details on mining subsidence in the Collie Basin available to base any design methodology on. Consequently, the investigation was conducted on a "Green fields" basis. Firstly, the mechanisms involved in the development of mining subsidence needed to be investigated and identified. It was then necessary to determine the effects that mining subsidence would have on mine and ground mass (specifically aquitards) structures and surface features. Once these two areas of work were completed, design criteria were formulated to manage the effects of mining subsidence by controlling the critical mechanisms of subsidence development.

The results from this study have greatly enhanced the level of understanding of the subsidence mechanisms involved, and allowed for the development of predictive models which can be used for the design of coal extraction by the panel/pillar mining method in the Collie Basin. Mine planning engineers can now use this design information to derive the most cost effective methods for the extraction of coal within the Collie Basin.

1.0 INTRODUCTION

Historical underground coal mining techniques in the Collie Basin - located in the south west of Western Australia (Figure 1.1) - had the underlying philosophy of maintaining stable roof and mining conditions to minimise groundwater ingress to the workings. Consequently, surface subsidence in the Collie Coal Basin in the period from the first recorded subsidence - at the Proprietary Colliery in 1902 (Figure 1.2) - to the 1980s, was relatively uncommon. Most cases of surface subsidence in the Collie Basin were of the discontinuous form; generally cave-ins over intersections or wide roadways in bord and pillar mining. This form of subsidence occurred predominantly at shallow depth where most of the overlying strata consist of soft clayey unconsolidated "Nakina sediments".

There was little concern for subsidence in these early times, as most of the collieries were sited below undeveloped bushland. It was only in isolated cases, such as the pot-hole subsidence that had developed near the railway line above the Proprietary colliery in 1928, and the development of cracks in a major road in the Collie district (above the Co-operative colliery, 1956), that subsidence became an issue. In October 1981, the potential for serious subsidence damage resulting from continuous trough forms of subsidence was further recognised, when the 6B East bord and pillar extraction panel in Western Collieries Limited's (WCL) WD-2 underground mine collapsed. The form of the 6B East subsidence was a trough-shaped depression with little surface expression. Maximum subsidence measured in this area was 0.7 m, and gave rise to much concern for the integrity of the water supply pipeline sited above the panel. This event initiated the first investigation into the causes of subsidence (by the author). This investigation was, however, relatively low-key and in the ensuing three years, there was minimal subsidence investigation; other than occasional check surveys of surface subsidence grids above secondary extraction panels (pillar splitting panels).

In 1984 WCL undertook an investigation of alternative mining practices to improve mine productivities. One of the more significant changes proposed was the adoption of the Wongawilli "total" extraction technique. This extraction method involves mining a series of splits or parallel bords, and lifting off fenders of coal on one side or on both sides of each split (see Figure 1.3). The fenders are typically 6 - 7 m wide and are sequentially mined in 4 to 5 m wide lifts along the splits until all available coal has been extracted.

COLLIE BASIN LOCATION PLAN

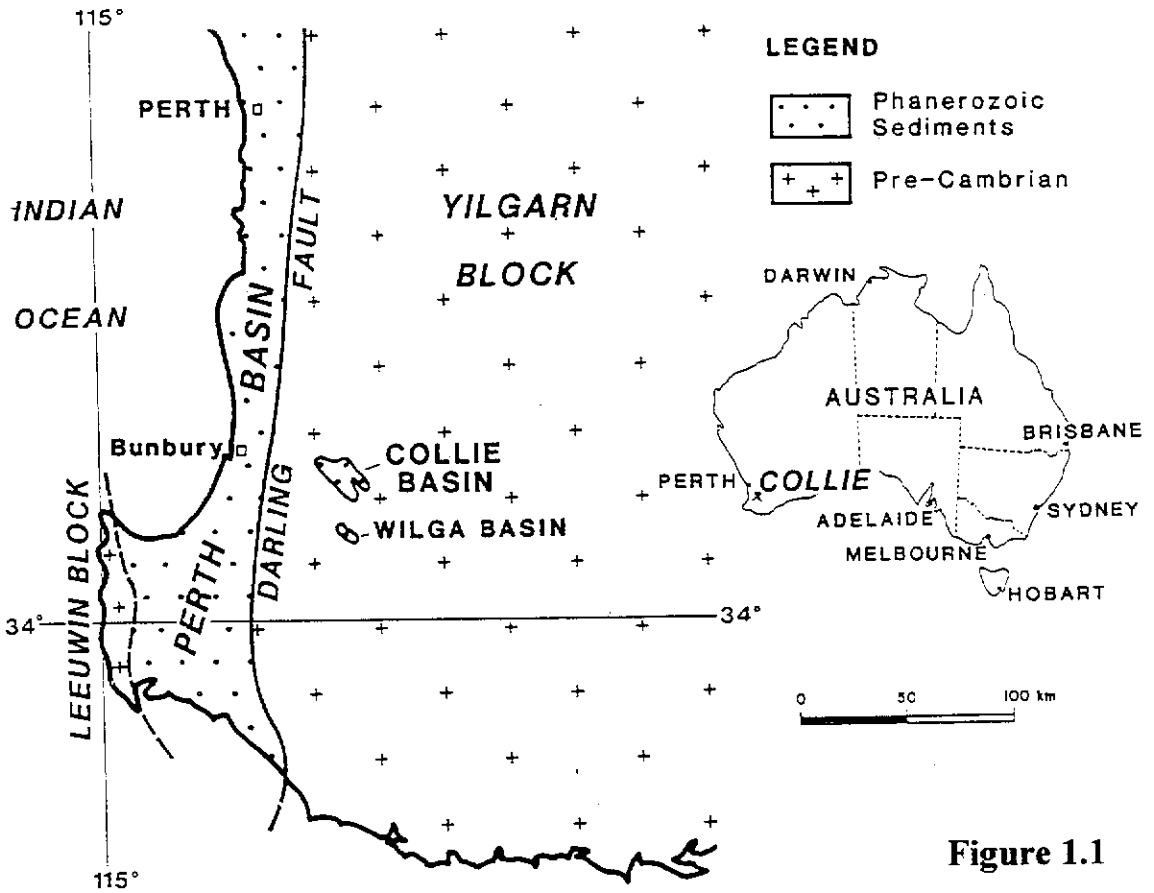

Figure 1.1

LOCATION OF CURRENT AND ABANDONED COAL MINES IN THE COLLIE BASIN

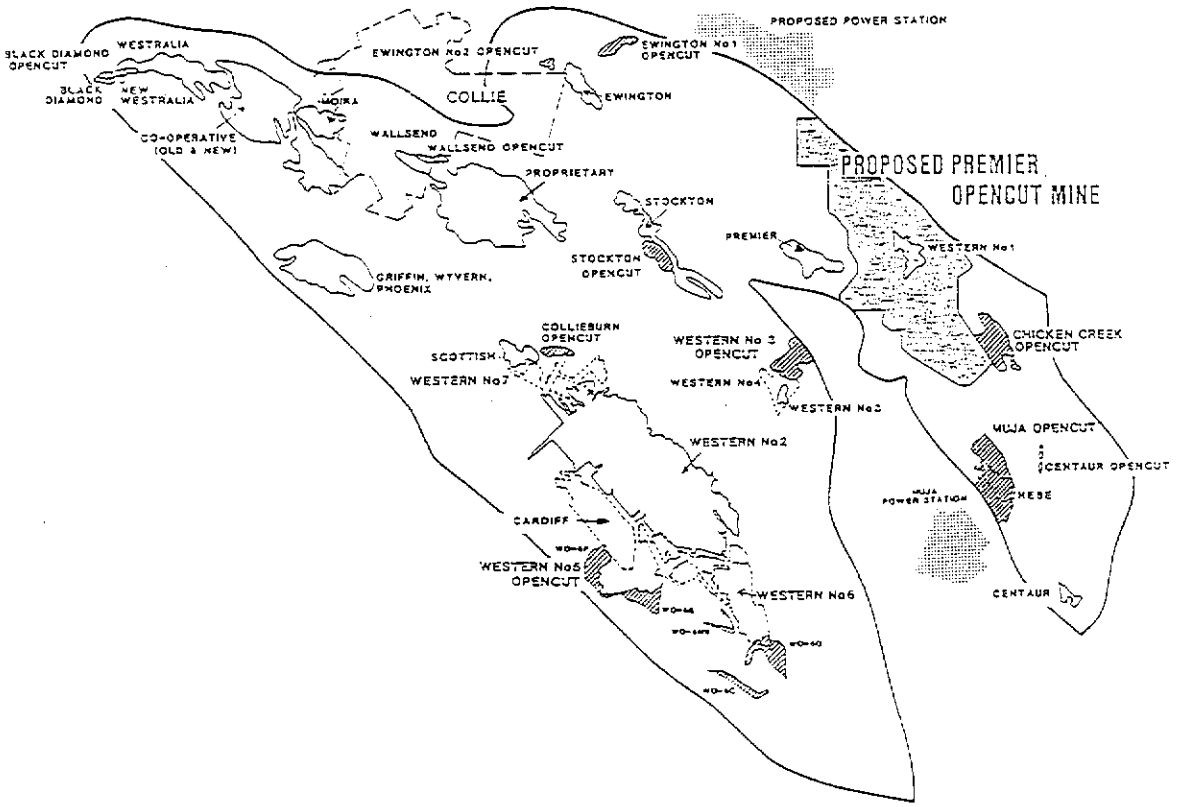

Figure 1.2

CONCEPTUAL DIAGRAM OF THE WCL WONGAWILLI COAL EXTRACTION METHOD

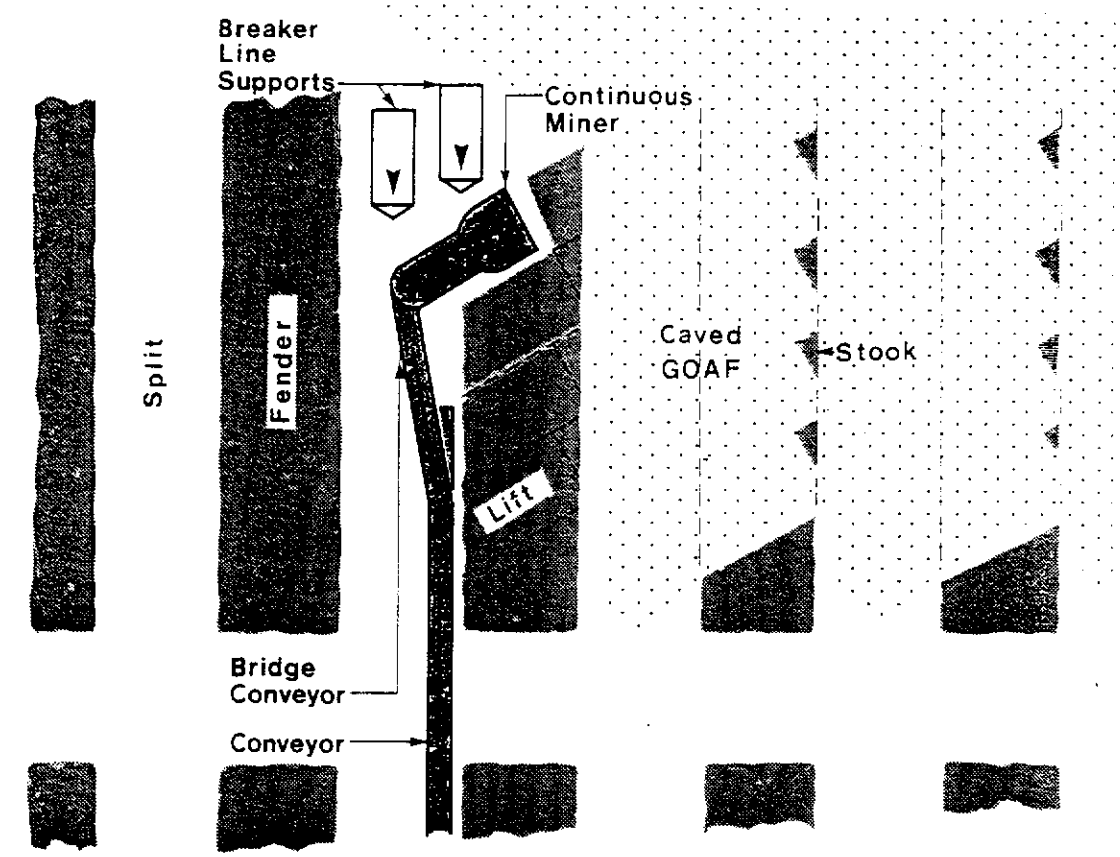

(a) One - way lifting

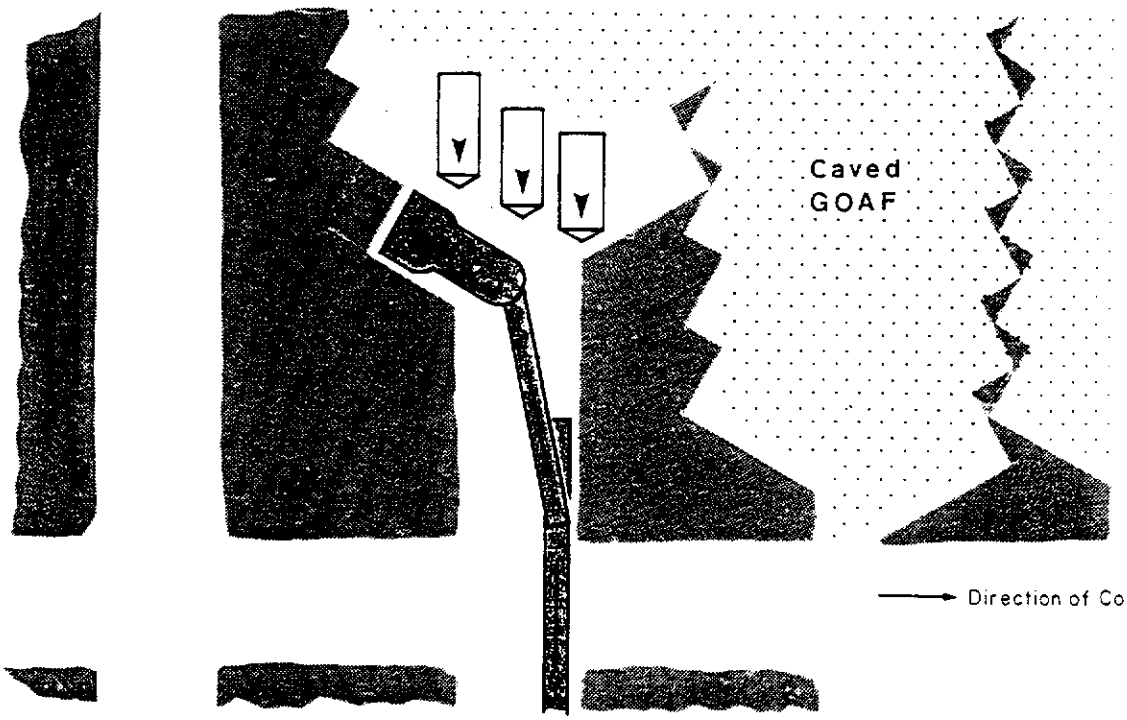

(b) Two - way lifting

Figure 1.3

This coal extraction technique had many benefits suited to the local conditions, the most attractive benefit being the potential to increase coal recovery, **by volume**, from 30 - 40% (as typically achieved in historical bord and pillar mines) to 70 - 80%, whilst using the existing mining equipment.

In 1985 a team of mining consultants visited Collie to investigate the full potential for mining coal in the Collie Basin. Of particular interest was the application of "total" extraction techniques in underground mines. One of the more significant concerns the specialists held after their site inspection was the apparent potential for the basin's weak sediments to develop ubiquitous discontinuous escarpment-type subsidence features such as deep, steep-sided pot-holes - in similar fashion to the historical bord and pillar subsidence. If correct, these forms of subsidence had serious implications for total extraction below significant surface features and subsurface aquifer systems located above much of WCL's remaining coal reserves.

As a result of these investigations, a trial "Wongawilli" extraction panel - ACIRL Panel - was set up to address the concerns held by the consultant mining group. Due to concern for the ramifications of escarpment-type subsidence, it was decided that each aquifer overlying the ACIRL panel should be drained/depressurised prior to extraction to minimise the risk of flooding the workings. An extensive surface and subsurface subsidence monitoring programme was also set up in an attempt to quantify groundwater and ground mass movements at all levels. If expert opinion was correct, WCL's underground mining options were limited. If incorrect there were far greater opportunities for underground coal extraction.

At the completion of the ACIRL trial total extraction panel, there was almost no visual evidence of mining subsidence, even though the maximum surface subsidence measured (~0.9 m) was approximately one third mining height (Hebblewhite and Humphreys, 1988). Clearly the level of "expert knowledge" of subsidence processes in the Collie Basin was inadequate, and more detailed investigation was required.

A significant point to arise from the trial extraction project was that large-scale ground water depressurisation was expensive and, if this level of "dewatering" was required for all aquifers above every panel, it would seriously impair the economic viability of total extraction of coal.

This raised the questions - to what vertical extent is "dewatering" required in the superimposed aquifers to prevent ground water influx to the underground mine workings?, and can mining subsidence be adequately managed to minimise the effects of ground movement on such important structures. If strata fracturing extends only to a defined height above the workings - according to the strata mechanical properties and subsidence mechanisms - then dewatering above the limit of fracturing would be unwarranted. (It should be noted that because of WCL's success in effectively draining water from each aquifer directly overlying the ACIRL panel, direct measurement of the subsidence effects on the aquifer systems could not be made from that trial.)

Following the successful implementation of the Wongawilli extraction method in the ACIRL panel, WCL altered long and short term mine planning to incorporate similar extraction panels wherever possible. Given the sensitive location of some of the extraction panels proposed, it was clear that the subsidence characteristics of the Collie Basin sediments needed to be investigated to, firstly, establish whether mining subsidence could be effectively managed, and subsequently, to develop a panel design approach such that coal extraction could proceed in the most cost-effective manner.

It was also considered necessary to research subsidence developed specifically from Wongawilli extraction because of the wider areas of unsupported ground created during fender extraction (between 13 to 20 m wide) compared to the more researched longwall coal extraction (which systematically mines thin slices of coal - 0.5 to 1 m wide). It was considered that the wider areas of collapse developed by the Wongawilli extraction system could potentially extend higher above the mine and therefore could be expected to have greater impact on superimposed features.

This requirement to research the local subsidence mechanisms, and the methods of prediction and management suited to subsidence resulting from Wongawilli extraction in the Collie Basin formed the basis of this research project. The specific aims, objectives and methodology used throughout the research project is discussed in the following Section.

1.1 AIMS AND OBJECTIVES OF RESEARCH PROJECT

The major objectives of the research program were to extend the knowledge of mining subsidence in the Collie Basin, and to develop a method of mine design which would allow for the extraction of coal from underground mines to proceed in the most cost-effective manner.

The specific aims of the research project were:

1) To develop a better understanding of the mechanisms involved with mining subsidence in the Collie Basin.

2) To develop a composite model (using empirical, mathematical and physical modelling techniques) which can adequately forecast the development of surface and subsurface subsidence and its effects for a wide range of mining conditions.

3) To establish a mining extraction approach and panel design criteria which can be used to manage the development of subsidence in the Collie Basin, within the limitations imposed by WCL's mining philosophies and equipment.

4) To design and then mine a trial total extraction panel according to design criteria established in points 2) and 3) to check the validity of the design system.

The scope of the program of work in this thesis only relates to ground movements due to mining subsidence. Investigations made towards prediction of rates of water flow into the mine workings have not been included in this thesis.

1.2 RESEARCH APPROACH / OUTLINE OF THESIS

The PhD thesis had the following research plan :-

1) Review literature published on subsidence characteristics, investigation and modelling.

2) Monitor surface and subsurface strata movements above a number of extraction panels to develop a better understanding of the mechanisms involved with subsidence development in the Collie Basin, then use this information to develop empirical subsidence prediction models.

3) Use numerical and physical modelling to further investigate the mechanisms of mining subsidence, particularly near the mining horizon and at the level of protective aquitard strata. It was proposed that if these forms of modelling could accurately reproduce field subsidence, they could be used to further enhance the empirical predictive models. It was considered best to attempt to base mine design criteria on empirical subsidence prediction models (developed from both field and modelling data) rather than using numerical or physical models for each panel design. In this way, the need to use costly and time consuming numerical and physical modelling would be minimised when designing future extraction panels.

4) Develop and then validate a mine design approach and design criteria for the management of mining subsidence in the Collie Basin (within the constraints imposed by the existing economics, mining equipment and geology). Validation was to be achieved by designing and extracting a trial Wongawilli extraction panel and monitoring the resultant subsidence to cross-check the subsidence predicted by the design model.

This thesis consists of five chapters. Each chapter represents a major phase of investigation and provides the methodology, results and conclusions for each phase. Each chapter has been divided into a number of relevant sub-sections, which form the basis of cross referencing in this document. The general content of each chapter is listed below.

Chapter 1 introduces the research topic and provides a summary of the scope of work within the study.

Chapter 2 describes the subsidence phenomenon in detail and summarises relevant work undertaken by other researchers in previous investigations on mining subsidence (in other mining regions as well as in the Collie Basin). This chapter also discusses the extent and relevance of previous work and identifies the need for specific research into mining subsidence in the Collie Basin; as undertaken by this doctoral thesis.

Chapter 3 pertains to the field investigation phase of the study. The approaches used to monitor subsidence are discussed, along with the results attained, the subsidence characteristics and processes observed, and the predictive models developed.

Chapter 4 describes the "laboratory" modelling phase of investigation. The observed factors that further enhance the empirical models (described in Chapter 3) are discussed, along with the limitations of each modelling method. Discussion is also provided for the potential of each modelling method to be used predict subsidence for complicated mining scenarios, that are not able to be catered for by empirical models.

Chapter 5 discusses the approaches used to develop panel extraction design criteria and describes the processes used to validate these design criteria.

The sixth and final chapter provides a summary of the major conclusions made from this research project and includes some recommendations for further work which could potentially enhance the results obtained from this study.

Where appropriate, specific details of each phase of investigation are given in the Appendices.

2.0 BACKGROUND TO THE RESEARCH PROGRAM

This Chapter provides a brief summary of the geological setting of the Collie Basin, and discusses work done previously by other researchers on topics related to the aims of this research project. The purpose of the information given within is to provide the reader with an understanding of both the general nature of this investigation, the subsidence phenomenon, and the extent to which this investigation represents original work in the field of subsidence prediction and modelling in the Collie Basin.

2.1 COLLIE BASIN - REGIONAL GEOLOGY

The Collie Basin is situated approximately 160 km SSE of Perth (Figure 1.1). It contains one of the few economic near-surface deposits of coal-bearing sediments in Western Australia. The origin of the basin has been discussed by a number of authors, e.g. Lord (1952), and Lowry (1976) and more recently Leblanc-Smith (1994).

The Collie Basin is a bilobate, asymmetrical structure containing a maximum thickness of around 1,500 m of Permian sediments, and covers an area of approximately 230 km^2. The Permian sediments are generally obscured from outcrop by a relatively thin veneer (typically between 10 and 30 m thick) of poorly indurated Tertiary continental gravels, sands and clays which is called the Nakina Formation. The coal measures are at least 1,050 m thick, and consist of three distinct coal-bearing horizons separated by relatively barren units (Figure 2.1, Lowry 1976):

- The basal coal measure, known as the Ewington Member, contains up to five major (>2 m) coal seams in a 60 m thick zone.
- The middle measure, the Collieburn or Premier Member, contains more than seven major seams in a 200 to 350 m thick zone.
- The top measure is known as the Cardiff Member and contains more than seven seams in a 160 m thick zone.

WCL were mining only two of these major coal seams by underground extraction methods at the time of the research project - the Wyvern seam and the Collieburn No.2 seam. A typical stratigraphic section above these two mining seams is given in Figure 2.2. WCL had three active underground mines - WD-2, WD-6, and WD-7. The WD-2 and WD-6 collieries were working the Wyvern seam, the WD-7 colliery was working the Collieburn No.2 seam.

COLLIE BASIN COAL SEQUENCES

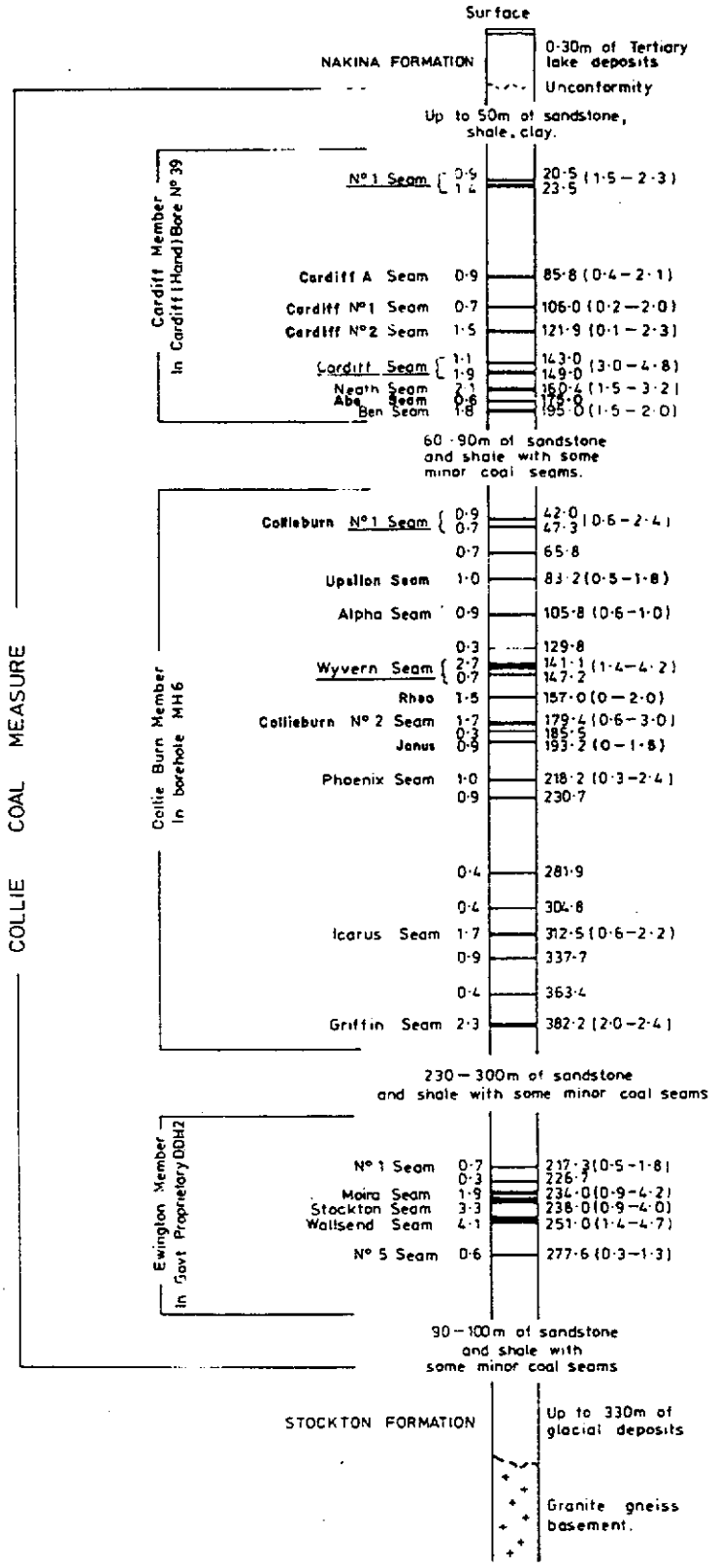

Figure 2.1

TYPICAL STRATIGRAPHY ABOVE WESTERN COLLIERIES' UNDERGROUND MINES

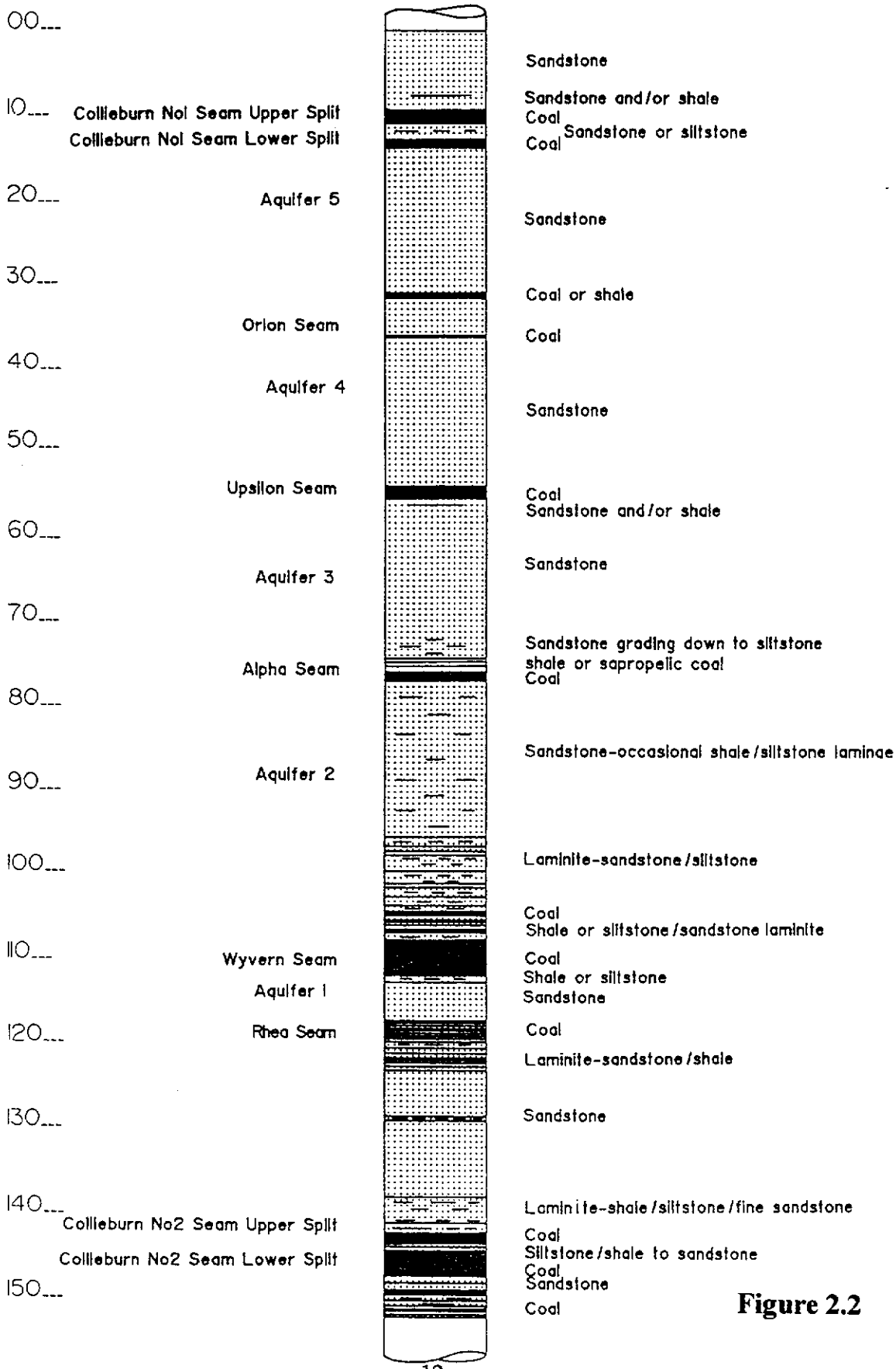

Figure 2.2

The interbedded sediments are generally cyclic, high energy fluviatile sandstones with thin gravel and conglomerate lenses. Silts and shales occur as overbank, lacustrine or paludal deposits. The coal seams are remarkably uniform in thickness and composition over considerable distances, although complex multiple splitting is known to occur (Hammond et al., 1983).

The principal overburden lithology is medium to very coarse grained, weakly cemented arkosic sandstone. The dominant detrital, constituents are quartz and kaolinised feldspar, both occurring as angular grains (Nikraz, 1991). A small proportion of kaolin matrix may be present, but the sandstone rock is commonly pitted, porous looking and cross-bedded. Finer grained sandstone are generally interbedded and many contain wisps or lenses of carbonaceous material. Grains from the shales show the same degree of angularity as the sandstone, but they vary in character, some being sandy, while others are carbonaceous (Nikraz, 1991). Shales cleave easily, and are usually micaceous (both Muscovite and Biotite). The coal is sub-bituminous and non-coking with low ash (typically 5 to 15%) and high moisture (typically 25 to 30%). Coal from the Collie Basin disintegrates on exposure and is subject to spontaneous combustion when stockpiled.

Complex faulting has played a major role within the Collie Basin with throws of up to 200 m being recorded. Consequently, in some areas one or two complete coal measures may be absent.

Structure, or rock mass defects, in the Collie Basin are generally simple features, are mostly widely spaced and have not affected mining significantly. Anomalies in the rock mass include:- faults, bedding planes, cleats, joints, underground caverns or vughs, and synclinal or anticlinal rolls.

Further details on the Collie Basin geology can be obtained from Leblanc-Smith (1994).

2.2 SURFACE FEATURES

The impact of steeply plunging topography on surface subsidence profiles has been well documented (e.g. Gurtunca & Bhattacharyya, 1992). However, as the surface topography in the Collie Basin depicts a mature landscape with shallow gullies and gently undulating hills, the natural slope of the surface is not expected to have a significant influence on mining subsidence in the region.

The majority of the surface above the total extraction panels planned for the near future was undeveloped bushland. Apart from barricading off some of the shallower areas from access to the general public, these areas did not represent much of a problem to total extraction. However, several mining areas did have significant surface structures, including:

- farmhouses and small residential settlements, and related public utilities,
- water supply pipelines for the Western Power's power station (Figure 2.3),
- sealed public roads and mine haulroads,
- a railway line used to service the coal mines, and
- an open cut coal mine (WO-5) and superstructure.

The panel design approach therefore needed to take account of the subsidence tolerance of each of these features to protect them from mining subsidence damage.

The dominant natural feature in the Basin is the South Branch of the Collie River, which meanders above most of WCL's deep mines.

2.3 REGIONAL HYDROGEOLOGY

The Collie Basin can be thought of as an interrelated groundwater system bounded by Archaean granite basement vertically subdivided into a number of superimposed aquifers by shale and coal seam aquitards. Simplistically, these aquifers can be considered to be separate entities, however, there is some interrelation at aquitard outcrops, and there is some minor hydraulic connection through faults and boreholes and through the aquitards.

Basin recharge is controlled by infiltration from channelled run-off, e.g. the Collie River South Branch, and direct infiltration through the highly permeable Nakina to the sub-cropping aquifers.

Aquifers comprise fine grained, to granular quartzose sandstones with little to no clay content. They can be detected geophysically by very low natural gamma counts [<50 American Petroleum Institute units (API), see Figure 2.4]. Moderately permeable material consists of silty/clayey sandstones with natural gamma counts of 50-150 API. Siltstones are generally low to moderately permeable aquifers with 100 - 150 API. Mudstone/shale (with >200 API) and coal (<50 API) represent system aquitards.

PIPELINE ABOVE ACIRL PANEL

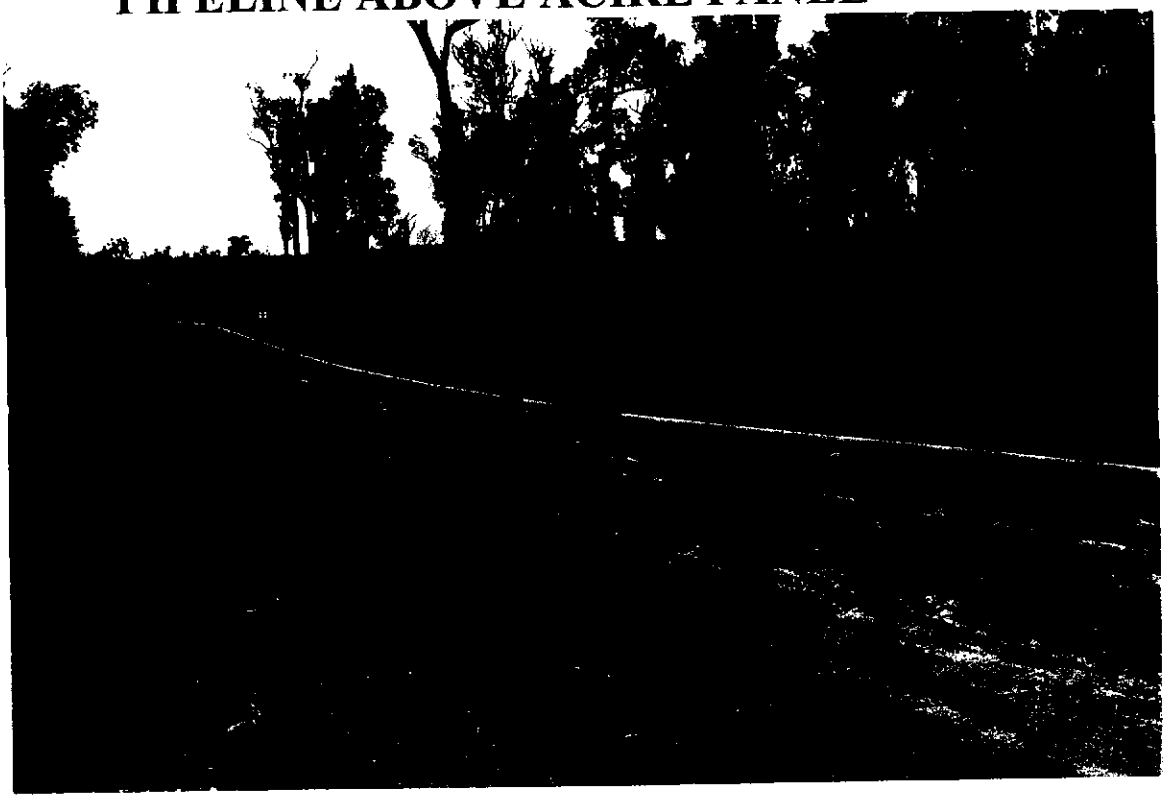

Figure 2.3

GEOPHYSICAL PLOT OF A TYPICAL AQUIFER SEQUENCE IN THE COLLIE BASIN

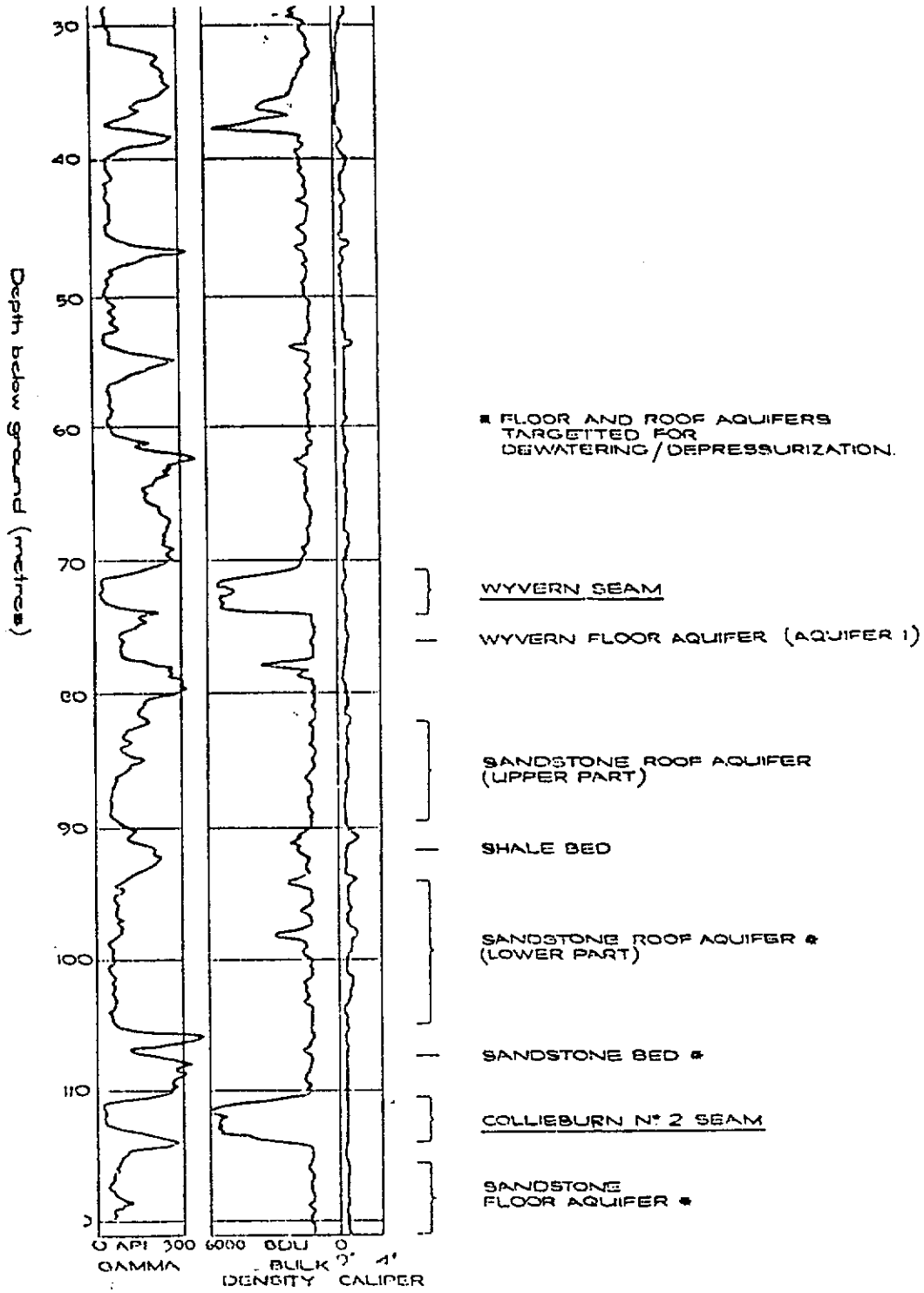

Figure 2.4

The coals can be separated geophysically from the sandstones by the bulk density sonde. Coals are represented by bulk density units (BDU) greater than 5000, while sandstone units are typically represented by BDU in the order of 1000.

In some locations water bearing strata can be in direct contact with the mined coal seams, however, in most cases aquitard barriers (of variable thickness) separate the coal from groundwater. The WD-7 and WD-6 mines commonly have 4 - 5 m of aquitard material in the roof and 0.5 to 1 m in the floor. The WD-2 mine typically has 8 m of roof aquitard. Both the WD-2 and WD-6 mines leave roughly 1 m of coal in the roof to improve mine stability; this coal septum also acts as additional aquitard material.

Heads of water within some aquifers can be very high; 80 and 98 m have been measured (Hebblewhite & Humphreys, 1988) in existing workings and water heads greater than 200 m are inferred in deeper, unmined areas. The effects of ground water on mining in the Collie Basin are described in detail in Misich et al., (1993)[2].

2.3.1 HYDROLOGICAL PROPERTIES

Within the sandstones of the main aquifers, are lenses of shale, siltstone, laminite beds, and coal which can restrict, but not prevent the vertical connection between separate sandstone lenses.

Particle size analyses on samples of drill-core, pump testing, and piezometer falling head tests indicate that each of the major aquifers associated with mining in the Collieburn 2 and Wyvern Seams will dewater adequately by gravity drainage using normal bore abstraction or mine drainage/sump pumping methods of dewatering.

Typical hydrological properties of aquifers in the Collie Basin are listed below (from Hammond et al., 1983):

- Permeability (K) > 1 to 5 $m^3/day/m^2$ (m/day)

  Permeability is calculated using Darcy's Law,

$$Q = \frac{K.A.H}{L} \qquad 2.3\ (1)$$

The rate of flow through an aquifer (Q) is proportional to the product of the coefficient of permeability (K), the area of the aquifer (A) and the hydraulic gradient (H/L), where

H is the head loss and L is the length of the flow path. In the Collie Basin a good, free draining aquifer is considered to have a permeability of at least 2 m/day (Hammond personal communication.)

- Storage coefficient (Sc) > 0.0001

  Sc = the volume of water released (V_r) per unit volume of the aquifer (V_b) for each unit change of head.

  $$= \frac{V_r}{V_b} \times H \qquad 2.3(2)$$

- Specific yield (Sy) > 15 to 20%

  Sy = the ratio of the volume, V_w, of the water that will drain by gravity from a rock that was initially saturated by the volume, V_b,

  $$\text{ie } Sy = \frac{V_w}{V_b} \times 100\% \qquad 2.3(3)$$

- Transmissivity (Ts) > 20 to 180 (m^2/day).

  Ts = the product of K and the aquifer's thickness, Kb. 2.3(4)

2.4 STRATA MECHANICAL PROPERTIES

The engineering properties of Collie Basin strata have been described in Hammond et al. (1983) to be dependent on:

- the original sediment composition and texture,
- weathering and erosion due to groundwater flow (past or present), and
- the proximity to faults, where sediments can be greatly disturbed and weakened.

Material strengths generally increase with depth, however, there are numerous exceptions to this rule. The degree of lithification increases in the proximity of coal seams, with weaker sandstones grading into relatively hard, black to grey carbonaceous shales and mudstones (aquitards).

Major coal seams are generally uniform in thickness and strength over large areas and typically dip gently to the south west. Interburden rock types, however, can vary over short intervals, both vertically and laterally. Accordingly, engineering properties can

vary from those of fine-grained, plastic sediments of low porosity to those of coarse-grained, cemented sediments devoid of fines, which are generally brittle and porous. There is also marked variation of engineering properties within the major lithologies (sandstones, shales, siltstones and laminites).

Table 2.1 lists typical values of compressive strength, elastic modulus, cohesive strength and friction angle for each major lithology of the Collie Basin sediments. This table demonstrates the general weak and plastic nature of Collie sediments and also illustrates that coal strengths are in the order of three to four times greater than non-coal lithologies. Therefore it can be expected that coal seams will tend to span across mine voids more than the non-coals during subsidence development which will lead to the development of bed separations at coal seam contacts.

Table 2.1 TYPICAL MECHANICAL PROPERTIES OF COLLIE BASIN SEDIMENTS

Lithology		UCS (MPa)	Elastic Modulus (MPa)	Cohesive strength (MPa)	Friction angle (deg.)
Sandstone	Range	0.2 - 16.4	100 - 1000		
	typical	5.2	500	0.5	32
Siltstone	Range	0.4 - 14.2	100 - 1500		
	typical	4.7	600	0.6	25
Laminite	Range	0.5 - 16.4	100 - 1500		
	typical	4.7	700	0.7	25
Shale	Range	2.0 - 14.9	100 - 2000		
	typical	7.0	1200	0.8	25
Wyvern	Range	7.1 - 26.4	1000 - 4000		
coal	typical	19.8	2000	2.0	42
Collieburn 2	Range	8.59 - 32.32	1000 - 4000		
coal	typical	20.50	2000	2.0	42

Using the ISRM (1978) classification for rock strength, the non-coal lithologies fall between extremely weak to weak rock, while coal is classified as weak rock. The strengths of the non-coals are much weaker than most other mining regions. For example, laboratory tests on sandstone bore core in the Ellalong Colliery in the

Cessnock area, New South Wales (NSW) by Wold and Pala (1986) gave UCS/Elastic modulus values between 58 / 7,700 MPa to 93 / 19,200 MPa (strong rock). Similar large variations exist between the two sites for shales; 37 / 4,500 MPa being recorded at Ellalong (medium strong rock) compared with 7 / 1200 MPa for Collie. However, coal strengths compare closely. Typical values for the Greta seam are 23.5 / 2,400 MPa which is very similar to those of the Wyvern and Collieburn 2 seams. The cohesive strength (c) of the Greta seam is 4.7 MPa and the angle of friction (ϕ) is 42°, which also compares well with the Collie coals. (There were no C and ϕ values quoted for the non-coals in the Cessnock coalfields.)

These results indicate that for constant stress, larger strains can be expected in Collie Basin sediments, and for constant strain, smaller stresses will be generated.

2.5 THE SUBSIDENCE PHENOMENON

The term subsidence, as applied to the earth's surface, normally refers to a given point sinking to a lower level (Whittaker & Reddish, 1989). Subsidence of any point is usually referred to as a vertical displacement, however, in most cases, horizontal movements also result from ground subsidence. The magnitude of subsidence is dependent on:

- the magnitude of the void, pressure or event responsible for subsidence,
- the position of any point (both laterally and vertically) in relation to this void, and
- the geological/geotechnical conditions of the particular site.

Examples and discussion of the effects of each of the above parameters or combinations of parameters are discussed in the following sections where relevant.

Subsidence events can be mining related and non mining related, and take the form of either continuous or discontinuous depressions. Discontinuous subsidence, is defined as ground movements with large-scale breaks in the ground surface such as step-like subsidence or deep, steep-sided pot-holes. This form of subsidence has the potential to totally destroy any surface features. Continuous deformation has no significant breaks at the ground surface, and the surface subsides gently to develop a "trough" shaped profile. Damage to surface features will depend on their position along the trough and on the maximum subsidence developed.

The final shape of surface subsidence can be influenced by a number of factors. These factors can be broadly classified into two groups:

- ground mass characteristics/properties, and
- mining influences.

To remain within the scope of this report, these factors have only been discussed briefly below.

2.5.1 FACTORS AFFECTING SUBSIDENCE (GROUND MASS)

It is well documented that subsidence characteristics in Australia, America, and Britain have significant differences. In fact, it is not uncommon that different mine sites from within similar geographical areas will have different subsidence characteristics (Kapp, 1982 demonstrated this). This variation can be put down to changes in local geology and engineering properties of the ground mass. A list of some of the more common ground mass factors controlling subsidence is given below.

Lithology / Geomechanical Properties

The effect of lithology on mining subsidence has been discussed by a number of investigators, e.g. Grond (1957) and Karmis et al. (1983). It is generally accepted that mining beneath argillaceous strata will manifest deeper subsidence profiles, whilst arenaceous materials generally tend to promote less subsidence for equivalent mining parameters. (Argillaceous strata consists predominantly of shales, claystones, whereas arenaceous materials are predominantly sandstones and conglomerates).

This could explain the large differences in maximum subsidence development between the more argillaceous sediments in the United Kingdom (90 to 100% mining height), and the more arenaceous sediments commonly in the USA and Australia (60 to 70% mining height). Arenaceous sediments typically account for between 80% and 95% of strata overlying the underground mines in the Collie Basin. Apart from above very shallow sites, the relatively small variation in lithology above existing mines, did not warrant an investigation into the effects of precise proportions of each rock type on the development of subsidence.

The presence of thick or geomechanically strong lithologies can greatly affect the caving processes and subsidence development (e.g. Krishna, 1989, Dunrud, 1984 and Galvin 1981). Stiffer or more "massive" material will deflect less, cave less readily, and potentially initiate less subsidence. Peng (1992) has provided subsidence "factors" depending on the proportion of hard/strong and soft/weak rock above the mined seam. This approach is not applicable for Collie Basin conditions, as similar ratios of maximum subsidence per unit of mining height have been observed (Misich, 1985)[1] with no strong rock, and in terms of the generic "standards" rock mass strength classifications, the variation in strength of sandstone is negligible.

For narrow mining panels/openings, the stability of the bridging beam is largely dependent on the three dimensional supportive effects of the panel abutments. In these instances plate theory is more appropriate. This conclusion is supported by Galvin (1981). The 3-dimensional plate effect was not considered to require investigation in this study as the proposed extraction panel widths were equal to or greater than the critical width (see Section 2.5.5.2), and could therefore be considered to be devoid of any edge effects.

When the rock fabric has inherent defects the strength of the material can be reduced proportionately, using one of several rock mass rating techniques, e.g. Bieniawski (1984). Care must be taken when using these correction factors if they are not derived from coal measures rocks.

Geological Structure

The presence of geological anomalies such as faults, caverns, infilled washouts, faults and joints, can greatly influence subsidence, as ground movement will tend to utilise lines of weakness and can result in steeper, sharper subsidence profiles. The main geological structures found within the Collie Basin and their likely influence on subsidence are discussed below.

Faulting

Kovago, 1986 classes faults in the Collie Basin into one of two types; mine boundary faults, and small, discontinuous faults. Boundary faults represent faulting which has displaced coal seams to such an extent that they terminate the mine workings in the direction they are encountered. (There are some locations where boundary faults have been mined through, however, these areas are towards the extremity of fault where the

throw is greatly reduced.) They are extensive in length and throw, many covering several kilometres. There are several boundary faults, (the more significant being the Wallsend, Stockton, Cardiff, and the McAlinden faults), however, they are spaced widely enough to allow relatively uncomplicated mining.

Discontinuous/small faults are faults with a maximum displacement of around 15 m. They can usually be mined through or around when encountered in the mine. Most of these faults are known as "sag" faults. Vertical displacement can diminish rapidly, often giving out within a pillar length. Discontinuous faults are commonly associated with boundary faulting, however, they can appear suddenly with little or no indication. Both types of faulting are generally oriented along strike (roughly 130 - 310 degrees) and have normal displacement. Their inclination is generally very steep, typically ranging from 5 to 55 degrees from the vertical.

There have been documented cases of faults acting as water conduits and creating many problems to mining, however, personal experiences with faults suggest that the majority of faults are "tight", allowing little transmission of water due to the type of infill or gouge material. Both types of faults can be associated with localised high horizontal stress fields, residual to the original ground movements, which can have a serious effect on the progress of mining. High horizontal stresses are not encountered in all cases.

The presence of faulting within the "zone of subsidence" can greatly affect both the depth and shape of the subsidence trough by providing a continuous plane of weakness for strata to mobilise against (as illustrated in Figure 2.5, from Bell, 1975). Detailed investigation of the effects of faulting by Donnelly and Reddish (1994) suggests that steps in the ground surface may not only be due to remobilisation of fault planes. Donnelly and Reddish observed (in British and Ukraine coalfields) that steps in subsided ground often occurred well outside the position where fault planes outcrop at the surface. They concluded that the cause was either slip along bedding within steep synclinal folds or across geological unconformities often associated with faults. This observation is very important in determining the potential for subsidence damage in critical areas (eg near townships).

INFLUENCE OF FAULTING ON SUBSIDENCE

(From Bell, 1975)

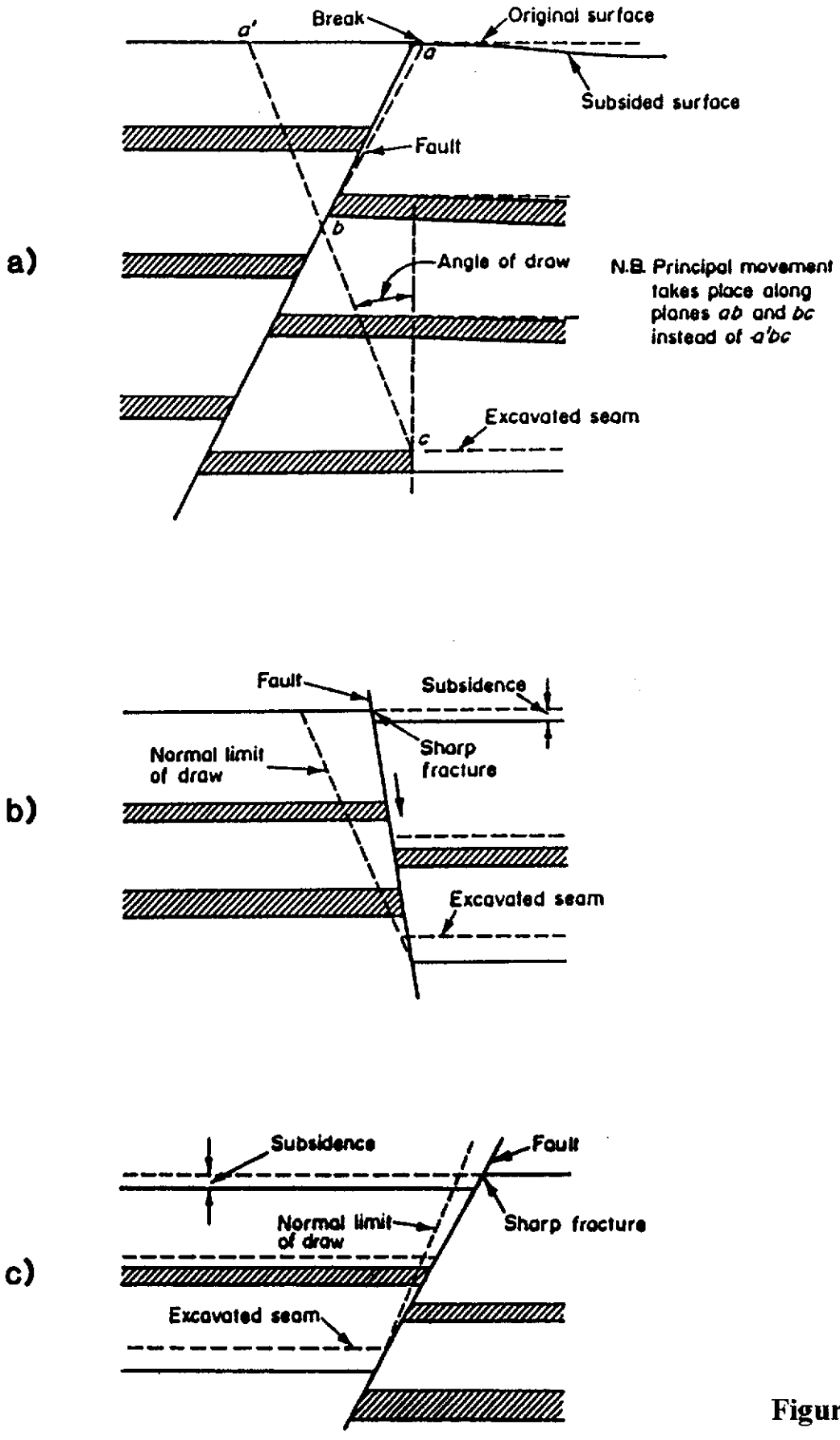

Figure 2.5

Two examples of fault-affected subsidence in Australia include:

- a stepped surface profile with anomalous horizontal strains at Hunter Valley No.1 Colliery, NSW (Kershaw et al., 1988), and
- a large crater or pot-hole in swampy ground at the extremity of the Cardiff Colliery in the Collie Basin. A more detailed account of this event is given in later in this Section.

The effects of faulting in the Collie Basin have not been researched in detail in this project as there are relatively few large scale faults within the mining areas of concern. Nonetheless, the potential for additional subsidence damage near faults needs to recognised.

Jointing and Cleating

Both jointing and main cleat are typically oriented within 10 degrees either side of North, and normal to both the bedding and to the strike of main dip (cleating being restricted to the coal seams). Joint sets are widely spaced and have had little impact on mining in general. Coal cleat is, on the other hand closely spaced and can significantly reduce the rock mass strength. For example, Wilson (1981) recommends a reduction factor of 1/6 for coal laboratory strength due to inherent cleating in coal seams.

Both joint and cleat sets are discontinuous to stepped and their surfaces are generally rough to slightly polished, planar and clean. Cleat sets also consist of less common butt cleating, normal to the main cleat, and a subset cleat oriented NW-SE. As these features are normally tight and have been infilled with pyrite, it is considered that they will have little impact on subsidence development in Collie, other than providing a smooth surface for discontinuous pot-hole subsidence to break back against.

Bedding Plane Weaknesses

Bedding plane weaknesses are commonly associated at interfaces between sandstone and fine grained carbonaceous material in several locations within the Collie Basin.

Laminated siltstone, sandstone and shale, along with most finely bedded mudstones and shales usually retain intact bedding. Inspection of core from diamond drilling programmes revealed few polished or slickensided surfaces in deep mine reserves (personal experience) in areas away from faulting.

It is obvious that the presence of any such weaknesses within the zone of subsidence will reduce resistance to shear and increase the potential for bed separation and caving and will consequentially result in a deeper sharper subsidence trough. The effect of layered/interbedded strata on bending characteristics of underground mine roof beams is well documented in Peng and Chiang (1984) and Stephansson (1971). This philosophy can obviously be applied directly to the subsidence phenomenon. The effect of layering on mining subsidence was considered, by the author, to be an important parameter to define - particularly for the physical modelling stage of the project.

Seam rolls

Synclinal/anticlinal rolls in underground reserves in the Collie Basin are usually gentle and pose few problems to mining, other than isolated small increases in horizontal stress or slight weakening of roof or floor material at the apex or base of the roll (Misich, 1991). Consequently these features are not expected to play a significant role in subsidence formation.

Underground Cavities

Underground cavities or "washouts"/vughs are encountered to varying degrees in all workings, generally limited to the shallower sections of the mines, close to the sub-crop (Kovago, 1985). The washouts show extreme variation in sectional outline, being bulbous, u-shaped or have very irregular steep sides and an irregular floor. They can be up to 6 m in width and 2-3 m high. Most vughs are filled with clay and fine grained sand. However, some vughs are only full of water and others are almost completely void. Some cavities follow along distinctive channels for hundreds of metres while others appear in isolation with little pre-warning of their existence.

It is obvious that the presence of any of these forms of geological structure will greatly affect the subsidence processes. Whittaker and Reddish (1989) give several accounts of severity of subsidence due to limestone cavities. The locations of such features is very irregular throughout the basin and will require careful mapping to account for their presence, which is outside the scope of this study.

Topography

Sloping seams and topography, although not generally affecting magnitudes of subsidence, will alter the position and shape of the subsidence trough. The most recognized method of accounting for sloping seams is taken from the Subsidence Engineers Handbook, by the NCB 1975. The effect of sloping topography on subsidence development in the east coast of Australia is also well documented by Shu (1990). More discussion has been provided in Section 2.2. Due to the relatively flat nature of the Collie Basin topography, these effects have not been investigated.

Ground water

The presence of ground water can greatly influence the general stability of the mine workings by applying increased vertical loading and pore pressure to the immediate roof. Conversely, the removal of ground water from pressurised aquifer systems is capable of inducing subsidence - through reconsolidation of the aquifer strata. Reconsolidation takes place through an increase in effective stress on the strata as the pore pressure is reduced. The magnitude of this type of subsidence is dependent on the compressibility of the strata (Helm, 1984).

The most noted case of subsidence due to fluid withdrawal in Australia is in the Latrobe Valley, Victoria, where a maximum subsidence of 2.25 m was recorded as a result of dewatering strategies adopted for open-cut lignite mining (Raisebeck, 1988).

A study of the influence of pore pressure variation on Collie Basin sediments by Evans et al. (1988) indicated that with artificially rapid pore pressure reduction by gravity drainage, some Collie sediments can break down, and undergo a volume reduction, resulting in ground subsidence. However, this work was done with exceedingly high and rapid pressure head losses. Natural drainage rates are orders of magnitudes less.

Nikraz (1991) continued research in this area, and found that the Collie sandstones have low compressibility and consequently subside very little after dewatering; the vertical deformation (Δh) of a prism of aquifer material was defined by Nikraz et al., (1995) as:

$$\Delta h = C_m . h . \delta P \qquad 2.5(1)$$

Where: C_m = a one-dimensional compaction coefficient,

h = the prism height, and

δP = the change in pore fluid pressure.

In an example given by Nikraz et al. (1995), the mean *in situ* compaction coefficient for one sample of sandstone was assumed to be 2.382×10^{-4}, which, when assuming a reduction in pore water pressure of 2.0 MPa and a 12.5 m thick aquifer, resulted in a vertical compaction of 0.006 m (6 mm).

Extrapolating this to the field, if hydrostatic conditions are assumed for a mine panel at 145 m depth (e.g. ACIRL panel), subsidence by compaction will occur in aquifers 1, 2, 3, 4, and 5 which are typically 8, 25, 15, 40 and 49 m thick respectively. If complete depressurisation occurs in each aquifer (from an initial standing water level of 20 m depth), the average reduction in pore pressure for each aquifer will be equivalent to the water head to the base of each aquifer less half the aquifer thickness. For example the reduction in pressure for aquifer 1 in this case equates to:

$$\frac{[145 + 8 \text{ (+ 4 m for the mine seam thickness)} - 20 - 4] \times 9.81}{1000} = 1.3 \text{ MPa} \qquad 2.5(2)$$

The average compression in aquifer 1 would therefore be:

$\Delta h_1 = 2.382 \times 10^{-4} \times 8 \times 1.30 = 3$ mm

Taking each aquifer in turn, the expected compaction for each interval is:

$\Delta h_2 = 2.382 \times 10^{-4} \times 25 \times 1.06 = 6$ mm

$\Delta h_3 = 2.382 \times 10^{-4} \times 15 \times 0.86 = 3$ mm

$\Delta h_4 = 2.382 \times 10^{-4} \times 40 \times 0.55 = 5$ mm

$\Delta h_5 = 2.382 \times 10^{-4} \times 49 \times 0.05 = 1$ mm

$\Delta h_{total} = \Delta h_1 + \Delta h_2 + \Delta h_3 + \Delta h_4 + \Delta h_5 = 18$ mm. 2.5 (3)

Because this value is much smaller, and expected to be more regional than mining subsidence it was assumed that this form of subsidence would have little impact on the any superimposed features. Consequently, this form of subsidence has not been included in this program of investigation.

2.5.2 FACTORS AFFECTING SUBSIDENCE (MINING)

It is obvious that mining subsidence cannot occur until there is a collapse of roof material into the workings. If coal extraction is planned to maintain permanent stability, then effectively, no large-scale subsidence can develop. Consequently, subsidence characteristics in any mining area are dependant on the nature and dimensions of ground collapse above underground workings - which is directly attributable to the mining method used at the minesite. There are a number mining related factors which influence subsidence characteristics, some of the more significant are listed below.

Mining/Extraction Width

As mentioned previously, the subsidence process can be likened to beam or plate theory. Thus it follows that the resultant subsidence depends largely on the span of collapsed ground. The larger the span (directly related to mining width), the greater the deflection. However, when a critical width is reached, there will be no subsequent increase in subsidence. This is discussed in greater detail in the following Section.

Mining/Extraction Height

The effect mining height has on subsidence needs little explanation. Simply, the greater the height of the mine void, the greater the deflection of superincumbent strata (subsidence). Mining heights in WCL's existing mines typically varied from 2.2 to 2.7 m, which is considered to be relatively consistent.

Percentage Extraction

The maximum subsidence due to coal mining depends on the percentage recovery of coal for the particular mining height over the area of extraction (Kapp, 1982). The higher the efficiency of coal removal, the greater the subsidence.

It has become practice in Australia to reduce the mining seam height by the percentage extraction and result in an "effective mining height" (Kapp, 1982). This effective height is then used in subsidence calculations. This is considered to be an acceptable approach for this study, as the Wongawilli extraction method leaves between 10 and 15% coal behind as small stooks which do not preclude the caving process. The exception to using this approach would be when sufficiently large pillars are left behind, which act as barriers to the development of subsidence.

Superimposed Mining

Greater subsidence is experienced when mining superimposed seams, the magnitude of subsidence depending on, largely, seam thickness and distance between seams (NCB, 1975). Most researchers suggest that subsidence for individual seams can be summated, although some cases have reported more subsidence than this.

Mining Direction

Mining direction in relation to seam dip, structure and minimum width can also influence subsidence mechanisms, as caving mechanisms will be affected. Orchard, 1973 comments that in Australia, maximum subsidence is achieved when the panel has progressed approximately 1/3 of the panel width. This is unlike that postulated by the NCB, where Smax should be above the centre of the panel. One possible reason for the discrepancy is the fact that it is common practice in Australia to commence mining from the down dip side. Due to the laws of gravity, the subsidence profile will be cast down-dip, according to the dip of the seam, and will be located within the first half of mining full panel width. There was insufficient data at this stage of the investigation to ascertain whether mining direction had influenced the shape of any subsidence profiles in the Collie Basin.

Remnant Coal

Remnant coal pillars such as stooks and chain or barrier pillars separating extraction panels can have a great influence on the resultant subsidence. Dunrud, 1984 supports this, observing that these unmined bodies of coal reduce the caving eight and consequently the total subsidence. Similar responses are reported in the SEH (1975) where a solid coal pillar with a width to depth ratio of 0.1 within the extraction area can reduce surface subsidence by up to 60%.

Stowage/Infill

Implementation of stowage or packing materials in and around gate roads to improve stress conditions will influence the caving process by reducing the volume the goafed material can occupy (NCB, 1975). This process can therefore be adopted for reduction of surface subsidence. The implementation of stowage principals is outside the economic limitations of mining in Collie.

Extraction Rates

The rate of coal extraction, or face advance will also affect the intermediate stages of subsidence, Dunrud (1984). It is expected that although the final magnitude of subsidence will not necessarily be affected by extraction rates, it is possible that the shape of subsidence troughs can be affected.

2.5.3 NON-MINING RELATED SUBSIDENCE

A number of processes unrelated to mining can induce surface subsidence. The potential for these processes to occur should be evaluated prior to mining to prevent unjust damage claims against mining companies. These processes can be experienced on both local and regional scales. The major causes of this type of subsidence are listed below:

- ground settlement through natural processes or the weight of structures,
- changes in fluid content of the soil or rock mass (e.g. swelling clays can alter ground elevation, or fluid abstraction can increase effective stresses and allow consolidation),
- erosional forces,
- chemical influences such as metallic corrosion,
- thermal effects which cause lateral strain at the surface,
- tectonic movements of the earth's crust which cause buckling at the surface, and
- the melting of ice in frozen ground.

These causes of subsidence are discussed in more detail by numerous authors including Kratzsch (1983), Whittaker and Reddish (1989), Barends et al., (1995). The most common cause of this type of subsidence is fluid withdrawal, for example gas, oil and ground water. Dewatering and pumping from aquifers for a prolonged period can, through reconsolidation, cause the surface to subside many metres; however, this is not applicable to the Collie Basin sediments - as discussed in Section 2.5.1.

Of these non-mining forms of subsidence, only changes in moisture content of the near surface clays appears to have had any impact on surface levels. Although the majority of clays in the Collie Basin are non reactive kaolinites, it has been established (by Hammond et al., 1983) that these materials can have a linear shrinkage value of 5 to

7%. Although the surficial clays within the vadose zone would probably never completely desiccate and thereby never realise their maximum shrinkage, cyclical "wetting and drying" is considered a potential source for some relatively minor natural ground movements. Field survey trials indicate that inclusive of survey error (established to be in the order of ±15 mm - see Appendix I.1), the seasonal variation of ground surface is in the order of ±30 mm. However, considering that this form of subsidence is occurring naturally, and cannot be effectively controlled, it was seen as being not relevant to the study. It was therefore concluded that non-mining subsidence did not require further investigation in this study. Non-mining subsidence is therefore not discussed further.

2.5.4 DISCONTINUOUS MINING SUBSIDENCE

In some circumstances, for example when mining takes place beneath weak or fractured strata and/or at shallow depths of cover, surface deformation can be expressed in a discontinuous/stepped form. The two main forms of discontinuous subsidence observed in the Collie Basin are:

- Steps in the ground where the ground slides on inclined planes or falls away from the panel edge (millimetres to metres deep). These steps are often associated with open cracks at the surface (millimetres to metres wide) at the point of maximum tensile strain, usually above the edge of the extraction panel.
- pot-holes, where localised ground collapse in the workings extend to the surface. These features are steep sided and usually circular in form.

In the Collie Basin these forms of discontinuous surface subsidence are generated by collapse of the mine roof (usually at roadway intersections) beneath shallow workings where the overlying strata are weak and provide little resistance to collapse. Prior to this investigation, there was nothing available to predict the limits of this form of subsidence In fact technical data on all forms of subsidence in the Collie Basin was very limited.

2.5.4.1 Historical Evidence of Discontinuous Subsidence in the Collie Basin

A search through government records revealed few documented details of subsidence, other than limited remarks in correspondence between mining and government bodies. Little interest was shown in surface subsidence unless it occurred near vital areas such main thoroughfares. Once identified they were simply filled in and additional supports installed in the mine immediately beneath and adjacent to the area of collapsed roof. Where pot-holing occurred in natural bushland, they were simply left standing to fill with water or debris. Although not well reported, it is evident that most of the subsidence that occurred prior to the 1980's was of the discontinuous form (pot-holing), resulting from the collapse of mine roof in the underground workings.

The frequency and location of discontinuous subsidence (mainly pot-holes) are very irregular and unpredictable. This observation is made by researches in other mining areas also (e.g. Burton 1988) and appears to be typical of these forms of subsidence. The dimensions of the pot-holes are also extremely variable, with hole depths as little as a few centimetres to several metres, and covering areas as small as one square metre, ranging up to one hectare. However, in general, the size and depth of pot-holes usually compares directly to the area of the collapsed mine roof and the mining height. They are usually very similar in appearance (being steep sided and circular - as in plates 1 & 2), however, some marked variations from the norm have been noted. A comprehensive list of sites where this form of subsidence has occurred is provided in Goldsmith et al. (1995). Two of the better documented cases of discontinuous subsidence are provided below.

The Cardiff Colliery

The largest of pot-holes to develop was over the old Cardiff workings near WCL's WO-5 open cut mine, where the upper sediments are known to be unconsolidated and water-saturated to greater depths. This well documented pot-hole, above No. 76 bord, was estimated to cover one hectare at the surface where the depth of cover was approximately 85 m (correspondence between the Joint Coal Board, and the Department of Mines dated 30 September 1947). The development of this subsidence feature was observed to occur in two stages of collapse. A brief description of the lithologies for the first 30 m above the seam is given below:-

DEPTH	LITHOLOGY
85.0 - 76.2 m	Soft sandstone. (This sandstone was expected to represent the extent of the first stage of collapse, as described by mine official.)
76.2 m - 64.0 m	Interbedded sandstones and shales
64.0 m - 62.4 m	White sandy clay
62.4 m - 55.2 m	Soft sandstone and quartz pebbles

The following account by R.L. Jack explains the sequence of events leading to the extra-ordinary subsidence/plug failure, which was thought to be due to the presence of beds of "slurry".

"First of all, pillars had been extracted right up against the 82 m up-thrown fault, which gave water freely. With the collapse of strata adjacent to the fault, the strata, instead of breaking small and choking, as in the previous falls, broke off in larger dimensions from the defined facings of the faulted ground. Water from the fault would more readily mix with the sandy stratum and would create more slurry than normally experienced. The size of the material falling as a result of the influence of the fault created larger cavities in the fallen material and allowed freer percolation of slurry."

"The manager later examined the surface, but found no surface depression had occurred. During this time heavy rains had been falling and created a water-filled swamp immediately above the roof fall. With the later surface collapse water from the creek and swamp entered the hole, carrying with it in suspension and solution, the sands and clay forming the upper section of the cover. The hole eventually plugged itself off and the waters accumulated in the cavity. On about the 15th August, the plug created at the bottom of the hole was washed out and the accumulated waters rushed into the mine. The hole stayed open for some time hence. "

This subsidence feature can no longer be seen as it was filled in by spoil dumps of the neighbouring WO-5 Mine. Other smaller, more typical, pot-holes that have occurred in the vicinity since and can still be seen. They are seasonally filled with water to ground surface level, and are at much shallower depth.

Several other small pot-hole features have also occurred in close proximity to the Cardiff colliery portal (at very shallow depths - less than 30 m). Many of these holes are purported to have occurred after extraction of "top" coal on retreat from the mine. (Top coal is the coal left in the roof - usually 1 m or so thick - to maintain roof stability as the mine was developed.) Personal communication by Fotakis (1985) with the local residents suggests that the majority of the pot-holes occurred only after the State Energy Commission began pumping water from the flooded mine.

The Hebe Colliery

A similar event to that of the large plug failure in the Cardiff Colliery occurred in 1965 at the old Hebe Mine in the Muja Sub-basin, where workings - approaching 200 m depth - intersected an uncemented borehole.

Extremely high water pressure within the roof aquifer systems resulted in inundation of the mine with ground water, taking with it any areas of loose unconsolidated sandstone that intersected the borehole from seam roof to the surface. The resultant inflow material was in the form of a "slurry". It appears that at least one of these stratigraphic zones of unconsolidated sandstone further intersected a channel of "washouts", which, as explained later, are usually filled with soft clay material and/or water and can extend for hundreds of metres. Consequently surface subsidence was noted tens of metres (laterally) from the borehole (personal communication with ex-mine manager Mr R Ferguson).

The combination of these events brought about the closure of the mine, and initiated the commencement of the Muja Open Cut in it current form.

In general, mining practices prior to, and at the time of the study restricted high percentage extraction at shallow depths to mine panels that were overlain by natural bushland, where any subsidence damage could be fenced off and rehabilitated comparatively simply. When mining beneath sensitive surface features, the mine is worked to ensure the roof and pillars remain stable, thus preventing large-scale collapses.

Due to the irregular nature of discontinuous subsidence detailed investigation of this form of subsidence in this study. However,a general discussion of the potential for discontinuous subsidence in the Collie Basin is given in Sections 3.1 and 3.3.

2.5.5 CONTINUOUS MINING SUBSIDENCE

The better documented and researched form of surface subsidence in most coal mining regions, is the continuous trough-shaped form (Figure 2.6) whereby the ground surface sags gently towards the centre of the extraction panel without any major shearing or stepping at the surface. The visual impact of continuous subsidence troughs on the surface is usually much less than the discontinuous forms.

Subsidence has been investigated formally since the 19th Century, and during this time many ideas have been formulated regarding the mechanisms of subsidence propagation. Fitzpatrick (1987) has divided these earlier investigations into Beam, Dome and Plastic ideology and provides an interesting summary of some of these investigations. A summary of Fitzpatrick's historical investigation for each of these ideologies is provided below.

Beam Theories

In the mid 1800's, Gonot provided a simple theory on the extent of surface subsidence expected above mines. His proposal, thought to have been derived from the work of Toillez, assumes that the subsidence effects due to extraction extended at right-angles to the dip of the seam, as shown in Figure 2.7. This was criticised in 1867 by both Schulz and Sparre when applied to steeply dipping seams, as the theory predicts that the subsided area would extend to infinity on the down-dip side of the panel. This is an unlikely situation considering field observations of angles of draw in various mining regions throughout the world.

Schulz thought that subsidence would develop along a line of break, and the `break' line would vary according to the geology; in sandstone the line of break would be vertical on the rise side and normal to the seam on the dip side; in limestone both lines would be vertical (Figure 2.8 a & b). Sparre on the other hand suggested that each layer of strata should be considered individually, and the break line for each bed could vary between vertical and normal.

A more detailed study carried out by Dumont in 1871 showed that Gonot's theory could be considered reasonably valid if the dip of the strata was less than 68°. Fitzpatrick claimed that Dumont's findings were tempered, though, by the fact that his area of investigation had been severely disturbed by previous mining.

CONTINUOUS SUBSIDENCE TROUGH ABOVE A SUPERCRITICAL WIDTH PANEL

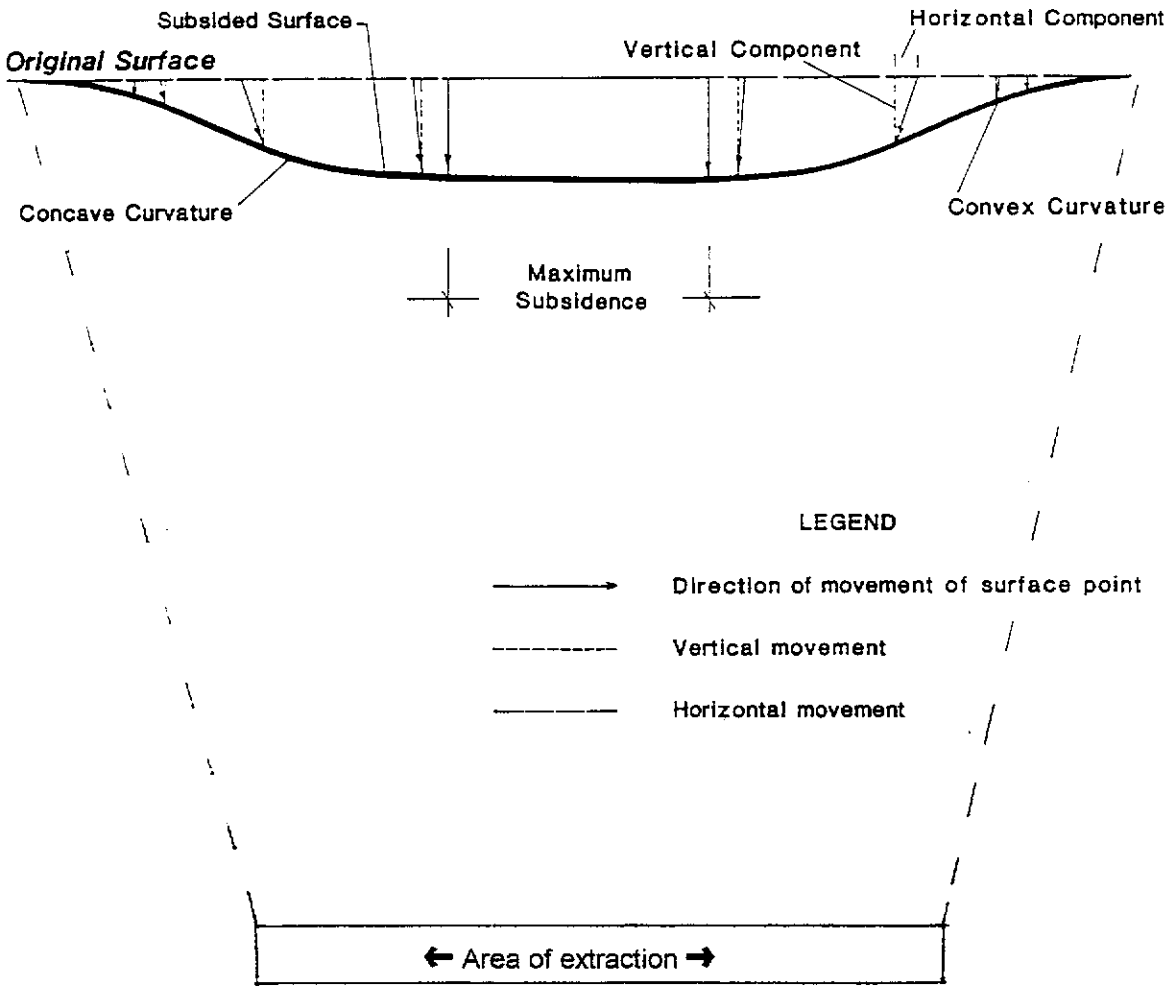

Figure 2.6

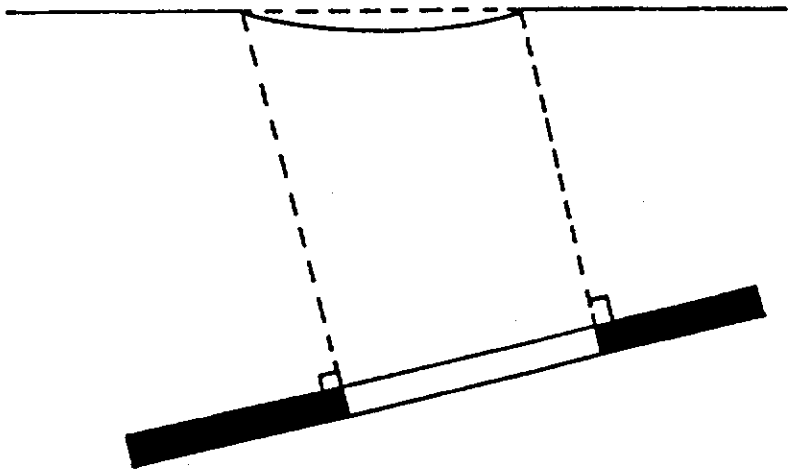

GONOT'S THEORY **Figure 2.7**

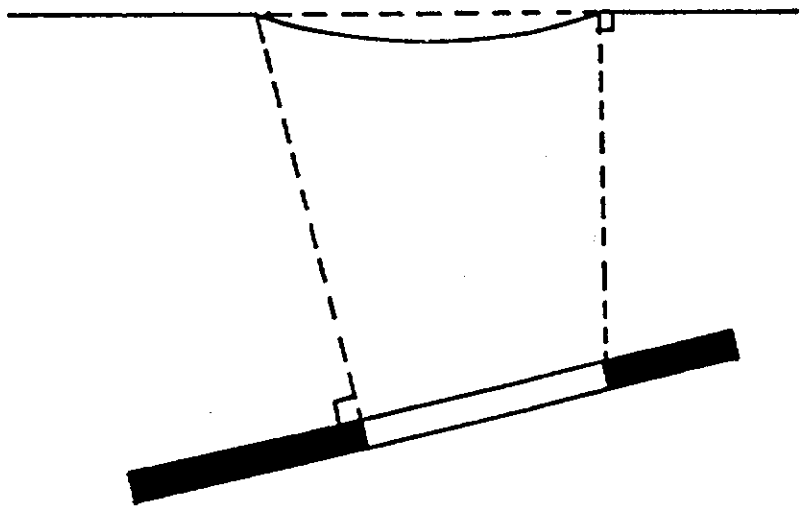

SCHULZ'S THEORY FOR SANDSTONE **Figure 2.8 a**

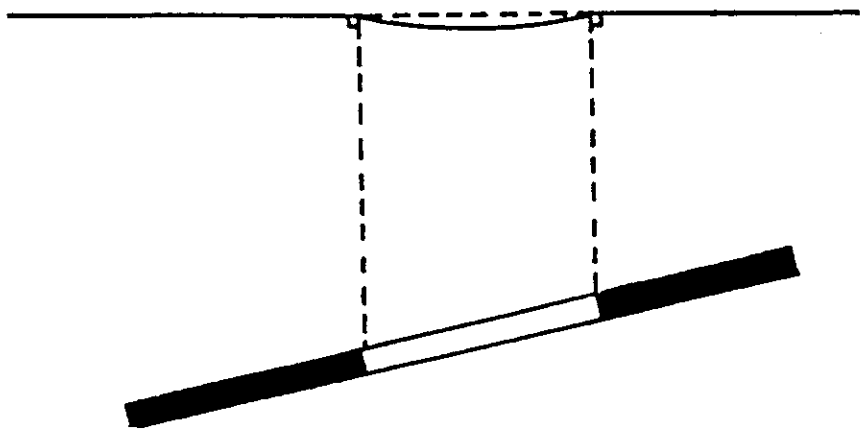

SCHULZ'S THEORY FOR LIMESTONE **Figure 2.8 b**

Further analysis by Jicinsky (1898) expanded the work of Schulz and Sparre by expressing the angle of the breakage plane (β) to the vertical in terms of the angle of dip of the worked seam.

i.e. $\beta = \theta/2$ when $\theta < 45°$

$X = 45° - \theta/2$ when $\theta > 45°$

where : β = angle of breakage plane (to the vertical), and

θ = angle of dip (to the horizontal).

Thus, according to his theory (illustrated in Figure 2.9), there is no subsidence outside the panel edge for a horizontal seam, which incorrectly assumes there to be no angle of draw. According to Fitzpatrick, Jicinsky was the first researcher to advocate the idea of the strata swelling (i.e. the modern concept of bulking) during subsidence development.

Lehmann's "Trough Theory" (Figure 2.10) has been described in Grond (1952), and is based on typical bending theory of stiff beams. The concept of zones of compression and extension are still used today, however, there is little evidence to support the 'anticline' depicted above the panel edge.

Dome or Arch Theories

In 1882 Rhiza improved upon the vertical theory by allowing for movements beyond the undermined area. He conceived of a `Dome of Tearing' based on static analysis of undercut rock (Figure 2.11). Briggs later acknowledged that this suggestion, along with the later work of Fayol, may be indicative of the preliminary stages of subsidence development, but had little value for subsidence prediction. It is not often that "tearing" is extended to the surface in deeper mines.

An interesting result of Fayol's work was the concept of a width/depth ratio (the basis of modern thinking in most countries) where the likelihood of surface damage increased as the width to depth ratio increased. Fitzpatrick (1987) states "his belief in the existence of a `harmless depth', though not alone in this (Jicinsky also suggested this), was naive, however, and not supported by general observations." The author concurs with this view.

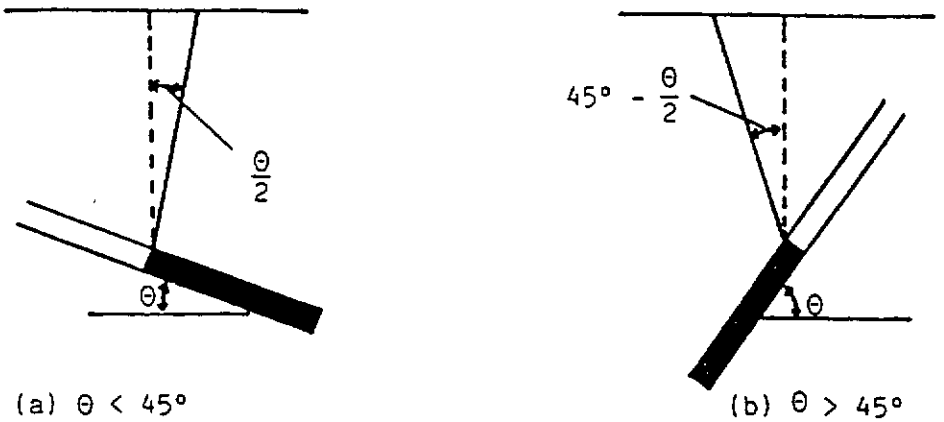

JICINSKY'S THEORY **Figure 2.9**

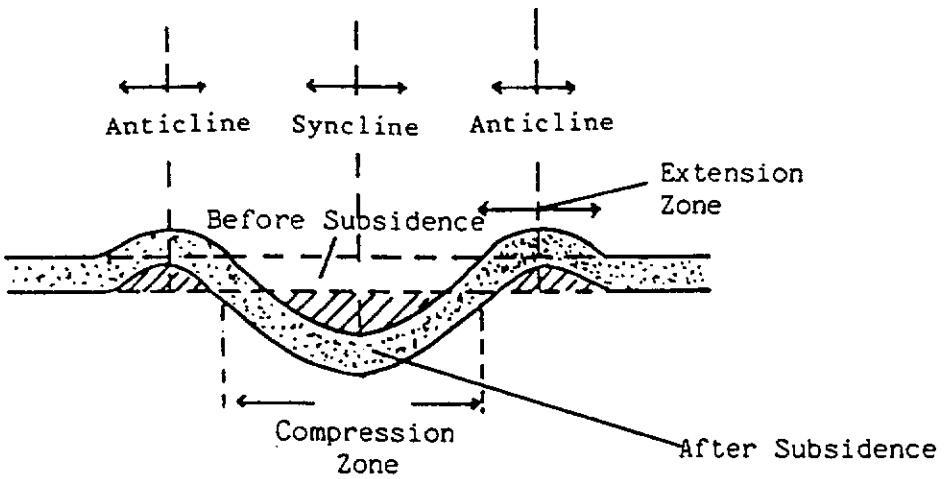

LEHMANN'S THEORY **Figure 2.10**

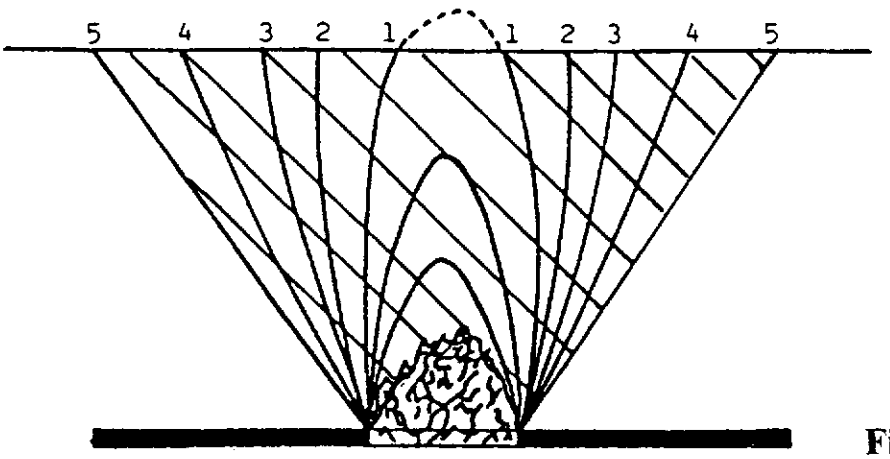

RHIZA'S THEORY **Figure 2.11**

Halbaum (1903) advocated a combination of a beam-type and a dome-type failure with the existence of a neutral axis in an overlying cantilevered beam (Figure 2.12) in order to explain the effects of subsidence. A major difficulty, however, was in deciding what effect layered strata would have on the position of the neutral axis. This remained undetermined, along with the effects of narrow extractions on the supposed `dead zone'.

Plastic Flow Theories

As early as 1899, Trompeter published work advocating the idea of a plastic or at least pseudo-plastic flow of material towards the excavation. The consideration of flow towards the extraction raises the concept of horizontal displacement in addition to vertical movement. Accordingly, the phrase `Trompeter's Zone' is well known in mining subsidence as the limit of the zone of subsidence - now defined by the angle of draw.

This very early research provides some insight into the staged development of current subsidence theories and illustrates how each researcher has contributed in some way, although not totally explaining the subsidence phenomenon. Hazine (1977) notably quoted Goldreich, claiming that `no-one will ever succeed in bringing the problem of subsidence into a system capable of being expressed by exact formulae'.

2.5.5.1 Initiation of Continuous Subsidence

Considering the above historical theories, and the work of many others, it is obvious that in order for continuous subsidence to develop, a void must be created below the surface which:

- is of sufficient dimension to initiate collapse or extensive relaxation of the roof, and all superincumbent strata leading to the surface (as for discontinuous subsidence), and
- has overlying strata with appropriate geomechanical properties to allow for "continuous" deformation of the ground surface.

MINING SUBSIDENCE ZONES
(According to Halbaum 1903)

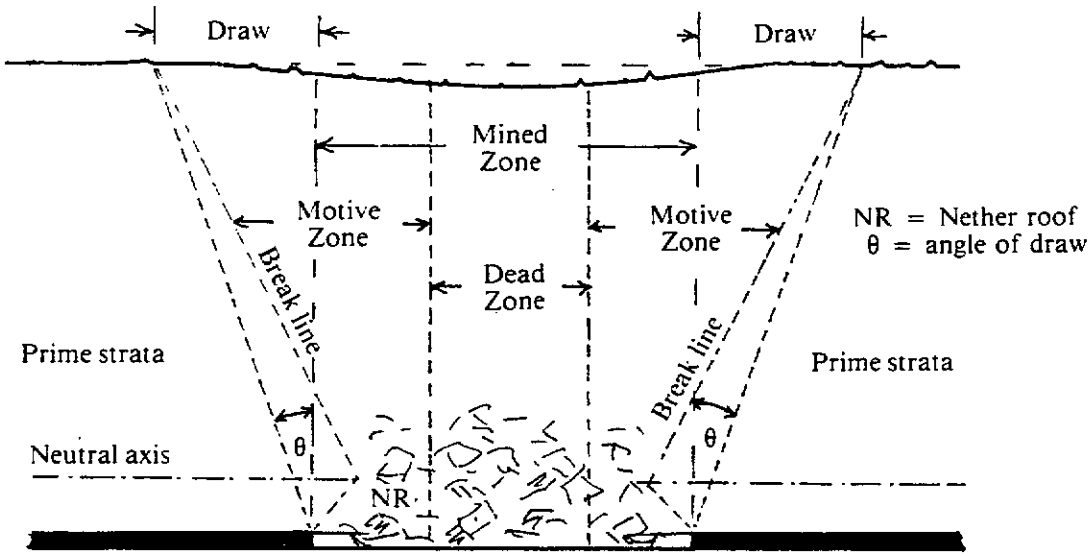

Figure 2.12

Previous work by Misich (1985)[2] identified two mechanisms leading to continuous subsidence trough formation due to mining in the Collie Basin:

1) "total" extraction of coal, and

2) panel collapse (creep).

"Total" extraction

Total extraction, by definition, is the removal of 100% of coal within the panel limits, however, this is rarely the case in practice. This term can be loosely applied to Wongawilli extraction where up to 15% of coal is left unmined as remnant stooks during fender lifting. The main feature of total extraction processes is that large spans of unsupported roof can be developed at various stages of extraction. When these spans reach a sufficient dimension, the immediate roof will collapse. The forces involved are tensile and shear stresses, which are largely dependent on the length of the roof beam. If one assumes that the driving mechanism of ground collapse is the stresses developed due to bending, then the idealised fixed beam equations (eg. Adler & Sun, 1976) can be used to estimate the stability of large spans of roof:

Max. tensile stress : $\sigma max = \frac{\gamma L^2}{2t}$ (at ends) 2.5 (4)

Max. Shear stress : $\tau max. = \frac{3\gamma L}{4}$ (at ends) 2.5 (5)

where: γ is the unit weight of the beam, given by ρg (N/m^3),
L is the beam length, and t is beam thickness.

When the roof beam or strong interburden layer is overlain by thinner or weaker strata then these members will tend to deflect downwards and load the immediate beam. This has the effect of increasing the unit weight of the beam, which, according to Adler & Sun (1976), can now be calculated by the equation:

$$W = \frac{E_1 t_1^2 (p_2 t_2 + \ldots + p_n t_n)}{E_1 t_1^3 + E_2 t_2^3 + \ldots + E_n t_n^3} \quad 2.5\ (6)$$

Where: n is the number of strata members above the initial beam,
E is the elastic modulus (N/m^2), and
p represents the unit weight of each beam (N/m^3)

It is considered by the author that a reduction in loading (p) of each sequential stratigraphic layer should be applied to Equation 2.5(6) as the length of each beam will lessen according to the shape of the "stress relief arch" above the bridging member (assuming that the loading on the supporting beam is attributable to the commonly acknowledged stress arching theory - e.g. Wilson, 1980).

As the tensile strength of intact rock is usually lower than the shear strength, roof beams tend to fail in tension. Once the initial failure has taken place, the caving of the immediate and upper roof, can be expeted to follow the cantilever theory, as the upper and immediate roof overhangs the void area (Unrug & Szwilski, 1982, provides explanation of cantilever-type caving of near-roof strata). The maximum stress in this case would be at the pivot of the cantilever - the coal seam abutment.

As the coal face advances, the length of the cantilever increases. This induces shearing and higher normal stresses according to the magnitude of the bending moment. The length of the cantilevering roof strata will increase until a critical length is reached at which the roof will collapse. Visual and audible observations in WCL's mines, indicate that the abutment pressure on the coal face reaches a peak just before caving occurs, which supports the cantilever theory. In this study, it was not possible to determine the critical cantilever length in the field, largely due to the effect of variable sizes and locations of remnant coal stooks.

When each split and fender is mined in succession, the individual collapses link to form a much larger area of unsupported material. Eventually, the area of collapsed and relaxed strata is sufficient to initialise surface subsidence.

It follows that if the colliery is overlain by a very stiff and/or massive layer of strata that can bridge across the panel abutments the development of surface subsidence is reduced (eg. Krishna, 1989).

Panel collapse/creep

Panel creep is a colloquial term which describes the manner in which large-scale collapses migrate *en masse* from one area of a mine to another. Such creeps can involve a small number of bords or complete panels; the rate of migration can be relatively slow or very sudden. There are many documented cases of such massive failures. One example occurred at the Hamilton Pit, at Glebe, NSW, a 20 ha area collapsed and in the process killed 11 mine worker (Anderson, 1993). In most

underground coal mine operations, creep is due to the size of coal pillars being insufficient to support the tributary cover load. The strengths of roof and floor material strengths, such as the Hawkesbury Sandstones in the eastern states of Australia, are much greater than coal strengths and when extensive areas of roof cave, there can be a large transfer of stress, through cantilever action, to the coal pillars. This redistribution of stress can exceed the strength of the coal pillars, which then collapse, usually in sequence radiating outward from the area of extraction.

To avoid this type of creep, the mine pillars are designed to be of dimension (mass strength) to be able to withstand the modified tributary loads. The ratio of the strength of the coal pillar mass to the tributary load is termed the factor of safety (FOS_C). The recommended design FOS_C, for the Collie Basin is 1.6 (Misich and Humphreys, 1988). This FOS_C corresponds to that given by Salamon and Oravecz (1967) for South African coalfields. This design criteria can be expressed as:

$$\mathbf{FOS_C} = \mathbf{Pillar\ Strength/Pillar\ Load} = \mathbf{1.6} \qquad 2.5(7)$$

The strength of coal pillars is estimated using a modified Hustralid/Salamon-Munro/Wagner pillar strength design criterion as described by Misich and Humphreys (1988). The pillar strength **(PS)** and pillar load **(PL)** are calculated by:

$$\mathbf{PS} = k \times \mathbf{(Weff/Wo)^{0.46}/(Mh/Mho)^{0.66}} \quad \text{(MPa)} \qquad 2.5(8)$$

$$\mathbf{PL} = \sigma 1 \div \mathbf{(1 - extraction\ ratio)}, \quad \text{(MPa)} \qquad 2.5(9)$$

where: $\sigma 1$ = the vertical stress due to weight of overlying strata,

Wo, **Mho** = 1 m, **Wp** = Pillar width (m),

k = UCS of 1 m^3 of coal - 6.5 MPa (Misich & Humphreys, 1988),

Weff (effective pillar width) = **4 x Ap/Cp** (m) (Wagner, 1980), 2.5(10)

Ap = Pillar area (m^2), **Cp** = Pillar circumference (m), and

Mh = Mining height, (m).

In the Collie Basin, however, the strengths of roof and floor materials can be up to an order of magnitude less than coal strengths. Consequently creep through failure of coal pillars is rare in Collie and has probably never occurred to any large extent within an extraction panel. This presumption is supported by the brief accounts given (by

Wilson 1943) of creeps that had occurred in four Collie coalfields collieries before 1940. It was noted in each case that significant roof or floor movement had occurred immediately before the ultimate closure of large areas of the mine.

Investigations by Misich (1985)[2] proposed two possible modes of panel collapse for the Collie Basin other than simple convergence of the overlying strata and failure of the coal pillars (Figure 2.13). These are:

1) Failure of roof or floor materials through bearing capacity being exceeded by tributary loads transferred through the under-sized pillars (Figure 2.13 b). This failure mechanism is similar to a foundation problem and is commonly called pillar "punching".

   The potential for bearing failure in underground mines was first assessed in an internal memorandum by Misich (1985)[2] using Terzaghi's relationship for ultimate bearing capacity (Qu) of foundations :-

   $$Qu = C.Nc + Yz.Nq + 0.5.Y.B.Ny \text{ (Smith, 1973),} \qquad 2.5(11)$$

   where C = cohesive strength of the material (MPa),

   Ny, Nc, and Nq are constants, dependant on the angle of internal friction,

   Y = the specific weight of the material (MN/m^3)

   B = pillar width (m)

Note : the term Yz.Nq will normally be zero unless the failure takes place in a weak bed some distance below the roof or floor contact.

The design criteria adopted for the design of minimum pillar width was:

$$Qu/PL \geq 3.0 \qquad 2.5(12)$$

2) When caving occurs on all sides of a pillar (through either excessively wide bords with insufficient support, or pillars punching differentially into the roof or floor), the resultant pillar consists of coal for the lower section and sandstone for the upper section (Figure 2.13 d).

MODES OF SUBSIDENCE INITIATION

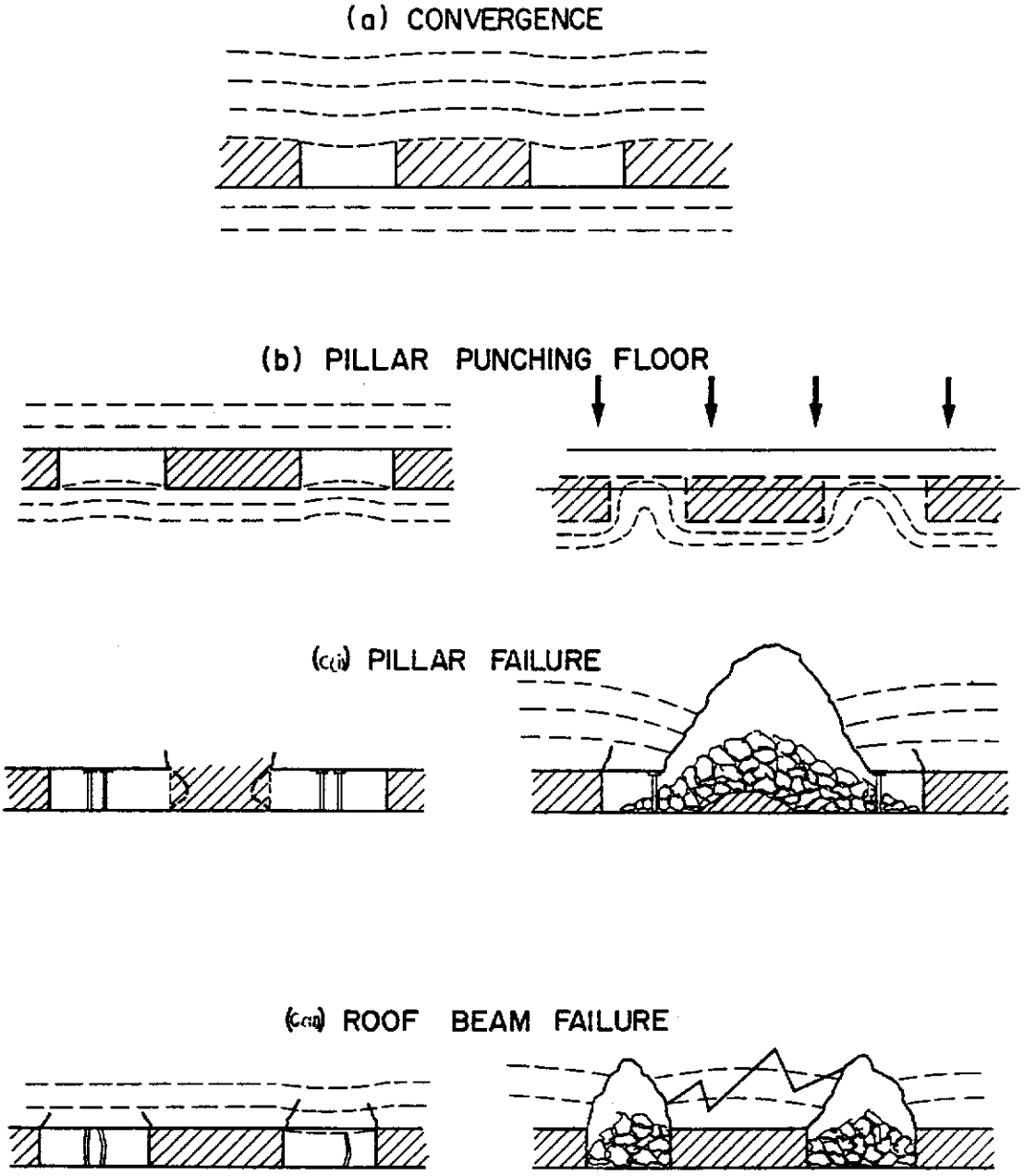

Figure 2.13

It is a combination of the weak sandstone in the composite pillar and a dramatic reduction in width to height ratio of the resultant pillar that causes failure. Once one pillar has failed, stresses are redistributed to adjacent roadways and pillars and the process continues, resulting in a creep. When the area of creep is of sufficient dimension, subsidence will occur.

At this stage of investigation this assumption could not be verified in engineering terms. Furthermore, the precise mechanisms and sequence of events leading to failure could not be established. It was acknowledged that further research was required. (This phase of investigation is described in Section 5.3.2.)

2.5.5.2 Surface Subsidence Trough Characteristics

Ideally, the subsidence trough is symmetrical to the middle of the panel at the point of maximum subsidence (Smax). Depending on panel width, each point leading away from Smax will have progressively less vertical displacement until there is no measurable subsidence.

Subsidence also involves lateral movements (Kratzsch, 1983) which also trend toward the centre of the panel or the point of Smax. These lateral movements are usually more destructive to surface features than vertical subsidence. In fact, subsidence troughs have a number of well-defined characteristics which are used to qualify subsidence in all mining regions. These subsidence trough characteristics or parameters are illustrated in Figures 2.14 a&b and listed below:

- critical width of extraction
- maximum subsidence
- angle of draw
- inflection point
- maximum tilt
- maximum horizontal strains
- curvature
- time dependency

SUBSIDENCE DEVELOPMENT FOR THE CRITICAL AREAS OF EXTRACTION

(From Brauner 1973)

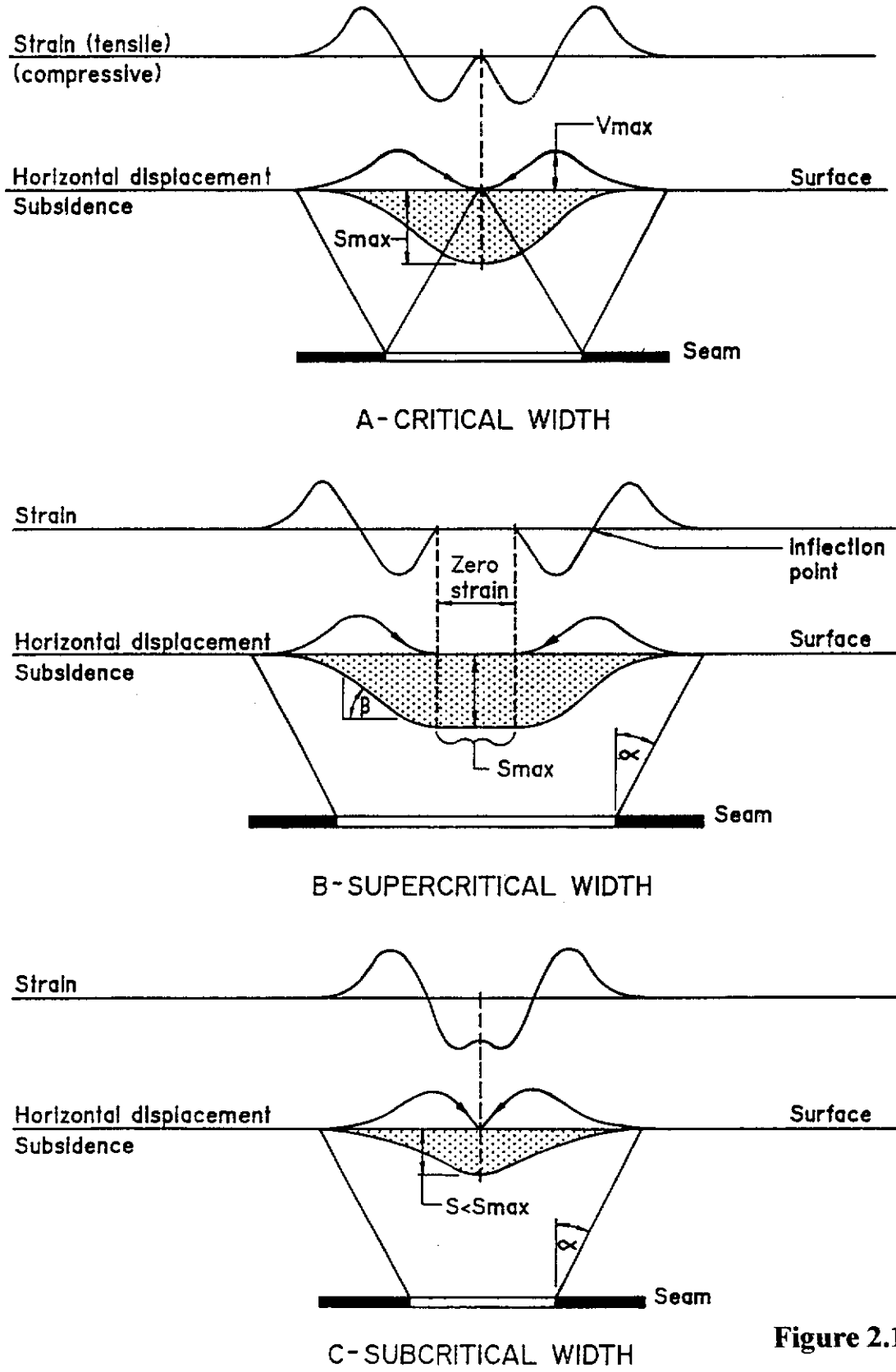

Figure 2.14

Prior to this research project, none of these parameters were well defined for the Collie Basin. The only definitive data available were from Misich (1985)[1] and Fotakis (1985), which were based largely on inferred subsidence data from panels that had already collapsed, and from Hebblewhite and Humphreys (1988) which described interim subsidence data from stage 1 of the ACIRL trial panel. (The assessment of subsidence in Hebblewhite and Humphreys (1988) was restricted to the provision of only the maximum subsidence recorded above sub-panel A of that panel. Full evaluation of the measured subsidence from the ACIRL panel was completed under the scope of the PhD thesis by the author.)

Each of the above eight subsidence characteristics is defined briefly in the following sub-headings.

Critical Width

Critical width is defined as the point where there is no increase in subsidence with increase in panel width. Subsidence profiles can be related to one of three extraction criteria: sub-critical, super-critical, and critical extraction widths (Figure 2.14 a & b).

Critical width extraction is where the ratio of panel width/depth of cover (W/H) typically equals 1.4 and represents the width at which the maximum possible subsidence is reached (Figure 2.14 a). It follows that in flat terrain, super-critical width panels, with W/H ratios greater than 1.4, develop a flat subsidence profile throughout the central section of the subsidence trough. Sub-critical panels, with W/H ratios less than 1.4 have a V-shaped subsidence profile (see Figures 2.14 b and c).

Maximum subsidence

The magnitude of Smax, Kratzsch, 1983 is dependent on:

- the effective height of extraction (T) = [Mh x Extraction Ratio] 2.5(13)
- depth of cover (H),
- extraction panel width (W), and
- the geology of the site.

Smax also determines the magnitude of the destructive horizontal movements, and therefore when subsidence control is required, panels are often designed to minimise Smax only. A number of British, American and Australian investigations have successfully reduced a large number of case history data to produce empirical/graphical charts for estimation of maximum strains and slopes from the predicted or measured Smax. Figure 2.15 - adapted from the plot given by NCB (1966) - compares the development of Smax with increasing W/H in panels mined in Collie prior to the research project, and other mining regions in Australia and the UK.

Angle of Draw

The angle of draw represents the angle from the panel edge to a point on the surface where there is no measurable subsidence (Figure 2.14 a). The point of zero "measurable subsidence" is difficult to establish due to natural seasonal movements and the accuracy of surveying techniques. In the Collie Basin this background error is in the order of ±30 mm. When seasonal background ground movements are unclear, this value is used as the limiting measurement of surface subsidence to determine the angle of draw.

Where seasonal effects are known, the limiting subsidence used for estimation of angle of draw is ±15 mm, which equates to survey error.

A similar approach has been used by Holla (1986) and Amadek & Jeran (1985) who proposed the use of either 0.1 ft vertical subsidence, 2 mm/m tilt, or 1 mm/m horizontal strain to define the limit of mine subsidence. The effect of background movement on the angle of draw can be minimised by altering the pre-mining survey according to the mean variance in reduced level, measured throughout one complete year, of stations located well outside the panel edge.

Other influences on the angle of draw (and other subsidence characteristics) include:-

- the seam dip,
- the surface topography,
- irregularly shaped panels (through design variation or mining problems), and
- bearing failure (pillar punching) or elastic deformation of the foundation materials beneath set-up road pillars, chain pillars and mini splits adjacent to each panel.

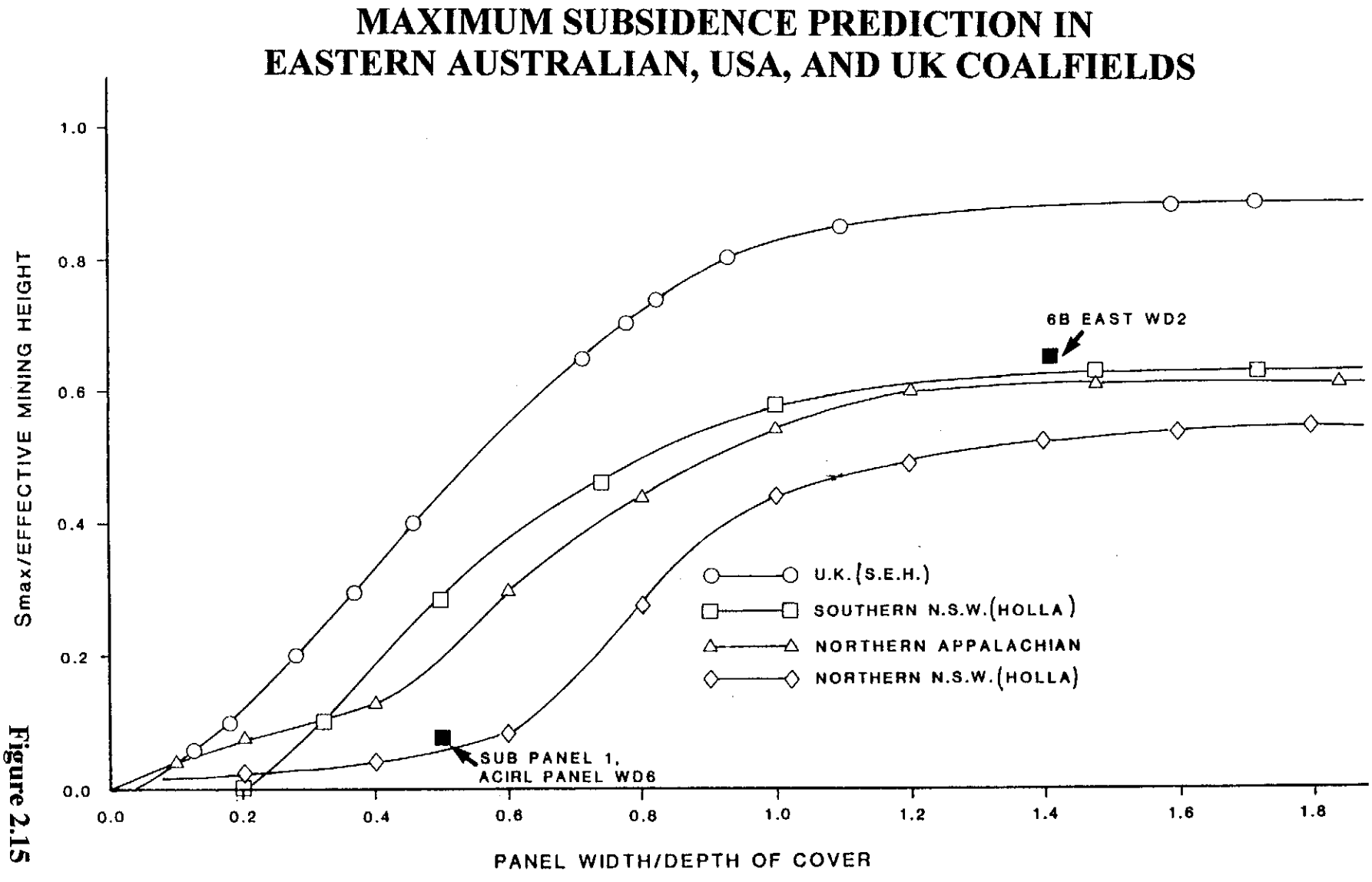
MAXIMUM SUBSIDENCE PREDICTION IN
EASTERN AUSTRALIAN, USA, AND UK COALFIELDS
Smax/EFFECTIVE MINING HEIGHT
PANEL WIDTH/DEPTH OF COVER
0.0
0.2
0.4
0.6
0.8
1.0
1.2
1.4
1.6
1.8
6B EAST WD2
SUB PANEL 1,
ACIRL PANEL WD6
U.K. (S.E.H.)
SOUTHERN N.S.W. (HOLLA)
NORTHERN APPALACHIAN
NORTHERN N.S.W. (HOLLA)

Figure 2.15

The effect of seam dip is well documented; the method most commonly used for estimation of the angle of draw affected by seam dip is the NCB (1975) approach. The requirement to investigate the effects of inclined seams in this study is considered unwarranted, due to the relatively consistent 1 in 12 dip of the working seams, and also due to the reported fact that the effect of dipping beds on displacing the maximum subsidence within weak overburden is small (Ren et. al., 1988). The effect of surface topography on mining subsidence is also well documented (e.g. Shu, 1990) ,however, in the Collie Basin topographical influences are considered to be minimal due to the gently undulating nature of the land surface.

Inflection Point

The inflection point represents the position of zero strain between maximum compressive and tensile strains at the panel edge (Figure 2.14). Its location commonly coincides with the point of maximum tilt. It is often reported that subsidence at the point of transition equates to one half of the maximum measured subsidence.

The importance of the inflection point to modelling is that it represents the point from which the shape of the subsidence profile is defined as concave toward the panel centre, and convex toward the limit of subsidence.

Some authors have reported migration of the point of inflection according to the W/H ratio. Holla (1986) in presenting subsidence data measured in the Eastern Australian Coalfields provides one example of this. There was insufficient data (prior to this research project) to comment on the applicability of Holla's findings to the Collie Basin strata.

Ground Tilt

Ground tilt is the change in elevation between two points at the surface divided by the distance between the points, and is commonly expressed in mm/m. The location of maximum tilt is inward of the panel edge (Figure 2.14 a) and usually coincides with the point of inflection. As discussed previously, the amount of tilt developed within subsidence troughs is primarily dependent on Smax.

Curvature

Ground surface curvature expresses differential vertical movements with respect to horizontal movements and has the dimension m^{-1} or ft^{-1}. Curvature is often expressed by its reciprocal, the "radius of curvature", where the smaller the radius, the greater the horizontal strain. (Common values of the radius of curvature are 1,000 to 2,000 m.) There are two forms of curvature (see Figure 2.14):

- convex curvature, where the subsided surface flexes across the panel boundary (coincidental with the area of tensile strain), and
- concave curvature, where the surface approaches the position of maximum subsidence (coincidental with the location of compressive strain).

Subsidence-horizontal strains can be proportional to subsidence curvature (e.g. Karmis et al 1985). This relationship is discussed below.

Surface Horizontal Strains

Horizontal strains are measured as the relative change in distance between two points and commonly expressed in millimetre change per metre ground length (mm/m). Surface strains can be either compressive (-ve) or tensile (+ve) and vary across the length of a subsidence trough.

Tensile strains are manifested as the ground surface is "stretched" across the position of the panel edge (convex curvature) and subsides toward the point of maximum tilt (Figure 2.14). Compressive strains are located between the point of maximum tilt to the position of maximum subsidence near the middle of the panel (concave curvature). Karmis et al. (1985) found that the relationship between curvature and strain for a number of US case data was:

$$0.92 \times (\text{curvature} \times 10^{4})^{0.5}. \qquad 2.5(14)$$

Again, there was insufficient field data prior to starting the research program to allow for any meaningful assessment of curvature/strain relationships for the Collie Basin sediments.

Time Dependency

The effects of time are perhaps the most uncertain factors in prediction of subsidence. Movements can begin days to years from extraction commencement and last weeks to years at completion. Time taken for full subsidence to occur depends largely on the length of the period of extraction, and the rate of advance (Brauner,1973).

Other factors affecting the duration of subsidence include:-

- strata litho-facies,
- depth of extraction,
- stowing/stowage type,
- previous workings,
- width of extraction, and
- the design of the mine (pillar and roadway width, roof support etc.).

Fotakis (1985) found that subsidence measured over time at the survey point HC 35 above 6B East Panel, WD-2 (in the Collie Basin) was relatively dynamic for some time after the initial ground movement; 80% Smax within 2 months, 95% within 3 months, and Smax finally occurring between 6 and 12 months afterwards. However, this observed time effect is personally considered to have been largely influenced by the time dependent form of creep which initiated the subsidence. It is considered that the 6B East panel time-lagged subsidence would not be representative of 'normal' total extraction subsidence development in Collie.

More detailed description of the characteristics of "continuous" subsidence troughs can be obtained from Peng (1992), NCB (1975), and Kratzsch (1983).

2.5.5.3 Historical Evidence of Continuous Subsidence in the Collie Basin

Although there are few reported cases of continuous subsidence, there is undoubtedly some areas where continuous trough-form surface subsidence would have occurred and has not been recorded or gone unnoticed (mining was mostly beneath native bushland and difficult to detect). Furthermore, these bushland areas were of little concern to the mine, nor the community and thus expensive and time consuming surveying of the surface would not be warranted.

Suspicion of subsidence trough surface deformation stems from personal knowledge of strata behaviour due to ground collapse in current workings. From historical records, extensive areas of ground collapse in workings occurred in many mines. These large areas of caving were both planned and unexpected. Planned caving occurred when the mines extracted pillars - usually toward the end of the life of the mine - by the "caving method" (as used in the Cardiff Colliery) or by pillar splitting. Unexpected caving resulted from insufficient mine planning/design for roof support or pillar

dimensions, usually in the form of a "creep".

In the document by Kovago (1986), recorded cases of creep, from within several mines dating from 1913 to 1940 were explained in varying detail. The area of influence of each creep varied greatly, from 0.7 to 11.0 Hectares of mine workings. Such large areas of collapse are certain to have subsided the surface to some extent. As would be expected however, recent inspections of the surface above such areas could not substantiate any forms of subsidence, as the topography is undulating and would disguise any surface movements, any tension cracks would certainly be infilled and covered with vegetation by now.

Three of the better noted cases of continuous subsidence during this period are summarised below.

Proprietary Colliery

In 1927, some concern was expressed for the stability of the Collie - Narrogin railway as roof falls in underground workings, initially mined in 1916, extended beneath the railway and subsidence cracking was noted on the surface (from correspondence between the Inspector of Mines and the State Mining Engineer dated 13 December 1927). The railway was reballasted, the surface closely monitored, and the offending bords were "well chocked up" to prevent further collapse. The ground stabilised following this remedial work and no further subsidence was detected. The average subsidence was estimated to be approximately 0.5 m (in correspondence from the Government Geologist held at the WA Department of Minerals and Energy, dated 11 December 1928).

Correspondence between the Mines' Inspector and the State Mining Engineer in December 1927 indicates the cause of the falls was due to swelling of a 6 m clay layer, 10 m from the surface, as winter rains percolated down (24 m above the mine). This is considered, by the author, to be an unlikely cause; it is more likely that it developed from a local creep. Comments from the Inspector of Mines and later the Government Geologist that the roof fall has "gone across" heavily supported bords (with no signs of pillar distress) is supportive of the author's view.

The extent of the roof falls was stated to be 110 m long, the coal pillars averaged 1.8 m high and were typically 7.3 m wide and 18.3 m long. The depth of cover varied from 37 to 49 m at this site.

Cardiff Colliery

Investigations into the cause of a partial rediversion of road No. 2020, over the Cardiff Colliery, some 20 years ago (by Fotakis, 1985) revealed that a large area of the surface had subsided, and, due to concern held for travellers, the road was closed until a safe route was constructed around the subsidence site. The cause of the subsidence was reported to be undersized pillars, resulting from the mine's pillar splitting strategy. A recent inspection of the area could only locate the wire ropes used to cordon off the area there were no signs of a depression.

Fotakis attempted to locate the original survey stations along the road and relevel the points, using a Geological Survey map, 1950. As the accuracy of original levelling was to the nearest 0.3 m, and the positioning of the coordinates of the stations to the nearest 3 m, there is potential for significant error in relevelling. The maximum subsidence measured from resurveying was 2.0 m.

The mining height of the Cardiff Colliery varied from 2.5 m to 4.7 m (full seam thickness) in extraction. Fotakis assumed that the miners removed "top" coal at this location and that the mining height would probably be 4.5 to 4.7 m (from borehole data). He therefore concluded the Smax/Mining height ratio (with reservation) to be :-

$$2.0/4.5 = 0.44$$

Fotakis however did not take into account unmined coal left in place during the mining process. If it is assumed that only 70% coal was extracted (the maximum extraction ratio for that type of mining), then according to Kapp (1982) the Smax/T ratio could be as high as:

$$2.0/(4.5 \times 0.7) = 0.63.$$

Assuming that the area of collapsed ground in the mine is 350 m (from measurements taken from an old local government plan), the W/H ratio must be greater than 1.4 and Smax is expected to have developed. (The depth, though unknown at this specific location, did not exceed 150 m at any point within the mine).

Co-operative Colliery

The Co-operative Colliery (Figure 1.2) ceased production in 1960. In 1956 surface cracking was detected in the main road to Perth and in a general area to the West of the Collie cemetery. A subsidence grid was installed over the area, at the request of the Inspector of Mines, and the surface was monitored over a two year period.

The maximum subsidence measured - which took some time to reach after the installation of the grid - was 1.32 ft (0.4 m).

As there are no details on the extent of the subsidence, or the mining parameters, and because the survey line was installed after surface movement was detected (which means that much of the subsidence would have already occurred), it is not possible to calculate the subsidence factor for this colliery. In fact it is interesting to note :-

- the only reason the area was detected was cracking in the main road, and
- time dependant response of subsidence. (Time dependency is discussed further in Section 3.1.9)

A more recent collapse of ground resulting in continuous subsidence being developed on the surface occurred in October 1981, above the 6B East panel in WCL's WD-6 colliery. This event has been reasonably well investigated by the author and Fotakis (1985). A summary of these investigations is provided below.

6B East Panel - WD-2 Colliery

The only information available from the surface subsidence over 6-B East was one survey point at roughly the centre of the panel, and the sequential lateral movements of each of the concrete support saddles along the State Electricity Commission water supply pipeline. (As the ground subsided, the supports moved laterally, according to their position in the subsidence trough.) The pipeline runs directly over the centre of the panel through its long axis and along seam strike. It was therefore possible to directly use the measured movements of the concrete supports to define lateral ground movements within the subsidence trough. This data was the best suite of information (prior to this study) from which a subsidence profile could be plotted and compared to profiles from other mining areas to ascertain whether any of the existing predictive profile functions could be used for Collie Basin subsidence.

To be able to plot a subsidence profile, three basic properties of the trough are required; Smax, the point of inflection, and the angle of draw or position where subsidence ceases.

Smax was determined using the survey station (HC45) which is off-set from the centre of the panel. Because the W/H ratio of the extraction panel was greater than 1.4, the subsidence profile was super-critical and Smax would have been achieved in the centre. From super-critical subsidence profiles in studies by the NCB (1975), the

percentage of Smax at the survey station would be approximately 94% of the subsidence expected at the true centre.

Thus the maximum subsidence would be 0.75 m. This equates to a 65% subsidence factor for the effective mining height (2.3 m x 50% E), which closely represents the value given by Kapp (1982) and calculated previously for the Cardiff Colliery.

The point of transition was determined from horizontal movements of the concrete supports, measured along the pipeline. It was identified as the point where the supports to the left had moved one way, and the supports to the right had moved the other. The transition point was determined to be 70 m from the centre of the panel, which is midpoint from the ribside to the panel centre.

The angle of draw was measured as the location where horizontal movement ceased outside the panel limits. The results indicated the limit of subsidence was some 120 m from the panel edge. The depth of cover at this point is 146 m, therefore the angle of draw was estimated to be:

$$\tan(x) = \frac{120}{146} = 39^\circ$$

This compared favourably with the limit angle on the side, where the limit point is 84 m from the edge of the goaf where the depth of cover is 108 m. This estimation of the angle of draw was later found to be excessive and is probably due to the effect of the pipeline stretching over a greater distance than the subsidence trough to more evenly distribute the tensile strains developed within the pipeline.

A subsidence curve was then drawn using the steps summarised below and assuming the ground surface to be flat and with a mean depth of cover (120 m).

1) A concave curve was drawn, with a near-flat base between the transition points on either side of the panel. The depth of the curve determined by Smax (0.75 m).

2) The concurve curve was straightened just prior to the point of transition at ½ Smax, representing the change from tensile to compressive strains. [Studies by Kapp (1982) and the NCB (1975) have found the transition point to represent the point where subsidence is half the maximum.] This straight section of the curve was reciprocated for the equivalent length beyond the transition point into tensile strain.

3) A convex curve was drawn from the end of the upper straight section of the curve, gradually sloping back to the limit of subsidence, finalising the curve.

To be able to compare this curve to other areas of differing mine parameters, it had to be fitted to a profile function (usually relating to dimensionless W/H ratios). Many profile functions, from a wide range of areas and reference material, were compared with the subsidence profile drawn for 6-B East Panel. It was found that none of these matched the Collie Basin data. It was thereby concluded that further research was required to develop a profile function which was more appropriate for the subsidence developed in the Collie Basin conditions.

2.5.5.4 Surface Subsidence Effects

According to Brauner (1973), ground deformations are 'allowable' if they cause little or no appreciable structural damage. The amount of allowable strain is dependent on the surface structure/feature and the surface soil/rock type.

In the case of continuous forms of subsidence, damage or undesirable modification to surface features can be attributable to any one or combination of vertical displacement, horizontal strains, tilts/slopes and curvature along the subsidence trough. Absolute vertical subsidence rarely causes direct damage to surface features, with the exception of those features dependant on drainage. Horizontal strains effect structures by creating tensile fractures, or shear (compressive) fractures and squeezing or buckling of structural elements. Damage will depend on structure type and its construction materials.

The slope of subsidence troughs can alter the gradient of roads, rivers, and gas and water mains. Subsidence can induce tilting of buildings, which can make them unsound, and can seriously disrupt industrial centres, for example, by affecting horizontally sensitive machinery such as hoists.

The direct effects of curvature on structures are:-

- Shear strain or distortion, defined as angular changes, that distort framed structures out of square.
- Bending, particularly along load-bearing walls. Concave curvature, for example, induces compression at the top of buildings.

Design limits differ between mining regions, as do the ground movement parameters used for establishing the subsidence design limits. Examples of subsidence tolerance and damage classifications for structures include the guidelines provided by NCB (1975, see Table 2.2) and the design and standards techniques for areas in eastern Australia, given by Bray & Branch (1988), and Holla & Hughson (1986). Further assessment of these design standards is not within the scope of this project.

As an example the (NCB, 1975) class of damage expected for a brickwork farmhouse, 15 m long, with 2.5 mm/m ground strain is estimated by the change in length (Δ l) of the ground beneath the structure. In this case it is calculated as:

$$\Delta l = \text{Structure Length (m)} \times \text{Expected Ground Strain (mm/m)} \quad 2.5(15)$$

i.e. $\Delta l = 15 \times 2.5 = 37.5 \text{ mm} = 3.75 \text{ cm}$,

so the second class of damage, namely "slight" must be expected.

TABLE 2.2 NCB MINE SUBSIDENCE DAMAGE CLASSIFICATION

Change in length (cm)	Class of Damage	DESCRIPTION OF DAMAGE TO STRUCTURE
0 - 3	**1**. Very slight	Hair cracks in plaster isolated fracture in the building not visible on the outside.
3 - 6	**2**. Slight	Several slight fractures showing inside the building. Doors, windows may stick slightly.
6 - 12	**3**. Appreciable	Slight fractures showing on outside of building. Windows sticking, service pipes may fracture.
12 - 18	**4**. Severe	Service pipes disrupted. Open fractures develop. Window and door frames distorted; floors sloping noticeably; some loss of bearing in beams.
> 18	**5**. Very severe	As above but worse, needs partial or complete rebuilding. Roof and floor beams lose bearing and need shaping up. Windows broken with distortion. Severe slopes on floors. Walls may buckle.

Regulations for mining beneath surface waters has also been well documented eg. Holla (1987), and Galvin & Anderson (1987). Further discussion on mine design for protection against inundation from bodies of surface water has been included in the following Section.

2.5.6 SUBSURFACE SUBSIDENCE

Research on subsurface subsidence has been minimal compared to surface subsidence investigations, largely due to the costs involved. However,several investigations have provided valuable information on the development of subsidence from seam level. For example Singh and Kendorski, 1981 identified four regions of subsurface ground movement (Figure 2.16).

1. A caving zone, where the strata immediately above the mined coal seam caves and fills the void left by coal extraction.
2. A partly fractured zone, where the strata are supported to some extent by the caved rock below, allowing this zone to sag and develop open cracks.
3. A zone of constraint, where beds are sufficiently confined by strata above and below to prevent the development of open fractures.
4. A surface zone, in the order of 15 m thick, where the strata are less constrained, and are therefore more susceptible to cracking from horizontal strains. This assumed depth of cracking compares well with Reynolds (1976) who considers that the extent of cracking is generally confined within the first 20 m. Observations by Misich (1985)[1] indicate that the depth of cracking (above 6B East Panel) did not exceed 2 m.

Halbaum, 1903 defined the subsurface as lateral zones above extraction panels (described previously). Although Halbaum's theory is considered to be generally sound, the positioning of the line of break is considered inaccurate. The point at the surface representing the limit of subsidence (the angle of draw) will experience minimal subsidence and thereby will not coincide with any line of break. Furthermore, the width of the "dead zone" will vary significantly, from almost a point in space for sub-critical width panels to massive areas for super-critical width panels.

Fritzche and Potts (1954) proposed a variation of Halbaum's theory, placing the line of fracture at the point of maximum tensile strain. This is considered to be more appropriate, and better matches field observations. Fritzche and Potts has also identified a vertically oriented "neutral zone", between zones of compression and relaxation, where there are no apparent strains.

GENERALISED STRATA BEHAVIOUR WITH MINING SUBSIDENCE

(After Singh & Kendorski, 1981)

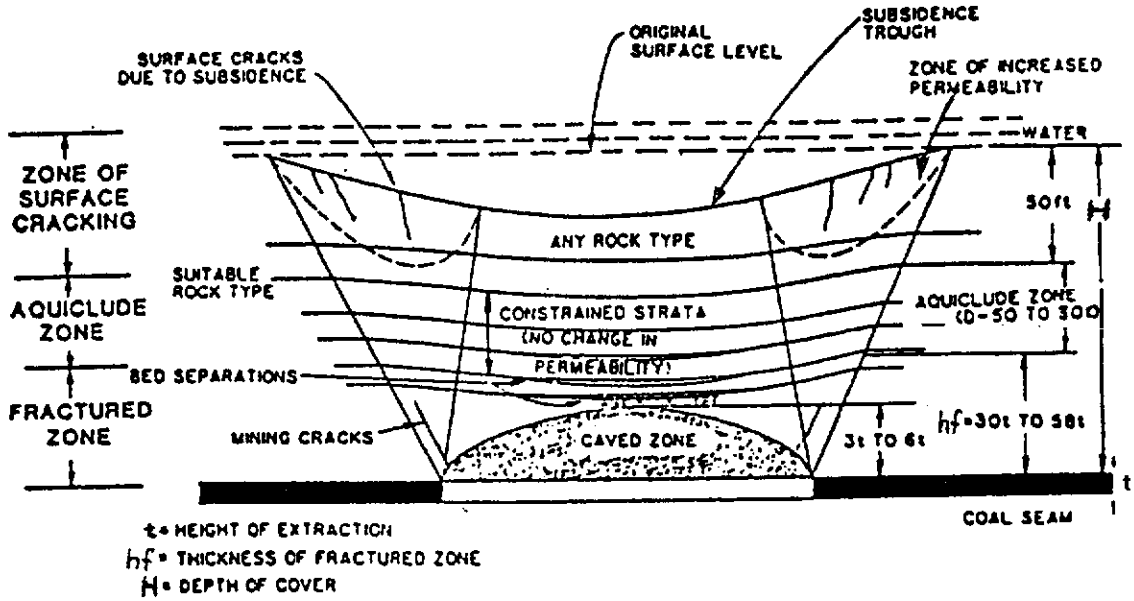

Figure 2.16

Their positioning of this zone, above the panel edge, however, does not match case studies (e.g. Holla, 1987), where the point of inflection varies significantly, depending on the panel W/H ratio. Kratzsch (1983) has accounted for the variation of the point of inflection in his model of subsidence development, placing it inside the panel edge. It is also noted that Kratzsch provides a similar shaped area of relaxation - termed zone of vertical expansion.

Of particular note in Fritzche and Potts' theory is the zone of full subsidence, which appears to be based on a line of caving. This is considered to be a more realistic assessment of the mechanisms of mine roof failure and subsidence development.

The proposal by Singh and Kendorski is also considered to be generally sound, with observations of caving in the mine and surface cracking matching personal observations in the Collie mines. However, the area designated as "Aquiclude zone" can be expected to experience a change in permeability at progressive stages of mining when this zone bends across the panel edge abutments - regardless of the confinement. It would be expected that stresses due to bending would, in most cases, exceed the flexural strength of these aquiclude/aquitard materials, which would cause them to crack in tension. This cracking must increase the aquiclude permeability, albeit at a reduced amount due to the confinement provided by the overlying strata.

The methods used by most researchers for investigating subsurface subsidence include numerical analyses, physical modelling and direct measurement of borehole extensometers. The more commonly used extensometery methods are discussed in detail in Appendix II. Examples of field data measurements can be obtained in several published literature including Holla (1989), Bhattacharyya and Gurtunca (1984), Shu (1990) and Potts (1964). It is evident from these investigations that subsurface subsidence development is variable between mining regions, and there is a large potential for installation problems and consequently monitoring error. Because of this variation, and the fact that previous investigations in other mining regions had been undertaken in relatively hard rock mass, it was considered necessary to specifically investigate Collie Basin subsidence.

2.5.6.1 Subsurface Subsidence Effects

Subsurface features of relevance to mining in the Collie Basin can be grouped into two categories; public utilities and aquifer systems.

Public Utilities

Subsurface public utilities prone to subsidence damage include services such as gas or water reticulation pipelines. Guidelines on the design of buried reticulation pipes - put forward by the Public Works Department NSW - suggest that pipe joints will need special design if the maximum expected ground strain exceeds 7 mm/m or when the average strain exceeds 4 mm/m. NSW Mine Subsidence Board requirements, for pipelines constructed in areas where excessive subsidence strains are to be developed, provide for the use of either flexible pipe or flexible pipe joints. The preferred flexible joint system incorporates a sliding rubber ring joint. Two examples of such joints are illustrated in Figure 2.17 from Thompson (1988).

An example on the potential for subsidence damage to water supply pipe is given as follows. Steel pipe used in construction of water supply pipeline is commonly type St 35 steel, with a maximum tensile stress of 240 MPa (Fotakis 1985). Assuming a factor of safety of 1.87 (after Kratsch, 1983) to allow for weld and manufacture problems, the maximum tensile stress permissible is 240/1.87 = 128 MPa.

As this type of steel has an elastic modulus (E) of approximately 210,000 MPa, the permissible lateral movement over a 6 m span is:-

$$\epsilon E = \sigma \qquad 2.5(16)$$

$$\text{I.e.} \quad \frac{(X-6)}{6} (210{,}000) = 128 \text{ MPa}$$

$$\simeq 4 \text{ mm or } 0.61 \text{ mm/m strain}$$

Using the estimated strain from 6B East panel subsidence as an example, the maximum tensile strain achieved was approximately 5.8 mm/m, which exceeds the maximum permissable strain calculated from Equation 2.5(16), but does not exceed the strain limit imposed by the New South Wales (NSW) Public Works Department.

Personal assessment of why the pipe remained in tact above the 6B East panel is that when the supportive concrete saddles failed, the pipe could effectively remain unaffected while the underlying concrete supports moved freely. The result is that the pipe is elongated across the full length of the panel with minimal tensile strains.

EXAMPLE OF UTILITY PIPELINE DESIGN TO CATER FOR MINING SUBSIDENCE

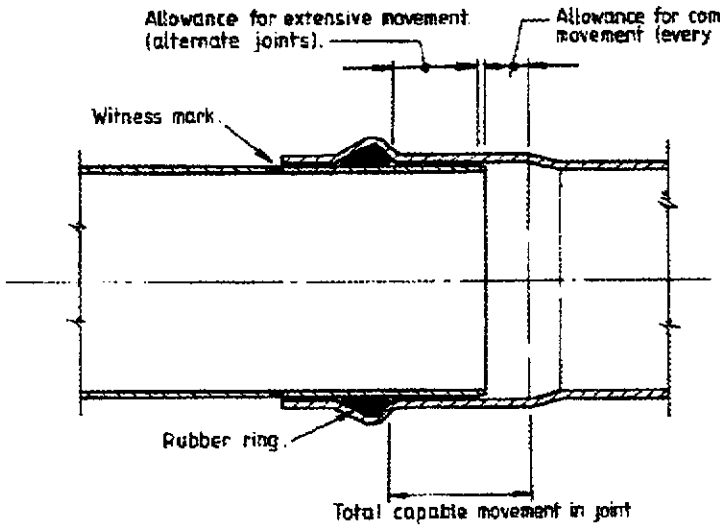

TYPICAL SKID TYPE
RUBBER RING JOINT

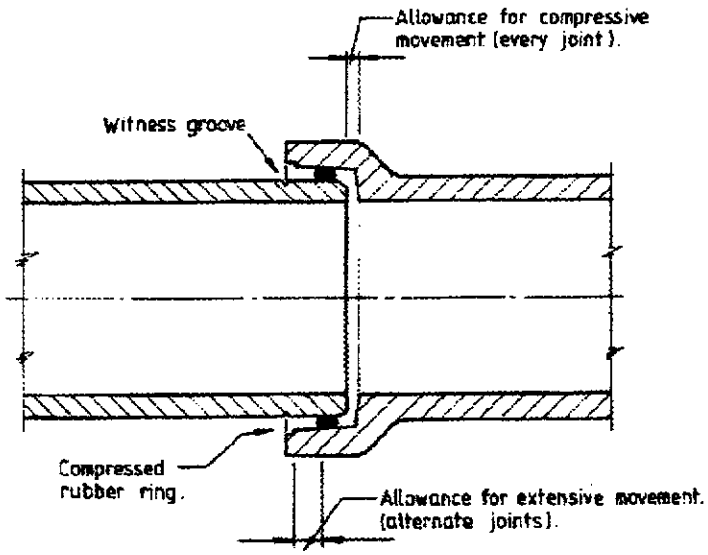

TYPICAL ROLLING RUBBER
RING TYPE JOINT

Figure 2.17

Aquifer Systems

The success of coal mining in the Collie Basin is largely dependent on the control of groundwater within the aquifer systems (Misich, 1993)[2]. In 1992, WCL's underground mines abstracted 13 tonnes of water for each tonne of coal mined (Hammond personal communication). Similar ratios have been reported in other mining regions, for example research by Fawcett (1986) lists water to coal tonnage ratios of 8 to 1 in inland regions in north east England, and 13 to 1 in one Kent colliery.

Water ingress to the workings can be sourced from either direct contact with a water-bearing body or conduit, or fractures developed through large scale ground collapse processes which can propagate tens of metres above the workings.

The main problems associated with groundwater ingress to a mine are:

- poor trafficking of mining machinery and difficult handling of mining equipment,
- additional costs and mine design restrictions associated with handling mine-water,
- mine stability problems, created by elevated water pressures on the mine workings,
- potential flooding of a mine, which may endanger life and result in mine closure.

From the experience gained during extraction of the ACIRL trial Panel, it was evident that depressurisation of each of the overlying aquifers in the deeper areas of the Collie Basin coal reserves was not economic. It was therefore necessary to establish whether such extensive depressurisation programs were infact required and whether or not any of the the higher aquifers could be left untouched prior to mining.

It has been established by numerous investigators, e.g Whittaker etal (1991), that the main controlling factors on the integrity of protecive aquitards was the width of extraction and the thickness of interburden between the mine workings and the aquifer and the concomitant strain at the aquitard level. Many attempts have been made to predict the tolerance or point of rupture of superimposed water-bearing bodies or underlying water-restraining layers. Most investigators have relied on the NCB's strain prediction for surface subsidence, whereby horizontal strains are calculated at specific horizons below the surface by assuming that the vertical separation between the mine and the specific horizon represents the full depth of cover to that point. This allows for the use of subsidence horizontal strain prediction curves provided by the NCB (1966, and 1975).

Wardell (1975) suggested a limiting horizontal strain (ϵ_{max})of 7.5 mm/m at the rockhead or bed of stored water in the eastern coalfields of Australia, while the NCB (1972) recommended a limit of 10 mm/m for the United Kingdom. Wardell used the NCB method to determine maximum surface strains, by substituting the parameter depth of cover (H) for the thickness of solid rock between the mine workings and the bed of stored water (D):

$$\epsilon_{max} = \frac{K.S_{max}}{D} \qquad 2.5\,(17)$$

where: D = thickness of solid rock between the mine and body of water (m),

K = an empirical tensile strain coefficient = 0.75,

S_{max} = 0.6 x effective mining height - T (m).

It follows, therefore that for super-critical panels, the minimum thickness of "solid rock" required is:

$$D = \frac{0.75 \times 0.6T}{0.0075} = 60.T \qquad 2.5(18)$$

Each of these design criteria is based on the premise that it is justifiable to calculate horizontal strains at any subsurface horizon as if that horizon was at the ground surface. This approach is considered to be empirical, and can only be used in site-specific cases. It has already been established that the ground surface is less confined and is prone to tensile cracking, whereas confined aquitards can be expected to develop much less and shallower cracking. Therefore these arbitrary limiting strains will depend on the type and nature of the surficial sediments at each site which are unlikely to bear any relation to the confined aquitard layer at depth.

It is also important to note that this limit does not take into account local variation in geology and the elastic/sealing properties of the particular water resistant layers. Galvin & Anderson (1986) gave evidence of the unsuitability of this method for shallow workings and expressed grave doubt for the use of the empirical tensile strain coefficient of 0.75. This doubt concerning the limiting strain index method is further strengthened by Whittaker et al., (1991) who found, in a number of case studies in the UK's north eastern coalfields, that "wet" longwall faces could develop with index strains in the range of 3 and 10 mm/m. The cover thickness between the mine workings in this region and the water-bearing aquifers varied between 85 and 310 m.

A further condideration when adopting the NCB limiting tensile strain index method is the different strain predictions obtained between the 1966 and 1975 editions of the NCB Handbook. It is understood that the limiting strain values, initially set up in The British Coal Instruction documentation, 1968/9 was based on the 1966 edition of the "Handbook" (Bigby and Osram, 1988), which predicts 40% more strain than the 1975 edition. Bigby and Osram, while not explaining the reason for the discrepancy between NCB data, recommend the use of the 1966 data. It would appear that the Bigby and Osram approach, being the more conservative, is the better suited for greenfield sites.

The publication by NCB (1972) also proposes a minimum interburden thickness when working under the sea equivalent to 43 times the extraction height plus 32 m. Application of such limiting interburden thicknesses in the Collie Basin would have serious implication for the use of any coal extraction techniques that initiate caving.

Furthermore, research carried out in the eastern Australian coalfields by Kapp (1982) Bhattacharyya and Gurtunca (1984) demonstrated that subsidence development above extraction panels in Australia was significantly different to that in the UK. This suggests that both the NCB curves and design criteria used to predict surface (and indirectly subsurface) subsidence strains are not valid in Australia. Bhattacharyya and Gurtunca (1984) concluded that to mine safely beneath bodies of water, the intervening strata should contain an adequate thickness of aquiclude (mudstones and clays which can absorb greater strain energy) free from open cracks and fissures as well at least one bed with low permeability. Additionally, there should not be any geological anomalies such as faults, fissures etc., along which water may flow. However,no quantitative design method or approach was forwarded in this research.

Further examples of research on the fracturing characteristics of strata in relation to aquifer systems are Garrity (1981 & 1983), Xiao et al. (1991), Fawcett (1986), and Jeffrey et al. (1991). Xiao et al., in summarising Garrity's work that investigated water inflows into longwall workings in the Northumberland and Durham coalfields in England, stated that there was a high risk of inflows when:

- Cover to the sea bed or the base of the Permian aquifer was less than 140 m or 100 m respectively.
- Faults with throws greater than 1 m connected the workings to the water source.
- The competence of the immediate roof strata was relatively high - particularly where the first 20 - 30 m contained less than about 35% of mudstones.

- Inadequate roof control allowed major roof breaks to develop.

Of these points, the last comment can be compared to Wongawilli extraction where caving takes place in up to 20 m wide increments, compared to the 0.5 to 1 m "continuous" collapse in longwall mining. It could therefore be expected that Wongawilli mining will produce greater surface and subsurface effects.

Xiao et al. concluded, through their work in the Horden, Blackhall, Wistow, Cotgrave and Clifton collieries in England, that there was a correlation between heavy water inflows and the proportion of weak, low permeability rocks in the immediate 30 m of strata above the mine workings. Inrushes were observed to occur when the percentage of these rocks is less than 30%. "Cover to the aquifer rocks is a less important parameter. When the percentage of weaker rocks is high, inflows do not occur even when aquifer rocks are in close proximity to the face." This statement appears to contradict those of others, however, the author tends to agree with this assessment more than the others' (this is discussed further later in this Section).

Once again, although general trends have been observed by these researchers, no design parameters have been provided.

The work by Fawcett (1986), although addressing the effect of aquitards on mine water flows as well as the flows through roof aquifers, was based on relatively simplistic finite difference and boundary element models with the immediate interburden being aquitard material of substantial thickness. It is considered that because of this the results gained from this research can only be used for indicative purposes. Nonetheless, some interesting trends were observed by Fawcett including:

- the interpretation that fractures giving rise to increased hydraulic conductivities were initiated by compressive failure ahead of the mining face and then subsequently opened by tension over the panel.
- The greater the mining height, the greater the height of caving.
- Lower elastic and shear moduli led to reduced fracture heights, conversely lower compressive strengths increased the height of fracture.
- The extent of mining subsidence damage in shallow panels was less; Fawcett put this down to the lower primitive and thereby induced stresses in the models.

- Reductions in fracture height were the result of the greater support provided by the additional closure between the roof and floor; closure increased with decreasing extraction thickness.
- Both Fawcett (1986) and Singh et al. (1985) demonstrated that a critical thickness of aquiclude from the aquifer (depending on the ratio of horizontal to vertical conductivity in the protective layer) was sufficient to control groundwater inflow to the mine horizon. The change from protected to unprotected flow occurred when the protective layer's thickness was less than 5% of the distance between the mine workings and the aquifer. These researchers also found that even after the aquiclude became fractured, water flows did not adopt open cavity (unity) conductivity, rather the fracture conductivity was in the order of 3×10^{-7} ms^{-1} or 0.026 m/day.

One of the major concerns with the application of this work to case studies is determination of the height of caving/fracturing, used to determine the required thickness of protective layers. Fawcett found that there was over 300% variation in fracture height prediction between the empirical methods; this is clearly inadequate for the purposes of this research study. Another concern was the application of fracture frequency to the cracked aquiclude as this could not be determined accurately. It was thereby concluded by Fawcett that much more detailed investigation was required to improve on his approach.

Jeffrey et al. (1991) used finite element modelling to predict the limit of rock fracturing in overlying aquifers. They suggested that the horizontal strain design criteria of 1mm/m tensile, and 2mm/m compressive strain (from Bai et al., 1990) applied to the noted ground movements and water inflow into Wistow colliery in England. It is interesting to note that the results from this study found that maximum strains were in fact oriented 60° to the bedding. Jeffrey et al. concluded that further investigation was required particularly in relation to the significance of the principal strain tensors, and the variation of geology and geomechanical properties. The latter suggestion for further work is considered as being critical before this method can be used. As stated in Section 2.6.4 and 4.1.1, there is serious concern for the ability of numerical models to be able to model subsidence at all mine sites at varying depths and geometries using one standard set of input parameters.

It has been common for previous researchers to investigate subsidence effects on lateral permeability of aquifers at specific intervals above the extraction horizon. Examples of this type of investigation are provided in Crane (1975), Kesseru (1977), Gvircman et al., (1977), and Booth (1994). Crane suggested that increases in permeability were limited to strata within 130 m above a 7.5 m high iron ore mine in Alabama. Kesseru found that in Hungary this zone of influence was slightly higher, being 25 times the mining height.

The research by Booth in Ohio, USA illustrated how aquifer water levels can lower temporarily due to bed separation below spanning strata. Water levels can return to pre-mining values once the advancing mine face has passed well beyond the point of measurement, and the bed separation reservoir closes up (through reconsolidation). Attempts were also made by Booth to qualify the changes in permeability of aquifers during the mining process. This research, though very interesting, is considered to be of limited use to this research project, as it has been demonstrated, from observations during the trial ACIRL panel, that water levels, once steeply drawn down, do not return to original values in the short term.

In general, considering the porous nature of the aquifer systems in the Collie Basin, it was the author's view that little value was to be gained in determining the impact of mining on the permeability of aquifers which are naturally very transmissive. The important parameter requiring definition was the maximum flexural strain of aquitards so any downward movement of water through the porous sandstone could be restricted.

In terms of mine design, some investigators have proposed the use of panel/pillar extraction methods (Figure 2.18 from Brauner, 1973) where relatively long but narrow panels are mined, separated by permanent pillars. By reducing the width of extraction in each of the sub-panels, the resultant subsidence is minimised and the subsidence effects reduced. The author concluded that this method of coal extraction was the best suited to mine set-up and ground conditions within WCL's leases. This method could be readily implemented as a slight variation of the ACIRL Wongawilli trial panel. No further capital expenditure was required, and the relatively small areas remaining for immediate extraction of coal were well suited to this form of extraction.

DIAGRAMMATICAL PRESENTATION OF PANEL/PILLAR MINING

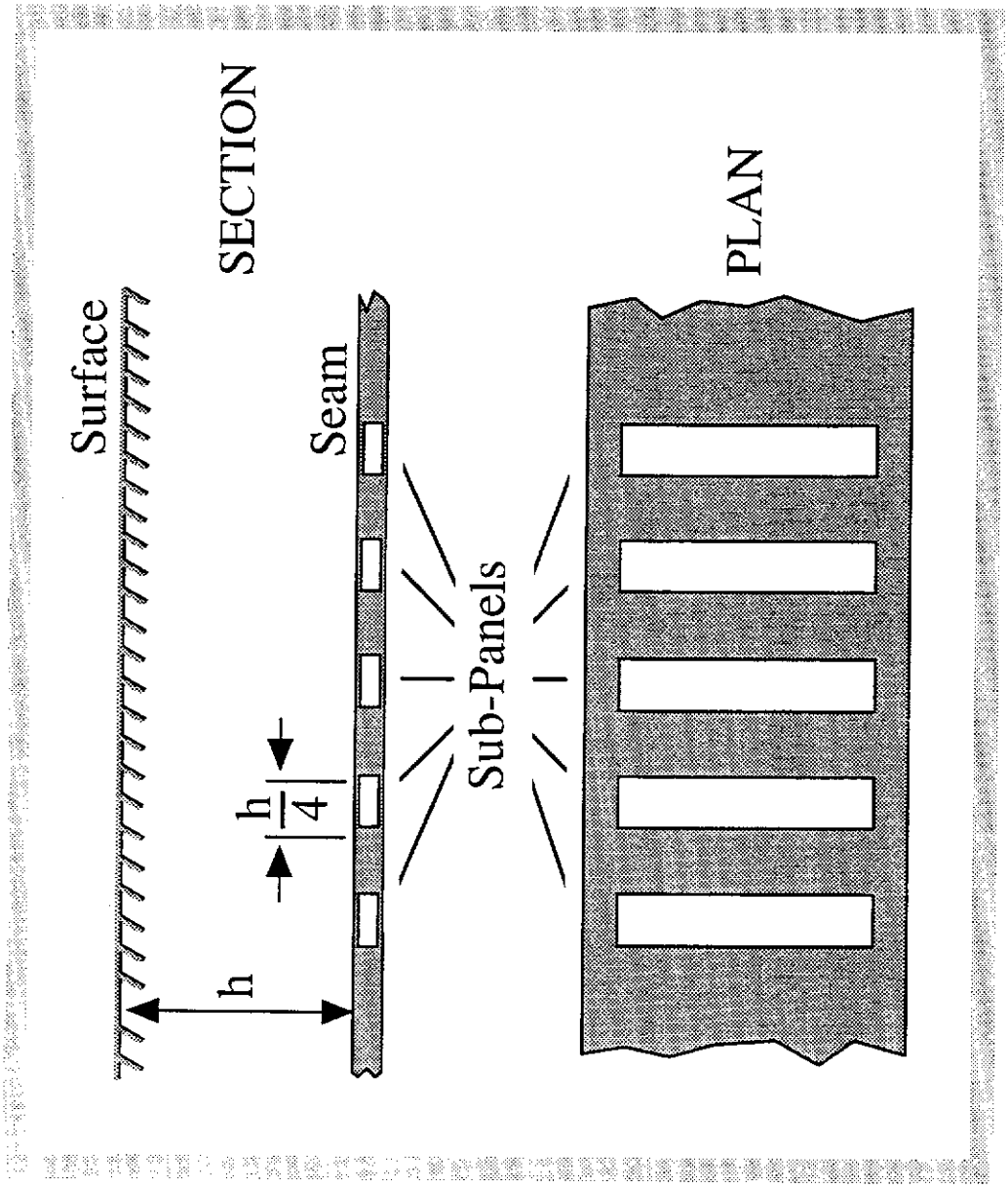

Figure 2.18

Kapp & Kennerly (1986) have listed design restrictions imposed on this form of mining by the New South Wales Dam Safety Committee (DSC) following the results of an inquiry by Reynolds (1977). The DSC guidelines for panel/pillar workings are summarised as; extraction panels beneath stored waters require cover depths (H) greater than 120 m, with panel widths no greater than 1/3(H). Intra-panel pillars separating the individual sub-panels are to be designed to the greater of 1/5(H), or 15 times the height of extraction. Holla (1987) proposed the following design limit; minimum cover depth 46 m, a maximum sub-panel width 0.4H, and a minimum intra-panel pillar width representing the greater of 0.12(H) or eight times the height of extraction. Holla (1987) further states that the panel/pillar system could be expected to work adequately for sub-panel widths up to 70% cover depth where Smax is restricted to less than 150 mm.

Both of these design criteria are obviously different, and it is not clear as to which one is more appropriate and why. If the DSC recommendations were to prove applicable to the Collie situation, total extraction would not be possible in much of the remaining WCL reserves. Furthermore, it was considered that these design panel widths, being based on W/H, were not well suited to the protection of Collie Basin aquitards.

If one considers a panel at 300 m depth, Holla's design criteria would allow for a sub-panel 120 m wide. From local knowledge, it can be expected that this width of extraction will result in large scale collapse which would probably crack several protective aquitards.

It was therefore concluded from the literature review, as per Cain et al. (1994), that much more detailed investigation was required to provide the mining engineer with a tool for accurately predicting aquifer responses to subsidence and thereby allowing for precise design of mining dimensions to manage groundwater inflows to the mines. This was seen to be one of the major components of Collie Basin subsidence requiring investigation. Consequently, a large proportion of this project has been dedicated to defining the effect of mining subsidence on aquitard integrity.

2.6 REVIEW OF SUBSIDENCE MODELLING METHODS

Because some of the major goals of the research project relied heavily on the use of artificial modelling, it was necessary to review the modelling methods used in other mining regions to establish which modelling techniques were most appropriate for the Collie Basin sediments, and which could meet the requirements of this project.

The art of subsidence prediction is believed to have begun in Europe in the early 1800's (Ingram etal, 1988). There have been numerous methods developed since then, each with its own limitations and applications.

Fitzpatrick (1987) states that because no early theory had proved itself conclusively better than the others, several dubious formulae were put forward, such as :-

$$S_{max} = (T - t(1-0.025H)(1-0.02H)) \quad \text{... O'Donahue} \qquad 2.6(1)$$

$$S_{max} = T_1 (1 - (H+6)/(6H+14)) \quad \text{... Louis} \qquad 2.6(2)$$

$$S_{max} = 400/(4+\sqrt{H}) \quad \text{... Briggs} \qquad 2.6(3)$$

where, S = maximum subsidence,

T = thickness of extraction, H = depth of working (in hundreds of feet),

t = thickness of compressed stowing, and $T_1 = T-t$

These formulae are clearly inadequate due to the omission of the width of extraction and the fact that they predict only vertical displacement. Their main role, along with other early theories, was to highlight the importance of the precalculation of mining subsidence and to increase the general understanding of the mechanisms involved.

Since then, the complexity and number of modelling techniques has increased dramatically and it would be impractical to discuss every one. Consequently only the more common subsidence prediction methods used by other researchers have been presented here. These modelling methods, are :-

- Empirically derived relationships,
- Profile and Influence functions,
- Numerical/mathematical methods,
- Physical models.

Profile and influence functions have been grouped with empirical models by most authors, such as Ingram et al. (1988), however, they have been separated in this study because they represent two different techniques of predicting the shape of subsidence troughs.

A summary of each of these methods and discussion of the suitability of each method to the Collie Coalfields has been provided in Sections 2.6.1 to 2.6.6. The modelling techniques chosen for use in the research project are provided in Section 2.7.

2.6.1 EMPIRICAL MODELS

There have been numerous studies on mining subsidence. In almost all cases, subsidence development has been shown to be primarily dependent on the mining parameters seam thickness, depth of cover and panel width. The relationships drawn between these parameters and subsidence development form the basis of nearly all empirical models. The aim of empirical models is to develop normalised "factors" to establish a dimensionless graph or equation which can predict subsidence for any range of mining conditions.

For example, in order to predict the maximum subsidence for any given extraction panel, the parameter subsidence is normalised as a dimensionless ratio of mining height (the maximum possible subsidence), and plotted against the mining parameter panel width which, in turn is normalised with depth of cover (W/H). Once such a relationship has been established, subsidence can be predicted for any combination of mining height, depth or width.

The most widely used empirical model for predicting maximum subsidence is the "UK" or NCB method, first published in 1966. This method is based on graphical solutions derived from numerous field measurements in Great Britain. (The 1966 NCB empirical chart used to predict maximum subsidence was given earlier in Figure 2.15). **Note** that an updated Smax nomogram is provided by NCB (1975) which allows for different rates of subsidence development above shallower panels. Within WCL's underground mining leases, the depth of extraction was mostly less than 300 m and the need for a similar plot was considered unwarranted. Consequently, the 1966 style nomogram was seen to be more applicable for this project.

Prediction of subsidence profiles is done in similar fashion. Ingram et al. (1988) describes three steps in predicting subsidence profiles with the NCB (1975) empirical method:

1) Selection of a subsidence factor/coefficient (Sf) from the nomogram based on the relation of panel width versus panel depth (given as Figure 3 by NCB, 1975).

2) Calculation of expected maximum subsidence by multiplying the subsidence coefficient by the extraction thickness.

3) Calculation of intermediate subsidence leading away from maximum subsidence using a nomogram (given as Figure 5 by NCB, 1975) which depicts the percentage of maximum subsidence according to the distance from

the centre of the panel.

Work by Kapp (1982), following on from the approach used by the NCB, suggests that the Sf for critical width panels in Eastern Australia is between 0.55 and 0.65 - compared to a typical Sf in the British coalfields of 0.9. In many of the coalfields in China and the USA, Sf is calculated as a function of the proportion of hard rock overlying the mine (eg Peng, 1992). Peng and Chiang (1984) suggest that the Sf for soft rock such as Collie Basin sandstone varies between 0.8 and 1.0, whereas the Sf in hard rock (> 70 MPa) can be expected to be between 0.45 to 0.6.

Comparing these documented Sf values against that measured in Collie for super-critical panels (estimated to be 0.63 for the Cardiff and 6B East Colliery) it is evident that the rock type factoring approach is not valid for local conditions. It is also obvious that the Brittish Sf is not suited to Collie Basin subsidence.

As surface subsidence strains and tilts are directly related to maximum subsidence (eg NCB, 1975), empirical models can also be formulated to predict maximum strains and tilts developed by subsided ground. The NCB's 1975 Subsidence Engineer's Handbook (SEH) provides a simplified nomogram for predicting maximum horizontal strains and tilts by empirical methods in the United Kingdom. This approach is considered to be valid, however, the researcher must also take into account the variation in subsidence that may occur due to other factors such as the coal seam dip or steep surface topography.

Shu (1990) adopted the NCB approach to develop a "theoretical" model which could be used to predict subsidence at both surface and subsurface horizons. His approach was to firstly predict the surface subsidence and then, in turn, the subsidence profile at each horizon below the surface by assuming the constant subsided volume theory (Kratzsch, 1983) where the cubic content of the trough at the surface equals the volume of convergence in the workings. Shu reported reasonable correlation with field results for sub-critical panels, however, this approach was not applicable for wider extraction, largely because this approach did not take into account any caving and the effect of bulking of the caved material. The accuracy of this theoretical model decreased closer to the seam.

Advantages ....

- There are no mathematical or mechanical assumptions made for this method. Empirical predictions are based on actual measured values. Variations in geology and goaf behaviour are automatically accounted for.

- The method is simple to use and gives predictions in an easy to manage form.

Disadvantages ....

- A large number of case studies, covering the complete range of mining scenarios, is required to develop a competent predictive model.
- Once an empirical model has been developed for a particular area, it can not be reliably applied to other mining locations.
- Irregular-shaped panels and panel edges cannot be accounted for accurately.

In summary, vertical subsidence and related subsidence parameters are dependent on the mine geometry, the mining methods used, and the caving and mechanical properties of the superincumbent strata for any particular site. Consequently, empirical models are site specific, and inaccuracies in subsidence predictions are commonplace when using pre-existing empirical charts from different mining regions, e.g. Adamek et al. (1987) and Munson and Eichfield (1980).

Therefore, in cases where it can be demonstrated that the site geology differs from the researched mining regions, separate studies should be conducted to develop empirical models unique to that site. However, in situations where there is very little information regarding subsidence and geological parameters, the U.K. method can be used as an indication of the maximum subsidence parameters expected.

2.6.2 PROFILE FUNCTIONS

Profile functions adapt a curve-fitting equation to a number of related parameters to define the shape of a given subsidence trough. Simple profile functions may only consider depth to be significant, whereas more advanced functions utilise many, if not all, significant parameters into account (as demonstrated by Whittaker & Reddish, 1989).

The profile function can be given simply as:

$$\mathbf{S = f(x).} \qquad 2.6(4)$$

The shape of the curve S is dependent on the function f(x) which is most often expressed in terms of:

1) the maximum subsidence (Smax),
2) the angle of draw (or critical radius of extraction R), and
3) the position of the point of inflection or horizontal distance from the panel centre.

There are numerous profile functions for each coal mining area throughout the world. The differences between each profile function relate directly to the variations of the function f(x), and the three principal factors given above.

Whittaker and Reddish (1989) has listed a selection of expressions of some of the more commonly used profile functions which they have subdivided into two groups; the first group includes functions which use the panel centre as the origin, the second uses the inflection/transition point as the origin. The author considers that of the two groups of profile functions, the inflection point method is more appropriate, as these profiles are calculated from a "hinge point" from which the shape of the trough can vary on either side. The location of the hinge point is usually well defined (eg Holla, 1987). Figure 2.19, taken from Whittaker and Reddish (1989), presents some examples of profile functions based on the point of inflection.

The terms used in the profile functions given in this Figure are:

x = Distance from centre of extraction,

R = Radius of critical area of extraction,

S = Maximum subsidence (Smax).

The expressions within **both** groups can be further grouped into three categories (Munson & Eichfield, 1980). These are:

- asymptotic (e.g. the Polish curve which utilises the error integral or its complement),
- non-asymptotic, or trigonometric, (e.g. the Donets coalfield - see Figure 2.19), and
- mixed form (e.g. the curve by Martos, for the Hungarian Coalfields in Figure 2.19).

Ground tilt and curvature can be derived by single differentiation and double differentiation, respectively, of the profile function equations defining the subsidence trough. Furthermore, if a relationship between curvature and horizontal strain can be formulated, as done by a number of researchers, e.g. Karmis et al (1985), profile functions can also be used to indirectly calculate surface strains.

Advantages ...

- Since the subsidence curve is defined by an equation, it is readily calculated.
- The method requires comparatively little site information to calculate the necessary constants. This is important when mining in greenfield sites.
- Geological variation is automatically taken into account.

PROFILE FUNCTIONS BASED ON TRANSITION POINT ORIGIN

Functions based on transition point origin

1. **Hyperbolic function:** King and Whetton (1957)

$$s = (S/2)\{1 - \tanh(\frac{2x}{R})\}$$

2. **Exponential function:** Martos (1958)

$$s = S\exp\{-0{\cdot}5\left[\frac{x+R}{R}\right]^2\}$$

3. **Donets trigonometrical function:** GIMS (1958)

$$s = (S/2)\{1 - \frac{x}{R} - \frac{1}{\pi}\sin(\frac{\pi x}{R})\}$$

4. **Trigonometrical function:** Hoffman (1964)

$$s = S\sin^2\{\frac{\pi}{4}(\frac{x}{R} - 1)\}$$

Figure 32 shows a comparison of equations (8) to (11) together with the UK SEH anticipated curve.

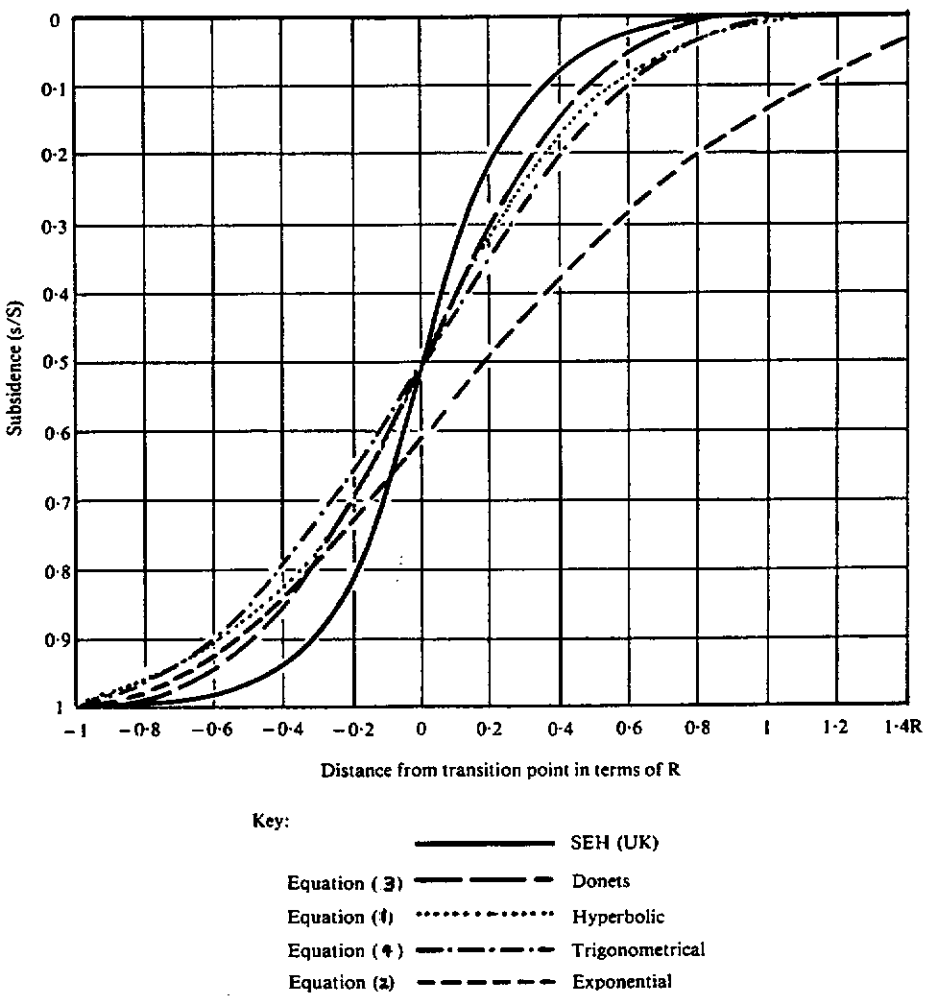

Figure 2.19

Notes:

1. Data used for SEH calculation: w = 140m, h = 100m, limit angle = 35°, transition point position = 0·8R from panel centre.
2. All calculations based on a critical extraction condition.

Disadvantages ....

- Irregular panel shapes and panel edge effects (eg pillar punching) are not taken into account.
- Profile functions are based on field data and are consequently site specific.

In summary, this method, like the empirical charts discussed above, is dependent on site specific subsidence parameters. It is therefore recommended that profile functions be used between mining regions with caution. When mining-related variables are consistent, factors such as panel edge effects and bearing failure are accounted for automatically by profile functions. This characteristic allows the profile method to have less variation between the predicted and measured profiles.

2.6.3 INFLUENCE FUNCTIONS

The basic concept of the influence method is to evolve a subsidence profile (or influence function) for an "infinitesimal cell" width of extraction, and sum the individual cell profiles - using the laws of superposition - to determine the final subsidence profile at the completion of the panel. Figure 2.20 (from Brauner, 1973) illustrates this concept. Figure 2.21 a illustrates the principle of profile functions. From this illustration, it can be seen that influence functions are based on the simplified function:

$$K_z = F(r) \qquad 2.6(5)$$

where K_z = the magnitude of influence of mined area dA on surface point P,

r = horizontal distance between position of P and the infinitesimal element dA. (Whittaker & Reddish, 1989)

It follows from the laws of superposition, that the extraction of an area A will result in a point at the surface subsiding by a magnitude **S** as expressed by the equation:

$$S = \int_A \int K_z(r)\, dA \quad \text{(Whittaker \& Reddish, 1989).} \qquad 2.6(6)$$

From Figure 2.21 a, it can be seen that the element directly under P contributes the most influence, and the function $K_z(r)$ is at a maximum when r = 0. With reference to Figure 2.21 b, in the situation when P is directly over the panel edge, the surface point experiences only half the full influence of the function, and consequently has half the maximum subsidence (S/2). This point also coincides with the point of inflection of the subsidence trough.

SUPERPOSITION OF INFINTESIMAL INFLUENCES

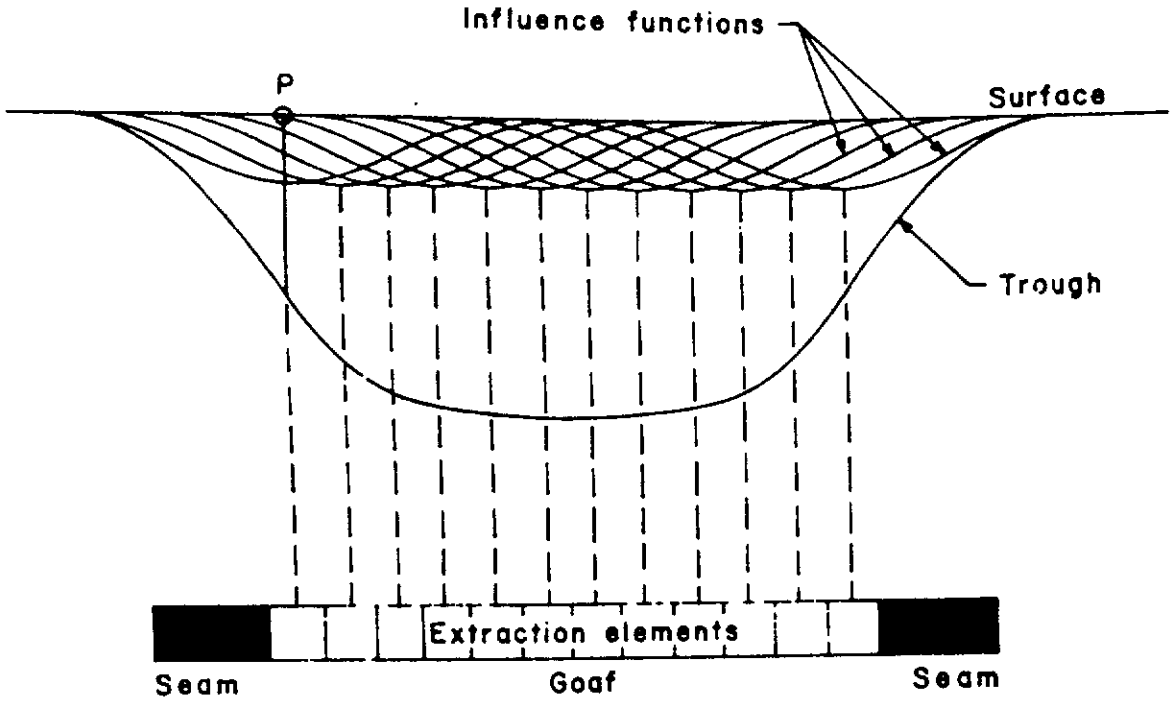

(From Brauner, 1973)

Figure 2.20

ILLUSTRATION OF THE PRINCIPLE OF INFLUENCE FUNCTIONS

(After Brauner 1973)

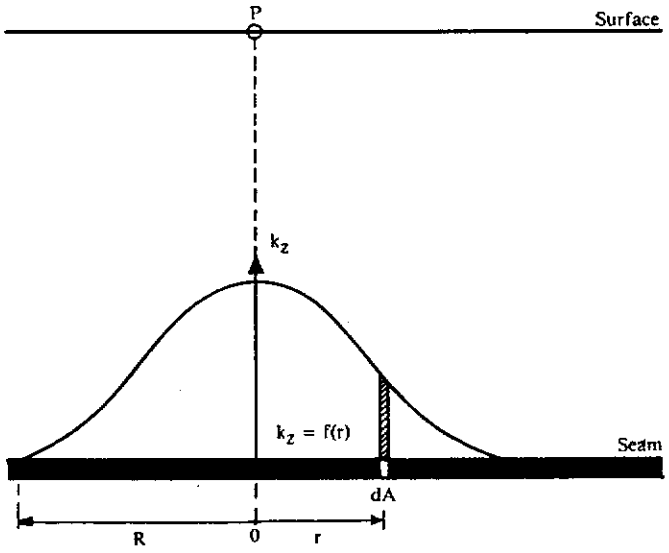

Figure 2.21 a

ILLUSTRATION OF PANEL EDGE SUBSIDENCE USING INFLUENCE FUNCTIONS

(After Brauner 1973)

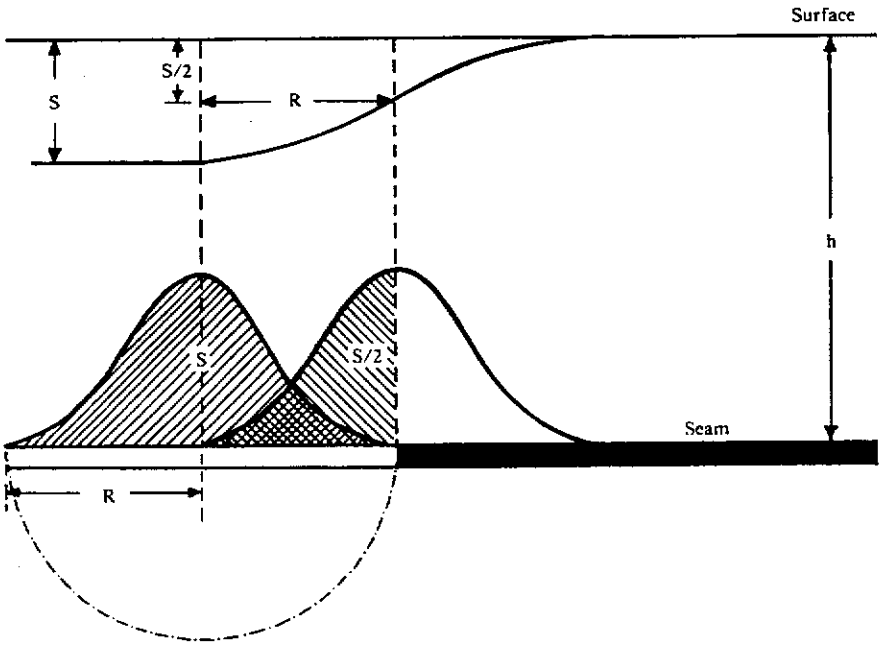

Figure 2.21 b

This represents a major drawback with this method, as it is well known that in many cases the point of inflection does not coincide with the panel edge. The subsidence curve established above 6B East panel is one such example. A correction factor needs to be applied to the final predicted profile function in these cases (e.g. Bahuguna et al., 1991). However,the correction factor cannot be predetermined and can only be applied confidently when significant field data exists.

Numerous influence functions have been developed e.g. the Keinhorst, Bals, Niemczyk, Beyer and Knothe functions to name a few. The difference between each function is the assignment of different values of influence to individual zones within the whole area of influence.

Bals' theory has achieved widest recognition and practical use in Europe. It is based on Newton's law of gravitation, where the area of each mined "cell" exerts an influence on a point on the surface inversely proportional to the distance from it. Two major factors affecting the resultant subsidence profile using Bals' theory are the angle of draw and the influence function, which is largely dependent on the "efficiency coefficient" of the partial area of influence. This is explained in detail by Adamek & Jeran, 1985.

Influence functions have also been popular in the USA, eg. in 1993 the Department of Mining and Minerals Engineering, Virginia, USA developed a commercially available system using a modification of Knothe's theory, which is based on the Gaussian function. This program has been reported to well represent the expected subsidence (personal communication J Craft 1993). Fitzpatrick (1986), whilst working for British Coal, claimed acceptable comparison of field data with influence function predictions.

Advantages ...

- The influence function method can account for odd-shaped panels and panels at varying width to depth ratios.
- It is also a relatively simple technique (once the function is established) to predict subsidence, involving less computing effort than complex numerical models.

Disadvantages ...

- Influence functions are considerably more difficult to apply than profile functions and more difficult to check and calibrate.

- Influence functions result in the position of half Smax and the point of inflection to be directly above the panel edge. This simplification of subsidence profiles is not applicable to many mining regions, such as the Collie Basin, as the shape of the subsidence trough is asymmetrical about the point of inflection - and not the panel edge. Correction factors have been applied with some success, however, this can over complicate the method.
- Influence functions are based on field data, and are consequently site-specific and can take much time to develop.

It was considered that these three disadvantages outweighed the advantages and consequently influence functions were not trialed for subsidence prediction in the Collie Basin.

2.6.4 NUMERICAL / MATHEMATICAL MODELS

Mathematical models basically simulate strata characteristics and behaviour in response to mining by giving discretised points/blocks representative material properties and calculating the resultant displacements, stresses and strains in relation to applied, resultant and/or virgin loads and constraints. Numerical models of numerous forms have been used with widely varying degrees of success over recent years.

The effectiveness of a mathematical model depends on three factors (Wardle, 1986):

1) the degree to which the model reflects the realities of the prototype,

2) the reliability of the input data, and

3) the accuracy of the numerical solution procedure.

Wardle, 1986 thus concludes that when modelling mining projects, the validity of the conceptual model will only become apparent "after the event".

It is apparent that no mathematical model has the capacity to simulate every aspect of subsidence. In particular the reaction of the failed, inelastic material within the caving zone and lines of shear, can only be approximated by numerical models. Furthermore, the geology of any mining site is rarely simple and modelling the mining environment, as it is *in situ*, becomes impractical.

Consequently results from mathematical modelling should be interpreted carefully.

Notwithstanding, a number of researchers have reported good representation of field **surface** subsidence by numerical modelling (e.g. Fitzpatrick, 1987). Bhattacharyya and Gurtunca (1984) demonstrated that although the results for the deeper stratigraphy (nearer the large strain caving regions) did not in any way represent the actual ground responses, they were able to reasonably approximate the final surface subsidence trough.

Holt (1988) demonstrated that it was acceptable to subjectively modify input parameters in computer codes in order to obtain a best fit surface subsidence prediction. The major concern with this approach is that any modelling "fudge factors" developed for a particular mine site are not transferrable to other sites or even other (nearby) panels of greater depth. Again, analytical modelling is highly reliant on field/empirical data, in this case for back-analysis purposes.

As there are many analytical models available for analysis of ground response due to mining, only the more popular models will be discussed in this report.

Finite Element/Finite Difference Models

It has been reported by several authors (eg Hoek etal, 1993) that, in practice, the finite element method is indistinguishable from the finite difference method, and that the two methods can therefore be discussed as one method of analysis. The difference between the two methods is largely the manner in which the two codes produce a suite of algebraic equations to solve for the stress/strain behaviour throughout the body of a model, although the resulting equations are the same (FLAC® version 3.0 user's manual). Both numerical methods have been used in many fields of research over several decades, particularly for civil engineering, and there been many studies on their application to the subsidence phenomenon. In this time, there has been numerous developments and refinements of each method, and consequently there are many forms of finite element/difference codes.

Until recently, with the refinement of the finite difference code FLAC®®, finite element techniques had largely superseded the closely related finite difference method. Discussion has therefore been provided from the side of finite element models.

Research in Australia on the use of finite element models (FEM) for coal mine design has been done largely by the C.S.I.R.O, and Australian Coal and Industry Research

Laboratories (ACIRL) in the 1970s and 1980s e.g. Puckett & Mikula (1984) and Mikula and Holt (1983).

There has also been useful work with FEM and subsidence in the UK, particularly at the University of Nottingham. Fitzpatrick et al. (1986) successfully applied non-linear, anisotropic FEM to longwall mining and subsidence (when Smax was approaching 100% mining height).

The basis for most FEM is the relationship between displacement, stresses and strains:

$$\mathbf{disp = FW}, \qquad 2.6(7)$$

where: W represents the system of loads applied to the body at certain points, and

F is the "flexibility" of the body. (The inverse of F is known as the stiffness of the body, Smith, 1971).

Displacement at any point within the mass depends on the position of the point in relation to the applied force and any applied restrictions, such as boundary edges. As each point is discretised sequentially they are thereby interconnected, which makes it possible to solve stresses and displacements throughout the mass by use of the matrix method.

The form of the flexibility or stiffness matrix used depends on the stress - strain relationship leading to and extending beyond failure of the material at any point.

In the linear elastic case, this relationship is given by:

$$\sigma_x = E\epsilon_x \qquad 2.6(8)$$

where: σ_x is the applied stress in the x direction,

E is the elastic modulus of the material, and

ϵ_x is the strain in the x direction.

Selection of the most appropriate material stress-strain curve is therefore critical to the success of FEM (and all mathematical modelling techniques). Figure 2.22 represents stress - strain curves for typical coal measure strata in the Eastern Australian coalfields (from Puckett and Mikula, 1984). It is seen from Figure 2.22 that the complete stress-strain curve is complex and is impractical to simulate exactly due to the considerable formulation problems which would make the numerical program inoperable.

TYPICAL STRESS-STRAIN CURVES FOR COAL MEASURE ROCKS IN THE NSW COALFIELDS (from Puckett & Mikula, 1984)

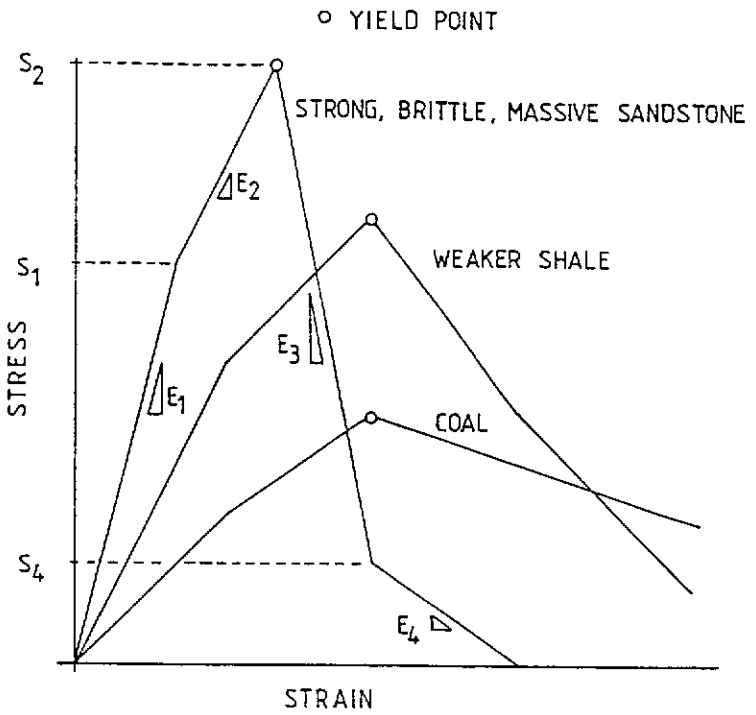

Figure 2.22

MOHR-COULOMB FAILURE CRITERION

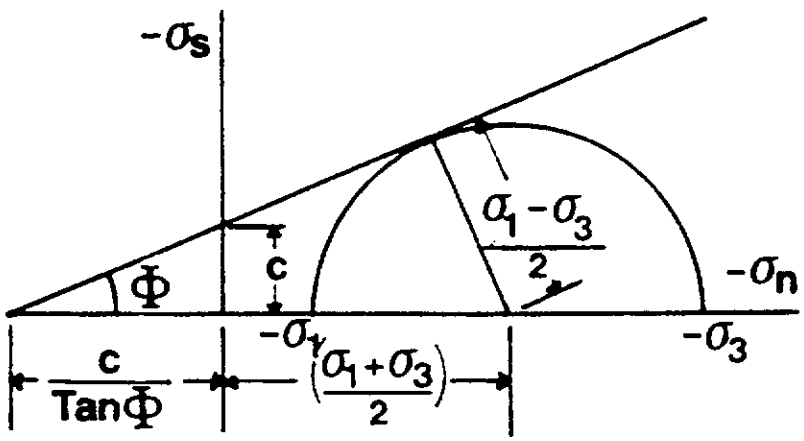

Figure 2.23

This inability to accurately simulate post-failure characteristics gives rise to error. The stress-strain models used in numerical methods therefore usually employ one of two material-type models; elastic, and elastoplastic.

Other more complex stress-strain models, e.g. the visco-elastic Kelvin and Maxwell models, which probably better represent the behaviour of natural materials, are unweildy and are therefore not suited for simple matrix solution.

Four of the most frequently used material failure criterion are the Tresca, Von Mises, Mohr-Coulomb (M-C), and Drucker-Prager models (D-P). The Tresca and Von Mises models are purely cohesive and are typically used to simulate metals or undrained clays. These models are considered by the author as being unsuited to mining subsidence studies. The M-C and D-P models are characterised by a cohesive - frictional yield strength and are used to describe the behaviour of soil or rocks.

The D-P criterion accounts for the intermediate principal stress σz while the M-C model is independent of σz and the normal and shear stresses can be simply represented by Figure 2.23. Because of its simplicity and better application to two-dimensional problems, the M-C failure criterion is usually favoured (e.g. Puckett and Mikula, 1984), however, some researchers, for example Hazen and Sargand (1988) have had some success with the D-P models.

The M- C representation indicates that a material is yielding if the shear strength (Ss):

$$Ss \leq C + N(\tan\phi), \qquad 2.6(9)$$

where C is the cohesive strength, N is the normal stress acting on the point, and ϕ is the angle of internal friction.

Once stresses and strains have been computed for each nodal point, they are compared to material property models for each lithology to assess whether the material at any point has yielded. The material strengths can then be upgraded accordingly (e.g. Fitzpatrick, 1986).

Advantages....

- Anisotropic and non-linear elastic media can be modelled.
- Complex geometries can be modelled.

- Several layers can be simulated within a stratigraphic section. This is a very important point for modelling the Collie Basin sediments, as there is a well-defined stratigraphy with greatly varying geomechanical properties.
- Variable surface and body forces are easily handled.
- Geological anomalies such as joints or faults can be modelled.
- Sequential mining steps can be simulated.

Disadvantages....

- Finite element analysis of ground masses do not cope well with areas of large displacement, such as caved and fractured zones immediately above an extraction panel. This problem can have a very significant impact on the resultant subsidence predictions.
- Boundary conditions at the perimeter of the model can have a significant effect on the final solution.
- FEM can take some time to set up and run due to the large number of discretised points. This problem has been restrictive in the past, however, with the development of sophisticated pre- and post-processing packages and faster computer processors, this problem is now of much less consequence.

Boundary Element Models

The term boundary element method is used to describe a class of numerical solution procedures that involve formulating a given stress-analysis problem in terms of boundary data rather than internal data (such as finite elements). The use of this method dates back to the work of Fredholm in 1906 (Wardle 1986). Boundary element models form a major part of what is generally termed integral methods in which the equations of elasticity that describe the behaviour in the rock mass, and its excavated boundary surfaces, can be transferred to an integral equation on the boundary surfaces alone. By discretising the boundary data, the integral equation reduces to a suite of algebraic equations. This method is particularly suited for the analysis of stress around deep underground excavations, as it does not require the imposition of artificial outer boundaries (as do other codes), as these boundary conditions are satisfied

automatically at infinity. (The numerical model is assumed to be of infinite dimension so that the numerical solutions can be 'closed' once equilibrium is achieved without the influence of any model boundaries.) Therefore, models of shallow excavations require that both the excavation boundary and the ground surface boundary must be discretised.

The main assumptions of the boundary element systems is that the rock mass is linearly elastic and in plane strain. Non-linear effects resulting from phenomena such as slip and separation of geological discontinuities or crushing of a mine pillar can be modelled, however, the inelastic behaviour is only modelled on a discontinuity or an excavation boundary. Hackett (1959) attributes the concept of displacement discontinuity elements to professor R Hill, of the University of Nottingham. The concept of these elements is to allow opposing nodal points to be able to move in different directions. Berry (1960) developed displacement discontinuity solutions for isotropic and cross-anisotropic media to model surface subsidence profiles.

The user's manual for the boundary element computer code BESOL by Crouch (1988) explains that although the program cannot actually model rock failure (being linear elastic), it can compute (intact rock strength) / (resultant stress) ratios, or " failure indices" for boundary points and any specified field points within the model body. The Mohr-Coulomb yield condition is often used in conjunction with the displacement discontinuity elements.

Boundary element methods are considered by some researchers to be generally more accurate than FEM because, with finite elements, the user subjectively applies elements of some simplified form and size. This action introduces an artificial stiffness to the FE model which does not really exist. In contrast, the boundary element method assumes the 'exact' solution inside the body which can produce a more accurate solution.

One of the improvements made to these models (such as MINLAY), is the inclusion of a "goafing element" to better represent the caved area immediately above the mine roof (personal correspondence McNabb, 1991). The number of goaf elements used in these models is dependent on the height of caving, the reconsolidation characteristics

of the mine goaf, and the stress-strain behaviour of this reconsolidated broken material. An alternative approach to including the effect of goaf in the subsidence process is to place a limiting convergence on the roof and floor materials. It is interesting to note that Edwards et. al. (1993) achieved better representation of field subsidence when a zone of "unbulked" material was included at the panel abutments. This non-bulking element is presumably reproducing the voids observed at panel edges during the caving process and results in less support being provided to the strata immediately above the panel edge.

The importance of bulking goaf on subsidence development can also be inferred from Salamon (1991), when describing how "stiff" goaf, with a high bulking factor provides greater support to the bridging strata and thereby reduces subsidence and load transfer to the abutments.

The influence of having no goaf bulking elements in earlier models is evident in the work of several researchers, e.g. Bhattacharyya and Gurtunca (1984) who found that the displacement discontimuity program MSEAMS (which did not have a goafing element) could reasonably predict subsurface subsidence at or near the surface, but not at greater depths.

Advantages .....

- As only the boundaries of the structures in the region of interest are discretised, boundary element systems have simple input and are relatively easy to use, unlike finite difference and FEM.
- Computation of complex problems is comparatively quick.
- Remote boundary conditions for infinite and semi-infinite regions are handled analytically, and hence no numerical approximations are made for this part of the problem.
- Hybrid programs such as BESOL/P5012 and MINLAY have the capacity to model non-linear effects such as slip and separation along geological discontinuities.
- Sequential mining can be simulated, and pillar crushing and artificial support can be

modelled.

Disadvantages .....

- Detailed stratification cannot be modelled in some cases.
- Only linear elastic characteristics can be used to simulate material behaviour of the general mass.
- Post-failure properties cannot be accurately simulated.

Stochastic (distinct element) Models

In stochastic models, a rock mass is represented as being completely broken by joints and fissures and acting as an accumulation of loose blocks of stone (Kratzsch, 1983). Block movement within such a large-scale and "mobile" deposit will tend to follow the laws of probability and will depend, to a relatively small extent, on the properties of the blocks.

This model can be readily applied to the caved zone immediately above an extraction panel. Large blocks tend to break loose when destressed by the mine void, and fall in rotation to occupy more volume (bulk).

Mathematical modelling of stochastic media is represented by Distinct Element models. The computational scheme proceeds by following the motion of blocks through a series of increments of displacement, controlled by a time-stepping algorithm (Kay, 1988). In Australia, two of the more commonly used distinct element software are UDEC and FEBLK. Sutherland et al. (1986), used the computer program RUBBLE and BLOCKS with some success.

Research by Bahuguna et al. (1991) suggests that the best application of this modelling technique is for stiff, well defined blocky strata. The author concurs with this assumption and concludes that stochastic models are not well suited to the application of modelling mining subsidence in the weak Collie Basin sediments.

Advantages.....

- The method can cope with large stresses and strains which the continuum models such as FEM, are largely incapable of.
- The behaviour of *in situ* goafed material can be more closely represented.

Disadvantages.....

- In order to obtain a realistic solution, the time-steps used must be very small, which results in large computational times.
- This method does not apply well to strata which are behaving elastically (e.g. above sub-critical width panels).
- Two-dimensional models, which assume infinite length in the z-direction, result in the development of infinitely long columns of "blocks", which cannot fully rotate as in the field.

The best approach to modelling subsidence would be to use hybrid models, such as FEBLK, which utilise finite element processes in conjunction with block motion theories, however, the problem of applying the correct number and area of blocks to represent the caving and fracturing zones still remains, as does the long column problem.

2.6.5 PHYSICAL MODELLING

Physical models represent simplified scaled models of complex prototype structures, and are manufactured with materials which best represent the mechanical properties of the prototype. The most common materials used to construct scaled models have been mixes of sand, plaster and water (Rowlands, 1990), however, a wide range of materials have also been used; from gelatin, as used by Kratzsch (1983), to natural materials sampled from the site of the prototype, as done by Sutherland (1986). When artificial rock or soil materials are used, the artificial material is termed ***equivalent material***.

Physical models can be designed to perform under 1 gravity(g) where model responses are developed from only the self weight of the model, or under elevated gravity such as base friction models where the frictional forces generated by a rotating base (eg Rowlands, 1990) generate higer gravitational forces, or centrifuge models where gravity forces are controlled by the speed of rotation of the model (e.g. Clark,1988). When modelling large depths of cover, external pressures can be applied to the perimeter of the model to reduce the model dimensions (e.g. Wold, 1984 and Stephan, 1989). The magnitude of applied forces is dependent on the field stresses, and the scaling between the prototype and the model. Each researcher has reported a certain amount

of success from their modelling, regardless of the construction materials or the method used to apply relevant body forces to the model. Most success has been recorded for models where the measured field subsidence is in the order of 100% "mining" height (e.g. Whittaker et al., 1984). Given that the Collie Basin subsidence is in the order of 63% mining height, it was considered that only the materials which allow some form of dilation or bulking should be investigated. The best representation of Collie Basin maximum subsidence found in the literature was 80% mining height by Sutherland, 1986 using natural materials. It was therefore considered that the best approach for the MERIWA study was to use either natural rock, or an appropriate sand/plaster synthetic material which could duplicate the natural material.

Given that the purpose of small scaled modelling is to replicate the behaviour of full-scale engineering structures, construction of the artificial model structures must be directly proportional to prototype dimensions and physical characteristics.

To correctly scale the model, firstly all the parameters involved in the engineering structure or process must be identified such that a functional relationship between the process (e.g. subsidence) and all the relevant parameters contributing to the process is established. Then, by adopting Buckingham's theory, this complex functional equation can be reduced to a series of independent dimensionless products, called (π) terms, on which to base model scaling. The model is then is then constructed such that similitude is maintained between the model and prototype for all of these π terms. Thus dimensional analysis represents a powerful tool which can be used to solve many complex problems.

Two examples of dimensional analysis for modelling of mining subsidence are given in Fitzpatrick (1987) and Whittaker and Reddish (1989). Both publications infer that subsidence is dependent on the mine geometry (G), the rock's unconfined compressive strength (UCS), tensile strength (TS), Poisson's ratio (v), and unit weight (W). Their resultant functional equation was:

$$\text{Subsidence (S)} = f(G,UCS,TS,E,v,W), \quad \text{or, because W= Rock density } (\gamma) \text{ x gravity(g),} \quad 2.6(10)$$

$$\text{Subsidence (S)} = f(G,UCS,TS,E,v,\gamma,g). \quad 2.6(11)$$

This can be rewritten in the general form:

$$f(S,G,UCS,TS,E,v,\gamma,g) = 0 \qquad 2.6(12)$$

As mentioned above, in order to simplify this complex function into terms that can be readily used in model scaling, a system of dimensionless π terms are developed. The first step is to reduce each parameter given in the functional Equation 2.6(12) to fundamental units of measure. This provides the number of "k" fundamental dimensions, and simplifies the process of development of the final system of dimensionless π terms. For example the parameters subsidence and geometry, material strength, elastic properties, and unit weight, have the respective fundamental units of Length (L), and mass, length and time ($ML^{-1}T^{-2}$). The number of fundamental units (k) = 3.

The remaining steps for reducing Equation 2.6(12) to an appropriate system of dimensionless variables are explained in note form below (from Jones and Kramadibrata, 1994):

1) Determine the number of dimensionless π terms given by n-k, where value "n" represents the number of parameters involved in the engineering process.

2) Select the "repeating" variables according to the following rules:

   - The repeating variables must include among them, all of the k fundamental units.
   - The dependent variable should not be used as a repeating variable.

3) In turn, assign each parameter listed in Equation 2.6(12) (but not including those selected as repeating variables in step 2) to each π term.

4) Find the exponents in each π term.

5) Write the equations in terms of the π terms and perform such algebraic operations as may be required to rearrange the terms into workable expressions.

Solving for the first step, the number of dimensionless π terms required is n-k = 5.

Satisfying the second step, the repeating variables chosen are G,UCS, and g.

Solving for the third step, the functional equation can now be expressed as:

$$f(\pi_1, \pi_2, \pi_3, \pi_4, \pi_5) = 0. \qquad 2.6(13)$$

Where, $\pi_1 = G^{a1}.UCS^{b1}.g^{c1}.S$, $\pi_2 = G^{a2}.UCS^{b2}.g^{c2}.TS$, $\pi_3 = G^{a3}.UCS^{b3}.g^{c3}.E$

$\pi_4 = G^{a4}.UCS^{b4}.g^{c4}.v$, and $\pi_5 = G^{a5}.UCS^{b5}.g^{c5}.\gamma$.

The fourth step requires solving for the exponents of each fundamental unit of measure in each of the five π terms.

	π_1	π_2	π_3	π_4	π_5	
M	$0+b_1+0+0 = 0$,	$0+b_2+0+1 = 0$,	$0+b3+0+1 = 0$,	$0+b_4+0+0=0$	$0+b_5+0+1$	$= 0$
L	$a_1-b_1+c_1+1 = 0$	$a2-b_2+c_2-1 = 0$	$a_3-b_3+c_3-1 = 0$	$a_4-b_4+c_4+0 = 0$	$a_5-b_5+c_5-3$	$= 0$
T	$0-2b_1-2c_1+0 = 0$	$0-2b_2-2c_2-2 = 0$	$0-2b_3-2c_3-2 = 0$	$0-2b_4-2c_4+0 = 0$	$0-2b_5-2c_5+0$	$= 0$

Solving for each π term:

π_1 ; b1 = 0, c1 = 0, a1 = -1

π_2 ; b2 = -1, c2 = 0, a2 = 0

π_3 ; b3 = -1, c3 = 0, a3 = 0

π_4 ; b4 = 0, c4 = 0, a4 = 0

π_5 ; b5 = -1, c5 = 1, a5 = 1

The final step is to derive n-k dimensionless terms from each of these lines of exponents, and write them as a functional equation from which to base the model scaling:

$\pi_1 = S/G$, $\pi_2 = TS/UCS$, $\pi_3 = E/UCS$, $\pi_4 = v$, $\pi_5 = G\gamma g/UCS$

and, $f(S/G, TS/UCS, E/UCS, v, G\gamma g/UCS) = 0$ 2.6(14)

This relationship can then be expressed as a system of dimensionless values in terms of the dependent variable (S):

$$S/G = \int(TS/UCS, E/UCS, v, G\gamma g/UCS). \qquad 2.6(15)$$

This function compares directly with that derived by Whittaker and Reddish (1989), page 441,

$$S/G = \int(TS/UCS, E/UCS, v, WG/UCS). \qquad 2.6(16)$$

It follows that if the model $_{(m)}$ is to truley represent the prototype structure $_{(p)}$:

$$S/G_{(m)} = S/G_{(p)} \quad 2.6(17)$$

$$TS_{(m)}/UCS_{(m)} = TS_{(p)}/UCS_{(p)}, \quad 2.6(18)$$

$$E_{(m)}/UCS_{(m)} = E_{(p)}/UCS_{(p)}, \quad 2.6(19)$$

$$v_{(m)} = v_{(p)}, \quad 2.6(20)$$

$$W_{(m)}.G_{(m)}/UCS_{(m)} = W_{(p)}.G_{(p)}/UCS_{(p)}. \quad 2.6(21)$$

Rearranging these terms, the following relationships for model similitude can be established:

$$S_{(m)}/S_{(p)} = G_{(m)}/G_{(p)}, \text{ the "geometric scale factor" (Whittaker and Reddish, 1989)} \quad 2.6(22)$$

$$TS_{(m)}/TS_{(p)} = UCS_{(m)}/UCS_{(p)} = E_{(m)}/E_{(p)} = WG_{(m)}/WG_{(p)}. \quad 2.6(23)$$

Note that the last term in Equation 2.6(23) is referred to as the "strength scale factor" by Whittaker and Reddish (1989).

Another example of the application of dimensional analyses is given by Sowers (1979) for simple problems in static plastic and elastic equilibrium. In this reference only two respective π terms need to be considered:

$$\pi_{strength} = \tau/\gamma.g.L, \quad 2.6(24)$$

$$\pi_{rigidity} = E/\gamma.g.L, \quad 2.6(25)$$

where, τ = shear strength of material.

If appropriate, the natural prototype material can be used to construct models and similitude can, in some cases, be met inherently. However, if these materials are not conducive for modelling, ***equivalent material*** must be used, and the task of obtaining true similitude, particularly for large scale destructive mining models, becomes extremely difficult if not impossible. For example in the series of dimensionless products given by Whittaker and Reddish above, a change in compressive strength of equivalent material will require equivalent changes in tensile strength, elastic modulus and the body dimensions if true similitude is to be met. Obert & Duvall (1967) considered that an equivalent material meeting all the requirements of similitude is "probably not attainable, at least no material of this kind has been reported." Indraratna (1990), Tomlin and Bicer (1988), and Hoek (1965), further support the conclusion that true similitude cannot be realistically obtained for all model parameters when using equivalent materials.

Furthermore the work done by Fitzpatrick (1987) at the University of Nottingham, found that when the modelled prototype is very large, the geometric scaling factor and the corresponding strength reduction factors required to maintain similitude in the model can result in an equivalent material which is very weak, and is "unlikely to behave like rock".

It is therefore highly improbable that an equivalent material can maintain true similitude for all these subsidence-relevant parameters.

Obert and Duvall (1967) state that "usually some compromise is necessary and first consideration should be given to matching the more important properties. Thus if the shear strength is considered to be the factor which will dominate failure in the prototype, the relationship:

$$\frac{Ss_{(p)}}{E_{(p)}} = \frac{Ss_{(m)}}{E_{(m)}}$$

should be satisfied and the other model strengths disregarded." Thus after the appropriate π terms have been establish, it is necessary to determine the most appropriate strength parameters of the prototype materials from which to base the models on.

The strength parameters presented by other researchers as being most applicable to the subsidence or mining processes vary. For example Wold (1984) included the use of tensile strength, whereas Stephan (1989) used the flexural strength. Whittaker and Reddish (1989) appear to have obtained adequate similitude for mining subsidence models by manufacturing equivalent materials scaled on unconfined compressive strength (UCS) and elastic modulus. The material property Poisson's ratio has been ignored, as it was considered to contribute little to the subsidence process, while the material property tensile strength appears to have been omitted - note on Page 442 of Whittaker and Reddish that only UCS and Young's Modulus strength parameters have been quoted as being tested for model similitude. Although Whittaker and Reddish do not provide any explanation for the omission of tensile strength, it is likely they either considered this term to be much less important than the UCS and elastic modulus for subsidence development, or that tensile strengths can be expected to change in proportion with variation in UCS. This is considered acceptable practice, if there is adequate supportive information.

Another important consideration for the construction of equivalent models is the application of "rock mass" strengths to model designs, rather than the laboratory strength test values. It is well documented that the strength parameters determined from small-scale laboratory tests can be significantly higher than the actual strength of materials in large scale natural structures. For example, Bieniawski (1984) and others have proposed rock mass reduction factors for hard rock, based on rock mass rating systems of fractured rock. Wilson (1982) provides some recommended rock mass reduction factors for coal fields strata. However, these reduction factors are not necessarily applicable to all strength parameters, and are generally based on site specific data. Misich and Humphreys (1988) and Misich (1988) recommend a strength reduction factor of approximately one third for compressive strength of coal, however, there is no requirement for a "rock mass" reduction of the weak sandstones that are generally devoid of fracturing/jointing. The ramifications for modelling is that the natural coal material may not behave correctly in models, as it does not represent the large scale rock mass properties.

Less than ideal scaling is therefore an inherent flaw in all physical models using equivalent materials. It follows therefore, that compromisation of scaling laws will lead to inaccuracies in the performance of the model, the size of the discrepancy being dependent on the importance of the role of the specific parameters being compromised in the physical processes.

Nonetheless, physical modelling has been used as an important tool for investigation of prototype performance and design in a large number of cases in all parts of the world (e.g. Whittaker and Reddish, 1989 - who reported good comparison between models and field results in the U.K. based on this simplified scaling approach, using a "strength scale factor" of 133.26). In view of some of the successful modelling results reported in several other coal mining regions, it was considered that physical modelling of the subsidence process of the weak Collie Basin sediments had good potential to fulfill the objectives of the research project.

The form of physical modelling proposed for project M165 was centrifuge modelling, largely because of its reported ability to obtain realistic stresses within critical areas of the model, introduce fluid flow and pore pressure, and because of the greatly reduced time needed to construct and run the models in comparison to other physical modelling techniques. A discussion of this modelling technique is provided below.

2.6.5.1 Centrifuge Modelling

The first documented case of the centrifuge modelling technique was in 1930, when Bucky (in the USA) used the method to assess deformation of rock beams in underground chambers, and Pokrovskii (in the USSR) looked at the stability of slopes in river banks. Although results proved favourable, interest in the technique - other than in the USSR - did not develop quickly due to the development of intricate computer modelling and the digital computer (Ko, 1988). Within the last two decades, interest in centrifuge modelling packages has increased, being fuelled by increasing awareness of the limitations of computer-based design methods.

Bucky and Fentress (1934) state "scalar models of any weighty structure will behave like its prototype if the model and prototype material are the same, and if the effective model weight is increased in the same proportion as its linear model dimensions are diminished. The effect of an increase in weight is obtained by substituting a centrifugal field of force for the gravitational field, the model being placed in a suitably designed centrifuge." In this way, the field stresses and resultant strains are closely represented by the scaled model throughout all stages of the test. This is the major advantage of the modelling method.

A geotechnical centrifuge is usually mounted in a temperature controlled, impact proof chamber and is operated remotely by a microcomputer which continuously monitors the performance and balance of the centrifuge during operation. Data acquisition is made possible by passing sheathed cable, connected to the model, through a series of slip-rings located in the central column of the centrifuge to data-logging computers. This allows for continuous, real-time data to be recorded and later transferred to personal computers for analysis.

Centrifugal acceleration of models, g(m), is dependent on the radius and speed of rotation around a central pivot and is calculated from the following relationship:

$$\mathbf{g(m) = V^2/y} \quad \text{(Hoek, 1965)} \qquad 2.6(26)$$

where g = accelerated gravities, V = linear velocity of the model, and
y = radius of rotation.

It is not possible to maintain true similitude of accelerated gravities throughout any centrifuge model as the radius of rotation of any point in the model will vary according to the distance of that point from the central pivot of the rotational arm of the centrifuge. This inaccuracy is commonly minimised by constructing the model so that the appropriate prototype gravity force is positioned at the mid-point of the model Hoek (1965). The percentage error between the top and bottom of centrifuge models of various depth and radius of rotation is illustrated in Figure 2.24 (from Hoek, 1965). It can be seen that in typical operating ranges (1.8 m radius of rotation, and 30 cm deep models), the error in stress distribution about the centre of the model is relatively small ($\leq$5%).

For this study it was considered more appropriate to replicate prototype stresses at the seam level to ensure that correct body forces were being imposed on the model in the region of caving to enhance correct caving and bulking.

Therefore, assuming the radius of rotation to the base of the model to be in the order of 1.8 m, the speed of rotation, using Equation 2.6(26), required to achieve 200 g is:

$$V = \sqrt{Gy} = \sqrt{200 \times 1.8} = 19 \text{ ms}^{-1}$$

At this speed, the model is travelling at $19 \div (2\pi \times 1.8) = 1.68$ revolutions per second. Thus a model 350 mm deep, will have a radius of rotation of 1.45 m at the model surface, and a corresponding linear velocity of $1.68 \times 1.45 \times 2\pi = 15.3 \text{ ms}^{-1}$. The resultant centrifugal force is; $15.3^2 \div 1.45 = 161$ g, which corresponds to a 20% variation between the surface and the base of the model. A model 200 mm deep will have a centrifugal force of 178 g, or 11% error at the surface.

This variation, though not ideal, was considered to be sustainable for the less important near surface subsidence (in terms of the objectives of modelling for the project).

Geotechnical centrifuge modelling, though not new, has rarely been used in full-scale underground mine modelling. This is largely because of:

- The limited ability of the centrifuge machine to provide sufficient accelerated gravity to sensibly model the stronger rocks found in typical coal measures in other parts of the world. [Clark, 1987 suggests that gravity forces in the range of 1000 to 3000 g would be required for such strata. McWilliams (1989) agreed with Clark,

MAXIMUM PERCENTAGE ERROR IN STRESS DISTRIBUTION AS A FUNCTION OF MODEL DEPTH AND CENTRIFUGE RADIUS (from Hoek, 1965)

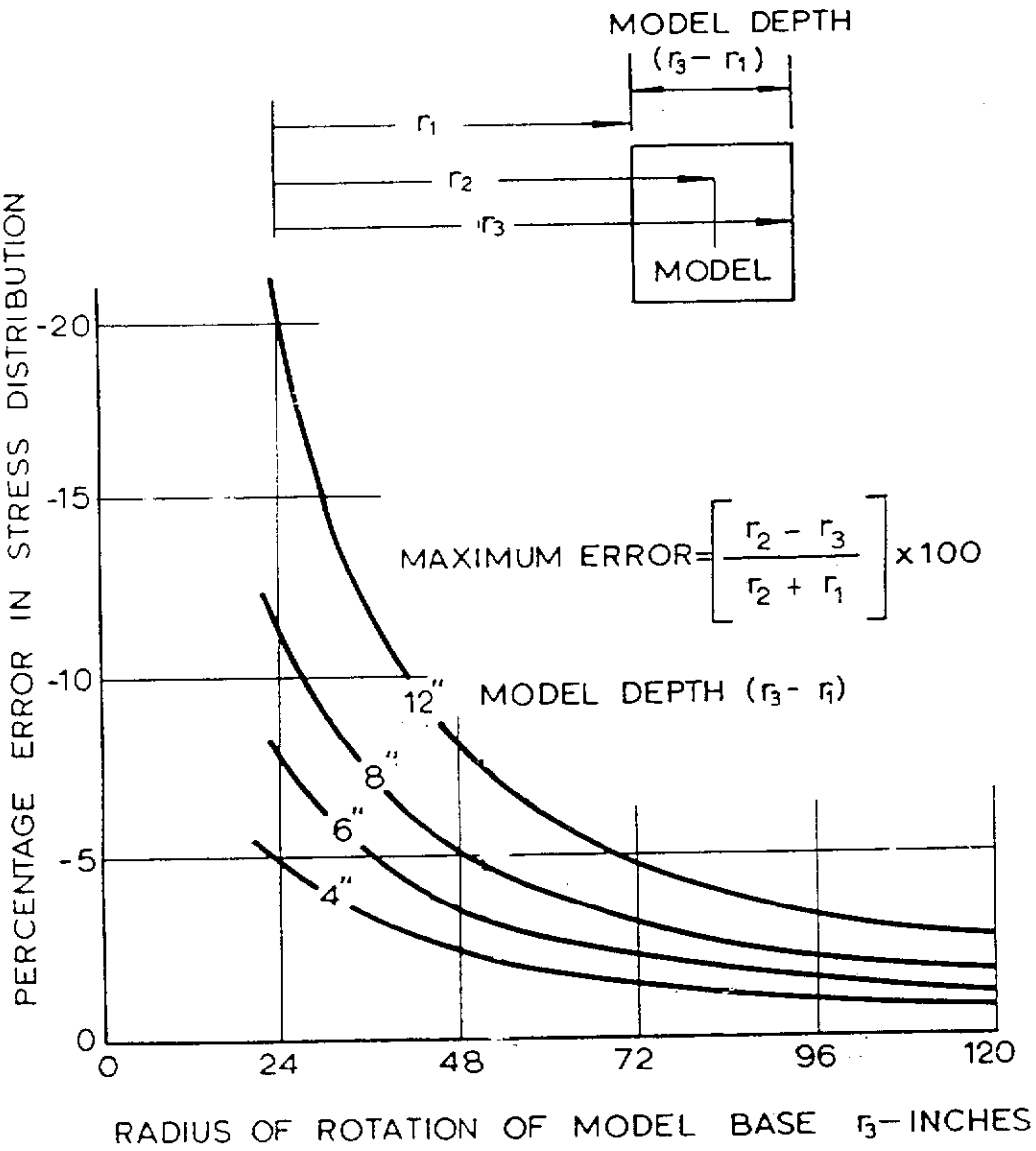

Figure 2.24

adding that a model payload of several short tons would be required. McWilliams states " such a machine does not exist today in the Western world." The cost of building such a machine and test model are considered prohibitive. This claim appears to be appropriate as Sutherland had to manually fracture the block of shale used in his models to obtain any meaningful subsidence results.]

- The fact that behavioural mechanisms in such high strength rocks are largely dependent on inherent rock fracturing, which is impractical to model accurately with small scaled models.

Consequently most mining related centrifuge studies have been limited to isolated elements such as tunnel linings (e.g. Moir 1979) and supported mine roof beams (e.g. Bucky 1931, Stephansson 1971 and Panek 1956). By far the majority of centrifuge tests have been developed for the investigation of soil mechanics problems.

At this point it would appear to be a fruitless exercise to model full-scale subsidence in any mining project; however, the opportunity to model the sediments in the Collie Basin was seen to represent a reasonable proposition as the strengths of the local sandstone material can be two orders of magnitude less than in other mining regions (see Section 2.4), there is a general paucity of rock mass fractures, and the depth of mining is relatively shallow.

Although several important characteristics of centrifuge modelling were gleaned from the many papers published on mining in clays or soils (e.g. Bolton et al., 1973, and Mair, 1979), as well a relatively small number of papers on rock mechanics investigations in mines, the authors were not able to locate any published work of the same scope or aims as proposed for the research project. The most applicable papers found included Sutherland (1982), Sutherland et al. (1984) (and a number of other papers by Sutherland), Howell and Jenkins (1985), and Mitchell (1991).

Sutherland et al. (1984) used slabs of Devonian shale taken from a minesite in Ohio to attempt to model mining subsidence in the early 1980's on their 25 ft centrifuge (McWilliams, 1989). This machine, using a swing platform to position the model, was capable of carrying a payload of over 1000 lb at 150 g acceleration. A total of three slabs of shale (UCS = 216 MPa) were used in the model, each being bonded together

using dental plaster. The completed model was 1.167 m long, 0.203 m wide and 0.511 m deep and operated at 150 g. Sutherland et al. (1984) overcame the problem of modelling strong rocks in the centrifuge by breaking the natural rock with chisels and hammers to introduce what was thought to be representative natural fracturing.

In order to represent the act of mining, Sutherland developed a series of hydraulic supports which could be lowered electronically at required intervals during the test. A total of 11 units were used each 102 mm wide and 203 mm deep, the drop height of each piston was 51 mm. The prototype dimensions represented by the model being a mine at 86.3 m cover depth with an excavation 15.24 m wide and 7.62 m high. The sequence chosen for lowering the supports was symmetric about the centerline of the model; first the centreline unit was dropped, followed by sequential symmetric pairs about the centerline.

In order to measure subsidence throughout the model, two types of transducers were implemented: firstly Linear Voltage Displacement Transducers (LVDT's), which were connected - through the viewing plate - to steel pins mounted 100 mm into the model; the second was a type of capacitance displacement transducer, using a sheet of aluminium foil placed on the surface of the model as a base for the transducers. When failure was observed at specific locations in the model, the steel pins were removed from those sites. The centrifuge test was stopped between each mining step to make additional photographic records.

Sutherland et al. (1984) recorded a final maximum prototype-equivalent subsidence of 6.10 m, which represents a subsidence factor of 6.10/7.62 = 0.80. (Note typical subsidence factors quoted by Amadek & Jeran, 1985 for the mid-east USA are 0.6.) The results gained from this test were only compared with the results attained from mathematical modelling of the surface (using analytical computer codes named RUBBLE and BLOCKS - Sutherland, 1986); no comparison was made to either measured or expected field data. No comparative data was provided for the subsurface subsidence predicted by the model. This lack of "real" data and exclusion of subsurface subsidence comparisons is considered to be a flaw in the experimental procedures in this study. It is well acknowledged by numerous researchers (e.g. Holt, 1988) that mathematical models can be made to represent any surface model with a

sufficient number of "fudge factors".

It was concluded by Sutherland et al. that although the centrifuge test rated as a success, the results were later proven, by mathematical modelling, to be largely dependent on the number and size of the fractured blocks in the model. Nonetheless, they concluded that " this weakness does not a priori invalidate the analysis".

Although the results gained from these tests were acceptable for their purposes, the use of their model tests for design purposes is questionable due to the method of crack enhancement in the model, and the disregard for similitude in shape, roughness and orientation of naturally occurring fractures in rock. It is also questionable what effect the steel monitoring pins inserted in the model had on the performance of the model.

Clark (1987), mentioned several successful applications of centrifuge modelling to salt mining, among which include physical properties of rock and behaviour of mine openings, and the mechanics of a Voussoir arch applied to mining by block caving, which could be extended easily to the mechanics of subsidence.

Howell and Jenkins (1987) studied pothole subsidence formations above relatively shallow rock salt mines in Cheshire, England, using the UMIT 100 g centrifuge. Cavities were created in the rock salt by lowering a series of "trapdoors" at the base of the model. The scaled model represented prototype ground masses 17 m deep and 55 x 34 m in area. The overburden material in the prototype situation was a series of unconsolidated gravels, sands, silts, clays and peat.

The combination of shallow mining depths and weak, unconsolidated materials in the prototype, allowed for reasonable similitude to be maintained within the centrifuge model, unlike other trials of subsidence modelling. The results from these tests gave favourable comparisons with field observations of rapid development of almost circular subsidence pot-holes. This trap-door approach was considered to be well suited to the simulation of mining for the Collie Basin research project.

Some reservations have been published about the inadequate scaling of material grain-sizes between the model and the prototype in large scale centrifuge models. For example, a 1 mm diameter grain of sand in a centrifuge model operating at 200 g is effectively 200 mm wide in the operating model. Depending on the type and purpose

of model, this exaggerated grain-size could greatly affect the performance of the model.

An investigation of this problem by Fuglsang & Krebs Ovesen (1988) acknowledges that discrepancies can occur with inadequate scaling of grain sizes. However,they found that this scale effect is not significant (in foundation related tests) when the model footing/average grain size ratio exceeds 30. In the case of mining models, this ratio would relate to the minimum dimensions of, say the trap-door element, representing a particular width of excavation. For example if a geometric scaling factor of 1:300 is used, a 13 m wide split/fender would be represented by a trap-door element 43 mm wide. In order to meet the above limiting grain size ratio, the maximum grain size of the model material would need to be less than 1.4 mm, which is easily achieved.

However, in terms of representing aquitard or sandstone material, the typical diameter of graded sand used for modelling is 0.3 mm, which equates to a prototype grain size of 60 mm gravel (as defined by Church, 1988) at 200 g. Although this is not totally unreasonable for the sandstone aquifers, this scaled grain dimension could affect crack propagation in the thinner aquitard material being modelled. In order to meet the above design criteria, the minimum thickness of aquitard strata in the model is 9 mm.

Physical modelling Advantages ....

Centrifugal and, in some cases large-scale physical modelling, can allow:

- the use of natural (prototype) materials to construct models, although most large-scale physical models usually consist of sand-plaster-water mixes,
- for continuity of loading after initial failure,
- modelling of reasonably complex geological structures,
- modelling of dynamic processes,
- (centrifuge models) the introduction of fluid flow,
- many types and numbers of mining sequences,
- the status of the model to be readily observed, both during testing and at the completion of a model test, which can be useful in determining types and mechanisms of fracturing.

Disadvantages ....

The major disadvantages of scaled physical models, including centrifuge models, include:

- Maintaining complete similitude of the material properties and applied loads for the model and prototype is difficult, if not impossible, particularly for artificial model materials. It is therefore unlikely that these models will exactly duplicate all the prototype responses and it is inevitable that some simplifications and compromises will be required. The resultant level of model accuracy will depend on the extent to which the isolated critical parameters of the process involved control the behaviour of the model.
- More expense and time is needed to design and construct models, although centrifuge model preparation is quicker (than large-scale 1 gravity models) due to their smaller size.
- Very deep or large structures cannot be modelled entirely due to the size restrictions of the model container. This is particularly true for centrifuge models..
- The effect of proportionately large grain size and grain shape in very small, scaled models is unclear.
- Rock mass defects are impractical to scale accurately in full scale mining models.
- It is difficult to apply a reduced rock-mass strength value for all material strength parameters from laboratory strength test results.

2.6.6 SUMMARY OF MODELLING METHODS

Empirically based prediction methods, including profile and influence functions, have been used more frequently than other methods due to their simplicity and the fact that they are based on reliable field data. Of the empirical methods, the functional approach is the most favoured (Bahuguna et al., 1991). However,in order to formulate a reliable empirical predictive method, large numbers of case studies are required. This could involve a period of many years which would be unacceptable to mine planners in

Greenfield sites. As a consequence, researchers usually trial other methods - such as numerical modelling - to assist with the design of coal extraction in mines.

Numerical modelling, using sophisticated computer codes, and physical modelling techniques can be used to evolve a predictive technique from minimal subsidence information. Physical, and to a lesser extent, numerical modelling can also address subsurface subsidence mechanisms. Numerical modelling in particular, has the ability to model a range of complex mining scenarios within a short period of time to allow the mining engineer to arrive at an optimum mine design in the most cost efficient manner.

These two modelling methods, however, also have restrictions to their usage, they cannot fully represent the complete mining/caving environment and the full suite of mechanical characteristics of the strata. Clark (1988) concluded that physical and mathematical modelling should be used in conjunction as the two methods complement each other. Clark considered that physical modelling should be "a fundamental step by itself in the analytical-design process" for the determination of the rock mass properties and engineering responses of rock masses.

Nonetheless, the deficiencies of these modelling techniques (particularly for subsidence modelling), require subjective modifications to model material properties and geology. Bahuguna et al. (1991) concur with this assessment, concluding that "the real problem remains again of determining the parameters afresh in each case and analysing the physical properties of rock layers on a large scale, which is normally beyond the means of mine operators". It is essential therefore to understand the limitations of application for each modelling technique before deciding which mathematical program or physical modelling method to use. Furthermore it is usually the case that verification of the suitability of these modelling assumptions and simplifications can only be accomplished after comparison with field data, in other words, all models need to be calibrated against known data. All subsidence prediction techniques are therefore site specific to some degree. Each method involves making some form of simplification or assumption of the complex field conditions which will probably not be applicable for other sites.

In Greenfield sites the author is therefore of the opinion that it is more efficient to firstly use empirical methods, such as the functional approach, from other mining areas with

similar geology and mining techniques to assist with the initial design of coal extraction panels. In relation to this research study, however, the author was not able to locate any published literature dealing with subsidence prediction in sediments similar to the weak water saturated strata in the Collie Basin. Furthermore, the empirical models available (eg NCB, 1975 and Brauner, 1973) did not adequately represent what limited field data existed in relation to subsidence in the Collie Basin. It was therefore considered essential to set up a comprehensive field monitoring program to obtain some real data from which predictive models could be calibrated against.

2.7 CONCLUSIONS FROM REVIEW OF PREVIOUS WORK

It was evident from the literature research that there has been a myriad of investigations of mining subsidence. It is also apparent that subsidence processes can differ widely from region to region, and it is most often the case that any subsidence predictive models produced from these investigations are site specific. Of the few Collie Basin subsidence observations recorded before this study, it was concluded that none of the predictive models available from other mining regions were appropriate for local conditions. This inconsistency between predictions made from existing predictive models and "green-field" subsidence development is not unique. Many researchers have reported problems with one or another model (eg Dunrud, 1984, and Bahuguna et al., 1991). It was evident that a site specific model needed to be developed so that accurate predictions of subsidence could be made for the local conditions.

Another concern for the introduction of total extraction was the potential to interconnect overlying water-filled aquifer systems with the mine workings during the caving/subsidence process. Although there has been many investigations into the effects of subsidence on aquifer systems (eg Wardell, 1975, and Singh et al., 1985), the author was again not able to locate any suitable modelling techniques which were applicable to the local conditions. It was therefore also evident that a site specific investigation was required to assess the effects of mining subsidence on aquifer systems in the Collie Basin. It was rationalised that, as the local aquifer sandstone is inherently porous (see Section 2.3.1), there was little to be gained from defining changes in permeability (of the sandstones) during the subsidence process - as done by a number of researchers, e.g. Fawcett (1986). The important parameter requiring

definition during subsidence development was considered to be the integrity of aquitard layers that separate vertical movement of large bodies of water.

This inconsistency with existing models, along with the general paucity of technical data available on the subsidence characteristics of the weak water-bearing Collie Basin sediments, and the need to manage mining subsidence to protect surface and subsurface features provided the impetus for this research project.

The first aim was to obtain sufficient field data on Collie Basin subsidence via a comprehensive investigation of both surface and subsurface subsidence. The requirement for accurate field data was paramount to the success of developing an understanding of the mechanisms leading to subsidence in the Collie Basin. It was seen as being critical that the field investigation was started as soon as possible, as a great amount of time is taken to set-up and mine an extraction panel.

The methods used to measure and evaluate field data are discussed in Chapter 3, Appendix I and Appendix II.

The second aim was to develop a site specific predictive model or modelling approach so that mine extraction could be suitably designed. For this project it was concluded that the best approach was to combine the use of empirical, numerical (using the boundary element/displacement discontinuity computer package SUBSOL), and physical (geotechnical centrifuge) modelling. Part of the intended approach was to use the centrifuge modelling to provide additional data for back-analysis of numerical models without relying solely on field data.

Of the empirical methods available, the profile function was selected, above influence functions, as being the most appropriate technique for prediction of the full subsidence trough. The main advantages with profile functions were that inflection points are not necessarily located above the panel edge, and the form of the profile function allows tilts and curvature to be calculated directly from the curve-fit equation. Although recent research (e.g. Bahuguna et al., 1991) suggests that the discrepancy with inflection point location for influence functions can be improved by applying weighed factors to the final subsidence profile, such additional manipulation of data was seen to be another source of error which would greatly increase the time spent on developing a reasonable predictive model.

Selection of the mathematical package SUBSOL was primarily based on the results of an investigation, by Kay et al. (1990), of the accuracy of a number of commercially available computer models for prediction of mining subsidence in Australia. The first conclusion made from this study was that none of the computer packages could accurately reproduce subsidence profiles measured in the field from the mining horizon through to the surface. Secondly, Kay et al. found that of all the mathematical packages tested, the model which best represented both surface and subsurface subsidence was the MINCAD Systems' (MINCAD) 3-D single seam displacement discontinuity computer software package MINLAY.

Since this investigation, the original computer program MINLAY had been improved sufficiently such that a second generation program, called SUBSOL was developed. SUBSOL was considered to be more able to represent subsurface subsidence and was therefore worthy of investigation. The more significant characteristics of this package are:

- SUBSOL has the ability to model layered stratigraphy (with or without surface topography), and incorporate large strain discontinuity elements at major geological interfaces such as coal seams, which have been identified to have a significant influence on the behaviour of Collie Basin sediments.
- SUBSOL has relatively simple to use pre- and post-processing packages to simplify set-up and manipulation of data.
- It is possible to model isotropic and anisotropic material properties with SUBSOL.
- SUBSOL can model non-linear, inelastic material properties at the excavation plane. This allows the modelling of pillar crush and compaction of goaf or fill. Although there is a certain amount of inflexibility with modelling this zone of subsidence, this option is valuable to modelling the subsidence phenomenon.
- Most other commercially available packages are 2-D systems. As modelling was to include irregular-shaped or narrow panels, a 3-D package was required.
- SUBSOL can incorporate complex "mining" steps and mine panel, pillar and roadway geometries. Each of these facets can have a significant impact on subsidence development.

It was proposed that should any secondary, small scale modelling be required, the elastic finite element program FESOL would be used where appropriate, largely due to its ease of use, availability and ability to represent complex shapes.

It was considered that, as the Collie Basin sediments are relatively weak, and the mining depths are comparatively shallow, the geotechnical centrifuge offered a useful technique for modelling the local subsidence processes from seam level through to the surface. It was anticipated that the centrifuge tests would provide useful information, particularly for strata in close proximity to the mine, which could be used to further develop mathematical and empirical models. The main advantage of this technique was the ability of the centrifuge to apply field-like stresses throughout the model at all stages of mining subsidence, to introduce fluid flow and pore pressure, and to reduce the time needed to construct and run the models in comparison to other physical modelling techniques.

A general summary of the modelling phase of the research project is presented in Chapter 4. Details of specific aspects of physical and numerical model development are provided in Appendices III, IV and V.

It was also identified that panel/pillar mining is the most appropriate method to manage subsidence within the economic and mining limitations existing at the time. However, the design criteria for such mining methods are limited and vary significantly, (eg Reynolds, 1977, and Holla, 1987). It was clear that a specific investigation into the design of panel/pillar extraction panels was required to ensure that safe, and economic mining practices could be established.

The approach used to develop and validate panel design criteria is presented in Chapter 5.

3.0 SUBSIDENCE MONITORING AND ANALYSES

The aim of this phase of research was to monitor subsidence development above a number of extraction panels (listed in Table 3.1) to provide base data for the development and validation of predictive models. The design, management and analysis of the data attained from this monitoring program was the sole responsibility of the author during his employment at WCL. A summary of the maximum surface subsidence parameters measured and the relevant geometry and depths of each of these panels is provided in Table 3.2. Details of individual panel set-up and extraction, monitoring and subsidence development are provided in Appendix I.

TABLE 3.1 EXTRACTION PANEL MONITORING DETAILS

	PANEL, MINE	MONITORING PARAMETERS
+	1) 6B East Panel, WD-2	(surface only)
%	2) ACIRL Panel (A & B), WD-6	(surface, subsurface & aquifers)
+	3) 2B West E1 Panel, WD-2	(surface only, aquifers "dry")
+	4) 2B West E2 Panel, WD-2	(surface only, aquifers "dry")
%	5) 2B West C Panel, WD-2	(surface only)
~~	6) Blue Panel, WD-6	(surface, subsurface & aquifers)
+	7) 2 South A Panel, WD-6	(surface & subsurface, aquifers"dry")
%	8) Red Panel, WD-6	(surface & aquifers)
+	9) 1 North Panel, WD-6	(surface & subsurface, aquifers "dry")
%	10) North West B3 Panel, WD-6	(surface, subsurface & aquifers)

%; panel W/H <1.4, ~~; panel W/H ≈ 1.4, +; panel W/H >1.4

A summary of the analyses of the results gained from these panels and the empirical models established to predict the form and dimension of subsidence in the Collie Basin is provided below. For consistency, the field monitoring has been presented into two separate phases - surface and subsurface subsidence monitoring.

TABLE 3.2
SUMMARY OF SUBSIDENCE MONITORING

PANEL	Smax (mm)	Mh (m)	% Extr	Smax /T	Width (W) (m)	Depth (H) (m)	W/H	Tilt max (mm/m)	Depth at Panel Edge (m)	Comp. strain (mm/m)	Tens. strain (mm/m)	Angle of Draw	Edge to Inflect. Dist(m)
2BWE1	200	2.5	85	0.09	15	32	0.47	22.0	-	-	-	-	-
2BWE1	1170	2.5	85	0.55	37	32	1.16	83.0	42	-	-	-	-
2BWE1	1290	2.5	85	0.61	59	32	1.84	87.0	42	-	-	12.0	-
2BWE1	1370	2.5	85	0.64	114	32	3.56	87.0	42	-	-	18.0	-
2BWE2	1320	2.4	90	0.61	80	55	1.45	63.0	55	22.0	21.0	-	-
2BWCA	853	2.5	90	0.38	48	60	0.80	97.0	60	-	-	-	-
2BWCB	937	2.5	90	0.42	52	59	0.88	64.0	60	-	-	-	-
RED1	24	2.6	80	0.01	39	160	0.24	0.0	160	-	-	-	-
RED2	50	2.6	80	0.02	60	160	0.38	0.9	160	-	-	-	-
RED2	115	2.6	80	0.06	80	160	0.50	1.5	160	1.4	1.1	-	-
RED2	254	2.6	80	0.12	80	160	0.50	3.0	160	2.5	1.6	22	-16
BLUE	50	2.7	90	0.02	52	142	0.37	1.0	150	-	-	-	-
BLUE	320	2.7	90	0.13	91	142	0.64	10.0	150	-	-	-	-
BLUE	560	2.7	90	0.23	105	142	0.74	14.0	150	-	-	-	-
BLUE	770	2.7	90	0.32	118	142	0.83	19.0	150	-	-	-	-
BLUE	900	2.7	90	0.37	131	142	0.92	-	-	-	-	-	-
BLUE	1020	2.7	90	0.42	145	142	1.02	-	-	-	-	-	-
BLUE	1290	2.7	90	0.53	160	142	1.13	26.4	150	14.4	16.5	25	25
ACIRL 1	41	2.7	90	0.02	50	150	0.33	-	-	-	-	-	-
ACIRL 1	50	2.7	90	0.02	62	150	0.41	1.1	153	-	-	-	-
ACIRL 1	170	2.7	90	0.07	75	150	0.50	2.9	153	0.5	0.7	27	5
ACIRL 2	890	2.7	90	0.37	106	140	0.76	19.5	138	13.4	12.3	27	-
2SA	290	2.5	90	0.13	30	56	0.54	-	-	-	-	-	-
2SA	670	2.5	90	0.30	42	56	0.75	-	-	-	-	-	-
2SA	1000	2.5	90	0.44	54	56	0.96	-	-	-	-	-	-
2SA	1150	2.5	90	0.51	66	56	1.18	-	-	-	-	-	-
2SA	1250	2.5	90	0.56	78	56	1.39	-	-	-	-	-	-
2SA	1310	2.5	90	0.58	91	56	1.63	55.0	69	24.0	25.0	18.0	10
2SA	1324	2.5	90	0.59	103	56	1.84	-	-	-	-	-	-
2SA	1421	2.5	90	0.63	136	56	2.43	57.2	69	24.0	31.0	22	10
6B EAST*	1000	2.65	60	0.63	200	120	1.67	18.8	129	6.8	5.6	39	-
1 NORTH	271	2.6	80	0.13	47	77	0.61	14.2	77	-	-	-	-
1 NORTH	802	2.6	80	0.39	64	77	0.83	33.4	77	-	-	23	-
1 NORTH	1125	2.6	85	0.51	82	77	1.06	45	77	-	-	23	-
1 NORTH	1229	2.6	85	0.56	100	77	1.30	50.1	77	24.7	22.3	23	13
1 NORTH	1275	2.6	85	0.58	117	77	1.52	50.9	77	-	-	23	13
1 NORTH	1301	2.6	85	0.59	134	77	1.74	52.1	77	44.1	22.7	23	13
1 NORTH	1314	2.6	85	0.59	160	77	2.08	52.3	77	-	-	23	13
1 NORTH	1313	2.6	85	0.59	212	77	2.75	52.3	77	-	-	23	13
1 NORTH	1318	2.6	85	0.60	390	77	5.06	52.3	77	50.6	22.3	23	13
1 NORTH	1386	2.6	90	0.59	450	77	5.84	52.3	77	50.4	22.1	25	13
1 NORTH	1434	2.6	90	0.61	507	77	6.58	52.9	77	49.4	22.5	26	13
NWB3_1	0	2.7	85	0.00	20	150	0.13	-	150	-	-	-	-
NWB3_1	16	2.7	85	0.01	40	150	0.27	-	150	-	-	-	-
NWB3_2	0	2.7	85	0.00	20	150	0.13	-	150	-	-	-	-
NWB3_2	25	2.7	85	0.01	40	150	0.27	-	150	-	-	-	-
NWB3_3	0	2.7	85	0.00	20	150	0.13	-	150	-	-	-	-
NWB3_3	35	2.7	85	0.02	40	150	0.27	-	150	-	-	-	-
NWB3_4	28	2.7	85	0.01	20	150	0.13	-	150	-	-	-	-
NWB3_4	25	2.7	85	0.01	40	150	0.27	-	150	-	-	-	-
NWB3_5	18	2.7	85	0.01	20	150	0.13	-	150	-	-	-	-
NWB3_5	18	2.7	85	0.01	40	150	0.27	-	150	-	-	-	-

* pillar split panel

Note: Subsidence parameters represent maximum values measured at incremental panel widths, and well after the completion of each panel. The subsidence recorded after any pillar robbing (within adjacent set-up roads on retreat from a panel) has not been included.

W = panel width (m), H = depth of cover (m), Mh = mining height (m), T = effective mining height(m)
Smax = maximum subsidence (mm), %Ext = percentage coal extraction

3.1 SURFACE SUBSIDENCE

In the majority of cases, subsidence was in the form of a continuous - gentle - trough with little or no visual impact on the ground surface. The exceptions were confined to some isolated areas above the shallow 2B West panels in WD-2. One area above the north eastern edge of 2B West E1 panel in particular had an open crack approximately 20 m long, 1 m wide and in the order of 5 m deep (see Figure 3.1). The depth of the crack, though not proven, was derived by placing a thin metal strip down the cracks. It is worthy to note that no significant additional water was pumped from the mine after heavy periods of rainfall.

Figure 3.2 provides the locations of each discontinuous pot-hole forms of subsidence featured above 2B West E1 panel. The timing and geometry of these features was random, taking from one or two days to months to show at the surface. It can be seen, however, that most of these discontinuous forms of subsidence occur near the panel edges, and toward the northern section of the panel.

Two explanations for the pot holes being located near the panel edge are:

- The panel edges represent the pivotal point for cantilevering of superincumbent strata. Due to the weak nature of the shallow sediments, a vertical shear can develop and extend to the surface above the pivotal coal abutments.
- Much of the perimeter of the panel is bounded by a number of setup roadways and older bord and pillar workings which provide additional space for the goafed material to rill into. This additional void retards the bulking process and, in turn reduces the support provided to the overlying, bridging strata, allowing the initial caving to extend higher into the overlying strata. Ultimately the near seam caving propagates through to the surface.

Further evidence supporting the latter mechanism can be seen where an 8 m deep pot-hole developed at the end of fender 4. This subsidence feature occurred after excavating and relocating the gob material which had partially buried the Alpine continuous miner. In the process of removal of the bulked waste, a much larger void was developed above the mine and, as a result, the collapse continued trough to the surface.

LARGE SCALE CRACKING ABOVE 2B WEST E1 PANEL

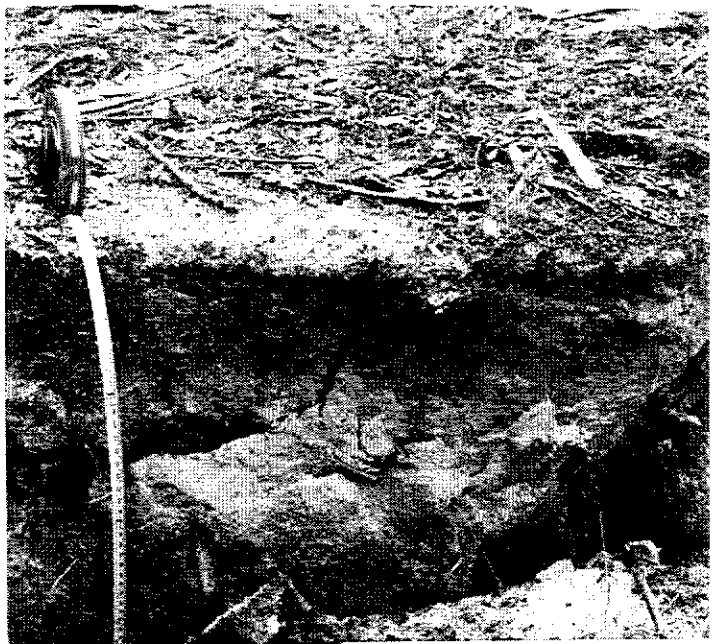

<<<< 0.4 m STEP IN SURFACE

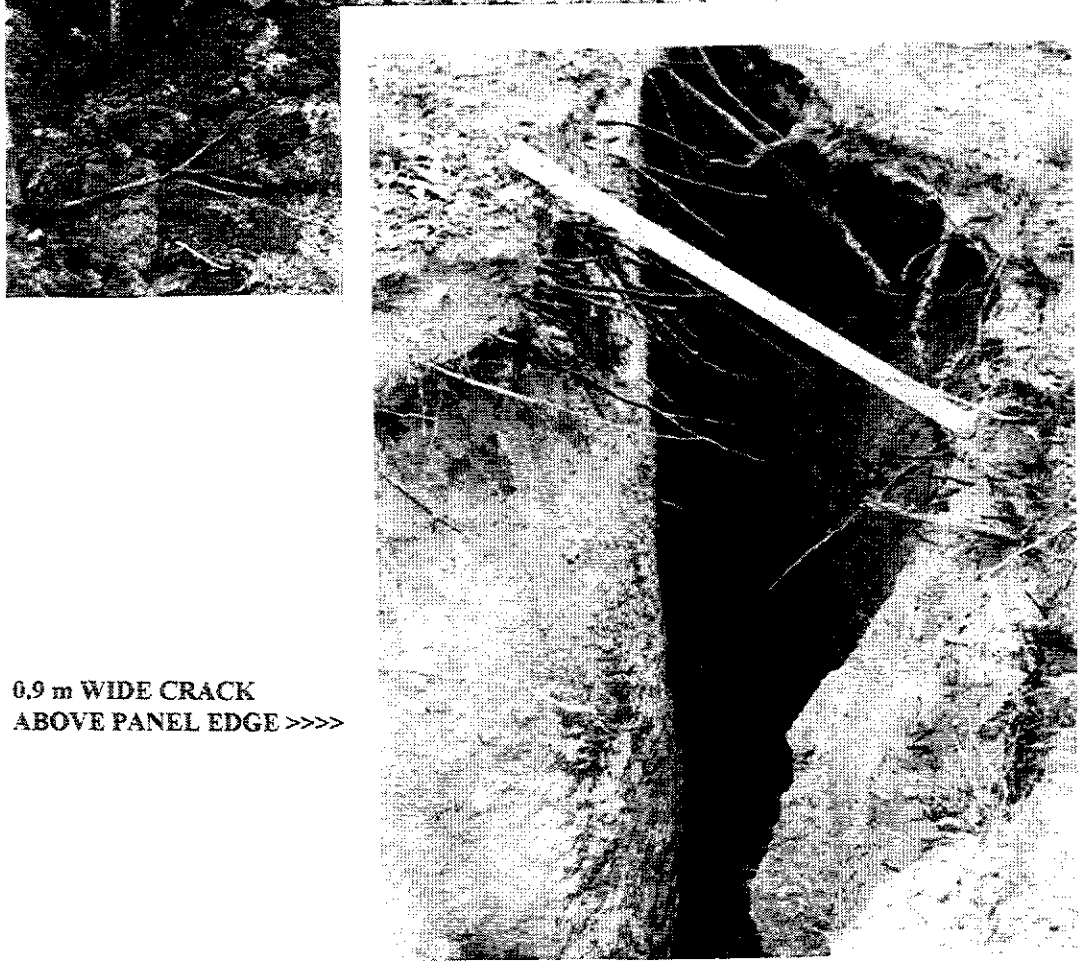

0.9 m WIDE CRACK
ABOVE PANEL EDGE >>>>

Figure 3.1

LOCATION OF DISCONTINUOUS SUBSIDENCE ABOVE 2B WEST E1 PANEL

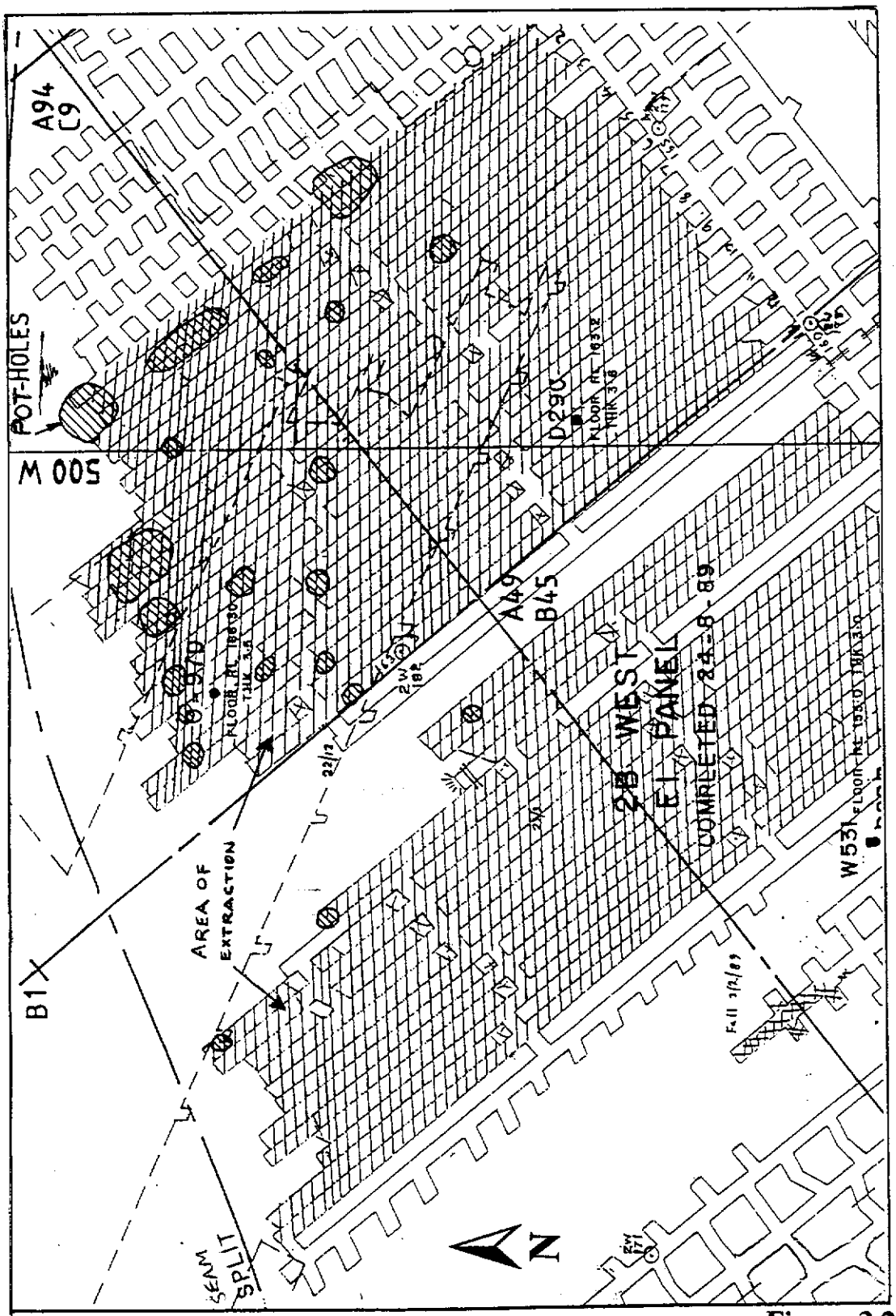

Figure 3.2

The development of this pot-hole would have been assisted by the extended time required to free the supports and the fact that extraction of fender 4 ceased here, thus permanently leaving the open void in the workings. Smaller pot-holes are also noted near intersections of roadways mined through fenders (to provide a second means of egress) during set-up of the splits. In many cases, the span of these intersections made total extraction of the fenders risky and forced the miners to leave stubs of unmined coal on either side to allow for safe passage across the intersection. These intersections were then often left open, providing additional void for neighbouring goaf to rill into.

There also appears to be a relationship between the general siting of the pot-holes to the north of the panel and the overlying geology. The strata above the northern section of the panel consists mainly of loose, leached white sands, which would be expected to be prone to large scale shear failure.

The southern section is slightly elevated and has lateritic outcrops, with thick underlying bands of ferruginous, plastic clays, extending down to 10 m beneath the surface. It is possible that the thick upper plastic clay layer, will tend to sag rather than rupture through to the surface. Another explanation could be that as the ground surface to the south is up to 10m higher (the cover depth is 42 m), the overburden may incorporate a stiffer aquitard member which may bridge across the caved zone. (This stiff layer could be oxidized or weathered out, in the shallower areas. The were no drill holes in the area which could be used to confirm this assumption.)

Another large pot-hole feature developed above the 2B West C1 panel in WD2. This feature formed as a result of the caved strata intersecting a pocket of loose, saturated sand, which liquefied and ran into the mine as a "slurry". The resultant subsidence feature was in the order of 8 m across and 9 m deep (Figure 3.3), which is far deeper than the height of excavation. This subsidence developed suddenly, as indicated by the "spray" of fine clayey material across the nearby vegetation. The depth of cover was approximately 60 m, which is far greater than the typical limiting depth for this type of subsidence in other areas in the Collie Basin.

Further analysis of pot-hole subsidence was not considered warranted at this stage, due to the lack of accurate details of the geology in the shallow areas.

DEEP SUBSIDENCE POT-HOLE RESULTING FROM A "SLURRY RUN"

Figure 3.3

As mentioned earlier, most subsidence above these extraction panels was of the continuous form, on which this research project is more focussed. These forms of surface subsidence generally followed consistent patterns of development, as explained later in this Section. However, peculiarities were observed above some panels, the more significant of these observations being:

- A hump, approximately 100 m long and 200 mm high, developed in the subsided ground above 1 North panel, about 25 m inside the panel edge (Figure 3.4), and between 85 and 65m depth. It is suggested that when the width of extraction reached 54 m, the unsupported mass subsided in one piece, and the hump developed at the surface where opposite lines of caving/shear (extending inwards from each panel abutment) intersect. It is expected that the overburden was compressed at this point and forced the loose surficial sands upward. (This shearing process is discussed further in Sections 3.2.5 and 3.3.) Assuming a shearing angle of 23° and a critical caving width of 54 m, the two planes of shear would be expected to intersect 64 m above the panel. This explains why the hump is not evident at depths less than 65 m and suggests that the compressive forces resulting from the intersecting lines of shear (that define the large scale "one-piece" collapse of ground) are sufficient to lift up to 20 m of sandy soil.

  A similar feature developed in the surficial sands above 2SA panel; the location of which was not accurately defined at the time. It is estimated that the depth of cover at this site was 60 m which suggests that either the angle of shear is lightly steeper above very shallow panels, or the critical width of extraction required to initiate the large scale one-piece collapse is less. Although the width of extraction required for the one-piece collapse above 2SA panel was 31 m, the overall width of collapsed ground was actually wider due to simultaneous collapse of bord and pillar workings immediately to the south of the panel. This collapse outside the panel was considered to be the result of elevated tributary loads at the panel abutments which allowed for the development of a "creep".

  A subsidence hump has been observed in at least one other region; in the Lake MacQuarrie District, NSW, Australia (Galvin & Anderson, 1986). However,no explanation of the feature was provided, and no panel details were given other than the depth of the panel being monitored varied between 45 and 120 m.

SUBSIDENCE HUMP ABOVE 1 NORTH PANEL WD6

Figure 3.4

- During extraction of fender #23 in 1 North panel, the JCM12 drum continuous miner cutting machine and three remote control mobile hydraulic breaker-line supports (BLS) were buried by a roof collapse. The JCM12 was recovered, however, two of the BLS were left in the collapsed ground mass. While repairs were being completed on the JCM12, it was decided to use the Voest Alpine #10 road-header continuous miner (A10) to complete extraction of the panel. The change in mine equipment to the A10 brought about slower rates of extraction (due to a less productive cutting action), but greater recovery of coal (due to the greater flexibility of the boom mounted cutter head on the A10). As a result of the higher percentage extraction of coal, there was greater surface subsidence above this section of the panel (see Figure 3.5).

- 1North was the first panel to trial the use of two-way lifting using the JCM12. Due to teething problems in the first two fenders, lifting off to the left was either not always possible or did not extend over the full width of the fender. This meant that the panel width varied by 6 m depending on location along the panel, and that a thin slice of coal (4-5 m) was left between the first two fenders extracted. As a consequence, surface subsidence was not noticed in 1 North panel until after 54 m (three partially completed splits) had been extracted. This initiating mining width was greater than observed during the extraction of previous panels.

- Surface cracking typically occurs within a zone from 8 to 15 m outside the panel edge. The depth of the tensile cracks was estimated to be between 0.5 to 2 m.

- The shape of the subsidence trough above the advancing edge of panels does not match the subsidence profiles at the trailing edge. This is best illustrated in Figure 3.5 which represents the development of surface subsidence with time above 1 North panel.

- The shape of the surface subsidence profile can be greatly affected by remnant coal left within the extraction panel. Examples of the effect of remnant coal can be noted by the irregular subsidence profiles above 2B West C, and 2B West E1 panels in the WD2 mine - see Figures I.26 a and I.16 a in Appendix I.

The typical trends and characteristics of continuous trough form of subsidence observed in the field study are summarised below in terms of the eight main characteristics of subsidence troughs - described in Section 2.5.5.2.

SURFACE SUBSIDENCE ABOVE 1 NORTH PANEL WD6

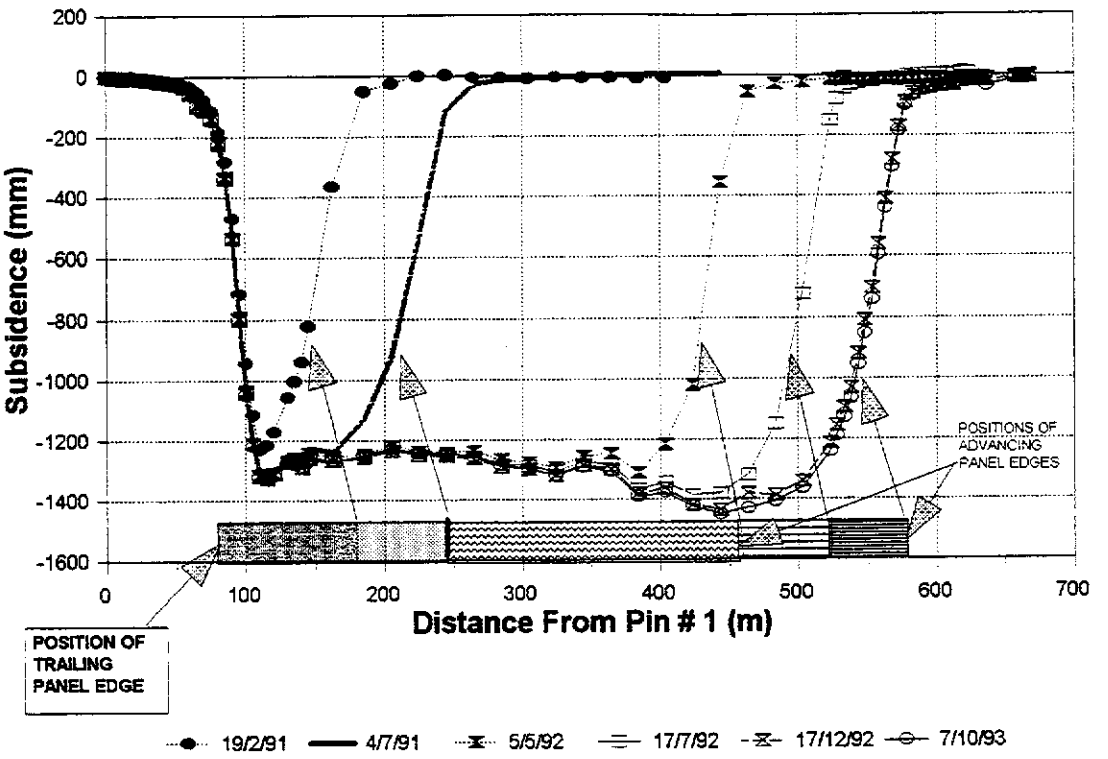

Figure 3.5

3.1.1 Maximum Subsidence

Maximum subsidence (Smax) is an important parameter for empirical modelling. Smax is used to predict maximum tilts, and strains and to determine the magnitude and ultimate shape of the surface subsidence trough. The greatest amount of trough-subsidence measured in the field study was 1.4 m above 2SA and 1North panels. As described earlier, the NCB (1966) and other researchers have established that Smax is dependent on the mining height, panel width and depth of cover and use these relationships to estimate Smax using a dimensionless nomogram (as given in Figure 2.15). The results from this study suggest that this approach is also valid for the Collie Basin (Figure 3.6). The resultant plot is considered to provide a tighter grouping of data when compared to those provided from other areas (eg Holla, 1985) and provides greater confidence that this family of data can be used to closely estimate Smax.

To assist with prediction of Smax, a bounding curve was fitted to the data. The use of a bounding envelope is considered to be more appropriate than fitting a curve of best fit through the data points because the enveloping curve provides a conservative prediction which automatically takes into account normal variation in mining methods and local geology. The equation adopted for estimating Smax in the Collie Basin (illustrated by Figure 3.6) is given as:

$$\mathbf{Smax = 0.63 \times T \times e^{(-12e\text{-}4(W/H))}} \qquad 3.1(1)$$

Where T = Effective mining height (m) - calculated as per Equation 2.5(13)

W = Panel width, and H = Mining depth of cover.

An interesting feature of this subsidence data is that the Smax/T versus W/H relationship is consistent for all panels, regardless of the depth of cover and whether or not the more lithified Permian sediments were present above the panel.

It is also interesting to note that Smax generally develops closer to the trailing panel edge. This has been also noted by other researchers; for example Ferrari (1996), who found that Smax occurred only 0.36 x H from the starting panel edge.

PREDICTION OF MAXIMUM SUBSIDENCE IN THE COLLIE BASIN

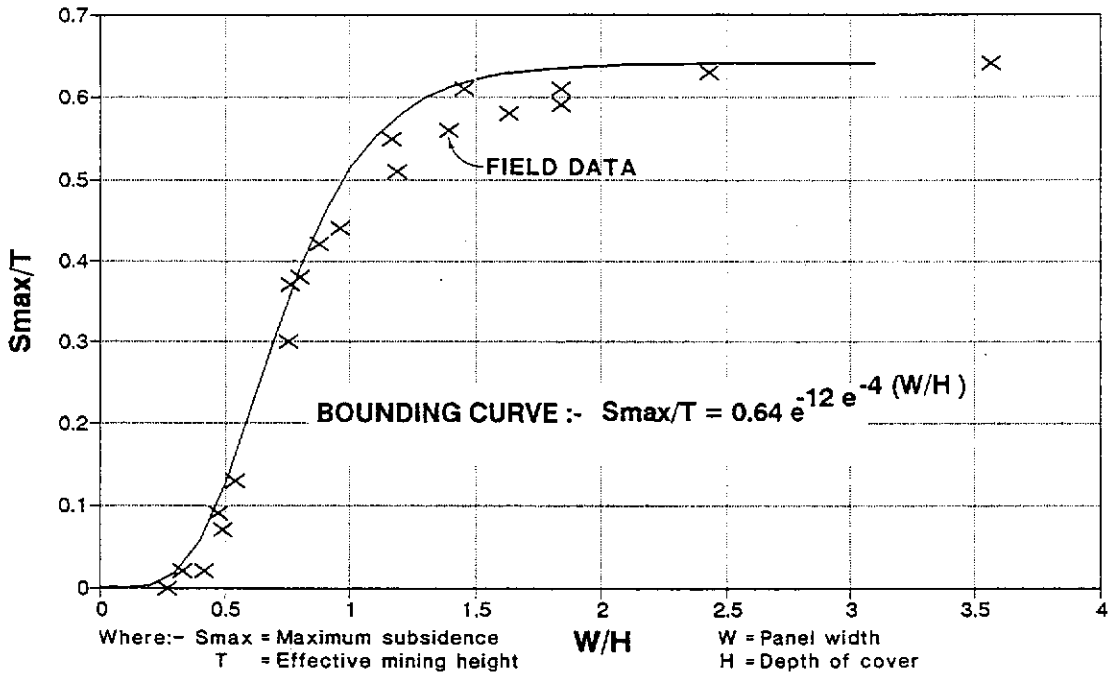

Figure 3.6

3.1.2 Critical Width

The results from field monitoring suggest that the definition of critical width in the Collie Basin, and that the limiting values for sub-critical and super-critical width panels differ from that given in the literature. Critical width is reached when the subsidence trough first develops a flatter profile within the central section of the trough (when the panel W/H ratio approximates 0.9). This flattened area is extended and deepens as the width of extraction increases and reaches super-critical width (to a W/H $\geq$ 1.7), when ultimate Smax is developed.

It has been interpreted that the point of initial critical width occurs when the panel width is sufficiently large that the subsidence trough is no longer influenced by the line of shearing. This timing equates to the panel width where the line of shear (measured as 23° from the vertical, and discussed in Sections 3.2 and 3.3), intersects the surface.

When critical width is first reached the subsidence that can be expected to be developed is in the order of 50% **effective** mining height. By the time the panel reaches super-critical width, the expected subsidence will have increased to 63% of effective mining height.

The mechanism by which subsidence can deepen beyond the initiation of a flattened trough is interpreted to be reconsolidation of the "dilated" collapsed/sheared ground which increases as the distance from the panel edge abutments to the panel centre increases. When a W/H ratio of 1.7 is reached, the full cover load is applied to the column of subsided ground and Smax is achieved. The process of shearing and reconsolidation is discussed in more detail in Sections 3.2 and 3.3.

This staged development of subsidence troughs differs from the published literature from other mining areas, where the initiation of a flat mid-section within the subsidence trough is coincident with the development of Smax (when the W/H=1.4 - see Figure 2.14). This local subsidence characteristic results in flatter subsidence profiles for narrower panels. This would be expected, as the extremely weak Collie Basin strata will tend to subside more readily than strata in other mining regions.

3.1.3 Angle of Draw

The angle of draw represents the angle measured (from the vertical) from the panel edge to a point on the surface where there is no measurable subsidence (Figure 2.14).

As mentioned in Section 2.5.1, the effect of seam dip and surface topography is expected to be minimal and has consequently been ignored. However, it has been established in Section 2.5.5.1 that bearing failure (pillar punching) or elastic deformation of the foundation materials beneath smaller pillars can influence the amount of subsidence developed. Therefore, in some locations where smaller pillars are sited immediately adjacent to the extraction panel, pillar punching can give rise to an extended angle of draw. Consequently, where pillar punching was interpreted to be impacting on the subsidence profile, the calculated angles of draw from these sites were not used in the case study database. An example of the effect of pillar punching is illustrated by the subsidence profile between Blue and ACIRL Panels (Figure 3.7), where approximately 200 mm subsidence had developed 57 m outside the edge of the Blue panel. At an equivalent distance from the edge of the ACIRL panel, which had larger pillars within the set-up roads, only 60 mm subsidence had developed.

The background surface movement, inclusive of survey error, is taken to be ±30 mm (Section 2.5.5.2). Movements less than this were not included in the determination of angles of draw, unless seasonal effects can be accounted for accurately. Where seasonal effects are known, the limiting subsidence used for estimation of angle of draw is ±15 mm, which equates to survey error. Other omissions from the angle of draw data base were made in areas where discontinuous subsidence had developed at the panel edges (eg 2BWE2 and 2BWC panels in the WD-2 colliery).

The range of angles of draw varied from 12° to 39°. Panels shallower than 60 m averaged 18°, while the mean angle of draw in the deeper panels was 25°(discounting 6 B East panel which was based inapropriately on the measurements of concrete supports beneath the water pipeline). These average values of angle of draw fall well within the statutory limitations for draw angle (35°). The Collie Basin angle of draw compares well with values quoted for NSW coalfields in eastern Australia - 26.5° by Holla, 1987. The assumed draw angle for the Northern Appalachians in USA is 25°, and 35° for the British coalfields.

SURFACE SUBSIDENCE BETWEEN ACIRL & BLUE PANELS - WD6

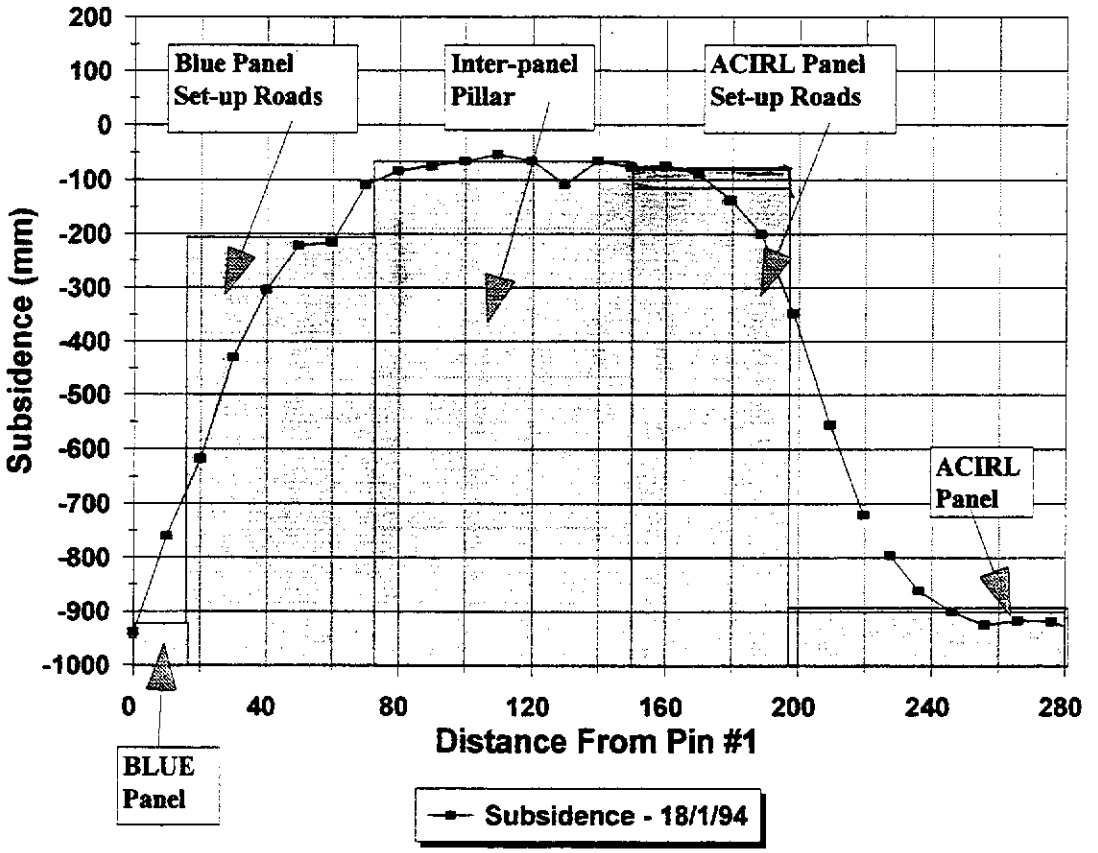

Figure 3.7

Misich (1991) recommended that the angle of draw to be used for mine design purposes in Collie should be a conservative 30°. More data has become available since that time, and it is now recommended that 25° be used for design purposes, provided the effect of seam dip, topography, and the potential for pillar punching are taken into account. It is recommended that, when the possibility for pillar punching exists, the angle of draw should be measured from the outer edge of the respective line of smaller pillars.

3.1.4 Inflection Point

The location of the inflection point can be used in empirical models to position subsidence profiles above extraction panels. The location of the inflection point was determined by identifying the point of zero strain, which also coincides with maximum tilt. In narrower panels, this point can be difficult to identify as the resultant surface strains are very small and the variation in strain due to monitoring accuracy can result in a set of data which meanders randomly about the zero strain axis. The accuracy of interpreted points of inflection can also be influenced by the subsequent lifting off of fender coal before the subsidence profile has settled. As a result, only the data from panel completion has been used for these analyses.

As for angle of draw data, inflection points above panel edges that were obviously affected by panel edge irregularities or pillar punching have not been included in the database.

A summary of the resultant set of field data is provided in Figure 3.8 a. From this data, it appears that the point of inflection can shift to a position outside the panel edge above narrower panels. This relationship is similar to that noted in coalfields in eastern Australia, and particularly in southern NSW (see Figure 3.8 b, from Holla, 1987). A bounding curve has been provided to estimate the position of the point of inflection according to the W/H ratio of the panel. This curve is represented by the equation:

$$X = H\left(0.17 - e^{-[2 \times (W/H + 0.5)^{1.8}]}\right) \qquad 3.1(2)$$

There is insufficient data to provide a well supported premise for the mechanism which allows the position of the influence function to shift outside the panel with smaller W/H ratios. More investigation is required to explain or disprove this observation.

PREDICTION OF INFLECTION POINT LOCATION IN THE COLLIE BASIN

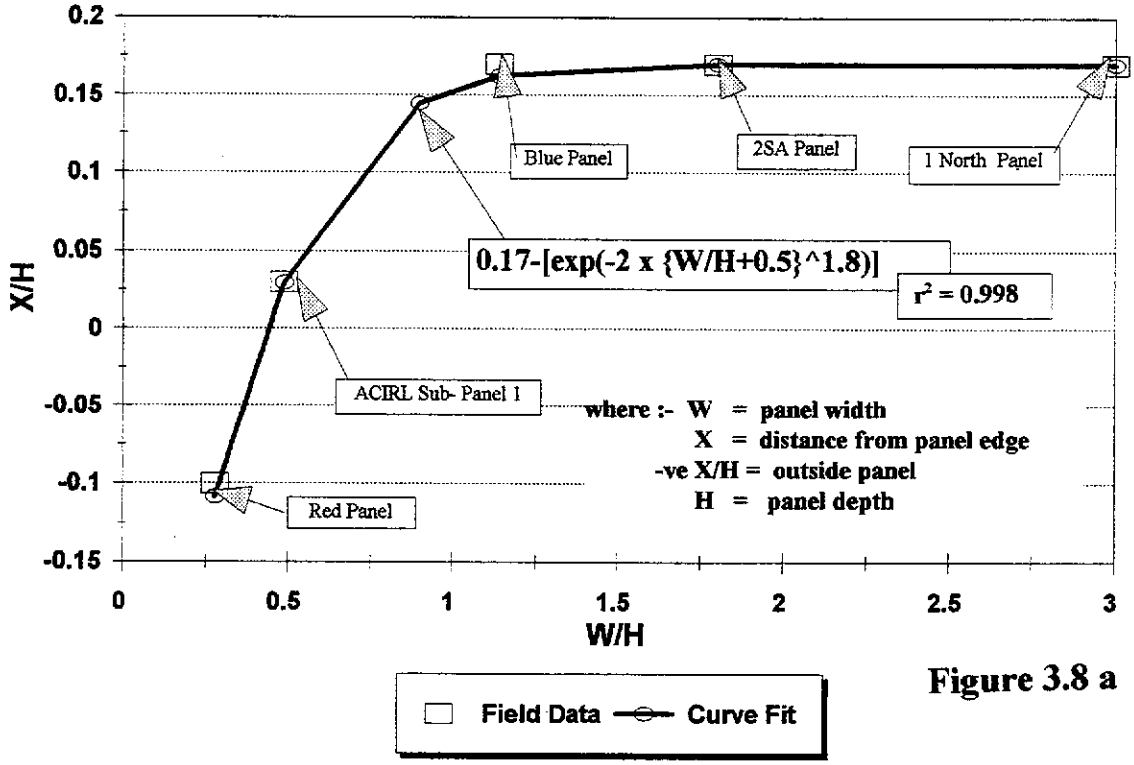

Figure 3.8 a

PREDICTION OF INFLECTION POINT LOCATION IN EASTERN AUSTRALIA

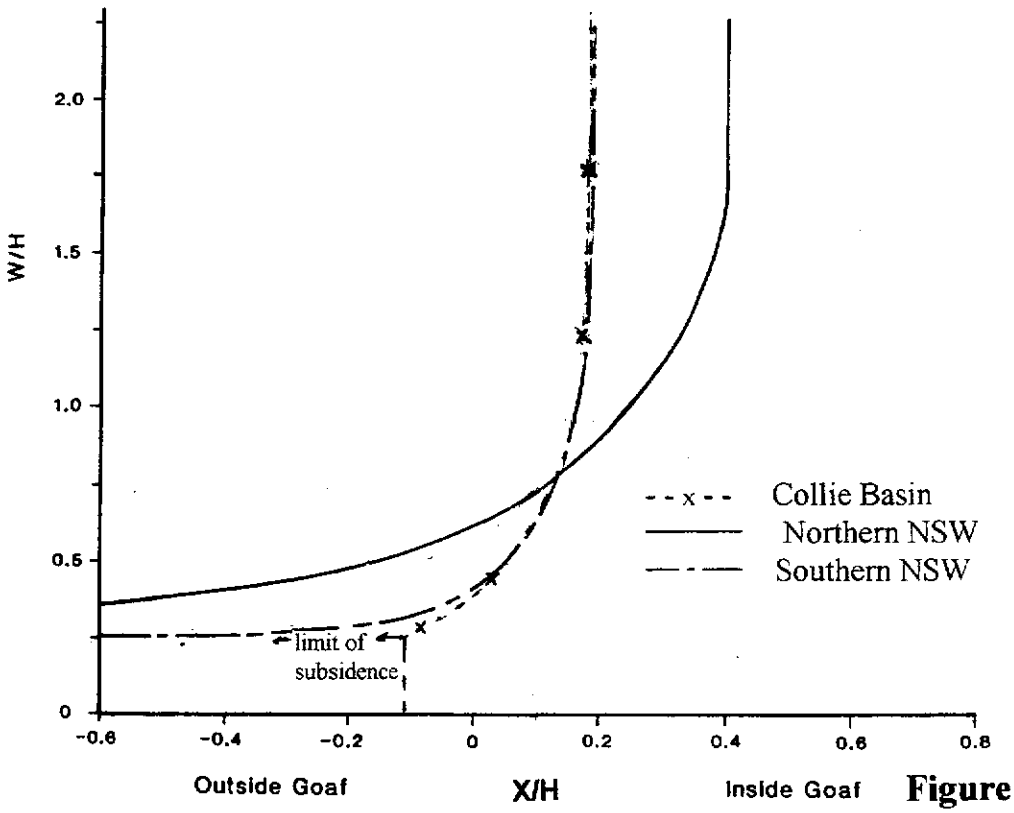

Figure 3.8 b

3.1.5 Subsidence Profiles

Before any subsidence effects on surface features can be foretold, the complete subsidence profile must be known or estimated prior to mining. As mentioned in Sections 2.6 and 2.7, the empirical profile function method was selected to be most suited for the requirements of this research project.

The approach used toward finding a suitable profile function for the Collie Basin sediments was to firstly evaluate the applicability of existing profile functions against the local field data. Then, if found that none of the existing functions were adequate, to a new site specific profile function would be developed for local conditions.

Existing profile functions chosen for back-analysis were those which incorporated the major factors influencing the shape of subsidence profiles. These factors are:-

- depth of cover
- panel width
- effective mining height, and
- proximity to a specified point (usually the panel centre or the inflection point).

A number of profile functions (selected from Whittaker and Reddish 1989) were plotted against field data to assess their applicability to the Collie Basin. Where existing profile functions did not explicitly relate to these parameters, (e.g. the NCB curve) the subsidence profiles were calculated for a standard width and depth.

The result was that none of the existing profile functions accurately represented Collie Basin profiles for the entire length of the subsidence trough. It was therefore evident that the Collie Basin sediments required a separate, site specific profile function.

The first step toward defining a site specific curve was to establish which form of profile function best suited the Collie data. Whittaker and Reddish (1989) subdivided profile functions into two groups. The first group includes functions which use the panel centre as the origin, the second uses the inflection point as the origin. It was decided that the inflection point-based functions were more appropriate due to the fact that the point of inflection was a "hinge point", between compressive and tensile strains. Furthermore, it had been established that the position of the point of inflection could be reasonably well predicted for a range of panel widths and depths.

The next step was to plot the field data in the form of a dimensionless nomogram to facilitate the prediction of subsidence for all mining width / depth scenarios. The form of the nomogram is illustrated in Figure 3.9 which includes the field data from all stages of mining in the ACIRL, BLUE and 2SA Panels. (These panels represented the most reliable data to that point in time.) It can be seen from Figure 3.9 that the field data are closely grouped, regardless of the width of extraction or mining depth. This gave greater confidence in the application of a profile function to the prediction of surface subsidence.

After trialing several forms of profile functions, the expression used for prediction of subsidence in the Collie Basin in the early stages of the research project was a tenth order polynomial, as described in Misich et al. (1991) and given below:

$$\text{Subs} = 0.53-[2.345(D/H)]+[0.985(D/H)^2]+[13.762(D/H)^3]-[14.660(D/H)^4]- \ldots$$
$$\ldots [53.183(D/H)^5]+[75.332(D/H)^6]+[88.275(D/H)^7]-[152.51(D/H)^8]- \ldots$$
$$\ldots [27.623(D/H)^9]+[76.061(D/H)^{10}] \qquad 3.1(3)$$

A comparison of this earlier profile function and those from other mining areas is given in Figure 3.10. It should be noted that the profile function represents a best-fit through these data, rather than the bounding (or worst case) envelop. The decision to use a best-fit curve was made because it was considered that the use of the worst case Smax prediction curve (Figure 3.6) would already provide a large degree of conservatism in profile prediction. The use of two worst case parameters in the prediction process would result in unrealistic subsidence.

The disadvantages with this polynomial profile function were that it is relatively cumbersome to deal with and although the resultant curve appears to represent a smooth trough, it can have small scale deviations. Consequently further research work was undertaken to find a "smoother" profile function which fits the field data equally well.

A hyperbolic tangent function was trialed, as used by Karmis et al. (1985) for the Appalachian coalfields in the USA and Kapusniak (personal communication, 1992) in Central Queensland. The best curve fit using this form of equation was:

$$S_{(D)} = \tfrac{1}{2}[1-\tanh(2.5D/B)] \cdot S_{max} \qquad 3.1(4)$$

COLLIE BASIN POLYNOMIAL PROFILE FUNCTION

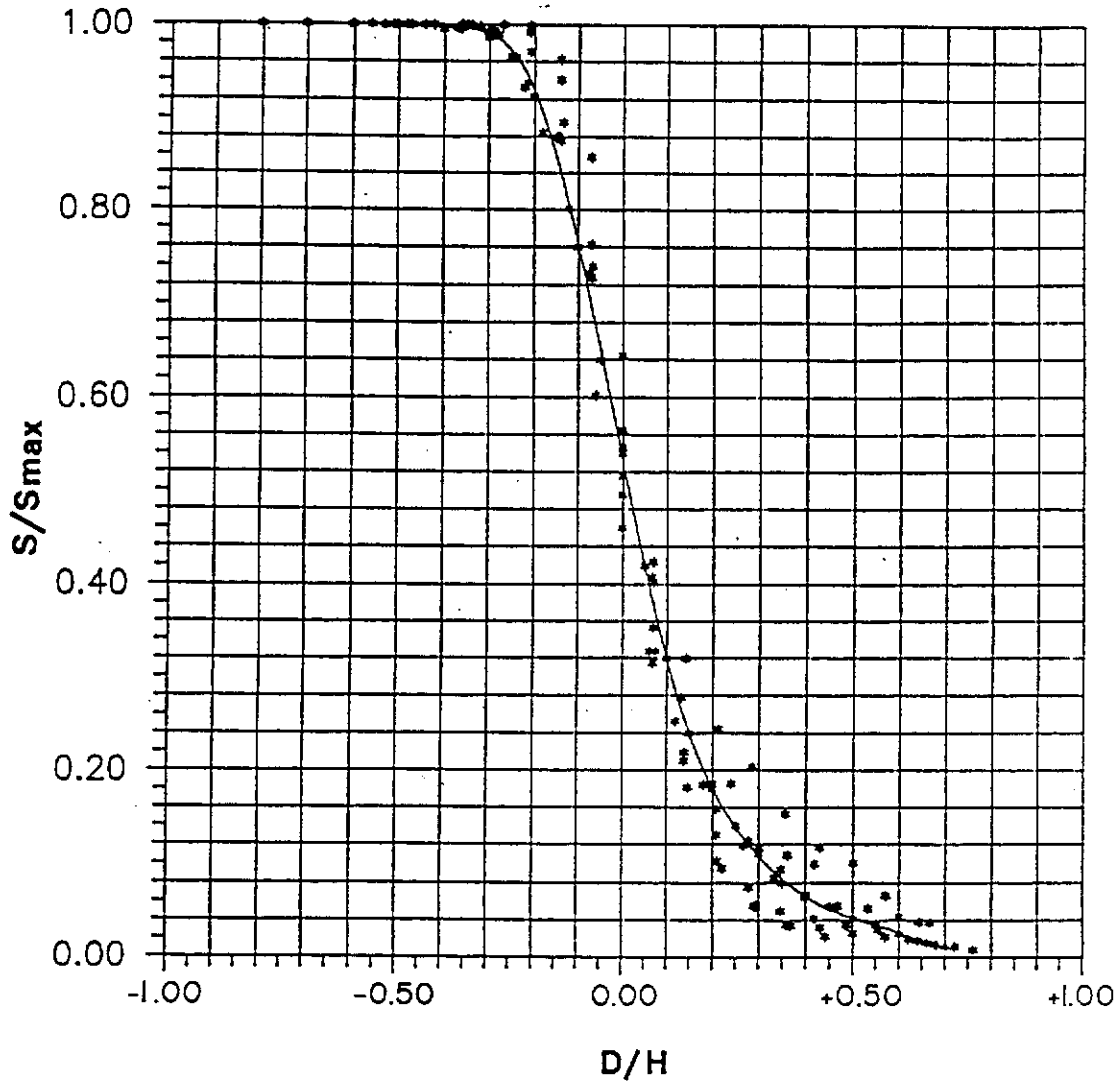

Equation for Line of Best Fit:-

$S/Smax = 0.53 - 2.3453\,(D/H) + 0.9848\,(D/H)^2 + 13.7622\,(D/H)^3 - 14.6598\,(D/H)^4 - 53.1826\,(D/H)^5 + 75.3316\,(D/H)^6 + 88.2752\,(D/H)^7 - 152.510\,(D/H)^8 - 27.6233\,(D/H)^9 + 76.0614\,(D/H)^{10}$

Equation Limits:- $-0.5 < (D/H) < 0.75$

Where:- D is the distance from the inflection point
H is the depth of cover
Smax is the predicted or measured maximum subsidence
S is the subsidence at any point on the surface

Figure 3.9

PROFILE FUNCTION COMPARISONS FOR SELECTED COAL MINING REGIONS

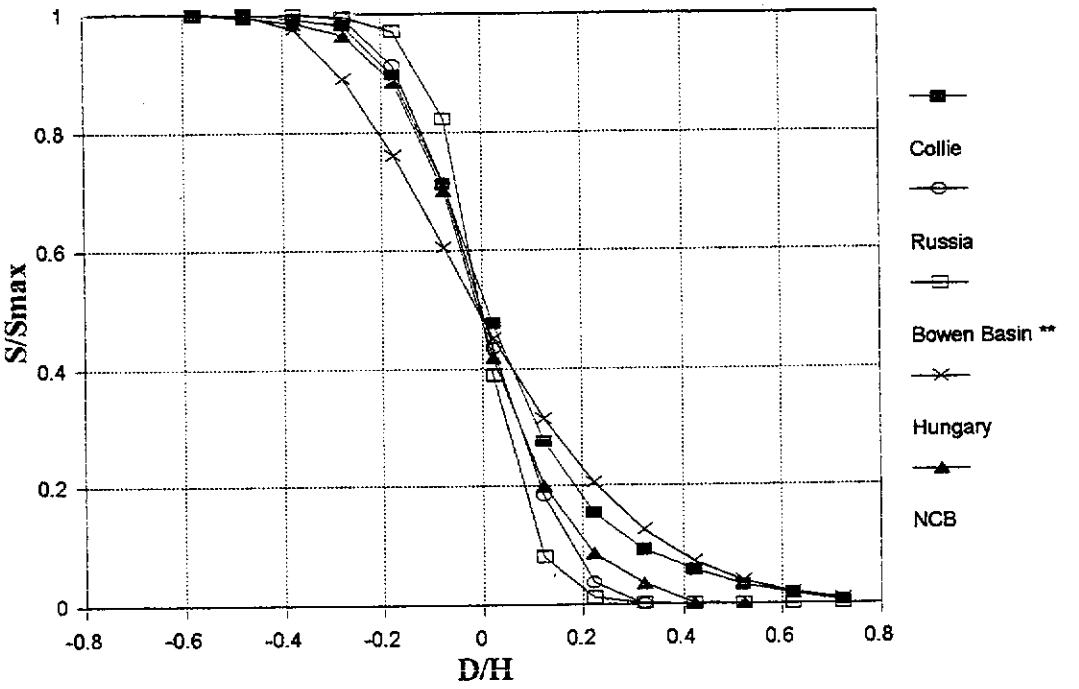

Equations:

Collie :- 0.53-[2.345(D/H)]+[0.985(D/H)^2]+[13.762(D/H)^3]-[14.660(D/H)^4]-[53.183(D/H)^5]+ . . . . .[75.332(D/H)^6]+[88.275(D/H)^7]-[152.51(D/H)^8]-[27.623(D/H)^9]+[76.061(D/H)^10]

Russia :- 0.5[1 - X/R - 1/3.14{sin(3.14X/R)}]

Bowen Basin** :- 0.5[1-Tanh(3.47X/R)] (From Kapusniak)

Hungary :- exp[-X^2/2D^2]

NCB :- Graphical

Where:- R = Radius of critical area of extraction
X = Distance from extraction centre
D = Distance from inflection point
H = Depth of cover

Figure 3.10

where, S_{max} = maximum subsidence derived from equation 3.1(1) given previously

$S_{(D)}$ = subsidence at any point D (m)

D = distance from inflection point, IP (m)

B = distance between point of maximum subsidence and the inflection point (m) (sometimes referred to as the critical subsidence radius) and can be expressed as a fraction of H,

B = ½[(W-2IP)H], and 3.1(5)

This function was published in Misich et al. (1992), however, after closer scrutiny, it was evident that this form of function did not fit the tensile region of the trough closely.

The profile function which provided the best-fit to the Collie Basin data was a form of double exponential. The double exponential provides for control of the location of the inflection point, the steep gradient of the curve near inflection, the magnitude of subsidence at inflection, and allows for asymmetrical subsidence profiles on either side of the point of inflection. From the literature reviewed, this form of profile function has not previously been used for subsidence prediction.

The profile function equation recommended for predicting subsidence in the Collie Basin is plotted in Figure 3.11 and given below:

$$\frac{Smax - s}{Smax} = 1 \times exp^{-9 \times exp^{-7 \times (D/H + 0.35)}} \quad 3.1(6)$$

$$i.e. \quad -s = Smax.\left[exp^{-9 \times exp^{-7 \times (D/H + 0.35)}}\right] - Smax$$

$$simplified: \quad -s = Smax.[F_1D] - Smax \quad 3.1(7)$$

where, S = subsidence at any point (m),

S_{max} = maximum subsidence (m), derived from Equation 3.1(1),

D = distance from inflection point, IP (m). -ve D represents points towards the middle of the panel, and

F_1D = a function of the variable D

$$= e^{-9 \times e^{-[7 \times (D/H + 0.35)]}}$$

SURFACE SUBSIDENCE PROFILE PREDICTION FOR THE COLLIE BASIN

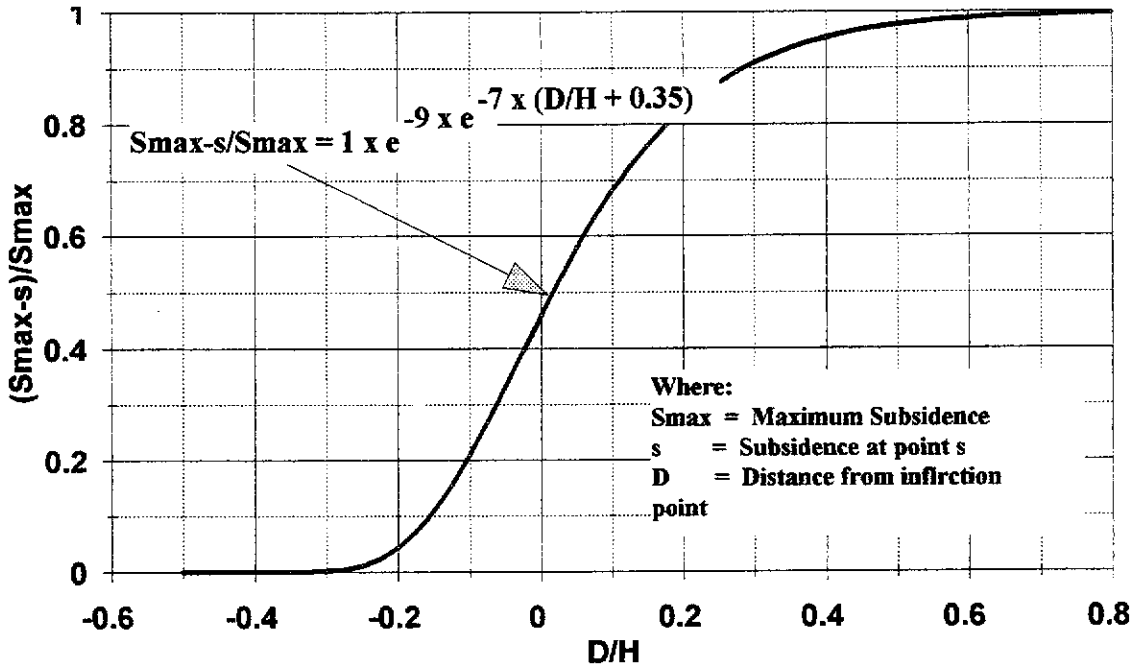

Figure 3.11 a

ILLUSTRATION OF DOUBLE EXPONENTIAL CURVE-FIT THROUGH FIELD DATA

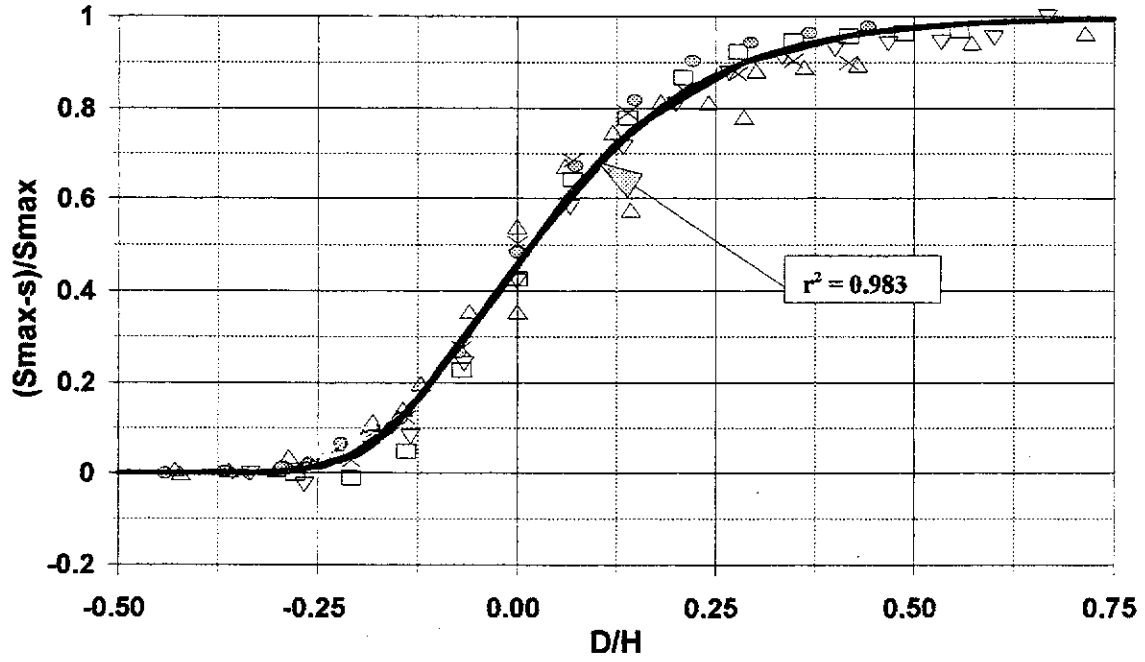

Figure 3.11 b

It can be seen that the value of dimensionless subsidence increases from absolute zero at D/H ≤ -0.35 (inside the panel) to 1 as D/H ≥ 1 (outside the panel edge). The Y-axis represents the difference between the surface subsidence and Smax at a given point, divided by the Smax; a value of zero represents full subsidence at a given point, conversely a value of 1.0 represents the position where there is no surface subsidence. The awkward structure of the terms used on the Y-axis has been derived so that the form of subsidence development is similar to the Smax prediction curve (Figure 3.6).

It can also be seen that the "tightness of fit" of the curve to the field data (see Figure 3.11 b) is good, as suggested by the statistical measure of curve fitting, the "sample coefficient of determination" (r^2), which equates to 0.98. Curve fitting was accomplished using the spreadsheet package Quattro Pro® (version 6 - from Novell Inc.), which optimises the coefficients in the profile function to the highest value of r^2 attainable.

As an example of the "representability" of this curve to predicting field subsidence, a comparative plot has been provided in Figure 3.12 between the calculated subsidence and the field results from 1North panel (which was mined after the development of this profile function). It can be seen that there is a reasonably good correlation between the two, although some variation is evident between the trailing and advancing edges of the panel. (This variation in subsidence between the trailing and leading edges is due to the different caving mechanisms at the opposing panel edges - see Section 3.3.)

An interesting feature of this curve is the manner in which it produces an angle of draw between 9 and 25° for increasing panel W/H ratios. (The position of limiting subsidence is defined as the point where there is less than 15 mm movement predicted. This approach is comparable to the method used to define subsidence limits in the field - assuming that the seasonal effects are known.) The ability of the profile function to maintain a realistic angle of draw is assisted by the shifting position of the inflection point for sub-critical panels - as illustrated in Figure 3.8.

The double exponential function is easily adaptable for use in computer spreadsheet packages and can be readily applied to subsidence functions from other mining regions. As an example, the Collie Basin profile function has been used to define subsidence profiles for Hungary, UK, Russian, Bowen Basin (as given in Figure 3.10), and Appalachian coalfields (as given in Karmis et al., 1985).

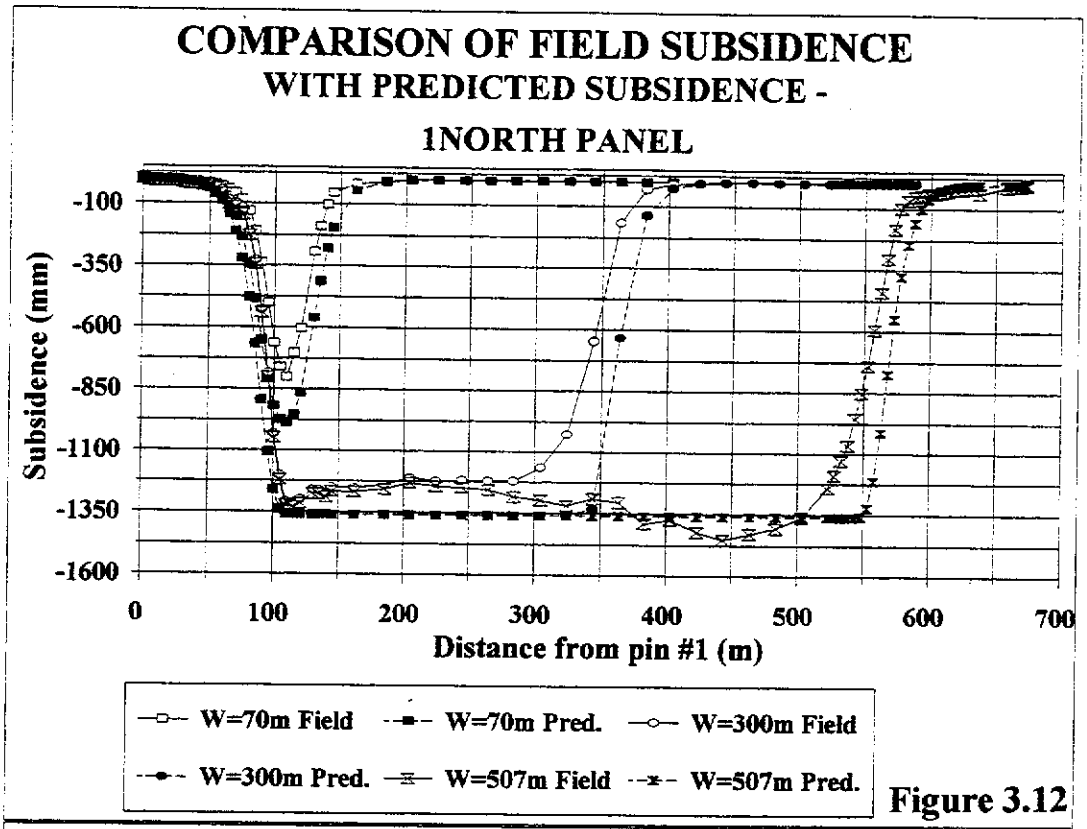

Figure 3.12

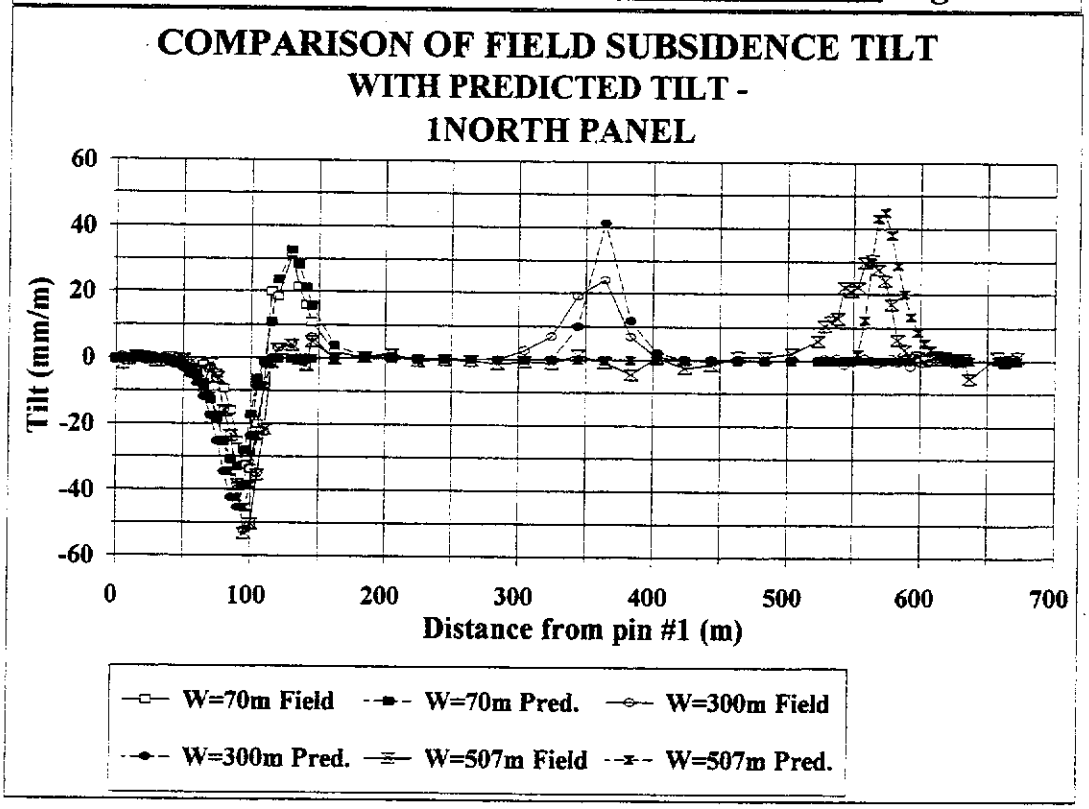

Figure 3.13

The comparability between curves can be described by the three exponents in the double exponential curve; the exponents of the first and second exponentials (α, and β), and the regulating exponent which is added to the independent variable D/H (λ) and multiplied to the second exponent - β. The comparative exponents are provided in Table 3.3. In order to compare subsidence plots, the form of Equation 3.1(6) has been adapted to suit the form of the existing functions; the comparative equation is:

$$1 - e^{-9 \times e^{[7 \times (D/H + 0.35)]}} \qquad 3.1(8)$$

TABLE 3.3 **COMPARISON OF DOUBLE EXPONENTIAL EXPONENTS**

Country/Mine region	Exponent α	Exponent β	Exponent λ	Curve fit r^2
Australia/Bowen Basin	6.0	13.8	0.16	0.99
Hungary	10.0	4.7	0.57	0.99
USA/Appalachian	9.0	8.0	0.33	0.99
UK	10.0	8.5	0.32	0.99
Australia/Collie	9.0	7.0	0.35	0.98

The shape of the subsidence trough is essentially controlled by the exponents α and β. The exponent α influences the width of the trough and the vertical positioning of the inflection point. The exponent α has more influence on the steepness of the subsidence trough and magnitude of subsidence at the point of inflection. It should be noted that although a perfect match was not determined for any of these comparative profiles (the Collie Basin profile tends to predict a slightly sharper subsidence trough in the concave section of the profile), these comparative coefficients do generally provide close representation for much of the subsidence profiles from each case area - as suggested by the high values of r^2. Nonetheless, this analysis helps quantify the variation observed between mining regions (as illustrated in Figure 3.10), for example the β coefficient of 4.6 in the Hungarian subsidence troughs results in a much flatter profile than other areas listed (even though the α exponent is not greatly dissimilar), and the steeper and narrower Bowen Basin subsidence troughs are defined by the low α and high β exponents).

It is interesting to note that even though the geological setting of the Collie Basin is quite different to the Appalachian coalfields, the form of the subsidence troughs is quite

similar.

It follows that, once the full subsidence profile is known the variation in ground tilt and curvature can also be determined by differentiation and double differentiation (respectively) of the subsidence profile - as discussed by Karmis et al. (1985) and given below.

3.1.6 Surface Tilt

The maximum tilt measured in the field study was 57.2 mm/m over 2 South A Panel in WD-6. Plots of the ground tilt at various stages of extraction in all panels are provided in Appendix I.

As mentioned previously, the ground tilt is directly proportional to the shape and depth of the subsidence trough. Therefore values of ground tilt can be calculated by differentiating the profile function [Equation 3.1(7)] given by:

$$\frac{dy}{dx} = \frac{63}{H}.exp^{-\left(7.\left[\frac{D}{H}+0.35\right]\right)}.exp^{-\left(9.exp^{-\left(7.\left[\frac{D}{H}+0.35\right]\right)}\right)}.Smax \qquad 3.1(9)$$

$$= \frac{63}{H}.exp^{\left(-7.\left[\frac{D}{H}+0.35\right]\right)}.\left[F_1D\right].Smax \qquad 3.1(10)$$

According to literature (eg Kratzch, 1983) maximum tilt is expressed at the point of inflection (or zero strain) - when D/H = 0. This is logical, as any strain in the trough would indicate a change in slope on the ground. In terms of the profile function, the point of inflection occurs when $d^2y/dx^2 = 0$. This equates to the point when the independent variable {D/H + 0.35} is equivalent to the natural logarithm of the first exponent (9) divided by the second exponent (7). Because the independent variable has an additive term of 0.35, the actual value of D/H at the point of inflection in the Collie Basin profile function is:

$$D/H = [\ln(9)/7] - 0.35 = -0.036$$

This small deviation from the theoretical position of D/H = 0 is a function of the curve fit error through the composite field data. This means that a panel 200 m deep will have its maximum tilt approximately 7 m further towards the middle of the panel from the true point of inflection.

As an example of the "representability" of this curve, a comparative plot between the calculated tilt and the field results from 1 North panel has been provided in Figure 3.13 (1 North panel was mined after the development of this profile function). It can be seen that, again, there is a reasonably good correlation between the two.

3.1.7 Ground Curvature

Curvature of the ground surface within a subsidence trough can be either convex or concave and is calculated by double differentiation of the profile function, Equation 3.1(7). The resultant curvature equation is:

$$\frac{d^2y}{dx^2} = \frac{441}{H^2}.\exp^{-\left(7.\left[\frac{D}{H}+0.35\right]\right)} . \exp^{-\left(9\,.\,\exp^{-\left(7.\left[\frac{D}{H}+0.35\right]\right)}\right)} . Smax + \qquad 3.1(11)$$

$$\frac{3969}{H^2} . \exp^{-\left(7.\left[\frac{D}{H}+0.35\right]\right)^2} . \exp^{-\left(9\,.\,\exp^{-\left(7.\left[\frac{D}{H}+0.35\right]\right)}\right)} .Smax$$

$$= \frac{dy}{dx} . \frac{7}{H} + \frac{3969}{H^2}.exp^{-\left(7.\left[\frac{D}{H}+0.35\right]\right)^2} .\left[F_1 D\right] Smax \qquad 3.1(12)$$

3.1.8 Surface Horizontal Strains

The approach used to predict horizontal strains was that used by the NCB (1975) and Karmis et al (1985), where the surface strains at given points along the subsidence trough will be directly related to the degree of flexure, or curvature of the surface. That is, the tighter the curve, the greater the degree of extension or compression, and therefore the greater the strain. (Concave curvature generating compressive strain, and convex curvature generating tensile strain.)

The relationship between curvature and strain is curiously site specific. It could be expected that a given curvature would give rise to an equivalent strain regardless of the location of the mine. It would appear that the strain generated along a subsidence trough is dependent on the local geological/geotechnical characteristics of the ground mass. Karmis et al. demonstrated large differences in the curvature - strain relationships between the United Kingdom and the USA. The reasoning for the variation between sites has not been investigated in this research project.

The procedure adopted to determine the Collie curvature-strain relationship is summarised below.

1) Firstly selected subsidence profiles were individually plotted against distance from a given reference point and a mathematical curve fitted through the data points. Curvatures throughout the trough were then calculated by double differentiation of the curve fit equation. The fitted curves were again derived using the optimising algorithm within the PC-based software package Quattro Pro® (version 6 - from Novell Inc.). The form of the curves used in each case was a double exponential equation. Example curves fitted to field subsidence data are provided in Figure 3.14, which present the profiles of subsidence grid lines D and A above the eastern edge of Blue panel, and line B above the northern edge of 2SA panel. (Again r^2 was greater than 0.99 in each fit.)

2) Maximum calculated curvatures for each profile were then plotted against measured maximum strains. The data set used for this calibration are presented in Table 3.3. This data has again been taken only from the earlier total extraction panels.

   It was decided to use only the maximum strains and curvatures because measurement error (of both strain and surface subsidence) had a more significant effect on the results when approaching the limits of subsidence and tended to cloud the relationship.

TABLE 3.3 **SURFACE CURVATURE Vs STRAIN CORRELATION DATA**

PANEL >>	ACIRL	ACIRL	ACIRL	BLUE	BLUE	BLUE	2SA
SURVEY LINE >>	E	E	F	A	B	D	A
Max. Calculated Tensile Curv. (m^{-1}) x 10^4	2.2	1.8	2.5	6.5	3.9	6.5	39
Max. Calc. Compressive Curv. (m^{-1}) x 10^4	3.1	3.8	4.8	12.4	8.3	12.5	73
Max. Measured Tensile Strain (mm/m)	5.5	3.8	4.4	3.2	7.5	16.5	32
Max. Measured Comp. Strain (mm/m)	5.3	8.0	5.6	7.4	12.1	14.4	23

ILLUSTRATION OF SURFACE SUBSIDENCE CURVE-FITTING FOR SELECTED PROFILES

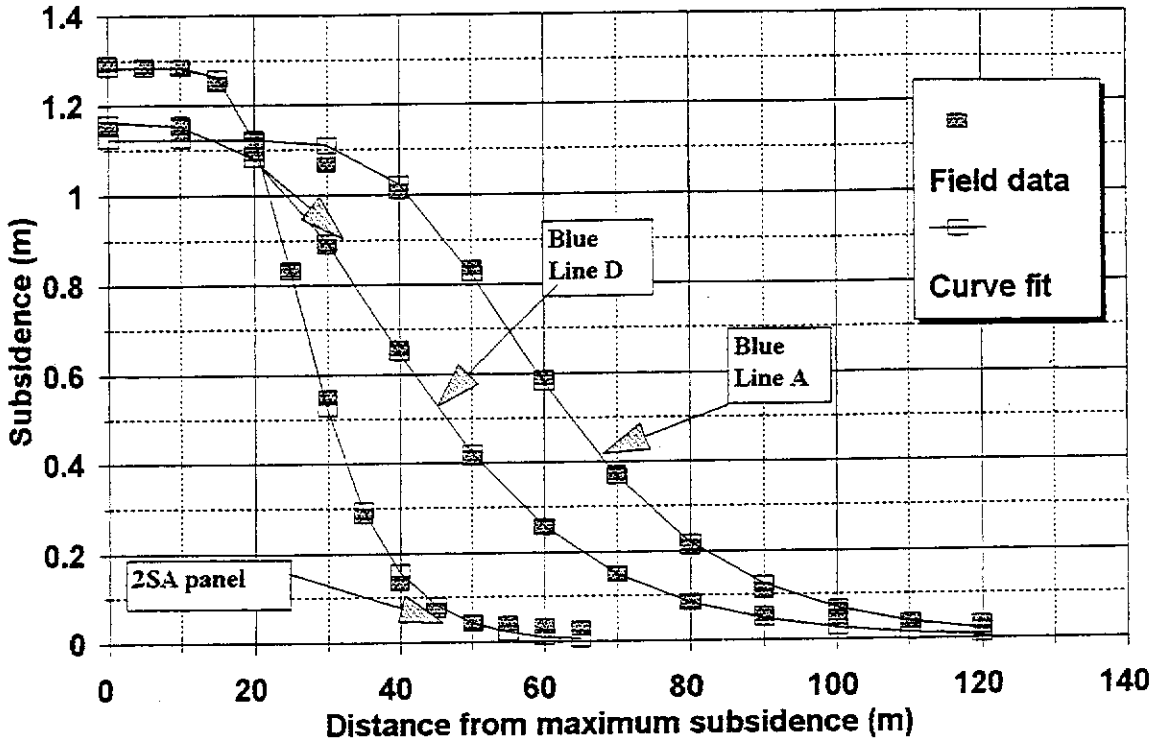

Figure 3.14

3) Using this plot, a mathematical relationship describing the bounding strain envelope for any given value of curvature was established.

The resultant plot of strain versus curvature is provided in Figure 3.15. It can be seen that there is a reasonable amount of scatter in these results, possibly because:

- the exact position of maximum strain rarely coincides with the exact location of surface survey points (which were used to establish the empirical relationship),
- of curve fitting error, and
- local variation in vegetation and surficial geology can effect individual measurements, for example tree roots or laterite capping can cause very localised large-scale movements.

Because of the scatter of data, it was necessary to fit a bounding curve to the Collie data. The resultant curve fitting equation for prediction of horizontal strain is:

$$\textbf{Strain (mm/m)} = 3.5\ (\text{curvature} \times 10^4)^{0.6} \qquad 3.1(13)$$

Figure 3.15 illustrates that the curvature-strain relationship for the Collie Basin is similar to that suggested for coal mining regions in the USA by Karmis et al. (1985).

As an example of the "representability" of this curve, a comparison between the calculated strain and field measurements from 1North panel has been provided in Figure 3.16. It can be seen that, there is again a reasonable correlation between the two. The apparent underestimation of compressive strains at the trailing edge, has been assumed to be due the presence of the surface "hump" that resulted at the intersection of two opposing lines of shear.

3.1.9 Time Dependency

It is a statement of the obvious that the development of subsidence with time is primarily dependent on the rate of advance of the mine face. With the Wongawilli extraction method, the rate of advance is stepped, with up to one month between each 13 or 20 m wide face advance. Furthermore, the timing between extraction cycles can vary greatly, depending on shift rosters and mining cycle problems etc.. Notwithstanding, the field results demonstrate that there is a component of time dependency for subsidence to firstly manifest itself on the surface, and secondly to reach equilibrium along the full subsidence trough once a given width has been mined.

CURVATURE / STRAIN RELATIONSHIP FOR THE COLLIE BASIN

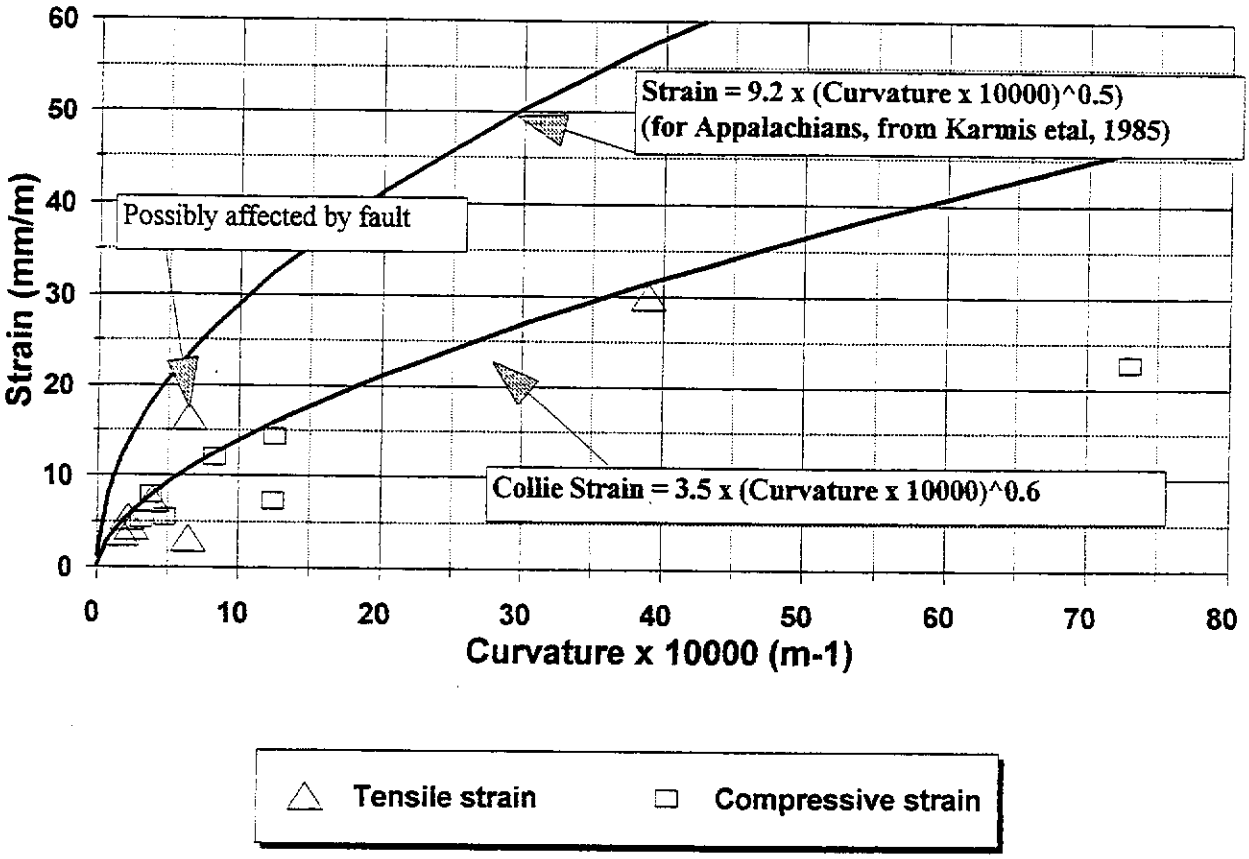

Figure 3.15

PREDICTED Vs MEASURED STRAIN
1 NORTH PANEL (507 m wide goaf)

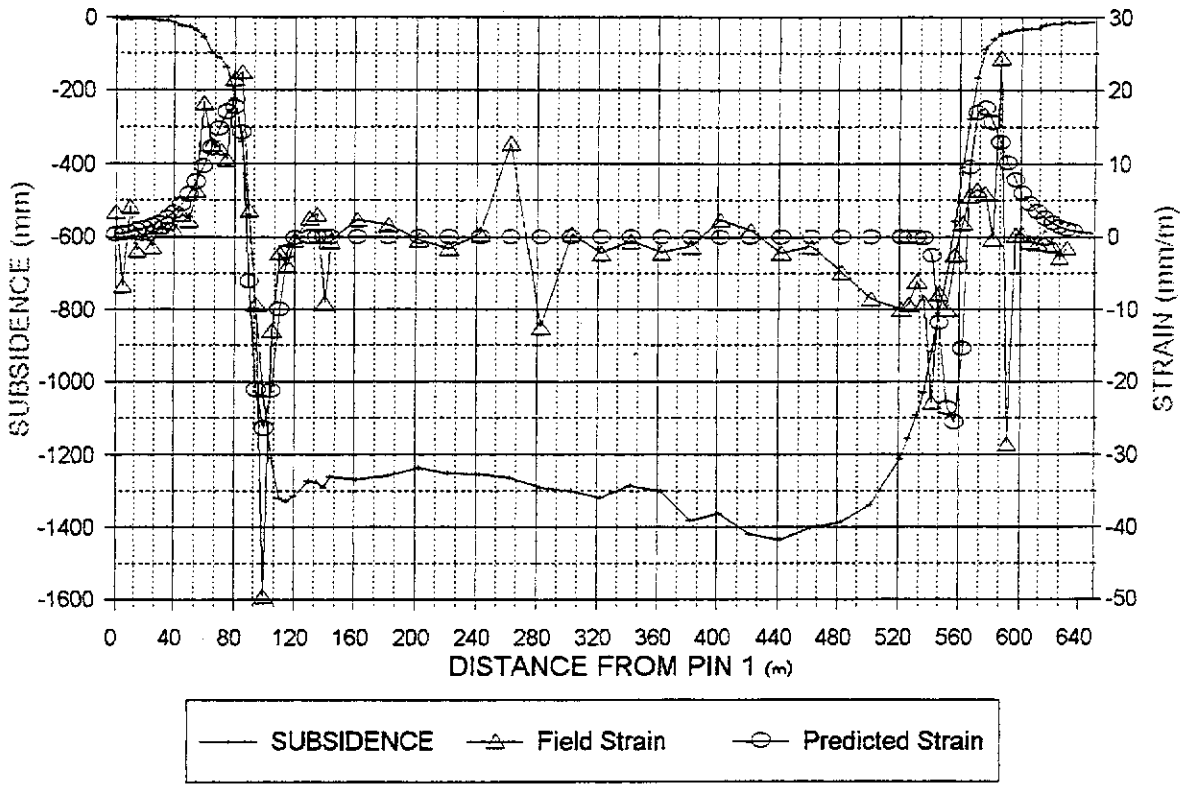

Figure 3.16

It is difficult to accurately define the time component for initiating subsidence with Wongawilli extraction as the rate of retreat mining along the fenders averaged around only 30 - 35 m per day over a five day week. This means that subsidence at a particular point above the panel can be within close proximity of the retreating face for long periods, making it difficult to establish the length of time taken to develop subsidence for a given width of extraction. (Subsidence effects will be observed as the fender lifting cycle approaches a given point above the panel - before coal is extracted beneath that point.)

An example of the time taken for subsidence to reach equilibrium - termed residual subsidence by Ferrari (1996) - is provided in Figure 3.17, where extraction of fenders 10 and 12, initially produces large increments in subsidence, followed by a slowing down of subsidence with time. It is noted that 80% of the subsidence due to the extraction of fender 10 (190 mm out of 240 mm) had developed within three days.

An additional 50 mm subsidence had occurred ten days later. It is estimated that only a further 30 mm would be expected to have developed if the panel had been left until subsidence reached equilibrium (before the extraction of the subsequent fender 11). If this is the case, then around 90% of the subsidence attributed to the extraction of fender 10 had occurred after two weeks.

These observations match those made above 2SA panel where surface expressions were noted on the (barricaded) bitumenised haulroad around two days after the mining face had passed below.

It is not feasible to estimate the length of time required to attain the additional 30 mm subsidence. However, it appears, from Figure 3.17, **that the amount of time dependent subsidence reduces as the panel widens**. This is best illustrated where the rate and magnitude of subsidence developed after the initial subsidence (attributed to fender 11) was much less than the rate for earlier fenders. Similarly, the equivalent point on the surface above the super-critical width 2SA panel had only an additional 20 mm (representing only an additional 1.5%) up to four years after mining ceased in the panel. In pillar splitting panels, the time taken to reach Smax can be up to a number of years, as measured in 6 B East panel in WD-6 colliery in 1983, and in the Proprietary colliery many years earlier (see Section 2.5.5.3).

SUBSIDENCE DEVELOPMENT WITH TIME (ABOVE BLUE PANEL) AT W669, W670 AND SURVEY PEG C33

GRAPH OF THE SUBSIDENCE OF THE DATUM PLATES FOR W669, W670 AND SURVEY PEG C33

(WD6 BLUE PANEL)

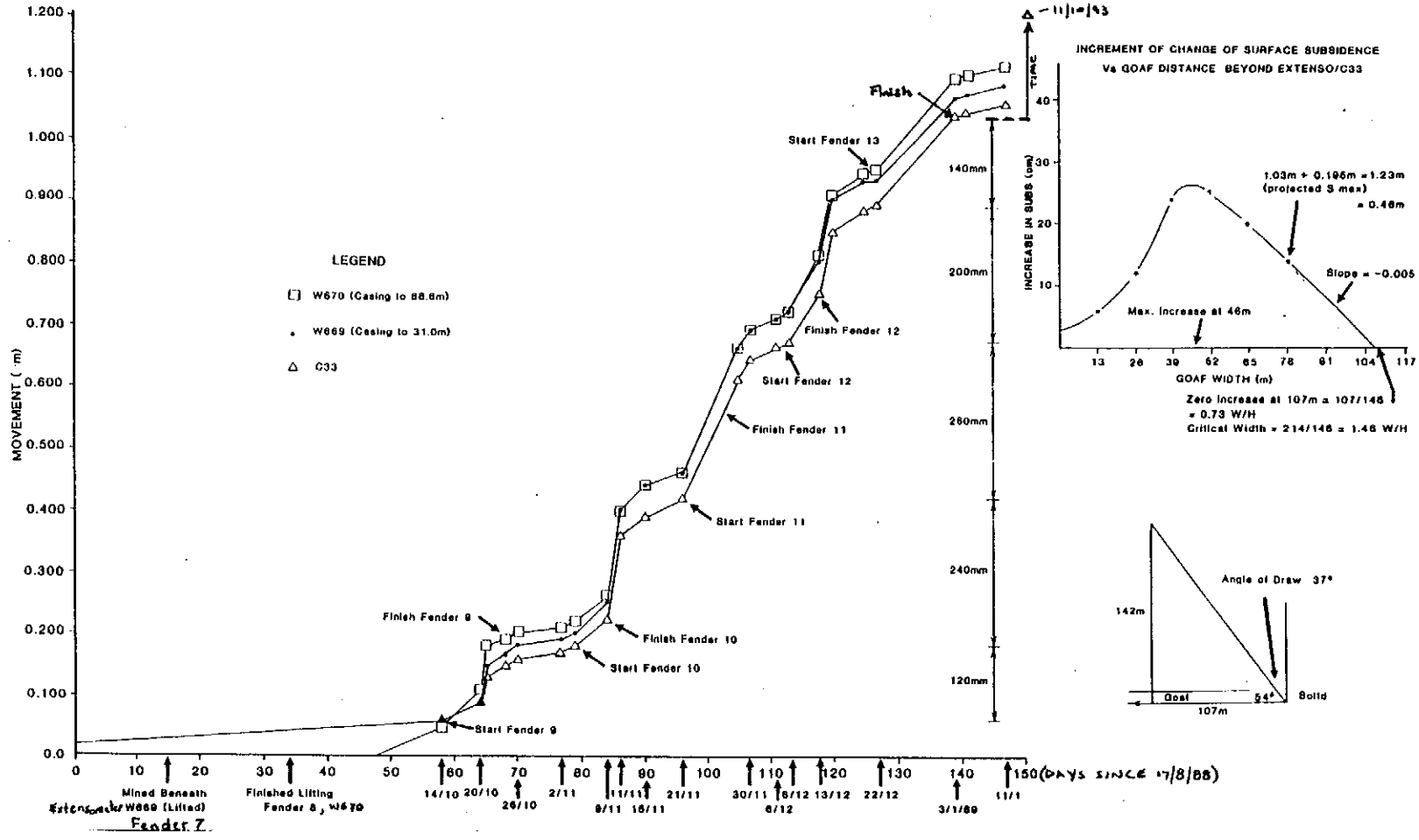

Figure 3.17

It is also evident that there is significantly more subsidence developed in the shallower 2SA panel when the advancing face initially passes beyond the point of measurement (the extensometer in this case). The maximum rate of subsidence development above 2SA panel occurred after the face was 22 m beyond the point of measurement (Figure 3.18).

By comparison, the maximum rate of subsidence above Blue panel occurred when the mining face had passed 46 m (3 ½ fenders) beyond the surface monitoring point (Figure 3.17).

Interestingly, the position of maximum rate of subsidence development above Blue panel equates to a face advance of 0.32 mining depth, compared to a W/H ratio of 0.39 for the 2SA panel. These W/H ratios are reasonably similar, considering the relatively wide increments in mining width for 2SA panel which would have greater impact on the W/H ratio at any particular time. It has therefore been interpreted that, apart from the mining rate, the rate of subsidence is affected by depth of cover **and** panel width. The first factor is expected, the second factor is probably driven by the elastic time-response of the upper spanning strata during the early stages of subsidence development (when W/H ratios are small). As the width of extraction increases, the spanning strata yield and full subsidence is manifested.

There has been no attempt to isolate the effects of these three variables (rate of advance, mining width and mining depth) to obtain a more definitive explanation of time dependent subsidence in the Collie Basin. This is because there is only 10% maximum variance of subsidence developed two weeks after fender extraction in all mining scenarios, which is of little value to the research project. Nevertheless, it is evident that time-dependant subsidence has a relatively short time span in the Collie Basin; probably due to the weak nature of the superincumbent strata which tends to subside more readily.

SUBSIDENCE DEVELOPMENT (ABOVE 2SA PANEL) AT SURVEY PIN B20

Surface subsidence for pin B 20 2SA PANEL

	Date >>	10-Aug-88	08-Mar-89	17-Mar-89	29-Mar-89	20-Apr-89	12-May-89	01-Jun-89	28-Jun-89	14-Jul-89	01-Aug-89	31-Aug-89	22-Sep-89	12-Oct-89
	Days >>	-210	0	9	21	43	65	85	112	128	146	176	198	
PIN 20	RL >>	197.770	197.770	197.770	197.76	197.750	197.727	197.580	197.240	196.810	196.635	196.530	196.480	196.46
subsidence	>>	0	0	0	10	20	43	190	530	960	1135	1240	1290	1310
panel width	>>	0.00	18.00	32.00	32.00	43.00	54.00	65.00	78.00	90.00	102.00	114.00	136.00	136.0
GED	>>	-68.00	-50.00	-36.00	-36.00	-25.00	-14.00	-3.00	10.00	22.00	34.00	46.00	68.00	68.0
incremental subsidence (mm)	>>	0	0	0	10	10	23	147	340	430	175	105	50	20

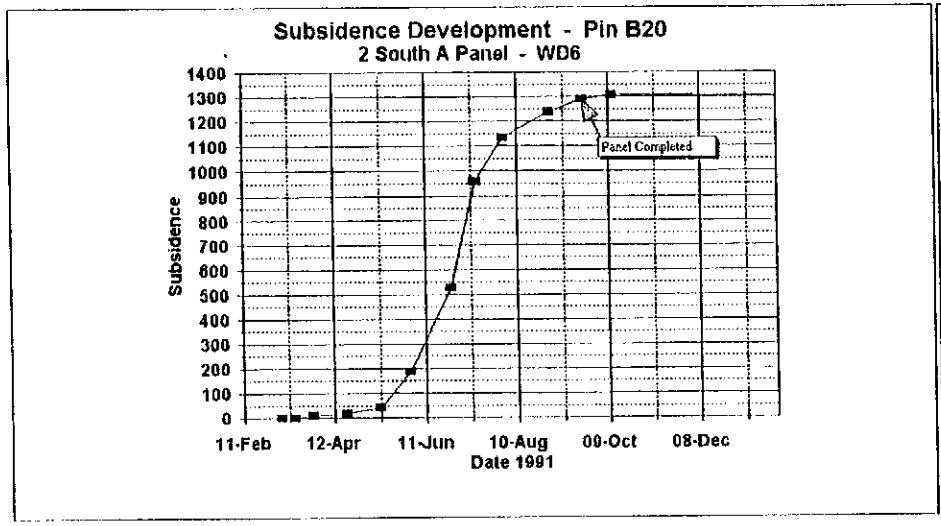

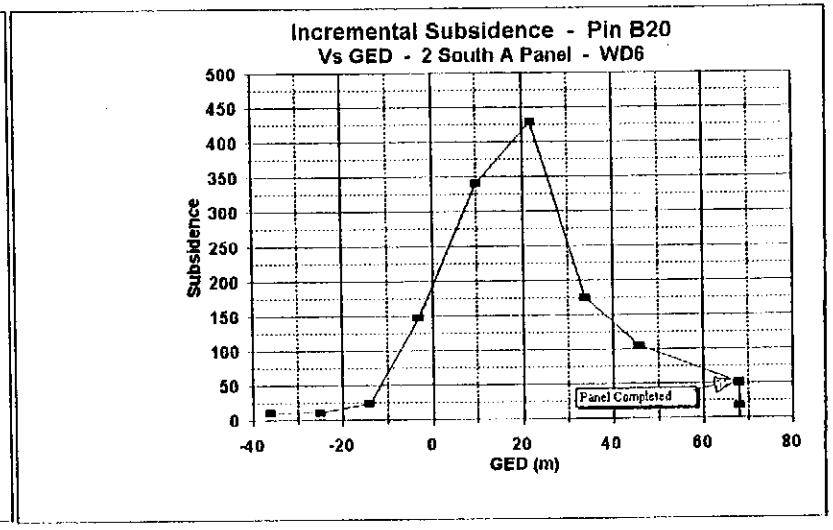

Figure 3.18

3.2 CONTINUOUS SUBSIDENCE (SUBSURFACE)

The purpose of this phase of investigation was to obtain a better understanding of the mechanisms leading to surface subsidence. It was considered that if the subsurface subsidence mechanisms can be rationalised from the seam to the surface, then surface subsidence predictive models could be used with more confidence. Additionally, it is not feasible that design criteria for the protection of the integrity of aquitards could be established unless the mechanisms leading to aquitard rupture are known.

There are numerous methods available - from each of the major coal regions of the world - for predicting **surface** subsidence. Subsurface subsidence models, on the other hand, are comparatively few and, particularly in terms of aquifer/aquitard assessment and design criteria, vary significantly (Bhattacharyya & Gurtunca, 1984).

Prior to site investigation, it was assumed that the expected process of ground movement would include an initial (primary) caving zone above the mine roof, after which the ground sags toward the caved/goaf area according to the elastic properties and thickness of each lithological layer. (Observations in WD-2 and WD-6 collieries suggest that primary caving extends only to the Marker Seam - typically 6 to 8 m above the seam). It was expected that stiff, massive aquitard strata would deflect less than the relatively plastic sandstones and that bed separations would develop at the base of the aquitards. Similar simplistic ground movement models have been proposed by other researchers, eg. Singh and Kendorski (1981) - see Figure 2.16. Significantly, though, prior to the author starting this program of research, no field data existed which could either verify these assumptions, or better explain the processes leading to the development of continuous subsidence in the extremely weak Collie Basin sediments.

In this study, subsurface subsidence has been measured using borehole extensometers (boreholes drilled from the surface and fitted with strategically placed anchors - usually installed within a major aquitard or coal stratum above the mining seam). The installation and monitoring processes of borehole extensometers are discussed in more detail in Appendix II.

The vertical movement of the anchors is measured as a distance relative to a datum plate at the surface and added to surveyed subsidence of the extensometer to give the change in reduced level (RL) for each anchor. It was initially proposed to use the change in separation between the anchors (expressed as vertical strains) to help

identify the critical strains on aquitards and thereby predict the potential for water inundation into the mine. This assumption is only valid if there is no significant differential lateral movement between interburdens (as this will tend to elongate the extensometer anchor positions in relation to the surface), and if each anchor has maintained good contact with the extensometer borehole wall with no anchor slippage.

The subsurface subsidence investigation was conducted in three stages:

1) The first stage involved the collection of field data from ACIRL, Blue and 2SA panels so that subsidence mechanisms could be identified, and aquitard integrity could be investigated.

2) The second stage was designed to answer questions that may arise from the preliminary stage (by specifically monitoring subsidence above 1North trial panel).

3) The third stage of subsurface investigation was set up to validate the performance of a trial extraction panel that was to be designed according to the limiting criteria developed from the first two stages of investigation. Research work associated with the final stage of investigation is discussed in Section 5.2.

The location of the extensometer anchors in each extensometer above the three panels used for the first stage of investigation are illustrated in Figures 3.19 to 3.21. (Note extensometer anchors below the Alpha Seam, above the ACIRL Panel, were not operational (due to installation problems.) The positions of the extensometers within each panel are illustrated in Figures I.1, I.4, I.5, I.7, and I.8 in Appendix I.

The results have been given as graphical plots of vertical displacement and strain relative to time and mining width. Strain has been plotted in two forms :-

> Cumulative strains, which represent the **total** strains measured between anchors as the goaf/extraction width increases. These plots illustrate the position and timing of maximum vertical strain and also represent the interburden as a continuum in relation to the position of the goaf.

> Incremental strains, which illustrate the **change** in vertical strain corresponding to the extraction of each individual fender/split. Movement attributed to the extraction of all previous fenders/splits is ignored. This plot is used to demonstrate the phases of strain development as the goaf edge approaches, then passes beneath, and finally as it extends beyond the position of the extensometer.

EXTENSOMETER ANCHOR INSTALLATION ABOVE ACIRL PANEL

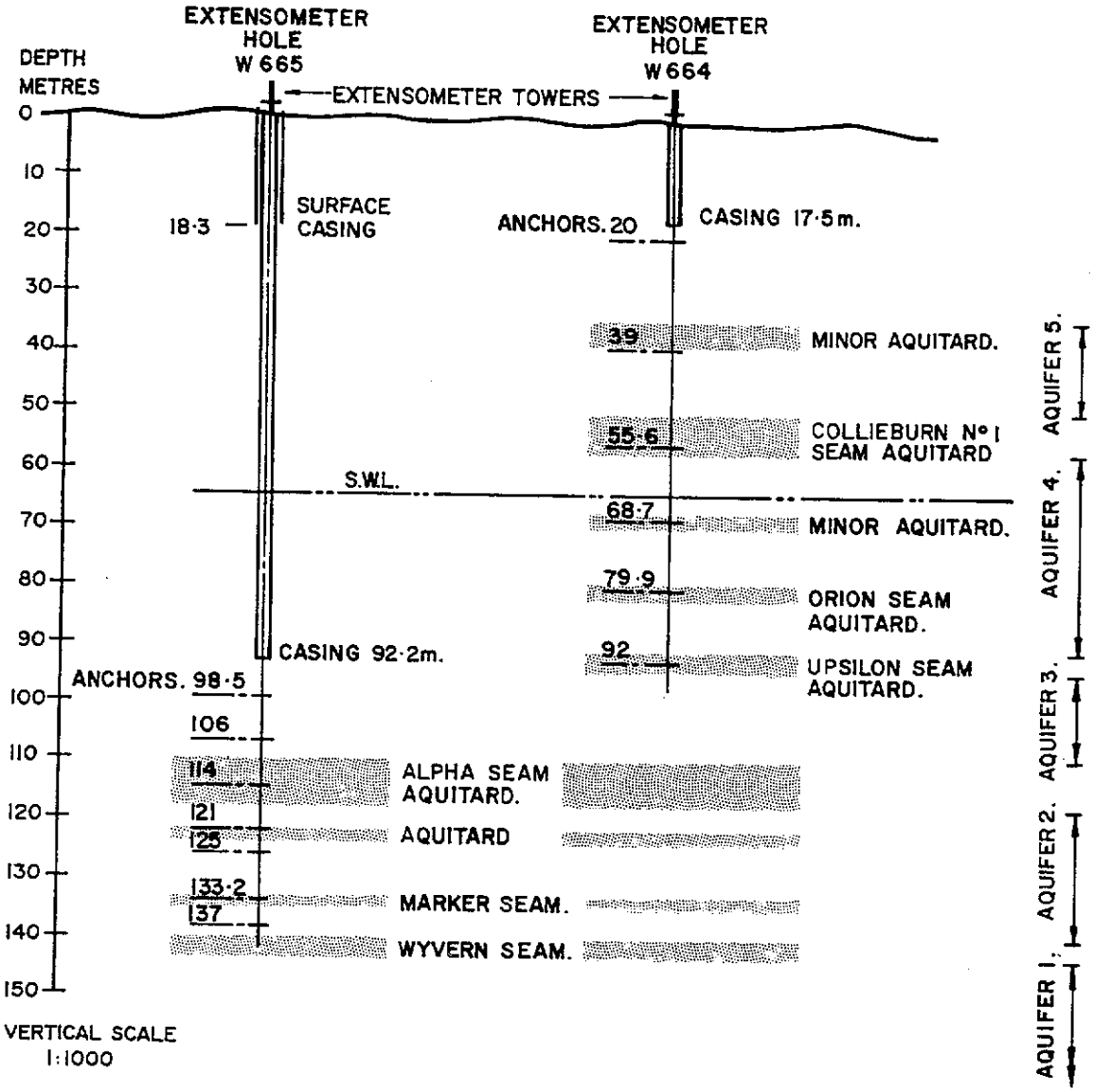

NOTE:
ONLY THE 98·5m ANCHOR IN HOLE W665 IS OPERATIONAL.

Figure 3.19

EXTENSOMETER ANCHOR INSTALLATION ABOVE BLUE PANEL

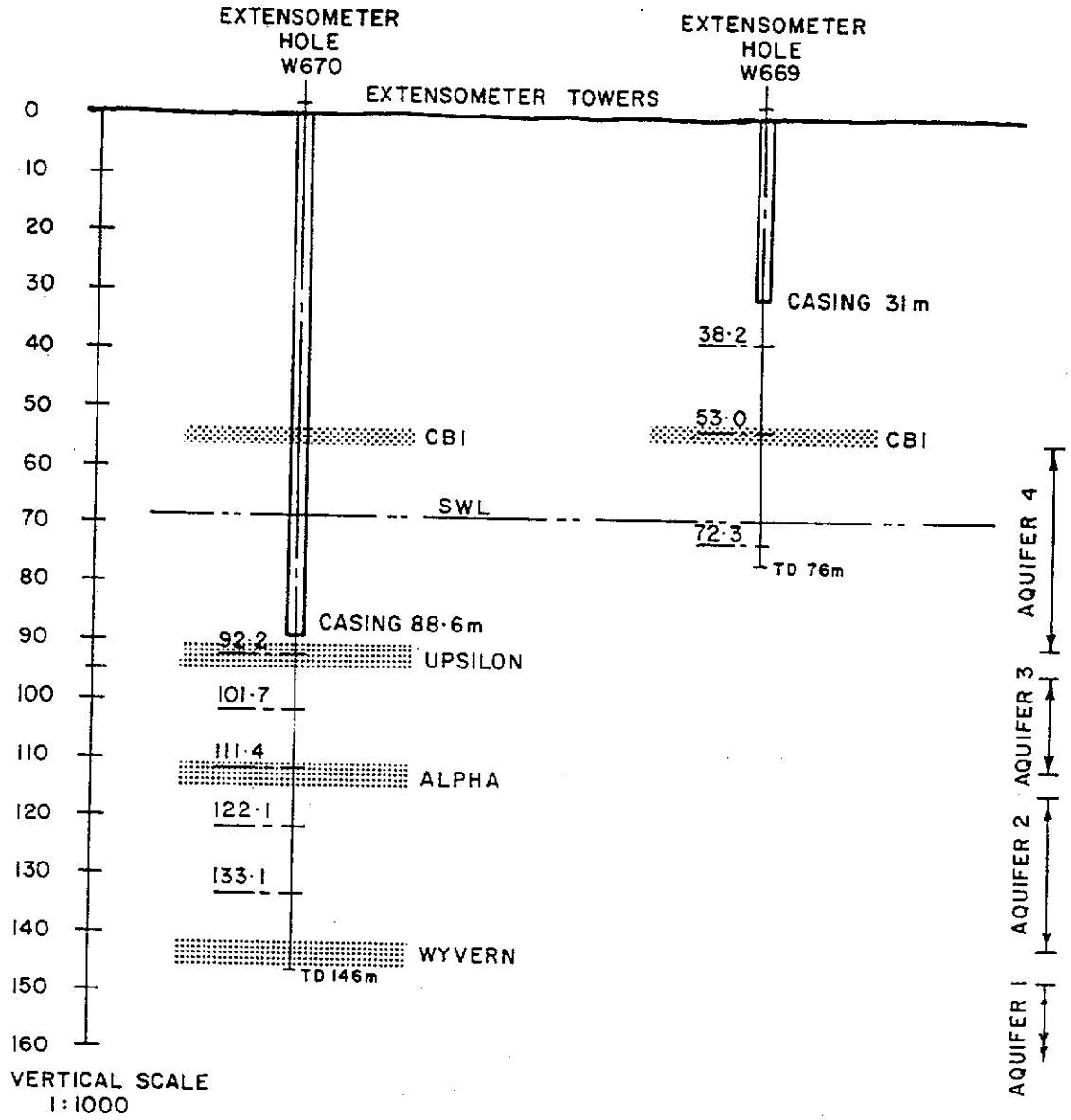

NOTE ANCHORS SET IN COAL SEAMS OR MINOR AQUITARDS (SHALES)

Figure 3.20

EXTENSOMETER ANCHOR INSTALLATION ABOVE 2SA PANEL

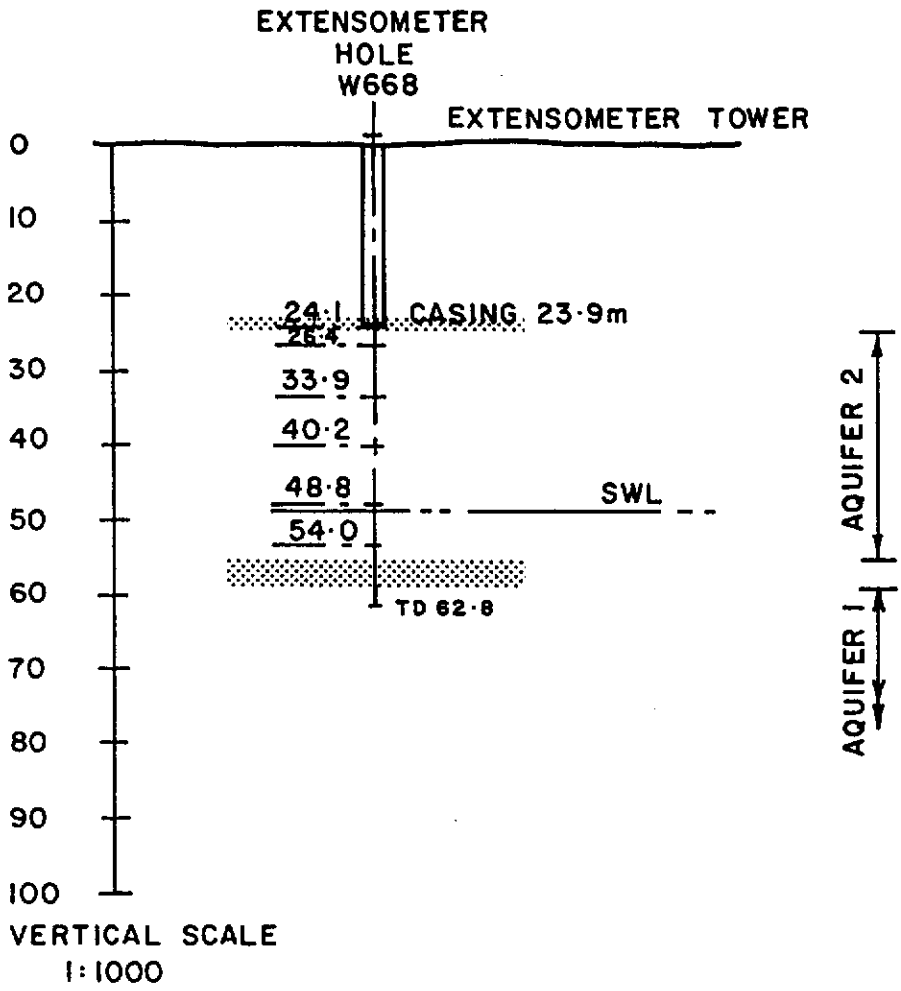

NOTE ANCHORS SET IN COAL SEAMS OR MINOR AQUITARDS (SHALES)

Figure 3.21

The results gained from this subsurface stage of investigation are provided and discussed in more detail than for the surface subsidence because subsurface subsidence is more complex and there are relatively few details on subsurface movements from other mining areas to compare against.

The main observations made from the subsurface investigations are firstly listed in note form for each individual panel, and then summarised and discussed in terms of the overall objectives.

3.2.1 ACIRL Panel

Subsurface subsidence investigations in the ACIRL panel were restricted to monitoring stresses and water flows in Sub-panel A, and extensometer measurement above Sub-panel B only. Irad-gauge stress-change cells were used to measure the redistribution of stress during extraction so that data could be gathered for more accurate design of coal fenders and pillars in future panels. The results of the stress monitoring are described in detail in Hebblewhite and Humphreys (1988) and Platt (1987) and summarised in Section 4.1.1.1 in this thesis.

The mine-water pumpage and aquifer ground water monitoring proved to be of little use for determining the impacts of mining subsidence on aquifers, as the depressurisation program effectively "drained" each aquifer above the panel. Water inflow was interpreted to originate from within the recharge area (within the ground water draw-down curve) immediately down-dip from the panel. There was consequently no discernible change in piezometric levels. At the time, it was considered not possible to establish whether the observed increases in mine water make came from any particular aquifer. Further discussion of the water make is provided in Section 5.1.

The major observations made from the extensometer monitoring above ACIRL sub-panel B (presented in Figures 3.22 to 3.26) are listed below:

- The maximum subsurface subsidence measured was only 24% (0.6 m) of the true mining height , compared to 19% at the surface of the extensometer. The point of maximum subsidence was recorded at the deepest functioning anchor - approximately 40 m above the seam. Note to convert these values to effective mining height, they need to be divided by the ratio of coal extracted from the panel (0.9 - see Table 3.2).

EXTENSOMETER ANCHOR MOVEMENTS (in RL) WITH TIME - ACIRL PANEL

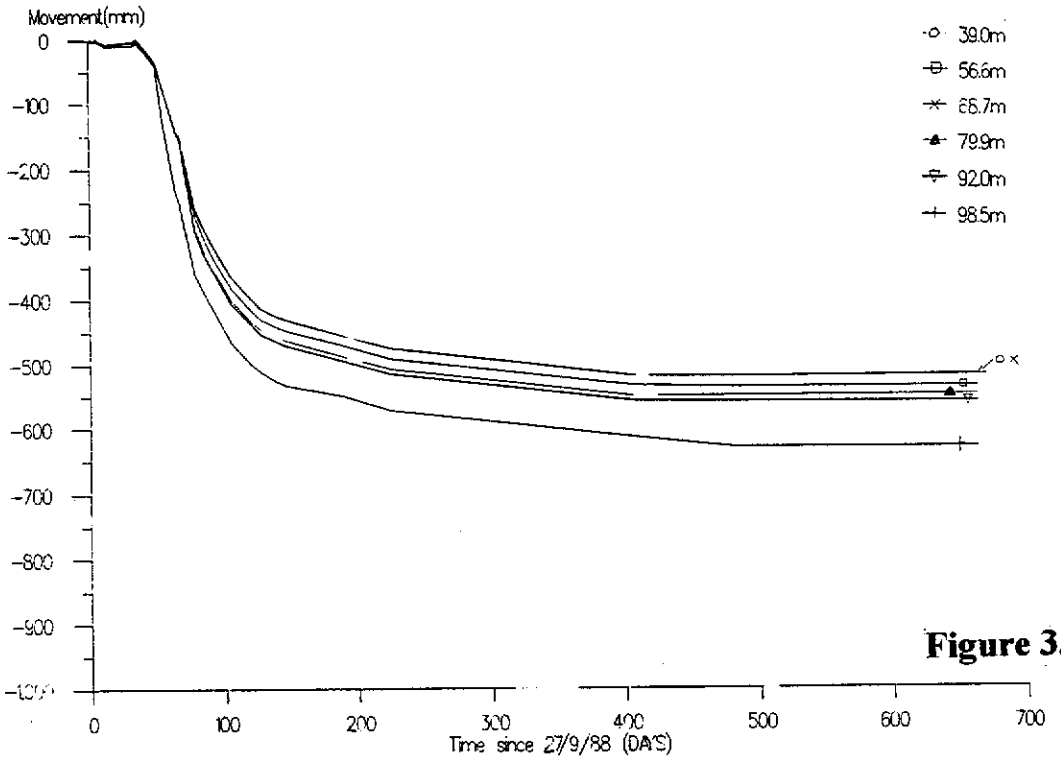

Figure 3.22

EXTENSOMETER ANCHOR MOVEMENTS (Relative to datum plate) WITH TIME - ACIRL PANEL

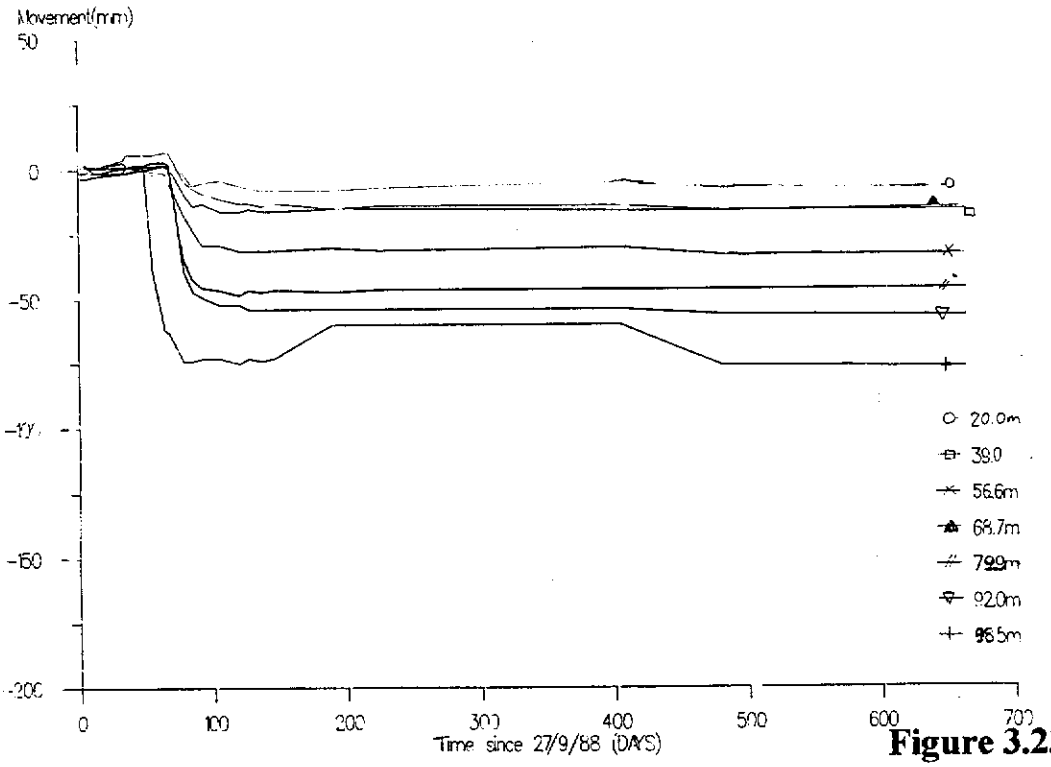

Figure 3.23

EXTENSOMETER ANCHOR MOVEMENT (in RL) Vs WIDTH OF EXTRACTION ACIRL PANEL

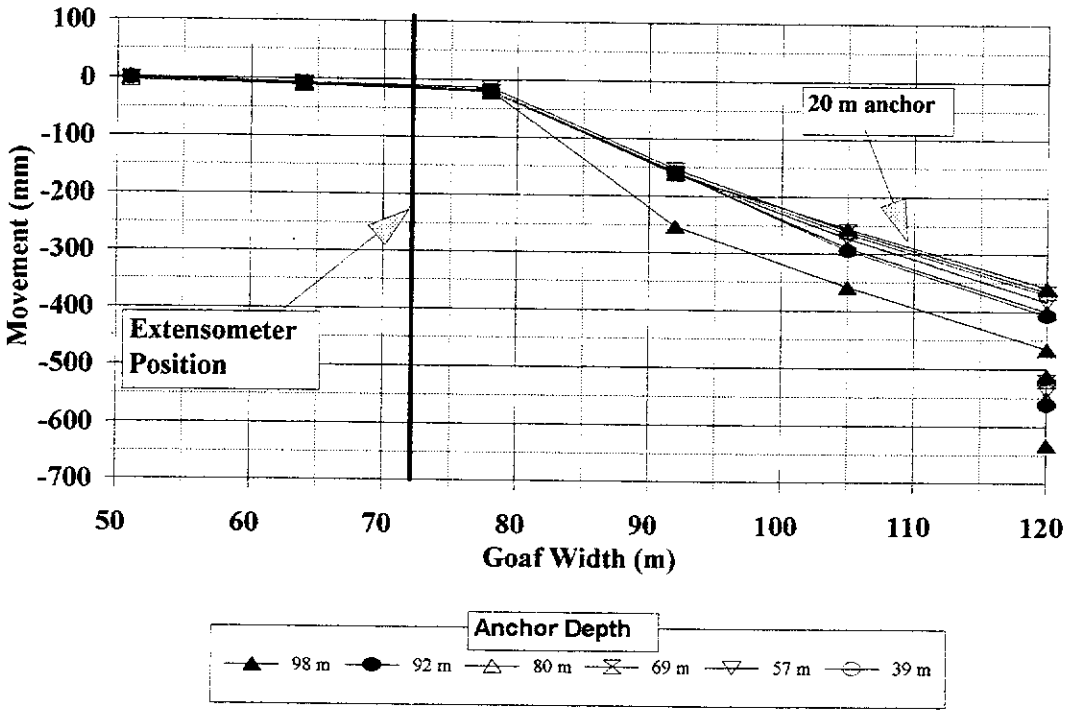

Figure 3.24

ACIRL PANEL SUBSIDENCE AS A PERCENTAGE OF MINING HEIGHT Vs GOAF ADVANCE RELATIVE TO EXTENSOMETER

(FROM 17/9/87 TO 12/7/89)

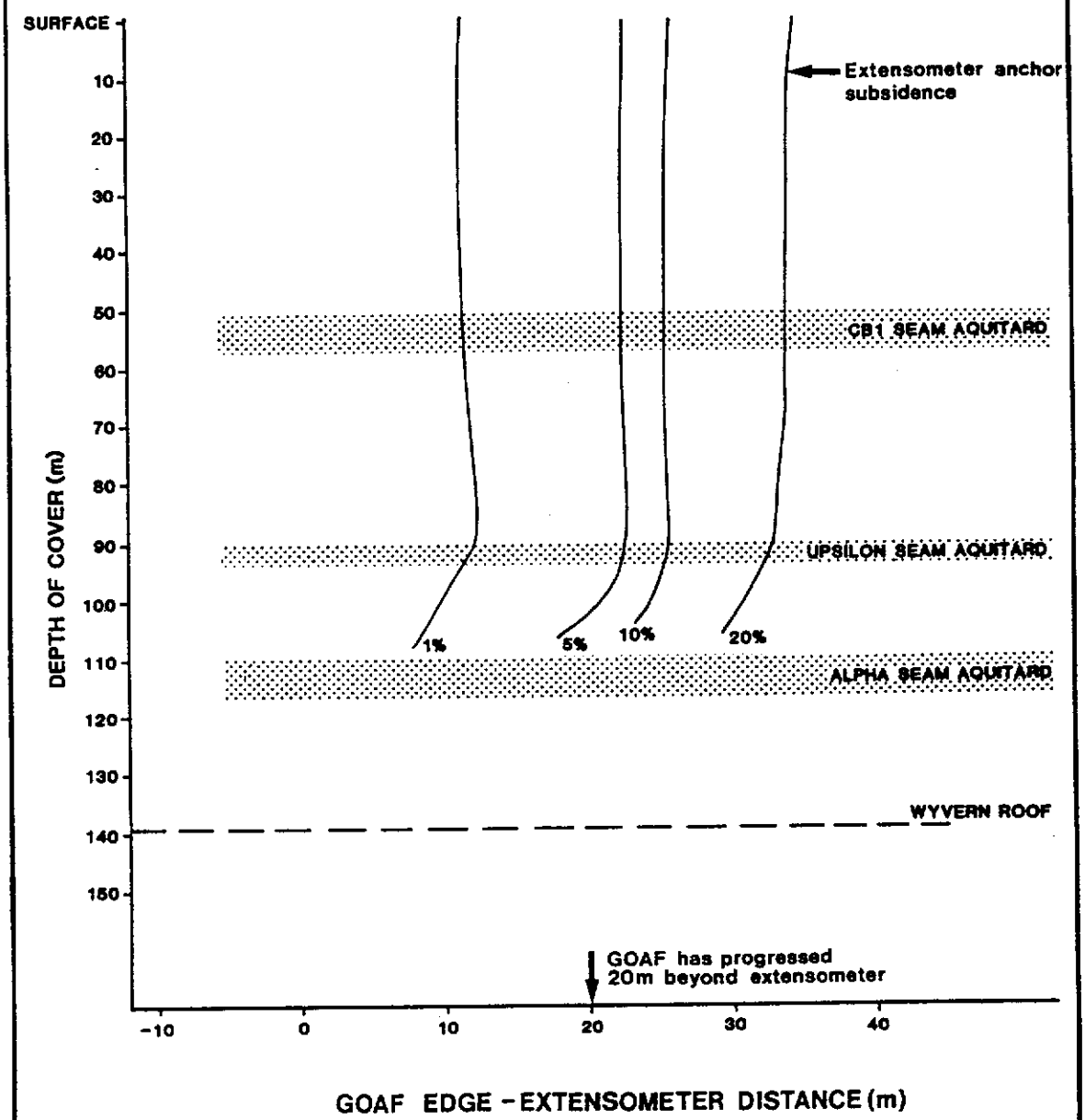

Figure 3.25

VERTICAL STRAIN Vs GOAF EDGE DISTANCE - ACIRL PANEL

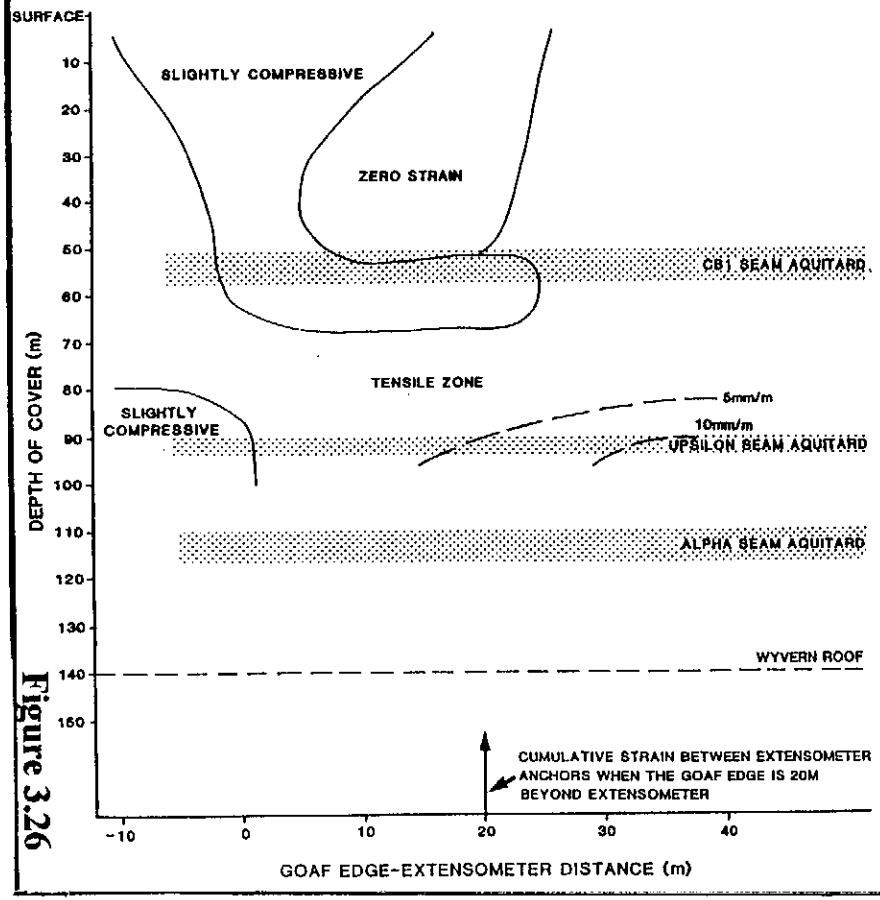

Figure 3.26

INCREMENTAL CHANGES IN VERTICAL STRAIN FOR EACH ADVANCEMENT OF THE GOAF EDGE ACIRL PANEL

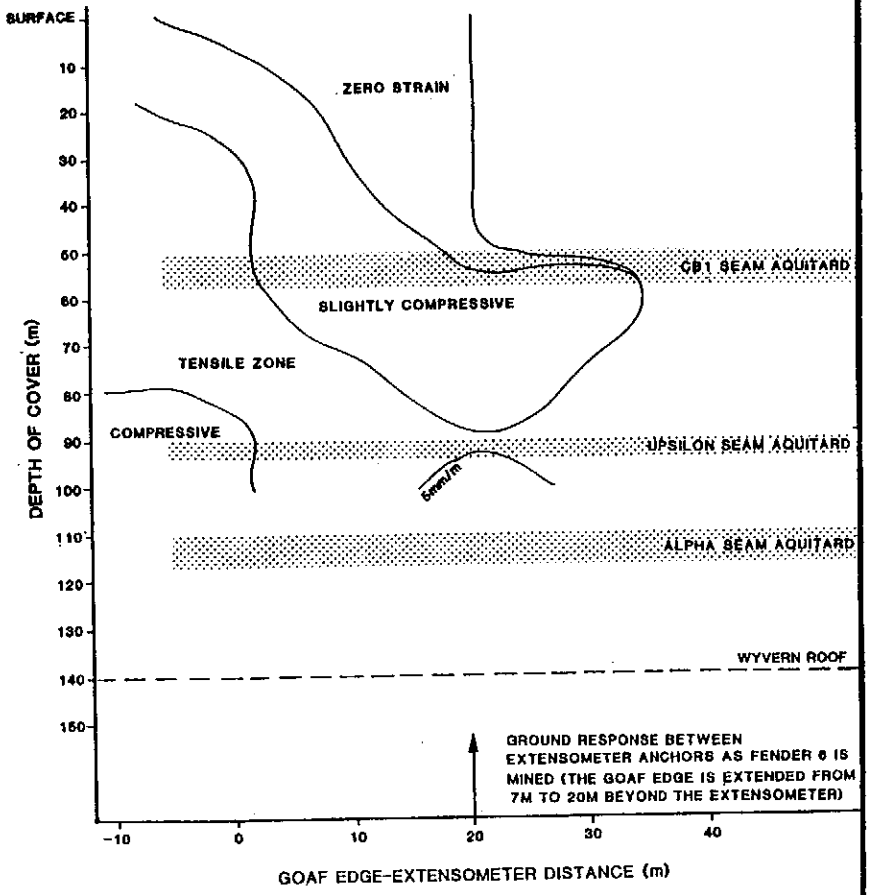

- The slope of the subsidence isopachs in Figure 3.25 are almost vertical above Upsilon Seam. This indicates that the strata from the surface to the Upsilon Seam is moving as one mass, for the limited panel development in sub-panel B. However, in the Alpha-Upsilon interburden, there does appear to be more subsidence with less goaf advance - as would be expected nearer to the Wyvern Seam. It should be noted that below the Upsilon Seam there is limited subsidence information; due to anchor installation problems.

- There was no discernible reconsolidation of the subsurface strata at any stage. This is illustrated by the plot of subsidence relative to the datum point (Figure 3.23) where the separation between each anchor was maintained well after completing the panel. The plot of incremental strains, given in Figure 3.26 b, provides further support of this assumption by the noted lack of compressive strains developed at any stage of mining. This would be expected of the upper strata in **sub-critical** panels.

- No significant vertical strain was measured in aquifer 3 until the goaf was 20 m past the position of the extensometer. Vertical strains are minimal in aquifers 4 and above (all horizons above the Upsilon Seam - see Figure 3.26). This supports the uniform movement assumption mentioned in the points above. The maximum vertical strain calculated was only 14.6 mm/m. It occurred in the Upsilon - Alpha interburden (aquifer 3) when the goaf had progressed to 33 m past the position of the extensometer.

- It is difficult to determine the effect, if any, the remnant fenders left within Sub-panel B had on subsidence development. More case data would be required before definitive conclusions could be formalised.

3.2.2 Blue Panel

The major observations made from the extensometer monitoring above Blue panel (presented in Figures 3.27 to 3.31) are listed below:

- The maximum subsurface subsidence is 51% (1.4 m) of the height of extraction, compared to 44% at the surface collar of the extensometer. This occurred at the anchor installed in aquifer 2 at 122 m (20 m above the working roof) when the goaf was 78 m past the extensometer - at panel completion. Note to convert these values to effective mining height, they need to be divided by the ratio of coal extracted from the panel (0.9 - see Table 3.2).

- The near-surface strata above Collieburn 1 seam, appears to have moved in one mass. This is assumption supported by :-

  > the shape of the subsurface subsidence contours (Figure 3.30) at depths less than 50 m being almost vertical,

  > the minimal strain measured from the surface to Collieburn 1 Seam (Figure 3.31 a).

- The maximum vertical strain measured was 22.5 mm/m tensile strain in the depth interval of 111.4 to 122.1 m. Tensile strains of 8 mm/m were measured in the interval corresponding to aquifer 4 (72 to 92 m, Figure 3.31 a).

- There is a zone of slight compression 25 - 40 m, above the seam as the goaf approached the extensometer Figure 3.31 a. This indicates "loading" of lower strata by cantilever action of the superincumbent strata across the goaf edge.

- There is a compressive zone in the upper sediments (Figure 3.31 a), possibly due to "drag" of the surface toward the goafed area.

- The plot of cumulative vertical strain (Figure 3.31 a) also demonstrates that the major aquitards are influencing the shape of the strain isopachs. This suggests that the sandstone strata in each aquifer is resting on the aquitards, and that the vertical strain is due to either bed separation or dilation of collapsed ground at the base of spanning aquitards. It was not possible, at this stage, to determine if there was bed separation or not.

EXTENSOMETER ANCHOR MOVEMENTS (in RL) WITH TIME - BLUE PANEL

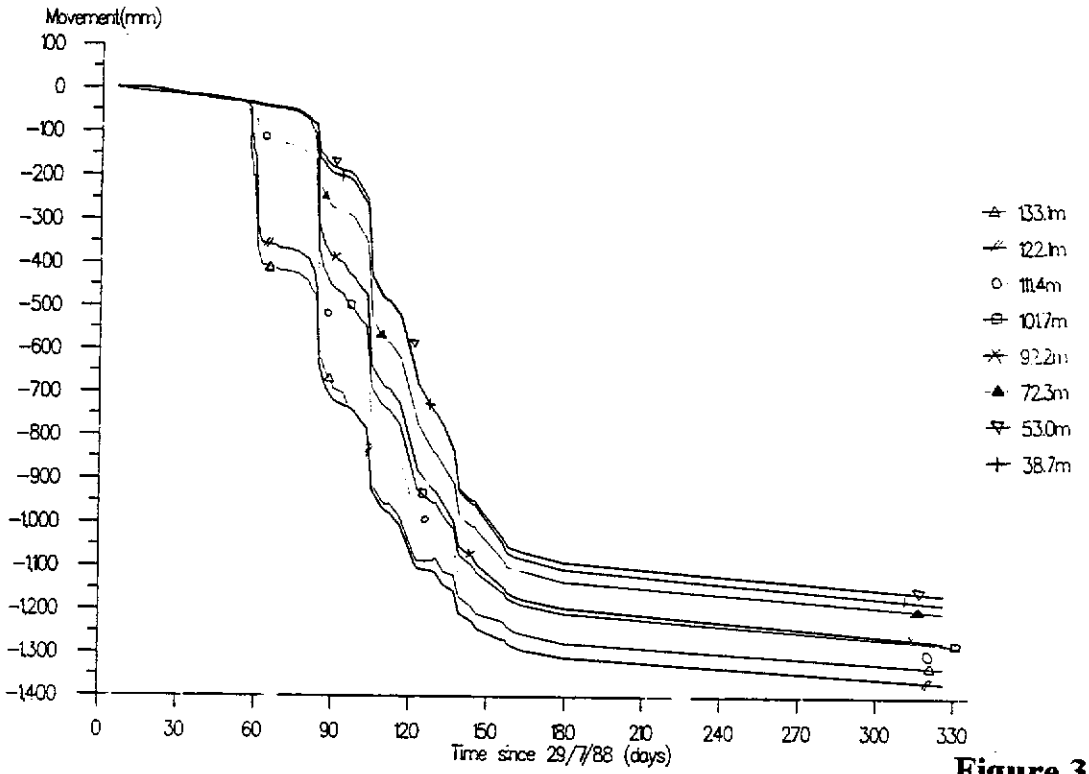

Figure 3.27

EXTENSOMETER ANCHOR MOVEMENTS (Relative to datum plate) WITH TIME - BLUE PANEL

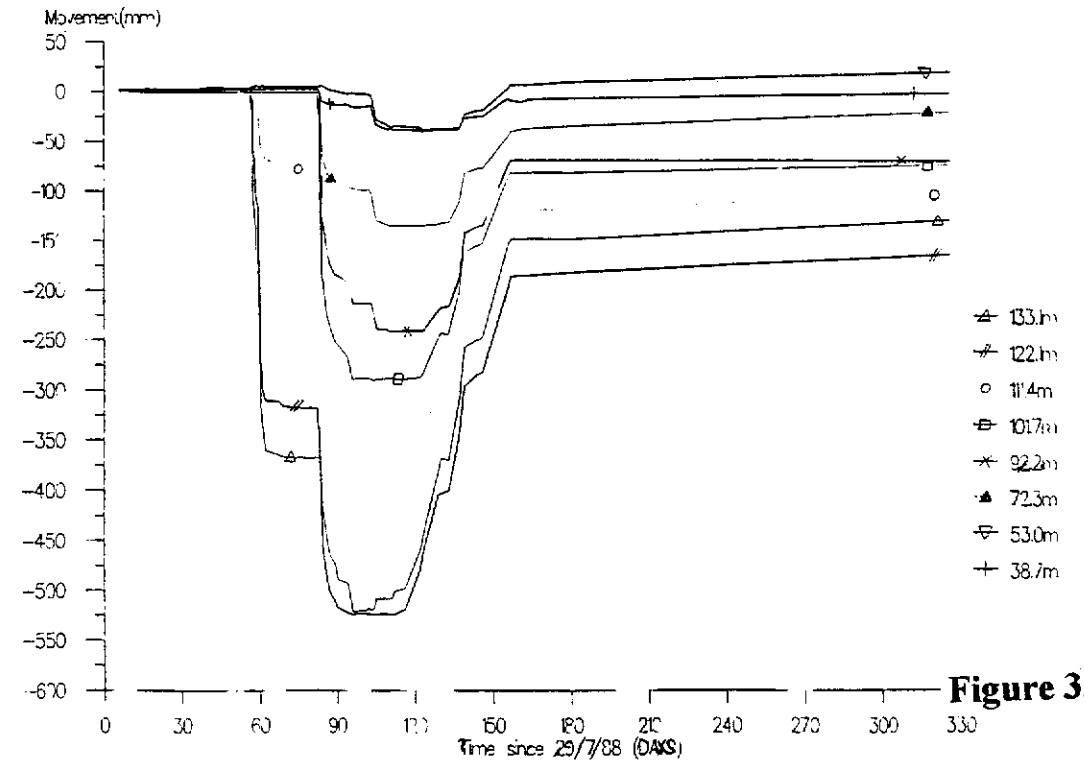

Figure 3.28

EXTENSOMETER ANCHOR MOVEMENT (in RL) Vs WIDTH OF EXTRACTION BLUE PANEL

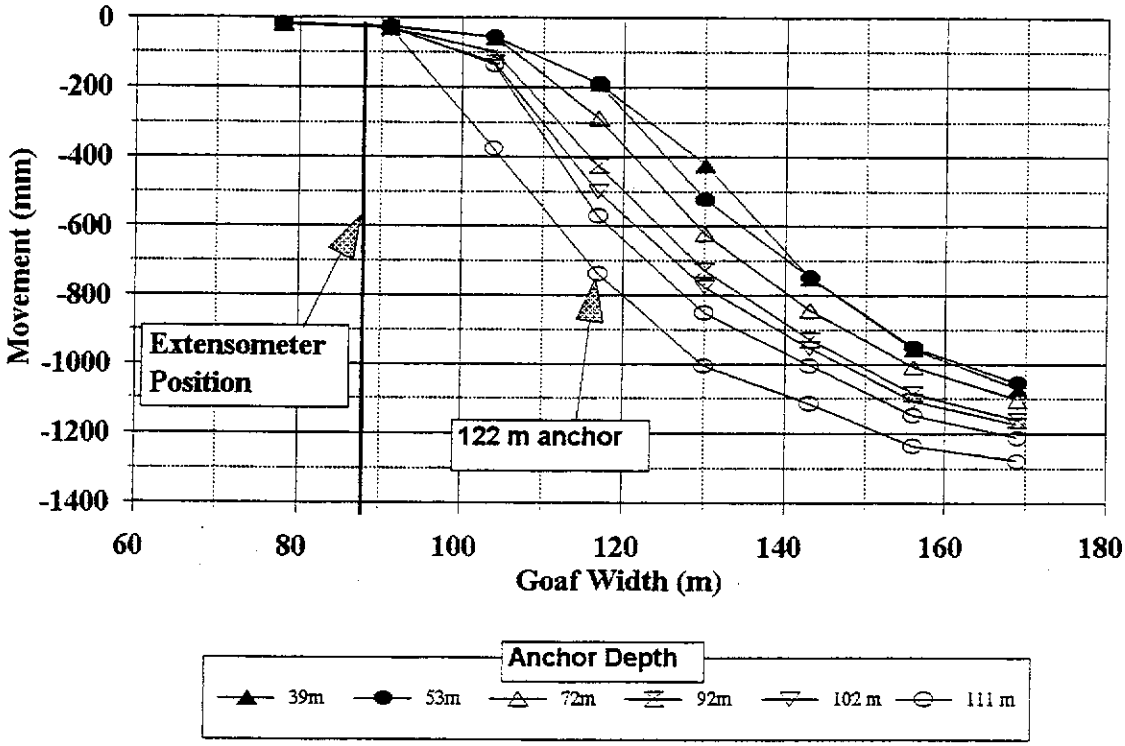

Figure 3.29

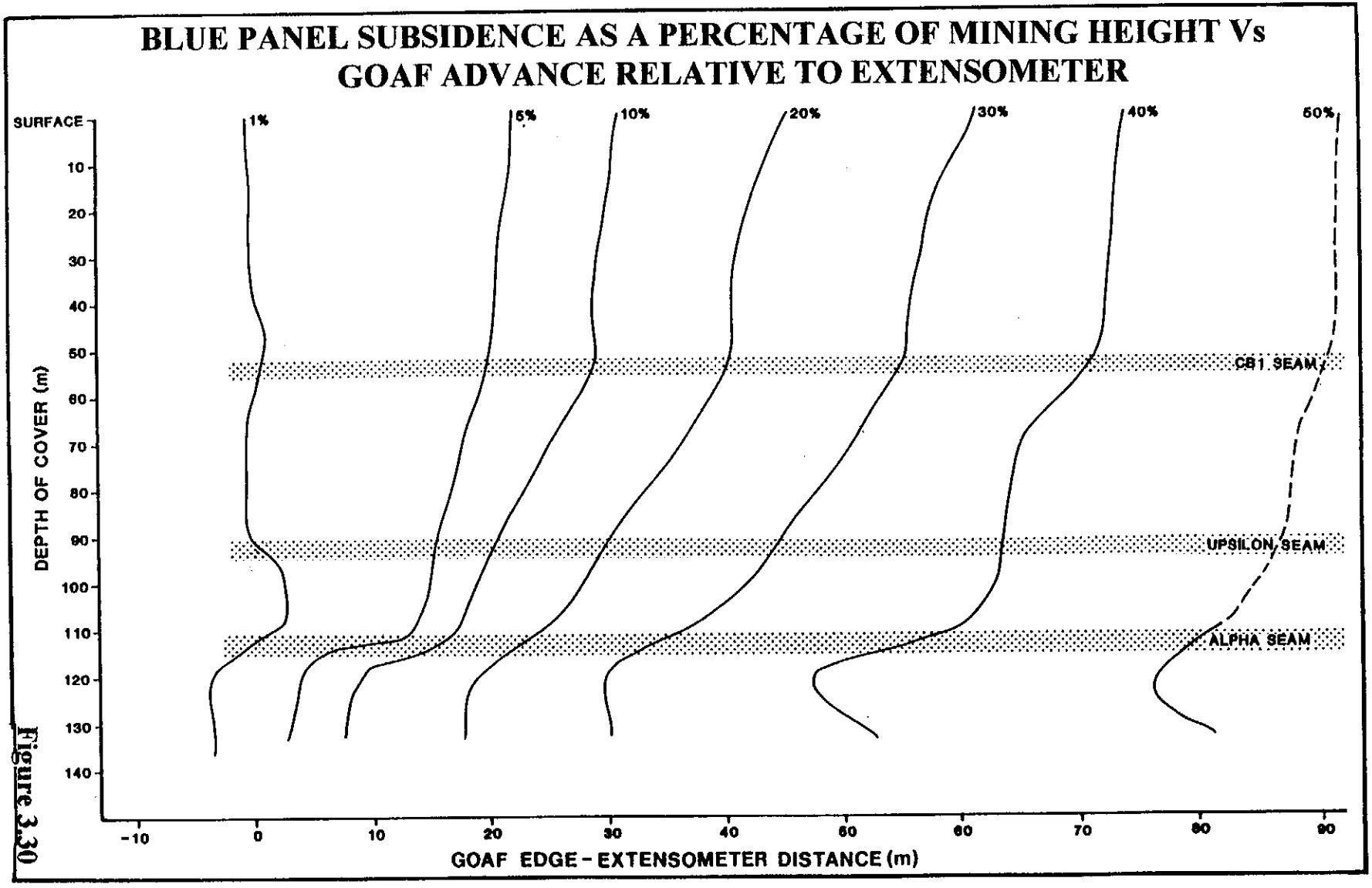
BLUE PANEL SUBSIDENCE AS A PERCENTAGE OF MINING HEIGHT Vs
GOAF ADVANCE RELATIVE TO EXTENSOMETER
SURFACE
DEPTH OF COVER (m)
10
20
30
40
50
60
70
80
90
100
110
120
130
140
1%
5%
10%
20%
30%
40%
50%
CB1 SEAM
UPSILON SEAM
ALPHA SEAM
-10
0
10
20
30
40
50
60
70
80
90
GOAF EDGE - EXTENSOMETER DISTANCE (m)

Figure 3.30

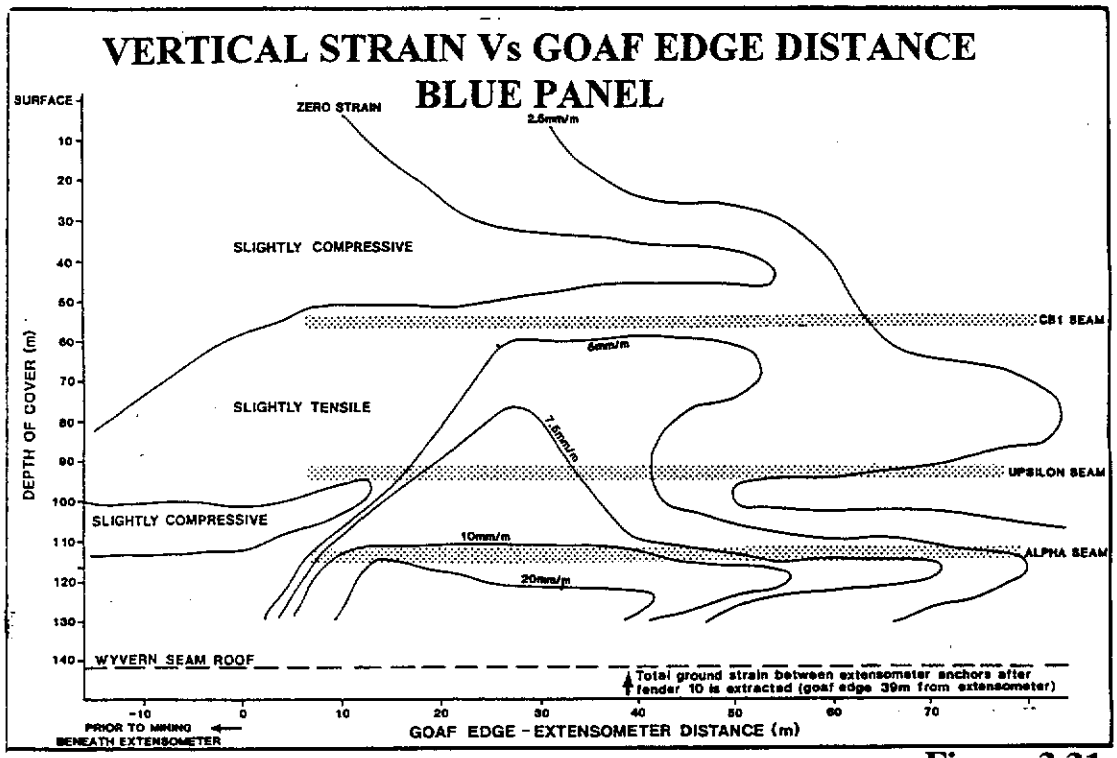

Figure 3.31 a

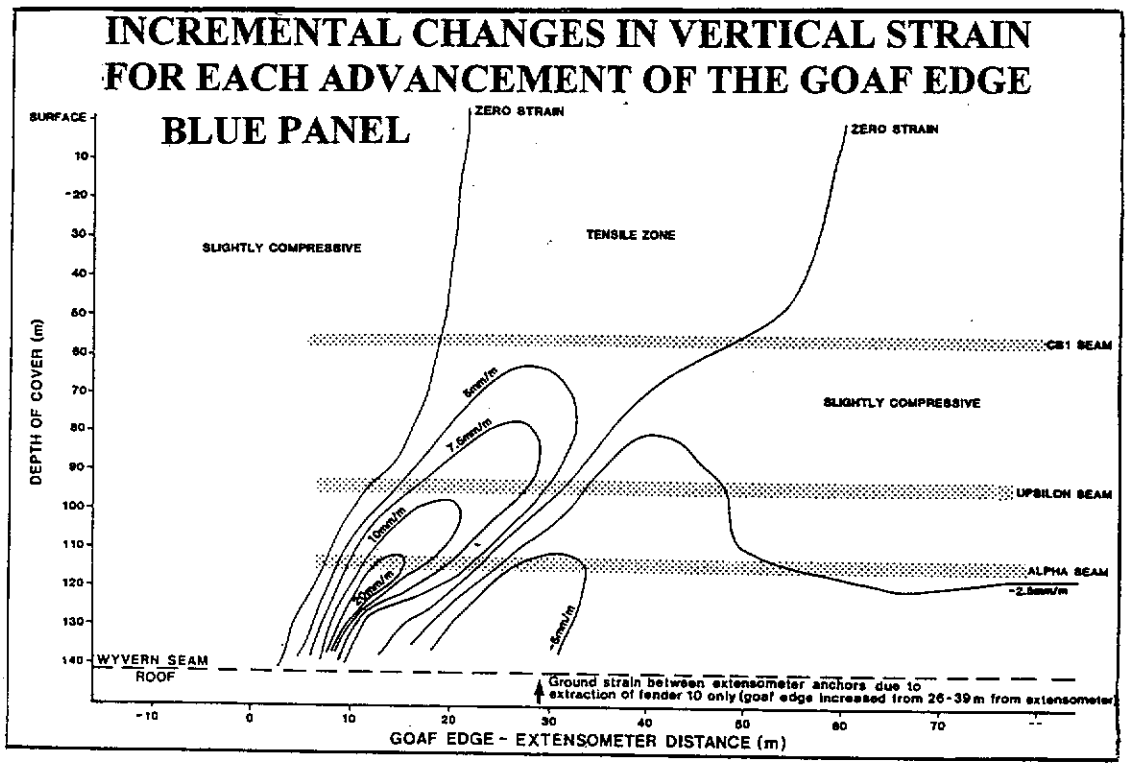

Figure 3.31 b

- Once the goaf extends beyond the extensometer position, the majority of subsurface strata undergoes tensile strain, of which a large proportion remains in tension from that point onwards (see Figure 3.31 a). This is because the magnitudes of tensile strains generated are greater than the reconsolidation strains developed as the goaf widens and recompacts.

  Figure 3.31 b - incremental strain Vs goaf width effectively highlights the dominant tensile strains developed during each stage of mining and demonstrates that :-

  > Tensile strain is confined to a wedge-shaped zone when the mining face is within a relatively small distance beyond the extensometer (the majority being experienced before the goaf extends beyond 40 m from the extensometer).

  > Compressive (-ve) strains - notably close to the seam - begin within two split/fender widths beyond the extensometer position. These compressive strains suggest reconsolidation and compaction of broken or "relaxed" strata in the goaf region. Figure 3.31, plotted against time demonstrates that after eighty days from 29/7/88, the vast majority of strain is compressive. Figure 3.28, which represents anchor movements relative to the datum plate, also illustrates the occurrence of compressive strains by the closing of the distance both between the individual anchors, and the anchors and the ground surface.

- The plot of anchor movements relative to the datum plate (Figure 3.28) also demonstrates the stepped sequencing of subsurface movements according to each fender/split extraction cycle.

- The deepest anchor - 133.1 m (9 m above the working horizon) appears to have been affected by the location of a relatively small stook beneath it. It was interpreted that this stook effectively retarded downward movement of this anchor as the anchor 10 m above subsided more - particularly in the early stages of goaf development.

- Subsurface subsidence is time dependent. Figure 3.26, which represents the anchor movements in reduced level, illustrates that subsidence was still increasing slightly some time after fender extraction was completed.

- There appears to be a relationship between subsurface subsidence and goaf - extensometer distance and height above mining horizon - as suggested by the left to right trending subsurface subsidence contours in Figure 3.30. This trend demonstrates more movement for less goaf development when closer to the seam - as would be expected - and is discussed further in Sections 3.2.5 and 3.3.

3.2.3 Two South A Panel

The field measurements for 2SA panel have been presented in the same fashion as for ACIRL and Blue panels in Figures 3.32 to 3.36 with the following major conclusions:

- Maximum subsurface subsidence measured was 54% of the height of extraction (1.35 m), or 60% of the effective mining height at the position of the extensometer.
- The shape of the subsurface isopachs (Figure 3.35) tends toward the vertical, which implies that the superincumbent strata is moving more or less as one mass in response to caving above the extracted seam, which is to be expected for plastic, shallow strata.
- Vertical tensile strains are relatively small, the maximum strain measured at any time being 8.3 mm/m between anchors at 33.9 and 40.2 m (in aquifer 3).
- Compressive strains are far greater and more extensive than for the other panels, as illustrated by Figure 3.36 a. The overlying strata is firstly being compressed by the forces induced by the action of cantilevering across the solid coal edge towards the goaf. The maximum compressive strain measured at the goaf edge was 6.4 mm/m - at a point 3 m above the seam. The probable cause of the greater compressive strains is that the shallower strata are more plastic and less consolidated and will deform more with less load.
- Major aquitards are influencing the distribution of vertical strains, as illustrated by the relatively flat cumulative vertical strain isopachs in Figure 3.36 a.
- Reconsolidation and compression of caved and/or "relaxed" strata occurs when the goaf had extended roughly two split/fender widths beyond the extensometer, as indicated by the incremental strain plot in Figure 3.36 b.

EXTENSOMETER ANCHOR MOVEMENTS (in RL) WITH TIME -2SA PANEL

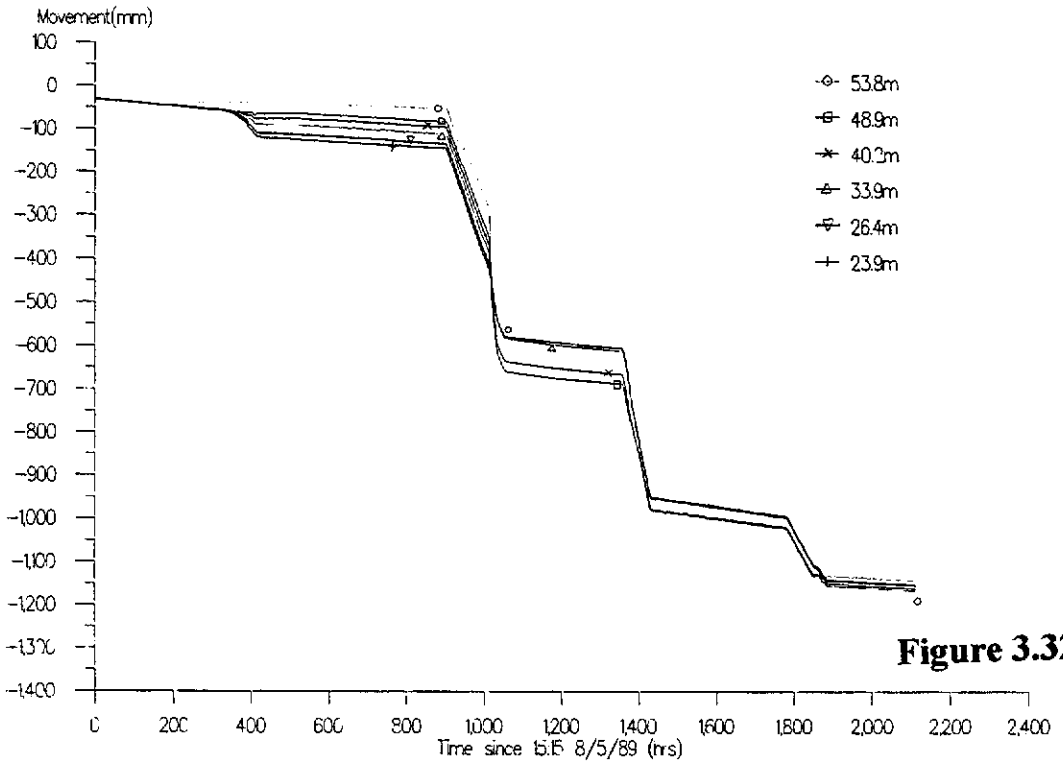

Figure 3.32

EXTENSOMETER ANCHOR MOVEMENTS (Relative to datum plate) WITH TIME - 2SA PANEL

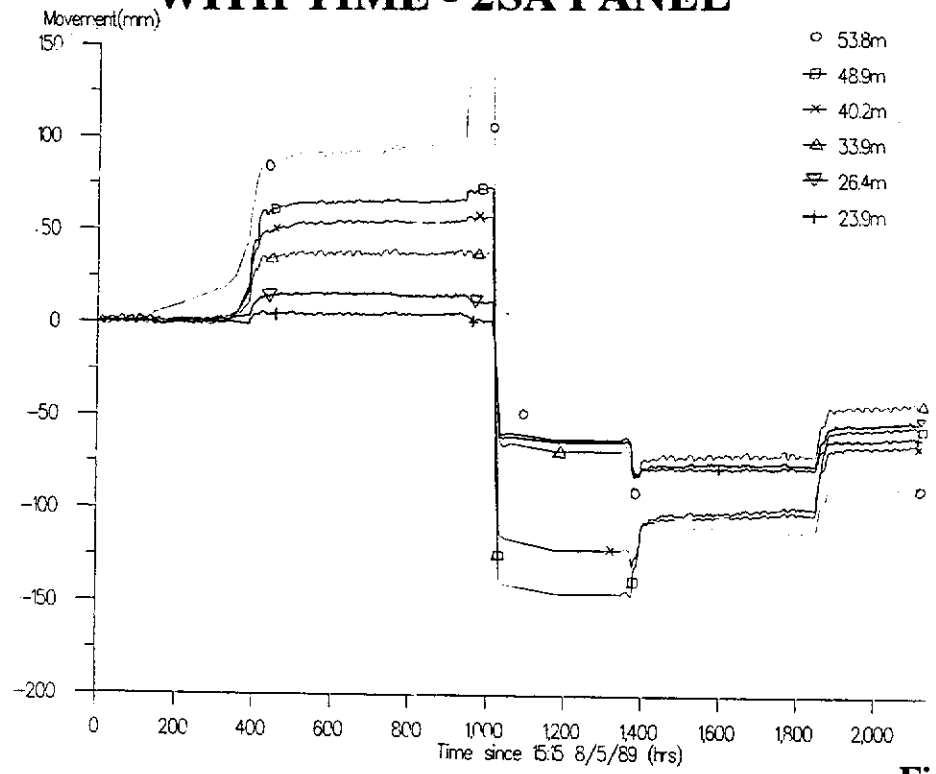

Figure 3.33

ANCHOR MOVEMENT (RL) Vs GOAF WIDTH
2 SOUTH A PANEL

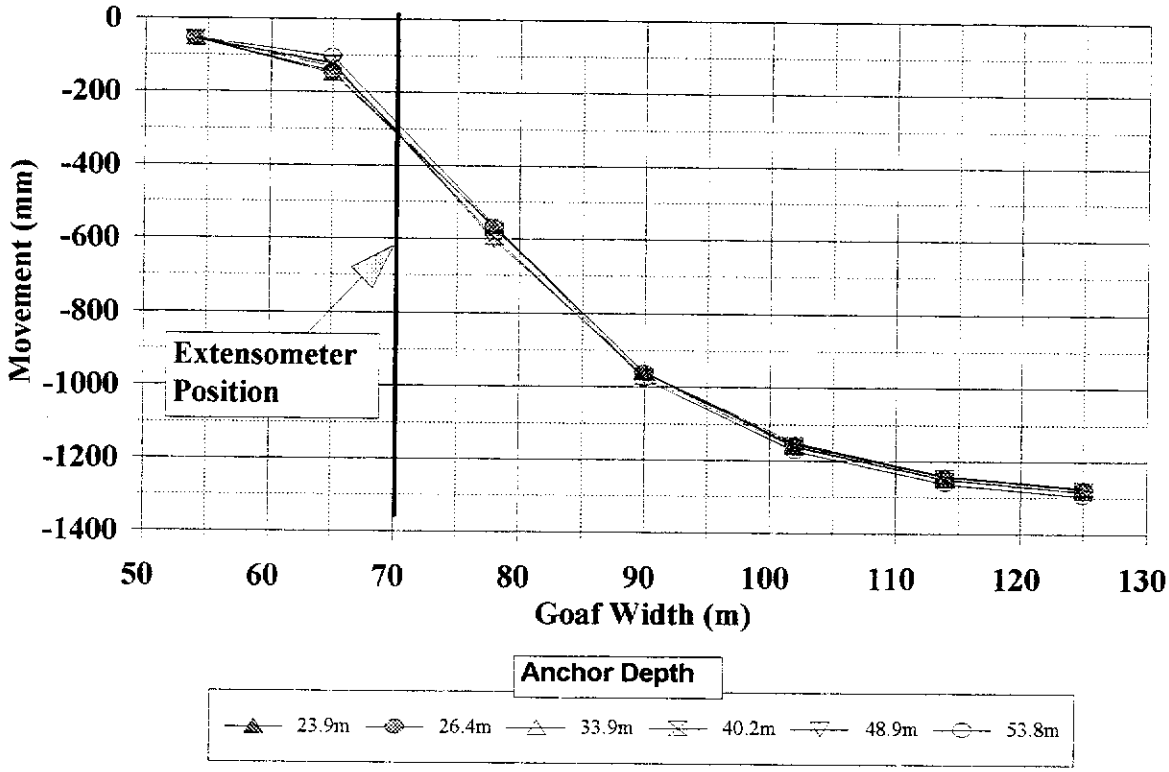

Figure 3.34

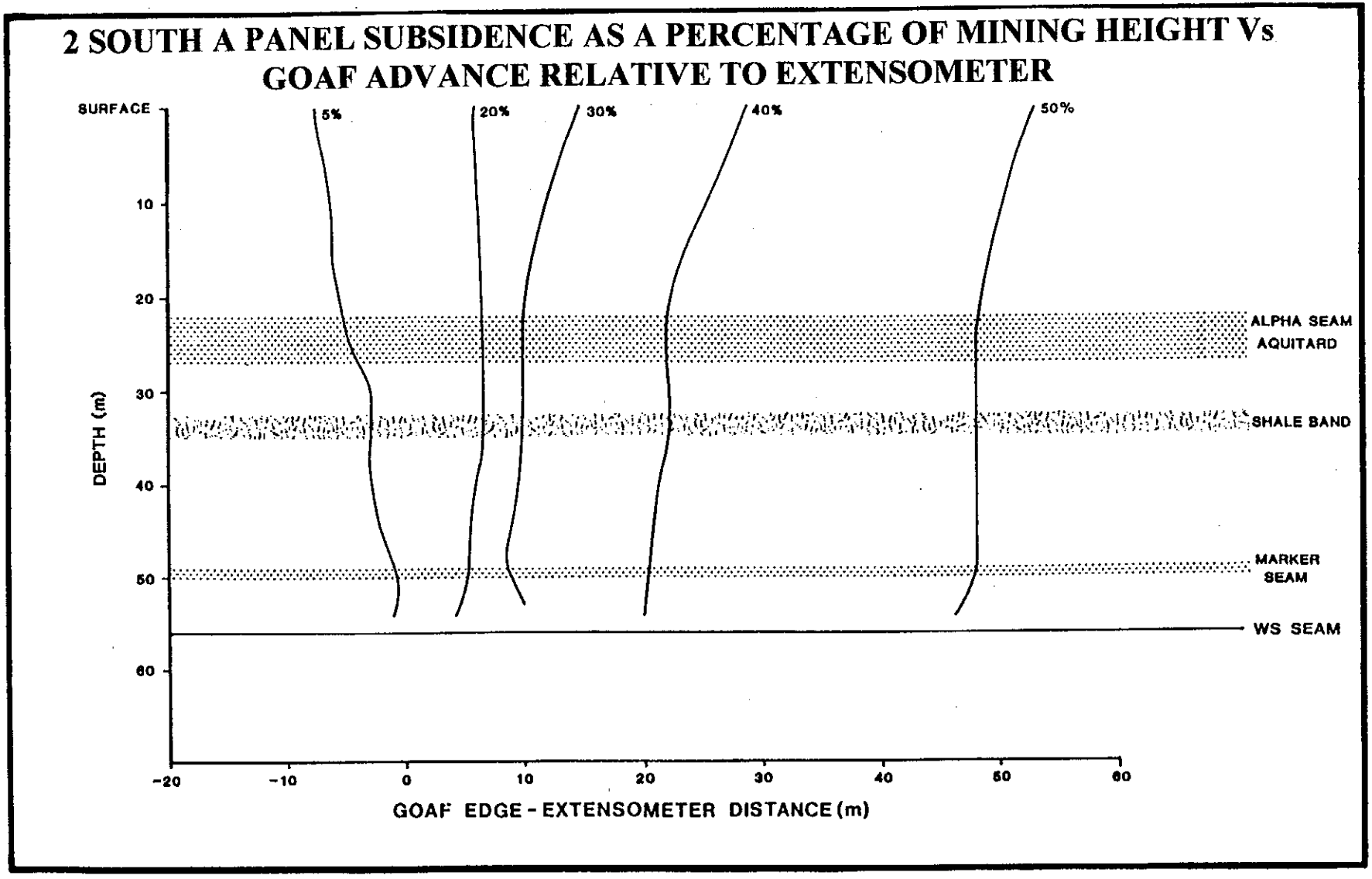
2 SOUTH A PANEL SUBSIDENCE AS A PERCENTAGE OF MINING HEIGHT Vs GOAF ADVANCE RELATIVE TO EXTENSOMETER
SURFACE
5%
20%
30%
40%
50%
10
20
30
40
50
60
DEPTH (m)
ALPHA SEAM AQUITARD
SHALE BAND
MARKER SEAM
WS SEAM
-20
-10
0
10
20
30
40
50
60
GOAF EDGE - EXTENSOMETER DISTANCE (m)

Figure 3.35

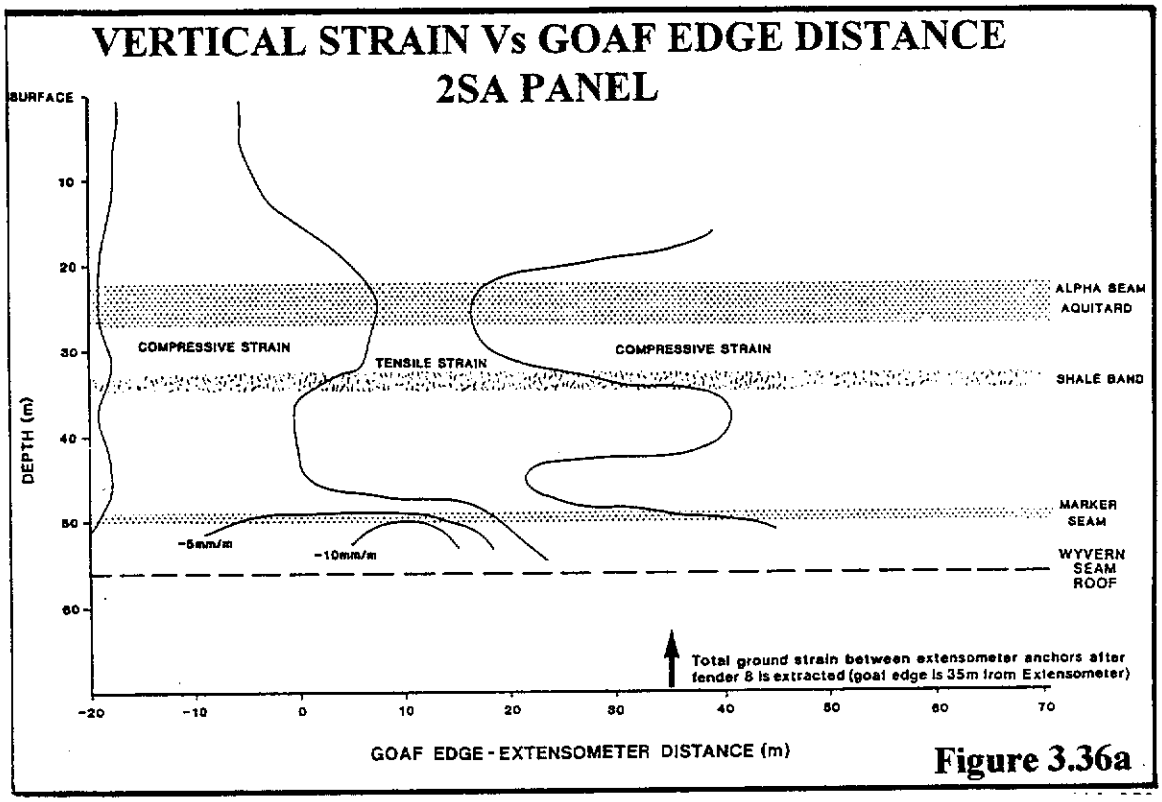

Figure 3.36a

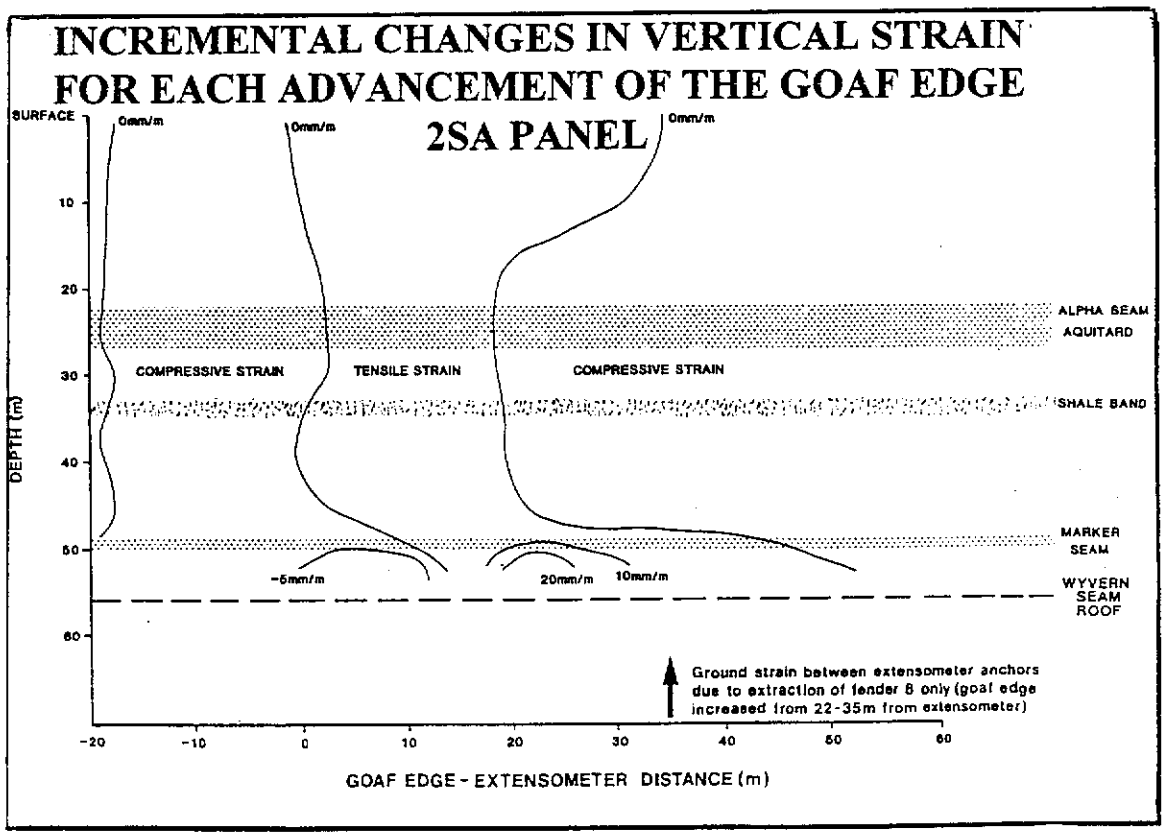

Figure 3.36b

- It appears that a stook had been left below the extensometer, as movements of the deepest anchor (at 53.8 m - 3 m above the working horizon) appear to have been retarded. Figure 3.36 b illustrates the effect of the "stook", where it can be seen that compressive strains continue to develop within the immediate roof area, until the goaf has extended to approximately 15 m beyond the extensometer position. It is interpreted that at this point the load transferred from the goaf edge exceeds the strength of the sandstone immediately above the coal stook and begins to yield. This zone can then move downwards (where previously the stook prevented this from occurring), and tensile strains can develop within the immediate roof.

- Immediately prior to the goaf edge reaching the extensometer, the distance between the extensometer anchors and the surface is reduced. This suggests that either the surface has subsided more than the subsurface, or the strata above the solid coal abutment has crushed. From the data available, it is not plausible to determine the precise factors contributing to this phenomenon. It is the author's opinion that the deeper weak sandstone is being crushed in this case.

- The apparent relationship between subsurface subsidence and height above the Wyvern seam **and** goaf width, as inferred by the Blue panel results in particular, is not clear in this panel. This variation from the Blue panel results can be expected as the 2SA panel is comparatively very shallow and the weaker superincumbent strata would tend to move more in unison, regardless of the height above the panel.

3.2.4 Horizontal Subsurface Movements

As referred above, the accuracy of subsurface subsidence measurements using anchors relies on there being no significant lateral shear within the subsidence profile. Should there be significant differential horizontal movement along stratigraphic horizons, the extensometer wires will be pulled laterally thus exaggerating the actual vertical subsidence and strain.

The phenomenon of horizontal **surface** strain is well documented, with the ground surface migrating toward the centre of the subsidence trough. Following from this, it is expected that lateral movement would occur in the subsurface strata also. This assumption is supported by the work of several authors (eg Kratzsch, 1983 who used finite element modelling to demonstrate the extent of lateral movement throughout the rock mass, and Conroy and Gyarmaty, 1982, who used geophysical techniques to attempt to monitor lateral defections down a borehole).

Further evidence of lateral subsurface movement is seen at the Latrobe Valley, Victoria, where dewatering bores with less than a 30 cm annulus between the rising main and the borehole wall were damaged by shearing (Raisebeck, 1988).

Local evidence of lateral movement includes :-

- the development of a constriction in borehole piezometer F4, sited over ACIRL Panel, which prevented a water level monitoring probe from being lowered down the hole past 38 m depth, and

- the extensometer tower servicing the deeper anchors above ACIRL panel was observed to be leaning away from the centre of the subsidence trough, as the goaf edge was located immediately below. This indicates that the casing at 90 m depth was being dragged laterally toward the caved zone a greater amount than the casing at the surface.

Although direct measurements were not attempted, it is considered that these lateral movements are relatively minor (having only affected the boreholes fitted with inflexible grouted pipes with an annulus of 26 mm). It can be estimated that the maximum lateral movement is in the range of 26 mm to 140 mm (the width of the annulus remaining in an open 150 mm extensometer hole with eight stainless steel cables). There must have been less than 140 mm lateral subsidence, otherwise all the cables would have been pulled simultaneously across the pulleys, by a consistent amount.

3.2.5 Discussion and Summary of Stage 1 Subsurface Subsidence Results

The main purpose of the first phase of the subsurface monitoring study was to develop:

- a better understanding of the mechanisms leading to surface subsidence so that predictive models defining the strata movement can be verified from the mine level through to the surface, and
- obtain information on the likely subsurface strains and movements at aquitard horizons above mine workings and relate these strains/movements to the potential of rupturing major aquitards and causing water inrushes into the mine.

In relation to these objectives, the following significant observations have been noted:

- It appears that remnant coal stooks and fenders can affect the caving and bulking of strata in the immediate vicinity of the goaf edge. This was noted where the lowest extensometer anchor (thought to be sited above a remnant stook) moved less than higher anchors in 2SA and Blue panels. It is not possible to quantify this effect, in terms of strata movements or size of stooks. The ramifications of the effects of remnant coal is that the application of any design criteria established from this study is likely to be site specific and may lead to inaccuracies if used to predict subsidence for other mining techniques such as longwall mining.
- The effect of chain pillars and barrier pillars on surface subsidence was also not clearly defined at this stage. Obvious humps can be detected from plots of surface subsidence above 2B West E1 and 2B West E2 panels - see respective Figures I.16, I.18, I.22 and I.26 in Appendix I. However, the final shape of the 0.9 m deep subsidence above the 13 m wide chain pillars in ACIRL panel was relatively flat. If all the coal was mined in the panel, the expected subsidence would be in the order of 1.5 m; so the chain pillar clearly did affect the subsidence, even though the flat profile would suggest otherwise. Another example of remnant coal fenders affecting surface subsidence was noted along a sealed roadway above 2SA panel where the regular shape of the subsidence trough was disrupted by a localised "hump". This hump - roughly 0.5 m high by eye - is located directly above a 20 m section of coal fender (7 m wide) left in the panel when difficult roof conditions developed in the split.

It has been interpreted that the shape of the subsidence trough will be more affected if the remnant coal or the sandstone above the coal remains intact. Collapse of the "pillar system" will result in full subsidence development, less an adjustment for the remnant coal left behind in this location. Collapse of pillar systems has been described in Section 2.5.5.1 as a mode of subsidence initiation. Further discussion of the stability of the "pillar system" is given in Section 5.3. At this stage, there was insufficient information to provide a definitive reduction factor in subsidence development above collapsed pillar systems of differing dimension. However, as a guide, the 890 mm surface subsidence above the 13 m wide pillar at 150 m depth (average) in ACIRL panel, represents a 36% reduction from what would be expected if all the coal between the two sub-panels was extracted. It is also interesting to note that the 7 m wide strip of remnant fender at 60 m depth in 2SA panel reduced the surface subsidence by 0.5 m, which also represents 64% of the expected Smax. The only other panel with a similar remnant pillar was Red panel, however, this pillar was left near the edge of the panel, and its effect would therefore differ.

The NCB (1975) has provided a predictive chart for estimating the effect of remnant pillars on surface subsidence. The graph, on page 23 of that publication, relates the subsidence reduction factor to pillar widths expressed as a ratio of depth of cover and suggests that for remnant pillars of width/depth of 0.1, the resultant subsidence would be in the order of 40% expected subsidence. This indicates that the weaker Collie Basin sediments tend to collapse more readily around solid coal pillars, thus allowing more subsidence - which is understandable. At this stage, there is insufficient field data to provide a graph for the Collie Basin, comparable to the NCB's empirical chart, for the full range of pillar width to depth dimensions.

- Vertical strains can be affected by the presence of major aquitards which appear to bridge slightly across the goaf area. The act of bridging strata raises doubt on the distributions and importance of vertical strain, as the majority of strain could be confined to the interval immediately beneath the stiffer aquitard horizon in the form of bed separation. For example, the maximum vertical strain measured was 22.5 mm/m - in aquifer 3 - above Blue Panel. The maximum vertical strain measured above aquifer 3 was 9.8 mm/m - in the lower half of aquifer 4 - (in the interval from 101.7 m - 111.4 m). Above aquifer 4 the maximum vertical strains reduce to 5.2 mm/m in aquifer 5, and were negligible in aquifer 6 strata.

- In close proximity to the panel edges, there is an undefined amount (greater than 25 mm and less than 140 mm) of lateral shear along what has been interpreted as major bedding surfaces. This lateral ground movement is supportive of composite beam theory, and is not expected to have unduly affected the extensometer movements above any of the panels.

- The maximum measured surface subsidence above 2SA and Blue panel (at the extensometers) was in the order of 50% of mining height (Figures 3.35 and 3.30). When the 2SA subsidence results are plotted as contour levels, the 50% S/T isopach can be seen to trend subvertically down from near the surface to the lowest anchor, suggesting that the majority of the bulking occurs below the lowest anchor. In the case of the 2SA extensometer, the lowest anchor is only 3 m above the mine, and this assumption is difficult to support. However,considering the fact that, in early stages of panel extraction, this lower anchor moved less than the anchor immediately above, it is likely that the caving and bulking took place either side of the extensometer anchor before the column of strata incorporating the extensometer ultimately collapsed.

- The results from Blue panel in particular, indicate a relationship between the development of subsurface subsidence and extraction width **and** height above the seam. To test this premise a nomogram has been produced for each panel in which the extensometer anchor subsidence (divided by the effective mining height) is plotted against the goaf-extensometer-distance (GED) divided by the height of each anchor (h) above the seam. (By normalising this data, subsurface movements could be more readily compared between panels of differing geometry and depth of cover.) These three plots (Figures 3.37 to 3.39) indicate the degree to which subsurface subsidence increases as the GED (or width of extraction) increases, and also demonstrate how there is less subsidence developed at incrementally larger distances above the seam.

  No explanation is required for the observed relationship with mining width, however, the relationship with height above the seam is less obvious. It can be inferred by the upward trend (from left to right) of each set of data measured after the extraction of each fender, where smaller GED/h values, representing anchors that are further from the mined seam, subside less, and larger GED/h, representing anchors closer to the seam, subside more - particularly when panels are narrow.

ACIRL PANEL EXTENSOMETER ANCHOR MOVEMENTS EXPRESSED AS A DIMENSIONLESS NOMOGRAM

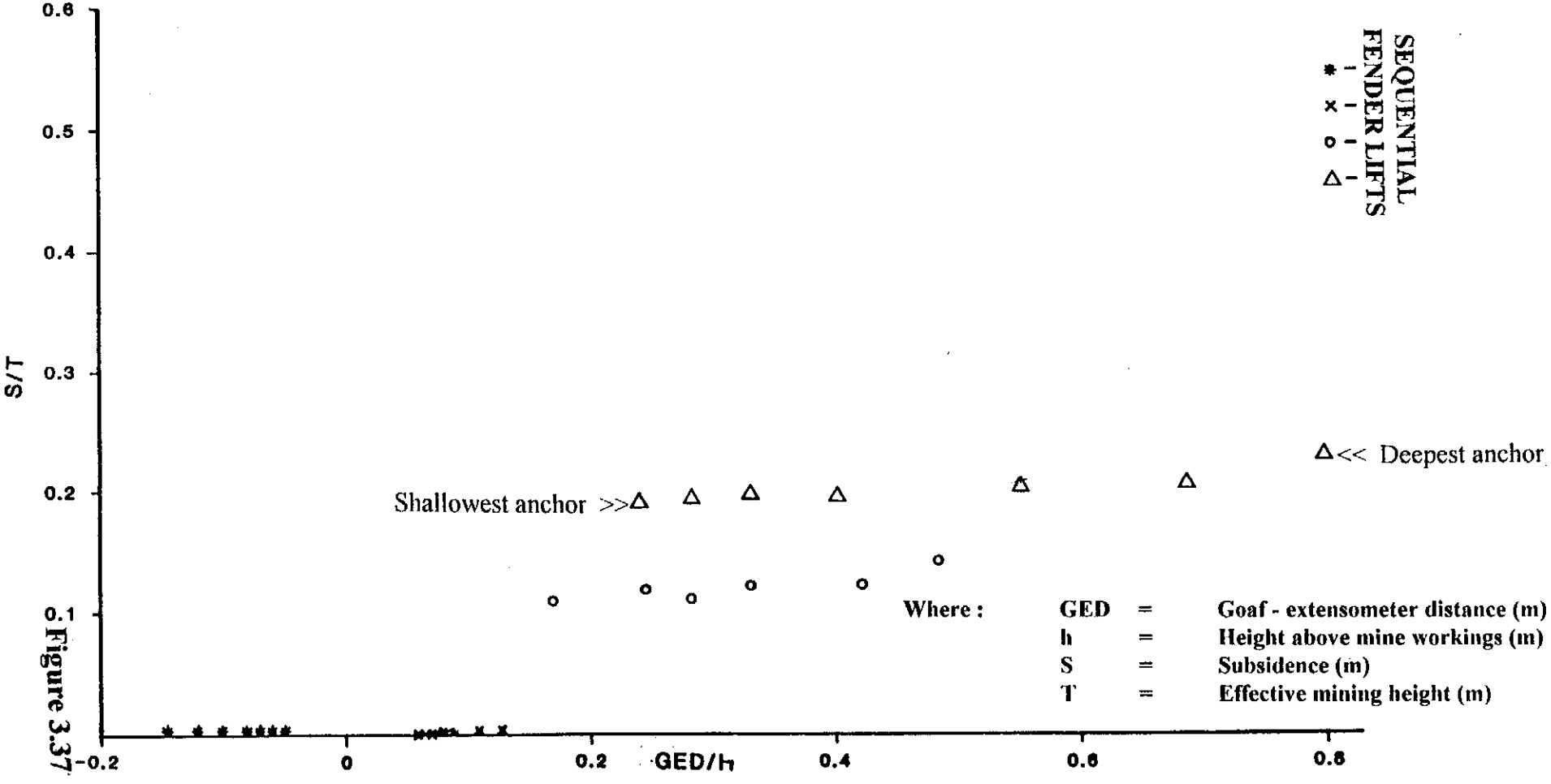

Figure 3.37

BLUE PANEL EXTENSOMETER ANCHOR MOVEMENTS EXPRESSED AS A DIMENSIONLESS NOMOGRAM

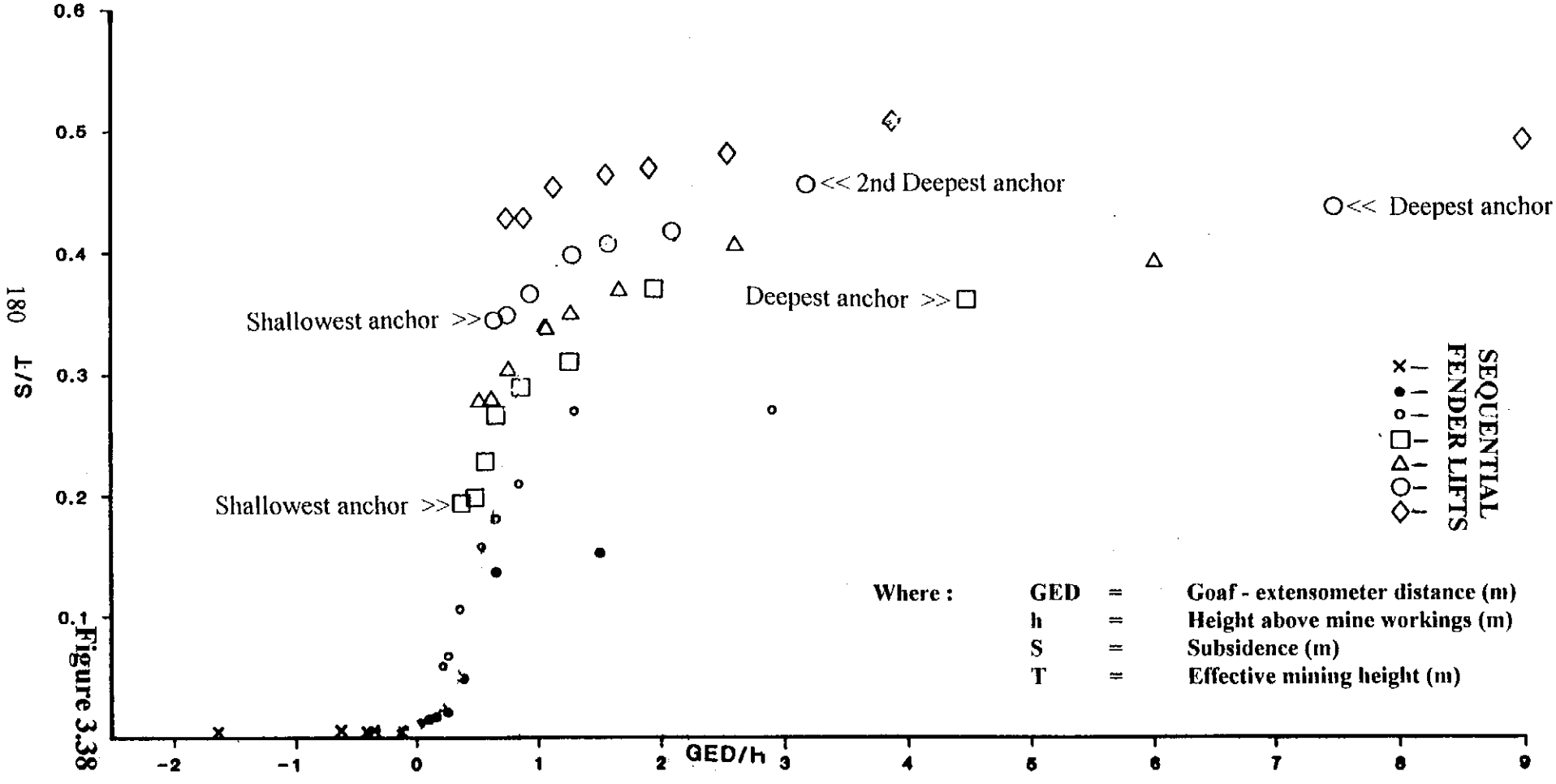

Figure 3.38

2SA PANEL EXTENSOMETER ANCHOR MOVEMENTS EXPRESSED AS A DIMENSIONLESS NOMOGRAM

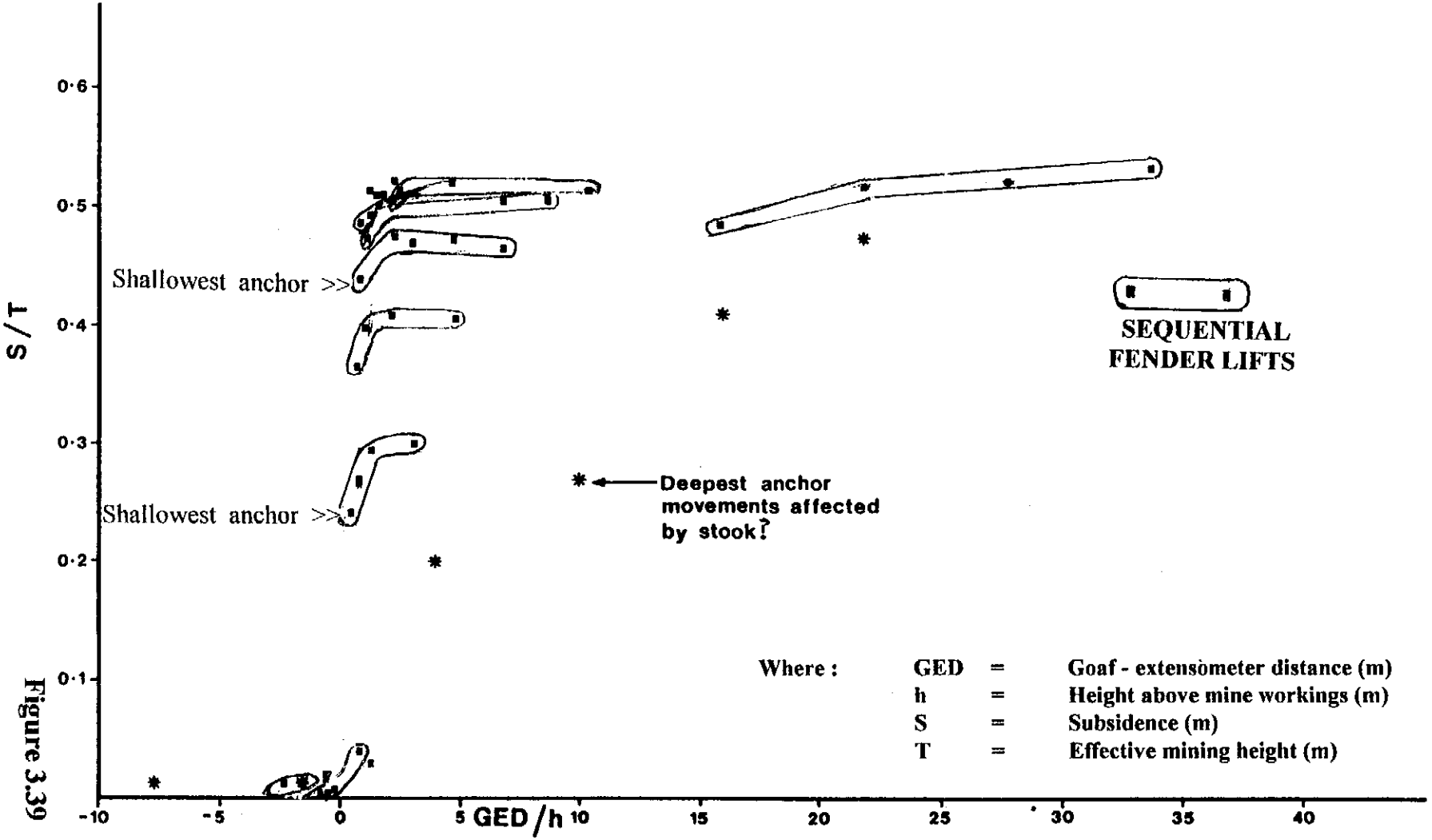

Figure 3.39

It is interesting to note that the data from 2SA panel, when plotted in this manner, displays a stronger trend with height above the seam than was observed when the data was plotted simply as subsidence versus goaf width (Figure 3.34) for each anchor.

- Of particular note from the field subsidence characteristics was the manner in which maximum vertical strains were confined within an angular zone from the mine roof towards the surface, resembling what would be thought of as a line of caving/shear (as noted in Figure 3.31 b). It was therefore postulated that the magnitude of vertical subsurface strains and therefore aquitard integrity was also governed by the relative proximity of any given point to this "line of shear".

  This line of shear concept is further illustrated by Figure 3.40, which plots the Blue panel subsurface subsidence as a normalised function of surface subsidence against GED. If it is assumed that the maximum variation between the surface and each subsurface horizon/anchor represents the point of shearing, the line of maximum separation (as indicated by the nadir of each curve in Figure 3.40) should be relatively consistent at each horizon above the seam. It can be seen that this is the case. It has been interpreted from Figure 3.40 that this line of shear occurs along an angular alignment corresponding to 23° from the vertical, projected from the panel edge. This compares well with the data from ACIRL panel, for example, when the GED was 20 m, the highest anchor to move significantly more than the surface was at 48 m above the mine, equating to a line of shear of 23°.

  Figure 3.40 also demonstrates that the variation between subsurface and surface subsidence is systematically reduced the closer the anchors are to the surface. This demonstrates another variation of the change in subsidence development (change according to the height above the seam) - discussed below.

- Due to the relative consistency of the data **trends** from the stage 1 study, an attempt was made to develop a chart for predicting subsurface subsidence from the mine horizon to the surface for panels of any dimension and depth of cover.

  At the time the only available subsurface data was from the ACIRL, 2SA, and Blue panels, of which the data from ACIRL and 2SA panels were considered to be of little value. (It was thought that subsidence above the 7 m wide coal fender left near the ACIRL panel extensometer may have influenced subsidence development, and the shallow, relatively unconsolidated, material above 2SA panel may be unrepresentative of caving at depth.)

SUBSURFACE SUBSIDENCE AS A RATIO OF SURFACE SUBSIDENCE

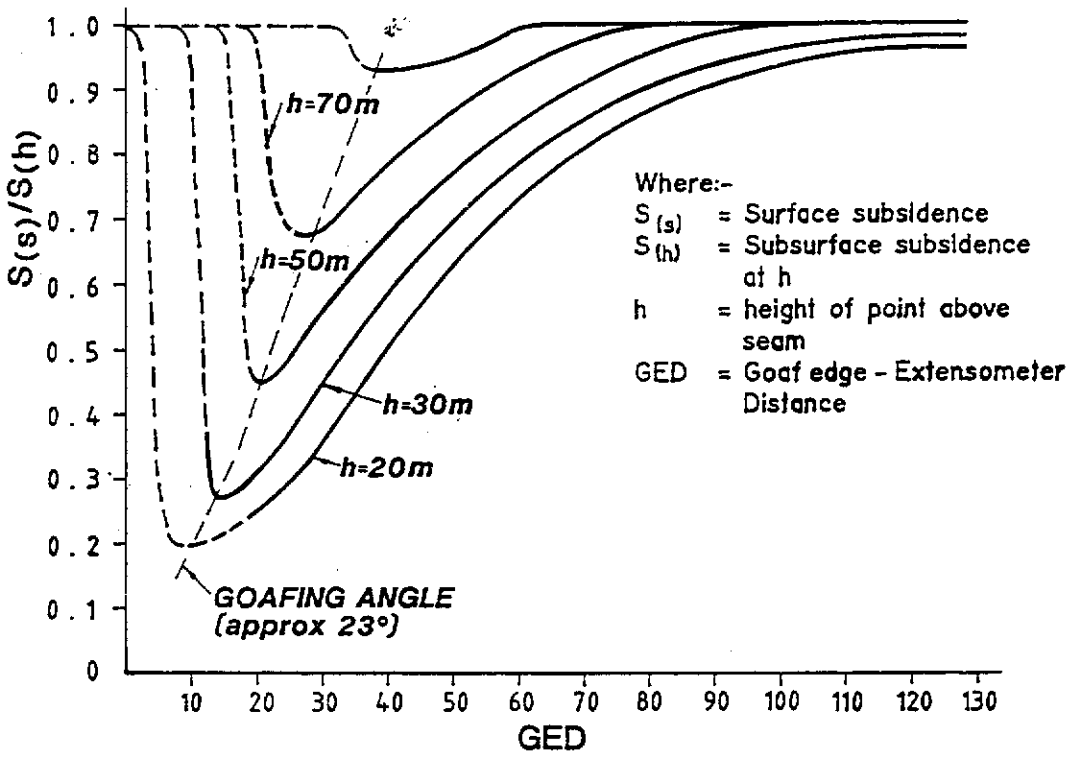

Figure 3.40

SUBSURFACE SUBSIDENCE PREDICTION - COLLIE BASIN

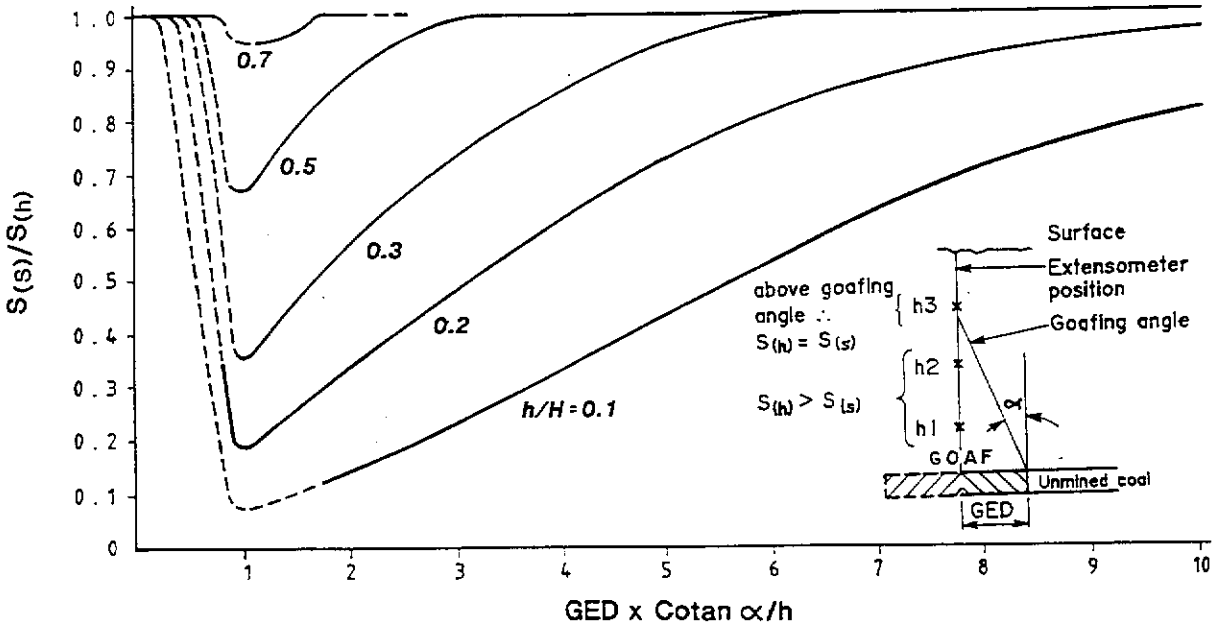

Where:- $S_{(s)}$ = Surface subsidence
$S_{(h)}$ = Subsidence at h above
GED = Goaf edge - Extensometer Distance
∝ = goafing angle (23°)
h = height above seam

Figure 3.41

Consequently, the investigation was based only on Blue panel data, which in itself is not ideal, as this panel is critical width (W/H = 1.14) and complete surface subsidence would therefore not have developed. However, it was thought that this would have minimal effect on the overall investigation because once critical width has been reached, the only information lacking would be the final stages of reconsolidation, which could probably be estimated from trends in the data.

After extensive manipulation of the data, it was established that the development of subsurface subsidence could be represented as a dimensionless nomogram (Figure 3.41), where:

- The X axis in this nomogram represents the position of the anchor at any horizon above the seam given in relation to the position of the line of shear [GED x Cotan(shear angle) ÷ height above worked seam (h)].
- The Y axis represents the ratio of surface subsidence (Ss), measured at the position of the extensometer, to the anchor subsidence (Sh) - as in Figure 3.40.

Each curve on the graph represents the position of an extensometer anchor expressed as a ratio of height above the worked seam (h) to the depth of cover (H). When this ratio is small, the respective anchors are nearer the seam. As the h/H ratio approaches unity, the respective anchor/aquitard is nearing the ground surface.

From this nomogram, a number of trends in subsidence development can be identified:

> When the dimensionless X-axis in Figure 3.41 reaches unity (equating to the position of the line of shear) the maximum separation between surface and subsurface subsidence is developed at all horizons.

> Prior to this line of shear reaching the position of the anchors/subsurface horizons (when the dimensionless X-axis in Figure 3.41 is less than 1.0) the trend is for the subsurface to move less than the surface. Note the data above the line representing Ss/Sh = 1.0 is not included due their insufficient quantity and quality.

> The further the anchor/subsurface horizon is below the projected line of shear, the greater the expectation for reconsolidation of the caved mass, and the greater the tendency for the subsurface to subside similarly to the surface.

The structure of the curves in Figure 3.41 are such that, knowing the **surface** subsidence at any point above an extraction panel, the **subsurface** subsidence at any horizon above the caved section of the panel can be predicted. In fact, after thorough investigation of these trends, it was found that the series of curves could be estimated mathematically as well as graphically. The form of the equation is:

$$Ss/Sh = (1/z \times \{GED \times \cot an\ \alpha/h\})^2 + a \times (1 - \exp [-k \times (\{GED \times \cot an\ \alpha/h\} - z)]) \quad 3.2(1)$$

Where:

Ss	=	surface subsidence,
Sh	=	subsidence at height (h) above the mine
GED	=	Goaf to Extensometer Distance
α	=	angle of shear
a, k, z	=	variables dependent on the h/H ratio of the anchor.

The relationships of each variable (a, k and z) with h/H are defined by the terms:

$$a = 1.004 - (h/H \times 0.039) \quad 3.2(2)$$

$$k = 1.6 \times \exp[-3.9 \times \exp \{h/H \times 5.1\}] \quad 3.2(3)$$

$$z = [2.4 \times \{1/(h/H \times 8.5)\}^{1.3}] + 0.95 \quad 3.2(4)$$

A comparison of the curves predicted by Equation 3.2(1) and the field data is presented in Figure 3.42. Generally, the predicted curves match reasonably well with the field data. It can be seen that there is a small error to the right hand side of the nadir of the curves representing anchors with a h/H ratio greater than 0.5 - where the predicted subsurface subsidence is slightly greater than surface subsidence. It is therefore recommended that a limiting Ss/Sh value of 1.0 be applied once the calculated Ss/Sh values reach 1.0.

It is possible to obtain better fits for each h/H curve, however, as it is necessary to develop a generic mathematical relationship for all potential anchor locations, the variables needed to represent a compromise between the statistical best fit and the observed best fit through the full range of data. When using statistical best fits the curves for the shallower anchors give rise to greater error.

COMPARISON OF CURVE FIT EQUATION TO SUBSURFACE SUBSIDENCE NOMOGRAM

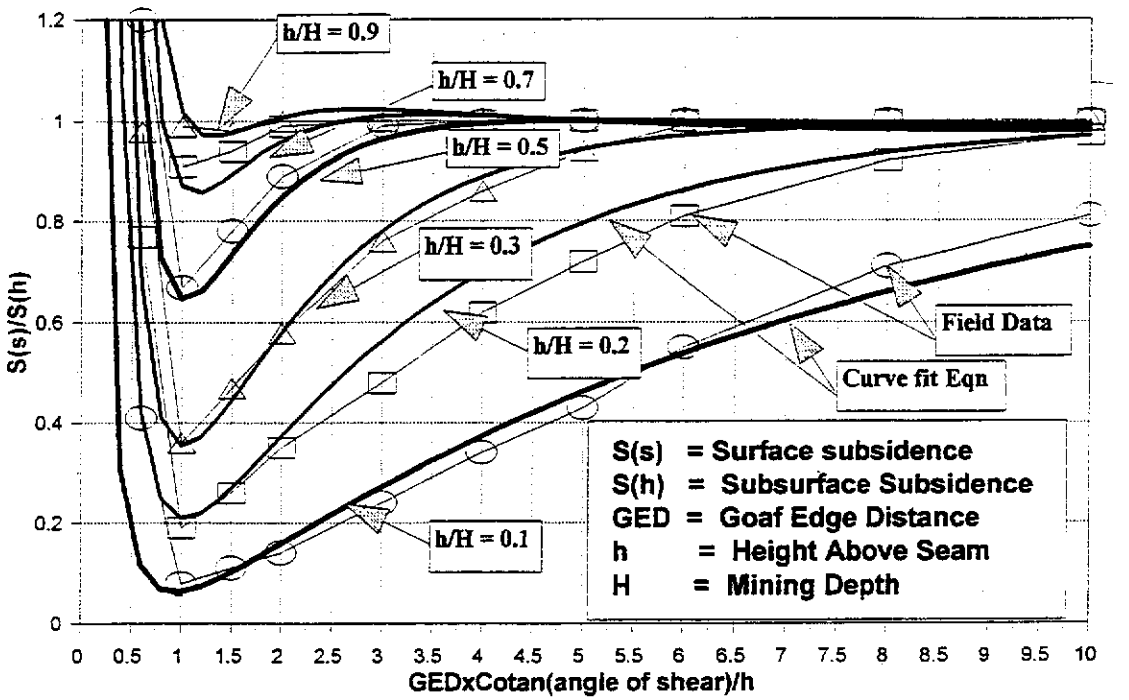

General form of equation = (1/z x GED x Cotan(AoS)/h)^2 + a[1-(0.64 x exp(-k{(GED x Cotan(AoS)/h) - z}))]

AoS = Angle of shear

Figure 3.42

The two main limitations of this predictive equation and nomogram are that subsurface subsidence cannot be determined until the panel is wide enough to express subsidence at the surface, and that the curves do not match **expected** Ss/Sh subsidence until the line of shear reaches and extends above the position of an anchor (until that particular horizon has sheared).

With regard to the second limitation, it can be expected that immediately prior to the line of shear reaching the position of an extensometer anchor, the surface will have subsided more than the anchor. Thus the Ss/Sh values would be greater than 1.0 and would tend to infinity for anchors where there is minimal subsurface subsidence compared to the surface subsidence. Although the curves generated by Equation 3.2(1) do display such trends, the field data from Blue and ACIRL panels do not show this expected trend. When the goaf edge was below the position of the Blue panel extensometer, and the surface subsidence was 52 mm, there was no differential subsurface subsidence, suggesting that the whole ground mass moved as one, by 52 mm.

It is interesting to note that the surface above the 2SA panel **did** converge on the extensometer anchors when the GED was 3 m short of the extensometer (as illustrated in Figure 3.32 between 180 and 800 hrs on the Y-axis). However, it is unclear to what extent this convergence is due to either near-surface subsidence or compression of the weak strata above the solid coal abutment (by elevated tributary loading). Elastic/plastic compression would be expected due to the elevated tributary loads at the panel abutment, similarly to that proposed by Heytenyi (1964) for beams on elastic foundations. Furthermore, when tributary loads exceed the shear strength of the abutment strata, crushing can be expected to take place.

Although the curves predicted by Equation 3.2(1) when {GED x cotan α / h} is less than 1.0 do follow a trend similar to that expected in the field, the shape of each curve above Ss/Sh = 1.0 does not compare with that expected in the field. It would be expected that before the line of shear reaches any particular anchor, (when {GED x cotan α / h} < 1.0), the Ss/Sh ratio will be less for anchors closer to the surface than anchors closer to the seam, rather than similar Ss/Sh values for all anchors as predicted by Equation 3.2(1). It is concluded that because there is inadequate field data for the early stages of subsidence development to compare against curve fitting equations, there would be little benefit from further refining the predictive equations at this stage.

3.2.6 Stage 2 Subsurface Subsidence Investigation - 1 NORTH B PANEL

The purpose of this stage of investigation was to further research any facets from stage 1 investigation requiring clearer definition. This was to be achieved by setting up specific monitoring strategies above another trial panel. Of the observations made in the stage 1 investigation, it was considered that the first objective would be to better define the development of subsidence during early stages of extraction. Another important goal was to cross-check the subsurface prediction nomogram developed from the stage 1 investigation. The only suitable extraction panel available for monitoring surface and subsurface subsidence was 1 North B Panel in the WD6 mine (1North panel). This panel was 507 m long and typically 330 m wide, and the cover depth varied from approximately 50 m to 100 m. The 1North panel was therefore well in excess of critical width and would be expected to develop maximum subsidence. As the panel was located below unimproved bushland, there was no need to design the panel to protect surface features.

The main disadvantages of this panel were that the panel was at shallow depth with few aquifers, and each of the superimposed aquifers had been drained for some time due to continual seepage into the surrounding mine bords. (At the position of maximum depth of cover, approximately 100 m at the southern boundary of the panel, only two "confined" aquifers - aquifers 2 and 3 - and one unconfined aquifer - aquifer 4 - were present. At depths shallower than 70 m only one confined aquifer - aquifer 2 - was present above the panel.) Thus detailed analysis of the effects of subsidence on the integrity of higher aquifer systems was not possible.

Two borehole extensometers were installed close to the panel edges (see Figure 3.43) to observe both narrow panel subsidence and near-panel-edge effects. They were positioned at the maximum possible depth of cover, and at the minimum allowable distance away from the southern edge of the panel to avoid panel edge effects from the southern abutment. The aim was to incorporate the maximum number of aquifers/aquitards within the superimposed stratigraphy; in this case, aquifers 2, 3, and 4 within the zone of investigation (Figure 3.44). The first extensometer (D212) was located 6 m inside the panel edge to investigate the caving/shearing characteristics at the edge of the panel. Of particular interest was the possible development of bed separations, the sequence of caving events, and the apparent crushing or shearing of strata above the panel abutments - as noted in 2SA panel.

BOREHOLE EXTENSOMETER AND SUBSIDENCE GRID LOCATION PLAN - 1 NORTH PANEL WD6

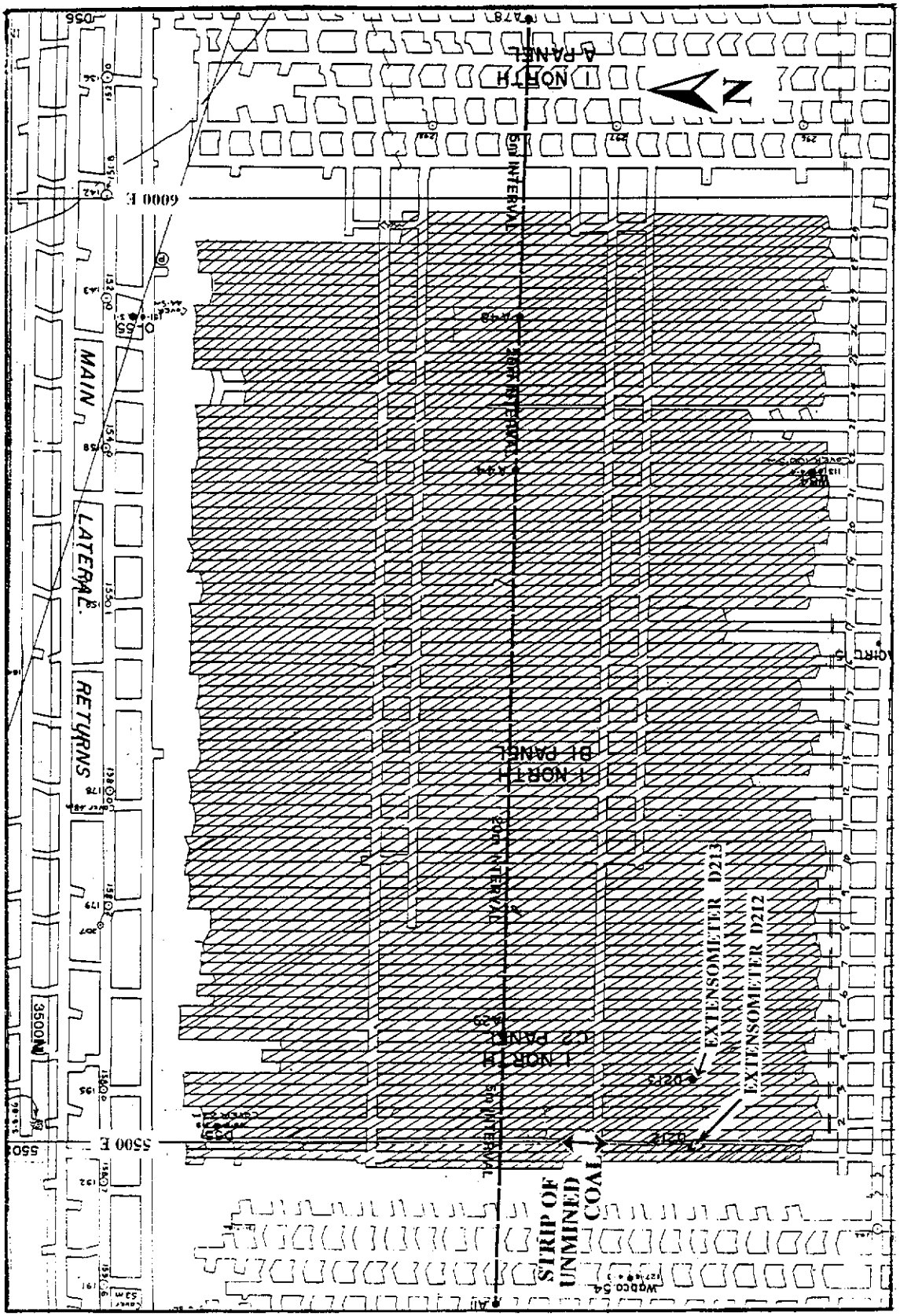

Figure 3.43

D212 AND D213 BOREHOLE EXTENSOMETER SET-UP 1 NORTH PANEL WD6

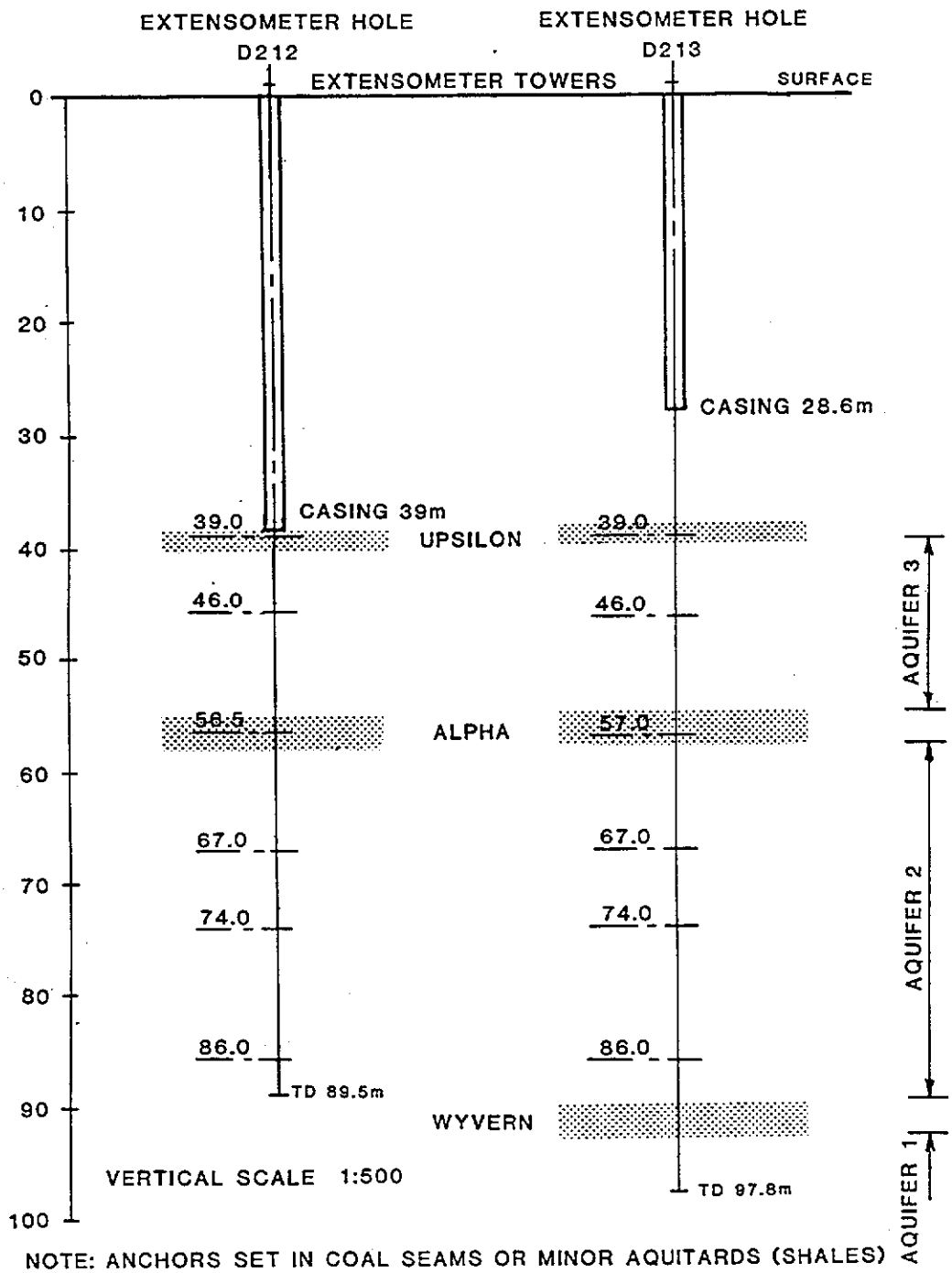

NOTE: ANCHORS SET IN COAL SEAMS OR MINOR AQUITARDS (SHALES)
NO STANDING WATER LEVEL DETECTED

Figure 3.44

The second consideration was to place both extensometers sufficiently far away from the southern abutment to avoid panel edge effects. The extensometers therefore needed to be installed where maximum subsidence would first be expected to be developed away from the panel edge. The projected location of this point of maximum subsidence was determined from Figure 3.11 as the point where the subsidence curve effectively reaches its nadir (at a distance 32% of the cover depth from the point of inflection). Assuming that the inflection point is located a horizontal distance inside the panel edge equating to 17% of mining cover depth (see Sections 2.5.5.2 and 3.1.4), the extensometer needed to be sited a horizontal distance of (0.32 + 0.17) x H from the panel edge. As the southern edge was approximately 100 m deep, the minimum distance the extensometer could be installed from this edge was 49 m. It was decided that a 10 m buffer be added to this distance to allow for any irregularities in the lengths of stubs left at the ends of panel splits - which was common in earlier panels. The resultant step-off distance (59 m) placed the extensometers at 92 m cover depth.

The horizontal distance between the western panel edge and the second extensometer is therefore: 92 x 0.49 = 45 m.

Due to the mining problems associated with trialing the JCM12, the left hand fender of the first split was not lifted off/extracted along much of the split. One of the places where the fender was not mined was opposite the extensometers. The distance separating the panel edge from the extensometer was 43 m, which is 2 m closer to the edge than planned. This, however, is interpreted to have had minimal impact on the quality of measured data as the change in subsidence predicted by the profile function [Equation 3.1(7)] for D/H > 0.29 is negligible.

The results from monitoring each borehole extensometer are illustrated in Figures 3.45 to 3.52. These plots present anchor movements as total subsidence (in Reduced Level) and as subsidence in relation to extensometer the datum point, plotted against both time, and goaf width.

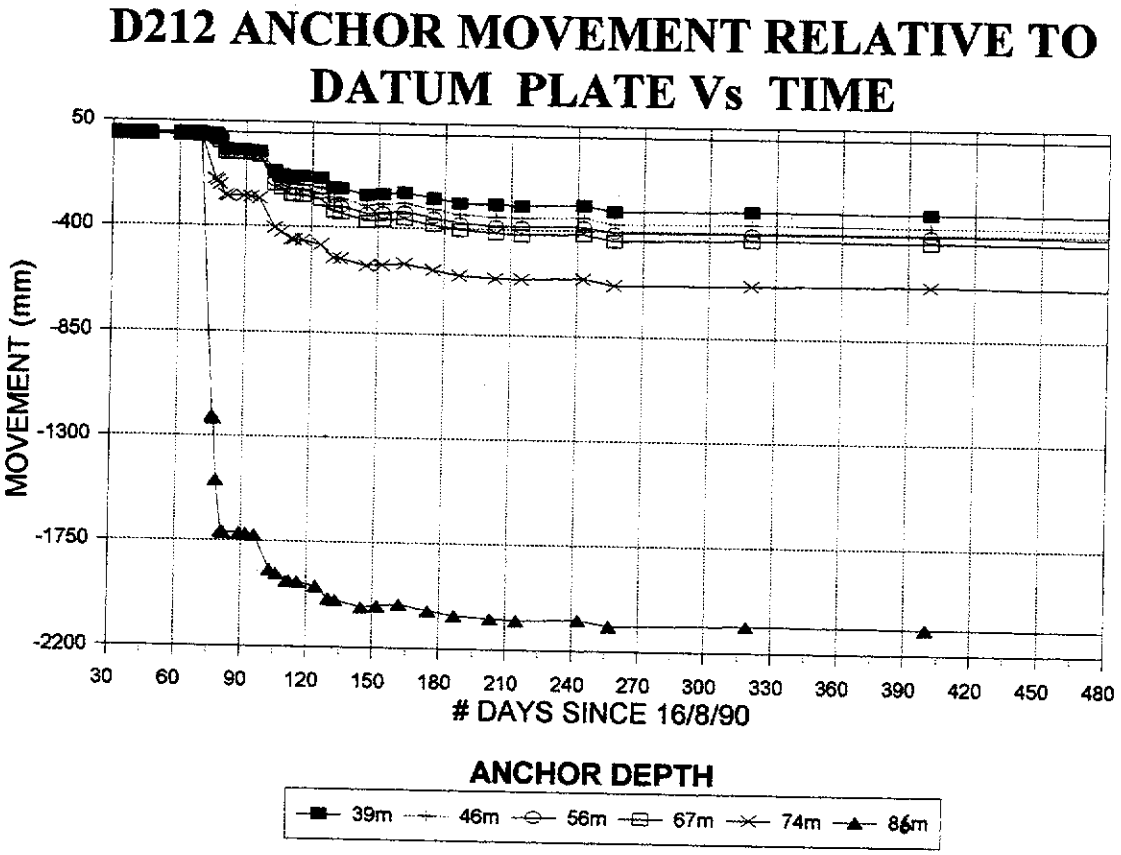

Figure 3.45

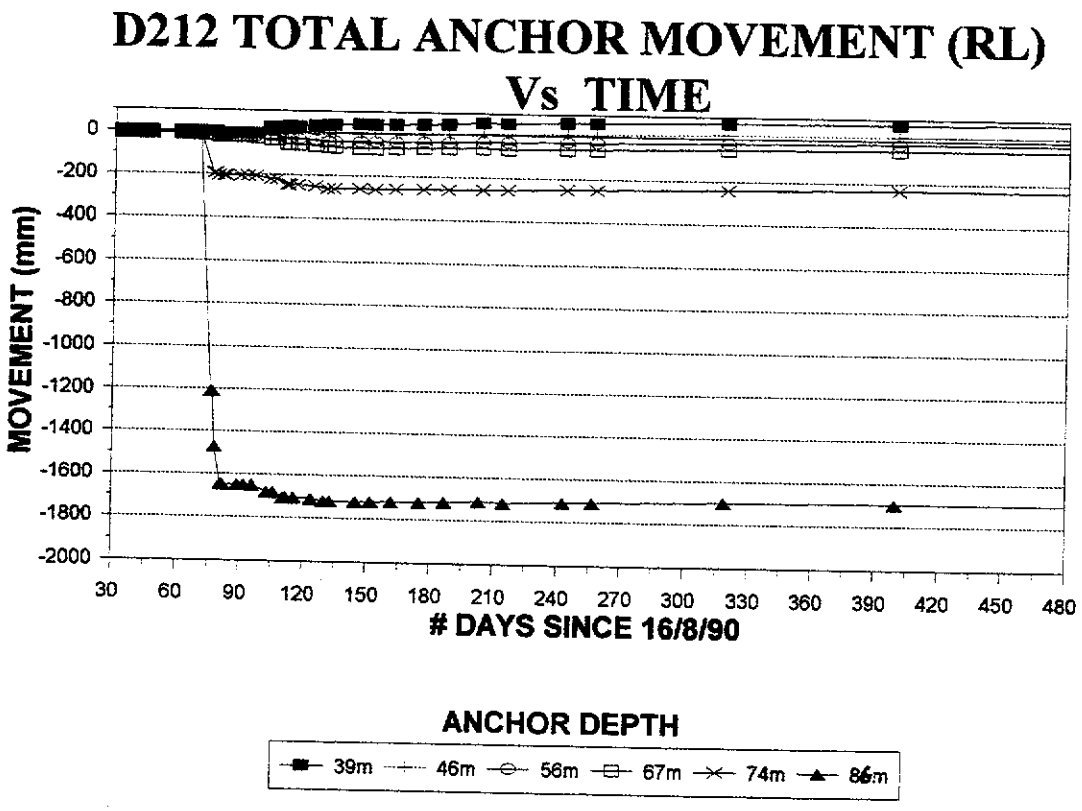

Figure 3.46

D212 ANCHOR MOVEMENT Vs GOAF WIDTH IN REDUCED LEVEL

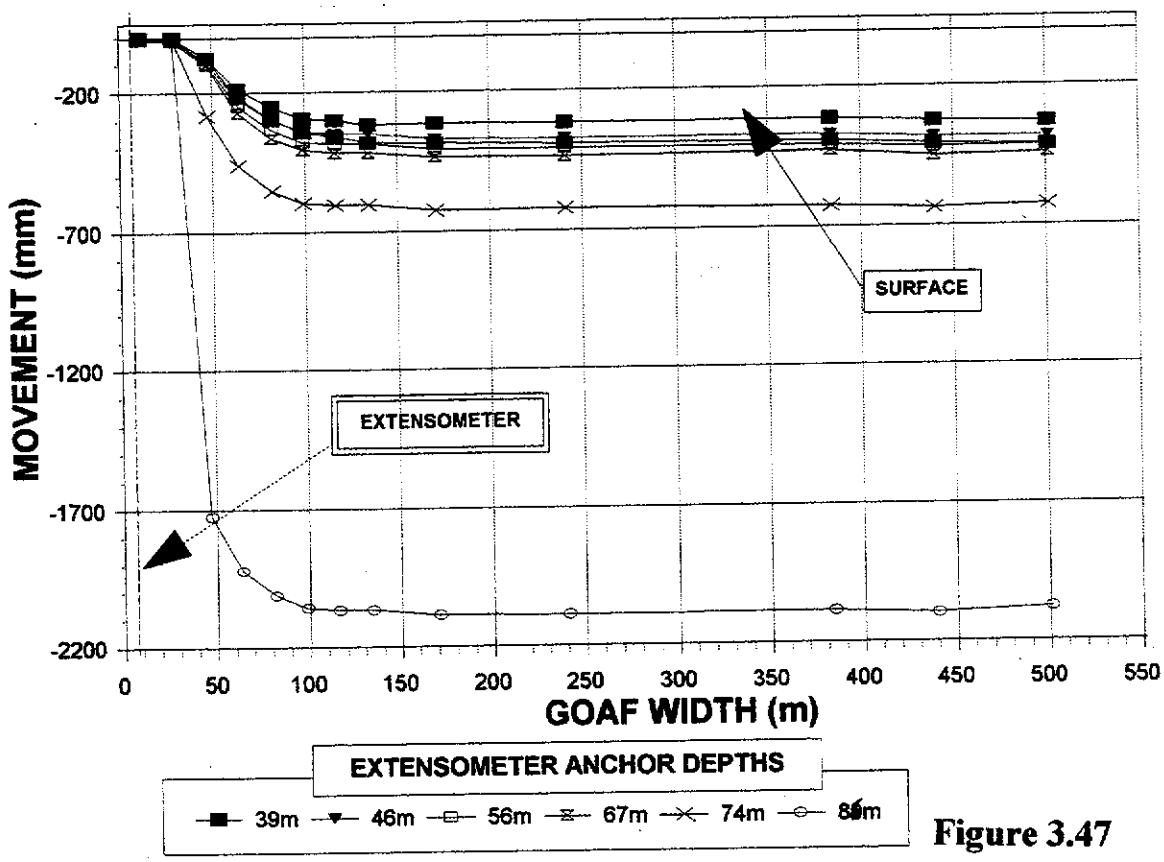

Figure 3.47

D212 ANCHOR MOVEMENT Vs GOAF WIDTH RELATIVE TO DATUM PLATE

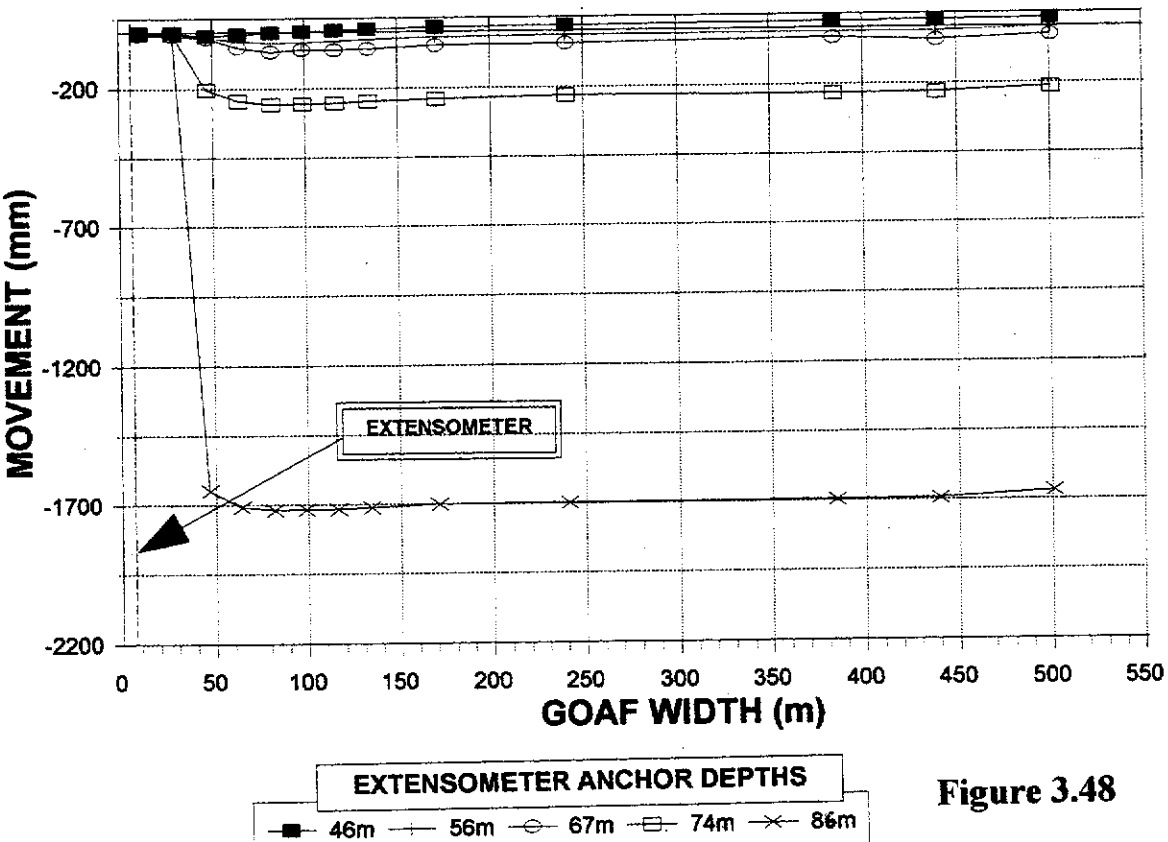

Figure 3.48

D213 ANCHOR MOVEMENT (RL) Vs TIME

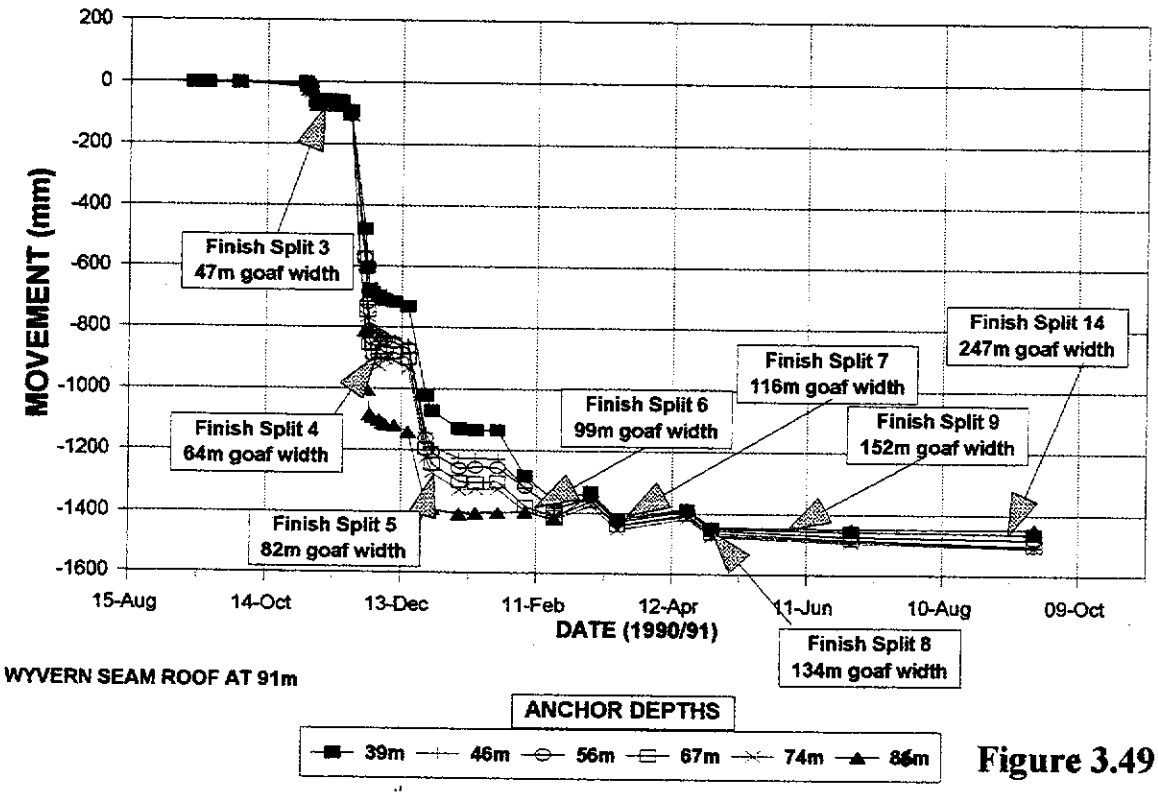

Figure 3.49

D213 ANCHOR MOVEMENT RELATIVE TO DATUM PLATE Vs TIME

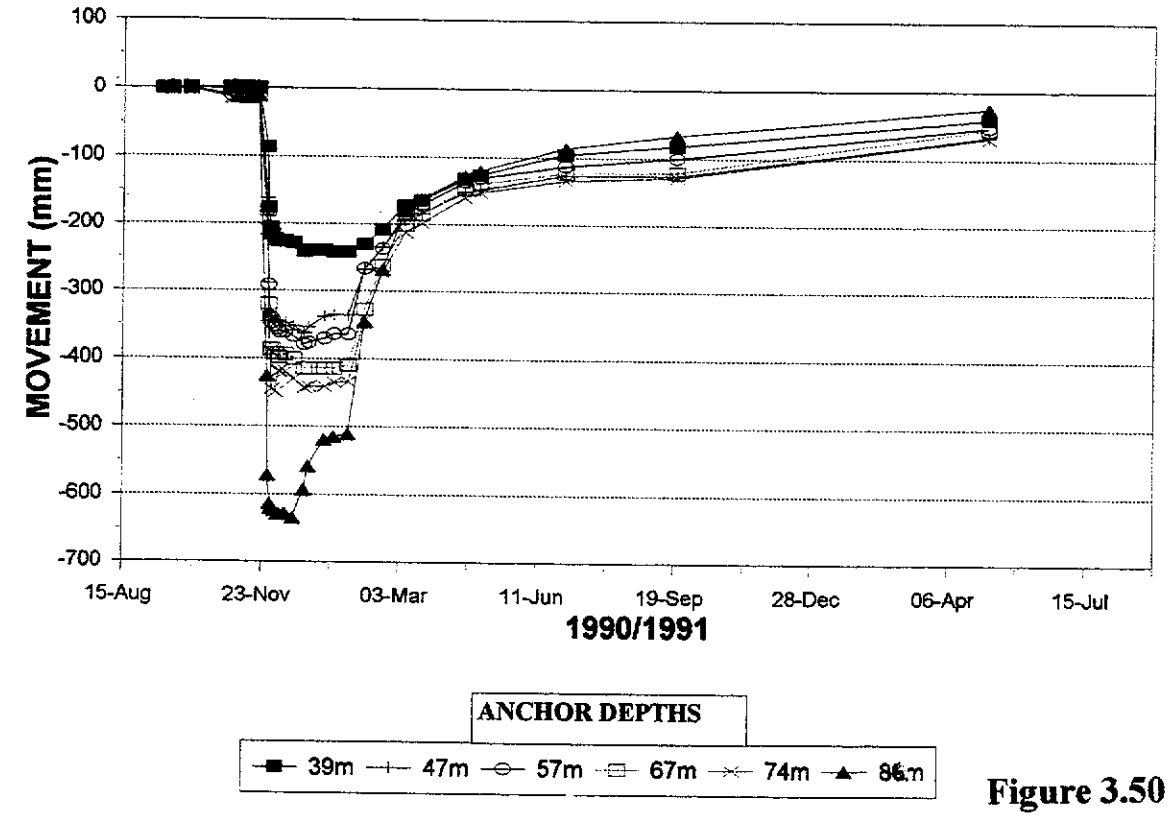

Figure 3.50

D213 ANCHOR MOVEMENT Vs GOAF WIDTH IN REDUCED LEVEL

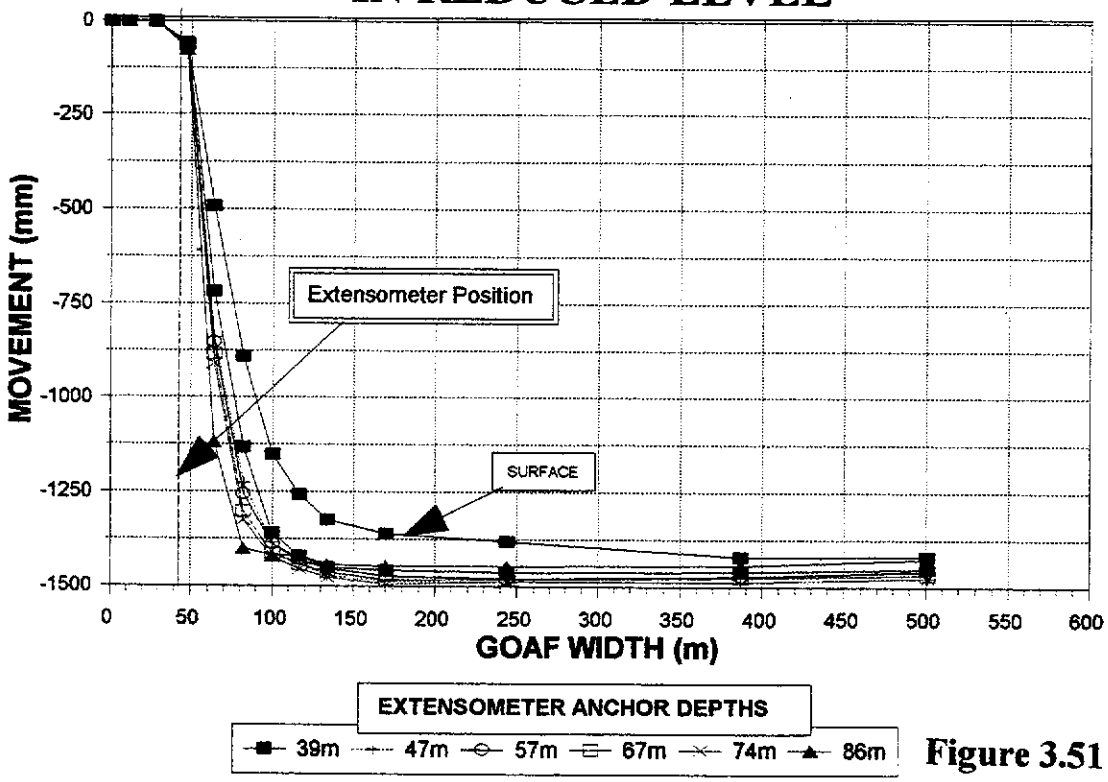

Figure 3.51

D213 ANCHOR MOVEMENT Vs GOAF WIDTH RELATIVE TO DATUM PLATE

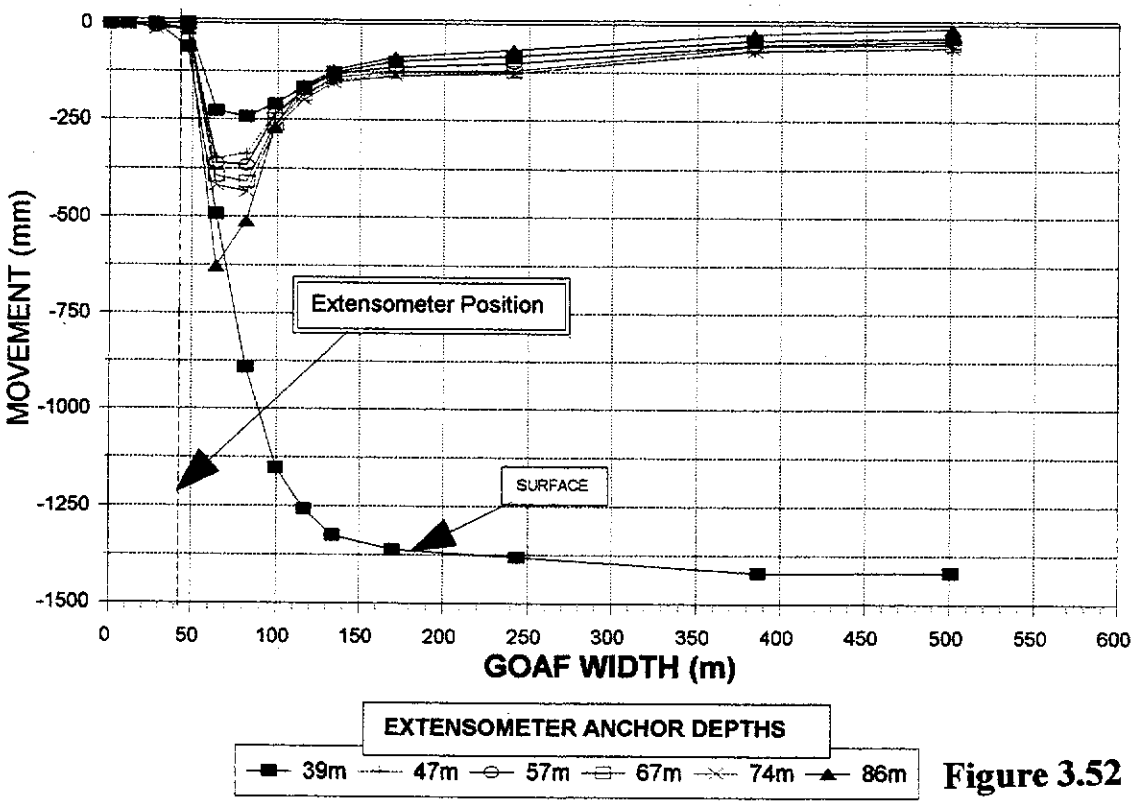

Figure 3.52

The main conclusions made from this phase of investigation are listed below:

- Large-scale subsurface subsidence was not noted in the extensometer recordings until the width of coal extracted from the panel reached 54 m. This subsidence-initiating extraction width is slightly greater than that observed in other panels of similar depth, however, the extent of support provided by the remnant slices of coal left in the first two fenders (2-4 m wide) cannot be determined.
- Figures 3.46 and 3.50, which represent anchor movements with time relative to the datum plate for each extensometer, illustrate that anchor separations occurring toward the panel edge tend to remain, whereas further toward the centre of the panel, the vertical separation between anchors reduce (as mining progresses) to distances approximating pre-mining conditions.
- The increase in separation between anchors, particularly near the surface, is considered to be largely due to shear dilation of the constituent sandstone grains within the general mass of strata. This is supported by Figure 3.40 which illustrates the angular trend in separation between successive anchors and the ground surface as the panel widens. If it is assumed that the overlying shallow, weak sandstone collapses and sags readily once the stiff aquitard has subsided (as would be expected by beam theory), then this increased separation is best explained by some form of dilation of the sediments. An example of shallow dilation can be noted in Figure 3.46, where the final separation between the 39 m and 56 m anchors of extensometer D212, located near the panel edge, is in the order of 150 mm. Another example of dilation can be seen in Figure 3.51, where the separation between the surface and shallowest anchor in extensometer D213 reached a maximum of approximately 200 mm at a goaf width of 80 m.
- The results plotted in Figure 3.45, in particular, indicate that the reason why Smax does not attain 100% mining height, is largely due to the bulking of caved strata within 6 m of the mine roof. This is evidenced by the fact that the lowest anchor (86 m deep, or 5 m above the mine roof) in extensometer D212 subsided approximately 2.0 m and maintained 1700 mm separation from the surface. If this anchor and cable unit were not affected by caving, then this subsidence represents 65% full mining height - 2.6 m. All extensometer anchors above this deepest anchor closely resembled the subsidence recorded at the surface (once the W/H ratio exceeds critical width).

  For future reference, this first caving of the roof has been termed **primary** caving.

- Whilst the general trends of subsurface subsidence at each of the aquitard horizons above 1North panel match well with the generic subsurface subsidence developed from previous extractions panels (see Figure 3.53), the individual curves of each nomogram do not overlay accurately. The major differences are:

  - The ratio of subsurface subsidence to surface subsidence in the early stages of panel extraction is less in the "generic" nomogram. This indicates that the ground mass above 1 North panel is tending to subside with either more surface subsidence or less subsurface subsidence at equivalent points. It is understandable that there is less variation between surface and subsurface subsidence, as more than 50% of the strata above 1 North panel was geologically logged as loose sand/stone and could not be "cored" during drilling. Details of laboratory testing provided in Appendix III illustrate that a triaxial test on a sample of loose "sandstone" taken from 52 m (13 m below the major aquitard Upsilon seam) had a shear strength of 39° and zero cohesion. This is only marginally greater than the shear strength of compacted waste dumps in the open cut (personal experience). Samples taken from shallower horizons gave slightly lower strengths.

    Less variation between surface and subsurface subsidence can also be expected as the two extensometers were located in the area of secondary ("one-piece") caving of ground (see the discussion regarding the development of a surface "hump" above 1North and 2SA panels given in Sections 3.1 and 3.3) which by definition collapses in one piece and bulks less, thereby initiating more subsidence higher in the sequence.

    It is also possible that this discrepancy may have been affected by the thin strip of coal left behind during extraction of fenders 1 and 2, which did not allow full caving until a significant width of extraction. Therefore more surface subsidence would have developed at the time of subsidence initiation.

  - The rate of reconsolidation between the surface and subsurface horizons is steeper in the generic nomogram which is based on the 150 m deep Blue Panel. This would be expected as the tributary loads must be greater in deeper panels.

COMPARISON OF 1 NORTH PANEL SUBSURFACE DATA AGAINST THE GENERIC SUBSURFACE SUBSIDENCE NOMOGRAM

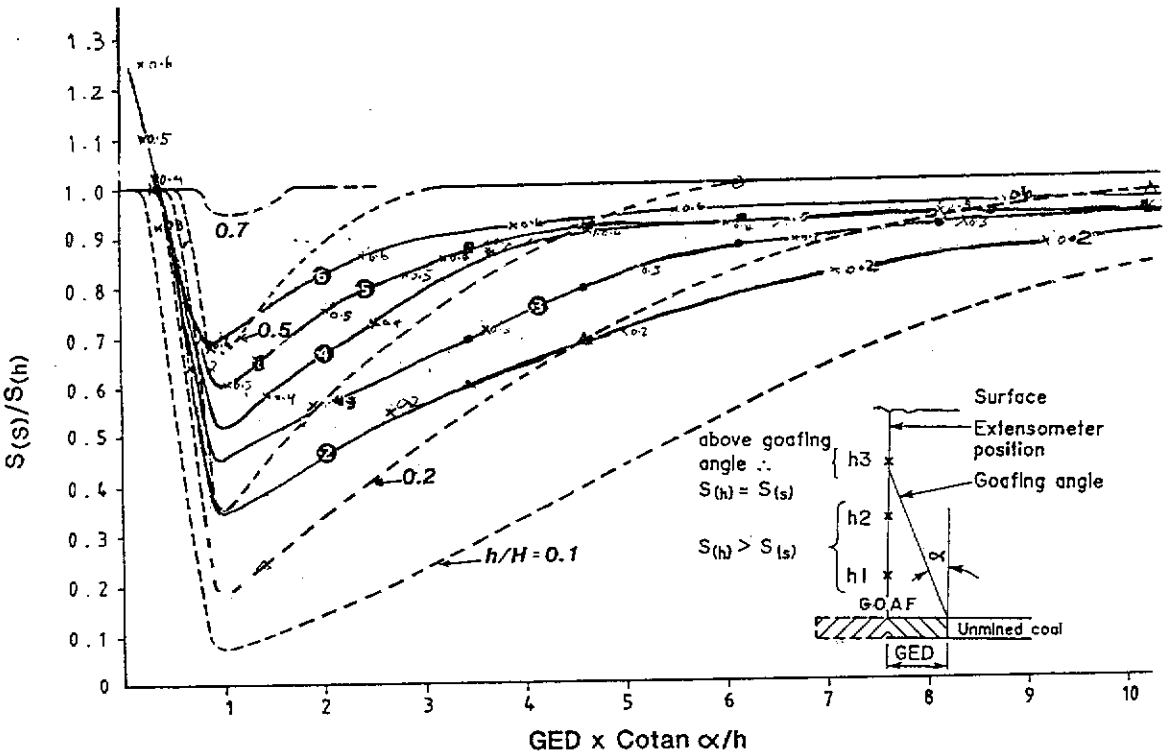

Figure 3.53

- In both nomograms the point where Ss/Sh is smallest (where the separation between subsurface anchors and the surface is largest) is where the GED x Cotan(Angle of shear)/h ratio approaches unity - see Figure 3.41 for a description of these terms.
- When the line of shear approaches any given point above the panel the rate of separation is very steep. This suggests that in this event the stratum in question is undergoing high strain energy and is therefore likely rupture in shear. Therefore a case can be made for defining the aquitard integrity by the ratio of GED x Cotan(Aos)/h.
- Once subsurface subsidence was initiated above 1 North panel, all the aquitards had subsided (and ruptured?) and the surface subsidence compressive hump (discussed in Section 3.1) developed. This indicates that the critical width for total failure of aquitards above this panel is between 34 and 54 m, although the effect of the remnant slice of fender at the start of the panel cannot be quantified.

3.3 FIELD STUDY CONCLUSIONS

The results from this field study have demonstrated that total extraction of coal in the Collie Basin (using the Wongawilli mining method), unlike the expert opinion provided before this research project, does not produce ubiquitous destructive pot-hole type subsidence. Infact, it is more common for the gentle subsidence trough form of subsidence to develop above total extraction panels. Furthermore, the local trough shape subsidence that is developed has many similar characteristics to that developed in other mining regions - e.g. the eastern Australian coalfields, and the Appalachian coalfields in the USA. One of the most notable comparisons between the three coal regions is a subsidence factor of 63% of effective mining height.

As for all other mining regions, the potential for surface subsidence to develop from the collapse of mine roof in the Collie Basin is dependent on the dimension of the collapse and the ability of the superincumbent strata to bridge across the collapse thus preventing deflection of the ground surface. Once an initiating width of extraction has been exceeded (field data suggest that the initiation width is approximately 25% depth of cover), surface subsidence will be manifested.

3.3.1 FACTORS AFFECTING SUBSIDENCE IN THE COLLIE BASIN

The shape of the subsided surface above mine workings is influenced by the geology (and depth of cover), the bulking characteristics of the collapsed ground, the presence of remnant coal, and the mine design, mining height, and extraction methods. In certain conditions, each of these parameters can control whether surface subsidence will be "discontinuous" or "continuous", although the primary factor controlling discontinuous subsidence is geology/depth of cover.

Geology

- The potential for discontinuous subsidence will be greatly reduced by the presence of a stiff, sufficiently thick, layer which can bridge across the collapsed ground and not shear at the edges. The best example of this effect is the subsidence noted above the Premier colliery. Here, the locations of the pot-hole subsidence has been clearly restricted to areas above of the lineament of the subcrop of a 2 m thick coal seam, 5 to 7 m above the mined Premier seam. At the Premier site, the limiting depth for discontinuous subsidence was between 15 and 20 m. Within WCL's underground mining leases, the presence of stiff strata is usually restricted to depths greater than 40 m. Therefore, at depths greater than 40 m, under normal geological and mining conditions in the Collie Basin, it can be expected that continuous subsidence will develop. (Note: The term shallow in the remaining paragraphs pertains to areas without a major aquitard/stiff layer above the mine workings.)

- The shape and form of surface subsidence above shallow workings can be influenced by the geology of the near surface strata. Mining areas with a predominance of Tertiary sands will have little resistance to shear and will therefore develop more discontinuous forms of subsidence.

- The presence of pockets or layers of unconsolidated, water-saturated strata can result in a "slurry" run into the mine. This can give rise to large potholes which can be many times deeper than the mining height (Figure 3.3). The presence of these materials is not widespread, however, it is common for pockets of this material to develop at the subcrops of coal seams.

- The presence of faults, relict tension joints or even tree roots can provide planes of weakness for shearing through to the surface. Resulting potholes can have

straight, almost smooth edges (as illustrated in lower section of the upper photograph in Figure 3.3, which is affected by relict jointing and tree roots).

Bulking characteristics of collapsed ground

When a section of ground collapses into the mine, the broken rock rotates randomly and occupies a greater volume (bulks). This bulking process reduces the maximum subsidence developed above an extraction panel. Results from 1North panel indicate that it is largely the bulking within the immediate 6 to 8 m of mine roof which reduces the maximum surface subsidence developed in the Collie Basin to 63% mining height. The effect of variable bulking on subsidence development has been demonstrated by:

- Very soft and wet overlying strata above 2B West E1 panel which did not bulk and thereby provided minimal support to the overlying strata and allowed pot-hole subsidence to develop. It follows that if no support is provided by the collapsed goaf, large-scale shearing can continue through to the surface.
- Rilling of goaf material into adjacent bord and pillar roadways. Such rilling can greatly reduce the bulking process and can result in discontinuous subsidence (at shallow depths of cover). This effect was again observed in 2B West E1 panel. The amount of rill lost to adjacent mine voids will depend on the frictional properties of the rill and the seam dip. A similar effect can be developed by removing caved material from the mine area (eg for retrieval of buried mine equipment.)
- Collapse at very shallow depths of cover, where the bulking process cannot be completed allowing caving to continue through to the surface. This process has been observed beneath a storage shed above the WD2 mine, where the depth of cover was in the order of 8 m in loose sands.

Remnant coal

The effect of unmined coal is far greater in shallow workings and it has been interpreted that the shape of the subsidence trough will be affected more if the remnant coal and the sandstone above the coal pillar remains intact. Collapse of any part of the "pillar system" will result in full subsidence development, less an adjustment for the amount of coal left in this location. Collapse of pillar systems has been described in Section 2.5.5.1 as a mode of subsidence initiation (see Figures 2.13 c & d). Further discussion of the stability of the "pillar system" is given in Section 5.3. At this stage, there was insufficient information to provide a definitive reduction factor for subsidence

development above collapsed pillar systems of differing dimension and depth of cover.

Two of the more significant effects of remnant pillars on shallow subsidence are described below:

- In shallow panels, the effective width of unmined coal (compared to the mine depth) is a more likely to be of large enough size to act as a limiting barrier for subsidence. For example, an 8 m wide pillar within a 30 m deep Wongawilli extraction panel, represents 26% of the cover depth. From Figure 3.11, the surface subsidence 8 m from the edge of a single extraction panel would be reduced to 25% of Smax. Using the additive subsidence approach from the NCB (1975), extraction immediately on the other side of the remnant pillar will effectively double the surface subsidence above each of the edges of the remnant pillar. The result is 50% Smax above the remnant coal, and a correspondingly uneven subsidence profile. An example of a remnant coal fender affecting surface subsidence was noted along the sealed roadway above 60 m deep 2SA panel where the regular shape of the subsidence trough was disrupted by a localised "hump". This hump - roughly 0.5m high by eye - was located directly above a 20m section of coal (7 m wide) left in the panel when difficult roof conditions developed in one of the panel splits.

- Solid coal at panel edges or larger remnant pillars in shallow workings can act as a shearing interface for weak, near-surface strata and can result in large-scale stepping of subsidence troughs (as observed above 2B West E1 and 2B West E2 panels). The angle of draw in these circumstances is steep.

  It appears that remnant coal stooks and fenders affect the caving and bulking of strata in the immediate vicinity of the goaf edge. This was noted above Blue and 2SA panels where the lowest extensometer anchor (thought to be sited above a remnant stook) moved less than higher anchors. It is not possible to quantify this effect, in terms of strata movements or size of stooks. The ramifications of the effects of remnant coal is that the application of any design criteria established from this study is likely to be site specific and may lead to inaccuracies if used to predict subsidence for other mining techniques such as longwall mining.

Mining Methods

- Variation in mining height and percentage extraction can affect the amount of subsidence developed; the greater the mining height and the more complete the extraction, the more the subsidence. This was effect was noted in 1 North panel by the greater subsidence developed above the areas extracted by the A10 continuous miner compared to the JCM12 continuous miner.

- The rate of coal extraction, and therefore roof collapse, can have a significant impact on surface subsidence. For example a steadily advancing longwall face (typically mining 0.5 to 1.0 m wide strips) can allow the superincumbent strata to fold down gradually and thereby result in minimal shear stresses. Wongawilli extraction, however, will collapse unsupported strips of ground up to 20 m wide at one time, and the mining face can remain in the same position along the panel for weeks, depending on the rate of split development. This results in large shear forces higher in the roof.

  It was also noted, to varying degrees in all panels, that subsidence development had not stopped completely between subsequent extraction cycles. Although this can affect the interpreted subsidence for any given mining width, it was established that 90% of subsidence occurs within two weeks. This period of time represents the minimum time between successive fender lifts; the typical interval between lifts is 3 to 4 weeks. Furthermore, the amount of time dependent subsidence diminishes as the width of extraction increases.

- The amount of subsidence developed from the collapse of old bord and pillar workings will depend on the percentage extraction of coal within the panel. The potential for such collapses of ground will depend on whether the mine proprietor has adopted the correct geotechnical design/approach for the particular conditions the mine is working in. Panel designs need to be aimed at permanent stability of the mine roof to prevent large scale exposure of weak sandstone above coal pillars. The design must also provide for coal pillars of adequate width to withstand tributary loads. Permanent stability cannot be guaranteed, however, as ground conditions can change markedly over time. For example, there maybe fluctuations in groundwater levels, deterioration of mine roof support (eg timber support) and immediate roof material, urban development introducing additional loading or vibration, surface or groundwater infiltration, or seismic events.

3.3.2 EMPIRICAL MODELLING FOR CONTINUOUS SUBSIDENCE

The field data collected suggests that the trough-form of subsidence develops systematically, with consistent subsidence characterics. The following characteristics of Collie Basin subsidence have been defined:

- Angle of draw = 25°.
- Maximum expected subsidence (the subsidence factor) is 0.63 times the effective mining height for super-critical width panels. The maximum expected subsidence can be estimated from the W/H ratio of the panel and the effective mining height by the equation: $$Smax = 0.63 \times T \times e^{(-12e-4(W/H))}, \quad 3.1(1)$$
- Critical width is met when the central section of the trough tends to flatten out. (Noted in Figure 3.6 when the rate of increase in Smax begins to slow - when the W/H ratio reaches approximately 0.9). Super-critical width is defined as being when the panel W/H ratio reaches 1.7 - from Figure 3.6). This variation from other research work has been supported by the results from subsurface investigations. It has been interpreted that critical width is a "stage of reconsolidation" which is reached when the line of shear (23 ° from the vertical) intercepts the ground surface. At this point, the panel W/H ratio is:

  2 x tan(23) = 0.85.

  This closely matches the estimate from Figure 3.6.

  Once this critical width is attained, a full column of collapsed ground is developed in the central section of the subsidence trough (as illustrated in Figure 3.53 b), and the full tributary load can be expressed onto the collapsed ground, thus allowing for greater rates of reconsolidation.
- The position of point of inflection, which "curiously" swings outside the panel edge for sub-critical width panels, can be estimated by the equation:

$$X = H(0.17 - e^{-[2 \times (W/H + 0.5)^{1.8}]}) \quad 3.1(2)$$

- As a result of the consistency of the data recorded, a predictive equation has been developed [Equation 3.1(7)] which can predict the full subsidence profile above any given extraction panel.

$$-s = Smax.\left[exp^{-6 \times exp^{-7 \times (D/H + 0.35)}}\right] - Smax \qquad 3.1(7)$$

One interesting feature of this function is the manner in which it will produce a flat profile once the Collie Basin critical width is achieved. When plotted in the form of Figure 3.11, it can be seen the location of maximum subsidence along the trough is reached at a distance of approximately 28% of the cover depth from the point of transition. The panel W/H ratio at this point is: 2 x (0.28 + 0.17) = 0.9, which equates to the position of critical width subsidence. Any points on the surface further away from the point of transition will have essentially the same amount of subsidence.

Through single and double differentiation of this function, the concomitant tilts and curvature at the ground surface can also be predicted [Equations 3.1(10), 3.1(12)]. Once the curvature is known, the horizontal strain on the ground surface can be calculated by the equation:

$$\textbf{Strain} = 3.5 \times (\textbf{Curvature} \times 10^4)^{0.6} \ \textbf{(mm/m)} \qquad 3.1(13)$$

The basis of the predictive tool is a double exponential profile function, which is dependant on mining height, mining width and depth of cover.

The accuracy of this predictive tool has been assessed by cross-checking subsidence predictions against the subsidence measured during the mining of a super-critical width "test" panel (1North panel). It was established that the profile function provides acceptable results for the trailing edge subsidence, but slightly over estimates the steepness of the subsidence profile at the advancing edge. This variation in the shape of subsidence troughs is thought to be due to the different caving mechanisms at the opposing ends of panels. It has been interpreted that a large proportion of strata at the trailing edge collapses in a vertical, one-piece, fashion once a critical span is reached (termed **secondary** caving); whereas the leading edge appears to collapse incrementally in cantilever fashion across the

already bulked goaf (termed tertiary caving - discussed further in Chapter 4). The trailing edge mechanism produces a steeper trough, the leading edge mechanism produces a more gently shaped trough above the panel edge. It is possible to develop two separate profile functions, however, it is recommended that the subsidence profile for the trailing edge be used as a worst-case estimate the leading edge subsidence profile.

Subsurface subsidence investigations have identified that the mechanisms leading to the development of surface subsidence involve four stages of downward ground mass movement (illustrated in Figure 3.54 a):

1) Small scale collapses of the immediate mine roof (typically 6 to 8 m high, termed **primary** caving) during fender lifting. The majority of the bulking which is attributable to establishing the subsidence factor of 0.63 occurs within this primary caving zone.

2) A large scale "one-piece" (**secondary**) collapse of the strata once a critical width/span, and the shear resistance of the bridging strata is exceeded. The height secondary caving appears to be limited to below the first major aquitard, however, there is insufficient data to conclusively prove this. Depending on the width of this secondary caving, and the range of cover depth, an uplifted hump can develop on the surface above the centreline of the excavation.

3) A triangular shaped translational sagging of strata from outside the edge of the panel towards the region of caving. The limits of this region are bounded by the angle of draw (averaging 25°), and the line of shearing (23°) - both measured from the vertical, and from the panel edge.

4) Sagging of strata, from the level of the first aquitard upwards, onto the secondary caving goaf, or onto the broken rock that became detached in the "cantilever slump" phase (described below), and ultimately onto the primary caving zone.

DIAGRAMMATICAL REPRESENTATION OF SUBSURFACE GROUND MOVEMENTS AND STRAINS

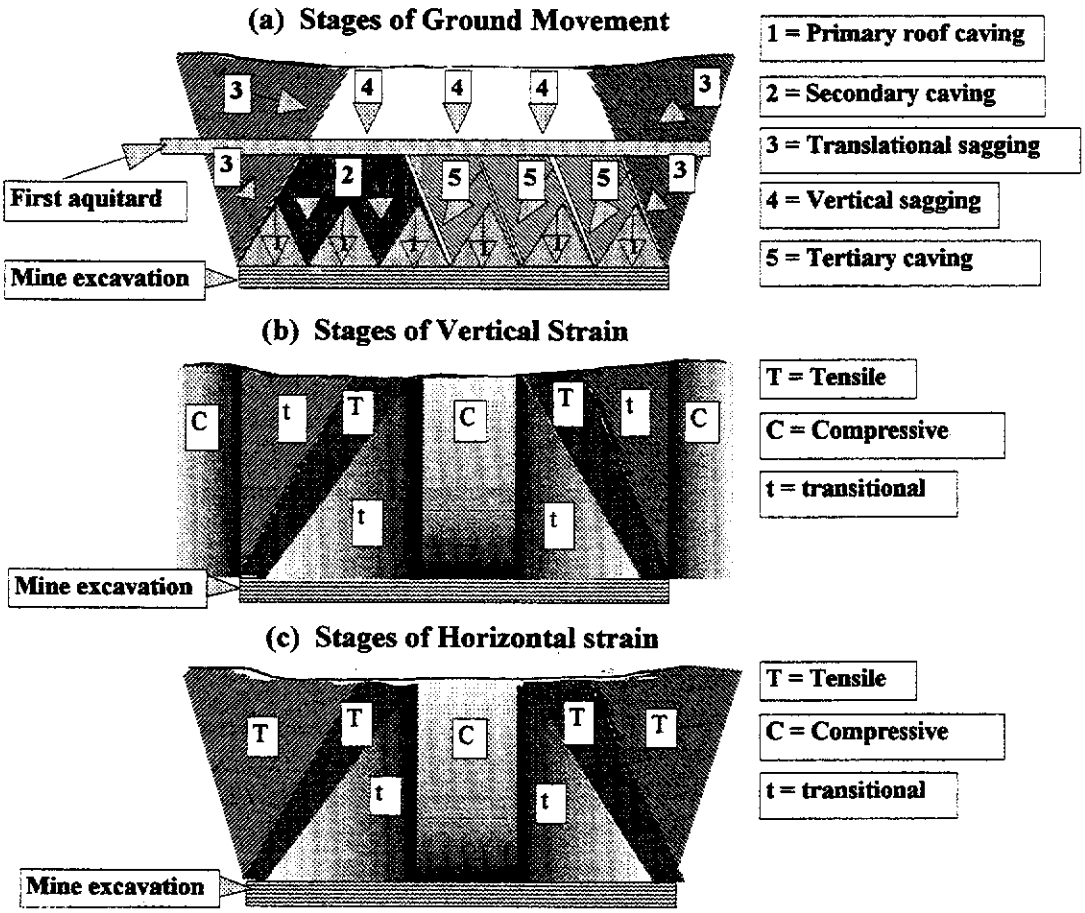

Figure 3.54

5) An incremental "cantilever slump" of strata below the first aquitard as the width of extraction is increased with subsequent lifts (beyond that width required to develop the one-piece secondary caving). The "free" end of the cantilever rests on the bulked goaf, generating a more gently sloped subsidence trough at the advancing edge - as illustrated by Figure 3.5. It appears that the line of shearing of this cantilever stage of ground movement also approximates 23°. Note: there was no direct evidence to indicate the exact mechanism involved with this mode of movement at this stage. This stage of ground movement is termed **tertiary** caving.

These ground mass movements give rise to corresponding zones of vertical and horizontal strains. Vertical strains can be categorised into three zones (illustrated in Figure 3.54 b):

i) A zone of compression from the point of minimal surface subsidence to the panel edge. The trend is for increasing strain toward the panel edge.

ii) An angular zone of extension where the overlying strata caves/subsides freely towards the goaf. This angular zone appears to be in the order of 20 m wide (widening near the surface) and extends from the panel edge at 23° from the vertical. Particularly near the surface, there is some "dilation" of the sheared sandstone during the subsidence process. The exact nature of this minor dilation could not be determined at this stage.

iii) A zone of recompression once all the strata has undergone shearing and is sufficiently distant from the panel edge [when W/H > 2 x tan(angle of shear) = 0.85] and cover load is fully redistributed onto the subsided strata. This zone of recompression matches well with the point of initial development of critical width, where the surface subsidence profile begins to flatten out, as mentioned above.

Between each zone, there are transition zones where ground movements trend from compression to tension, and from bulked caved/sheared mass to reconsolidated ground.

Although it was not possible to accurately establish the stages of horizontal movements/strains during the field investigation, a best guess interpretation has been provided as a base for further investigation. The interpreted zones of horizontal subsurface movements (and consequent strains) associated with the vertical zones of

subsidence given above are illustrated in Figure 3.54 c and listed below:

i) A zone of extension (between the limit of subsidence and the line of shearing), where the superincumbent strata stretch across the solid coal abutment and sag toward the centre of the panel. When combined with the zone of vertical compression at the edges of the panel, a zone of translational torsion is developed. The trend is for increasing tension from the line of minimum subsidence to the line of shear.

ii) A transitional zone, beneath the line of shear, where there is minimal reconsolidation of the collapsed strata .

iii) A zone of horizontal (and vertical) compression, from the intercept of the line of shear with the ground surface toward the middle of the panel, with zero horizontal strain above the absolute centre of the panel.

- A generic nomogram and predictive equation [Figure 3.41 and Equation 3.2(1)] have been developed for estimating the magnitude and shape of subsurface subsidence for mining at variable depths and widths. The basis of this predictive tool is the relationship of subsurface movements to the proximity of the subsurface angle of shear and the subsidence at the surface. (Outside the angle of shear, there is less subsurface subsidence than surface subsidence; when the projected line of shear coincides with a given point below the surface, maximum subsurface subsidence develops; once the angle of shear has passed any given point, the separation between the surface and subsurface horizons reduces through reconsolidation towards pre-mining distances.)

The fact that the surface subsidence observations can be explained by subsurface subsidence measurements has provided a reasonable degree of confidence for the conclusions made from this stage of the study.

In relation to the investigation of subsidence effects on aquitard integrity, there was limited information other than some vertical strains measured at aquitard horizons and water flows into ACIRL panel. What the vertical strains mean in regard to aquitard integrity is not certain. As stated in Section 2.5.6.1, historically, the integrity of water resistant strata has been defined by horizontal strain.

Field observations on the integrity of the Alpha Seam aquitard (the basal unit of aquifer 3) are not definitive. For example, the piezometric water levels in aquifers 3 and 4 did not drop significantly at any stage of extraction in piezometer boreholes surrounding both ACIRL and Blue panels. However, increased water make (recorded after the extraction of the second fender in ACIRL Subpanel 1) suggests that aquifer 3 had been penetrated [Hebblewhite and Humphreys, 1988]. Conversely, surface water that had ponded above 2SA panel and was noticed to disappear down tension cracks on the surface did not add to the water make in the mine. This indicates that the Alpha seam aquitard remained intact.

Given the limited aquitard related field data available at this stage, it was considered that before any meaningful panel design criteria could be developed for the prevention of aquitard rupture, further investigation was required. It was proposed to use both numerical, physical and additional field investigation to assist with this objective (detailed in Chapter 4). An account of the work done towards establishing the tolerance limits of aquitards, and developing adequate panel design criteria is provided in Section 5.1 and 5.3.

It was therefore also concluded that developments made in surface and subsurface subsidence definition and prediction - to this stage of investigation - represent a major advance in the level of understanding of subsidence mechanisms in the Collie Basin sediments. However, it was recognised that the data collected to this stage was restricted to relatively simple panel geometries with similar mining heights and relatively shallow depths of cover. Furthermore, it was evident that there was insufficient information from which to develop design techniques to predict the effective stability of remnant coal pillars within panels, and their consequential impacts on surface subsidence.

Consequently, a program of work was proposed to investigate the potential to develop an all encompassing strategy from which the effects, magnitude and shape of surface and subsurface subsidence can be predicted with an acceptable level of accuracy for any mining scenario. This extension of work is described in the following chapters.

4.0 PROJECT MODELLING

It was concluded from the literature review that each of the subsidence prediction techniques are, to varying degrees, "site specific" in their application. Each modelling method involves some form of simplification or assumption of the prototype conditions which does not necessarily apply to other sites. The aim of the modelling phase of the project was to use mathematical and physical modelling conjunctively to compliment the strengths and weaknesses of each technique and hopefully produce a better balanced predictive/design tool.

It was proposed to conduct the modelling phase of investigation as a parametric study to isolate and quantify the critical subsidence parameters, and use the information gained from this study to better develop empirical models.

The mathematical modelling package selected to address this phase of the project was the MINCAD Systems' developed boundary element/displacement discontinuity software package SUBSOL. The specific features of the program relative to the aims of the research project are discussed in the following Section. Some minor modelling was proposed for specific tasks later in the project using finite element codes. The physical modelling technique proposed was the geotechnical centrifuge, specifically the Acutronic 661 machine located at UWA.

4.1 NUMERICAL MODELLING

Prior to researching the merits of SUBSOL, the author investigated the potential for using a finite element model (FEM), developed by the University of Nottingham, specifically for subsidence prediction. This program had been used by several researchers to successfully reproduce field subsidence and subsidence curves given by the NCB (e.g. Fitzpatrick 1987). The more significant features of the Nottingham FEM include:

- The ability to model anisotropic and cross-anisotropic (transversely isotropic) materials,
- The ability to model elasto-plastic material,

- The inclusion of a "mined-out" element which is used to approximate the void created by coal extraction. By providing these elements with low elastic modulus before 'failure" and a high modulus after "failure", excessive closure of the mined element is prevented.
- A number of stratigraphic horizons can be modelled.

The author found, whilst working with Dr D. Reddish and Professor B. Whittaker at the Nottingham University in 1991, that although the model was very flexible, and mathematically well attuned to the subsidence process, it could not accurately reproduce the Collie Basin subsidence from the mine through to the surface for panels nearing or greater than critical width. This discrepancy was considered to be mainly due to the inability of the program to represent the caved/bulked area which reduces the surface subsidence to 63% of the effective mining height. The exact causes for the variations could not be determined, however, as the author was only on site (in Nottingham) for three weeks. It is understood that since this time, Nottingham University has made several modifications to the FEM code, and it may now be able to account for the caving area more successfully.

However, better results were attained for the prediction of surface subsidence when the author modelled a series of narrow panel/pillar (sub-critical width) panels. The FEM predicted 240 mm subsidence for two 40 m wide sub-panels separated by a 20 m wide pillar with minimal interaction between each area of extraction. At the time this was considered to be a good result (though recent field tests suggest that maximum subsidence is in the order of 60 mm for similar widths of extraction). It is thought that the reason the FEM was able to provide a better representation of subsidence above narrow panels is the lesser reliance of the subsidence process on the bulking goaf and inelastic qualities of near seam caving for sub-critical panels. Shu (1990) also attained better model results (using the displacement discontinuity element-based computer code MSEAMS) for sub-critical width panels less than 0.4 W/H. Shu provided no specific reasoning for his observations, however, Seneviratne (1987) explains that for panel W/H ratios less than 0.25, subsidence is comparatively small and elastic. At W/H ratios greater than 0.25, Seneviratne thought that there is greater inelastic deformation.

It should be noted that the panel/pillar trial at Nottingham was only a preliminary test to help assess whether this extraction method had potential to work in the weak Collie Basin sediments. As the panel/pillar model results showed that there would be minimal subsidence, the author had greater confidence with trialing the method before the event.

Considering the limited time spent at the Nottingham University, this modelling experience was considered very positive for the modelling proposed for the remainder of the project, and particularly so for modelling of narrow panels.

As the SUBSOL software was not commercially available, and because it still had some "bugs" within the code at the time, it was intended to use the software on a bureau service, where all the model input parameters and design parameters were provided by the author, and the running of the models was completed by MINCAD Systems. Data output was to be returned to the author by mail after each stage of the modelling for evaluation.

Presentation and discussion of the calibration stage of this investigation has been summarised from a draft calibration report provided by MINCAD, additional information provided by MINCAD as requested by the author, and personal communication and analysis of data received.

The general development of SUBSOL and set-up details of each model are provided in detail in Appendix V to minimise the amount of supportive detail in the main body of the thesis. A brief description of the mechanics of SUBSOL and similar programs is given in Section 2.6.4.

4.1.1 Calibration of SUBSOL

The intention was to firstly calibrate the model against subsidence data previously measured above two completed extraction panels (ACIRL and 2SA panels) and then check the predicted subsidence from the "calibrated" model against subsidence measured above another extraction panel in the process of being mined (1 North panel). The two calibration panels chosen were considered to be appropriate for the purpose of the exercise as ACIRL panel was comparatively deep(140 m), and had a

complex mine set-up, and 2SA panel was comparatively shallow (56 m) with a higher proportion of extremely weak rock mass above it (the geometrical and geological details of each panel are discussed in more detail later in this Section and Appendix V). The reason for adopting this calibration approach was to assess whether the general assumptions made for input parameters in each model could apply equally to models at varying depth and stratigraphy.

"Calibration" of the model input parameters within the specific limitations of the SUBSOL software was done by MINCAD with some cross-reference to the author. Although calibration of the numerical model was a major component of this phase of the investigation, for the purpose of the research, there was seen to be little benefit gained by personally "tweaking" a software package developed by others for such a small stage of the overall project.

It was planned that once the SUBSOL model was "calibrated", a series of parametric studies would be run remotely by electronically mailing set-up data files developed by the author to MINCAD who would 'run" the models on their equipment. (As part of the funding provided by MERIWA, MINCAD Systems visited the author and provided a copy of the pre-processing package for SUBSOL for the author's use.) It was proposed that the results gained from this parametric stage would be used to establish more rigorous empirical models, covering a wide range of mining scenarios and thus minimise the reliance on expensive modelling for the prediction of subsidence and subsidence effects. The first mine model processed using SUBSOL was developed personally, with the assistance of Mr K McNabb of MINCAD Systems.

It was proposed that if SUBSOL could not be accurately calibrated to represent the subsurface subsidence then rigorous mathematical modelling (of any of the commercially available codes) would proceed no further, and the research study would continue, using subsidence parameters derived from only field and physical modelling investigation. This judgement was founded on published literature (eg Bahuguna et al., 1991), personal communication with leading computer consultants, and personal experience with a wide range of computer codes which suggested that the complete subsidence phenomenon is too complex for mathematical modelling.

4.1.1.1 ACIRL Test Panel

An oblique view of the ACIRL panel (as discretised in the model) is provided in Figure 4.1. This three dimensional (3-D) view also illustrates the position of the aquitards/stiff strata overlying the panel. A plan view of the overall panel is provided in Figure 4.2; the finer details of the discretised model layout and "mining steps" of each sub-panel are depicted by Figure 4.3. The ACIRL panel represents a complex mine geometry for modelling. It was developed as two separate sub-panels, mined in different directions and separated by a row of chain pillars that were approximately 13 m wide. Furthermore, mining problems in the second sub-panel resulted in sections of fender coal being left unmined (Figure 4.3). Another important feature of the panel was the development of set-up roadways around the panel for personnel and equipment access and mine ventilation and drainage. As some of the pillars between these roadways were observed to be prone to pillar punching, these peripheral workings needed to be incorporated into the model.

The surface subsidence predicted for each sub-panel by SUBSOL are presented in Figure 4.4 as shaded contours superimposed on an exaggerated vertical scale. The 3-D axis or gnomon indicates north is the negative X direction and east is positive in the Y direction. Figure 4.4 shows an overall view of subsidence above the ACIRL test panel as viewed from the northeast. Figure 4.5 represents a detailed view of the northeast region of sub-panel B as viewed from the southwest. The effect of the remnant coal at the edge of sub-panel B is illustrated by the uneven profile at the edge of the subsidence trough (in the lower right hand corner).

Figure 4.6 a shows a longitudinal section through the subsidence profile running south-north across the panel. The unconnected square and triangle marker points represent subsidence readings taken above an equivalent section above the panel (subsidence grid-line D), on the 10/12/87 and 20/1/89. The 1987 readings were taken before the subsidence profile had fully developed and while the profile was being influenced by the presence of the chain pillars separating the two sub-panels.

SUBSOL MODEL LAYOUT FOR ACIRL PANEL - WD6

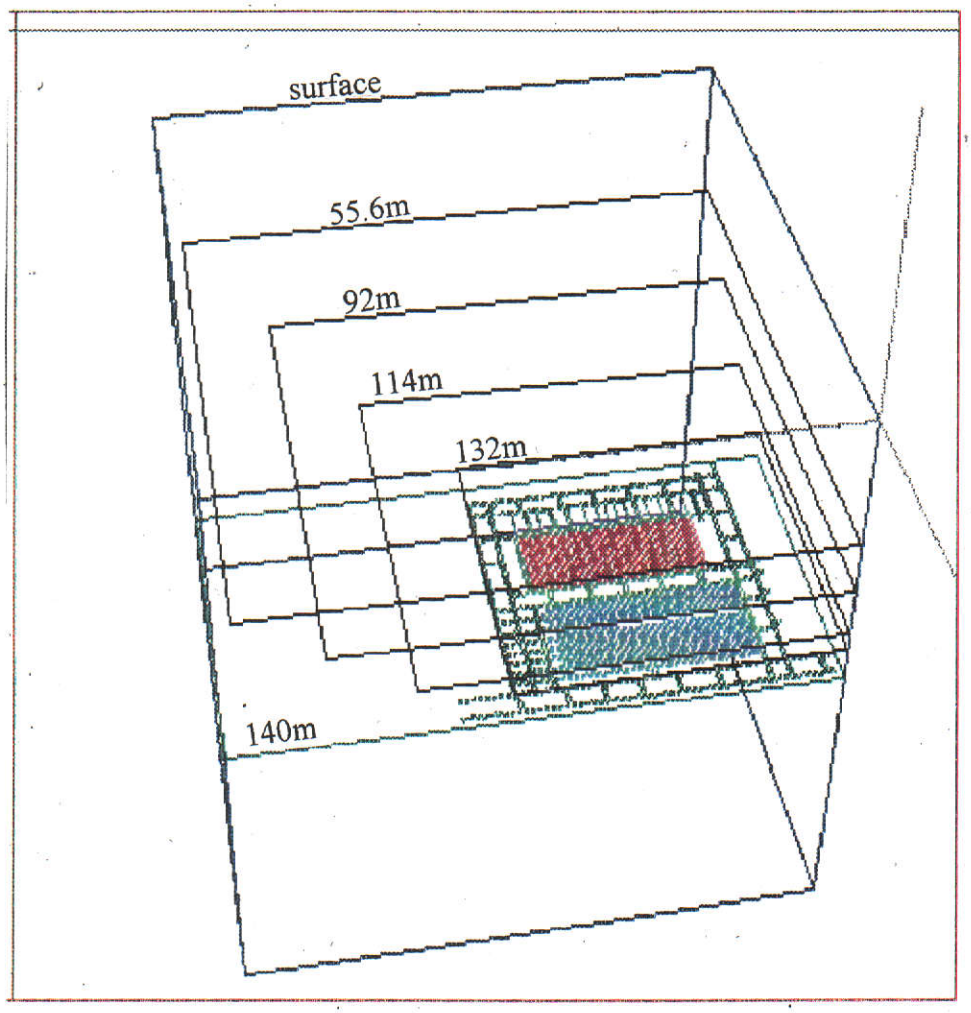

Discretised Model in 3D

Figure 4.1

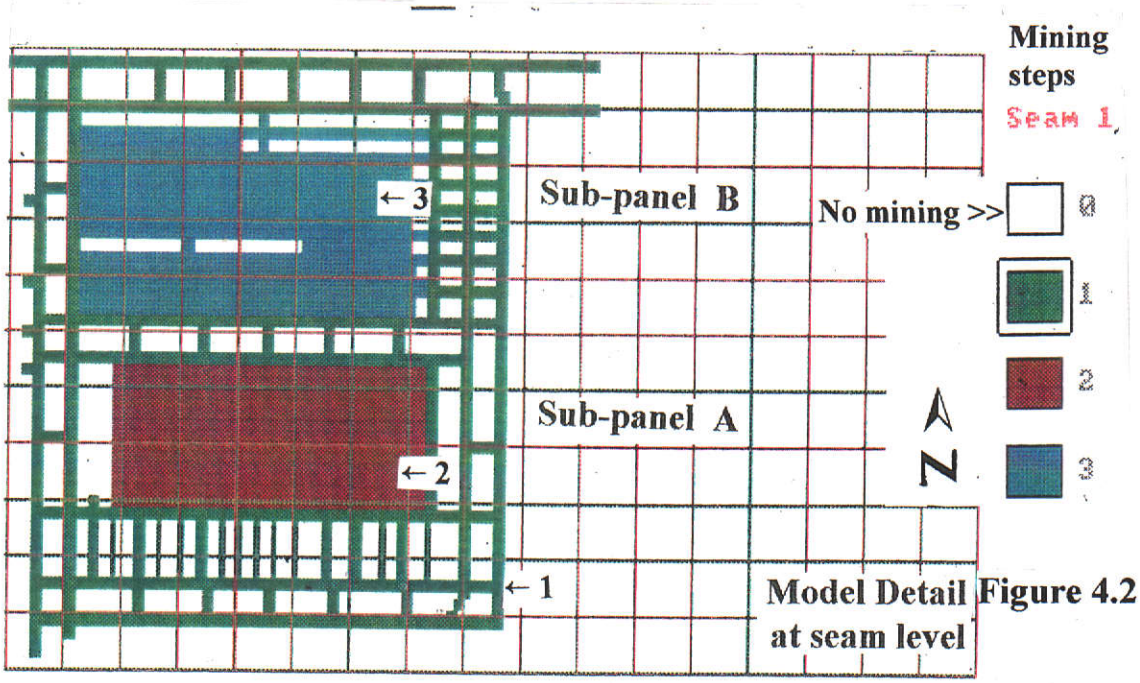

Figure 4.2

SUBSOL MINING ELEMENT DETAIL FOR ACIRL PANEL MODEL

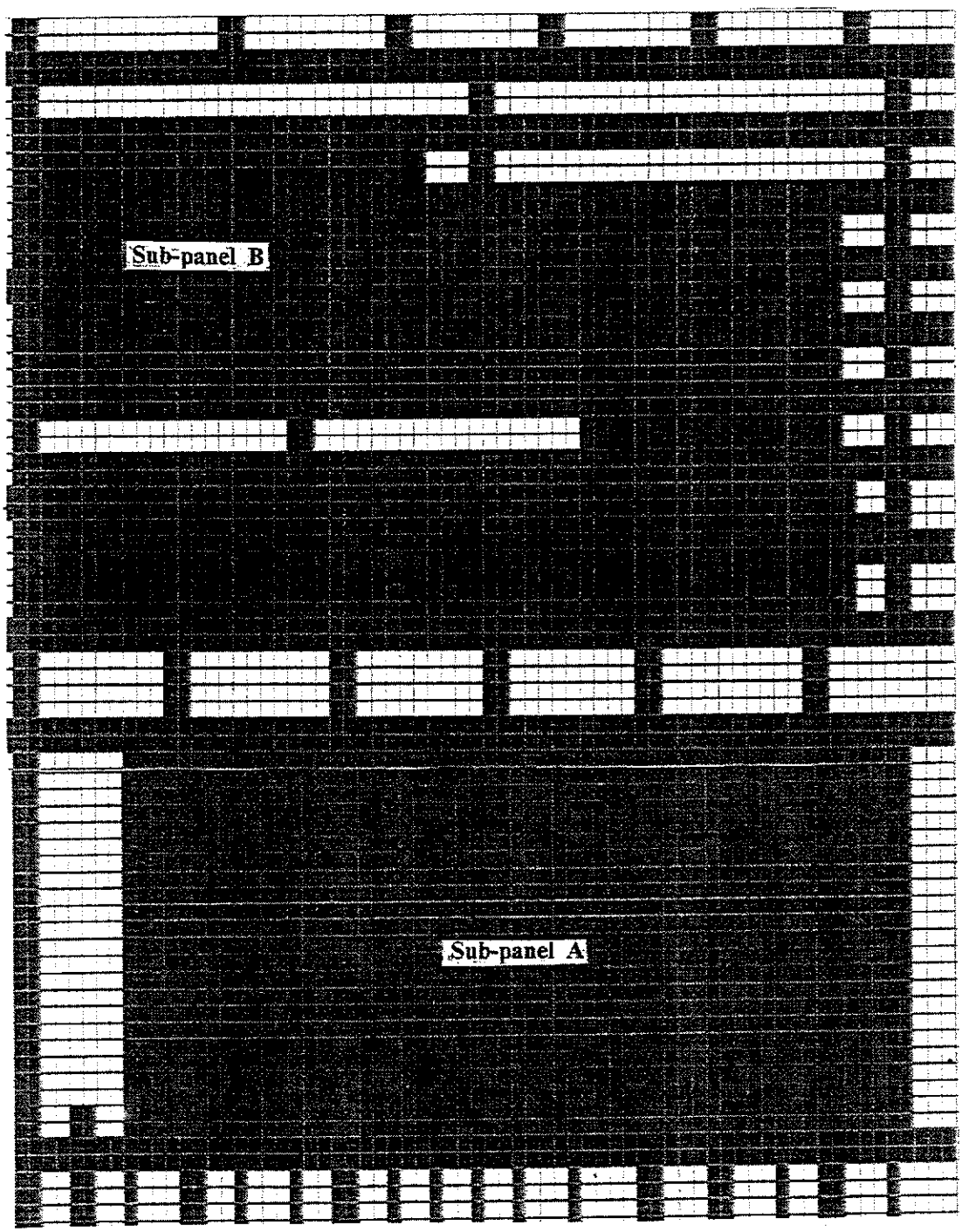

Figure 4.3

SUBSOL PREDICTED SURFACE SUBSIDENCE ABOVE ACIRL PANEL

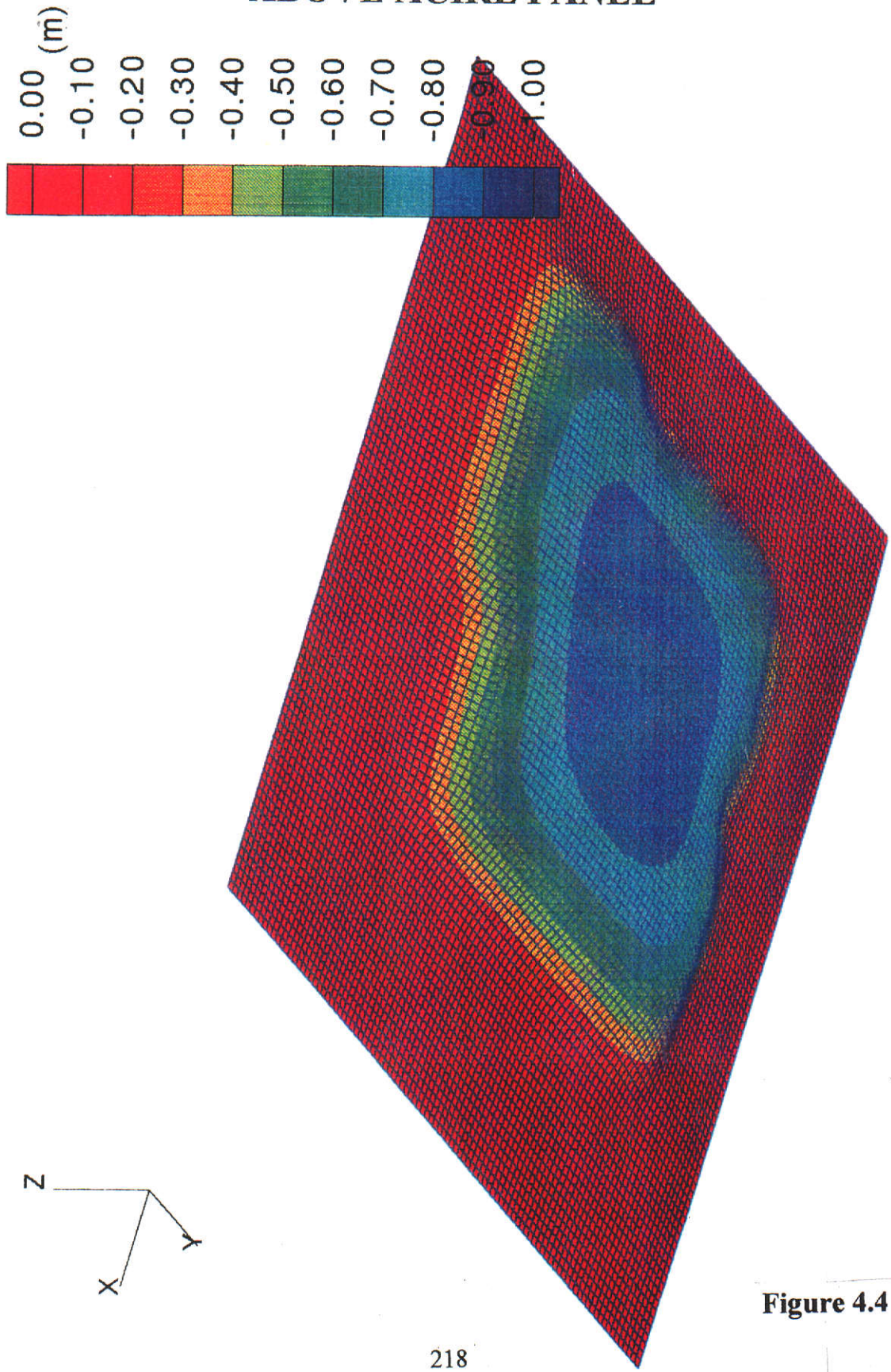

Figure 4.4

SUBSOL PREDICTED SUBSIDENCE ABOVE THE NORTH NORTH EAST CORNER OF SUB PANEL B

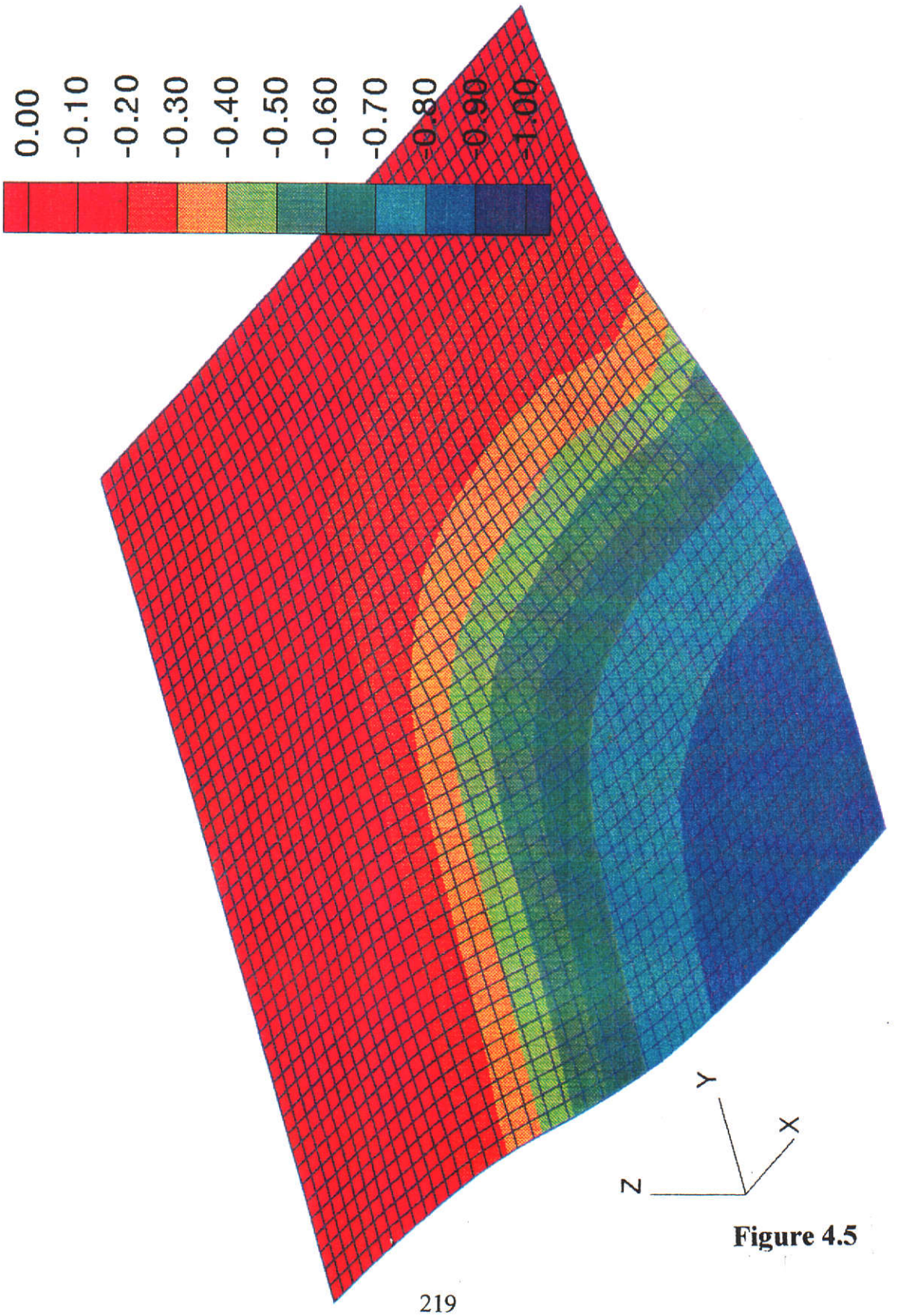

Figure 4.5

COMPARISON OF PREDICTED AND MEASURED SUBSIDENCE ABOVE THE ACIRL PANEL

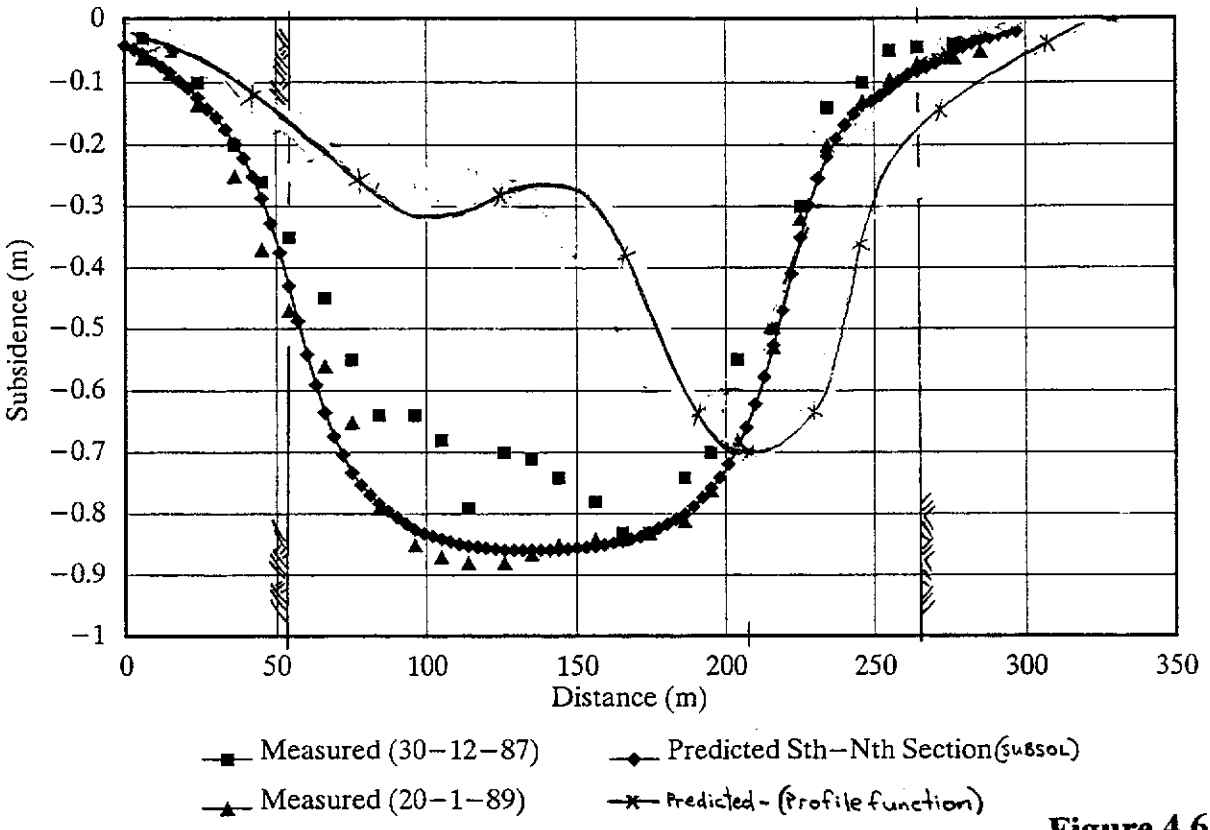

Figure 4.6 a

(Profile Function)

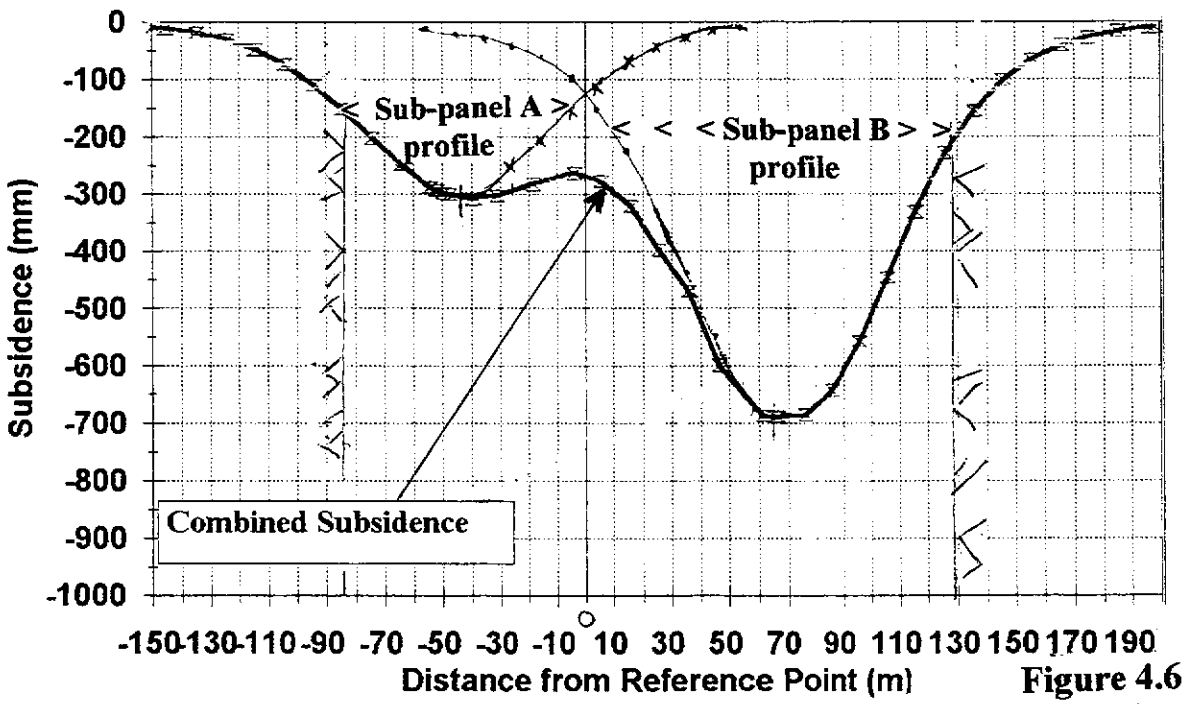

Figure 4.6 b

It can be seen in Figure 4.6 a that SUBSOL closely matches the field surface subsidence, whereas the profile function method does not. Note that the profile function subsidence trough was determined by firstly calculating the subsidence for each individual sub-panel [using Equation 3.1(7)]. Then each profile is plotted separately and the final subsidence profile determined by summing the subsidence overlap between each sub-panel (after the NCB, 1975) - as illustrated by Figure 4.6 b. The resultant maximum subsidence using the Collie Basin profile function and overlap approach is 0.7 m compared to 0.86 m predicted by the SUBSOL model and 0.89 m in the field.

It is suggested that either the coal pillar, or the strata above, has collapsed under elevated tributary load and thereby effectively combined the two areas of extraction to develop significantly more subsidence than would otherwise be expected above the inter-panel pillar. The effect of a collapsed pillar system cannot be predicted by the profile function. Note: if the chain pillar was mined out, the maximum subsidence would be in the order of 1.5 m.)

In-mine observations suggest that it was the strata immediately overlying the chain pillars which collapsed, and not the coal. Prior to the sealing off of access to the first sub-panel and chain pillar, there was very little evidence of pillar stress (eg. slabbing) whereas high pitched soundings were "noted" to come from some distance above the immediate roof. This interaction of separate goafed areas by failure of strata above intra-panel pillars is discussed in more detail in Sections 5.1 and 5.3.

It was also interesting to note that the SUBSOL model's calculated subsidence gave lower curvature and tilt above the edge of sub-panel A (attributed to the "punching" of set-up pillars into the floor) than measured and calculated in other panels - see following Sections. SUBSOL was also able to accurately predict subsidence across the unmined coal fenders in the north-eastern corner of the panel, where the remnant coal was limiting the amount of subsidence near the panel edge. (Note that the profile function was calculated assuming that all fenders were extracted from within the panel boundary.)

To supplement calibration of the model, the on-seam stresses measured during extraction of fenders 6 and 2 in sub-panel A (see Figure 4.7 from Platt, 1987) were compared to those calculated by SUBSOL (Figures 4.8 and 4.9).

STRESS MEASUREMENTS IN SELECTED FENDERS IN ACIRL PANEL - WD6

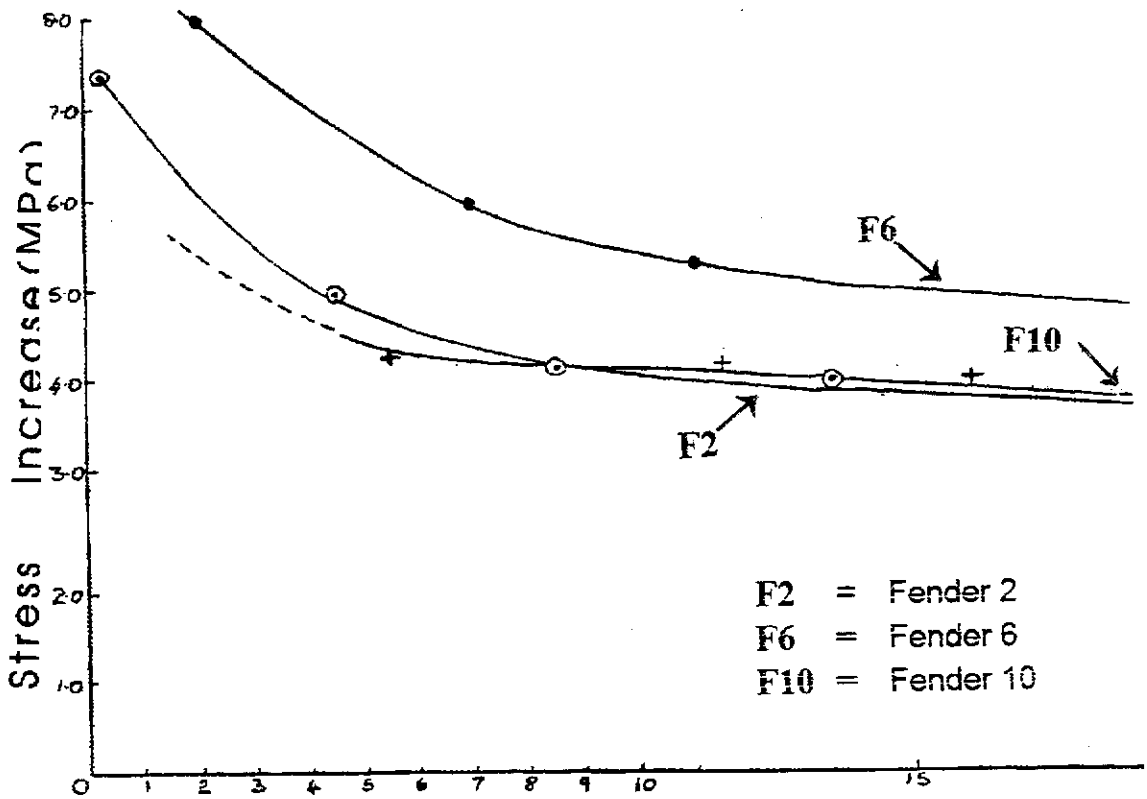

Distance between stress cell and mining end of fender (m)

(From Platt, 1987)

Figure 4.7

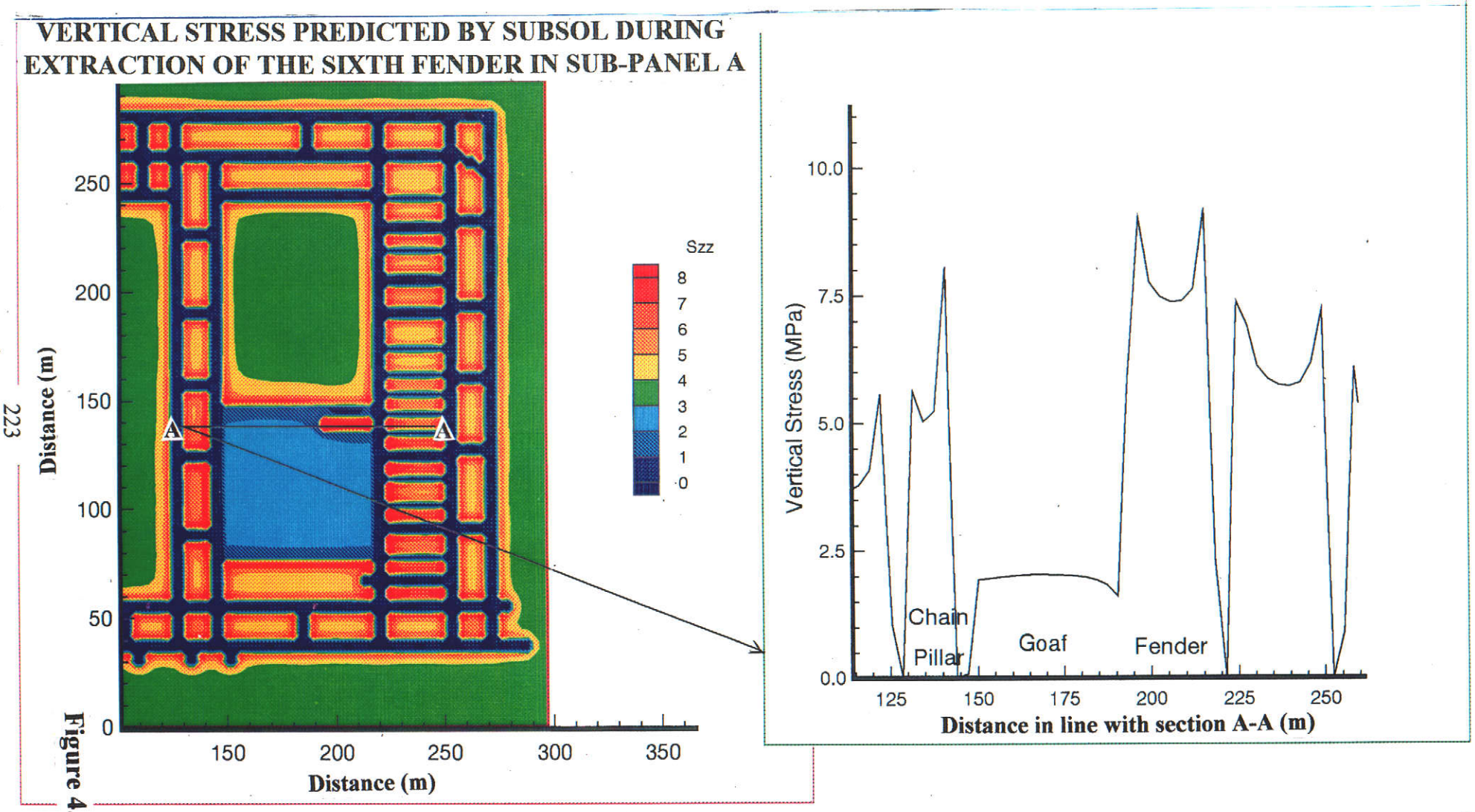
VERTICAL STRESS PREDICTED BY SUBSOL DURING EXTRACTION OF THE SIXTH FENDER IN SUB-PANEL A
Distance (m)
250
200
150
100
50
0
150
200
250
300
350
Distance (m)
A
A
Szz
8
7
6
5
4
3
2
1
0
Vertical Stress (MPa)
10.0
7.5
5.0
2.5
0.0
Chain Pillar
Goaf
Fender
125
150
175
200
225
250
Distance in line with section A-A (m)

Figure 4.8

VERTICAL STRESS PREDICTED BY SUBSOL DURING EXTRACTION OF THE SECOND FENDER IN SUB-PANEL A

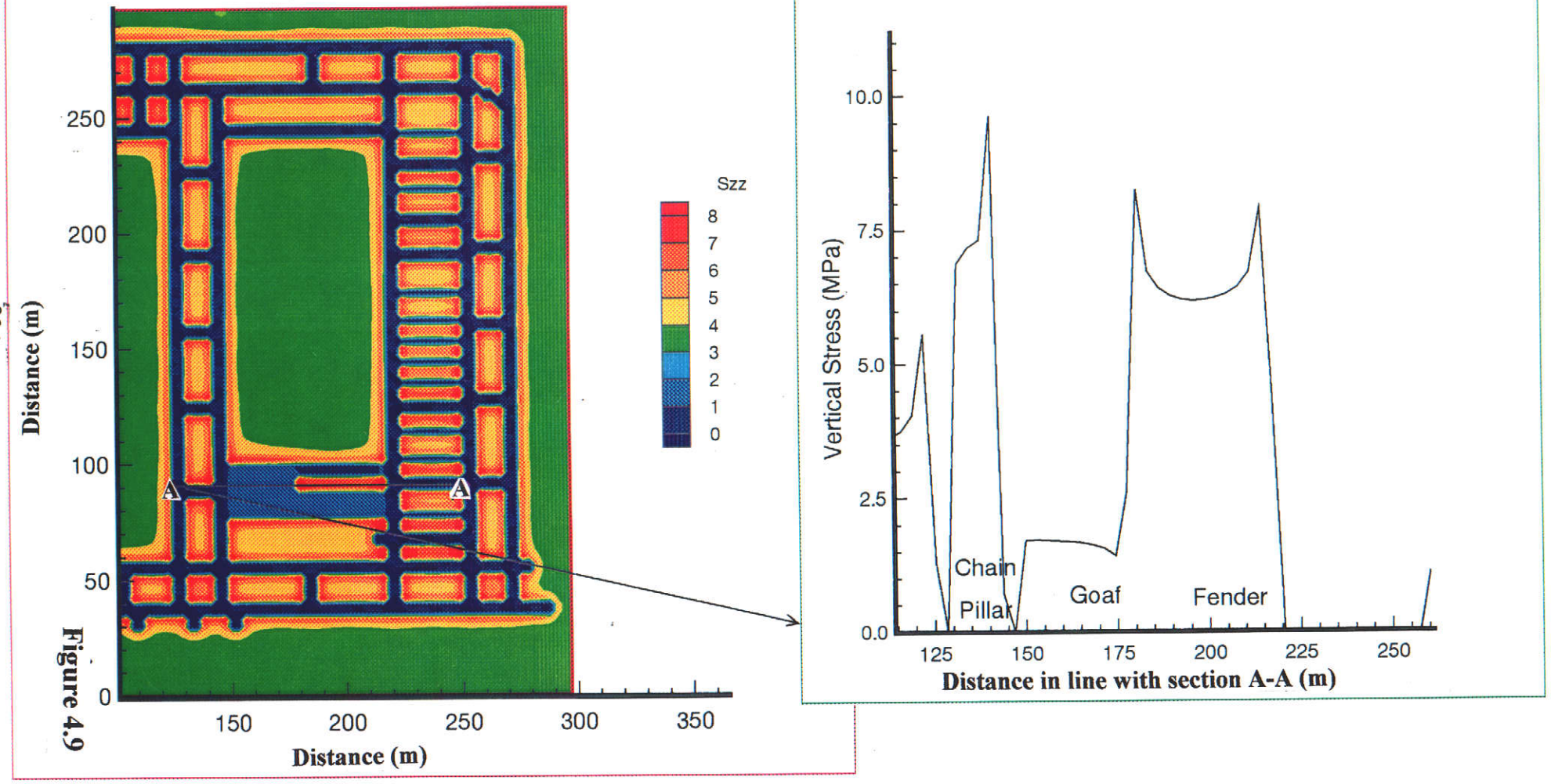

Figure 4.9

Note that the in-mine stress was monitored using "Irad gauges" which can only measure the change in stress from the time of installation. The total stress can be estimated by adding 3.0 MPa to the measured stress; based on the assumption that the pre-mining vertical stress is equivalent to ρgH. (Where H = 140 m, and ρ = 2.2 t/m^3 - from Hammond et al., 1983 - has been assumed). The stress cells were installed 14 m from the end of each of the 2nd, 6th and 10th fenders.

These figures demonstrate that the model and field stresses compare reasonably well. For example, Figure 4.8, representing the stresses calculated by SUBSOL during extraction of the sixth fender in sub-panel A (along section A-A oriented longitudnally through the sixth fender), illustrates that the calculated vertical stress 14 m from the end of the 18 m long stub of unmined fender (4 m from the goaf) is approximately 8.2 MPa. Measured stress change within the sixth fender stub, at the equivalent stage of extraction and distance from the goaf edge, extrapolated from Figure 4.7, was approximately 7 MPa. The stress level calculated by SUBSOL is therefore in the order of 18% less than the total stress measured/inferred in the mine. In comparison, SUBSOL stress predictions across fender 2, when there is 35 m coal remaining in the fender - see Figure 4.9 - suggest that at 21 m from the goaf edge, the expected stress would be in the order of 6.3 MPa. The change in stress measured at an equivalent stage during extraction of fender 2 was approximately 3.5 MPa. Thus the total stress calculated by SUBSOL in this case is only 3% less than the total stress measured/inferred in the mine. Taking into consideration the inherent error in stress monitoring (as demonstrated by the 20% lower stress measured by the stress cell in fender 10 compared to fender 6 - see Figure 4.7), the SUBSOL stress values are considered quite acceptable.

It was therefore concluded that the SUBSOL model had suitably represented both the surface subsidence trough measured above the ACIRL panel, and on-seam stresses within the panel. No comment could be provided on the ability of the model to represent subsurface subsidence characteristics as MINCAD provided no details of the subsurface subsidence above the ACIRL panel. Nonetheless, these results strongly supported the initial proposal to attempt to establish a mathematical model for prediction of subsidence for complex mining scenarios.

4.1.1.2 Two South A (2SA) Panel

The development roadways and bord and pillar workings surrounding 2SA panel (Figure 4.10) were not included in the model for simplicity. Their effect at this shallow depth of cover on the overall subsidence profile was seen to be negligible (other than the collapsed roadways to the south of the panel). The cover depth modelled was 56 m which represents the average depth. The depth of cover *in situ* varies from 70 m at the western edge to 50 m at the eastern edge. The set-up and input parameters used for the 2SA model are detailed in Appendix V.

Figure 4.11 portrays a 3D-view of the predicted surface subsidence of the North-West corner of the 2SA panel as would be seen if viewed from the southeast. This Figure illustrates the impact of a remnant fender (7 m wide) left within the panel due to operational difficulties. In this case, the narrow remnant fender and superimposed strata are not crushed out by the superincumbent loads above this shallow panel, and a subsidence hump is developed within the subsidence profile. The magnitude of this hump in the model surface is approximately 0.5 m, which compares favourably with that observed in the field.

Figure 4.12 a represents the predicted surface subsidence along a longitudinal section running North-South across the fully extracted, 140 m wide panel (Line B). Figure 4.12 b compares the SUBSOL profile, the field data, and the profile function profile across the western edge of the panel - Line A. It can be seen that there is a strong similarity between:

- the maximum subsidence measured in the field and the two predictive models (-20 mm for SUBSOL and +20 mm for the profile function), and
- the subsidence profile curvatures across the panel edges.

However,there is marked variation between predicted subsidence profiles and field data at the panel edges along Line B. This is due to a large body of remnant coal fender remaining near the northern edge, and some collapse of bord and pillars workings immediately to the south of the panel (see Figure 4.10). These variations in the mine plan were not modelled in SUBSOL.

Verbal communication with MINCAD suggests that, apart from when the very first fenders were extracted, there was effectively no bed separation noted in the model. (No printed evidence was provided.) This model response matched field observations.

2SA PANEL LAYOUT AND SUBSIDENCE GRID LOCATION PLAN

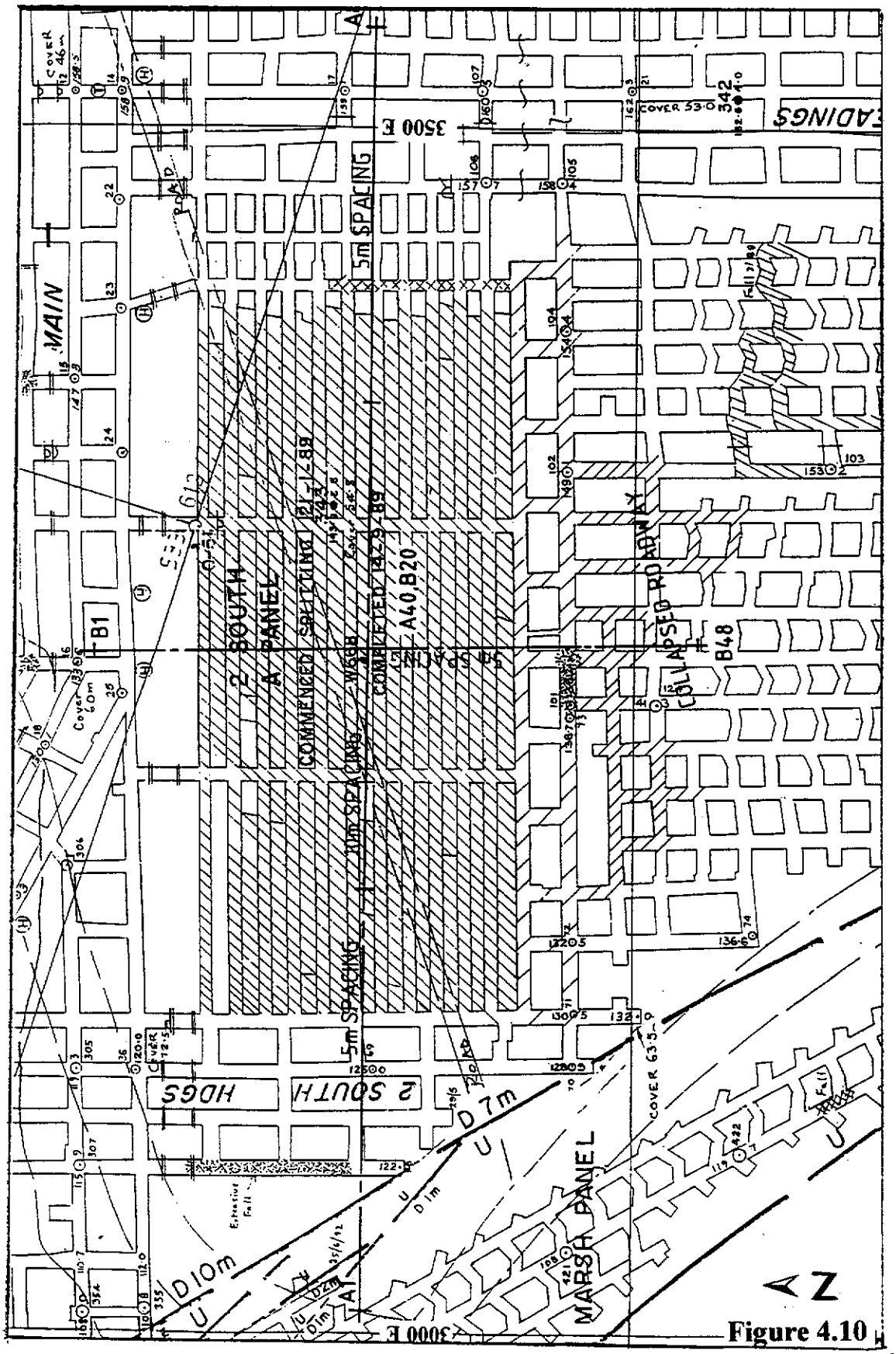

Figure 4.10

SUBSOL PREDICTED SURFACE SUBSIDENCE ABOVE THE NORTH-WEST CORNER OF 2SA PANEL

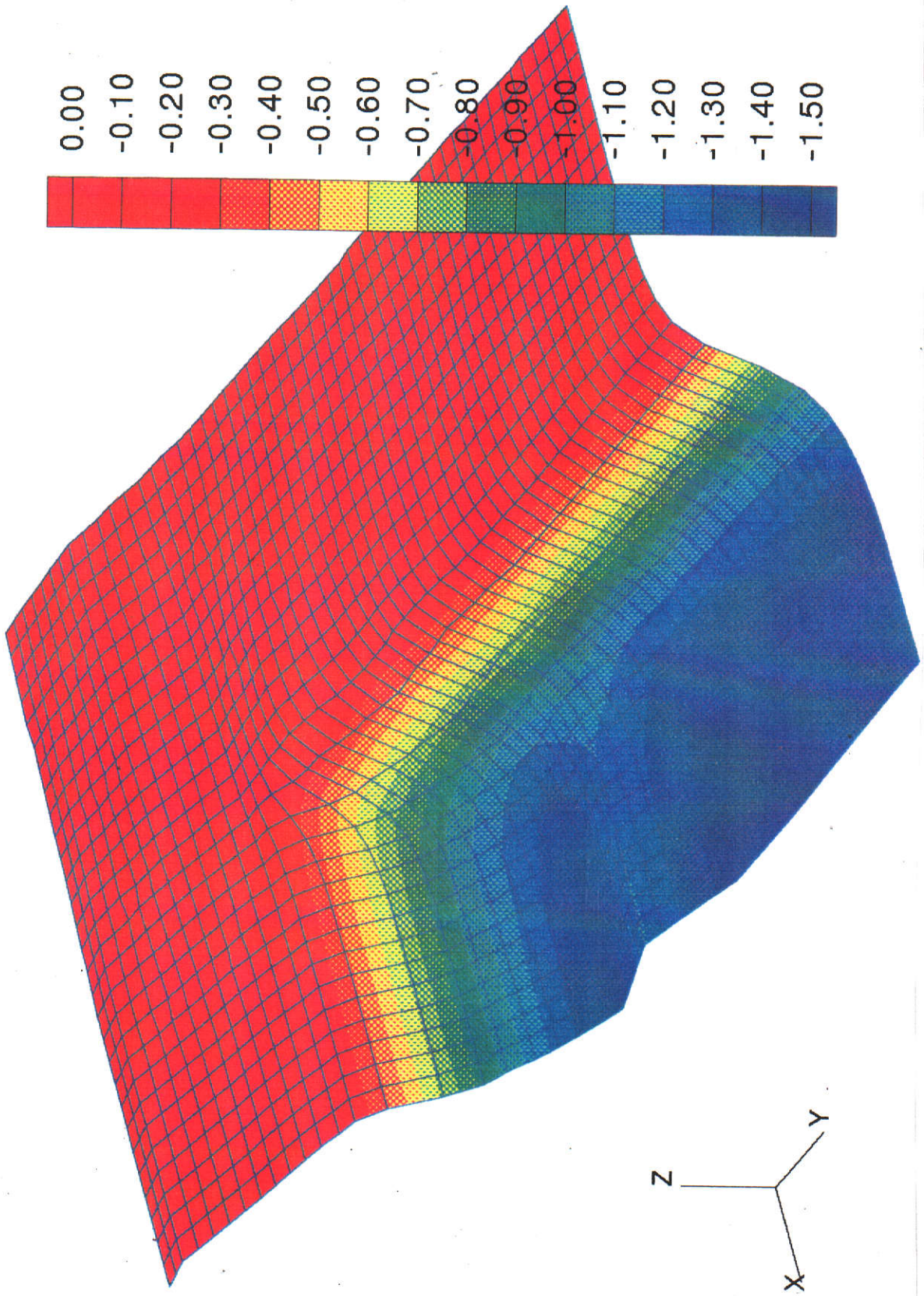

Figure 4.11

NORTH-SOUTH SECTION OF SUBSOL PREDICTED SUBSIDENCE ABOVE 2SA PANEL

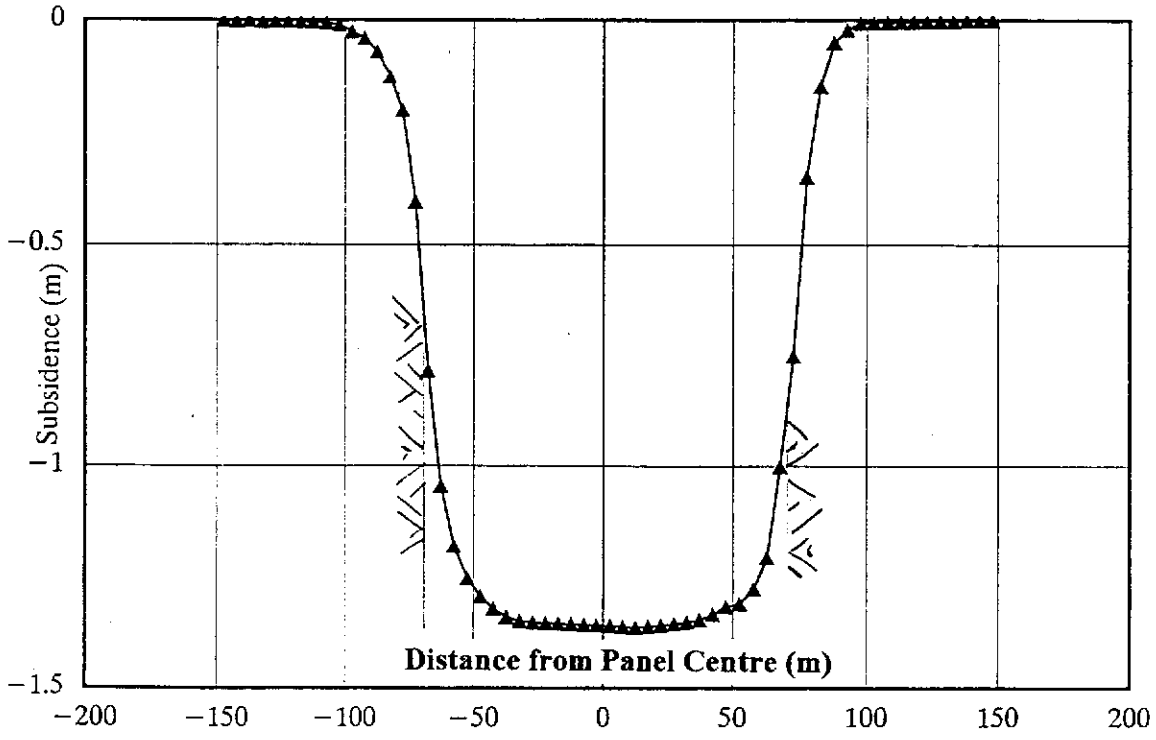

Figure 4.12 a

COMPARISON OF MEASURED AND PREDICTED SUBSIDENCE - 2SA PANEL WD6 AFTER 140m FACE ADVANCE

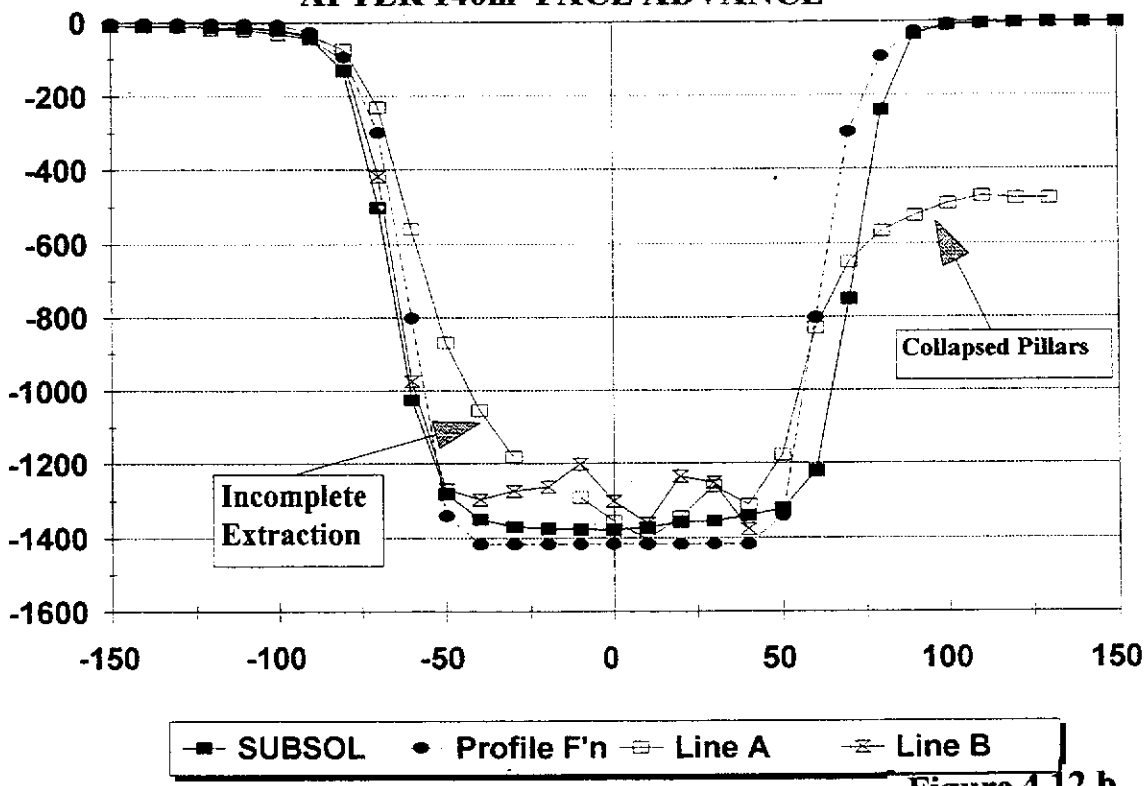

Figure 4.12 b

It can again be concluded that considering the simplistic set-up of the panel in the 2SA model, SUBSOL had sufficiently represented the development of surface subsidence above the 2SA panel. This is seen as a significant result, as this panel is very shallow (60 m), and has considerably different stratigraphy to the majority of strata above the ACIRL panel (described in detail in Appendix V).

4.1.1.3 Cross-checking Model Calibration - 1North Panel

A plan view of the panel layout and the actual range of cover depth is provided in Figure 3.42; extraction monitoring details are provided in Table 3.1 - Section 3.0. This panel, unlike the other two test case panels, used two-way split/fender lifting (see Figure 1.3 in Section 1.0).

For this model 'run', MINCAD were requested to provide subsidence data at significant levels above the mine horizon so that a better assessment could be made of the model's capability to represent the development of subsurface subsidence. Of particular interest was the ability to model the curvature and strain of the aquitards across the panel edge.

The model output for surface subsidence has been presented in Figures 4.13 and 4.14. Figure 4.13 represents a view from the east of the panel of the predicted surface subsidence after 40 m of face advance from the western edge. Figure 4.14 a represents a sectional plot of predicted surface subsidence along the west-east axis of the panel (for critical width conditions) after the face has advanced 140 m.

A comparison of the field subsidence profiles to those predicted by the SUBSOL model and profile function is illustrated in Figure 4.14 b. It is noted that some variation exists between the predictions from the two models and the field data, and that the profile function subsidence almost fits mid-point between the SUBSOL and field subsidence. The main variations with the field data are:

1) The width of the subsidence trough is greater.

2) The difference between the measured maximum subsidence and that predicted by SUBSOL is approaching 200 mm. (Note that the profile function over estimates maximum subsidence by only 60 mm.)

3) The shape of the profile function and SUBSOL subsidence troughs above the advancing/leading edge are steeper than the field data.

SUBSOL PREDICTED SURFACE SUBSIDENCE ABOVE 1 NORTH PANEL (40m Extraction)

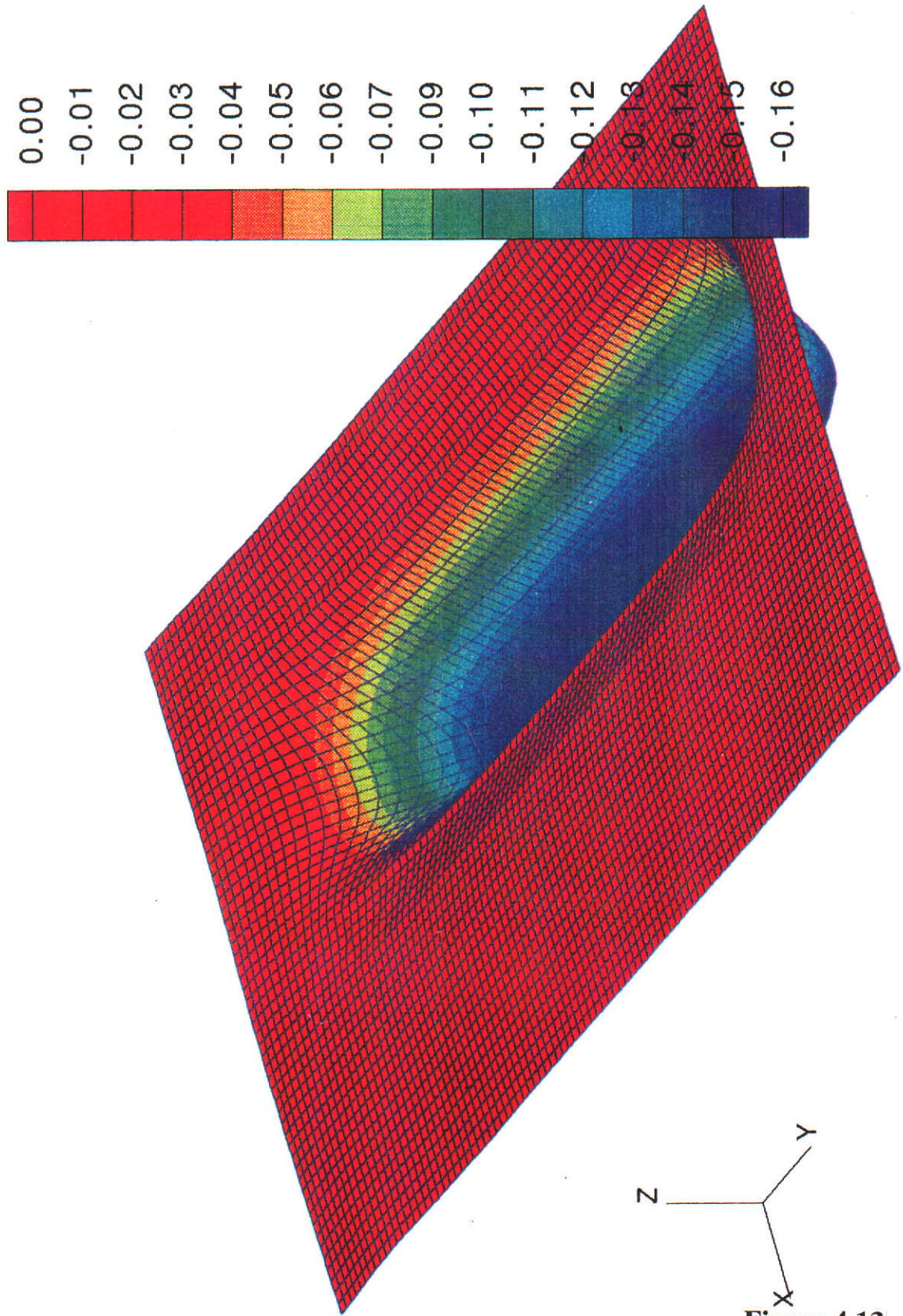

Figure 4.13

WEST-EAST SECTION OF SUBSOL PREDICTED SUBSIDENCE ABOVE 1 NORTH PANEL

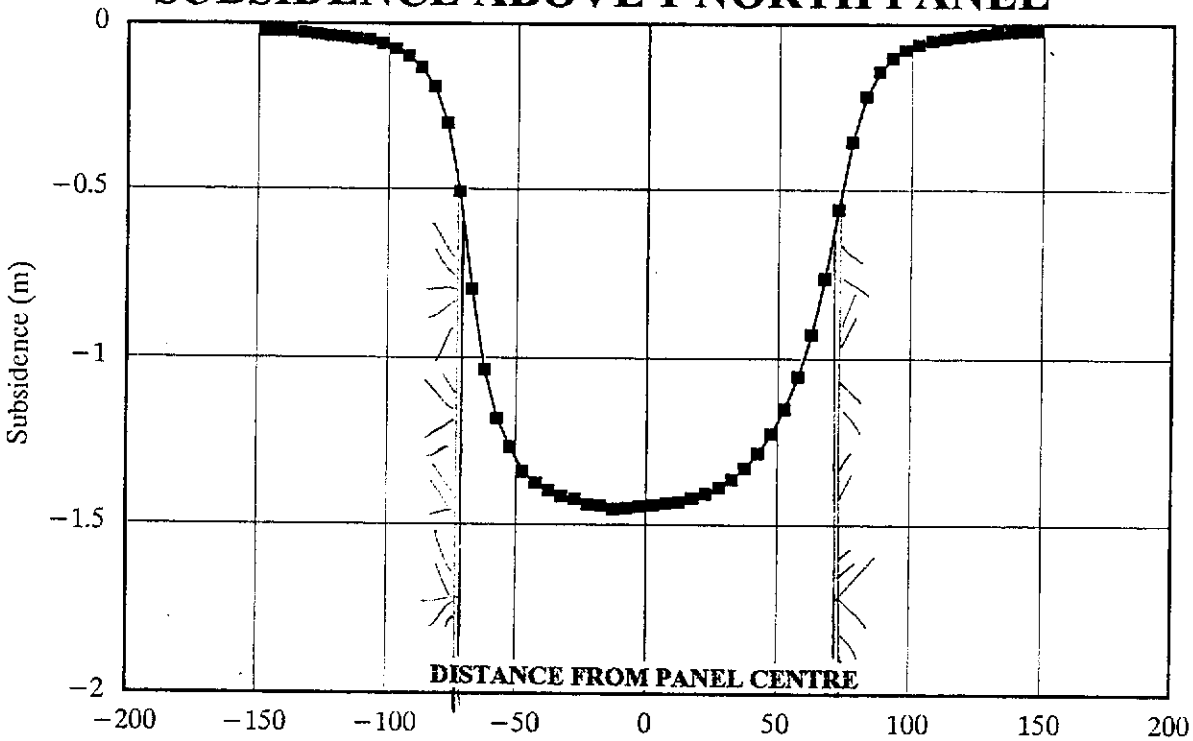

Figure 4.14 a

COMPARISON OF MEASURED AND PREDICTED SUBSIDENCE ABOVE 1 NORTH PANEL

PANEL WIDTH = 140m

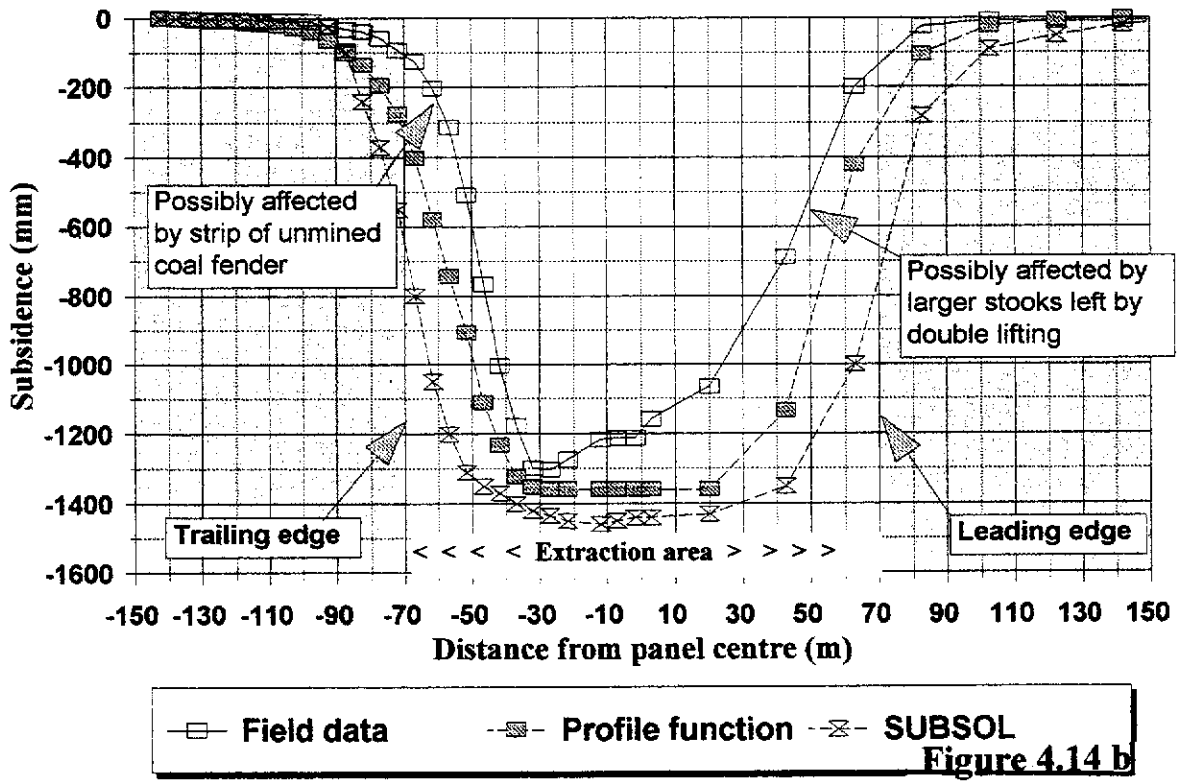

Figure 4.14 b

It is thought that the larger variation between the field and predicted subsidence at the leading edge is due to:

- the effect of the caving process at the advancing goaf edge being different and more time dependent than caving at the trailing edge. As discussed in Sections 3.2 and 3.3, the ground collapse at the trailing edge occurs more suddenly, and as one mass, whereas the leading edge caves more gently, in cantilever fashion. This probably allows for more bulking nearer the mine workings, and thereby establishes a flatter slope towards the leading edge subsidence trough.
- the probable effects of the larger remnant stooks, left by two-way lifting compared to one-way lifting (as illustrated in Figure 1.3), would have on the caving process near the panel edges.

This variation at the trailing edge is not considered important as, in the long term, subsidence profiles tend to steepen (see Figures 3.5 and 3.12).

The significance of the greater width of predicted subsidence and the greater maximum subsidence predicted is not clear. It is possible that the remnant coal allows the overhanging strata to bridge further across the panel edge before subsiding, however, it is also possible that there could be a discrepancy with some input parameters in SUBSOL. Given that the profile function subsidence trough is based on case history data, and also gives rise to a wider trough, it is assumed that the discrepancy in width of subsidence trough is caused by the remnant coal. The larger maximum subsidence may be due to a simple error of underestimating the area of coal left behind in the stooks, thus increasing the effective mining height [estimated from Equation 2.5(13)] used to calculate Smax.

As a preliminary check of the **subsurface** subsidence calculated by SUBSOL, MINCAD supplied the author with graphical subsidence data (Figure 4.15) extracted from the model representing a 140 m wide panel. This plot presents contours of the bed separation, as predicted by SUBSOL, between the first aquitard above the mine workings (the Alpha seam) and the sandstone aquifer immediately below.

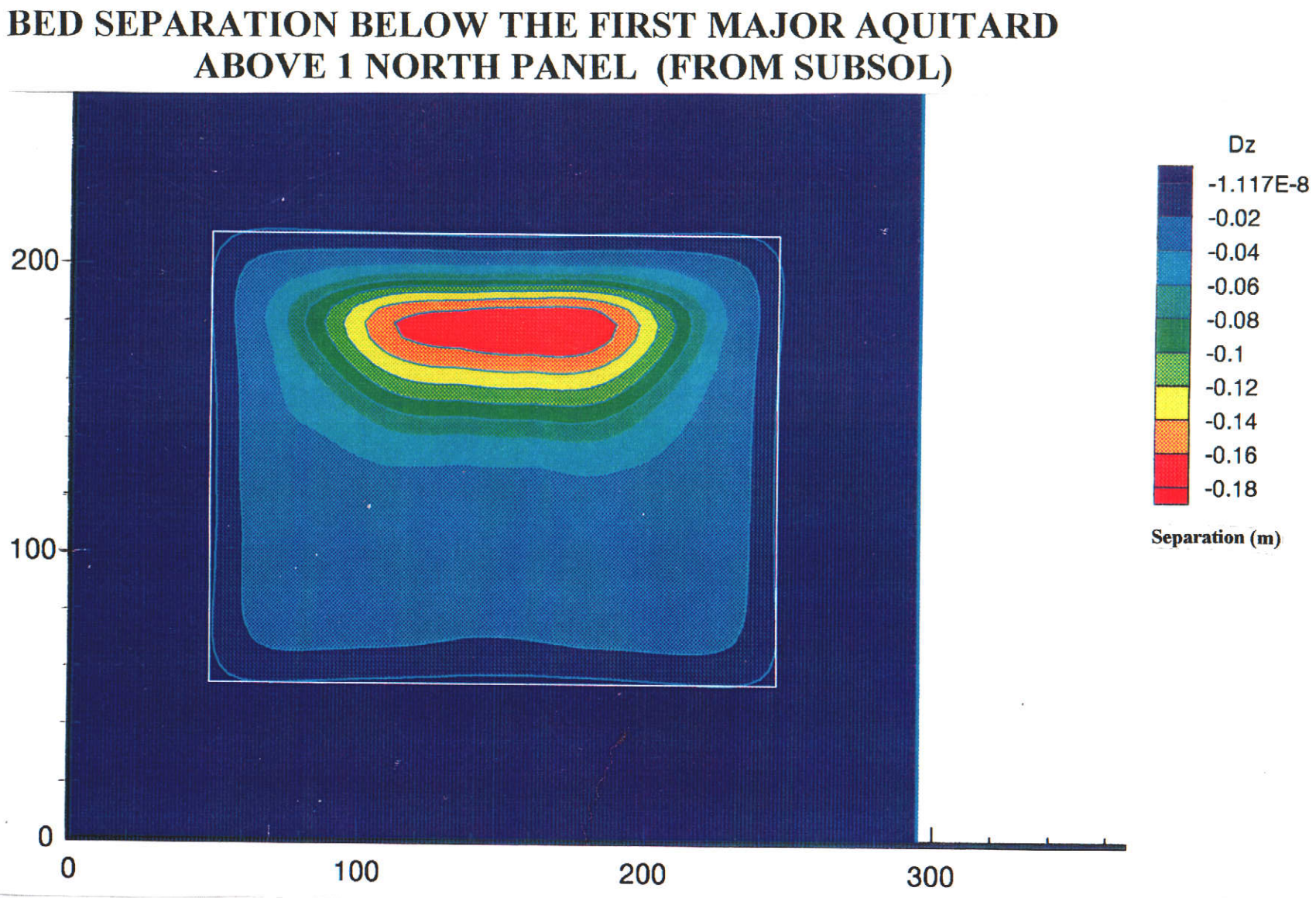
BED SEPARATION BELOW THE FIRST MAJOR AQUITARD
ABOVE 1 NORTH PANEL (FROM SUBSOL)
Dz
-1.117E-8
-0.02
-0.04
-0.06
-0.08
-0.1
-0.12
-0.14
-0.16
-0.18
Separation (m)
200
100
0
0
100
200
300

Figure 4.15

Comparison of the field data with the SUBSOL bed separation (presented in Figure 4.16) indicates that although the maximum separation is similar, the shape of separation profiles is different. This suggests that the model does not accurately represent the subsurface subsidence curvature (and concomitant strains) of the aquitards. Therefore the SUBSOL model could not be used to predict the impact of subsidence on aquifer systems. It is considered that the reason for the inadequate shape of the bed separation profile is due to the model's inability to accurately represent the strata properties within and immediately adjacent to the line of shear or caving zones.

Following this negative result, it was decided that no further tests would be run with the SUBSOL model as alterations would be required to be made to the existing calibrated model to match subsurface field data. It was considered that because the success of previous SUBSOL models were based on a number of critical assumptions, any alteration of these assumptions for the 1North model would require altering the input in earlier models. The new model output would then invariably differ from the measured surface subsidence and on-seam stresses. Further calibration of the ACIRL and 2SA models would be required which would greatly exceed the time and budgetary restraints of this project. It was concluded that the time and funds remaining did not warrant further investigation of SUBSOL.

4.1.1.4 SUBSOL Calibration Summary

The following listed points summarise the more significant conclusions made from the the stage 1 attempt to calibrate SUBSOL to the Collie Basin sediments:

- The model was proven to be able to suitably represent surface subsidence for a range of mining depths, mining geometries, and superimposed stratigraphies. The impressive feature of the model was its apparent ability to simulate the surface subsidence above panel edges affected by, in particular, rows of small set-up road pillars, unmined areas of fender, and inter-panel pillars.

COMPARISON BETWEEN SUBSOL AND MEASURED BED SEPARATION ABOVE 1 NORTH PANEL

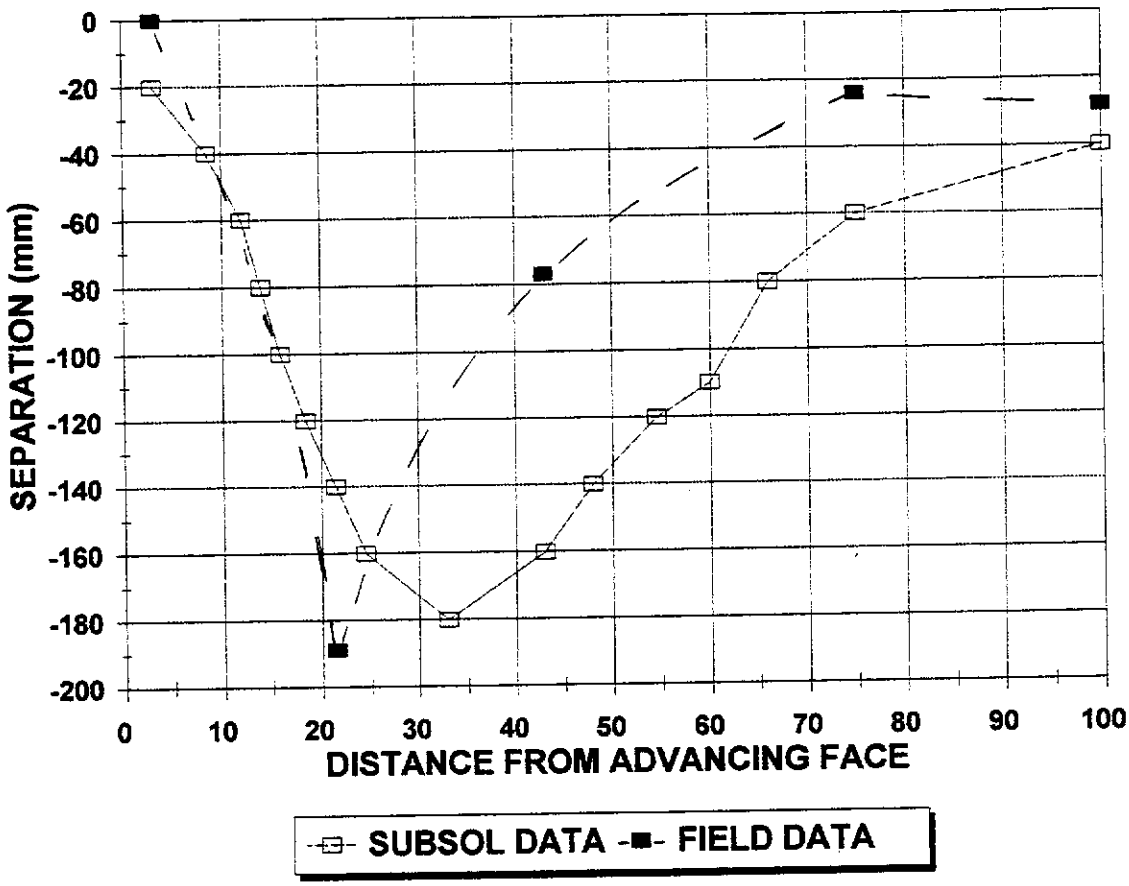

Figure 4.16

- SUBSOL could also, at least for the ACIRL panel, well represent on-seam stresses. This could be of great importance for design of pillar, fender and mine opening dimensions in future panels.

- SUBSOL modelling indicates that the aquitards are the prime geological factor controlling subsidence formation. This assumption was based on the requirement to set the mode of failure by the amount of separation at the displacement discontinuity/base of the aquitard (discussed in Appendix V). The aquitards initially bridge across the collapsed ground before subsequently "failing" and settling on the underlying layers. The deformation characteristics of the **aquifers** are a secondary parameter as they only have the potential to slump down when not restrained by the aquitards. This information compares well with the field data.

- It follows that differential bending of successive layers results in an opening being formed between the two bridging layers. The ultimate width of parting primarily depends upon the height of the respective parting above the excavation plane, however, it can also be affected by the number of partings put in the model (personal correspondence McNabb, 1993). As separation can only be developed at locations where displacement discontinuity elements were placed, the amount of bed separation predicted at a particular horizon is also dependent on the number of parting's put into in the model. This is seen as a fault with SUBSOL.

- SUBSOL could not match the shape of the subsurface subsidence, particularly adjacent to the goafing edge. It is therefore considered that SUBSOL, in its current form, cannot be used for accurate determination of the likely effects of subsidence on aquifer systems.

- It was necessary, when modelling the aquitard layers within the model, to adopt only the thickness of the coal and not include the thickness of shales and silts which make up the full thickness of an aquitard. The inclusion of silts, shales and coals resulted in excessive bridging and muted subsidence profiles.

- The numerical modelling also confirmed the important role that the goaf has on subsidence for the supercritical conditions at Collie. The model suggests that the goaf takes load rapidly - probably due to the relatively plastic nature of the overlying sediments which quickly deflect and come to rest on the goafed material, and also due to the rapid rate of reconsolidation of the goaf material. This characteristic of rapid loading of the goaf has also been inferred from the stress monitoring results from the ACIRL Test Panel, where low stress increases were reported during fender isolation and extraction (Platt, 1987). Low stresses infer that the goaf is absorbing a significant proportion of the tributary load.

- Because any failed beds rapidly deflect down onto the goaf, the model predicts that a supercritical width panel will have a central region where there is no open bedding plane partings between the goaf zone and the surface. This central zone is surrounded by "edge" zones where bridging strata will produce partings which will remain open to varying magnitudes and areal extent. This observation appears to also match field data, although it has been interpreted that the increased separation measured in the field is possibly due to dilation.

It was therefore concluded, from the analyses of the results provided, that the mathematical program SUBSOL has merit for the prediction of both on-seam stresses and surface subsidence for a wide range of mining conditions. However, in its present form SUBSOL cannot be used to accurately predict subsurface subsidence and strains above the panel edge (where it is of most importance for estimating the likely impact of subsidence on aquitards). Although some improvement of the model is considered possible, the author, in similar fashion to Bahuguna et al. (1991) has serious doubts that <u>any</u> numerical technique can suitably represent the full range of elastic and inelastic strata response to mining, and particularly along the line of shear.

Consequently, it was decided that the research project should not proceed with detailed parametric investigation of subsidence mechanisms and effects using numerical modelling.

4.2 PHYSICAL (CENTRIFUGE) MODELLING

Reiterating earlier comments, it was considered that the problems associated with physical modelling of mine subsidence in other mining regions would in general, not apply to this project as the Collie Basin sediments are weak, and the mining depths are comparatively shallow. It was anticipated that centrifuge modelling would provide useful information, particularly for caving strata in close proximity to the mine, which could be used to further enhance predictive models. However, there was still some doubt that centrifuge modelling could adequately meet the requirements of the program of research. It was therefore decided that the centrifuge modelling program be divided into two stages:

1) A feasibility stage or pilot study to assess the applicability of centrifuge modelling to the requirements of the project. Should the pilot study prove unsuitable to meet the objectives of the project, centrifuge modelling would discontinue.

2) A parametric stage in which a series of models would be constructed and operated to assess the mechanisms and characteristics of subsidence pertinent to the total extraction of coal in the Collie Basin. The intention was to use relevant data from these tests to provide supportive evidence for, and further develop existing empirical models.

4.2.1 FEASIBILITY/PILOT STUDY - PHASE 1TESTING

When the initial proposal was put forward to UWA centrifuge managing staff, it was agreed that there was potential to simulate mining of coal by underground methods within the limitations of the geotechnical centrifuge at UWA. The centrifuge manager at that time, Mr K Stone, had recently been involved in a "trap-door" study at the geotechnical centrifuge centre in Cambridge University, whereby a trap-door submerged in sand was lowered remotely during a centrifuge test at accelerated gravity forces (Stone, 1987). It was envisaged by Mr Stone that a similar system could be used for this study. Similar trap-door systems have also been developed by several other researchers (e.g,. Sutherland, 1986, Howell & Jenkins, 1983, Vardoulakis et al., 1981), and each had worked efficiently at accelerated gravities. It was proposed to

extend this approach to incorporate a number of adaptable hydraulic piston "trap-doors" and develop a comprehensive actuator system which could sequentially lower individual pistons at accelerated gravities of up to 200 g when and where required.

The responsibility for the design and construction of the trap-door system and equivalent materials in the pilot study tests (given in more detail in Appendix III) was given to UWA staff, within the guidelines provided by the author. The general set-up and operation/control of the centrifuge model was the responsibility of UWA staff. An example of the centrifuge in use, and the general set-up of a model on the centrifuge is provided in Figures 4.17 and 4.18. Suitably scaled models are mounted on a swinging platform attached to the end of the centrifuge "arm". The base of the swinging platform is 1.8 m from the central pivot of the centrifuge which, given the maximum speed of rotation of the Acutronic machine, can induce a maximum centrifugal acceleration of 200 g on a payload (scaled model) of 200 kg. As the model is rotated, the swinging platform realigns the model by 90 degrees to end up spinning horizontally, in the same plane as the centrifuge arm. This realignment allows full centripetal force to be transmitted through the model as would be in the field. It can be seen in Figure 4.17 (from UWA promotional records) that the model is in the process of being either "spun up" or "ramped down".

Aims of Feasibility/Pilot Study

The principal aims of the pilot study may be summarised as:

1. To design and develop a mechanical system to both operate efficiently and to simulate Wongawilli extraction methods on a geotechnical centrifuge.
2. To assess the feasibility of modelling Collie Basin sediments and their response to mining in a reduced-scale centrifuge model.
3. To investigate the feasibility of monitoring both surface and subsurface movements in the model.

A description of the model construction and results from each of the pilot study tests is discussed below.

40G - TONNE ACUTRONIC CENTRIFUGE AT THE UWA

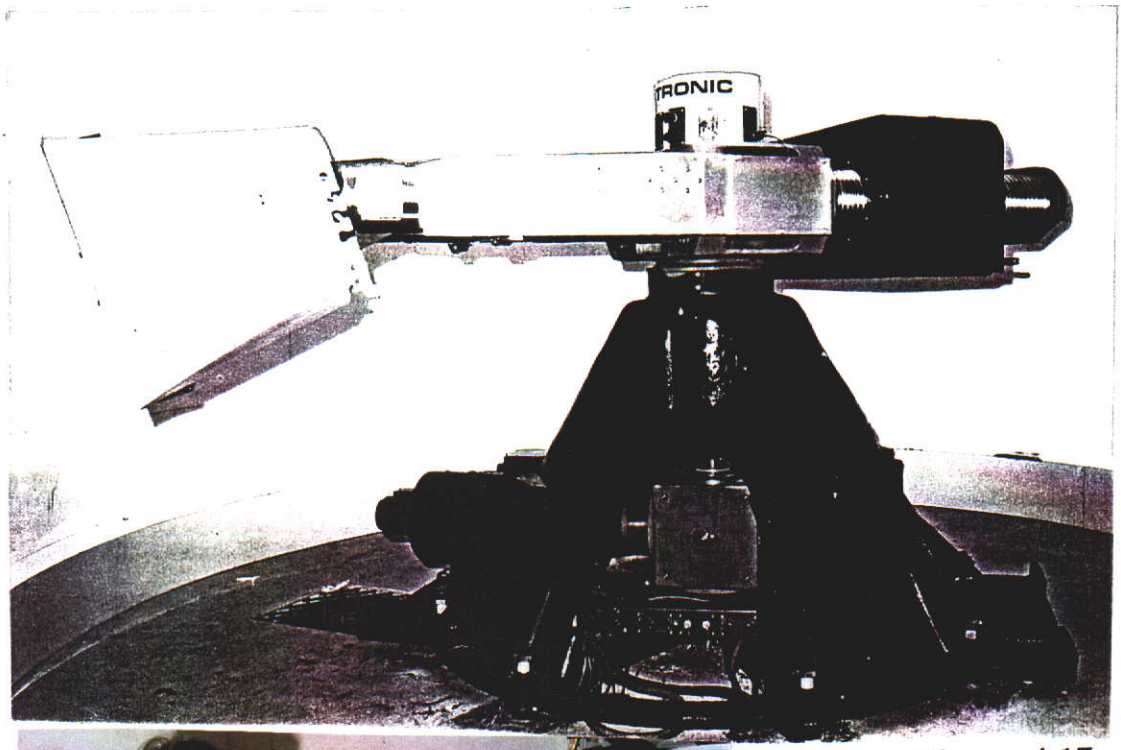

Figure 4.17

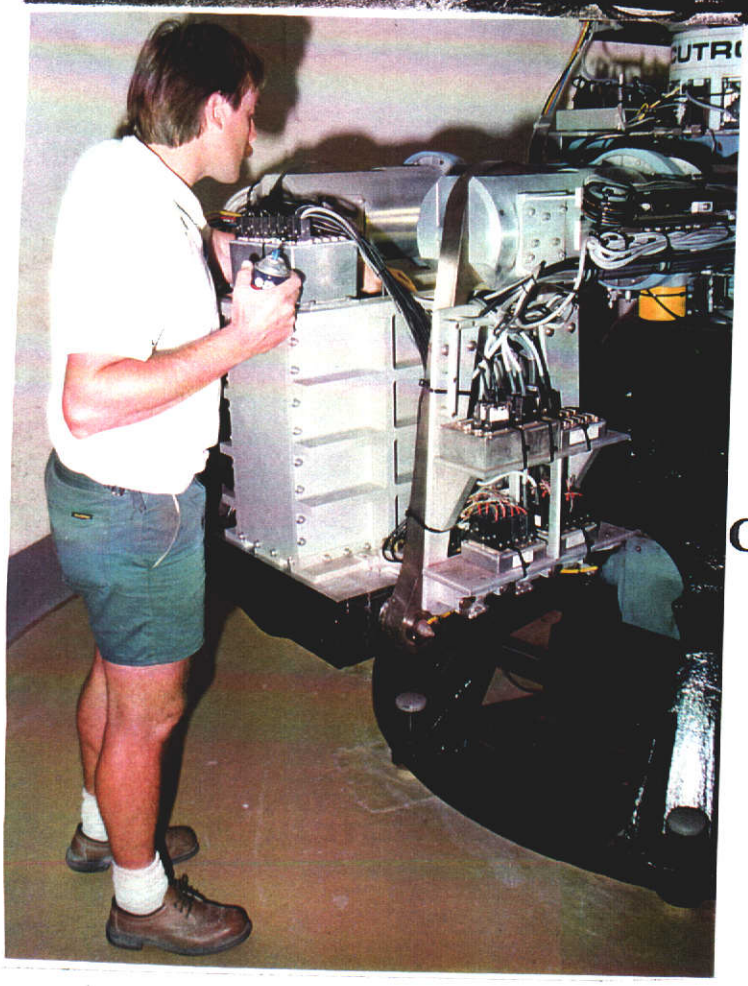

CENTRIFUGE MODEL
STRONG - BOX AND
CONTROL UNITS

Figure 4.18

A total of four centrifuge model tests were conducted to achieve the aims of the pilot study. The first two tests (Westcoll1 and Westcoll2) were aimed at proof testing the main infrastructure and individual mechanical elements of the centrifuge model package, and to assess whether mining induced subsidence could be successfully modelled within a small container at elevated gravity forces. The third and fourth tests (Westcoll3 and Westcoll4) were constructed to investigate methods of potential subsidence measurement, the feasibility of reproducing the material characteristics of the Collie Basin in such small models, and the impact of Wongawilli-type coal extraction with and without stooks.

4.2.1.1 Design of Pilot Study Models

In order to conduct a series of four tests that would provide comparable data between each test, it was necessary to design the models to meet two criteria. The first criteria was the size restriction of the existing centrifuge strong box. The second was that the mining elements needed to be engineered so that they could work effectively at accelerated gravities, were compatible with both the size restrictions of the model box, and could also be easily enlarged or reduced (to represent different mining widths) without large increases in costs or time. Flexibility within the overall system was an essential prerequisite for the pilot study models to also minimise the costs and timing of future parametric tests.

Design of Equivalent Material Model Dimensions

The first step was to determine the most appropriate field/prototype extraction panel to base the model on and then to determine the required scaling factors of the model. It was best that the prototype panel should be of supercritical width so that full subsidence would develop, and shallow so that it would fit better within the 390 mm wide, 650 mm long, and 300 mm deep model strong-box. The panel best meeting this criteria was WCL's 60 m deep extraction panel 2SA.

In regard to the scaling of the model, the author decided to adopt the same principals as Whittaker and Reddish (1989), and discussed in Section 2.6.5, due to the high level of success they had with subsidence physical modelling studies. Summarising their work, Whittaker and Reddish established that subsidence was dependent on a number

of critical parameters, and presented these as a functional equation:

Subsidence (S) = f(G,UCS,TS,E,v,W),

where W= Rock density (γ) x gravity(g) 2.5(24)

In order that these critical parameters could be used for designing synthetic materials which maintain similitude with the prototype materials, Whittaker and Reddish derived a dimensionless functional equation:

$$S/G = \int(TS/UCS, E/UCS, v, WG/UCS). \quad 2.5(29)$$

(A description of each of the above terms is provided in Section 2.6.5)

It follows that if the model (m) is to truley represent the prototype structure (p), then:

$$S/G_{(m)} = S/G_{(p)}, \quad 2.5(30)$$

$$TS_{(m)}/UCS_{(m)} = TS_{(p)}/UCS_{(p)}, \quad 2.5(31)$$

$$E_{(m)}/UCS_{(m)} = E_{(p)}/UCS_{(p)}, \quad 2.5(32)$$

$$v_{(m)} = v_{(p)}, \quad 2.5(33)$$

$$W_{(m)}.G_{(m)}/UCS_{(m)} = W_{(p)}.G_{(p)}/UCS_{(p)}. \quad 2.5(34)$$

Rearranging these terms, the following relationships for model similitude can be established:

$S_{(m)}/S_{(p)} = G_{(m)}/G_{(p)}$, the "geometric scale factor", and 2.5(35)

$$TS_{(m)}/TS_{(p)} = UCS_{(m)}/UCS_{(p)} = E_{(m)}/E_{(p)} = WG_{(m)}/WG_{(p)} \quad 2.5(36)$$

Note that the last dimensionless term in 2.5(36) is referred to as the "strength scale factor" by Whittaker and Reddish (1989).

As the 300 mm depth of the model would be further reduced by the height of the "mining" pistons and support platform (designed to be in the order of 85 mm) to be fixed to the base of the strong-box, it was decided to scale the mine prototype depth (60 m) down to 200 mm in the model.

It follows, therefore that the geometric scale factor for subsidence is defined by the term $G_{(m)}/G_{(p)}$ [Equation 2.5(22)] = 1/300 (1 m in the model equates to 300 m in the prototype).

Design of Mining Elements

It was then necessary to design the number and dimensions of each "mining element" to fit within the size limitations of the model box according to the geometric scale determined above. The resultant design was an assemblage of 18 individual hydraulic actuator units. Each actuator composes a circular piston unit with a rectangular top cap. The plan dimensions of the top cap were 45 mm wide by 68 mm long, which represented a prototype area of 13.5 m by 20.4 m at 1:300 scale. The width of the top-caps corresponded to the prototype mining width of "one-way lifting" - see Figure 1.3. The length of the top-cap represents a 20 m long section of split/fender. Although the lifting cycle in the mine progresses in a series of 4 m wide strips, it is not unusual for up to 20 m of lifted fender/split to hang up before collapsing. Therefore, the dimensions of the top-caps were considered to represent the mining cycle reasonably well.

The actuator units were arranged three deep by six across in the centrifuge strong box to provide a simulated extraction area of 81 x 61 m or 4,680 m^2. Figures 4.19 a) to c) (from Stone and Brown, 1993) illustrate the design details of a typical actuator unit and Figure 4.19 e) and Figure 4.20 shows the arrangement of the actuator units in the centrifuge strong box and the conceptual actuator solenoid control system respectively. If the model is considered as a slice through the centre of the panel, as is typically done for mathematical modelling, the area of extraction being represented by the model is 122 m long by 81 m wide.

The final number and arrangement of the actuators corresponds to a W/H ratio of: $81/60 \approx 1.4$, which represents a critical width panel and therefore can be expected to develop close to full subsidence. The direction of advance of mining (increasing panel width) was across the face of the model from right to left (see Figure 4.19 d).

The throw of the actuator units in all pilot study tests was designed to be 8.3 mm, which represented a prototype mine extraction height of 2.5 m.

The actuator units were designed to cater for the provision of stooks by allowing circular columns to remain standing as the actuator cap is lowered (also illustrated in Figures 4.19 a-e). These stooks/columns could be removed if not required, i.e. for a modified "longwall" mining simulation. The two 9 mm diameter columns each represented 64 mm^2 which corresponds to approximately 4% of the total "area of extraction", and represents 96% extraction. This represented what was considered the maximum possible extraction ratio for any individual area of extraction.

MINING SIMULATION ACTUATOR SYSTEM

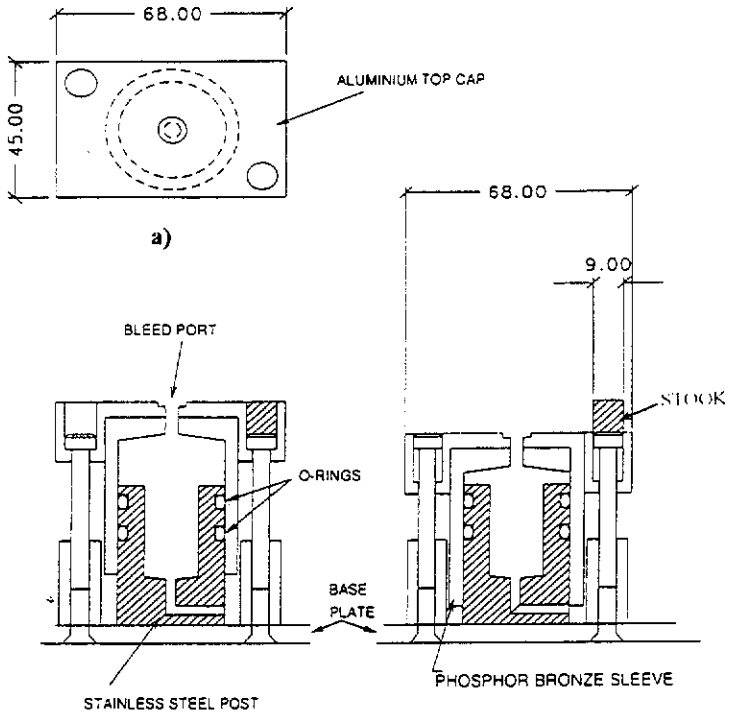

a) Plan of actuator top cap;
b) Section through raised piston actuator; **c) Section through lowered piston actuator**

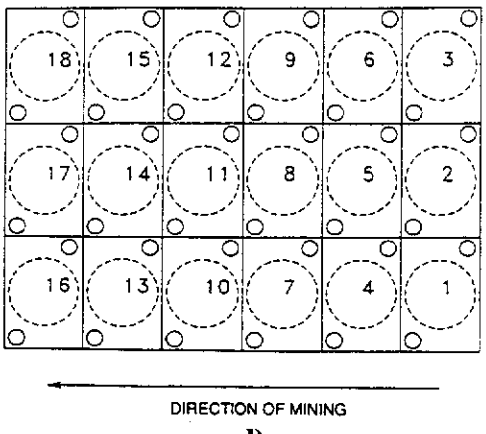

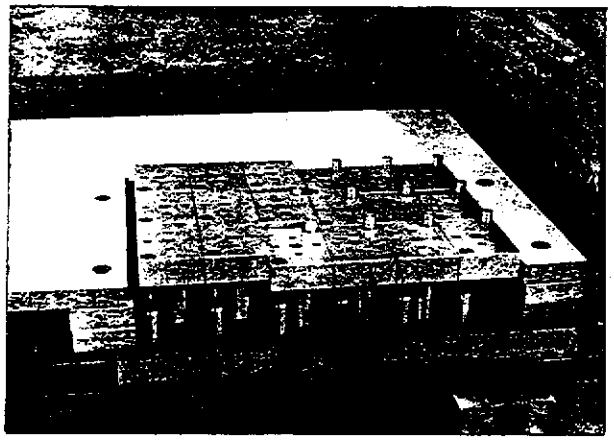

d) Plan of actuator assemblage; **e) Photograph of mining actuators in strong-box**

(after Stone and Brown)

Figure 4.19

CONCEPTUAL DIAGRAM OF ACTUATOR CONTROL SYSTEM

(modified from Stone & Brown 1993)

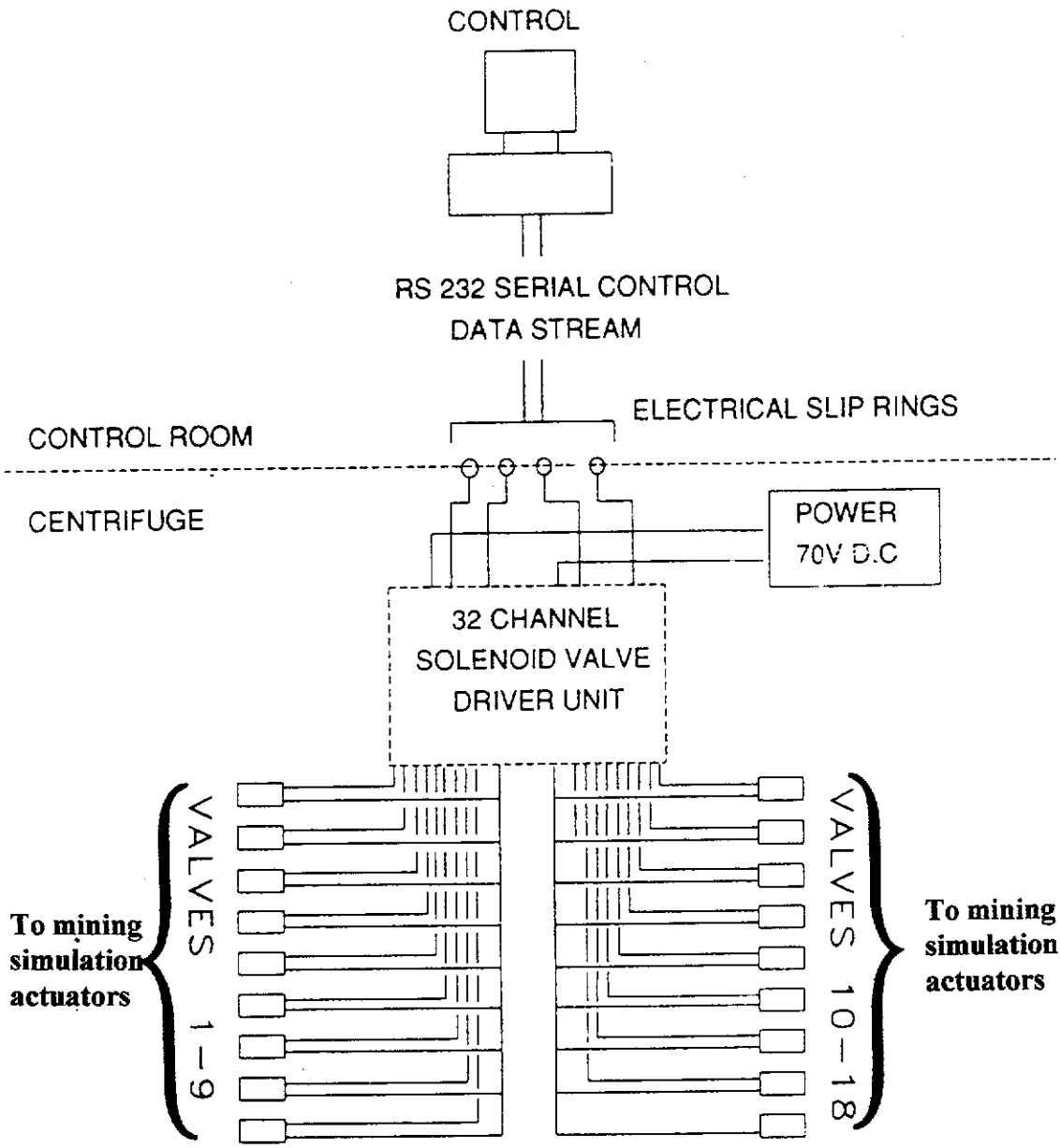

Figure 4.20

Design of Test Model Equivalent Materials

Before the models were constructed, it was necessary to establish which strength parameters should be used to develop the subsidence modelling on. As mentioned above it was decided for the feasibility/pilot study to develop the model in similar fashion to Whittaker and Reddish (1989).

Furthermore, because of the relative uncertainty of the level of success achievable in the feasibility/pilot study, it was decided that the additional time and costs involved for a detailed investigation into developing a more site specific design approach was not warranted.

It was considered that if the results gained from the pilot study supported the cost and time for further investigation of equivalent material modelling, then these pilot test results could be post-rationalised in terms of equivalent mixes of materials. In this way, even if the design criteria for equivalent materials was to change, the results from the pilot study could provide useful data for the purpose of the study.

The implication of constructing the pilot study model at 1:300 scale is that, by similitude, all dimensionless terms defined by length/dimension are affected by the same ratio; the most obvious parameter being the strength of the model material.

Again, using the approach given by Whittaker and Reddish (1989), the strength scale factor - see Equation 2.5(23) in Section 2.6.5 - can be determined from:

$$[W]G_{(m)}/[W]G_{(p)},$$

where: W = Rock density (γ) x gravity(g). 2.5(24)

It follows that, as the geometric scaling term $G_{(m)}/G_{(p)}$ used above equals 1/300, the strength scaling factor is:

$$[\gamma_{(m)}.g_{(m)}].1 \;/\; [\gamma_{(p)}.g_{(p)}].300$$

If it is assumed that the bulk density of the model materials equals the bulk density of the prototype materials, and that the centrifuge model will be operated at 150 gravities (g) the strength scaling factor becomes:

$$1 \times 150 \div 1 \times 300 \quad = \quad ½$$

This means that in order to maintain similitude, the model strength parameters must be half that of the prototype.

As discussed in Section 2.6.5, Poisson's ratio and tensile strength have (successfully) not been included in the modelling design process by Whittaker and Reddish. Based on their work, these parameters have consequently been omitted from the pilot study scaling process. The critical model strength parameters used for the pilot study were therefore the UCS and Elastic modulus of the strata.

Details of the actual materials used and the equivalent materials made for the pilot study tests can be found in Appendix III.1, along with some preliminary studies of the strength characteristics of various sand/gypsum mixtures which were performed in conjunction with this phase of the project. The model construction details for each test are discussed in the relevant Sections below.

4.2.1.2 Centrifuge Test Westcoll1

Objective - To trial the actuator assembly and proof test all mechanical elements of the geotechnical centrifuge.

Model Construction - A 10 mm thick slab of 3:1 gypsum/sand mixture was cast in an external mould, and after curing, placed in the strong box immediately above the piston actuators. From the strength test results presented in Table III.1 in Appendix III.1, this equivalent material mix gives a UCS strength of 2.3 MPa and an elastic modulus of 832 MPa. At half scale this equates to a UCS of 4.6 MPa and an elastic modulus of 1664 MPa in the prototype, which fits within the range of UCS properties for mine roof shale (as given in Table 3.1) in the Collie Basin, however, the elastic modulus is slightly higher than the typical prototype values.

For the purpose of the feasibility study, this discrepancy in similitude of the modulus was considered unimportant. It was acknowledged, however, that further investigation of appropriate material mixes would be required should the study proceed to phase II.

Once the precast slab had been placed in the strong box, 200 mm of fine sand, average particle size 300 microns, was "rained" into the strong box onto the gypsum/sand slab immediately above the actuators. At approximately 20 mm intervals, thin horizontal bands of dyed sand were placed to facilitate observation of the model deformation. There was no attempt to maintain similitude between the mechanical

properties of this sand layer and the prototype overburden as both the first two tests were mostly for systems testing. A summary of the model is provided below:

Model Type - 3 dimensional - ½ extraction panel (see Figure 4.19 e)

Operating Force - 150g

Scale - 1:300

Effective Mining Dimensions	**Model Dimensions**	**Prototype Dimensions**
1. Cover depth		200 mm 60 m
2. Individual actuators	45 x 68 mm	13.5 x 20.4 m
3. Total excavation dimension	270 x 204 mm	81 x 61 m
4. Effective mining height		8.3 mm 2.5 m

5. Mining sequence> Drop time = 5 sec, Wait time = 30sec. for individual actuators and 2 minute wait between rows of actuators.

Data Collection - Visual only:

i) during testing, through a perspex window fitted in the side of the strong box. Visual contact was made via mini CCD cameras connected to a television/video system.

ii) post- testing, following disassembly of strong box and model

Stooks - Yes

Mining Direction - Right to left

Results - Due to voltage leakage down the power slip rings, some problems were encountered in dropping all the actuator units for test Westcoll1; only 15 of the 18 units were successfully dropped. Video evidence showed that some sagging of the roof slab occurred, but the post-test investigation revealed that the model had remained essentially intact, the gypsum/sand slab was being supported by the stooks and upright pistons. Although there was some evidence of the stooks starting to punch through the strength of the roof slab was sufficient to with hold the pressures from the sand overburden when supported by stooks and irregularly spaced unlowered pistons.

Conclusions - The actuator units and general assemblage seem to work well, some modifications were required to the wiring. It was possible that the roof slab may have been too strong. No fracturing developed.

4.2.1.3 Centrifuge Test Westcoll2

Objective - Check wiring modifications and remove stooks to assess caving/sand rill behaviour.

Comments - This test was constructed to the same standards of Westcoll1. The power supply to the actuator unit solenoid valves was modified such that power was provided via a step down transformer located on the centrifuge arm supplied from mains power, delivered through a heavy duty slip ring (Stone & Randolph, 1991). The dropping order of the actuator units is shown in Figure 4.19 d, but from left to right. This test utilised the unbroken roof slab used in the previous test.

Results - Video monitoring of this test showed an initial spanning of the roof slab over 2 rows of lowered pistons (≈26 m prototype width) but with significant sagging of the roof slab occurring. At the instant of dropping the first unit of the third row, (unit 7-Figure 4.19 d), a collapse of the roof slab occurred. The collapse of the roof slab led to the development of shear bands in the overlying sand extending to approximately the centre of the model. The angle of shearing dilation in the sand, was measured to be 22-23° from the edges of the goaf (see Figure 4.21).

Tension and compression zones could be identified on the surface of the model by respective cracks and ridges through the layer of paint sprayed on the model surface prior to testing (see Figure 4.22).

Post-test excavation of the sand revealed that the gypsum roof slab had collapsed in two stages; an initial "one-piece" collapse three actuator pistons wide, followed by progressive collapses representing the width of one actuator cap for each mining step (see Figure 4.23). This figure also illustrates the curved shape of fracturing of the roof slab at the limits of each area of "extraction".

Conclusions - The centrifuge actuator system worked well and resultant collapses, shear and cracking from a simple model appear to have similarity with field observations. Further tests are required using more representative material types in the model.

POST-TEST PHOTOGRAPH OF CENTRIFUGE TEST WESTCOLL 2

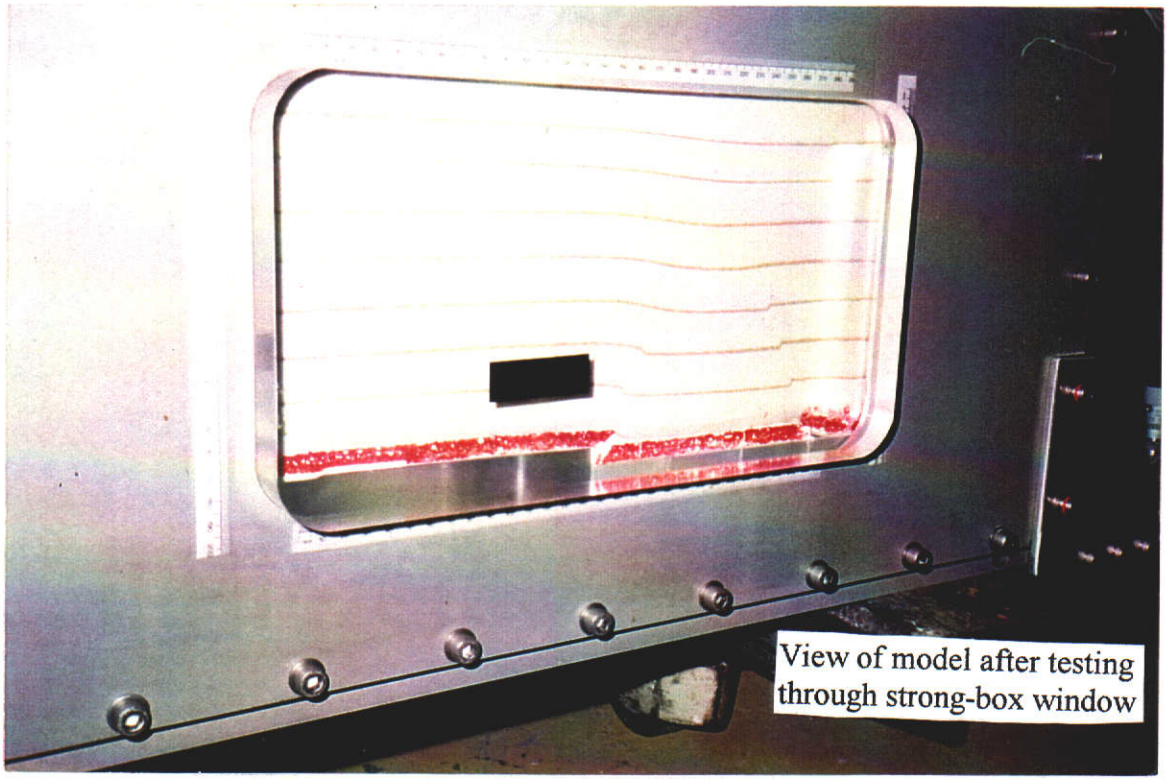

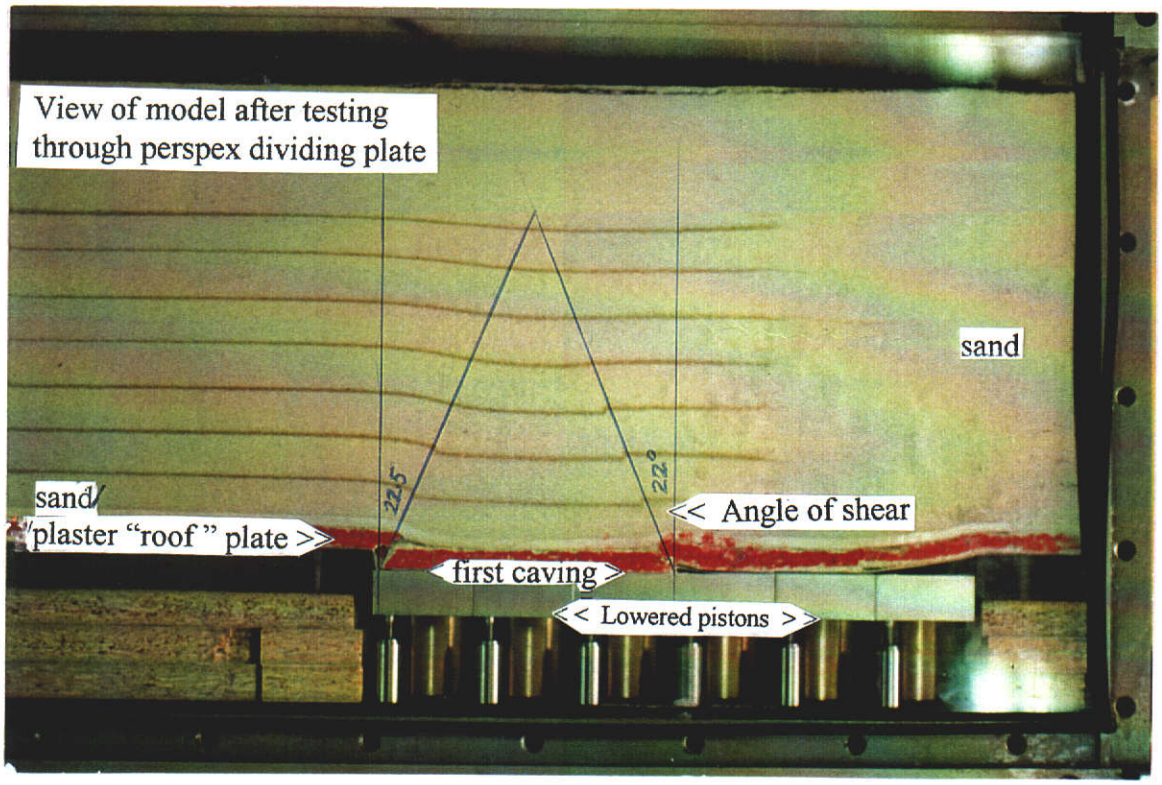

Figure 4.21

POST-TEST PHOTOGRAPH OF THE SURFACE OF CENTRIFUGE TEST WESTCOLL 2

Figure 4.22

POST-TEST PHOTOGRAPH OF THE ROOF SLAB OF CENTRIFUGE TEST WESTCOLL 2

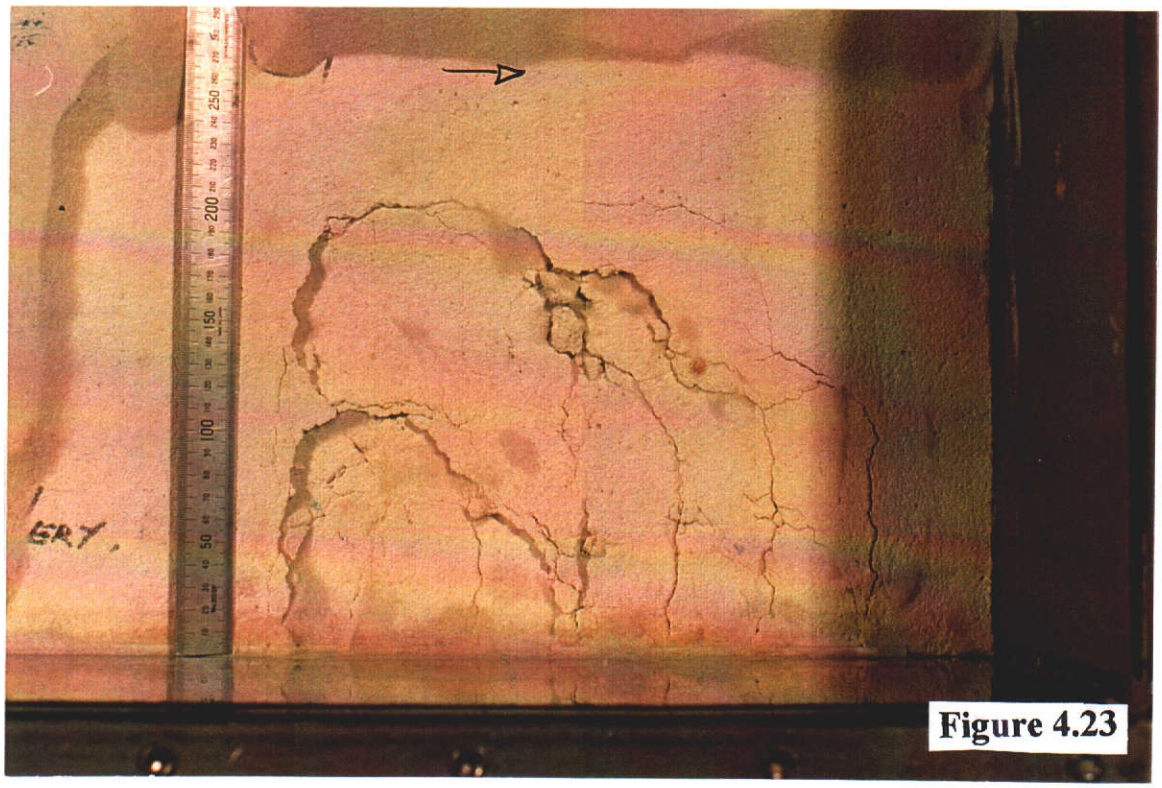

Figure 4.23

4.2.1.4 Centrifuge Test Westcoll3

Objective - The principal objective of this test was to assess the potential of simulating the subsidence and mechanical characteristics of the Collie Basin sediments in the model. In order to achieve this aim, it was necessary to base the Westcoll3 model on an existing extraction panel with a large suite of surface and subsurface subsidence field data to compare against movements measured in the centrifuge model. It was also decided to model an extraction panel at shallow depth and with simple geology to keep costs to a minimum and stay within the size and weight limitations of the centrifuge equipment. As mentioned previously, the extraction panel which best met these criteria was 2SA panel in the WD-6 colliery. The dimensions of this panel were approximately 300 m x 140 m at a typical depth of 60 m. This panel was therefore of super-critical width and can be expected to have developed maximum subsidence.

A secondary objective was to investigate the effects of remnant fender "stooks" on the caving and subsidence processes. The actuator units in Westcoll3 did not have stooks included, thus representing true 100% extraction. The following test, Westcoll4 included stooks to better represent Wongawilli extraction.

Model Make-up - The synthetic material strength and stratigraphy used for this test was based on information attained from drill holes in the immediate vicinity of the 2SA extraction panel. The model stratigraphy is illustrated in Figure 4.24.

A series of tests were conducted on varying plaster/sand/water mixes to obtain the appropriate scaled strength "equivalent material" for the model. The procedures used, and results achieved from these tests, are given in Appendix III.1. The responsibility of constructing the model according to the scaling requirements and equivalent material strength tests was given to UWA geotechnical centrifuge staff. The scaling criteria used for this test (and Westcoll4) were identical to those in the previous tests.

CENTRIFUGE MODEL WESTCOLL3 STRATIGRAPHI SECTION AND EQUIVALENT MATERIAL MIXES

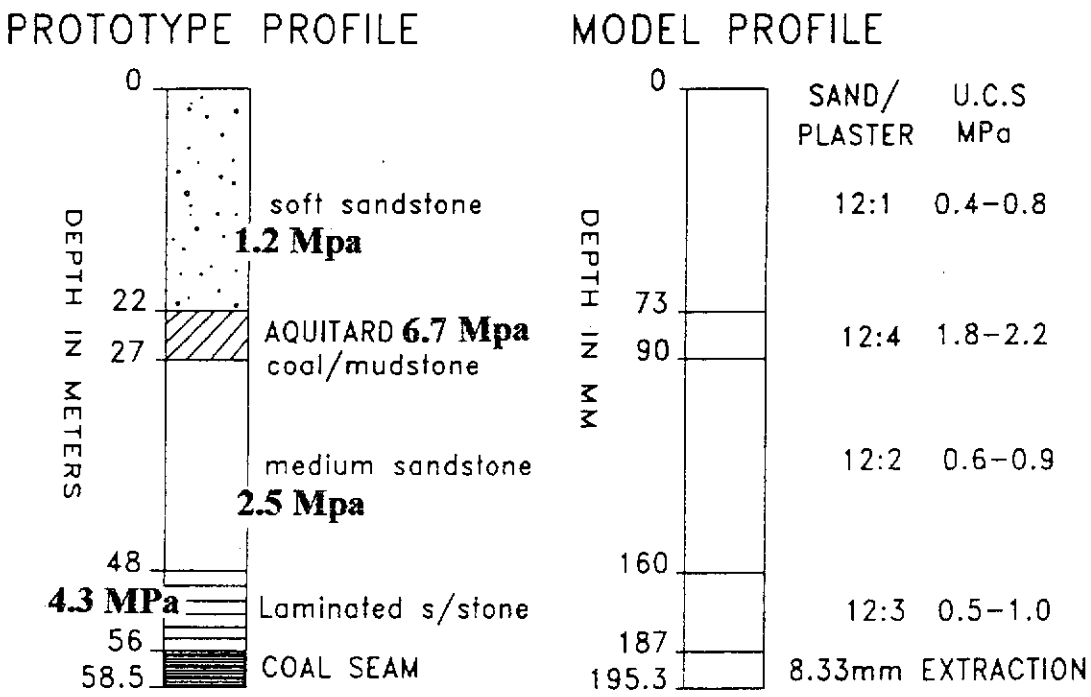

Figure 4.24

At the time of the pilot study, it was thought that one of the key elements to successfully replicate the prototype situation was to develop a technique to represent the laminated structure of the mine roof. After some trial and error, this lamination was achieved by successively casting thin layers of gypsum/sand mixtures and by sprinkling a small amount of dry sand onto the surface of each hardened mixture before the next layer was cast. (The use of the dry sand between individual cast layers was a variation of the method used for the subsidence modelling at the University of Nottingham under 1 gravity, where fine sawdust is used - B Whittaker, personal communication, 1991. From personal observations at the Nottingham Mining Engineering laboratories, this method worked reasonably well for producing laminated strata, and for absorbing free water on the surface of each layer.) The net result of this technique was to produce a 27 mm thick laminated roof stratum with definitive horizontal planes of weakness 2 - 3 mm thick. (Laboratory bending tests on laminated beams later demonstrated that this practice was inadequate for the construction of equivalent materials as it frequently resulted in totally debonded laminations which reduced the flexural strength of the material - see Appendix III.2.)

Three more uniform gypsum/sand mixtures were then cast, in appropriate thicknesses, to represent the more massive layers above the WD-6 mine roof. Figure 4.24 shows the model stratigraphic profile used in the Westcoll3 and Westcoll4 tests and the associated plaster/sand mixtures used for each stratum.

In all, four prototype material layers were modelled; an upper soft sandstone (UCS=1.2 MPa) down to 22 m from the surface (to 73 mm in the model), then a coal/mudstone aquitard (UCS=6.7 MPa) from 22 to 27 m (73 - 90 mm), then a slightly stronger sandstone (UCS=2.5 MPa) from 27 to 48 m (90 - 160 mm), and finally the laminated sandstone/shale roof material (UCS=4.3 MPa) from 48 to 56 m (160 - 187 mm from the surface of the model).

After the synthetic model material had been cast into the strong box, the front face of the strong box was removed and a uniform grid of dots and horizontal lines painted onto the model face. The use of marker rods embedded in the model, as per Sutherland (1984), was considered to be inappropriate; it was important that there was no interference to the caving process in this test. The top surface of the model was also sprayed black to highlight the expression of any surface subsidence. The general layout of the model and equivalent prototype mining parameters are summarised

below:

Model Type - 3 dimensional - ½ extraction panel

Operating Force - 150g

Mining Parameters	**Model Dimensions**	**Target Prototype Dimensions**
1. Cover depth	187 mm	56 m
2. Individual actuators	45 x 68 mm	13.5 x 20.4 m
3. Total excavation	270 x 204 mm	81 x 61 m
4. Effective mining height	8.3 mm	2.5 m
5. Mining sequence	Drop time = 5sec, Wait time = 30sec. for individual actuators and 2 min. wait between rows of actuators.	

Note: Due to an oversight in scaling calculations, the target prototype dimensions were not met (see Comments section below).

Data Collection - Subsidence data was collected from the test with the following methods:

1. Laser profiling of the surface before and after testing. The laser unit emits an infra-red laser beam from its source onto the surface of the model and captures reflected beam signals. The time delay between emitting and receiving the signal pulses relates to a vertical distance from the source. The output from the laser detection unit is directly connected via a RS-232 plug to a computer which runs the data recording and storage software. The laser unit is mounted on an aluminium frame approximately 400 mm long which rests on the top of the strong-box and can be moved at a controlled, constant rate either vertically and laterally as required. Movement is initiated by a screw fed, motor driven, actuator. Discussion of the laser set-up is given in Appendix IV.13.
2. Visual:
    a) during testing - through the perspex window (via a CCD camera/video).
    b) post-test - following disassembly of model:
        i) crack tracing
        ii) marker dots and line tracing

Stooks - No

Mining Direction - Right to left

Comments - It should be noted that the actual strength scaling factor required to maintain similitude is not ½ scale as reported earlier and in Stone et al. (1991) and assumed for tests Westcoll1 & 2, as there was some variation between the model and prototype material bulk densities. (The typical prototype bulk density near 2SA panel is 2.00 t/m^3, whilst the sand/plaster material is typically 1.61 t/m ^{3} which relates to a variation of approximately 20%.) This means that the forces acting on the seam level are not 150 times the prototype because the equivalent material is lighter than the prototype strata. By adopting the same principles given by Equation 2.5(23), the actual strength-scaling-factor that would be required with the lower density material would be:

$$\gamma_{(m)}.g_{(m)}.G \;/\; \gamma_{(p)}.g_{(p)}.G \quad = \quad 1.61 \times 150 \times 1 \div 2.00 \times 300 \quad = \quad 1/2.5.$$

Therefore the model actually represents prototype materials that are 2.5 times greater. However, as illustrated by the range of UCS values given in Figure 4.24 for each sand:plaster mix, the scaled prototype strengths were still reasonably represented by the mixes used in the model. For example, the 12:1 mix used for the upper sandstone equates to UCS between 0.4 and 0.8 MPa. If a mid-range equivalent material UCS value of 0.6 MPa is scaled by a factor of 2.5 then the prototype strength being represented is 1.5 MPa which is close to the desired prototype strength of 1.2 MPa.

It should also be noted that the equivalent prototype UCS of the mine roof laminite (between 0.5 and 1.0 MPa) is much less than the required 4.3 MPa. It is considered that this discrepancy between scaled model dimensions and prototype dimensions, though possibly affecting the results, was not important to the purpose of the pilot study. This discrepancy was corrected in future models and model construction was specifically designed and itemised by the author from this point onwards; the general construction and set-up of the model remained within the duties of UWA staff.

It was decided to reverse the direction of mining for these tests - from left to right in the previous tests - to right to left to observe if any end effects were developing. Figure 4.25 a illustrates how the model looked in the strong-box immediately prior to and after testing.

PRE-TEST PHOTOGRAPH OF THE FRONT OF CENTRIFUGE TEST WESTCOLL 3

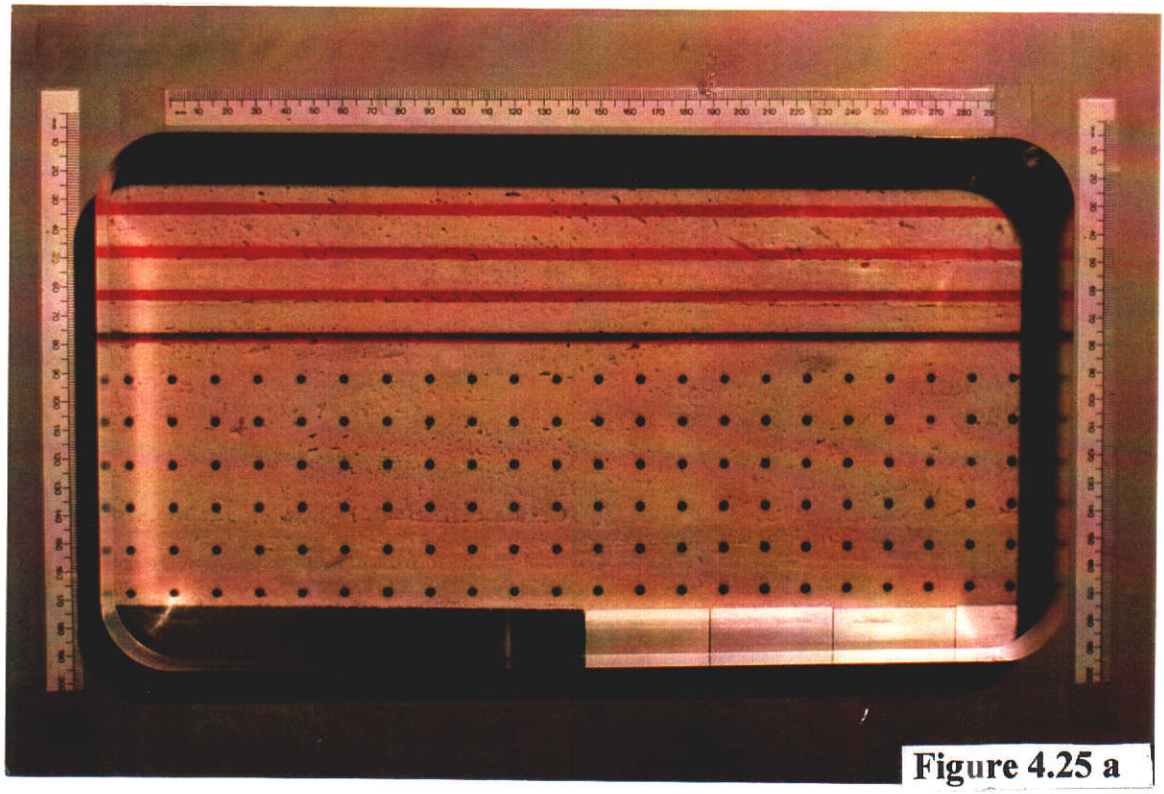

Figure 4.25 a

POST-TEST PHOTOGRAPH OF THE FRONT OF CENTRIFUGE TEST WESTCOLL3

(Cracks enhanced by tracing)

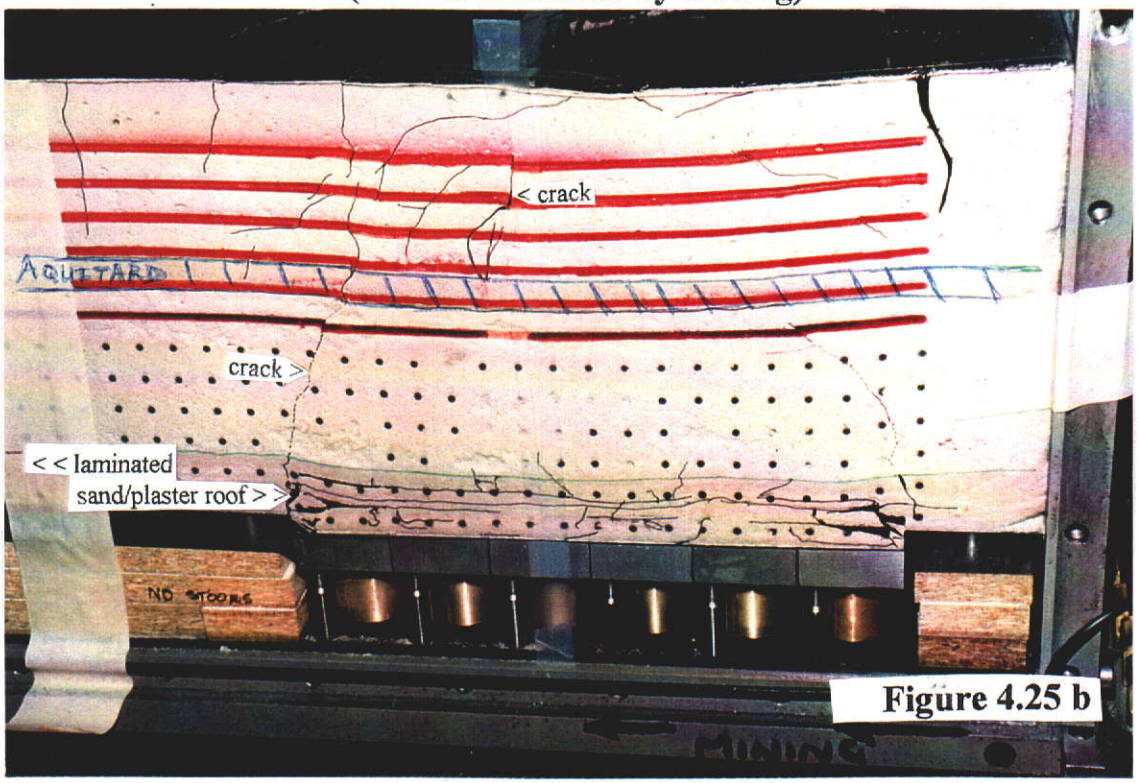

Figure 4.25 b

Results - The actuator assembly and accompanying system worked well. Video observations of the model test showed that an equivalent material laminated roof stratum had been successfully prepared. Definite caving, fracturing and bending sequences could be identified throughout the "extraction" process via the perspex window. Traces of the cracking evident on the exposed faces of the model and the aquitard layer after the test was completed and the model strong-box dismantled are provided in Figure 4.25b and 4.26 and 4.27. Measured caving angles at the panel edges ranged between 18 and 25 degrees for the trailing and advancing edges respectively, which compare reasonably well with field data (Section 3.2).

It was interpreted that the caving processes of the immediate roof compared reasonably well with goafing mechanisms seen in mine workings. However, there did not appear to be any development of a definite, continuous shearing plane above the first aquitard, as interpreted from field measurements. This lack of a definite shearing plane was consistent with all centrifuge tests.

Traces of the cracking developed on the equivalent material aquitard layer demonstrated:

- A series of near parallel cracks representing shearing along the alignment of each row of actuator units. These cracks generally appear to have sequentially opened and closed as the "mining face" passes beneath and extends beyond any position. Some cracks did remain open towards the panel edges.
- Cracks at the edges of "extraction" limits were both wide (2 - 3 mm) and had vertically displaced edges.
- Both compressional and tensional cracks were evident. Compression cracks are denoted by raised triangular shapes disseminating from a crack trace - see Appendix IV.
- Curved/semi circular shearing (in plan) at the extraction panel edges.

Although the large magnitudes and apertures of traced cracking were not expected from field measurements, it was not possible to discount them. The ramifications of such movements on aquifer interconnection are obvious.

POST-TEST TRACING OF THE SURFACE OF CENTRIFUGE TEST WESTCOLL 3

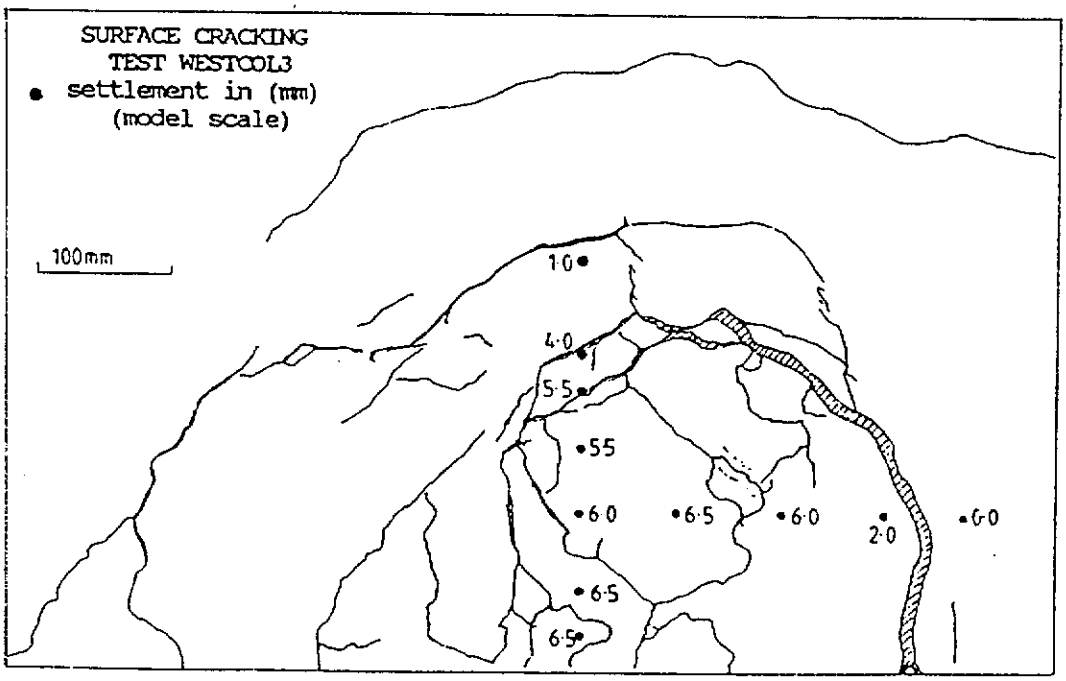

Figure 4.26

POST-TEST TRACING OF THE AQUITARD OF CENTRIFUGE TEST WESTCOLL 3

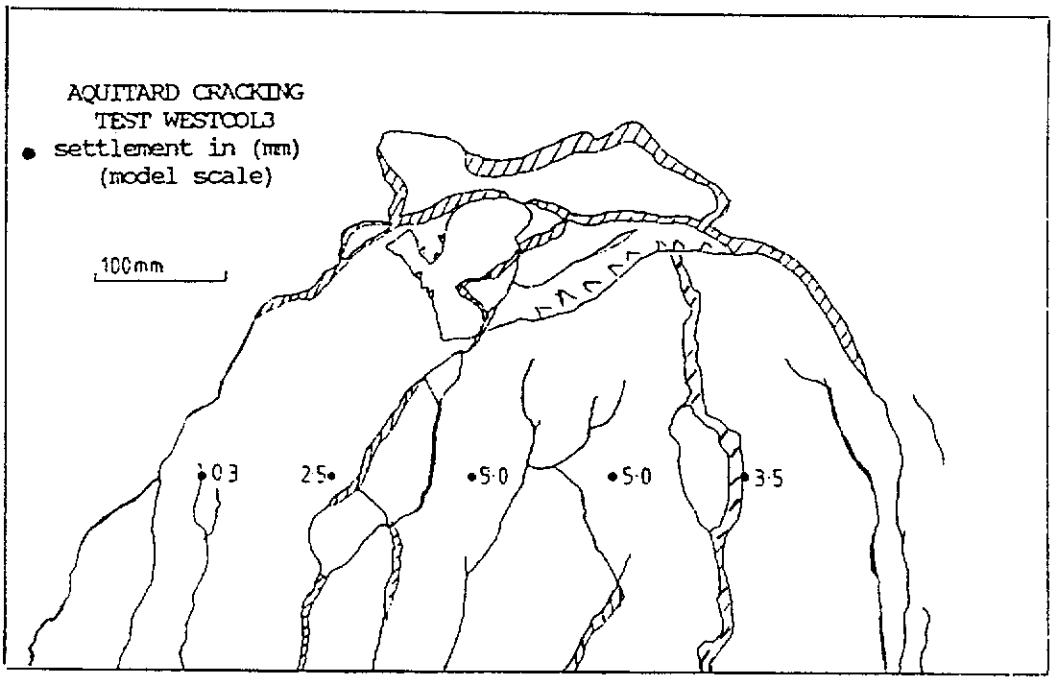

Figure 4.27

Surface cracking (Figure 4.26) appeared to be a direct reflection of the shearing, bending and cracking occurring at the stiffer aquitard. (This would be expected.) Cracking on both the aquitard and model surface was much more severe on the side near the trailing edge.

Laser Profiles - Two laser profiles were successfully trialed along the surface of the model, orthogonally bisecting each other above the mid-point of the extraction panel. An attempt was also made to profile the surfaces of the aquitard layer and the laminated mine roof stratum. Profiling was attempted both during construction of the model, and after the test was completed. Subsidence was calculated as the difference between the data recorded both before and after testing. It was found to be impractical to try using the laser at the mine roof horizon after testing. The results of the laser profiling are also presented in Figures 4.26 and 4.27, being represented as spot heights taken at regular intervals across these sections after dissection of the model.

It was interpreted from these results that although the shape and surface features of the final subsidence trough did not fully comply with field data (due to the presence of the large open cracks and somewhat stepped surface), the magnitude of subsidence measured by the laser profiling was reasonably similar to what would be expected for this test. (The maximum subsidence measured by laser profiling was 6.5 mm, which represents 78% of the mining height - compared to 63% mining height expected in the field). Considering the relatively limited research and detail put into fabrication of the equivalent materials used in the pilot study, this was interpreted as a favourable result.

Conclusions - All mining simulation procedures worked well. Model subsidence compares reasonably well with field measurements considering the rudimentary scaling applied. The caving characteristics of the laminated roof material appeared reasonable, however, there was some doubt about the apparent caving, cracking and bending characteristics of the remainder of the equivalent materials. Nonetheless, visual evidence suggests that subsidence development through flexural shear is the controlling factor.

From observations made during the test, it appears that the actuator drop intervals were adequate for the test. After close scrutinisation of the video screen during testing, it was evident that all movement within the model had ceased after one minute.

4.1.2.5 Centrifuge Test Westcoll4

Objective - The aim of this test was to assess the effect of leaving "stooks" in the panel by comparing the results of this test against those obtained in Westcoll3 and in the process attempt to better represent the prototype situation.

As a result, the test was made to closely represent Westcoll3, with the exception that stooks were introduced into the piston top caps.

Results - **Comparison of Model Responses (Westcoll3 and 4)**

Comparison of subsidence as measured by the laser transducer shows that the maximum surface and aquitard settlements recorded for both tests were fairly similar, (78% effective mining height as indicated in Figures 4.26 to 4.29). Although the magnitudes of subsidence are similar, the traces of model face and surface crack patterns (Figures 4.25b and 4.30) illustrate that the area affected by the extraction process is greater for extraction without stooks, and although the general shape of the subsided region is similar for both tests, the surface and subsurface expressions (i.e. visible cracks), are more pronounced/stepped for the "no stooks" case.

These results suggest that the Wongawilli-associated stooks are affecting the manner in which the immediate roof blocks detach from the undisturbed strata and collapse into the goaf. In test Westcoll3 it appears that the roof blocks are caving more suddenly, and vertically with distinct shearing edges (as seen in the comparison between Figures 4.27 and 4.29 at the aquitard level) and hence more pronounced cracking develops. Furthermore, shearing - though not definitive - is readily apparent above the aquitard in Westcoll3 (no stooks), whereas in Westcoll4 (with stooks) there is no discernible shearing above this aquitard. Regardless of these varying effects, the measured caving/shearing angles at the panel edges compared well in both tests (ranging between 18 and 25° for the trailing and advancing edges respectively), and also compare reasonably well with field data (Sections 3.2 and 3.3).

An interesting feature to note in the Westcoll4 test is the development of a hump on the surface of the model at roughly the midpoint above the first three pistons. The location of this hump is almost identical to that observed in Westcoll2. In fact, considering the geometric scaling factor of 1:373, this hump phenomenon also closely matches the hump noted in the field above 1North panel (see Section 3.1), where it was located at the mid-point of large-scale "secondary" caving after three fenders were extracted.

POST-TEST TRACING OF THE SURFACE OF CENTRIFUGE TEST WESTCOLL 4

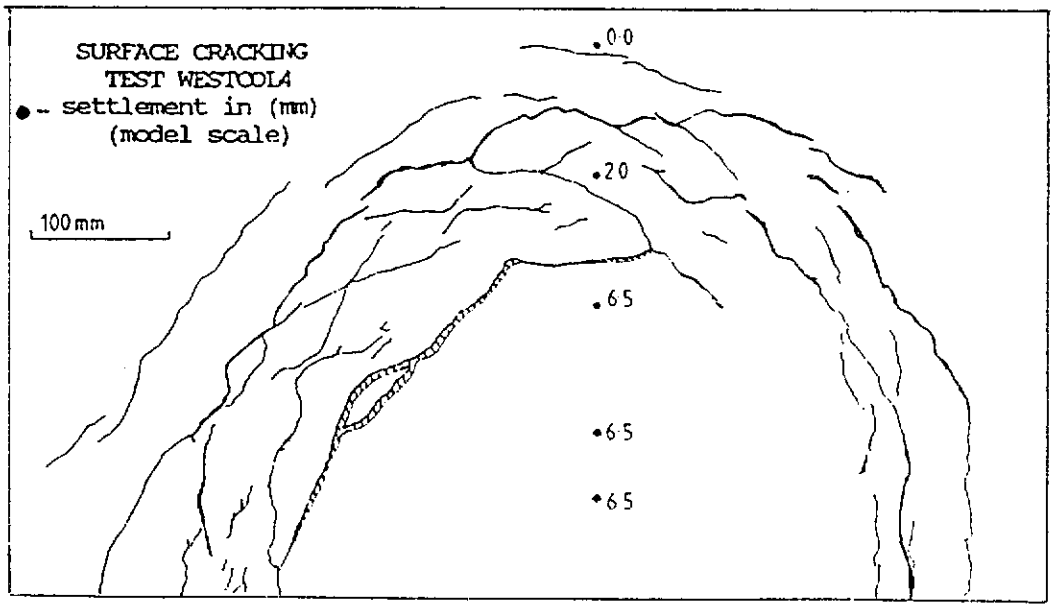

Figure 4.28

POST-TEST TRACING OF THE AQUITARD OF CENTRIFUGE TEST WESTCOLL 4

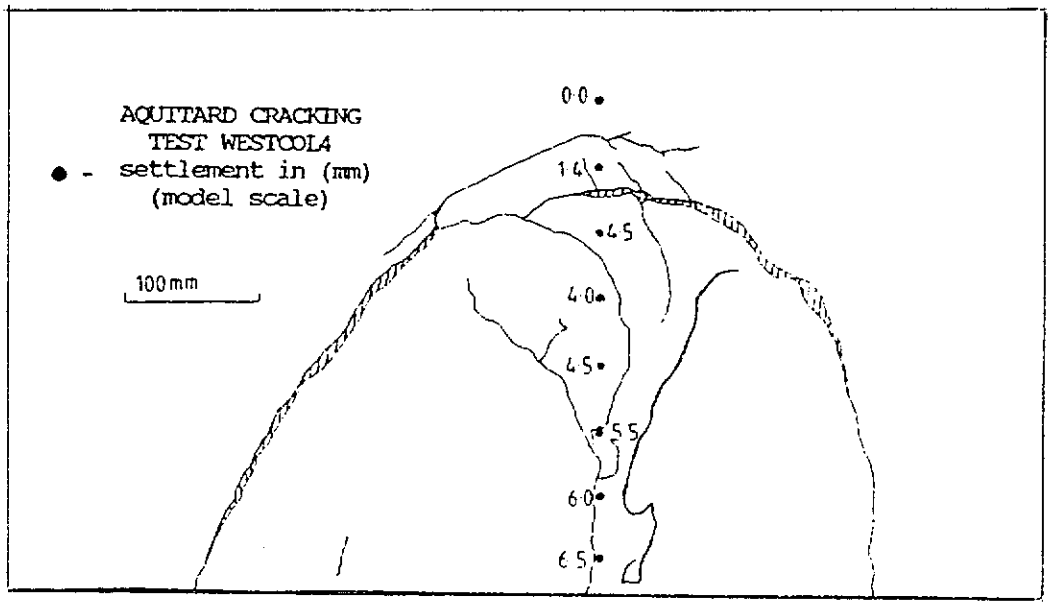

Figure 4.29

POST-TEST PHOTOGRAPH OF THE FRONT AND TOP OF CENTRIFUGE TEST WESTCOLL4

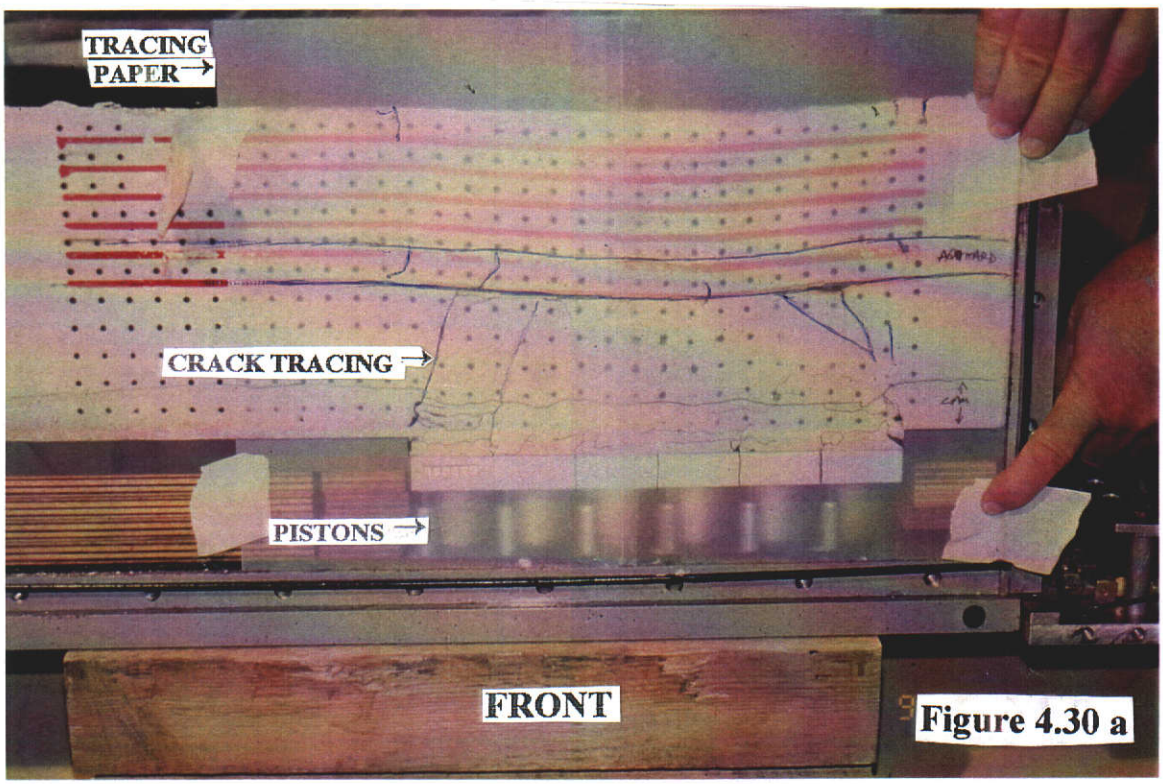

Figure 4.30 a

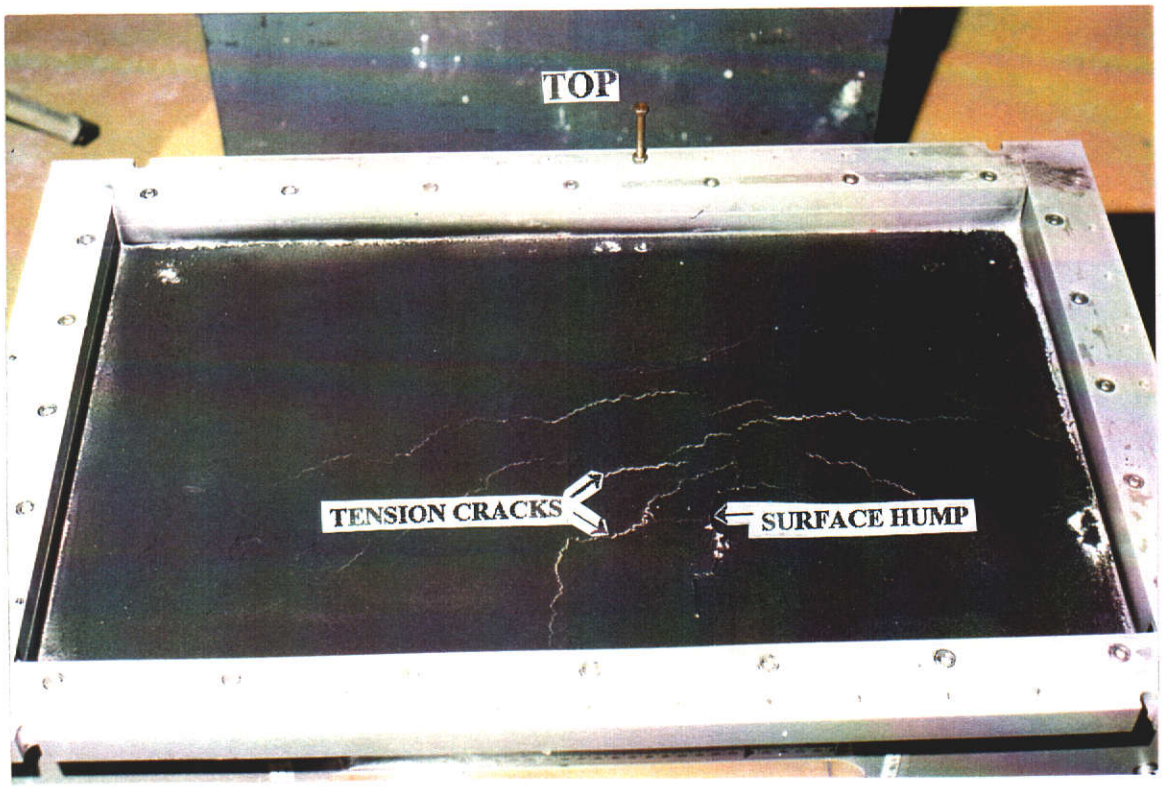

Figure 4.30 b

This hump was only noted within an area between 65 and 85 m depth of cover along the direction of split driveage, after the panel width reached 54 m, representing a W/H interval of 0.64 to 0.83. In the 182 mm deep model the width of extraction represented by lowering 3 x 45 mm actuators corresponds to a W/H of 0.74. Curiously, however, there was no obvious shearing plane leading to this hump in the model.

It is worth noting that in the paper by Stone et al. (1991) it was claimed that the Westcoll3 test represents a longwall panel with no stooks. This is not completely true, as longwall faces tend to advance more steadily, in 0.5 - 1 m increments, and not in 13 m wide segments. The results for Westcoll3 may, however, be likened to a longwall face when the mine stops advancing for a period of time and consequently allows a clearly defined shearing edge to develop.

Another point to note from the paper by Stone et al. is that the laser spot height subsidence given at the aquitard level in both tests is generally less than the surface level. This is clearly not possible, the difference being put down to:

a) plaster from the superimposed strata being left on the surface of the aquitard,

b) an error in laser profile calibration, and/or

c) an inability of the laser to give accurate readings on granular, angular material.

In this case, it was probably a combination of all three. In later tests it was found to be very difficult to obtain an accurate calibration factor for laser signals on uneven, dull, granular surfaces. In test Westcoll4 in particular, it was not possible to establish a continuous, clean, undisturbed surface after separation of individual layers (necessary for profiling). **Subsurface** laser profiling was hence not attempted in future tests.

Another result claimed by Stone et al. was the successful implementation of a laminated roof material, based on the observed caving (Figures 4.31 a) and laser-measured subsidence. However,the photograph of the caved roof in Figure 4.31 b, with the broken material removed, suggests that the immediate roof material has essentially slumped in one mass - equivalent to the dimension of each piston top-cap. Furthermore, the measured subsidence at the face of the model approximated 100% of the mining height - see Figure 4.32. At the time this excessive subsidence was thought to be due to the localised crushing of the front skin of the model which allowed the dots to displace downwards separately within the thin annulus between the model block and the perspex window. More value was placed on laser readings at the time.

POST-TEST PHOTOGRAPH OF THE CAVED ROOF OF CENTRIFUGE TEST WESTCOLL4

(Blockiness enhanced during dismantling)

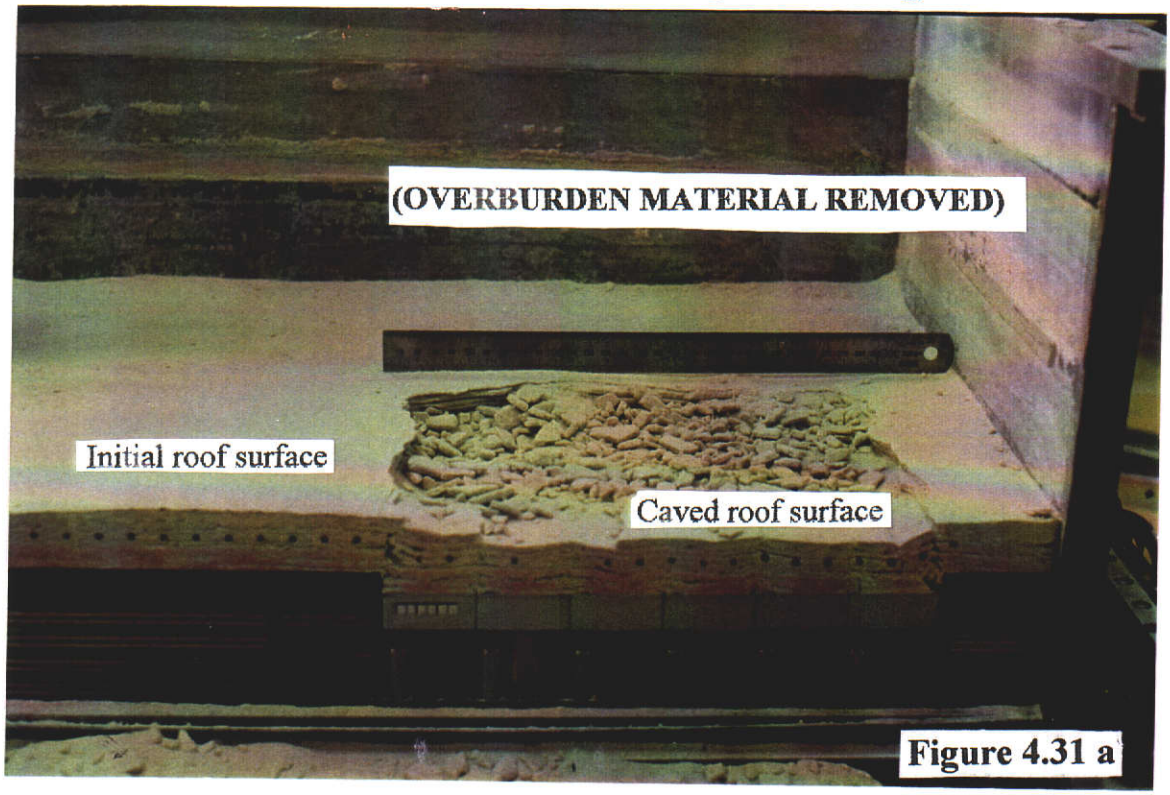

Figure 4.31 a

POST-TEST PHOTOGRAPH OF CAVED ROOF OF CENTRIFUGE TEST WESTCOLL4

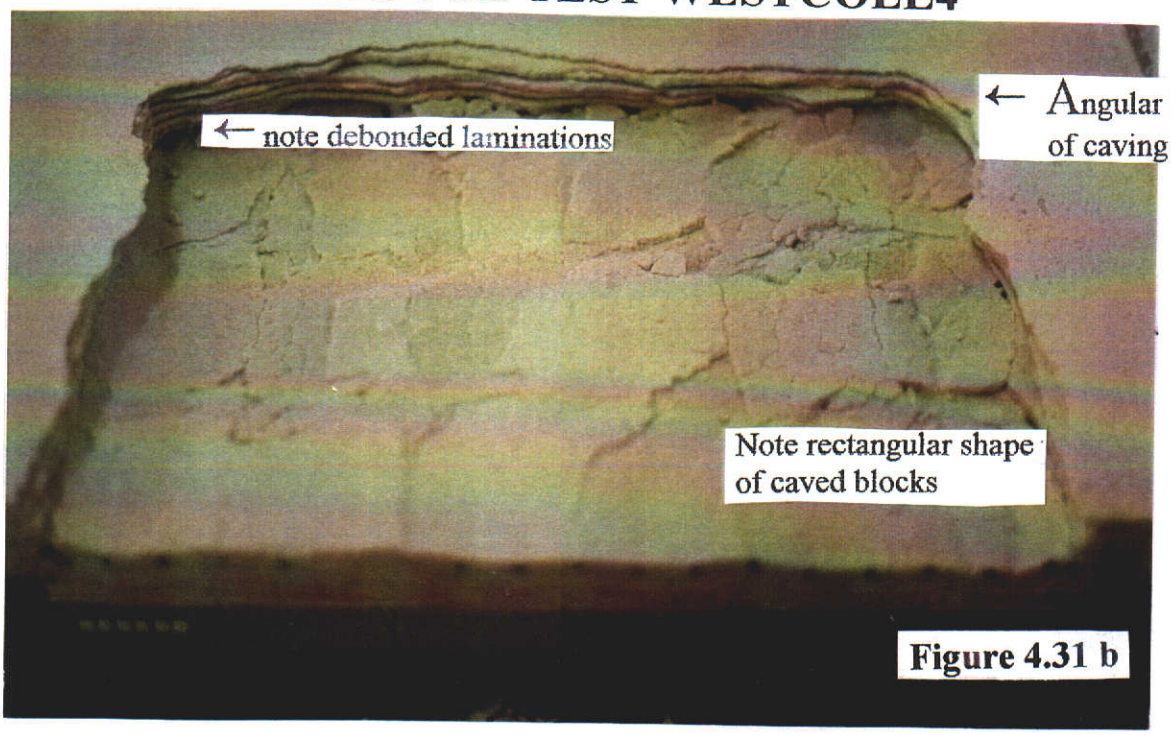

Figure 4.31 b

POST-TEST TRACING OF THE FACE OF CENTRIFUGE MODEL WESTCOLL4

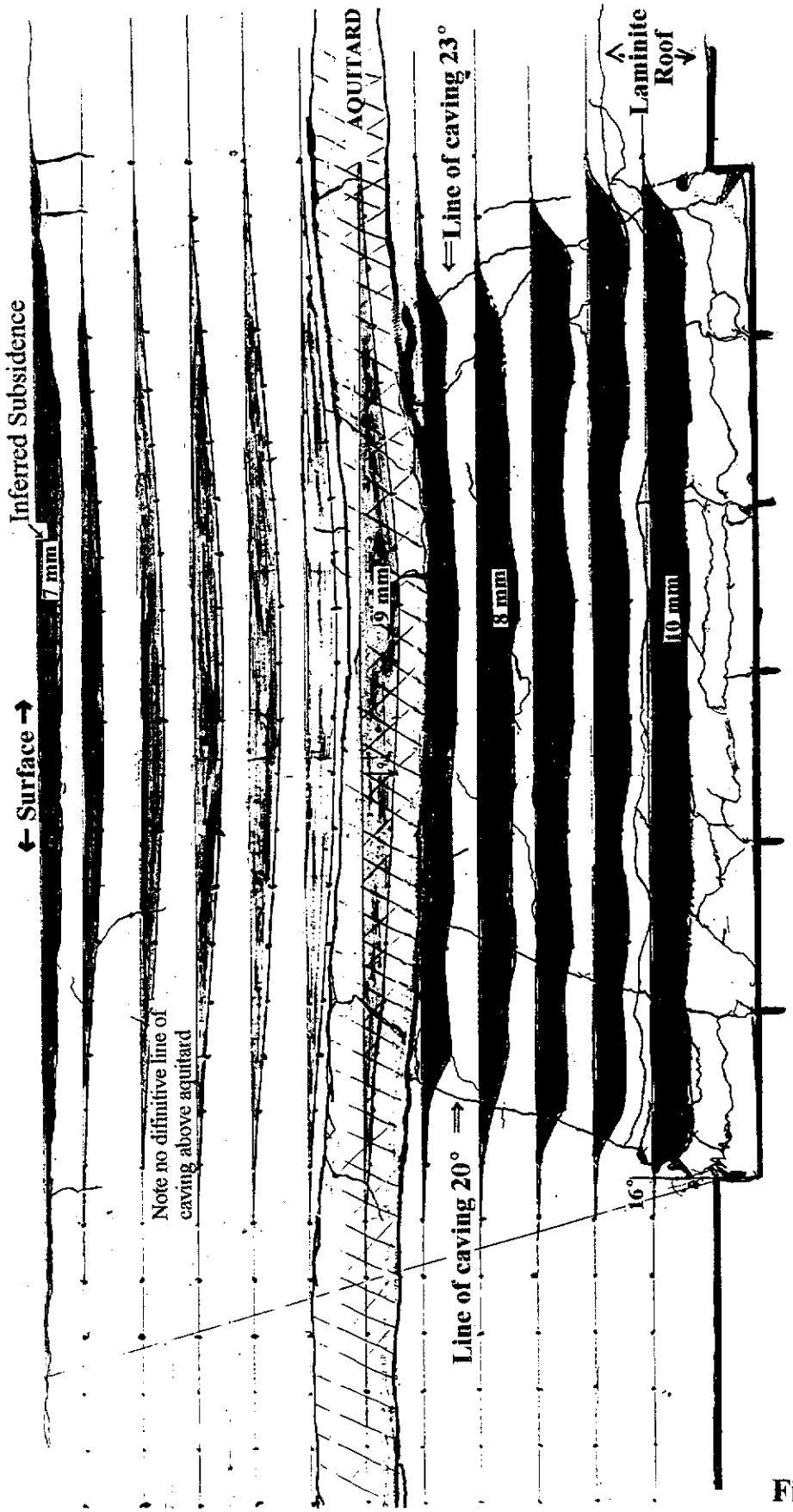

Figure 4.32

These results indicated that in all future tests, where the Wongawilli coal extraction method is to be emulated, it is necessary to incorporate "stooks" within the top-caps.

4.2.1.6 Conclusions - Pilot Study

The following list represents the more significant results:

1) The actuator units, which simulate the extraction of coal, work well - even at highly accelerated gravities.

2) Maximum subsidence measured (by laser profiling) in the final two models (6.5 mm) represents 78% of the drop height of the pistons, which is within 15% of the subsidence factor measured in the field (63% of mining height).

3) Cracking and buckling patterns in the model were not dissimilar to those detected in the field above 1North extraction panel (apart from Westcoll3, which had no stooks in the model).

4) Fracturing processes are largely reduced in tests where "stooks" are left in place following "extraction".

5) It appears, from the limited investigation done, that equivalent materials can be used to represent *in situ*/prototype material, however, more work is required in this area.

6) Data acquisition methods worked well, however, some doubt has been raised over the accuracy of laser profiling. Spraying all model surfaces with paint and the model face with dots assisted somewhat. A more direct approach is required to evaluate the behaviour of aquitards during the extraction process (e.g. strain gauges).

It was therefore concluded that the phase 1 - pilot study - tests had demonstrated that the geotechnical centrifuge modelling technique had potential for use as a tool to investigate mining subsidence, and that most goals for the pilot study were met. These interim results suggested that the project could proceed to the second phase of study.

4.2.2 CENTRIFUGE STUDY - PHASE 2

It was envisaged that the results from the phase 2 centrifuge testing would be used to assist with the further development of empirical models which may, on completion, be used to predict subsurface subsidence and therefore subsidence effects on aquifer systems for a range of mining conditions, such as:

- varying depths of cover (and stratigraphy),
- with and without saturated strata, and
- using different mining approaches (e.g. varying extraction widths, larger mining height and panel/pillar mining).

It was considered that if a generic empirical model could be achieved, centrifuge modelling would only be required to assess subsurface movements for atypical mining conditions in any future extraction panels. The actions used to address these aims are given below.

Equipment Modification and Development

As a consequence of the results gained from Phase 1 and the projected study proposals, it was considered that the following equipment modifications and developments needed to be investigated:

1. Development of an automated surface profiling system to monitor subsidence of the model surface during the centrifuge model tests. (This was found to be impractical within the project's funding framework).
2. Replacing one complete side of the existing strong box with a perspex window to allow deformations of the entire model face to be viewed. (It was decided not to proceed with this due to concern for the potential of excessive flexure of a full length window which would impact on caving processes and preclude modelling of confined aquifers within the model).
3. To help quantify the general response and timing of any rupture of subsurface aquitards during testing, it was proposed to incorporate the use of strain gauges, glued directly onto the upper surface of the aquitards. This was tested and worked well. The gauging equipment and application methodology is summarised in Appendix IV.11.
4. Increase the number of stooks to one on each corner of the actuator caps to better represent two-way lifting. (This objective was achieved).
5. Machine additional actuator units and modify top caps so that the dimensions of

each cap can be readily altered to represent required scaled mining widths or heights. (The latter was accomplished).

6. Manufacture either a suitable extension to the height of the strong box in order to model greater depths, or a new "plane strain" box with a "free-to-move" face on both the front and back of the model. This would allow modelling to be simplified to represent only a slice of strata (through the middle of the panel).

   The size of the model strong-box and actuator units at the time of phase I testing, allowed for a maximum model height of approximately 220 mm. At 200 g and a scaling factor of 1:200, an extension of 80 mm in height of the strong-box would be required in order to model the preferred depth of cover (60 m - which includes aquifer 3 and its aquitard (Alpha Seam) some 35 m above the Wyvern Seam). At 150 g the required extension of the strong-box is even greater. The resultant mass of a 1/g scale model required for *in situ* materials testing in either case exceeds the capacity of the machine.

   Consequently, it was decided (by the author) to manufacture a "plane strain" strong box to model only a plane section of the complete extraction panel. This reduces the weight of the *in situ* material model and therefore permits greater depths to be modelled. The design and layout of the plane strain box and mining actuator pistons are given in Figures 4.33 a and 4.34 b (from UWA records), which illustrate that the width of the plane strain box has been reduced to 200 mm (from 390 mm), and the depth of the box increased to 450 mm (from 300 mm).

   The plane strain box was designed by UWA engineering staff and built by engineering contractors in accordance with the requirements set out by the author to meet the objectives proposed for the study. One drawback with the plane strain box is that it is not possible to include irregular-shaped panels or panel corners and thus three dimensional analyses cannot be studied. However, for the purpose of the study this was not required.

7. Purchase/manufacture of a pressure bag system for application of surcharge forces for simulation of greater depths. (This did not eventuate due to time restrictions and delays in completing strategic parts of the subsidence study).

DESIGN OF PLANE STRAIN CENTRIFUGE MODEL CONTAINER (STRONG BOX)

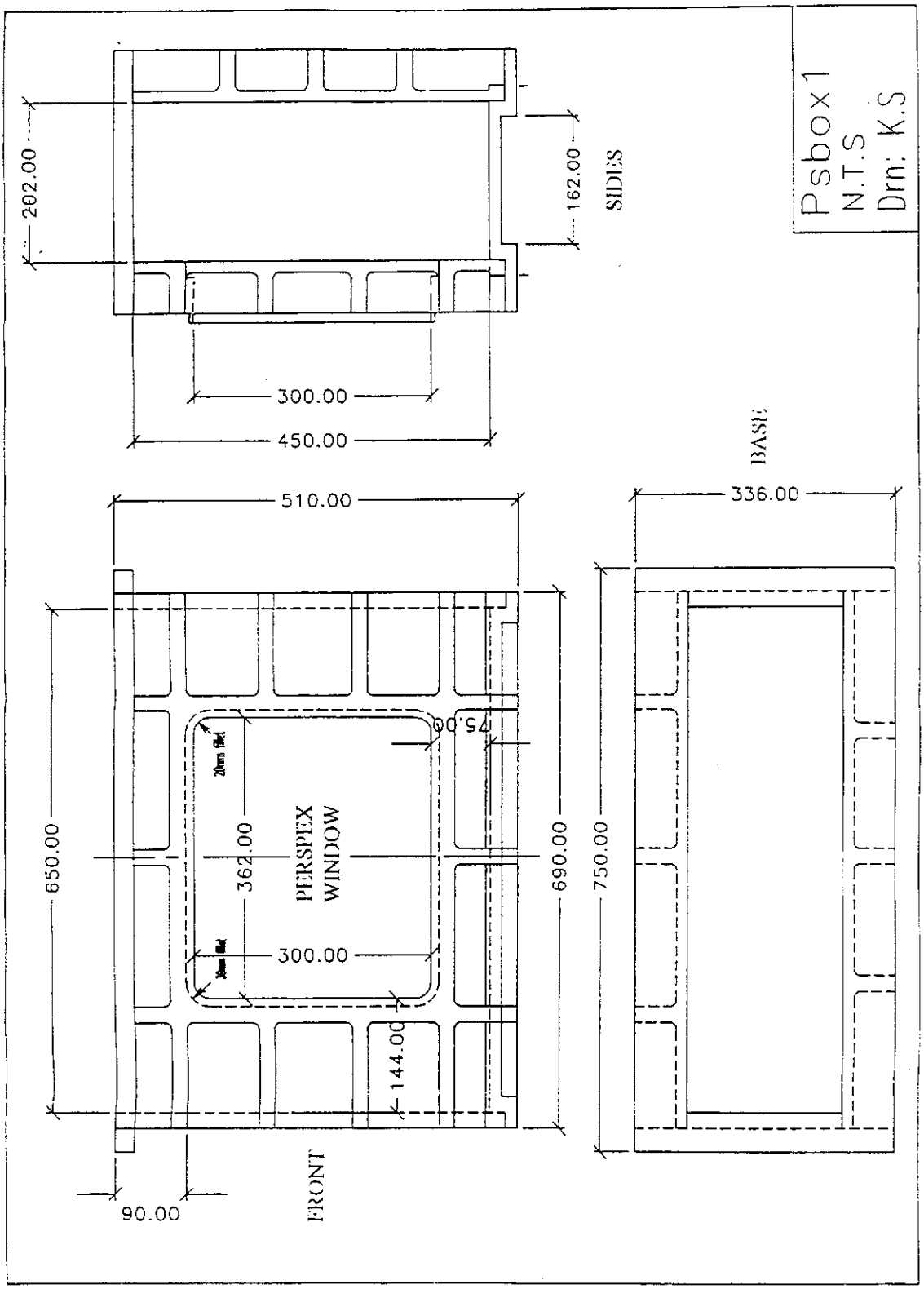

Figure 4.33 a

PLAN LAYOUT OF PLANE STRAIN CENTRIFUGE MODEL CONTAINER (Strong-box)

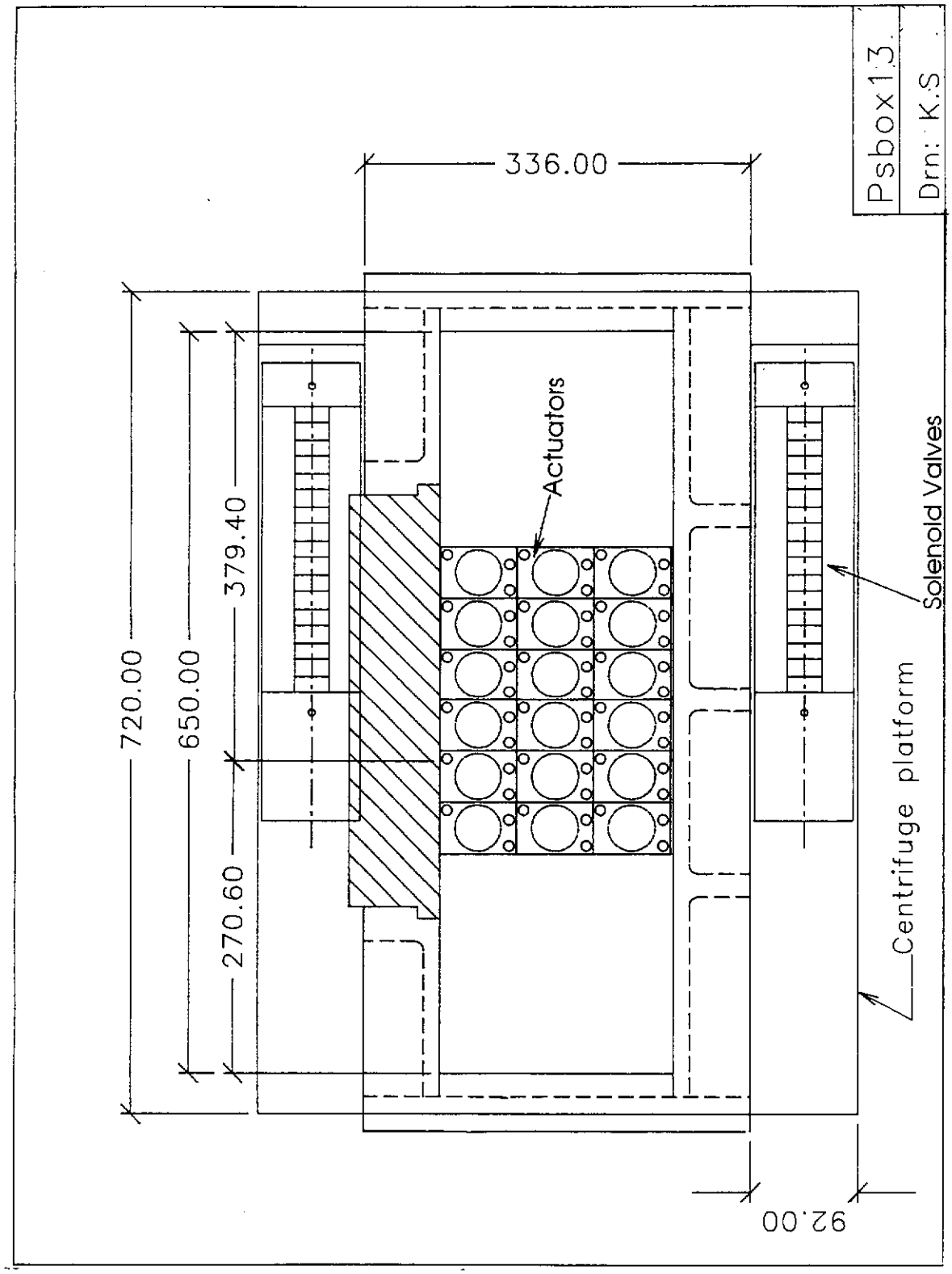

Figure 4.33 b

4.2.2.1 Model Scaling Investigation

One of the conclusions made from the pilot study was that the mixing of synthetic materials and model construction technique used could be greatly improved and needed further investigation. This material construction work is discussed in Appendix III. Before any detailed laboratory testing was carried out, it was necessary to confirm that the parameters defining the functional equation for subsidence development in the pilot study were sufficient for designing model synthetic materials to accurately represent Collie Basin sediments. This functional equation, taken from Whittaker and Reddish, 1989, and described in detail Section 2.6.5 is:

Subsidence (S) = f(G,UCS,Ts,E,v,W),

where W = Rock density (γ) x gravity(g), G = geometry of all structures,
UCS = Unconfined compressive strength, Ts = Tensile strength,
E = Elastic modulus, and v = Poisson's ratio.

It is only when the model is a true replica of the prototype that one can assume that the model's caving, fracture and subsidence patterns will be identical to the prototype.

This requirement necessitated further investigation of published literature on subsidence modelling. In the process, some of the major modelling laboratories in Australia, Europe and England were visited personally to help expedite the modelling phase. During these investigations, it was found that several other parameters and material qualities were noted as contributing factors to the subsidence process and should be included in the functional equation for this study. These **additional** parameters, and the reasoning for their inclusion in the functional equation for the stage II study are listed below:

The parameter **strain** [ϵ] was included as it governs whether the aquitard material will yield in bending, as observed in laboratory bending tests - see Appendix III. In reality, however, there is little control over this parameter in physical modelling.

The parameter **extraction ratio** [Er] was included because of the well documented effect the remnant coal left within extraction panels (e.g. Kapp, 1982). The effect of residual coal was also noted during the extraction of the first trial panel - 1 North panel in the WD6 mine. Due to problems with equiment, the last five splits were mined with an AM 50 machine which is able to extract up to 10% more by volume than the JCM 12 used in the earlier sections of the panel. The measured subsidence above the latter section of the panel also increased by 10% - see Figure 3.5.

It was recommended that the **frictional properties** [⌀] of the model be included, as this can influence the angle of shear, which will affect, in turn, the tributary loading on panel edge abutments.

The parameter **body force** [Q] (throughout the model) should be included, as it is a particularly important component in tributary loading redistribution and the bulking and reconsolidation of goaf material.

The parameter **time** [t] has been included because of the well published influence of time on subsidence development (e.g. Whittaker and Reddish, 1989, NCB, 1975, and Brauner, 1973[1]). The importance of time in this project was that the correct timing of extraction sequences could be established so that subsequent mining steps were not influencing subsidence still being developed from previous mining steps.

The importance of the **bulking factor** [Bf] to the development of subsidence cannot be understated. The results from the mathematical modelling stage of the research project were largely dependent on the "goafing element". Subsurface subsidence monitoring in 1North panel indicated that upward of 90% of bulking occurs within the first 6 to 8 m above the seam. This bulked mass provides support for the overlying strata, and helps prevent caving extending to much greater heights.

It was proposed that the beam bending/shear force theory in bedded strata is the most applicable mechanism to explain subsidence processes and therefore the flexural [Fs] and shear strength [Ss] along bedding are the most important material properties to be modelled. This assumption is supported by the discussion given in Section 2.5.5.1 and the results of 3-dimensional mathematical modelling (discussed in detail in Section 4.1.1.4) using the MINCAD computer software program SUBSOL. The SUBSOL modelling demonstrated that yielding of successive layers of strata above the mining horizon was dependant on the mechanical strength and thickness of each layer, the width of bed separation and the height above the workings, all of which are representative of laminated beam theory and dependant on flexural strength. This assumption is further supported by the mine design research done in Essen, Germany, by Stephan (1989) with large 1g physical models (typically 4 m long x 3 m wide x 3 m in height) at prototype depths in excess of 800 m.

Beam or plate theory has been used by several researchers to describe the shape of subsidence profiles (with varying success). Two examples include Salustowisz's analytical method (Lama et al., 1986), and Dunrud, 1984, using the work done earlier by Sherwood and Taylor, 1957, and Kunz, 1957. Furthermore, Galvin (1981) found that the spanning qualities of massive dolerite above longwall panels could be explained by beam theory.

The importance of shear strength across bedding is also supported by Dunrud, 1984, who states "rock masses derive much of their strength from confining stresses and attendant increases in frictional resistance across bedding, stratification, joints or faults. Strength of rock masses therefore are often reduced near mine openings and downwarped zones."

The final form of the functional equation was therefore:

$$f(S, \epsilon, E_r, \varnothing, v, E, UCS, Ts, Q, t, B_f, \gamma, Ss, G, Fs, g) = 0 \qquad 4.2(1)$$

				Units of measure
Where	1)	S	= Subsidence at any point	L
	2)	ϵ	= strain	-
	3)	E_r	= Extraction ratio	-
	4)	$\varnothing$	= angle of friction	degrees
	5)	v	= Poissons ratio	-
	6)	E	= elastic modulus	M,L^{-1},T^{-2}
	7)	UCS	= Compressive strength	M,L^{-1},T^{-2}
	8)	Ts	= Tensile strength	M,L^{-1},T^{-2}
	9)	Q	= body forces	M,L,T^{-2}
	10)	t	= time	T
	11)	B_f	= bulking factor of goaf	-
	12)	γ	= density	M,L^{-3}
	13)	Ss	= shear strength(along bedding)	M,L^{-1},T^{-2}
	14)	G	= geometry	L
	15)	Fs	= flexural strength	M,L^{-1},T^{-2}
	16)	g	= gravitational force	L,T^{-2}

Note that the term G relates to the geometry of all relevant terms defined by the measure of length, e.g. depth, width, length, mining height, height above the seam etc.

Once this equation was established, the second requirement was to manipulate these parameters to develop a series of dimensionless products from which to base the scaling of centrifuge models on. Using the theory of dimensional analysis, described in Section 2.6.5, each of the above parameters (n) needs to be simplified to its basic units of measurement to establish the number of components (k) involved (or rank of the dimensional matrix). In this case the units of measurement which cover all the above parameters are *mass*, *length* and *time* (k = 3). Each of the parameters above is then manipulated with the other parameters into n-k dimensionless π terms. Using the parameters listed above, the number of dimensionless π terms required is:16-3=13.

Satisfying the second step, the repeating variables chosen are G, Fs, and g.

Solving for the third step, the functional equation can now be expressed as:

$$f(\pi_1, \pi_2, \pi_3, \pi_4, \pi_5, \pi_6, \pi_7, \pi_8, \pi_9, \pi_{10}, \pi_{11}, \pi_{12}, \pi_{13}) = 0. \qquad 4.2(2)$$

Where: $\pi_1 = G^{a1}.Sf^{b1}.g^{c1}.S$ $\pi_2 = G^{a2}.Fs^{b2}.g^{c2}.\epsilon$ $\pi_3 = G^{a3}.Fs^{b3}.g^{c3}.Er$

$\pi_4 = G^{a4}.Fs^{b4}.g^{c4}.\phi$ $\pi_5 = G^{a5}.Fs^{b5}.g^{c5}.v$ $\pi_6 = G^{a6}.Fs^{b6}.g^{c6}.E$

$\pi_7 = G^{a7}.Fs^{b7}.g^{c7}.UCS,$ $\pi_8 = G^{a8}.Fs^{b8}.g^{c8}.Ts,$ $\pi_9 = G^{a9}.Fs^{b9}g^{c9}.Q$

$\pi_{10} = G^{a10}.Fs^{b10}.g^{c10}.t,$ $\pi_{11} = G^{a11}.Fs^{b11}.g^{c11}.Bf.$ $\pi_{12} = G^{a12}.Fs^{b12}.g^{c12}.Ss$

$\pi_{13} = G^{a13}.Fs^{b13}.g^{c13}.\gamma$

The fourth step requires solving for the exponents of each fundamental unit of measure in each of the above π terms. This process can be simplified by firstly isolating terms which are inherently dimensionless. In this case there are five inherently dimensionless terms:

$\Pi_2 = \epsilon$ $\Pi_3 = Er$ $\Pi_4 = \phi$ $\Pi_5 = v$ $\Pi_{11} = Bf$

The steps leading to the derivation of the exponents in each remaining Π term are provided below:

	M		L		T	
π_1	$0+b_1+0+0$	$= 0,$	$a_1-b_1+c_1+1$	$= 0,$	$0-2b_1-2c_1+0$	$= 0.$
π_6	$0+b_6+0+1$	$= 0,$	a_6-b_6+c-1	$= 0,$	$0-2b_6-2c_6-2$	$= 0.$
π_7	$0+b_7+0+1$	$= 0$	$a_7-b_7+c_7-1$	$= 0,$	$0-2b_7-2c_7-2$	$= 0.$
π_8	$0+b_8+0+1$	$= 0,$	$a_8-b_8+c_8-1$	$= 0,$	$0-2b_8-2c_8-2$	$= 0.$
π_9	$0+b_9+0+1$	$= 0,$	$a_9-b_9+c_9+1$	$= 0,$	$0-2b_9-2c_9-2$	$= 0.$
π_{10}	$0+b_{10}+0+0$	$= 0,$	$a_{10}-b_{10}+c_{10}+0$	$= 0,$	$0-2b_{10}-2c_{10}+1$	$= 0.$
π_{12}	$0+b_{12}+0+1$	$= 0,$	$a_{12}-b_{12}+c_{12}-1$	$= 0,$	$0-2b_{12}-2c_{12}-2$	$= 0.$
π_{13}	$0+b_{13}+0+1$	$= 0,$	$a_{13}-b_{13}+c_{13}-3$	$= 0,$	$0-2b_{13}-2c_{13}+0$	$= 0.$

Solving for the exponents in each π term and arranging them in their respective dimensionless products gives:

	π term coefficients						Resultant dimensionless term
π_1 ;	b_1	$= 0,$	c_1	$= 0,$	a_1	$= -1,$	S / G
π_6 ;	b_6	$= -1,$	c_6	$= 0$	a_6	$= 0,$	E / Fs
π_7 ;	b_7	$= -1,$	c_7	$= 0,$	a_7	$= 0,$	UCS / Fs
π_8 ;	b_8	$= -1,$	c_8	$= 0,$	a_8	$= 0,$	Ts / Fs
π_9 ;	b_9	$= -1,$	c_9	$= 0,$	a_9	$= -2,$	$Q / Fs.G^2$
π_{10} ;	b_{10}	$= 0,$	c_{10}	$= ½,$	a_{10}	$= -½,$	$t.\sqrt{g} / \sqrt{G}$
π_{12} ;	b_{12}	$= -1,$	c_{12}	$= 0,$	a_{12}	$= 0,$	Ss / Fs
π_{13} ;	b_{13}	$= -1,$	c_{13}	$= 1,$	a_{13}	$= 1,$	g.γ.G / Fs

Thus the functional equation describing all the relevant parameters for subsidence development has been simplified to a complete set of independent dimensionless products:

$$f\left[\frac{S}{G}, \epsilon, Er, \varnothing, \nu, \frac{E}{Fs}, \frac{UCS}{Fs}, \frac{Ts}{Fs}, \frac{Q}{FsG^2}, \frac{t.g^{1/2}}{G^{1/2}}, B_f, \frac{g.\gamma.G}{Fs}, \frac{Ss}{Fs}\right] = 0 \qquad 4.2(3)$$

$$\text{or} \quad \frac{S}{G} = \left[\epsilon, Er, \varnothing, \nu, \frac{E}{Fs}, \frac{UCS}{Fs}, \frac{Ts}{Fs}, \frac{Q}{FsG^2}, \frac{t.\sqrt{g}}{\sqrt{G}}, B_f, \frac{g.\gamma.G}{Fs}, \frac{Ss}{Fs}\right] \qquad 4.2(4)$$

Where there is variation between the prototype and individual model parameters, the correct scaling for individual parameters can then be calculated simply by balancing out the relevant π term.

However, as described below, some of these terms do not require special attention for scaling as they will be accounted for automatically in the scaling process. Therefore, the final requirement was to establish which of these terms were considered to be "critical" to the model scaling process, and those which could be effectively ignored.

If it is assumed that the dimensionless parameters $\varnothing$, ϵ, B_f inherently maintain similitude between the prototype and the model (e.g. $\varnothing_{(m)} = \varnothing_{(p)}$,) then these terms can be ignored. As the Poissons ratio is unlikely to have any great effect it too can be ignored (Whittaker et al., 1985). If one considers that the mechanism of failure within subsidence processes is tensile, not compressive, and that tensile strength is another form of flexural strength, then terms including compressive and tensile strength can also be ignored.

This leaves six dimensionless π terms:

$$E_r, \quad \frac{E}{Fs}, \quad \frac{Ss}{Fs}, \quad \frac{Q}{Fs.G^2} \quad \frac{G.\gamma.g.}{Fs} \text{ and } \quad \frac{t.g^{½}}{G^{½}}$$

Considering that the Q term cannot be practically controlled in the model once the centrifuge model is being run, and that it is reasonable to assume that if all other critical dimensionless terms are scaled correctly, the body forces will be correct by default, it can also be ignored. The critical functional equation for which similitude should be maintained where possible is therefore :

$$\frac{S_{ubs}}{G} = f_2\left\{E_r, \quad \frac{E}{Fs}, \quad \frac{Ss}{Fs}, \quad \frac{G.\gamma.g}{Fs}, \quad \frac{t.g^{½}}{G^{½}}\right\} \qquad 4.2(5)$$

As the geometric scaling factor ($S_{(m)} / S_{(p)} = G_{(m)} / G_{(p)}$, from Whittaker and Reddish, 1989) for the proposed centrifuge models was essentially fixed by the scaling relationship between the actuator caps and extraction widths, the critical scaling parameters available to maintain adequate similitude are the material strengths and accelerated weight/gravity forces. The design of centrifuge models was therefore based on the dimensionless scaling factor:

$$\frac{G.\gamma.g.}{Fs} \qquad 4.2(6)$$

where $\frac{G.\gamma.g.}{Fs}_{(m)} = \frac{G.\gamma.g}{Fs}_{(p)}$ and

$$\frac{Fs}{Fs}_{(m)}_{(p)} = \frac{G.\gamma.g}{G.\gamma.g}_{(m)}_{(p)} \quad \text{(strength scale factor)} \qquad 4.2(7)$$

It can be seen that, the scaling for the other two strength-based dimensionless terms in Equation 4.2 (5) are set automatically once the scaling ratio for this term has been established.

For example:

$$\frac{E_{(m)}}{E_{(p)}} = \frac{Fs_{(m)}}{Fs_{(p)}} \qquad 4.2(8)$$

Similarly, if the model is restricted to a particular size (the linear scale factor is known), the required operating gravity force can be determined. Likewise, the system can be influenced by varying the density of material used in the model.

Note that the density of equivalent materials cannot be used in isolation to alter the model similitude because any variation in density also changes the material strength (as illustrated by the laboratory test results given in Appendix III.2). In order to obtain the required flexural strength for any particular stratigraphy, a certain mixture of sand, water and plaster must be used and these clearly defined mixtures govern the final bulk density of the equivalent material. It is possible to introduce additional higher density sand particles (e.g. garnet sand) to alter the density to maintain similitude, however, this would require further detailed and complex laboratory strength testing (P Bolton personal communication, 1991). This was beyond the scope of this study.

Therefore the design mixture for each equivalent material had to be established by adopting a complex iterative approach whereby the final mixture, representing a known flexural strength, also satisfied the requirement for bulk density such that the correct body forces were applied to the model. The resultant flexural strength is not a direct scaling of the gravity force and geometric scale, rather a compromise value depending on the resultant density of the critical mix of materials.

As can be seen by the results provided in Table III.2 in Appendix III.2, the densities of sand/plaster materials varies from 1.1 to 1.67 t/m^3 depending on the percentage of sand in the mix. Furthermore, when resultant material densities are plotted against the percentage sand used, it was evident that there is a certain proportionality between the two variables. Consequently, it was attempted to fit a curve/equation to the data to simplify the iterative process for model construction/scaling. The equation derived to estimate the density of equivalent materials in the models is:

$$\textbf{Density} = 4.24 - 3.11 \times \exp^{-(\text{Ratio})^{0.6}/22)} \qquad 4.2(9)$$

where Ratio = the ratio of sand to plaster (by weight) in the mix.

More details on the density : sand/plaster relationship of equivalent materials are provided in Appendix III.

An example of the scaling approach for equivalent materials is given below.

Taking the 1North panel as an example, the flexural strengths of each of the major prototype strata are:

Coal Aquitards - 3.39 MPa

Sandstone Aquifers - 0.46 MPa

Overburden - No tests were completed due to problems with preparing weak overburden material. In this case it would be better to use *in situ* material in the model.

Knowing that the width of extraction of each fender in 1North Panel is 20 m and that the proposed width of the actuator caps for the equivalent material tests is 68 mm, the geometric scale factor is:

$G_{(m)}/G_{(p)}$ = 0.068 / 20 m = 1/304,

Given that the strength scale factor ($Fs_{(m)}/Fs_{(p)}$) for each stratigraphic member is determined from the relationship given in Equation 4.2(7), the required model flexural strength for each layer of material is:

$$Fs_{(m)} = \frac{G.\gamma.g_{(m)}}{G.\gamma.g_{(p)}} . Fs_{(p)} \qquad 4.2(10)$$

Therefore, for the sandstone aquifer material, assuming $\gamma_{(m)}$ = 1.61 t/m^3 and $\gamma_{(p)}$ = 2.00 t/m^3:

$$Fs_{(m)} = \frac{1/304 \times 1.61 \times 200\ Fs_{(p)}}{1.85 \times 1 \times 1}$$

$$Fs_{(m)} = 0.53\ Fs_{(p)} = 0.24\ \text{MPa}$$

The next step was to manufacture an equivalent material of the correct mix of sand, plaster and water to achieve the required 0.24 MPa flexural strength. In similar fashion to the derivation of the density estimation curve, the strengths of each test mould of equivalent material were plotted against the ratio of sand to plaster in each test mix and a mathematical relationship derived between the two variables Ratio and flexural strength. (Note that the water added to each mix was kept consistent at 18% total mix weight.) The following equation was derived to estimate the equivalent material flexural strength from any given sand:plaster mix (explained in more detail in Appendix III.2):

$$F_s = 4.0 \times \exp^{-(0.88 \times \text{Ratio}^{0.55})} \qquad 4.2(11)$$

In the example given, it follows that the required equivalent material sand:plaster mix ratio to obtain a flexural strength of 0.24 MPa is >> 9:1

This sand-plaster mix cross-checks well against the estimated density calculated by Equation 4.2(9) and the assumed $\gamma_{(m)}$.

For true similitude, the same scaling approach must also apply to the π terms E/Fs. and Ss/Fs. In fact this requirement represents the major concern with this functional equation; that the equivalent material used in the model must attain the required Elastic modulus **and** shear strength with the same mixtures of materials that meet the required flexural strength. From the results provided in Table III.2 and III.3 in Appendix III.2, a sand:plaster mix of 9:1 will result in an equivalent elastic modulus in the order of 120 MPa. Given that the elastic moduli for the three samples of natural material tested are between 74 and 233 MPa, this is considered to be acceptable scaling for the sandstone aquifer material. The bedding plane shear strength assessment was based on a direct shear test on a 1 - 2 mm thick layer of sand/plaster mix between a block of natural sandstone and shale. Table III.5 (sheets 5 - 7) indicates that the shear strength parameters of the interface equivalent material is given by a friction angle of 30°, and an cohesive strength of 25 kPa. Again, this was considered to fit adequately within the range of shear strengths for weak sandstone material in the Collie Basin (based on

confidential laboratory tests conducted by WCL).

It can be argued, however, that the laboratory strength values given above represent small-scale laboratory strength test data, which should be reduced accordingly to better represent the strength of discontinuous rock-masses. For example, Hoek et al. (1993) suggested a reduction factor of 0.45 for compressive strengths of hard rock with widely spaced joints, and Wilson (1983) suggested a reduction factor of 0.14 for weaker rocks. However,as described in Hammond etal 1983, there is very few defects in Collie Basin sediments. Furthermore, work by Misich (1988) on back-analysis of slope failures in WCL's W05-B open cut suggested that there should be no reduction of laboratory strengths for non-coals in the Collie Basin (where drill core loss is minimal and core sampling is correctly representative of the overall mass). On a practical note, a reduction in compressive strength by a factor of 0.14 for a 1.0 MPa sandstone, as suggested by Wilson (1983), will result in an unrealistic near-soil material which is unacceptable for modelling rock-like material.

Support for this assumption that reduction factors are unrealistic for the very weak rocks in Collie Basin is inferred by Pells and Ferry (1983) who found that the sample preparation and testing standards for UCS and Brazilian strength testing were unnecessarily stringent. Pells and Ferry purposefully tested a range of materials, with a variable quality of sample preparation. Their results demonstrated relatively insignificant variation in the strengths tests on weak rock and large deviation for strong rock (rock greater than 50 MPa). This supports the author's findings that the laboratory strength determined for very weak rock is much less affected by defects in the rock sample.

Chappell, 1987 further demonstrated that there was minimal variation of deformation moduli between samples of weaker coal measures rocks (other than shale) with and without jointing.

Therefore, considering the inherent extremely weak nature of the Collie Basin sandstone sediments (Section 2.4) and the general paucity of joints, it was concluded that there should be no reduction factor applied to this aquifer material and that the approach to designing the correct mix for sandstone aquifers - given above - is appropriate.

However, in the case of the much stiffer coal strata, natural cleavages are ubiquitous and therefore require reduction to a suitable rock mass strength. Wilson (1983) suggested a reduction factor of 0.2 for UCS of coal. Local research has established that a rock mass strength reduction factor of approximately 0.3 is required for the design of mine pillars in the Collie Basin (Misich and Humphreys, 1988). For this study, the local reduction factor has been applied to coal modelling and it is assumed that the compressive rock mass strength of coals is 6.5 MPa. As illustrated in Figure III.5, a rock mass UCS of 6.5 MPa equates to a flexural strength in the equivalent materials of 1.75 MPa. Assuming the model material density will be equivalent to a field density of coal (1.35 t/m^3), the required model flexural strength [from Equation 4.2(9)] is:

$$Fs_{(m)} = \frac{1/304 \times 1.35 \times 200\ Fs_{(p)}}{1.35 \times 1 \times 1}$$

$$Fs_{(m)} = 0.66 \times 1.75$$

$$= 1.2 \text{ MPa.}$$

and the required sand:plaster mix - using Equation 4.2(11) - is 1.75:1.

By inserting this sand:plaster ratio into the density estimation equation [4.2(9)] an estimated density of 1.32 t/m^3 is attained which also cross-checks well with the assumed density (1.35 t/m^3) used to define the required flexural strength of aquitard material. Therefore the 1.75:1 sand:plaster mix is appropriate for maintaining similitude of the flexural strength of aquitard materials.

In terms of elastic modulus, an equivalent material with 1.8 : 1 sand/plaster (Table III.3) can be expected to possess a modulus of 1,845 MPa, which represents minimal reduction in the modulus of coal from the accepted laboratory value of 2,000 MPa (Misich et al., 1991). It is therefore most likely that the model's elastic modulus is somewhat excessive; when considering the 0.69 strength scale reduction factor required for the model **and** the 0.3 rock-mass strength reduction required for UCS of coals. (Although Kramadibrata and Jones (1993) and Chappell (1987) suggest that the modulus of some materials is not significantly affected by size effects.)

In an attempt to obtain a more accurate representation of elastic modulus in the model, it was decided to try using kaolin clay as the binding matrix, however, this material completely altered the behaviour of the synthetic material. It was then decided to accept the conclusion reached by Obert and Duvall (1967) that ideal similitude is unlikely to be met with equivalent materials and that further investigatory tests seeking perfect similitude would be futile.

Nonetheless it was considered that as the stiffer model aquitard material was within the range of laboratory moduli, it could at worst only emphasise the effect of the large variation between aquitard and aquifer material strengths without greatly impacting on the results.

In relation to similitude of time, it follows from the equation given below, that the time scale factor required for the model is represented by:

$$t_{(m)} = t_{(p)} \times \left(\frac{g/G_{(p)}}{g/G_{(m)}} \right)^{1/2} = (g_{(p)}/g_{(m)})^{1/2} \times (G_{(m)}/G_{(p)})^{1/2} \times t_{(p)} \qquad 4.2(12)$$

$$= t_{(p)} \times \sqrt{1/300} \times \sqrt{1/200}$$

$$= t_{(p)} / 245$$

During earlier investigations into subsidence prediction (given in Section 3.1.9), it was established that 80% of the mine subsidence had occurred within 60 - 72 hours of completion of mining of a complete fender. The remaining 20%, however, could take several months to develop. Considering the excessive model run-time required to represent up to 6 months, it was considered that 80% of total subsidence was more than adequate for this phase of the centrifuge study. It was rationalised that if it could be demonstrated that subsidence effects were not settled at any stage of the early tests, then model run-time would be increased to account for the time-dependent subsidence.

Therefore if it is assumed that the minimum possible time to mine a 20 m long section of coal from a Wongawilli fender is 2 hours, the length of time between lowering of individual pistons is: 120/245 min $\approx$ 30 sec. Similarly, the length of time between lowering each row (representing the 60 hrs required for 80% subsidence to develop) is: 3600/245min. $\approx$14.5 min

Both of these time scale factors were within reasonable scope for centrifuge modelling, however, there was some concern, initially, for the lengthy total spin times required to lower all six rows of pistons in each test (approximately 93 minutes).

Summarising the equivalent material scaling investigation it was considered that, although there was some deviation from true similitude with elastic modulus of the model's aquitard material, these scaling terms adequately represented the processes of subsidence development and met, within reason, similitude between the model and prototype. It was therefore decided to proceed with the full testing proposal, applying these scaling terms to all **equivalent material** tests.

However, given the program of modelling proposed, it was determined that the best approach would be to firstly use *in situ* rock material, obtained from within the mine, to test modelling criteria. If realistic data was obtained from these *in situ* material tests, these results could be used as base-line data for the proposed parametric **equivalent material** tests. Consequently, a series of three *in situ* material tests were completed first, followed by an iterative series of six equivalent material tests which were used to assess the effects of mining height, width, water filled aquifers, and processes involved in panel/pillar coal extraction.

The objectives and conclusions made from each test are discussed below. In order to condense this Section, the specific details of model construction and the measurements and observations made during and after testing (which were used to form the main conclusions listed) are detailed in Appendix IV. This approach has been adopted for all Phase II tests, although more information has been provided for the earlier tests in the text so that the reader has a better understanding of the nature of the models.

4.2.2.2 Centrifuge Test PS01

Objective of test PS01 - To use intact blocks of "*in situ* material" to:

- Assess the suitability of using naturally occurring rock in centrifuge models. If field observations can be verified by *in situ* material tests, these test results can be used as the basis for the parametric equivalent material tests proposed for the remainder of the project.
- Observe the effect of using an aquitard thickness that corresponds to the thickness of all aquitard materials - not just the coals.
- To observe the effect of mining narrower split/fenders.

Model construction - Because natural materials were being used, the only parameters requiring scaling were the geometric scaling factor and time (time scaling is discussed later). Given the size restrictions of the centrifuge strong-box, the optimum scaling factor was 1:200 [as per Equation 4.2(6)]. To maintain similitude, it follows that this geometric scaling factor requires that the model be operated at 200g.

The 45 mm wide top caps represent a prototype equivalent mining width of only 9 m per fender which is atypical for one-way lifting (it is normally 13 m). The complete panel width was 54 m which represents a critical width panel (54/59 = 0.92). Therefore the PS01 test could not develop full subsidence.

Large block samples were selected (from active underground mining areas 1 North Panel and 2SA Panel) as being representative of typical sandstone and aquitard materials. Selection of suitable blocks for testing was very difficult. Firstly, they had to be at least 200 x 200 x 650 mm, but not too large to handle. There could be no defects in them, and the shape of the block had to be regular in order to obtain the required cut block dimension in each direction.

Each block was cut to the dimensions of the strong-box (±8 mm) and the required layer thickness (± 2 mm) at a stone mason establishment in Perth (WA Marble and Granite). For this test, two sandstone blocks were cut, both 130 mm (26 m in the prototype) thick, and one 35 mm (7 m) thick cannel coal slab was cut.

The model was made in three distinct layers, the two sandstone blocks (representing aquifers) being separated by the slab of cannel coal (aquitard). The depth of cover and stratigraphy in the model approximated to that in 2SA Panel (See Figure 4.24) as in previous tests in the pilot study. The model aquitard width of 35 mm represents the full thickness of the aquitard, including coals, shales and laminites in the Alpha seam aquitard in the field. It was not clear at this stage whether these materials should be included in the model as being part of the aquitard. (No SUBSOL modelling had been completed to this stage.) Nonetheless, it was decided that a thicker aquitard in the first test - provided it worked - would give useful information regarding bending and bridging characteristics of the coal in comparison to other tests with correctly scaled aquitard thicknesses. It was also not certain whether a thinner plate of cannel coal (5-8 mm thick - representing only the thickness of coal) could withstand rigorous handling during cutting, strain gauging, and placement in the box and laying another block on top.

At the interfaces between the actuators and the first sandstone block, the top of the aquitard slab and the bottom of the upper sandstone block, and the bottom of the aquitard slab and the top of the lower sandstone block, a thin layer of sand, plaster and water mix was placed. The purpose of the sand/plaster mix was to fill gaps developed by cutting aberrations between blocks. It was also used to fill the gaps between the edges of the centrifuge box and the sawn blocks of *in situ* material for this test and all remaining *in situ* material tests. The mix used for the infill material was: 600 g sand, 335 g plaster, and 270 g water.

This particular mix was used because it best represented shear strength (from laboratory tests - see Appendix III.2) of *in situ* laminated material in the area - typically 30° friction and 25 kPa cohesion.

The nature of the bedding in the sandstone block was discontinuous and wispy. Compressive strength tests (also given in detail in Appendix III.2) demonstrate that the average UCS value of the wispy, fine to medium-grained sandstone material is 1.5 MPa, which confirms that the rock sample is within the typical range of material strengths at shallow depths of cover.

In order to measure subsidence throughout the model during testing, the face of the model was painted with black dots (typically 1-2 mm in diameter) by spraying gloss paint through a 0.6 mm thick tin plate with holes drilled on a 15 mm grid. The appearance of the model before testing is illustrated in Figure 4.34 a.

PRE-TEST PHOTOGRAPH OF CENTRIFUGE MODEL PS01

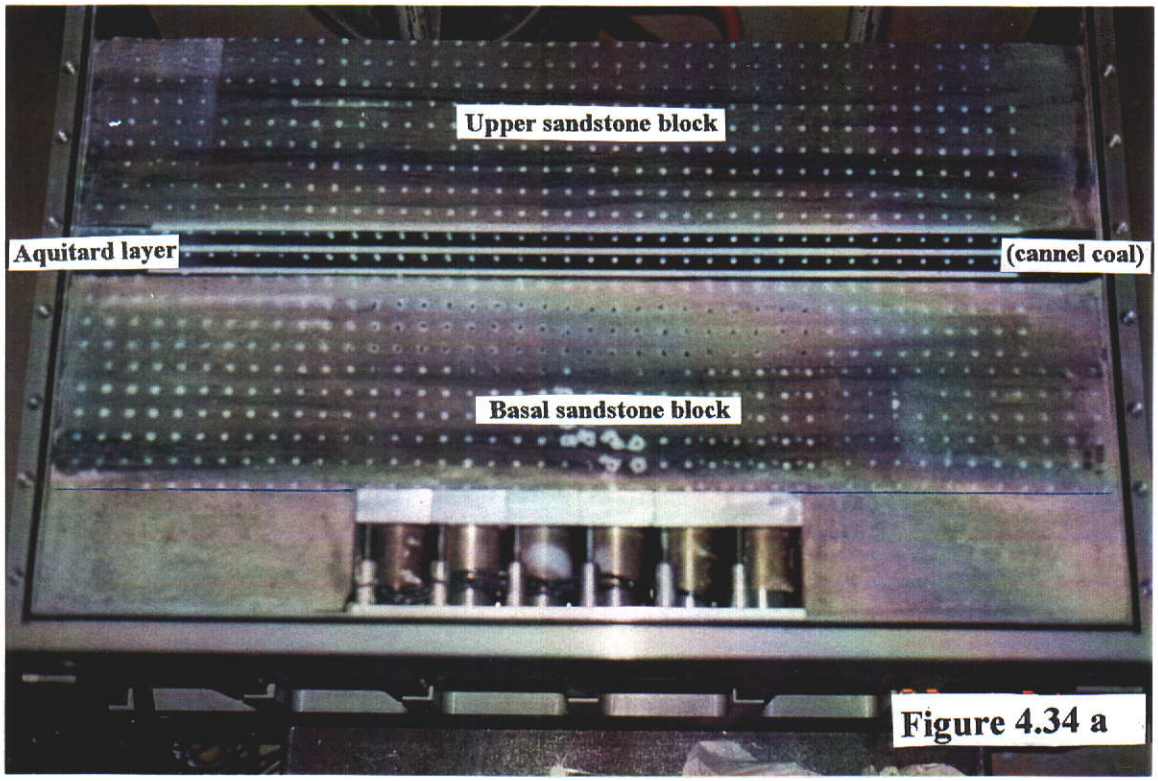

POST-TEST PHOTOGRAPH OF CENTRIFUGE MODEL PS01

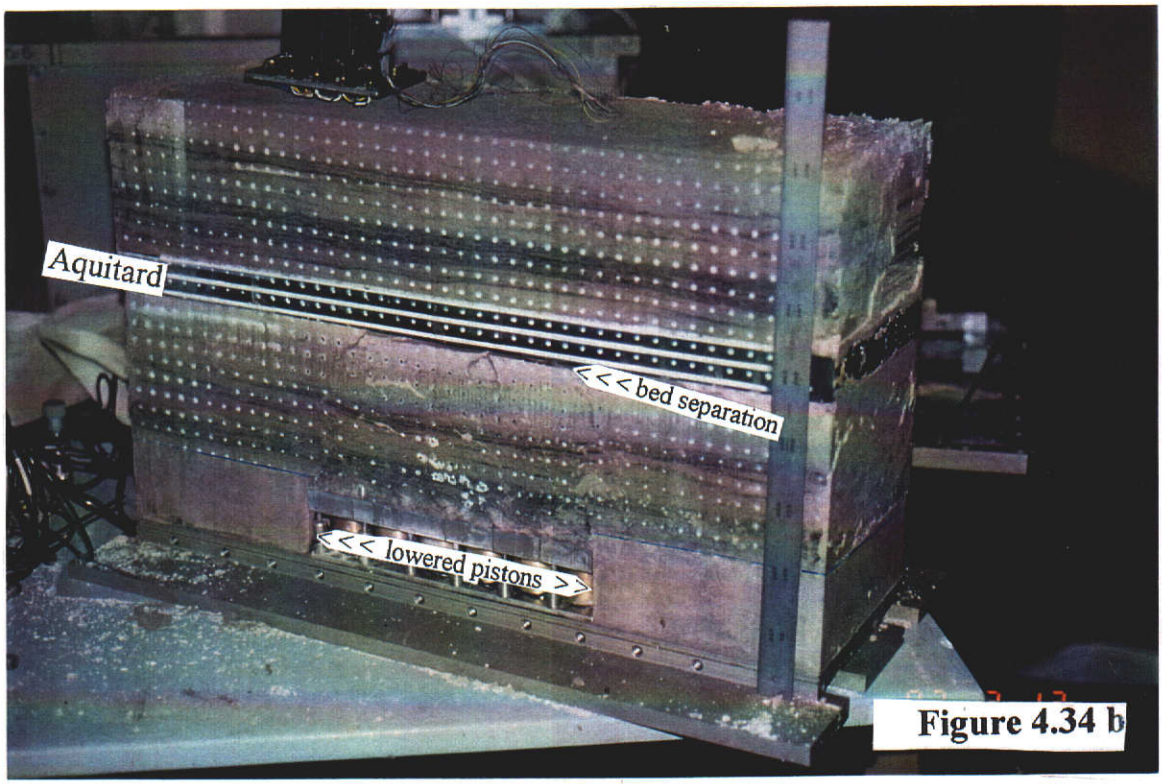

Each black dot was "digitised" using the computer software package ACCUware which "grabs" specific images (e.g. dark spots of specific size) from individual video frames recorded by CCD camera during the test. Details of the ACCUware processing package and "frame grabbing" are given in Appendix IV.10. This approach was used for all future tests.

In order to assess the influence of subsidence on the aquitard layer, strain gauges were fixed (by epoxy resin) to the top surface of the aquitard slab. The gauges used were an inexpensive wire in a paper carrier type - see Appendix IV.11. Other forms of gauges, such as etched foil on a polyamide or epoxy backing, were not considered necessary because the nature of testing was quick and destructive. There was no need to use the more precise, expensive gauges for long term "stability" of the gauges.

Positioning of the gauges on the aquitard blocks was assisted by carefully measuring and marking out the precise location of all gauges on the surface of the slab. This sped up the process and reduced the error in location of the gauges. In test PS01, only seven strain gauges were installed, which left some large gaps between strain gauges. (In the *in situ* material tests only one junction box, connecting the strain gauges to the computer operated recording unit, was available which could only take up to ten channels. In later tests, the number of both the terminals and junction boxes were increased to provide a more continuous representation of the strain across the full length of aquitard above the "extraction panel".)

In test PS01 the gauges were set up for a ± 2000 μ strain tolerance - see Appendix IV.11. The gauges in all other tests were configured to withstand a strain variance of ± 4000 μ strain. This higher strain output tolerance in latter tests allowed for wider ranges of measurement, though slightly less accurate.

Observations - A detailed list of observations made from this test is provided in Appendix IV.1. A summary of the main observations is provided in note form below:

- This test proved that *in situ* material could be used for simulation of mining subsidence in the Collie Basin within the geotechnical centrifuge.
- The thick aquitard layer had a significant effect on the development of subsidence. There was no measurable subsidence above the aquitard block. A wide bed

separation developed above the weaker basal block of sandstone as it collapsed and separated from the bridging aquitard (Figure 4.34 b and 4.35 a & b). This observation, to some extent, supports the school of thought of subsidence development according to beam theories - mentioned in Section 2.5.5.1.

- The shape of the line of shear/caving at the **leading** panel edge was curved during early stages (Figure 4.36) of extraction. This does not match observations within the mine, and field data from extensometer monitoring. The variation is thought to be due to the thick aquitard bridging across the caved area, resulting in lower vertical pressures at the caving abutments at these early stages of collapse. However, the line of shear/caving at the **trailing** edge is in the order of 23° (Figures 4.35 a and 4.36); this closely represents the angle of shear measured in the field. It is also interesting to note that after all pistons were lowered, the line of shear/caving at the advancing edge suddenly became sub-vertical. This is probably due to the increase in stress transferred to the advancing abutment exceeding the strength of the material below the aquitard at the caving edge.
- A tensile crack was noted on the lower edge of the spanning aquitard after all pistons were lowered (equating to 54 m extraction in the prototype), once the strata at the leading edge, beneath the aquitard, was sheared sub-vertically. It can therefore be inferred that the thicker aquitard can support a span, represented by the length of the bed separation in the model (illustrated in Figure 4.35 a to be 222 mm, or 44 m in the prototype).
- A lower subsidence factor was evident (0.56 x T) at the top of the caved sandstone in this test. This can also be explained by the lower vertical pressures being transferred to the goaf because of the bridging aquitard, thus reducing recompaction.
- It appears that a yielding strain of 20 mm/m, as assumed from laboratory testing of confined compressive strength (triaxial) tests (by Misich et al., 1991), is not valid for tensile/flexural yielding strains in the prototype. A yielding strain in the order of 2.0 mm/m appears to be more applicable (Figure 4.37). This yielding strain is similar to the value given by Farmer and Altounyan (1980) for rock masses in the United Kingdom (2.5 mm/m).
- No significant handling problems were experienced with using a relatively thin (35 mm) aquitard slab.

POST-TEST BED SEPARATION BENEATH AQUITARD - CENTRIFUGE MODEL PS01

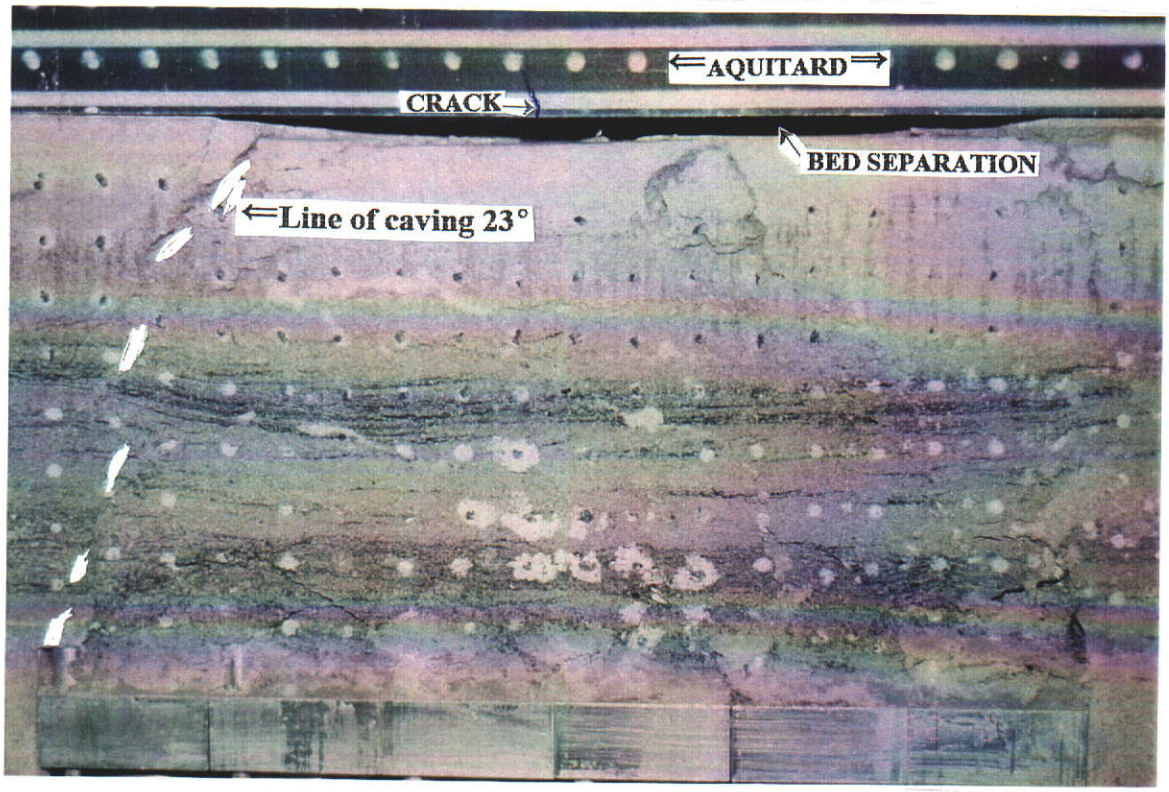

Figure 4.35 a

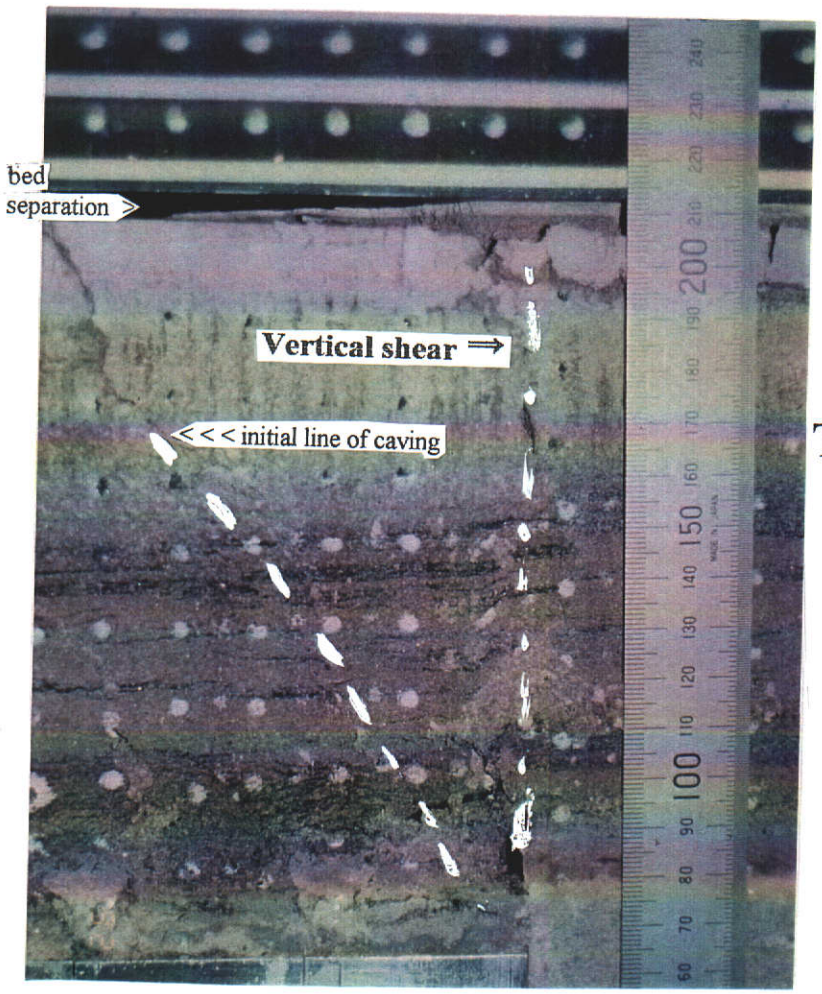

CAVING AT THE LEADING EDGE OF CENTRIFUGE MODEL PS01

Figure 4.35 b

SUMMARY OF THE CAVING SEQUENCES OF CENTRIFGUGE TEST PS01

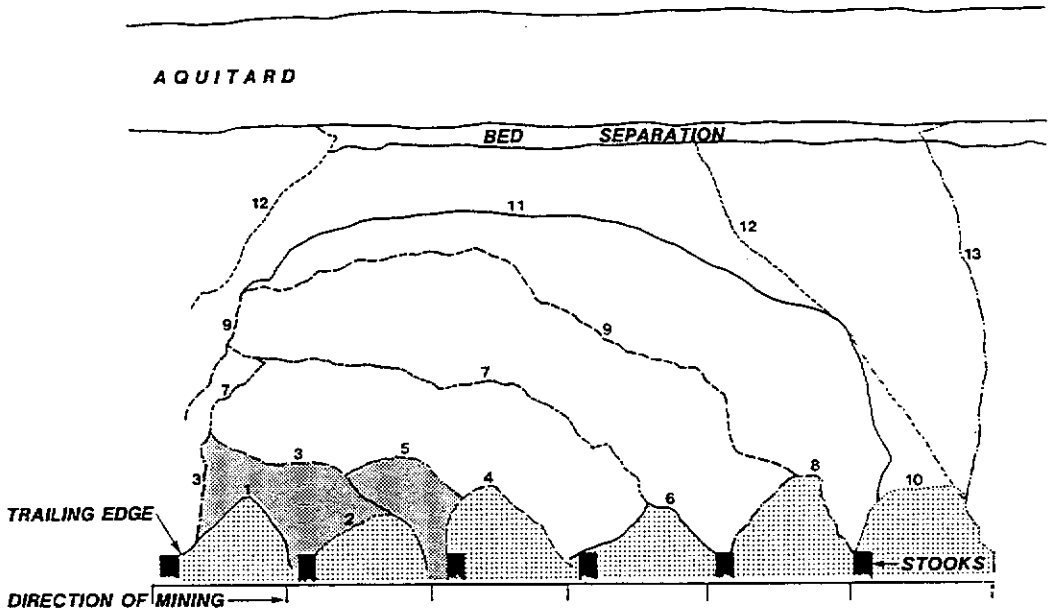

Figure 4.36

STRAIN GAUGE DATA - CENTRIFUGE MODEL PS01

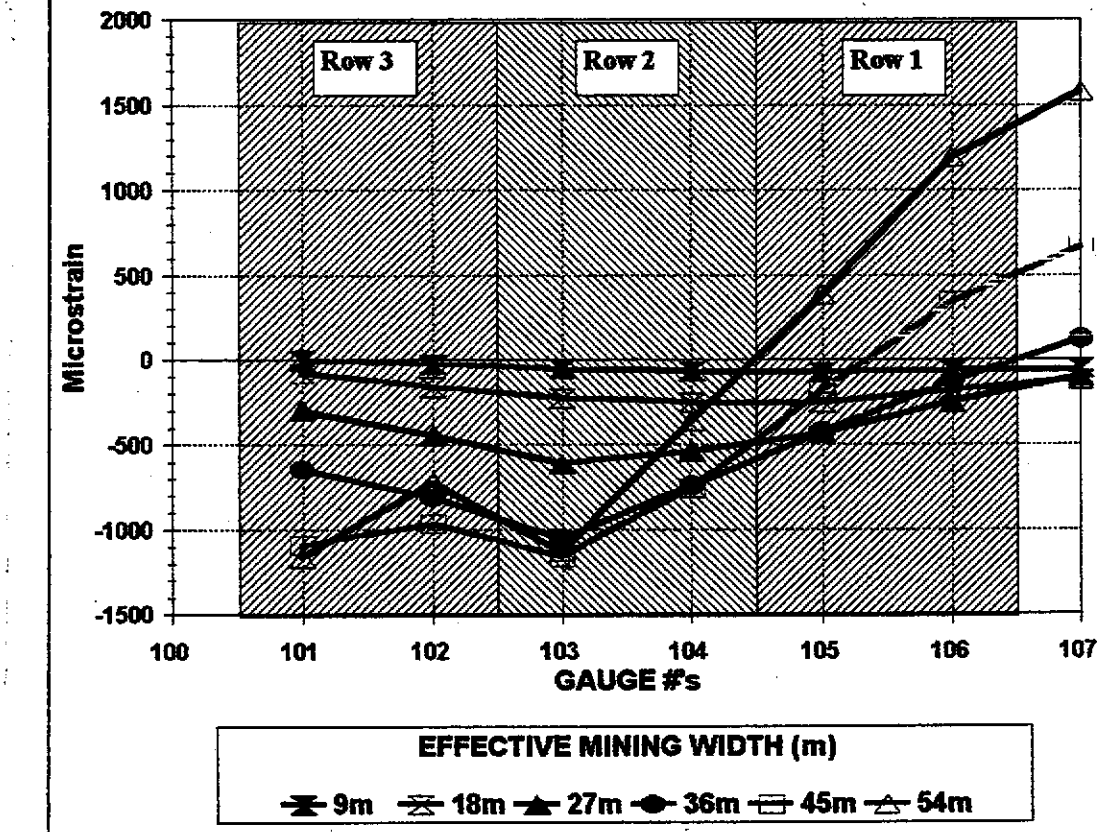

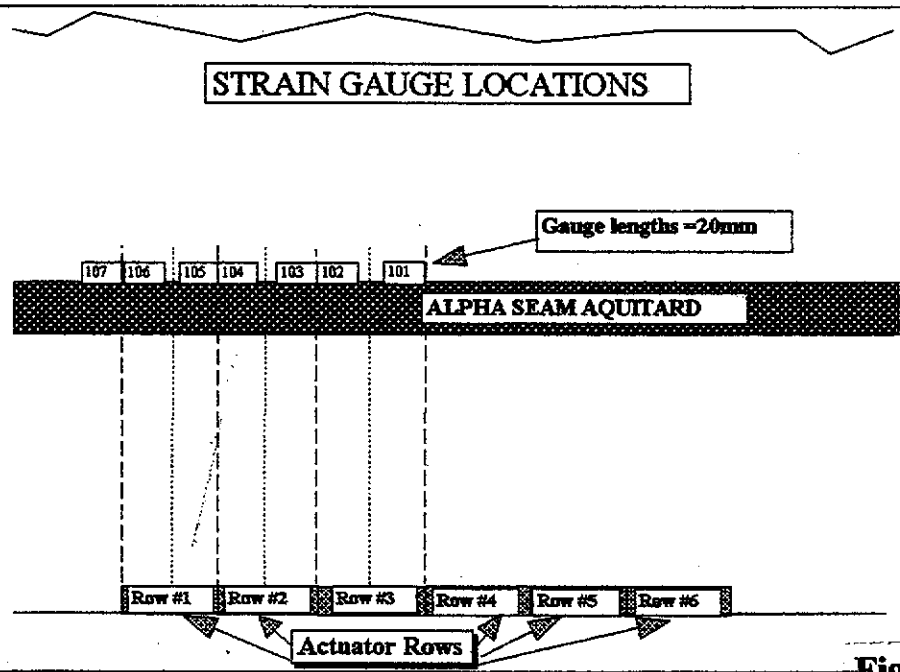

Figure 4.37

- The high silt and clay fraction within the *in situ* material allows the goaf material to reconsolidate and "re-knit" (Figure 4.38). Thus, although the goaf material will be more porous, there is little likelihood that open fractures will develop which would provide a clear conduit between any superimposed water-bearing bodies and the mine. This evidence is supported by the consistent, but not catastrophic, mine-water inflows in the WCL underground workings at varying stages of extraction.
- The accuracy of frame grabbing from video film was inadequate. It was considered that an improvement in either the standard of lighting or tracer dots was required if the ACCUware frame grabbing package was to be used for detailed analysis.
- The timing of the sequence of lowering actuators for this test seem adequate as strain gauge data had peaked prior to the subsequent lowering of each row of pistons. It was therefore proposed to use identical drop sequences for the other two *in situ* material tests proposed.

4.2.2.3 Centrifuge Test PS02

Objective - To assess the caving performance of a sandstone block devoid of bedding laminations. If the controlling mechanism of subsidence development was beam theory, then it would be expected that a "massive" block of sandstone (of similar strength) with no obvious bedding weaknesses would cave differently to that in PS01.

Model Construction - This model was constructed similarly to PS01 with the following variations:

1. The bottom sandstone block was 146 mm thick (which better represents the thickness of aquifer 2 in the prototype) and did not have any visible formal bedding.
2. The thickness of the cannel coal/aquitard layer was reduced to 8 mm (from 35 mm in PS01), which is a more realistic scaled prototype thickness of 1.6 m of coal aquitard.
3. In order to improve the accuracy of frame grabbing, the complete front of the model was firstly painted white, then after drying, jet black dots were painted on the model through the template to provide better contrast.

- The high silt and clay fraction within the *in situ* material allows the goaf material to reconsolidate and "re-knit" (Figure 4.38). Thus, although the goaf material will be more porous, there is little likelihood that open fractures will develop which would provide a clear conduit between any superimposed water-bearing bodies and the mine. This evidence is supported by the consistent, but not catastrophic, mine-water inflows in the WCL underground workings at varying stages of extraction.
- The accuracy of frame grabbing from video film was inadequate. It was considered that an improvement in either the standard of lighting or tracer dots was required if the ACCUware frame grabbing package was to be used for detailed analysis.
- The timing of the sequence of lowering actuators for this test seem adequate as strain gauge data had peaked prior to the subsequent lowering of each row of pistons. It was therefore proposed to use identical drop sequences for the other two *in situ* material tests proposed.

4.2.2.3 Centrifuge Test PS02

Objective - To assess the caving performance of a sandstone block devoid of bedding laminations. If the controlling mechanism of subsidence development was beam theory, then it would be expected that a "massive" block of sandstone (of similar strength) with no obvious bedding weaknesses would cave differently to that in PS01.

Model Construction - This model was constructed similarly to PS01 with the following variations:

1. The bottom sandstone block was 146 mm thick (which better represents the thickness of aquifer 2 in the prototype) and did not have any visible formal bedding.
2. The thickness of the cannel coal/aquitard layer was reduced to 8 mm (from 35 mm in PS01), which is a more realistic scaled prototype thickness of 1.6 m of coal aquitard.
3. In order to improve the accuracy of frame grabbing, the complete front of the model was firstly painted white, then after drying, jet black dots were painted on the model through the template to provide better contrast.

COMPACTED GOAF MATERIAL
CENTRIFUGE MODEL PS01

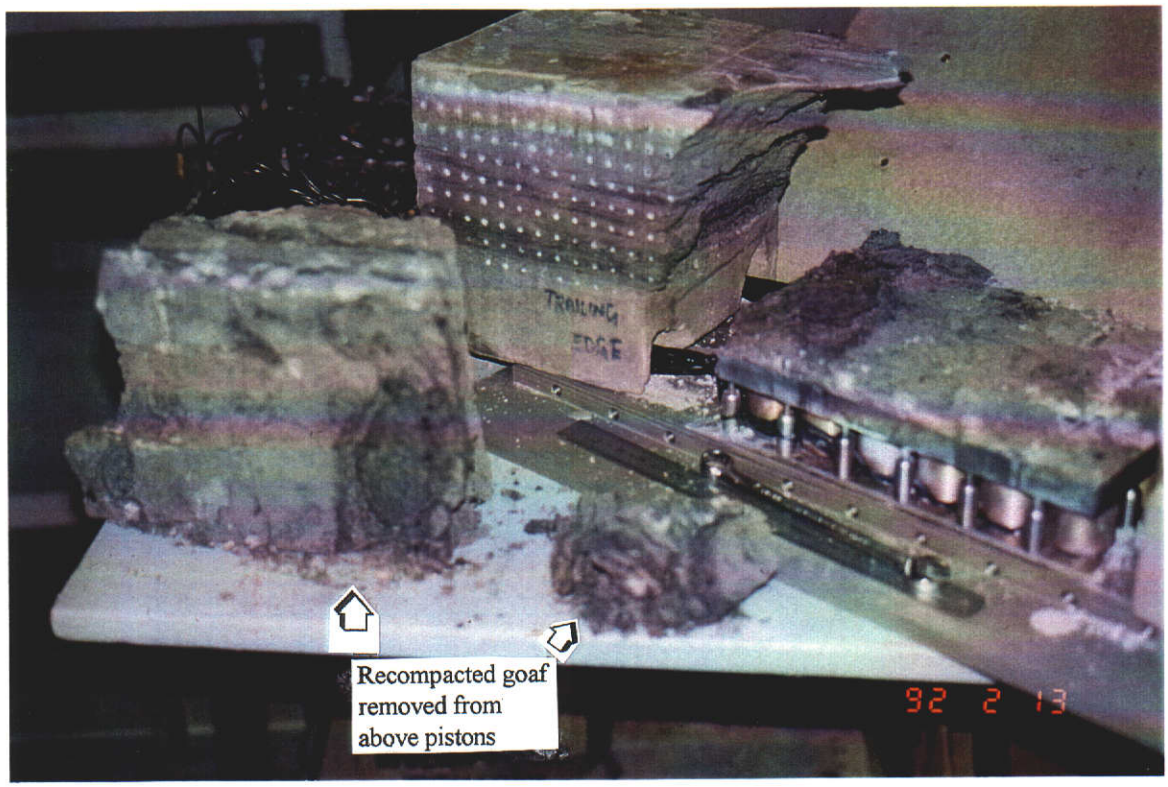

Figure 4.38

4. The piston top caps were widened to 67.5 mm to correspond to a more representative split/fender width of 13.5 m. The effective panel width was 6 x 13.5 = 81 m which equates to a W/H ratio of 1.4, making this test "critical" width under the Collie definition.

The upper sandstone block used in Test PS01 was used again as the upper block for this model. This was possible, as the bridging aquitard in the earlier test prevented the upper block from subsiding and the sandstone block was therefore not damaged by subsidence.

Comments - Unlike the previous models, the thickness of the PS02 aquitard block represents only the width of coal and cannel coal within the Alpha seam aquitard; the presence of shale and siltstone units was ignored. The importance of restricting the aquitard thickness in the model to only the thickness of coals in the aquitards was highlighted by initial results from the SUBSOL numerical modelling which had become available immediately prior to construction of this test. SUBSOL modelling showed that when the model aquitard thickness equated to the coal thickness only, the resultant **surface** subsidence profiles more closely matched field results (see Section 4.1.1 and Appendix IV.2). This observation compares well with the PS01 test results, where there was no surface subsidence noted above the thick aquitard.

This supports earlier assumptions that the non-coals are only passive members in the subsidence process, and the coal seams act as reinforcement within the overall mass. From this point onwards, the thickness of aquitard in all models approximated only the interpreted thicknesses of coal within the composite aquitards.

No problems were encountered with handling the thin (8 mm) aquitard layer. Handling was assisted by clamping a flat wooden board to the aquitard. Cutting the slab had some problems initially, however, these were solved after several attempts. A 3 mm spacer was placed in the sawn cut and pressure applied to the free edge. Two operators were required for the sawing process.

Finding the best block of sandstone which met the requirements of this test took several hours to locate. The difficulty was to firstly find a physically manageable lump of rock of sufficient size in all dimensions to adequately fill the plane strain strong box once it is trimmed to size. Secondly, it was to have no obvious bedding planes, and yet not possess large, very coarse-grained particles of silica; the concern with the particle

size was that at 200 g, 5 mm wide grains of silica sand would correspond to 1 m boulders, which would be unacceptable. The resultant block had a maximum particle size of 1 mm which still represents atypical-sized sandstone grains at 200 g, however, the proportion of these particles was visually low within the overall mass of the block. No sieve analyses were done on this block.

Thirdly, the block had to be of similar strength to the previous block, and of similar moisture content. It is obvious that the strength of the specific block is difficult to determine in underground mines. In order to obtain a reasonable idea of the material strength, a Robinson point load index tester was taken underground to test irregular lumps of material found adjacent to the blocks. To better assess the strength of the in situ material selected, UCS tests were performed at a NATA registered laboratory. The results of these tests are given in Appendix III.2.

Comparison of UCS tests on samples of the *in situ* material blocks for the PS01 and PS02 tests suggest that, given the natural variation in test samples for each type of sandstone, the compressive strengths were reasonably similar; the average UCS of each sandstone block was approximately 1.46 MPa. However, it can be seen that even with careful selection processes, the intact strength of the material within the blocks can vary by more than 30%. The potential effects such variation in strength could have on small-scale centrifuge models is obvious.

Observations - The appearance of the model at the completion of the test is illustrated in Figure 4.39 a and b. The main observations made from this test are listed below, more detail is provided in Appendix IV.2.

- During the test, no significant caving occurred until some time after all rows of pistons were lowered. Then - probably after the stooks began to "punch" into the sandstone - some small scale primary caving of the immediate roof occurred across the base of the model. Large-scale secondary caving of the remainder of the block then followed within 30 seconds of the initial collapse. What appeared to be happening was that the flexural strength of the "massive" sandstone block (with no obvious bedding weakness) was sufficiently higher in this model to allow the thick sandstone beam to bridge across the excavation from stook to stook.

POST-TEST POTOGRAPH OF THE FRONT OF CENTRIFUGE MODEL PS02

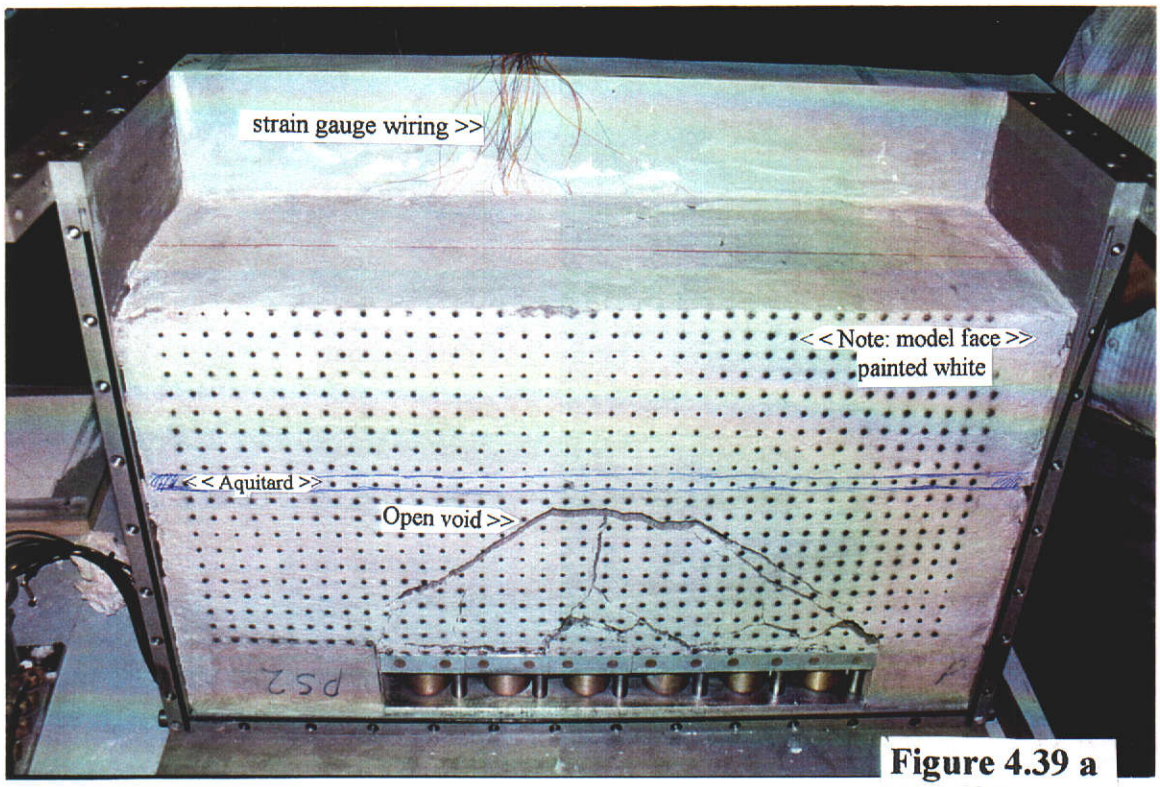

Figure 4.39 a

POST-TEST PHOTOGRAPH OF THE REAR OF CENTRIFUGE MODEL PS02

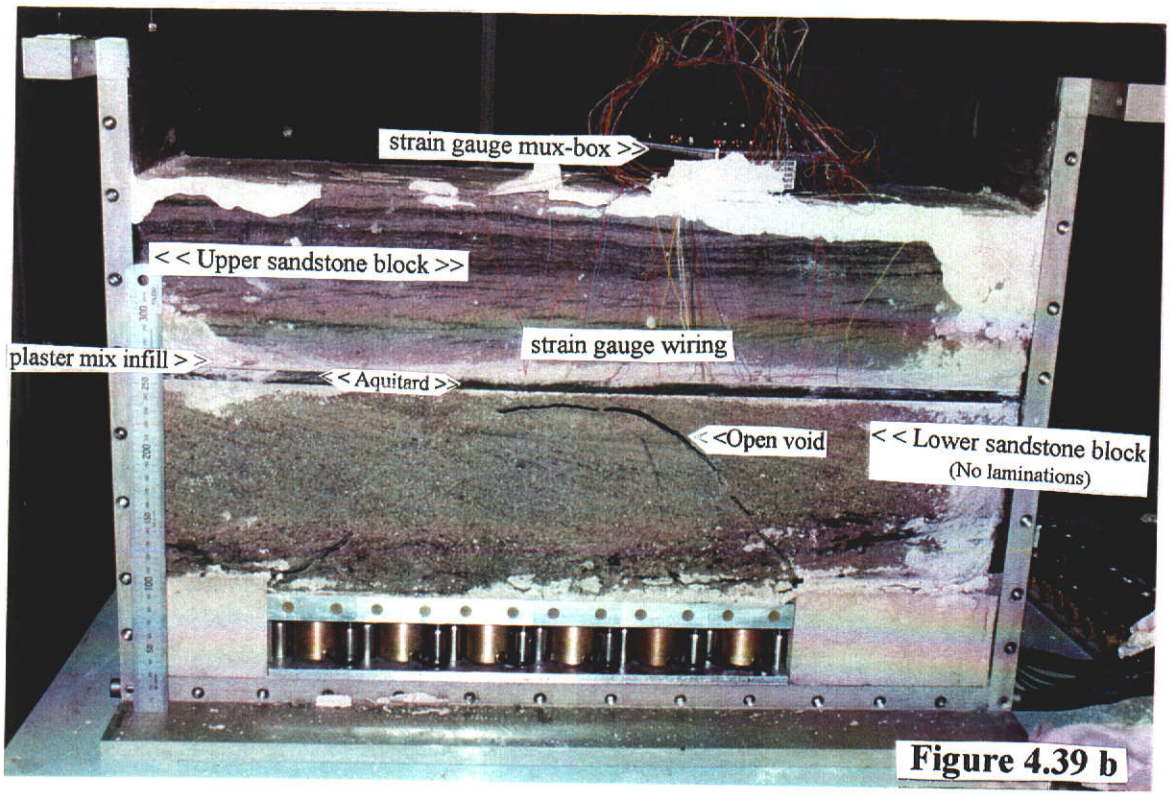

Figure 4.39 b

- It is postulated that the angle of caving of massive materials differs from well-bedded materials. The ultimate collapsed mass in this test essentially broke off in one piece, with a central tensile fracture from the base of the block to the top of the broken triangular slab (Figure 4.39 a) and a very low angle of caving at the goaf edges (~40° - see Figure 4.40 a & b). This assumption of lower angles of caving for more massive strata is also inferred by Wilson (1982).

- The height of "secondary caving" did not extend to the top of the basal block, finishing 3 mm below the aquitard. A gap of 6 - 12 mm was maintained between the collapsed goaf and the intact sandstone. This represents a bulking factor of between 50% and 100% of "mining" height. No discernible subsidence was measured above the level of the aquitard.

- Very little flexure of the aquitard and strata immediately above the collapsed ground was noted and only small flexural strains were measured on the top of the gauged aquitard (Figure 4.41). The maximum compressive and tensile strains measured were 0.62 mm/m and 0.68 mm/m respectively even though the scaled area of mining was greater and the thickness of the aquitard was significantly less than test PS01. Both maximum values are well within the yielding strain for cannel coal, which is also supported by the fact that no cracks were noted within the aquitard. It has been assumed that the reason for the small strains on the aquitard is that the uncaved triangular overhang above the goaf (illustrated by Figures 4.40 a & b) is of sufficient stiffness and strength to support the aquitard in a similar fashion to a building gable. Further discussion of the effect of caving overhang is provided in Section 5.1.

4.2.2.4 Centrifuge Test PS03

Objective - To assess the caving performance of sandstone blocks with well defined, continuous bedding laminations. It was considered that a block would meet this criteria if such bedding extended across the model for at least the middle 2/3 the block to allow for the possibility of bridging of stiffer laminations. This test was aimed at further investigating the influence of the bridging aquitard, and the bedding in sandstones on subsidence.

POST-TEST PHOTOGRAPHS OF THE LOW CAVING ANGLE AND SUPPORTIVE OVERHANG - PS02

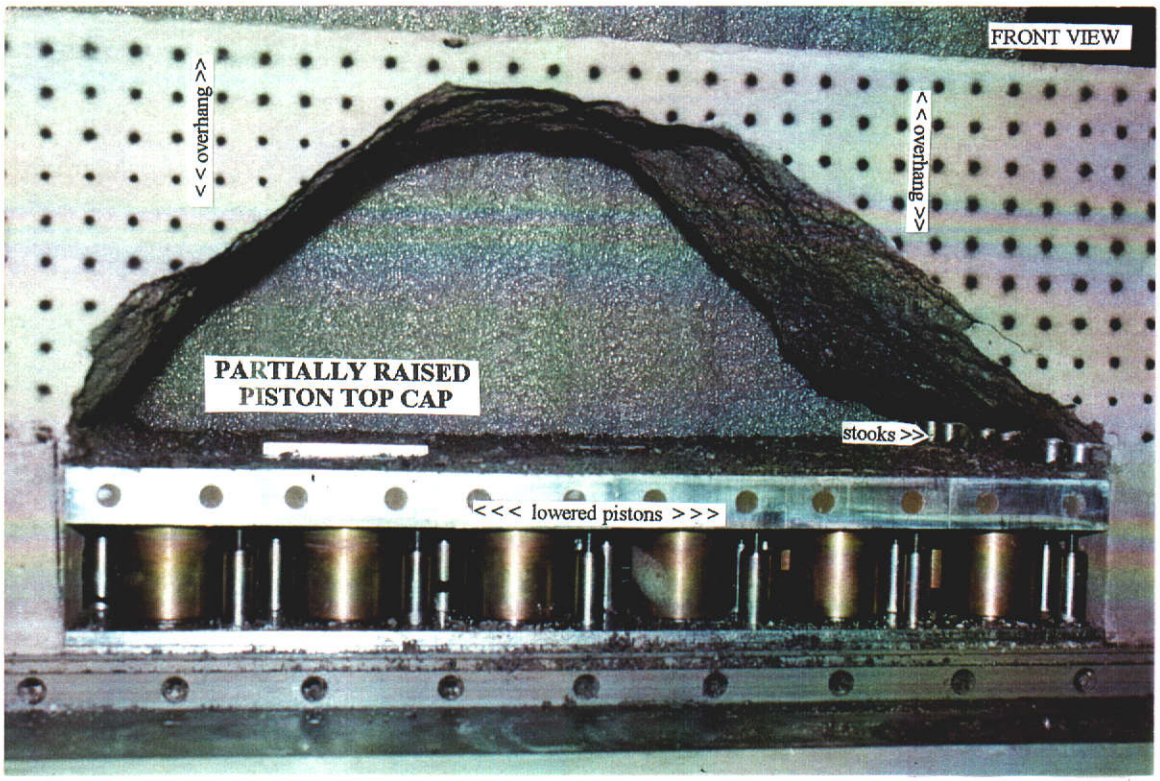

Figure 4.40 a

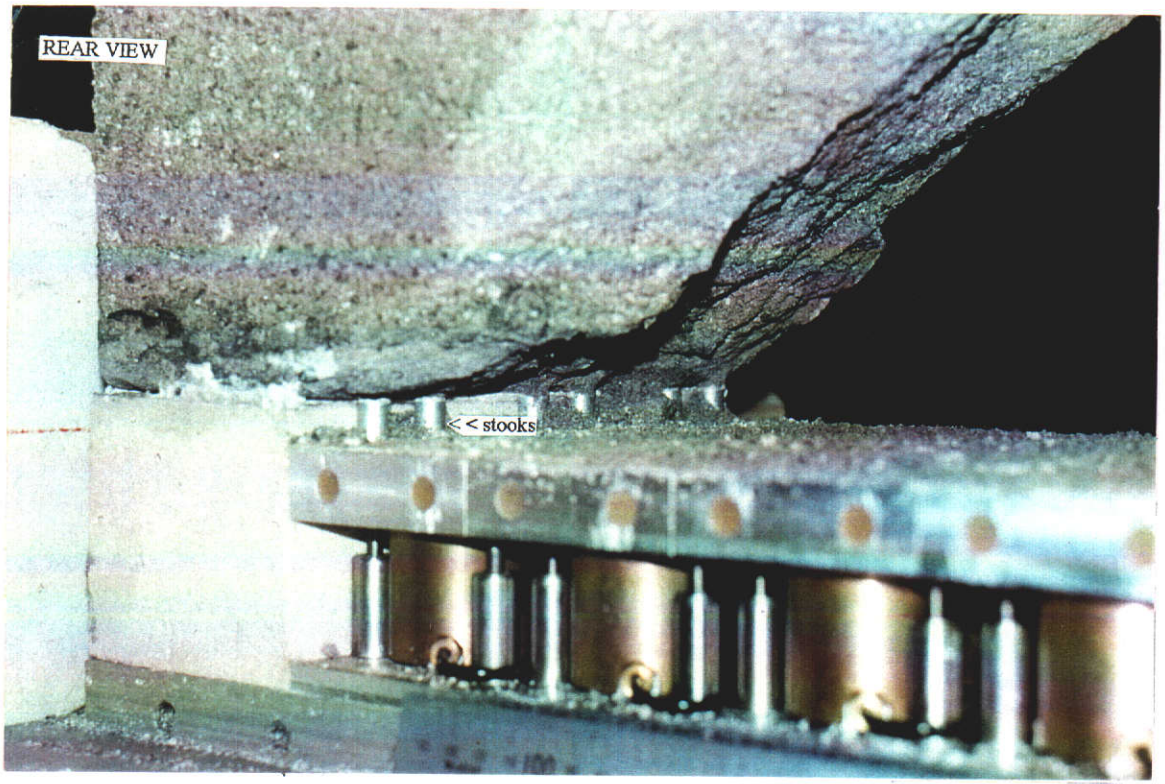

Figure 4.40 b

STRAIN GAUGE DATA - CENTRIFUGE MODEL PS02

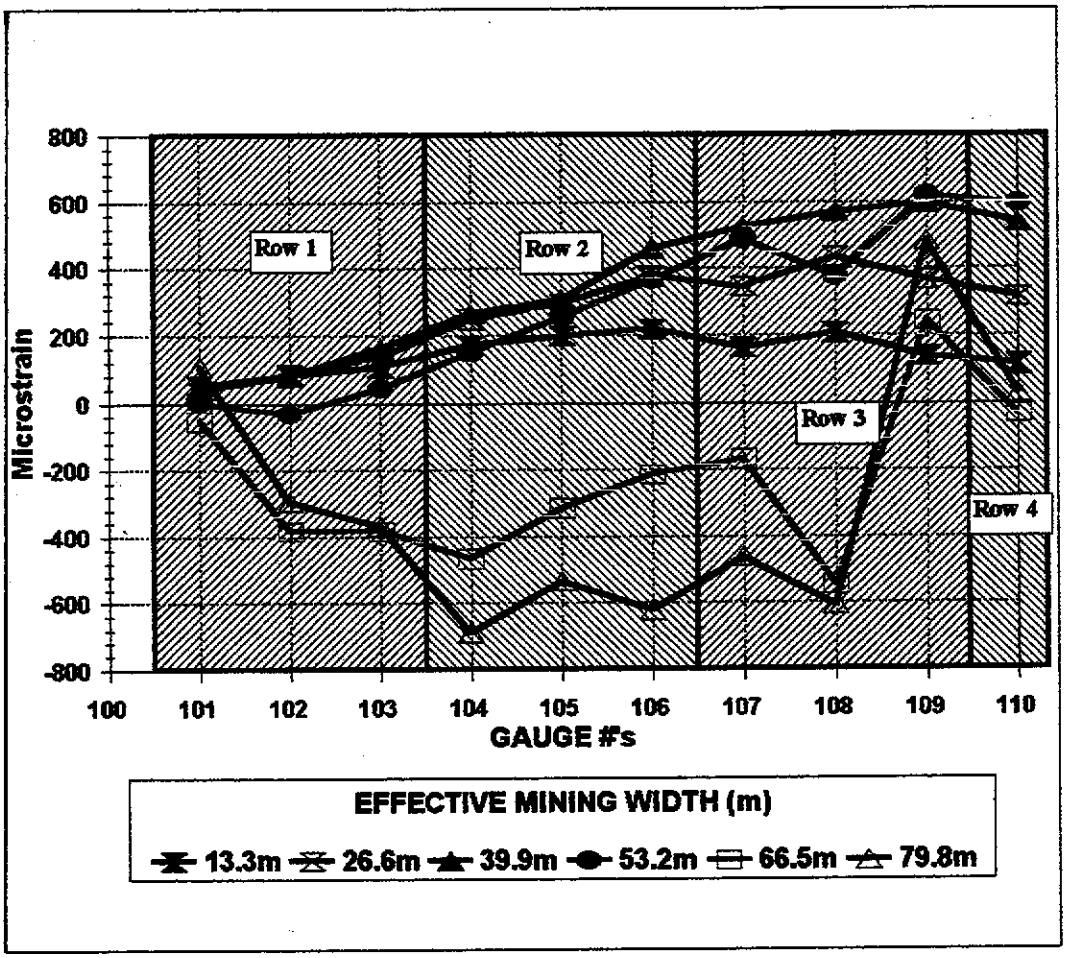

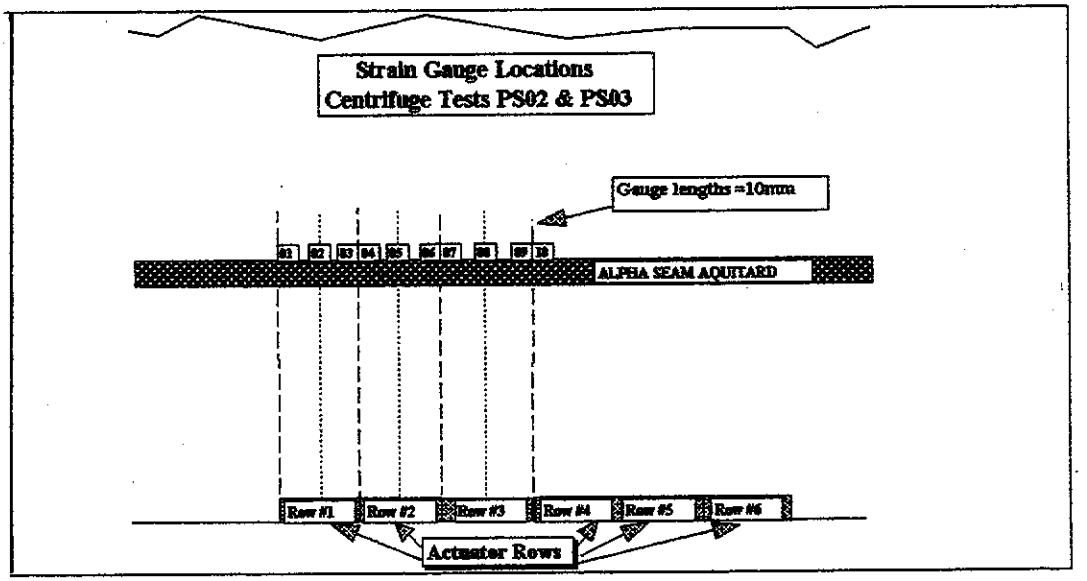

Figure 4.41

Comments - Due to concern that surface subsidence in the centrifuge models could be influenced by using blocks of semi-lithified material as the upper overburden, it was decided that this test would incorporate actual Nakina overburden material, typically found in the upper 30 m of Collie basin stratigraphy. This material was sampled from the WO-5 mine, which at certain locations, is sited above the WD6 Mine. (This material was therefore considered to be representative of the general overburden in the 2SA "prototype" panel area.)

The sample of overburden was sieved to remove the larger grains of quartz which may have influenced the performance of the model. The grain size selected to be acceptable for scaling purposes, was minus 0.5 mm.

Problems associated with sample selection for the immediate roof block in this test were even more demanding than for previous tests due to the additional selection criteria for continuous bedding across the length of the block.

The stringent selection criteria for strength was not put into practice for selecting this block. Only visual comparison of the materials (based on almost 10 years experience in the Collie area) was used to select a block with similar strength to the earlier tests.

Model Construction - The construction procedure used for this model was similar to that used for PS02, except:

- The basal sandstone block had well defined bedding, though the distribution of the laminations within the block was irregular - with bedding thicknesses ranging from sub-millimetre to + 20 mm. The final block thickness after cutting was 137 mm. This is slightly narrower than the previous block, however, such variation could not be helped as sample selection and preparation was restrictive.
- A 135 mm layer of compacted, sieved (<0.5 mm), overburden material from WO-5B Open-cut was placed immediately above the aquitard layer. This material was compacted at optimum moisture content (9% - as determined by Misich, 1988) to a bulk density of 1.9 t/m^3 (matching the bulk density of overburden in the field).
- The thickness of the cannel coal (aquitard) layer thickness was inadvertently reduced to 5 mm - due to cutting problems.

Observations - A detailed list of observations made from this test is provided in Appendix IV.3. A summary of the main observations is provided in note form below:

- In general, the height of primary caving observed in this test was 50% lower than that interpreted in prototype conditions. It would seem that the thickness of laminations is critical to the caving mechanisms during a geotechnical centrifuge model test. This again supports the process of beam theory subsidence development.
- The subsidence factor measured in the model was approximately 23% greater than that measured above 2SA panel. This suggests that either goaf consolidation is greater or bulking processes were not replicated in the model. Two possible causes for this discrepancy are a lack of block formation and block rotation during primary caving (which, in turn, reduces the bulking factor of the goaf), and a lack of floor heave in the model (the model is founded on an aluminium base). It is considered that the smaller bulking factor has the most impact, as it follows that floor heave in mining areas where subsidence equates to 100% mining height must be negligible.
- All forms of caving cease at the height of the first aquitard beam of sufficient thickness, or strength, that can bridge across the line of shear at the caving edge (Figure 4.42). This model suggests that the minimum thickness of aquitard required to trunkate the line of shear is in the order of 1 m (5 mm in the model). It was noted that a sub-vertical plane of shear had developed through the aquitard at some stage after the line of shear was initially bridged. This indicates that the line of shear could break through a thinner aquitard, and continue the tertiary caving process into strata higher above the mine.
- Once the caving edge is bridged, the shape of the subsided mass above the aquitard becomes more gently curved, even if the aquitard is sheared through as in this case. This "softening" effect was also noted in Westcoll4 (see Figure 4.32).
- Post-test observation suggested that during testing, the *in situ* overburden material, underwent a significant amount of consolidation. As this consolidation would obviously mask the true surface subsidence, laser profiling was therefore not attempted for this test. This consolidation was to be clarified in future tests.
- Although it is possible to develop a sub-vertical shear through the complete thickness of the aquitard, there is no evidence which suggests that an open fracture will develop. This is an important observation in regard to water passage through the subsided mass from overlying aquifers.

POST-TEST PHOTOGRAPH OF THE LEADING EDGE AT THE REAR OF CENTRIFUGE MODEL PS03

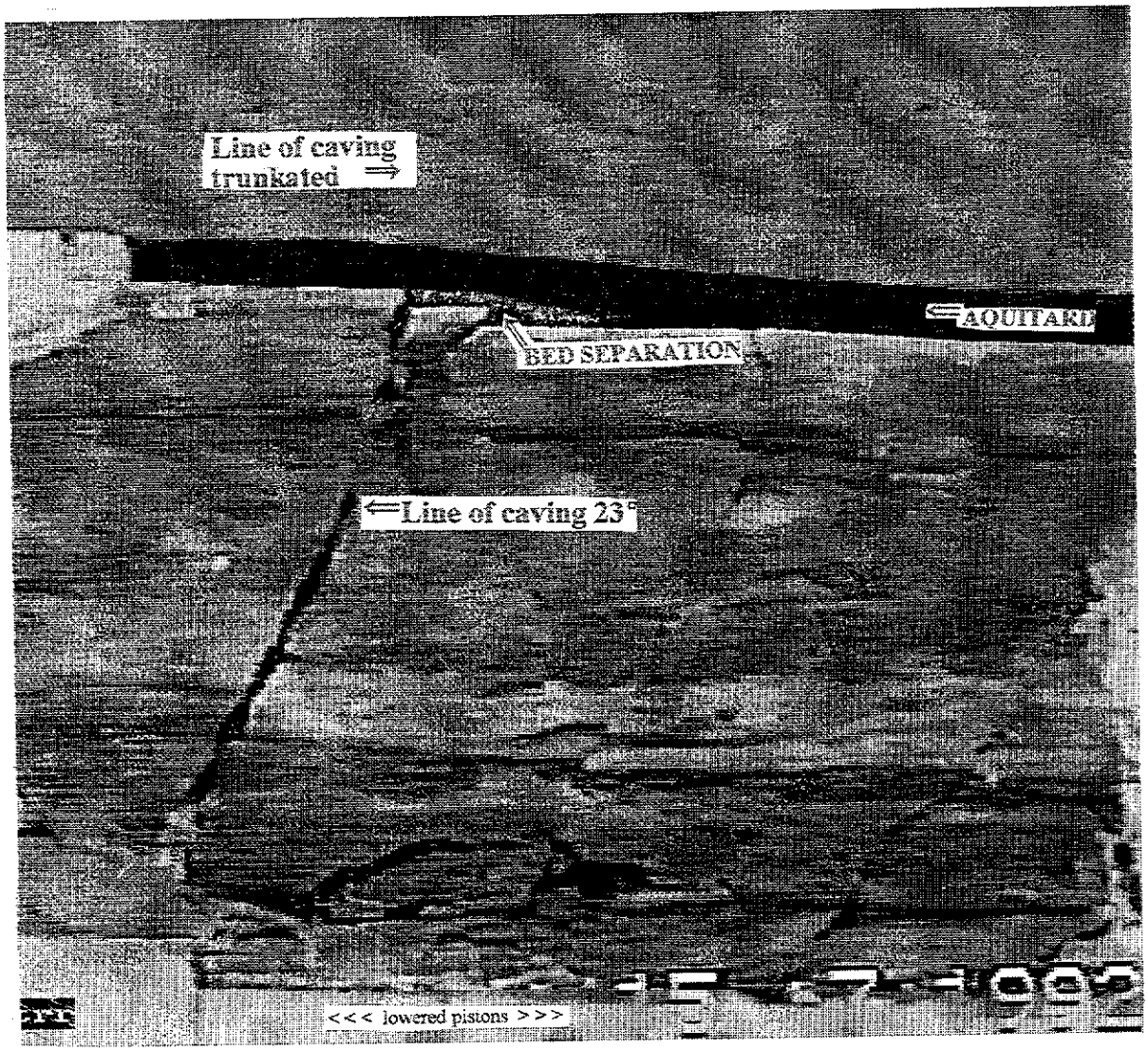

Figure 4.42

- It has been interpreted from Figure 4.43, which represents the aquitard strain data recorded during testing, that the yielding tensile strain of the cannel coal aquitard was in the order of 2 mm/m. There was no cracking observed from the video footage in the aquitard until the fourth row of pistons was lowered (representing 54.4 m width). Prior to this point (when the width of mining was effectively 40.8 m), the maximum strain recorded was approaching 2 mm/m.

4.2.2.5 Summary of *In situ* Material Tests

The most significant results to come out of the plane strain *in situ* material models are:

- The caving characteristics of sandstone in the Collie Basin are largely dependent of the inherent bedding. Massive bedding structures appear to have greater apparent flexural strength. This characteristic is supported by beam theory, where tensile stress reduces proportionally with effective beam thickness [see Equation 2.5(4). It is to be noted, however, that although the beam theory is, in principal, a major component in subsidence development, no researcher has been able to use this theory to accurately predict subsidence [although many have tried - e.g. Krishna (1991) who investigated subsidence development above a bord and pillar mine in the Ranigunj coalfield, India]. This assumption supports the use of flexural strength in dimensional analyses, and also suggests that it is important that the bedding of materials is adequately scaled within the physical models.
- Selection of suitable blocks of *in situ* material is extremely difficult, if not impractical, particularly as the best source of material is at the relatively unstable edge of the caved goaf.
- The material strengths of test samples cored from within these large blocks of *in situ* material can vary markedly, thus illustrating the difficult task in obtaining repeatability for *in situ* material tests.
- Coal aquitards more than 1 m thick have the ability to span across the caved edge, thus reducing the amount of shear through the overlying sediments (Figure 4.42). This mechanical characteristic of the stiffer aquitard promotes continuous subsidence trough formation and restricts the development of pot-hole subsidence. This phenomenon also prevents the development of open conduits along lines of shear which may otherwise interconnect overlying aquifers to the mine.

STRAIN GAUGE DATA - CENTRIFUGE MODEL PS03

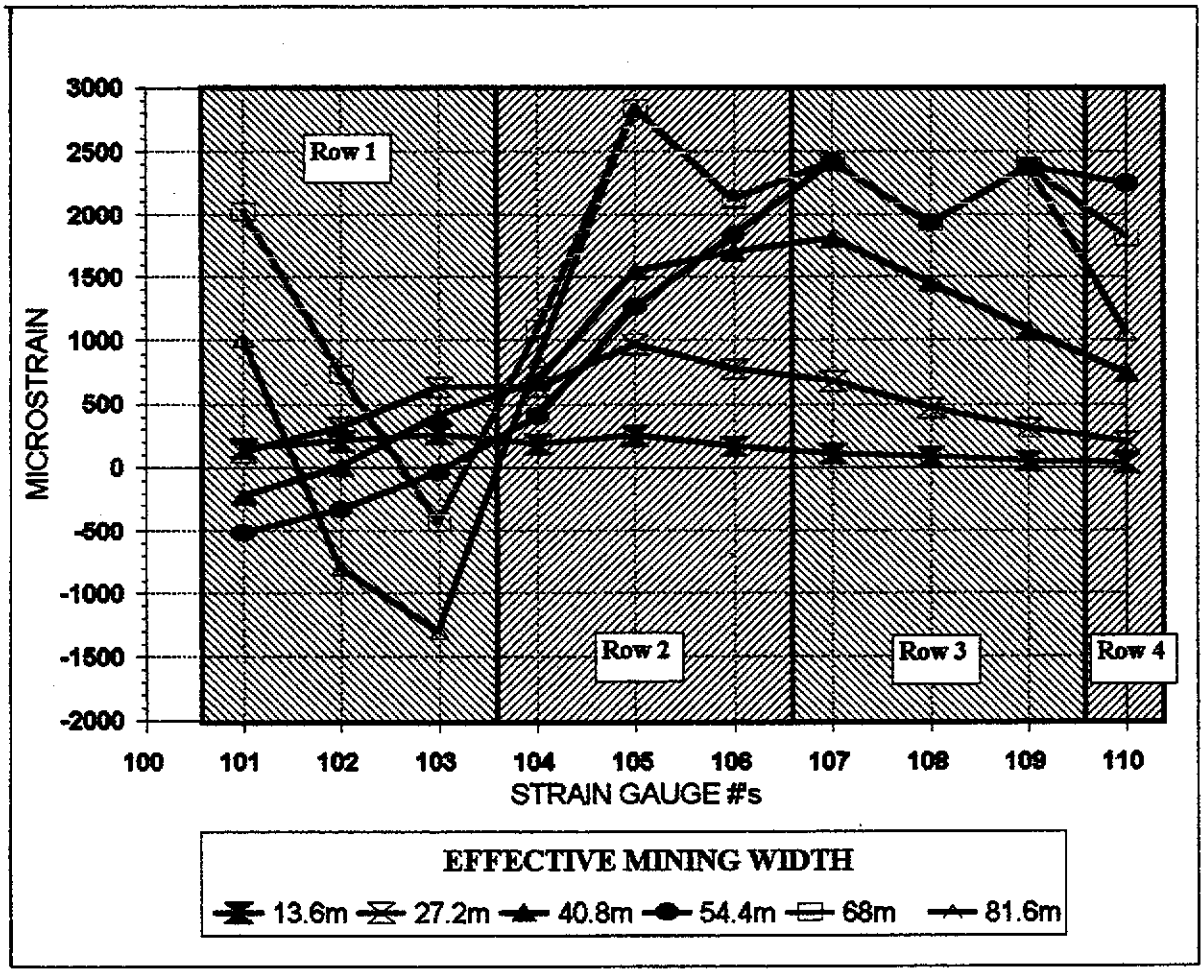

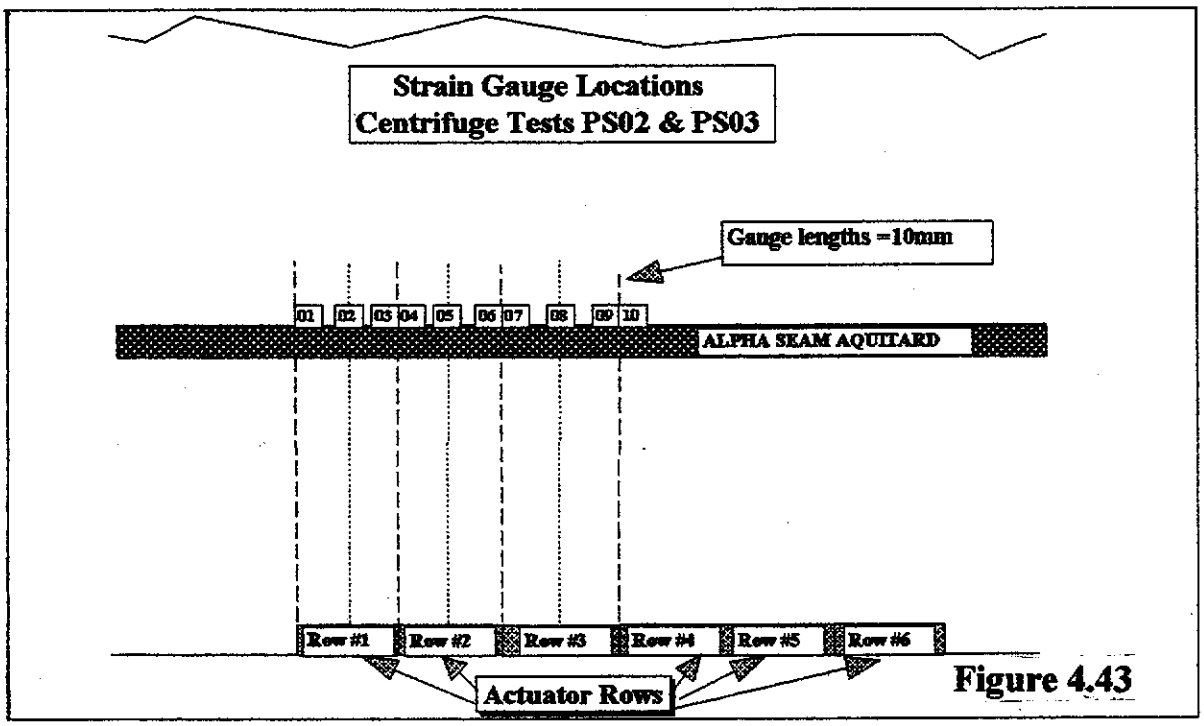

Figure 4.43

- The yielding flexural bending strain of coal aquitards is estimated to be 2 mm/m.
- The angle of subsidence shearing/caving is 23°, which supports field measurements.
- The shape of the subsidence profile and magnitude of aquitard strains is also influenced by the support provided by the underlying (triangular) caved overhang at the abutments of the goaf to the bridging aquitards.

4.2.2.6 Centrifuge Test PS04

Objective - To develop an "equivalent material" model for comparison with "*in situ* material" tests, and to better assess the discrepancy between maximum subsidence measured in the previous test, and that surveyed in the field. An additional aquitard/aquifer sequence was added to whether there would be any changes in subsidence mechanisms from one aquitard to the next.

Model Construction - Prior to construction of the first equivalent material test, a comprehensive investigation was undertaken to establish the most suitable:

- mechanical parameters to scale the equivalent material model on,
- equivalent material constituents, and
- mixing and curing procedures to develop a representative equivalent material model.

The results of the first point of investigation is discussed above in Section 4.2.2.1. This investigation established that modelling must be based on a system of dimensionless terms incorporating the critical subsidence parameters extraction ratio, elastic modulus, flexural strength, geometry and time. The resultant critical functional equation is:

$$\frac{S_{ubs}}{G} = f_2 \left\{ E_r, \frac{E}{Fs}, \frac{Ss}{Fs}, \frac{g.G.v.}{Fs}, \frac{t.g^{½}}{G^{½}} \right\} \qquad \text{[Eqn. 4.2(5)]}$$

The results of investigation pertaining to the other two points are summarised in Appendix III.2. In brief, it was found that the most suited materials for modelling were mixes of sand, water and building plaster. All mixing and curing procedures were firstly established by the author using facilities at the UWA, then when the author was satisfied that adequate representability and repeatability of equivalent materials could be maintained by the procedures adopted, the responsibility of constructing models was given to UWA technicians (in particular Mr J. White). All models were constructed as per the guidelines set out by the author (see Appendix III and IV) for each test.

Comments - The strain gauge wiring was fixed incorrectly along the long axis of the PS04 model aquitards, and grouped together as a mass of wiring, rather than being taken back, individually, to the rear of the box as for all other tests . (Figure 4.44 illustrates the strain gauge set-up for tests PS04 and PS05). This change in gauge installation was made by a contract technician who at the time was unsupervised and decided to alter the proven system without consultation.

The fault was detected prior to completion of the model, however, as the model was 90% complete at that point, it was decided to finish construction and run a full test. Concern was held that the longitudinally glued wires would give additional support to the aquitard beams and thus reduce the superincumbent loading on lower aquitards and goafed material.

The thickness of each block varied slightly from that proposed across the length of the model. This variation appeared to be ± 2 mm for aquitard, and ± 5 mm for aquifers.

It was proposed that the drop height be 8 mm (2.4 m in the prototype), however, during the test, the piston top-caps actually dropped 14 mm - which represents the maximum stroke of the pistons. This fault was corrected by the next test.

In order to assist with determining the influence of specific parameters on subsidence, the model stratigraphy was simplified to comprise of essentially three components; weak aquifer material, stiff coal aquitard layers and overburden - as per test PS03.

Observations - It was decided not to rigorously evaluate the subsidence troughs developed during the PS04 model (due to the concern with the incorrectly glued strain gauge wires) until a second, replica model, was constructed - PS05 - with wires glued in the standard configuration and operated so that both sets of results could be used as a comparison. It was considered that PS04 results would be unrepresentative of the prototype subsidence mechanisms. However,a number of interesting points were observed during this test, these are discussed briefly below:

- It was demonstrated that with Wongawilli extraction, it is possible to develop less subsidence immediately above the mine horizon than at some distance above the mine roof due to the sequencing of extraction and localised ground collapse (see Figure 4.45). This unusual event is supported by field evidence.

STRAIN GAUGE LAYOUT FOR CENTRIFUGE MODELS PS04 AND PS05

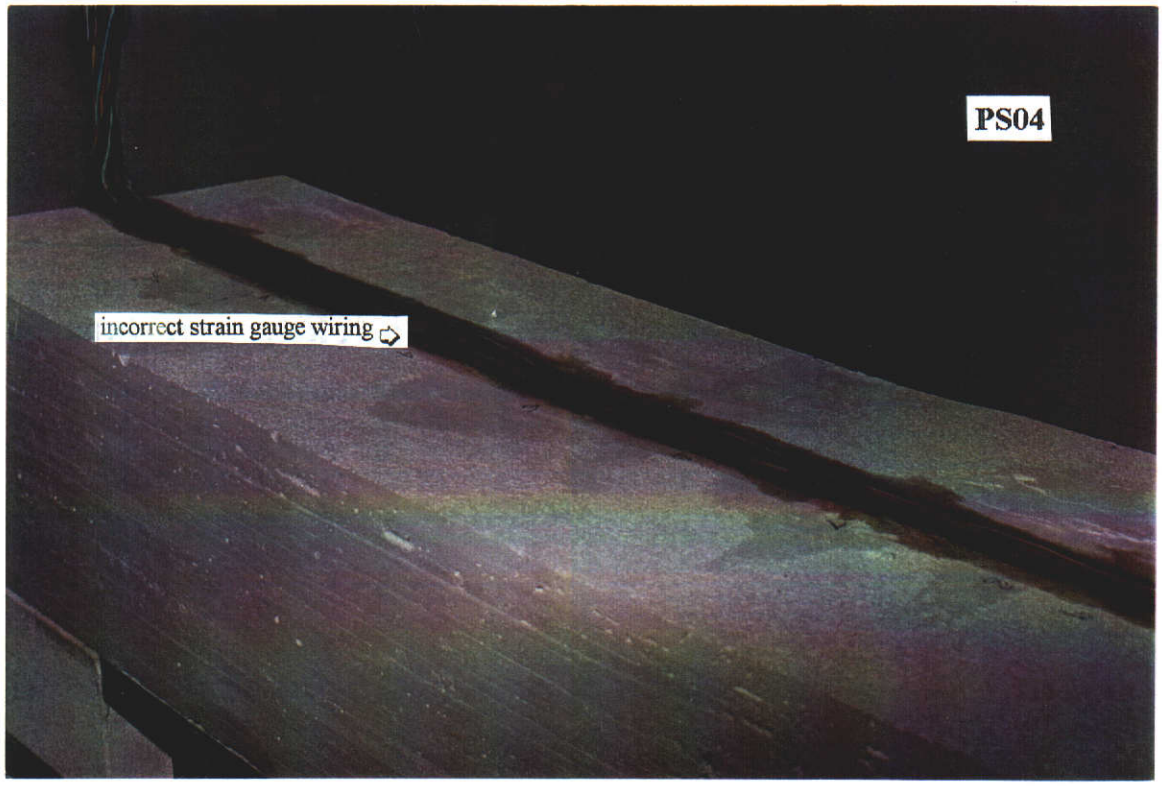

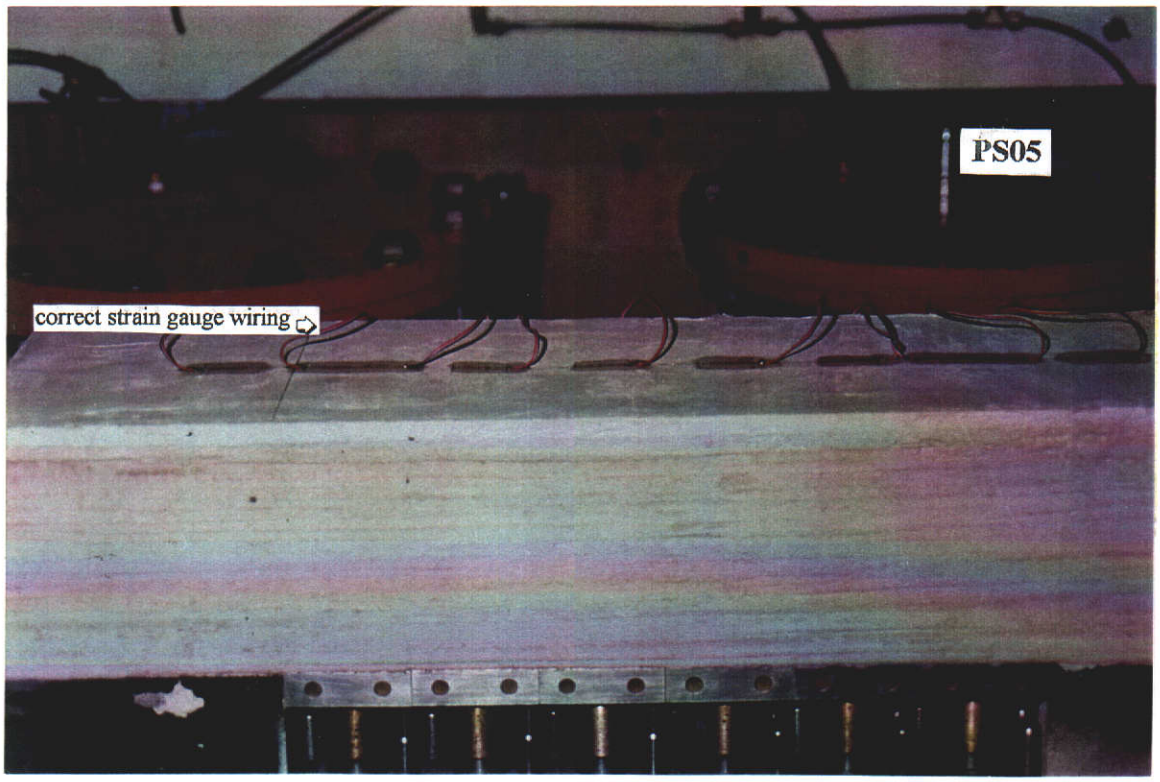

Figure 4.44

POST-TEST PHOTOGRAPHS OF CENTRIFUGE MODEL PS04

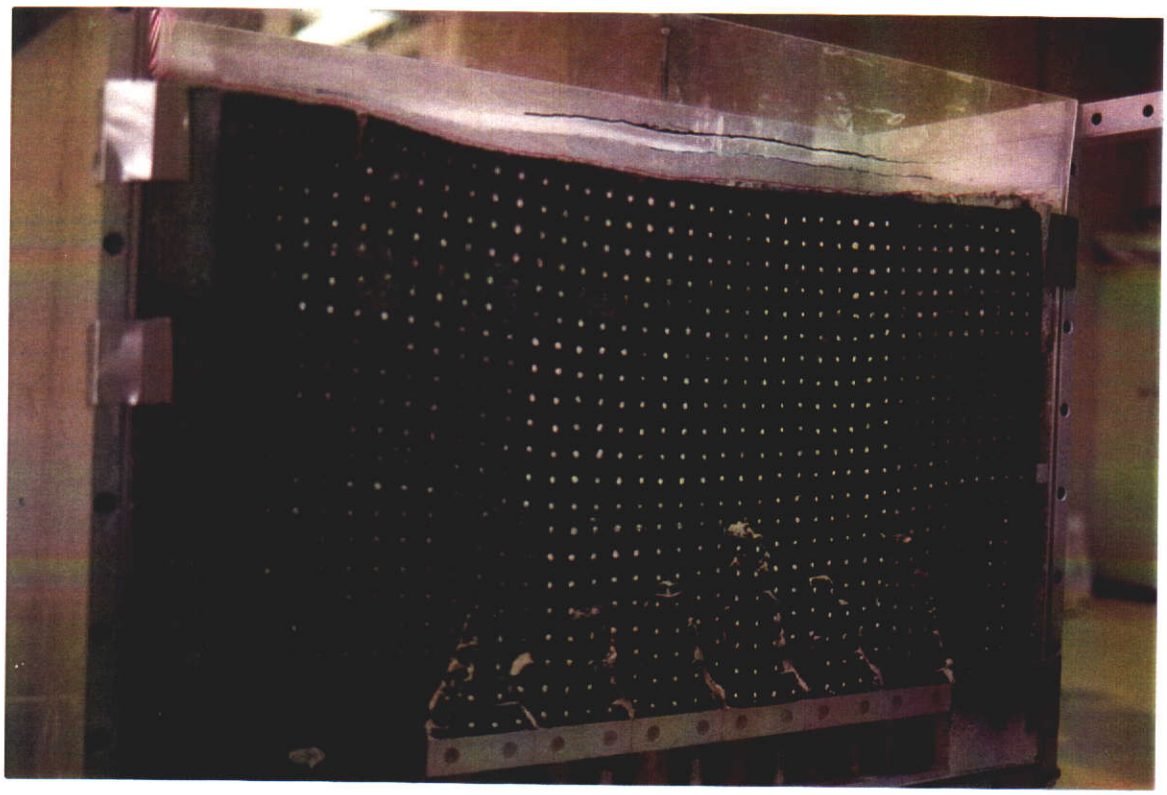

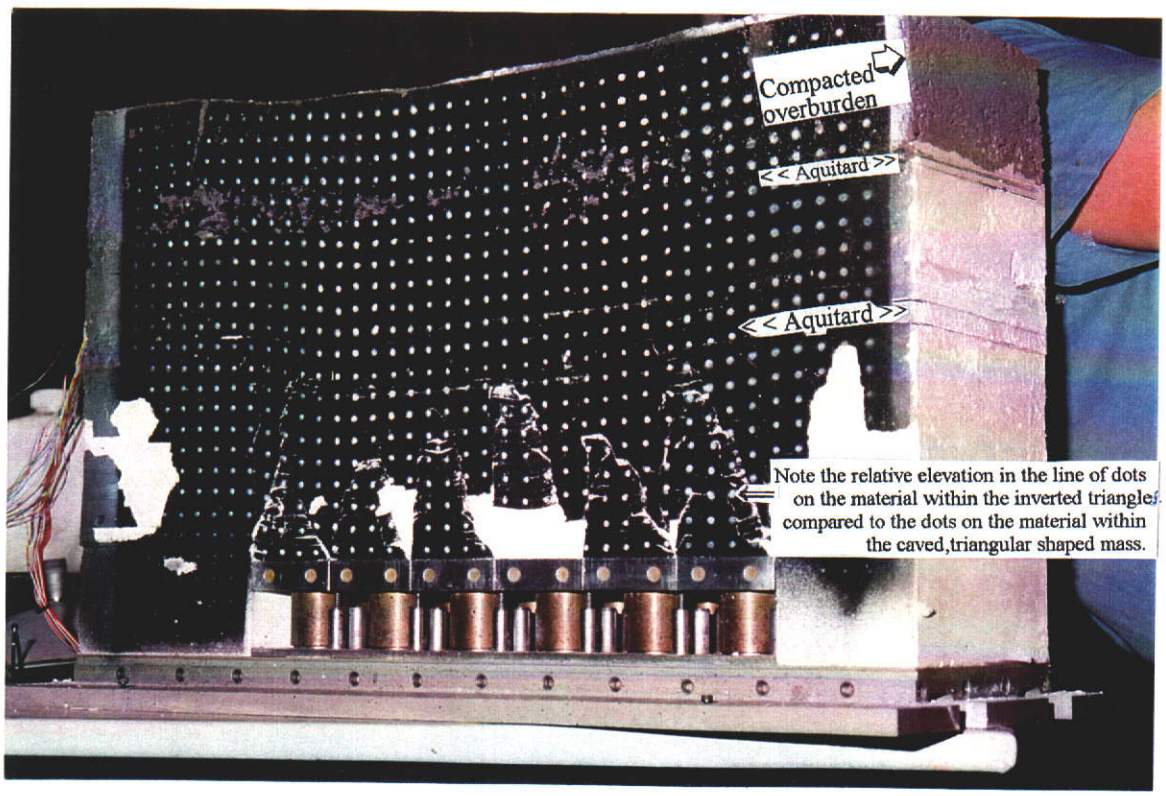

Figure 4.45

- Laser profiling of the model surface after test completion showed significant variation both between duplicate profiles, and along each subsidence trough profile where many "spikes" were interpreted by the laser. Although the general trend of subsidence was identifiable, this variation made it impractical to fit an appropriately accurate curve to the subsidence profile for calculation of curvature and strain.

  It was therefore decided that laser testing in future tests would be misleading. Furthermore, the edge effects near the surface on the right hand side of the model (noted by larger cracking at the surface, and the gap between the model and strong box walls as the model edge sagged inwards) also misrepresent surface subsidence.

- Aquitard cracking was fairly symmetrical, and although some crack dilation was noted, at no point did the crack develop into an open fissure. Some cracking - interpreted from high tensile strains recorded at various stages during the test (plotted in Figures 4.46 a, b and c) - could not be visibly detected. This lack of crack detection has been interpreted as being due to the "re-knitting" of cracks as the subsidence 'wave' passes and the aquitard changes from being in tension to being in compression. The subsidence wave is not a new phenomenon, and has been reported by many researchers from various parts of the world (eg. Dunrud, 1984), however, the supportive evidence of subsurface recompression of fractures is an important point when considering the potential for large-scale innundation of groundwater.

- There was an unusually large height of primary caving. This has been interpreted as being due to scaling of already weak prototype sandstones which tends to promote soil-like behaviour of equivalent materials or possibly variable distribution of binder throughout the weaker aquifer mix.

4.2.2.7 Centrifuge Test PS05

Objective - To duplicate test PS04 and establish whether the strain gauge wires had any influence on the performance of the model and further investigate the unexpected large heights of primary caving and subsurface subsidence.

Comments - Because the main purpose of this test was to establish what the effects of placing the strain gauge wires along the long axis of the model were, PS05 was constructed in identical fashion to PS04, with the exception of the placement of the strain gauge wiring.

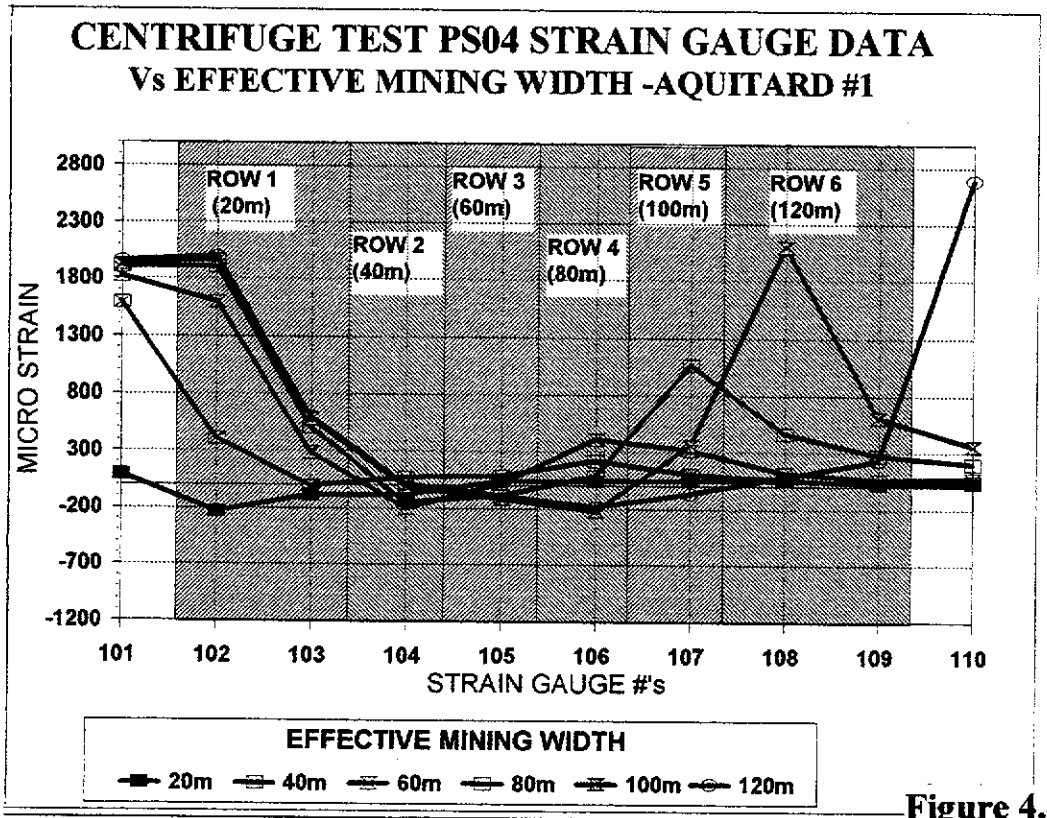

Figure 4.46 a

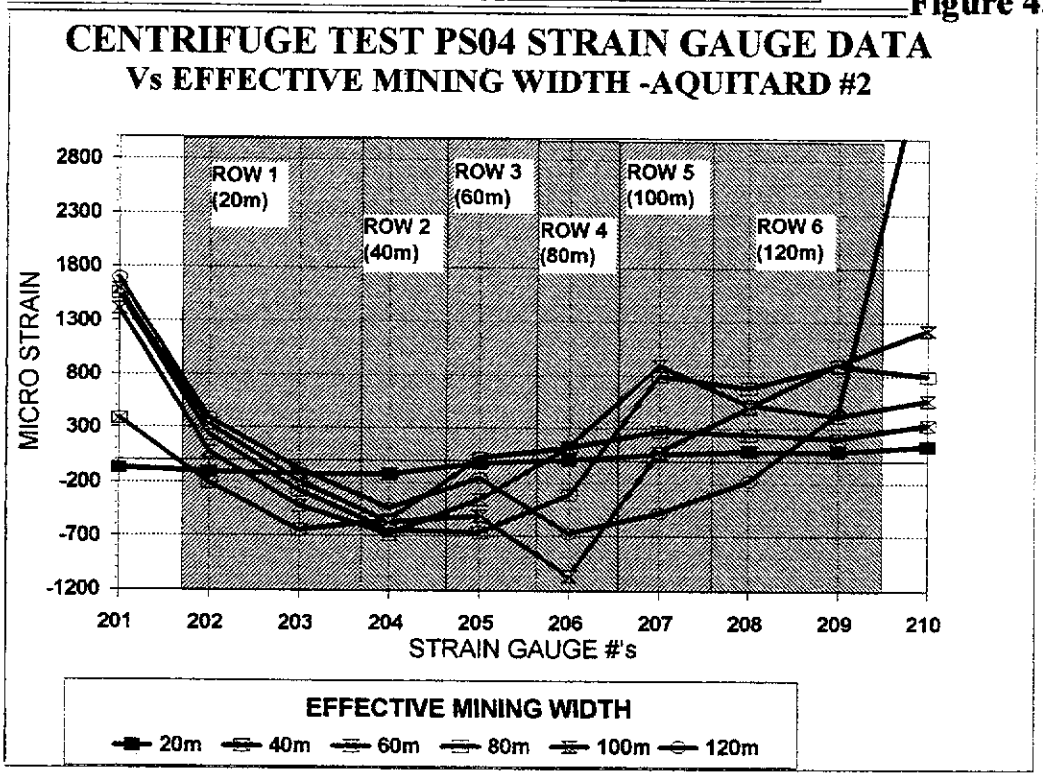

Figure 4.46 b

STRAIN GAUGE LAYOUT - CENTRIFUGE MODEL PS04

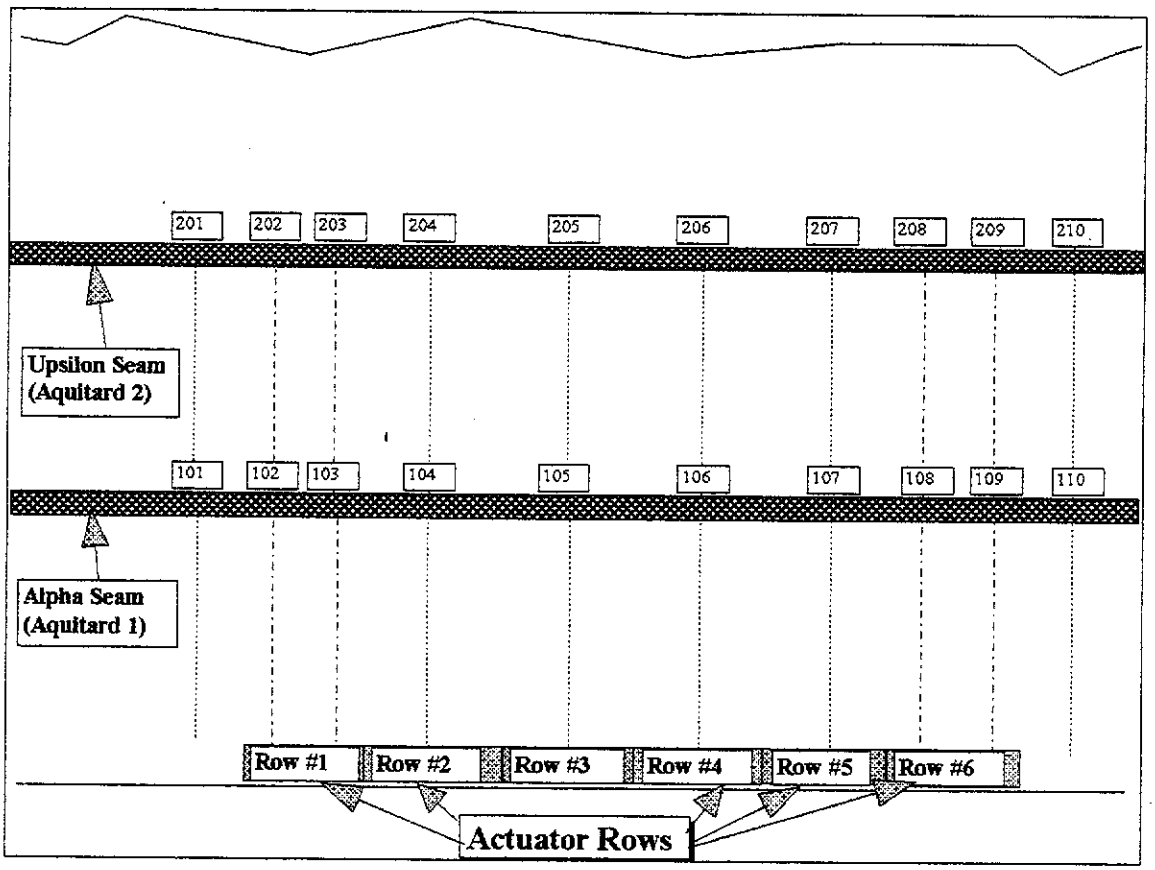

Figure 4.46 c

During the initial spin-up of the model, a light bulb "fixed" to the side of the centrifuge box dislodged and shattered against the actuator solenoid valve rack. A piece of broken glass pierced the black polyethylene hose feeding the front actuator on the extreme right hand side (RHS) of the model. This actuator consequently dropped immediately, thus initiating "mining" on the RHS. It was then decided to proceed with the test, mining from right to left, which is the reverse of PS04.

As it turns out, during the uncontrolled collapse of the front RHS actuator, some debris prevented the middle actuator in the same row (hidden from view) from lowering. This severely restricted the development of subsidence, particularly in the early stages.

Observations - A detailed list of observations made from this test is provided in Appendix IV.5. A summary of the main observations is provided in note form below:

- Higher strains measured during the PS05 test indicate that the strain gauge wires in the previous test have significantly influenced the subsidence processes. From this point onwards, the normal wiring configuration was strictly enforced.
- One of the edge pistons did not drop. This had a significant impact on the behaviour of the model and the effect of increasing mining width on subsidence development could not be established for this test either.
- It was again evident that large open vertical cracks did not develop during the test, even with the development of large-scale shearing and excessive subsidence.
- Although there was no evidence of bed separation above the first aquitard, the magnitudes expected (0.1 to 0.2 m in the prototype = 0.3 mm to 0.6 mm in the model) would probably not be able to be detected either visually, or within the standard error of the ACCUware software.
- The maximum surface subsidence in the model approximated the full height of "mining". It was therefore considered that the use of centrifuge modelling (using the existing configuration of mining elements, and methods of fabrication of equivalent materials) for accurate predictive purposes was not practical. It appears that the main fault with this modelling technique is the inability to reproduce large-scale rotational movements in the caved zone.

  One possible option to check whether equivalent material centrifuge models can actually represent the caving and bulking process in larger scale models would

have been to redesign the base plate and actuator system to incorporate many more pistons and therefore reduce the area of caving. Another option would have been to introduce an artificial blocky material in the immediate roof horizon which may have been able to better represent bulking. However, thorough investigation of the bulking actions was beyond the budgetary constraint of this project and was seen to have no guarantee of working. [The author had serious doubt about the effect of such high scaling factors (300:1) on critical, large strain, defect-dependent movements.] On top of this, the length of time estimated to undertake such a program of investigation was considered to be unacceptable as the testing schedule was already well behind. Consequently, these possibilities were not investigated further.

It was therefore concluded that the existing centrifuge modelling layout was unsuitable for accurate prediction of subsidence profiles, due primarily to the poor representation of bulking goaf. However, it was considered that the modelling technique provides a good visual account of the likely subsidence mechanisms for a wide range of mining scenarios; the most favourable feature of the modelling technique was the ability of the collapsed ground to provide restraint to the edges of caved masses. It was considered that despite the bulking problem this modelling method had sufficient merit for further testing because the lower bulking factor would provide worst-case subsidence development and any findings made would only err on the side of conservatism.

This conclusion and approach to centrifuge modelling is supported by Iglesia et al., (1991) with their experimentation with trap-door simulation of mining below jointed rock in centrifuge models. They concluded that centrifuge modelling of materials with large scaled discontinuities could not meet the laws of similitude and provides a serious obstacle for centrifuge modelling. Such large scale discontinuities can be compared with bedding planes in the subsidence models, and the large strain caving mechanisms fundamental to the subsidence process. Iglesia et al., however, emphasise, with their final comment on the use of centrifuge modelling for such studies, that centrifuge modelling when geared toward investigation of the basic mechanisms, and not direct simulation of site specific prototypes, can provide valuable information towards understanding the prototype response to mining.

Consequently it was decided to continue with the physical modelling program for another four tests to qualitatively assess the effect of:

- coal extraction by panel/pillar mining methods,
- extracting greater mining heights, and
- mining beneath saturated aquifers.

The tests developed for investigation of these issues are discussed in detail in the following Sections. It was recognised that although accurate design parameters would most likely not be derived from these tests, the opportunity to obtain visual evidence on these issues, was considered as being potentially valuable to the study.

4.2.2.8 Centrifuge Test PS06

Following rationalisation of all field data and subsidence modelling, it was concluded, given the economic viability of underground mines at the time, that the overriding factor for profitability of total extraction was dependent on the amount of water ingress into the mine. It was established, through personal contact with WCL management, that in order to maintain profitability, groundwater inflow should be minimised (to less than 2000 m^3/day) if Wongawilli "total extraction" methods were to be used (Misich et al., 1993[2]). It was also proposed that the only realistic way in which this could be achieved was to mine by panel/pillar methods (as illustrated by Figure 2.18, in Section 2.5.6.1). The success of the panel/pillar mining technique relies on both the restriction of subsidence from individual sub-panels, and the interaction between separate sub-panels, so that the resultant subsidence is within the tolerance level of the superimposed aquitards. It is possible that uncontrolled interaction between the individual goafs would generate significantly more subsidence and therefore rupture the protective aquitards, with serious implications.

Following from work by Misich (1985[2]), with the establishment of the panel creep mechanism of subsidence development (discussed previously in Section 2.5.5.1 and later in Section 5.3), it was thought that the panel/pillar method had potential for elevated tributary loads to collapse the weak sandstone column above intra-panel coal pillars (developed by caving on either side, see Figure 4.47). In this event, greater subsidence would obviously be developed and the general safety of the operations could be jeopardised.

CONCEPTUAL CAVING MECHANISM ABOVE INTRA-PANEL PILLARS FOR PANEL/PILLAR MINING

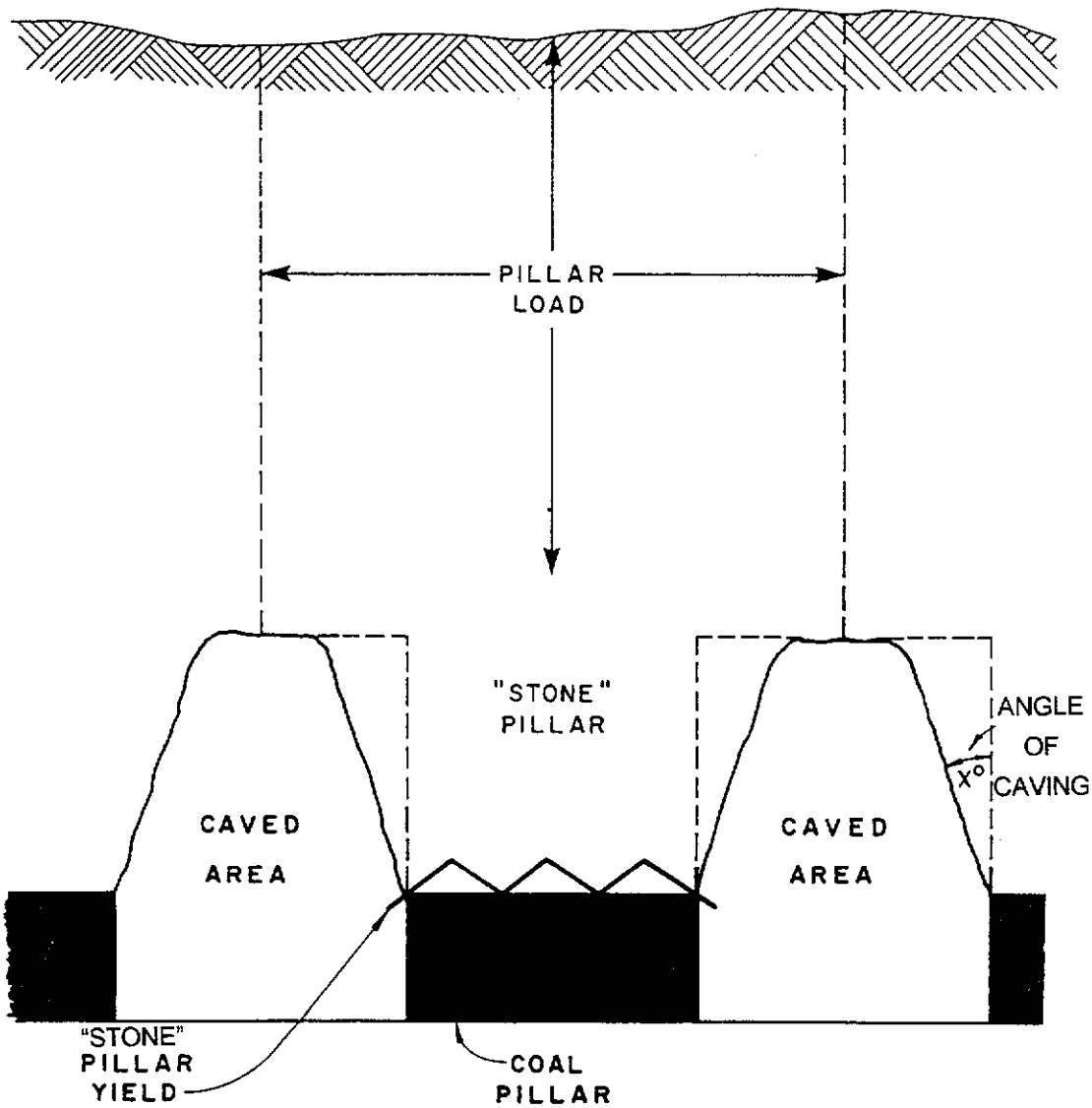

Figure 4.47

Due to concern for the significant ramifications of this form of collapse during mining, it was decided to use the geotechnical centrifuge to investigate the potential for interaction between adjoining sub-panels.

It was decided to use centrifuge modelling for investigation of sub-panel interaction (rather than mathematical modelling) because of :

- the inability of mathematical models to accurately represent the caving process and goaf edge characteristics in the subsidence process, and

- the success of centrifuge modelling for representing the angles of shear and the demonstrated ability of the model goaf to provide support to the caved edges and spanning aquitards. It was considered that the lack of bulking of the model goaf material would probably provide less support for the first bridging aquitard, than in the field, however at worst, this would provide a conservative estimate of this interaction.

The model details and analyses are summarised below.

Objective - To model a panel/pillar extraction panel and assess the potential for interaction of separate areas of subsided ground between individual sub-panels.

Comments - It was recognised that the proposed model design was very conservative (considering the expected lack of bulked goaf) and that there was a risk that the results may have proven unduly negative because of this, however, due to the high level of concern held for minimising groundwater ingress into the mine workings, this approach was considered to be justifiable.

The row of intra-panel pillars was modelled by not lowering the third row of pistons. This resulted in two sub-panels (one 40 m wide, the other 60 m wide) separated by a 20 m wide pillar.

Once the fourth row of pistons was lowered (representing two 40 m wide sub-panels separated by a 20 m wide intra-panel pillar), the middle row of pistons dropped unexpectedly. This unexpected event is attributed to the additional loading on the

actuator system developed by having fully caved ground on either side. This additional load exceeded the burst pressure of the hydraulic piston's thin polyethylene feeder tubes with the result that the tubes perforated, releasing hydraulic pressure and subsequently lowered the row of pistons representing the intra-panel pillar. From video evidence, the timing of this event appeared to be gradual at first, with ultimate collapse occurring (suddenly) about 25 seconds after the 4th row of pistons was lowered.

Observations - A detailed list of observations made from this test is provided in Appendix IV.6. A summary of the main observations is provided in note form below:

- Even though the results from this test were not ideal, the low levels of strain (Figures 4.48 a,b,c,d) and minimal subsidence noted prior to the untimely collapse of the intra-panel pillars provided some confidence to trial the NWB3 panel as planned (with the necessary water management safeguards installed should the unexpected happen).
- A more rigorous testing procedure was required for checking the condition of the model components before testing.
- The method used to represent standing pillars within the model (by leaving a row of pistons in an active, upright position) was not adequate. It was evident that further proposed panel-pillar tests would require a more secure method of including permanent intra-panel pillars in the model.
- The yielding strain for equivalent aquitard material confined within the model is interpreted as 0.8 mm/m in tension and 0.7 mm/m in compression (see Appendix IV.6). By comparison, these yielding strains compare reasonably closely with the laboratory beam test yielding strains for beams of natural coarse sandstone (0.8 mm/m - see Table III.2, Appendix III.2), measured during the investigation into modelling materials prior to the Phase II centrifuge study. This yielding strain probably represents an acceptable aquitard rock mass limiting strain, considering that the yielding strains for the *in situ* aquitard material tested in the laboratory is ~2 mm/m, and that a one third reduction factor is required for aquitard rock mass material strengths (discussed in Section 4.2.2.1).
- Sub-panel widths of 40 m with intra-panel pillars 20 m wide appear to be suited for total extraction beneath undrained strata above the Wyvern seam. However, it is not clear - due to the collapse of the middle row of pistons in the model - what effects a 60 m wide sub-panel would have on the process.

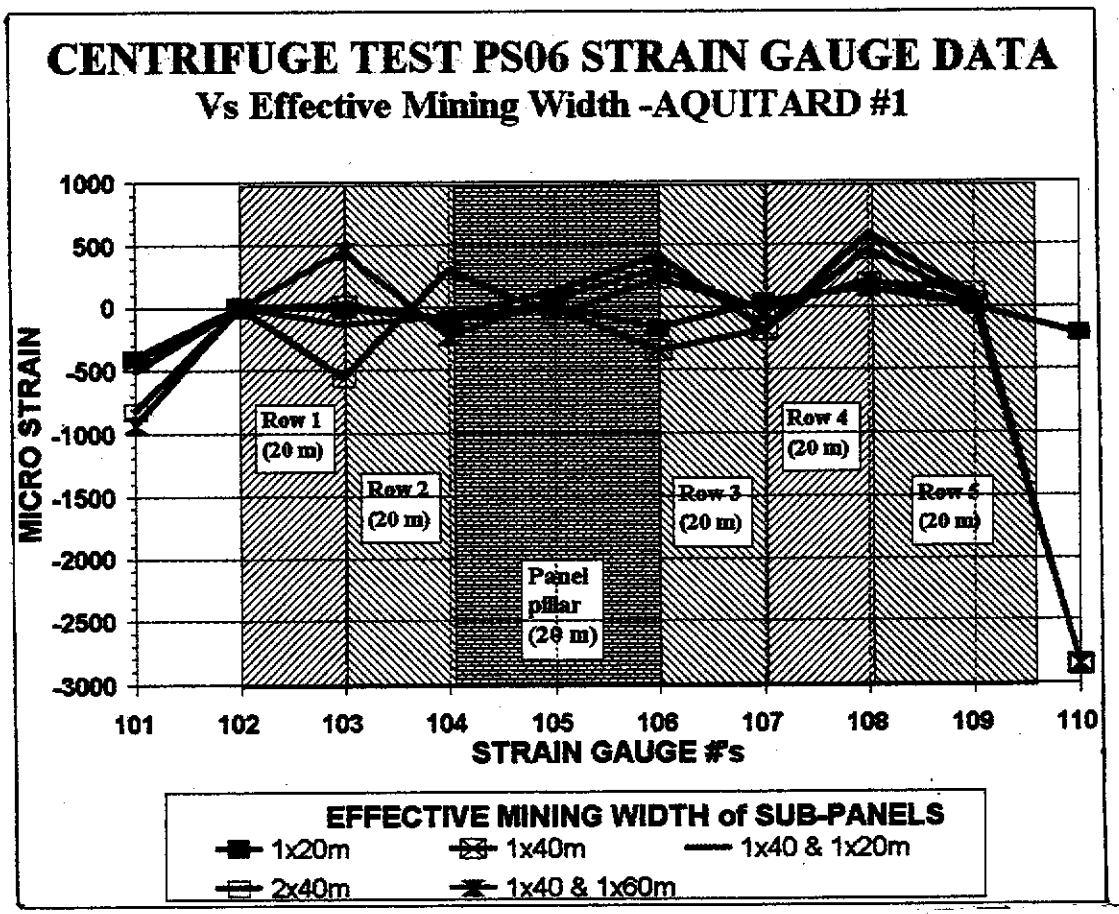

Figure 4.48 a

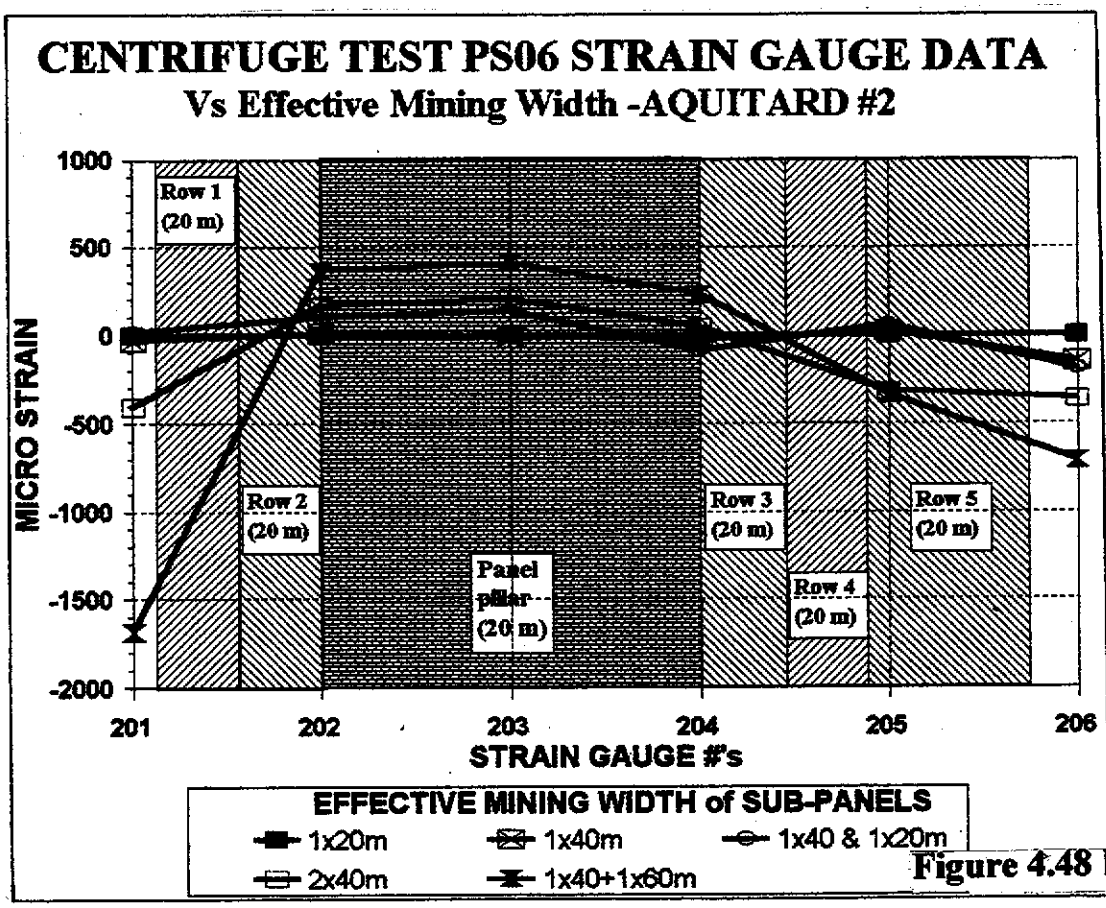

Figure 4.48 b

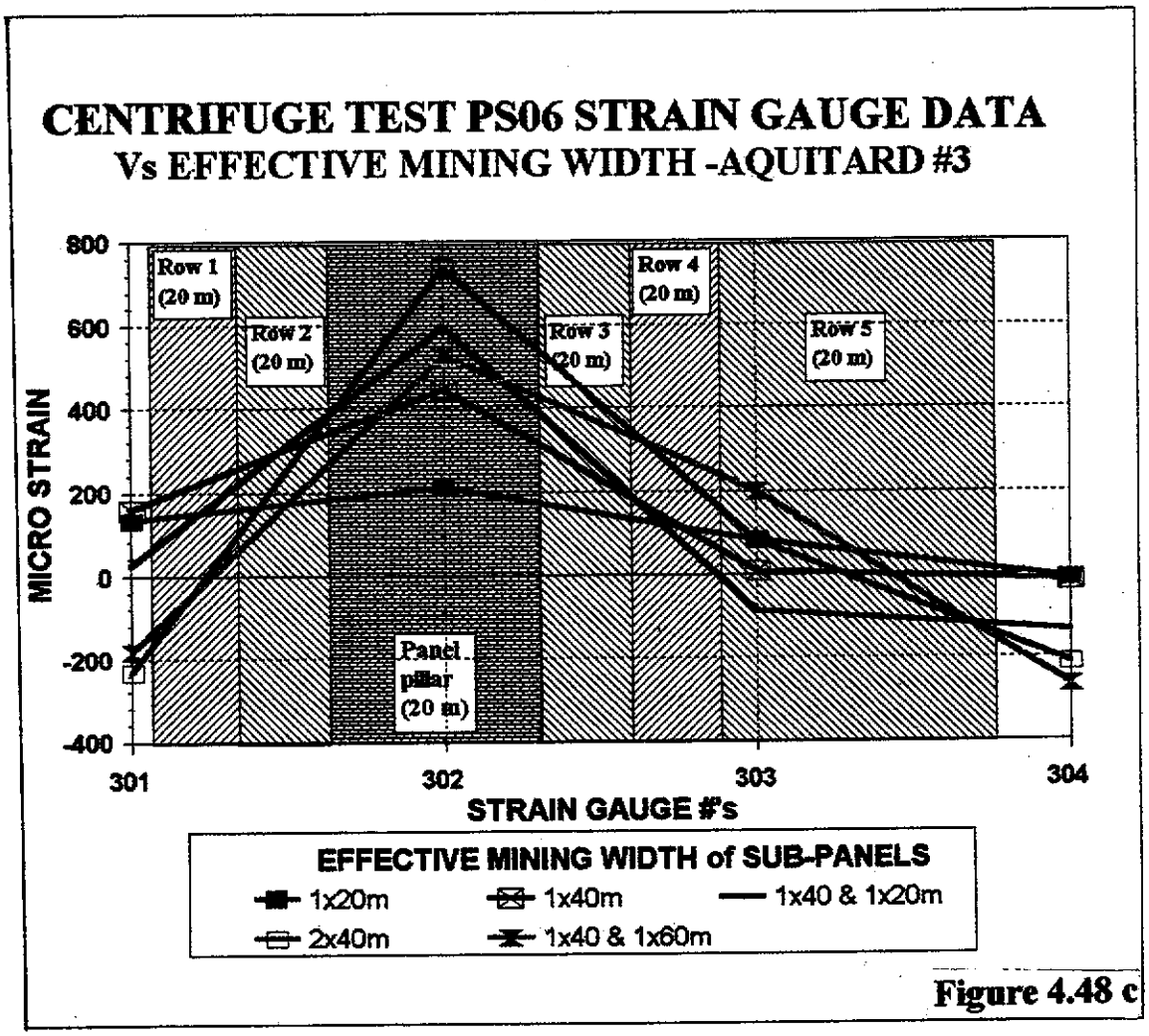

Figure 4.48 c

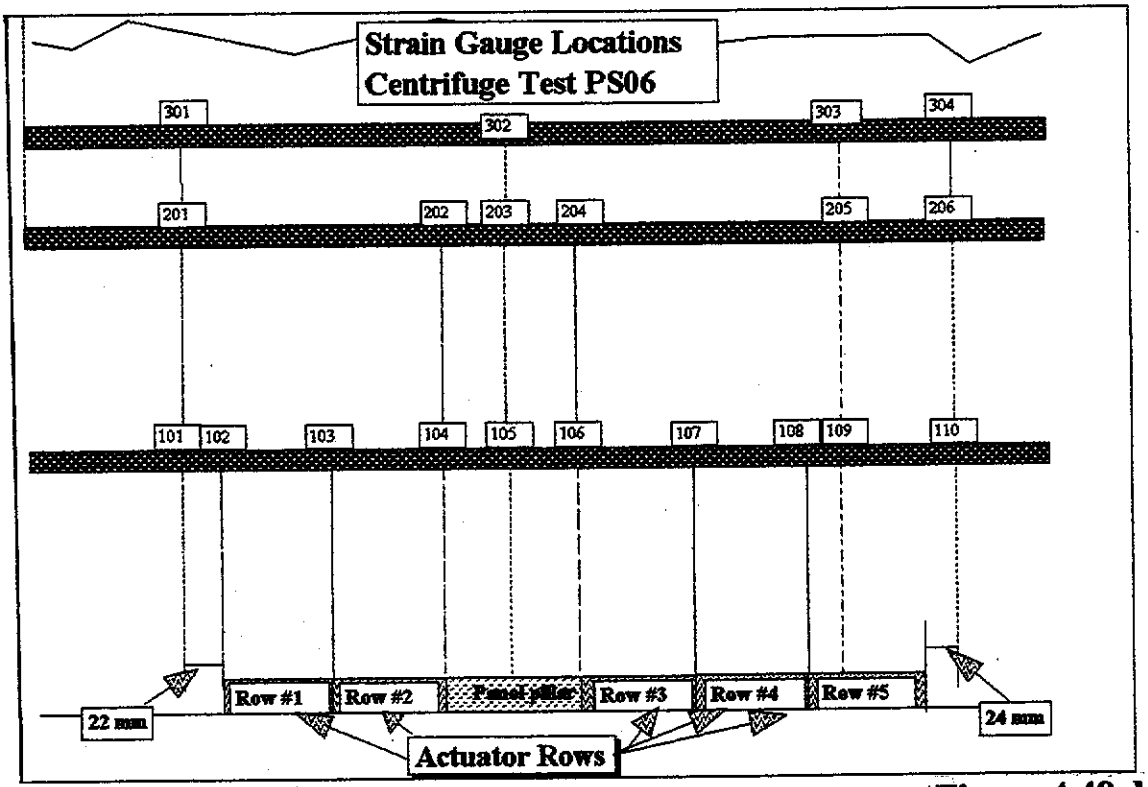

Figure 4.48 d

4.2.2.9 Centrifuge Test PS07

Objective - To assess the effect of greater heights and widths of extraction, and the inclusion of an additional aquitard on subsidence development of panel/pillar extraction systems.

Comments - Because of the problems with the rupture of the hydraulic piston feeder tubes connected to the pistons in the previous test, it was decided that the "pillar" pistons should remain fully lowered with "spacers" fixed on top each piston to represent the scaled height of intra-panel pillars.

The effective "mining height" in this model, and all remaining models was increased to to 4.2 m, which approximates the maximum thickness of the Wyvern seam in the WCL mine leases. This inceased mining height was achieved by increasing the throw of the piston top caps to 14.2 mm.

It was also decided to strain gauge the actuator pistons so that load redistributions could be measured during testing. Of particular interest was the load transfer onto the intra-panel pillars, and advancing mine edge. It was thought that although the bulking characteristics of the model were poor, the expected higher redistributions of load could be used for conservative pillar design etc.

It was devised that the most appropriate method to measure loads was to use strain-gauging techniques on the individual hydraulic pistons, where load is calculated according to the elastic modulus of the piston and the measured strain by the following relationships:

$$\sigma = \frac{F}{A}, \text{ and} \qquad 4.2(13)$$

$$\sigma = E.\epsilon. \qquad 2.5(16)$$

where: σ = vertical pressure (MPa), E = elastic modulus (MPa),
A = cross-sectional area of piston (m), and ϵ = measured strain.

The construction and design details of the load cells are given in Appendix IV.12. Figures 4.49 and 4.50 portray the set-up of the load cells within the model and the calibration weights used to check the performance of the load cells during operation of the centrifuge.

LOAD CELL ARRANGEMENT FOR CENTRIFUGE TESTS PS07 - PS09
(TOP CAPS REMOVED)

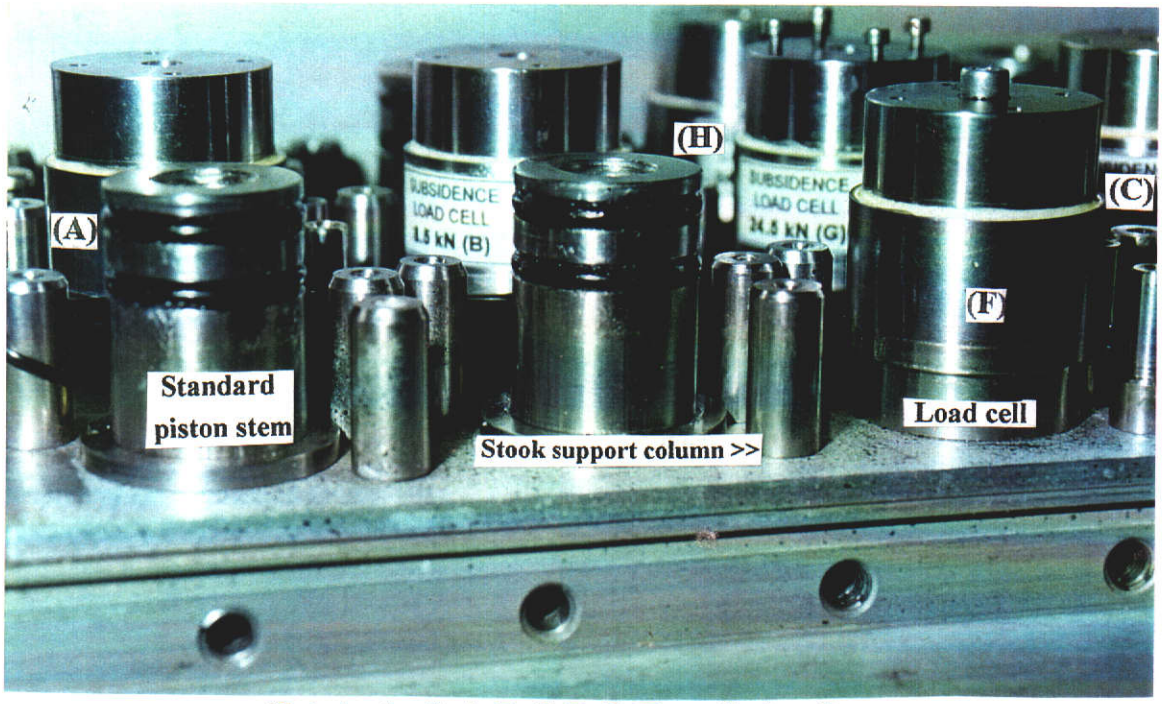

(Only load cells A, B, C, F, G, H are displayed)

Figure 4.49

LOAD CELL CALIBRATION WEIGHTS

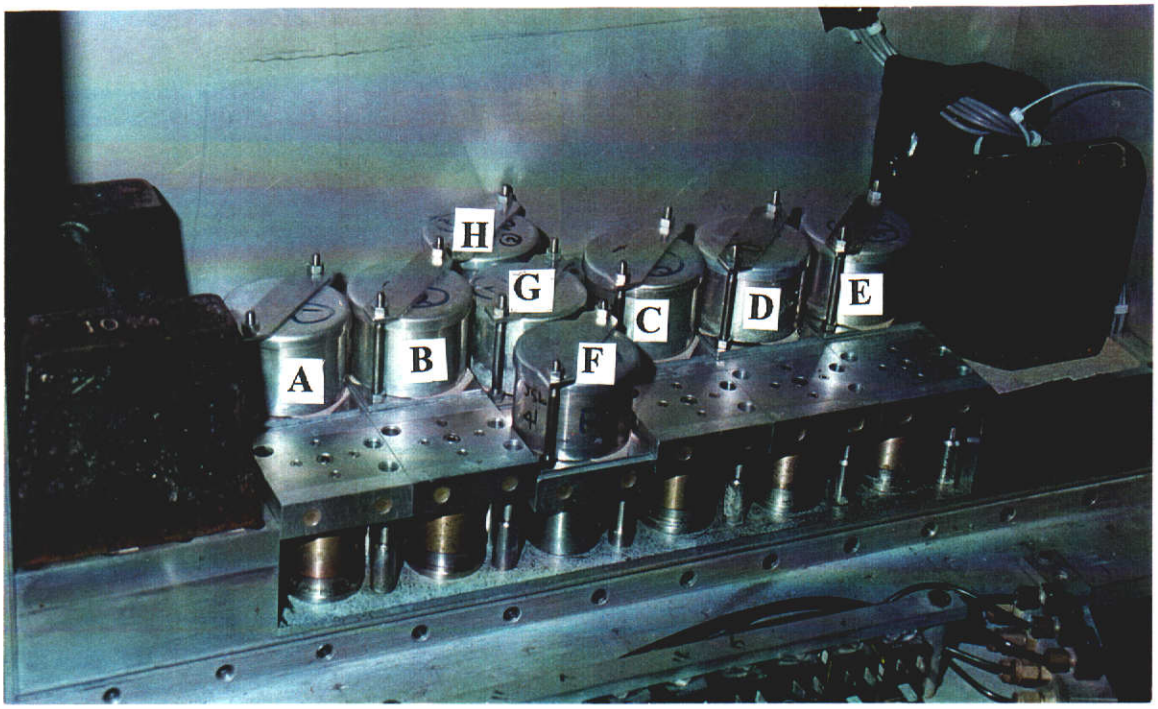

Calibration weights clamped at corresponding load cell positions.

Figure 4.50

This test (PS07) and those remaining were constructed to include equivalent materials that represented the semi-lithified silts and shales associated with aquitards and mine roof. The inclusion of these layers was considered to be important for the proposed modelling of water-filled aquifers, planned for the next centrifuge test (PS08). It was thought that if water was applied to the sand layer in direct contact with the porous aquifer material the effective strength of the stiff aquitard layers would be softened. Consequently, these less porous layers (representing the prototype roof material above coal seams) were introduced to minimise the impact of pressurised "groundwater. Again, the model make up is described in greater detail in Appendix IV.8. It was also thought that the main cause for the abnormally high extension of primary caving in tests PS04 and PS05 was the fact that the immediate roof consisted of scaled, extremely weak, aquifer material which is more prone to collapse.

After the test was completed, an error in the location of the aquifer 4 aquitard - the Upsilon seam - was noted. This incorrect placement resulted from a typographical error (from the author) which positioned the Upsilon seam at the Orion seam level. (The Orion seam, located approximately mid-point in aquifer 4, is not a recognised aquitard - Hebblewhite and Humphreys, 1988). It was decided to repeat the modified stratigraphy in the next two tests so that parametric studies (into the effect of water in the aquifers and a narrower intra-panel pillar) could be assessed appropriately.

Conclusions - The general set-up of the model both before and after testing is illustrated in Figures 4.51 a and b. A summary of the more interesting conclusions made from the results of PS07 are given below:

- An unsupported span of aquitard material material (with an open void below) developed after extraction of the first sub-panel. Before any additional mining, this span cracked in tension at the bottom edge of the aquitard (Figure 4.52). In fact, the yielding strains on aquitard #1 were exceeded after the second row of pistons was lowered in both sub-panels. The strain values noted during this test were at least twice those measured in the comparative test PS06 which had approximately half the mining height of test PS07.
- The timing of the tensile fracture of the Alpha seam aquitard also coincided with a crushing of the underlying wedge of caving overhang (Figure 4.52). It is interpreted that this overhang was acting as a form of support to the aquitard (in similar fashion to model PS02) prior to it being crushed. It has also been interpreted that the combination of increased loading and the ultimate length of the aquitard beam (increased by some failure of the triangular overhang) exceeded the flexural strength of the aquitard, thus causing it to yield in tension.

PRE-TEST PHOTOGRAPH OF CENTRIFUGE MODEL PS07

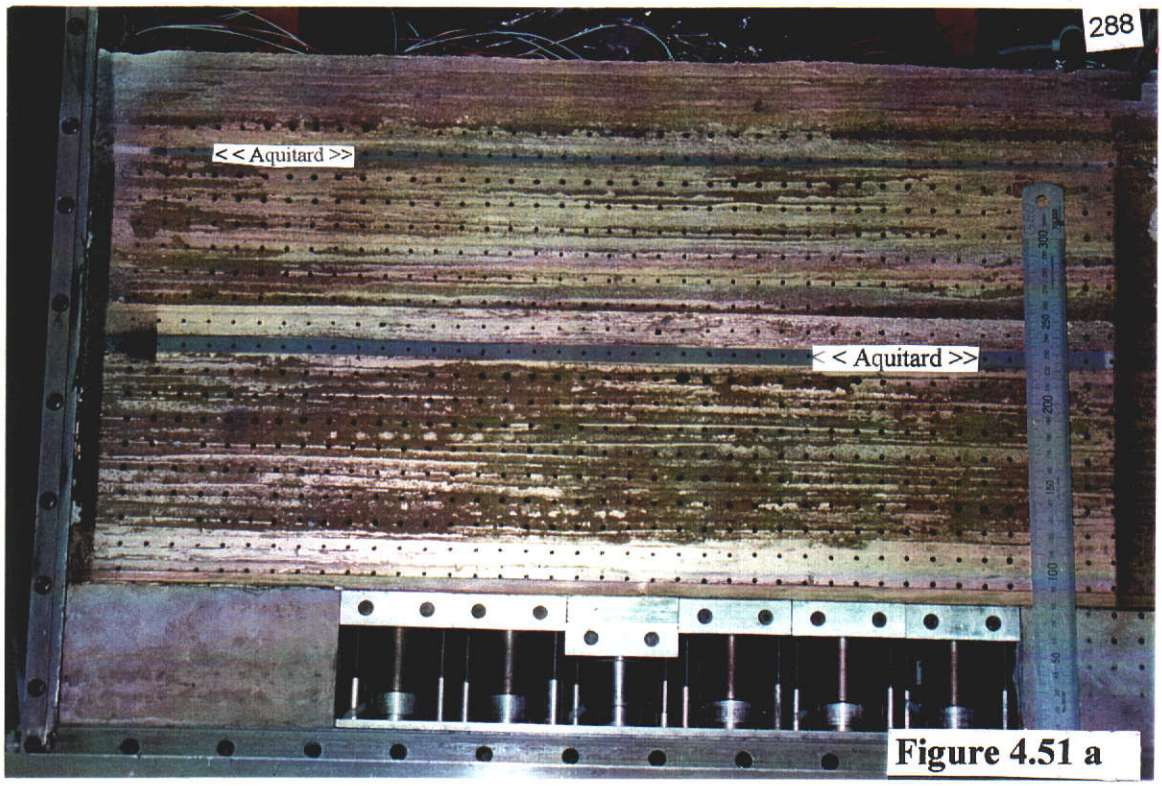

Figure 4.51 a

POST-TEST PHOTOGRAPH OF CENTRIFUGE MODEL PS07

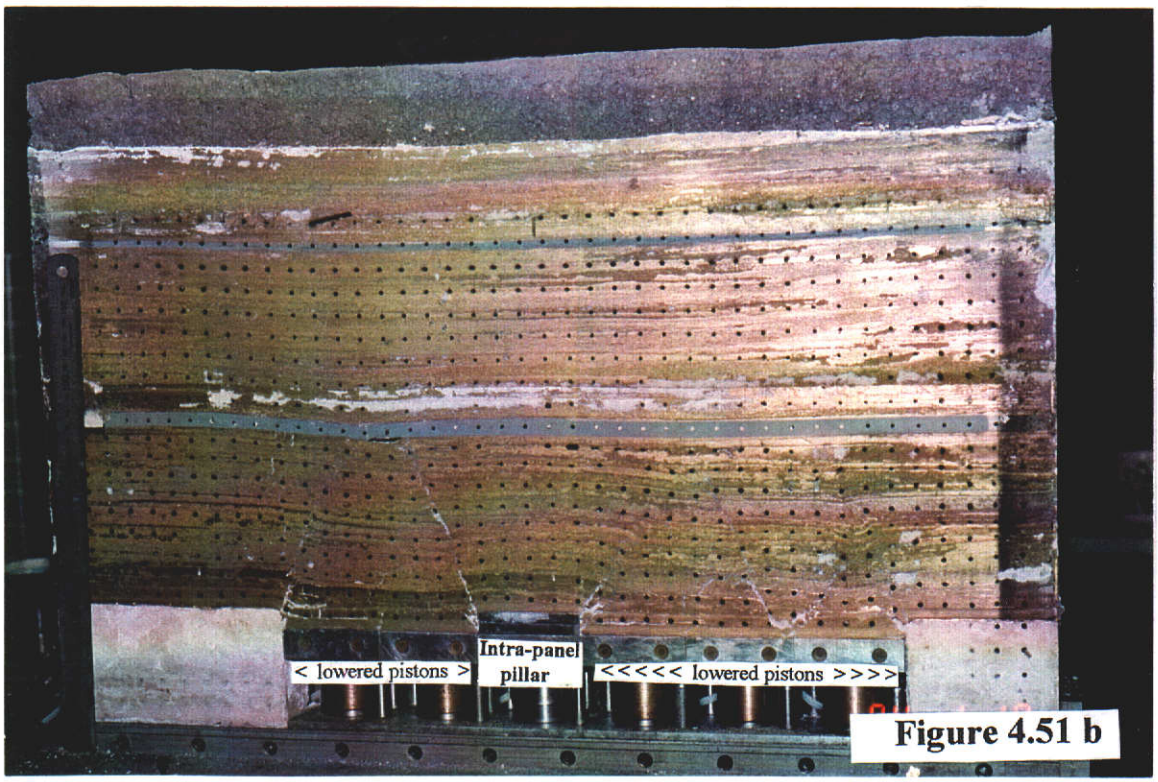

Figure 4.51 b

ILLUSTRATION OF CRUSHED OVERHANG BELOW THE FIRST AQUITARD - CENTRUFUGE MODEL PS07

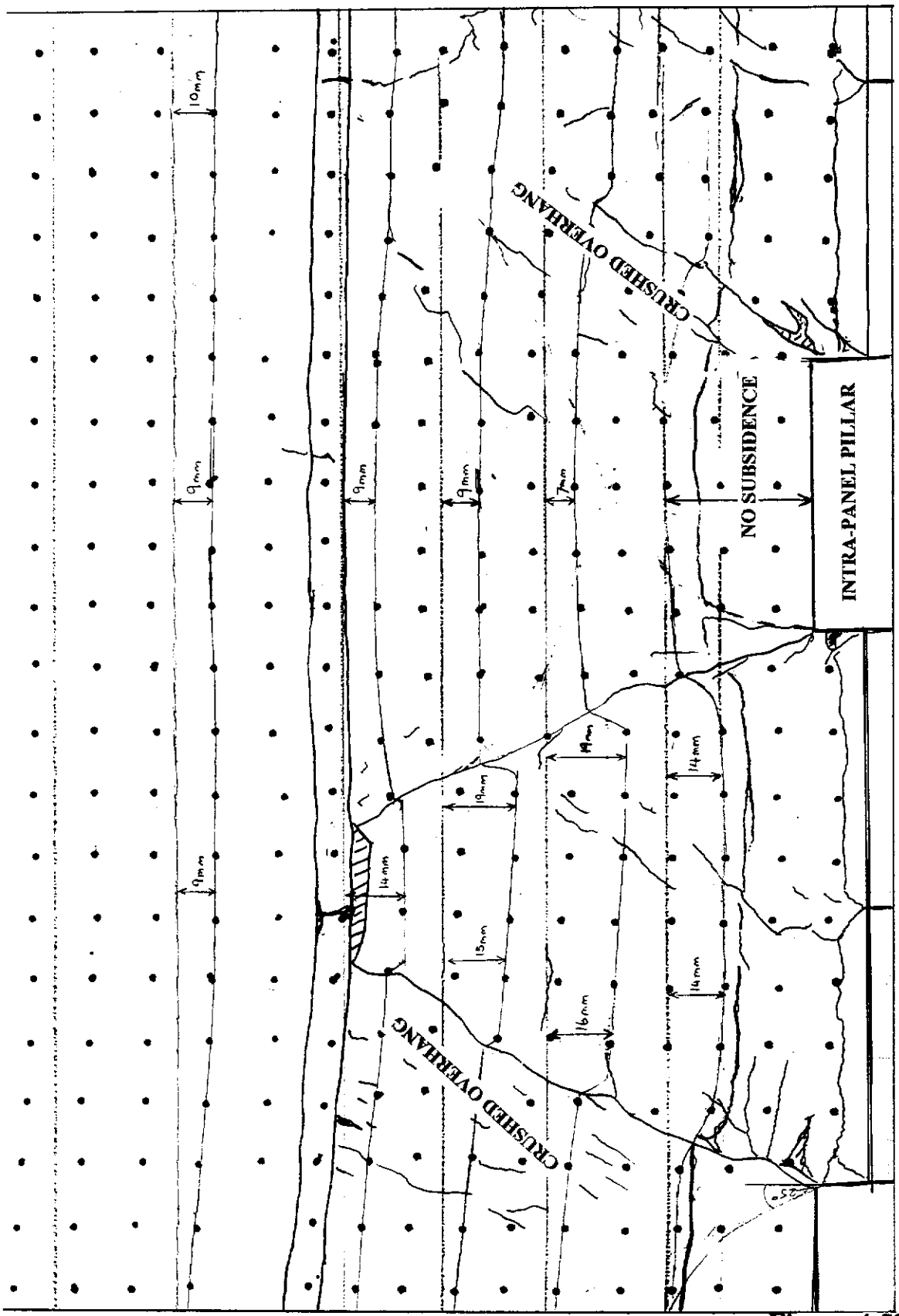

Figure 4.52

The effect of the triangular caving overhang is discussed in greater detail in Section 5.1, where finite element analysis was used to assess the impact of an elastic, triangular-shaped overhang on subsidence of an aquitard beam. This work, along with the practical demonstration in the centrifuge model, probably accounts for the problems previous researchers have had with using beam theory to explain the subsidence process.

- Load cell data suggests that the integrity of the intra-panel pillar support system had been generally maintained. As illustrated diagrammatically by Figure 4.53, the average load taken by the intra-panel pillar load cells increased throughout the test with the exception of the slightly reduced load measured when the second and fourth rows of pistons were lowered. It was expected that if the pillar system had completely failed, then the superincumbent load would drop back to pre-mining loads. It was considered possible that the reductions in load may have occurred as a result of either the tributary load being transferred onto the goaf in each sub-panel, or the crushing of the weaker strata above the pillar which spread the load more evenly throughout the model.

- Although the load cell data suggests that the pillar system has generally remained in tact, there was 9 mm subsidence measured in the weak aquifer material directly above the pillar (Figure 4.52) which suggests otherwise. This subsidence was initiated when two 40 m wide sub-panels had been "mined" on either side of the intra-panel pillar. This unexpected subsidence increased to approximately 60% mining height when three rows of pistons were lowered in the second sub-panel. The additional subsidence has been attributed to consolidation/crushing of the scaled weak interburden material above the immediate roof strata over the intra-panel pillar. This form of consolidation/crushing has been observed in the field above the panel abutment of the shallow 2SA panel. In this field case study the deepest anchor was measured (temporarily) to be 150 mm closer to the surface (than before mining) when the goaf edge was adjacent to the extensometer.

  It is considered possible that although the sandstone above the intra-panel pillar may have yielded, it did so in a controlled manner, with full confinement on both sides. This confinement may have allowed post-mining loading to be maintained on the pillar. (This assumption needs to be confirmed with further investigation.)

DIAGRAMMATICAL VIEW OF LOAD CELL VALUES CENTRIFUGE TEST PS07

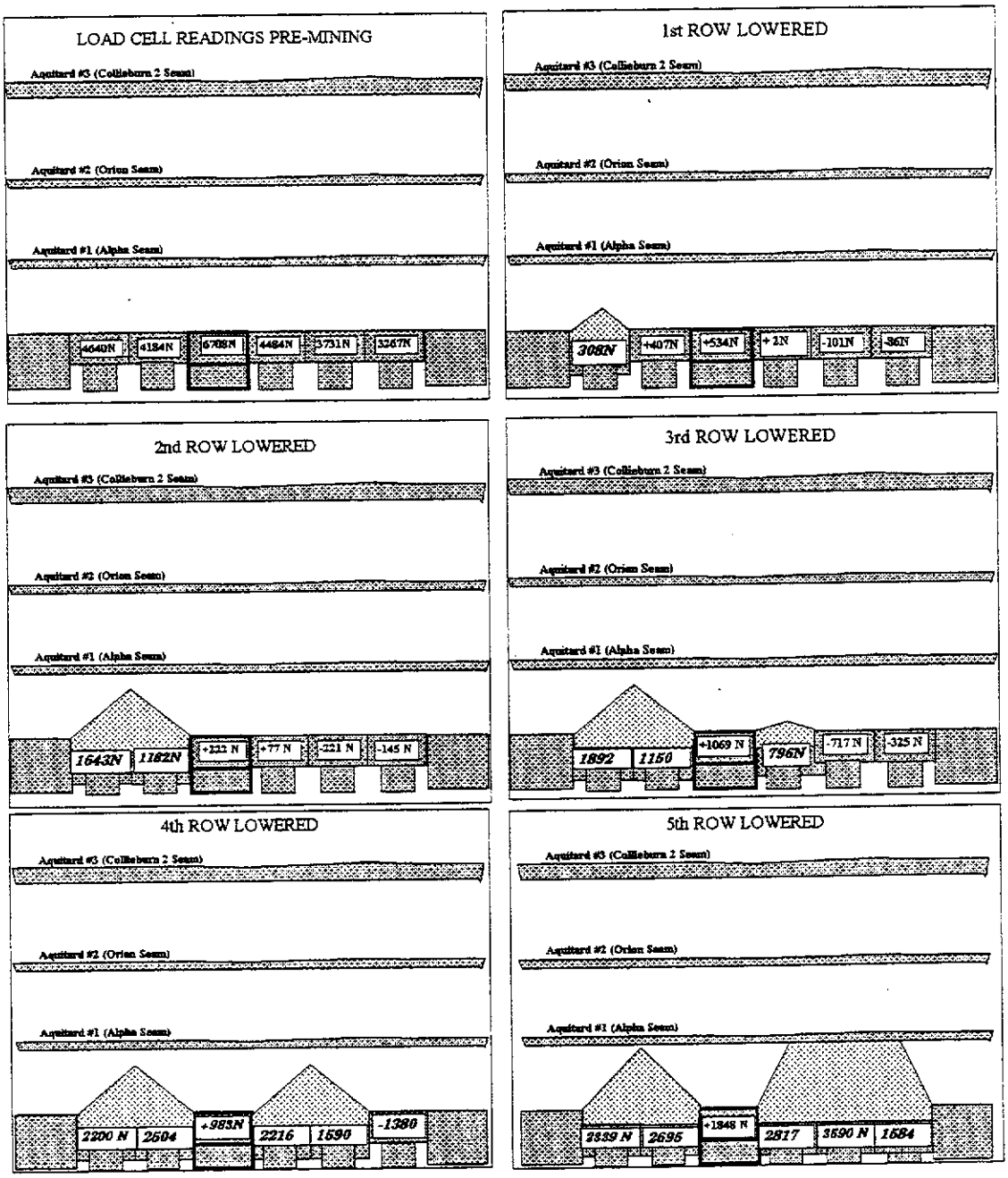

Note :- Loads are given as : a) total loads for lowered actuators, and
b) load variance from pre-mining loads
for unlowered actuators

Figure 4.53

This consolidation/crushing phenomenon was not observed in the (later) NWB3 panel field trial, and, assuming similitude has been maintained, could be attributed to one or a combination of the greater mining height, the lack of bulking of goaf material, the lower scaled strength of the already weak sandstone.

It was evident that more detailed investigation was required if the precise mechanisms of subsidence developement and load transfer above intra-panel pillars were to be better understood.

- Maximum subsidence measured above sub-panel one, the intra-panel pillar, and sub-panel two are 9 mm, 9 mm and 10 mm respectively. In terms of mining height, these deflections represent 63%, 63% and 70% of the maximum possible movement. It is interesting to note that the 67 mm wide pillar represents 19% of cover depth. A similar reduction in maximum subsidence resulted above pillar widths of approximately 10% cover depth in the field (e.g. above the ACIRL panel chain pillars).

  This additional subsidence above the PS07 model pillars appears to have reduced the subsidence effects on aquitards 2 and 3 compared to PS06 (according to strain gauge data - see Figures 4.54 a to d). This would be expected, as the resultant subsidence trough is flatter across the length of the model.

- Load cell measurements also suggest that the tributary loading angle with 40 m goaf on either side of the intra-panel pillars is 5° (see Appendix IV.7) and not the 23° assumed by the shearing angle measured in the field and the *in situ* material centrifuge tests. This steeper angle of loading could be explained by a combination or any of the following; the tributary loading changing once any crushing occurs at the abutments, frictional self-support at the junction of the opposing two masses of triangular overhang at the goaf edge, or the lower material strength and potentially poorly distributed binder in the model's weak sandstone.

- It is suggested from the load of only 307 N on the "mobile" load cell A (equating to a vertical weight less than the weight of the top-cap) immediately after it had been lowered that frictional resistance between top-caps can reduce the effective load measured by the load cells. It is also possible that this could also be contributing to the lower than expected tributary loading angles given above.

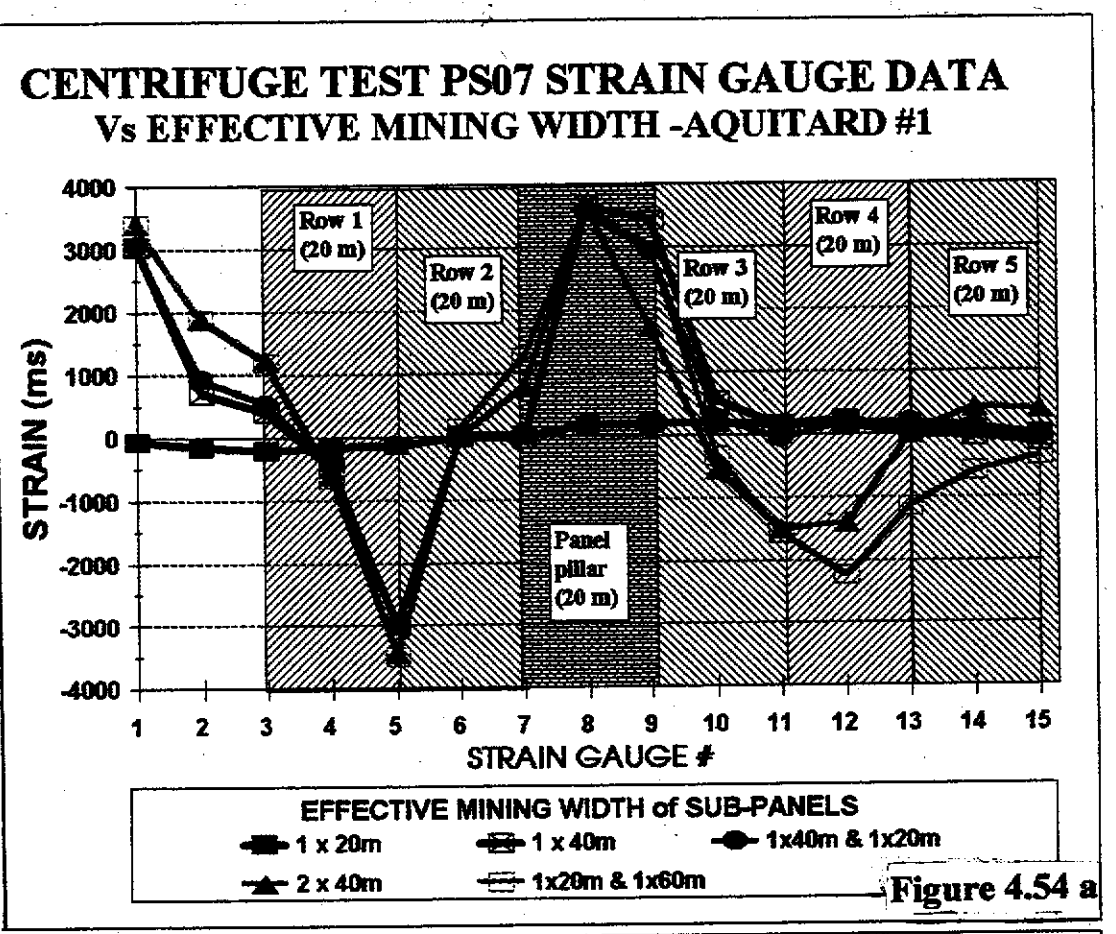

Figure 4.54 a

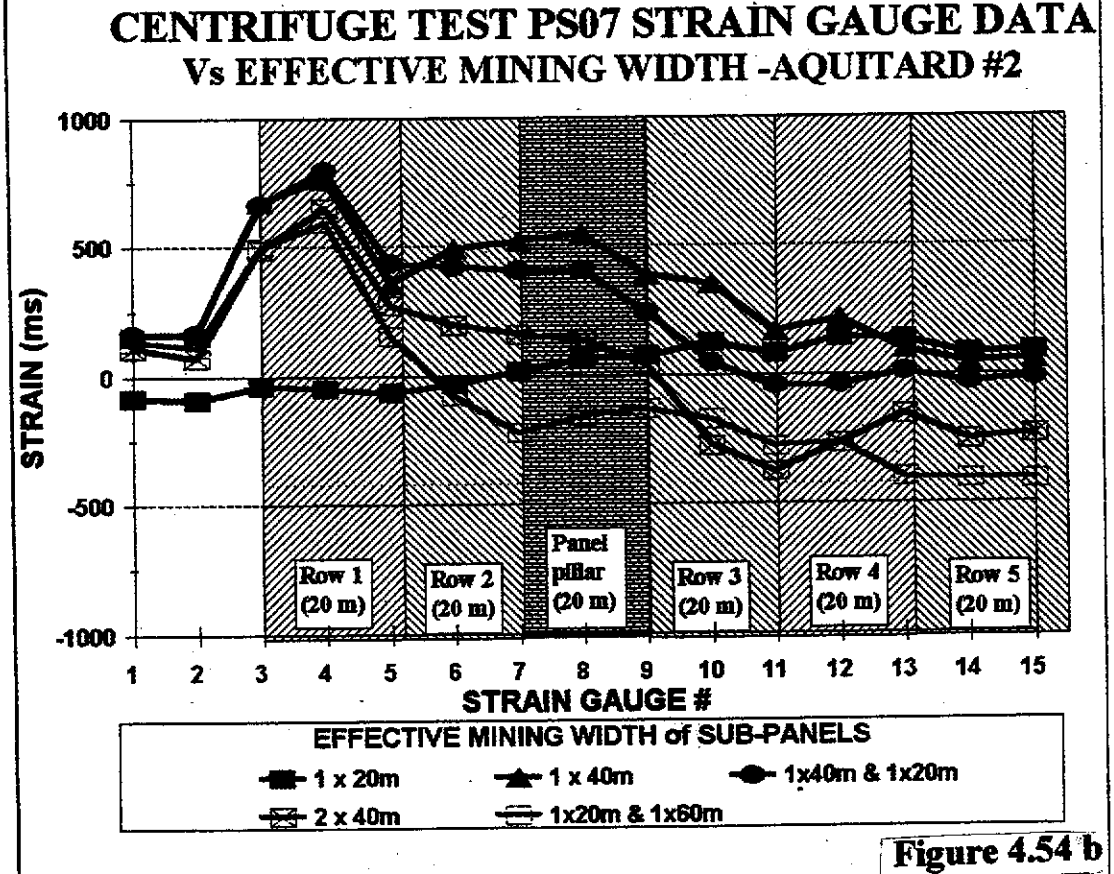

Figure 4.54 b

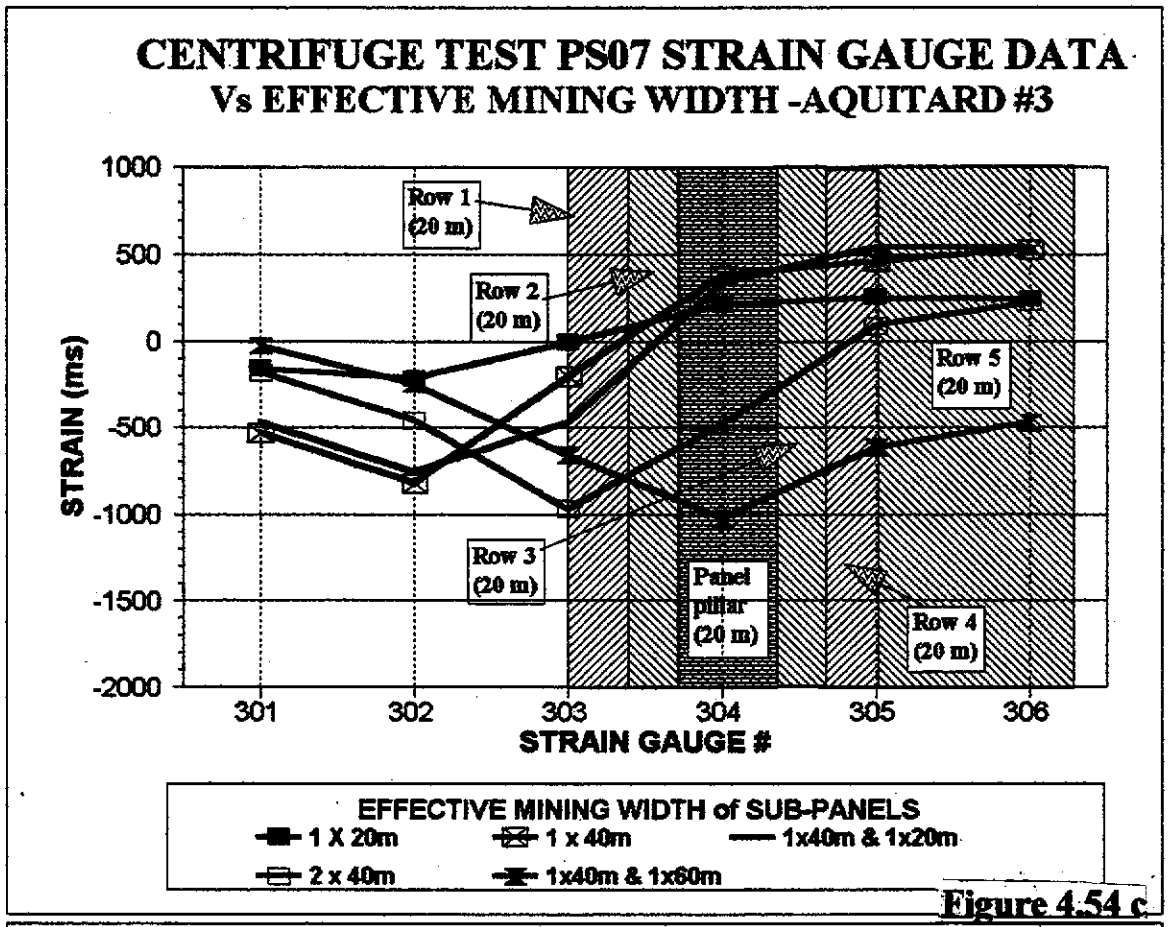

Figure 4.54 c

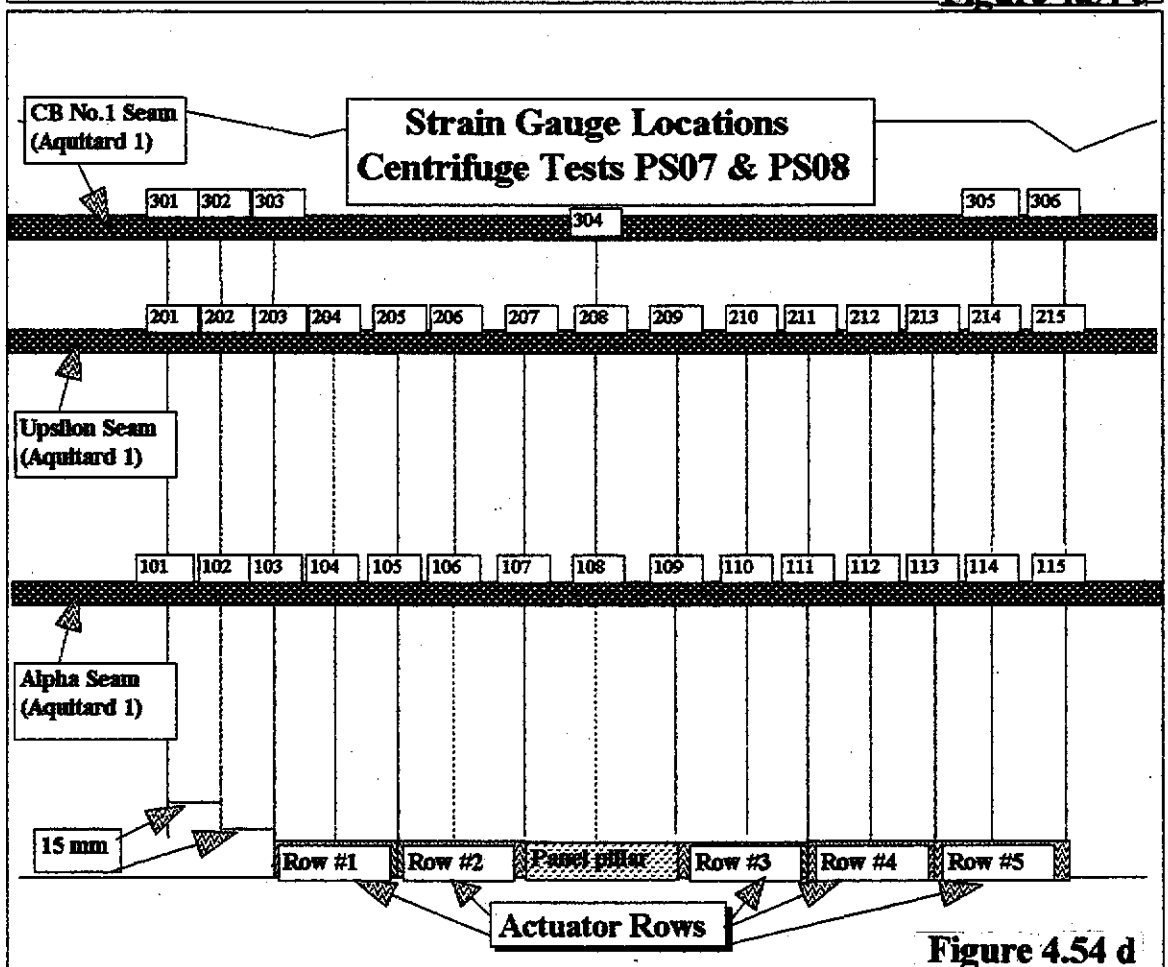

Figure 4.54 d

- The middle three intra-panel load cells noted 13% additional load than expected prior to "mining". It is possible that because the intra-panel pillars were stiffer than the adjacent "mining" actuators they accepted more load.
- The weak aquifer sandstone in this model has undergone some consolidation during spin-up, in similar fashion to the loose overburden (though at a far smaller amount). The effect of this phenomenon on the model's performance is not known, however, if the overall strength of the weak sandstone has been reduced by this consolidation, it could have an impact on the shearing of the sandstone and the consequent angle of tributary loading. The rate of consolidation was later defined to be approximately 0.03 mm per millimetre of weak sandstone aquifer material.
- There appears to be less load transferred to the load cells nearer the advancing edge, indicating that the leading load cells are within a slight stress shadow. For example the middle load cell in the second sub-panel (load cell D) had more tributary load redistributed onto it (3590 N) than the load cell at the edge of the panel (1584 N - cell E) after all pistons were lowered - see Figure 4.53.

  This would be expected as this middle load cell is further away from the supporting abutments on either side of the panel and suggests that the tributary load is now being transferred through the goaf. This stress-shadow observation would also be expected in the field, at the leading/advancing panel edges, where the shallower-dipping subsidence profiles (see Figure 3.5) are observed.

Summarising the performance of the load cells, it was apparent that the measured sequences of load transfer offered the opportunity for greater understanding of the behaviour of the models and warranted further investigation. Consequently, the two additional tests (PS08 and PS09) were completed with load cell measurements as planned.

4.2.2.10 Centrifuge Test PS08

Objective - To evaluate the effect of water pressure in weak sandstone aquifers on the subsidence processes of the Collie Basin sediments.

Comments - Water was introduced into the model via external stand-pipes (see Figure 4.55) which were mechanically anchored to the sides of the centrifuge strong-box and individually connected to each loose sand layer within the model. The adding of water was delayed to immediately prior to the test spin-up to minimise the effect of any water seepage either prior to or during the test. (It was noted during cutting of large moulded blocks of equivalent material for PS04 that water absorption delaminated some layers, and greatly reduced the material strength).

The intention was that the column of water, being isolated within the sand aquifer (which was enclosed in neoprene rubber - Figure 4.56), would apply pressure to the model according to the head of water and the accelerated gravity force (200 g). The height of the columns of water applied to each sand layer in the model (150 mm) were scaled to represent 30 m of head in the prototype (which relates to the typical groundwater levels within aquifers 3 and 4 in the NWB3 panel area).

Conclusions - This test has been regarded as a failure as it did not achieve any of its objectives. Two major problems were encountered.

Firstly the sealing methods used in an attempt to keep the water isolated within the loose sand beds (as mentioned above) did not work adequately under 200 g, allowing water to leak into the body of the model during the early spin-up stages. This leakage resulted in a softening of the equivalent material, which could no longer be used for comparison with PS07. Moisture contents measured in the aquifer equivalent material reached 13% compared to 2 - 4% in the previous models.

Secondly, the first piston in sub-panel #1 did not lower fully. This greatly affected the caving process above the panel.

Comparison of the PS08 test with PS07 results is therefore not meaningful.

STAND-PIPE CONFIGURATION
CENTRIFUGE MODEL PS08

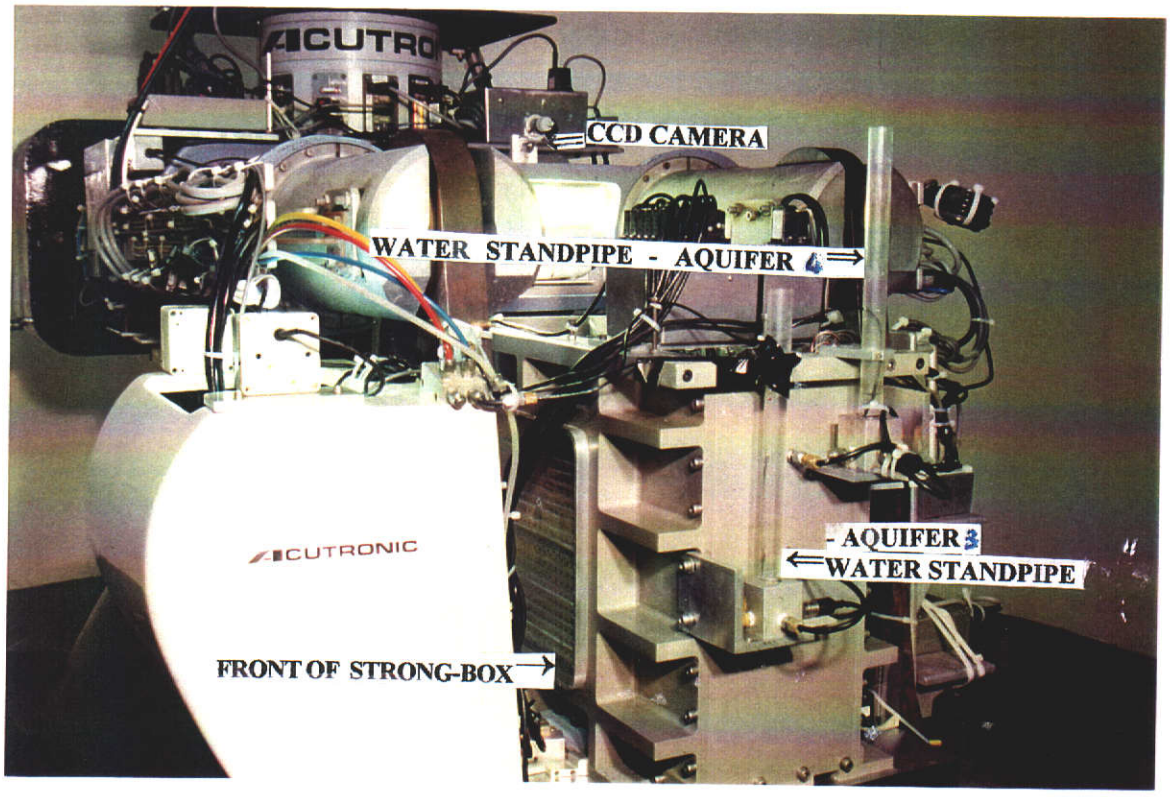

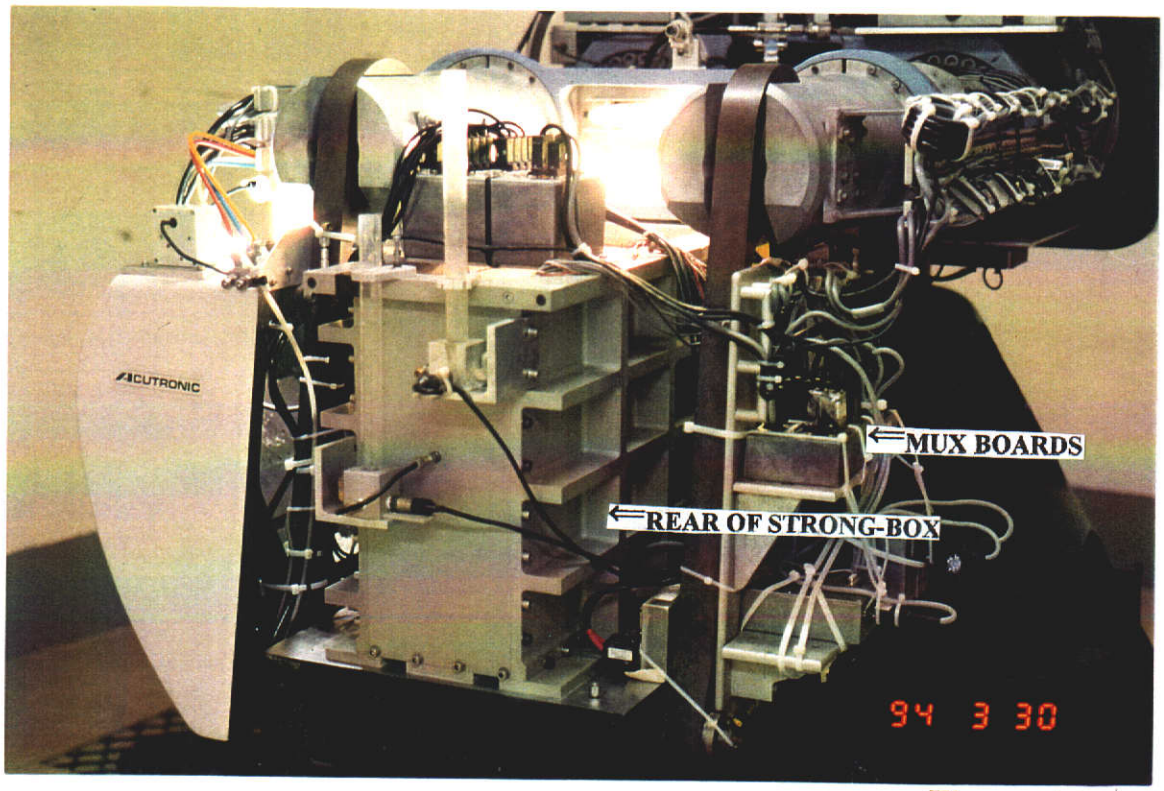

Figure 4.55

WATER FILLED AQUIFER CONSTRUCTION CENTRIFUGE MODEL PS08

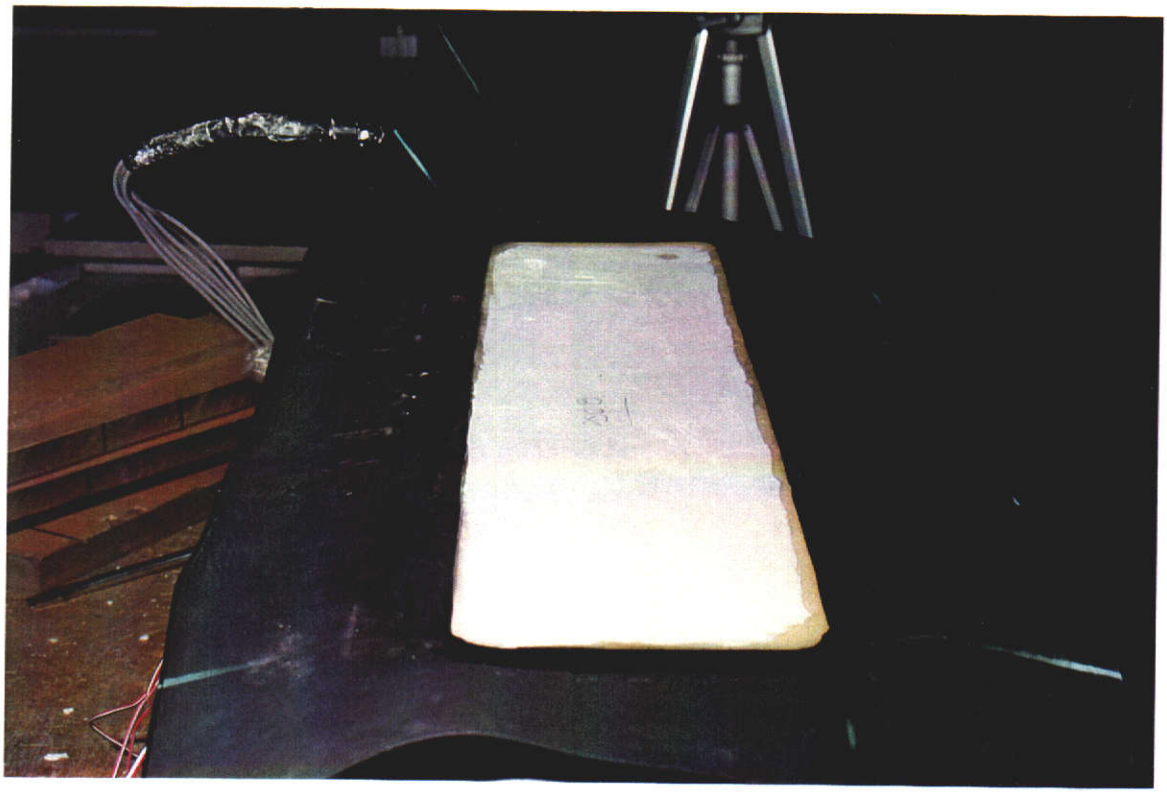

a) Neoprene Rubber Gasket Cut to Shape

Figure 4.56

b) Isolated Aquifer after Dismantling

4.2.2.11 Centrifuge Test PS09

Objective - To evaluate the potential for collapse of the pillar support system above narrower intra-panel pillars.

Comments - At the time of the design of the trial panel/pillar extraction panel (NWB3 panel), the author held concern for the potential of the weak sandstone column above the coal pillar to rupture due to excessive tributary loading. However, conflicting opinion by geomechanical experts in the eastern Australian coalfields (personal communication) suggested that this phenomenon was not realistic due to the expected confining pressures provided by the goaf (which would significantly increase the shear strength of the sandstone). If such a collapse did occur, the resultant subsidence would most likely exceed the subsidence tolerance limits of the overlying aquifers - as per test PS06 - and could thereby flood the mine workings. On the other hand, if this type of collapse was not feasible, it was possible that the design widths of intra-panel coal pillars could be reduced to make better use of the finite coal reserves.

The lack of bulking in the model was seen as being conservative to the cause, as a fully compacted model goaf in the immediate vicinity of the excavation plane would provide better constraint to the uncaved sandstone column formed above the intra-panel pillar.

Every attempt was made to construct PS09 the same as PS07. The only variation designed into the model was a reduction in width of the top caps representing intra-panel pillars. The reduction (from 65 to 45 mm) represents an intra-panel pillar width of 13 m in the prototype.

Observations - Figures 4.57 a and b illustrate the general appearance of the model before and after testing. A detailed list of observations made from this test is provided in Appendix IV.9. A summary of the main observations is provided in note form below:

- It is possible that the weak column of sandstone developed by vacing on either side of the intra-panel coal pillars can collapse catastrophically. Within seconds of lowering the first row of pistons in the second sub-panel, the sandstone above the aluminium spacers (representing the coal pillars) collapsed. This collapse eventually resulted in a maximum surface subsidence of approximately 12 mm, which represents 85% of the mining height.

PRE-TEST PHOTOGRAPH OF CENTRIFUGE MODEL PS09

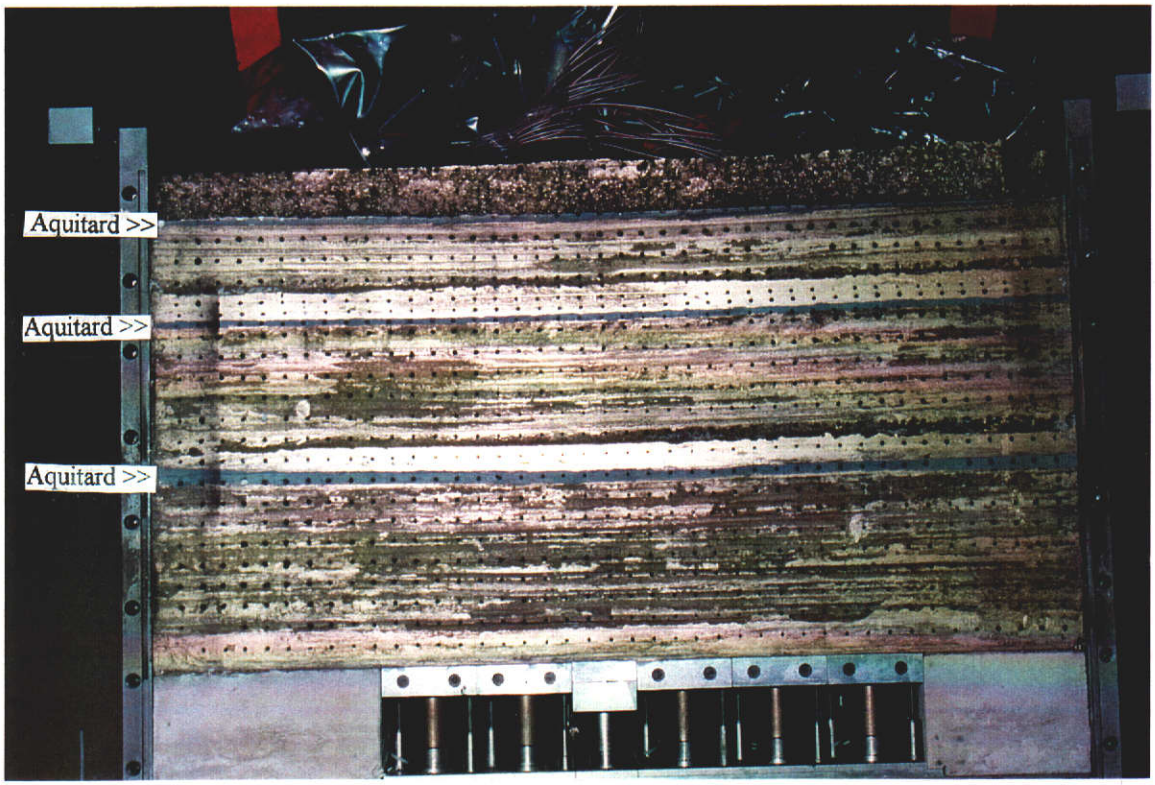

Figure 4.57 a

POST-TEST PHOTOGRAPH OF CENTRIFUGE MODEL PS09

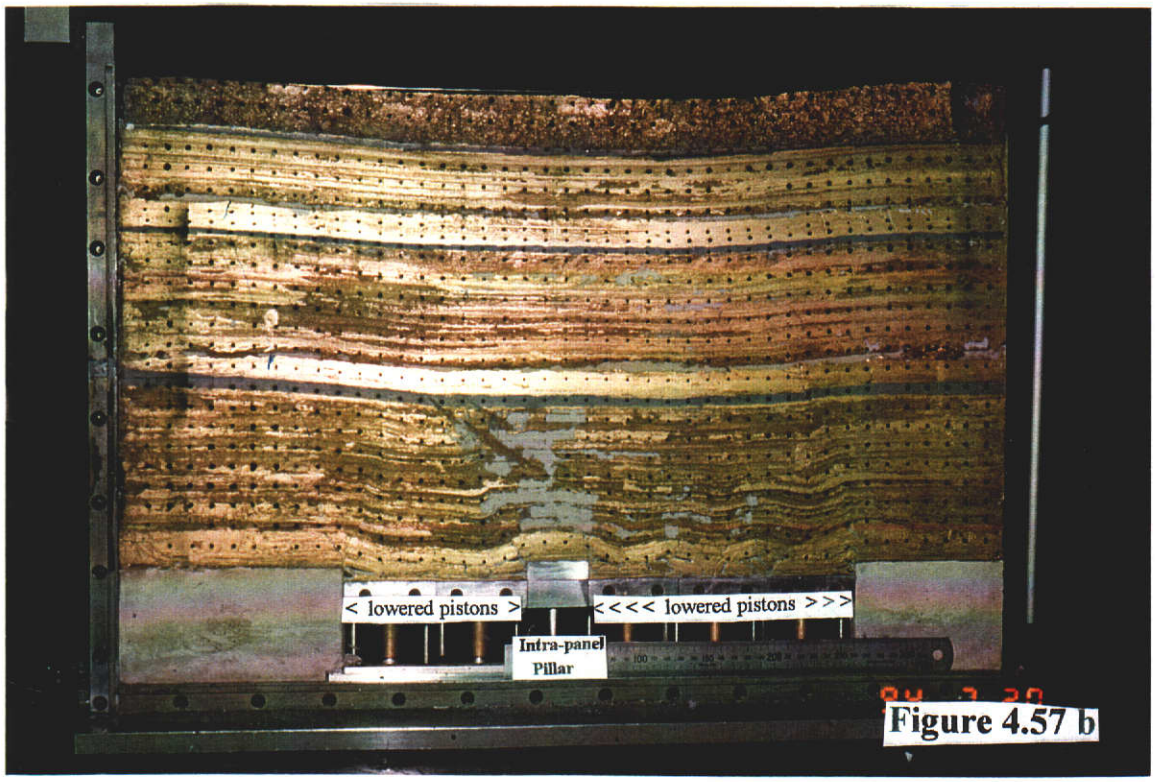

Figure 4.57 b

This compares with the PS07 subsidence where only 9 mm convergence was measured above the intra-panel pillars. The subsidence developed above the pillar is portrayed by Figure 4.58 as displacement vectors. This Figure illustrates that the major line of shear was oriented toward the RHS of the intra-panel pillar, or the side of least confinement.

- The ramification of this additional subsidence is the likely rupturing of the protective aquitards and greater potential for damage to surface features.
- The collapse of the superincumbent sandstone column above the intra-panel pillar produced a flatter subsidence profile. This is supported by the lower aquitard tensile strains measured above the intra-panel pillar in this test (see Figure 4.59 a to d) compared to PS07.
- Given the different ground mass response to mining in this test, the load cell results still trended similarly to PS07 (Figure 4.60). This suggests that reasonable degree of repeatability can be achieved with equivalent materials in centrifuge tests. However, conflicting evidence was noted by the different manner of caving above sub-panel #1 in the two tests, with PS07 developing a wide cavity beneath aquifer #1 and PS09 not doing so.
- In similar fashion to test PS07, the triangular overhang above the caved zone has crushed under the elevated redistributed loads - see Figure 4.61.
- The tributary loading angle has again been calculated to be in the order of 6° - see Appendix IV.9.
- Evidence suggests that near the edge of the panel and within close proximity to the ground surface, there is some dilation of loose sand. The maximum dilation measured in the model was 2 mm which represents 0.6 m dilation in the field prototype. This form of dilation, once developed does not appear to reconsolidate at any stage during testing. Although this near-surface dilation is evident in the field (e.g. the 150 mm separation between the shallowest anchors in 1North panel extensometer D212 - see Figure 3.54), the magnitudes of dilation in the model are well in excess of field measurements. It is possible that the greater dilation noted in the model surface was due to the 20% reduction in gravity loading at the model surface for 350 mm deep models (as discussed in Section 2.6.5.1).

DISPLACEMENT ABOVE THE INTRA-PANEL PILLAR - CENTRIFUGE MODEL PS09

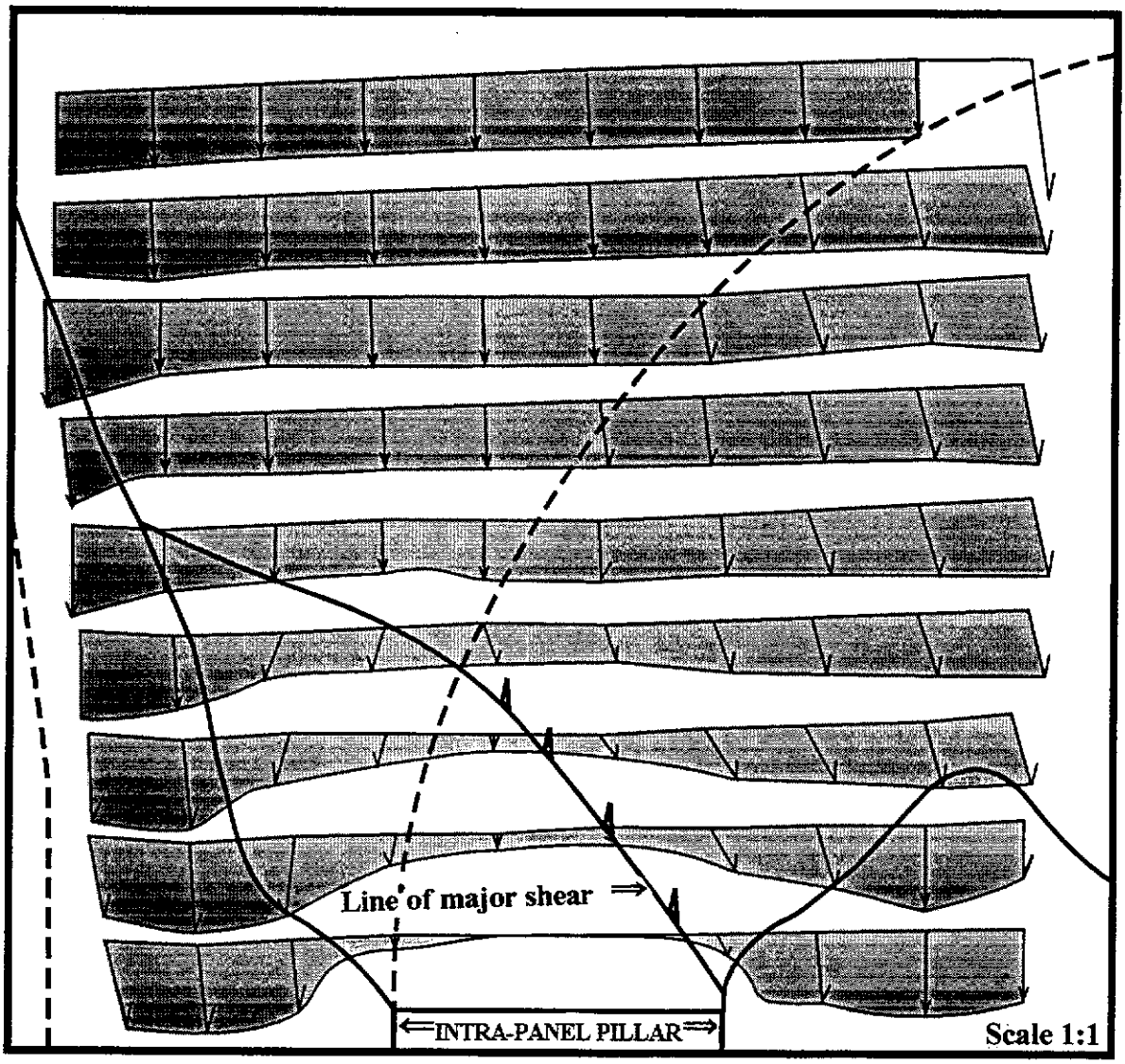

Note that the displacement vectors are divided into zones of directional movement

vertical movement - ↓ movement to the left - ↙ movement to the right - ↘

Figure 4.58

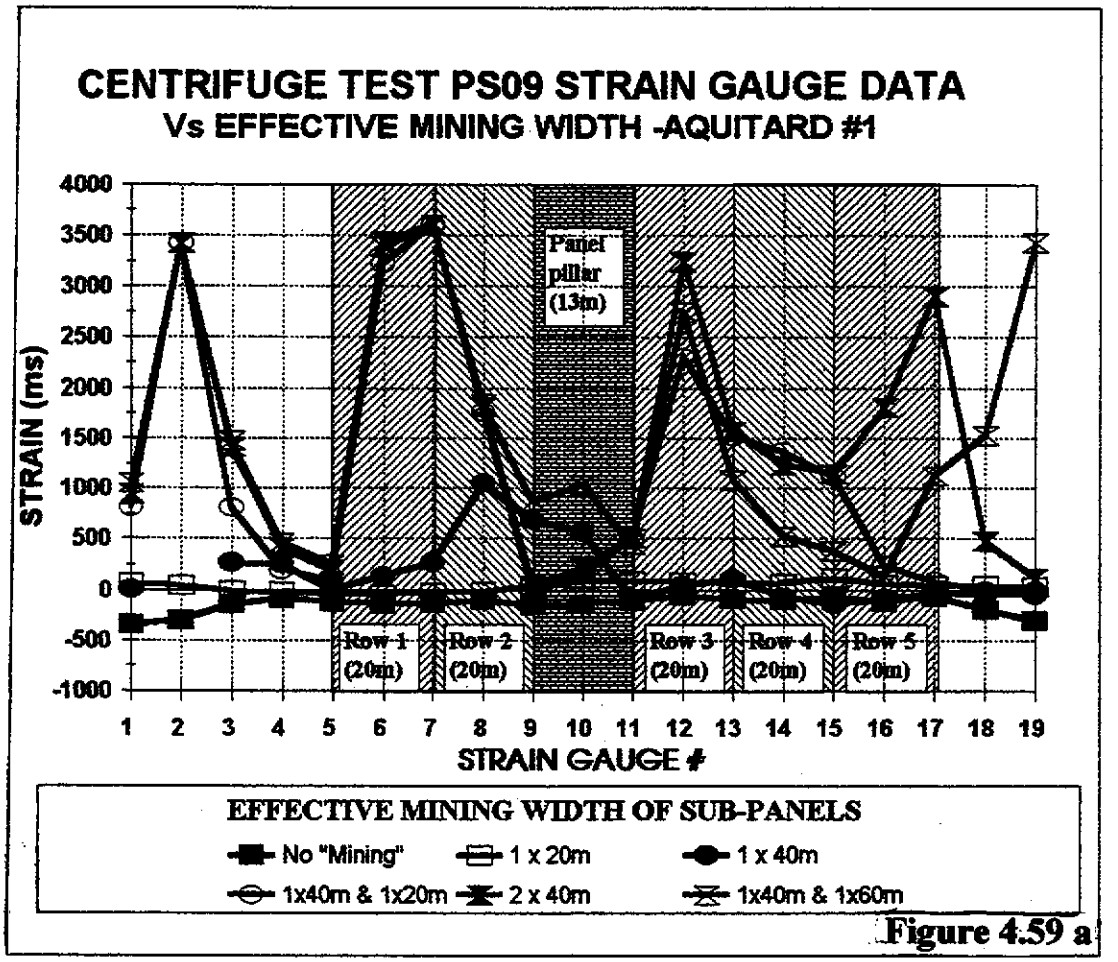

Figure 4.59 a

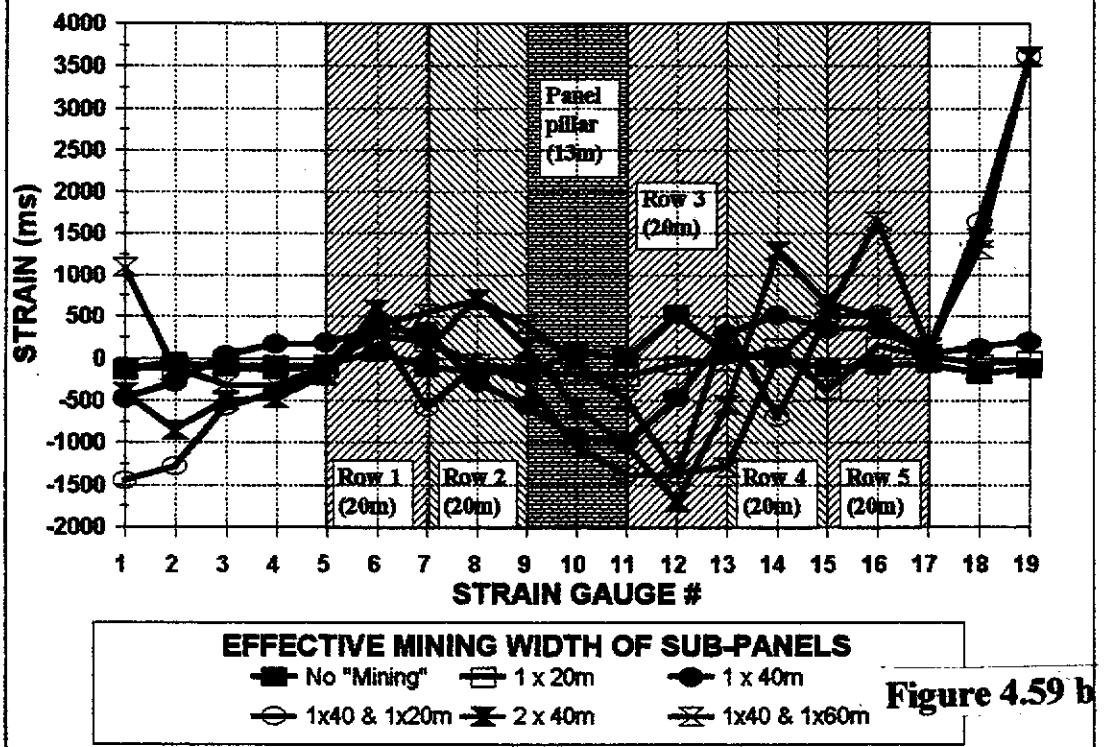

Figure 4.59 b

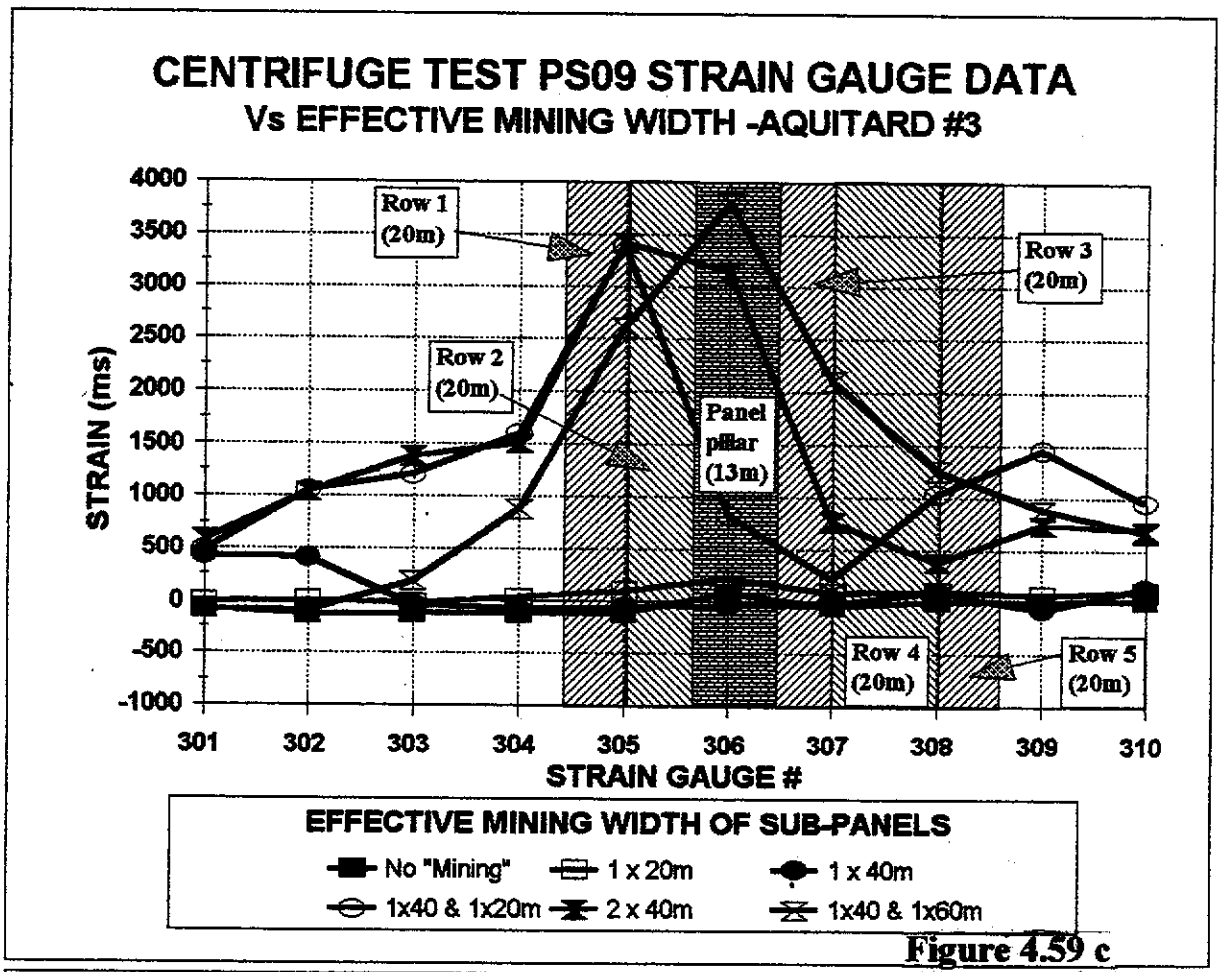

Figure 4.59 c

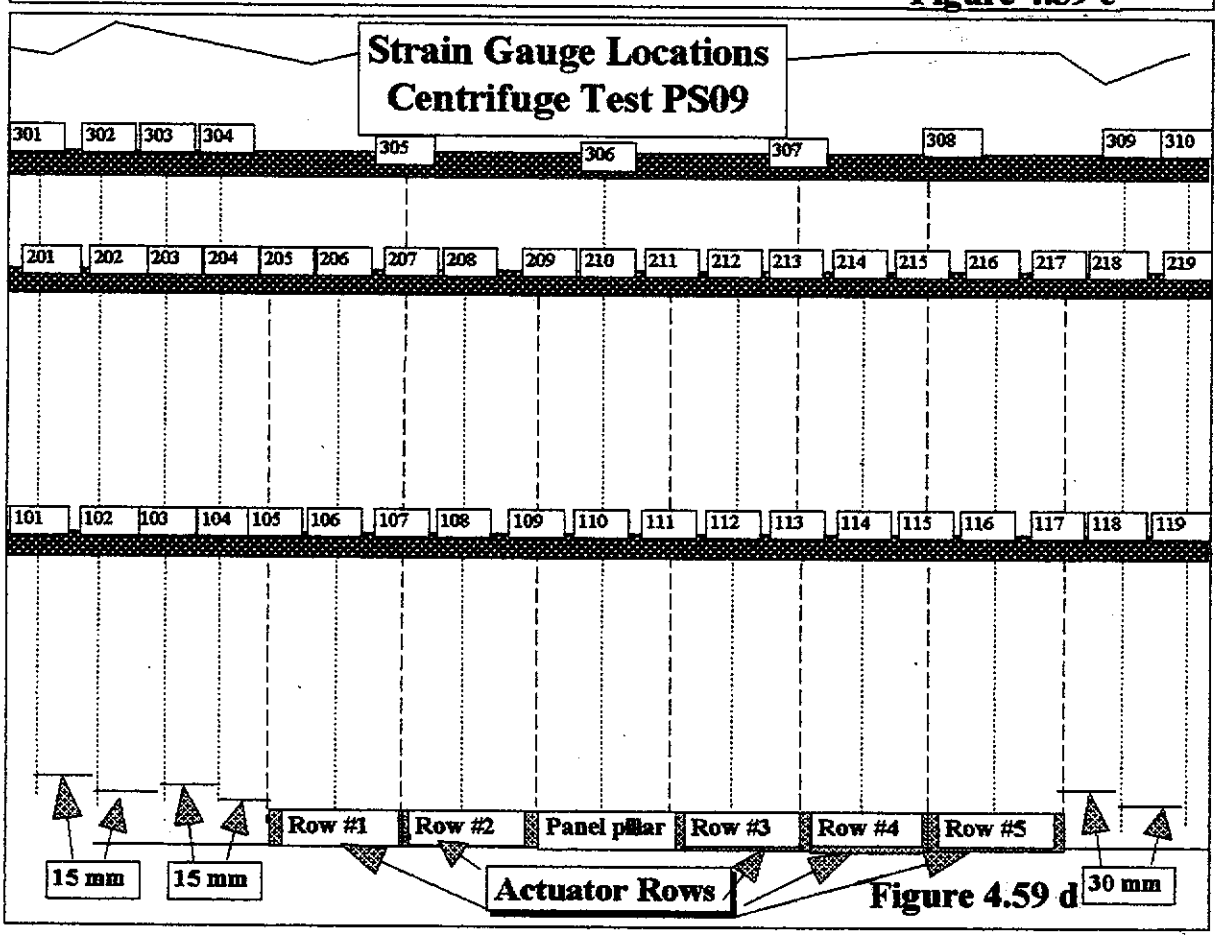

Figure 4.59 d

DIAGRAMMATICAL VIEW OF LOAD CELL VALUES CENTRIFUGE TEST PS09

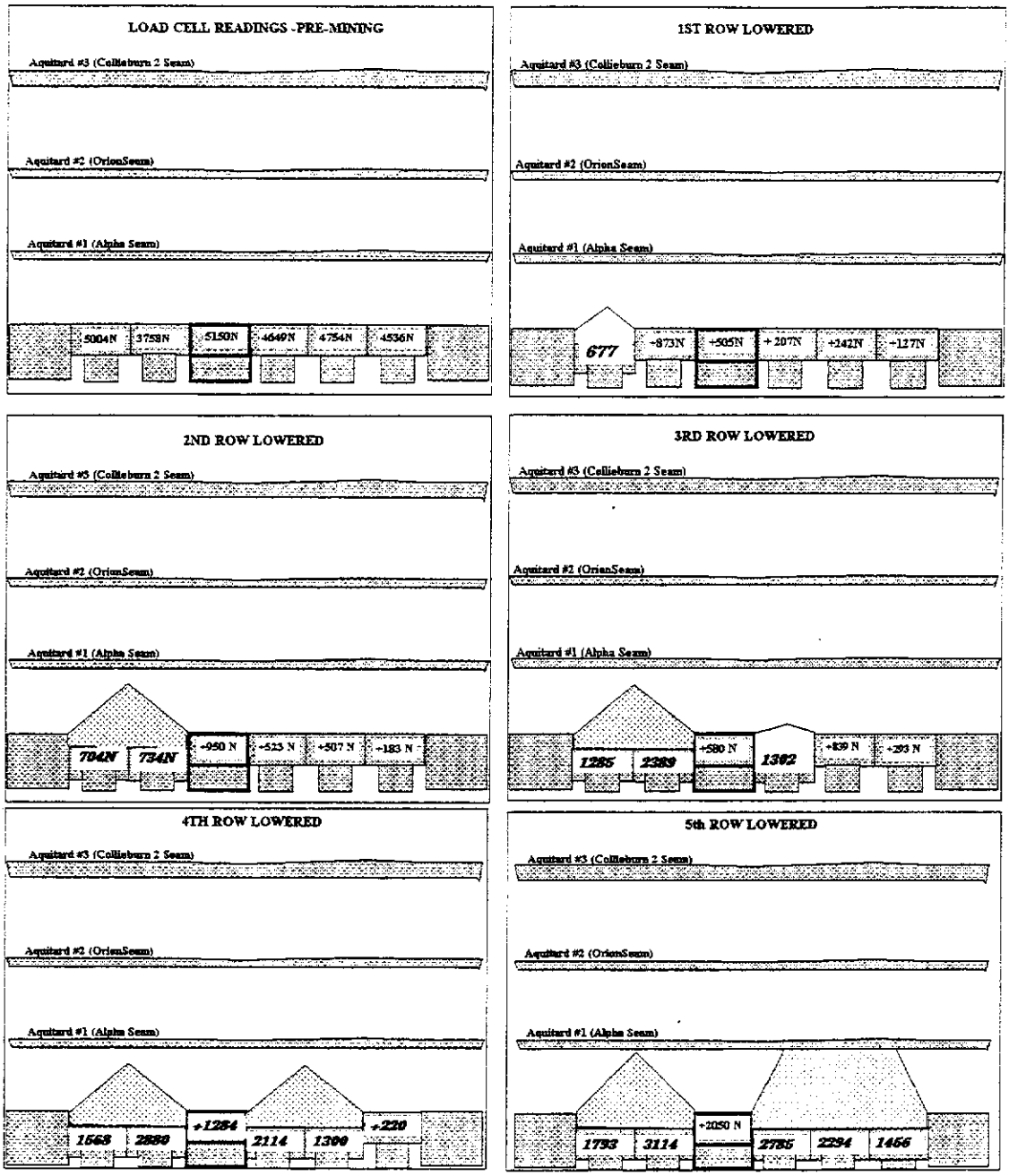

Note : Loads are Given as :- a) Total loads for lowered actuators, and
b) Load variance from pre-mining loads for unlowered actuators

Figure 4.60

ILLUSTRATION OF CRUSHED OVERHANG BELOW THE FIRST AQUITARD - CENTRIFUGE MODEL PS09

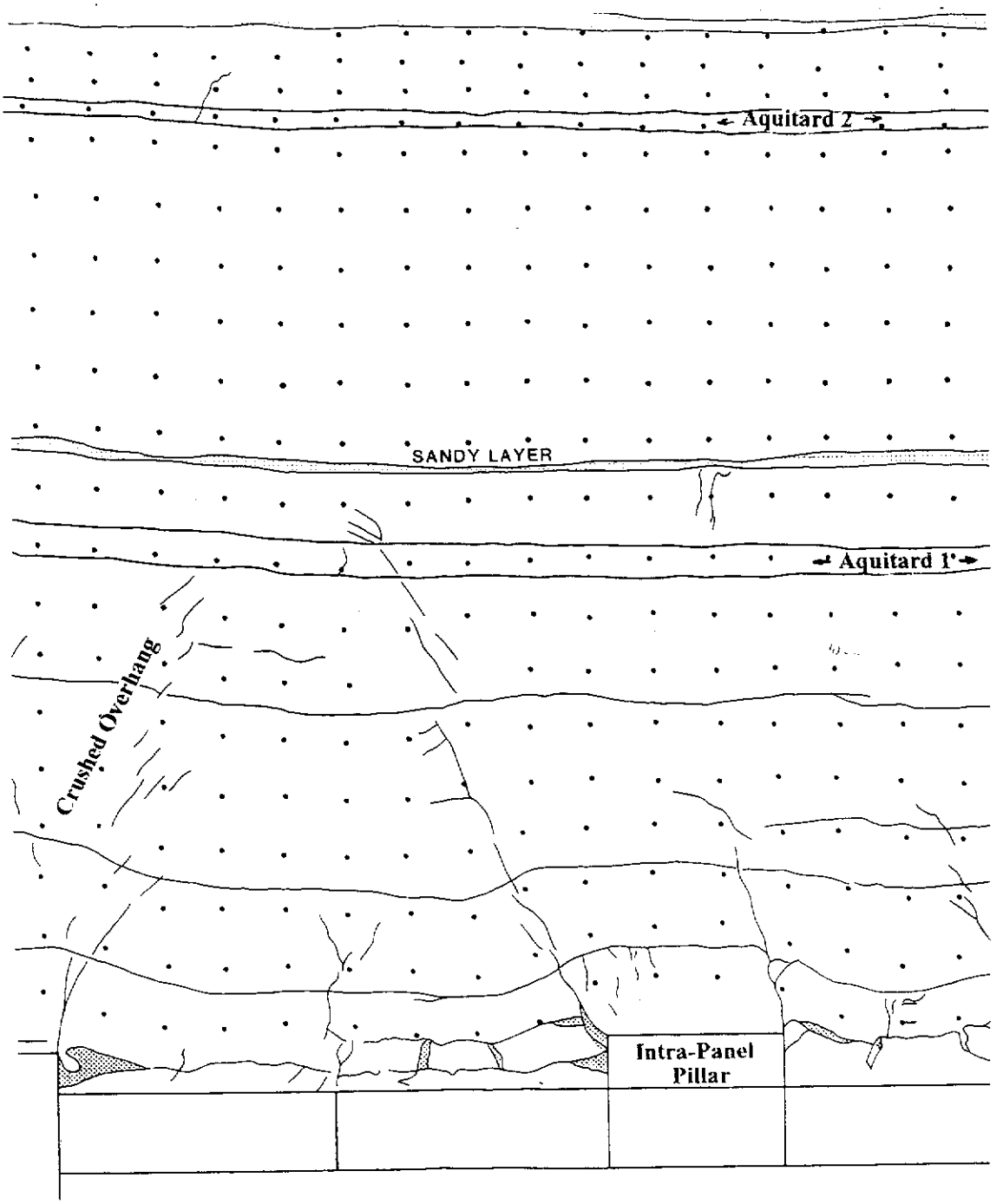

Figure 4.61

- For the first time in the equivalent material models a displaced crack developed through aquitard #1 above the edge of the second sub-panel (Figure 4.57 b), however, there was no evidence which suggested that this crack actually opened during or after the test.

4.2.2.12 Conclusions / Summary of Centrifuge Investigations

In summary, part the way through the investigations it was found that, with the current configuration of the "mining" piston actuator assembly, the geotechnical centrifuge was not able to represent the bulking of goafed material immediately above the mine roof. The result was that the surface subsidence developed by the models was up to 100% of mining height, compared to 63% in the field. Consequently, it was not justified to use the measured model subsidence for parametric design purposes as originally intended. Emphasis was then shifted to using the centrifuge modelling technique for investigation of subsidence *mechanisms* only. This investigatory approach for centrifuge modelling has also been accepted as the best use of the modelling technique by Iglesia et al., (1991) for his work on large scale "mine" models.

By adopting this approach, a number of important facets of subsidence development were successfully investigated. A brief summary of each centrifuge test is provided in Table 4.1, and the more significant observations made from subsidence modelling of the Collie Basin sediments are discussed below.

The main findings made from the centrifuge study can be divided into two groups:

1) general modelling limitations and trends, and

2) sustainable findings relevant to coal mining activities in the Collie Basin.

In regard to modelling limitations and trends, the most significant observations made during the study were:

- When using natural materials in the models, the rock mass similitude is not met for the aquitard coals, but can be expected to be met reasonably well with the extremely weak Collie Basin sandstones. This is because the rock mass behaviour/strength of coal is significantly different from the behaviour of small (eg centrifuge model size) samples of coal. Typically, coal rock mass cleavages and other forms of weakness which affect their behaviour and overall strength are inherently ubiquitous.

TABLE 4.1 SUMMARY OF GEOTECHNICAL CENTRIFUGE TESTS

TEST ID	PRINCIPAL TEST AIMS	MODEL TYPE	MODEL SCALE	MODEL DIMENSIONS L x B x H (mm)	EXTRACTION DIMENSIONS L x B x H (mm)	AQUITARDS MODELLED	DATA COLL.	# STRAIN GAUGES	MAJOR RESULTS
WESTCOLL 1	Test actuators	Equivalent Material 1/2 panel	1:300	650 x 390 x 200	270 x 204 x 8.3	Nil	CCD Tracing	Nil	System generally worked well, however 3 pistons did not drop. Problems with power slip ring. No caving occurred as a result.
WESTCOLL 2	Test actuators	Equivalent Material 1/2 Panel	1:300	650 x 390 x 200	270 x 204 x 8.3	Nil	CCD Tracing	Nil	System worked well; all pistons dropped, and the roof subsided. A compressive hump was noted on the model surface. A line of shear was evident in the lower half of the model.
WESTCOLL 3	Test artificial material	Equivalent Material 1/2 Panel	1:373	650 x 390 x 187	270 x 204 x 8.3	Alpha	CCD, Tracing Laser	Nil	Caving characteristics OK. Laser subsidence measured as 78% piston drop height. Large open subsidence cracks noted on the model surface and at the aquitard level. Some apparent shearing near the model surface.
WESTCOLL 4	Repeat above include stooks	Equivalent Material 1/2 Panel	1:373	650 x 390 x 187	270 x 204 x 8.3	Alpha	CCD Tracing Laser	Nil	Laser results similar to Westcoll3. Subsidence pattern was curved at panel edges. Less cracking was noted throughout the model. The caving angles match field data. A subsidence hump was noted on the surface - after first caving occurred.
PS01	Test insitu material	Insitu Material Plain strain	1:200	650 x 201 x 295	270 x 201 x 12.5	Overly thick Alpha	CCD, Trace Laser Strain g.	7	A definite caving pattern was identified. No surface subsidence developed. The aquitard bridged across the goaf; bed separation occurerd below the aquitard. A tensile crack developed at the mid point of the lower side of the bridging aquitard.
PS02	Use sandstone with no bedding	Insitu Material Plain strain	1:200	650 x 201 x 284	270 x 201 x 12.5	Alpha	CCD, Trace Laser Strain g.	10	No significant caving occurred until all pistons were lowered. No subsidence developed. The caving angle was much lower. The aquitard was being supported by the low angled caved overhang. Differences in caving due to no bedding in sandstone.
PS03	more defined bedding	Insitu Material Plain strain	1:200	650 x 201 x 277	270 x 201 x 12.5	Alpha	CCD, Trace Laser Strain G.	10	First caving occurred after 4 rows of pistons had been dropped. Caving more angular. Maximum subsidence = 80% piston drop height. Caving angles similar to field data. The aquitard trunkated the line of shear. The aquitard yield strain was 2 mm/m.
PS04	Equivalent mat'l based on flexural strength	Equivalent Material Plain strain	1:300	650 x 201 x 318	402 x 201 x 14	Alpha Upsilon	CCD Tracing Strain G	20	Poor wiring practice affected subsidence development. Subsidence factor = 86% drop h No open cracks on aquitards. Caving heights were much larger than insitu material.
PS05	Repeat of above test with improved wiring	Equivalent Material Plain strain	1:300	650 x 201 x 318	402 x 201 x 12	Alpha Upsilon	CCD Tracing Strain G	20	Caving patterns varied from test PS04. Subsidence factor = 100% drop height. Problems with edge piston; this affected subsidence development.
PS06	Panel/pillar investigation	Equivalent Material Plain strain	1:300	650 x 201 x 362	134 x 201 & 201 x 201 x 8.4	Alpha Upsilon	CCD Tracing Strain G	20	Indication that the sandstone pillar above the intra-panel coal pillar would remain in tact. The hydraulic lines feeding the "pillar" hydraulic pistons ruptured, and the pillars lowered
PS07	Repeat PS06; larger ext. height More Aquitards	Equivalent Material Plain strain	1:300	650 x 201 x 348	134 x 201 & 201 x 201 x 14.1	Alpha Orion Collieburn 1	CCD, Trace Load Cell Strain G	36	There was no pillar failure, but there was some consolidation of sandstone materials. An unsupported span concept is developed. The caved overhang supports the aquitard. The tributary loading theory is questionable.
PS08	Repeat PS07; saturated aquifer	Equivalent Material Plain strain	1:300	650 x 201 x 351	134 x 201 & 201 x 201 x 14.1	Alpha Orion Collieburn 1	CCD, Trace Load Cell Strain G	36	This test failed due to a water leak in the model. One piston did not lower; this greatly affected the subsidence development. More consolidation was noted above the pillars.
PS09	Repeat PS07; narrower intra-panel pillar	Equivalent Material Plain strain	1:300	650 x 201 x 350	134 x 201 & 201 x 201 x 14.1	Alpha Orion Collieburn 1	CCD, Trace Load, Laser Strain G	48	The sandstone above the intra-panel coal pillar collapsed. Significantly more subsidence developed. There was evidence of near surface dilation of sand grains. It appeared that the tributary loading approximates an angle of 6 degrees.

Small samples of coal cannot replicate this rock mass effect. Conversely, a general paucity of rock mass defects, and the relatively small variation between the defect strength and intact material strength in the extremely weak Collie Basin **sandstones** means that these materials could be used with better effect in models.

The ramification of this conclusion is that it would be very difficult to adequately represent subsidence mechanisms within stiff rocks in other mining regions that are largely dependent on the inherent defects of the rock mass. Furthermore, the selection of blocks of natural material having consistent material characteristics throughout each block and between blocks is very difficult if not impractical for parametric studies in coal measures strata.

- It was also evident that perfect similitude was not attainable for all material parameters when using equivalent materials to construct models. Nonetheless model behaviour, based on the design criteria used to construct centrifuge models in this study (extraction ratio of "coal", model geometry, flexural strength, shear strength, density, and elastic modulus of the materials), appeared to well represent the line of shear and aquitard performance of that noted in the field.

- The large "equivalent prototype" size of the individual top-caps used does not allow for the formation and rotation of blocky materials within the caved material. This lack of bulking results in subsidence up to 100% of mining height and bending stresses and strains in excess of those developed in the prototype. Consequently, conclusions drawn from the shape and magnitudes of measured subsidence profiles can only be qualitative.

- Similitude is also not met in regard to the performance of the model with time. The time-dependent subsidence effects, well known by most researchers (e.g. Kratzsch, 1973), were not observed during testing. In this study, ground movements and strains steadied within 30 seconds of a mining step, equivalent to 1.7 hrs in the prototype. This can possibly be explained by the ineffective bulking achieved by the modelling. (The time dependent subsidence in the field possibly being largely due to recompaction of bulked goafed material over time and the consequent change in support provided to the overlying strata.)

- During the operation of the centrifuge tests the model's weak sandstone aquifer material can undergo consolidation. Up to 10 mm of consolidation has been interpreted at the model surface. The rate of consolidation appears to be 0.03 mm per millimetre thickness of weak aquifer material. It is possible that this consolidation process can result in a reduction of material strengths. The potential for weakening of equivalent materials by consolidation was not investigated during this study.
- With the current configuration of the strong-boxes at the UWA's geotechnical centrifuge centre, it is not practical to observe near surface behaviour during testing for the depth of models tested.
- Apart from the frame grabbing and laser profiling of surface subsidence, the data collection methods proved adequate. (Though good use was made of frame grabbing data in instances where accuracy was of less concern - eg. the subsidence vector plot in Figure 4.58.)
- When thick, stiff aquitard beams bridge across caved ground, the shape of the underlying edge of collapsed ground is more curved and develops at a lower angle. This is probably due to the lower tributary load on the caved overhang, allowing the caving edge to assume a more arched shape - typical of primary caving geometry. Once the bridging aquitard begins to yield, the tributary load is transferred to the underlying caving overhang which subsequently shears in a more linear fashion. Although this observation makes sense, there is no direct evidence of this happening in the field. (This phenomenon would be very difficult to measure in the field).
- Although there is no direct proof, it appears that greater heights of caving can be expected to develop with larger heights of extraction. This can cause some localised crushing of the goaf overhang, and thereby develop larger areas of unsupported mass at the aquitard level. This can lead to premature rupture of the bridging aquitard. However, it is not clear from the existing models, if correctly bulking materials would reduce these effects.
- There was no evidence of bed separations occurring above the first aquitard in any model (although the model-scale of bed separations measured in the field are

difficult to detect visually). It appears that large scale collapse only reaches the base of the first major aquitard which bridges across the caved zone and allows the upper material to sag gently downwards. This sagging effect is more evident when extraction is wider.

- Inherent bedding has a significant effect on the caving characteristics of the overlying roof material in the models. Massive sandstones (with little or no apparent bedding or of high shear strength), in accordance with beam theory, tend to withstand greater superincumbent loads and therefore bridge across larger open mine voids. A good example of this was observed in centrifuge test PS02, where the sandstone roof aquifer had no obvious bedding and only caved into two large blocks after all pistons were lowered. It is therefore important that physical models adequately represent the bedding of the sediments. This also confirms the findings of investigations of other researchers (e.g. Iglesia, 1991).

- Inconclusive evidence exists that suggests that the standard tributary area loading theory might not be applicable to panel/pillar mining. This loading theory is crucial to the design of intra-panel widths. More research is required into this matter, as there was a number of anomalies associated with the centrifuge models.

- Finally, the assumption made from analyses of field data that subsidence develops in five well-defined stages (see Section 3.3) has been confirmed. The following additional details have been provided for the three zones involving collapse of ground, and the central vertical sagging zone:

  a) The primary caving zone in the immediate roof is typically less than 12 m high (depending on mining height) and occurs shortly after the extraction of each fender lift. (Note field data suggests that the limit of primary caving is between 6 and 8 m above the mine roof in 2.5 m high workings.)

  b) The secondary caving zone, at the start of the extraction panel, where the ground mass tends to cave as one large mass (typically once a critical width of 40 m has been extracted), can extend vertically 30 m to the first aquitard. The form of the collapse is usually triangular and is defined by the angle of shear (23°).

  c) The zone of tertiary caving, where large blocks of material subside in a cantilever / rotational-type collapse, follows on from the advancing edge of the

"one-piece" collapse and is extended in stepped form with the extraction of subsequent fenders. The shape of the collapsed ground in this zone is rhomboidal and parallel with the line of shear. This zone of collapse is defined vertically by the interval between primary caving and the first aquitard layer that can truncate the caving edge. This rhomboidal mass provides support for bridging strata.

d) The sagging zone, from the first aquitard and above, is allowed for by the bridging of the stiff aquitard layer across the caving edge. The superincumbent strata can then slump rather than cave onto the bridging aquitard. Sagging is also enhanced by the gradual yielding of the triangular-shaped caved overhang beneath the abutments of the bridging aquitard. Evidence from centrifuge test PS03 suggests that the minimum thickness of aquitard required for adequate bridging across the line of shear is in the order of 1.0 m.

Zones listed in a), b), and c) above are large strain horizons that involve large scale cracking and caving. Zone d) has comparatively little strain, and the width of any cracking that develops is largely dependent on the amount of of vertical constraint. Two zones of constraint can be defined in zone d):

1) A zone of high constraint where, other than tensile cracking, minimal open fracturing develops. This zone lies between the first spanning beam/aquitard and the base of the unconsolidated overburden material. .

2) A zone of minimal constraint, which allows for the development of deeper open cracking at the ground surface. This zone is also susceptible to shear dilation of loose sands.

Note that the results attained from the centrifuge modelling did not allow for the translational sagging zone, above the panel edge and away from the caving zones, to be better defined than has been interpreted from field data (see Section 3.3).

- The yielding flexural tensile strain for both the confined (centrifuge model) and unconfined (laboratory bending tests) natural aquitard coal material is 2 mm/m. The yielding strain is 0.8 mm/m for the aquitard equivalent material when confined within the model. It was observed during testing, that once the panel is sufficiently wide the yielding strains of aquitards, and presumably sandstones, at all horizons

are exceeded. Therefore these aquitards could be expected to at least become leaky.

In regard to the sustainable developments pertinent to mining, the following listed points describe the most significant findings made during the study:

- During operation of the centrifuge tests, it was evident that the Wongawilli system has unique caving processes. Therefore, all empirical models established should only be considered to be **directly** applicable to these mining conditions. If anything other than Wongawilli extraction techniques are used in the Collie Basin, the existing models will require modification and further research. Three of the more significant differences from other total extraction methods include:
  - It is possible to develop less subsidence closer to the mine workings than at some distance above the mine roof - as observed by borehole extensometer anchor measurements and the "wavey" subsidence profiles in the caving zone in the centrifuge models. It has been demonstrated that, after each mining step, the immediate roof caves in the form of an "inverted V" (primary caving - see Figure 3.54). When two adjacent fenders have been extracted, a "V shaped" triangular mass of material is developed between the two areas of primary caving (coincidently at the stook line). This triangular mass of material is, to some extent, supported by primary caving on either side and therefore subsides less.

    This effect of this differential movement is dissipated within the first 30 m above the mine workings by localised crushing of the general ground mass in the collapsed zone, resulting in an even subsidence profile above the middle portion of the panel, as would normally be expected.
  - The presence of stooks and remnant coal pillars can influence the immediate caving and subsidence mechanisms. For example centrifuge test Westcoll3 (with no stooks) had significantly greater cracking of aquitards, and the model surface than Westcoll4 (with stooks). This provides good support for the inference made about the cause of the variation in field subsidence above remnant coal left in 1North panel compared to that predicted by the empirical and SUBSOL models (in Section 4.1.1.3).
  - Wongawilli extraction develops sequential strips of coal up to 20 m wide.

When these wide spans collapse, there is a greater impact on the caving of the upper strata. The effect that collapses of large spans can have on the overlying strata is best illustrated by the atypical shear dislocation through the Alpha seam aquitard in centrifuge test PS09, immediately after the massive collapse of the sandstone column developed above intra-panel "coal" pillar. A similar, though less obvious effect was observed after secondary caving in test PS03. (Field data supporting this observation includes the subsidence hump developed above 1 North Panel - see Section 3.2.6).

- Aquitards (or more particularly the coal within the aquitard) act as reinforcement within the weak sandstone. These layers of reinforcement bridge across the line of caving and therefore retard development of the shearing plane through the overlying sediments. It can be expected that this phenomenon helps prevent the development of pot-hole subsidence. Consequently, the development of pot-hole subsidence can be expected to be limited to depths of cover where there are no consistently thick horizons (<1.0 m) of coal aquitard material within the interval between the mine roof and the surface.

  Within the WCL mine leases, this typically restricts pot-hole development to depths of cover less than 40 m. However, it is important to note that where large-scale geological/structural anomalies exist within the superimposed strata, pot-hole subsidence can develop at much greater depths. For example, collapsed ground above pillar splitting in the Cardiff colliery, adjacent to a "mine boundary" fault and below soft swampy sediments, mobilised the ground mass through to the surface at over 80 m depth of cover. This mobilised material rushed into the mine and developed a pot-hole feature extending for approximately 2 acres (Lord, 1952). Another example of anomalous pot-hole formation was observed at the 2B West C panel in the WD2 colliery (at 60 m depth). This panel was located adjacent to a dominant "wash-out" structure. The mining method used in this panel was Wongawilli extraction.

- The magnitude of flexural stress etc. that will develop within a bridging aquitard is dependent on the amount of support given by the underlying (triangular) goaf overhang, as well as the thickness and strength of the bridging aquitard. Elevated tributary abutment loads can tend to crush the weaker underlying strata, thus softening the abutment below the spanning aquitard and reducing the bending strains.

- It is postulated that a small portion of the field subsidence factor is due to dilation of the constituent grains of quartz - particularly near the surface - where consolidation pressures are less. This assumption is supported by the results gained in centrifuge tests Westcoll3 and PS09, by the development of a hump in the surface above 1North panel, and by the increase in separation between the shallowest anchors in extensometer D212. It is proposed that the staged collapses of ground produced by Wongawilli-style extraction will dilate the coarser grained, extremely weak sandstones more than standard longwall extraction.

  It is also postulated that this dilation along the line of shear is a contributing factor to the shape of the subsidence trough above the inside panel edge.

- Even though an additional 36% subsidence developed in the geotechnical centrifuge models, compared to field observations, no open vertical cracks were observed either between aquitards or within the goaf material itself. Some open bed separations were noted immediately beneath the first aquitard, however, these horizontal voids do not pose any threat to the vertical transport of water into the mine workings. This modelling observation has also been inferred from field observations, where relatively deep surface cracking in the swampy area above the 2SA panel did not allow the large volumes of pooled winter rains into the mine.

- The results gained from modelling two separate 40 m wide sub-panels (at 120 m depth), separated by a 20 m wide intra-panel pillar in the centrifuge test PS06 indicated that the panel-pillar method could be used successfully in the Collie Basin (before the trial panel NWB3 was successfully mined).

- It has been demonstrated that the column of sandstone developed above the coal intra-panel pillars, as a result of caving on either side of the intra-panel coal pillar, can collapse if not of sufficient width to withstand the tributary load. The collapse of this sandstone column results in additional subsidence which can generate higher tensile strains at the surface and aquitard horizons. The additional subsidence developed from the collapse of the sandstone column therefore provides greater potential for unwanted groundwater to enter the mine workings and additional damage to surface features. It has been interpreted that this mode of failure is similar to that responsible for most of the historical creeps in the Collie Basin - see Section 2.5.5.

In conclusion, the results gained from the centrifuge study have provided some useful supportive information regarding general subsidence mechanisms in the Collie Basin. Some important "unknowns", particularly along the line of shear, have been answered, and others identified as requiring further investigation.

It is therefore considered that geotechnical centrifuge modelling can be a useful tool for investigation of mining problems in some circumstances. However, centrifuge modelling, like all physical and numerical modelling methods, has a number of limitations which must be qualified before embarking on such a program of investigation.

The most significant limitation is that it is unlikely that complete similitude will be met for all parameters involved with large scaled mining models. The performance of the model and the success of the investigation is therefore ultimately dependent on:

- The degree of influence (in the prototype) of the parameters not meeting similitude.
- The primary objectives of the investigation.

In this case, a reasonable level of similitude was met for the intact mechanical properties of the extremely weak Collie Basin sediments, however, a major problem was encountered with the inability of the model material to bulk at the mine roof horizon after primary caving. This lack of similitude in bulking precluded the use of the model for precise measurements of surface and subsurface subsidence for design purposes. It can be considered, however, that the lack of bulking of caved roof would have represented a conservative worst-case scenario which would only have highlighted the critical subsidence processes, without changing them significantly. This assumption is partly supported by the observed shearing angles and shearing processess in the models which appeared to reasonably match field observations, and the behaviour of intra-panel pillars under loading also seemed to be plausible.

There was also some concern held for the pre-test consolidation of the weaker sandstone aquifer materials during initial "spin-up" of the model. It has not been established conclusively whether the strength of these weaker materials has been reduced during consolidation, however, from the realistic angles of shear and subsidence mechanisms observed, it does not appear to have had a significant performance on the model.

5.0 MINE PLANNING FOR SUBSIDENCE CONTROL IN THE COLLIE BASIN

The aim of this (final) phase of investigation was to develop appropriate extraction panel design criteria for the management of mining subsidence by panel/pillar mining methods in the Collie Basin.

It was established in Chapter 2 that there are two general forms of subsidence in the Collie Basin - discontinuous and continuous. In regard to the discontinuous forms of subsidence, the exact form, dimensions and timing of this type of subsidence is still not predictable; however, it is now possible to determine whether there is any potential for discontinuous subsidence to develop. Firstly, under normal geological conditions, this form of subsidence is limited to depths where there are no major aquitards within the overlying strata. This limiting depth has been arbitrarily set at 40 m, however, in some locations, bridging strata is known to exist at much shallower depths. The 40 m limit should be used in cases when there is limited knowledge of the stratigraphy above a panel.

Secondly, discontinuous subsidence will only develop if the site has one of a list of prerequisite mining conditions - see Section 3.3. Because accurate prediction of discontinuous forms of subsidence is not practical, it is recommended to adopt a remedial/after-the-event approach unless there are very important structures overlying the panel, in which case the mine plan should be designed for "permanent" stability. Three examples of methods used to prevent or rehabilitate discontinuous subsidence in Collie are listed below:

- In August 1992 the author successfully filled inaccessible mine workings beneath WCL's core shed, using a slurry of clayey overburden from the WO-5 open cut.
- In April 1992, WCL and Western Australian Department of Minerals and Energy (DME), using a concept devised by the author, set up a system of subsidence monitoring for prediction and prevention of subsidence in an abandoned mine 15m beneath a public road. Wooden chocks were installed beneath suspect areas of mine roof and remote roof convergence monitors were installed in better ground with wide roadways to any detect collapses of ground that may require additional roof support to prevent mining subsidence. If a collapse of ground was detected by the remote monitoring, it was proposed to use WCL's mines rescue personnel to implement the required remedial actions where required. This work is described in

- Where a site has one or more of the pre-requisite ground conditions needed for the development of discontinuous subsidence (as listed in Section 3.3), the surface has been barricaded off from public use until after mining has finished and the surface has been rehabilitated. (To date these forms of subsidence - resulting from WCL coal extraction - have been restricted to bushland or WCL leasehold land where public access is already restricted).

Remedial and preventative works for this form of subsidence in other areas is well documented, for example the Proceedings from the Conference on Mine Subsidence in Urban and Developed Areas (Richmond, 1993) provides a large number of relevant case studies which would be of interest to the reader.

In regard to continuous-trough forms of subsidence, damage to surface and subsurface features usually results from a change in ground curvature and the corresponding strains developed. It follows, therefore, that if this curvature can be controlled, then the concomitant effects on the ground mass or structures will also be controlled. Two basic methods have been identified which can be used to reduce the curvature of subsidence troughs:

- Reducing maximum subsidence (e.g. by infilling mine voids or mining narrower panels).
- Softening the "sharp" subsidence profile above the edge of extraction panels (e.g. by leaving "yield" pillars immediately adjacent to the extraction panel abutments, or in thick seams - by mining successive strips of coal with vertically and inwardly staggered edges as done at the Rudnik coal mine in Velejne, Slovenia).

In Collie the most appropriate method for controlling mining subsidence damage is to extract coal in a series of narrow panels (panel/pillar mining - see Figure 2.18). This conclusion was based largely on the economics of each alternative, which essentially precluded any method that added to the running cost of the operations - such as the purchase of new equipment. These cost-efficiency analyses are not presented here.

After detailed evaluation of all modelling during the research project, and all available data, a rudimentary design method was established for the panel/pillar method of mining. Rather than discussing its evolution separately, the design method is discussed in terms of the approach used to design a trial panel that was mined to validate this design method.

5.1 TRIAL PANEL DESIGN

The area selected to be most suited for trialing panel/pillar extraction was the North West B3 Panel in WD6 colliery (NWB3 Panel - Figure 5.1), largely because it was close to super-critical width - 200 m minimum width at 144 m depth. A trial panel/pillar panel less than critical width would be both short and narrow and the ground movements for any given mining width would be clouded by the end effects between panel abutments.

Another favourable feature of the NWB3 Panel was that the overlying aquifers were only partially depressurised, and could therefore still provide valuable information on the effect of mining subsidence on aquitard integrity.

In order to extract coal efficiently, it was required to establish the maximum width of extraction allowable for each of the individual sub-panels (so as to reduce subsidence development), and the minimum intra-panel pillar width (required to prevent any significant interaction between each sub-panel). The following describes the approach used to design for each of these parameters.

1) **Establish the maximum extraction width.**

The first task was to obtain all relevant information about the superincumbent strata and surface features and to establish subsidence tolerance limits for anything needing to be safeguarded against subsidence damage. In this case there was a requirement to protect both a sealed open-pit haulroad sited directly above the panel (Figure 5.1), and the Alpha seam aquitard (which separates the mine from aquifer 3), approximately 30 m above the mine workings. (Aquifers 1 & 2 in the mine floor and immediate roof respectively had been depressurised by previous bord and pillar mining activity around the panel).

For the protection of the haulroad and its drainage features, it was established that the maximum allowable subsidence was 100 mm. By using the equation:

$$Smax = T \times 0.64e^{-12e^{-4(W/H)}} \qquad 3.1(1)$$

detailed in Section 3.1.1, the maximum width of extraction allowable to limit Smax to less than 100 mm with a 2.7 m mining height and 85% extraction was established (54 m).

NWB3 PANEL LAYOUT & EXTENSOMETER BOREHOLE LOCATION PLAN

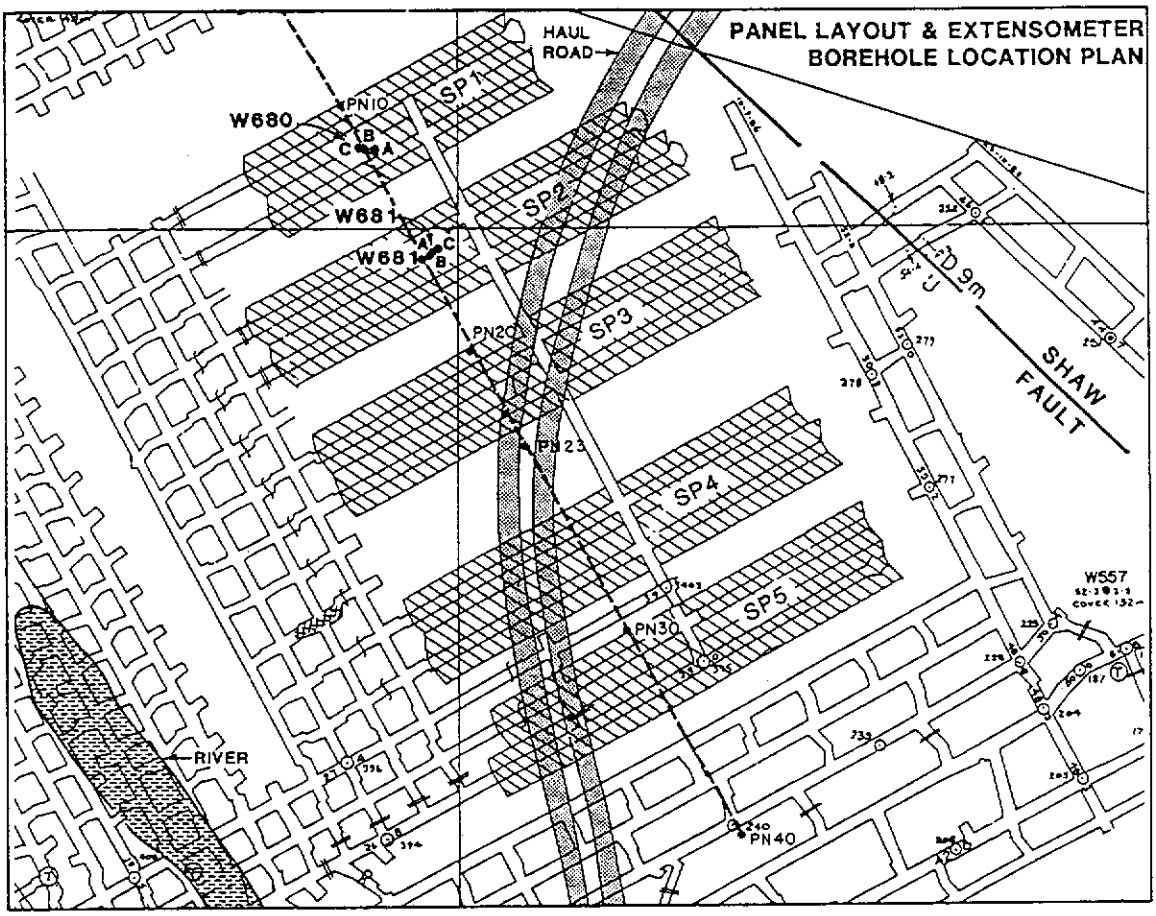

Figure 5.1

Designing the mine to maintain the integrity of the protective aquitard, however, is not as straightforward. It was concluded, in Section 2.5.6.1 that the published design criteria for aquitard rupture available at the time of the research project did not meet the requirements of this study. Consequently a specific program of work was required to assess whether an appropriate design approach could be established for the Collie Basin.

Following assessment of field data, two approaches were proposed to assess the integrity of aquitards. The first method was derived in 1991 (Misich et al., 1991) and is based on the horizontal strains at aquitard horizons. The use of this design approach has since been discontinued, for reasons explained later. However, the approach used and advancements made towards refining this method are still discussed in this Section for the potential benefit of further investigation. The second approach, developed much later, was based on shearing angles through the overlying strata. The methodology used to develop this design approach is also discussed later in this Section.

The basis of the first design approach was derived from observations of the anchor movements in the two-part extensometers above Blue panel (Figure 5.2), where the degree of flexure/curvature of each subsurface subsidence trough above the panel edge decreased incrementally for sequentially higher anchors. This observation, along with the well documented fact that strain is directly proportional to the curvature of the subsidence trough at the surface (e.g. Karmis et al, 1985), led to the premise that a measure of aquitard integrity could be derived from the magnitudes of curvature at each aquitard horizon. Therefore even if the aquitard is infinitely thin, unless the subsurface subsidence trough exceeds a limiting curvature it should maintain its integrity.

An interesting variation on this assumption was observed by the author during a study visit to the Rudnik Lignita Colliery in Velenje, in the Slovenian coalfields, where 100 m of coal has been mined from a 150 m thick seam of lignite by multi-slice longwall methods. Measured subsidence in September 1990 was in the order of 80 m and was increasing with the mining of each subsequent longwall slice (personal communication M Veselic, 1990).

INTERPRETED SUBSURFACE SUBSIDENCE PROFILES - BLUE PANEL (COLLIE BASIN)

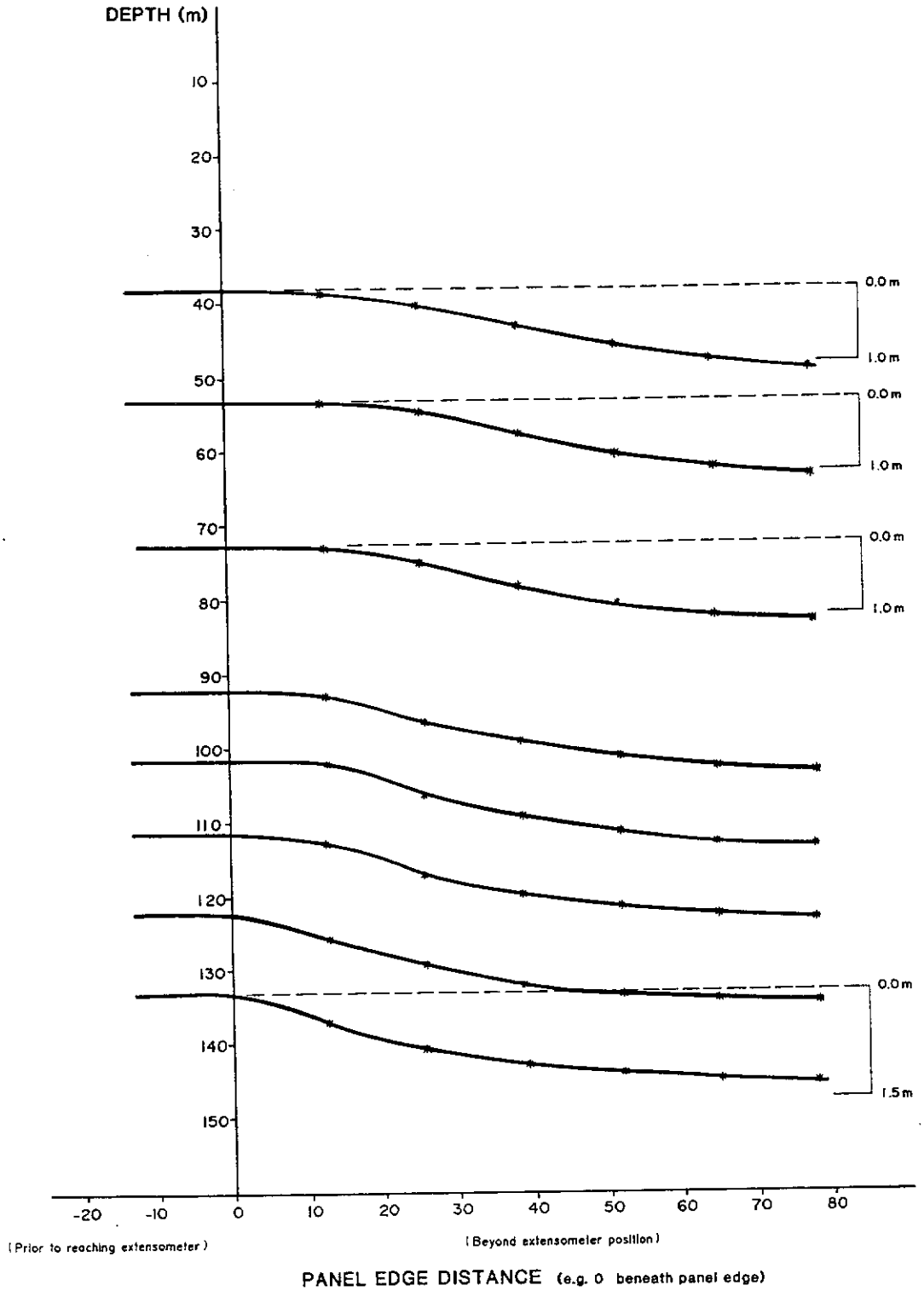

Figure 5.2

The 80 m deep subsidence resulted in a 50 m deep lake being formed on the surface above the extraction panel, with sheared face escarpments 3-4 m high around the perimeter of the lake. The tensile strains developed would exceed by far the tolerance limits of any material, however, the mine workings do not flood. This can be explained by the fact that the superincumbent strata consist of predominantly weak, swelling clays which re-knit with minimal confining pressure (equivalent to 8 m cover depth) thus preventing the flow of water along shear planes (Kocar et al., 1987, and Janezic, 1987). In this case, it is the post-failure characteristics of the clays which prevent inundation.

The limiting strain on Collie Basin aquifer materials was not known before this research study. The author initially used **confined** compressive strength tests (triaxial) on core samples of aquitard materials for limiting strains (Misich et al., 1991), the results from these tests indicated a yielding strain of 21 mm/m. It was acknowledged that the mode of failure of the triaxial tests was shear rather than flexural bending, however, it was considered, at that time, that this **confined** testing data would provide acceptable limits for first pass investigation. Particularly if the design criteria could be back-analysed against field data. By comparison, Xiao et al. (1991) state that the limiting tensile strain for most rocks is 1 mm/m, and Farmer and Altounyan (1980) accepted a yielding tensile strain of 2.5 mm/m for coal measure rocks. From the results in this study the limiting tensile strain for the aquitard material in the Collie Basin has been estimated to be 2 mm/m (Sections 4.2.2.12 and 4.2.2.2).

It was rationalised that if maximum curvature could be predicted from subsurface profiles with a known maximum subsidence at any horizon above the extraction panel, then the maximum strains could also be estimated. To assess the relationship between maximum subsidence and subsurface curvature, the first step was to plot anchor subsidence against the distance from the goaf edge in each panel. Curve fitting functions were then adapted to each subsidence profile so that curvature could be calculated by double differentiation of the profile function. Two curve-fit methods were used to cross-check the results, polynomial and double exponential algorithms. The curve fitting approach used was the same as that discussed in Section 3.1.8.

Examples of exponential curve fitting are provided in Figures 5.3, 5.4, 5.5 which represent extensometer anchor subsidence across the panel edge for selected anchors above Blue 2SA panel and 1North panels. The **polynomial** curve fitting required a number of "dummy" points to be added to the data, through what was considered to represent the most realistic shaped subsidence across the panel edge. This approach was necessary as the polynomial best fit curve (using GRAPHER® from Golden Software) tended to meander between the widely spaced X-axis datum points.

To simplify prediction of subsurface strains, it was decided to assess only the **maximum tensile** curvatures and strains, as it is widely recognised that the tensile strains are responsible for damage to water resistent layers - e.g. Wardell (1975.) The value of compressive strain, and the positioning of maximum tensile strain was considered irrelevant.

As can been seen by the data presented in Table 5.1, there is a reasonable amount of scatter of calculated curvatures between each of the curve-fit methods and between each panel.

TABLE 5.1 SUBSURFACE SUBSIDENCE PROFILE CURVE-FIT CURVATURES

PANEL								
ACIRL	20.0	39.0	56.6	68.7	79.9	92.0	98.5	Anchor depth (m)
H =140	0.51	0.52	0.54	0.52	0.55	0.56	0.62	Smax (m)
Poly/DExp	7/**12**	7/**13**	7/**14**	7/**13**	14/**13**	14/**14**	15/**14**	Curvature m^{-1} x 10^4
BLUE	38.7	53.0	72.3	92.2	101.7	111.4	122.1	Anchor depth (m)
H = 142	1.09	1.08	1.12	1.18	1.19	1.23	1.30	Smax (m)
Poly/DExp	14/**11**	14/ **11**	22 /**12**	34 /**14**	40/ **17**	33 /**17**	36 /**20**	Curvature m^{-1} x 10^4
2SA	23.9	26.4	33.9	40.2	48.9	53.8		Anchor depth (m)
H = 56	1.29	1.28	1.28	1.30	1.29	1.32		Smax (m)
Poly/DExp	82/**31**	82/**32**	82/**33**	122/ **37**.	122/**38**	122/**37**		Curvature m^{-1} x 10^4
1NORTH	39	46	56	67	74	86		Anchor depth (m)
H = 91	1.46	1.51	1.48	1.50	1.51	1.45		Smax (m)
Poly/DExp	47/**27**	62/**43**	62/**47**	71/**54**	72/**57**	112/107		Curvature m^{-1} x 10^4

CURVE FIT EQUATION FOR THE SUBSIDENCE PROFILE OF THE 92 m ANCHOR IN EXTENSOMETER W669/W670 - BLUE PANEL

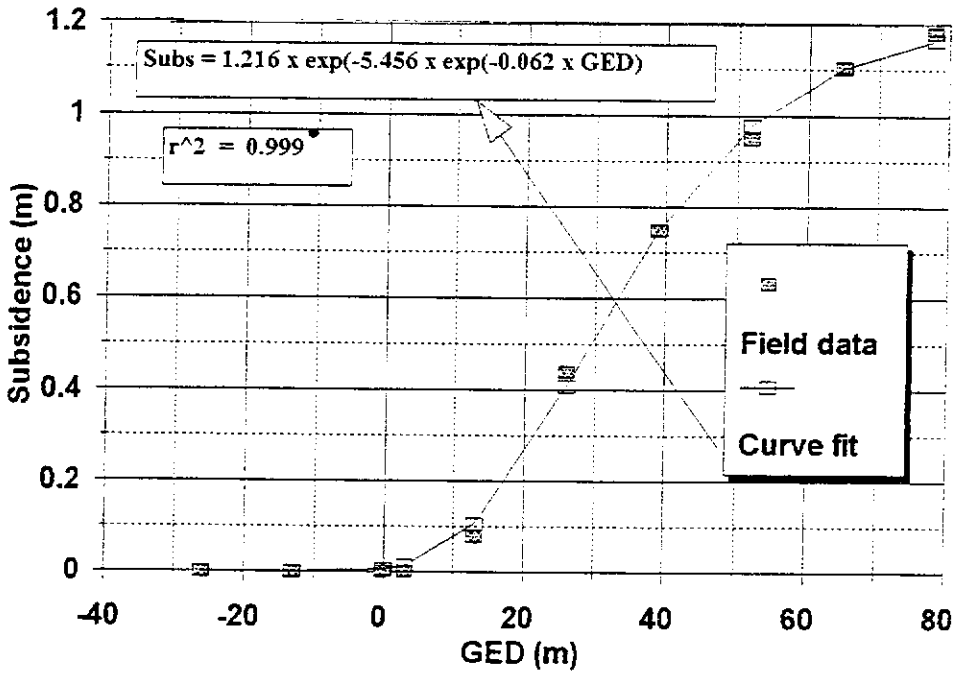

Figure 5.3

CURVE FIT EQUATION FOR THE SUBSIDENCE PROFILE OF THE 49 m ANCHOR IN EXTENSOMETER W668 - 2SA PANEL

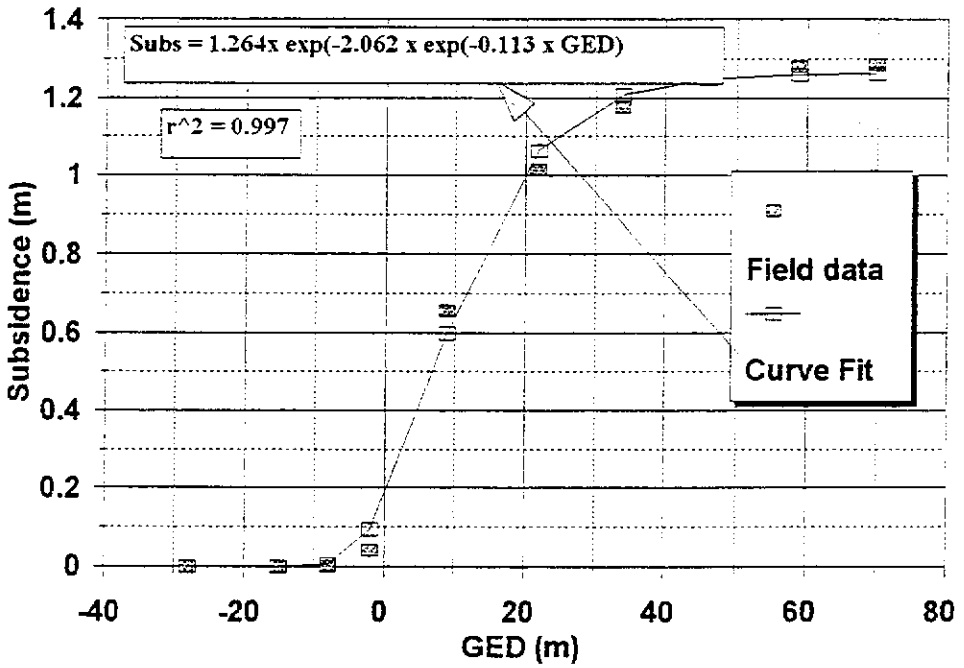

Figure 5.4

CURVE FIT EQUATION FOR THE SUBSIDENCE PROFILE OF THE 74 m ANCHOR IN EXTENSOMETER D213 - 1NORTH PANEL

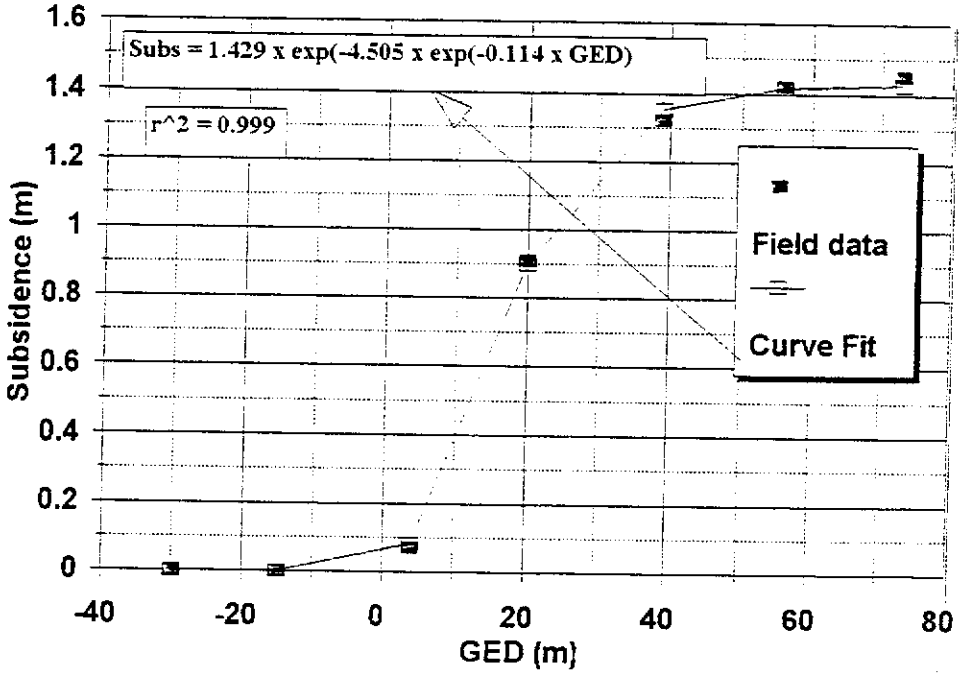

Figure 5.5

CALCULATED CURVATURE Vs MAXIMUM SUBSURFACE SUBSIDENCE AT VARYING h/H RATIOS FOR ALL EXTENSOMETERS

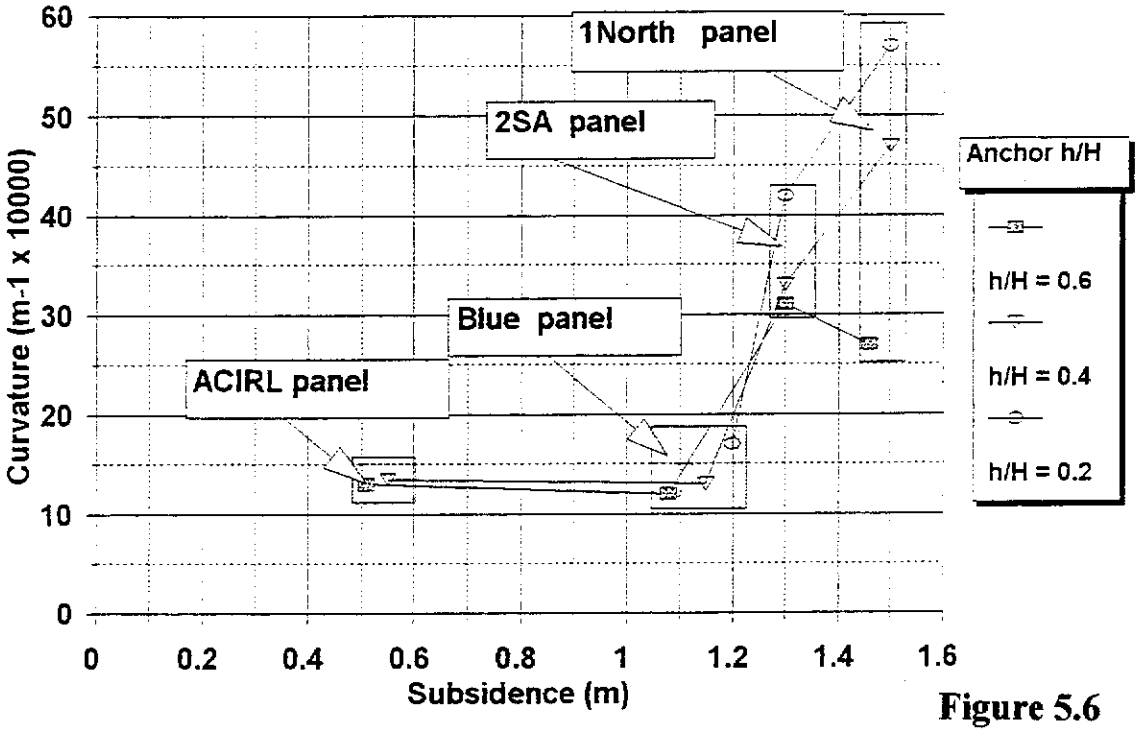

Figure 5.6

This variation can be explained by:

- variation in the relative location of the extensometers with respect to each incremental fender lift,
- the effects of remnant coal (eg the unmined fenders in ACIRL panel), and
- curve fitting error of subsidence profiles. Polynomial curve-fits generally produced higher curvature than the double exponential curve-fits. This is considered to be due to the manner in which the multi-variant polynomial can be made to fit around tight bends, and the fact that the double exponential curves were fitted only to the relatively few (as low as five) data points and not the additional interpreted/dummy data as was required to be introduced for the polynomial algorithm.

Although the coefficient of determination (r^2) for each fitted curve was greater than 0.99, this variation between the curve-fitting tools was seen to be a source of error which needs reconciliation should further studies on the curvature/strain be instigated.

Figure 5.6 presents the curvature/strain data at varying h/H values for all panels. It can be seen that although there are general trends for curvature to decrease with decreasing h/H, and to increase with increasing subsidence, these trends are not consistent enough to develop a design criteria from all the data.

It was also recognised that the general curvature/strain aquitard integrity prediction approach had some limitations:

- Irregular panel shapes and panels of W/H ratios less than 0.25 (that do not generate "measurable" surface subsidence) cannot be accounted for accurately. For example, a 400 m deep panel will only develop surface subsidence when the panel width exceeds 60 m, however, it is postulated that a 60 m goaf is likely to result in the yielding of at least the protective aquitard beneath aquifer 3.
- The method needs to be validated against a wide variation in stratigraphy, depth of cover, water pressure, and mining height.
- The curvature/strain relationships are based on measurements on the unconfined ground surface. It is questionable whether these correlations can be transposed to confined subsurface strata.

Further investigation of this method was undertaken during the physical and mathematical modelling stages to attempt improve the level of understanding of this concept, however, this program of work proved unsuccessful, largely due to

- the physical and mathematical modelling not being able to accurately represent the caving/bulking region and the shape of sub-surface profiles, and
- the inability to accurately measure beam/aquitard deflection profiles for comparison with measured strains (Appendix III.2) during four point bending tests and centrifuge modelling.

Consequently, this method was not developed through to a multi-faceted design criteria, even though a rudimentary curvature design model (provided by Misich et al., 1991) cross-checked well against the measured aquifer responses to the extraction of Red panel in WD-6 colliery. Further analysis of field and modelling data has since identified a more straight-forward method for designing panel widths to control groundwater inflow into underground workings in the Collie Basin. This alternative design approach, based on the concept of critical span, is discussed below.

Critical Span Design method

It was interpreted from centrifuge test PS01, where the thicker aquitard was noticed to bridge across the caved zone (Figure 4.35) an then crack in tension when a critical span was reached, that the mechanism of rupture of the aquitard closest to the mine workings was largely dependent on:

1) The dimensions of the unsupported span of the aquitard, developed by collapse of the underlying strata, and defined by the shearing angle of the collapsed ground.
2) The flexural properties (and thickness) of the aquitard.
3) The mechanical properties of the strata immediately below the bridging aquitard which provide support at the abutments of the stiffer bridging layer.

In order to obtain an appreciation of what effects the strata underlying the aquitards may have on the integrity of spanning aquitards, a low key investigation was conducted using a two dimensional finite element computer program. The package used was FESOL,

from Crouch Research Inc.

In this investigation, the FESOL models were set-up to represent a mine at 80 m depth with only Alpha seam aquitard above the mine. The structure of the models were simplified to consist of a 35 m interburden between the mine horizon and the 2.5 m thick aquitard, and a weak, plastic overburden 42.5 m thick (Figure 5.7). An "open cavity", representing the caved zone was created by discretising the model's quadratic element (eight noded) mesh in a series of blocks surrounding the area designated as having caved, thus leaving a void in the centre of the interburden mesh. The mesh was generated using FESOL's pre-processing module PREPPY, and had horizontal constraints applied at the edges and vertical constraints at the model base. The model forces were based on simple gravity loading.

Although FESOL can incorporate more complex material models such as the Drucker-Prager yield criterion, this series of modelling was, for simplicity, based on orthotropic elastic materials. The material properties required as input by FESOL in this case are elastic modulus, poisson's ratio, and material density. The respective elastic moduli were 500 MPa for the softer overburden, and 2000 MPa for the aquitard. The elastic moduli used for these materials were arbitrarily selected as being representative of the stratigraphy in the field, based on data provided in Table 2.1 and personal experience. For the purpose of the exercise, there was no requirement to be more definitive. The elastic modulus of the interburden material beneath the aquitard was varied in each FESOL model from 800 to 2,000 to 20,000 MPa (800 MPa is a more typical value for this material). The values of Poisson's ratio used were 0.3, 0.28, and 0.25 for each respective strata, and the model input densities were 2.15 t/m^3 for sandstone and 1.3 t/m^3 for the coal aquitard. There was no attempt to assess the stresses and strains throughout the model, as the purpose of this low-key study was only to demonstrate the impact of caved overhang on the shape (curvature) of subsided aquitards.

Two series of tests were developed, one to assess the effect of the presence of triangular shaped overhang (above the abutment of the caved zone, as illustrated in Figure 5.7 b) at the base of the bridging aquitard, the other to assess the effect of stiffer interburden overhang on the bending characteristics of the aquitard.

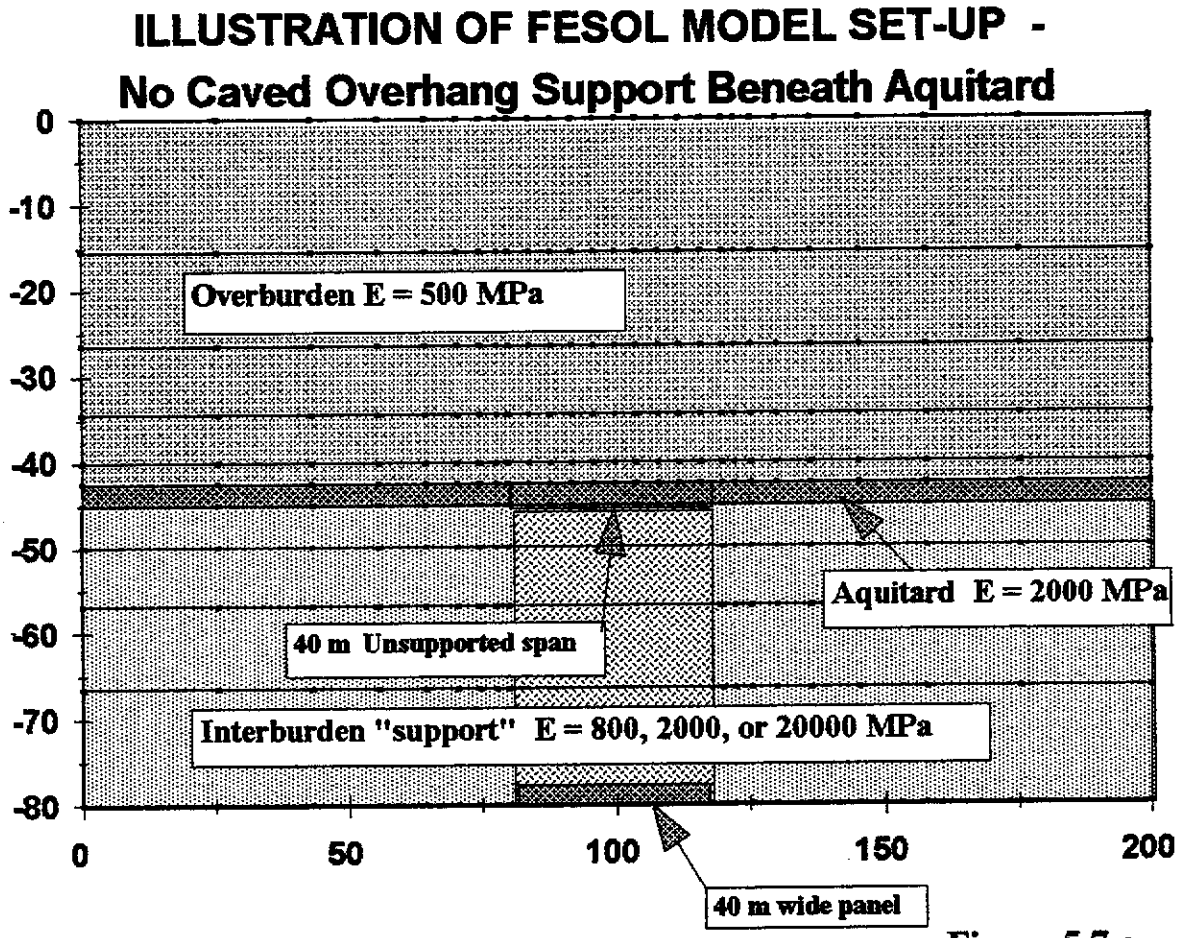

Figure 5.7 a

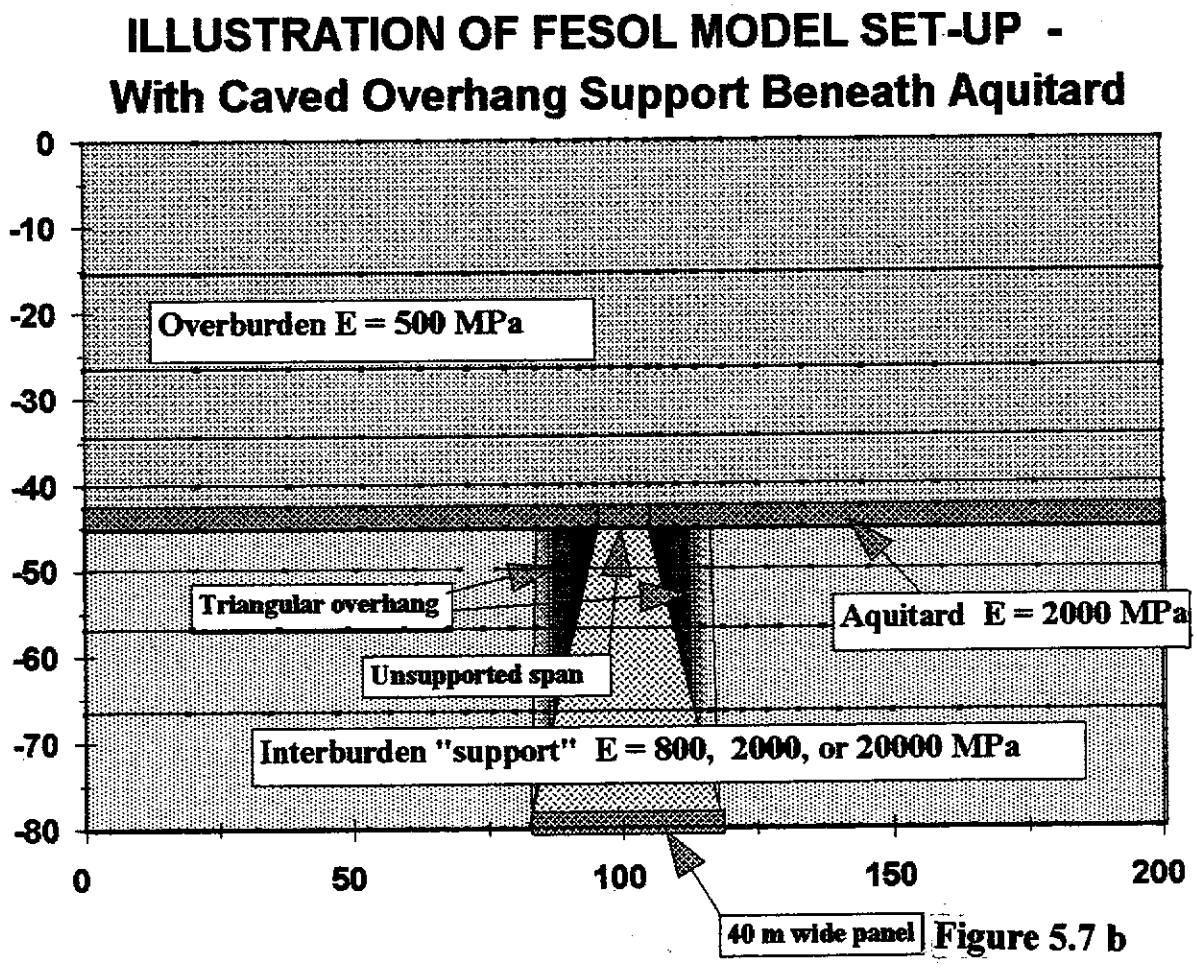

Figure 5.7 b

The first test incorporated three models, one with a 40 m wide panel and vertical caving (Figure 5.7 a), one with a 40 m wide panel and caved overhang (Figure 5.7 b), and another with a 70 m wide panel and caved overhang (similar to Figure 5.7 b). Comparison of the results from the first two 40 m wide models (illustrated in Figure 5.8 a) shows that the overhang firstly reduced the subsidence at the aquitard level by more than 50%, and secondly resulted in a flatter subsidence profile.

The combined effect would be to reduce the bending stresses on the aquitard, and thereby less potential for the aquitard to yield in tension. This effect of producing a flatter, or less curved profile is better illustrated with comparison of the latter two models, which both have an effective unsupported span of 40 m at the aquitard horizon. Although the aquitard subsides more above the 70 m wide panel (as would be expected), the apparent curvature across the resultant 40 m aquitard span in this model is less than that developed by the model with a 40 m span above a 40 m wide panel (with no caved overhang).

A similar "softening" of the subsidence trough is observed for models with more plastic interburden. Figure 5.7 b illustrates that for very stiff interburden, the subsidence trough is down-thrown steeply across the overhang, and in comparison the two more plastic models allowed the aquitard to sag more gently. It appears that the overhang, though not providing massive support for the aquitard (seen by the additional 40% subsidence in the 70 m wide panel), provides a "softer" and wider base at the span abutments from which the aquitard can subside more gently.

Nonetheless, if it is assumed that the mechanical properties of the aquitards and underlying material in the Collie Basin are reasonably consistent (at depth), then the parameter which essentially determines the integrity of aquitards is the length of the unsupported aquitard beam. Therefore the philosophy of panel design for maintaining aquitard integrity was to restrict the panel width so that the "unsupported span" of the protective aquitard (as illustrated by Figure 5.9) does not exceed its critical width.

After devising this concept, a comprehensive literature search of this subject was undertaken. It was found that a similar span concept had been developed by Galvin (1981). Galvin's work included an investigation of the effects of the spanning of strong, thick layers of dolerite above total extraction panels in the South African coalfields.

EFFECT OF CAVING OVERHANG SUPPORT ON AQUITARD SUBSIDENCE

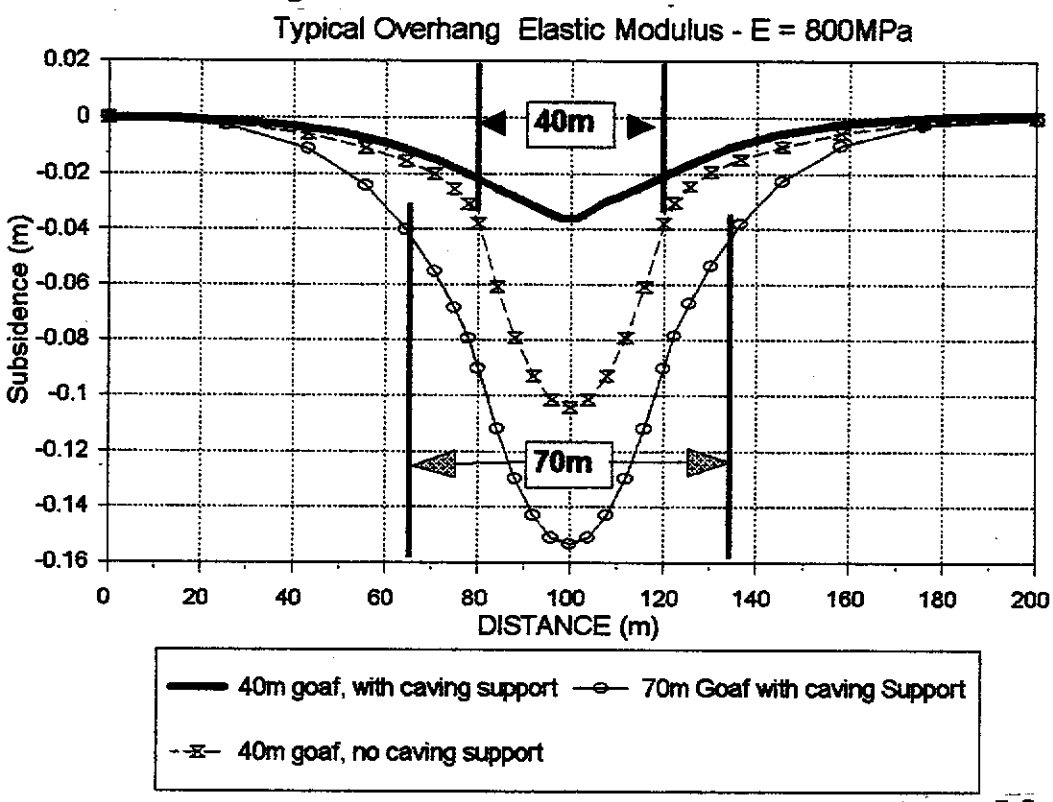

Figure 5.8 a

EFFECT OF CAVING OVERHANG MODULUS ON AQUITARD SUBSIDENCE

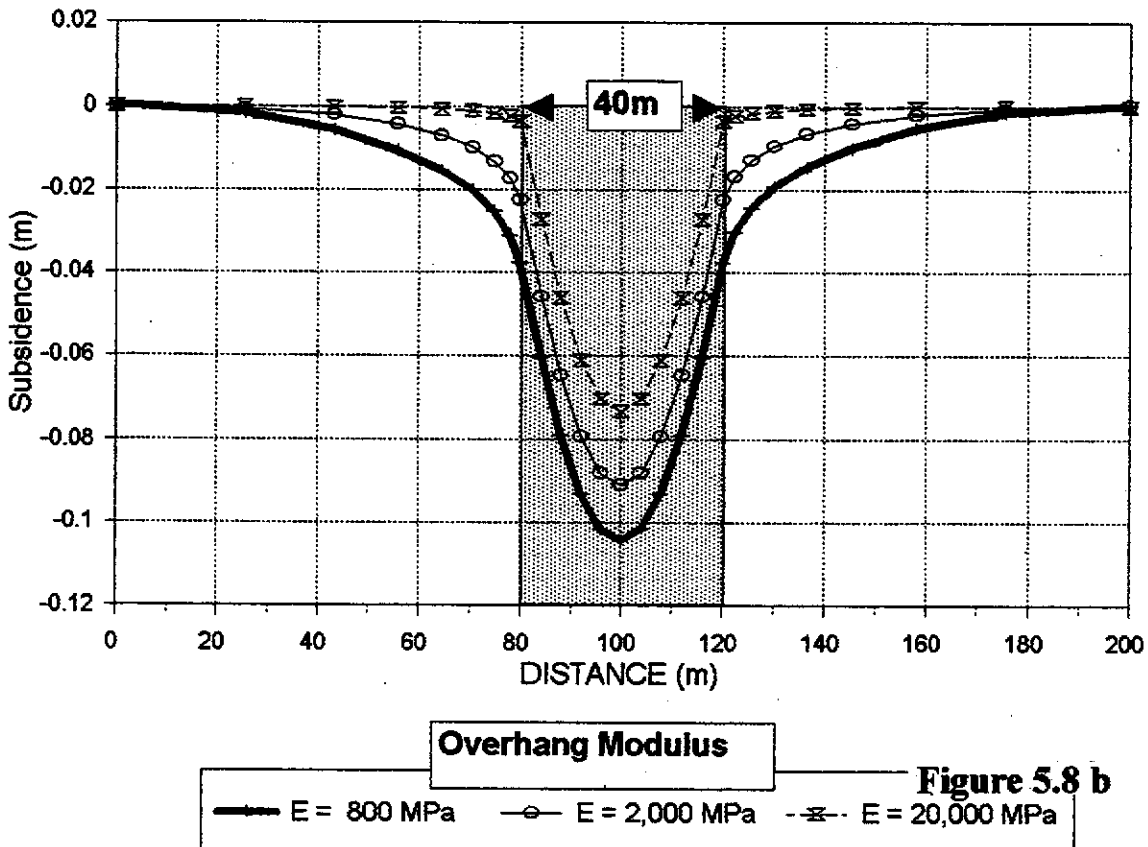

Figure 5.8 b

ILLUSTRATION OF THE UNSUPPORTED AQUITARD SPAN CONCEPT AND AQUIFER DRAINAGE

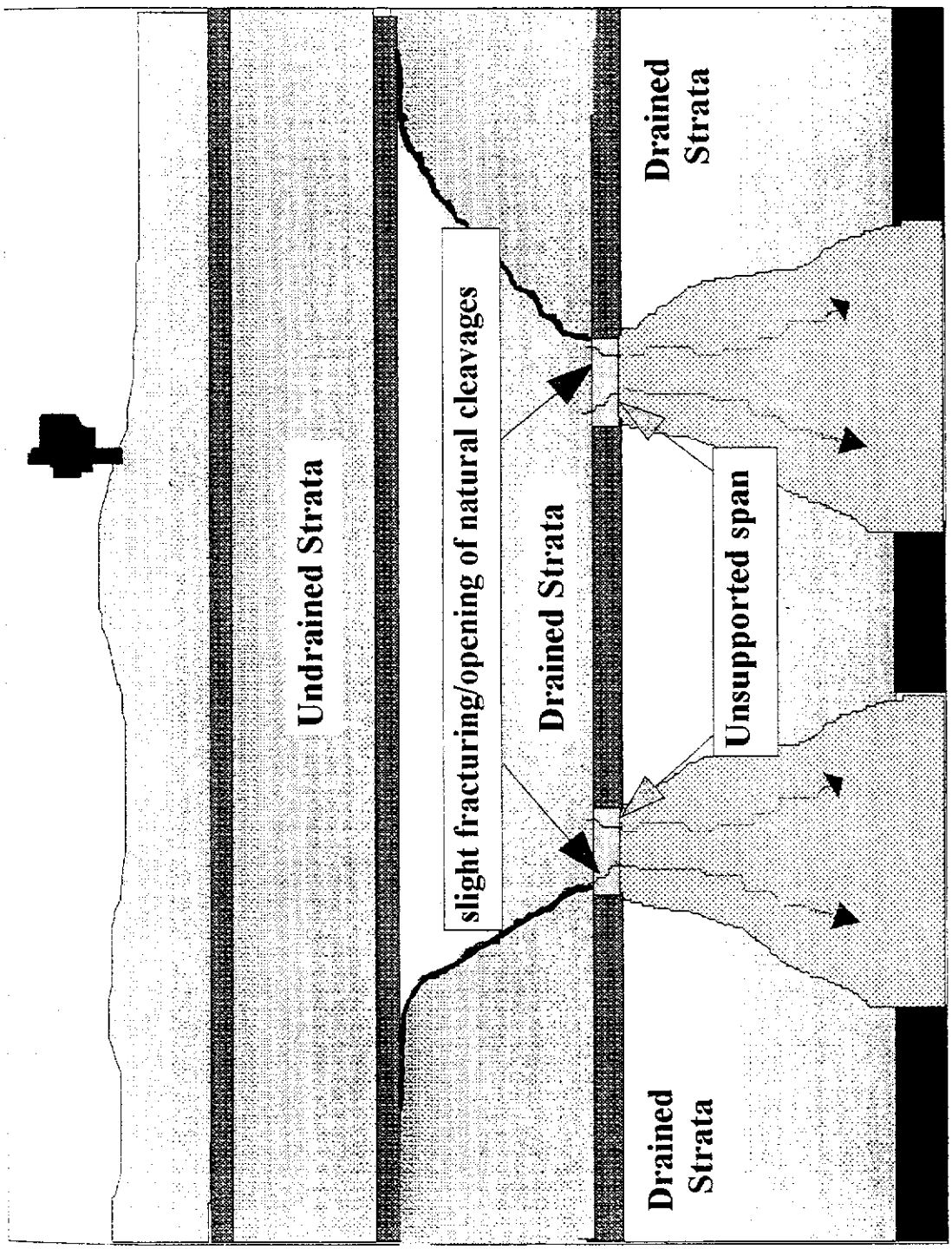

Figure 5.9

Thick dolerite sills were found to be able to bridge across collapsed ground developed from coal extraction, and form spans up to several hundred metres wide. These large spans would then induce very high on-seam stresses - at the abutments - which had a significant impact on the productivity of the mines. In some cases the associated problems were forcing collieries to adopt less efficient bord and pillar mining techniques.

Galvin concluded that total extraction mining was possible beneath such thick sills, provided the width of the mine panel was sufficiently large to ensure that the spanning limits of the sills were exceeded, thus inducing total failure of the bridging beams/plates of dolerite.

Galvin proposed that the minimum width of mining required to induce failure of the dolerite could be estimated from the following equation:

$$\text{Design panel width} = \sqrt{[1165t_D - 935 . \frac{t_D^2}{D_D}] + 2t_p \text{Tan}(\beta - 90)} \text{ (m).} \qquad 5.1(1)$$

where: t_p = interburden thickness between the base of the sill and the mine,

(D_D) = depth of the base of the dolerite below surface,

t_D = the thickness of the dolerite sill, and

(β) = caving angle.

Once failure had been induced, Galvin found that normal subsidence stress conditions prevailed for the remainder of extraction.

No attempt was made by Galvin to quantify this concept in terms of prediction of mining subsidence or aquitard integrity. It has been assumed that, as water ingress would obviously impact on mine production rates and profitability, subsurface aquifers were either not of concern or not present in these South African coalfields.

For interest, if the results and model parameters from centrifuge test PS01 are applied to Galvin's equation for estimating the maximum effective span of a dolerite sill the expected maximum effective span (Seff) for a "sill"/aquitard 7 m thick and 26 m below the surface is:

$$\text{Seff} = \sqrt{\{1165(7) - [935(7)^2/(26+7)]\}}$$

$$= 82 \text{ m, almost twice the PS01 test value (44 m).}$$

If the typical thickness of coal and cannel coal in the Alpha seam aquitard - 2.4 m - is substituted in the above equation, the design dolerite span equates to 51 m, which is far greater than the yielding spans observed in the field (5 to 10 m). It must be noted that this approach has been used by Galvin to establish the point of total rupture of the bridging beam to allow full subsidence development. For this research study, it is more important to establish the point when the aquitard loses its sealing properties.

Historical evidence in the WCL open cut highwalls (personal experience) indicated that over time, an unsupported aquitard span in excess of 5 m began to develop open cracks along cleavage planes, and that a 10 m span always led to failure of aquitards of similar thickness to those above WCL's underground mines. This practical evidence is supported by the results from the computer modelling package SUBSOL which was "successfully" calibrated to represent Collie Basin **surface** subsidence and on-seam stresses. During calibration of SUBSOL (detailed in Section 4.1) it was found that Collie Basin subsidence characteristics, were best represented when the iterative failure criterion was set to the development of an unsupported aquitard span one or two full elements wide. In the case of the ACIRL panel it was 2x3 m wide elements, which effectively allowed for limiting spans between 6 and 8 m to develop in the model before "failure" occurred. For 1North and 2SA panels, the allowable limit was 1x5 m wide element, which represented a limiting span between 5 and 9 m width.

Interestingly, field data suggests that the "unsupported span" concept can be applied to all aquitards above the mine horizon and does not only apply to the first bridging aquitard with caving immediately beneath. For example, piezometric water levels and panel-water pumpage rates measured during the extraction of Red panel, illustrated in Figures 5.10 and 5.11, suggest that as the width of extraction increases, the number of aquitards and aquifers rupturing also increases. (Aquitard rupture is inferred by the changes in water head in each aquifer.)

RED PANEL AQUIFER WATER LEVELS

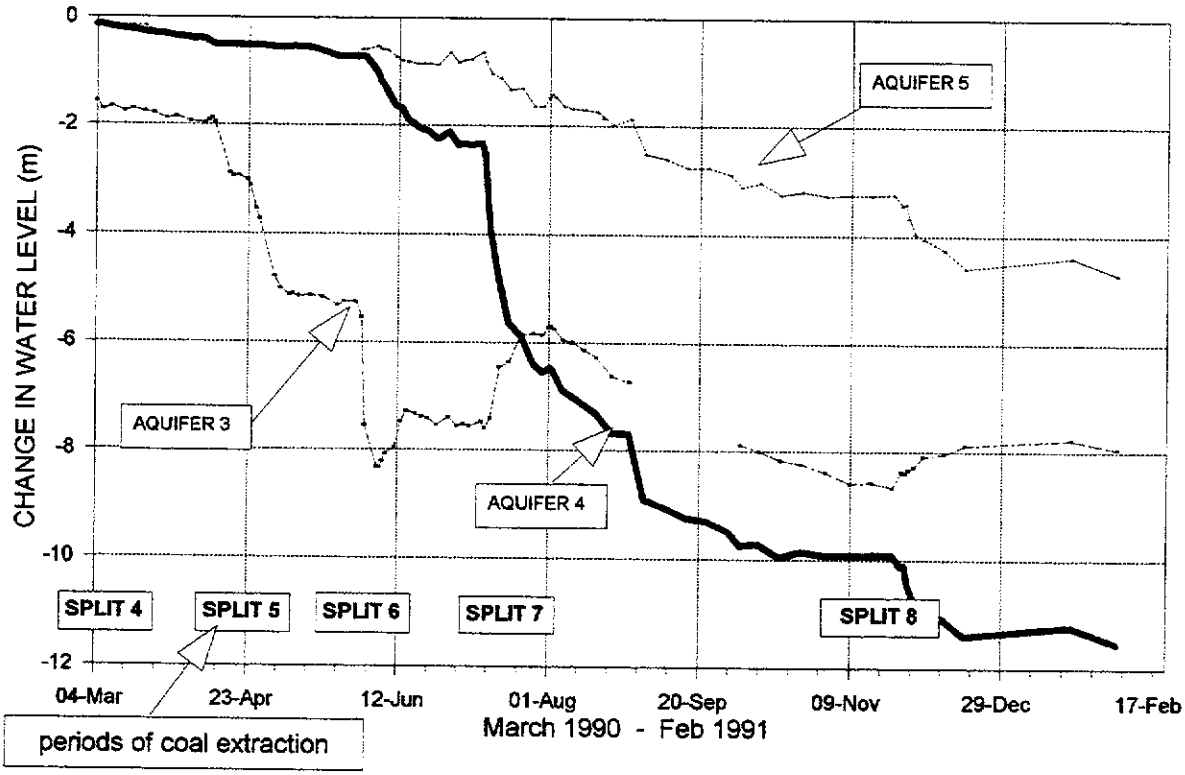

Figure 5.10

RED PANEL WATER MAKE

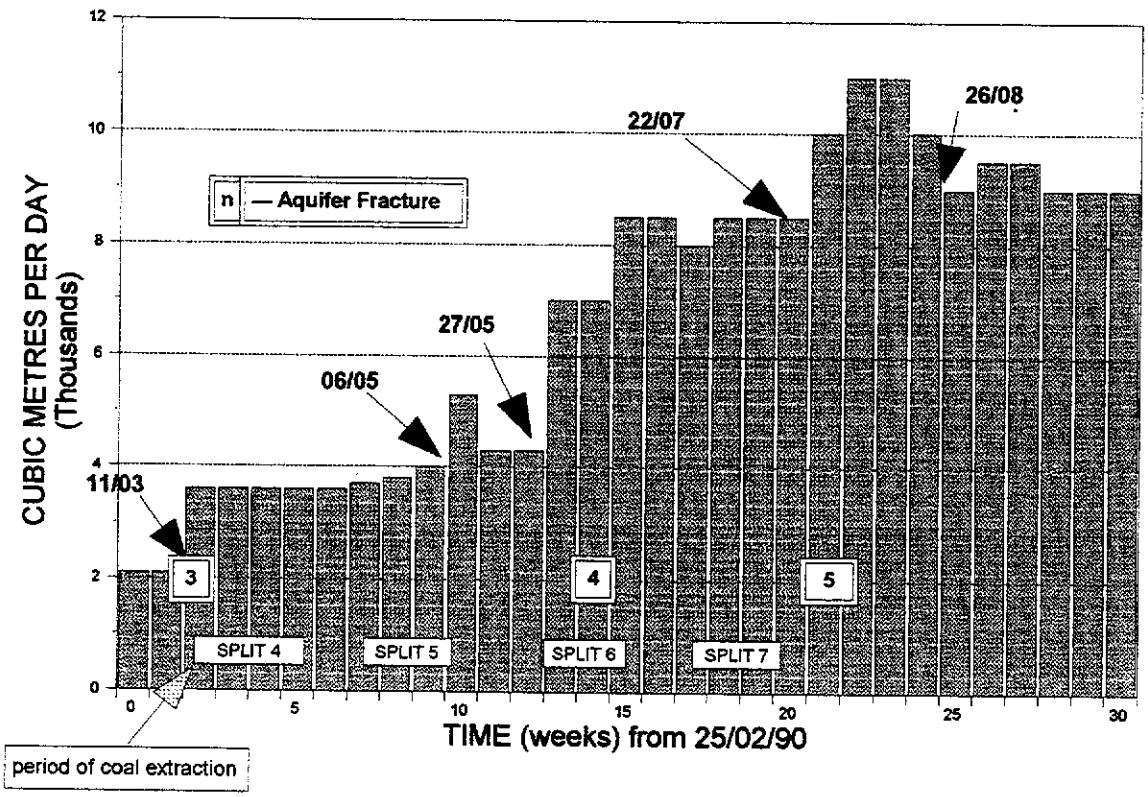

Figure 5.11

The following relevant conclusions are drawn from the Red panel water monitoring data:

- The Alpha seam, at the base of aquifer 3, was ruptured after the mining sequence had developed two separate 40 m wide sub-panels (after Split 5 had been mined).
- The Upsilon seam, at the base of aquifer 4 cracked after the width of extraction in the second sub-panel reached 58 m (after Split 6 had been mined).
- The Collieburn #1 seam at the base of aquifer 5 became "slightly leaky" when the second sub-panel reached 58 m width (although it is possible that some of the drop in water level was due to the lowering of the ground mass) and began to show significant signs of rupture after the width of the second sub-panel had reached 78 m (after Split 7 had been mined). No discernible effects could be detected by the mining of split 8, which increased the extraction width to 100 m. Note that, due to mining problems, long sections of fender coal were left from split 8 which has probably retarded caving.

Assuming that an "unsupported span" of 5 m (developed according to the angle of shear - 23° - measured from the vertical, from the panel edges) is required before the aquitards begin to rupture, the design extraction panel widths to maintain sealing characteristics of aquitards are calculated as:

$$W_{ext} = 2h.Tan\ (\propto) + 5 \qquad 5.1(2)$$

where $\propto$ = angle of shear (23°), and

h = height of aquitard above the panel.

Given that the respective distances to the top of each protective coal aquitard located sequentially above Red panel are 33, 63, and 86 m, the design extraction widths would equate to 33 m for the Alpha seam, 57 m for the Upsilon seam, and 78 m for the Collieburn #1 seam.

Each of these design widths compare well against the field observations (see Figure 5.10); the Alpha seam aquitard rupturing after 40 m, the Upsilon seam aquitard losing its sealing properties after 58 m, and the Collieburn #1 seam becoming leaky after 78 m of extraction. This was considered to be a very positive result, however, there was concern that the increment in panel width is relatively coarse (by mining up to 20 m wide fender/splits) for back-analysis purposes. It was possible that aquitard rupture may have also occurred at slightly narrower widths of extraction.

For cross-checking purposes, the only other panel with reliable mine water data was ACIRL panel. However,because the aquifers immediately **above** this panel were essentially drained (the source of the water-make in ACIRL panel was from recharge points at each aquifer horizon immediately down-dip from the panel), identification of aquifer responses by piezometric recording was not feasible. Cross-checking was therefore attempted by comparing the aquifer response/mine water pumpage relationships for Red Panel, with the pumpage rates from ACIRL Panel. It was considered that the timing of aquitard rupture could be roughly estimated from the pumpage rates alone.

The mine water pumpage data used for this back-analyses was taken from the report by Hebblewhite and Humphreys (1988), which provided a graph of the pumpage rates versus time in relation to periods of fender extraction (Figure 7.25 in that report). Table 5.2 summarises the sequencing of increasing mining width, mine water-make and interpreted aquitard response from both ACIRL and Red Panels. The data beneath the column titled 'Interpolated Aquitard Rupture' in Table 5.2 represents the aquitards interpreted as being ruptured after the mining of each split. The last column positions the intercept of the two lines of shear that extend from each panel abutment, thus reflecting the vertical position where an "unsupported span" would begin to be developed.

TABLE 5.2 WATER MAKE FROM ACIRL & RED PANELS

Split #	Effective Mining Width (m)		Additional Water Make(m^3/day)		Interpolated Aquitard Rupture		Height of projected shear angle(m)	
	ACIRL	Red	ACIRL	Red	ACIRL	Red	ACIRL	Red
1	18	20	0	0	2	2	21	24
2	31	40	600	200	2,3	2	36	47
3	44	-	600	200	2,3	2	53	47
4	57	40 + 20	1200	1700	2,3,4	2,3	68	47
5	70	40 + 40	1800	2200	2,3,4,5	2,3	83	47
6	75	40 + 60	1800	6000	2,3,4,5	2,3,4	88	71
7	75	40 + 80	1800	8000	2,3,4,5	2,3,4,5	88	94
8	75	40+80 +15	1800	7000	2,3,4,5	2,3,4,5	88	94

[Note that: Extraction in Red panel was accomplished by two-way lifting off each split (in 20 m wide increments), whilst one-way lifting was used in ACIRL panel (13 m wide mining steps). Due to mining problems, Red panel was effectively mined in three discrete sub-panels, each separated by unmined strips of coal fender. The total post-mining water make was 4900 m^3/day in ACIRL panel and 9000 m^3/day in Red panel.]

The following listed points represent the most significant observations made from of the above data:

- When the length of extraction advance in ACIRL panel reached the width of sub-panel A (75 m - after split #6 was mined), the volume of mine water make levelled out even though the length of extraction was still increasing. This observation supports the use of the minimum dimension of any panel to determine the integrity of a bridging aquitard.
- The differences noted between the volumes of water make in each panel is attributed to the fact that the aquifers above ACIRL Panel were largely dewatered prior to the commencement of extraction.
- The widths of extraction responsible for initiating aquitard rupture in ACIRL panel do not appear to completely match the above design criterion. Alpha seam (~29 m above the workings above ACIRL panel) is interpreted to have ruptured after the width of extraction reached 31 m, Upsilon seam (~48 m above) ruptured at 57 m goaf width, and Collieburn 1 seam (~81 m above) yielded at 70 m width. The above design criteria [Equation 5.1 (2)] estimates that the maximum allowable panel widths are 30, 46, and 74 m for each aquitard respectively. It appears, therefore, that a more suitable design criterion is:

$$W_{ext} = 2h.Tan\ (\propto) + 0 \qquad 5.1(3)$$

In the Collie basin, Equation 5.1(3) can be reduced to:

$$W_{ext} = 0.85h \qquad 5.1(4)$$

Therefore, the respective design limits for each aquifer correspond to 25, 41, and 69 m.

This (zero span) design criterion is further supported by observations made during the centrifuge test PS07 where it was seen that the edges of the caved overhang below the first bridging aquitard tended to crush (see Figure 4.52), thus increasing the effective width of the "unsupported span". The crushing of the overhang material did not appear to develop in other tests when the projected lines of shear from each panel edge intersected below the position of the bridging aquitard.

The influence of the position of the line of caving on subsidence is made more apparent when compared against extensometer anchor movements at varying heights above the seam (as in Figure 3.45 a). It has been interpreted that the maximum separation between a point on the surface and a point/anchor immediately below occurs when the position of the line of shear is coincident with the position of the anchor point. It would be expected that if the aquitards were bridging across the goaf to any great extent, the form of the U-shaped curve in Figure 3.45 a would be flatter at the base and shifted to the right.

Although the literal application of the term "unsupported span" is questionable for coal aquitards further above the mine (it was inferred from centrifuge testing and field data that there was no bed separation above the first aquitard above the mine), the design terminology has been kept as it is a simple concept to visualise.

Therefore the design width of extraction of the sub-panels in relation to the Alpha seam, 33 m above the NWB3 test Panel was:

$$33 \times 0.85 = 28 \text{ m}$$

It follows that if the width of extraction is designed so that the closest aquitard remains intact, then all higher aquitards must, by default, remain intact and can therefore be ignored for panel design purposes.

As mentioned previously, the resultant geometry of the test panel was governed to a large extent by previous mining in the area. Further design restrictions were imposed by the need to satisfy management's production requirements which were dependent on mining 6 m wide "splits" with 7 m wide "fenders" lifted on either side of each split.

Consequently, the trial panel design incorporated five individual 40 m (2 x 20 m) wide sub-panels, each separated by 20 m wide intra-panel pillars.

Because the planned 40 m wide sub-panels exceeded the recommended design width of 28 m by more than 40%, the author included drainage and sump facilities into the panel design to accommodate the expected inflow of groundwater into the workings from aquifer 3. No water ingress was expected from aquifer 4 as the design criteria for this aquitard allows for a 54 m wide sub-panel which is significantly greater than the designed 40 m wide sub-panels.

Application of this design approach to case studies at Wistow Colliery (Bigby and Osram, 1988) suggest that the angle of shear above three separate 45 m wide panels, when water infiltrated the mine from an aquifer approximately 80 m above, is in the order of 16°. When the width of extraction in subsequent panels was reduced to 40 m, there were no further inrushes of water. A similar angle of shear can be interpreted from Klenowski and Phillips (1988) above the Central Colliery in the Bowen Basin. This publication reports that water inrush occurred after the 200 m wide panel had advanced 40 m. The height of the closest aquifer was 70 m above the mine. The author considers that although these angles of shear are not unreasonable, it is not known whether the difference in apparent shear is due to the effect of longwall mining removing 100% of coal compared to 85 to 90% in Wongawilli extraction.

Comparison of the NCB and Collie Basin aquitard integrity prediction methods. The requirement for the site specific aquitard span design criteria can be illustrated by comparing the allowable panel widths determined from the critical span method with that from the more commonly used NCB method.

To be consistent with the local conditions, the Collie Basin profile function [Equation 3.1(7)] has been substituted for the empirical subsidence prediction nomogram used in NCB design method (using the NCB, 1966 publication as suggested by Bigby and Osram, 1988). The concomitant strains have been calculated by double differentiation of the profile function and application of the curvature/strain relationship derived for the Collie Basin, as described in Section 3.1 (using Equations 3.1(11) and 3.1(13) respectively). It follows that by using the Collie Basin approach, panel design

can be based on either the limiting horizontal strain (2 mm/m), or the subsidence profile curvature which gives rise to this limiting strain. The limiting curvature can be calculated from Equation 3.1(13), where it can be seen that the limiting strain of 2 mm/m is reached when the modified NCB-type subsidence profile curvature is:

$$2 = 8\,(\text{curv.} \times 10^4 \div 4)^{0.6}$$

$$\text{i.e. } (\text{curv.} \times 10^4) = [0.25 \times (4^{0.6})]^{1.67} \qquad 5.1(5)$$

$$\text{curv.} \times 10^4 = 0.4\ m^{-1}$$

The use of a curvature design criteria will reduce the design procedure by one step. However, the value of limiting curvature is less obvious to the design engineer than a limiting strain. Limiting strain has been used in this case.

The allowable panel widths predicted from the two methods for hypothetical aquitards at 30, 60, 100 and 200 m above a mine with a 2.6 m mining height and 85% extraction are presented in Table 5.3.

TABLE 5.3 COMPARISON OF DESIGN WIDTHS OF EXTRACTION USING THE MODIFIED NCB AND CRITICAL SPAN DESIGN METHODS.

	Allowable Panel Widths (m)			
AQUITARD HEIGHT (h) >>	**30 m**	**60 m**	**100 m**	**200 m**
Modified NCB Profile design method >>	5	15	32	91
Critical Span design method >>	25	51	85	170

The results provided in Table 5.3 indicate that:

- The critical span method allows for greater widths of extraction than the modified NCB method.
- In deeper panels, the difference between the two methods reduces. This is because the NCB method relies on the W/H ratio at the aquitard surface; the greater the depth (H), the less the subsidence for any given width. It is considered that this observation represents a possible flaw with the critical span method, as it

it is possible that the shape and extent of shearing also changes at heights greater than 90 m above the mine. (Note that the critical span method has been verified to approximately 90 m above Red panel.) However, with the relative close proximity of aquifers above areas proposed for mining in the Collie Basin, the critical span method will always allow for greater widths of extraction.

It is also interesting to note that, if the NCB (1966) design criteria are used instead of the Collie Basin criteria in the modified NCB approach, the subsidence generated by the allowable widths of extraction, as defined by the critical span method, would be expected to develop maximum strains of 42, 21, 13 and 6 mm/m for the 30, 60, 100 and 200 m high aquitards respectively. This further illustrates the effect of increasing depth/height, and indicates that the design criteria for the NCB method should change with height above the seam.

One obvious difference between both design approaches is that the critical span method, as it currently stands, does not take into account the effect of variable mining extraction height. This does not have a significant implication for WCL, however, as the mining methods used in Collie allow for a maximum mining height of less than 3 m, and a minimum height of around 2 m. The typical height of extraction is 2.6 m, which is what the design method has been based on.

It is therefore considered that the unsupported span concept is appropriate for the Collie Basin conditions.

B. Establish the **minimum intra-panel pillar widths**

The intra-panel pillars need to be of sufficient width to withstand elevated superincumbent loads resulting from extraction on either side. Two modes of pillar collapse have been identified; firstly collapse of the coal itself, and secondly collapse of the column of sandstone formed above the coal pillar by caving on either side (similar to that illustrated in Figure 2.13 c & d). If the intra-panel pillar support "system" was to collapse by either mechanism, there would be an increase in final subsidence which could damage superimposed surface and subsurface features. Additional subsidence

could also result if the intra-panel coal pillar abutment loads were to exceed the roof or floor materials' bearing capacity causing the pillars to "punch" into the roof or floor strata. The intra-panel pillars must therefore be designed for long-term stability for the whole "pillar system".

Firstly, a suitable design Factor of Safety had to be adopted for the design of the intra-panel coal pillars (FOS_{ipC}) which ensures the required long term stability of the complete pillar support system. It has been shown in Section 2.5.5.1 that the design Factor of Safety of standard coal mine pillars (FOS_C), given by Salamon and Oravecz (1967) for South African coalfields is:

$$\mathbf{FOS_C} = \mathbf{Pillar\ Strength/Pillar\ Load} \qquad 2.5(7)$$

$$= \mathbf{1.6}$$

Using a modified Salamon/Hustralid/Munro/Wagner strength criterion, the pillar strength **(PS)** is calculated by:

$$\mathbf{PS} = k \times (Weff/Wo)^{0.46} / (Mh/Mho)^{0.66} \quad (MPa) \qquad 2.5(8)$$

where: **Wo**, **Mho** = 1 (m), **Wp** = Pillar width (m)

k =compressive strength of 1 m^3 of coal - 6.5 MPa (Misich & Humphreys, 1988),

Weff (effective pillar width) = **4 x Ap/Cp** (m) (Wagner, 1980), 2.5(10)

Ap = Pillar area (m^2), **Cp** = Pillar circumference (m), and

Mh = Mining height (m).

The pillar load **(PL)** is calculated by the tributary area theory, which, for bord and pillar workings can be simplified to:

$$\mathbf{PL} = \sigma 1\ (1\text{-extraction ratio}) \quad (MPa), \qquad 2.5(9)$$

where: **σ1** = vertical load due to gravity.

However, for pillars in development entries in between extraction panels, the tributary load is represented by the area of uncaved strata above the panel, as illustrated by Figure 4.48.

For these pillars, Salamon and Oravecz recommend that a FOS_{ip_c} of 2.0 be adopted. (Though the exact reasoning for the higher FOS for the intra-panel pillars is not provided by Salamon and Oravecz.) As it has been established (by Misich and Humphreys, 1988, and through numerous panel designs done by the author) that the design FOS_C to prevent collapse of coal pillars developed from standard bord and pillar workings in the Collie Basin was also 1.6 (Section 2.5.5.1), it is also concluded that it was reasonable to assume a FOS_{ipC} of 2.0 for the collie Basin.

In the trial case study, because pillar width was predesigned to be 20 m, it was necessary to check that the corresponding FOS_{ipC} - again using Equation 2.5(7) - met the proposed design limit of 2.0. The pillar load and strength of the 20 m wide intra-panel coal pillar was calculated using Equations 2.5 (8) and 2.5 (9).

Using this approach for the trial case study, the calculated FOS_{ipC} (for 20 m wide, 100 m long intra-panel pillars with 40 m sub-panels on either side) was 2.1 which was accepted as being adequate for preliminary design.

It is also necessary to design the coal pillar to have sufficient bearing area so as to prevent failure of the roof and floor material. The design criterion adopted for the Collie Basin sediments was a modified Terzaghi/Hansen formula (Scott, 1980, and Stacey & Page, 1986) with a design FOS against bearing failure (FOS_B) of 3.0; established by Misich (1985)[2]. The FOS_B is calculated by:

$$\mathbf{Qult/PL} \qquad 2.5(12)$$

Where:

$$\mathbf{Qult} = \mathbf{c.N_c} + \mathbf{q_o.N_q} + \gamma\mathbf{.0.5.Wp.N_\gamma}, \qquad 2.5(11)$$

c = cohesive strength kPa, and

$\mathbf{N_c}$, $\mathbf{N_\gamma}$ & $\mathbf{N_q}$ are functions dependent on frictional properties of roof or floor material.

In the case study, with floor material properties (being the weakest), of c = 700 kPa and angle of internal friction = 30°, the resultant FOS_B for a 20 m wide intra-panel pillar is well in excess of the design limit of 3.0 for bearing failure, which further supported the use of 20 m wide intra-panel pillars.

As noted in Figure 5.1 the final configuration of the extraction panel was altered from the original design due to problems with the stability of an intersection after it was stripped to better align the belt bord. The result was this split was not mined and the lifting sequence was shifted along by 20m. This lateral shift then placed the last intra-panel pillar mid-point to where a 5.0 m wide return airway had already been mined through the lower section of the panel. This effectively reduced the pillar to two separate 7.0 m wide strips. Using the design criterion above, the estimated strength of a 7.0 m wide pillar is 11.6 MPa [from Equation 2.5(8)] and assuming tributary loading (as illustrated in Figure 4.48, but with caving on only one side of the pillar), the pillar stress is 8.0 MPa. This equates to a FOS of 1.4, which is slightly lower than the acknowledged FOS_c of 1.6 and much less than the previously accepted FOS_{ipc} of 2.0. However, it was considered that providing the roof above the return airway was suitably supported to prevent roof collapse/primary caving (and exposure of the sandstone), the effective width of the sandstone column is maintained at 20 m and would thereby meet the design FOS_{ipc}.

In regard to bearing failure below the pillar, the FOS_B calculated for a 7 m wide pillar was approximately 2.9, which is marginally acceptable for normal design purposes.

Another influencing factor on the design of the NWB3 Panel was that the WD-6 mine and open pit haulroad were scheduled to close (due to diminishing reserves) within, at the most, two and five years respectively. Very long term stability of the whole "pillar system" was therefore not required. Considering the temporary nature of the extraction panel and superimposed features, the slightly lower FOS_B and FOSc design parameters were accepted as being adequate.

The main concern with the middle roadway was that, should the immediate roof above the return airway collapse, it would predicate the development of a column of sandstone which could potentially collapse and thereby combine the caved areas above the last two sub-panels. After discussing the potential ramifications of roof collapse above the middle bord with WCL management, the author recommended that wooden crib supports ("pig-styes") be installed at 10 m intervals along the bord (as illustrated in Figure 5.12).

PHOTOGRAPH OF WOODEN "PIGSTYES" AND COAL RIBS ALONG THE BORD MINED THROUGH THE FINAL INTRA-PANEL PILLAR

a) wooden pigstyes

b)Rib spall (note the roof fall in the background)

Figure 5.12

5.2 NWB3 FIELD TRIAL RESULTS and DESIGN CRITERIA VALIDATION

In order to evaluate the success of the trial panel, a number of monitoring facilities were set up, as for previous panels. The installation of the monitoring devices and discussion of monitoring results are discussed below.

A novel approach was taken for subsurface monitoring above the NWB3 trial panel, whereby a single extensometer anchor and piezometer was installed within individual boreholes. Drilling in each of these boreholes was stopped once the hole had penetrated the top 1/3 of each targeted major aquitard. Anchors and piezometers were then installed at the base of each borehole and sealed off from higher aquifers using cement slurry so that each aquitard/aquifer could be specifically targeted and monitored. The anchor cable was isolated from the cement by placing it within 20 mm PVC over the full length of the hole (the pipe was resting on the anchor). The configuration of the monitoring bores is illustrated in Figure 5.13 a & b.

The main reasons for this novel installation process were:

- to maintain the integrity of the respective aquitards separating the four superimposed aquifers,
- to minimise drilling costs (in this way the comparatively inexpensive "HQ" reverse circulation drilling could be used rather than 6" mud rotary holes and the cementing process was straight forward and involved minimum rig down-time.)

Two sets of monitoring bores were installed, the first was above sub-panel one, the second above sub-panel two. The sub-panel two monitoring bores were installed to check for variation in ground response between successive panels, and/or if there was any interaction between the sub-panels. Piezometers were not installed in duplicate in each sub-panel because of their close proximity. Any change in piezometric heads due to fracturing of the aquitards above sub-panel 1 would be duplicated simultaneously by piezometers above the second sub-panel. The location of each monitoring borehole is illustrated in Figure 5.1.

CONTRUCTION OF MONITORING BORES ABOVE SUB-PANEL #1 NWB3 PANEL

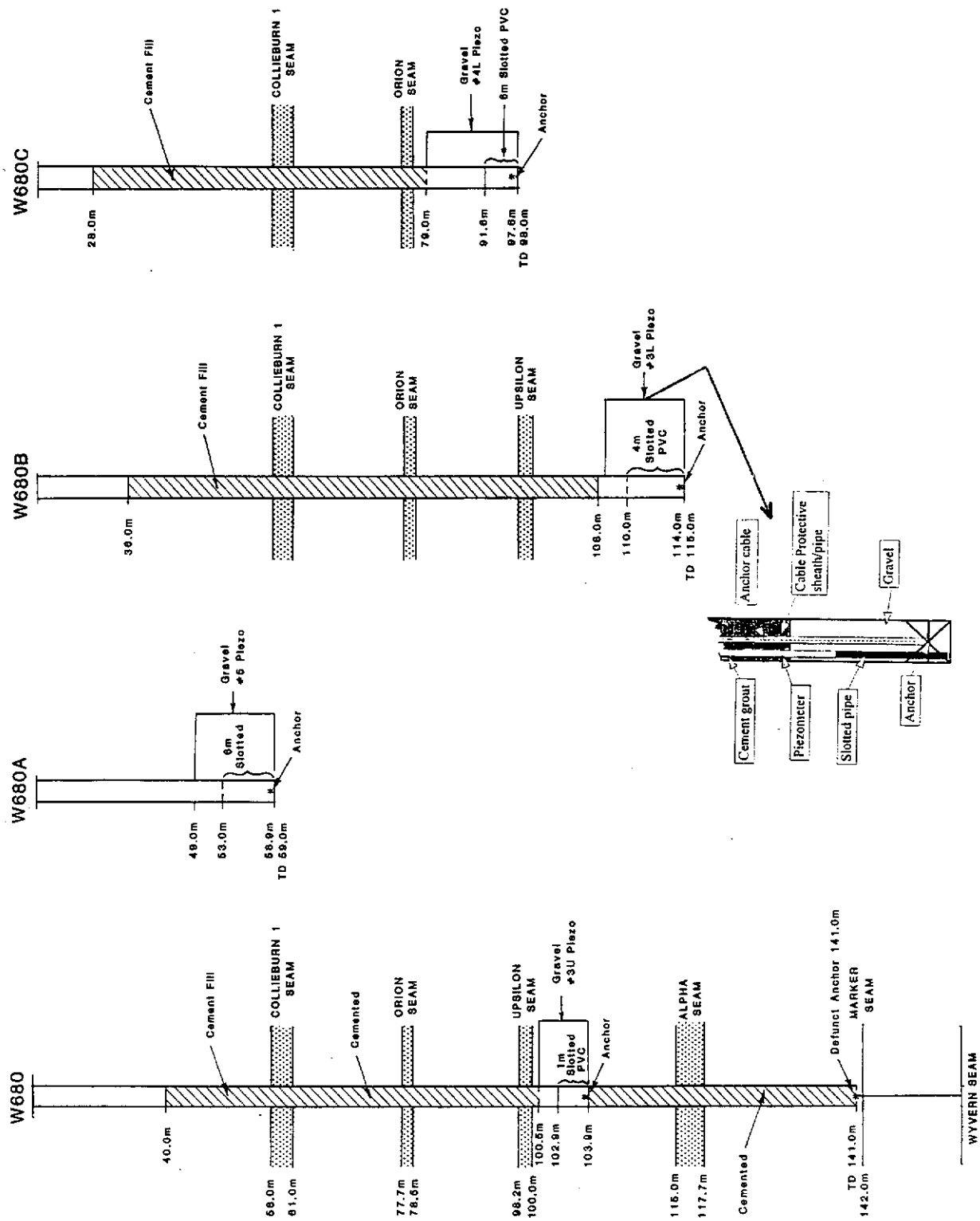

(NOT TO SCALE) **Figure 5.13 a**

CONTRUCTION OF MONITORING BORES ABOVE SUB-PANEL #2 NWB3 PANEL

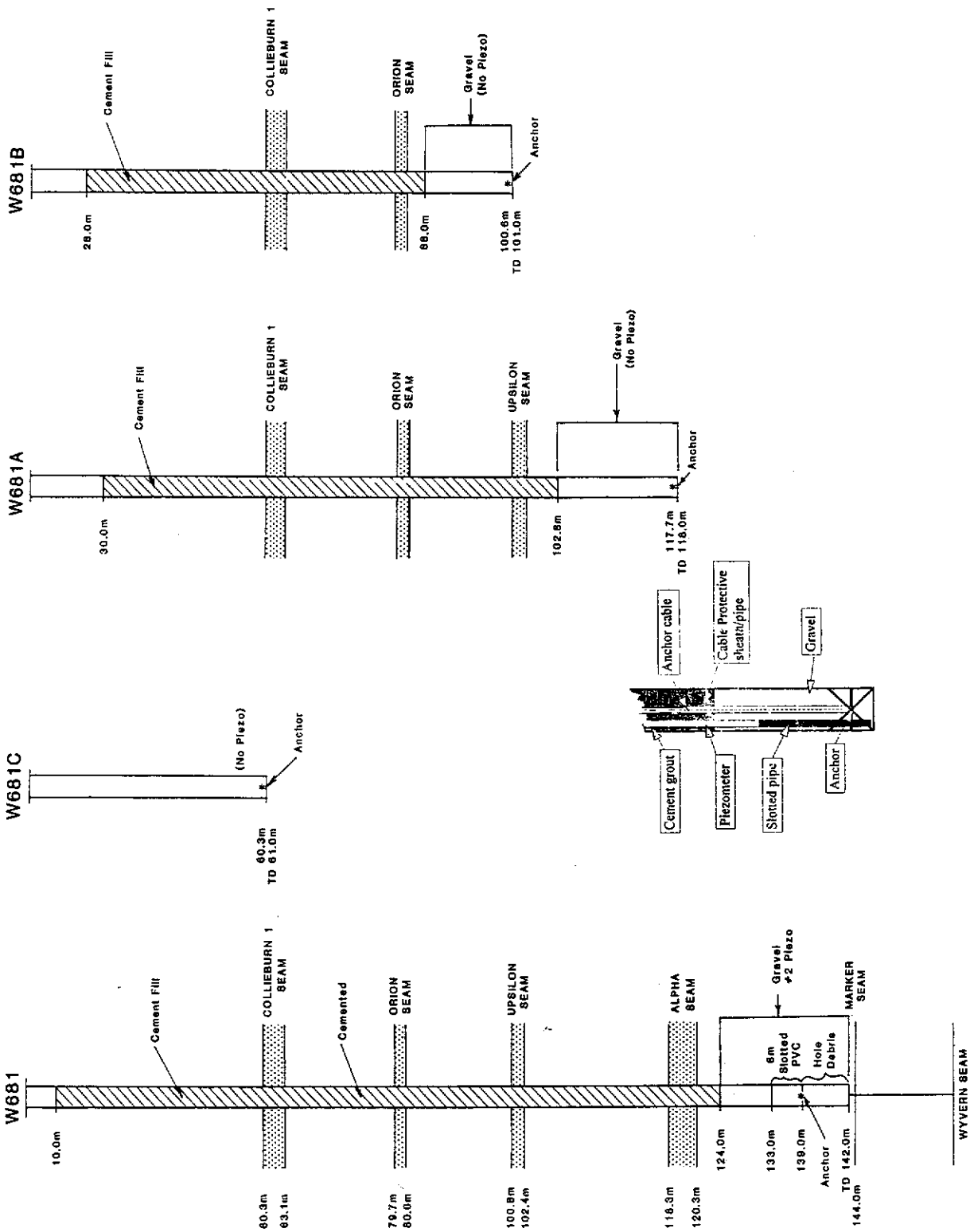

(NOT TO SCALE) **Figure 5.13 b**

Water levels and anchor movements were measured at daily intervals during periods of "lifting" and at weekly intervals during split development. Water measurements were made using a standard, manually operated, tape dip-meter which emits a high pitched noise when the sensor contacts water, completing an electrical circuit.

Extensometer movements were also recorded manually by measuring the distance between the base of the 10 kg weight (connected to each extensometer anchor by 7 by 7 strand stainless steel wire cable) and a datum point. In order to simplify measurement, the wire cable was placed over a pulley, as in all other extensometer installations used previously, see Appendix II.

A line of surface subsidence survey stations (1.4 m long star-pickets at 20 m intervals) was also installed above the panel. These star pickets were not installed to previous standards because of the expected minimal subsidence, rather they were hammered either to refusal or to 0.5 m above ground. Each picket was surveyed immediately prior to subsequent "lifting" of each split in the sub-panels.

The monitoring data retrieved from this trial panel are presented in Figures 5.14 and 5.15. The main observations made from this data and from within the mine are listed below:

- There were no signs of deterioration of the coal haulroad at any stage during or after mining.
- Surface subsidence has been limited less than 50 mm, which is only marginally above the standard error resulting from seasonal fluctuations of the ground surface and survey accuracy.
- Water ingress into the mine was kept below 600 m^3/day (apart from a three week period when water inflow reached 630 m^3/day, Figure 5.15). This constant flow rate was first reached after the extraction of the second sub-panel; most of this water has been interpreted to have come from aquifer 3.
- From Figure 5.15, it appears that aquifer 3 groundwater leaked through the Alpha seam after the extraction of sub-panel 1, representing an extraction width of 40 m.

SURFACE SUBSIDENCE NWB3 PANEL WD6 AT THE COMPLETION OF EACH "SUB PANEL"

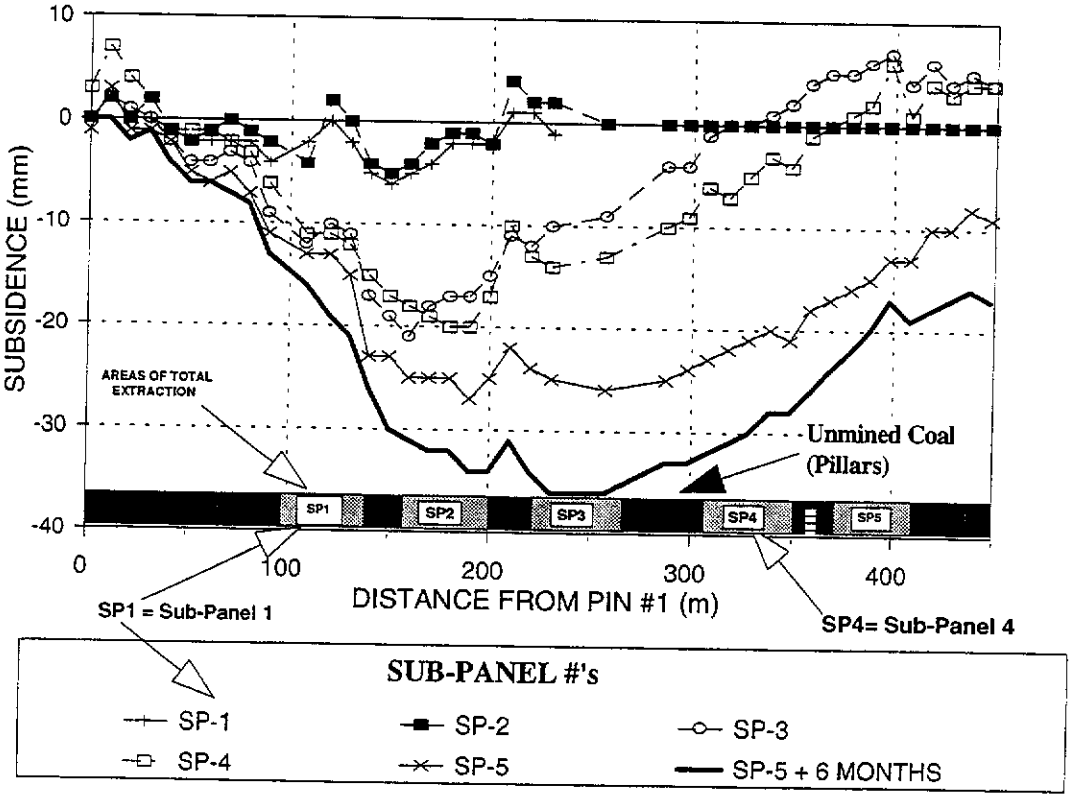

Figure 5.14

CHANGE IN SWL-PIEZOMETER W680/681 AND MINE WATER MAKE - NWB3 PANEL WD6

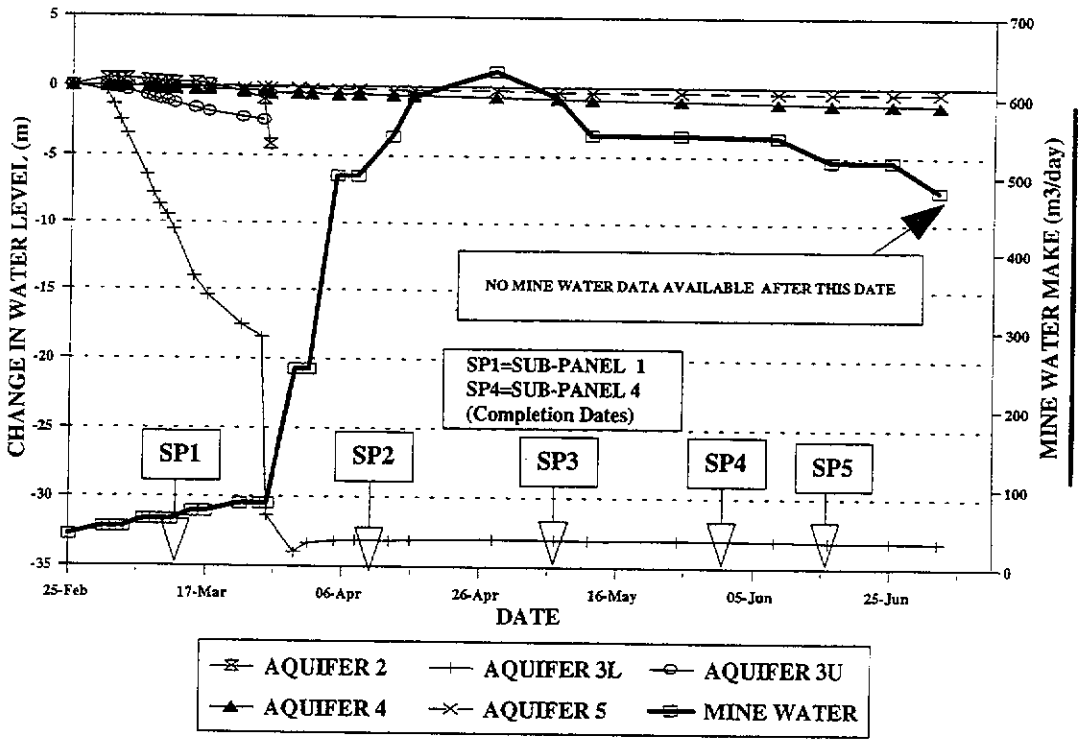

Figure 5.15

- It is apparent that the point of "rupture" of the Alpha seam's water resistant qualities is not dependent on large scale failure of the aquitard. It has been interpreted that groundwater leakage occurs once the line of shear intersects the base of the aquitard, possibly due to the lack of confinement which could open inherent cleavages within the coal aquitards (as illustrated in Figure 5.9). This assumption is supported by the insignificant surface subsidence measured (less than 5 mm) above sub-panel 1 at the time the Alpha seam aquitard ruptured - see Figure 5.15

  Furthermore, the separation between the extensometer anchor in the aquifer 3 lower aquitard (Alpha seam) and the ground surface (Figure 5.16) above sub-panel 1 was only 6 mm (total aquitard subsidence of 11 mm) and even less above sub-panel 2, suggesting that the Alpha seam aquitard had remained physically intact with an unsupported span of:

  $$40 - 2(\tan\alpha)33 = 12 \text{ m.} \qquad 5.2\ (1)$$

  It is interesting to note that for an aquitard 30 m above the mine, the allowable panel width derived by the modified NCB design method (5 m in Table 5.3), will give rise to 6 mm subsidence.

  This suggests that the aquitard curvature/strain method (discussed in Section 5.1) could also be adapted for the prediction of aquitard integrity - once there is sufficient data to accurately predict the subsurface subsidence for narrow panels, before surface subsidence is manifested.

  The observation of a spanning aquitard is similar to the subsurface subsidence observed in 1North panel, where the Alpha 2 seam collapsed only after three lifts had been extracted (when the panel was 54 m wide). Prior to this point, there was no discernible surface or subsurface subsidence in either of the extensometer anchors in 1North panel. At the time, it was not known whether the strip of coal left behind during early stages of extraction in that panel had any effect on caving. It now appears that if it did, it would only have been slight, and that the critical mining width before the Alpha seam can be expected to collapse/fail comprehensively is between 40 m and 54 m, with unsupported aquitard spans somewhere between 12 m and 26 m.

EXTENSOMETER ANCHOR MOVEMENTS RELATIVE TO SURFACE DATUM NORTHWEST B3 PANEL

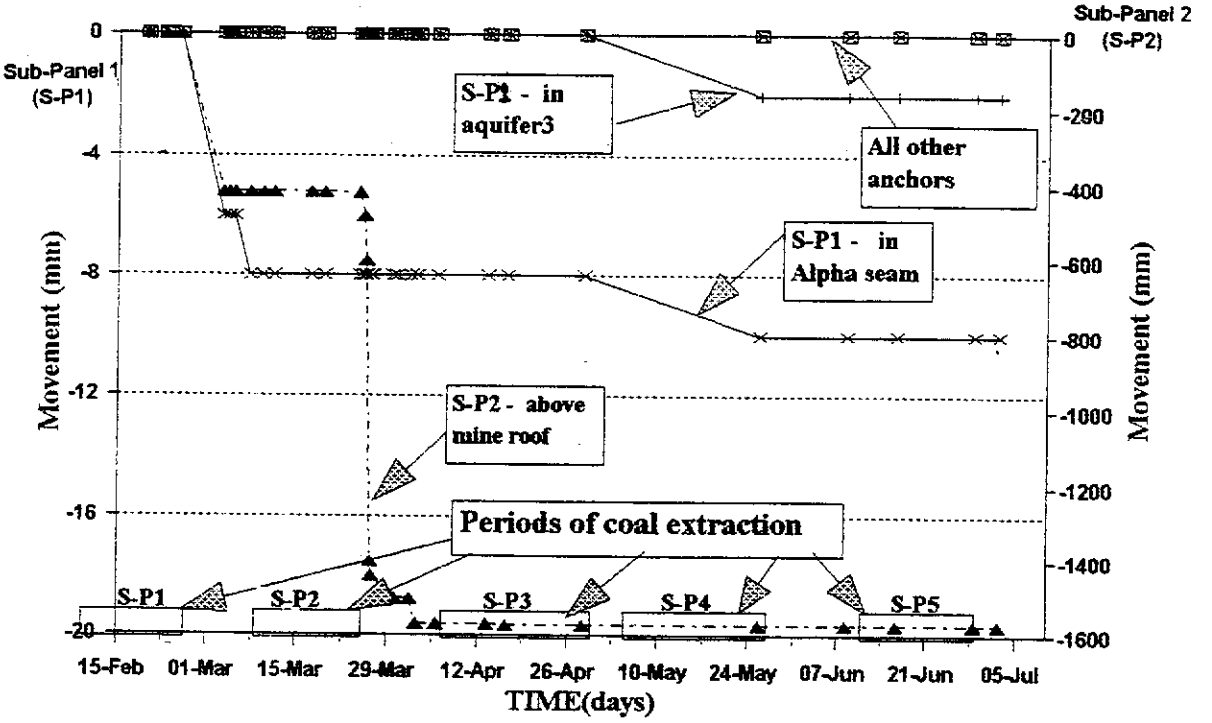

Figure 5.16

- The results in Figure 5.14 also illustrate that less surface subsidence has been measured above sub-panel 1 than the other sub-panels. From Figure 5.1 it can be seen that sub-panel 1 was only 130 m long and, at 150 m depth, represents a W/H ratio of 0.9. It is therefore possible that the Alpha seam is receiving additional support from the head-end abutments on either side of the panel and therefore subsided less. The other sub-panels, being 200 m long would not be influenced by head-end effects.

- The integrity of coal/shale aquitards of aquifers 4 and 5 above the mine workings was kept in tact - no discernible change in water level was detected in these aquifers.

- There is insufficient evidence to conclude whether or not ground movements would have ceased since the last period of measurement, however, given the very small magnitudes of subsidence to date, this is of little concern.

- The consistent level of "noise" emanating from the ribs of coal fenders and the consistent "effort" used in cutting coal indicated that the intra-panel pillars were more than adequately absorbing the elevated tributary loads.

- The impact of mining a roadway into the barrier/intra-panel pillar between sub-panels 4 and 5 was minimal. Mine conditions within this roadway had remained "good" for at least six months, other than some rib spalling in the intersection with the lateral return airway. After this time the NWB3 area was sealed off for ventilation purposes and the mine conditions could not be monitored. These good in-mine conditions also suggest that the design dimensions of the intra-panel pillars were well matched to the ground mass response to mining.

- The only large-scale anchor movement noted was 1.6 m subsidence at a height of 9 m above the mine roof in sub-panel 2. This suggests that all caving/shearing occurred within the first sandstone aquifer (somewhere within 33 m of the mining horizon) and supports the earlier assumption that the majority of bulking occurs in the first 6 - 8 m above the seam.

It was therefore concluded that the criteria established for the *design of maximum widths of sub-panels* within a Wongawilli panel/pillar extraction panel were valid for local conditions. The only factors requiring further investigation were considered to be the design of intra-panel pillars, the effect of variable mining height, and mining beneath aquitards at greater depths.

The actual benefit of the latter two investigations is probably limited. It has been demonstrated that the protective aquitards beneath aquifers 3, 4, & 5 will be ruptured with relatively narrow extraction widths, and it is likely that as the cost of coal extraction by Wongawilli methods after the rupture of these aquitards would be prohibitive. Given that the typical mining heights in WCL mines are 2.2 m in the Colliebum No.2 seam and 2.7 m in the Wyvern seam, it would probably be difficult to account for any variation in field observations between the two mining heights.

Further investigation into the *design of the intra-panel pillars* was considered to have some merit. It was not clear whether narrower intra-panel pillars could be left to support the tributary load. It is obvious that the cost efficiency of this form of mining will be influenced by the width of pillar left within the panel. A summary of the work done towards developing better intra-panel pillar designs is provided below.

5.3 "SANDSTONE COLUMN"/PILLAR INVESTIGATION

Due to the serious ramifications of potential failure of pillar systems through collapse of the sandstone column exposed by caving on either side of coal pillars (as illustrated in Figures 2.13 c and 4.47), an investigation was initiated which looked directly at this issue. It was proposed to investigate the potential for this form of large-scale collapse, with the intent of developing a design criteria which specifically addresses the mode of failure of the sandstone. The approach used in this investigation was to conduct a series of geotechnical centrifuge tests to examine the potential for such an event occurring, and to back-analyse known areas of panel "creep" through extensive roof beam collapse (as illustrated in Figure 2.13 d) in the mine. As a result of these investigations, two tentative design criteria have been proposed for establishing the

minimum width of intra-panel pillars.

The first design criteria, described in Section 5.3.1, represents a variation of the design approach adopted for the FOS_{ipc} [Equation 2.5(7)] using coal pillar strengths and dimensions to calculate the minimum pillar width. The variation, described below, pertains to the application of the tributary loading to the intra-panel pillars during certain stages of extraction.

The second design approach, described in Section 5.3.2, is based on the assumption that the stability of the sandstone column is dependent on the height of caving in the immediate roof (and thus the height of the sandstone pillar), the rock mass strength of the sandstone column, and the modified tributary loading.

5.3.1 DESIGN CRITERIA (1) (Intra-panel Coal Pillar)

It has already been established in Section 5.1 that a design FOS_{ipC} of 2.1 was adequate to maintain stability of the entire pillar support system between the two fully goafed 40 m wide sub-panels in the 150 m deep trial NWB3 panel, however, the precise design FOS_{ipC} has yet to be determined. Taking the information gained from the field and scaled modelling into consideration, two important points require notice:

1) It has been demonstrated that major failure can occur with limited extraction on one side of the pillar and large-scale extraction on the other (as illustrated diagramatically by Figure 5.17).

2) It is postulated that in cases where large goafed areas exist on both sides of intra-panel pillars - in this case 40 m or more each side - the constraining pressure provided to both the superincumbent sandstone column and coal pillar by the goaf material will increase the apparent strength of the pillar.

It follows therefore that the design FOS_{ipC} should be calculated for the case with a fully collapsed goaf on one side and first caving on the other side of the pillar.

Re-assessing the FOS_{ipC} of the NWB3 trial panel, where the 20 m wide intra-panel pillars remained in tact, the resultant FOS_{ipC}, at an equivalent stage of caving is increased from 2.1 to 2.6.

ILLUSTRATION OF TRIBURAY LOAD CONCEPT FOR PANEL/PILLAR MINING

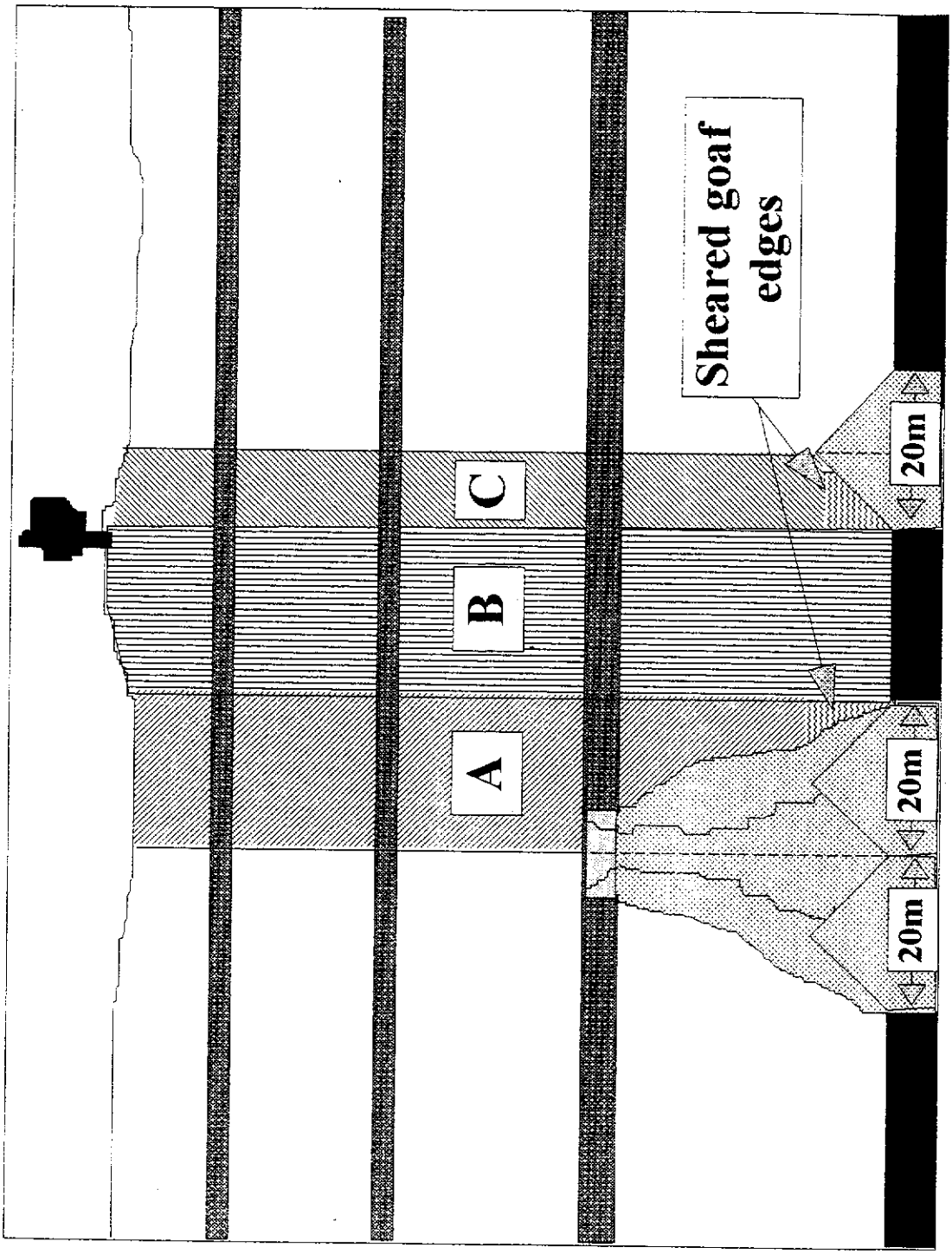

Figure 5.17

Two case studies of collapsed sandstone pillars are provided by the subsided 6B East and 4 West panels in the WD-2 mine (Figures 5.18 & 5.19). In the 6B East extraction panel, the mining company WCL was undertaking secondary extraction by driving 6.3 m wide "splits" through the middle of the large group of pillars within the panel. The original dimensions of the pillars were typically 12 to 13 m wide and 19 to 23 m long; after "splitting" the pillars the average dimensions were 12.7 m wide by 7.8 m long (see Table 5.4). Once the area of secondary extraction in sub-panel B had reached 140 x 150 m (approximately half the total area of the panel), several roof falls were noted at the minimally supported intersections of the split pillars. After about one week (personal communication, Mr A Sandford) these falls became more prevalent and appeared to be "creeping" toward the working face. The panel was then abandoned.

During the following two weeks or so, during regular inspections of the panel, access throughout the panel was diminishing until the panel was sealed off, preventing any access. In October 1981, a few months after panel closure, subsidence was noted on WCL's dual carriageway haul road. Following joint work by the author, WCL surveyors, and Mr Fotakis, it was established that the subsidence had developed across the whole panel, including the unsplit pillars.

Fotakis (1985) found that a survey station - HC45 - installed by the Department of Lands and Surveys (see Figure 5.19) above the unsplit side of the panel had subsided approximately 0.7 m. Further analysis by Misich (1985)[1] estimated that 1.0 m subsidence could have been expected above the split pillar section of the panel. For interest, assuming 65% extraction from the pillar-split panel, and a mining height of 2.5 m the subsidence factor for the 1.0 m of subsidence equates to 0.62 which approximates the subsidence factor determined for total extraction panels.

Back analyses of the loading on these pillars and their resultant factors of safety indicates that the FOS_c for the coal pillars in the split and unsplit sub-panels are 1.5 and 2.5 respectively. These FOS_c are either much greater than or marginally less than the design FOS_c for permanent stability (1.6). These high FOS_c, and in-mine observations (that the coal pillars themselves were not being overstressed), suggest that it was the sandstone columns, created by cave-ins of the mine roof on either side of the coal pillars, that collapsed as a "creep".

COLLAPSED AREA IN 6B EAST PANEL397

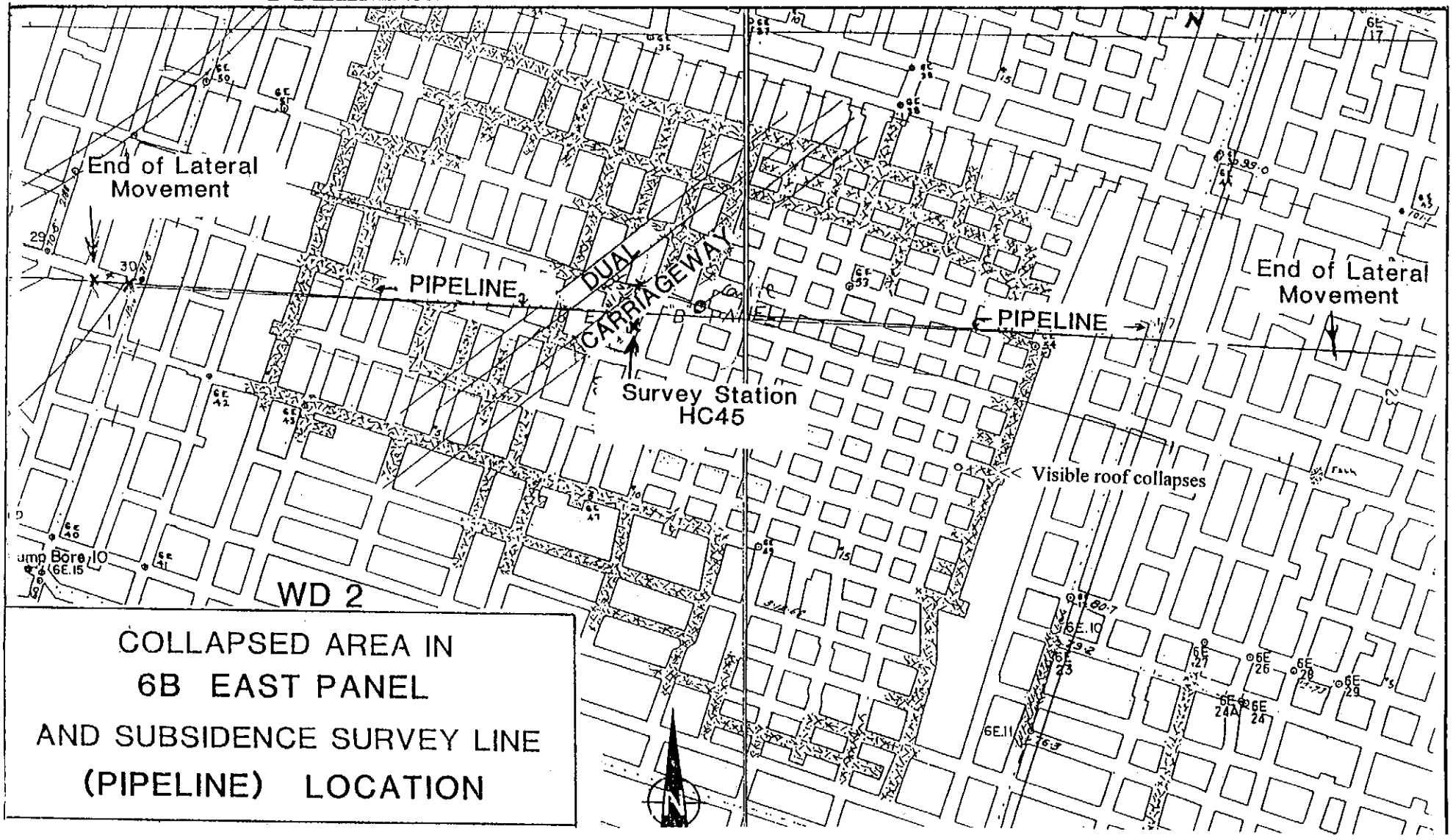

397

Figure 5.18

COLLAPSED AREA IN 4A WEST PANEL398

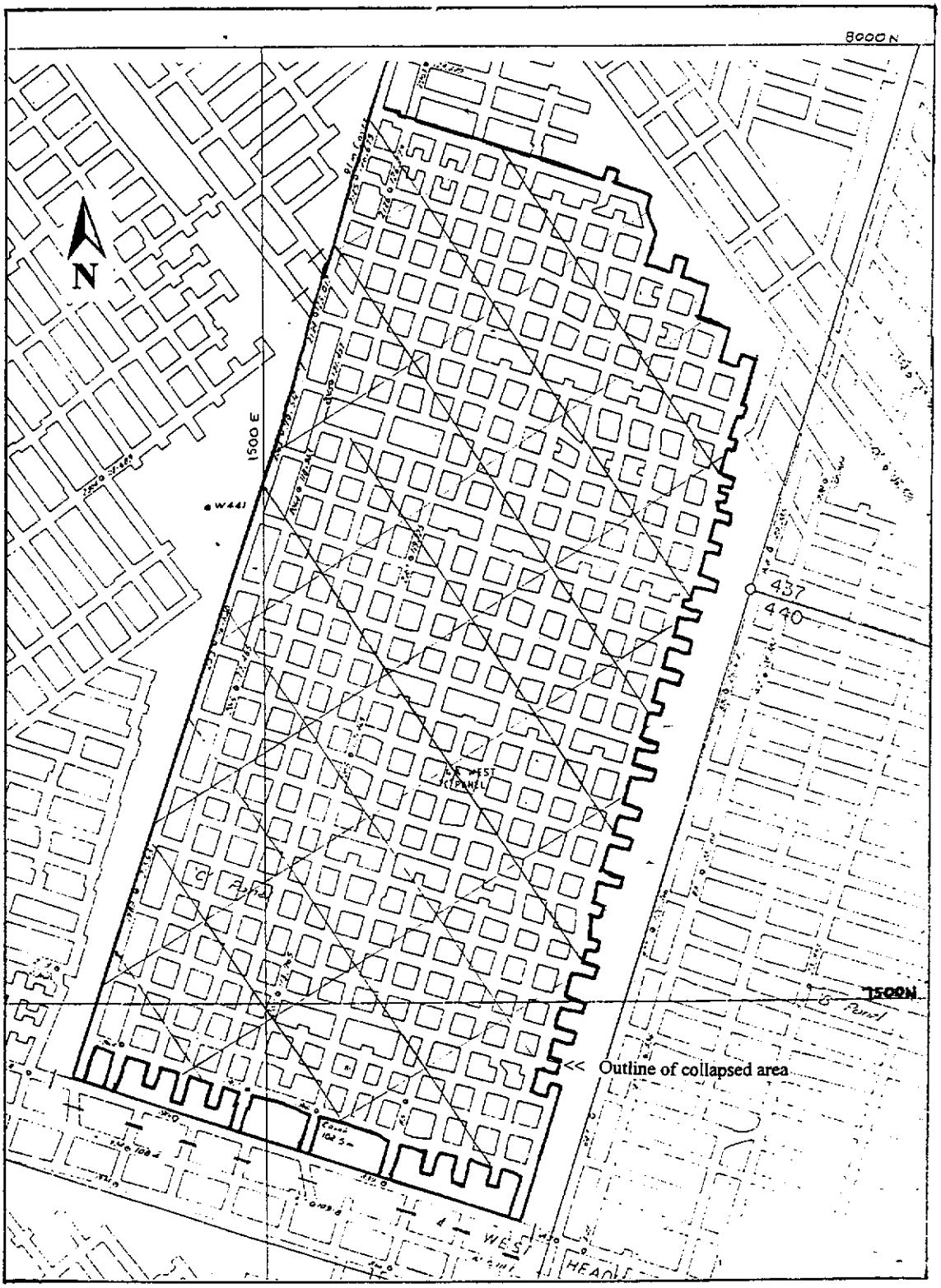

Figure 5.19

TABLE 5.4

6B East Panel WD2
Pillar Dimensions

Sub-Panel A

Pillar #	Width (m)	Length (m)	Pillar #	Width (m)	Length (m)
1	11	19	26	12	24
2	12	19	27	12	23
3	12	19	28	12	23
4	12	22	29	9	21
5	12	22	30	10	19
6	12	23	31	10	19
7	12	23	32	11	22
8	12	20	33	11	24
9	11	18	34	11	23
10	11	19	35	11	23
11	11	22	36	11	20
12	11	24	37	11	18
13	10	23	38	11	19
14	10	23	39	11	22
15	11	20	40	11	24
16	11	18	41	11	23
17	11	19	42	12	23
18	11	22	43	11	20
19	12	24	44	11	18
20	13	23	45	11	19
21	12	23	46	11	22
22	13	20	47	11	24
23	14	18	48	11	23
24	12	19	49	12	23
25	12	22			
Avg.	11.3	21.3			

Sub-Panel B

Pillar #	Width (m)	Length (m)	Pillar #	Width (m)	Length (m)	Pillar #	Width (m)	Length (m)
1	11	6	26	9	5	51	12	7
2	12	6	27	9	7	52	12	8
3	12	7	28	9	7	53	11	9
4	12	7	29	10	9	54	11	9
5	12	8	30	11	8	55	11	8
6	12	8	31	11	8	56	12	8
7	12	8	32	11	8	57	12	8
8	12	8	33	11	8	58	11	9
9	12	8	34	11	8	59	11	9
10	12	8	35	12	10	60	11	8
11	12	10	36	12	8	61	12	7
12	12	9	37	12	7	62	12	5
13	12	6	38	12	5	63	12	8
14	12	6	39	12	7	64	11	9
15	12	7	40	12	8	65	11	9
16	12	7	41	12	9	66	11	8
17	12	8	42	12	9	67	12	8
18	12	8	43	12	8	68	11	8
19	12	8	44	12	8	69	12	9
20	12	8	45	12	8	70	12	9
21	12	10	46	12	9	71	12	8
22	12	10	47	12	9	72	11	7
23	12	9	48	12	8	73	10	5
24	12	9	49	12	7	74	9	8
25	99	7	50	12	5	75	10	7
Avg.	12.7	7.8						

It is interesting to note that the creep continued across into the unsplit sub-panel where the FOS_c of the coal pillars was 2.5, which is well in excess of the design FOS_c (1.6) recommended in Sections 2.5.5.1 and 5.1 and the FOS_{ipc} (2.1). This collapse is considered to be due to the elevated vertical loading at the interface of the two sub-panels once the pillar-split side of the 6B East panel fully collapsed (through creep). Once total collapse has occurred, additional loading from the material above the line of shear (projected from the seam to the surface - as illustrated by Wilson, 1980) is transferred to the abutment pillars. The difference between vertical loading from standard tributary theory and the additional loading resulting from total collapse is:

Standard vertical load (PLv)

$$PLv = 21.1 \times H \times [Lp + Wct] \times [Wb + Wp] \quad 5.3(1)$$

$$= 21.1 \times 116 \times [21.3 + 5.5] \times [6.8 + 11.3]$$

$$= 1{,}187 \text{ MN or } 4.9 \text{ MPa.}$$

Standard vertical + Caving load (PLvc)

$$Plvc = Plv - [21.1 \times H \times (Lp+Wct) \times 0.5Wb] + [21.1 \times (Lp+Wct) \times (0.5 \times \tan 23 \times H^2)] \quad 5.3(2)$$

$$= 1187 - 73.4 + [1615]$$

$$= 2729 \text{ MN or } 11.3 \text{ MPa.}$$

Where: H = Cover depth, Wp = Pillar width,

Lp = Pillar length, Wb = Bord width, and

Wct = Cut-through width.

Given that the strength of a typical pillar [from Equation 2.5(8)] in this panel is:

$$PS = 6.5 \times Weff^{0.46}/Mh^{0.66}$$

$$= 6.5 \times 14.8^{0.46} / 2.5^{0.66}$$

$$= 12.3 \text{ MPa,}$$

This additional load reduces the FOSc to 12.3 / 11.3 = 1.1. This low FOSc indicates that once the creep has initiated in the split sub-panel, the coal pillars are reasonably close to yield. In this circumstance, it is possible that the coal pillars themselves may

have yielded, however, in-mine observations do not suggest that this is the case.

A full appraisal of the 6B East panel pillars is presented in Table 5.5. Note that the origin and discussion of the values given in the columns titled **'S/STONE'** (sandstone) are provided in the following Section.

The magnitude of subsidence above the second pillar splitting case study - '4 West' panel (230 m wide by 500 m long - Figure 5.19) - could not be determined as there were no survey reference points above the panel. Evidence of subsidence occurring was in the form of long narrow cracks, oriented parallel with the panel edge (Fotakis, 1985).

Back-analysis of the stability of panel pillars (also presented in Table 5.5), indicate that subsidence initiation was not prevented by coal pillars with a FOS_c of 2.37. Interestingly, there are numerous panels with pillar FOS_c less than 2.37 which have not collapsed. The reason why these two particular panels have subsided is because the splits driven through the initially large pillars were excessively wide for the local conditions and were inadequately supported. With time, many of the wide splits and bords collapsed, thereby developing a panel in which the superincumbent loads are being supported by weak columns of relatively unconfined sandstone.

For interest, back-analysis of the failure of the extrapolated 13 m wide sandstone column with a 4.2 m mining height in centrifuge test PS09 (when failure occurred with a 40 m goaf on one side and a 20 m goaf on the other side at an extrapolated depth of 105 m) the resultant FOS_{ipC} of the (assumed) coal pillar was 2.2.

Taking these points into consideration, and in the absence of further testing and case data, it is suggested that a design FOS_{ipC} of 2.6 be used when designing for the long-term stability of pillars when extensive caving is expected on either side of the pillars.

When panel/pillar methods are to be employed, the design FOS_{ipC} is to be calculated according to tributary area theory with limited extraction on one side of the pillar and large-scale extraction on the other, which represents the most susceptible scenario for collapse of the sandstone column.

TABLE 5.5

Back-Analysis of Pillar Collapses in 6B East and 4 West Panels, WD2

	SUB_PANEL B		SUB_PANEL A			
	COAL	S/STONE	COAL	S/STONE	COAL	S/STONE
	6B EAST				4 WEST	
BORD WIDTH (m)	6.8	6.8	6.8	6.8	6.0	6.0
CUT-THRU WIDTH (m)	6.3	6.3	5.5	5.5	6.5	6.5
BORD C/LINE DIST.(m)	19.5	19.5	18.1	18.1	17.5	17.5
C/T C/LINE DIST.(m)	14.1	14.1	26.8	26.8	17.5	17.5
PILLAR LENGTH (m)	7.8	7.8	21.3	21.3	11.0	11.0
PILLAR BREADTH (m)	12.7	12.7	11.3	11.3	11.5	11.5
Effective Width (m)	9.7	9.7	14.8	14.8	11.2	11.2
EXTRACTION RATIO	65%	65%	50%	50%	59%	59%
DEPTH OF COVER (m)	116	109	116	109	100	94
MINING HEIGHT (m)	2.5	7	2.5	7	2.3	6
"PILLAR" UCS (MPa)	6.5	4.5	6.5	4.5	6.5	4.5
O/B DENSITY (kgf/m3)	2110	2110	2110	2110	2110	2110
PILLAR STRENGTH (MPa)	10.08	3.54	12.25	4.30	11.42	4.2
LOAD ON PILLAR (MPa)	6.66	6.26	4.84	4.55	5.12	4.71
Width/Height Ratio	3.12	1.11	4.52	1.61	4.78	1.83
FACTOR OF SAFETY	***1.5***	***0.6***	***2.5***	***0.9***	***2.3***	***0.9***

5.3.2 DESIGN CRITERIA (2) (Sandstone Pillar)

The above design criterion FOS_{ipc} can be only described as an empirical solution, whereby the excessive dimensions of the coal pillars, by default, account for the potential for failure of weak strata above the coal (once exposed by caving on either side of the pillar). It is recognised that traditional pillar design criteria, such as these can be misleading for design of intra-panel pillars with weak superimposed strata. For instance, if the mine planner needs to improve the design FOS_{ipc} and decides to reduce the mining height, by say 0.5 m, within a very thick coal seam, this will not necessarily reduce the potential for collapse of superincumbent sandstone columns developed by caving on either side of the intra-panel coal pillars. A second tentative design approach was then investigated which is aimed more directly at the mechanism of failure above the intra-panel coal pillars.

Put briefly, this concept is similar to the design criteria used for coal pillars in the preceding Section, except the strength and height terms used in the design equation pertain to the sandstone column (pillar height is determined by the height of caving of the immediate mine roof), and the design FOS_{ips} is reduced to account for confinement pressure provided by the goaf. Discussion on these variations is provided below.

The height of 'roof caving' above the Wyvern seam has been observed to almost always stop at the "Marker" seam, which is located at a consistent height above the mine roof within panel sized areas, and typically between 6 and 8 m above the Wyvern roof throughout the WCL mines. In the 6B East panel, the Marker seam was consistently in the order of 7 m above the worked Wyvern seam and in the 4 West area the Marker seam was 6 m above the mine horizon. It is worthy to note that the height of caving - to the marker seam - also approximates the theoretical caving height calculated by the equation (modified from Peng and Chiang, 1984):

$$\textbf{Caving Height} = Mh/(Ko-1) \qquad 5.3(3)$$

where: Mh = mining height (typically 2.6 m), and

Ko = goaf swell factor (measured to be 1.32 for weak sandstone from the Premier minesite - given in Figure V.1, Appendix V).

It is possible that, in other sites where a specific stiff horizon defining the height of roof caving is absent, that the above relationship may be used to establish the height of the sandstone column.

The strength of the sandstone has been given an arbitrary value of 4.5 MPa, which is slightly below the typical strength of Collie Basin sandstone as listed in Table 2.1. (Note that it is not required to reduce laboratory strength of sandstones to represent rock mass strengths - as it is for coals. This has been discussed in greater detail in Section 4.2.2.1.)

One difficulty with this approach is the application of a sandstone pillar width to determine pillar strength, as the shape of the superincumbent sandstone column is influenced by a triangular mass formed by the angle of shear. However, it is proposed that under elevated vertical loading, this triangular mass can shear off subvertically, resulting in a more rectangular shaped pillar. This observation (made during geotechnical centrifuge tests) suggests that the width of the coal pillar can be used for the width of the sandstone column for design purposes.

It is also proposed that this failed wedge of material, along with the caved goaf on either side would provide additional confinement to the superincumbent sandstone column and thereby increase its mass strength. Therefore the requirement to have a conservative design FOS is less appropriate. For reference, the FOS_{ips} for the 4 West panel and each sub-panel in the 6B East panel are given in Table 5.5 under the columns titled "S/Stone". It is evident that the FOS_{ips} in each case, are less than 1.0. This observation agrees well with standard geotechnical criteria for predicting failure of structures.

Further support for reducing the sandstone column design criteria is given by back-analysis of the trial panel case study NWB3 panel, where the sandstone column remained in tact, and the corresponding FOS_{ips} was 1.2.

It is therefore recommended that a FOS of 1.2 be applied for the design FOS_{ips}.

NOTE : The design criteria for the intra-panel sandstone columns is only tentative at this stage. Further work is required to provide more supportive evidence for this approach over a wider range of mining scenarios.

5.4 SUMMARY OF THE RECOMMENDED EXTRACTION PANEL DESIGN APPROACH IN THE COLLIE BASIN

The basis of panel design is to firstly predict the complete subsidence profile above the extraction panel and then to iteratively design the panel dimensions until the relevant characteristics of the predicted subsidence troughs do not exceed the tolerance limits of a given structure. The derivation of the subsidence profile is accomplished by following three steps. Firstly the maximum subsidence (Smax) is estimated for any given extraction panel according to the effective mining height (T), width (W) and depth of cover (H) using Equation 3.1(1):

$$Smax = T \times 0.64 \times e^{-12e^{-4(W/H)}}$$

Secondly, the point of inflection is determined from Equation 3.1(2):

$$X = H\left[0.17 - e^{-[2 \times (W/H + 0.5)^{1.8}]}\right]$$

The subsidence at any point on the surface can then be calculated in relation to the distance of that point from the point of inflection (allowing for the complete shape of the subsidence trough to be determined) by the profile function given in Equation 3.1(7):

$$-s_{(mm)} = [e^{-9 \times e^{-7 \times (D/H + 0.35)}} - 1] \times Smax$$

This profile function can then be used to predict tilt and curvature at any point along the subsidence trough (as done by Karmis, 1985), by single differentiation and double differentiation of the profile function respectively (as given in Sections 3.1.6 and 3.1.7). Horizontal strains can then be predicted using the relationship between curvature and strain given in Equation 3.1 (13):

$$\text{Strain} = 3.5 (\text{curv.} \times 10^{4})^{0.6} \text{ (mm/m)}$$

These predicted subsidence parameters (vertical deflection, tilt, curvature and strain) can then be used to predict the likely damage to specific surface features. Some of the more accepted models for surface subsidence damage classification are listed in the 1972 NCB publication, and by Peng (1992). Germanis & Smith (1973) lists some Australian design criteria for subsidence.

The mine designer, through the use of appropriate subsidence damage classification criteria, can then derive the optimum panel dimensions by iteratively modifying the panel geometry until the magnitudes of the predicted surface subsidence are within tolerable limits for each overlying structure.

Design for protection of aquitard integrity in the Collie Basin is based on the "supported span" concept, whereby the maximum width of extraction (Wext) is estimated by Equation 5.1(3):

$$\mathbf{Wext = 2h \times \tan(\alpha)}$$

Where: h = the height of the aquitard above the seam, and

α = the angle of shear

The application of the "unsupported aquitard span" concept for estimating aquitard integrity in other mining areas will depend largely on the aquitard's thickness and geomechanical properties. This concept is also significantly influenced by the geomechanical properties of the underlying interburden and the presence of large-scale geological discontinuities. For example:

- Massive, strong lithologies with minimal defects can span very large distances and greatly reduce the resultant subsidence magnitudes and effects.
- Very soft, plastic aquitard strata - usually weak clays - can absorb large strain energy and have the capacity to "re-knit" with minimal confining pressure, thereby maintaining the integrity of the aquitard.
- Weak interburden material forming the caved overhang which supports the base of bridging aquitards can crush, thereby increasing the unsupported span.

If panel/pillar mining methods are to be employed, the width of pillar between each sub-panels must be designed to adequately support the elevated tributary loads.

Firstly intra-panel coal pillars must meet the design criterion:

$$\mathbf{FOS_{ipc} = PS/PL = 2.6} \qquad 5.4(1)$$

Where: $\mathbf{PS} = k \times (Weff/Wo)^{0.46}/(Mh/Mho)^{0.66}$ (MPa), 2.5(8)

$\mathbf{PL} = (A+B+C).\gamma.\ 10^{-6}/Wp$ (MPa), 5.4(2)

A+B+C are tributary load components as per Figure 5.18,

γ = unit weight of superincumbent strata, MN; **Wo**, **Mho** = 1 m,

Wp = Pillar width (m), **Mh** = Mining height (m),

k = compressive strength of 1 m^3 of coal, which in Collie is 6.5 MPa;

Weff= **4 x Ap/Cp** (m) (Wagner, 1980), 2.5(10)

Ap = Pillar area (m^2), and **Cp** = Pillar circumference, (m).

Secondly the coal pillar must have sufficient bearing area so as to prevent bearing failure of the roof or floor material. The design criterion adopted for the Collie Basin was a modified Terzaghi/Hansen formula (Scott, 1980, Stacey & Page, 1986) with a design FOS against bearing failure (FOS_B) of 3.0. The FOS_B is calculated by:

$$\mathbf{Qult/PL} \qquad 2.5(12)$$

Where $\mathbf{Qult.} = \mathbf{c.N_c} + \mathbf{q_o.N_q} + \gamma\mathbf{.0.5.Wp.N_\gamma}$, 2.5(11)

c=cohesive strength kPa, and $\mathbf{N_c}$, $\mathbf{N_\gamma}$ & $\mathbf{N_q}$ are functions dependent on frictional properties of the roof or floor material.

Once these design criteria have been met it is possible to mine a well supported narrow roadway (less than 5.5 m wide) longitudinally through the intra-panel pillar, provided the design criteria $FOS_B \geq 3.0$, and $FOS_c \geq 1.6$ [- Eqn. 2.5(7)] are met. Note that FOS_c is calculated in the equivalent way as FOS_{ipc}.

For complex mine geometries, such as odd-shaped panels or adjacent bord and pillar workings, it is recommended that the three dimensional program SUBSOL be utilised to obtain a more accurate estimate of the likely stresses and strains at the mining horizon and resultant surface subsidence. This modelling design work should be able to be completed in conjunction with MINCAD Systems on a "bureau service" charge. SUBSOL, in its current form, is not recommended to be used for assessment of the integrity of aquitards. Further investigation is required before the shape of the subsurface horizons can be predicted with sufficient accuracy.

6.0 CONCLUSIONS

The mechanisms and characteristics of mining subsidence in the weak and water-saturated sediments of the Collie Basin have been investigated both in the field, and the laboratory. The results from the field study have demonstrated that total extraction of coal in the Collie Basin (using the Wongawilli mining method), unlike the expert opinion provided before this research project, does not produce ubiquitous destructive pot-hole type subsidence. In fact, it is more common for the gentle subsidence-trough form of subsidence to develop above extraction panels. Furthermore, the trough-shaped subsidence that is developed in Collie has many similar characteristics to subsidence troughs developed in other mining regions - e.g. the eastern Australian coalfields, and the Appalachian coalfields in the USA. One of the more notable comparisons between the three coal regions is a subsidence factor of 63% of effective mining height for super-critical width panels.

As for all other mining regions, the potential for surface subsidence to develop from the collapse of mine roof in the Collie Basin is dependent on the dimension of the collapse and the ability of the superincumbent strata to bridge across the collapse to prevent deflection of the ground surface. Once an initiating width of extraction has been exceeded (Collie Basin field data suggest that the initiation width is approximately 25% depth of cover for trough-shaped subsidence), surface subsidence will be manifested.

The shape of the subsided surface above mine workings is influenced by the bulking characteristics of the collapsed ground, remnant coal, geology (and depth of cover), and the mine design, mining height, and extraction methods. In certain conditions, each of these parameters can control whether surface subsidence will be "discontinuous" or "continuous". Although this study has not been able to predict the magnitude, timing and dimension of discontinuous subsidence, the author (in Section 3.3) has been able to identify a range of pre-requisite conditions for the initiation of discontinuous subsidence.

Of these pre-requisite conditions, the primary factor controlling discontinuous subsidence is geology/depth of cover. Under normal geological conditions, this form of subsidence is limited to depths where there are no major aquitards within the overlying strata. A generic limiting depth has been arbitrarily set at 40 m, after which

it can be expected that the strata will include a bridging (aquitard) layer with at least 1.5 m of coal and the potential for discontinuous subsidence to develop is minimal. In some locations, bridging strata is known to exist at much shallower depths; the 40 m limit will not apply in these instances. It is recommended that the 40 m design limit be used in cases when there is limited knowledge of the stratigraphy above a panel.

Field data collected during the study suggests that the trough-form of subsidence develops systematically, with consistent subsidence characteristics. The following characteristics of Collie Basin subsidence have been defined:

- Angle of draw = 25°.
- The maximum subsidence (Smax) expected to develop above super-critical width total extraction panels is 63% of the effective mining height. The maximum expected subsidence for any width panel can be estimated from the relationship between the ratio of panel width (W) and depth of cover (H), and the effective mining height (T), given by the equation:

$$\mathbf{Smax = 0.63 \times T \times e^{(-12e\text{-}4(W/H))}} \qquad 3.1(1)$$

  Where T = mining height multiplied by the % extraction of coal.

- Critical width is met when the central section of the trough first tends to flatten out. (Noted when the rate of increase in Smax begins to slow - when the W/H ratio reaches approximately 0.9). Super-critical width is defined as being when the panel W/H ratio reaches 1.7). This variation from other research work has been supported by the results from subsurface investigations. It has been interpreted that critical width is a "stage of reconsolidation" which is reached when the line of shear (23 ° from the vertical) intercepts the ground surface.

  Once this critical width is attained, a full column of collapsed ground is developed in the central section of the subsidence trough (as illustrated in Figure 3.53 b), and the full tributary load can be expressed onto the collapsed ground, thus allowing for greater rates of reconsolidation and ultimate Smax to be achieved.

- The location of the point of inflection can be estimated by the equation:

$$X = H\left[0.17 - e^{-[2 \times (W/H + 0.5)^{1.8}]}\right] \qquad 3.1(2)$$

where X = distance from the panel edge (-ve = outside the panel, +ve = inside the panel)

- The magnitude of horizontal strain on the ground surface across the subsidence profile has been shown to be dependent on the curvature of the subsidence profile. It can be calculated by the equation:

$$\text{Strain} = 3.5 \times (\text{Curvature} \times 10^4)^{0.6} \quad \text{(mm/m)} \qquad 3.1(13)$$

- The consistency of this field data has allowed for the development of a profile function (see Section 3.1.5) that can be used to predict the magnitude and shape of surface subsidence troughs, and the concomitant tilts and strains for a range of mining geometries. The profile function that provided the best-fit to the Collie Basin data was a form of double exponential:

$$-s = Smax.\left[exp^{-\theta \times exp^{-\gamma \times (D/H + 0.35)}}\right] - Smax \qquad 3.1(7)$$

where: S_{max} = maximum subsidence derived from Equation 3.1(1) (m),

S = subsidence at any point (m), and

D = distance from in flection point, IP (m). -ve D represents positions located toward the middle of the panel on the subsidence trough.

From the literature reviewed, a **double** exponential profile function had not previously been used for subsidence prediction.

Subsidence prediction is therefore dependent on four input parameters:

- panel width,
- **effective** mining height,
- depth of cover above the mine workings, and
- distance from the point of inflection.

The subsidence prediction procedure, defined in detail in Section 3.1, is to:

I) Estimate the maximum subsidence using Equation 3.1(1).

2) Define the location of the inflection point (as a distance from the panel edge) using Equation 3.1(2).

3) Establish the complete subsidence profile using the site-specific double exponential profile function [Equation 3.1(7)].

Once the profile of the subsidence trough is known, the concomitant tilts, curvatures and strains can be calculated, from which the damage due to subsidence can be predicted. Ground tilt and curvature is calculated respectively by single and double differentiation of the double exponential profile function.

$$\frac{dy}{dx} = \frac{63}{H}.exp^{-\left(7.\left[\frac{D}{H}+0.35\right]\right)}.exp^{-\left(9.exp^{-\left(7.\left[\frac{D}{H}+0.35\right]\right)}\right)}.Smax$$

$$= \frac{63}{H}.exp^{\left(-7.\left[\frac{D}{H}+0.35\right]\right)}.\left[F_1D\right].Smax \qquad 3.1(10)$$

$$\frac{d^2y}{dx^2} = \frac{441}{H^2}.\exp^{-\left(7.\left[\frac{D}{H}+0.35\right]\right)}.\exp^{-\left(9.\exp^{-\left(7.\left[\frac{D}{H}+0.35\right]\right)}\right)}.Smax +$$

$$\frac{3969}{H^2}.\exp^{-\left(7.\left[\frac{D}{H}+0.35\right]\right)^2}.\exp^{-\left(9.\exp^{-\left(7.\left[\frac{D}{H}+0.35\right]\right)}\right)}.Smax \qquad 3.1(11)$$

Strain is determined from the site specific relationship between curvature and strain [Equation 3.1(13)].

These predictive models have been compared against field measurements taken above the trial extraction panel (1 North panel) in the WD6 mine and match reasonably well.

The trends involved in the development of **subsurface** subsidence have also been identified and a tentative method/equation established from which the magnitude of subsidence at any horizon below the surface (within the collapsed zone) can be estimated. The main factor controlling the amount of subsurface subsidence is the

relative position of any given point with respect to the line of shear. The difference between subsurface and surface subsidence is greatest when the line of shear (projected from the panel edge towards the middle of the panel) is coincident with any given point above the area of extraction. As the panel edge is extended, the line of shear passes above the given point, and the difference in magnitude of subsidence between the specific subsurface point and the surface reduces. The form of the predictive equation is:

$$Ss/Sh = (1/z \times \{GED \times \cot \alpha/h\})^2 + a \times (1 - \exp [-k \times (\{GED \times \cot \alpha/h\} - z)])$$

Eqn. 3.2(1)

Where: Ss = surface subsidence,

Sh = subsidence at height (h) above the mine

GED = Goaf to Extensometer Distance

α = angle of shear (23°)

a, k, z = variables dependent on the h/H ratio of the anchor.

The relationships of each variable (a,k and z) with h/H are defined by the terms:

$$a = 1.004 - (h/H \times 0.039) \quad 3.2(2)$$

$$k = 1.6 \times \exp[-3.9 \times \exp \{h/H \times 5.1\}] \quad 3.2(3)$$

$$z = [2.4 \times \{1/(h/H \times 8.5)\}^{1.3}] + 0.95 \quad 3.2(4)$$

It is evident from Equation 3.2(1) that subsurface subsidence can only be predicted once surface subsidence has developed above the given subsurface point.

This particular phase of subsurface investigation, detailed in Section 3.2.5 and 3.2.6, requires further field studies before the complete shape of subsurface subsidence troughs can be accurately predicted. (There is insufficient data defining the magnitude of subsurface subsidence that develops before the line of shear encroaches on any given point.)

It is recommended that, at this stage, these empirical models only be applied to coal extraction by the Wongawilli method. The major difference with this mining technique

is the manner in which the width of extraction is increased by between 13 and 20 m wide increments, resulting in a stepped sequence of subsidence development. Another variation is that the Wongawilli method typically leaves between 10 and 15% of unmined coal behind (in area) as "stooks" which affects the near-seam caving processes.

The laboratory phases of investigation have attained variable degrees of success. Physical modelling, using the geotechnical centrifuge at The University of Western Australia, did not prove suitable for accurate representation of the magnitudes of subsidence developed at any level above the mine. The reason for the discrepancy is that the centrifuge models could not reproduce bulking of collapsed ground in the primary caving zone.

Nonetheless this modelling technique still proved to be a useful component of the research project. Several important observations were made from these physical models which reinforced assumptions derived from earlier field monitoring studies. The following list of points include those observations that are considered to be not affected significantly by the bulking similitude problems. These include:

- Even though greater subsidence was developed in the centrifuge models, open vertical cracks did not develop below the surface at any stage of subsidence development in phase 2 testing. The significance of this observation is that, other than in very shallow mine workings or areas where significant geological anomalies exist (such as faults or wash-outs), the risk of every body of water above an extraction panel being directly connected to the mine workings is minimal.

- The amount of subsidence and concomitant strain developed at any horizon above the area of extraction will be governed by both the mechanical properties of the spanning beams/aquitards and the caved overhang material supporting the beams.

- The main mechanism responsible for prevention of pot-hole (discontinuous) subsidence above the mine workings has been identified. Firstly, it is required that a major aquitard is present above the mine that can bridge across the goaf and truncate the caving edge. As the abutment loads increase, the potential for continuation of the line of shearing through the bridging aquitard is minimised by crushing of the weaker overhang material beneath the abutments of the bridging

aquitard. This crushing produces a flatter subsidence profile and lower shear strain within the aquitard at the caving abutment.

- When mining by panel/pillar methods, sandstone columns are developed above the intra-panel pillars by caving on either side of the intra-panel coal pillars. These sandstone pillars are susceptible to collapse if their cross-sectional area is not sufficient to withstand the elevated tributary loads.

- Some dilation of the sand/sandstone near free surfaces (e.g. immediately beneath a major spanning aquitard or the ground surface) will occur through the process of shearing during subsidence development. It is postulated that the dilation of surficial sands, particularly toward the line of shear affects the shape of the subsidence profile.

- The centrifuge tests have demonstrated that, within the zone of primary caving, greater magnitudes of subsidence can develop higher above the mine roof than closer to the mine roof. This peculiarity is a function of the Wongawilli extraction method and further suggests that the empirical models developed in this project are suited only to this method of extraction. Above the limit of primary caving, the sequence of subsidence developed is relatively consistent.

Further use of centrifuge modelling is considered limited until a method can be found to achieve repeatable, representative goafing/bulking characteristics of the immediate roof strata in the models and a number of other problems are solved (see Section 6.1).

The three-dimensional mathematical model SUBSOL was not suitable for accurately predicting the subsidence profiles and strain of aquitards above the extraction panels and therefore also failed meet all the objectives of the research project. Literature searches, personal experience and communication with other analytical software distributors, suggest that the prediction of ground movements of this nature is not feasible with any of the computer codes currently available.

However,the computer program's estimations for stresses at the mining horizon and surface subsidence did compare well with field data. It is recommended that this software be used for prediction of surface subsidence and on-seam stresses for

extraction panels with complex panel dimensions and/or complex combinations of primary and secondary extraction. The ability of the program to iteratively simulate any combination of mining steps is a powerful tool for optimising the mining method whilst controlling surface subsidence to within required limits.

A low-key investigation (using the numerical package FESOL) has further illustrated the importance of the caved overhang material on the development of subsidence. Stiffer caved overhang strata and weaker ground masses with vertical lines of shear (with no caved overhang) will produce steeper subsidence profiles, and increase the risk of aquitard rupture. Conversely, plastic overhang material will produce flatter subsidence profiles and therefore less horizontal strain on the aquitards horizons.

It has also been established that the panel/pillar mining technique is the most appropriate method for management of mining subsidence in the Collie Basin, given the mining conditions and limitations at the time of the investigation. It has been demonstrated in Chapter 5 that if panel/pillar mining is to be employed by the mine, two critical design elements need to be defined:

- The maximum width of individual sub-panels such that the subsidence tolerance limits of critical features superimposed either above or below the ground surface are not exceeded.
- The minimum width of intra-panel pillars and panel set-up pillars. These critical pillars must:
    - be of adequate width to reduce the combined subsidence overlap between each sub-panel, and/or
    - remain intact and prevent collapse the superincumbent sandstone column that develops once caving occurs on either side of the coal pillar, and
    - prevent roof or floor bearing failures.

    Inadequate pillar design will result in significantly more subsidence than desired.

Design methods have been derived so that each of these panel/pillar design parameters can be calculated (discussed in detail in Chapter 5). The design methods used for pillar

dimensions are based on the work of a number of other researchers (including Terzaghi, Salamon, and Wagner). A variation on pillar design has been proposed for the design of intra-panel pillar widths. The variations include the use of a modified tributary area concept, and the dimensions of sandstone pillars (developed by primary caving on either side of the intra-panel pillar) to determine the stability of the pillar system. Although the concept has been supported by field and laboratory data, further work is required to validate the design criteria over a range of mining scenarios.

A new design approach, based on an "unsupported span" concept, has been established for the prediction of aquitard integrity. This design concept (discussed in Section 5.1) is based on the assumption that once the line of shear intersects the position of the aquitard, the aquitard becomes unsupported and inherent fractures will open. In the Collie Basin, this occurs when the panel width is 0.85 times the height of the protective aquitard above the mine horizon (h). It is postulated that in other mining regions, where the spanning aquitards are stronger, or contain less cleavage, large unsupported span can develop before the integrity of the aquitard will be compromised. Curiosly, though, back-analysis of water inrushes at Wistow and Central Collieries (in England and Queesnsland respectively) occurred after the width of mining had reached 0.57 x h. It is postulated that this difference between apparent angles of shear is a result of the greater amount of coal extracted by longwall extraction which induces greater load at the mine abutments.

These design strategies and models have been validated by the successful mining of the NWB3 trial "panel/pillar" panel in the WD-6 mine. This panel required mining subsidence to be adequately managed for the protection of both a sealed mine haulroad, and the integrity of a number of aquitards above the mine.

Extensive monitoring of ground and water movements during extraction of this trial panel has demonstrated that surface subsidence could be kept to less than 50 mm, and groundwater inflow into the mine reduced to 500 m^3 per day (down from as much as 12,000 m^3/day measured in previous extraction panels). These results, rated as highly successful by the WCL management, suggest that these predictive models and mining design strategies are well suited to the Collie Basin sediments.

It has therefore been concluded that this research project has been very successful. The level of understanding of the processes involved with the development of mining subsidence in the "Green fields" Collie Basin has been greatly increased. It is now possible to predict the magnitudes and effects of surface and subsurface subsidence so that the design of coal extraction from underground mining in the Collie Basin can be optimised within the economic restraints at each mine site.

6.1 RECOMMENDATIONS / FUTURE WORK

During the course of investigation, a number of aspects of each of the three modelling phases of the project were identified as requiring further investigation:

1) **Physical (centrifuge) modelling**

It was established that subsidence generated from the centrifuge tests greatly exceeded that measured in the field. The reason for this additional subsidence has been largely put down to a lack of bulking by the material in the primary caving zone. Therefore, if centrifuge modelling is to be used at a later date, it is essential that an adequate method is introduced such that the process of bulking of the immediate roof strata is better represented. One possibility would be to introduce an artificial blocky material within the primary caving zone.

Test results suggest that loose surficial strata can dilate along the line of shear, thus slightly modifying the shape of the subsidence profile. However, this shear dilation could not be quantified from the results gained. It is recommended that the shear dilation process be further investigated to establish the degree of influence it has on subsidence development.

Centrifuge load cell results suggest that the tributary loading theory is conservative. To optimise pillar design criteria, this should be further investigated. Further studies could include putting load cells on all mining elements and below panel edge abutments and include more representative materials in the foundation beneath the actuators. **An integral part of such further studies would be to accurately define the effect of consolidation (of the modelling materials during spin-up and operation) on the strength and mechanical properties of models.**

It has been established that the integrity of the aquitards is largely dependent on the support provided by the caved-edge overhang. The effect of the caved edge on subsidence mechanisms and bending strains, particularly with different interburden materials needs to be further assessed.

It is considered that centrifuge modelling would be less beneficial in hard rock materials than it has been for the weak Collie Basin strata. This is due to the greater dependence of the behaviour of hard rock on inherent rock mass structures. Achieving adequate similitude would therefore be very difficult.

2) **Mathematical Modelling**

The 3-D computer software package SUBSOL was able to be calibrated against surface subsidence and on-seam stresses for a wide range of panel depths and panel set-up complexity. However, the SUBSOL model, as it currently stands, was unable to accurately represent subsurface subsidence during all stages of panel extraction. Potential improvements to the computer code SUBSOL include:

Developing a better failure criterion (e.g. flexural strength instead of bed separation/unsupported span) to trigger the sequential ground mass response to mining subsidence.

Developing the code to allow for iteration procedures to be halted momentarily to extract strategic output at any level within the model data as the model solves towards equilibrium for each mining step. In this way the full sequence of subsidence development can be measured.

Given that groundwater is a potential source of loading in the rock mass, it would be useful to develop a sustainable method for simulation of water pressure in the model.

3) **Field Investigation**

The methods used to monitor surface and subsurface subsidence have been rated as being highly successful and have provided the author with crucial data for the development of empirical models for the prediction and management of mining subsidence.

However, the achievements made from this thesis would be complimented with additional surface and subsurface subsidence monitoring above extraction panels with:

- varying widths of intra-panel and remnant coal pillars,
- a larger variation in sub-panel length and width,
- 100% extraction (eg. Longwall or Shortwall extraction),
- greater depths of cover - to investigate the validity of the design criteria against higher aquifers, and
- larger heights of extraction.

It should be noted that the true benefit of further investigation of the latter two points is questionable due to the relatively small variation in seam thickness in WCL's two underground mines, and the fact that the economics of Wongawilli extraction are poor when the protective aquitard below aquifer 3 is completely ruptured.

It would also be of advantage to investigate the effect of varying thicknesses of stiff (aquitard) strata on the subsidence development. This work would be necessary to establish the required minimum thickness of bridging strata to prevent large scale shearing/caving from extending through to the surface, and thereby prevent discontinuous subsidence from developing.

Benefit would also be gained from a specific investigation targetted at the prediction of rates water flow into mines once aquitards have ruptured.

REFERENCES

Note that references listed below are used in both the main body and the appendix of the dissertation.

Adamek V. & Jeran P.W. (1985). Evaluation of Surface Deformation Characteristics Over Longwall Panels in the Northern Appalachian Coalfield. Proc. Symp. 'State-of-the-Art of Ground Control in Longwall Mining and Mining Subsidence', American Inst. Min., Metall. & Petroleum Engineering, New York, pp 183 - 197.

Adamek V. & Jeran P.W. (1985). Precalculation of Subsidence Over Longwall Panels in the Northern Appalachian Coalfield. Proc. Symp. Bureau of Mines Information Circular 9042, United States Dept. Of The Interior, pp 34 - 53.

Adamek V., Jeran P.W. & Trevits M.A. (1987). Predictions of Surface Deformations over Longwall Panels in the Northern Appalachian Coalfield. Report of Investigations 9142, U.S. Bureau of Mines, 19 p.

Adler L. & Sun M.C. (1976). Ground Control in Bedded Formations. *Bulletin Virginia Polytechnique Institute of Resources Division* No. 28, 266 p.

Alexander I.G. & Fraser C.J. (1975). Experiences in the Measurement of Rock Dilation With Three-Depth, Rod Type Borehole Extensometers. Proc. 2nd Australian & New Zealand Conf. On Geomechanics. Brisbane, pp 281 - 286.

Alligaier F.K. (1982). Surface Subsidence Over Longwall Panels in the Western United States. Proc. Symp. 'State-of-the-Art of Ground Control in Longwall Mining and Mining Subsidence' American Inst. Minining, Metallurgy & Petroleum Engineering, New York, pp199 - 209.

Allen D.R. (1969). Collar and Radio-active Bullet Logging for Subsidence Monitoring. Dept. Of Oil Properties, City of Long Beach, California.

Amstad C.H., and Koppel J. (1977). A Multihead Borehole Rod Extensometer Design. Proc. Symp. On Field Measurements in Rock Mechanics, Zurich.

Anderson I. (1993). Case Studies of Buried Continuous Miners and Fatal Pillar Extraction Accidents in NSW, Dec 1993. RR1/93, University of New South Wales.

Bahuguna P.P., Srivastava, A.M.C., & Saxena, N.C. (1991). A Critical Review of Mine Subsidence Prediction Methods. *Mining Science and Technology*, 13, Elsevier Science Publishers B.V. Amsterdam, pp 369-382.

Bai M., Elsworth D., Li Z., and Tomlin N. (1990). Evaluation of Stress and Displacements in Discretely Layered Media. *Int. Journal Rock Mechanics Mineral Science and Geomechanics.* Vol 27, No.1, pp 23 - 31.

Barends F.B.J, Brouwer F.J.J, and Schroder F.H. (Eds) (1995). Land Subsidence - Proc. 5th Int. Symp. on Land Subsidence, Vol 1&2. The Hague, The Netherlands.

Bell F.G. (1975) *Site Investigations in Areas of Mining Subsidence.* Newnes - Butterworths, London.

Bhattacharyya A.K. & Gurtunca R.G. (1982). Sub-surface Subsidence Investigations West Cliff Colliery Progress Report to August 1982.

Bhattacharyya A.K. & Gurtunca R.G. (1984) National Energy Research, Development and Demonstration Program, End of Grant Report. Investigation of Sub-Surface Subsidence. N.S.W. Dept. Mineral Resources.

Bieniawski Z. T. (1982). Improved Design of Room and Pillar Coal Mining. Final Report, US Department of Energy. Grant No. DE-FG01-78ET-11428. 164 p.

Bieniawski Z. T. (1984). Rock Mechanics Design in Mining and Tunneling. AA Balkema, Rotterdam and Boston, 1984.

Bigby D.N. (1988). Surface Monitoring of Weighting Conditions on United Kingdom Longwall Coalfaces. Source unknown, pp 23 - 33.

Bigby D.N. and Osram J.S. (1988). Longwall Working Beneath Water. Coal International, April 1988, pp 26 - 28.

Bolton M.D., English R.J., Hird C.C. & Schofield A.N. (1973). Ground Displacements in Centrifuge Models. Proc. 8th Int. Conf. On Soil Mechanics and Foundation Engineering, Vol.1, pp 65-70.

Brauner G. (1973). Subsidence Due to Underground Mining (In Two Parts). US Bureau of Mines, Information Circular 8571. U.S. Dept. of the Interior, Washington, USA, 56 p & 46 p.

Brauner G. (1973). Calculation of Ground Movements in European Coalfields. Proc. Symp. 'Subsidence In Mines' Aust. Inst. Min. Metall., Illawarra Branch, pp 10/1 - 10/8.

Bray I.J. & Branch B.E. (1988). Design of Buildings for Mine Subsidence. Proc. Conf. on Buildings and Structures Subject to Mine Subsidence. Newcastle Div. Institute of Engineers, paper #2, 9 p.

Brice S.J., Hopkins R.S., Swindells C.F., and Thompson A.G. (1992). Subsidence Monitoring at the Scottish Colliery, Collie, Western Australia. Proc. Western Australian Conference On Mining Geomechanics. Kalgoorlie WA, June 1992, pp 439 - 444.

Brown E.T & Trollope D.H (1970). Strength of a Model of Jointed Rock. *J. Soil Mechanics Foundations Div. American Soc. Civ. Engineers.* 96 SM6, 1935 -1949.

Bucky P.B. (1931). Use of Models for the Study of Mining Problems. *Transactions of the American Institution of Mining and Metallurgical Engineers*, Tech. Pub., 425, pp 3-28.

Bucky P.B. & Fentress A.L. (1934). Applications of Principles of Similitude to Design of Mine Workings. *Transactions of the American Institute of Mining and Metallurgical Engineers*, 109, pp 25 - 50.

Burland J.B. & Moore J.F.A. (1973). The Measurement of Ground Displacement Around Deep Excavations. Proc. Symp. Field Instrumentation Brit. Geotech. Soc. Part I, pp 70 - 84.

Burton B.W. (1988). Mine Subsidence at Grass Roots. Proc. Conf. on Buildings and Structures Subject to Mine Subsidence. Newcastle Div. Institute of Engineers, paper #4, 20 p.

Cain P., Forrester, D.J. & Cooper R. (1994). Water Inflows at Phalen Colliery in the Sydney Coalfield and Their Relation to Interaction of Workings. Proc. 5th Int. Mine Water Congress Nottingham UK Sept 1994, pp 83 - 95.

Chappell B.A. (1987) Predicted and Measured Rock Mass Moduli. *Mining Science and Technology*, 6 (1987) pp 89-104. Elsevier Sci. Pub.

Church H.K. (1988). *Excavation Planning Reference Guide*. McGraw-Hill Engineering Reference Guide Series.

Clark G.B. (1988). Centrifugal Testing in Rock Mechanics. *Centrifuges in Soil Mechanics*. Craig, James and Scholfield (eds). 1988 Balkema, Rotterdam. ISBN 90 6191 800 6, pp 187 - 198.

Conroy P.J. & Gyarmaty J.H. (1982). Planning Subsidence Monitoring Programs Over Longwall Panels. Proc. Symp. 'State-of-the-Art of Ground Control in Longwall Mining and Mining Subsidence',American Inst. Min., Metall. & Petroleum Eng., New York, pp 225 - 234.

Crane W.R. (1975). Subsidence and Its Relation to Drainage in the Red Iron Mines of the Birmingham District, Alabama. *Transactions of the American Institute of Mining and Metallurgical Engineers*, 72, pp 837 - 869.

Craft J.L. & Crandall T.M. (1988). Mine Configuration and Its Relationship With Surface Subsidence. Proc. Conf. Mine Drainage and Surface Reclamation, U.S. Bureau of Mines.

Crouch Research Inc. (1988). *The FESOL System. User's Guide*. Minnesota, USA.

Crouch S.L. & Starfield A.M. (1983). *Boundary Element Methods in Solid Mechanics*. Allen & Unwin, London.

Donnelly L.J. & Reddish D.J. (1994). The Development of Surface Steps During Mining Subsidence: "Not Due to Fault Reactivation". *Engineering Geology* 36, Elsevier Science, The Netherlands, pp 243 - 255.

Dunrud C.R. (1984). Coal mine subsidence - Western United States. *Geological Society of America, Reviews in Engineering Geology*, 6, pp 123-150.

Edwards J.L., Swan D.B., McNabb K.E., and Wardle L.J. (1993) Mine Design Considerations for Surface Subsidence Control. Proc. 12th Int. Conf. On Ground Control in Mining. West Virginia. Peng S.S. ed., pp 385 - 386.

Einstein H.H. & Hirschfeld R.C. (1973). Model Studies on Mechanics of Jointed Rock. *J. Soil Mechanics & Foundations.* Div. American Soc. Civ. Engineers. 99, SM3, pp 229 - 248.

Evans A.W., Kawecki M.A. & Nikraz H. (1988). Influence of Pore Pressure Variation on Sandstone Behaviour and Its Contribution to Subsidence and Strata Behaviour Interpretation in the Collie Basin. West. Aust. Mining & Petroleum Research Institute Western Australia, Report No.35, 25 p.

Farmer I.W. & Altounyan, P.F.R. (1980). The Mechanics of Ground Deformation Above a Caving Longwall Face. Proc. 2nd Int. Conf. on Ground Movement and Structures. University of Cardiff, 1980, pp 75-91.

Fawcett R.J. (1986). Studies on the Prediction of Groundwater Inflow to Longwall Coal Faces. PhD thesis dissertation, University of Nottingham, England, 285 p.

Ferrari C.R. (1996). Case for Continuing Coal Mining Research. *Mining Technology,* June 1996, pp 171 - 176.

Fitzpatrick D.J., Reddish D.J. & Whittaker B.N. (1986). Studies of Surface and Sub-surface Ground Movements Due to Longwall Mining Operations. Dept. Mining Engineering University of Nottingham, England.

Fitzpatrick D.J. (1987). Modelling of Mining Subsidence Mechanisms and Prediction of Ground Movements. PhD Thesis Dept. Mining Engineering University of Nottingham, England, 168 p.

Fotakis D. (1985). Subsidence in the Collie Basin. Masters Thesis (B.Min.Eng.), Western Australian School of Mines. Curtin University of Technology WA, 121 p.

Fritzche C.H. & Potts E.L.J (1954) *Horizon Mining.* George Allen and Unwin Ltd. London.

Galvin J. M. (1981). The Mining of South African Thick Coal Seams - Rock Mechanics and Mining Considerations. PhD Thesis, University of Witwatersrand, Johannesburg, South Africa, 336 p + appendices.

Galvin J.M. & Anderson K.G. (1986). The Design of Multi-Seam Workings at Shallow Depth Under Tidal Waters. Proc. Symp. Ground Movement and Control Related to Coal Mining, pp 352 - 361.

Galvin J.M. (1988). Surface Subsidence Mechanisms Theory and Practice. *The Coal Journal* No.19, pp 11 - 25.

Garrity P. (1981) Effects of Mining on Surface and Subsurface Water Bodies. PhD thesis, University of Newcastle upon Tyne.

Garrity P. (1983). Water Flow Into Undersea Mine Workings. *International Journal Mining Engineering.*1, pp 237-251.

Germanis E. & Smith G.W. (1973). Criteria for Design and Tolerance of Structures and Services to Subsidence Movements. Proc. Sym. 'Subsidence In Mines ' Aust. Inst. Min. Metall., Illawarra Branch, pp 12/1 - 12/8.

Goldsmith C.R., Brice S.J. & Evans A.W. (1995). An Investigation of the Controls on Shallow Subsidence in the Collie Basin. MERIWA Report No 140.

Gonot and Dumont (1871). Des Affaisements du sol Produits par L'exploitation Houillere. Liege.

Grond G.J.A (1952) A Critical Analysis of of Early and Modern Theories of Mining Subsidence and Control. Dept. Of Mining, University of Leeds.

Gurtunca R.G. & Bhattacharyya A.K. (1988). Modelling of Surface Subsidence in the Southern Coalfield of New South Wales. Proc. 5th Aust-N.Z. Conference on Geomechanics, Sydney, pp 346 - 350.

Gvircman B.Y (1977). Undermining Water Reservoirs Without Risk. Nedra, Moscow, 174 pp (in Russian).

Halbaum (1903). Longwall Workings. The Action, Influence and Control of the Roof in Longwall Workings. *Trans. of the Institute of Mining Engineers*, Vol. XXVII pp 205 - 228.

Hammond G. A., Misich I.J., and Boyd G. (1983). Geotechnical Report - WCL & Dampier Region. Internal report to WCL.

Haycocks C., Karmis M. & Ehgartner B. (1982). Multiple Seam Mine Design. Proc. Symp. 'State-of-the-Art of Ground Control in Longwall Mining and Mining Subsidence', American Inst. Min., Metall. & Petroleum Eng., New York, pp 59 - 65.

Hazen G.A., & Sargand S.M. (1988) Methods for Assessing Effects of Longwall Mining on Surface Subsidence. *Mining Engineering*, June 1988, pp 451 - 454.

Hazine H.I. (1977). A Study of the Development of the Surface Strains Produced by Mining Subsidence. Master of Philosophy, University of Nottingham.

Hebblewhite B. & Humphreys D. (1988). Underground mining research in the Collie Coalfield, Western Australia, NERDDP Project No. 644.

Hedley D.G.F (1969). Design Criteria for Multi-wire Borehole Extensometer Systems. Proc. 1st Canadian Symp. On Mine Surveying and Rock Deformation Measurements, New Brunswick, Canada, pp 349 - 377.

Helm D.C. (1984). Field-based Computational Techniques for Predicting Subsidence Due to Fluid Withdrawal. Geological Society of America Reviews in Engineering Geology Vol. VI, pp 1 - 22.

Heytenyi M. (1964). *Beams on Elastic Foundations* Vol. XVI, University of Michigan, Pub. Ambassador Book Limited, 255 p.

Hoek E. (1965). The Design of a Centrifuge for the Simulation of Gravitational Force Fields in Mine Models. *J. South African Institute Mining & Metallurgy*. Vol.65, No. 9, pp 455-487.

Hoek E., Kaiser P.K., & Bawden W.F. (1995). *Support for Underground Excavations in Hard Rock Mines*. AA Balkema, Rotterdam, 215 p.

Holla L. (1987). *Mining Subsidence in New South Wales.* Vol.1 & Vol.2 Dept. of Mineral Resources New South Wales, 32 p.

Holla L. (1989). Investigation Into Subsurface Subsidence. National Energy Research, Development and Demonstration Program. Commonwealth Dep. of Primary Industries and Energy, 189 p.

Holla L., Hughson R.A. & Sutherland G.A. (1986). Subsidence Legislation, Engineering, and Management. *Monograph Series No.12 Australasian Coal Mining Practice*, Aust. Inst. Min. & Metall., Sydney, pp 117 - 127.

Holla L. (1987). Design of Mine Workings Under Surface Waters in New South Wales. *Bulletin Australian Institute Minining Metallurgy*, 292, pp 45 - 50.

Holt G.E., Mildon A.D. & Fletcher K.L.(1984). Monitoring the Effects of Coal Extraction under the Great Western Railway near Bell, N.S.W. Proc. Fifth Aust. Tunnelling Conference, Sydney, Oct., pp 170 - 175.

Holt G.E. (1988). The Prediction of Multi-seam Subsidence Using a Finite Difference Program on a Desktop Computer. Proc. Conf. on Buildings and Structures Subject to Mine Subsidence. Newcastle Div. Institute of Engineers, Aug. 1988, pp 1 - 7.

Howell F.T. & Jenkins P.L. (1983). Centrifuge Modelling of Salt Subsidence Features. Source unknown, pp 193 - 201.

Hustralid W.A. (1976) A review of Coal Pillar Strength Formulas. *Rock Mechanics*, Vol. 8 1976, pp 115 - 145.

Iglesia G.R. (1991). Trap Door Experiment With Simulated Jointed Rock. Proc. Centrifuge 1991. Balkema Rotterdam.

Indraratna B. (1990). Development and Applications of a Synthetic Material to Simulate Soft Sedimentary Rocks. *Geotechnique*, 40 (2), pp 189-200.

ISRM (1978). Suggested methods for the quantitative description of discontinuities in rock masses. *International Journal of Rock Mechanics and Mining Sciences and Geomechanical Abstracts*, 15, pp 319 - 368.

ITASCA Consulting Group Inc. (1993) *FLAC Fast Lagrangian Analysis of Continua Version 3.2. Volume 1: User's Manual.* Minneapolis, Minnesota, USA.

Janezic S. (1987). Studija Za Resevanje Problematike Varnega Odkopavanja In Dolocitev Kriterijev Za Projektiranje In Odkopavanje Premoga Pod Vodonosnimi Plastmi V Jamah RLV. Rudnik Lignita Velenja. Geoloski Zavod Ljublana, 104 p.

Jeffrey R.J., Summers J.W., and North M.D. (1991). The Numerical Analysis of Deformation in Relation to Minewater Ingress at Wistow Colliery. Proc. 4th Int. Mine Water Congress, Ljubljana, Slovenia, September 1991, pp 73-84

Johnston I.W. & Choi S.K. A Synthetic Soft Rock for Laboratory Model Studies. Geotechnique 36, No.2, pp 251 - 263.

Jones O. & Kramadibrata S. (1985). An Excavating Power Model for Continuous Surface Miners. Submitted for publication Bulletin Australian Institute Mining & Metallurgy, 1995, 16 p.

Joseph P.G., Einstein H., & Whitman R.V. (1987). "A Literature Review of Geotechnical Centrifuge Modelling with Particular Emphasis on Rock Mechanics." Report to Air Force Service Centre, Tyndall Air Force Base, Report No. DACA88-86-D-0013.

Kapp W.A. (1982). A Review of Subsidence Experiences in the Southern Coalfield New South Wales, Australia. Proc. Symp. 'State-of-the-Art of Ground Control in Longwall Mining and Mining Subsidence', American Inst. Min. Metall. & Petroleum Eng., New York, pp 167 - 182.

Kapp W.A. (1984). Mine Subsidence in the Newcastle District, New South Wales. Source unknown, pp 331 - 340.

Kapp W.A. & Kennerly (1986). Subsidence and Strata Control Under Stored waters in the Southern Coalfield New South Wales. Proc. AUSIMM Symp. on Ground Movement and Control Related to Coal Mining, pp 341 - 151.

Kapusniak S. (1990). Internal report to Western Collieries LTD.

Karmis M., Triplett T., Haycocks C., and Goodman G. (1983). Mining Subsidence and Its Prediction in the Appalachian Coalfield. Proc. 24th US Symp. On Rock Mechanics., Texas University, pp 665 - 675.

Karmis M., Triplett T. & Schilizzi P. (1985). Recent Developments in Subsidence Prediction and Control for the Eastern U.S. Coalfields. Dept. Mining and Minerals Engineering, Virginia Polytechnic Institute and State University, pp 713 - 721.

Karmis M. (1989). Predicting Subsidence With a Computer. COAL, December 1989, pp 54 - 61.

Kay D. (1988). Prediction of Subsidence Ground Movements using Mathematical Modelling Techniques. Subsidence Research Steering Committee, NSW, 55 p.

Kay D. (1990). Angus Place Subsidence Modelling - Joint case Study. Report to sponsors, edited by New South Wales Dept. of Minerals and Energy, 58 pages plus appendices.

Kesseru Z. (1977). Recent Investigations and Some Observations on Protecting Layers. Pub. Of the Hungarian Mining Research Institute. Budapest, Hungary.

Klenowski G. & Phillips R.N. (1988). Determination of Groundwater Inflow From Longwall Mining, German Creek, Bowen Basin, Queensland. Proc. 3rd Mine Water Congress, Melbourne, Australia, pp 21 - 29.

Ko H. (1988). Summary of State-of the Art in Centrifuge Model Testing. *Centrifuges in Soil Mechanics*, Craig, James & Schofield (eds). Balkema, Rotterdam, pp 11-18 .

Kocar F., Veselic M., Ribicic M, Mramor J., Tamse M. (1987). Kriteriji Varnega Odkopavanja Premoga Pod Vodonosimi Plasimi V Jamah RLV. Titovo, Velejne, 1987, 108 p.

Kovago A. (1986). A History of Roof Failures in the Collie Basin. Internal report to Western Collieries LTD.

Kramadibrata S. and Jones I.O. (1993). Size Effect on Strength and Deformability of Brittle Intact Rock. Proc. 2nd International Workshop on Scale Effects in Rock Masses. Lisbon, Portugal, 25 June 1993, pp 277 - 284.

Kratzsch H. (1983). *Mining Subsidence Engineering*. Springer -Verlag, New York, 543 p.

Krishna R. (1989). Correlation of Surface Subsidence With Deformation Parameters in Underground and Intervening Strata. Indian Institute of Technology. Kharagpur, 98 p.

Krishna R. (1991). Measurement of Sub-surface Strata Behaviour in Bord and Pillar Mining: A Case Study. *J. Mining Science & Technology*, 13, pp 337 - 349.

Kunz K.S. (1957). *Numerical Analysis*: New York, McGraw-Hill.

Lajtai E.Z. (1967). The Influence of Interlocking Rock Discontinuities on Compressive Strength (Model Experiments) , source unknown.

Lama R.D., Moxon P., Shu D.M. (1986) Prediction of Subsidence Due to Longwall Mining at Westcliff Colliery. Proc. Symp. Ground Movement and Control Related to Coal Mining. AUSIMM - Illawarra Branch, pp 311-323

Lawrence W. (1986). Mathematical Modelling of Wongawilli Extraction, ACIRL panel, Western No 6 Colliery. ACIRL report to Western Collieries Ltd.

Lord J. H. (1952). Collie Mineral Field. *West Australian Geological Survey, Bulletin No.105.*

Lowry D.C. (1976). Tectonic History of Collie Basin, Western Australia. *Geological Society of Australia.* 23, 95-104.

McWilliams P.C. (1989). Bureau of Mines Geotechnical Centrifuge Research - A Review. U.S.B.M. Information circular 9218, 19 p.

Mair R.J. (1979). Centrifugal Modelling of Tunnel Construction in Soft Clay. PhD thesis, University of Cambridge.

Meyers A.G. (1993) The Determination of Rock Mass Strength for Engineering Design. PhD Thesis, University of Adelaide.

Mikula P.A. & Holt G.E. (1983). Prediction of Mine Subsidence in Eastern Australia by Mathematical Modelling. Proc. Int. Congress on Rock Mechanics Melbourne, Australia, pp E119 - E126.

[1]Misich I.J. (1985). Subsidence Report - 6B East Panel WD2 Mine. Internal memorandum to Western Collieries Ltd..

[2]Misich I. (1985). Investigation Into Creep in Underground Mines. Internal Memorandum to Western Collieries Ltd..

Misich I. & Humphreys D. (1988). Pillar Design Criteria. Internal Memorandum to Western Collieries Ltd..

Misich I. (1988). Investigation Into C17 Block Slope Failure - WO-5. Internal Memorandum to Western Collieries Ltd..

Misich I. (1991). Summary of Subsidence Investigations. Internal Memorandum to Western Collieries Ltd..

Misich I., Evans, A. & Jones O. (1991). Control & Strata Investigations to Allow Total Extraction of Coal by Underground Methods in the Collie Basin (Western Australia). Proc. 4th Int. Mine Water Congress, Ljubljana, Slovenia, September 1991, pp 131 - 146.

Misich I., Evans A. & Jones O. (1992). Subsidence Prediction From the Beginning - Collie Coal Basin (Western Australia). Proc. 11th Conf. Ground Control in Mining, Wollongong, New South Wales, July 1992, pp 443 - 451.

[1]Misich I. Evans A. & Jones O. (1993). Subsidence Prediction and Management in Collie (Western Australia). Proc. Conf. On Mining Subsidence in Urban and Developed Areas Rock Springs Wyoming, Sept. 1993, pp 1 - 9.

[2]Misich I, Hammond G, Evans A & Jones O, and MacPherson R. (1993). Mining coal in water bearing strata in Western Australia. Proc. International Conference on Environmental Management, Ge-water and Engineering Aspects. Wollongong, New South Wales, Australia, February 1993. A.A Balkema Rotterdam, pp 635 - 649.

Misich I. Evans A & Jones O. (1994). Subsidence Prediction and Management in the Collie Coalfields (Western Australia) Proc. Third International Conference on Environmental Issues and Waste Management in Energy and Mineral Production. Perth, Western Australia, pp 303 - 310.

Misich I., Evans A. & Jones O. (1995). Subsidence Prediction and Management in Collie (Western Australia). Proc. 5th Int. Symp. on Land Subsidence. The Hague, Netherlands, 16 - 20 Oct 1995, pp 175 - 185.

Mitchell R.J. (1991). Sill Mat Evaluation Using Centrifuge Models. *Mining Science and Technology*, 13, pp 301-313.

Munson D.E., Eichfield W.F. Evaluation of European Empirical Methods for Subsidence in U.S. Coalfields. B.U.S.A.R, 23 p.

Myers R.H. (1986). *Classical and Modern Regression with Applications.* PWS Publishers, Boston, Massachusetts.

National Coal Board (1966) *Subsidence Engineers' Handbook.* Mining Department, National Coalboard, Doncaster.

National Coal Board (1972) Design of Mining Layouts. Mining Department, National Coalboard, Doncaster.

National Coal Board (1975) *Subsidence Engineers' Handbook.* Mining Department, National Coalboard, Doncaster, 111 p.

Nikraz H. (1991). Laboratory Evaluation of the Geotechnical Design Characteristics of the Sandstone Aquifers in the Collie Basin. PhD thesis, Curtin University of Technology, 312 p.

Nikraz H., Press M. & Evans A. (1995). Prediction of land subsidence caused by mine dewatering. Proc. Fifth Int. Symp. On Land Subsidence. The Hague, October 1995. IAHS Publ. No. 234, pp 197 - 206.

Obert & Duval (1967). *Rock Mechanics and the Design of Structures in Rock.* John Wiley & Sons Inc. Sydney.

Orchard R.J. (1964). Partial Extraction and Subsidence. Proc. Meeting of the Southern Counties Institute of Mining Engineers, London, pp 417 - 428.

Orchard R.J. (1973). Some Aspects of Subsidence in the UK. Proc. Sym. 'Subsidence In Mines ', Aust. Inst. Min. Metall., Illawarra Branch, pp 3/1 - 3/8.

Pells P.J.N. & Ferry M.J. (1983). Needless Stringency in Sample Preparation Standards for Laboratory Testing of Weak Rocks. Proc. Int. Cong. Rock Mechanics, Melbourne, 1983, pp A 203 - A 207.

Peng S.S. & Chiang H.S. (1984). *Longwall Mining*. John Wiley & Sons Inc. U.S.A.

Peng S. (1992). *Surface Subsidence Engineering*. Braun Brumfield Inc. Ann Arbour M.I., 161 p

Platt P.E. (1987). Geotechnical Investigations Into The Modified Wongawilli Extraction System at Western No.6 Colliery. Masters degree project, University of New South Wales, 123 p.

Potts E.L.J. (1964). Current investigations in rock mechanics and strata control. Proc. 4th Int. Conf. on Strata Control and Rock Mechanics, New York, May 4-8 1964.

Puckett G.A. & Mikula P.A. (1984). Development of Geotechnical Mathematical Modelling Techniques for Coal Mine Design. Published Report 84-5, A.C.I.R.L., North Ryde, Sydney.

Raisbeck D. (1988). Surveillance of Structures in the Latrobe Valley. Proc. Conf. on Buildings and Structures Subject to Mine Subsidence. Newcastle Div. Institute of Engineers. Aug. 1988, paper #9, 6 p.

Reddish D. (1984). Study of Ground Strain in Relation to Mining Subsidence. PhD Thesis, Nottingham University, England.

Reynolds R.G. (1976). Coal Mining Under Stored Water. Report on Inquiry into Coal Mining Under or in the Vicinity of Stored Waters, New South Wales Government Printer.

Richmond T.C. *[Editor]* (1993). Proceedings of the Conference on Mine Subsidence in Urban and Developed Areas. Presented by Abandoned Mine Land Division Wyoming Department of Environmental Quality, Rock Springs ,Wyoming, 385 p.

Ringis J. (1976). The Use of Gamma-Ray Logging to Measure Sub-surface Subsidence. Geological Survey Rep. GS 1976/317 Geol. Surv. New South Wales, Dept. Of Mines.

Rowlands D. (1990). Establishing a Design Rationale for Partial Extraction Coal Mining Systems. Commonweath of Australia NERDD Report / EG91/968, 68 pages plus appendices.

Salamon M.D.G. & Oravecz K.I. (1967). *Rock mechanics in coal mining.* Contract report to the Coal Mining Research Controlling Council. Chamber of Mines South Africa.

Salamon M. (1991) Behaviour and Design of Coal Pillars. *The Australian Coal Journal No. 32*, pp 11 - 22.

Scott C.R. (1980). *An Introduction to Soil Mechanics and Foundations.* Applied Science Pub., London, 406 p.

Seneviratne P. (1987) Design of Partial Ectraction Systems for Mining in New South Wales. PhD dissertation, University of New South Wales.

Sherwood G.E.F & Taylor A.E. (1957). *Calculus*, Englewood Cliffs, New Jersey, Prentice Hall Inc.

Shu D. (1990) Studies of Surface and Subsurface Subsidence Movements Due to Underground Coal Mining. PhD dissertation University of New South Wales, 362 p.

Singh R.N., Hibbert S., and Fawcett R.J. (1985). Numerical Calculation of Groundwater Inflow Into Longwall Coal Faces. Proc. 2nd Int. Mine Water Congress IMWA, Granada Vol.1, pp 541 - 552.

Singh T.N. & Kendorski F. (1981). Strata Disturbance prediction for Mining Beneath Surface Water and Waste Impounds. Proc. 1st Conf. on Ground Control in Mining. West Virginia University, July 1981.

Smith G.N. (1971). *An Introduction to Matrix and Finite Element Methods in Civil Engineering.* Applied Science Pub. London.

Smith G.N. (1973). *Elements of Soil Mechanics for Civil and Mining Engineers.* 3rd. Edition, Granada Publishing LTD., London.

Sowers G.F. (1979) *Introductory Soil Mechanics & Foundations*, 4th Ed. Collier MacMillan.

Stacey T.R. & Page C.H. (1986). *Practical handbook for underground rock mechanics.* Trans Tech Publications. Clausthal, Germany, 144 p.

Stephan P.C.W. (1989). Entwicklung und Erprobung Eines Modellprufstandes zur Losung Driedimenionaler Gebirgsmechanischer Aufgaben im Steinkohlentiefbau. Phd dissertation (in German), Clausthal University of Technology, Germany, 251 p.

Stephansson O. (1971). Stability 0f Single Openings in Horizontally Bedded Rock. *Engineering Geology*, 5, pp 5-71.

Stimpson B. (1970). Modelling Materials for Engineering Rock Mechanics. *International Journal Rock Mechanics & Mineral Science*, 7, pp 77 - 121.

Stone K.J.L., Randolf M.F. & Jewell R.J. (1991). Feasibility study for centrifuge modelling of coal extraction in the Collie Basin. Report to Western Collieries Ltd.

Stone K., Jewell R. & Misich I. (1991). Modelling Surface and Subsidence Over Coal Mines. Proc. 5th Mine Tunnelling Conf., Christchurch, New Zealand.

Stone K. & Wood M. (1987). Model Studies of Soil Deformations Over a Moving Basement. Report No. CUED/D-SOILS/TR197 Cambridge University Engineering Dept. May 1987, 7 p.

Stone K. & Brown T. (1993). Simulation of Ground Loss in Centrifuge Model Tests. *Geotechnical Testing Journal*, June 1993. American Society for Testing and Materials Phil. PA.

Sutherland H.J. (1986). Program Review: Subsidence and Roof Stability Analysis for the Extraction and *In situ* Processing of Fossil Fuels. 10(4), pp 313-389.

Sutherland H.J. & Munson E. (1982). Complimentary Influence Functions for Predicting Subsidence Caused by Mining. Proc. 23rd. Symp. in Rock Mechanics on Issues in Rock Mechanics, AIME, pp 1115 - 1121.

Sutherland H.J., Heckes A.A. & Taylor L.M. (1984). Physical and Numerical Simulations of Subsidence Above High Extraction Coal Mines. Proc. Conf. Design and Performance of Underground Excavations. ISRM/BGS Cambridge, 1984.

Thompson R. (1988). Pipeline Design in Mine Subsidence Areas. Proc. Conf. on Buildings and Structures Subject to Mine Subsidence. Newcastle Div. Institute of Engineers, paper #3, 5 p.

Tomlin N. & Bicer N. (1988) The Application of Physical Modelling to the Undersea Mining Conditions at Kozlu Mine in Turkey. Proc. 3rd Int. Mine Water Congress. Melbourne Australia, October 1988, pp 371 - 381.

Unrug K. & Szwilski T.B. (1982). Methods of Roof Caveability Prediction. Proc. Symp. State-of-the-Art of Ground Control in Longwall Mining and Mining Subsidence, American Inst. Min., Metall. & Petroleum Eng., New York, pp 13 - 29.

U.S. Bureau of Mines (1985). Mine Subsidence Control. Proc. Bureau of Mines Technology Transfer Seminar, Pittsburgh. Information Circular 9042.

Vardoulakis I., Graf B & Gudehus G. (1981). Trap-Door Problem With Dry Sand: A Statical Approach Based Upon Model Test Kinematics. *International Journal for Numerical and Analytical Methods in Geomechanics*, 5, pp 57-78.

Veselic M. & Enichlmayr E. (1988). Water Inrush Protection Criteria and Dewatering Scheme at Sakog Brown Coal Mine, Trimmelkam, Austria. Proc. 3rd Int. Mine Water Cong., Melbourne, Australia, pp 583 - 588.

Wagner H. (1980). Pillar design in coal mine. *Journal South African Insitute of Mining & Metallurgy*, 80, pp 37-45.

Wardell K. & Partners (1975). Mining Under Tidal Waters. New South Wales Ministry For Mines and Power, Ref. KW/EM/3757.

Wardle L.J. (1986). Boundary Element Methods for Stress Analysis of Tabular Excavations. PhD Thesis, Univ. of Queensland.

Wardle L.J. & Enever J.R. The Application of the Displacement Discontinuity Method to the Planning of Mine Layouts. Proc. 5th. Int. Congress on Rock Mechanics, Melbourne, pp E61-E69.

Wardle L.J. & McNabb K.E. (1985). Stress Monitoring During Extraction in 8 North Panel, Lalem No.1 Colliery South Blackwater, QLD. Report No.60, C.S.I.R.O. Division of Applied Geomechanics, Syndal, Melbourne, Victoria.

Whittaker B.N. (1982). A Review of Progress with Longwall Mine Design and Layout. Proc. Symp. State-of-the-Art of Ground Control in Longwall Mining and Mining Subsidence, American Inst. Min., Metall. & Petroleum Eng., New York, pp 77-84.

Whittaker B.N. & Reddish D.J. (1989). *Subsidence Occurrence Prediction and Control.* Elsevier, New York, 528 p.

Whittaker B.N., Reddish D.J. & Fitzpatrick D.J. (1985). Ground Fractures Due to Longwall Mining Subsidence. Dept. Mining Eng. Univ. Nottingham, England.

Whittaker B.N., Reddish D.J. & Sun G.X. (1991). Subsurface Strata Changes Due to Longwall Mining. Final report to British Coal Corp., Bretby, Staffs. DE 15OQD, May 1991.

Whittaker B.N. & Woodrow G.J.M. (1977). The Constant Tension Strain Wire Borehole Extensometer and Its Application to Instrumentation of Underground Openings. Proc. Symp. On Field Measurements in Rock Mechanics, Zurich.

Wilson A.H. (1980). The Stability of Underground Workings in the Soft Rocks of the Coal Measures. PhD. Thesis, Nottingham Univ. England, 187 p.

Wilson A.H. (1982). Pillar Stability in Longwall Mining. Proc. Symp. State-of-the-Art of Ground Control in Longwall Mining and Mining Subsidence, American Inst. Min., Metall. & Petroleum Eng., New York, pp 85 - 95

Wilson R. C. (1943). The Collie Coalfield Its Problems and Its Economic Importance. Paper presented to the Royal Society of Western Australia, July 13, 1943, pp 41-42.

Wold M.B. (1984). Physical Model Study of Caving Under Massive Sandstone Roof Conditions at Moura, Queensland. CSIRO Div. Geomechanics Report No. 57.

Wold M.B. & Pala J. (1986). Three-dimensional stress changes in pillars during longwall mining at Ellalong Colliery. Report No. 65. CSIRO Div. Geomechanics. Mt Waverly, Victoria, 44 p.

Xiao G.C., Irvin R.A. & Farmer I.W. (1991) Use of Database in Ground Control to Identify Weightings and Water Inflows. Proc. 10th International Conference on Ground Control in Mining. Morgantown, West Virginia. Peng S.S. ed.,pp177 - 183.

TABLE OF CONTENTS

APPENDIX V

LIST OF FIGURES

LIST OF TABLES

APPENDIX I

SUBSIDENCE MONITORING

I.1 SURFACE SUBSIDENCE SURVEYING

Surface subsidence was measured by surveying lines of fixed points anchored into the surface. The survey method used was either an engineer's spirit level/ survey staff or Electronic Distance Measurement (EDM) equipment. Measurement of each survey line commenced from a reference point well outside the influence of the extraction panel (outside the angle of draw) to avoid closing error arising from movement of the base station. The positioning of reference points can vary, depending on the sequencing of nearby areas of extraction, and to take into account the possibility of pillar punching or pillar collapse (Section 2.5.5.1) outside the panel area to be extracted.

Subsidence grid lines are levelled at the end of each mining cycle, immediately prior to the commencement of "lifting" of subsequent fenders. The frequency and timing of levelling is not regular, as it is dependent on the progress of mining. The level of repeatability achieved for the survey monitoring was ± 15 mm.

Lateral movements are measured using a steel tape stretched between the centre-punched marks of each survey station (star picket). The timing of monitoring lateral movement is usually such that it coincides with the completion of mining of a major section of the panel and some time well after panel completion (once noted subsidence has ceased). These lateral measurements are then used to calculate horizontal strains consequent to surface subsidence. Strains are calculated as the change in distance between any two adjacent pins, divided by the bay length (distance between the two pins) and reported in millimetres per metre.

I.2 SUBSIDENCE GRID INSTALLATION

Subsidence grid lines are installed with the view of minimising costs without compromising the quality of data retrieved. Consequently, the number of grid lines and survey stations installed above a particular panel depend on the depth of cover and the geometry of the extraction panel. Plans of the layout of each panel and subsidence grids installed are given in Figures I.1 to I.8.

For the earlier, rectangular-shaped panels, two grid lines were installed at the surface through each major axis of the panel (eg. 2SA panel - Plan I.5). For irregularly shaped panels, an additional survey grid line was optionally installed, centrally through the irregularity (eg. Line D above Blue panel - see Plan I.4). 1 North and NWB3 panels, however, had only one subsidence grid line installed - in the direction of advancing panel length. It was found that survey lines oriented across the panel were affected by pillar punching of the smaller set-up pillars at one end and irregular lengths of mining at the other end.) Where required, subsidence lines were offset from above the centre of the panel to minimise the effect of any remnant pillars left at the intersections of Wongawilli splits and panel ventilation bords.

The ground surface above all panels was relatively flat; therefore the subsidence profiles measured during the trial were not influenced by steeply dipping topographical features.

The spacing of survey stations within each subsidence grid was either 5, 10 or 20 m. This represents a variation from recommendations by the NCB (1975) and L. Holla (1987), which suggest a spacing of 1/20 x depth of cover. This variation arose because of the high number of survey stations required to meet the NCB standards for total extraction panels at depths of cover less than 100 m (eg. above 2B West E1 panel in WD2, which averages 35 m cover). It was decided to limit the distance between survey pins to 5 metres for panels with a depth of cover less than 100 m and 10 metres for panels greater than 100 m deep.

For very long panels (>400 m) such as 1 North panel, the spacing of subsidence grid stations in the central section of the panel was widened to 20 m to reduce surveying times and expenses. The length of the subsidence grid lines were designed to ensure surveying encompasses the complete subsidence profile within the angle of draw. The typical horizontal distance that subsidence grids are extended beyond

panel limits is 0.7 times the mining depth of cover.

The method employed for installation of the survey grid lines is as follows:

i) Subsidence grid lines are marked out and, where required, 3 m wide strips are cleared along the length of the lines.

ii) Survey points are then surveyed in at the correct intervals and orientation relative to the panel below.

iii) Holes, 1.5 m deep and 75 mm diameter, are drilled for each survey station using a post-hole auger.

iv) Each hole is then filled with cement slurry, and 1.5 m long star pickets are then pushed in place.

v) Each star picket is then centre punched and labelled with aluminium permatags.

An example of a survey subsidence grid line is given in Figure I.9.

I.3 SURFACE SUBSIDENCE MONITORING RESULTS

Rather than provide a copious amount of survey data in tabulated form, the subsidence monitoring data has been presented as a series of graphs of vertical subsidence, tilt and horizontal strain. Access to raw data will require special permission from WCL.

Results have been provided only for those total extraction panels extracted during the period of research, and those specifically used for developing subsidence models. These panels are listed in Table I.1. Monitoring above each panel includes any combination of surface, subsurface and groundwater monitoring. The scope of monitoring in each panel was dependent on budgetary restraints, and whether the overlying strata had been "drained" prior to the commencement of total extraction mining. Groundwater monitoring data has only been provided for Red Panel and NWB3 panel. Recorded data from ACIRL panel can be obtained from Hebblewhite and Humphries (1988). No meaningful water measurements were obtained from Blue panel which can be presented in this thesis - largely due to the drainage effect of ACIRL panel on the adjacent Blue panel.

Table I.1 **EXTRACTION PANEL MONITORING**

		PANEL, MINE	MONITORING
%	1)	ACIRL Panel (A & B), WD6	(surface, subsurface & aquifers)
+	2)	2B West E1& E2 Panels, WD2	(surface only, aquifers "dry")
%	3)	2B West C Panel, WD2	(surface only)
~~	4)	Blue Panel, WD6	(surface, subsurface & aquifers)
+	5)	2 South A Panel, WD6	(surface & subsurface, aquifers"dry")
%	6)	Red Panel, WD6	(surface & aquifers)
+	7)	1 North Panel, WD6	(surface & subsurface, aquifers "dry")
%	8)	North West B3 Panel, WD6	(surface, subsurface & aquifers)

%; subcritical width panel, ~~; critical width panel, +; super-critical width panel

Maximum subsidence values, measured at incremental stages of extraction, and also well after the completion of each extraction panel, have been provided in Table 3.2. It should be noted that in some instances, WCL undertook a program of pillar extraction in adjoining bord and pillar workings (eg. Blue panel Laterals - see Figures I.1 and I.4) once extraction in the main panels was completed. In these cases, the subsidence recorded once pillar extraction had commenced have not been included in the Table. The graphical results given below may show greater values of subsidence than given in Table 3.2, however, as explained, the subsidence measured following the commencement of pillar extraction have been ignored in this study.

A summary of the extraction sequence for each panel has been included to provide the reader the opportunity to compare the measured subsidence at any given date against the equivalent panel width.

Attention has been drawn to any variation from the subsidence development "norm" by annotation on the graphs. The annotation, when viewed in conjunction with the plans of each panel, provide adequate explanation for the cause of the variation. Consequently, there has been no detailed written commentary provided in the text.

Note that the strain measurements have not been undertaken with the same frequency as the survey levelling. This was because strain measurement is labour intensive. Strain has only been measured at critical periods uring panel development.

No strain values have been provided for Red panel, other than Line C, as Line C was considered to be the most favourably oriented to the direction of panel advance. In some panels, some survey lines have had no strain measurements taken, other than the initial readings taken on installment. These areas with no strain information are typically restricted to shallow panels (eg. 2BWE2 panel in WD-2) where discontinuous forms of subsidence developed. It was not considered warranted to measure strains in areas where the surface has been greatly disturbed.

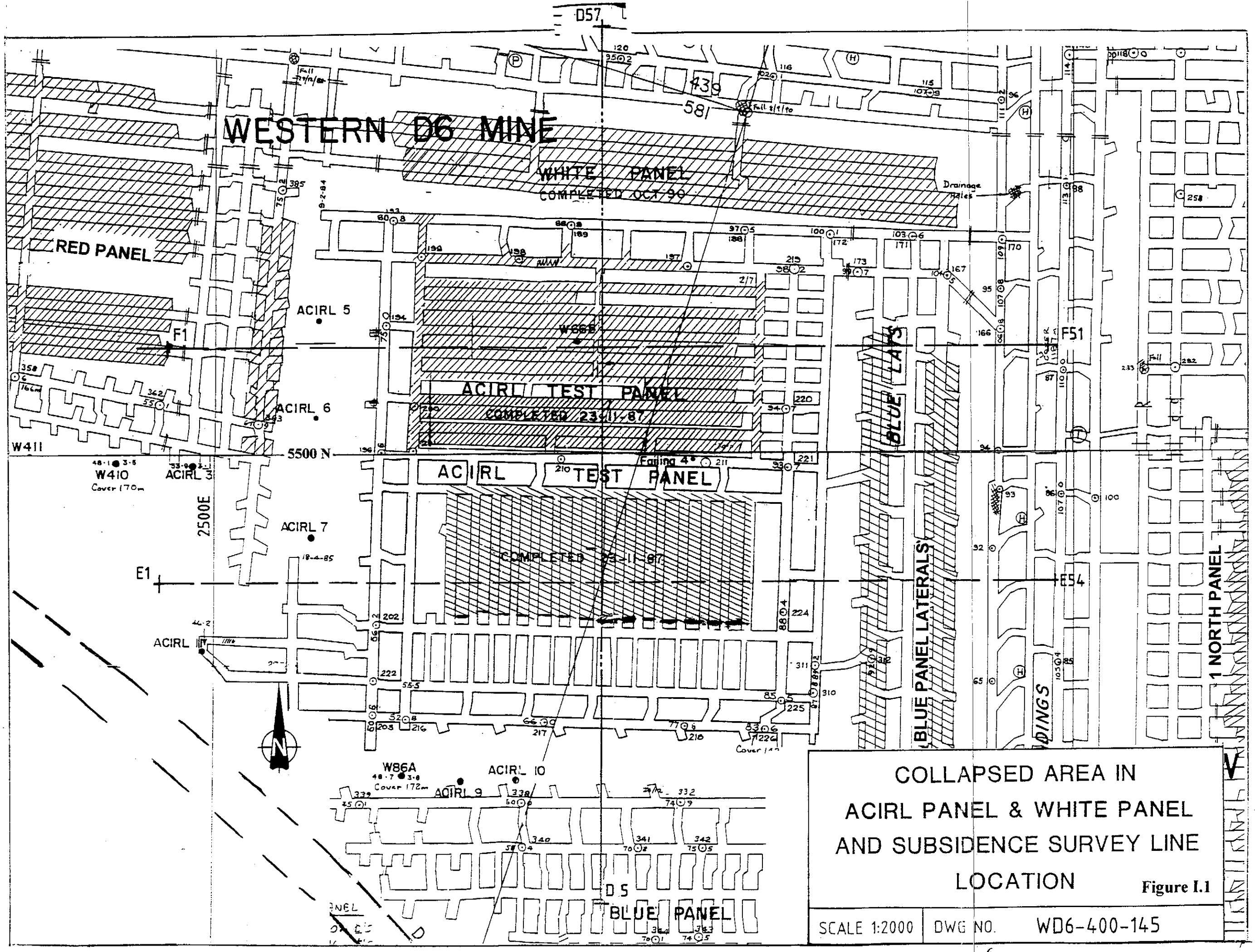

COLLAPSED AREA IN
ACIRL PANEL & WHITE PANEL
AND SUBSIDENCE SURVEY LINE
LOCATION

Figure I.1

SCALE 1:2000	DWG NO. WD6-400-145

2B WEST E1 PANEL

B1

C1

A98

SPLIT LINE

SINK HOLES

A94
C9

500 W

D29D

W539

CB2-7C

FLOOR RL 192·1
THK 2·8

CB2-7B
FLOOR RL 191·0
THK 1·1

CB2-7A
THK 1·8

W533

D29
FLOOR RL 176·5
THK 3·6

D29O
FLOOR RL 166·30
THK 3·5

22/12

2W 182

A49
B45

D29C
FLOOR RL 163·2
THK 3·8

C49

W532 FLOOR RL 178·1
THK 3·6

D29T

2B WEST
E1 PANEL
COMPLETED 24-8-89

Fall 2/12/89

W531 FLOOR RL 153·0 THK 3·0

D29R

HDGS

HILLE

10000 N

B83

D29P
183·9 3·5

E60

W665

W535

D29H
178·4 3·8

B101,E39

2B WEST
E2 PANEL
COMPLETED 15-12-89

Position of Vugh Area

Assumed

E1

D124
143·4 3·2

B108

HDGS

2 WEST

WD2 MINE

N

COLLAPSED AREA IN
2B WEST E1 & E2 PANELS
AND SUBSIDENCE SURVEY LINE
LOCATION

Figure I.2

SCALE 1:2000 | DWG NO. WD2-400-119

WD2 MINE

COLLAPSED AREA IN
2B WEST C PANEL
AND SUBSIDENCE SURVEY LINE
LOCATION

Figure I.3

SCALE 1:2000 | DWG NO. WD2-400-120

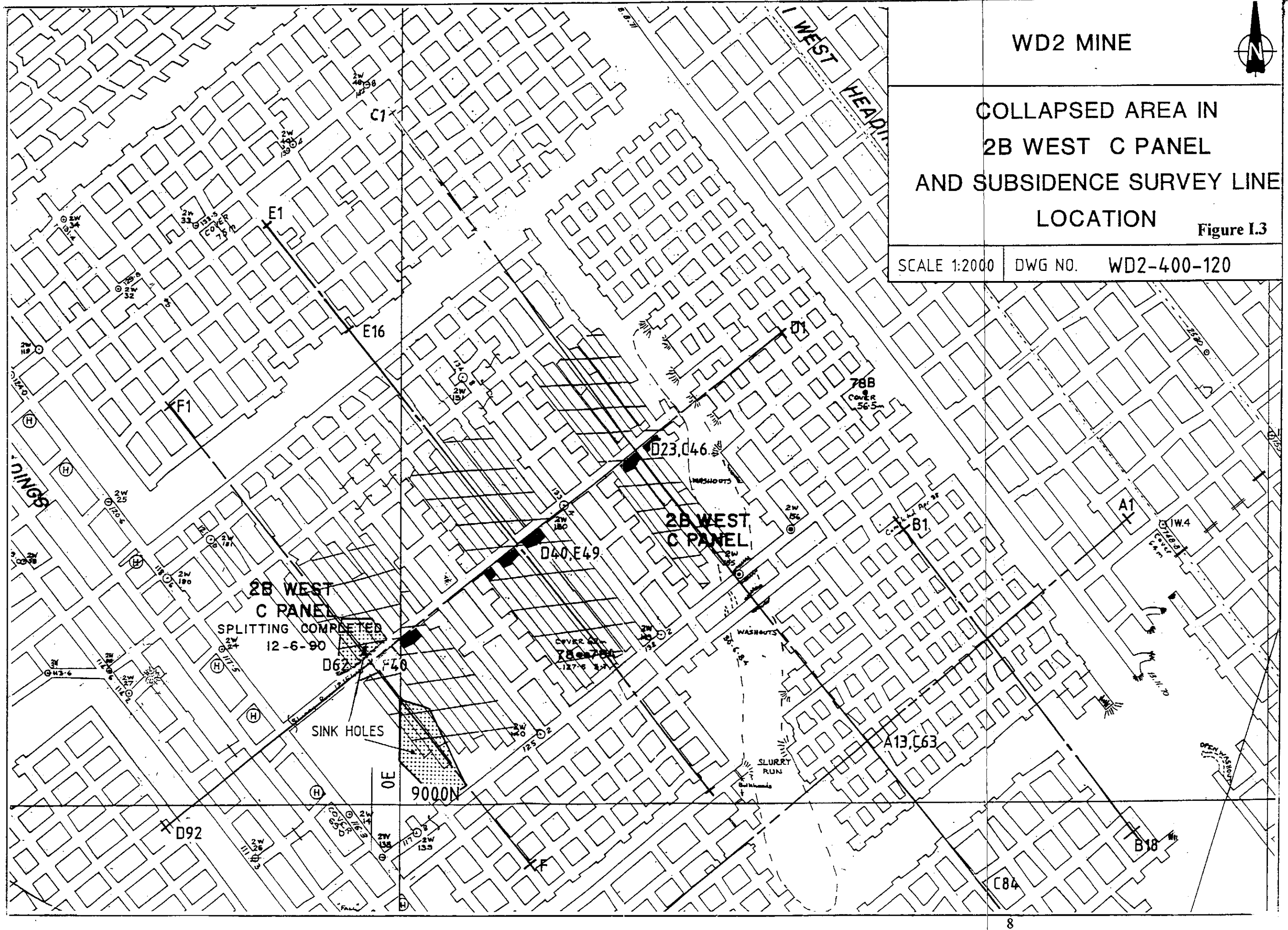

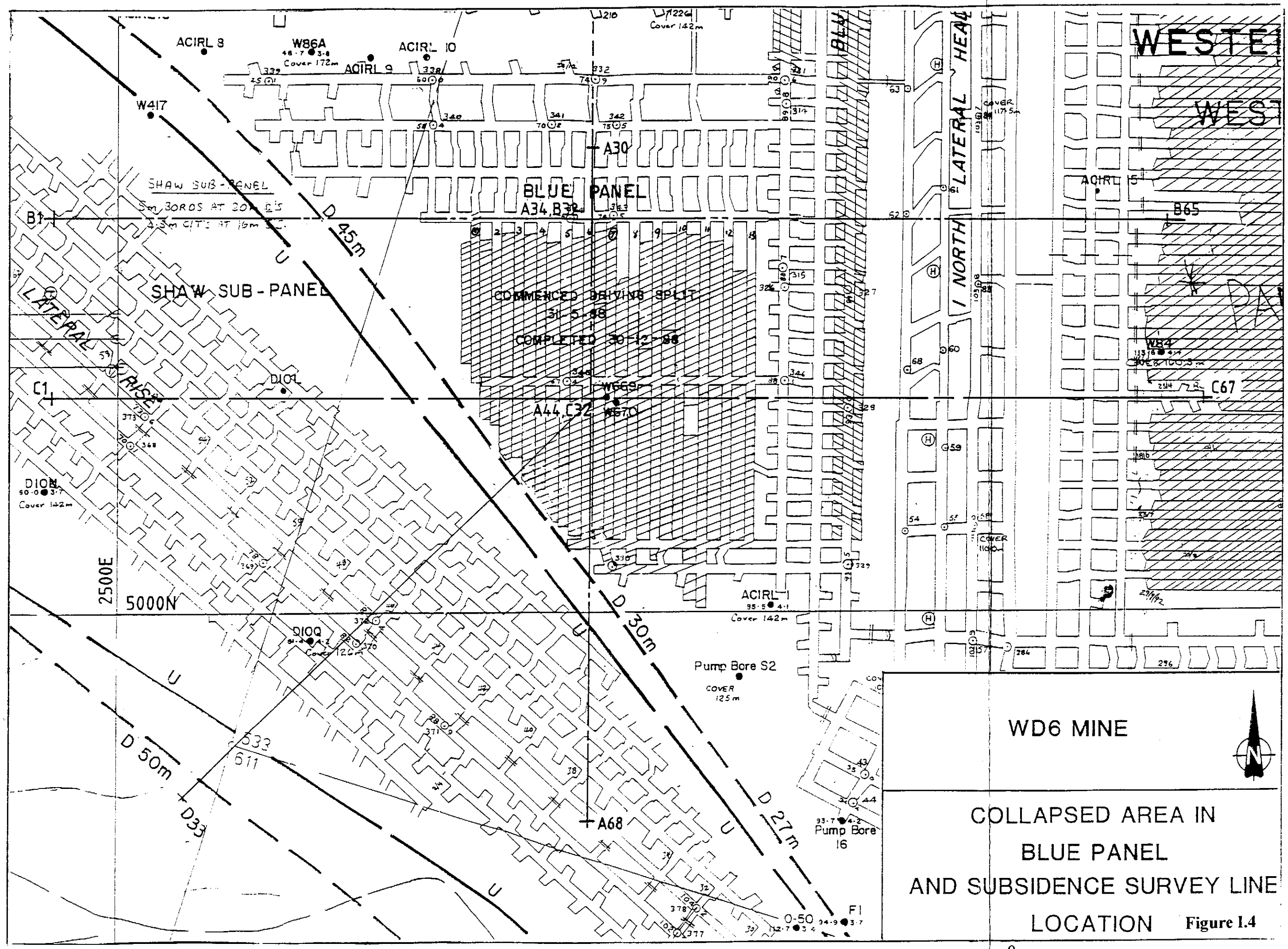
ACIRL 8
W86A
ACIRL 10
ACIRL 9
W417
SHAW SUB-PANEL
3m BOROS AT 30m C's
4.5m CITS AT 18m C.
B1
SHAW SUB-PANEL
BLUE PANEL
A34, B32
A30
COMMENCED DRIVING SPLIT
31-5-88
COMPLETED 30-12-88
W669
W670
A44, C32
LATERAL RISE
DIOL
C1
DION
Cover 142m
D 45m
U
LATERAL HEAD
NORTH
ACIRL 5
B65
C67
W84
WESTE
WEST
2500E
5000N
DIOQ
Cover 125m
ACIRL 1
Cover 142m
Pump Bore S2
COVER 125m
D 30m
D 27m
D 50m
D35
533
611
A68
0-50
F1
Pump Bore 16
WD6 MINE
N
COLLAPSED AREA IN
BLUE PANEL
AND SUBSIDENCE SURVEY LINE
LOCATION

Figure I.4

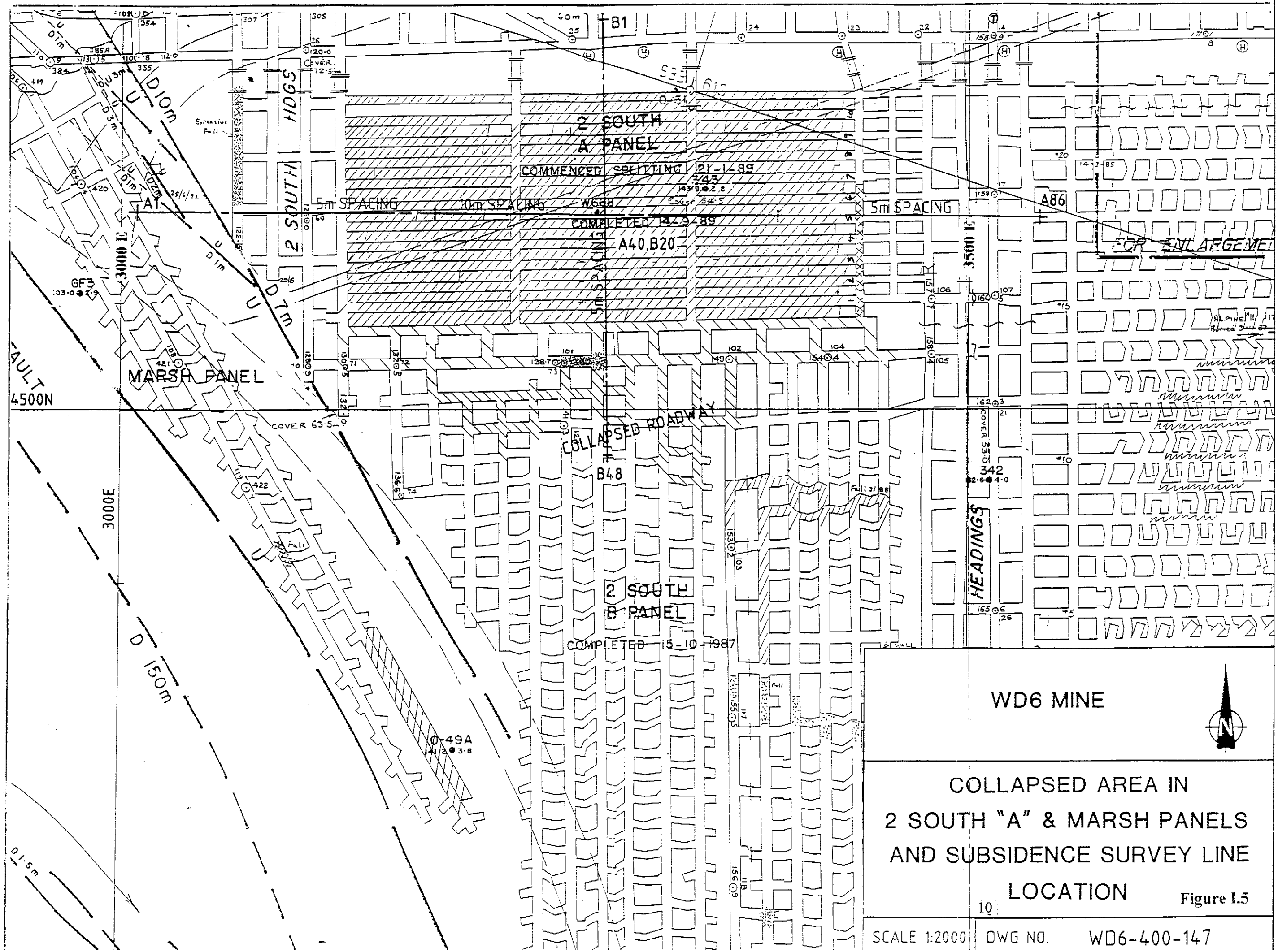
2 SOUTH
A PANEL
COMMENCED SPLITTING 21-1-89
5m SPACING
10m SPACING
W668
COMPLETED 14-9-89
A40,B20
5m SPACING
5m SPACING
A86
A1
3000 E
3500 E
MARSH PANEL
FAULT
4500N
COLLAPSED ROADWAY
B48
2 SOUTH
B PANEL
COMPLETED 15-10-1987
HEADINGS
HIDGS
2 SOUTH
3000E
D 150m
D 15m
D 10m
D 7m
D 1·5m
GF3
0-49A
FOR ENLARGEMENT
WD6 MINE
COLLAPSED AREA IN
2 SOUTH "A" & MARSH PANELS
AND SUBSIDENCE SURVEY LINE
LOCATION
Figure 1.5
SCALE 1:2000
DWG NO. WD6-400-147

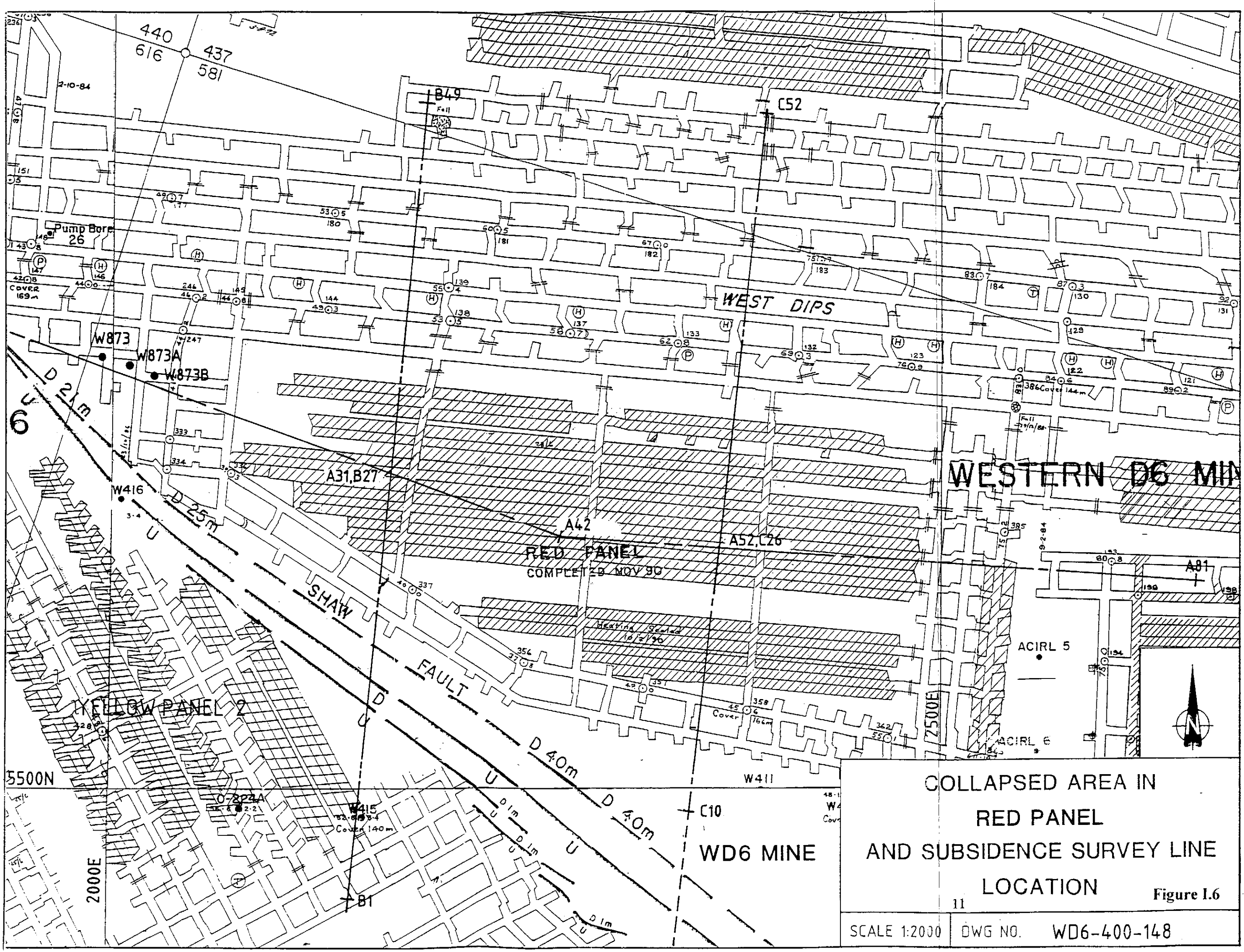

COLLAPSED AREA IN RED PANEL AND SUBSIDENCE SURVEY LINE LOCATION

Figure I.6

SCALE 1:2000	DWG NO. WD6-400-148

COMPLETED SEPT. 1992

6000 E

5500 E

3000 N

⇦5 m survey station spacing⇨

⇦20 m survey station spacing⇨

⇦5 m survey station spacing⇨

A1

A78

A48

A26

Extensometer D212

Extensometer D213

1 NORTH LATERAL HEADINGS

1 NORTH PANEL

AQH11

N12

N11

N10

N09

COLLAPSED AREA IN 1 NORTH PANEL AND SUBSIDENCE SURVEY LINE LOCATION

Figure I.7

SCALE 1:2000 | DWG NO. WD6-400-151

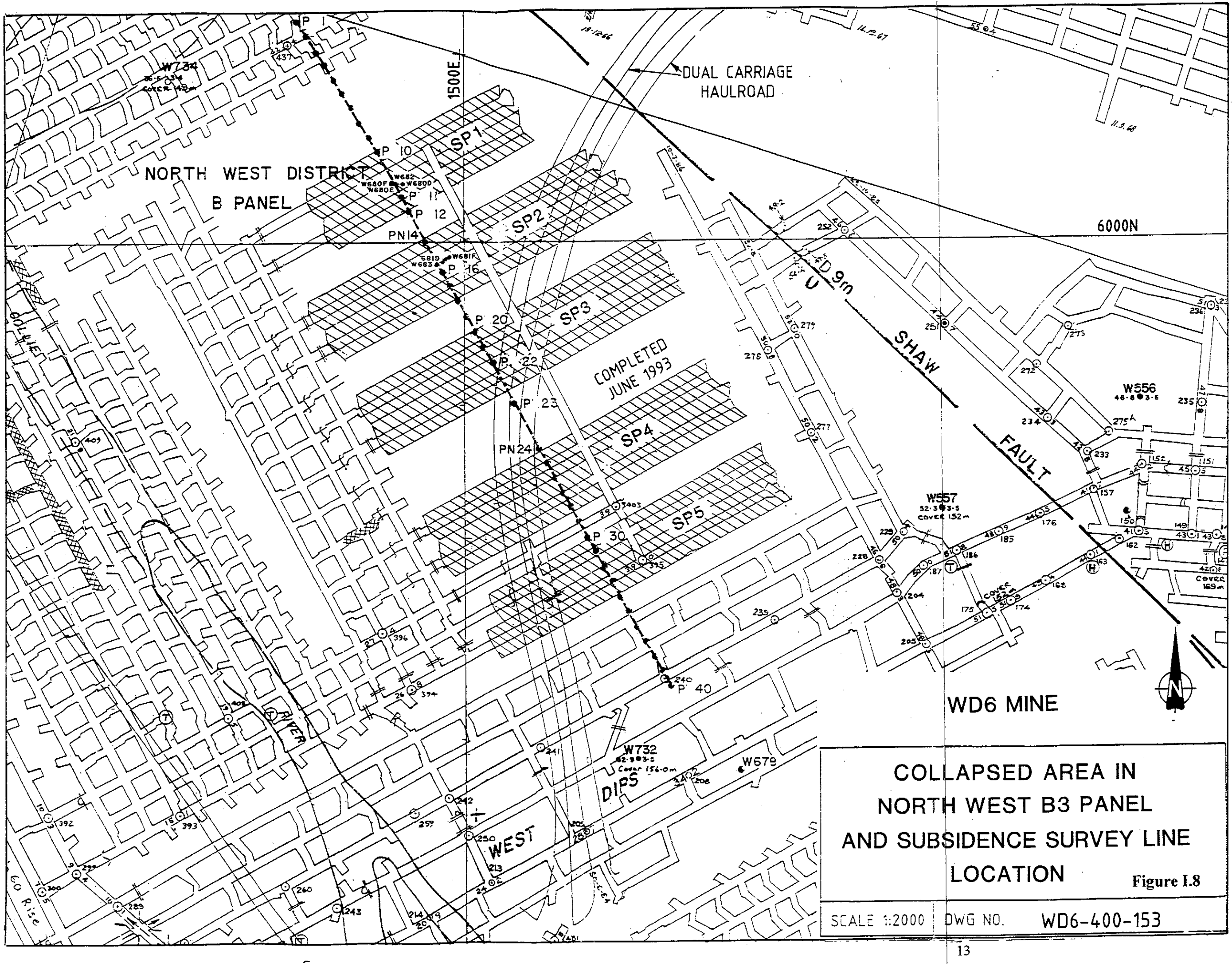

WD6 MINE

COLLAPSED AREA IN NORTH WEST B3 PANEL AND SUBSIDENCE SURVEY LINE LOCATION

Figure I.8

SCALE 1:2000 | DWG NO. WD6-400-153

PHOTOGRAPH OF A SUBSIDENCE GRID LINE THROUGH BUSHLAND

Figure I.9

TABLE I.2

LIFTING PROGRESS
ACIRL SUBPANEL 1 WD6
(10 ALPINE)

DATE	SPLIT #		GOAF LENGTH/ /WIDTH (m)
	1	START	
10/12/86	1	FINISH	75 / 13
	2	START	
17/12/86	2	FINISH	75 / 26
	3	START	
14/01/87	3	FINISH	75 / 39
	4	START	
22/01/87	4	FINISH	75 / 52
	5	START	
02/02/87	5	FINISH	75 / 65
	6	START	
09/02/87	6	FINISH	78 / 75
	7	START	
17/02/87	7	FINISH	91 / 75
	8	START	
26/02/87	8	FINISH	104 / 75
	9	START	
09/03/87	9	FINISH	117 / 75
	10	START	
24/03/87	10	FINISH	130 / 75
	11	START	
26/03/87	11	FINISH	143 / 75
	12	START	
03/04/87	12	FINISH	156 / 75
	13	START	
13/04/87	13	FINISH	169 / 75
	14	START	
05/05/87	14	FINISH	182 / 75

LIFTING PROGRESS
ACIRL SUBPANEL 2
(10 ALPINE)

DATE	SPLIT #		GOAF WIDTH (m)
	1	START	
20/7/87	1	FINISH	22
	2	START	
27/8/87	2	FINISH	38
	3	START	
09/09/87	3	FINISH	51
	4	START	
28/09/87	4	FINISH	64
	5	START	
23/10/87	5	FINISH	78
	6	START	
11/11/87	6	FINISH	92
	7	START	
27/11/87	7	FINISH	105

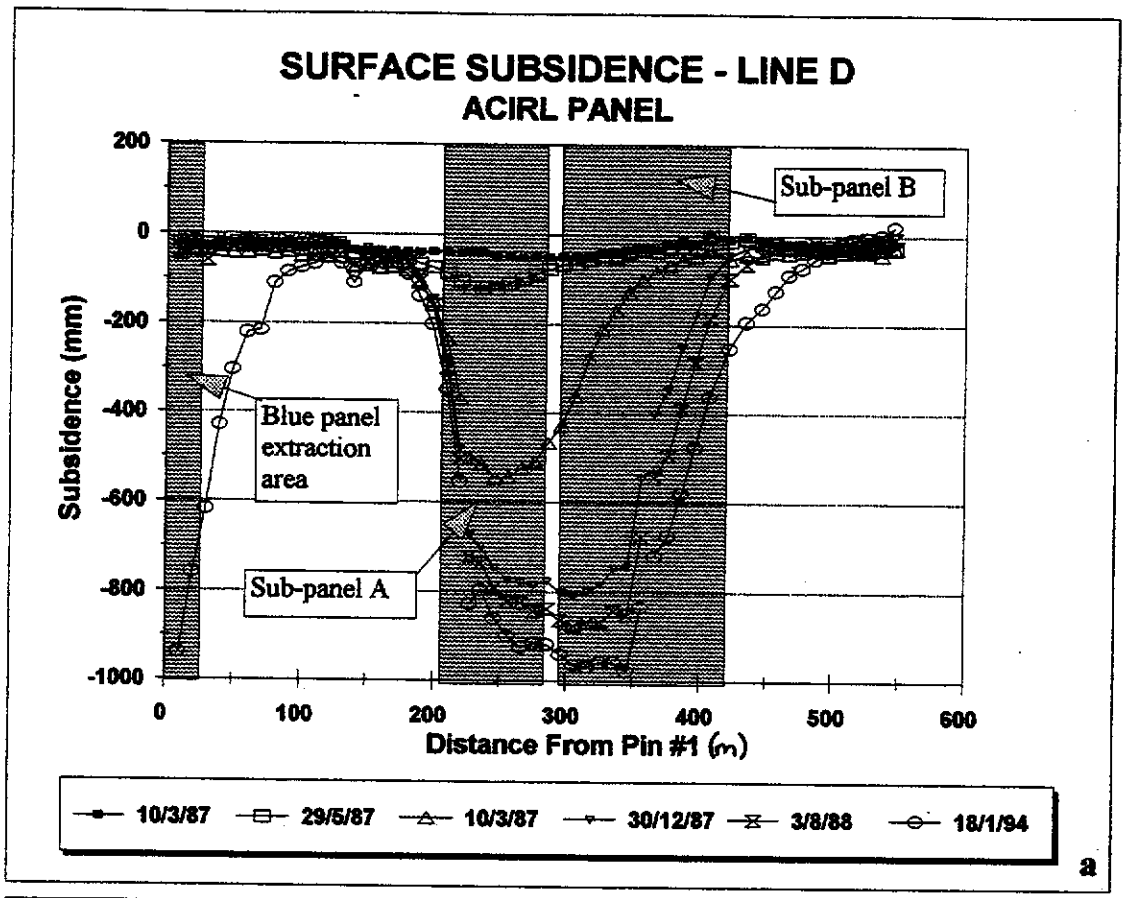
SURFACE SUBSIDENCE - LINE D
ACIRL PANEL
Subsidence (mm)
200
0
-200
-400
-600
-800
-1000
Blue panel extraction area
Sub-panel A
Sub-panel B
0
100
200
300
400
500
600
Distance From Pin #1 (m)
10/3/87
29/5/87
10/3/87
30/12/87
3/8/88
18/1/94
a

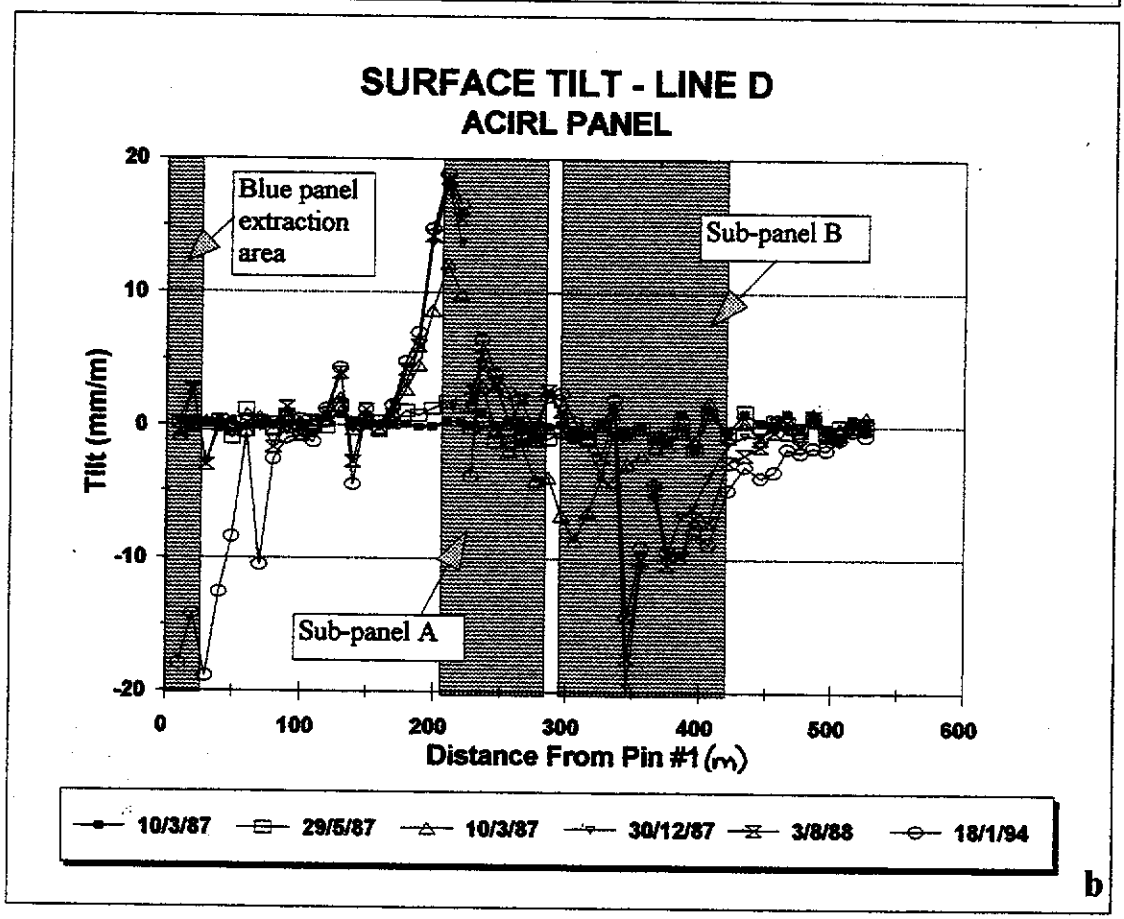
SURFACE TILT - LINE D
ACIRL PANEL
Tilt (mm/m)
20
10
0
-10
-20
Blue panel extraction area
Sub-panel B
Sub-panel A
0
100
200
300
400
500
600
Distance From Pin #1 (m)
10/3/87
29/5/87
10/3/87
30/12/87
3/8/88
18/1/94
b

Figure I.10

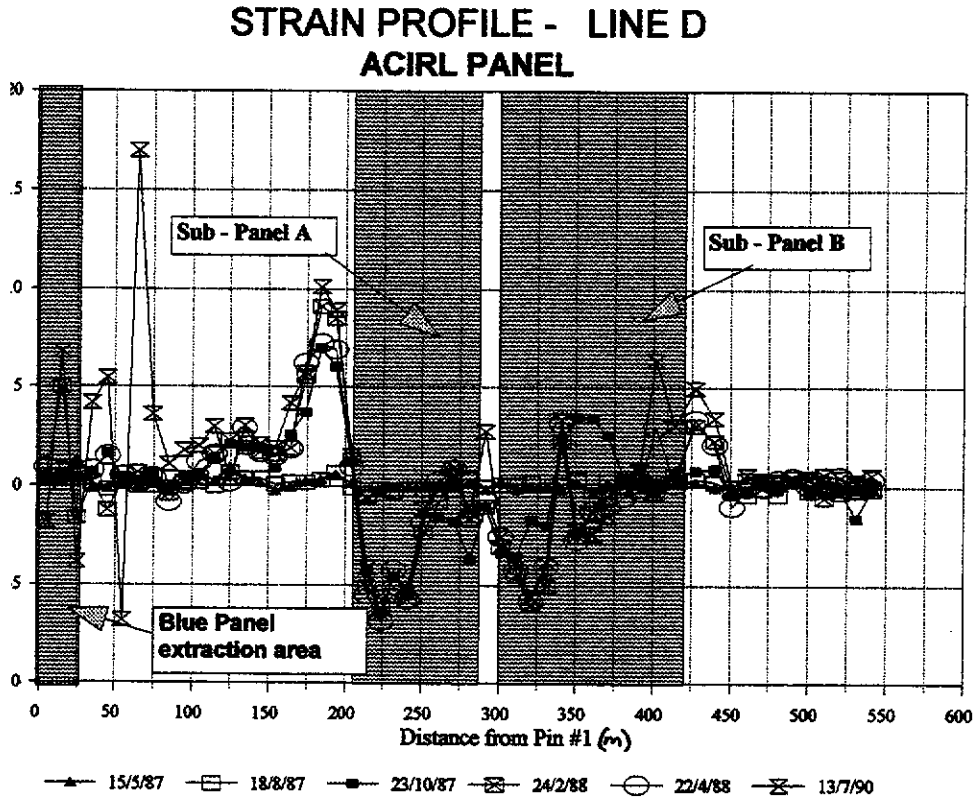
STRAIN PROFILE - LINE D
ACIRL PANEL
Sub - Panel A
Sub - Panel B
Blue Panel
extraction area
0
50
100
150
200
250
300
350
400
450
500
550
600
Distance from Pin #1 (m)
15/5/87
18/8/87
23/10/87
24/2/88
22/4/88
13/7/90

Figure I.11

TABLE I.3 LINE D STRAIN MONITORING - ACIRL PANEL

Date>	09-May-85	15-Nov-86	29-Nov-86	30-Dec-86	03-Feb-87	15-May-87	18-Aug-87	23-Oct-87	24-Feb-88	22-Apr-88	13-Jul-90	18-Jan-94
Days>	0	555	569	600	635	736	831	897	1021	1079	1891	3176
	MEASUREMENTS GIVEN AS DISTANCE BETWEEN SURVEY PEGS											
1-2	9.977	9.978	9.978	9.978	9.979	9.979	9.978	9.982	9.982	9.986	9.959	9.953
2-3	10.010	10.014	10.012	10.012	10.012	10.012	10.011	10.015	10.060	10.017	10.078	
3-4	9.916	9.921	9.920	9.920	9.919	9.920	9.921	9.926	9.900	9.922	9.878	
4-5	10.028	10.033	10.031	10.028	10.030	10.027	10.029	10.035	10.030	10.036	10.070	10.046
5-6	9.852	9.847	9.845	9.868	9.864	9.851	9.850	9.868	9.840	9.867	9.906	9.893
6-7	9.997	10.001	10.001	9.998	9.996	10.000	9.999	10.000	10.000	10.002	9.929	
7-8	10.003	10.003	10.001	10.003	10.004	10.003	10.003	10.006	10.010	10.005	10.173	
8-9	9.960	9.967	9.967	9.959	9.958	9.963	9.965	9.967	9.960	9.964	9.996	9.962
9-10	9.994	9.996	9.996	9.996	9.990	9.994	9.993	9.993	9.990	9.986	10.005	10.020
11	10.028	10.030	10.280	10.030	10.028	10.030	10.029	10.033	10.030	10.029	10.046	10.039
12	9.978	9.984	9.984	9.984	9.978	9.983	9.982	9.984	9.980	9.990	9.998	9.987
13	10.004	10.005	10.003	10.008	10.013	10.007	10.004	10.018	10.020	10.020	10.034	9.998
14	10.067	10.071	10.071	10.071	10.074	10.077	10.074	10.088	10.090	10.069	10.071	
15	9.891	9.893	9.893	9.893	9.895	9.895	9.895	9.910	9.910	9.920	9.921	
16	9.963	9.966	9.964	9.967	9.965	9.965	9.967	9.982	9.980	9.980	9.984	9.995
17	9.984	9.982	9.982	9.985	9.979	9.982	9.985	9.993	10.000	9.999	10.003	10.003
18	10.011	10.013	10.013	10.008	10.008	10.011	10.013	10.037	10.030	10.030	10.053	10.054
19	9.945	9.948	9.946	9.948	9.945	9.948	9.947	9.962	10.000	10.007	10.002	9.986
20	8.998	9.000	9.001	9.001	8.997	9.001	9.001	9.061	9.080	9.063	9.089	9.089
21	9.965	9.970	9.972	9.920	9.971	9.971	9.972	10.025	10.050	10.034	10.054	
22	11.035	11.039	11.039	11.037	11.034	11.037	11.034	11.049	11.050	11.046	11.052	
23	10.031	10.028	10.028	10.023	10.019	10.025	10.026	9.988	9.980	9.976	9.990	
23-25	7.899	7.897	7.899	7.901	7.898	7.898	7.898	7.848	7.850	7.845	7.848	7.830
26	8.517	8.517	8.519	8.518	8.515	8.517	8.515	8.478	8.470	8.481	8.479	8.486
27	10.058	10.058	10.060	10.055	10.053	10.058	10.057	10.006	10.000	10.000	10.004	9.987
28	9.963	9.967	9.965	9.963	9.963	9.963	9.962	9.950	9.940	9.945	9.952	9.928
29	9.938	9.940	9.935	9.940	9.939	9.939	9.937	9.923	9.930	9.941	9.937	9.950
30	10.080	10.084	10.082	10.081	10.078	10.080	10.078	10.062	10.090	10.089	10.086	10.072
31	10.046	10.050	10.054	10.046	10.048	10.049	10.050	10.009	10.030	10.030	10.034	10.036
32	10.010	10.007	10.009	10.008	10.004	10.009	10.010	10.000	10.000	10.003	10.038	9.998
33	9.880	9.882	9.882	9.880	9.877	9.883	9.881	9.847	9.850	9.855	9.855	9.855
34	9.985	9.986	9.986	9.986	9.985	9.984	9.986	9.950	9.940	9.943	9.947	9.947
35	9.990	9.995	9.993	9.995	9.989	9.990	9.992	9.973	9.930	9.932	9.934	9.946
36	9.880	9.882	9.882	9.871	9.878	9.880	9.879	9.860	9.830	9.840	9.842	
37	10.057	10.057	10.057	10.052	10.055	10.056	10.058	10.081	10.080	10.089	10.091	
38	10.045	10.049	10.049	10.043	10.047	10.047	10.049	10.080	10.020	10.018	10.023	10.014
38-40\	9.943	9.943	9.943	9.941	9.938	9.940	9.941	9.977	9.930	9.931	9.919	
41	10.055	10.057	10.057	10.060	10.057	10.057	10.058	10.081	10.050	10.045	10.040	9.998
42	10.015	10.018	10.018	10.014	10.013	10.017	10.015	10.020	10.020	10.010	10.018	10.013
43	10.116	10.118	10.118	10.113	10.108	10.119	10.115	10.126	10.120	10.114	10.124	10.101
44	10.817	10.812	10.810	10.812	10.813	10.815	10.814	10.820	10.820	10.850	10.886	
45	14.352	14.352	14.350	14.352	14.353	14.355	14.353	14.360	14.360	14.354	14.396	
46	12.432	12.437	12.437	12.438	12.436	12.435	12.437	12.442	12.470	12.474	12.494	12.453
47	12.172	12.171	12.169	12.180	12.179	12.172	12.175	12.183	12.200	12.198	12.214	12.157
48	10.132	10.138	10.136	10.136	10.130	10.131	10.130	10.128	10.130	10.122	10.132	10.121
49	9.976	9.971	9.973	9.971	9.971	9.975	9.972	9.975	9.980	9.976	9.982	9.977
50	10.156	10.162	10.164	10.156	10.154	10.158	10.155	10.160	10.160	10.156	10.159	10.152
51	9.918	9.920	9.910	9.916	9.914	9.918	9.914	9.917	9.920	9.922	9.921	9.936
52	9.935	9.937	9.935	9.937	9.933	9.938	9.940	9.939	9.940	9.940	9.940	
53	10.016	10.018	10.016	10.012	10.012	10.014	10.014	10.015	10.020	10.017	10.021	
54	9.465	9.471	9.471	9.466	9.465	9.468	9.465	9.462	9.460	9.470	9.471	9.469
55	10.563	10.562	10.565	10.564	10.563	10.564	10.562	10.562	10.560	10.569	10.568	10.576
56	10.022	10.023	10.024	10.025	10.020	10.021	10.024	10.006	10.020	10.022	10.025	10.032
57	10.001	10.001	10.001	10.001	9.998	10.005	10.001	10.000	10.000	10.005	10.007	10.004

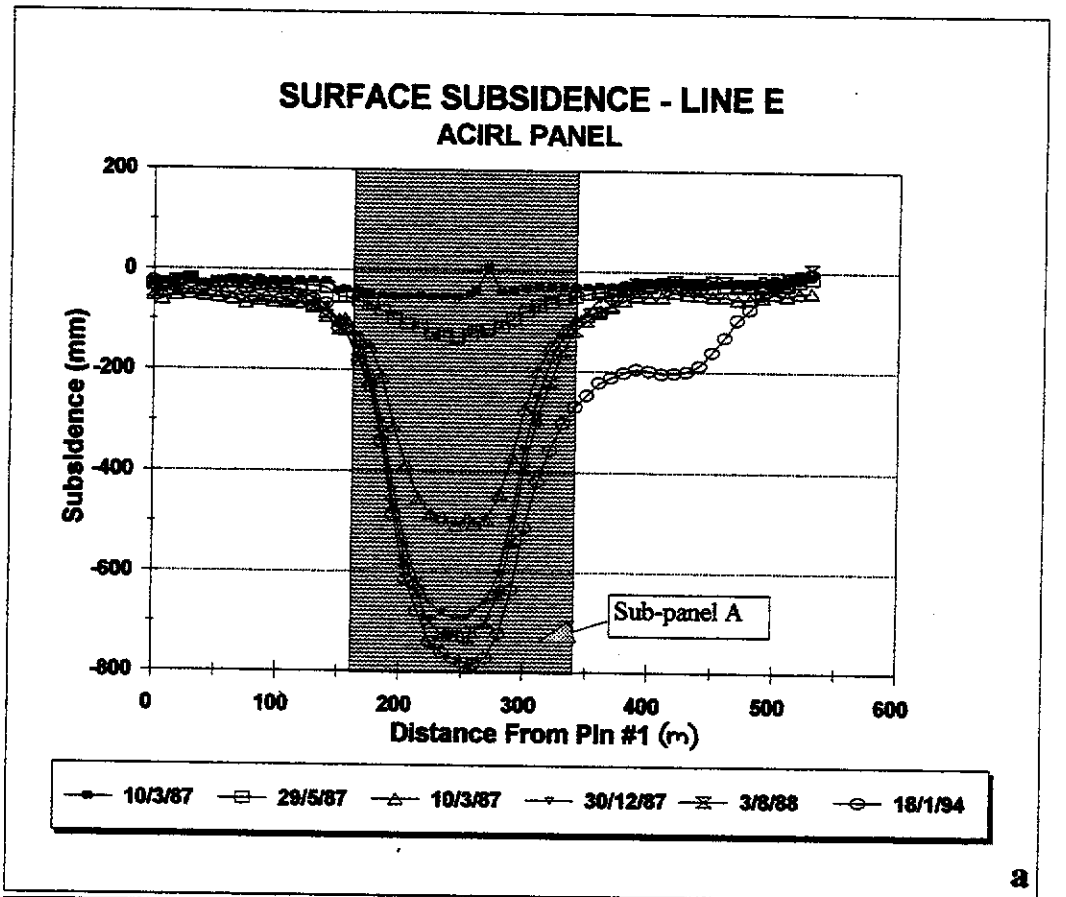
SURFACE SUBSIDENCE - LINE E
ACIRL PANEL
Subsidence (mm)
200
0
-200
-400
-600
-800
0
100
200
300
400
500
600
Distance From Pin #1 (m)
Sub-panel A
10/3/87
29/5/87
10/3/87
30/12/87
3/8/88
18/1/94
a

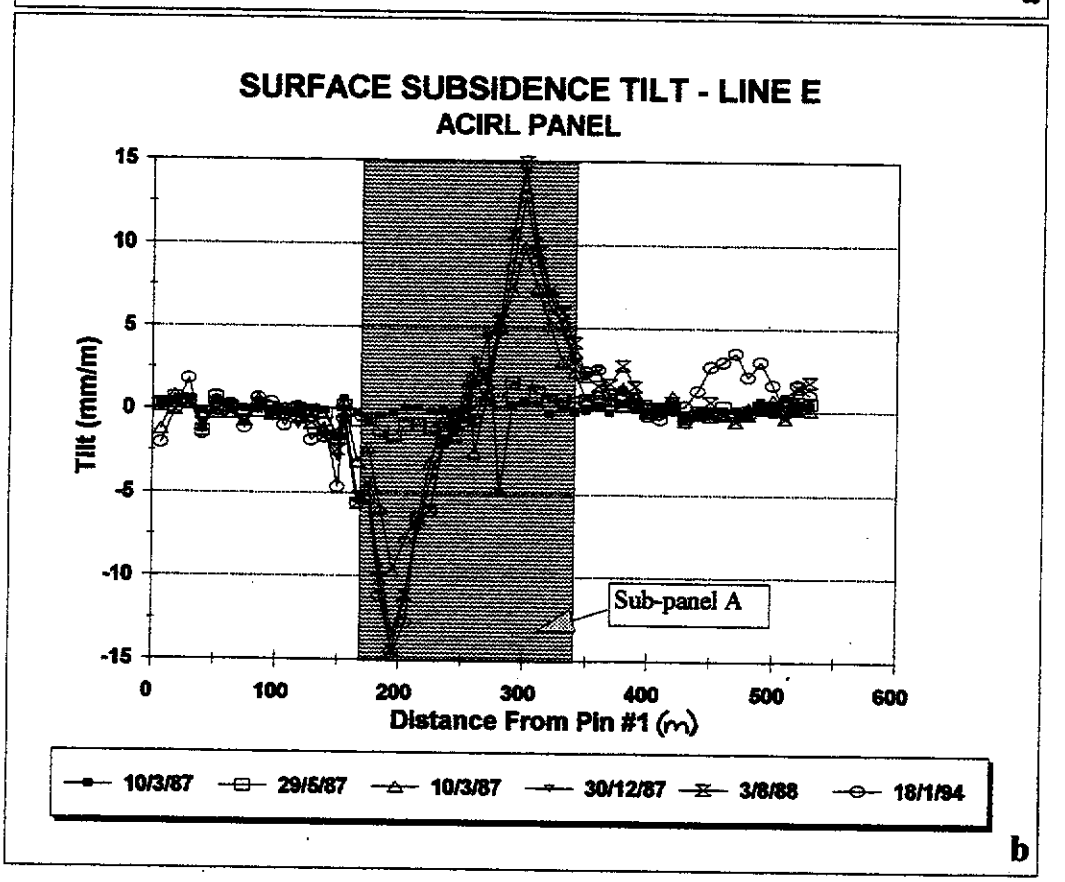
SURFACE SUBSIDENCE TILT - LINE E
ACIRL PANEL
Tilt (mm/m)
15
10
5
0
-5
-10
-15
0
100
200
300
400
500
600
Distance From Pin #1 (m)
Sub-panel A
10/3/87
29/5/87
10/3/87
30/12/87
3/8/88
18/1/94
b

Figure I.12

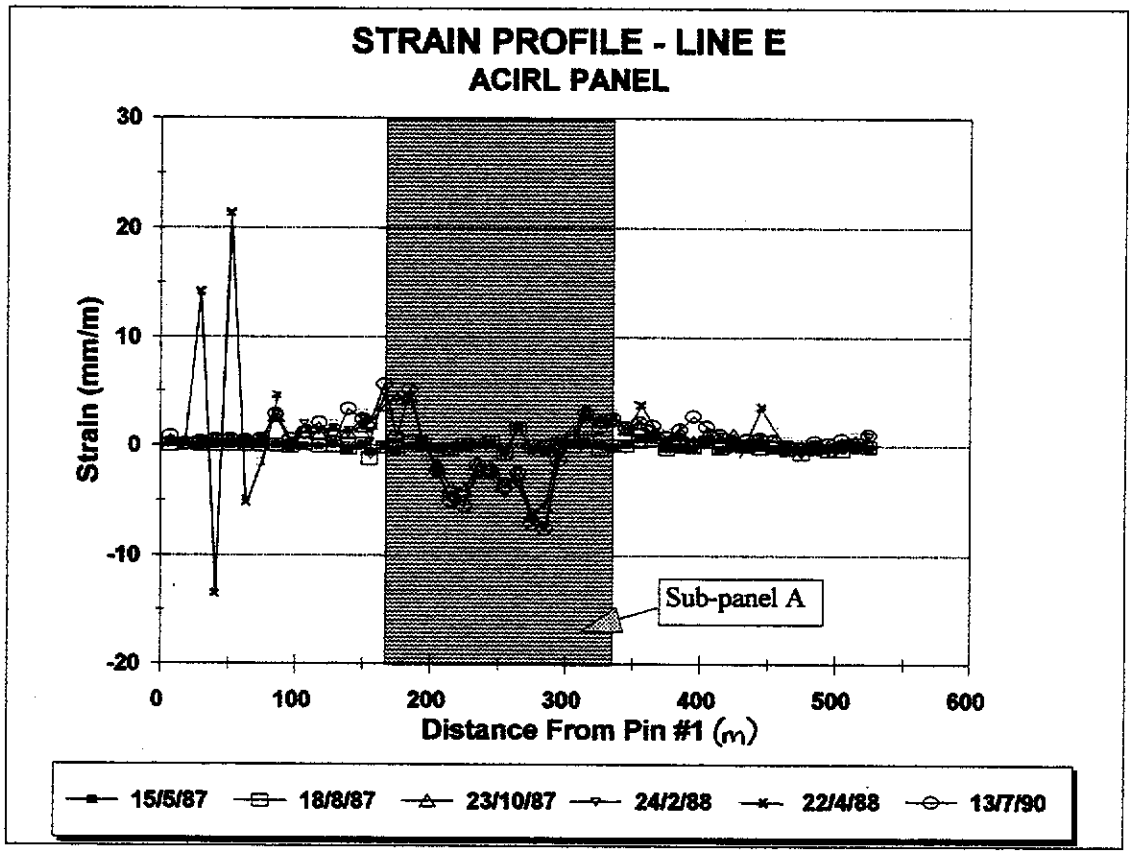
STRAIN PROFILE - LINE E
ACIRL PANEL
Strain (mm/m)
30
20
10
0
-10
-20
0
100
200
300
400
500
600
Distance From Pin #1 (m)
Sub-panel A
15/5/87
18/8/87
23/10/87
24/2/88
22/4/88
13/7/90

Figure I.13

TABLE I.4 **LINE E STRAIN MONITORING - ACIRL PANEL**

Date >	09-May-85	15-Nov-86	30-Dec-86	03-Feb-87	15-May-87	18-Aug-87	23-Oct-87	24-Feb-88	22-Apr-88	13-Jul-90	18-Jan-94
Days >	0	555	600	635	736	831	897	1021	1079	1891	3176
	MEASUREMENTS GIVEN AS DISTANCE BETWEEN SURVEY PEGS										
1-2	7.207	7.208	7.208	7.208	7.208	7.207	7.210	7.210	7.211	7.213	7.202
2-3	11.149	11.150	11.150	11.150	11.150	11.150	11.150	11.150	11.150	11.150	
3-4	11.238	11.238	11.238	11.238	11.238	11.238	11.240	11.242	11.398	11.242	
4-5	11.025	11.025	11.025	11.025	11.025	11.025	11.030	11.031	10.875	11.031	
5-6	10.926	10.926	10.926	10.926	10.926	10.926	10.930	10.932	11.160	10.932	
6-7	11.437	11.437	11.437	11.437	11.437	11.437	11.440	11.442	11.376	11.442	
7-8	11.047	11.047	11.047	11.047	11.047	11.047	11.050	11.053	11.030	11.053	
8-9	11.108	11.108	11.108	11.108	11.108	11.108	11.138	11.140	11.160	11.140	
9-10	10.748	10.748	10.748	10.744	10.745	10.746	10.750	10.750	10.751	10.754	10.728
11	10.649	10.649	10.650	10.649	10.648	10.650	10.662	10.670	10.659	10.661	10.678
12	11.125	11.125	11.123	11.124	11.124	11.124	11.137	11.140	11.141	11.148	11.146
13	10.683	10.683	10.685	10.683	10.684	10.682	10.697	10.700	10.704	10.686	
14	10.958	10.960	10.954	10.957	10.953	10.955	10.971	10.970	10.973	10.995	
15	10.763	10.765	10.761	10.765	10.764	10.765	10.782	10.790	10.795	10.789	
16	4.938	4.937	4.936	4.931	4.935	4.932	4.948	4.940	4.945	4.948	
17	11.027	11.027	11.025	11.025	11.026	11.025	11.068	11.080	11.087	11.089	11.083
18	8.952	8.955	8.955	8.945	8.947	8.950	8.990	8.990	8.954	8.959	8.969
19	9.945	9.947	9.947	9.944	9.944	9.948	9.990	9.990	10.000	9.996	9.991
20	10.020	10.018	10.022	10.018	10.018	10.021	10.023	10.020	10.011	10.023	10.021
21	10.041	10.040	10.048	10.036	10.037	10.036	10.023	10.020	10.015	10.018	10.034
22	9.989	9.994	10.001	9.987	9.988	9.986	9.951	9.940	9.936	9.939	9.918
23	9.989	9.986	9.992	9.993	9.989	9.990	9.948	9.940	9.944	9.934	9.955
24	10.047	10.047	10.052	10.045	10.047	10.047	10.030	10.020	10.028	10.029	10.010
25	10.048	10.051	10.054	10.045	10.050	10.051	10.029	10.020	10.026	10.025	10.031
26	9.954	9.954	9.956	9.947	9.949	9.947	9.920	9.910	9.918	9.916	9.907
26-28	9.965	9.965	9.965	9.984	9.982	9.980	9.940	9.930	9.934	9.940	
29	10.137	10.136	10.142	10.135	10.132	10.136	10.074	10.070	10.065	10.065	10.070
30	10.123	10.120	10.128	10.119	10.117	10.122	10.067	10.050	10.040	10.046	10.037
31	9.770	9.775	9.779	9.771	9.774	9.772	9.770	9.760	9.761	9.757	9.753
32	10.037	10.038	10.038	10.038	10.038	10.036	10.051	10.040	10.043	10.042	10.036
33	9.941	9.942	9.944	9.949	9.945	9.946	9.970	9.970	9.979	9.971	9.945
34	10.445	10.443	10.447	10.440	10.445	10.441	10.470	10.470	10.472	10.462	10.449
35	9.924	9.924	9.924	9.923	9.923	9.924	9.948	9.950	9.954	9.949	9.943
36	9.527	9.527	9.527	9.527	9.528	9.527	9.542	9.540	9.540	9.543	9.542
37	9.976	9.978	9.982	9.978	9.983	9.980	9.992	10.000	10.013	9.997	9.978
38	9.790	9.790	9.797	9.796	9.796	9.795	9.800	9.800	9.807	9.808	9.794
39	10.145	10.140	10.140	10.143	10.142	10.142	10.146	10.150	10.158	10.153	10.182
40	10.024	10.025	10.025	10.024	10.023	10.024	10.037	10.030	10.035	10.039	
41	9.986	9.984	9.986	9.985	9.984	9.985	9.990	9.990	9.988	10.013	10.014
42	9.996	10.000	10.000	10.000	10.001	10.000	10.007	10.000	10.014	10.014	9.998
43	10.021	10.020	10.018	10.021	10.017	10.019	10.026	10.030	10.034	10.031	10.012
44	10.029	10.025	10.031	10.032	10.029	10.030	10.040	10.030	10.025	10.032	10.013
45	9.928	9.925	9.931	9.928	9.926	9.928	9.930	9.930	9.935	9.934	9.913
46	10.023	10.024	1.000	10.022	10.022	10.021	10.028	10.030	10.059	10.030	10.014
47	10.053	10.052	10.053	10.050	10.051	10.052	10.058	10.050	10.067	10.058	10.044
48	9.928	9.928	9.928	9.926	9.926	9.926	9.925	9.930	9.933	9.927	9.943
49	10.058	10.055	10.055	10.054	10.054	10.051	10.058	10.050	10.060	10.056	10.031
50	9.977	9.974	9.974	9.975	9.974	9.975	9.977	9.980	9.976	9.981	9.991
51	9.925	9.920	9.925	9.922	9.923	9.921	9.925	9.920	9.922	9.927	9.951
52	10.036	10.031	10.031	10.034	10.033	10.032	10.038	10.040	10.040	10.042	10.057
53	10.012	10.011	10.014	10.015	10.013	10.014	10.016	10.010	10.021	10.011	10.008
54	10.031	10.029	10.030	10.030	10.029	10.030	10.034	10.040	10.043	10.041	10.026

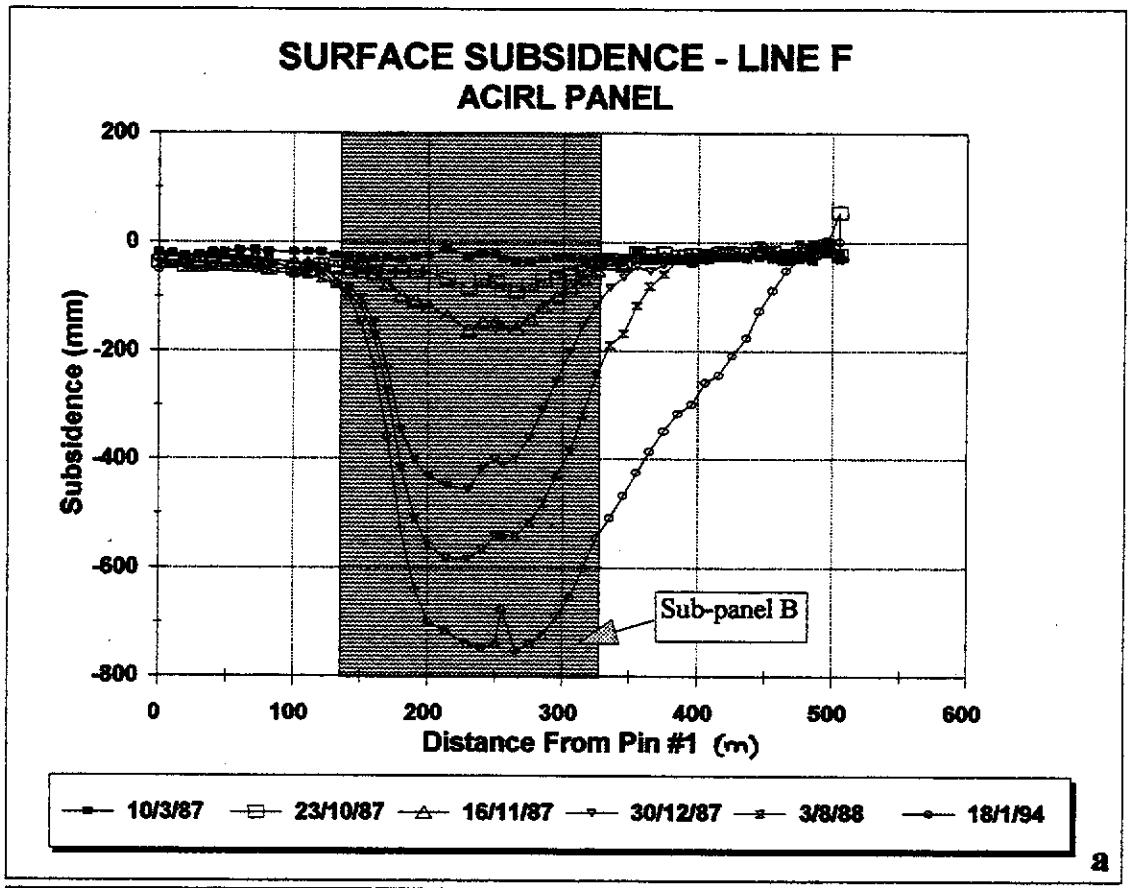
SURFACE SUBSIDENCE - LINE F
ACIRL PANEL
Subsidence (mm)
200
0
-200
-400
-600
-800
0
100
200
300
400
500
600
Distance From Pin #1 (m)
Sub-panel B
10/3/87
23/10/87
16/11/87
30/12/87
3/8/88
18/1/94
a

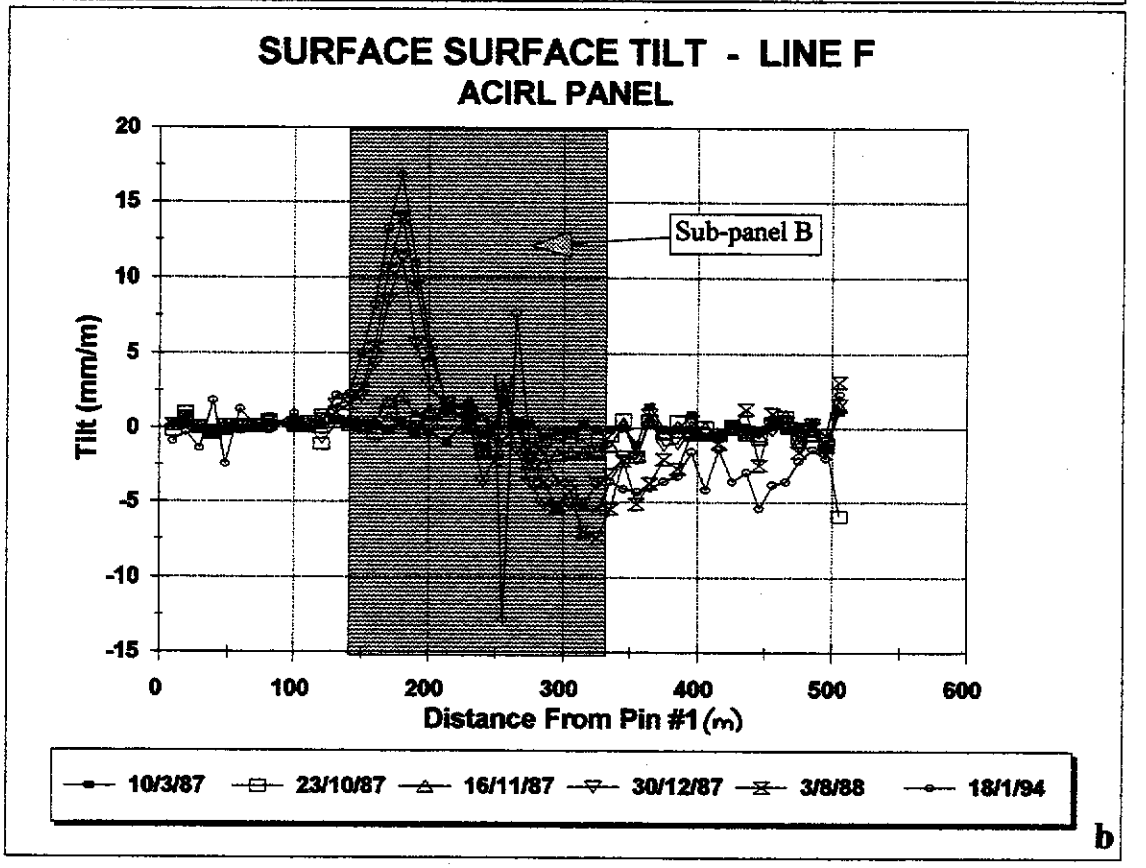
SURFACE SURFACE TILT - LINE F
ACIRL PANEL
Tilt (mm/m)
20
15
10
5
0
-5
-10
-15
0
100
200
300
400
500
600
Distance From Pin #1 (m)
Sub-panel B
10/3/87
23/10/87
16/11/87
30/12/87
3/8/88
18/1/94
b

Figure I.14

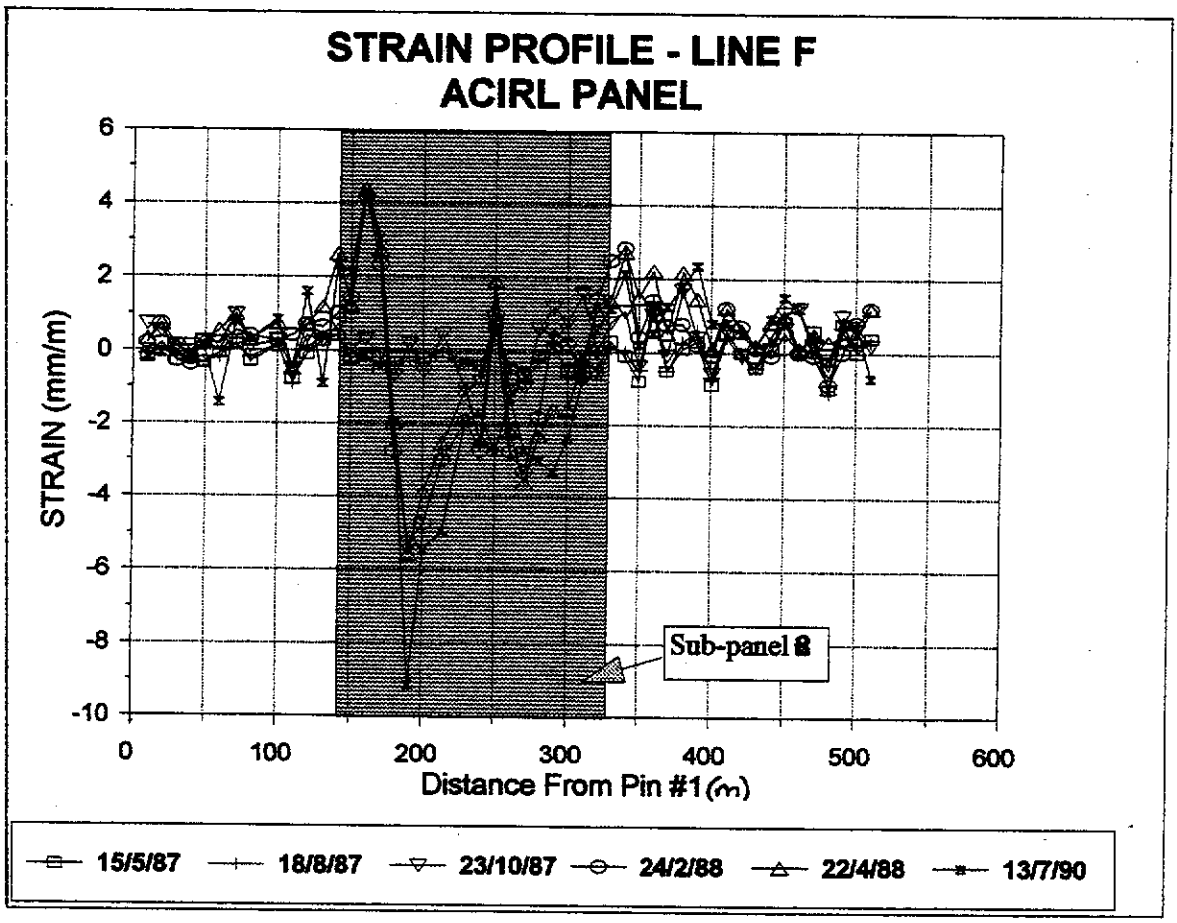
STRAIN PROFILE - LINE F
ACIRL PANEL
STRAIN (mm/m)
6
4
2
0
-2
-4
-6
-8
-10
0
100
200
300
400
500
600
Distance From Pin #1 (m)
Sub-panel 8
15/5/87
18/8/87
23/10/87
24/2/88
22/4/88
13/7/90

Figure I.15

TABLE I.5 LINE F STRAIN MEASUREMENTS - ACIRL PANEL

Date >	09-May-85	15-Nov-86	03-Feb-87	15-May-87	18-Aug-87	23-Oct-87	24-Feb-88	22-Apr-88	13-Jul-90	18-Jan-94
Days >	0	555	635	736	831	897	1021	1079	1891	3176
Pin #	MEASUREMENT GIVEN AS DISTANCE BETWEEN SURVEY PEGS (m)									
1-2	10.008	10.009	10.006	10.006	10.007	10.015	10.010	10.011	10.006	9.994
2-3	9.883	9.885	9.880	9.885	9.883	9.888	9.890	9.890	9.882	9.892
3-4	10.153	10.152	10.151	10.150	10.151	10.154	10.150	10.154	10.155	10.145
4-5	9.834	9.834	9.832	9.832	9.832	9.835	9.830	9.832	9.832	9.835
5-6	9.028	9.030	9.026	9.025	9.025	9.030	9.030	9.030	9.029	9.028
6-7	11.158	11.160	11.156	11.157	11.156	11.160	11.160	11.164	11.142	11.135
7-8	11.334	11.335	11.337	11.336	11.336	11.345	11.340	11.345	11.343	11.339
8-9	10.126	10.126	10.122	10.123	10.124	10.127	10.130	10.129	10.129	10.086
10	19.025	19.031	19.027	19.027	19.028	19.030	19.030	19.039	19.041	19.023
11	9.926	9.922	9.918	9.918	9.917	9.921	9.930	9.921	9.921	9.926
12	10.023	10.023	10.023	10.022	10.024	10.027	10.030	10.030	10.039	10.011
13	10.943	10.945	10.949	10.946	10.947	10.946	10.950	10.956	10.933	10.954
14	9.940	9.947	9.942	9.944	9.944	9.947	9.950	9.966	9.963	9.953
15	9.017	9.016	9.014	9.015	9.014	9.018	9.030	9.028	9.036	9.023
16	10.038	10.038	10.037	10.037	10.036	10.041	10.080	10.082	10.082	10.080
17	9.887	9.886	9.883	9.882	9.884	9.886	9.910	9.914	9.917	9.933
18	10.148	10.151	10.145	10.145	10.144	10.141	10.120	10.128	10.128	10.080
19	10.053	10.053	10.052	10.050	10.051	10.055	10.000	9.997	9.961	9.980
20	10.068	10.068	10.065	10.066	10.066	10.062	10.020	10.029	10.013	9.990
21	13.340	13.347	13.336	13.338	13.340	13.346	13.300	13.306	13.274	13.260
22	16.091	16.072	16.092	16.085	16.087	16.074	16.060	16.074	16.060	16.051
23	10.519	10.516	10.513	10.515	10.513	10.510	10.490	10.493	10.501	10.483
24	10.020	10.026	10.029	10.027	10.027	10.028	10.030	10.039	9.992	9.992
24-26	10.068	10.065	10.065	10.063	10.062	10.057	10.040	10.046	10.055	10.031
27	9.923	9.926	9.918	9.917	9.915	9.913	9.890	9.887	9.896	9.880
28	9.958	9.958	9.955	9.957	9.955	9.964	9.940	9.935	9.928	9.916
29	9.954	9.955	9.954	9.955	9.956	9.966	9.960	9.938	9.921	9.909
30	10.048	10.042	10.045	10.043	10.041	10.056	10.050	10.032	10.024	10.019
31	10.087	10.084	10.084	10.085	10.083	10.103	10.080	10.085	10.079	10.056
32	9.736	9.730	9.733	9.731	9.729	9.736	9.750	9.747	9.742	9.742
33	10.105	10.112	10.105	10.108	10.106	10.113	10.130	10.119	10.117	10.080
34	9.922	9.923	9.922	9.921	9.922	9.933	9.950	9.949	9.943	9.927
35	10.036	10.026	10.030	10.028	10.031	10.032	10.040	10.051	10.038	10.020
36	9.956	9.963	9.970	9.968	9.970	9.966	9.970	9.978	9.961	9.956
37	9.633	9.630	9.625	9.628	9.628	9.632	9.640	9.638	9.645	9.651
38	10.562	10.560	10.565	10.563	10.565	10.580	10.570	10.585	10.581	10.559
39	10.208	10.215	10.210	10.211	10.214	10.212	10.210	10.223	10.232	10.200
40	10.101	10.096	10.093	10.092	10.094	10.095	10.100	10.102	10.109	10.090
41	9.898	9.899	9.902	9.903	9.902	9.904	9.910	9.910	9.906	9.890
42	10.023	10.023	10.023	10.023	10.022	10.022	10.030	10.029	10.028	10.001
43	9.979	9.978	9.974	9.975	9.975	9.975	9.980	9.981	9.980	9.970
44	10.771	10.771	10.770	10.772	10.774	10.776	10.770	10.780	10.781	10.751
45	9.265	9.270	9.271	9.273	9.273	9.275	9.270	9.274	9.279	9.290
46	9.940	9.940	9.941	9.940	9.941	9.952	9.940	9.941	9.952	9.941
47	9.991	9.995	9.999	9.997	9.995	9.993	9.990	9.996	9.991	9.989
48	10.089	10.085	10.079	10.079	10.078	10.084	10.080	10.092	10.087	10.109
49	9.990	9.990	9.997	9.998	9.997	10.000	9.990	9.994	9.998	10.001
50	9.982	9.982	9.982	9.982	9.984	9.989	9.990	9.986	9.989	9.998
51	9.968	9.966	9.976	9.972	9.971	9.970	9.980	9.980	9.961	9.959

TABLE I.6

LIFTING PROGRESS

2B WEST E1 PANEL WD2

(10 ALPINE)

DATE	SPLIT #		GOAF WIDTH (m)	
26/05/88	1	START		
01/06/88	1	FINISH	15	
16/06/88	2	START		
21/06/88	2	FINISH	28	
06/07/88	3	START		
11/07/88	3	FINISH	37	
20/07/88	4	START		Fender truncated
25/07/88	4	FINISH	47	BLS buried
10/08/88	5	START		
18/08/88	5	FINISH	59	
30/08/88	6	START		
05/09/88	6	FINISH	70	
16/09/88	7	START		
23/09/88	7	FINISH	82	
11/10/88	8	START		
14/10/88	8	FINISH	94	
01/11/88	9	START		Trouble with first 30m
07/11/88	9	FINISH	105	of lifting when lowering
17/11/88	10	START		BLS. Roof breaking and sand
21/11/88	10	FINISH	114	rilling around supports.
05/12/88	11	START		Cover only 30m here.
08/12/88	11	FINISH	126	
20/12/88	12	START		No roof problems
23/12/88	12	FINISH	138	

Note: no progress data recorded for the second stage of the panel.

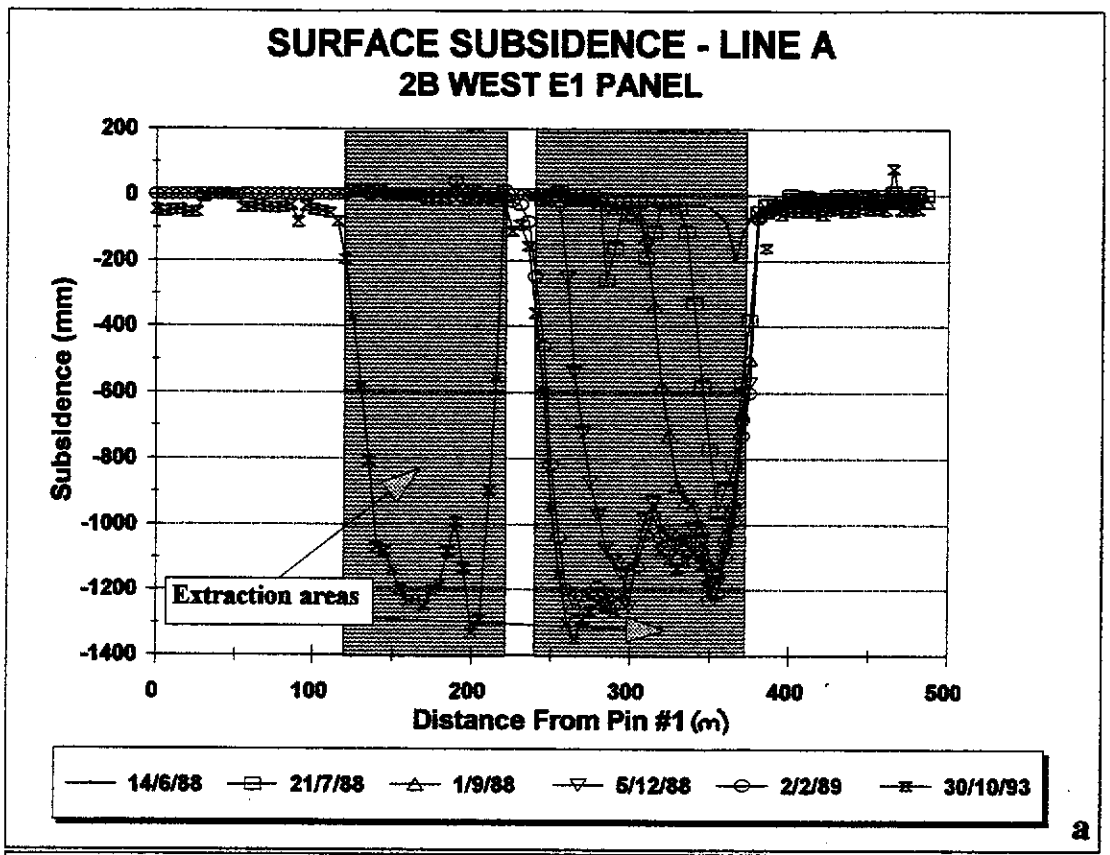
SURFACE SUBSIDENCE - LINE A
2B WEST E1 PANEL
Subsidence (mm)
200
0
-200
-400
-600
-800
-1000
-1200
-1400
Extraction areas
0
100
200
300
400
500
Distance From Pin #1 (m)
14/6/88
21/7/88
1/9/88
5/12/88
2/2/89
30/10/93
a

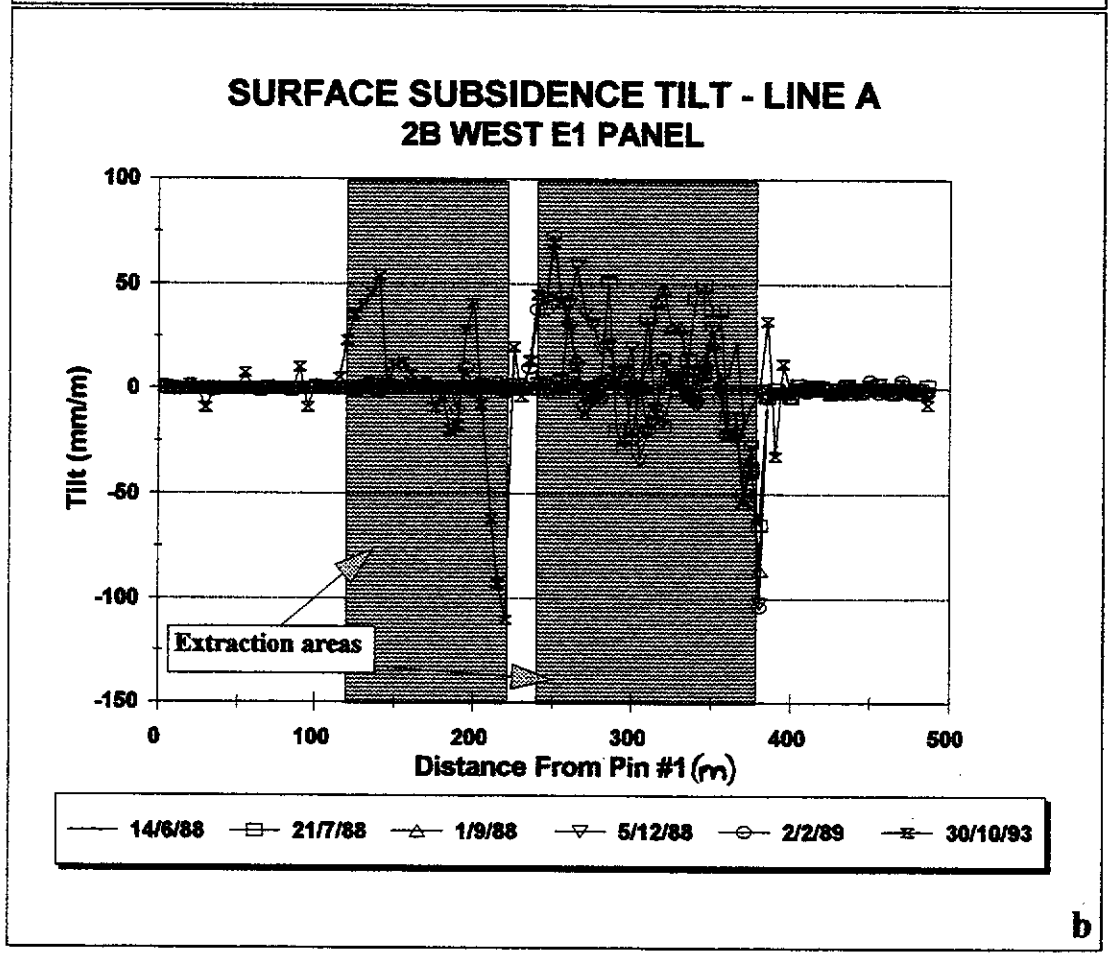
SURFACE SUBSIDENCE TILT - LINE A
2B WEST E1 PANEL
Tilt (mm/m)
100
50
0
-50
-100
-150
Extraction areas
0
100
200
300
400
500
Distance From Pin #1 (m)
14/6/88
21/7/88
1/9/88
5/12/88
2/2/89
30/10/93
b

Figure I.16

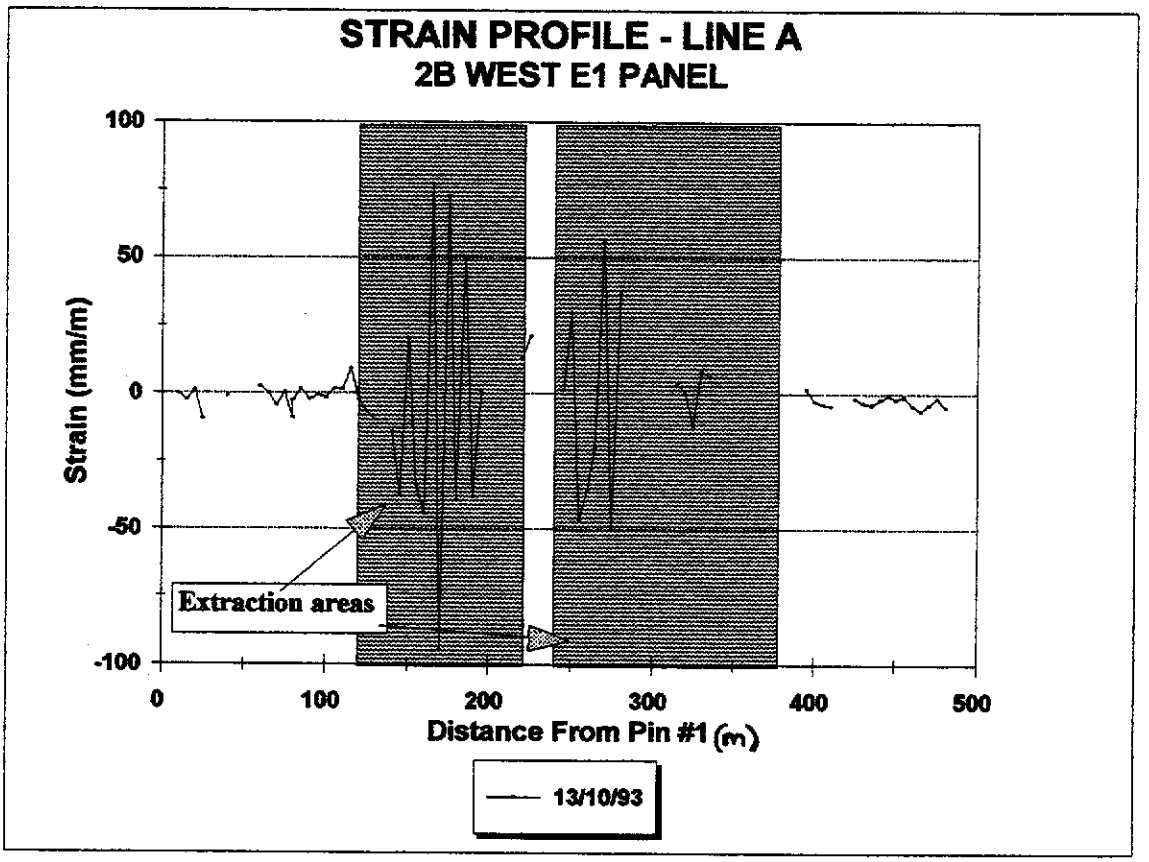
STRAIN PROFILE - LINE A
2B WEST E1 PANEL
100
50
0
-50
-100
Strain (mm/m)
Extraction areas
0
100
200
300
400
500
Distance From Pin #1 (m)
13/10/93

Figure I.17

TABLE I.7 LINE A STRAIN DATA - 2B WEST E1 PANEL.		
Date >	13-Apr-88	13-Oct-93
Days>	0	2009
PIN #	MEASUREMENTS GIVEN AS DISTANCE BETWEEN SURVEY PEGS	
1-2	5.033	
2-3	5.042	5.041
3-4	4.923	4.911
4-5	5.075	5.082
5-6	5.075	5.028
6-7	4.901	
7-8	5.116	
8-9	4.983	4.979
9-10	4.947	
11	5.112	
12	4.983	
13	4.950	4.962
14	5.010	5.011
15	4.982	4.961
16	5.005	5.007
17	5.039	4.995
18	4.970	4.958
19	4.993	5.001
20	5.085	5.075
21	4.939	4.936
22	5.025	5.018
23	4.970	4.979
23 -24	5.024	5.032
25	4.964	5.011
26	4.993	4.982
27	5.137	5.104
28	4.955	4.907
29	4.846	9.743
30	5.066	4.996
31	5.048	4.861
32	4.930	5.031
33	5.115	4.943
34	4.964	4.744
35	4.776	5.145
36	5.176	4.687
37	4.806	5.155
38	5.177	4.974
39	4.943	5.191
40	5.013	4.822
41	4.882	4.885
42	5.099	6.173
43	6.400	3.682
44	3.680	
45	4.942	
46	5.016	5.082
47	5.054	5.161
48	5.029	
49	4.480	
50	5.518	4.892

TABLE I.7 LINE A STRAIN DATA - 2B WEST E1 PANEL.		
Date >	13-Apr-88	13-Oct-93
Days>	0	2009
PIN #	MEASUREMENTS GIVEN AS DISTANCE BETWEEN SURVEY PEGS	
51	4.944	4.952
52	4.984	5.134
53	5.165	4.925
54	4.930	4.754
55	4.958	4.861
56	4.916	5.191
57	5.169	4.911
58	4.887	5.069
59	5.033	
60	4.958	
61	4.984	
62	5.033	
63	4.987	
64	4.974	
65	5.008	5.028
66	5.018	5.020
67	5.035	4.977
68	5.007	5.049
69	5.026	5.059
70	5.004	
71	4.981	
72	5.000	
73	4.983	
74	5.078	
75	4.987	
76	4.852	
77	5.091	
78	5.000	
79	5.042	
80	4.976	
81	5.014	5.024
82	4.875	4.862
83	5.043	5.025
84	5.021	5.000
85	5.048	
86	4.986	
87	4.959	4.952
88	5.007	4.991
89	5.020	5.001
90	5.061	5.051
91	4.928	4.926
92	5.111	5.103
93	4.946	4.942
94	4.998	4.977
95	4.991	4.961
96	4.996	4.976
97	5.246	5.239
98	5.569	5.543

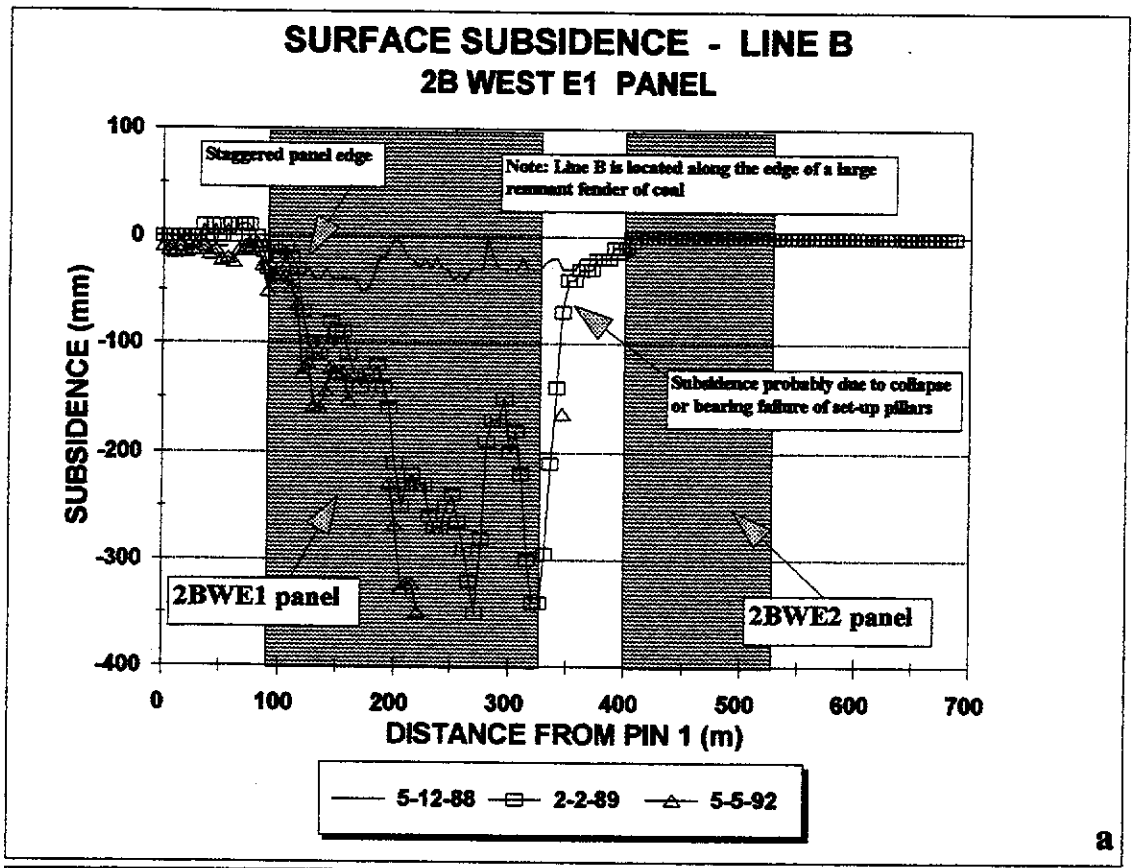
SURFACE SUBSIDENCE - LINE B
2B WEST E1 PANEL
SUBSIDENCE (mm)
DISTANCE FROM PIN 1 (m)
Staggered panel edge
Note: Line B is located along the edge of a large remnant fender of coal
Subsidence probably due to collapse or bearing failure of set-up pillars
2BWE1 panel
2BWE2 panel
5-12-88
2-2-89
5-5-92
a

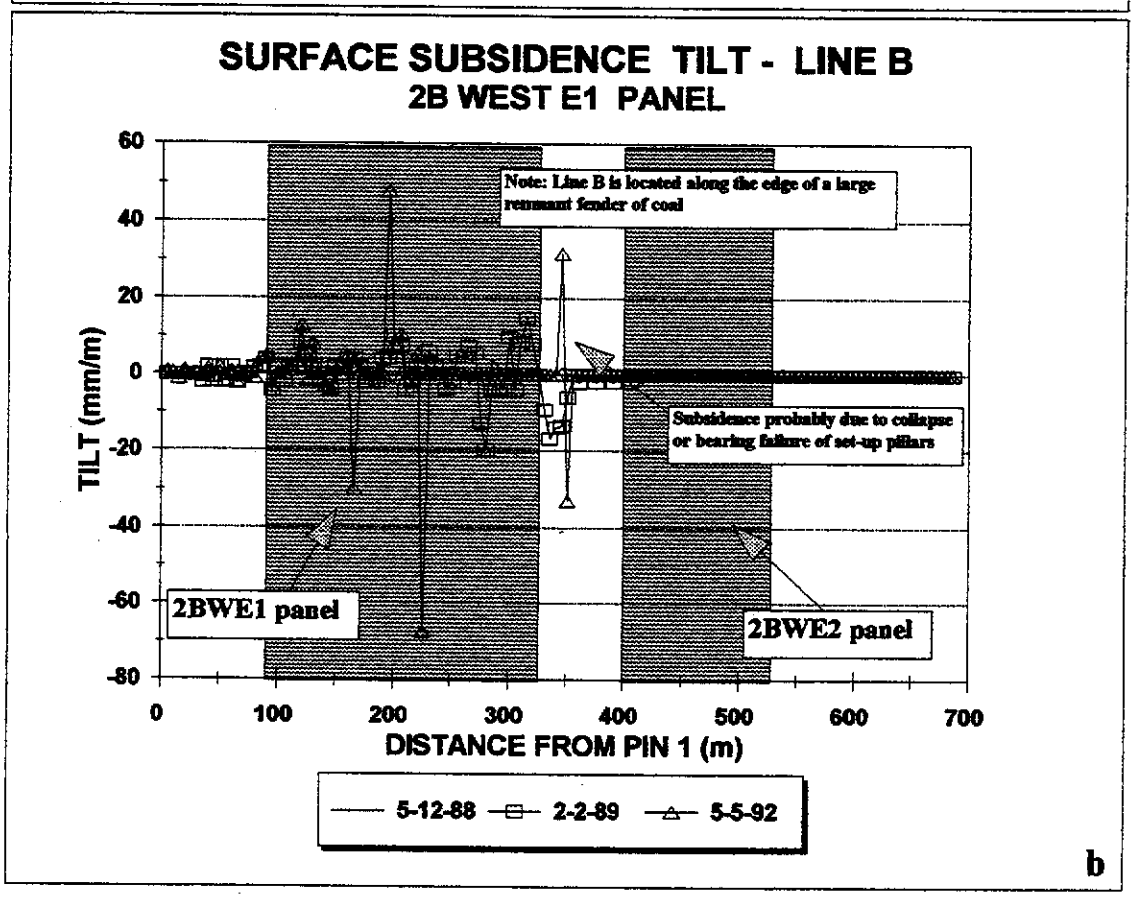
SURFACE SUBSIDENCE TILT - LINE B
2B WEST E1 PANEL
TILT (mm/m)
DISTANCE FROM PIN 1 (m)
Note: Line B is located along the edge of a large remnant fender of coal
Subsidence probably due to collapse or bearing failure of set-up pillars
2BWE1 panel
2BWE2 panel
5-12-88
2-2-89
5-5-92
b

Figure I.18

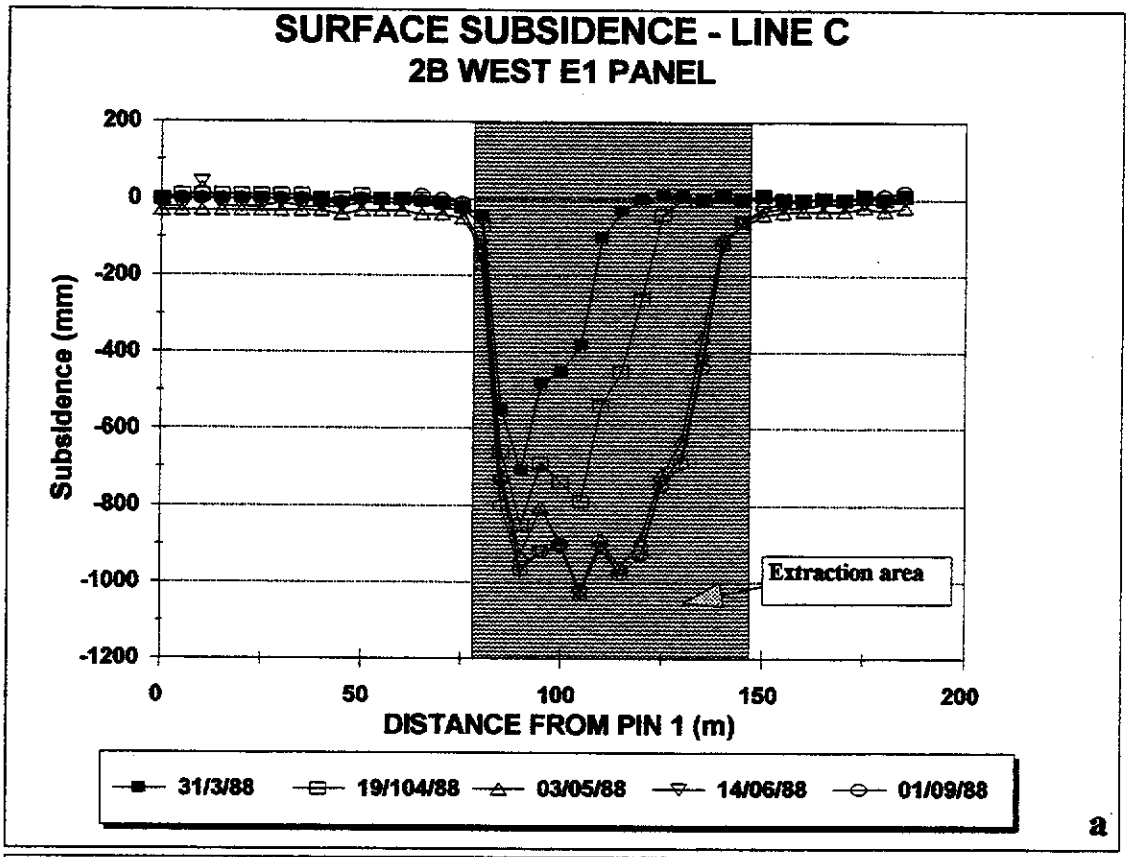
SURFACE SUBSIDENCE - LINE C
2B WEST E1 PANEL
Subsidence (mm)
200
0
-200
-400
-600
-800
-1000
-1200
0
50
100
150
200
DISTANCE FROM PIN 1 (m)
Extraction area
31/3/88
19/104/88
03/05/88
14/06/88
01/09/88
a

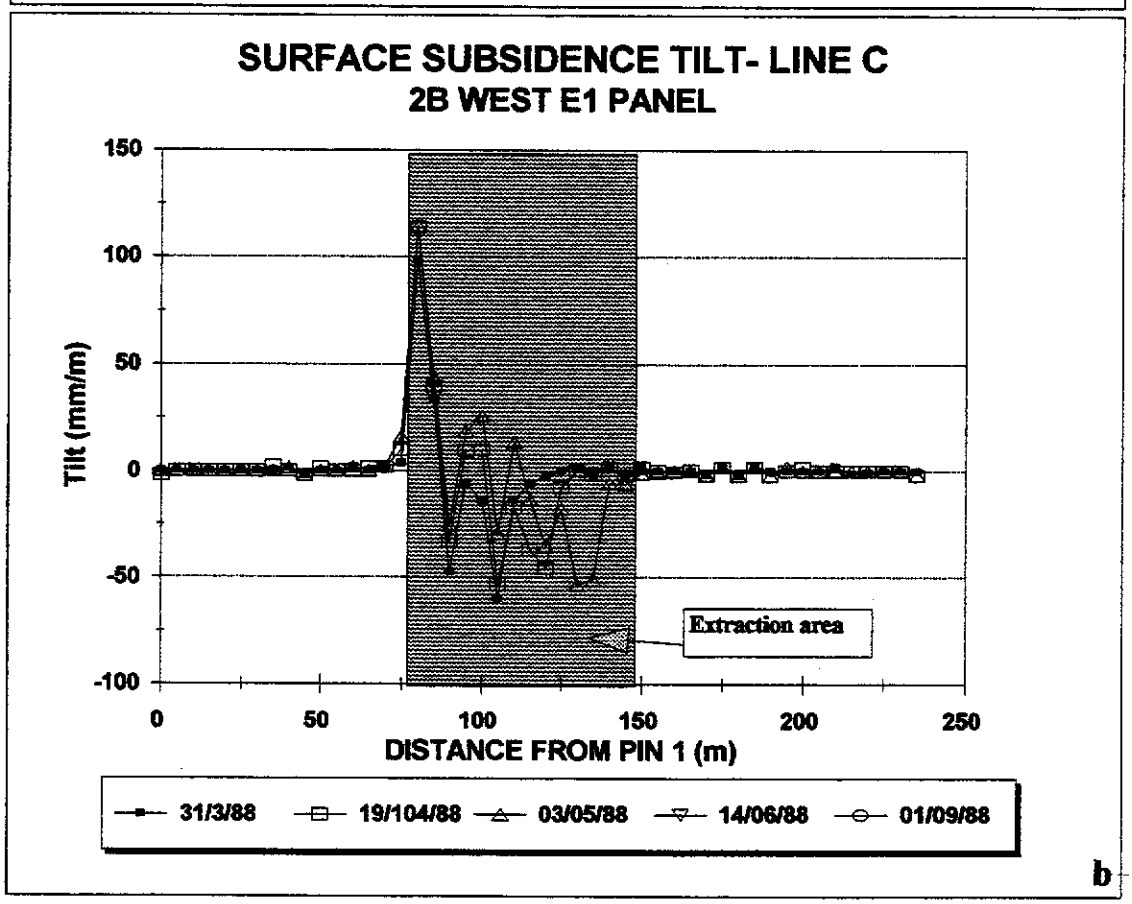
SURFACE SUBSIDENCE TILT- LINE C
2B WEST E1 PANEL
Tilt (mm/m)
150
100
50
0
-50
-100
0
50
100
150
200
250
DISTANCE FROM PIN 1 (m)
Extraction area
31/3/88
19/104/88
03/05/88
14/06/88
01/09/88
b

Figure I.19

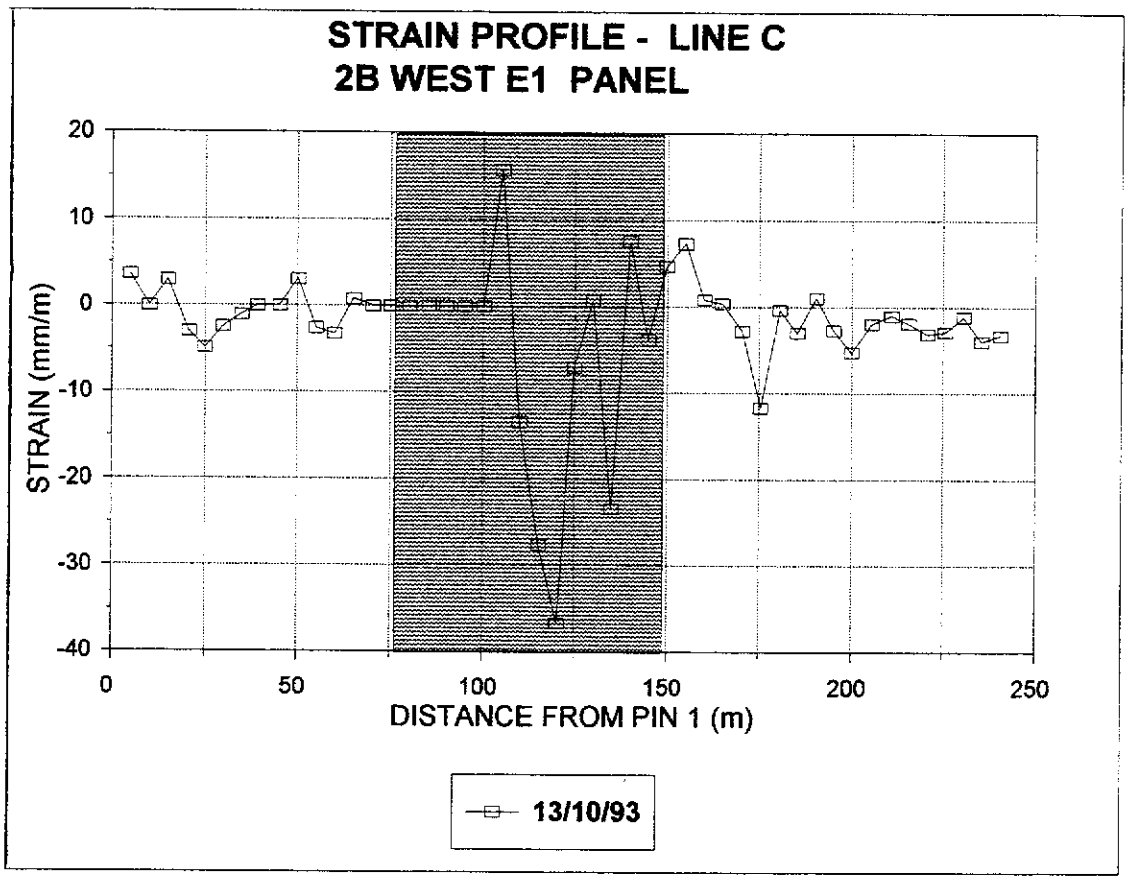
STRAIN PROFILE - LINE C
2B WEST E1 PANEL
STRAIN (mm/m)
20
10
0
-10
-20
-30
-40
0
50
100
150
200
250
DISTANCE FROM PIN 1 (m)
13/10/93

Figure I.20

TABLE I.8 LINE C STRAIN MONITORING - 2B WEST E1 PANEL

Date >	13-Apr-88	13-Oct-93
Days >	0	2009
PIN #	MEASUREMENTS GIVEN AS DISTANCE BETWEEN SURVEY PEGS	
1-2	4.968	4.986
2-3	5.011	
3-4	5.041	5.056
4-5	5.566	5.549
5-6	4.436	4.414
6-7	5.000	4.988
7-8	4.989	4.984
8-9	4.300	
9-10	6.095	
11	4.735	4.750
12	4.999	4.986
13	4.996	4.980
14	5.034	5.038
15	5.067	
16	5.012	
17	4.995	
18	5.188	
19	4.762	
20	4.835	
21	5.218	
22	5.028	5.107
23	4.674	4.611
24	5.124	4.983
25	5.132	4.944
26	4.788	4.754
27	4.984	4.988
28	5.031	4.913
29	5.060	5.098
30	4.981	4.962
31	4.728	4.750
32	5.389	5.429
33	4.950	4.954
34	4.749	4.751
35	5.438	5.423
36	5.094	5.034
37	5.074	5.072
38	4.904	4.889
39	5.038	5.043
40	4.740	4.727
41	4.800	4.775
42	5.578	5.567
43	5.274	5.269
44	4.650	4.641
45	5.178	5.162
46	4.725	4.711
47	5.058	5.052
48	5.031	5.011
49	5.028	5.011

TABLE I.9

LIFTING PROGRESS

2B WEST E2 PANEL WD2

(10 ALPINE)

DATE	SPLIT		GOAF WIDTH (m)
05/09/89	1	START	
13/09/89	1	FINISH	15
20/09/89	2	START	
25/09/89	2	FINISH	31
29/09/89	3	START	
11/10/89	3	FINISH	46
18/10/89	4	START	
23/10/89	4	FINISH	61
30/10/89	5	START	
03/11/89	5	FINISH	75
10/11/89	6	START	
16/11/89	6	FINISH	91
27/11/89	7	START	
01/12/89	7	FINISH	107
ONE WAY LIFTING			
06/12/89	8	START	
08/12/89	8	FINISH	129
14/12/89	9	START	
18/12/89	9	FINISH	145

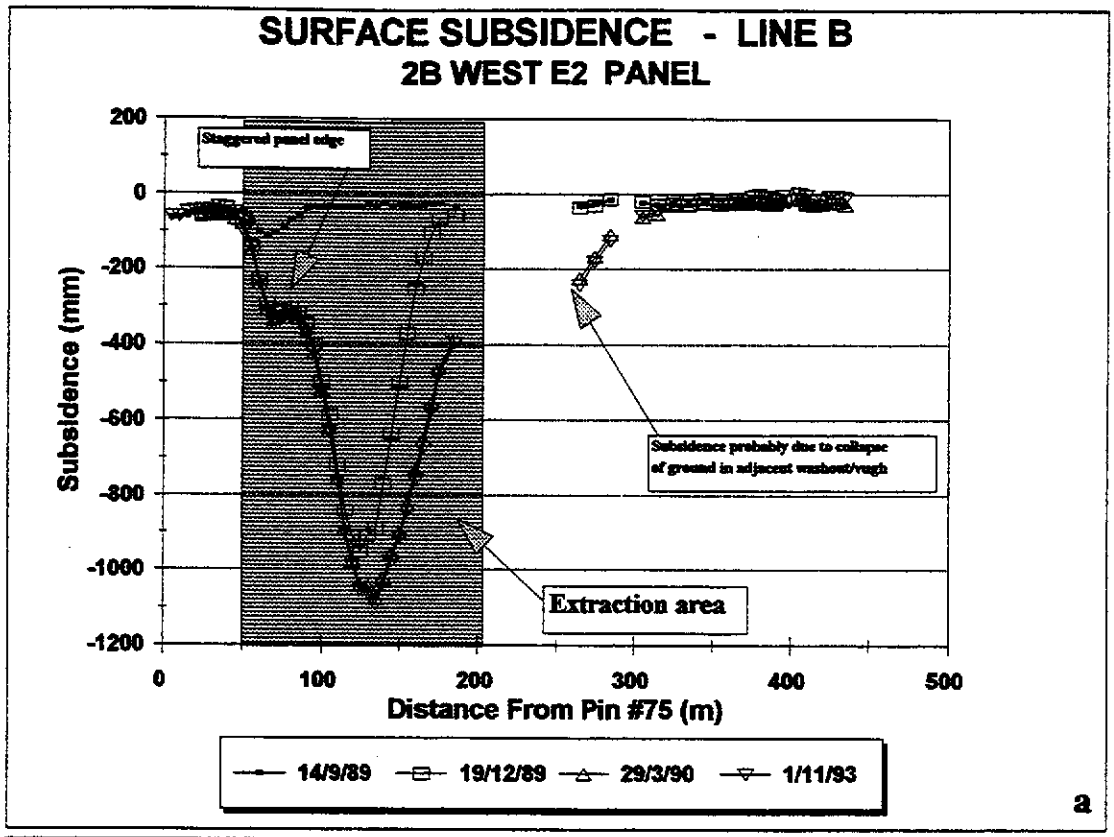
SURFACE SUBSIDENCE - LINE B
2B WEST E2 PANEL
Staggered panel edge
Subsidence probably due to collapse of ground in adjacent washout/vugh
Extraction area
Subsidence (mm)
200
0
-200
-400
-600
-800
-1000
-1200
0
100
200
300
400
500
Distance From Pin #75 (m)
14/9/89
19/12/89
29/3/90
1/11/93
a

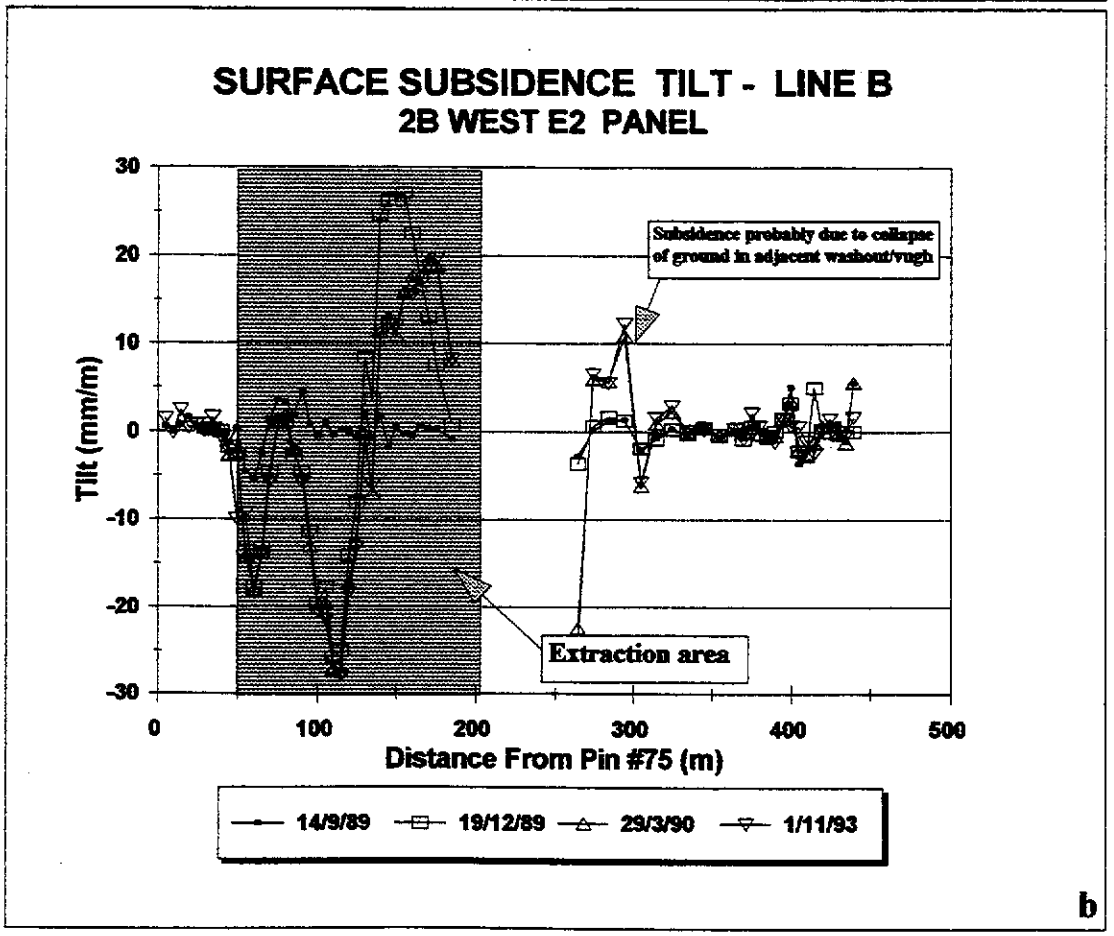
SURFACE SUBSIDENCE TILT - LINE B
2B WEST E2 PANEL
Subsidence probably due to collapse of ground in adjacent washout/vugh
Extraction area
Tilt (mm/m)
30
20
10
0
-10
-20
-30
0
100
200
300
400
500
Distance From Pin #75 (m)
14/9/89
19/12/89
29/3/90
1/11/93
b

Figure I.21

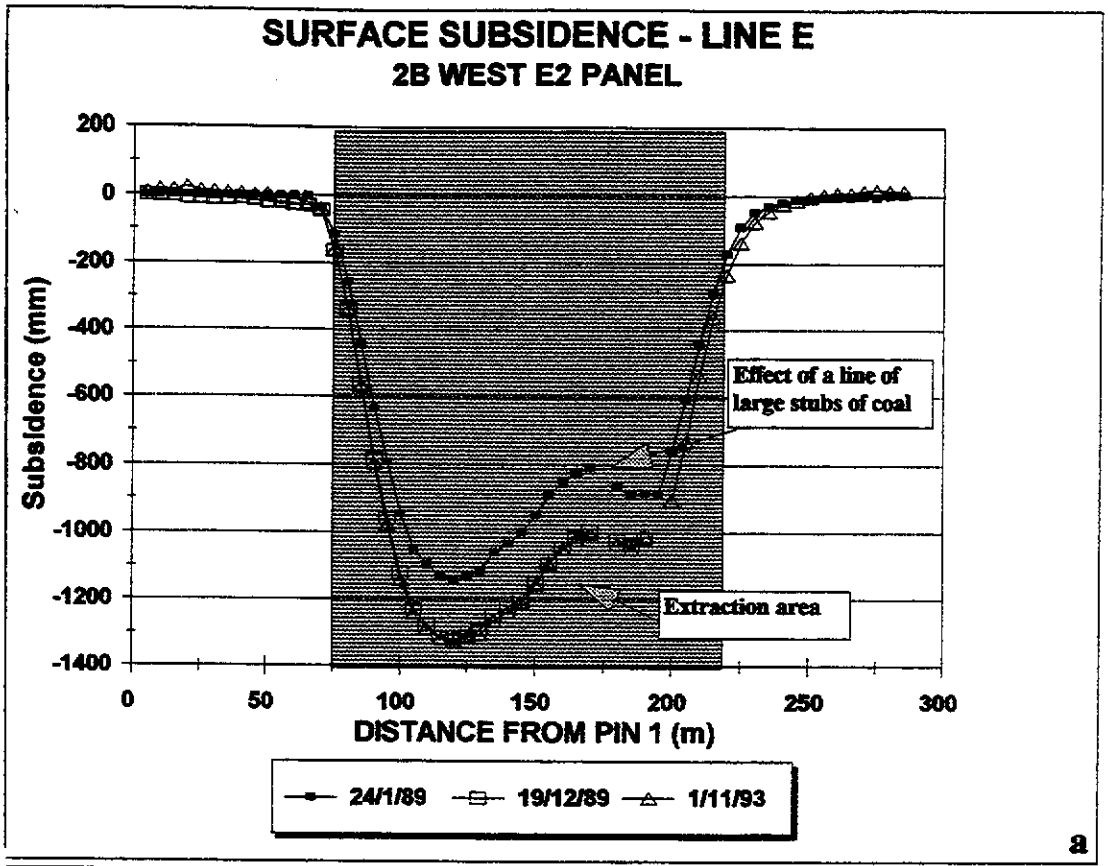
SURFACE SUBSIDENCE - LINE E
2B WEST E2 PANEL
Subsidence (mm)
200
0
-200
-400
-600
-800
-1000
-1200
-1400
0
50
100
150
200
250
300
DISTANCE FROM PIN 1 (m)
Effect of a line of large stubs of coal
Extraction area
24/1/89
19/12/89
1/11/93
a

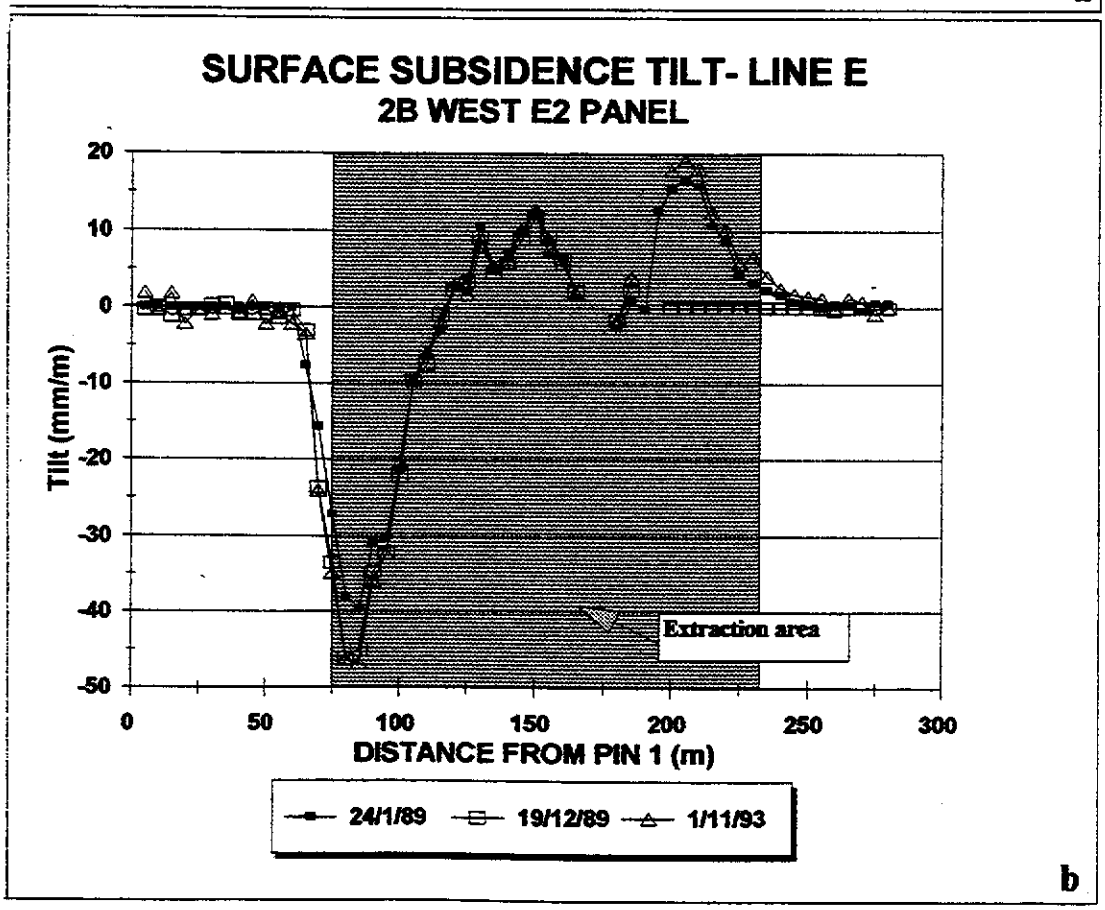
SURFACE SUBSIDENCE TILT- LINE E
2B WEST E2 PANEL
Tilt (mm/m)
20
10
0
-10
-20
-30
-40
-50
0
50
100
150
200
250
300
DISTANCE FROM PIN 1 (m)
Extraction area
24/1/89
19/12/89
1/11/93
b

Figure I.22

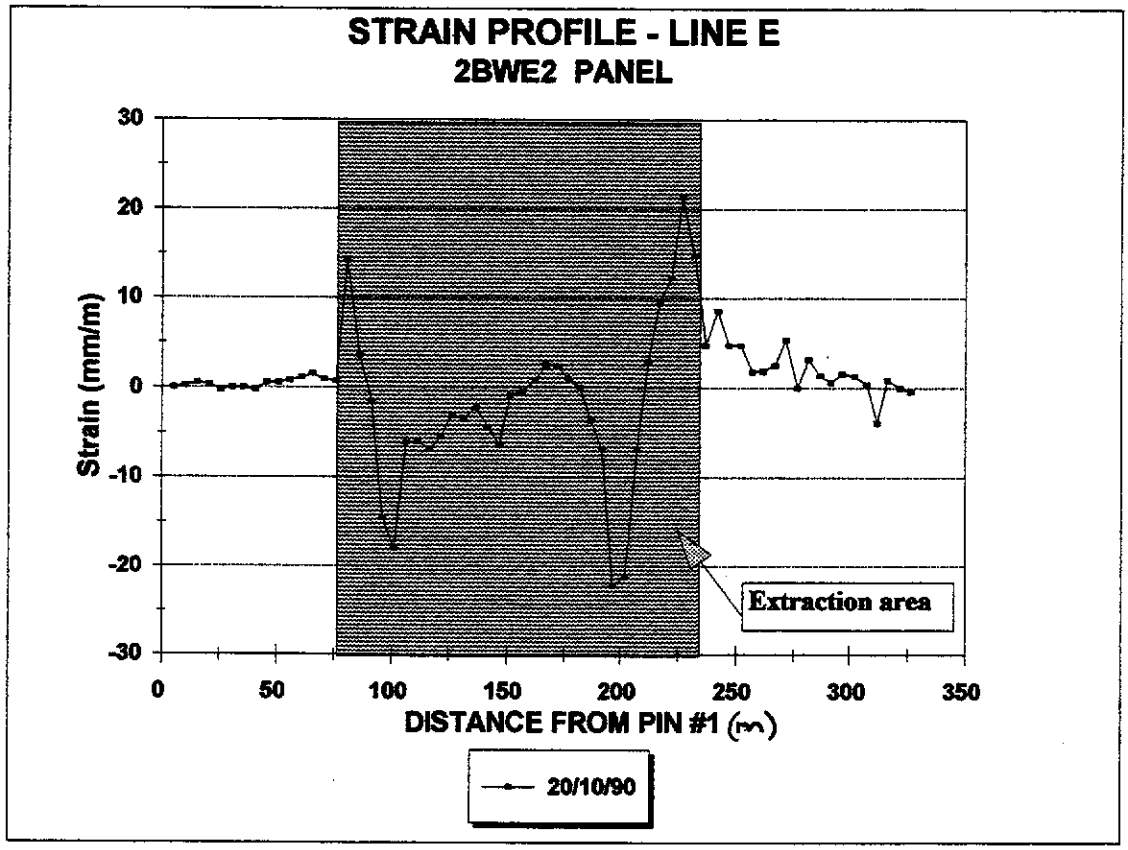
STRAIN PROFILE - LINE E
2BWE2 PANEL
Strain (mm/m)
30
20
10
0
-10
-20
-30
0
50
100
150
200
250
300
350
DISTANCE FROM PIN #1 (m)
Extraction area
20/10/90

Figure I.23

TABLE I.10 LINE E STRAIN MONITORING 2BWE2 PANEL.

Date >		28-Sep-89	02-Oct-90
Days >			
Pin #	DISTANCE BETWEEN SURVEY PEGS (m)		
1-2		5.240	5.240
2-3		4.894	4.895
3-4		5.235	5.238
4-5		5.426	5.428
5-6		4.631	4.630
6-7		5.166	5.166
7-8		4.948	4.948
8-9		4.969	4.968
9-10		5.066	5.069
11		5.132	5.135
12		5.035	5.039
13		5.200	5.206
14		4.503	4.510
15		5.167	5.172
16		5.205	5.209
17		4.805	4.874
18		5.347	5.366
19		5.172	5.164
20		4.838	4.768
21		5.053	4.962
22		5.147	5.116
23		5.045	5.015
24		4.960	4.926
25		5.027	5.000
26		4.989	4.974
27		5.054	5.037
28		5.095	5.084
29		5.024	5.002
30		5.166	5.133
31		4.904	4.900
32		5.316	5.314
33		5.004	5.008
34		5.146	5.159
35		4.998	5.010
36		4.801	4.806
37		5.083	5.083
38		4.953	4.935
39		5.112	5.077
40		4.812	4.705

TABLE I.10 LINE E STRAIN MONITORING 2BWE2 PANEL.

Date >		28-Sep-89	02-Oct-90
Days >			
Pin #	DISTANCE BETWEEN SURVEY PEGS (m)		
40 - 41		5.367	5.253
42		4.984	4.950
43		4.974	4.988
44		5.120	5.169
45		4.888	4.948
46		4.917	5.022
47		5.122	5.198
48		4.921	4.944
49		5.247	5.292
50		4.681	4.703
51		5.125	5.149
52		5.060	5.069
53		4.794	4.803
54		5.187	5.200
55		4.705	4.730
56		5.002	5.002
57		4.780	4.795
58		5.097	5.104
59		4.912	4.915
60		4.953	4.961
61		5.136	5.143
62		5.277	5.279
63		4.658	4.640
64		4.652	4.656
65		5.272	5.272
66		5.010	5.008
67		4.958	4.957
68		5.121	5.125
69			
70			10.250
71		4.832	4.834
72		5.037	5.041
73		5.052	5.054
74		5.007	5.009
75		3.689	3.691
76		6.130	6.133
77		4.892	4.900
78		5.454	5.461
79		6.443	6.441
80		3.450	3.451

TABLE I.11

LIFTING PROGRESS

2B WEST C PANEL WD2

(10 ALPINE)

DATE	SPLIT #		GOAF WIDTH (m)
21/12/89	1	START	
24/01/90	1	FINISH	10
05/02/90	2	START	
12/02/90	2	FINISH	28
19/02/90	3	START	
26/02/90	3	FINISH	47
07/03/90	4	START	
20/03/90	4	FINISH	18
27/03/90	5	START	
04/04/90	5	FINISH	36
11/04/90	6	START	
30/04/90	6	FINISH	54
04/05/90	7	START	
11/05/90	7	FINISH	18
18/05/90	8	START	
26/05/90	8	FINISH	36
05/06/90	9	START	
11/06/90	9	FINISH	54

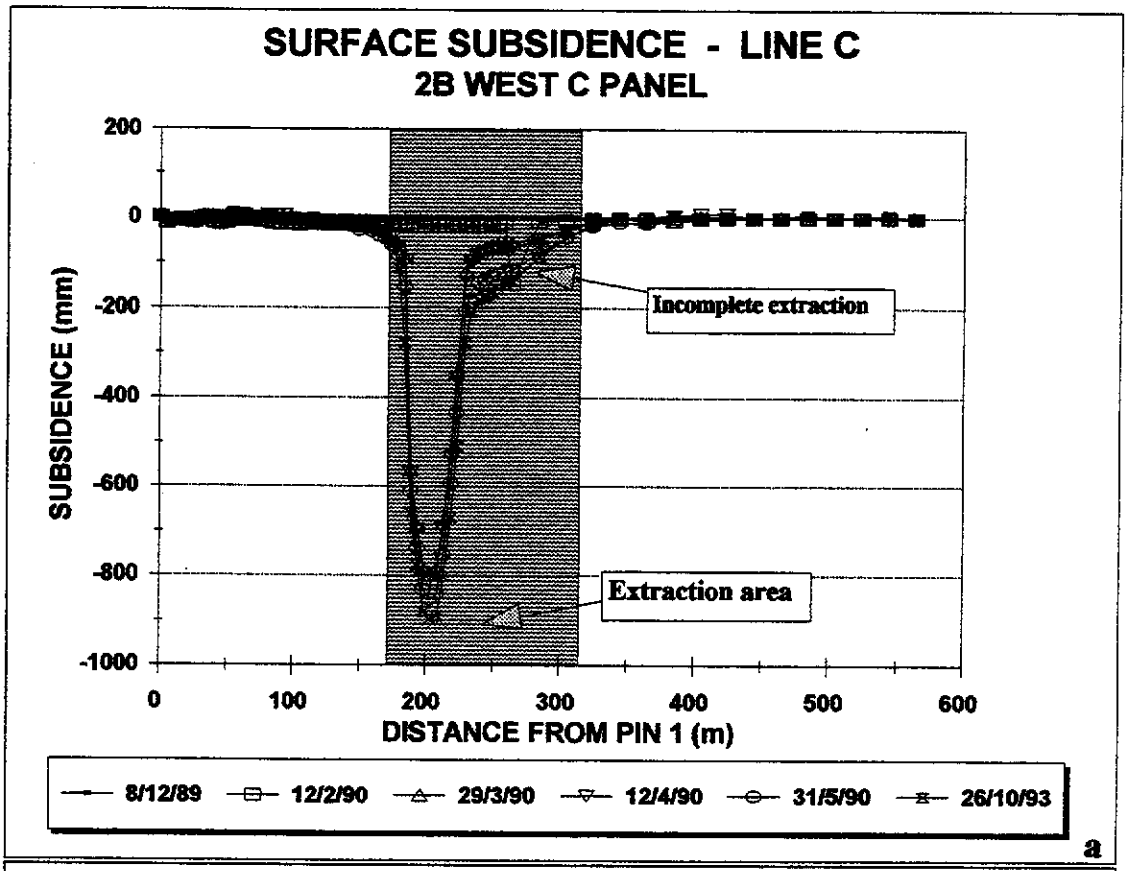
SURFACE SUBSIDENCE - LINE C
2B WEST C PANEL
SUBSIDENCE (mm)
200
0
-200
-400
-600
-800
-1000
0
100
200
300
400
500
600
DISTANCE FROM PIN 1 (m)
Incomplete extraction
Extraction area
8/12/89
12/2/90
29/3/90
12/4/90
31/5/90
26/10/93
a

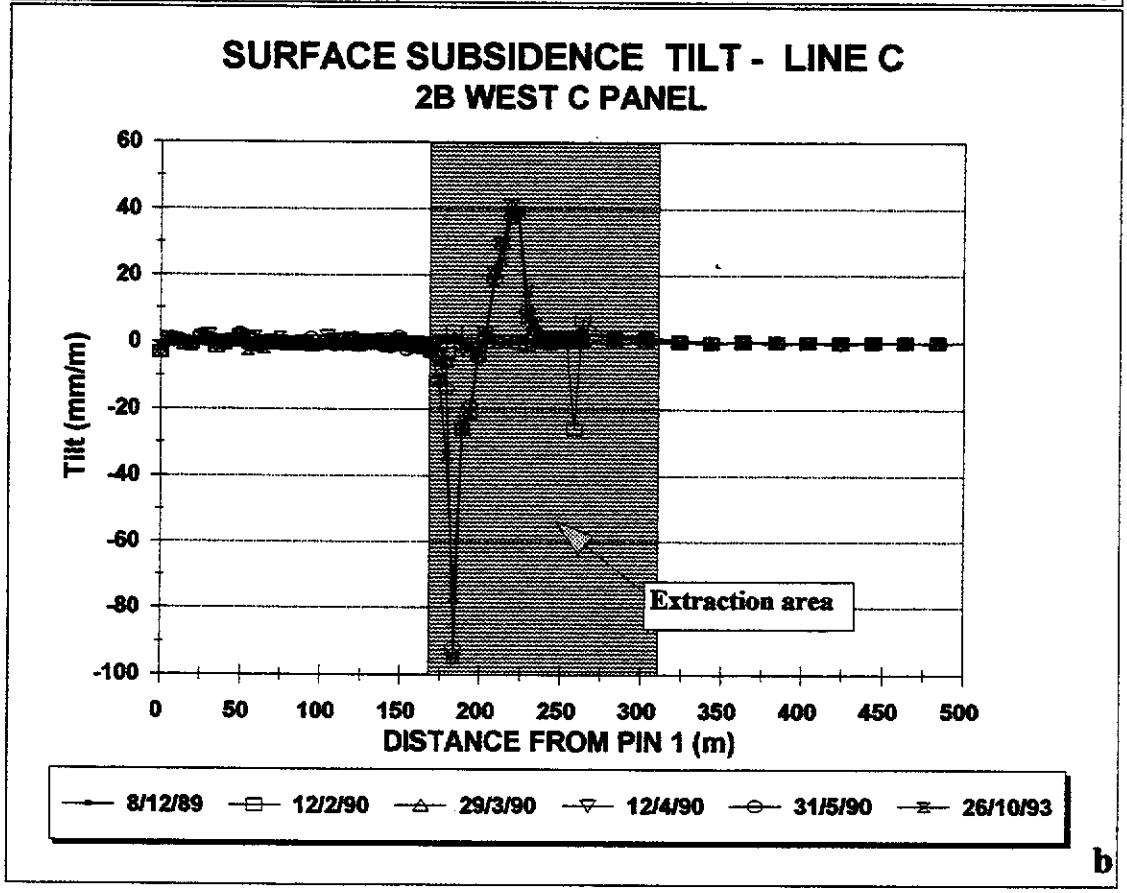
SURFACE SUBSIDENCE TILT - LINE C
2B WEST C PANEL
Tilt (mm/m)
60
40
20
0
-20
-40
-60
-80
-100
0
50
100
150
200
250
300
350
400
450
500
DISTANCE FROM PIN 1 (m)
Extraction area
8/12/89
12/2/90
29/3/90
12/4/90
31/5/90
26/10/93
b

Figure I.24

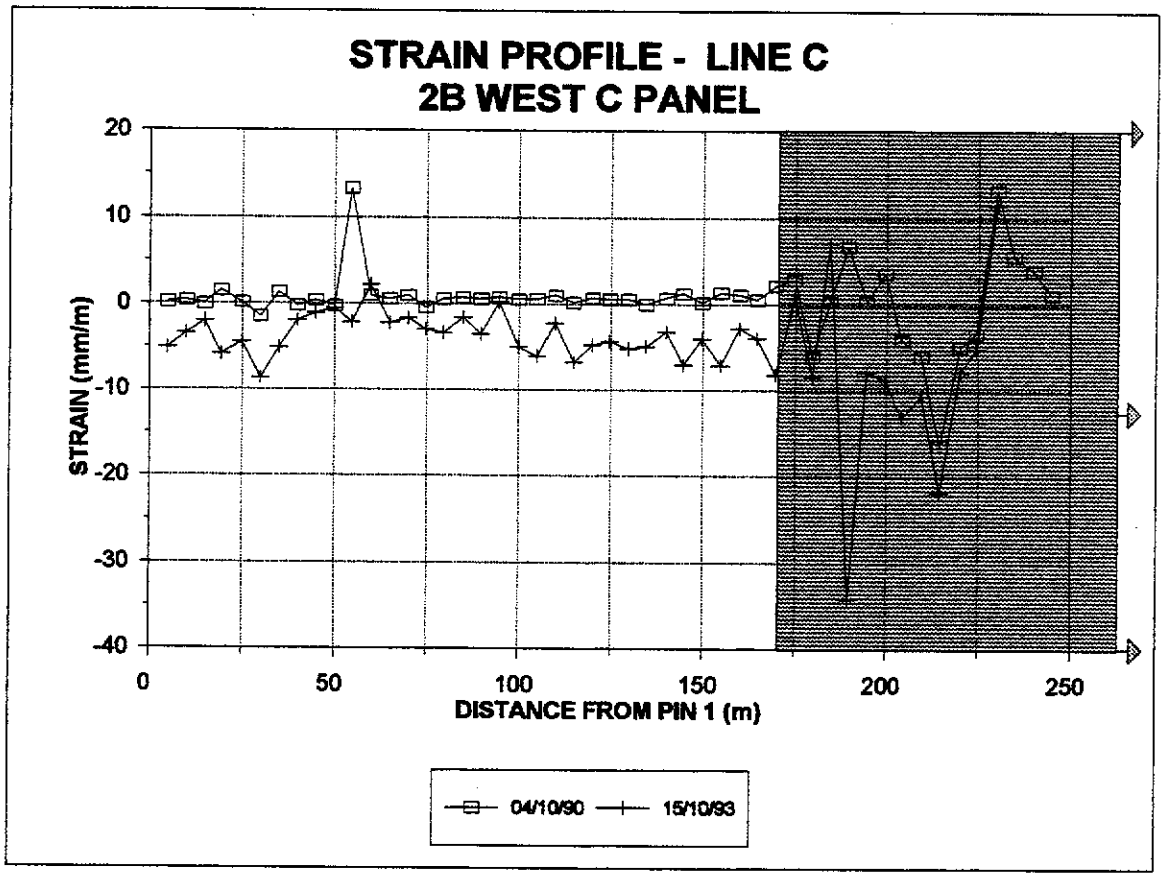
STRAIN PROFILE - LINE C
2B WEST C PANEL
STRAIN (mm/m)
20
10
0
-10
-20
-30
-40
0
50
100
150
200
250
DISTANCE FROM PIN 1 (m)
04/10/90
15/10/93

Figure I.25

TABLE I.12 LINE C STRAIN MONITORING 2B WEST C PANEL			
Date >>	13-Dec-89	04-Oct-90	15-Oct-93
Days >>	0	295	1402
PIN #	DISTANCE BETWEEN SURVEY PEGS (m)		
1-2	4.962	4.963	4.937
2-3	5.011	5.013	4.994
3-4	5.011	5.011	5.001
4-5	4.448	4.455	4.422
5-6	5.576	5.577	5.551
6-7	4.885	4.878	4.843
7-8	5.086	5.093	5.060
8-9	5.019	5.018	5.009
9-10	4.872	4.874	4.867
11	5.246	5.245	5.243
12	4.491	4.551	4.481
13	5.121	5.126	5.132
14	5.112	5.115	5.101
15	5.021	5.026	5.013
16	4.852	4.850	4.838
17	4.805	4.808	4.789
18	5.207	5.211	5.199
19	4.866	4.869	4.849
20	4.958	4.962	4.959
21	5.256	5.259	5.230
22	4.959	4.962	4.929
23	4.838	4.843	4.827
24	4.983	4.984	4.949
25	5.173	5.177	5.148
26	4.871	4.874	4.850
27	5.106	5.109	5.079
28	4.846	4.846	4.822
29	5.386	5.390	5.369
30	4.669	4.675	4.636
31	5.131	5.132	5.110
32	4.970	4.977	4.935
33	5.175	5.181	5.161
34	4.768	4.771	4.749
35	4.975	4.986	4.934
36	5.080	5.095	5.084
37	4.985	4.955	4.943
38	4.832	4.834	4.867
39	5.154	5.189	
40	4.994	4.996	4.977
41	4.880	4.898	4.955
42	4.681	4.662	4.837
43	5.350	5.318	4.619
44	4.931	4.850	5.293
45	5.554	5.527	4.823
46	4.283	4.269	5.510
47	5.796	5.873	4.261
48	4.561	4.587	5.863
49	5.202	5.223	9.753
50	4.824	4.830	4.818
51	4.952	4.963	4.937
52	4.910	4.895	4.880
53	4.956	4.957	4.944
54	5.225	5.227	5.218

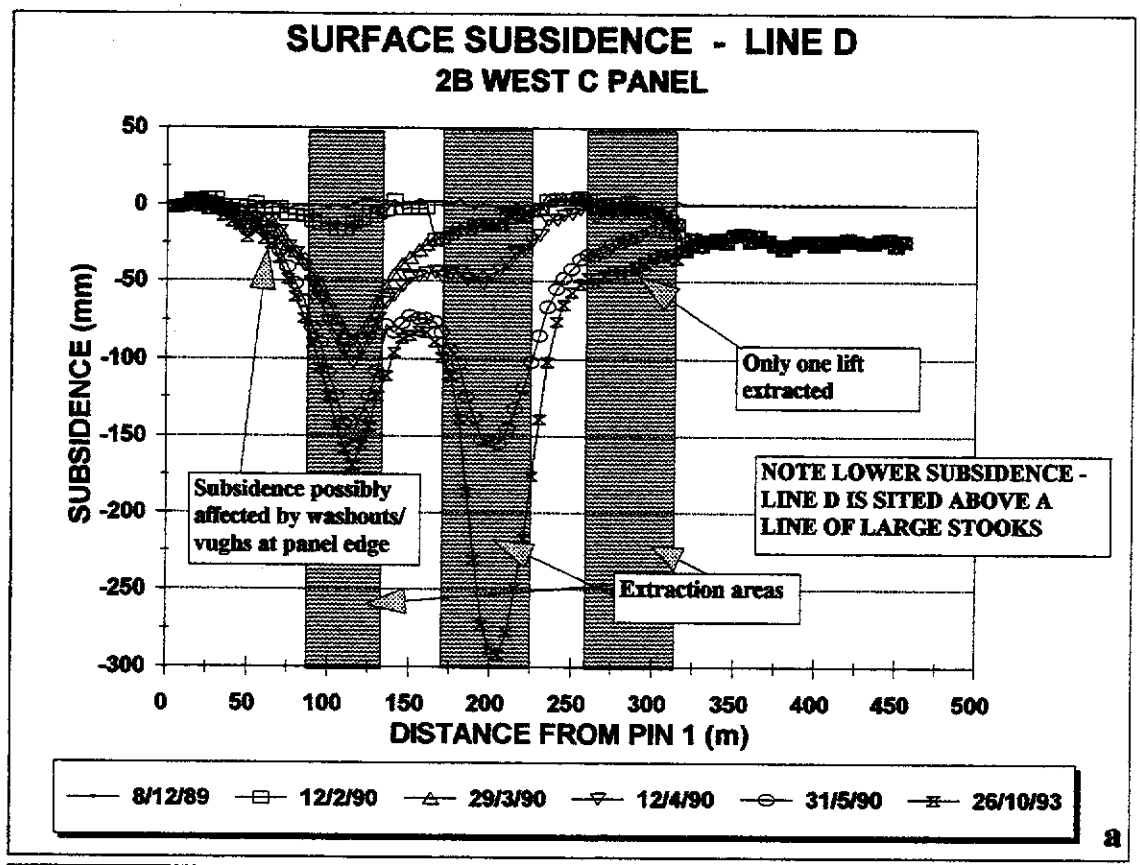
SURFACE SUBSIDENCE - LINE D
2B WEST C PANEL
SUBSIDENCE (mm)
50
0
-50
-100
-150
-200
-250
-300
0
50
100
150
200
250
300
350
400
450
500
DISTANCE FROM PIN 1 (m)
Only one lift extracted
NOTE LOWER SUBSIDENCE - LINE D IS SITED ABOVE A LINE OF LARGE STOOKS
Subsidence possibly affected by washouts/ vughs at panel edge
Extraction areas
8/12/89
12/2/90
29/3/90
12/4/90
31/5/90
26/10/93
a

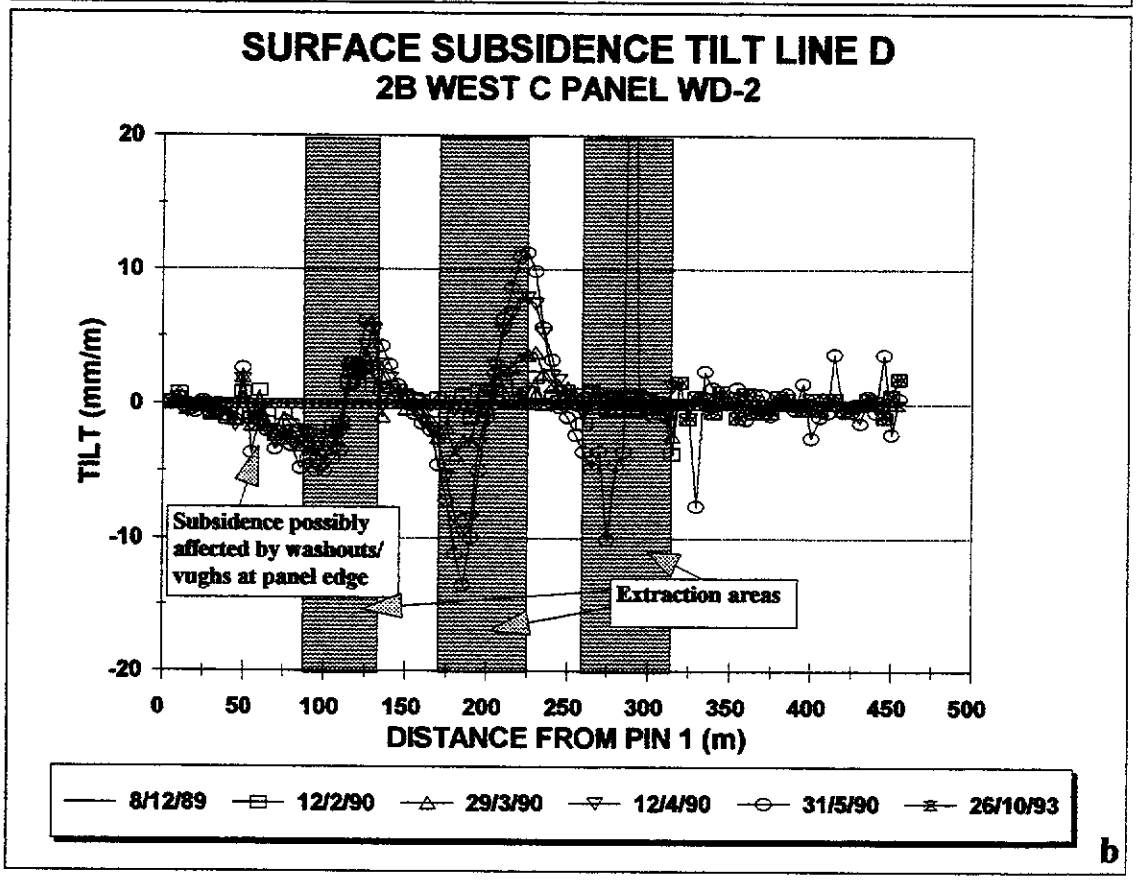
SURFACE SUBSIDENCE TILT LINE D
2B WEST C PANEL WD-2
TILT (mm/m)
20
10
0
-10
-20
0
50
100
150
200
250
300
350
400
450
500
DISTANCE FROM PIN 1 (m)
Subsidence possibly affected by washouts/ vughs at panel edge
Extraction areas
8/12/89
12/2/90
29/3/90
12/4/90
31/5/90
26/10/93
b

Figure I.26

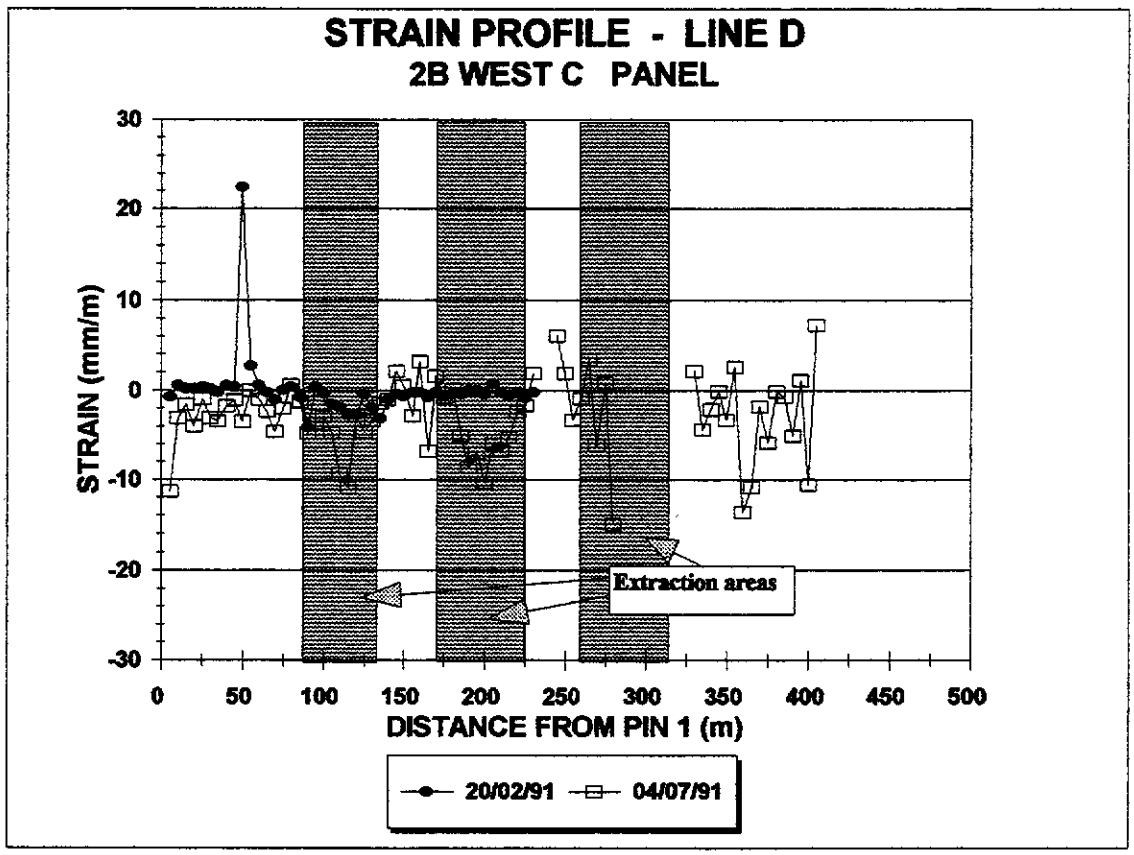
STRAIN PROFILE - LINE D
2B WEST C PANEL
STRAIN (mm/m)
30
20
10
0
-10
-20
-30
0
50
100
150
200
250
300
350
400
450
500
DISTANCE FROM PIN 1 (m)
Extraction areas
20/02/91
04/07/91

Figure I.27

TABLE 1.13
LINE D STRAIN MONITORING C PANEL

Date >	13-Dec-89	13-Mar-90	15-Oct-93
Days >	0	90	1402
PIN #	DISTANCE BETWEEN SURVEY PEGS (m)		
1-2	5.533	5.529	5.470
2-3	5.096	5.099	5.080
3-4	4.900	4.901	4.892
4-5	4.681	4.682	4.662
5-6	5.161	5.163	5.156
6-7	4.961	4.962	4.946
7-8	4.555	4.554	4.540
8-9	5.453	5.456	5.444
9-10	4.938	4.940	4.933
11	4.581	4.684	4.565
12	5.466	5.481	5.466
13	5.071	5.074	5.066
14	4.934	4.933	4.923
15	4.713	4.708	4.691
16	5.264	5.264	5.254
17	4.829	4.831	4.832
18	5.403	5.399	5.396
19	4.818	4.798	4.795
20	4.989	4.991	4.971
21	4.786	4.784	4.772
22	5.269	5.261	5.244
23	4.882	4.873	4.836
24	5.146	5.132	5.090
25	5.197	5.183	5.183
26	4.729	4.727	4.707
27	4.802	4.793	4.786
28	5.179	5.163	5.172
29	4.852	4.847	4.847
30	5.108	5.106	5.119
31	4.670	4.667	4.673
32	5.302	5.301	5.287
33	4.772	4.771	4.787
34	5.483	5.479	5.446
35	4.384	4.383	4.391
36	5.148	5.145	5.144
37	5.728	5.726	5.729
38	4.569	4.567	4.546
39	4.895	4.895	4.853
40	5.035	5.035	5.000
41	4.671	4.669	4.623
42	5.322	5.326	5.290
43	5.202	5.201	5.167
44	4.752	4.749	4.727
45	5.213	5.212	5.201
46	4.708	4.704	4.700

TABLE 1.13
LINE D STRAIN MONITORING C PANEL

Date >	13-Dec-89	13-Mar-90	15-Oct-93
Days >	0	90	1402
PIN #	DISTANCE BETWEEN SURVEY PEGS (m)		
46 - 47	4.972	4.971	4.982
48		4.971	5.266
49	5.237	4.971	4.461
50	4.450	4.971	5.388
51	4.946	4.971	4.976
52	5.188	4.971	5.198
53	4.821	4.971	4.805
54	5.022	4.971	5.018
55	5.058	4.971	5.075
56	4.841	4.971	4.811
57	5.220	4.971	5.224
58	5.032	4.971	4.956
59	4.800	4.971	
60	4.795	4.971	
61	5.417	4.971	
62	5.901	4.971	
63	4.399	4.971	
64	4.610	4.971	
65	4.920	4.971	
66	4.704	4.971	
67	5.387	4.971	
68	4.892	4.971	4.903
69	5.002	4.971	4.980
70	5.212	4.971	5.201
71	4.814	4.971	4.813
72	4.882	4.971	4.866
73	5.133	4.971	5.147
74	5.004	4.971	4.936
75	5.452	4.971	5.393
76	4.827	4.971	4.818
77	5.222	4.971	5.192
78	5.072	4.971	5.071
79	4.959	4.971	4.955
80	5.147	4.971	5.121
81	4.803	4.971	4.809
82	5.072	4.971	5.018
83	4.874	4.971	4.909
84	4.624	4.971	4.551
85	5.415	4.971	5.408
86	5.373	4.971	5.363
87	4.942	4.971	4.788
88	5.047	4.971	5.039
89	4.875	4.971	4.852
90	5.210	4.971	5.200
91	4.491	4.971	4.497
92	4.706	4.971	4.695

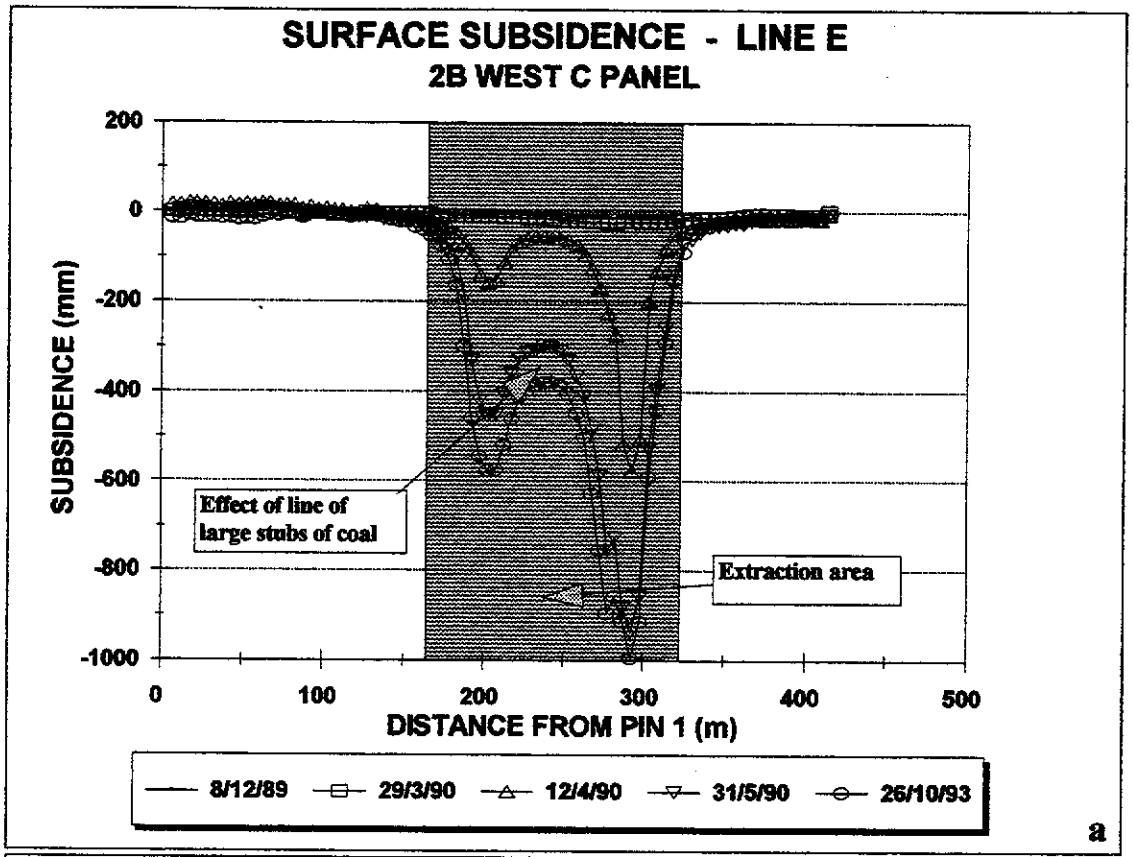
SURFACE SUBSIDENCE - LINE E
2B WEST C PANEL
SUBSIDENCE (mm)
200
0
-200
-400
-600
-800
-1000
0
100
200
300
400
500
DISTANCE FROM PIN 1 (m)
Effect of line of large stubs of coal
Extraction area
8/12/89
29/3/90
12/4/90
31/5/90
26/10/93
a

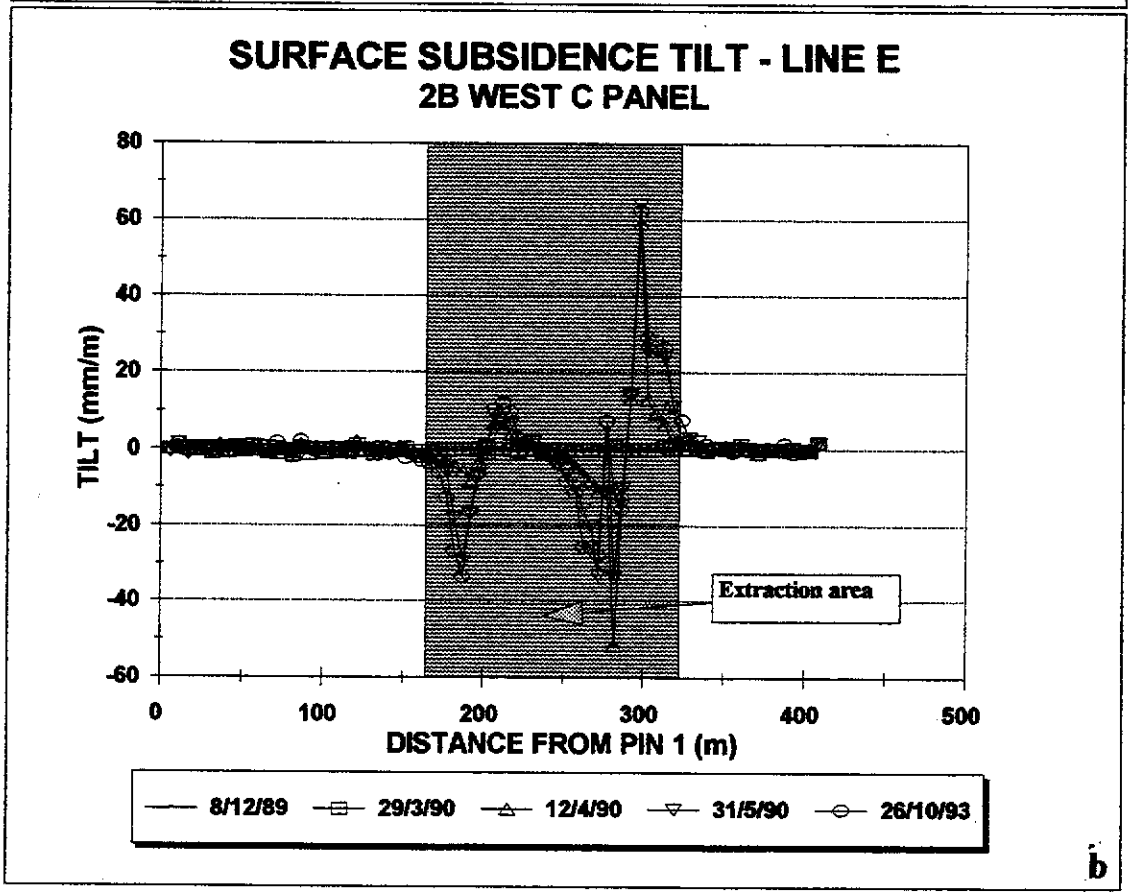
SURFACE SUBSIDENCE TILT - LINE E
2B WEST C PANEL
TILT (mm/m)
80
60
40
20
0
-20
-40
-60
0
100
200
300
400
500
DISTANCE FROM PIN 1 (m)
Extraction area
8/12/89
29/3/90
12/4/90
31/5/90
26/10/93
b

Figure I.28

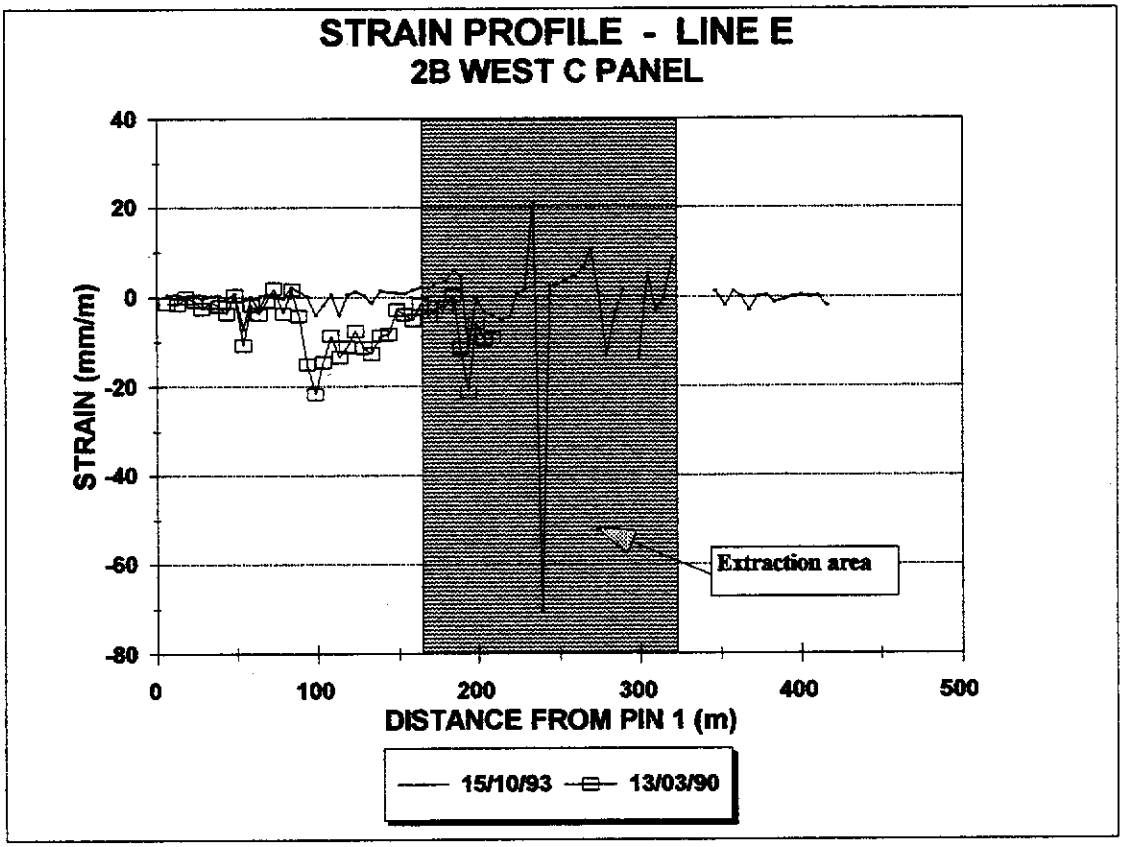
STRAIN PROFILE - LINE E
2B WEST C PANEL
STRAIN (mm/m)
40
20
0
-20
-40
-60
-80
0
100
200
300
400
500
DISTANCE FROM PIN 1 (m)
Extraction area
15/10/93
13/03/90

Figure I.29

TABLE I.14

LINE E STRAIN MONITORING C PANEL

Date >	13-Dec-89	13-Mar-90	15-Nov-93
Days >	0	90	1433
PIN #	DISTANCE BETWEEN SURVEY PEGS (m)		
1-2	6.548	6.551	6.540
2-3	5.223	5.226	5.215
3-4	5.410	5.410	5.410
4-5	4.453	4.455	4.450
5-6	5.374	5.372	5.361
6-7	4.895	4.896	4.890
7-8	5.010	5.012	5.000
8-9	5.068	5.067	5.050
9-10	5.327	5.331	5.330
11	4.680	4.647	4.630
12	4.829	4.829	4.821
13	5.079	5.065	5.060
14	4.504	4.507	4.500
15	5.848	5.852	5.860
16	4.930	4.929	4.912
17	4.711	4.721	4.719
18	5.254	5.261	5.233
19	4.859	4.860	4.787
20	4.903	4.884	4.797
21	5.048	5.039	4.975
22	4.982	4.985	4.939
23	5.093	5.073	5.025
24	5.046	5.049	4.990
25	5.028	5.034	4.990
26	4.761	4.763	4.707
27	5.354	5.347	5.287
28	5.111	5.118	5.067
29	4.823	4.828	4.783
30	5.074	5.079	5.060
31	4.948	4.952	4.929
32	4.893	4.901	4.868
33	5.353	5.364	5.345
34	4.545	4.554	4.526
35	5.796	5.814	5.783
36	5.063	5.080	5.052
37	4.463	4.489	4.465
38	5.051	5.075	4.994
39	4.748	4.696	4.647
40	5.262	5.260	5.232
41	4.991	4.975	4.944

LINE E STRAIN MONITORING C PANEL

Date >	13-Dec-89	13-Mar-90	15-Nov-93
Days >	0	90	1433
PIN #	DISTANCE BETWEEN SURVEY PEGS (m)		
42	4.880	4.859	4.836
43			5.144
44	5.199	5.173	4.837
45	4.885	4.863	4.980
46	4.998	5.000	5.157
47	5.148	5.158	4.782
48	4.787	4.888	5.234
49	5.258	4.888	4.731
50	4.741	4.752	4.910
51	4.900	4.914	5.329
52	5.323	5.343	5.359
53	5.341	5.366	4.775
54	4.756	4.786	4.929
55	4.875	4.926	4.969
56	5.000	5.005	4.980
57	5.081	5.015	4.994
58	5.047	5.029	
59	4.710	4.718	4.720
60	5.192		
61	5.369	5.294	5.293
62	5.210	5.237	5.209
63	5.106	5.091	5.098
64	5.314	5.314	5.307
65	5.217	5.261	5.244
66	5.421		5.562
67	5.458		5.431
68	5.244		5.148
69	5.190		5.129
70	5.884	5.891	5.875
71	5.671	5.661	5.594
72	4.683	4.689	4.672
73	5.065	5.065	5.056
74	5.279	5.264	5.239
75	5.440	5.441	5.429
76	5.235	5.237	5.229
77	5.425	5.419	5.418
78	5.500	5.497	5.484
79	5.309	5.309	5.300
80	5.050	5.052	5.050
81	5.332	5.332	5.323
82	5.425	5.426	5.425
83	5.340	5.330	5.323

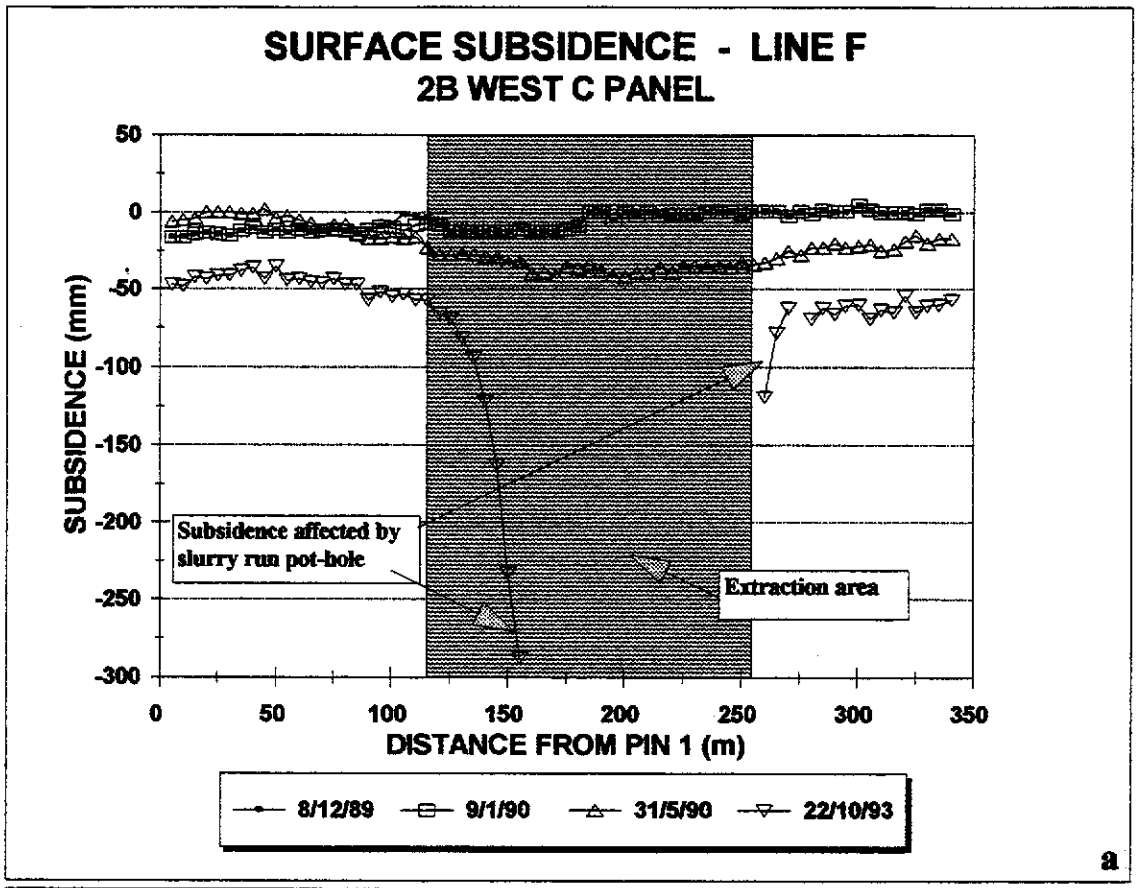
SURFACE SUBSIDENCE - LINE F
2B WEST C PANEL
SUBSIDENCE (mm)
50
0
-50
-100
-150
-200
-250
-300
0
50
100
150
200
250
300
350
DISTANCE FROM PIN 1 (m)
Subsidence affected by slurry run pot-hole
Extraction area
8/12/89
9/1/90
31/5/90
22/10/93
a

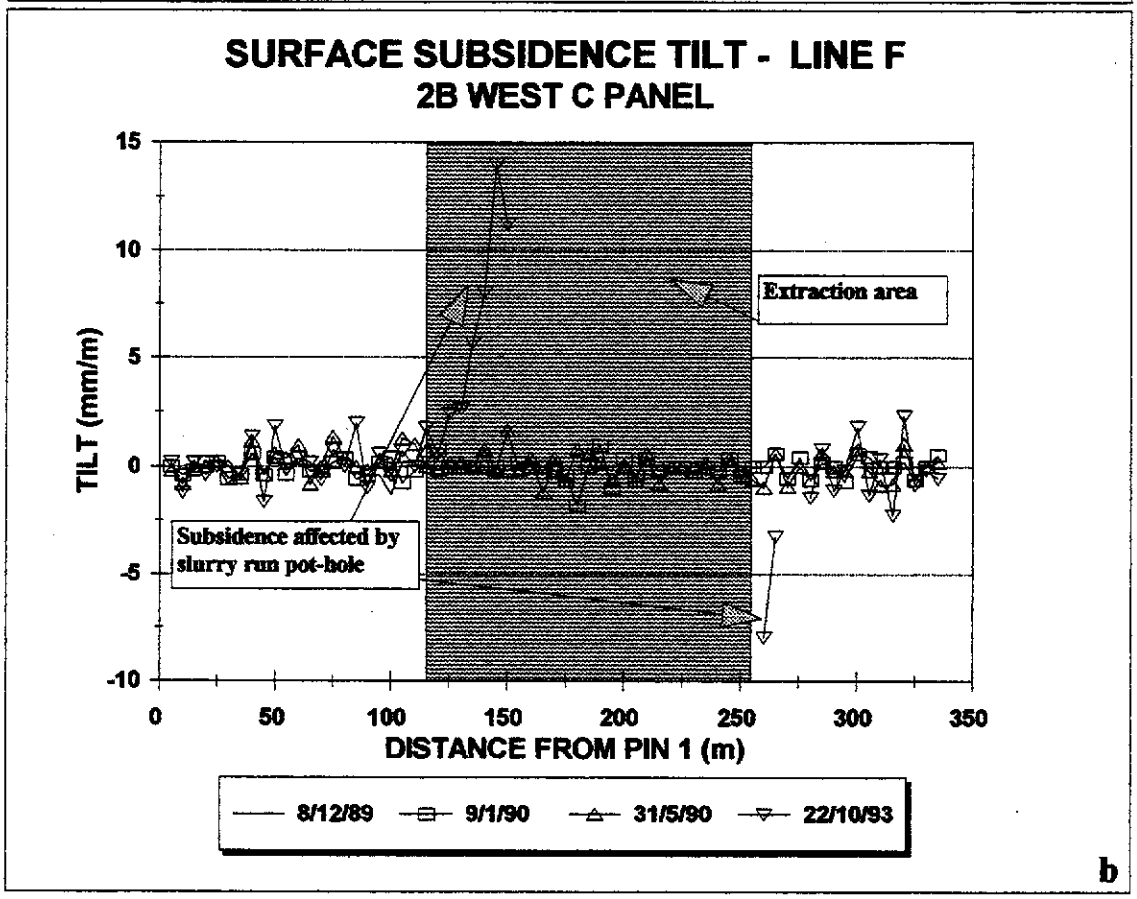
SURFACE SUBSIDENCE TILT - LINE F
2B WEST C PANEL
TILT (mm/m)
15
10
5
0
-5
-10
0
50
100
150
200
250
300
350
DISTANCE FROM PIN 1 (m)
Extraction area
Subsidence affected by slurry run pot-hole
8/12/89
9/1/90
31/5/90
22/10/93
b

Figure I.30

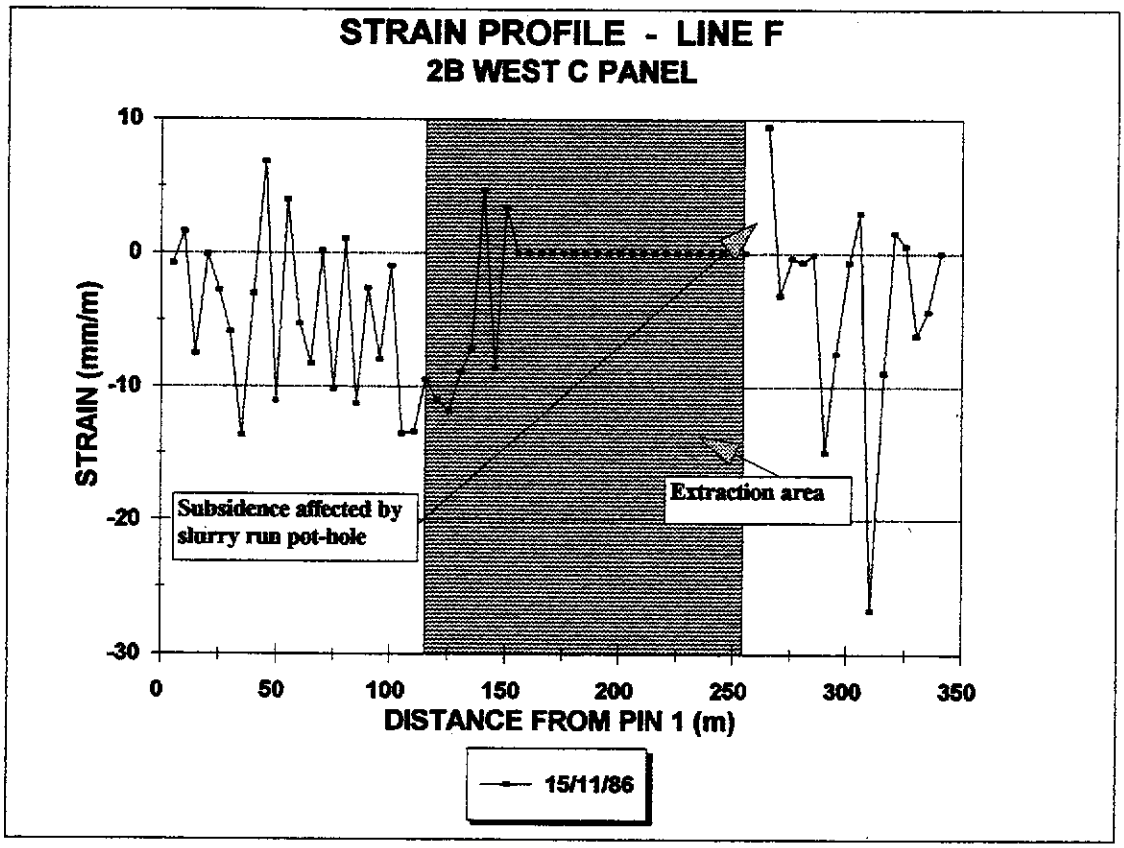
STRAIN PROFILE - LINE F
2B WEST C PANEL
STRAIN (mm/m)
10
0
-10
-20
-30
0
50
100
150
200
250
300
350
DISTANCE FROM PIN 1 (m)
Subsidence affected by slurry run pot-hole
Extraction area
15/11/86

Figure I.31

TABLE I.15	LINE F STRAIN MONITORING C PANEL	
Date >	13-Dec-89	15-Oct-93
Days >	0	1402
PIN #	DISTANCE BETWEEN SURVEY PEGS (m)	
1-2	5.134	5.130
2-3	4.943	4.951
3-4	4.935	4.898
4-5	5.169	5.168
5-6	4.913	4.899
6-7	4.720	4.692
7-8	5.102	5.032
8-9	5.262	5.246
9-10	5.033	5.067
11	4.829	4.775
12	4.889	4.908
13	5.160	5.133
14	5.165	5.122
15	4.927	4.928
16	4.881	4.831
17	5.128	5.133
18	5.053	4.996
19	4.996	4.983
20	4.983	4.944
21	4.986	4.981
22	4.630	4.567
23	5.339	5.268
24	4.889	4.843
25	5.073	5.017
26	5.206	5.144
27	4.974	4.930
28	4.914	4.879
29	4.921	4.944
30	5.105	5.061
31	4.998	5.015
32	4.902	4.887
33	5.005	
34	5.170	
35	4.895	
36	4.946	
37	4.894	
38	5.059	
39	5.098	
40	5.105	
41	4.922	
42	5.004	
43	4.836	
44	5.208	
45	4.987	
46	5.005	
47	4.876	
48	4.880	
49	5.186	
50	4.850	
51	5.083	
52	4.950	
53	4.952	
54	5.147	5.196
55	4.928	4.913
56	5.322	5.320
57	4.698	4.695
58	4.860	4.859
59	5.011	4.936
60	4.638	4.603
61	5.786	5.782
62	4.969	4.984
63	4.521	4.400
64	5.705	5.654
65	4.844	4.851
66	4.737	4.739
67	4.733	4.704
68	5.134	5.112
69	5.573	5.582

TABLE I.15

LIFTING PROGRESS

BLUE PANEL WD6

(10 ALPINE)

DATE	SPLIT #	GOAF WIDTH (m)
07/06/88	1 START	
10/06/88	1 FINISH	13
17/06/88	2 START	
24/06/88	2 FINISH	26
05/07/88	3 START	
07/07/88	3 FINISH	39
18/07/88	4 START	
22/07/88	4 FINISH	52
02/08/88	5 START	
08/08/88	5 FINISH	65
18/08/88	6 START	
24/08/88	6 FINISH	78
02/09/88	7 START	
09/09/88	7 FINISH	91
20/09/88	8 START	
28/09/88	8 FINISH	104
14/10/88	9 START	
24/10/88	9 FINISH	117
03/11/88	10 START	
09/11/88	10 FINISH	130
23/11/88	11 START	
29/11/88	11 FINISH	143
08/12/88	12 START	
13/12/88	12 FINISH	156
22/12/88	13 START	
30/12/88	13 FINISH	169

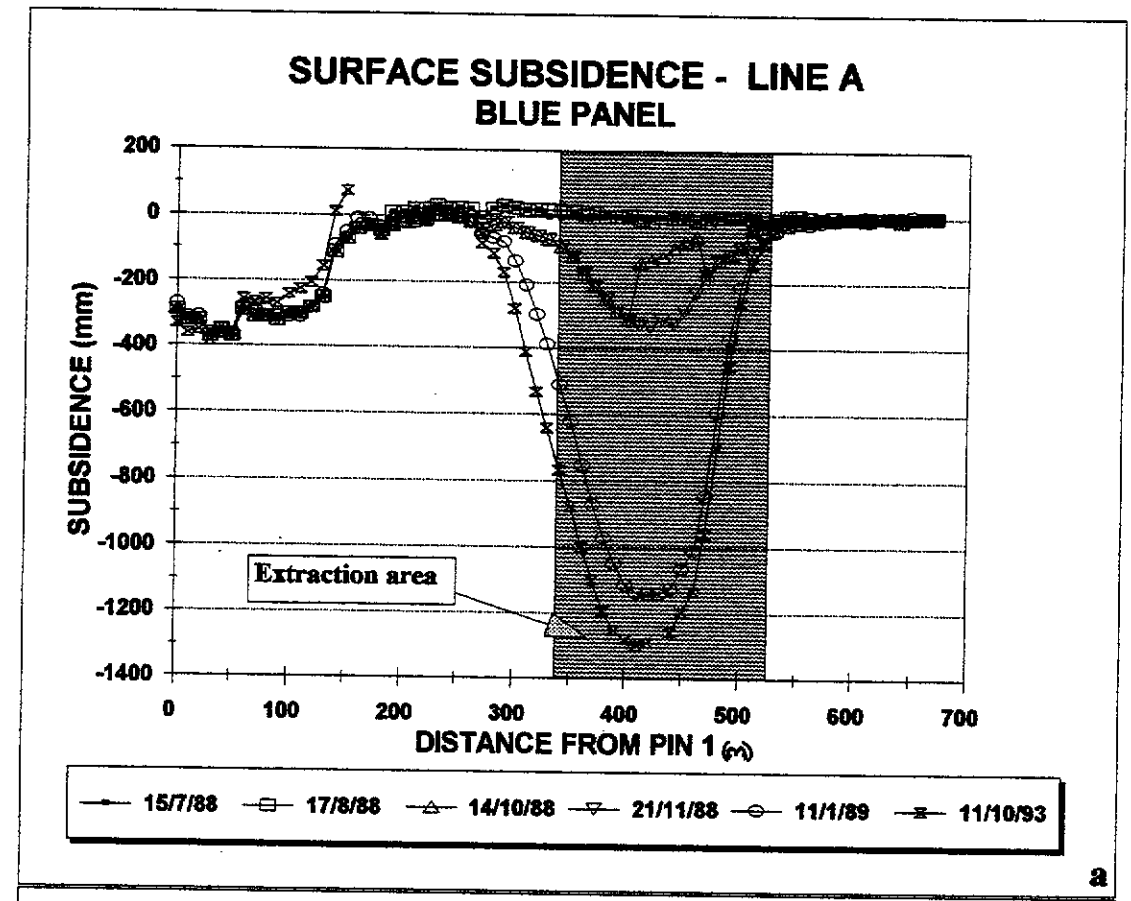
SURFACE SUBSIDENCE - LINE A
BLUE PANEL
SUBSIDENCE (mm)
200
0
-200
-400
-600
-800
-1000
-1200
-1400
Extraction area
0
100
200
300
400
500
600
700
DISTANCE FROM PIN 1 (m)
15/7/88
17/8/88
14/10/88
21/11/88
11/1/89
11/10/93
a

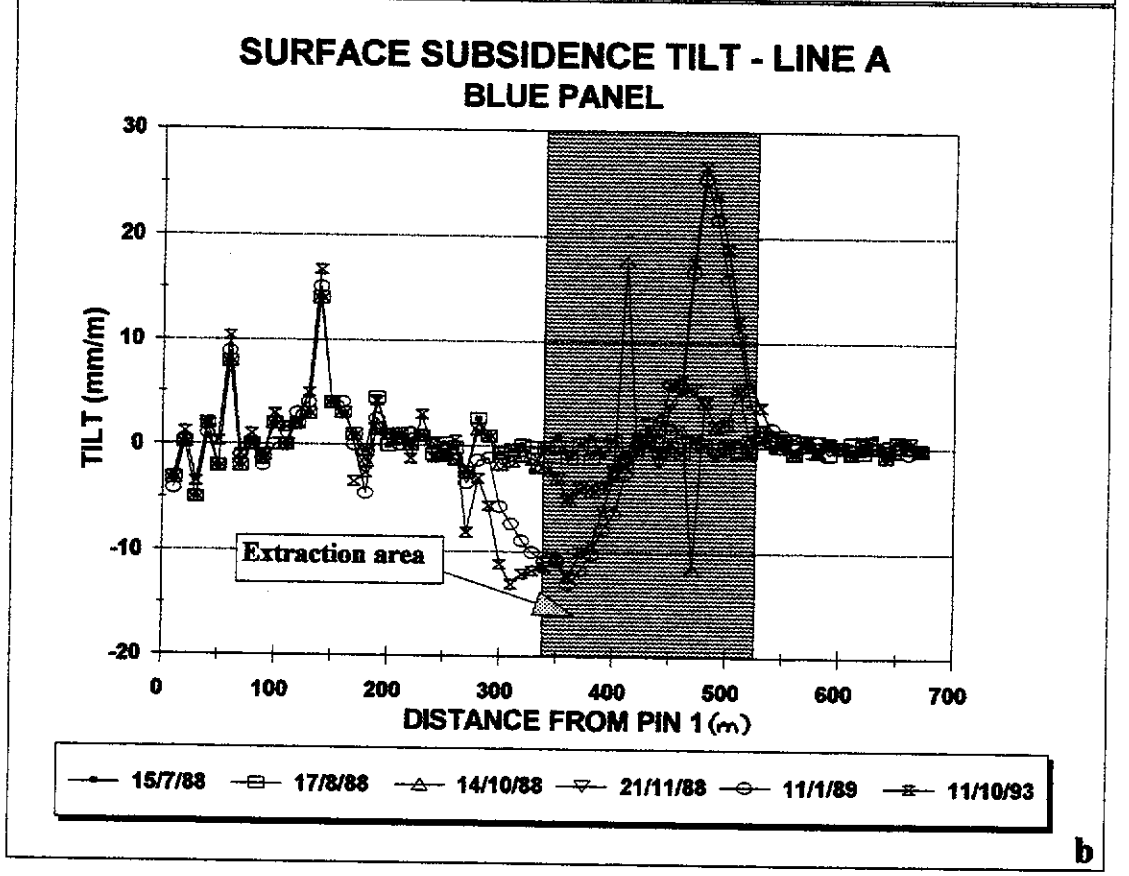
SURFACE SUBSIDENCE TILT - LINE A
BLUE PANEL
TILT (mm/m)
30
20
10
0
-10
-20
Extraction area
0
100
200
300
400
500
600
700
DISTANCE FROM PIN 1 (m)
15/7/88
17/8/88
14/10/88
21/11/88
11/1/89
11/10/93
b

Figure I.32

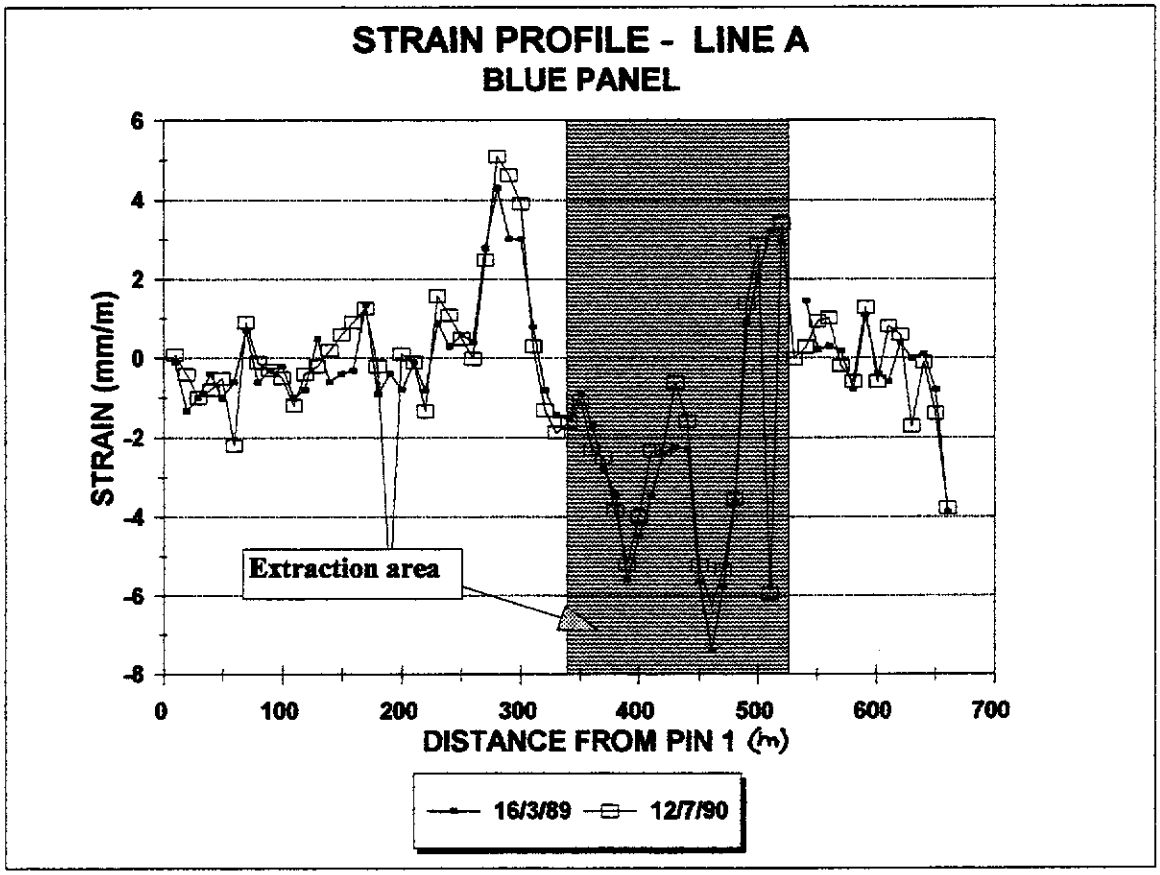
STRAIN PROFILE - LINE A
BLUE PANEL
STRAIN (mm/m)
6
4
2
0
-2
-4
-6
-8
0
100
200
300
400
500
600
700
DISTANCE FROM PIN 1 (m)
Extraction area
16/3/89
12/7/90

Figure I.33

TABLE I.16
LINE A STRAIN MONITORING
BLUE PANEL

Date >	06-Apr-88	16-Mar-89	12-Jul-90
Days >			
PIN #	DISTANCE BETWEEN SURVEY PEGS (m)		
1-2	10.063	10.062	10.064
2-3	9.776	9.763	9.772
3-4	10.055	10.045	10.045
4-5	9.971	9.967	9.963
5-6	9.990	9.980	9.985
6-7	10.096	10.090	10.074
7-8	9.916	9.923	9.925
8-9	9.834	9.828	9.833
9-10	10.095	10.092	10.092
11	10.135	10.133	10.130
12	10.124	10.114	10.112
13	9.987	9.979	9.983
14	10.119	10.124	10.117
15	9.934	9.928	9.936
16	10.100	10.096	10.106
17	9.876	9.873	9.885
18	10.196	10.210	10.209
19	9.949	9.940	9.947
20	9.977	9.973	9.919
21	9.953	9.945	9.954
22	10.261	10.260	10.260
23	9.755	9.747	9.742
24	10.096	10.105	10.112
25	10.012	10.015	10.023
26	10.037	10.043	10.042
27	9.804	9.808	9.804
28	10.054	10.082	10.079
29	10.184	10.228	10.236
30	9.935	9.965	9.981
31	9.962	9.992	10.001
32	10.078	10.086	10.081
33	9.943	9.935	9.930
34	9.091	9.078	9.074
35	11.207	11.190	11.189
36	10.084	10.075	10.073
37	10.027	10.010	10.004
38	10.053	10.025	10.028
39	9.869	9.835	9.831
40	10.033	9.977	9.981
41	10.054	10.009	10.014
42	9.885	9.851	9.862
43	10.041	10.017	10.018
44	9.829	9.807	9.823
45	10.087	10.064	10.071
46	10.125	10.068	10.072
47	9.865	9.792	9.803
48	9.923	9.866	9.870
49	9.886	9.850	9.851
50	10.092	10.101	10.106
51	10.070	10.091	10.099
52	9.958	9.990	9.899
53	10.277	10.307	10.312
54	9.962		10.060
55	10.243	10.258	10.246
56	9.545	9.547	9.554
57	9.694	9.697	9.704
58	10.343	10.345	10.341
59	10.098	10.090	10.092
60	10.024	10.035	10.037
61	10.130	10.126	10.124
62	9.898	9.892	9.906
63	10.111	10.115	10.117
64	9.960	9.960	9.943
65	9.977	9.978	9.976
66	10.067	10.059	10.053
67	10.067	10.028	10.029
68	10.067	10.583	10.593

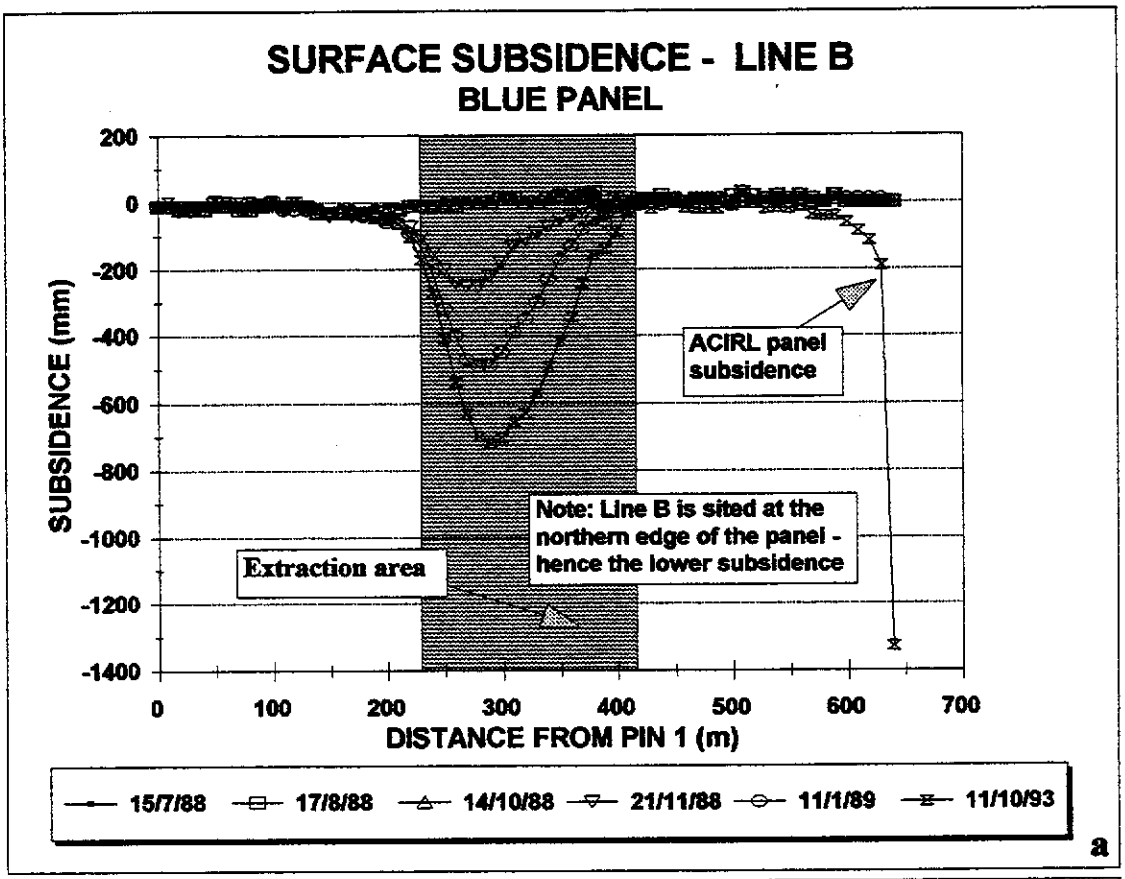
SURFACE SUBSIDENCE - LINE B
BLUE PANEL
SUBSIDENCE (mm)
200
0
-200
-400
-600
-800
-1000
-1200
-1400
0
100
200
300
400
500
600
700
DISTANCE FROM PIN 1 (m)
ACIRL panel subsidence
Note: Line B is sited at the northern edge of the panel - hence the lower subsidence
Extraction area
15/7/88
17/8/88
14/10/88
21/11/88
11/1/89
11/10/93
a

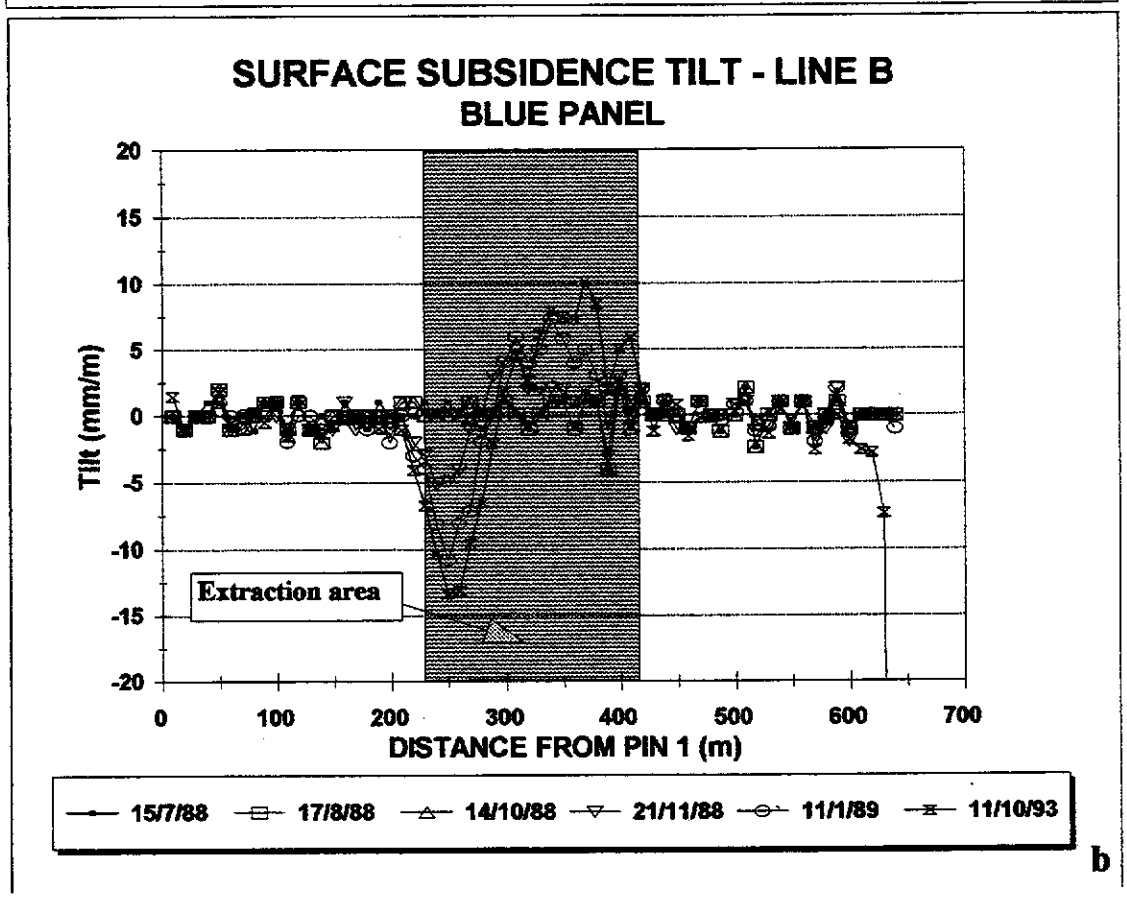
SURFACE SUBSIDENCE TILT - LINE B
BLUE PANEL
Tilt (mm/m)
20
15
10
5
0
-5
-10
-15
-20
0
100
200
300
400
500
600
700
DISTANCE FROM PIN 1 (m)
Extraction area
15/7/88
17/8/88
14/10/88
21/11/88
11/1/89
11/10/93
b

Figure I.34

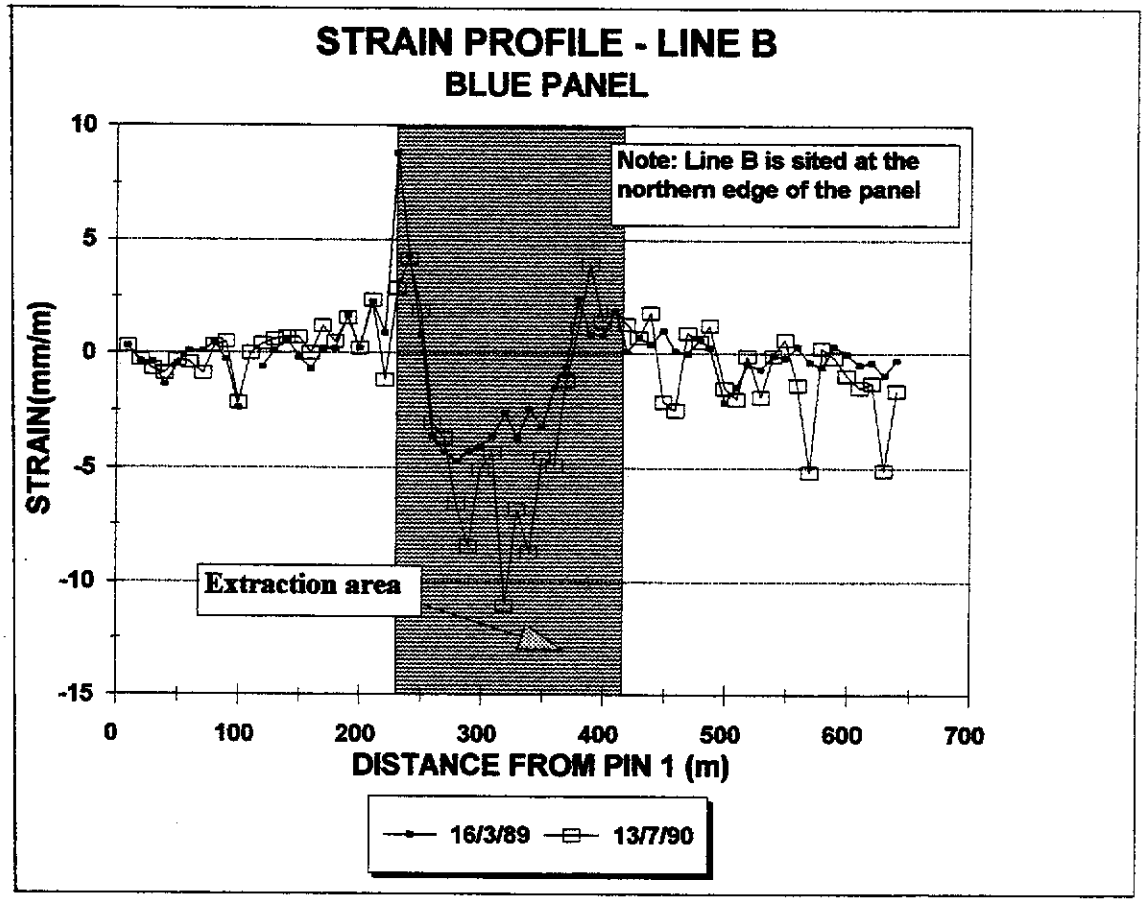
STRAIN PROFILE - LINE B
BLUE PANEL
Note: Line B is sited at the northern edge of the panel
Extraction area
STRAIN(mm/m)
10
5
0
-5
-10
-15
0
100
200
300
400
500
600
700
DISTANCE FROM PIN 1 (m)
16/3/89
13/7/90

Figure I.35

TABLE L17
LINE B STRAIN MONITORING
BLUE PANEL

Date >	06-Apr-88	16-Mar-89	13-Jul-90
Days >	0	344	828
PIN #	DISTANCE BETWEEN SURVEY PEGS (m)		
1-2	9.592	9.595	9.595
2-3	10.011	10.007	10.008
3-4	9.989	9.985	9.982
4-5	10.016	10.002	10.007
5-6	9.886	9.881	9.883
6-7	9.955	9.956	9.951
7-8	10.994	10.995	10.984
8-9	9.168	9.172	9.171
9-10	9.933	9.930	9.938
11	9.715	9.692	9.694
12	10.264		10.317
13	9.966	9.960	9.970
14	10.005	10.006	10.011
15	9.926	9.932	9.933
16	10.042	10.040	10.049
17	9.955	9.948	9.955
18	9.900	9.902	9.912
19	9.908	9.910	9.913
20	10.190	10.207	10.206
21	9.761	9.763	9.763
22	10.159	10.182	10.183
23	10.022	10.031	10.010
24	10.107	10.196	10.136
25	9.780	9.822	9.821
26	10.170	10.178	10.189
27	9.856	9.820	9.826
28	9.752	9.710	9.716
29	10.209	10.161	10.142
30	10.069	10.026	9.984
31	9.862	9.822	9.812
32	10.137	10.100	10.093
33	10.043	10.017	9.932
34	9.995	9.958	9.927
35	9.554	9.531	9.471
36	10.343	10.310	10.296
37	10.027	10.012	9.978
38	9.954	9.948	9.942
39	9.910	9.934	9.921
40	9.921	9.929	9.960
41	10.085	10.093	10.099
42	9.934	9.953	9.953
43	10.108	10.109	10.121
44	9.907	9.914	9.914
45	9.937	9.941	9.955
46	9.992	10.002	9.971
47	10.107	10.108	10.082
48	9.836	9.836	9.845
49	9.931	9.937	9.936
50	8.061	8.063	8.071
51	12.562	12.535	12.543
52	9.610	9.596	9.591
53	8.452	8.448	8.451
54	11.515	11.507	11.493
55	9.895	9.894	9.894
56	9.907	9.905	9.913
57	10.065	10.068	10.051
58	10.069	10.065	10.017
59	9.882	9.876	9.884
60	9.975	9.978	9.973
61	10.212	10.212	10.202
62	10.034	10.029	10.019
63	9.954	9.950	9.941
64	10.193	10.183	10.141
65	9.799	9.796	9.783

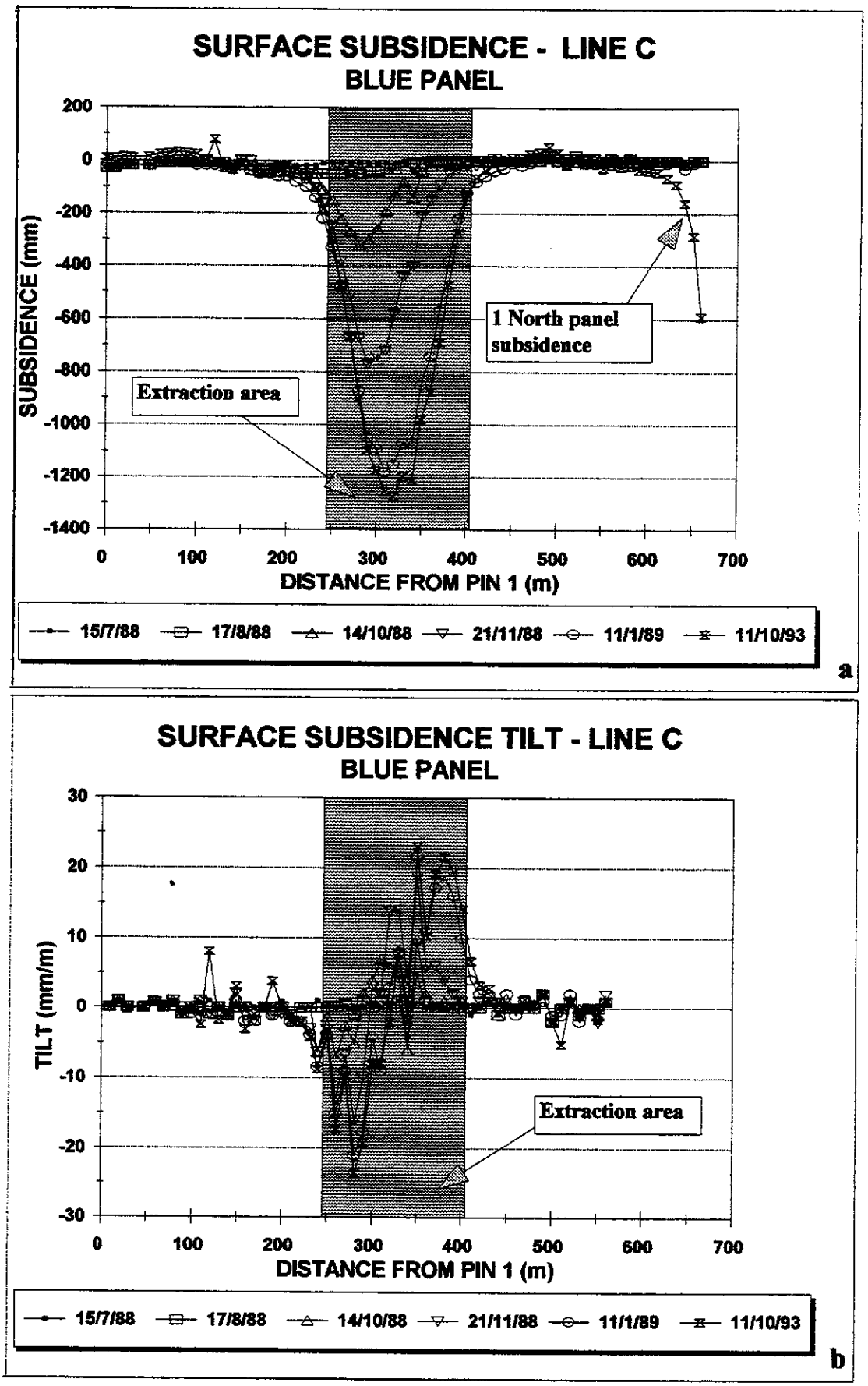
SURFACE SUBSIDENCE - LINE C
BLUE PANEL
SUBSIDENCE (mm)
200
0
-200
-400
-600
-800
-1000
-1200
-1400
0
100
200
300
400
500
600
700
DISTANCE FROM PIN 1 (m)
1 North panel subsidence
Extraction area
15/7/88
17/8/88
14/10/88
21/11/88
11/1/89
11/10/93
a
SURFACE SUBSIDENCE TILT - LINE C
BLUE PANEL
TILT (mm/m)
30
20
10
0
-10
-20
-30
0
100
200
300
400
500
600
700
DISTANCE FROM PIN 1 (m)
Extraction area
15/7/88
17/8/88
14/10/88
21/11/88
11/1/89
11/10/93
b

Figure I.36

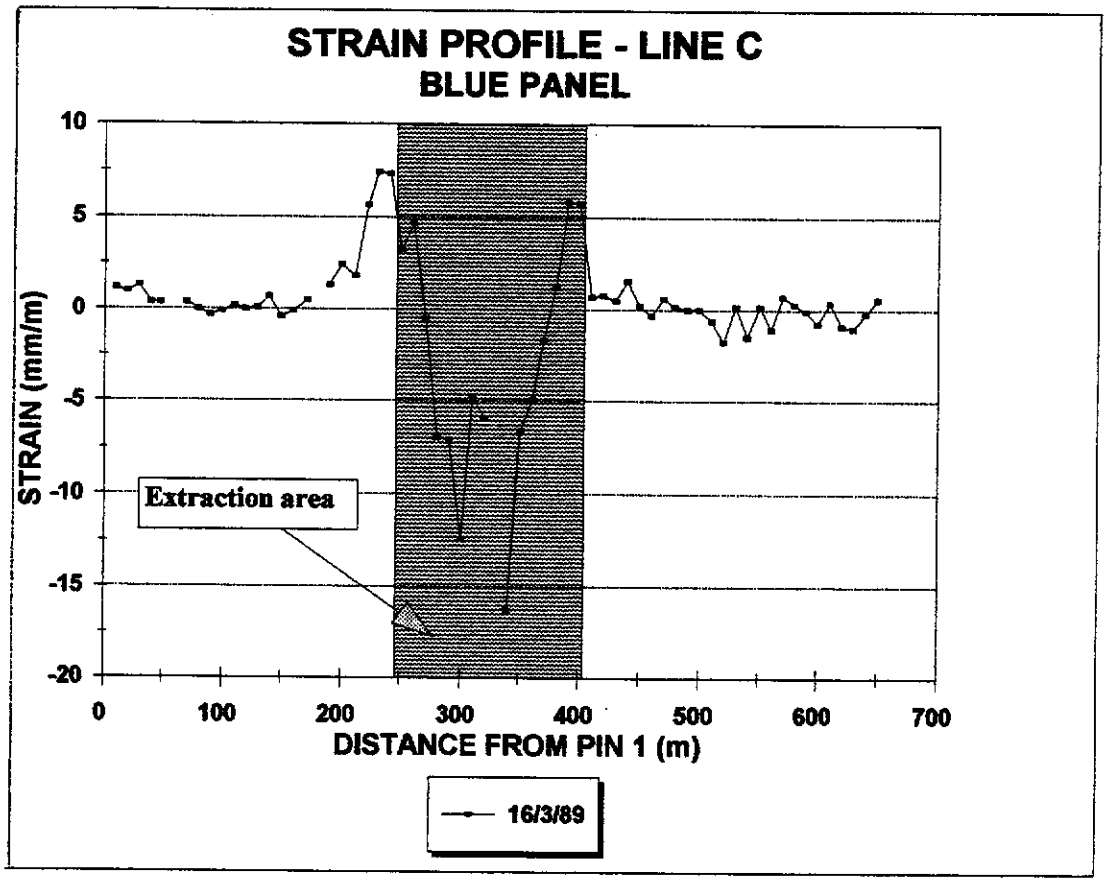
STRAIN PROFILE - LINE C
BLUE PANEL
STRAIN (mm/m)
10
5
0
-5
-10
-15
-20
Extraction area
0
100
200
300
400
500
600
700
DISTANCE FROM PIN 1 (m)
16/3/89

Figure I.37

TABLE I.18
LINE C STRAIN MONITORING
BLUE PANEL

Date >	06-Apr-88	16-Mar-89	12-Jul-90
Days >	0	344	827
PIN #	DISTANCE BETWEEN SURVEY PEGS (m)		
1-2	9.370	9.381	9.378
2-3	10.058	10.068	10.062
3-4	9.706	9.719	9.722
4-5	10.168	10.172	10.167
5-6	8.050	8.053	8.053
6-7	12.230		12.243
7-8	10.014	10.018	10.018
8-9	10.035	10.035	10.031
9-10	9.919	9.916	9.917
11	10.108	10.107	10.085
12	9.863	9.865	9.873
13	10.065	10.065	10.061
14	9.938	9.939	9.931
15	9.957	9.964	9.967
16	9.982	9.978	9.985
17	10.190	10.189	10.190
18	9.908	9.913	9.897
19	12.360		11.544
20	8.811	8.823	8.827
21	9.415	9.438	9.445
22	10.296	10.315	10.292
23	10.918	10.980	10.989
24	10.602	10.681	10.652
25	8.152	8.212	8.182
26	10.406	10.440	10.451
27	9.651	9.696	9.690
28	10.073	10.068	10.076
29	10.402	10.330	10.308
30	9.660	9.592	9.602
31	9.907	9.784	9.762
32	10.086	10.038	10.046
33	9.835	9.777	9.786
34	9.976		
35	10.270	10.103	10.096
36	9.799	9.734	9.722
37	10.030	9.981	9.977
38	10.216	10.199	10.182
39	9.874	9.887	9.897
40	9.984	10.042	10.053
41	10.040	10.098	10.051
42	9.901	9.908	9.904
43	10.000	10.008	9.985
44	10.063	10.068	10.078
45	9.997	10.013	10.018
46	9.832	9.834	9.840
47	10.011	10.008	10.015
48	9.996	10.002	10.006
49	10.090	10.092	10.101
50	10.031	10.031	10.037
51	9.767	9.767	9.769
52	9.854	9.848	9.813
53	10.256	10.238	10.244
54	9.911	9.913	9.911
55	10.239	10.224	10.203
56	10.040	10.042	10.042
57	10.238	10.227	10.234
58	9.701	9.708	9.700
59	9.858	9.861	9.876
60	10.234	10.233	10.241
61	9.553	9.546	9.551
62	9.910	9.914	9.912
63	10.302	10.293	10.294
64	9.894	9.884	9.889
65	9.759	9.757	9.761
66	10.183	10.189	10.187
67	10.186	10.183	10.180

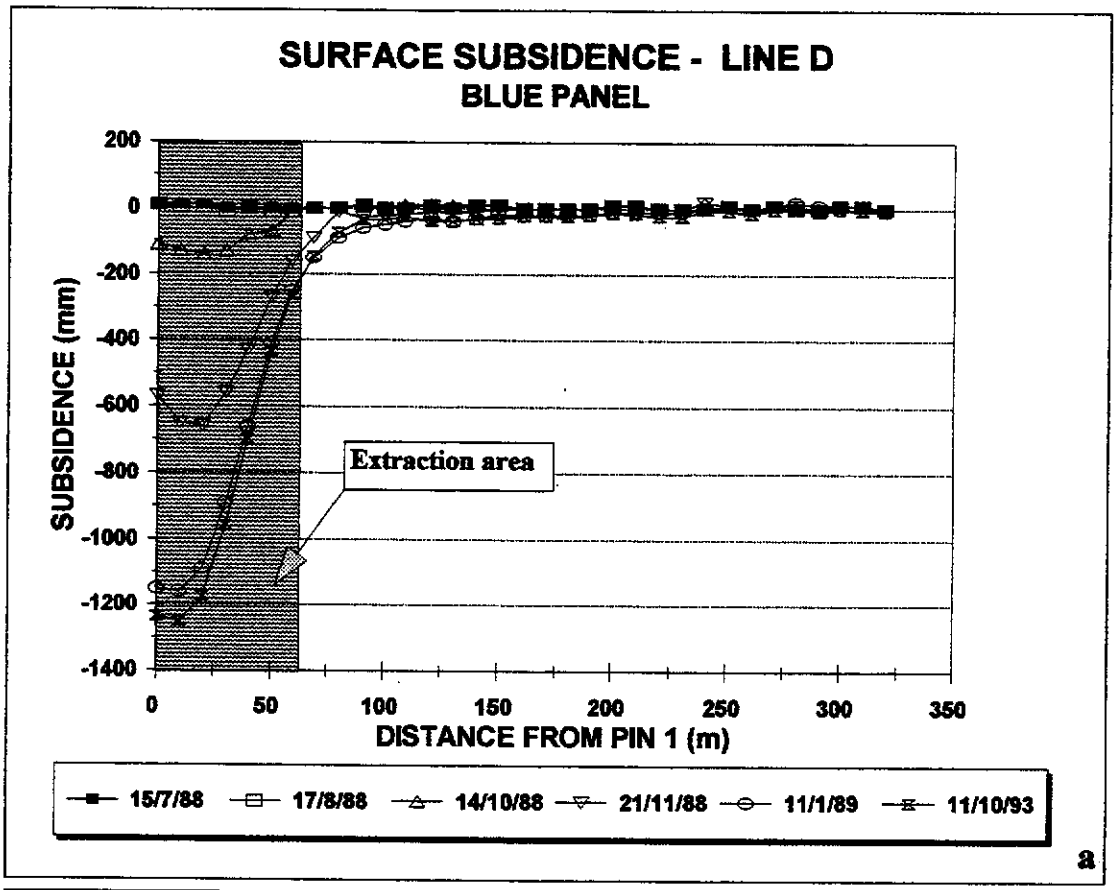
SURFACE SUBSIDENCE - LINE D
BLUE PANEL
SUBSIDENCE (mm)
200
0
-200
-400
-600
-800
-1000
-1200
-1400
Extraction area
0
50
100
150
200
250
300
350
DISTANCE FROM PIN 1 (m)
15/7/88
17/8/88
14/10/88
21/11/88
11/1/89
11/10/93
a

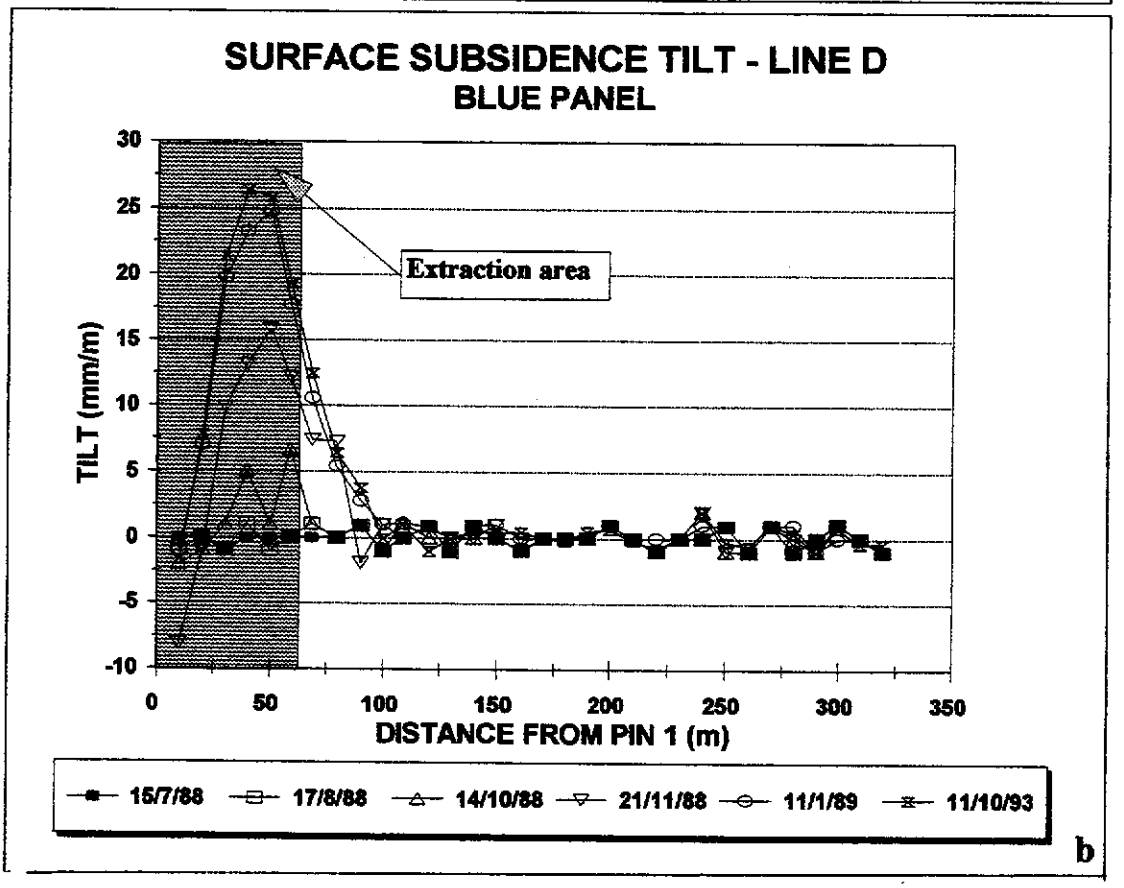
SURFACE SUBSIDENCE TILT - LINE D
BLUE PANEL
TILT (mm/m)
30
25
20
15
10
5
0
-5
-10
Extraction area
0
50
100
150
200
250
300
350
DISTANCE FROM PIN 1 (m)
15/7/88
17/8/88
14/10/88
21/11/88
11/1/89
11/10/93
b

Figure I.38

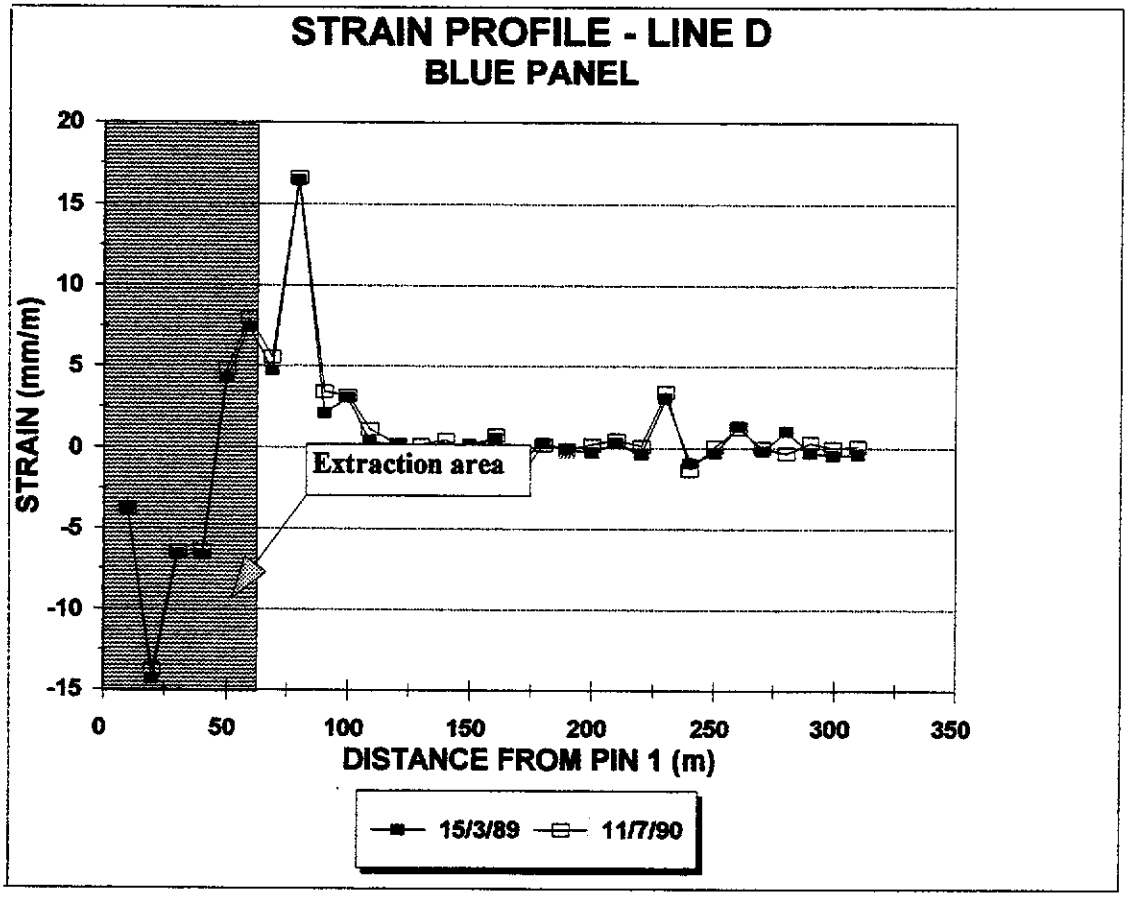
STRAIN PROFILE - LINE D
BLUE PANEL
STRAIN (mm/m)
20
15
10
5
0
-5
-10
-15
Extraction area
0
50
100
150
200
250
300
350
DISTANCE FROM PIN 1 (m)
15/3/89
11/7/90

Figure I.39

TABLE I.19
LINE D STRAIN MONITORING
BLUE PANEL

Date >	06-Apr-88	16-Mar-89	11-Jul-90
Days >	0	344	826
PEG #	DISTANCE BETWEEN SURVEY PEGS (m)		
1-2	9.904	9.867	9.867
2-3	10.026	9.882	9.888
3-4	10.129	10.062	10.064
4-5	9.884	9.818	9.821
5-6	10.088	10.131	10.137
6-7	9.015	9.082	9.087
7-8	9.463	9.508	9.516
8-9	11.006	11.187	11.189
9-10	10.549	10.571	10.585
11	9.798	9.828	9.829
12	8.923	8.926	8.933
13	11.544	11.546	11.546
14	9.485	9.484	9.487
15	10.289	10.289	10.294
16	9.720	9.722	9.718
17	10.707	10.713	10.715
18	9.741	9.733	9.724
19	9.669	9.672	9.671
20	9.793	9.792	9.792
21	10.206	10.203	10.208
22	10.074	10.077	10.079
23	10.046	10.042	10.047
24	9.940	9.970	9.974
25	9.906	9.897	9.893
26	10.430	10.427	10.431
27	9.890	9.903	9.902
28	10.021	10.019	10.021
29	9.803	9.813	9.800
30	10.122	10.119	10.125
31	9.089	9.085	9.089
32	10.141	10.137	10.142
33	9.964	9.958	9.964

TABLE I.20

LIFTING PROGRESS

2 SOUTH A PANEL WD6

(10 ALPINE)

DATE	SPLIT #		GOAF WIDTH (m)
23/01/89	1	START	
10/02/89	1	FINISH	18
24/02/89	2	START	
02/03/89	2	FINISH	31
05/04/89	3	START	
13/04/89	3	FINISH	43
27/04/89	4	START	
03/05/89	4	FINISH	54
18/05/89	5	START	
26/05/89	5	FINISH	65
14/06/89	6	START	
20/06/89	6	FINISH	78
30/06/89	7	START	
07/07/89	7	FINISH	90
20/07/89	8	START	
26/07/89	8	FINISH	102
15/08/89	9	START	
22/08/89	9	FINISH	114
04/09/89	10	START	
04/09/89	10	FINISH	125
11/09/89	11	START	
14/09/89	11	FINISH	136

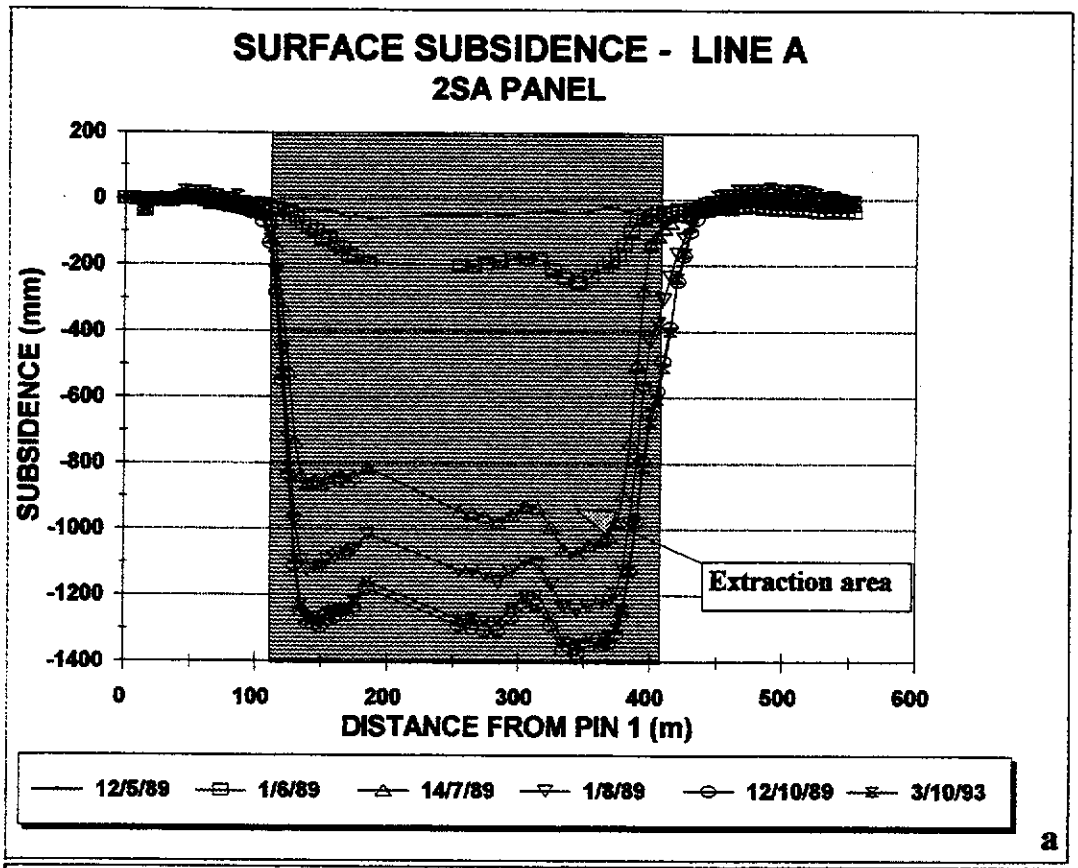
SURFACE SUBSIDENCE - LINE A
2SA PANEL
SUBSIDENCE (mm)
200
0
-200
-400
-600
-800
-1000
-1200
-1400
0
100
200
300
400
500
600
DISTANCE FROM PIN 1 (m)
Extraction area
12/5/89
1/6/89
14/7/89
1/8/89
12/10/89
3/10/93
a

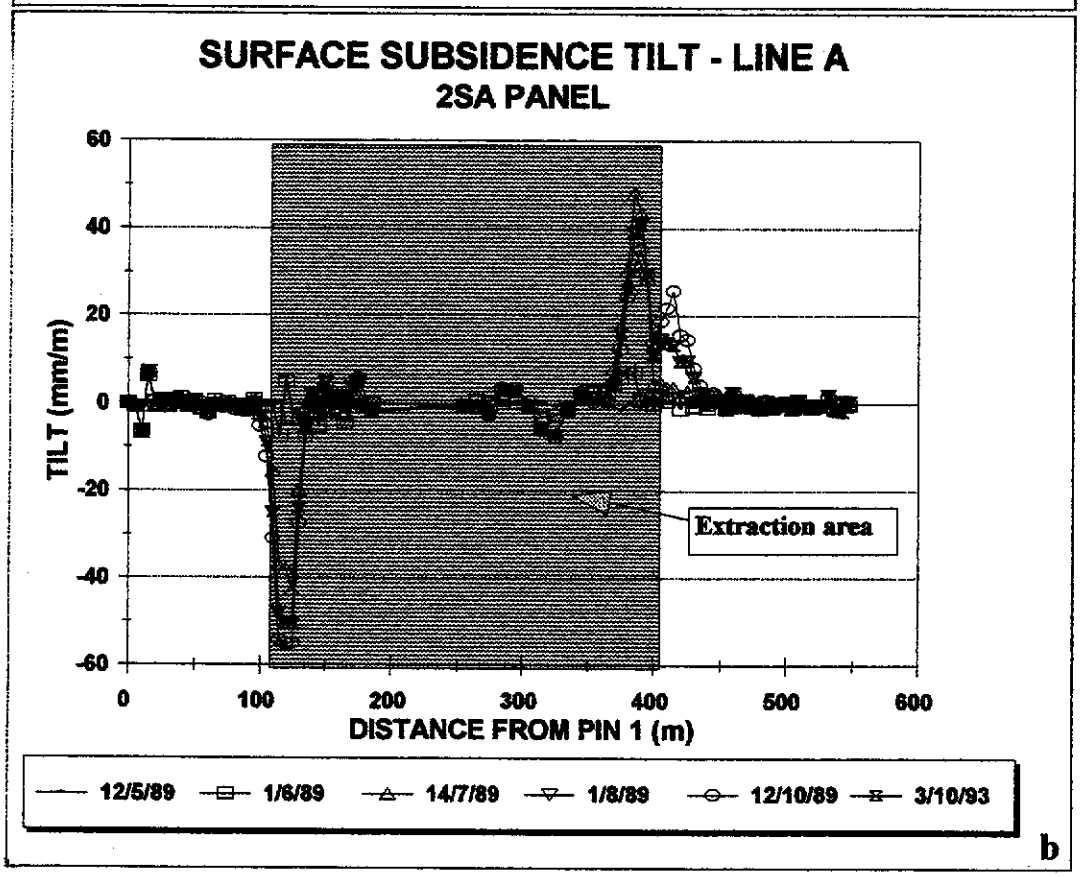
SURFACE SUBSIDENCE TILT - LINE A
2SA PANEL
TILT (mm/m)
60
40
20
0
-20
-40
-60
0
100
200
300
400
500
600
DISTANCE FROM PIN 1 (m)
Extraction area
12/5/89
1/6/89
14/7/89
1/8/89
12/10/89
3/10/93
b

Figure I.40

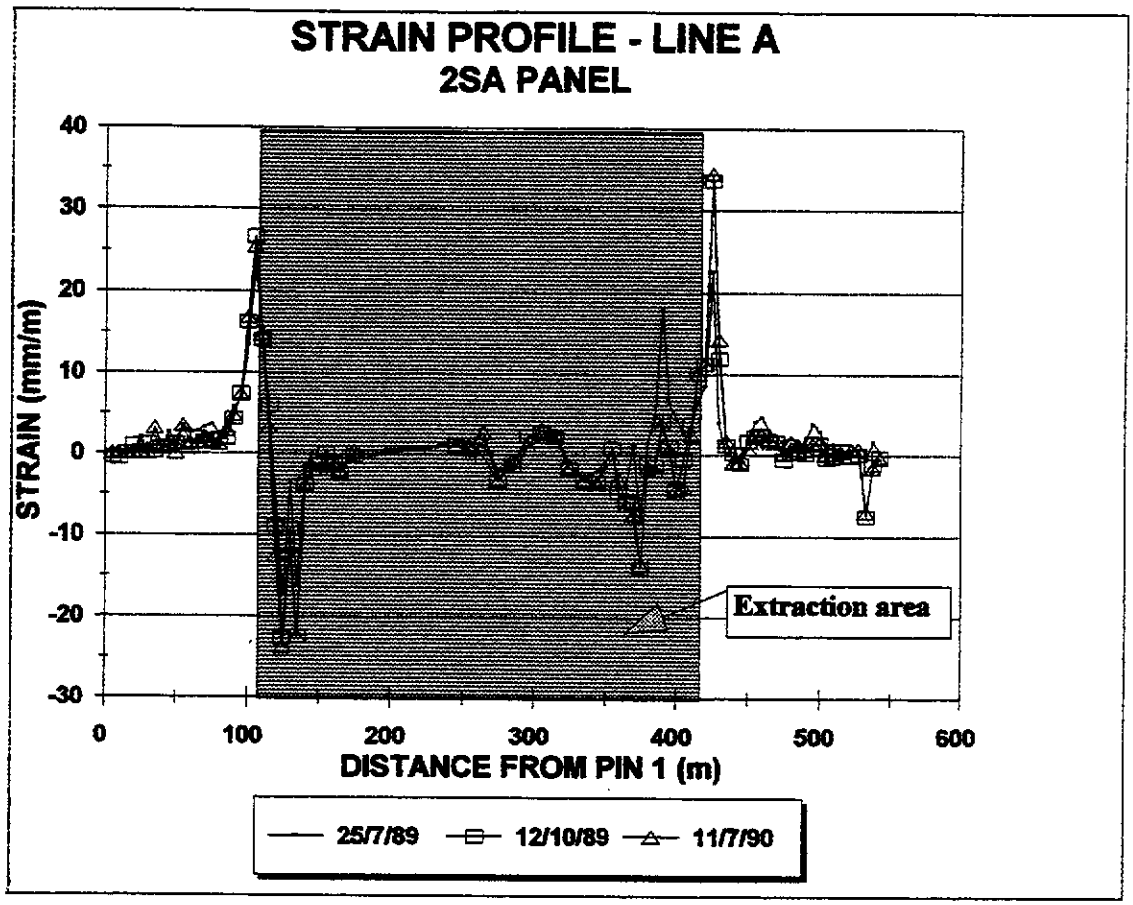
STRAIN PROFILE - LINE A
2SA PANEL
STRAIN (mm/m)
40
30
20
10
0
-10
-20
-30
0
100
200
300
400
500
600
DISTANCE FROM PIN 1 (m)
Extraction area
25/7/89
12/10/89
11/7/90

Figure I.41

TABLE I.21
LINE A STRAIN MEASUREMENTS
2 SOUTH A PANEL.

Date >	19-Feb-89	25-Jul-89	12-Oct-89	11-Jul-90
Days >	0	156	235	507
PEG #	DISTANCE BETWEEN SURVEY PEGS (m)			
1-2				
2-3				
3-4	5.016	5.016	5.014	5.016
4-5	4.905	4.905	4.902	4.905
5-6	5.212	5.212	5.212	5.212
6-7	4.978	4.978	4.983	4.978
7-8	4.923	4.933	4.924	4.923
8-9	5.025	5.025	5.031	5.025
9-10	5.100	5.100	5.101	5.116
11	4.926	4.926	4.929	4.930
12	5.077	5.090	5.081	5.082
13	5.023	5.030	5.029	5.023
14	4.953	4.970	4.957	4.970
15	4.957	4.970	4.960	4.963
16	5.096	5.110	5.106	5.103
17	4.874	4.890	4.881	4.884
18	5.062	5.080	5.070	5.069
19	5.158	5.170	5.167	5.164
20	4.905	4.920	4.914	4.919
21	4.892	4.920	4.913	4.915
22	5.066	5.100	5.104	5.103
23	5.042	5.110	5.124	5.127
24	4.867	4.980	4.997	4.991
25	4.904	4.980	4.973	4.976
26	5.183	5.210	5.214	5.200
27	5.012	4.980	4.967	4.949
28	4.966	4.880	4.853	4.848
29	4.878	4.860	4.833	4.822
30	5.103	5.020	4.988	4.988
31	5.170	5.159	5.150	5.149
32	4.753	4.753	4.743	4.746
33	5.192	5.189	5.185	5.182
34	4.903	4.903	4.903	4.895
35	5.065	5.064	5.059	5.058
36	4.881	4.874	4.869	4.870
37	9.932	9.925	9.930	9.935
38	69.835	69.940	69.905	69.910
39	10.020	10.036	10.025	10.029
40	9.774	9.784	9.770	9.799
41	10.210	10.190	10.176	10.177
42	10.110	10.089	10.094	10.102
43	10.130	10.139	10.152	10.141

TABLE I.21
LINE A STRAIN MEASUREMENTS
2 SOUTH A PANEL.

Date >	19-Feb-89	25-Jul-89	12-Oct-89	11-Jul-90
Days >	0	156	235	507
PEG #	DISTANCE BETWEEN SURVEY PEGS (m)			
43-44	9.734	9.752	9.759	9.763
45	10.113	10.138	10.134	10.138
46	9.748	9.737	9.731	9.732
47	10.404	10.374	10.369	10.371
48	9.243	9.223	9.212	9.210
49	10.500	10.505	10.509	10.495
50	4.825	4.807	4.802	4.810
51	5.230	5.210	5.200	5.197
52	4.845	4.850	4.816	4.809
53	5.173	5.130	5.101	5.103
54	4.972	4.980	4.967	4.964
55	5.116	5.140	5.109	5.106
56	4.941	5.030	4.962	4.960
57	5.078	5.110	5.083	5.081
58	4.858	4.880	4.837	4.837
59	4.787	4.800	4.784	4.768
60	5.321	5.340	5.341	5.334
61	4.967	5.000	5.017	5.017
62	4.977	5.020	5.033	5.033
63	4.899	5.010	5.064	5.068
64	5.040	5.060	5.100	5.112
65	5.100	5.100	5.106	5.109
66	5.133	5.140	5.134	5.128
67	4.628	4.620	4.623	4.624
68	5.169	5.180	5.178	5.173
69	4.900	4.920	4.911	4.912
70	4.907	4.930	4.919	4.920
71	5.165	5.180	5.174	5.175
72	4.848	4.860	4.856	4.857
73	5.343	5.340	5.340	5.344
74	4.899	4.900	4.905	4.907
75	4.843	4.850	4.845	4.849
76	5.102	5.110	5.103	5.105
77	5.160	5.180	5.168	5.167
78	4.636	4.650	4.643	4.643
79	5.124	5.130	5.122	5.124
80	4.933	4.940	4.934	4.932
81	5.054	5.050	5.057	5.056
82	7.528	7.530	7.527	7.533
83	4.960	4.960	4.960	4.964
84	5.252	5.250	5.212	5.215
85	4.922	4.930	4.916	4.914
86	4.988	4.990	4.987	4.986

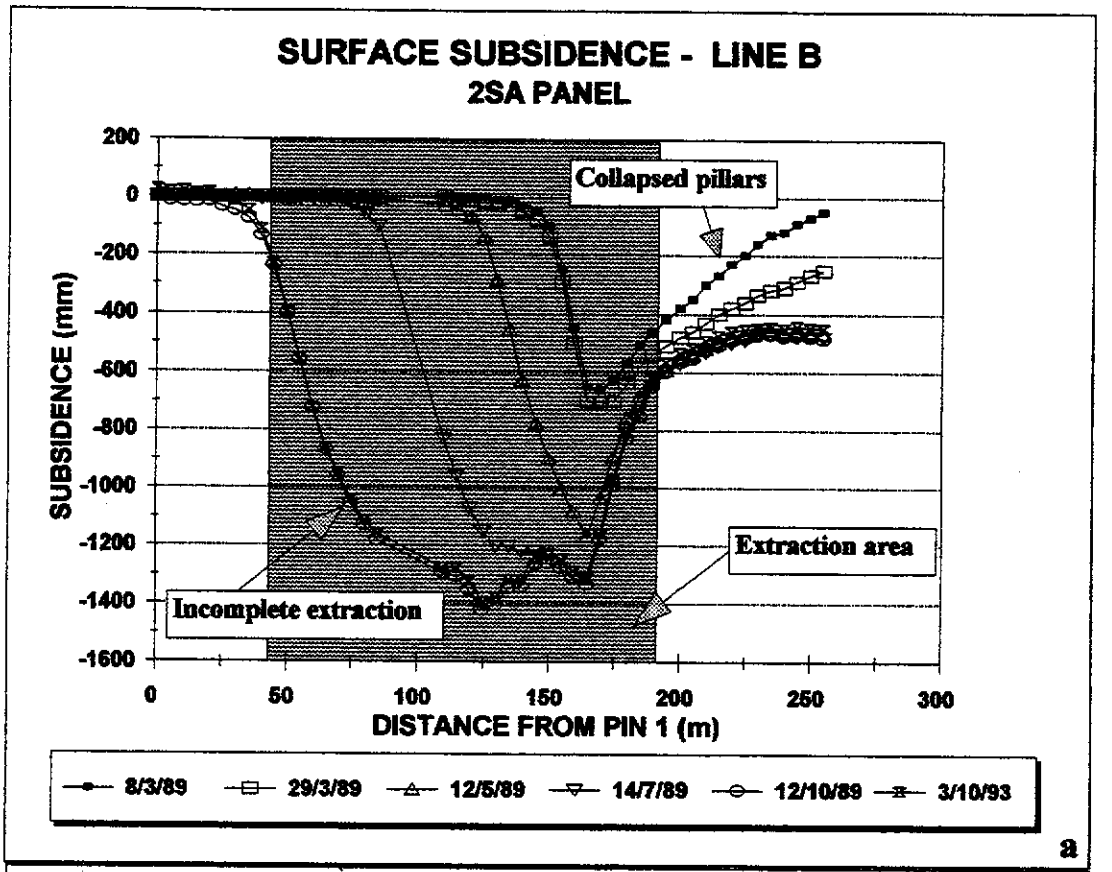
SURFACE SUBSIDENCE - LINE B
2SA PANEL
SUBSIDENCE (mm)
200
0
-200
-400
-600
-800
-1000
-1200
-1400
-1600
Collapsed pillars
Extraction area
Incomplete extraction
0
50
100
150
200
250
300
DISTANCE FROM PIN 1 (m)
8/3/89
29/3/89
12/5/89
14/7/89
12/10/89
3/10/93
a

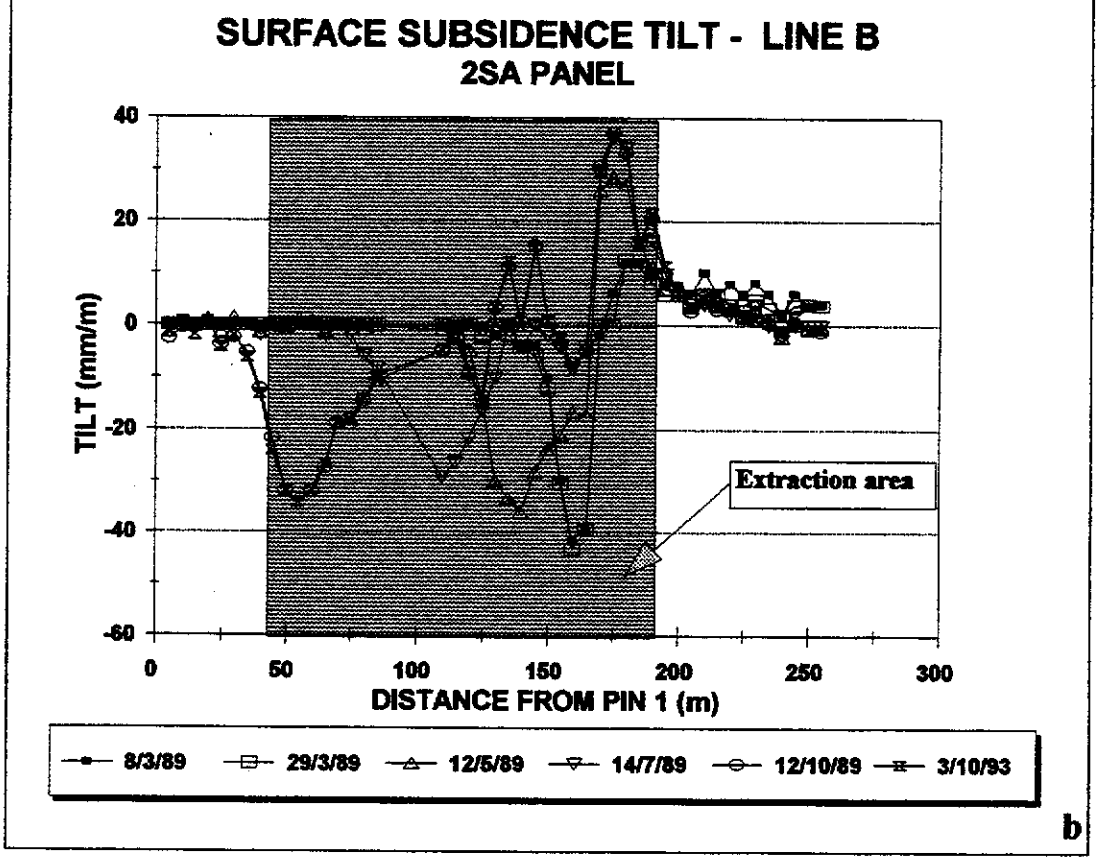
SURFACE SUBSIDENCE TILT - LINE B
2SA PANEL
TILT (mm/m)
40
20
0
-20
-40
-60
Extraction area
0
50
100
150
200
250
300
DISTANCE FROM PIN 1 (m)
8/3/89
29/3/89
12/5/89
14/7/89
12/10/89
3/10/93
b

Figure I.42

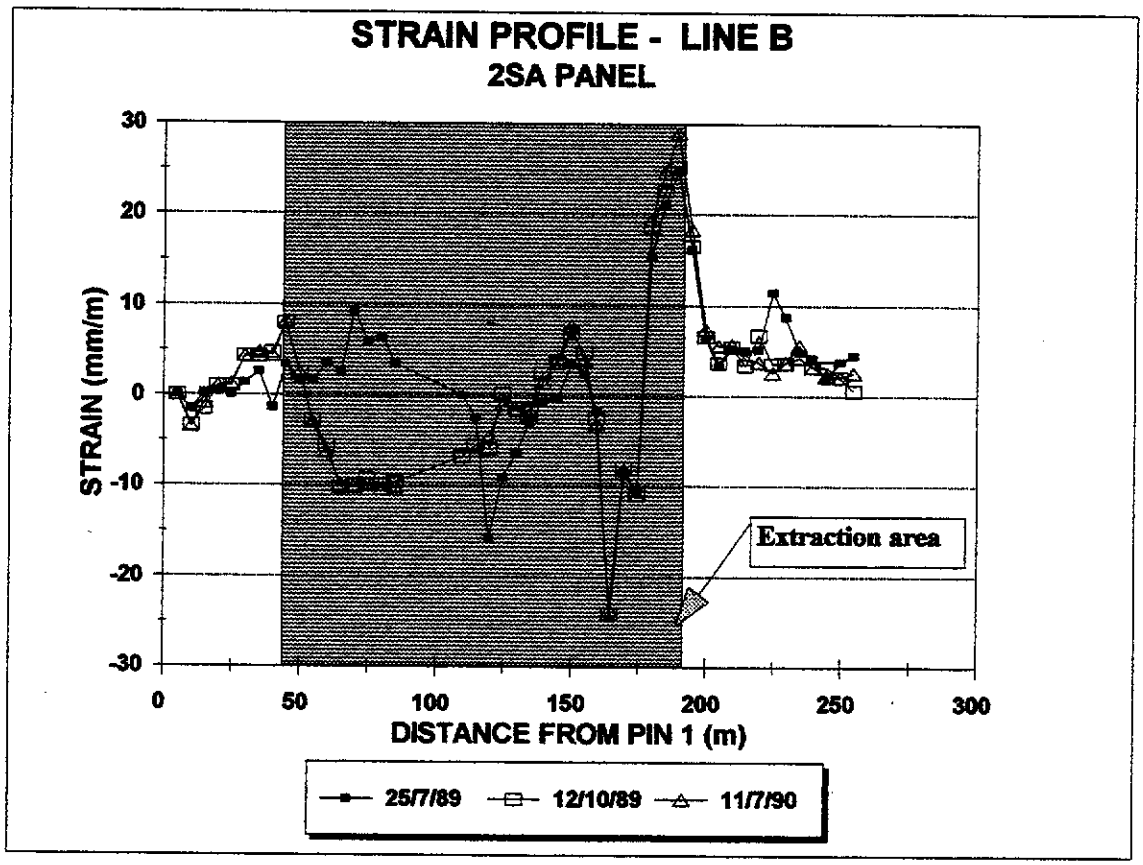
STRAIN PROFILE - LINE B
2SA PANEL
STRAIN (mm/m)
30
20
10
0
-10
-20
-30
0
50
100
150
200
250
300
DISTANCE FROM PIN 1 (m)
Extraction area
25/7/89
12/10/89
11/7/90

Figure I.43

TABLE I.22
LINE B STRAIN MONITORING
2 SOUTH A PANEL

Date >	19-Feb-89	25-Jul-89	12-Oct-89	11-Jul-90
Days >	0	156	235	507
PEG #	DISTANCE BETWEEN SURVEY PEGS (m)			
1-2	5.000	5.000	5.000	5.000
2-3	5.178	5.170	5.161	5.160
3-4	4.599	4.600	4.592	4.595
4-5	4.968	4.970	4.973	4.973
5-6	5.030	5.030	5.035	5.036
6-7	5.083	5.090	5.105	5.105
7-8	5.027	5.040	5.049	5.051
8-9	5.007	5.000	5.031	5.029
9-10	4.754	4.770	4.792	4.793
11	5.192	5.200	5.205	5.205
12	4.752	4.760	4.739	4.738
13	5.201	5.220	5.172	5.168
14	5.167	5.180	5.114	5.116
15	4.785	4.830	4.737	4.736
16	5.090	5.120	5.043	5.040
17	5.187	5.220	5.135	5.133
18	4.883	4.900	4.836	4.833
19	24.980	24.980	24.810	
20	4.912	4.900	4.885	
21	5.050	4.970	5.020	5.027
22	4.955	4.910	4.956	4.950
23	4.962	4.930	4.955	4.954
24	5.035	5.020	5.027	5.024
25	4.823	4.820	4.835	4.830
26	5.202	5.200	5.221	5.223
27	5.042	5.060	5.077	5.081
28	4.988	5.000	5.012	5.008
29	4.808	4.800	4.796	4.793
30	5.075	4.950	4.953	4.955
31	5.114	5.070	5.073	5.072
32	4.974	4.920	4.920	4.919
33	4.944	5.020	5.036	5.040
34	4.946	5.050	5.058	5.068
35	4.898	5.020	5.022	5.040
36	5.078	5.160	5.162	5.171
37	5.167	5.200	5.201	5.205
38	4.844	4.860	4.862	4.871
39	4.914	4.940	4.941	4.942
40	5.005	5.030	5.022	5.026
41	5.044	5.070	5.078	5.063
42	5.042	5.100	5.060	5.055
43	4.917	4.960	4.935	4.935
44	4.936	4.960	4.957	4.964
45	4.989	5.010	5.005	5.005
46	4.901	4.910	4.917	4.912
47	5.250	5.270	5.261	5.261
48	5.037	5.060	5.040	5.050

TABLE I.23

LIFTING PROGRESS

RED PANEL WD6

(10 ALPINE)

DATE	SPLIT #		GOAF WIDTH (m)
04/12/89	1	START	
13/12/89	1	FINISH	18
30/01/90	2	START	
09/02/90	2	FINISH	39
--	3	START	
--	3	FINISH	
28/02/90	4	START	19
20/03/90	4	FINISH	
04/04/90	5	START	
04/05/90	5	FINISH	38
23/05/90	6	START	
15/06/90	6	FINISH	58
08/07/90	7	START	
01/08/90	7	FINISH	79
7/11/90	8	START	
7/12/90	8	FINISH	13

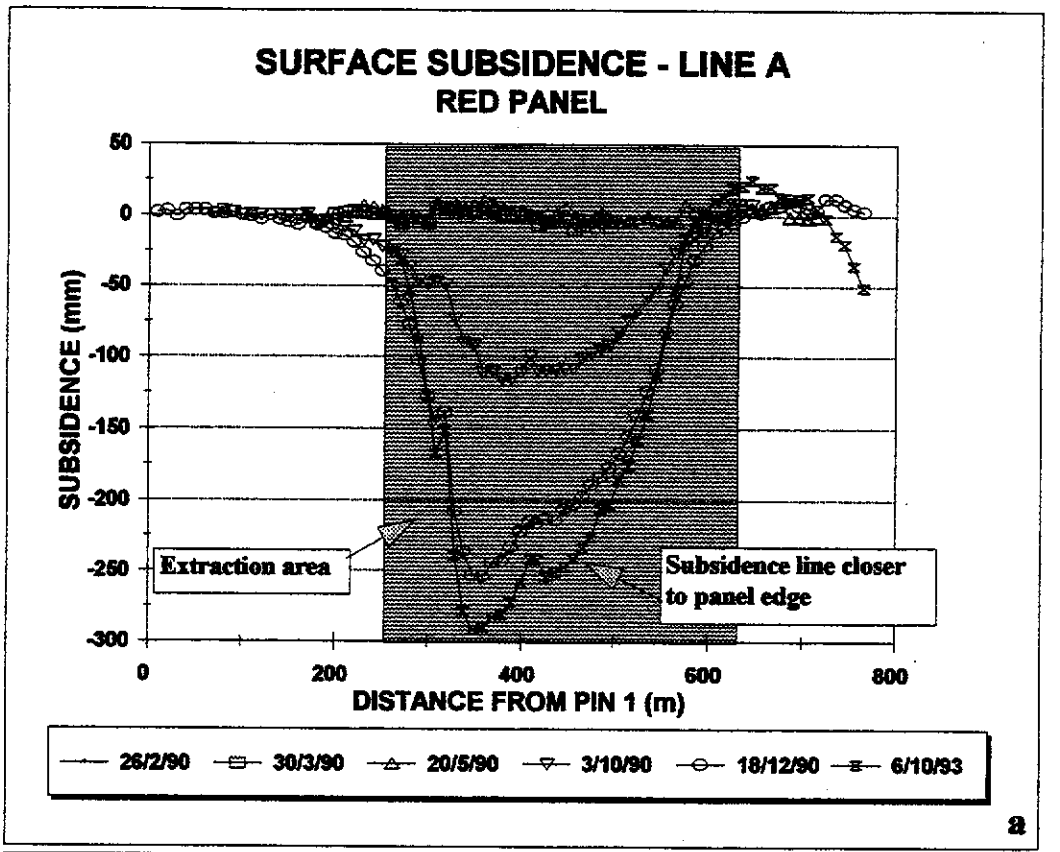
SURFACE SUBSIDENCE - LINE A
RED PANEL
SUBSIDENCE (mm)
50
0
-50
-100
-150
-200
-250
-300
0
200
400
600
800
DISTANCE FROM PIN 1 (m)
Extraction area
Subsidence line closer to panel edge
26/2/90
30/3/90
20/5/90
3/10/90
18/12/90
6/10/93
a

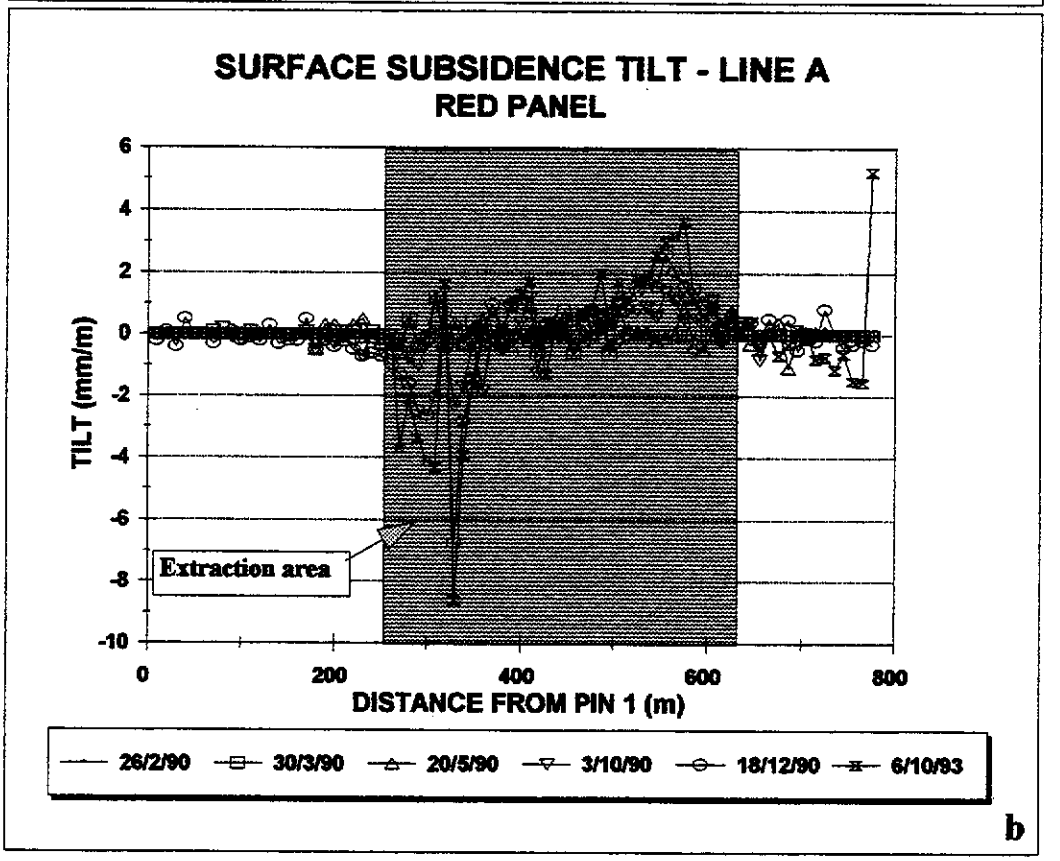
SURFACE SUBSIDENCE TILT - LINE A
RED PANEL
TILT (mm/m)
6
4
2
0
-2
-4
-6
-8
-10
0
200
400
600
800
DISTANCE FROM PIN 1 (m)
Extraction area
26/2/90
30/3/90
20/5/90
3/10/90
18/12/90
6/10/93
b

Figure I.44

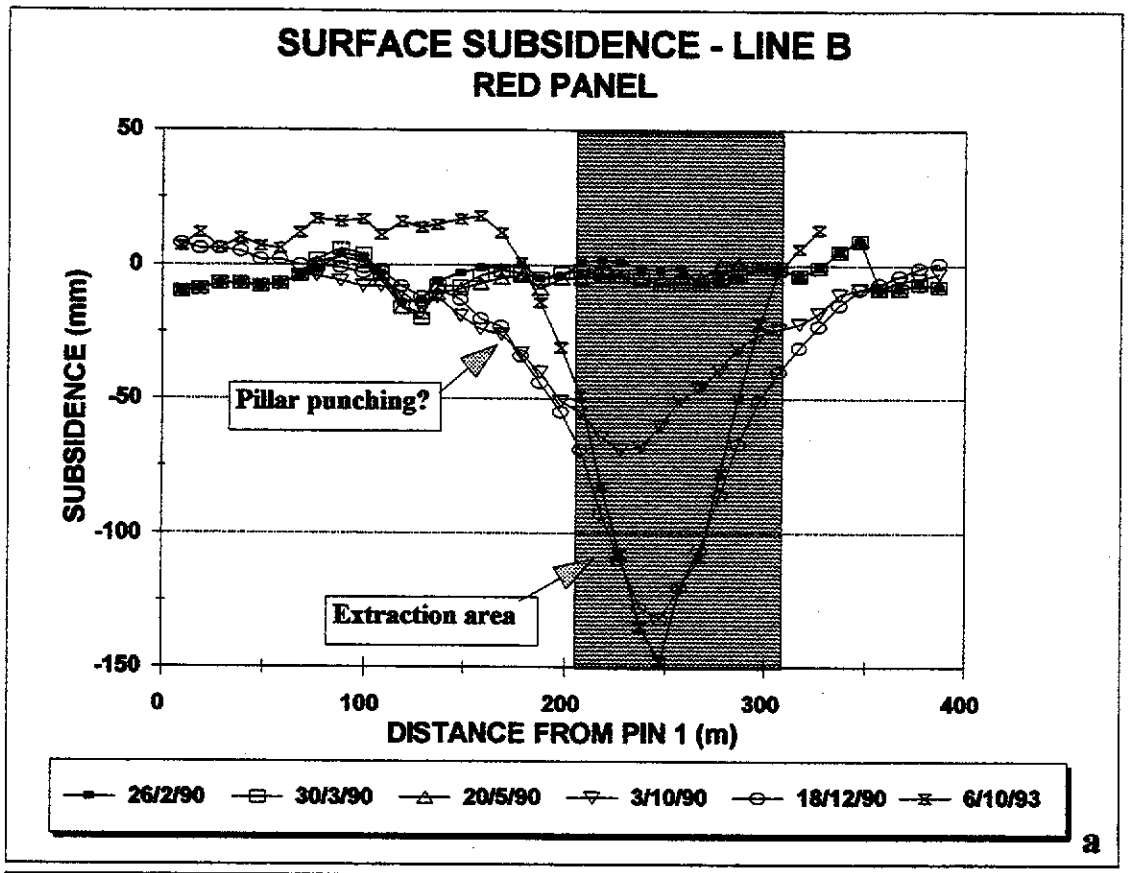
SURFACE SUBSIDENCE - LINE B
RED PANEL
SUBSIDENCE (mm)
50
0
-50
-100
-150
Pillar punching?
Extraction area
0
100
200
300
400
DISTANCE FROM PIN 1 (m)
26/2/90
30/3/90
20/5/90
3/10/90
18/12/90
6/10/93
a

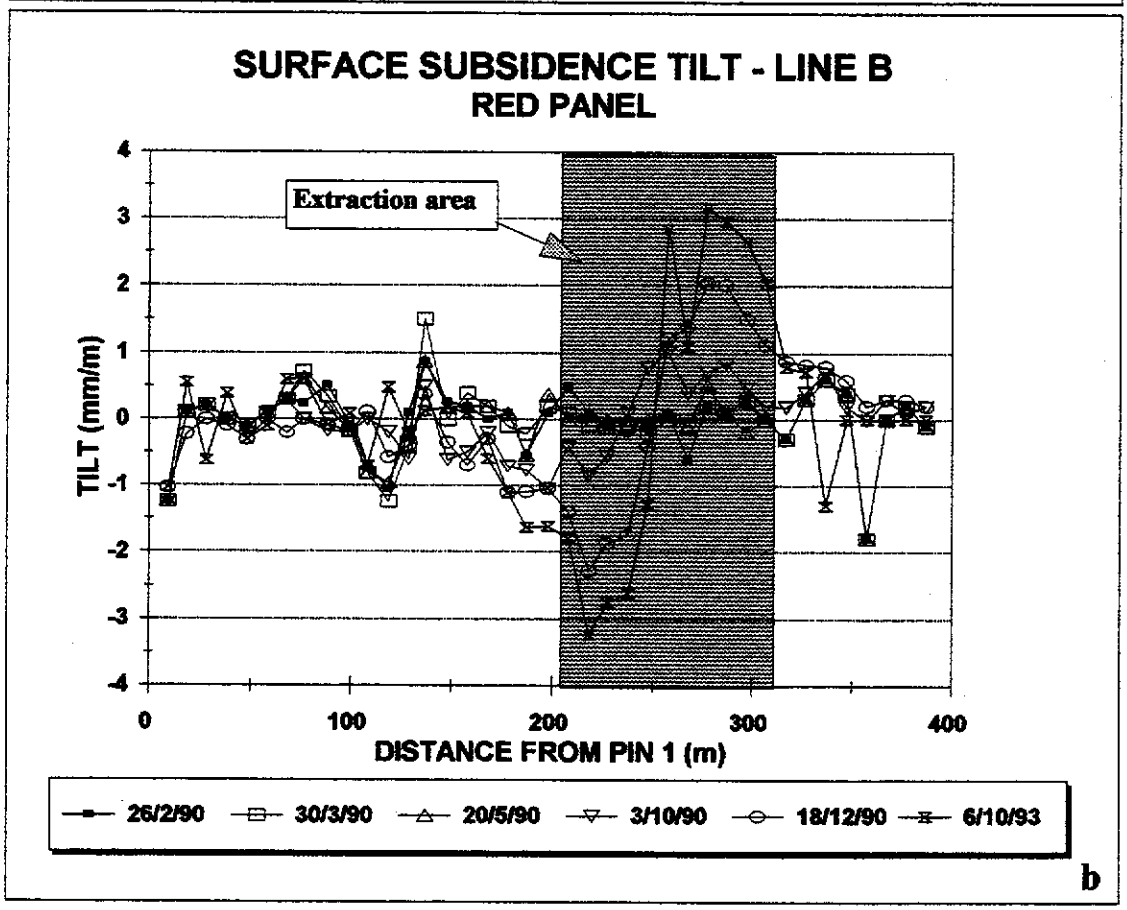
SURFACE SUBSIDENCE TILT - LINE B
RED PANEL
TILT (mm/m)
4
3
2
1
0
-1
-2
-3
-4
Extraction area
0
100
200
300
400
DISTANCE FROM PIN 1 (m)
26/2/90
30/3/90
20/5/90
3/10/90
18/12/90
6/10/93
b

Figure I.45

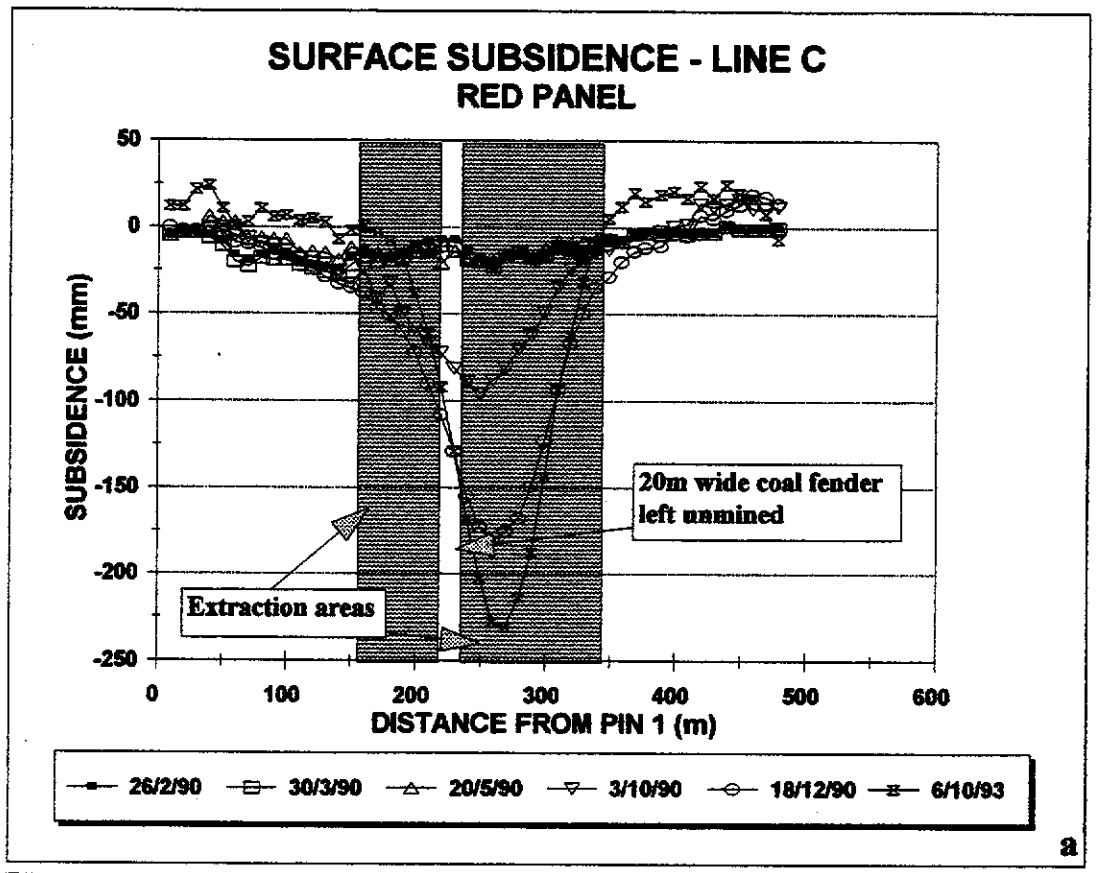
SURFACE SUBSIDENCE - LINE C
RED PANEL
SUBSIDENCE (mm)
50
0
-50
-100
-150
-200
-250
0
100
200
300
400
500
600
DISTANCE FROM PIN 1 (m)
20m wide coal fender left unmined
Extraction areas
26/2/90
30/3/90
20/5/90
3/10/90
18/12/90
6/10/93
a

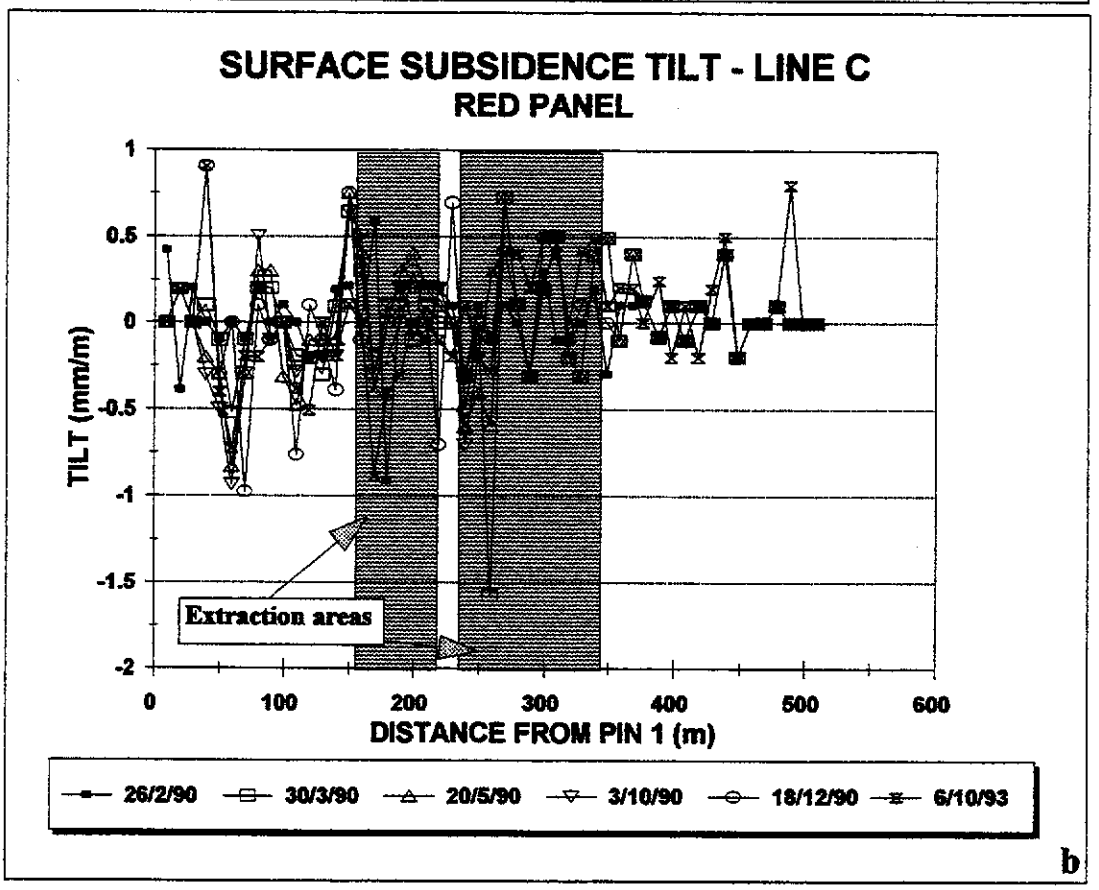
SURFACE SUBSIDENCE TILT - LINE C
RED PANEL
TILT (mm/m)
1
0.5
0
-0.5
-1
-1.5
-2
0
100
200
300
400
500
600
DISTANCE FROM PIN 1 (m)
Extraction areas
26/2/90
30/3/90
20/5/90
3/10/90
18/12/90
6/10/93
b

Figure I.46

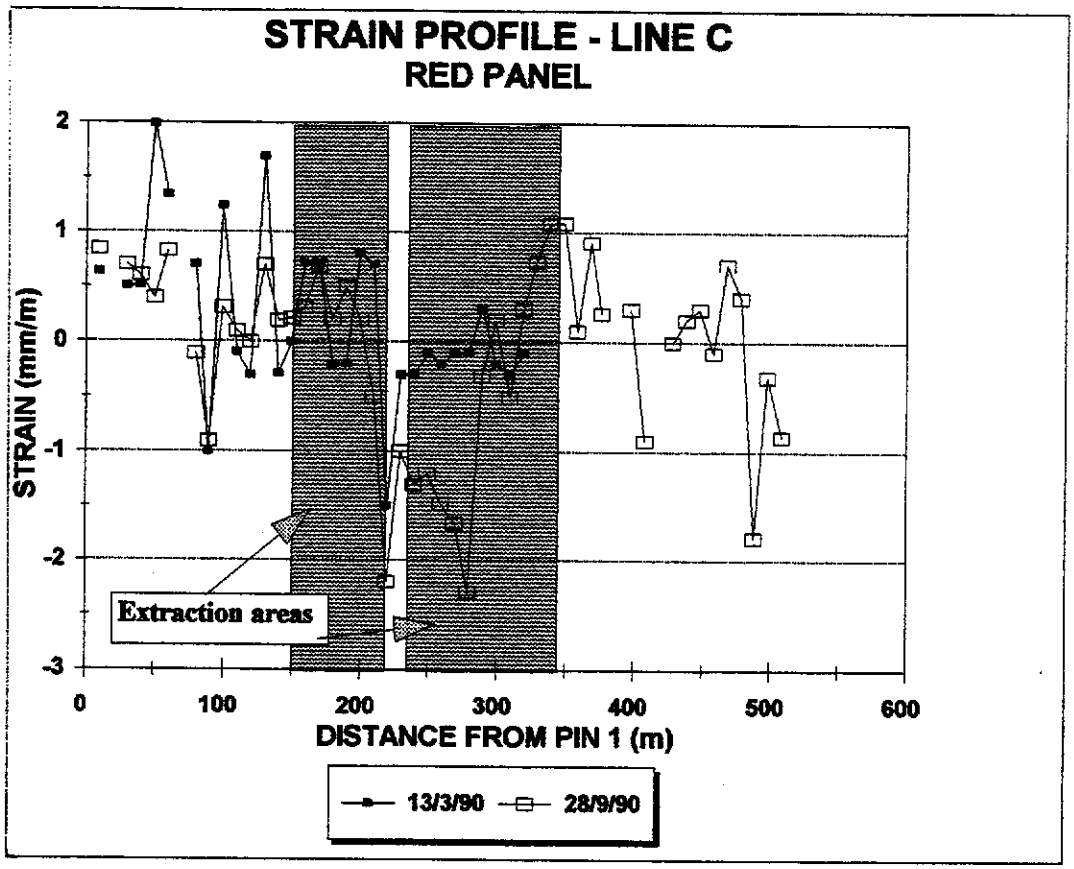
STRAIN PROFILE - LINE C
RED PANEL
STRAIN (mm/m)
2
1
0
-1
-2
-3
0
100
200
300
400
500
600
DISTANCE FROM PIN 1 (m)
Extraction areas
13/3/90
28/9/90

Figure I.47

TABLE I.24

LINE C STRAIN MONITORING RED PANEL

Date >	13-Dec-89	13-Mar-90	28-Sep-90
Days >	0	90	289
PEG #	DISTANCE BETWEEN SURVEY PEGS (m)		
1-2	9.492	9.498	9.500
2-3	10.333		
3-4	9.993	9.998	10.000
4-5	9.932	9.937	9.938
5-6	10.050	10.070	10.054
6-7	9.656	9.669	9.664
7-8	10.258		
8-9	9.964	9.971	9.963
9-10	9.938	9.928	9.929
11	9.673	9.685	9.676
12	10.521	10.520	10.522
13	9.866	9.863	9.866
14	10.030	10.047	10.037
15	10.355	10.352	10.357
16	9.322	9.322	9.324
17	9.819	9.826	9.822
18	10.160	10.167	10.167
19	9.885	9.883	9.887
20	9.977	9.975	9.982
21	9.934	9.942	9.936
22	10.000	10.007	9.995
23	9.989	9.974	9.967
24	10.048	10.045	10.038
25	9.960	9.957	9.947
26	9.946	9.945	9.934
27	10.145	10.143	10.130
28	9.639	9.638	9.623
29	10.029	10.028	10.006
30	9.777	9.780	9.774
31	10.045	10.043	10.047
32	9.978	9.975	9.973
33	9.980	9.979	9.983
34	9.574		9.581
35	10.186		10.197
36	10.142		10.153
37	9.775		9.776
38	9.932		9.941
39	7.638		7.640
40	12.298		
41	10.013		10.016
42	10.010		10.001
43	9.994		
44	10.045		10.045
45	9.945		9.947
46	10.058		10.061
47	10.067		10.066
48	9.953		9.960
49	9.973		9.977
50	10.048		10.030
51	9.572		9.569
52	10.453		10.444

TABLE I.25

LIFTING PROGRESS 1NORTH PANEL WD6

DATE	SPILT #	PANEL WIDTH AT EXTENSO/ GRID LINE (m)	CONTINUOUS MINER #
03-Aug-90	1 START		13 JEFFREY
24-Aug-90	1 FINISH	9 / 15	
11-Sep-90	2 START		"
26-Sep-90	2 FINISH	29 / 35	
18-Oct-90	3 START		"
02-Nov-90	3 FINISH	47 / 53	
13-Nov-90	4 START		"
26-Nov-90	4 FINISH	64 / 70	
10-Dec-90	5 START		"
27-Dec-90	5 FINISH	82 / 88	
23-Jan-91	6 START		"
06-Feb-91	6 FINISH	99 / 105	
19-Feb-91	7 START		13 JEFFREY
07-Mar-91	7 FINISH	116 / 122	
20-Mar-91	8 START		"
17-Apr-91	8 FINISH	134 / 140	
03-May-91	9 START		"
17-May-91	9 FINISH	152 / 158	
31-May-91	10 START		"
14-Jun-91	10 FINISH	171 / 177	
02-Jul-91	11 START		"
14-Jul-91	11 FINISH	188 / 194	
08-Aug-91	12 START		13 JEFFREY
08-Aug-91	12 FINISH	206 / 212	
18-Aug-91	13 START		"
29-Aug-91	13 FINISH	224 / 230	
10-Sep-91	14 START		"
17-Sep-91	14 FINISH	241 / 247	
30-Sep-91	15 START		"
10-Oct-91	15 FINISH	258 / 264	
21-Oct-91	16 START		13 JEFFREY
30-Oct-91	16 FINISH	276 / 282	
16-Nov-91	17 START		"
21-Nov-91	17 FINISH	294 / 300	
08-Jan-92	18 START		14 JEFFREY
23-Jan-92	18 FINISH	312 / 318	
12-Feb-92	19 START		"
21-Feb-92	19 FINISH	330 / 336	
02-Mar-92	20 START		"
11-Mar-92	20 FINISH	348 / 354	
20-Mar-92	21 START		"
27-Mar-92	21 FINISH	366 / 372	
07-Apr-92	22 START		"
15-Apr-92	22 FINISH	384 / 390	
01-May-92	23 START		14 JEFFREY
08-May-92	23 FINISH	401 / 407	
22-May-92	24 START		"
01-Jun-92	24 FINISH	418 / 424	
11-Jun-92	25 START		"
18-Jun-92	25 FINISH	436 / 442	
28-Jun-92	26 START		"
06-Jul-92	26 FINISH	451 / 457	
15-Jul-92	27 START		"
23-Jul-92	27 FINISH	467 / 473	
01-Sep-92	28 START		10 ALPINE
26-Sep-92	28 FINISH	484 / 490	
18-Oct-92	29 START		10 ALPINE
29-Oct-92	29 FINISH	501 / 507	

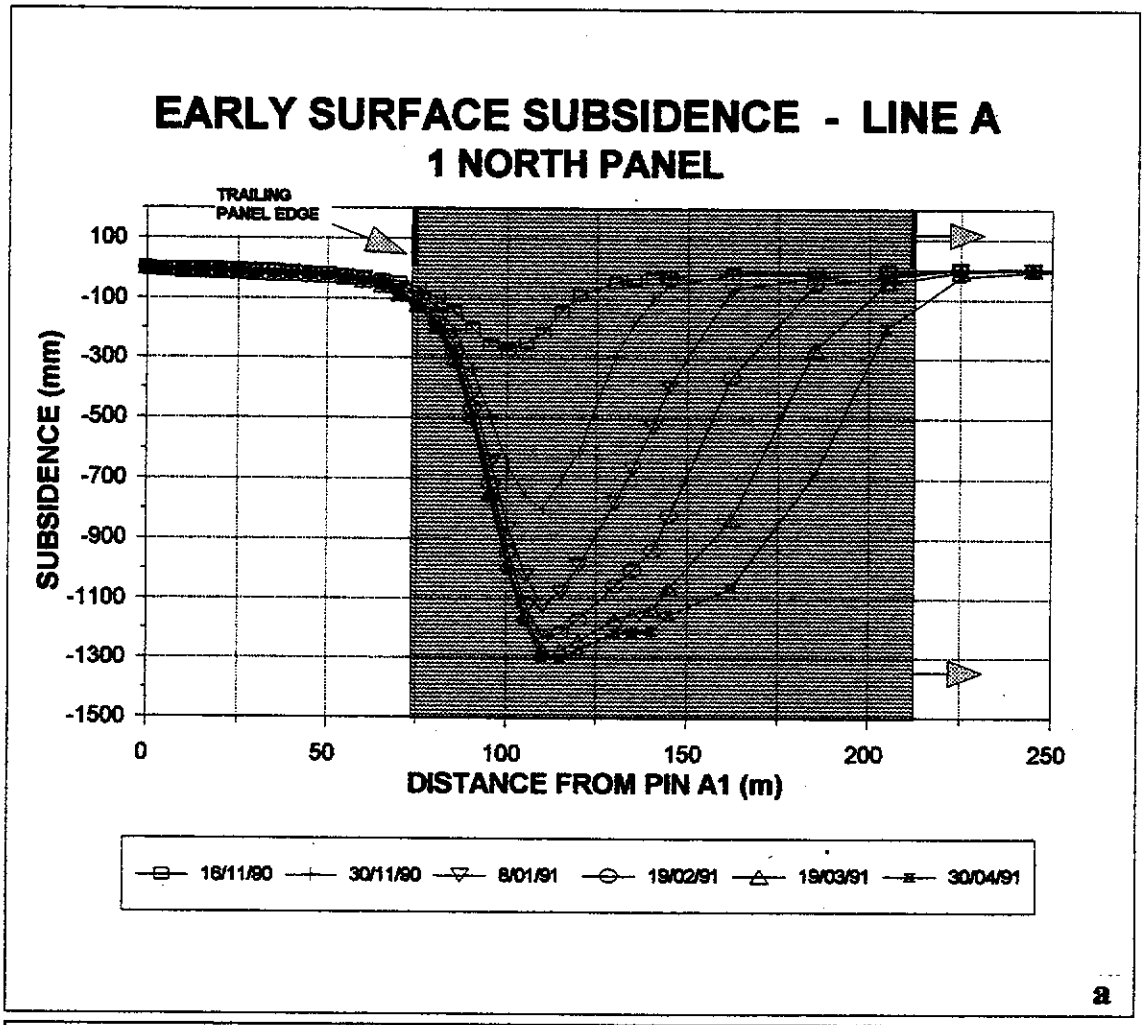
EARLY SURFACE SUBSIDENCE - LINE A
1 NORTH PANEL
TRAILING PANEL EDGE
SUBSIDENCE (mm)
100
-100
-300
-500
-700
-900
-1100
-1300
-1500
0
50
100
150
200
250
DISTANCE FROM PIN A1 (m)
16/11/90
30/11/90
8/01/91
19/02/91
19/03/91
30/04/91
a

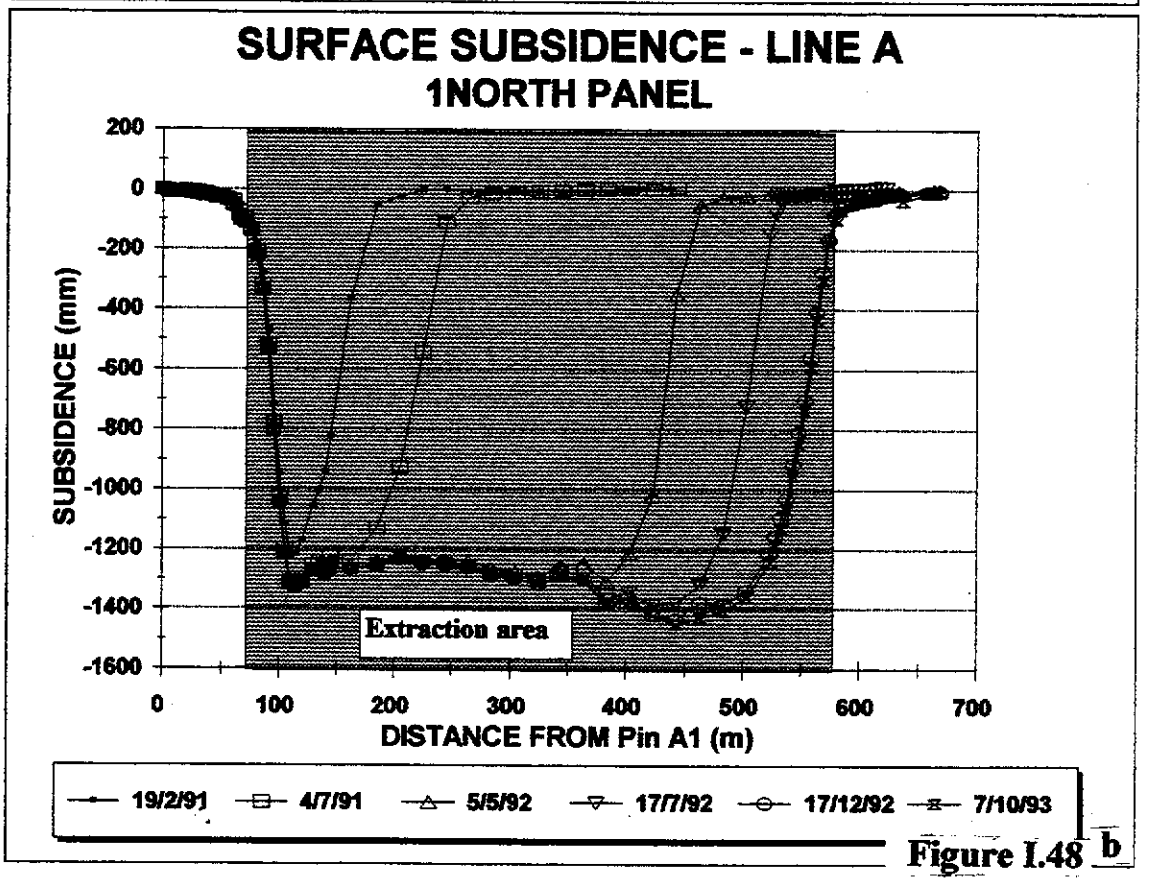
SURFACE SUBSIDENCE - LINE A
1NORTH PANEL
SUBSIDENCE (mm)
200
0
-200
-400
-600
-800
-1000
-1200
-1400
-1600
Extraction area
0
100
200
300
400
500
600
700
DISTANCE FROM Pin A1 (m)
19/2/91
4/7/91
5/5/92
17/7/92
17/12/92
7/10/93
b

Figure I.48

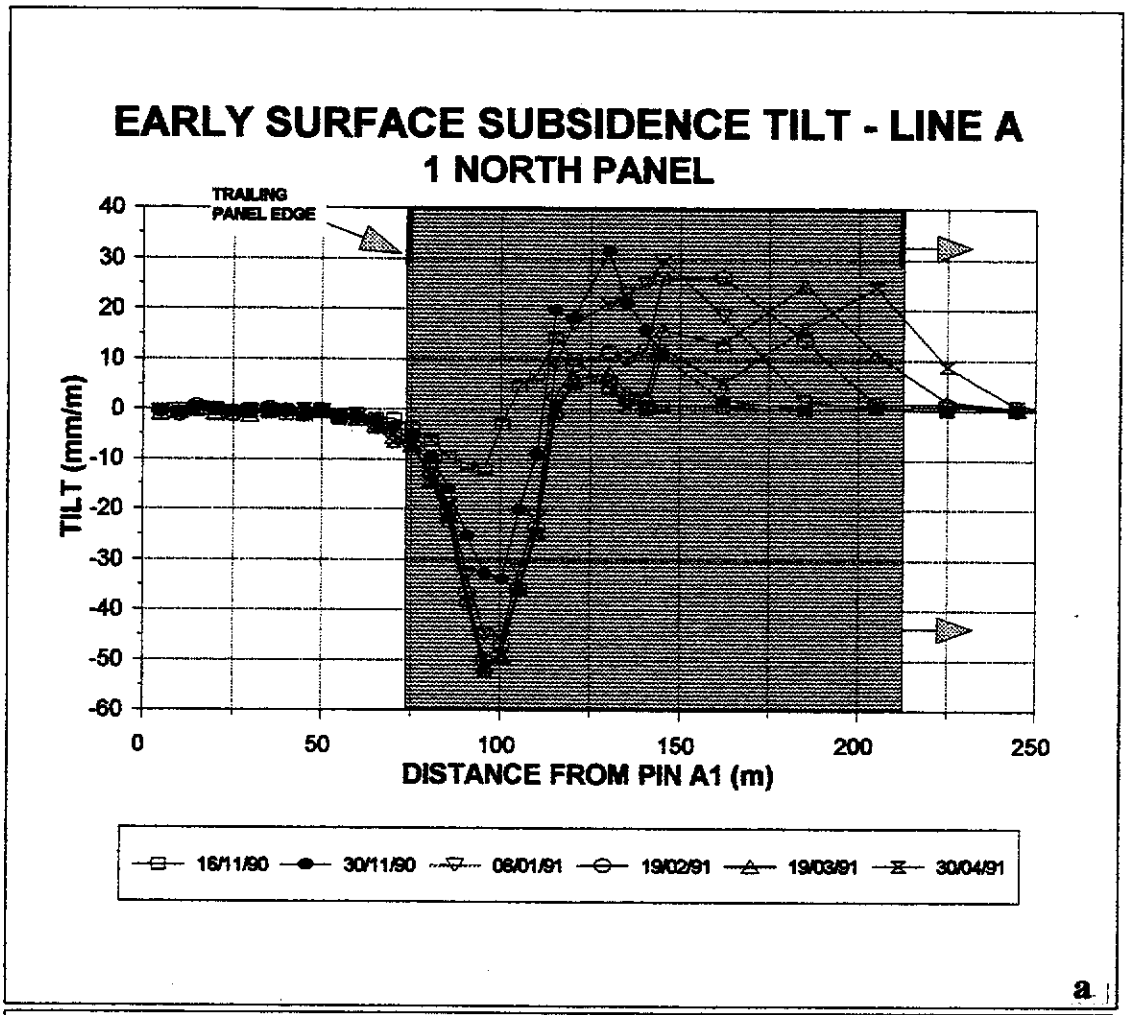

a

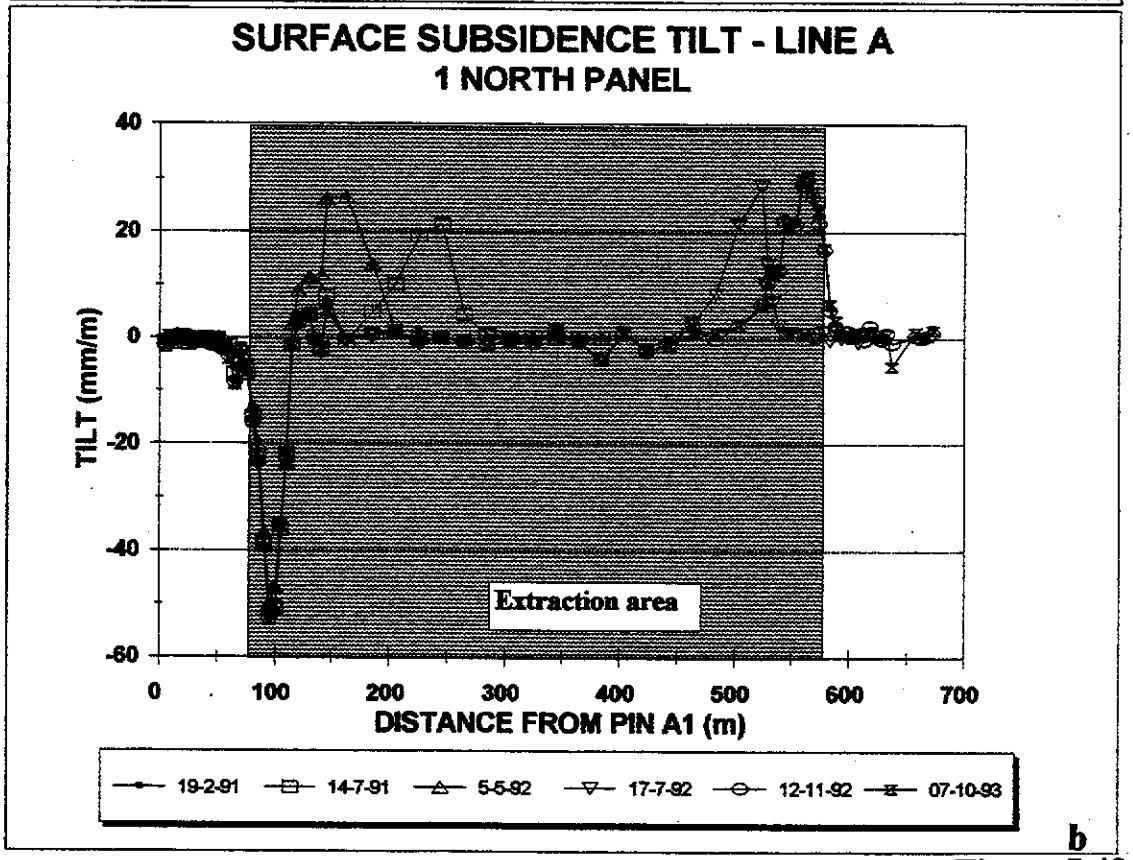

b

Figure I.49

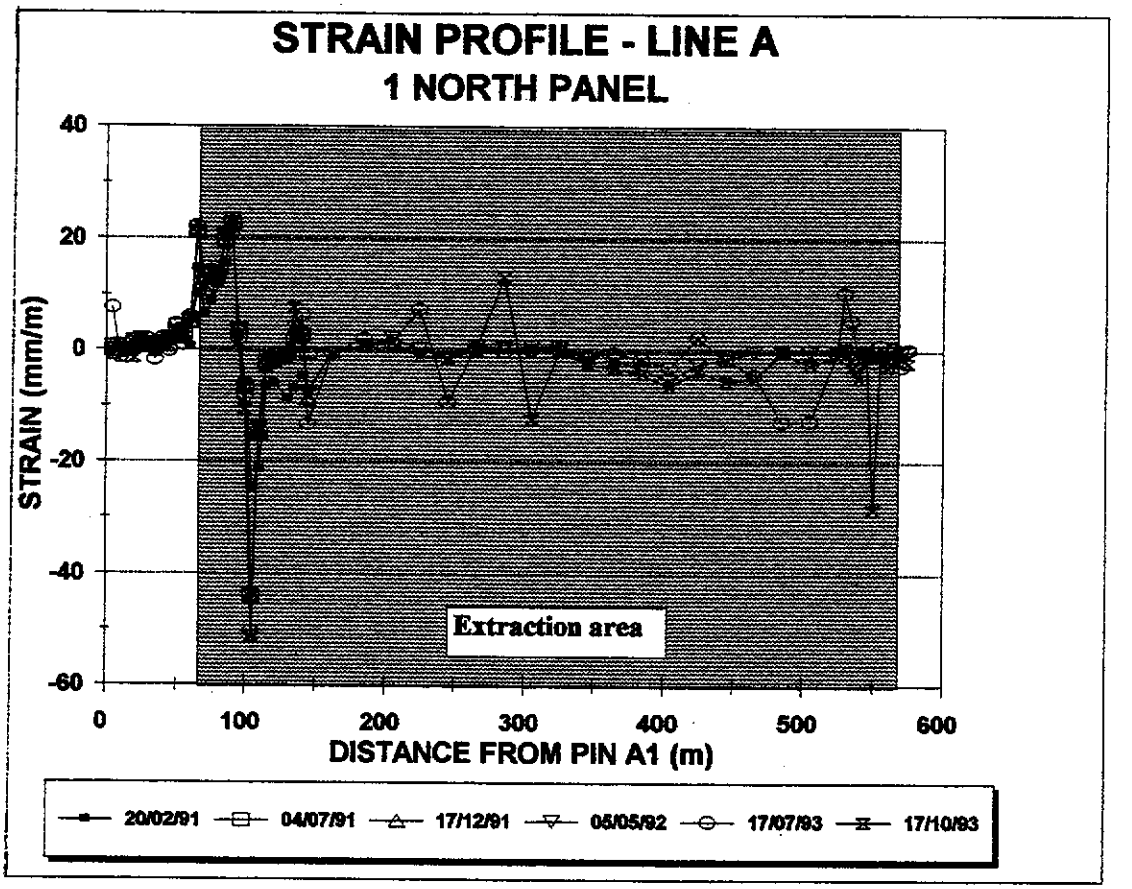
STRAIN PROFILE - LINE A
1 NORTH PANEL
STRAIN (mm/m)
40
20
0
-20
-40
-60
Extraction area
0
100
200
300
400
500
600
DISTANCE FROM PIN A1 (m)
20/02/91
04/07/91
17/12/91
05/05/92
17/07/93
17/10/93

Figure I.50

TABLE I.26

LINE A STRAIN MONITORING 1NORTH PANEL

Date >	17-Aug-90	20-Feb-91	04-Jul-91	17-Dec-91	04-May-92	05-May-92		30-Jun-92	17-Jul-92	23-Sep-92	12-Nov-92	24-Feb-93	07-Oct-93
Days >	0	187	321	487	626	627		683	700	768	818	922	1147
PEG #	DISTANCE BETWEEN SURVEY PEGS (m)												
					TAPE	EDM	DIFF						
1-2	4.863	4.862	4.863	4.867	4.866	4.887	21	4.893	4.900		4.880	4.880	4.858
2-3	5.235	5.236	5.235	5.235	5.235	5.224	-11	5.212	5.228		5.200	5.200	5.240
3-4	4.949	4.949	4.949	4.948	4.949	4.950	1	4.976	4.942		4.970	4.970	4.947
4-5	5.039	5.044	5.045	5.045	5.047	5.025	-22	5.012	5.047		5.030	5.030	5.032
5-6	4.917	4.919	4.920	4.922	4.927	4.927	0	4.923	4.922		4.920	4.920	4.925
6-7	4.746	4.750	4.752	4.752	4.752	4.748	-4	4.756	4.755		4.740	4.740	4.752
7-8	5.362	5.361	5.365	5.367	5.362	5.357	-5	5.362	5.353		5.370	5.370	5.360
8-9	4.875	4.881	4.881	4.883	4.880	4.885	5	4.871	4.885		4.880	4.880	4.883
9-10	5.025	5.032	5.035	5.036	5.036	5.027	-9	5.033	5.024		5.030	5.030	5.027
11	5.034	5.046	5.050	5.051	5.055	5.044	-11	5.038	5.057		5.050	5.050	5.046
12	4.998	5.006	5.011	5.012	5.015	5.016	1	5.010	5.003		5.010	5.010	5.017
13	4.859	4.862	4.883	4.884	4.885	4.888	3	4.896	4.888		4.890	4.890	4.887
14	5.057	5.131	5.164	5.167	5.167	5.160	-7	5.167	5.169		5.150	5.150	5.163
15	4.957	4.969	5.011	5.011	5.016	5.017	1	5.002	5.007		5.020	5.020	5.019
16	5.048	5.092	5.115	5.115	5.112	5.116	4	5.129	5.119		5.110	5.110	5.117
17	5.155	5.215	5.230	5.229	5.222	5.224	2	5.213	5.225		5.210	5.210	5.223
18	4.816	4.891	4.910	4.912	4.915	4.916	1	4.900	4.914		4.920	4.920	4.915
19	5.017	5.129	5.131	5.133	5.134	5.129	-5	5.137	5.121		5.130	5.130	5.127
20	4.931	4.944	4.949	4.951	4.947	4.943	-4	4.957	4.941		4.950	4.950	4.938
21	4.915	4.888	4.883	4.883	4.881	4.866	-15	4.867	4.874		4.870	4.870	4.862
22	5.102	4.976	4.877	4.877	4.878	4.844	-34	4.853	4.845		4.850	4.850	4.840
23	4.913	4.808	4.839	4.843	4.844	4.847	3	4.832	4.838		4.850	4.850	4.844
24	5.051	5.017	5.039	5.041	5.044	5.028	-16	5.040	5.042		5.040	5.040	5.037
25	5.210	5.179	5.200	5.202	5.201	5.198	-3	5.202	5.201		5.190	5.190	5.201
26	9.923	9.838	9.918	9.916	9.913	9.908	-5	9.913	9.916		9.920	9.920	9.906
27	4.827	4.794	4.835	4.845	4.847	4.864	17	4.858	4.829		4.840	4.840	4.864
28	5.433	5.408	5.448	5.452	5.448	5.445	-3	5.454	5.467		5.450	5.450	5.445
29	4.541	4.465	4.539	4.501	4.506	4.505	-1	4.499	4.481		4.500	4.500	4.506
30	17.244				17.237	17.242	5	17.235	17.235		17.235	17.235	17.237
31	22.700				22.717	22.720	3	22.755	22.748		22.755	22.748	22.717
32	20.025				20.070	20.057	-13	20.061	20.052		20.060	20.060	20.051
33	19.827				19.834	19.822	-12	19.819	19.975		19.820	19.820	19.807
34	21.020				20.995	20.985	-10	20.967	20.825		20.990	20.990	20.992
35	19.827				19.845	19.826	-28	19.835	19.837		19.835	19.837	19.829
36	19.745				19.756	19.731	-25	19.737	19.745		20.000	20.000	20.007
37	20.110				20.127	20.118	-9	20.122	20.114		19.860	19.860	19.861
38	20.080				20.094	20.067	-27	20.086	20.084		20.090	20.090	20.081
39	19.884				19.841	19.819	-22	19.833	19.867		19.840	19.840	19.835
40	20.040				20.012	19.953	-59	20.015	20.034		20.030	20.030	19.978
41	19.821				19.559	19.510	-49	19.572	19.593		19.580	19.580	19.540
42	19.545				19.444	19.427	-17	19.497	19.488		19.520	19.520	19.421
43	20.290				20.243	20.166	-77	20.276	20.340		20.340	20.340	20.219
44	19.950				19.924	19.921	-3	19.922	19.921		19.970	19.970	19.841
45	20.284				20.284	20.290	6	20.200	20.200		20.240	20.240	20.185
46	19.975				19.975	19.999	24	19.787	19.721		19.950	19.950	19.972
47	19.936				19.936	19.903	-33	19.846	19.687		19.840	19.840	19.888
48	19.908				19.908	19.893	-15	20.028	19.905		19.740	19.740	19.890
49	5.010				5.010	5.012	2	5.020	5.063	4.960	4.960	4.964	5.013
50	4.996				4.996	4.985	-11	4.991	5.024	4.968	4.950	4.961	4.982
51	4.940				4.940	4.932	-8	4.928	4.930	4.912	4.910	4.911	4.916
52	5.075				5.075	5.076	1	5.082	5.070	5.036	5.030	5.027	5.074
53	5.045				5.045	5.032	-13	5.049	5.038	4.994	4.930	4.955	4.901
54	5.069				5.069	5.068	-1	5.058	5.075	5.049	5.030	5.024	5.066
55	4.919				4.919	4.904	-15	4.902	4.911	4.925	4.870	4.902	4.906
56	5.042				5.042	5.021	-21	5.029	5.045	5.065	5.030	5.046	5.035
57	4.930				4.930	4.936	6	4.932	4.917	4.959	4.940	4.940	4.931
58	5.021				5.021	5.006	-15	5.022	5.023	5.071	5.050	5.052	5.011
59	4.908				4.908	4.895	-13	4.906	4.903	4.924	4.940	4.945	4.904
60	5.000				5.000	4.995	-5	4.986	4.989	5.008	5.030	5.049	4.980
61	5.041				5.041	5.041	-0	5.033	5.029	5.044	5.040	5.051	5.030
62	4.988				4.988	4.982	-6	4.980	4.955	5.980	5.110	4.990	4.965
63	5.033				5.033	5.039	6	5.033	5.048	5.035	4.890	5.033	5.039
64	4.958				4.958	4.953	-5	4.951	4.937	4.959	4.960	4.957	4.947
65	4.948				4.948	4.943	-5	4.944	4.946	4.949	4.950	4.951	4.944
66	5.003				5.003	4.993	-10	5.007	4.984	5.005	5.000	5.005	4.978
67	5.064				5.064	5.057	-7	5.020	5.044	5.065	5.060	5.063	5.042
68	4.970				4.970	4.955	-15	4.972	4.942	4.970	4.970	4.970	4.955
69	4.905				4.905	4.897	-8			4.909	4.900	4.906	4.895
70	5.034				5.034	5.061	27			5.035	5.020	5.020	5.035
71	4.156				4.156	4.155	-1				4.150	4.150	4.136
72	20.854					9.216							
73					20.854	0.000				20.870	20.820	20.820	20.683
74	4.015				4.015	30.048				4.015	4.010	4.010	4.003
75	5.057				5.057	5.052				5.059	5.057	5.059	5.035

NOTE THAT A TRIAL USING THE EDM TO MEASURE HORIZONTAL DISTANCE WAS NOT SUITABLY ACCURATE.

TABLE L.27

LIFTING PROGRESS

NORTH WEST B3 PANEL

(14 JEFFREY)

DATE	SPLIT #	GOAF WIDTH (m)	
08-Feb-93	1 START		
13-Feb-93	1 FINISH	20	
			S-P1
21-Feb-93	2 START		
27-Feb-93	2 FINISH	40	
08-Mar-93	4 START		
14-Mar-93	4 FINISH	20	
			S-P2
21-Mar-93	5 START		
26-Mar-93	5 FINISH	40	
07-Apr-93	7 START		
13-Apr-93	7 FINISH	20	
			S-P3
20-Apr-93	8 START		
29-Apr-93	8 FINISH	40	
07-May-93	11 START		
14-May-93	11 FINISH	20	
			S-P4
21-May-93	12 START		
27-May-93	12 FINISH	40	
11-Jun-93	14 START		
17-Jun-93	14 FINISH	18	
			S-P5
29-May-93	15 START		
04-Jun-93	15 FINISH	36	

S-P1 = SUBPANEL 1

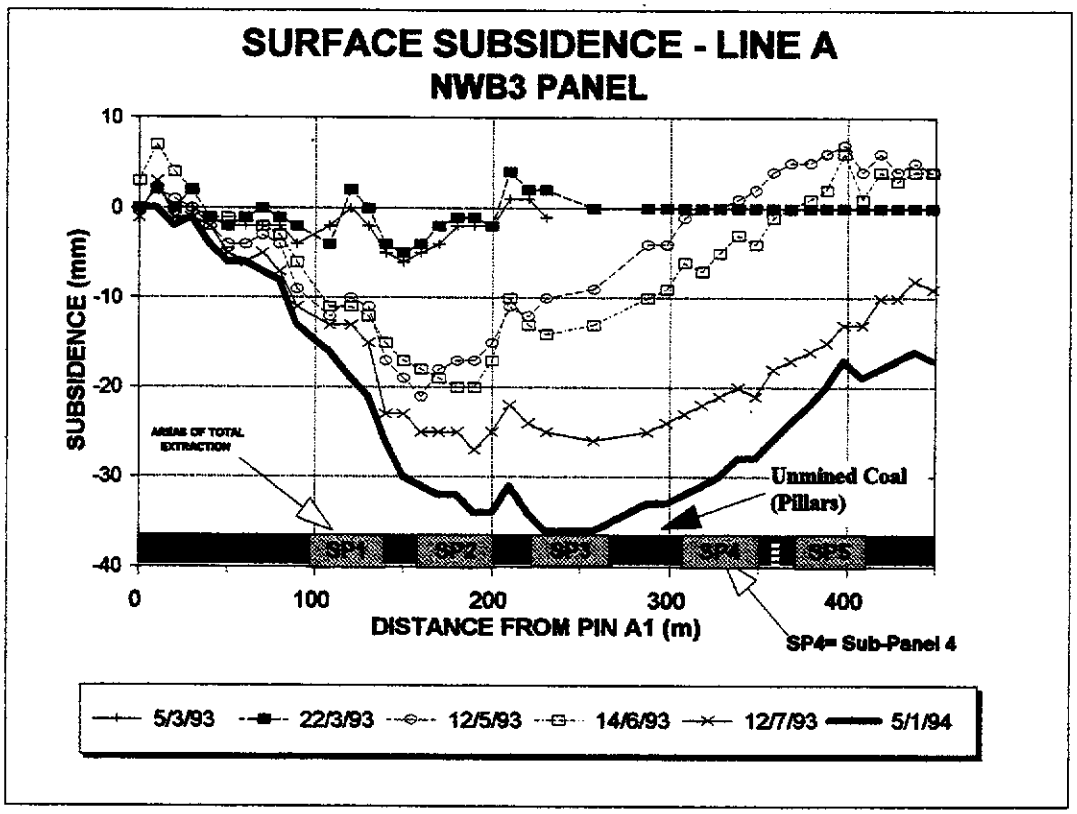
SURFACE SUBSIDENCE - LINE A
NWB3 PANEL
SUBSIDENCE (mm)
10
0
-10
-20
-30
-40
0
100
200
300
400
DISTANCE FROM PIN A1 (m)
AREAS OF TOTAL EXTRACTION
Unmined Coal (Pillars)
SP4= Sub-Panel 4
5/3/93
22/3/93
12/5/93
14/6/93
12/7/93
5/1/94

Figure I.51

APPENDIX II

SUBSURFACE SUBSIDENCE MONITORING

Over the years, there have been mainly five methods (Bhattacharyya & Gurtunca, 1984) used to measure subsurface subsidence. These methods are:

- Time domain reflectometry
- Borehole radio active anchors and Gamma-ray logging
- Borehole rod extensometer
- Borehole magnetic extensometer
- Borehole wire extensometer

The following paragraphs explaining the basic principals of these methods have been modified from Bhattacharyya and Gurtunca (1984).

Time Domain Reflectometry (TDR) uses a coaxial electrical cable grouted in a borehole from the surface to the extraction horizon (Peng, 1978). Any movement of the subsiding strata either cuts off or creates faults in the cable at the position of movement. A voltage signal which has a very fast rise time is sent down the cable and the signal is reflected back up from the closest fault in the cable and received by a detector at the surface. A cathode ray tube or oscilloscope is usually used for the display of the signal.

TDR cable can be installed as deep as 6,000 m and can resolve faults to within 15 mm on short, high quality cables. The main disadvantage of this method is that if a large break occurs high in the cable, no readings can be gained from the lower strata. It appears to be necessary (Rowlands, 1990) to establish a relationship for shear displacement and reflection coefficients for different lengths of cable to maintain reasonably accurate readings.

Borehole Radio Active Anchors and Gamma-ray Logging involves the embedding of radio active markers into the strata along the axis of a borehole. The displacement of the subsiding markers is determined by lowering a gamma-ray logging tool into the hole. When a gamma-ray logging tool or a probe moves inside the borehole, it detects the gamma-rays emitted from the marker sources and these signals are

recorded on paper charts or digitally in conjunction with the measurements from a depth counter.

The gamma-ray logging method is widely used to determine the thickness and approximate composition of the formations intersected by a borehole (Ringis, 1976). The accuracy of this type of measurement depends upon the following variables:

- The shape and amplitude of the deflections recorded on the gamma-ray log.
- The logging speed.
- The time constant of the detector.
- The instrument sensitivity.
- The nature of the source, including its volume and its distance from the detector.

When this method has been applied in the past (e.g. Allen,1969) for subsurface subsidence measurements, Cobalt-60 bullets have been used. These bullets are fired through the casing pipe into the borehole wall. A special gun is required to fire the sources and this makes the process very expensive. The penetration of the radioactive bullets into the strata depends on the amount of charge in each bullet and also the hardness of the strata. In soft strata, excessive penetration can make detection of the radiation source difficult. On the other hand, special care must also be taken to ensure adequate penetration in hard rock. Problems occur when some of the radioactive 'shot' is eroded out of its original position and lodges at any position farther down the hole.

The method of gamma-ray logging with radioactive markers has the following advantages:

- The system of logging does not require skill to install the equipment and the equipment is easy to operate.
- The system can be used in corrosive conditions.
- Many markers can be installed and monitored in one borehole.

The disadvantages of the method are:

- Knowledge of the nature of the strata is needed to position the radioactive bullets to the prescribed penetration depth.

- A special gun is required to fire the bullets into the strata and this is an expensive operation.
- A central opening is required along the full length of the borehole for the passage of the gamma-ray logging probe.
- The measuring runs to great depths consume a lot of time.
- The method cannot be used in environmentally sensitive areas.

A borehole rod extensometer system consists mainly of anchors, steel rods and a measuring head. The rods are usually inserted in plastic tubes or run through nylon bearings to reduce friction between the different parts (Hoek and Brown,1980). The annulus between the plastic tube and the borehole sides is also grouted. The rods are therefore not bound to the rock mass along its length and any movement of the rock mass at the anchor point relative to the borehole collar will be transferred via the anchor and rod to the borehole collar.

A light oil was used by Alexander and Fraser (1975) to fill the air space between the rods and the plastic tube to prevent corrosion.

Mechanical dial gauges or electronic displacement transducers can be used at the collar as the measuring head. Electronic type measuring heads can be used to measure larger displacements but their installations are expensive. The sensitivity of the mechanical and tele-electronic type reading devices was reported as 0.01 mm (Amstad and Koppel, 1977).

The rod-type extensometers are extensively used to measure the displacement around underground tunnels, caverns and in sub-surface strata.

This method is limited to monitoring subsidence at only shallow depths because of the restriction in rod lengths. Up to six anchors have been installed in one borehole, the number being dependent on the diameter of the borehole and of the rods (Whittaker and Woodrow, 1977).

The magnetic type extensometer consists of annular-shaped permanent magnets placed around either a mechanical type anchor (e.g. Krishna, 1991) or central P.V.C tube within a borehole and grouted (Bhattacharyya & Gurtunca, 1984). The magnets

move with the rock mass and their positions are determined by logging with a Reed type electrical switch mounted on a probe at the end of a survey tape.

Before installation, the magnets are usually coated with epoxy resin or an enamel paint to prevent corrosion. In some cases, the magnets are encapsulated in neoprene rubber and subsequently coated with a sealing compound. The magnets are then mounted in a holder made from a short length of P.V.C tube. The central P.V.C guide tube is first placed in the borehole to provide guidance and protection for the reed switch. The magnet holder, with fitted strong springs, is attached to the insertion tool and lowered down the borehole. The insertion tool is withdrawn from around the magnet holder at the required depth of the borehole and the springs then jam into the borehole wall to hold the magnet in place. The magnets are permanently bonded to the wall of the borehole by injecting grout in the annulus between the P.V.C tube and the borehole wall (Burland et al., 1972).

The accuracy of the magnetic extensometer method is ±0.5 mm which is adequately sensitive for measuring sub-surface movements. The equipment is also durable, relatively easily installed and capable of measuring large deformations. However, problems can be experienced with lowering the detection tool down the borehole at various stages of subsidence development, and inadequate radial coverage of the magnets around the borehole wall to affect the detection unit.

Borehole Wire Extensometers

The basic principle of the borehole wire extensometer measuring system is to fix one end of the measuring wires or tapes to the walls of boreholes at selected depths, using one of many types of anchor, and to fix the other end to an extensometer at the borehole collar. The axial displacement of the anchor is determined by measuring the gauge length of the attached wire relative to a fixed point on the extensometer. Where more than one wire is installed, the anchors require axial holes to allow free passage of the wires from anchors already installed at greater depths within the borehole (Hedley, 1969).

There are two basic anchor mechanisms, mechanically set or hydraulically set. The mechanically set is the most commonly used. Caliper type anchors are more suitable

where the strata are particularly weak and significantly influenced by water (Whittaker and Woodrow, 1977), such as in the Collie Basin.

An example of a caliper borehole anchor is the device used by Oravecz and Salamon (1973) in South Africa. The anchor is set in the borehole by activating a spring after the anchor is lowered to the desired position. A special insertion device is used to hold the shells compressed while the anchor is lowered into position. The release mechanism of the insertion device is activated by a wire rope. This type of anchor is useful in slightly oversized holes and at locations subject to tensile strain (Oravecz, 1977). On the other hand, it has the disadvantage of requiring a wire rope for disengaging the anchor from the insertion piece and this also makes the installation difficult in deep boreholes.

The extensometer is the instrument used to measure changes in the gauge length of each wire relative to a fixed seat at the collar anchor and thus the displacements of the relevant anchor attached to the strata within the borehole. The instrumentation can be set up to take measurements automatically by data logging systems, or manually. Typical arrangements involve measurements of the change in position of either a tensioned wire within a graduated frame, or a weight attached to the end of the anchor wire which is placed over a pulley.

The mechanical-type anchor was considered to be the most suited to the conditions pertinent to this project. This type of anchor was considered to be more cost efficient to install, more reliable, and better able to handle short or long term variation in hole diameter than the other anchors. The general setup of this system is described in greater detail below.

II.1 RESEARCH PROJECT BOREHOLE WIRE EXTENSOMETER SET-UP

The form of the anchors used in this project can be described as a wire brush (Figure II.1) attached to a 2 mm gauge, 7 x 7 multi-stranded stainless steel wire. The thin gauged wire is placed over a pulley arrangement on the surface "tower" and a 10 kg weight attached to the end of the wire so that the weight hangs just above a datum plate. The pulley arrangement allows for unhindered movement of the anchor.

The mechanics of the anchor results in the bristles being forced upward as the anchor is being pushed down the hole, during installation, to the target depth. Upon reaching the target depth, a 10 kg weight is attached to the free end of each anchor's cable. The upward force induced on the anchor's bristles (by the 10 kg weight) prevents the anchor from sliding further down the hole.

The main favourable features of the anchor include:

- An "open" structure, which allows groundwater and some erosional debris to pass through the anchors without disruption.
- The oversized wire bristles can tolerate large variations in hole diameter without affecting the integrity of the anchorage.
- The anchors are low cost, and quick and easy to install. This allows for the installation of several anchors down each hole.
- The open structure of the anchors also allows the extensometer boreholes to be left open, thus eliminating the costs of cement-filling the holes for multi-anchor extensometers. This factor, along with the speed of installation, also greatly reduces drilling costs which account for more than 90% of total costs associated with subsurface subsidence investigations.

It was decided to generally place the anchors within the stiffer aquitard material as the extremely weak, water saturated sandstone, can be subject to high erosional forces from cascading groundwater. It was considered possible that in partly pressurised aquifers, the erosional forces could "blow out" the diameter of the open extensometer boreholes, allowing the anchors to move freely without contact with the borehole walls.

Subsurface movement can be measured as a change in distance from the bottom of the weight to the datum plate (Figure II.2 a), or as a change in electrical resistance if the pulley is fitted with a multi-turn potentiometer as the spindle of the pulley (Figure II.2 b - described in more detail below). Total subsidence is determined by adding these differential movements to changes in reduced level (RL) of the datum plate - levelled at regular intervals by WCL surveyors.

In areas where the overlying aquifers are partly depressurised, extensometer boreholes must be designed to avoid connection between the mine and the

pressurised aquifer. Two design approaches were used in this study. The first was to drill two 152 mm diameter holes using mud-rotary methods. The first hole was drilled to the base of the deepest pressurised aquifer, and the second drilled through to the mine roof. The second (deeper) borehole is cased and sealed off with cement in the upper section of the hole (from below the depth of the shallower hole). In this way, the two boreholes are independent of each other, and at the same time maintain continuity of anchor positioning from the surface to the mine. This method was used for the extensometers above ACIRL and Blue panels.

The other design approach used was to drill individual HQ [(100 mm) reverse-air circulation] holes for each anchor, and seal each hole with portland cement slurry from immediately above the anchor. (The anchor cable is lowered down the hole within a 25 mm diameter PVC pipe to provide a void for free movement of the cable within the cement seal.) This extensometer design keeps all aquifers separate and prevents interconnection via the extensometer. This design approach, used for the narrow NWB3 sub-panels, also allows for a piezometer to be installed in the same hole. This method is not recommended for wide panels, where the researcher is interested in monitoring the staged development of subsidence as the panel widens. In such cases, the lateral movements will shear through the cemented cable, rendering the extensometer inoperable.

The merits of each method are dependent on the objectives of the study, and the costs of drilling (and drilling standby for cementing). A more detailed description of the set up for the second extensometer design approach has been given in Section 5.2 in the main body of the thesis.

The configuration of each extensometer is illustrated in Figures II.3 to II.8. The location of each extensometer within the panel is denoted in Figures I.1, I.4, I.5, I.7, and I.8 respectively. A summary of the subsurface monitoring for each panel is provided in Tables II.1 to II.5. Graphical plots of these subsurface data have been provided in Section 3.2.

Note that the subsurface data for panels with two separate extensometers (namely ACIRL and Blue panels) has been combined and presented as if only one extensometer was installed above each panel.

Once again the frequency of monitoring is governed by the progress of mining within the panel. Measurements are generally taken weekly, until the fender extraction mining face nears the location of the extensometer and monitoring can be increased to twice daily or more; depending on the position of the goaf edge in relation to the extensometer.

During the early stages of mining, subsurface subsidence above 1 North panel and 2 South A panel was monitored continuously every two hours, using a data logger powered by a 12 volt car battery. The data logger was programmed to read the electrical current across rotary potentiometers connected to each pulley supporting each anchor's cable. (The central spindle from the potentiometer was used as the hub of the pulley.) As the extensometer anchors move, the cable pulls down on the pulley and thereby rotates the spindle of the potentiometer by an amount equivalent to the movement of the anchor. This rotation alters the electrical resistance measured through the potentiometer (by the data logger). The change in resistence can then be used to directly quantify the movement of the anchor.

Data is stored in the memory of the logger and down-loaded onto computer disk using a communications package operated by a portable computer.

The results from the 1 North panel automated monitoring are plotted in Figure II.9. It has been concluded that, given the hours of work in the mines (two shifts from 8 am to 10 pm Monday to Friday), manual readings takenaccording to the proximity of the mining face, were more than adequate.

DIAGRAMMATICAL REPRESENTATION OF EXTENSOMETER ANCHORS

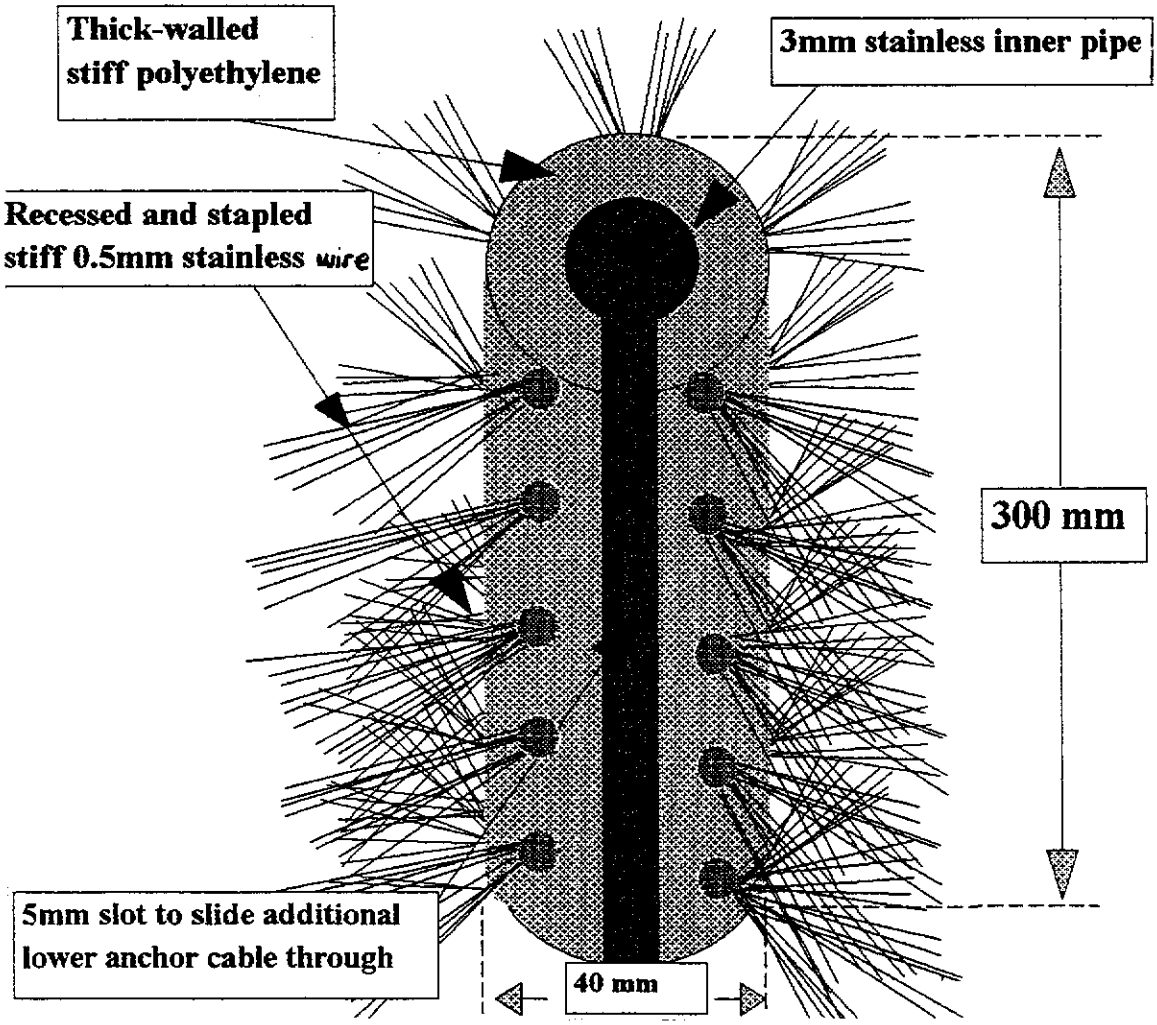

Figure II.1

PHOTOGRAPHS OF BOREHOLE EXTENSOMETERS

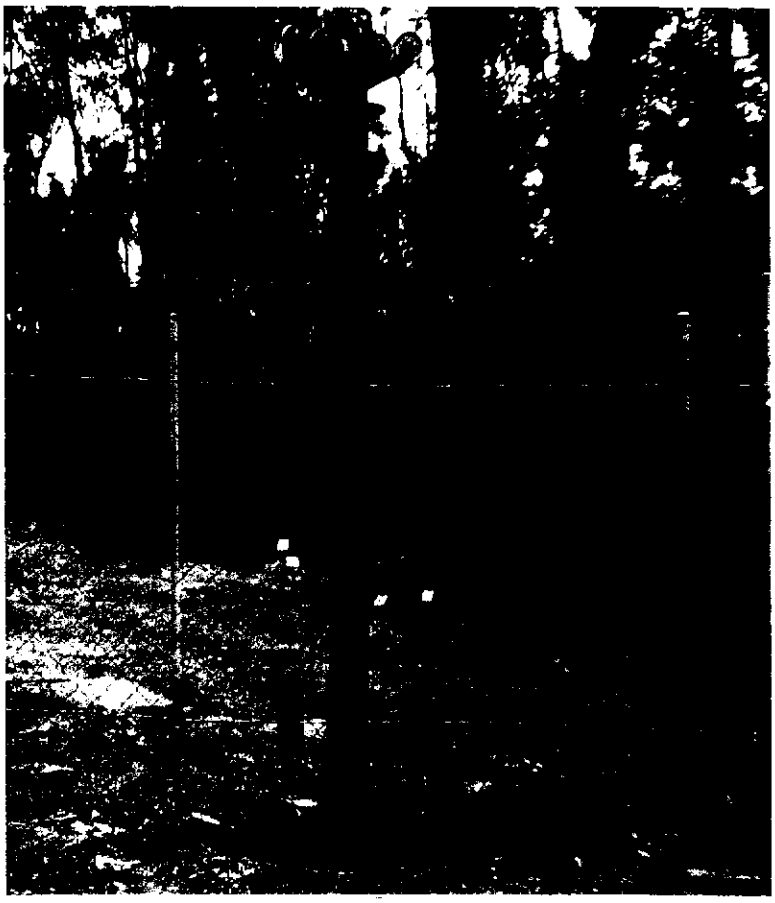

a) Extensometer D213 manual recording set-up

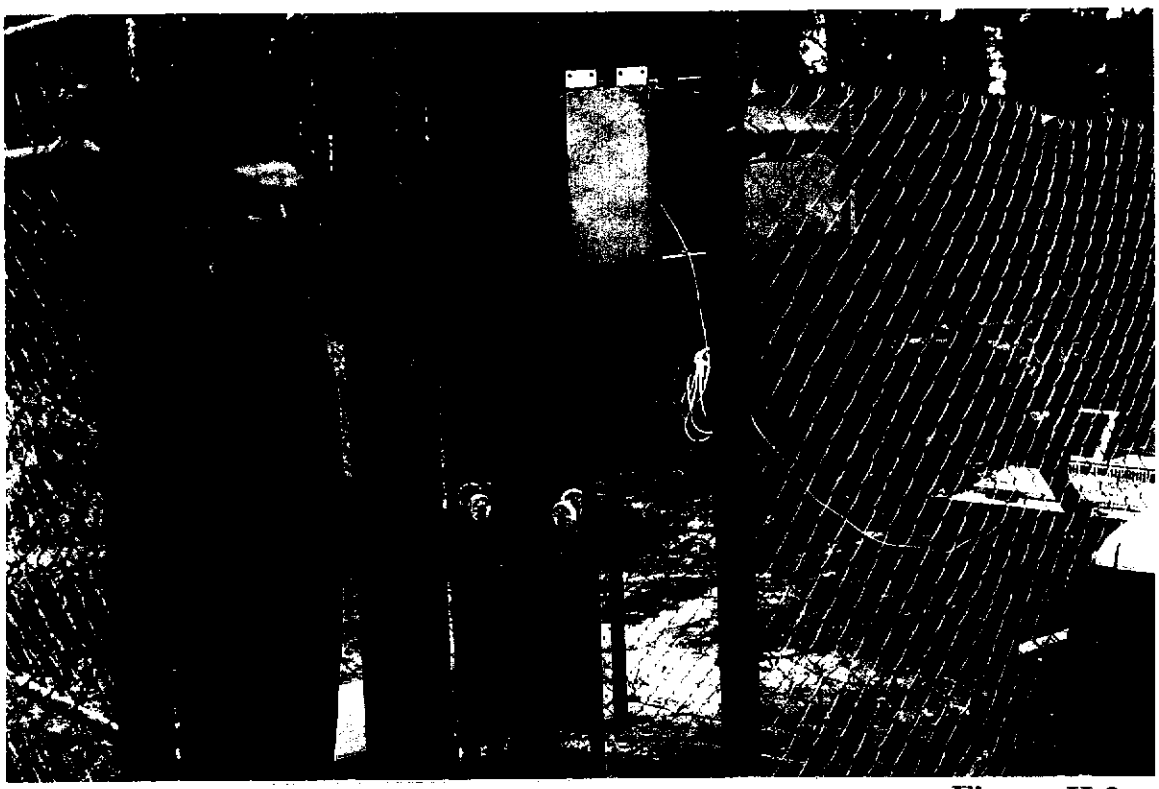

b) Extensometer D212 automatic recording set-up

Figure II.2

EXTENSOMETER ANCHOR INSTALLATION ABOVE ACIRL PANEL

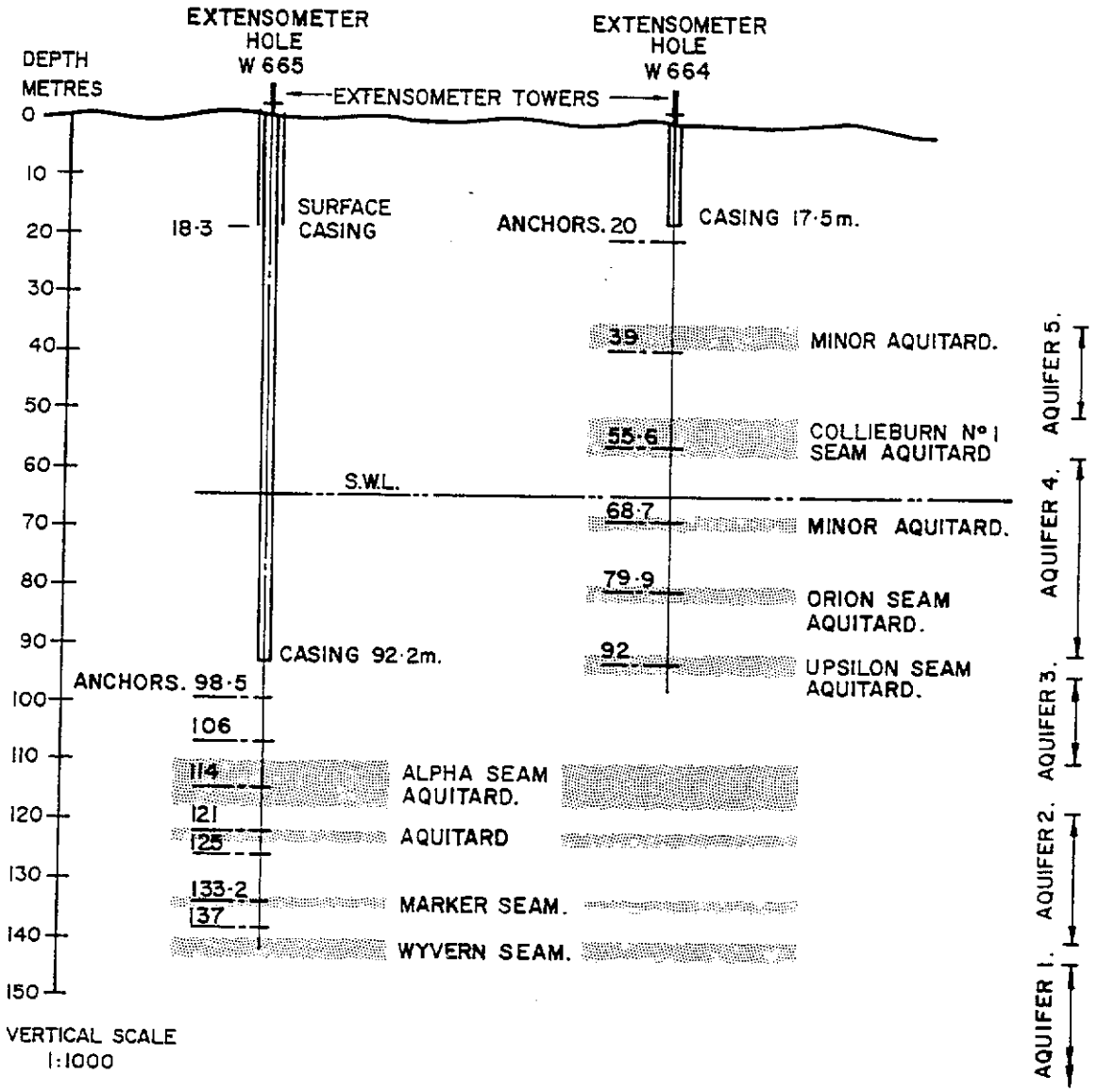

NOTE:
ONLY THE 98·5m ANCHOR IN HOLE W665 IS OPERATIONAL.

Figure II.3

EXTENSOMETER ANCHOR INSTALLATION ABOVE BLUE PANEL

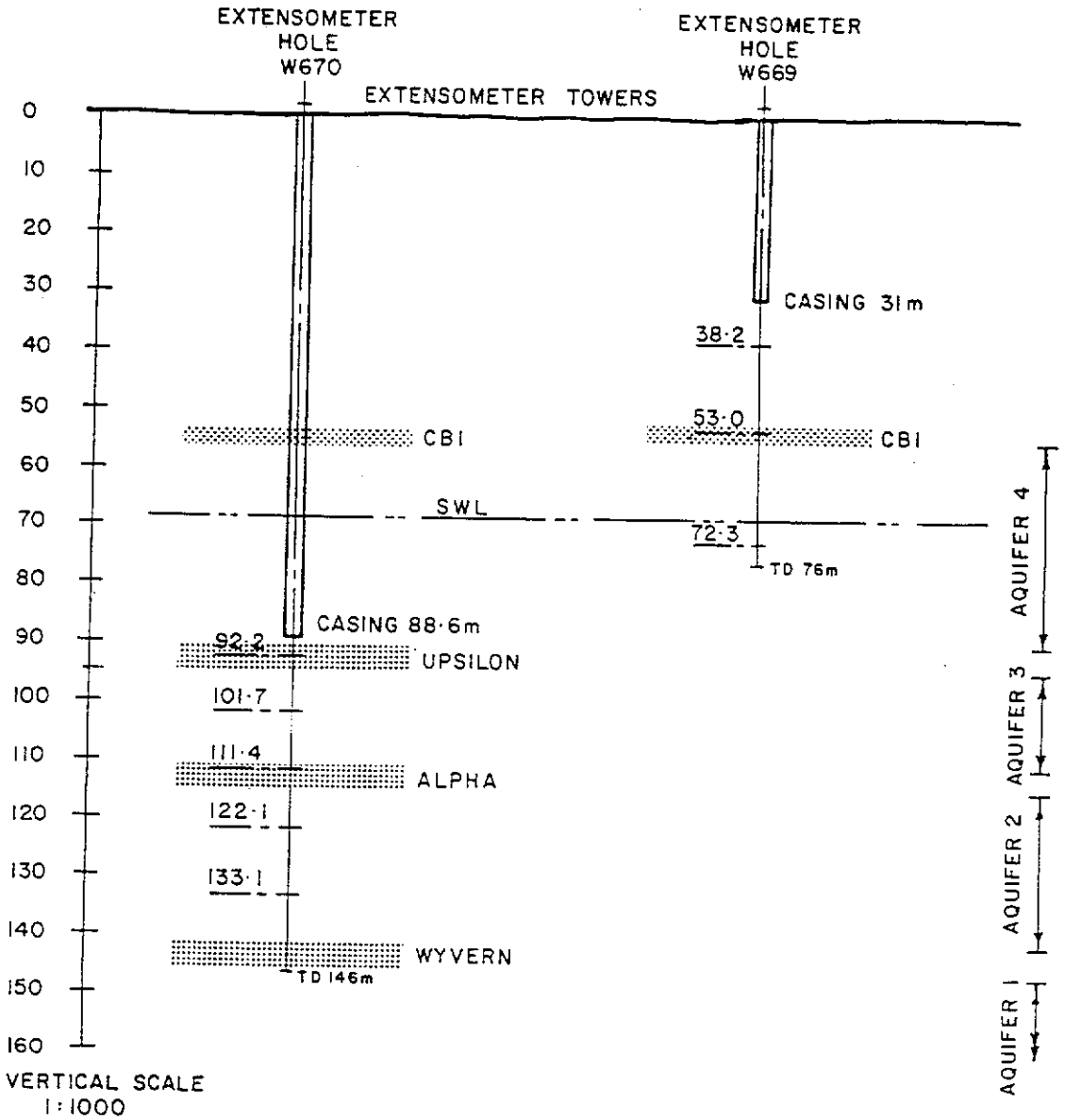

NOTE ANCHORS SET IN COAL SEAMS OR MINOR AQUITARDS (SHALES)

Figure II.4

EXTENSOMETER ANCHOR INSTALLATION ABOVE 2SA PANEL

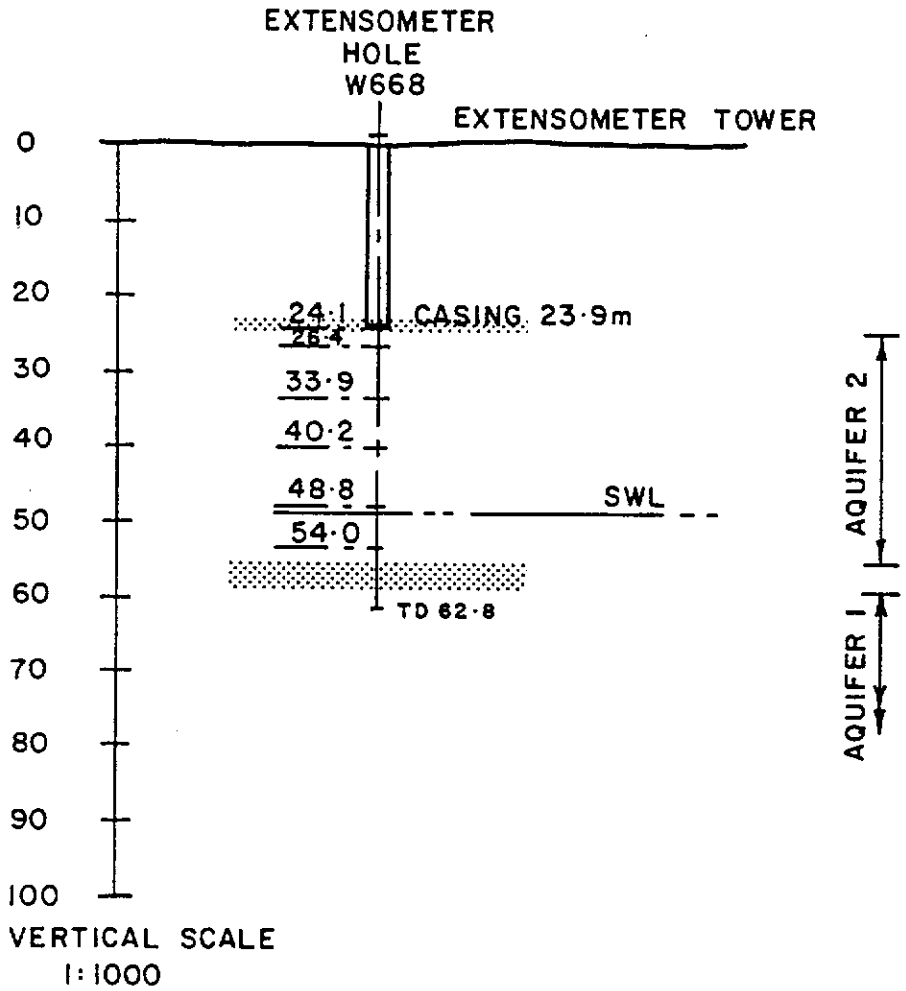

NOTE ANCHORS SET IN COAL SEAMS OR MINOR AQUITARDS (SHALES)

Figure II.5

D212 & D213 BOREHOLE EXTENSOMETER SET-UP
1 NORTH PANEL WD6

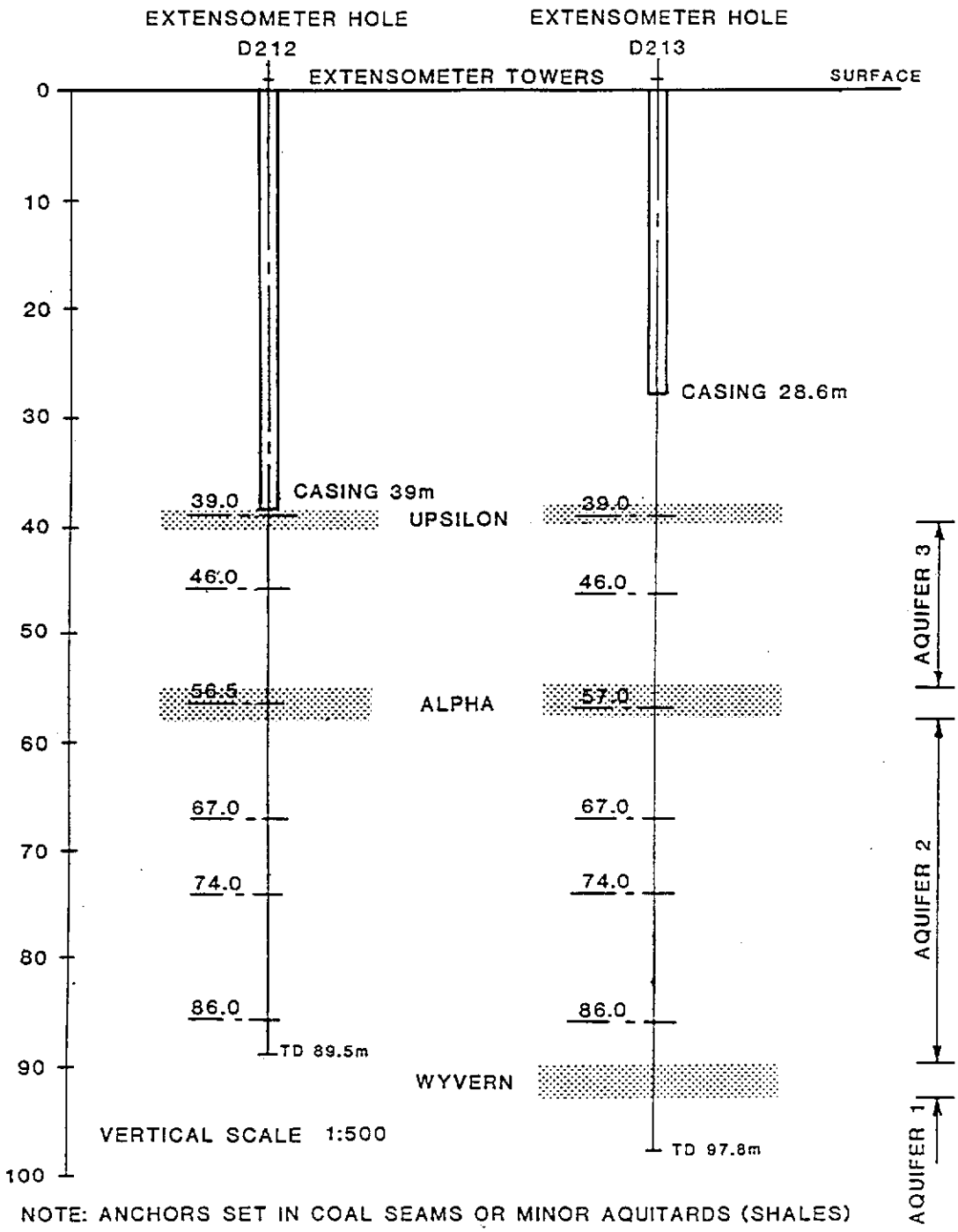

NOTE: ANCHORS SET IN COAL SEAMS OR MINOR AQUITARDS (SHALES)
NO STANDING WATER LEVEL DETECTED

Figure II.6

CONTRUCTION OF MONITORING BORES ABOVE SUB-PANEL #1 NWB3 PANEL

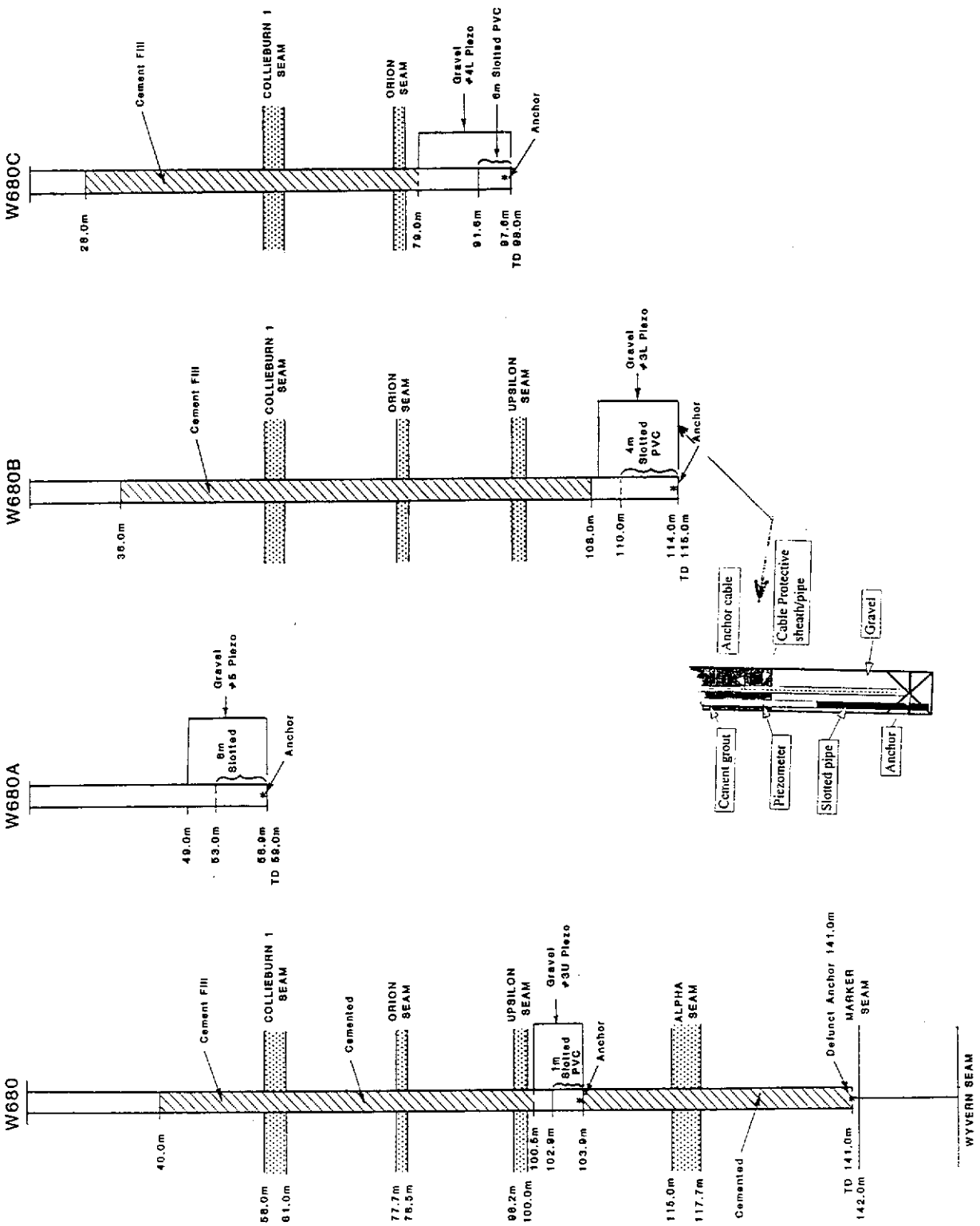

(NOT TO SCALE)

Figure II.7

CONTRUCTION OF MONITORING BORES ABOVE SUB-PANEL #2 NWB3 PANEL

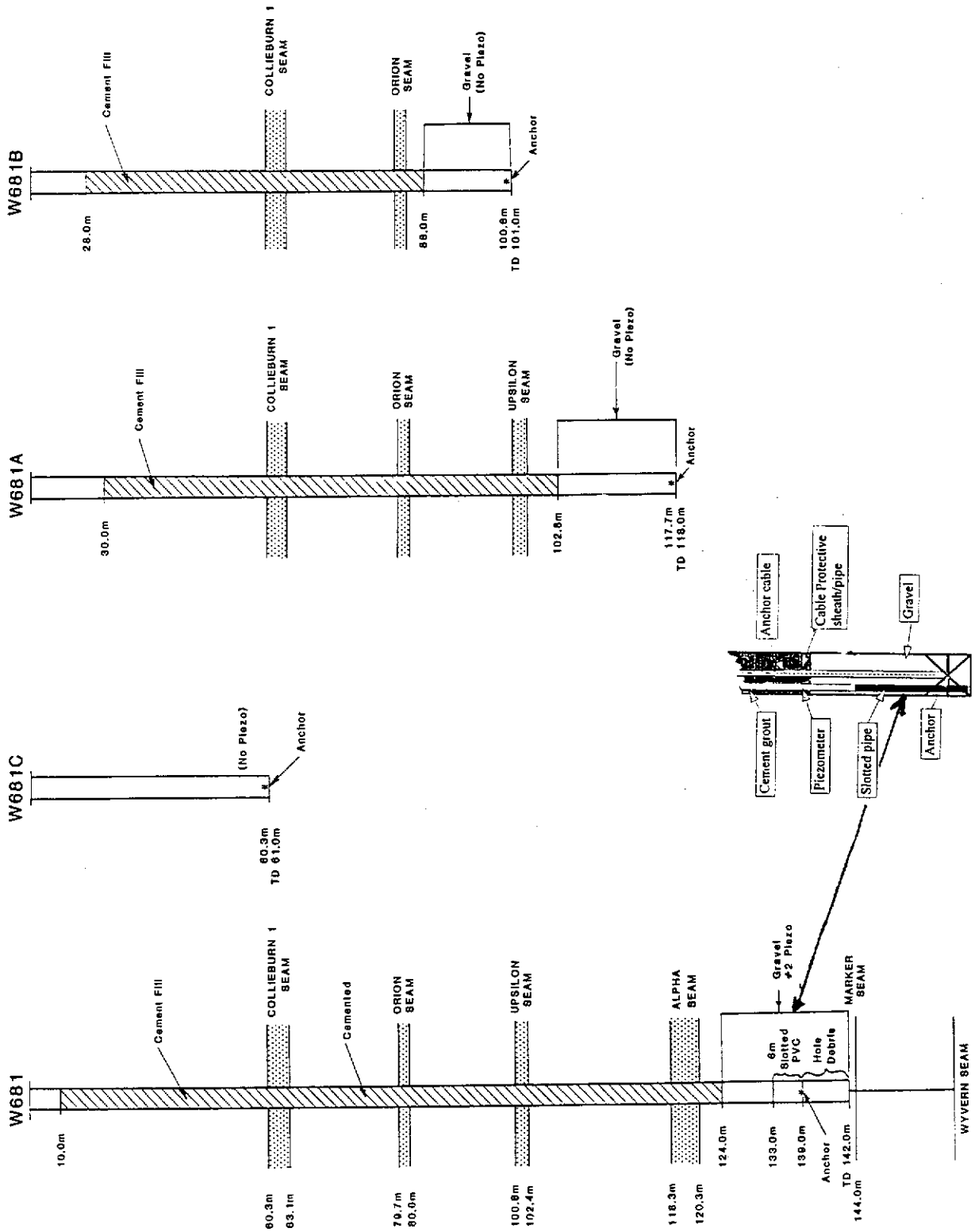

(NOT TO SCALE) **Figure II.8**

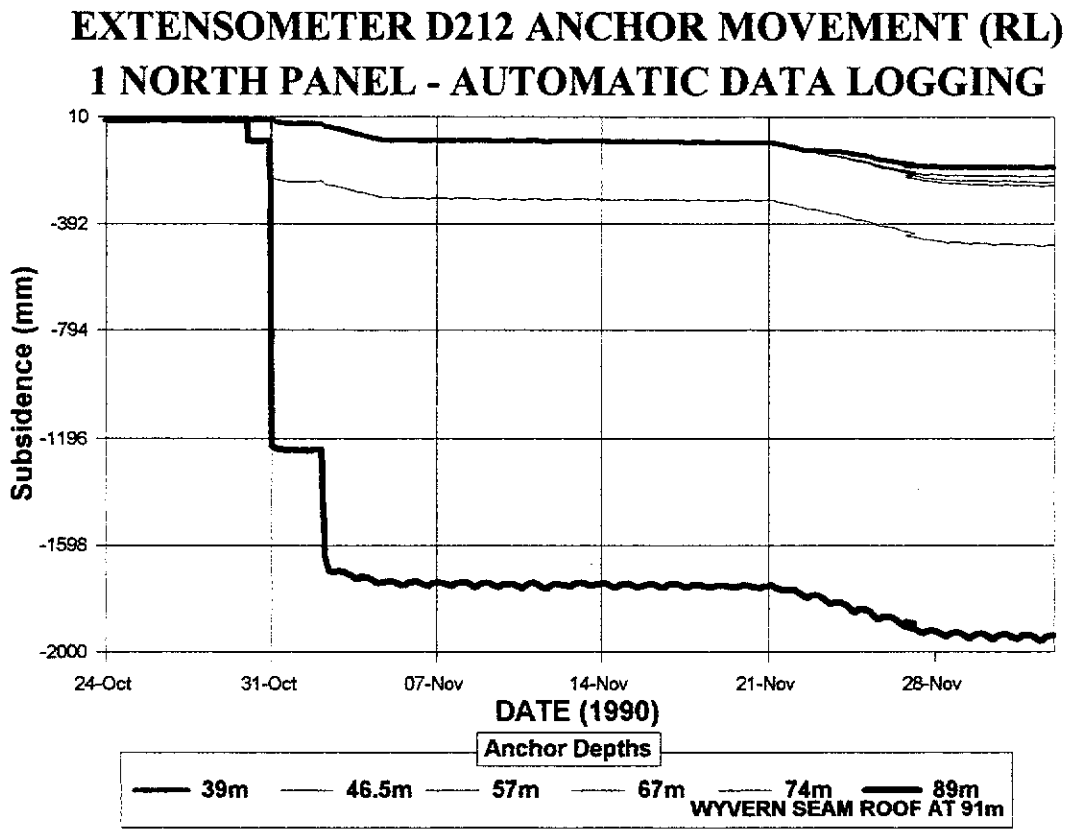
EXTENSOMETER D212 ANCHOR MOVEMENT (RL)
1 NORTH PANEL - AUTOMATIC DATA LOGGING
Subsidence (mm)
10
-392
-794
-1196
-1598
-2000
24-Oct
31-Oct
07-Nov
14-Nov
21-Nov
28-Nov
DATE (1990)
Anchor Depths
39m
46.5m
57m
67m
74m
89m
WYVERN SEAM ROOF AT 91m

Figure II.9

TABLE II.1

ACIRL PANEL ANCHOR MOVEMENT RELATIVE TO DATUM PLATE

MANUAL RECORDINGS

DATE	Goaf Width	Days	ANCHOR DEPTHS (m) -98.5	-92.0	-79.9	-68.7	-56.6	-39.0	- 20.0	Inferred Datum Plate Movement W665	W664	PIN F23 SUBS.
			Movement (mm)									
17-Sep-87		0	0	0	0	0	0	0	0	0	0	0
18-Sep-87		1	0	0	-3	-1	-1	0	1	0	0	0
22-Sep-87	51	5	2	1	-3	-1	0	1	2	0	0	0
29-Sep-87	64	12	-1	0	-2	1	-1	1	1	9	8	8
20-Oct-87		33	-1	1	-1	4	1	3	1	7	6	6
22-Oct-87		35	1	1	0	6	1	1	1	6	5	5
28-Oct-87	78	41	1	2	0	6	0	0	-1	20	20	10
05-Nov-87		49	1	2	0	6	0	0	0	42	42	30
11-Nov-87		55	-38	3	1	6	0	0	0	84	68	55
20-Nov-87		64	-62	3	2	7	-1	2	-2	170	146	125
23-Nov-87	92	67	-63	2	1	7	0	1	-1	190	160	160
04-Dec-87	105	78	-74	-39	-34	-4	-17	-9	-1	285	255	245
11-Dec-87		85	-74	-47	-42	-7	-23	-14	-6	315	285	285
11-Dec-87		85	-74	-47	-42	-7	-23	-14	-6	315	285	285
18-Dec-87		92	-73	-49	-45	-9	-29	-13	-5	342	310	310
31-Dec-87	120	105	-73	-52	-46	-11	-29	-16	-4	393	355	360
15-Jan-88		120	-75	-52	-48	-13	-31	-16	-6	425	387	385
22-Jan-88		127	-73	-54	-46	-13	-31	-15	-7	438	400	400
01-Feb-88		137	-74	-54	-47	-14	-31	-16	-8	450	410	410
10-Feb-88		146	-73	-54	-46	-13	-31	-16	-8	460	418	418
24-Mar-88		189	-60	-54	-47	-15	-30	-15	-8	490	442	442
28-Apr-88		224	-60	-54	-46	-14	-31	-15	-7	512	462	462
26-Oct-88		405	-60	-54	-46	-14	-30	-16	-5	555	505	505
09-Jan-89		480	-76	-56	-46	-16	-33	-16	-7	555	505	505
11-Jul-89	120	663	-77	-57	-46	-15	-33	-16	-7	555	505	505

NOTE: Extensometer is 71 m from chain pillar

TABLE II.2

BLUE PANEL ANCHOR MOVEMENTS RELATIVE TO DATUM PLATE MANUAL RECORDINGS

Date	Days	Goaf Width (m)	ANCHOR DEPTHS (m) Movement (mm) 38.7	53.0	72.3	92.2	101.7	111.4	122.1	133.1	SURFACE & DATUM PLATE MOVEMENTS (mm) Pin C33	W699	W670
29-Jul-88	0	52	0	0	0	0	0	0	0	0	0	0	0
04-Aug-88	6		1	1	1	1	0	2	1	-1	0	0	0
15-Aug-88	17	65	1	2	3	-1	-1	1	-1	0	20	20	20
01-Sep-88	34	78	1	1	2	-1	-1	2	-1	-1	38	38	38
05-Sep-88	38		3	3	2	0	0	2	1	-1	40	40	40
07-Sep-88	40		2	4	2	-1	-2	1	0	-3	42	42	42
14-Sep-88	47		2	3	2	-1	-1	2	-1	-1	48	48	48
20-Sep-88	53	91	1	2	3	-1	0	1	0	-1	52	52	52
23-Sep-88	56		2	3	3	-1	-1	2	-1	-2	56	56	56
24-Sep-88	57		1	4	3	-1	0	2	-12	-36	57	57	57
24-Sep-88	57		1	4	3	-1	1	-3	-59	-106	57	57	57
25-Sep-88	58		2	4	3	-1	0	-11	-83	-137	59	59	59
25-Sep-88	58		2	5	4	-1	1	-22	-103	-162	59	59	59
26-Sep-88	59		2	5	4	-1	0	-22	-116	-162	60	60	60
27-Sep-88	60		2	4	3	-1	1	-59	-269	-318	61	61	61
28-Sep-88	61		1	5	2	0	0	-63	-301	-339	62	62	62
29-Sep-88	62		2	4	2	-1	1	-70	-311	-360	63	63	63
04-Oct-88	67		0	4	2	-1	0	-71	-311	-364	68	68	68
06-Oct-88	69		2	4	2	-1	0	-77	-316	-366	70	70	70
10-Oct-88	73		2	4	2	-1	0	-78	-317	-367	72	72	72
13-Oct-88	76	104	2	4	2	-1	0	-79	-318	-367	77	77	77
17-Oct-88	80		2	4	3	-1	1	-78	-318	-368	94	94	94
18-Oct-88	81		2	4	2	-1	0	-78	-318	-367	100	100	110
19-Oct-88	82		2	4	2	-1	1	-88	-318	-367	105	105	120
20-Oct-88	83		1	4	1	-1	-26	-108	-350	-367	108	108	128
20-Oct-88	83		1	6	1	-9	-32	-114	-353	-370	108	108	128
20-Oct-88	83		0	5	-1	-17	-39	-116	-352	-366	108	108	128
21-Oct-88	84		-10	5	-65	-120	-171	-262	-445	-412	140	160	190
21-Oct-88	84		-10	5	-67	-126	-179	-268	-452	-411	146	166	196
21-Oct-88	84		-10	5	-66	-129	-183	-276	-456	-415	150	170	200
23-Oct-88	86		-12	2	-84	-164	-227	-317	-491	-453	160	180	207
24-Oct-88	87		-13	1	-87	-175	-236	-331	-502	-465	170	190	210
26-Oct-88	89		-14	0	-92	-185	-252	-341	-512	-474	180	200	220
27-Oct-88	90		-14	0	-93	-185	-255	-349	-518	-489	182	202	222
31-Oct-88	94		-13	-3	-97	-193	-267	-357	-523	-493	188	208	228
02-Nov-88	96	117	-16	-2	-98	-214	-290	-358	-525	-522	190	210	230
04-Nov-88	98		-16	-3	-99	-213	-289	-358	-524	-521	200	220	240
07-Nov-88	101		-16	-3	-100	-214	-289	-358	-524	-521	228	250	266
08-Nov-88	102		-15	-4	-99	-213	-289	-358	-524	-518	234	260	272
09-Nov-88	103		-15	-4	-103	-214	-289	-362	-525	-520	240	270	280
10-Nov-88	104		-25	-17	-118	-226	-291	-364	-525	-519	315	330	345
11-Nov-88	105		-34	-29	-130	-239	-290	-364	-525	-508	380	420	420
15-Nov-88	109		-38	-34	-134	-239	-289	-364	-524	-508	410	460	460
16-Nov-88	110		-38	-36	-135	-242	-289	-364	-525	-508	415	465	465
17-Nov-88	111		-38	-37	-135	-242	-289	-364	-525	-508	420	469	469
18-Nov-88	112		-39	-35	-135	-241	-290	-364	-525	-501	424	472	472
22-Nov-88	116	130	-39	-36	-135	-241	-290	-364	-520	-498	460	505	505
28-Nov-88	122		-40	-37	-135	-241	-288	-362	-480	-459	590	635	635
29-Nov-88	123		-41	-40	-135	-241	-285	-347	-463	-445	612	660	660
05-Dec-88	129		-39	-38	-134	-220	-250	-295	-405	-381	675	725	725
06-Dec-88	130		-39	-38	-133	-218	-244	-294	-404	-368	680	730	730
09-Dec-88	133	143	-40	-39	-132	-217	-245	-293	-401	-370	706	760	760
13-Dec-88	137		-39	-37	-111	-187	-204	-251	-346	-308	770	820	830
15-Dec-88	139		-28	-24	-83	-143	-163	-209	-297	-258	870	920	930
20-Dec-88	144	156	-26	-20	-78	-136	-156	-197	-285	-250	900	950	960
21-Dec-88	145		-26	-20	-78	-135	-155	-197	-284	-250	910	950	970
22-Dec-88	146		-26	-20	-78	-135	-154	-194	-283	-247	920	960	980
01-Jan-89	156	169	-8	2	-46	-74	-88	-127	-198	-154	1030	1057	1090
02-Jan-89	157		-10	5	-41	-70	-83	-120	-187	-149	1040	1070	1100
03-Jan-89	158		-10	5	-41	-70	-84	-120	-187	-148	1050	1080	1110
06-Jan-89	161		-12	5	-39	-70	-83	-120	-186	-149	1060	1086	1120
09-Jan-89	164		-9	5	-38	-70	-83	-120	-186	-148	1065	1093	1126
24-Jan-89	179		-8	8	-36	-70	-83	-120	-183	-149	1090	1118	1145
20-Jun-89	326		-4	17	-23	-72	-76	-105	-166	-131	1170	1200	1220

NOTE: Extensometer 78 m from panel edge

TABLE II.3

2 SOUTH A PANEL ANCHOR MOVEMENT RELATIVE TO DATUM PLATE MANUAL RECORDINGS

Date	Days	Goaf Width (m)	ANCHOR DEPTHS (m) Movement (mm) 23.9	26.4	33.9	40.2	48.9	53.8	Surface (W668)
08-Mar-89	0	32	0	0	0	0	0	0	0
05-May-89	58		0	0.5	-0.5	0	0	0	0
08-May-89	61		0	0	0	0	0	0	0
12-May-89	65		0	0.5	-0.5	1	0	-0.5	36
17-May-89	70	55	0	0	-0.5	1	0	0.5	55
22-May-89	75		0	0.5	0	1.5	1	1	85
24-May-89	77		0.5	1.5	1.5	2.5	2.5	6	124
29-May-89	82		2	7	17.5	27	30	45.5	130
02-Jun-89	86		1.5	7	17.5	27	30	45.5	135
08-Jun-89	92		2	8	18.5	28	32	45.5	142
16-Jun-89	100	68	1.5	7	19	27	30.5	48.5	150
19-Jun-89	103		0	5.5	17.5	27.5	35	70.5	270
19-Jun-89	103		-6	-7	-12.5	-18	-34	6.5	390
20-Jun-89	104		-30.5	-33	-44.5	-61	-70	-21.5	410
21-Jun-89	105		-31	-34	-37.5	-63	-72	-27	515
26-Jun-89	110		-31.5	-34.5	-37.5	-63	-72	-30	519
27-Jun-89	111		-32	-34.5	-38.5	-63.5	-72	-30	523
28-Jun-89	112		-32	-35	-38.5	-64	-72.5	-30.5	528
30-Jun-89	114	79	-32	-35	-38.5	-63.5	-71.5	-30	533
03-Jul-89	117		-32	-35	-38.5	-64	-72	-30	537
04-Jul-89	118		-34	-37	-44	-65	-73	-32.5	540
05-Jul-89	119		-42	-45	-46	-66	-65	-51.5	650
06-Jul-89	120		-40	-41.5	-40.5	-55	-52	-56	760
07-Jul-89	121		-40	-41	-39.5	-55	-53	-57	873
10-Jul-89	124		-40	-40.5	-39.5	-54.5	-50	-57.5	886
15-Jul-89	129		-40	-40.5	-39.5	-54.5	-52	-58	902
21-Jul-89	135	92	-40	-41	-39.5	-54	-48	-58.5	920
26-Jul-89	140		-32	-29	-24.5	-35	-29	-46.5	1086
04-Aug-89	149		-32	-28	-23.5	-35	-28	-46	1115
11-Aug-89	156		-32	-28	-23.5	-34	-28	-46	1120
18-Aug-89	163	104	-30	-25.5	-20.5	-31.5	-24	-43.5	1130
24-Aug-89	169		-24.5	-19	-14.5	-25	-18.5	-36.5	1205
29-Aug-89	174		-24	-18	-14.5	-24.5	-18	-36.5	1215
01-Sep-89	177		-24	-18	-14.5	-24.1	-17.5	-37	1220
05-Sep-89	181	116	-24	-18	-14.5	-24.5	-17.5	-37	1225
07-Sep-89	183		-18	-12.5	-8.5	-18	-12	-31.5	1235
11-Sep-89	187		-17	-11	-7.5	-17	-10.5	-30.5	1260
13-Sep-89	189	129	-12.5	-6	-2.5	-12.5	-6	-25.5	1270
15-Sep-89	191		-11.5	-5	-1	-11.5	-5	-24	1270
18-Sep-89	194		-11.5	-4.5	-1	-11	-4.5	-24	1273
22-Sep-89	198		-11	-4.5	-0.5	-11	-4	-23.5	1276
27-Sep-89	203		-10.5	-4	-0.5	-10.5	-4	-23.5	1280
29-Sep-89	205	140	-10.5	-4	-0.5	-10.5	-4	-23.5	1282
24-Jul-90	503		-10	-3	0.5	-10	-3	-22.5	1285

NOTE: Extensometer 70 m from panel edge.

TABLE II.4

1 NORTH ANCHOR MOVEMENTS RELATIVE TO DATUM PLATE

MANUAL READINGS EXTENSOMETER D212

DATE	Days	Goaf Width (m)	ANCHOR DEPTHS 39.0m	46.0m	56.0m	66.8m	74.0m	86.0m	Surface datum plate
			Anchor movements (mm)						
16-Aug-90	0	9	0.0	0.0	0.0	0.0	0.0	0.0	0
17-Aug-90	1		0.0	0.0	0.0	0.0	0.0	0.0	0
20-Aug-90	4		0.0	0.0	0.0	-1.0	0.0	0.0	0
21-Aug-90	5		0.0	0.0	0.0	0.0	0.0	0.0	0
22-Aug-90	6		-4.0	1.0	-2.0	-8.0	-2.0	-6.0	0
07-Sep-90	22		1.0	1.0	-2.0	-8.0	-3.0	-3.0	0
12-Sep-90	27		1.0	1.0	-2.0	-8.0	-3.0	-3.0	0
18-Sep-90	33		1.0	0.0	-2.0	-9.0	-4.0	-4.0	0
24-Sep-90	39		2.0	0.0	-2.0	-9.0	-4.0	-4.0	0
25-Sep-90	40	64	2.0	-1.0	-3.0	-9.0	-4.0	-6.0	0
25-Sep-90	40		2.0	-1.0	-2.0	-9.0	-4.0	-5.0	0
26-Sep-90	41		2.0	0.0	-2.0	-9.0	-4.0	-6.0	0
02-Oct-90	47		2.0	0.0	-2.0	-9.0	-4.0	-6.0	0
16-Oct-90	61		2.0	0.0	-3.0	-11.0	-5.0	-6.0	0
20-Oct-90	65		1.0	0.0	-2.0	-10.0	-5.0	-7.0	0
25-Oct-90	70		2.0	0.0	-5.0	-13.0	-9.0	-14.0	0
31-Oct-90	76		2.0	0.0	-5.0	-14.0	-194.0	-1210.0	-4
01-Nov-90	77		2.0	0.0	-6.0	-14.0	-192.0	-1211.0	-13
02-Nov-90	78	47	-7.0	-10.0	-14.0	-20.0	-204.0	-1470.0	-18
05-Nov-90	81		-7.0	-13.0	-16.0	-21.0	-204.0	-1646.0	-63
06-Nov-90	82		-6.0	-14.0	-18.0	-20.0	-204.0	-1648.0	-68
13-Nov-90	89		-6.0	-13.0	-18.0	-21.0	-204.0	-1648.0	-68
16-Nov-90	92		-6.0	-13.0	-18.0	-21.0	-204.0	-1648.0	-70
20-Nov-90	96		-4.0	-13.0	-18.0	-24.0	-205.0	-1650.0	-74
27-Nov-90	103	64	25.0	-6.0	-17.0	-33.0	-219.0	-1682.0	-186
30-Nov-90	106		25.0	-6.0	-17.0	-33.0	-219.0	-1682.0	-203
05-Dec-90	111		20.0	-6.0	-30.0	-53.0	-243.0	-1706.0	-210
06-Dec-90	112		30.0	-7.0	-31.0	-54.0	-244.0	-1704.0	-211
10-Dec-90	116		29.0	-7.0	-32.0	-55.0	-244.0	-1706.0	-213
18-Dec-90	124		34.0	-6.0	-34.0	-59.0	-250.0	-1712.0	-224
24-Dec-90	130		38.0	-6.0	-39.0	-65.0	-260.0	-1720.0	-268
27-Dec-90	133	82	40.0	-5.0	-38.0	-67.0	-260.0	-1720.0	-273
08-Jan-91	145		43.0	-4.0	-38.0	-71.0	-258.0	-1722.0	-302
15-Jan-91	152		42.0	-3.0	-38.0	-70.0	-260.0	-1720.0	-297
25-Jan-91	162		44.0	-2.0	-38.0	-69.0	-258.0	-1718.0	-292
07-Feb-91	175	99	48.0	0.0	-36.0	-67.0	-256.0	-1718.0	-318
19-Feb-91	187		50.0	2.0	-36.0	-63.0	-256.0	-1716.0	-340
07-Mar-91	203	116	60.0	6.0	-32.0	-61.0	-254.0	-1712.0	-353
19-Mar-91	215		58.0	6.0	-32.0	-65.0	-254.0	-1716.0	-355
16-Apr-91	243	134	64.0	10.0	-28.0	-61.0	-248.0	-1710.0	-355
30-Apr-91	257		64.0	10.0	-28.0	-61.0	-248.0	-1710.0	-379
01-Jul-91	319	171	74.0	18.0	-20.0	-49.0	-240.0	-1700.0	-384
20-Sep-91	400	241	76.0	20.0	-16.0	-45.0	-232.0	-1698.0	-389
05-May-92	628	384	80.0	24.0	-14.0	-45.0	-234.0	-1694.0	-402
23-Sep-92	769	484	82.0	26.0	-12.0	-45.0	-232.0	-1692.0	-403
30-Oct-93	1171	501	84.0	30.0	-2.0	-29.0	-214.0	-1668.0	-410

NOTE: Extensometer is 6 m from panel edge

TABLE II.5

1 NORTH ANCHOR MOVEMENTS RELATIVE TO DATUM PLATE
MANUAL READINGS EXTENSOMETER D213

DATE	Days	Goaf Width (m)	ANCHOR DEPTHS 39.0m	46.0m	56.0m	66.8m	74.0m	86.0m	Surface datum plate
			Anchor movements (mm)						
12-Sep-90	0	9	0.0	0.0	0.0	0.0	0.0	0.0	0
18-Sep-90	6		0.0	0.0	2.0	-1.0	-2.0	-1.0	0
02-Oct-90	20	29	1.0	1.0	0.0	-1.0	-1.0	1.0	0
31-Oct-90	49	47	1.0	0.0	-10.0	1.0	-14.0	-1.0	0
01-Nov-90	50		1.0	-1.0	-4.0	0.0	-15.0	0.0	-10
02-Nov-90	51		1.0	-1.0	-4.0	-1.0	-14.0	0.0	-20
05-Nov-90	54		1.0	-5.0	-11.0	0.0	-14.0	-13.0	-60
06-Nov-90	55		3.0	-5.0	-11.0	0.0	-14.0	-13.0	-60
13-Nov-90	62		2.0	-5.0	-10.0	-1.0	-15.0	-14.0	-61
16-Nov-90	65		2.0	-1.0	-10.0	-1.0	-12.0	-13.0	-62
20-Nov-90	69		2.0	-2.0	-11.0	0.0	-13.0	-11.0	-93
27-Nov-90	76	64	-86.0	-162.0	-181.0	-181.0	-209.0	-424.0	-390
28-Nov-90	77		-176.0	-288.0	-292.0	-319.0	-338.0	-571.0	-430
29-Nov-90	78		-206.0	-334.0	-339.0	-386.0	-388.0	-613.0	-470
30-Nov-90	79		-216.0	-338.0	-348.0	-386.0	-444.0	-620.0	-471
03-Dec-90	82		-223.0	-344.0	-352.0	-392.0	-448.0	-623.0	-477
05-Dec-90	84		-226.0	-346.0	-357.0	-397.0	-418.0	-628.0	-483
06-Dec-90	85		-226.0	-348.0	-360.0	-398.0	-417.0	-628.0	-487
10-Dec-90	89		-226.0	-348.0	-360.0	-393.0	-418.0	-627.0	-491
16-Dec-90	95		-229.0	-352.0	-367.0	-399.0	-429.0	-634.0	-504
24-Dec-90	103		-241.0	-362.0	-379.0	-413.0	-442.0	-592.0	-780
27-Dec-90	106	82	-240.0	-354.0	-376.0	-413.0	-440.0	-558.0	-831
08-Jan-91	118		-240.0	-338.0	-370.0	-413.0	-440.0	-518.0	-888
15-Jan-91	125		-242.0	-336.0	-364.0	-413.0	-434.0	-514.0	-890
25-Jan-91	135		-242.0	-336.0	-364.0	-409.0	-433.0	-510.0	-891
06-Feb-91	147	99	-230.0	-268.0	-266.0	-327.0	-342.0	-346.0	-1052
19-Feb-91	160		-208.0	-234.0	-236.0	-261.0	-272.0	-268.0	-1151
07-Mar-91	176	116	-172.0	-194.0	-186.0	-201.0	-212.0	-180.0	-1160
19-Mar-91	188		-164.0	-184.0	-172.0	-185.0	-198.0	-162.0	-1256
19-Apr-91	219	134	-132.0	-152.0	-136.0	-147.0	-160.0	-128.0	-1256
30-Apr-91	230		-126.0	-148.0	-130.0	-139.0	-152.0	-120.0	-1323
01-Jul-91	292	171	-96.0	-126.0	-112.0	-123.0	-134.0	-86.0	-1360
20-Sep-91	373	241	-82.0	-126.0	-100.0	-121.0	-128.0	-66.0	-1380
05-May-92	601	384	-40.0	-66.0	-52.0	-55.0	-68.0	-24.0	-1420
23-Sep-92	742	484	-40.0	-66.0	-50.0	-57.0	-68.0	-26.0	-1397
30-Oct-93	1144	501	-34.0	-58.0	-40.0	-49.0	-58.0	-8.0	-1418

NOTE : Extensometer is 45 m from panel edge.

TABLE II.6 D212 EXTENSOMETER ANCHOR MOVEMENTS (AUTOMATIC RECORDINGS)

DATE	TIME	Hours from	CHANGE IN ANCHOR POSITION RELATIVE TO DATUM PLATE						Surface Subs.
1990		1.38pm 15/8/90	39.0m	46.0m	56.0m	66.8m	74.0m	86.0m	(mm)
15-Aug	03:38 PM	2	0.00	0.00	0.00	0.00	0.00	0.00	0
	07:38 PM	6	0.06	0.28	-1.00	0.32	0.72	0.76	0
	11:38 PM	10	-0.30	1.04	-1.04	0.36	0.88	0.88	0
	03:38 AM	14	-0.58	1.72	-1.12	0.32	0.80	0.84	0
	07:38 AM	18	-0.18	1.84	-1.12	0.16	0.52	0.48	0
	11:38 AM	22	-0.18	2.68	0.12	-0.08	0.12	0.08	0
	03:38 PM	26	-0.14	2.36	0.16	-0.72	0.28	0.24	0
	07:38 PM	30	-0.38	2.56	-0.04	-0.56	0.60	0.56	0
	11:38 PM	34	-0.70	1.76	-0.32	-0.44	0.88	0.92	0
	03:38 AM	38	-2.34	2.04	-0.08	-0.08	1.32	1.36	0
	07:38 AM	42	-3.66	1.64	0.12	-0.20	1.00	1.12	0
	11:38 AM	46	-0.26	1.84	0.76	-0.32	0.00	0.04	0
	03:38 PM	50	0.02	1.72	0.72	-0.40	0.32	0.44	0
	07:38 PM	54	0.02	2.00	-0.12	-0.08	0.80	0.96	0
	11:38 PM	58	0.22	2.28	-0.56	-0.08	0.76	0.96	0
	03:38 AM	62	0.30	2.04	-0.56	-0.04	0.68	1.00	0
	07:38 AM	66	-1.26	2.00	-1.16	-0.84	0.04	0.16	0
	11:38 AM	70	0.18	1.84	0.72	-0.20	0.60	0.72	0
	03:38 PM	74	0.30	1.68	0.68	-0.08	0.88	1.04	0
	07:38 PM	78	0.62	2.00	1.08	0.36	1.32	1.48	0
	11:38 PM	82	0.26	2.28	0.84	0.08	1.08	1.24	0
	03:38 AM	86	0.14	2.04	0.80	0.20	1.24	1.40	0
	07:38 AM	90	0.46	2.00	0.28	0.36	1.40	1.56	0
	11:38 AM	94	0.46	1.84	1.48	0.08	0.92	1.04	0
	03:38 PM	98	0.54	1.68	1.56	0.16	1.00	1.12	0
	07:38 PM	102	0.74	1.36	1.24	0.40	1.52	1.68	0
	11:38 PM	106	0.74	1.56	1.04	0.40	1.48	1.72	0
	03:38 AM	110	0.74	1.76	1.00	0.44	1.56	1.80	0
	07:38 AM	114	-0.50	2.04	0.20	0.36	1.44	1.60	0
	11:38 AM	118	0.06	1.64	1.16	-1.16	-0.52	-0.44	0
	03:38 PM	122	0.10	1.32	1.16	-1.04	-0.04	0.08	0
	07:38 PM	126	0.50	0.96	1.44	-1.44	0.48	-0.28	0
	11:38 PM	130	0.14	1.12	0.72	-1.08	-0.08	0.08	0
	03:38 AM	134	-0.30	1.12	0.76	-1.16	-0.08	0.08	0
	07:38 AM	138	-0.38	0.52	0.84	-1.76	0.16	0.28	0
	11:38 AM	142	0.34	1.24	0.32	-2.40	-1.08	-1.04	0
	03:38 PM	146	0.50	1.24	0.44	-2.88	-0.84	-0.76	0
	07:38 PM	150	0.54	0.44	0.52	-2.52	-0.48	-0.40	0
	11:38 PM	154	0.70	0.72	-0.12	-4.00	-0.04	0.00	0
	03:38 AM	158	0.66	1.00	0.00	-3.72	0.24	-0.60	0
	07:38 AM	162	0.58	0.84	0.08	-3.64	0.32	-0.52	0
	11:38 AM	166	0.70	1.12	0.72	-3.08	0.40	0.00	0

05-Sep	10:38 AM	501	0.30	0.84	0.20	-4.32	-0.80	-0.28	0
	02:38 PM	505	-0.30	0.96	1.24	-3.88	-0.32	0.24	0
	06:38 PM	509	0.18	1.08	0.88	-2.80	-0.08	0.64	0
	10:38 PM	513	0.26	0.96	0.92	-2.56	0.16	0.88	0
	02:38 AM	517	0.26	0.84	0.80	-2.36	0.40	1.12	0
	06:38 AM	521	0.02	0.76	0.52	-2.92	-0.08	0.60	0
	10:38 AM	525	-0.54	2.36	0.08	-4.20	-0.64	-0.12	0
	02:38 PM	529	-0.42	2.60	1.04	-3.80	-0.16	0.36	0
	06:38 PM	533	-0.10	3.32	0.60	-3.08	-0.36	0.24	0
	10:38 PM	537	0.06	1.84	0.72	-2.76	-0.08	0.52	0
	02:38 AM	541	-0.06	1.76	0.64	-2.92	-0.24	0.36	0
	06:38 AM	545	-0.06	1.76	0.60	-2.96	-0.24	0.36	0
	10:38 AM	549	-0.46	2.72	0.24	-3.84	-1.12	-0.56	0
12-Sep	01:38 PM	672	-0.72	2.88	-0.15	-3.12	-0.67	-0.22	0
	03:38 PM	674	-0.80	2.72	-0.46	-3.12	-0.68	-0.20	0
	07:38 PM	678	-0.38	2.32	-0.58	-2.68	0.08	0.60	0
	11:38 PM	682	-0.26	2.20	-0.44	-2.36	0.08	0.52	0
	03:38 AM	686	-0.18	1.48	-0.32	-2.24	-0.32	0.12	0
	07:38 AM	690	-0.26	1.32	-0.36	-2.36	-0.44	-0.04	0
	11:38 AM	694	-0.86	2.64	-1.04	-3.84	-0.96	-0.52	0
	03:38 PM	698	-0.70	2.92	-0.08	-3.00	-0.88	-0.68	0
	07:38 PM	702	-0.18	2.68	0.08	-2.96	0.16	0.40	0
	11:38 PM	706	-0.06	2.16	-0.28	-2.52	0.48	0.40	0
	03:38 AM	710	-0.10	2.12	-0.28	-2.56	0.32	0.44	0
	07:38 AM	714	-0.14	1.60	-0.32	-2.52	-0.28	-0.08	0
	11:38 AM	718	-0.90	2.36	-0.24	-4.04	-0.84	-0.68	0
	03:38 PM	722	-0.78	2.36	-0.08	-3.24	-1.04	-0.80	0
	07:38 PM	726	-0.42	2.16	0.28	-2.32	-0.08	0.12	0
	11:38 PM	730	-0.30	2.12	0.24	-3.08	0.08	0.32	0
	03:38 AM	734	-0.30	1.96	-0.44	-3.00	0.16	0.40	0
	07:38 AM	738	-0.26	1.48	-0.44	-2.96	0.24	0.48	0
	11:38 AM	742	-0.42	1.44	-0.60	-3.24	-0.04	0.20	0
	03:38 PM	746	-0.46	1.52	-0.64	-3.20	0.00	0.20	0
	07:38 PM	750	-0.26	1.64	-0.44	-2.60	0.36	0.36	0
	11:38 PM	754	-0.06	1.68	-0.28	-2.36	-0.16	0.12	0
	03:38 AM	758	-0.18	1.36	-0.36	-2.44	-0.24	0.04	0
	07:38 AM	762	-0.30	1.28	-0.40	-2.56	-0.32	-0.08	0
	11:38 AM	766	-0.50	2.52	-0.72	-3.12	-0.84	-0.68	0
	03:38 PM	770	-0.70	3.04	1.12	-3.36	-0.60	-0.12	0
	07:38 PM	774	-0.34	3.24	1.48	-2.60	-0.16	0.36	0
	11:38 PM	778	-0.26	2.80	1.56	-2.36	-0.24	-0.04	0
	03:38 AM	782	-0.34	2.40	1.56	-2.36	-0.32	-0.08	0
	07:38 AM	786	-0.42	2.44	1.52	-2.44	-0.44	-0.20	0
	11:38 AM	790	-0.74	3.24	1.08	-3.44	-1.20	-0.16	0
	03:38 PM	794	-0.38	3.12	1.48	-2.52	-0.40	-0.16	0
	07:38 PM	798	-0.34	3.12	1.52	-2.48	-0.36	-0.16	0

11:38 PM	802	-0.38	3.08	1.48	-2.52	-0.40	-0.20	0
03:38 AM	806	-0.34	3.08	1.52	-2.48	-0.36	-0.12	0
07:38 AM	810	-0.30	3.08	1.56	-2.44	-0.28	-0.08	0
11:38 AM	814	-0.58	3.04	1.28	-3.04	-0.88	-0.72	0
03:38 PM	818	-0.54	2.92	1.32	-3.04	-0.84	-0.24	0
07:38 PM	822	-0.38	2.68	1.48	-2.52	-0.40	-0.20	0
11:38 PM	826	-0.34	2.60	1.56	-2.44	-0.32	-0.12	0
03:38 AM	830	-0.30	2.52	1.56	-2.44	-0.32	-0.08	0
07:38 AM	834	-0.38	2.36	1.48	-2.56	-0.40	-0.20	0
11:38 AM	838	-0.50	2.52	1.32	-2.88	-0.72	-0.52	0
03:38 PM	842	-0.74	2.36	1.12	-3.28	-1.12	-0.28	0
07:38 PM	846	-0.30	2.92	1.56	-2.40	-0.28	-0.04	0
11:38 PM	850	-0.22	2.68	1.64	-2.04	0.12	0.28	0
03:38 AM	854	-0.10	1.96	1.00	-2.64	0.32	0.56	0
07:38 AM	858	-0.34	2.12	0.80	-3.08	-0.08	0.12	0
11:38 AM	862	-0.78	2.44	1.16	-3.20	-1.00	-0.88	0
03:38 PM	866	-0.98	1.32	0.88	-3.76	-1.56	-1.40	0
07:38 PM	870	-0.46	1.52	1.52	-2.40	-0.24	-0.04	0
11:38 PM	874	-0.38	0.88	0.72	-2.32	-0.12	0.12	0
03:38 AM	878	-0.46	0.92	0.68	-2.44	-0.24	-0.04	0
07:38 AM	882	-0.50	1.12	0.60	-2.56	-0.36	-0.16	0
11:38 AM	886	-0.90	1.92	1.08	-3.36	-1.16	-1.00	0
03:38 PM	890	-0.86	1.36	1.08	-3.44	-1.28	-0.84	0
07:38 PM	894	-0.54	1.52	1.40	-2.60	-0.48	-0.28	0
11:38 PM	898	-0.42	1.48	1.56	-2.36	-0.20	0.00	0
03:38 AM	902	-0.46	1.36	1.48	-2.48	-0.28	-0.04	0
07:38 AM	906	-0.50	1.36	1.48	-2.56	-0.44	-0.20	0
11:38 AM	910	-0.86	2.12	1.08	-3.36	-1.16	-0.96	0
03:38 PM	914	-0.78	2.36	1.20	-3.08	-0.92	-0.72	0
07:38 PM	918	-0.50	2.04	1.48	-2.52	-0.40	-0.16	0
11:38 PM	922	-0.30	2.68	0.80	-2.16	-0.04	0.20	0
03:38 AM	926	-0.30	2.52	0.84	-2.12	0.00	0.24	0
07:38 AM	930	-0.42	2.44	0.72	-2.40	-0.28	-0.04	0
11:38 AM	934	-0.90	2.40	1.08	-3.44	-1.20	-1.00	0
03:38 PM	938	-0.70	2.56	1.24	-3.08	-0.92	-0.76	0
07:38 PM	942	-0.58	2.24	1.40	-2.64	-0.56	-0.32	0
11:38 PM	946	-0.66	2.16	1.32	-2.76	-0.64	-0.44	0
03:38 AM	950	-0.46	2.32	1.52	-2.48	-0.32	-0.12	0
07:38 AM	954	-0.42	2.24	1.44	-2.40	-0.24	-0.04	0
11:38 AM	958	-0.78	2.60	1.16	-3.00	-0.84	-0.68	0
03:38 PM	962	-0.86	2.44	1.12	-3.32	-1.16	-1.00	0
07:38 PM	966	-0.34	2.68	0.76	-2.36	-0.08	0.12	0
11:38 PM	970	-0.26	3.00	0.88	-2.96	-0.60	-0.12	0
03:38 AM	974	-0.26	3.00	0.84	-2.96	-0.84	-0.32	0
07:38 AM	978	-0.42	3.40	0.68	-3.32	-1.16	-0.44	0
11:38 AM	982	-0.66	2.72	0.40	-2.72	-0.60	-0.76	0

	03:38 PM	986	-0.90	2.52	0.16	-3.44	-1.28	-1.44	0
	07:38 PM	990	-0.54	2.08	0.24	-2.56	-1.28	-1.08	0
	11:38 PM	994	-0.38	2.32	-0.16	-3.16	-1.00	-0.80	0
	03:38 AM	998	-0.30	1.40	-0.04	-3.04	-0.88	-1.52	0
	07:38 AM	1002	-0.46	1.32	-0.12	-3.20	-1.04	-1.68	0
	11:38 AM	1006	-0.94	2.08	-0.76	-3.76	-2.16	-2.00	0
	03:38 PM	1010	-1.06	2.00	-0.04	-4.04	-2.64	-2.64	0
	07:38 PM	1014	-0.50	2.20	-0.36	-2.84	-1.48	-1.36	0
	11:38 PM	1018	-0.34	0.60	-0.20	-3.32	-1.08	-1.84	0
	03:38 AM	1022	-0.38	0.60	-0.24	-3.36	-1.12	-1.80	0
	07:38 AM	1026	-0.38	0.60	-0.24	-3.40	-1.28	-1.84	0
	11:38 AM	1030	-0.94	1.04	-0.24	-4.00	-2.52	-2.48	0
	03:38 PM	1034	-0.82	1.04	0.20	-4.32	-2.40	-3.00	0
	07:38 PM	1038	-0.50	0.76	-0.40	-3.12	-1.68	-1.60	0
	11:38 PM	1042	-0.26	0.08	-0.16	-3.60	-1.24	-2.04	0
	03:38 AM	1046	-0.22	-0.84	-0.08	-3.56	-1.20	-1.96	0
	07:38 AM	1050	-0.38	-0.88	-0.32	-3.60	-1.36	-2.04	0
	11:38 AM	1054	-1.14	0.20	-0.24	-4.40	-2.92	-2.92	0
	03:38 PM	1058	-1.10	-0.12	-0.16	-3.60	-2.52	-2.92	0
	07:38 PM	1062	-0.46	-0.28	0.56	-3.56	-1.88	-1.80	0
	11:38 PM	1066	-0.38	-0.88	-0.36	-3.84	-1.36	-2.16	0
	03:38 AM	1070	-0.34	-1.60	-0.20	-3.56	-1.16	-1.88	0
	07:38 AM	1074	-0.46	-1.72	-0.28	-3.84	-1.56	-2.16	0
	11:38 AM	1078	-1.26	-0.56	-0.36	-4.52	-2.96	-2.92	0
	03:38 PM	1082	-1.26	-0.56	-0.36	-4.36	-2.32	-2.88	0
	07:38 PM	1086	-0.74	0.72	0.20	-3.44	-1.96	-1.96	0
	11:38 PM	1090	-0.66	0.24	-0.60	-3.20	-1.68	-1.68	0
	03:38 AM	1094	-0.70	0.12	-0.60	-3.24	-1.60	-1.80	0
	07:38 AM	1098	-0.70	0.08	-0.60	-3.32	-1.60	-2.44	0
	11:38 AM	1102	-1.14	0.92	-1.04	-4.08	-2.36	-2.36	0
	03:38 PM	1106	-1.10	1.24	-0.96	-3.80	-2.24	-2.24	0
	07:38 PM	1110	-0.86	1.28	-0.72	-3.24	-1.76	-1.72	0
	11:38 PM	1114	-0.82	1.56	-0.68	-3.24	-1.64	-2.28	0
	03:38 AM	1118	-0.70	1.52	-0.56	-3.52	-1.44	-2.28	0
	07:38 AM	1122	-0.78	1.32	-0.60	-3.84	-1.52	-2.36	0
	11:38 AM	1126	-0.94	1.44	-0.80	-4.24	-1.92	-2.80	0
	03:38 PM	1130	-0.90	1.52	-0.72	-4.20	-1.88	-2.72	0
	07:38 PM	1134	-0.78	1.56	-0.64	-3.92	-1.64	-2.48	0
	11:38 PM	1138	-0.74	1.60	-0.60	-3.80	-1.52	-2.36	0
	03:38 AM	1142	-0.82	1.52	-0.68	-3.92	-1.60	-2.44	0
	07:38 AM	1146	-0.86	1.48	-0.68	-3.96	-1.68	-2.52	0
	11:38 AM	1150	-1.02	1.60	-0.78	-4.44	-2.08	-2.40	0
25-Oct	04:38 PM	1707	-1.10	-0.56	-0.96	-4.32	-2.12	-1.76	0
	08:38 PM	1711	-1.14	-0.12	-0.56	-3.64	-1.44	-1.00	0
	12:38 AM	1715	-1.06	-0.52	-1.28	-3.44	-1.36	-0.80	0
	04:38 AM	1719	-1.02	-0.56	-1.24	-3.36	-2.00	-0.68	0

	08:38 AM	1723	-1.18	-0.60	-1.40	-3.72	-2.36	-1.08	0
	12:38 PM	1727	-1.54	0.84	-1.04	-4.24	-2.88	-1.72	0
	04:38 PM	1731	-1.66	0.52	-1.00	-4.40	-2.16	-1.84	0
	08:38 PM	1735	-1.06	0.56	-1.24	-3.32	-1.96	-0.64	0
	12:38 AM	1739	-0.78	-2.36	-1.20	-3.72	-1.52	-0.92	0
	04:38 AM	1743	-0.62	-3.04	-1.88	-3.72	-2.20	-0.72	0
	08:38 AM	1747	-1.14	-2.00	-2.20	-4.60	-3.04	-1.68	0
	12:38 PM	1751	-1.66	-2.64	-1.92	-5.28	-2.96	-1.68	0
	04:38 PM	1755	-1.66	-3.60	-2.04	-5.20	-2.96	-1.68	0
	08:38 PM	1759	-1.10	-2.60	-1.44	-4.16	-1.88	-1.32	0
	12:38 AM	1763	-1.02	-2.64	-1.36	-3.92	-1.68	-1.12	0
	04:38 AM	1767	-1.14	-2.76	-1.48	-4.16	-1.84	-1.36	0
	08:38 AM	1771	-1.34	-2.44	-1.68	-4.48	-2.28	-1.80	0
	12:38 PM	1775	-1.58	-1.12	-1.88	-5.00	-2.80	-1.52	0
	04:38 PM	1779	-1.58	-1.56	-1.92	-5.04	-2.88	-1.60	0
	08:38 PM	1783	-1.18	-1.68	-1.48	-4.12	-1.88	-1.00	0
	12:38 AM	1787	-1.22	-1.48	-1.52	-4.04	-1.80	-1.28	0
	04:38 AM	1791	-1.22	-1.48	-1.52	-4.08	-1.88	-1.32	0
	08:38 AM	1795	-1.34	-0.56	-1.64	-4.40	-2.20	-1.72	0
	12:38 PM	1799	-1.34	-0.28	-1.64	-4.40	-2.24	-1.76	0
	04:38 PM	1803	-1.34	0.04	-1.64	-4.44	-2.24	-1.80	0
	08:38 PM	1807	-1.14	-0.28	-1.48	-3.88	-1.68	-1.16	0
	10:38 PM	1809	-1.18	-0.48	-2.36	-3.84	-2.56	-1.16	0
	12:38 AM	1811	-1.18	-0.48	-2.36	-3.84	-2.52	-79.88	0
	02:38 AM	1813	-1.22	-0.48	-2.40	-3.96	-2.64	-80.04	0
	04:38 AM	1815	-1.34	0.56	-2.32	-4.24	-2.96	-80.52	0
	06:38 AM	1817	-1.50	0.28	-1.76	-4.64	-2.48	-81.08	0
	08:38 AM	1819	-1.62	-0.64	-1.96	-5.12	-2.92	-80.80	0
	10:38 AM	1821	-1.78	-1.28	-2.16	-5.36	-3.16	-81.16	0
	12:38 PM	1823	-1.82	-0.96	-2.08	-5.12	-2.92	-80.84	0
	02:38 PM	1825	-1.50	-1.80	-1.80	-4.60	-2.36	-80.00	0
	04:38 PM	1827	-1.30	-2.64	-1.60	-4.20	-1.96	-80.36	0
	06:38 PM	1829	-1.22	-2.88	-1.64	-4.08	-1.92	-80.12	0
	08:38 PM	1831	-1.22	-2.84	-2.32	-4.00	-2.60	-80.04	0
	10:38 PM	1833	-1.22	-2.88	-2.20	-4.12	-2.72	-80.16	0
	12:38 AM	1835	-1.30	-3.80	-2.48	-4.24	-217.48	-1224.24	-1
	02:38 AM	1837	-1.42	-3.24	-2.60	-4.04	-218.28	-1226.24	-3
	04:38 AM	1839	-1.46	-3.12	-2.64	-4.00	-218.28	-1226.24	-5
	06:38 AM	1841	-1.54	-2.28	-2.72	-3.96	-218.68	-1227.84	-7
31-Oct	03:38 PM	1850	-1.48	-1.52	-3.60	-3.88	-218.68	-1227.84	-13
	07:38 PM	1854	-1.42	-1.52	-3.44	-3.60	-217.88	-1225.84	-13
	11:38 PM	1858	-1.34	-2.20	-3.40	-3.48	-217.88	-1225.44	-13
	03:38 AM	1862	-1.42	-2.28	-3.48	-3.56	-219.08	-1226.24	-13
	07:38 AM	1866	-1.46	-2.32	-3.48	-3.68	-218.28	-1226.64	-13
	11:38 AM	1870	-1.58	-2.04	-4.56	-3.96	-218.68	-1228.64	-13
	03:38 PM	1874	-1.66	-2.08	-4.60	-4.04	-219.08	-1229.84	-13

	07:38 PM	1878	-1.34	-2.52	-5.16	-4.32	-217.88	-1225.84	-13
	11:38 PM	1882	-2.18	-2.84	-5.08	-4.12	-217.48	-1225.84	-13
	03:38 AM	1886	-2.18	-3.88	-5.16	-4.92	-217.48	-1225.44	-13
	07:38 AM	1890	-10.70	-11.28	-13.88	-11.96	-227.48	-1619.84	-15
	11:38 AM	1894	-11.02	-11.00	-13.40	-11.92	-229.08	-1676.64	-17
	03:38 PM	1898	-10.90	-12.56	-13.36	-12.12	-226.68	-1679.04	-21
	07:38 PM	1902	-10.50	-12.68	-12.92	-11.00	-227.08	-1669.84	-25
	11:38 PM	1906	-10.46	-12.68	-12.92	-10.64	-226.68	-1667.04	-28
	03:38 AM	1910	-10.50	-12.96	-12.96	-10.44	-226.68	-1666.64	-31
	07:38 AM	1914	-10.94	-12.28	-13.40	-11.24	-227.88	-1671.84	-34
	11:38 AM	1918	-11.38	-13.24	-13.88	-12.00	-229.08	-1678.24	-37
	03:38 PM	1922	-11.42	-13.44	-13.96	-12.68	-230.28	-1684.24	-42
	07:38 PM	1926	-10.58	-12.40	-13.08	-11.08	-227.08	-1670.64	-45
	11:38 PM	1930	-10.38	-11.80	-12.88	-10.68	-226.68	-1668.64	-49
	03:38 AM	1934	-10.38	-11.76	-12.84	-10.36	-226.28	-1666.64	-53
	07:38 AM	1938	-10.74	-10.80	-13.20	-11.12	-227.48	-1672.24	-56
	11:38 AM	1942	-11.30	-12.32	-13.76	-11.88	-229.08	-1678.64	-59
	03:38 PM	1946	-11.30	-12.60	-13.72	-11.84	-229.08	-1678.24	-62
	07:38 PM	1950	-10.86	-11.20	-13.40	-11.04	-227.48	-1671.84	-64
	11:38 PM	1954	-10.62	-12.08	-13.92	-10.64	-226.68	-1669.44	-65
	03:38 AM	1958	-10.58	-11.60	-13.80	-10.36	-226.28	-1668.24	-66
	07:38 AM	1962	-10.74	-10.72	-14.00	-10.88	-227.08	-1672.24	-66
	11:38 AM	1966	-11.30	-12.60	-14.60	-11.80	-229.88	-1680.64	-66
	03:38 PM	1970	-11.26	-12.32	-14.56	-11.92	-229.88	-1682.24	-66
	07:38 PM	1974	-10.74	-12.52	-14.00	-10.84	-227.88	-1672.24	-66
	11:38 PM	1978	-10.62	-11.76	-13.84	-10.88	-227.08	-1669.44	-66
	03:38 AM	1982	-10.54	-12.32	-13.80	-11.00	-226.68	-1667.04	-66
	07:38 AM	1986	-10.98	-11.52	-14.28	-11.84	-228.28	-1674.24	-66
	11:38 AM	1990	-11.38	-13.84	-14.84	-12.68	-229.88	-1681.44	-66
06-Nov	03:38 PM	1994	-11.18	-14.28	-14.96	-13.28	-231.08	-1686.24	-66
	07:38 PM	1998	-10.98	-13.04	-14.32	-11.96	-228.28	-1675.84	-66
	11:38 PM	2002	-10.82	-13.72	-14.12	-11.48	-227.48	-1671.84	-66
	03:38 AM	2006	-10.78	-14.04	-14.08	-11.48	-228.28	-1672.64	-67
	07:38 AM	2010	-10.94	-13.20	-14.24	-11.88	-228.28	-1675.44	-67
	11:38 AM	2014	-11.34	-12.76	-14.68	-12.44	-229.48	-1680.24	-67
	03:38 PM	2018	-11.50	-13.32	-14.84	-12.92	-230.28	-1684.24	-67
	07:38 PM	2022	-10.98	-12.68	-14.32	-11.84	-228.28	-1675.04	-67
	11:38 PM	2026	-10.74	-12.32	-14.00	-11.40	-227.48	-1671.44	-67
	03:38 AM	2030	-10.66	-13.12	-14.00	-11.12	-227.08	-1669.04	-67
	07:38 AM	2034	-10.78	-12.44	-14.28	-11.52	-227.88	-1672.64	-67
	11:38 AM	2038	-11.42	-13.88	-14.84	-12.52	-229.88	-1680.64	-67
	03:38 PM	2042	-11.66	-13.60	-15.08	-13.48	-231.88	-1688.64	-67
	07:38 PM	2046	-11.02	-12.60	-14.44	-12.24	-229.08	-1678.24	-67
	11:38 PM	2050	-10.66	-13.60	-14.88	-11.64	-228.28	-1673.44	-68
	03:38 AM	2054	-10.50	-13.72	-14.72	-11.28	-228.28	-1670.64	-68
	07:38 AM	2058	-10.78	-13.60	-14.96	-11.64	-228.68	-1673.04	-68

	11:38 AM	2062	-11.42	-13.44	-15.64	-12.64	-230.68	-1681.84	-68
	03:38 PM	2066	-11.78	-14.16	-16.00	-13.52	-232.28	-1688.64	-68
	07:38 PM	2070	-11.02	-13.48	-14.68	-12.44	-230.28	-1679.84	-68
	11:38 PM	2074	-10.82	-13.68	-15.00	-12.00	-229.48	-1675.84	-68
	03:38 AM	2078	-10.74	-14.08	-15.00	-11.96	-230.68	-1675.84	-68
	07:38 AM	2082	-10.70	-13.96	-14.92	-12.00	-229.48	-1675.84	-68
	11:38 AM	2086	-11.38	-13.92	-15.64	-13.20	-231.08	-1683.44	-68
	03:38 PM	2090	-11.90	-15.96	-16.16	-14.12	-233.48	-1691.84	-68
	07:38 PM	2094	-10.82	-14.68	-15.16	-12.64	-230.68	-1680.24	-68
	11:38 PM	2098	-10.34	-14.20	-14.68	-11.76	-229.08	-1673.44	-68
	03:38 AM	2102	-10.22	-14.32	-14.60	-11.52	-228.68	-1671.84	-68
	07:38 AM	2106	-10.42	-14.36	-14.84	-12.04	-229.48	-1675.44	-68
	11:38 AM	2110	-11.98	-16.12	-16.36	-13.52	-232.28	-1687.84	-68
	03:38 PM	2114	-11.94	-16.44	-16.28	-14.20	-233.48	-1693.44	-69
	07:38 PM	2118	-10.78	-15.16	-15.16	-12.68	-230.68	-1681.04	-69
	11:38 PM	2122	-10.22	-14.16	-14.56	-11.96	-229.48	-1674.64	-69
	03:38 AM	2126	-10.18	-14.08	-14.48	-11.96	-229.48	-1675.04	-69
	07:38 AM	2130	-10.34	-13.96	-14.64	-12.32	-229.88	-1677.84	-69
	11:38 AM	2134	-10.42	-13.52	-14.68	-12.32	-229.88	-1679.04	-69
	03:38 PM	2138	-10.74	-13.52	-15.08	-12.84	-231.08	-1683.84	-69
	07:38 PM	2142	-10.26	-12.56	-14.48	-11.68	-228.68	-1674.64	-69
	11:38 PM	2146	-10.14	-12.24	-14.60	-12.04	-228.28	-1671.04	-69
	03:38 AM	2150	-9.74	-12.64	-15.12	-11.80	-227.48	-1668.64	-69
	07:38 AM	2154	-9.98	-12.12	-15.40	-12.36	-228.28	-1673.04	-69
	11:38 AM	2158	-10.50	-12.12	-15.88	-13.16	-229.88	-1680.24	-69
13-Nov	03:38 PM	2162	-10.40	-13.52	-15.96	-13.32	-230.68	-1681.44	-69
	07:38 PM	2166	-10.30	-12.44	-15.56	-12.60	-229.08	-1675.44	-69
	11:38 PM	2170	-10.22	-13.80	-15.52	-12.36	-229.08	-1672.64	-70
	03:38 AM	2174	-10.10	-13.20	-15.44	-12.00	-228.68	-1670.64	-70
	07:38 AM	2178	-10.62	-11.24	-15.96	-12.80	-230.28	-1677.04	-70
	11:38 AM	2182	-11.06	-13.48	-16.36	-13.68	-231.88	-1683.84	-70
	03:38 PM	2186	-11.26	-15.12	-16.68	-13.80	-232.28	-1685.04	-70
	07:38 PM	2190	-10.74	-14.64	-16.12	-12.80	-229.88	-1677.04	-70
	11:38 PM	2194	-10.54	-14.40	-15.84	-12.44	-229.48	-1673.84	-70
	03:38 AM	2198	-10.38	-14.52	-15.88	-12.24	-229.08	-1671.84	-70
	07:38 AM	2202	-10.82	-13.04	-16.32	-13.04	-230.68	-1678.24	-70
	11:38 AM	2206	-11.26	-15.20	-16.72	-13.84	-231.88	-1684.64	-70
	03:38 PM	2210	-11.22	-15.96	-16.64	-13.72	-231.88	-1684.24	-70
	07:38 PM	2214	-10.94	-15.64	-16.36	-13.16	-230.68	-1679.84	-70
	11:38 PM	2218	-10.66	-15.76	-16.04	-12.68	-229.88	-1675.84	-70
	03:38 AM	2222	-10.70	-15.80	-16.08	-12.76	-230.68	-1676.64	-70
	07:38 AM	2226	-10.66	-15.72	-16.08	-12.80	-229.88	-1677.04	-70
	11:38 AM	2230	-11.26	-13.56	-16.68	-13.80	-231.88	-1685.04	-70
	03:38 PM	2234	-11.94	-15.56	-17.40	-14.16	-232.68	-1687.84	-70
	07:38 PM	2238	-10.90	-14.44	-16.24	-12.88	-230.28	-1677.04	-70
	11:38 PM	2242	-10.90	-13.80	-16.28	-12.76	-229.88	-1675.84	-70

	03:38 AM	2246	-11.02	-13.88	-16.36	-12.84	-231.48	-1676.64	-70
	07:38 AM	2250	-10.94	-13.28	-16.32	-12.96	-230.28	-1677.84	-70
	11:38 AM	2254	-11.14	-12.92	-16.56	-13.32	-231.08	-1681.44	-72
	03:38 PM	2258	-11.78	-14.28	-17.20	-13.80	-231.88	-1685.04	-72
	07:38 PM	2262	-11.38	-14.08	-16.76	-12.84	-230.28	-1677.04	-72
	11:38 PM	2266	-11.42	-14.12	-16.80	-12.68	-230.68	-1676.24	-72
	03:38 AM	2270	-11.18	-14.60	-16.52	-12.36	-229.08	-1673.44	-72
	07:38 AM	2274	-11.54	-14.32	-16.92	-13.16	-230.68	-1679.84	-72
	11:38 AM	2278	-11.78	-14.08	-17.16	-13.56	-231.88	-1683.44	-72
	03:38 PM	2282	-11.82	-13.44	-17.16	-13.52	-231.48	-1683.04	-72
	07:38 PM	2286	-11.46	-13.88	-16.76	-12.92	-230.28	-1677.84	-72
	11:38 PM	2290	-11.54	-13.92	-16.80	-12.92	-231.48	-1678.24	-72
	03:38 AM	2294	-11.38	-13.68	-16.68	-12.76	-229.88	-1676.64	-73
	07:38 AM	2298	-11.54	-13.88	-16.84	-13.08	-230.68	-1679.04	-73
	11:38 AM	2302	-11.70	-13.16	-17.00	-13.44	-231.08	-1682.24	-73
	03:38 PM	2306	-11.86	-13.48	-17.20	-13.68	-231.88	-1683.84	-73
	07:38 PM	2310	-11.34	-14.08	-16.64	-12.72	-229.88	-1678.64	-73
	11:38 PM	2314	-11.22	-13.76	-16.52	-12.40	-229.48	-1676.24	-73
	03:38 AM	2318	-11.30	-13.76	-16.60	-12.56	-229.48	-1677.84	-73
	07:38 AM	2322	-11.50	-13.76	-16.80	-12.96	-230.28	-1681.04	-73
	11:38 AM	2326	-11.62	-13.88	-16.92	-13.28	-231.08	-1683.44	-73
20-Nov	03:38 PM	2330	-11.56	-14.76	-17.16	-13.60	-231.88	-1686.64	-73
	07:38 PM	2334	-11.46	-13.68	-16.76	-12.88	-230.28	-1680.24	-73
	11:38 PM	2338	-11.30	-13.88	-16.56	-12.60	-229.88	-1678.64	-73
	03:38 AM	2342	-11.14	-14.24	-16.52	-12.20	-228.68	-1675.44	-73
	07:38 AM	2346	-11.22	-13.68	-16.64	-12.60	-229.48	-1678.64	-76
	11:38 AM	2350	-11.62	-14.76	-16.96	-13.24	-231.08	-1683.84	-79
	03:38 PM	2354	-11.66	-14.24	-17.00	-13.28	-230.68	-1684.24	-82
	07:38 PM	2358	-11.54	-14.16	-16.84	-12.96	-230.28	-1681.44	-86
	11:38 PM	2362	-11.30	-14.92	-16.60	-12.52	-229.48	-1677.84	-89
	03:38 AM	2366	-11.06	-14.88	-16.40	-12.16	-228.68	-1675.04	-92
	07:38 AM	2370	-11.26	-13.32	-16.64	-12.76	-230.28	-1679.84	-96
	11:38 AM	2374	-11.66	-15.04	-17.16	-13.56	-231.48	-1686.24	-99
	03:38 PM	2378	-12.06	-16.08	-17.52	-14.44	-233.08	-1693.44	-102
	07:38 PM	2382	-8.02	-14.20	-16.24	-13.12	-230.68	-1682.24	-105
	11:38 PM	2386	-2.46	-12.24	-13.44	-11.96	-228.28	-1678.64	-108
	03:38 AM	2390	-1.18	-11.60	-13.16	-11.56	-227.48	-1676.64	-112
	07:38 AM	2394	-0.54	-10.48	-13.40	-12.08	-228.28	-1682.24	-115
	11:38 AM	2398	1.38	-11.24	-13.24	-12.44	-229.88	-1689.84	-118
	03:38 PM	2402	4.38	-11.68	-11.40	-12.32	-231.48	-1698.24	-121
	07:38 PM	2406	8.26	-8.88	-10.08	-11.00	-229.08	-1689.04	-124
	11:38 PM	2410	10.38	-8.76	-9.84	-10.52	-228.68	-1687.44	-127
	03:38 AM	2414	10.58	-8.48	-9.88	-10.92	-228.68	-1687.44	-130
	07:38 AM	2418	11.34	-8.48	-10.80	-11.56	-230.68	-1691.84	-133
	11:38 AM	2422	11.06	-10.40	-12.08	-13.48	-232.68	-1702.24	-136
	03:38 PM	2426	11.06	-10.20	-12.20	-15.32	-236.68	-1713.04	-139

	07:38 PM	2430	11.66	-10.08	-11.44	-13.60	-233.48	-1699.44	-142
	11:38 PM	2434	12.98	-9.68	-11.84	-13.92	-233.48	-1696.64	-145
	03:38 AM	2438	13.50	-9.56	-11.64	-13.52	-233.08	-1694.24	-148
	07:38 AM	2442	13.74	-9.36	-11.92	-14.96	-234.68	-1699.44	-151
	11:38 AM	2446	12.98	-10.92	-13.84	-17.04	-237.88	-1710.64	-156
	03:38 PM	2450	12.90	-10.84	-13.88	-18.04	-239.48	-1717.44	-160
	07:38 PM	2454	13.66	-10.36	-13.16	-16.48	-236.68	-1705.04	-163
	11:38 PM	2458	14.26	-9.84	-12.48	-15.76	-235.48	-1700.64	-166
	03:38 AM	2462	14.42	-9.56	-12.28	-15.68	-235.88	-1699.84	-169
	07:38 AM	2466	14.14	-9.56	-12.52	-16.68	-236.28	-1703.04	-172
	11:38 AM	2470	15.30	-9.32	-14.00	-17.68	-238.28	-1710.24	-175
	03:38 PM	2474	15.70	-10.20	-13.68	-18.40	-239.48	-1718.24	-178
	07:38 PM	2478	18.22	-7.80	-12.88	-17.00	-237.88	-1706.64	-182
	11:38 PM	2482	19.30	-6.56	-12.84	-18.16	-238.68	-1705.44	-185
	03:38 AM	2486	20.22	-6.12	-13.40	-19.00	-240.28	-1705.84	-189
	06:38 PM	2477	21.90	-5.00	-14.44	-21.88	-243.48	-1712.24	-193
27-Nov	07:38 AM	2490	23.10	-4.60	-16.76	-25.40	-249.08	-1723.44	-196
	11:38 AM	2494	23.82	-7.32	-19.04	-28.68	-252.68	-1732.64	-198
	03:38 PM	2498	24.42	-5.36	-19.08	-28.80	-251.48	-1723.04	-200
	07:38 PM	2502	24.70	-3.64	-20.40	-29.92	-252.68	-1720.64	-200
	11:38 PM	2506	24.78	-4.48	-21.28	-31.28	-253.88	-1720.64	-200
	03:38 AM	2510	25.46	-4.08	-21.60	-32.72	-255.48	-1725.84	-201
	07:38 AM	2514	25.14	-5.72	-22.88	-34.40	-258.68	-1733.84	-201
	11:38 AM	2518	24.86	-7.76	-24.20	-36.08	-261.08	-1741.04	-201
	03:38 PM	2522	25.58	-5.84	-23.48	-35.40	-258.28	-1729.44	-202
	07:38 PM	2526	25.86	-5.76	-23.20	-34.80	-257.08	-1726.24	-202
	11:38 PM	2530	25.82	-5.84	-24.08	-35.36	-258.28	-1725.04	-202
	03:38 AM	2534	25.46	-4.76	-24.52	-37.04	-259.88	-1731.44	-202
	07:38 AM	2538	25.06	-6.96	-25.64	-37.88	-262.28	-1739.04	-202
	11:38 AM	2542	24.42	-7.76	-26.08	-39.72	-264.68	-1747.84	-203
	03:38 PM	2546	25.18	-6.12	-25.28	-38.76	-261.88	-1734.64	-203
	07:38 PM	2550	25.62	-6.56	-24.96	-38.16	-261.48	-1730.24	-203
	11:38 PM	2554	25.82	-6.36	-24.80	-37.96	-261.48	-1729.04	-203
	03:38 AM	2558	25.70	-6.16	-25.08	-38.36	-261.88	-1732.64	-203
	07:38 AM	2562	26.06	-6.28	-26.52	-40.36	-264.68	-1741.84	-203
	11:38 AM	2566	25.42	-7.72	-27.00	-41.40	-267.08	-1750.24	-203
	03:38 PM	2570	26.18	-6.28	-26.20	-39.76	-263.88	-1737.44	-203
	07:38 PM	2574	26.50	-6.16	-25.96	-39.08	-263.08	-1733.04	-203
	11:38 PM	2578	26.66	-5.40	-25.68	-38.92	-262.28	-1730.24	-203
	03:38 AM	2582	26.42	-4.60	-26.08	-40.28	-263.48	-1735.84	-203
	07:38 AM	2586	25.90	-5.96	-26.72	-41.20	-265.88	-1743.04	-203
	11:38 AM	2590	25.42	-8.52	-27.96	-42.08	-267.48	-1749.84	-203
	03:38 PM	2594	26.06	-6.72	-27.20	-40.48	-264.68	-1737.44	-203
	07:38 PM	2598	26.34	-5.64	-26.88	-39.84	-263.48	-1733.44	-205
	11:38 PM	2602	26.70	-5.84	-26.60	-39.68	-263.08	-1731.44	-205
	03:38 AM	2606	26.38	-4.80	-27.08	-40.68	-265.08	-1737.04	-205

	07:38 AM	2610	25.66	-7.28	-27.76	-42.64	-268.28	-1746.24	-205
	11:38 AM	2614	25.42	-7.48	-28.24	-44.32	-270.28	-1754.64	-205
	03:38 PM	2618	26.18	-6.64	-27.64	-42.44	-267.08	-1740.64	-205
	07:38 PM	2622	26.62	-6.24	-27.44	-41.72	-265.88	-1735.84	-205
	11:38 PM	2626	26.66	-6.04	-27.36	-41.36	-265.08	-1733.04	-205
	03:38 AM	2630	26.50	-5.96	-27.60	-42.00	-266.28	-1737.04	-205
	07:38 AM	2634	25.90	-6.20	-28.24	-42.96	-267.88	-1745.04	-205
	11:38 AM	2638	25.94	-6.60	-28.12	-42.76	-267.88	-1744.24	-205
	03:38 PM	2642	26.26	-5.08	-27.72	-41.96	-267.08	-1738.24	-207
	07:38 PM	2646	26.34	-5.40	-27.60	-41.72	-266.68	-1736.64	-207
	11:38 PM	2650	26.38	-5.40	-27.56	-41.52	-266.28	-1735.04	-207
	03:38 AM	2654	26.26	-4.64	-27.88	-42.08	-267.08	-1738.24	-207
	07:38 AM	2658	26.02	-8.74	-29.42	-38.26	-263.50	-1751.90	-207
05-Dec	01:38 PM	2688	26.70	-8.70	-30.46	-40.18	-265.50	-1756.30	-207
	05:38 PM	2692	28.06	-8.94	-30.18	-39.62	-264.30	-1751.90	-207
	09:38 PM	2696	28.22	-9.38	-29.98	-39.18	-263.50	-1748.70	-207
	01:38 AM	2700	28.30	-8.78	-29.90	-38.94	-263.10	-1747.10	-207
	05:38 AM	2704	26.70	-4.72	-29.12	-45.08	-269.88	-1745.04	-207
	09:38 AM	2708	28.06	-4.96	-28.84	-44.52	-268.68	-1740.64	-207
	01:38 PM	2712	28.22	-5.40	-28.64	-44.08	-267.88	-1737.44	-209
	05:38 PM	2716	28.30	-4.80	-28.56	-43.84	-267.48	-1735.84	-209
	09:38 PM	2720	28.10	-4.08	-29.00	-44.52	-268.68	-1740.64	-209
	01:38 AM	2724	27.74	-5.56	-29.36	-45.36	-270.28	-1747.04	-209
	05:38 AM	2728	27.90	-6.40	-30.12	-45.84	-271.08	-1751.44	-209
	09:38 AM	2732	28.46	-5.64	-29.68	-44.64	-269.08	-1742.24	-209
	01:38 PM	2736	28.94	-5.56	-29.40	-44.08	-267.88	-1738.24	-209
	05:38 PM	2740	29.06	-6.12	-29.32	-43.92	-267.88	-1737.84	-209
	09:38 PM	2744	28.70	-5.68	-29.72	-44.72	-269.08	-1742.64	-209
	01:38 AM	2748	28.26	-6.12	-30.16	-45.52	-270.68	-1748.64	-209
	05:38 AM	2752	28.06	-6.08	-30.16	-45.56	-270.68	-1749.04	-211
	09:38 AM	2756	28.50	-5.96	-29.68	-44.64	-269.08	-1743.04	-211
	01:38 PM	2760	28.86	-5.88	-29.56	-44.20	-267.88	-1738.24	-211
	05:38 PM	2764	28.98	-4.96	-29.32	-43.76	-267.48	-1735.44	-211
	09:38 PM	2768	28.58	-4.32	-29.80	-44.64	-268.68	-1741.84	-211
	01:38 AM	2772	28.30	-6.64	-30.04	-45.32	-270.28	-1747.44	-211
	05:38 AM	2776	27.94	-7.32	-30.36	-46.12	-271.48	-1753.44	-211
	09:38 AM	2780	28.50	-5.92	-29.68	-44.60	-268.68	-1741.84	-211
	01:38 PM	2784	28.94	-5.84	-29.40	-44.08	-267.88	-1738.64	-211
	05:38 PM	2788	29.10	-5.76	-29.40	-43.88	-267.48	-1736.64	-211
	09:38 PM	2792	28.90	-5.44	-29.76	-44.56	-268.68	-1741.44	-211
	01:38 AM	2796	28.42	-6.24	-30.12	-45.48	-270.28	-1747.44	-211
	05:38 AM	2800	27.98	-7.84	-30.48	-46.28	-271.88	-1754.24	-211
	09:38 AM	2804	28.50	-6.12	-29.72	-44.88	-269.48	-1744.24	-213
	01:38 PM	2808	29.06	-5.64	-29.40	-44.04	-267.88	-1738.24	-213
	05:38 PM	2812	29.14	-5.00	-29.28	-43.84	-267.48	-1736.24	-213
	09:38 PM	2816	28.86	-4.60	-29.56	-44.56	-268.68	-1741.44	-213

TABLE II.7

NWB3 ANCHOR MOVEMENTS RELATIVE TO DATUM PLATE
MANUAL READINGS - VARIOUS EXTENSOMETERS

DATE	DAYS	SUB-PANEL 1 ANCHOR DEPTHS(m)			SUB-PANEL 2 ANCHOR DEPTHS(m)			
		98	104	115	60.3	100.6	117.7	139
		Anchor movement (mm)						
19-Feb	0	0	0	0	0	0	0	0
22-Feb	3	0	0	0	0	0	0	0
24-Feb	5	0	0	0	0	0	0	0
03-Mar	12	0	0	-6	0	0	0	-416
04-Mar	13	0	0	-6	0	0	0	-416
05-Mar	14	0	0	-6	0	0	0	-416
07-Mar	16	0	0	-8	0	0	0	-416
09-Mar	18	0	0	-8	0	0	0	-416
11-Mar	20	0	0	-8	0	0	0	-416
17-Mar	26	0	0	-8	0	0	0	-416
19-Mar	28	0	0	-8	0	0	0	-416
24-Mar	33	0	0	-8	0	0	0	-418
25-Mar	34	0	0	-8	0	0	0	-480
25-Mar	34	0	0	-8	0	0	0	-600
26-Mar	35	0	0	-8	0	0	0	-1400
26-Mar	35	0	0	-8	0	0	0	-1440
29-Mar	38	0	0	-8	0	0	0	-1496
30-Mar	39	0	0	-8	0	0	0	-1500
01-Apr	41	0	0	-8	0	0	0	-1500
02-Apr	42	0	0	-8	0	0	0	-1568
05-Apr	45	0	0	-8	0	0	0	-1568
13-Apr	53	0	0	-8	0	0	0	-1568
16-Apr	56	0	0	-8	0	0	0	-1572
28-Apr	68	0	0	-8	-2	0	0	-1572
25-May	95	0	-2	-10	-2	0	0	-1572
08-Jun	109	0	-2	-10	-2	0	0	-1572
16-Jun	117	0	-2	-10	-2	0	0	-1572
28-Jun	129	0	-2	-10	-2	0	0	-1572
02-Jul	133	0	-2	-10	-2	0	0	-1572

NOTE: Ex..tensometers are approximately 20m from the panel edge.

TABLE II.8

NORTHWEST B3 PANEL AQUIFER WATER MONITORING DATA

	SUB-PANEL 2				SUB-PANEL 1				Mine Water
DATE	Water Depth Aq. #2	Water Depth Aq.#3	Water Depth Aq.#4	Water Depth Aq.#5	Water Depth Aq.#3L	Water Depth Aq.#3U	Water Depth Aq.#4L	Water Depth Aq.#5	Make (m3/day)
25-Feb-93	-119.36	-90.54	-41.69	-15.14	-75.65	-72.95	-42.38	-30.57	40
02-Mar-93	-122.39	-90.58	-41.70	-15.15	-76.00	-73.00	-42.40	-30.60	50
03-Mar-93	-122.56	-90.60	-41.72	-15.16	-77.00	-73.10	-42.42	-30.62	50
04-Mar-93	-122.72	-90.77	-41.75	-15.17	-78.10	-73.21	-42.45	-30.63	50
05-Mar-93	-122.80	-90.87	-41.74	-15.17	-79.09	-73.30	-42.44	-30.62	50
08-Mar-93	-122.97	-91.22	-41.77	-15.18	-82.09	-73.65	-42.49	-30.64	60
09-Mar-93	-123.03	-91.40	-41.81	-15.18	-83.41	-73.82	-42.54	-30.65	60
10-Mar-93	-123.05	-91.52	-41.88	-15.21	-84.30	-73.94	-42.60	-30.68	60
11-Mar-93	-123.04	-91.58	-41.83	-15.19	-85.07	-74.02	-42.59	-30.65	60
12-Mar-93	-123.05	-91.73	-41.82	-15.19	-86.16	-74.17	-42.61	-30.66	60
15-Mar-93	-123.01	-92.13	-41.84	-15.19	-89.62	-74.56	-42.63	-30.67	70
17-Mar-93	-122.95	-92.31	-41.84	-15.19	-91.07	-74.78	-42.63	-30.66	70
22-Mar-93	-123.02	-92.68	-41.82	-15.16	-93.15	-75.16	-42.68	-30.72	80
25-Mar-93	-123.04	-92.78	-42.00	-15.14	-94.06	-75.38	-42.70	-30.65	80
26-Mar-93	-123.54	-97.02	-42.05	-15.14	-106.92		-42.88	-30.65	80
30-Mar-93	-123.65	-102.50	-42.12	-15.18	-109.62		-42.86	-30.70	250
01-Apr-93	-123.75	-102.60	-42.20	-15.22	-108.98		-42.90	-30.74	250
05-Apr-93	-123.88	-102.72	-42.28	-15.24	-108.81		-42.97	-30.78	500
08-Apr-93	-123.87	-102.69	-42.28	-15.22	-108.75		-42.93	-30.74	500
13-Apr-93	-123.95	-102.95	-42.31	-15.21	-108.77		-43.01	-30.86	550
16-Apr-93	-123.95	-102.91	-42.33	-15.27	-108.72		-43.00	-30.79	600
28-Apr-93	-124.00	-102.94	-42.54	-15.27	-108.65		-43.08	-30.78	632
07-May-93	-124.52	-103.08	-42.64	-15.33	-108.68		-43.19	-30.88	600
12-May-93	-124.32	-103.20	-42.72	-15.35	-108.69		-43.25	-30.91	552
25-May-93	-123.85	-103.22	-42.85	-15.36	-108.68		-43.33	-30.91	552
08-Jun-93	-124.15	-103.35	-43.07	-15.40	-108.70		-43.49	-30.95	550
16-Jun-93	-124.27	-103.43	-43.11	-15.40	-108.77		-43.54	-30.94	520
25-Jun-93	-125.08	-103.39	-43.22	-15.45	-108.77		-43.59	-30.98	520
02-Jul-93	-125.18	-103.41	-43.26	-15.42	-108.81		-43.63	-30.97	482
28-Jul-93	-125.18	-103.41	-43.26	-15.42	-108.81		-43.63	-30.97	428
03-Aug-93	-125.12	-103.51	-43.62	-15.47	-108.78		-43.85	-30.06	428
26-Aug-93	-125.18	-103.43	-43.70	-15.49	-108.81		-43.88	-30.01	
28-Sep-93	-125.24	-103.22	-43.91	-15.51	-108.81		-44.00	-30.06	
26-Oct-93	-125.28	-103.04	-44.07	-15.63	-108.79		-44.11	-31.10	
01-Mar-94	-125.81	-102.93	-45.04	-16.42	-108.81		-45.00	-31.75	

NOTE: CHANGES IN WATER LEVEL ARE CALCULATED AFTER SUBSIDENCE HAS BEEN SUBTRACTED FROM THE CHANGE IN WATER LEVEL

TABLE II.9

RED PANEL AQUIFER WATER LEVEL DATA

DATE	Aquifer 3 Water level (m)	Aquifer 4 Water level (m)	Aquifer 5 Water level (m)	Change in Aquifer 3 level (m)	Change in Aquifer 4 level (m)	Change in Aquifer 5 level (m)
06-Feb-90	112.66	148.46	153.87	0	0	0
07-Feb-90	112.62	148.43	153.81	-0.04	-0.03	-0.06
13-Feb-90	112.61	148.38	153.78	-0.05	-0.08	-0.09
16-Feb-90	112.51	148.26	153.66	-0.15	-0.2	-0.21
20-Feb-90	112.51	148.3	153.7	-0.15	-0.16	-0.17
27-Feb-90	111.39	148.31	153.71	-1.27	-0.15	-0.16
28-Feb-90	111.41	148.31	153.71	-1.25	-0.15	-0.16
04-Mar-90	111.1	148.31	153.71	-1.56	-0.15	-0.16
06-Mar-90	110.94	148.31	153.71	-1.72	-0.15	-0.16
09-Mar-90	111.01	148.28	153.71	-1.65	-0.18	-0.16
13-Mar-90	110.92	148.25	153.71	-1.74	-0.21	-0.16
16-Mar-90	110.96	148.22	153.71	-1.7	-0.24	-0.16
20-Mar-90	110.91	148.19	153.71	-1.75	-0.27	-0.16
23-Mar-90	110.88	148.17	153.6	-1.78	-0.29	-0.27
27-Mar-90	110.78	148.14	153.57	-1.88	-0.32	-0.3
30-Mar-90	110.82	148.11	153.54	-1.84	-0.35	-0.33
04-Apr-90	110.73	148.08	153.51	-1.93	-0.38	-0.36
09-Apr-90	110.7	148.05	153.48	-1.96	-0.41	-0.39
10-Apr-90	110.76	148.02	153.45	-1.9	-0.44	-0.42
11-Apr-90	110.79	147.99	153.42	-1.87	-0.47	-0.45
12-Apr-90	110.71	147.96	153.39	-1.95	-0.5	-0.48
17-Apr-90	109.78	147.95	153.37	-2.88	-0.51	-0.5
18-Apr-90	109.72	147.95	153.37	-2.94	-0.51	-0.5
20-Apr-90	109.73	147.95	153.37	-2.93	-0.51	-0.5
23-Apr-90	109.65	147.95	153.37	-3.01	-0.51	-0.5
24-Apr-90	109.54	147.95	153.37	-3.12	-0.51	-0.5
26-Apr-90	109.12	147.95	153.37	-3.54	-0.51	-0.5
27-Apr-90	108.93	147.95	153.39	-3.73	-0.51	-0.48
02-May-90	107.88	147.91	153.36	-4.78	-0.55	-0.51
04-May-90	107.66	147.91	153.36	-5	-0.55	-0.51
07-May-90	107.53	147.91	153.36	-5.13	-0.55	-0.51
08-May-90	107.56	147.94	153.36	-5.1	-0.52	-0.51
10-May-90	107.52	147.91	153.36	-5.14	-0.55	-0.51
14-May-90	107.53	147.91	153.36	-5.13	-0.55	-0.51
18-May-90	107.5	147.84	153.29	-5.16	-0.62	-0.58
23-May-90	107.35	147.74	153.18	-5.31	-0.72	-0.69
25-May-90	107.42	147.74	153.18	-5.24	-0.72	-0.69
29-May-90	107.41	147.74	153.21	-5.25	-0.72	-0.66
31-May-90	107.13	147.74	153.29	-5.53	-0.72	-0.58
01-Jun-90	105.12	147.74	153.29	-7.54	-0.72	-0.58
05-Jun-90	104.35	147.45	153.35	-8.31	-1.01	-0.52
06-Jun-90	104.34	147.28	153.29	-8.32	-1.18	-0.58
07-Jun-90	104.45	147.23	153.29	-8.21	-1.23	-0.58
08-Jun-90	104.6	147.13	153.28	-8.06	-1.33	-0.59
11-Jun-90	104.7	146.82	153.15	-7.96	-1.64	-0.72
13-Jun-90	105.19	146.79	153.08	-7.47	-1.67	-0.79
15-Jun-90	105.39	146.58	153.06	-7.27	-1.88	-0.81

18-Jun-90	105.34	146.46	153.03	-7.32	-2	-0.84
20-Jun-90	105.29	146.4	153.03	-7.37	-2.06	-0.84
22-Jun-90	105.26	146.36	153.03	-7.4	-2.1	-0.84
25-Jun-90	105.13	146.22	153	-7.53	-2.24	-0.87
29-Jun-90	105.27	146.35	153.23	-7.39	-2.11	-0.64
02-Jul-90	105.11	146.1	153.05	-7.55	-2.36	-0.82
04-Jul-90	105.15	146.13	153.1	-7.51	-2.33	-0.77
06-Jul-90	105.11	146.09	153.11	-7.55	-2.37	-0.76
10-Jul-90	105.19	146.14	153.24	-7.47	-2.32	-0.63
11-Jul-90	105.07	145.94	153.06	-7.59	-2.52	-0.81
13-Jul-90	105.26	144.52	152.84	-7.4	-3.94	-1.03
16-Jul-90	106.21	143.6	152.77	-6.45	-4.86	-1.1
19-Jul-90	106.31	142.82	152.55	-6.35	-5.64	-1.32
23-Jul-90	106.82	142.59	152.57	-5.84	-5.87	-1.3
27-Jul-90	106.83	142.07	152.24	-5.83	-6.39	-1.63
30-Jul-90	106.81	141.92	152.24	-5.85	-6.54	-1.63
01-Aug-90	106.95	141.98	152.42	-5.71	-6.48	-1.45
02-Aug-90	106.97	141.98	152.47	-5.69	-6.48	-1.4
03-Aug-90	106.91	141.89	152.42	-5.75	-6.57	-1.45
06-Aug-90	106.72	141.58	152.23	-5.94	-6.88	-1.64
09-Aug-90	106.67	141.47	152.2	-5.99	-6.99	-1.67
13-Aug-90	106.53	141.31	152.18	-6.13	-7.15	-1.69
17-Aug-90	106.4	141.15	152.14	-6.26	-7.31	-1.73
22-Aug-90	106.05	140.79	151.9	-6.61	-7.67	-1.97
28-Aug-90	105.94	140.76	152.01	-6.72	-7.7	-1.86
02-Sep-90		139.55	151.35		-8.91	-2.52
09-Sep-90		139.4	151.26		-9.06	-2.61
16-Sep-90		139.21	151.11		-9.25	-2.76
23-Sep-90		139.15	151.11		-9.31	-2.76
30-Sep-90		138.96	150.98		-9.5	-2.89
04-Oct-90	104.78	138.7	150.75	-7.88	-9.76	-3.12
10-Oct-90	104.67	138.75	150.84	-7.99	-9.71	-3.03
17-Oct-90	104.5	138.5	150.61	-8.16	-9.96	-3.26
24-Oct-90	104.43	138.6	150.67	-8.23	-9.86	-3.2
01-Nov-90	104.28	138.53	150.6	-8.38	-9.93	-3.27
09-Nov-90	104.07	138.53	150.61	-8.59	-9.93	-3.26
16-Nov-90	104.1	138.54	150.61	-8.56	-9.92	-3.26
23-Nov-90	104	138.55	150.63	-8.66	-9.91	-3.24
26-Nov-90	104.29	138.34	150.43	-8.37	-10.12	-3.44
27-Nov-90	104.27	138.36	150.45	-8.39	-10.1	-3.42
28-Nov-90	104.33	138.03	150.19	-8.33	-10.43	-3.68
30-Nov-90	104.39	137.74	149.92	-8.27	-10.72	-3.95
03-Dec-90	104.58	137.62	149.82	-8.08	-10.84	-4.05
10-Dec-90	104.63	137.37	149.61	-8.03	-11.09	-4.26
17-Dec-90	104.79	137.05	149.28	-7.87	-11.41	-4.59
21-Jan-91	104.9	137.23	149.48	-7.76	-11.23	-4.39
05-Feb-91	104.72	136.93	149.17	-7.94	-11.53	-4.7

TABLE II.10

RED PANEL WATER MAKE

WEEK ENDING	WEEKS SINCE 4/3/90	Water make cubic metres per day
04-Mar-90	0	2100
11-Mar-90	1	2100
18-Mar-90	2	3600
25-Mar-90	3	3600
01-Apr-90	4	3600
08-Apr-90	5	3600
15-Apr-90	6	3600
22-Apr-90	7	3700
29-Apr-90	8	3800
06-May-90	9	4000
13-May-90	10	5300
20-May-90	11	4300
27-May-90	12	4300
03-Jun-90	13	7000
10-Jun-90	14	7000
17-Jun-90	15	8500
24-Jun-90	16	8500
01-Jul-90	17	8000
08-Jul-90	18	8500
15-Jul-90	19	8500
22-Jul-90	20	8500
29-Jul-90	21	10000
05-Aug-90	22	11000
12-Aug-90	23	11000
19-Aug-90	24	10000
26-Aug-90	25	9000
02-Sep-90	26	9500
09-Sep-90	27	9500
16-Sep-90	28	9000
23-Sep-90	29	9000
30-Sep-90	30	9000

APPENDIX III

CENTRIFUGE MODELLING

EQUIVALENT MATERIALS TESTING

III.1 PILOT STUDY TESTS - PHASE I

It was not the intention to perform a detailed material testing program for this initial pilot study. In order to determine the requirements of a full-scale testing program, the factors which influence the strength characteristics of the synthetic rock material needed to be quantified, which was out of the scope of this phase of testing. However it was necessary to perform a limited number of tests to establish reasonably representative mixtures of sand, water, and gypsum which would allow the centrifuge system to be assessed; i.e. mixtures which were likely to respond adequately to the extraction process and induce reasonable loads on the mechanical components.

From the initial studies performed, it was found that the following factors influence the strength characteristics of gypsum/sand mixtures:

i) The percentage of plaster and sand in the mix.

ii) The amount of water used in the mix.

iii) The amount of curing time allowed after mixing and before testing.

iv) The degree of vibro-compaction during placement of the mix.

Whilst factors i) and iii) are intuitively obvious, factors ii) and iv) are worthy of further comment. Firstly, the amount of water added to the mix is fairly critical. Enough water must be added to complete the hydration process, however, if there is excess water (free water), then as the sample is dried, free water evaporates and leaves voids which reduce the strength of the sample. Efficient vibration of the mix during

placement inthe moulds can alleviate this problem by closing the voids occupied by free water which then tends to flow to the top and bottom of the sample. Similarly, any entrapped air is also expelled from the sample.

Having established these initial influencing factors, several tests were performed in a standard fashion using various percentage mixtures, by weight, of sand, gypsum and water. Several castings of each mix were made in cylindrical moulds (75.4 mm in diameter and 153.4 mm in length) and unconfined compression tests were performed after allowing a curing time of one week. Table III.1 below (from Stone et al., 1991) summarises the tests performed during the early stages of the pilot study.

Table III.1 UCS Test Results for Various Sand/Plaster/Water Mixes

	PERCENTAGE BY WEIGHT				
MIX ID	SAND	PLASTER	WATER	UCS (MPa)	MODULUS (MPa)
A 1.5:1	47.4	31.6	20.9	6.0	1316
B (3:1)	60.7	20.2	18.9	2.32	832
C (4.8:1)	64.8	16.2	18.9	0.8	191
D (5:1)	75.2	15.7	10.0	0.65	-

For the model tests Westcoll1 and Westcoll2, mix B was used for the roof slab. It was evident, at this early stage, that by careful choice of design mixtures it is possible to produce representative strengths for the model rock.

Other Materials

The Westcoll1 and Westcoll2 models had a layer of fine sand (with an average particle size of 300 microns - see Figure III.1) above the gypsum/sand roof slab (of mix B). It should be noted that this sand was also used in the roof slab. Figure III.2 shows the results of a direct shear test performed on a medium dense sample of this sand. The corresponding peak and residual friction angles obtained from the test are 35 and 31 degrees respectively (Stone et al., 1992). These values compare reasonably well with the peak friction angle for sandstone material in the Collie Basin (as given in Table 2.1).

III.2 EQUIVALENT MATERIALS TESTING - PHASE II INVESTIGATION

From early centrifuge tests using insitu material, it was clear that the variability of natural materials can have a significant impact on caving behaviour. This observation, along with the physical limitations of the centrifuge equipment at UWA, thus necessitated the use of equivalent materials to be able to develop and successfully complete the full range of models proposed for the phase II study.

It is obvious that the success or otherwise of modelling of prototype structures with synthetic material depends on the ability of the equivalent material to represent the mechanical characteristics of the prototype.

Following Phase I modelling, it was recognised that the equivalent material "standards" needed tighter control. Two aspects in particular required better definition:

i) the critical mechanical properties for which the equivalent material must maintain similitude, and

ii) a stringent mixing procedure from which a reproducible product could be fabricated at all times. For example, early attempts at equivalent material modelling (Westcoll3 & Westcoll4) were not able to remove air trapped in the mix during the mixing process. Figure III.3 illustrates the high number of air pockets within the centrifuge model Westcoll3.

Consequently, a comprehensive literature review was undertaken to address these issues. The review also included visits to some of the leading modelling and /or subsidence research facilities. (Including Bochum University, Germany; ISMES in Bergamo, Italy; Cambridge University, England; CSIRO in Melbourne, Australia; Nottingham University, England; University of West Virginia, USA; and GMBH in Essen, Germany.)

Summarising the results from the review of the work of other researchers, it was established that, inclusive of the mechanical strength parameters used in phase 1 modelling (UCS and elastic modulus), physical modelling should also be based on the flexural and shear strength of the strata and bedding (Section 4.2.2.1).

Flexural strength would logically appear to be the most appropriate due to the nature of collapse in the subsidence processes. As discussed in Section 2.5.5.1, subsidence is initiated by collapse of the "roof beam", which is largely dependent on the span of the beam, the vertical loading on the beam, and its flexural strength. It is also reported in several mining locations that thick, very strong layers of conglomerate can span the zone of initial caving and either prevent or significantly limit subsidence development. Two examples of bridging by thick, stiff strata above caved extraction panels are given by Krishna (1989) in Indian coalfields and Galvin (1981) in South African coal mining regions. This phenomenon is obviously supportive of the beam theory for subsidence development, and it therefore follows that the critical factor in the development of subsidence is the flexural strength of the strata.

Once these critical subsidence parameters were identified, it was necessary to conduct a detailed investigation into the manufacture of equivalent materials. These investigations were needed to establish the most appropriate mix procedures, ingredients, and proportions required for any particular prototype lithology within a given model geometry according to the laws of similitude. This investigation is summarised below.

III.3 CONSTRUCTION OF EQUIVALENT MATERIALS

In order to establish a consistent product, there are essentially three components of the construction cycle which require tight control. These are listed below:

1. Raw Materials
2. Mixing Procedures
3. Curing and Storing Procedures.

Raw Materials

Comprehensive research on mixing procedures for scaled modelling of earth structures highlighted the need to establish the most applicable ingredients for manufacture of equivalent materials. Many researchers throughout the world (e.g. Stimpson, 1970) have established their own criterian for equivalent materials.

However, there are basically three components in an equivalent material.

1. A filler - forming the body of the artificial material. Fillers can be almost anything from sawdust to glass beads to sand and clay.

2. A bonding agent or bonder - typically either cement, fly ash, dental plaster or plaster of Paris.

3. A mixing medium which:

   a) gives a workable texture of the equivalent material, and

   b) can act as a chemical component in the bonding process.

   In almost all cases, the medium used is water. There are a few exceptions; for example ISMES (in Bergamo, Italy), often use a type of vegetable oil with plaster. ISMES found that the oil greatly reduces the number of air pockets, and gives a more pliable mix. The drawback is the low final strength of the oil-based material (personal communication 1991) which could not reach the strength of the prototype aquitard material.

A number of attempts were made at constructing equivalent materials to meet the similitude requirements of modelling. After the phase I tests, a trial using kaolin clay as the main body of the artificial material was conducted. It was decided to trial kaolin because this material is the natural bonding agent for the weak sandstones, and represents the major component in the Collie Basin mudstones. It was thought that if the natural components of insitu material could be used to construct the equivalent materials, then better similitude would be obtained between the model and the prototype. A similar approach was used by Johnston & Choi (1986), where crushed mudstone was used in conjunction with Portland cement. The mudstone was crushed manually with a rubber pestle and mortar so that a larger particle size was attained than the constituent mudstone particles. Because the Portland cement takes approximately 90 days to reach a constant strength, Johnston and Choi included a calcium chloride accelerator to speed up the setting process. Rapid-setting cement was found to produce unstable mixes that were more ductile than the natural mudstone. This approach was not considered appropriate for this study because the main aim was to reduce the particle size in the model material.

The kaolin tests were, however, unsuccessful due largely to the high quantity of water required in the initial mixture to obtain a malleable mix. This resulted in irregular hydration of the kaolin, several days curing time, and high linear shrinkage on drying. Consequently it was decided no longer to use kaolin in the equivalent material mixes.

Following consultation with leading researchers in England, Germany, Italy and Australia, and review of the published literature (e.g. Lajtai, 1967; Stimpson, 1970; Brown and Trollope, 1970; Einstein & Hirschfield, 1973; Reddish, 1984; Indraratna, 1990; and Rowlands, 1990), it was decided that the most appropriate mix ingredients for this study were those used in the Phase 1 tests:

- plaster of Paris (Hardy's International Hardwall plaster)
- fine, graded sand (300μm)
- tap water.

However, it was clear that the mixing and curing procedures needed to be improved.

Mixing Procedures

Mixing procedures used by researchers throughout the world are widely variant. Early attempts at obtaining a reproducible, consistent mix proved very frustrating. After many trials with mixing techniques, and air pocket control, it was found that the simplest and best method was a slight variation of the methods adopted by B. Whittaker in the UK (personal communication, 1990), and A.G. Meyers (1990) in Australia .

The mixing procedure finally adopted was:

i) measure out the required proportions of sand, plaster and water (by weight) for any particular layer

ii) mix the sand and plaster together uniformly

iii) place the water in a sufficiently sized mixing bowl with an automatic, variable speed mixer

iv) add the dry mix slowly to the water, ensuring the mix does not form lumps at any stage

v) pour the mix into the mould

vi) lightly vibrate the mould and mix for 5 seconds.

Some researchers (e.g. Johnston & Choi,year unknown, and the ISMES research centre Bergamo, Italy - personal communication) have successfully implemented hydraulic tamping of the freshly mixed specimens in enclosed compartments fitted with porous bases to drive out excess water and obtain a better consolidated, more consistent and reproducible mix. This technique was trialed early for initial moulded beam tests; however, it was quickly discarded as it became clear that the best method for constructing the model was to develop the layers within the strong-box. Tamping within the strong-box was impractical for the budgetary constraints of the project.

As discussed in Section 4.2.2.5, following evaluation of the three insitu material tests, it was clear that the performance of any stratum above a total extraction panel was greatly dependent on bedding.

Consequently, it was decided that future models using equivalent materials should be cast in several layers. The nominal layer thickness was 5 mm (1.5 m in the prototype), which was based on typical maximum stratification thicknesses in the Collie sandstones, and practical limitations for applying thinner layers to large models.

Accordingly, it was decided that the original - one layer - cast beam tests be supplemented with layered beam tests to assess the effect, if any, of laminations in equivalent materials.

When fabricating a laminated or layered equivalent material, the best result is achieved when successive layers are added prior to final setting/hardening of the lower layer. This promotes better adhesion between laminations.

In some mixes, with higher sand to plaster ratios, the time for initial curing and placement of successive layers can be advanced by using a hair dryer or equivalent which can direct hot air across the exposed surface of the top layer. The results of these tests are given in the following section.

Curing and Storing

Unconfined compressive strengths of equivalent materials from the mixing/testing studies in the pilot study were highly variable. In particular, the strengths of these materials appeared to change with time (Figure III.4). This variability was attributed to differences in moisture content of the tested cylinders. The variation in moisture content in the pilot study was considered to be due to:

- the fact that initial curing was done "on the bench" at variable diurnal temperatures,
- the drying time not being consistent for all mixes, which resulted in variable moisture contents at testing,
- cast cylinders being stored on the bench, and therefore subject to variable diurnal temperatures and humidity.

Subsequent research into curing and storage of laboratory test samples also demonstrated that curing procedures are widely variant. Literature published by Indraratna (1990) and Meyers (1990), pointed out three major procedures needing control:

a) the final curing temperature must not exceed 46°C.

b) drying/curing is completed when a consistent or desired moisture content is attained, and

c) storage of laboratory specimens should be in sealed, plastic bags, preferably in humidity controlled rooms.

Therefore the approach adopted for the second phase of the project was to:

- Let the mixes cure in the moulds for at least 2 hours prior to dismantling the moulds.
- Measure the wet weight of beams immediately prior to placing in the drying oven.
- Place the sample beams in the drying oven, set at 40°C.
- Check regularly for changes in weight of the beam, removing the beam when the moisture content reaches 2% of the asymptote of the dry mass (according to Indraratna, 1990, any further desiccation can be deleterious to the sample).

- Place the beams in a sealed plastic bag and store in a constant temperature, humidity room.

By adopting these guidelines for all three aspects of fabricating equivalent materials (ingredients, mixing, and curing/storage control), acceptable repeatability has been achieved, and equally important, a representative equivalent material established. It was found that a reasonable relationship can be formed between the proportions of sand and plaster in each mix for the UCS and flexural strengths (using a constant proportion of water 18%) with the accepted, simple mixing technique. The details of testing procedures and results are given in the following section.

III.4 MATERIAL STRENGTH TESTS

Equivalent material related testing

As mentioned previously, in order to establish the appropriate scaled equivalent material for the models, a series of UCS and flexural strength tests were conducted on beams made from a range of sand/plaster and water mixes and compared to flexural tests on "insitu material" beams. In order to better represent the yielding strain due to flexure/curvature, four point bending strength tests were conducted. The dimensions of the beams were 300 mm long x 50 x 50 m in section, in accordance with the requirements for AS 2733 -1984 testing procedure for flexural strength.

The results for the flexural strength of insitu material and equivalent materials are summarised in Tables III.2 and III.3; UCS test results have also been included for comparison. (Table III.4 lists the laboratory UCS test details for the samples taken from the blocks of insitu material used in centrifuge models PS01 - PS03). The equations derived from the beam testing results, and used to estimate the variation of material strength indices with variable plaster ratios (illustrated in Figure III.5) are given below:

$$F_s = 4.0 \times \exp^{-(0.88 \times Ratio^{0.55})} \qquad 4.2(11)$$

$$UCS = 9.0 \times \exp^{-(0.35 \times Ratio^{0.96})} \qquad III.3(1)$$

where; ratio = sand:plaster ratio (by weight), F_s = flexural strength, and

UCS = Unconfined Compressive Strength.

Concurrent to establishing the mechanical strengths of materials, the bending characteristics and development of subsequent horizontal surface strains from early stages of the tests through to failure were also investigated. Therefore much effort was put into establishing an efficient way in which both strains and beam deflections could be measured whilst loading the beams in a controlled fashion. A test rig was established which allowed for reasonable access to the top and bottom of the sample beams for easy implementation of measurement devices. The dimensions and main features of the test rig are illustrated in Figure III.6, along with the method of calculation of flexural strength.

The beam tests were generally conducted in accordance with AS 2733 - 1984 with the exception that loading was not done at a constant rate; rather, it was applied in definitive increments to identify any hysteresis or relaxation of the beam at any stage of loading. It was also thought to be more important to allow for any time/bending effects to develop during testing rather than use a consistently increasing load which could result in the failure of the beams at an artificially high value. A typical loading cycle used for tests is illustrated in Figure III.7.

The researcher initially trialed laser distance measurement (described in more detail in Appendix IV.13) and mechanical dial gauges (Figure III.8 a) to quantify the bending of test beams; however, these proved too clumsy and took some time to set up. Furthermore, laser readings appeared to be irregular. The one and only trial - with a cannel coal beam - gave several spikes along the beam surface (Figure III.9). As these could not be explained adequately, laser profiling was not trialed again. It was then decided to use LVDT's to measure beam deflections (Figure III.8 b). The initial intent for this program of research was to measure the shape or curvature of the aquitard surface as the beam tests progressed through to failure and relate these curvatures to measured strains. If a relationship between curvature subsidence and strain could be developed, then it would be possible to estimate the strain on a aquitard horizon for any given subsidence [subsurface subsidence being calculated by Equation 3.2(1)].

This approach, however, proved to be impractical as the number of LVDT's which could be successfully installed above the beams was limited, and as a result required much interpolation between individual points of measurement. Imperfections in the bedding of natural materials also resulted in local "hot spots" which lifted out of

synchrony with the remainder of the beam. These local "hot spots" on the surface of a beam could also explain the irregular readings obtained from laser profiling in Figure III.9.

It was then attempted to predict the onset of failure of the from the maximum deflection at the top and centre of the beams and compare these deflections with measured strains. This approach adopts a similar approach to the method developed by Misich et al (1991) for the prediction of aquitard strains during various stages of subsidence development where the maximum horizontal tensile strain is interpolated from the maximum subsidence - either measured or inferred - at any horizon above the seam. It was considered that if it could be proven in practice that standard beam theory can be applied to these materials, then this would further support the assumption by Misich et al (1991) and could assist in interpretation of rupture of aquitards during the centrifuge tests. Consequently, beam deflection measurement for the equivalent ensuing materials only targetted the maximum deflections prior to failure.

The measured maximum deflections, given in Table III.2, illustrated that the amount of deflection at failure is dependent on the strength of the beam being tested. This relationship was evident for both equivalent material beams and beams cut from insitu material. The stronger the beam the more the sustainable deflection. Tables III.5 to III.11 summarise the beam deflection data for given applied loads leading toward ultimate failure of the in situ material beams. The results have also been summarised in graphical form in Figures III.9 to III.16. (Note that deflections were measured at close intervals during each test with the use of an automatic data logging system. The resultant data files for each test are excessively large to present all the recorded data in tabular form. Also note that the data files for the coarse sandstone and laminated sandstone beam #2 were corrupted and only maximum data has been recoreded.)

The flexural yielding strains for the insitu material tested are included in Table III.2. (Strain gauge type and installation is discussed - in terms of the strain gauging used in centrifuge tests - in Appendix IV.11.) Although some problems were encountered initially with the near surface defects of the finely laminated sediments, these were overcome somewhat by coating the beam surface with epoxy resin. The yielding strains measured for coal aquitards, and massive and finely laminated sandstones,

are 2.0 mm/m 0.8 mm/m and 0.48 mm/m respectively. (Note that strains were measured at close intervals during each test with the use of an automatic data logging system. The resultant data files for each test are excessively large to present all the data in tabular form, and as a consequence, only the yielding strains have been provided.)

The horizontal strain measured during testing is summarised in tabular form in Tables III.12 and III.13 and graphically in Figures III.17 and III.18. (Note that only the maximum strain was measured in the coarse sandstone test fitted with strain gauges. Also note that the third cannel coal beam failed in two stages. The first was along a thin bedding ply on the top side of the beam. Loading was continued from this point, until ultimate failure was achieved. Calculation of failure stresses for the second stage of failure used the thinner (semi-failed) section of the beam.)

Flexural yielding strains of prototype materials and synthetic materials with equivalent strength compare differently. For example the maximum strain measured prior to the yield of an equivalent sandstone material mix with a flexural strength of 0.54 MPa was 0.41 mm/m, whereas the maximum deflection of insitu sandstone material with a flexural strength of 0.41 MPa was 1.2 mm. The "confined" yielding strain of aquifer material is not known. The "confined" yielding strains of synthetic aquitard material in operating centrifuge models is 0.8 mm/m (see Section 4.2.2.8). This compares to yielding strains of insitu aquitard material of 2 mm/m - both confined (in centrifuge test PS03) and unconfined (in beam bending tests).

This variation in yielding strains for the synthetic aquitard material is considered acceptable, as the rock mass strength reduction factor for coal materials is 0.3 (discussed in Section 4.2.2.1). The significance of the lower synthetic sandstone aquifer yielding strain is not clear, as the weak sandstone materials do not require a "rock mass reduction" in strength (Section 4.2.2.1). There were no strain measurements taken on these materials in the centrifuge models. Nonetheless, it was considered that if the yielding strains were weaker, the model would behave as a conservative estimate of the prototype.

The results listed in Table III.4 illustrate that flexural strengths for laminated beams (with a reasonable amount of bonding between layers) are equivalent to flexural strengths of beams with no bedding. This effect is best illustrated by the results for

the 2:1 mixtures. Conversely, laminated beams with debonded layers can have significantly weaker flexural strengths (as exemplified by the variability of results in the 0:1 mixture beams). It was found that these debonded layers tended to detach from the main beam, thus reducing the sectional area and inducing artificially high bending stress.

In fact, it was evident that bedding imperfections inherent within both the insitu and equivalent material had a significant effect on the bending moments/curvature of beams. Even when using only maximum deflections, the effect of these imperfections on surficial movements of small scale beams is too great to allow a meaningful relationship to be developed between maximum deflection and horizontal strain.

It is considered that a better test would be to vertically confine the beams and conduct a similar suite of four point bending tests on these confined beams. It was probable that the flexural strength of bedded materials is significantly improved by confinement. Some considerable time was spent investigating the potential for developing such tests; however, it was found that given the time and budget constraints for this project, these tests had to be omitted.

As discussed in Section 4.2.2.1, it is also essential to provide adequate similitude for modelling material densities. In order to predict the likely density of an equivalent material for a given sand:plaster raio (material strength), a predictive curve was fitted to the density data listed in Table III.4 for the range of sand:plaster mix ratios tested. The resultant equation, depicted by Figure III.17, is given as:

$$\text{Density } (\gamma)\ (t/m^3) = 4.24 - 3.11 \times \exp^{-[(\text{Ratio})^{0.6}/22]} \qquad 4.2(9)$$

where Ratio = the ratio of sand to plaster (by weight) in the mix.

It can be seen that there is some divergence between the calculated and measured densities at sand:plaster ratios around 4.0. This divergence is probably due to the change in the make-up of the mix as fine plaster particles are replaced by the coarser sand particles. This significance of this divergence is considered to be small, as the models did not require a sand:plaster mix of 4.0.

Prior to testing the in situ material centrifuge models, the requirements of fill material between individual blocks of strata was also investigated. It was considered that

without any fill, it would not be possible to achieve a suitable shear strength at the interface of the separate insitu material blocks, or individually cast blocks of equivalent material. According to MINCAD's initial investigations, and from discussion provided in Section 4.2.2.1, shear strength across bedding, was critical to the succes of modelling the subsidence process.

After a number of mixes of sand:plaster:water were trialed a suitable, workable mix was determined. This mix was then tested between two slabs of insitu material (one coal and one sandstone slab) to determine the shear strength of the mix. The results, given in Table III.11 indicate that the shear strength of the mix is:

Cohesion - 25 kPa, Friction - 30°.

It was considered, from personal experience in the Collie Basin, that this mix adequately represented the typical interface shear strength between coals and sandstones.

An additional shear test was provided to assess what the shear strength of the interface would be without the fill material. This test, again listed in Table III.12, demonstrates that without the fill material the shear strength drops significantly to:

Cohesion - 0 kPa, Friction - 25°.

The filling mix (600 g of sand, 270 g of water, 335 g of plaster) was hence used for all centrifuge modelling.

Bore core Testing - 1North Panel

Prior to the calibration of SUBSOL, it was necessary to establish a full suite of mechanical properties for the complete stratigraphic section above 1North Panel as there was minimal geotechnical data available in this area. (The 1North panel was to be used as a back-analyses of calibrated models from ACIRL and 2SA panels - see Section 4.1.1.) In order to minimise costs it was decided to use the extensometer holes D212 and D213 as sources of core. The approach to coring was to drill the first hole (D212) using mud-rotary/diamond boring techniques and attempt to retrieve as much core as possible. The termination depth of this hole was at the marker seam, approximately 6 m above the Wyvern seam. The second hole (D213) was drilled in two stages; the first using reverse circulation air (RC) drilling techniques down to the

Marker seam followed by mud-rotary/diamond drilling "tail". The termination depth of this hole was 8 m below the Wyvern seam floor. The diamond tail section of the borehole was sealed with cement slurry to prevent water influx into the mine workings from the superimposed strata.

The purpose for drilling in this manner was that the first hole would be used to detect areas of poorly consolidated ground which could not be sampled by diamond drilling. These measured intersections of core loss were then carefully sampled in the second hole by collecting the return samples from the RC drill rig's cyclone.

Core recovery was achieved in each borehole by triple tube wire-line techniques, using HQ sized drill bits and barrels. Core recovery was generally good, except for the first 30 m or so in the unconsolidated Nakina formation.

Laboratory tests on the highly disturbed RC material were achieved by reconsolidating the samples by standard compaction techniques to the densities determined from the core samples from D212 and down-hole geophysical data.

All test results are presented in Table III.13.

TYPICAL GRADING CURVE FOR MODEL SAND

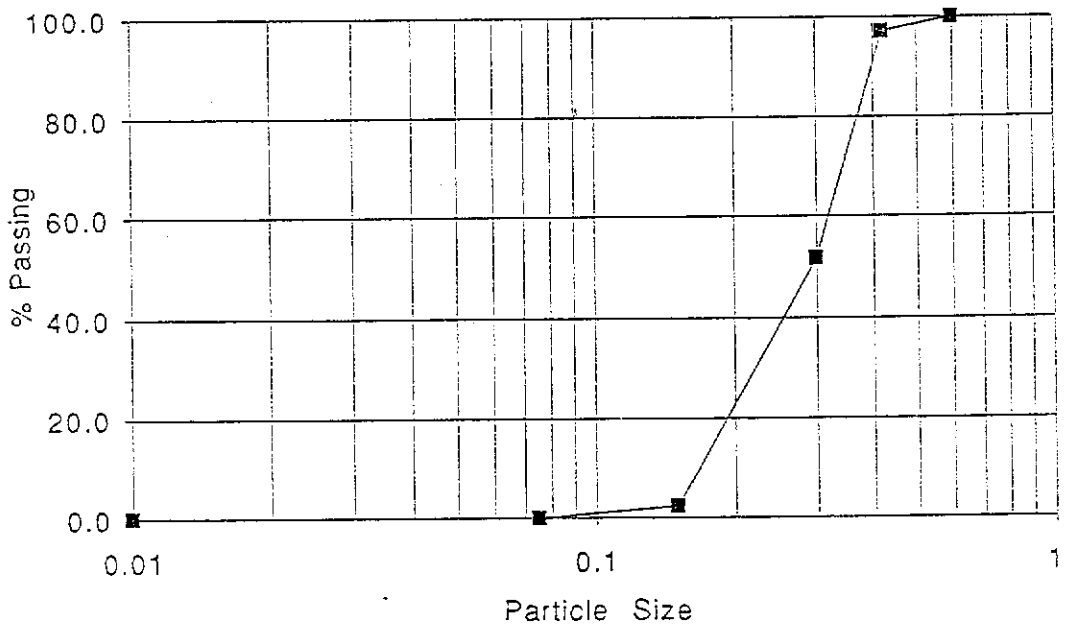

Figure III.1

DIRECT SHEAR TEST FOR MODEL SAND

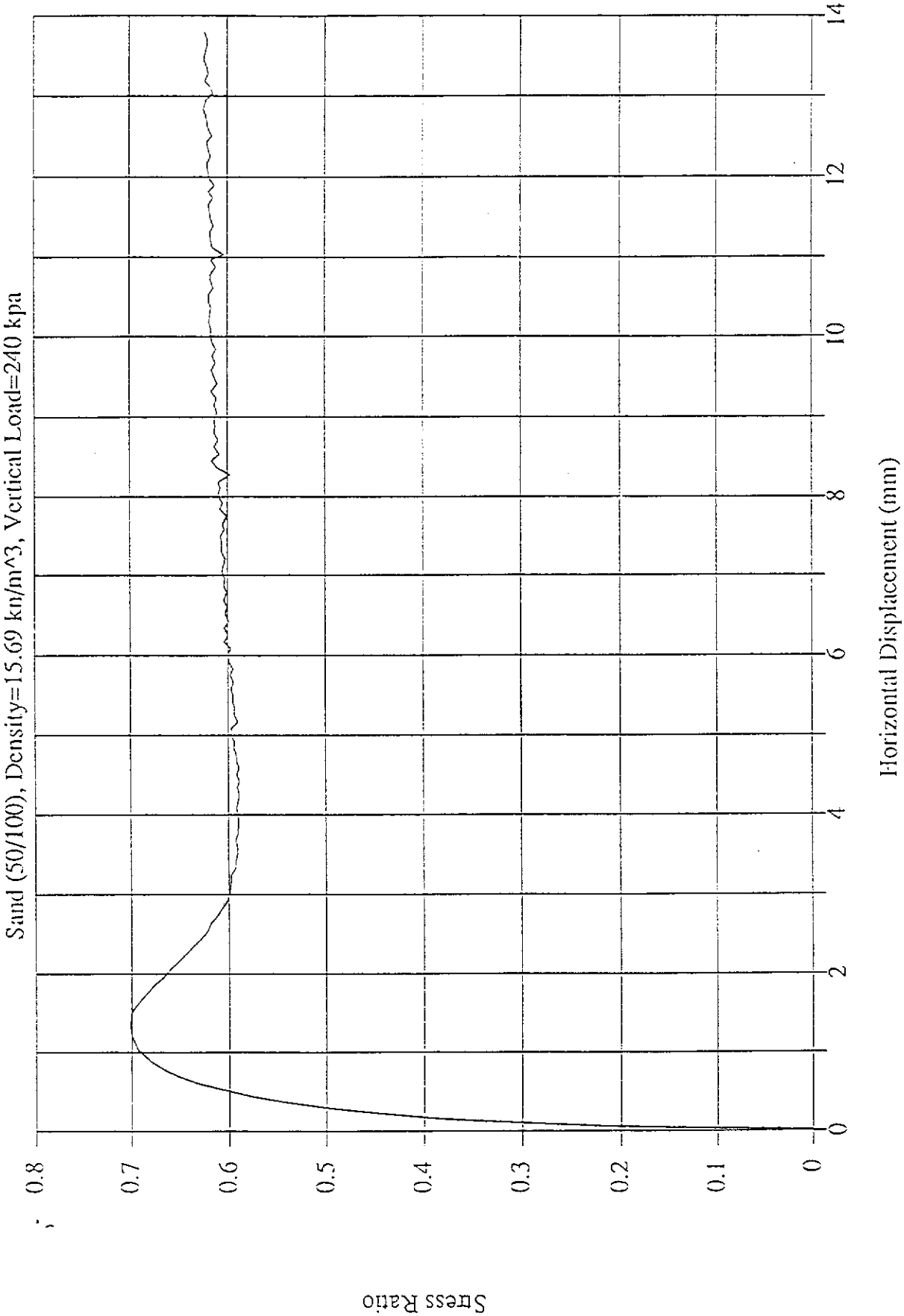

Figure III.2

ILLUSTRATION OF AIR POCKETS WITHIN EARLY MODEL MIXES

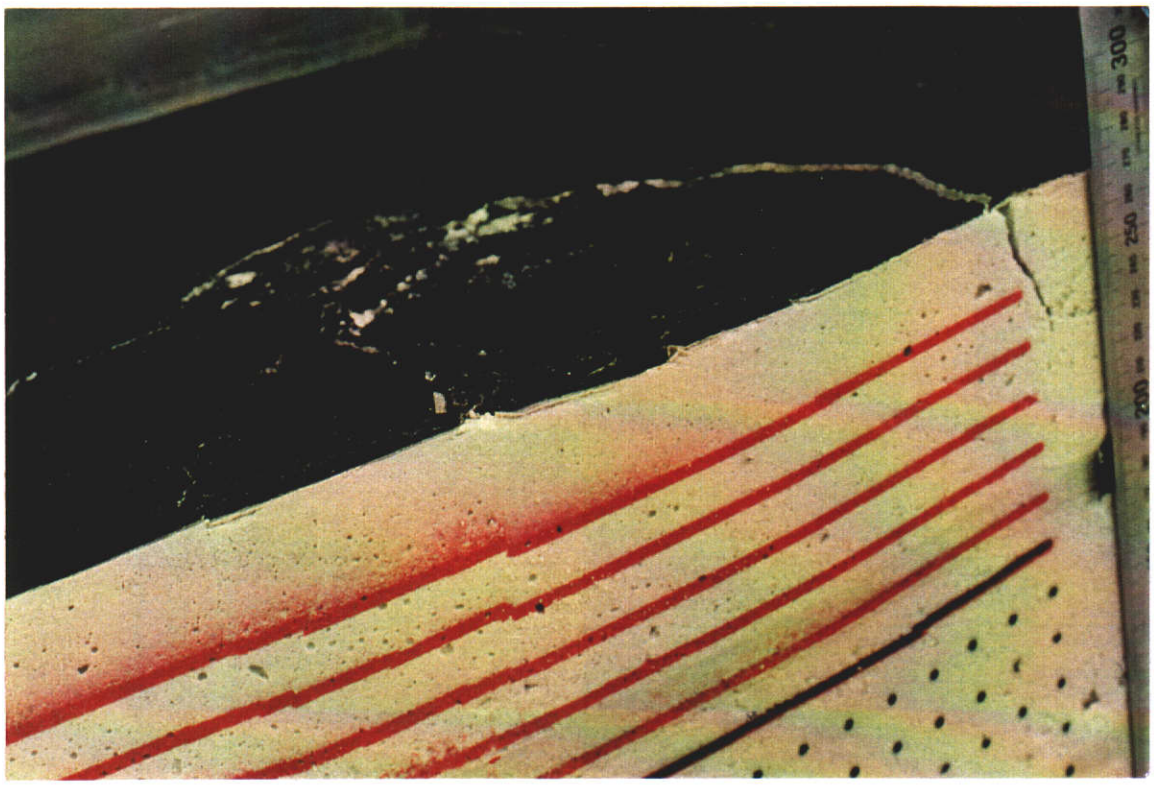

Figure III.3

VARIATION IN COMPRESSIVE STRENGTH WITH TIME IN EARLY MODEL MIXES

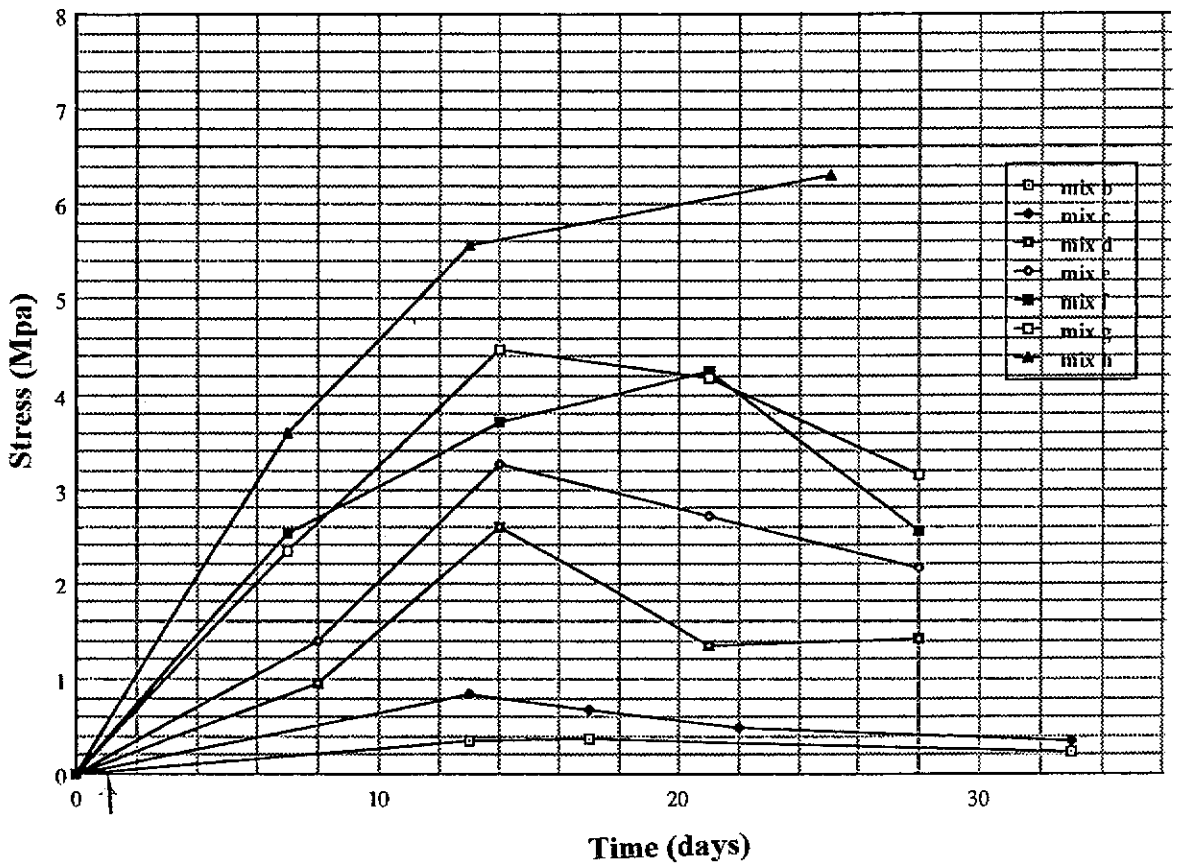

Figure III.4

UCS & FLEXURAL STRENGTH Vs SAND : PLASTER RATIO FOR ALL TESTS

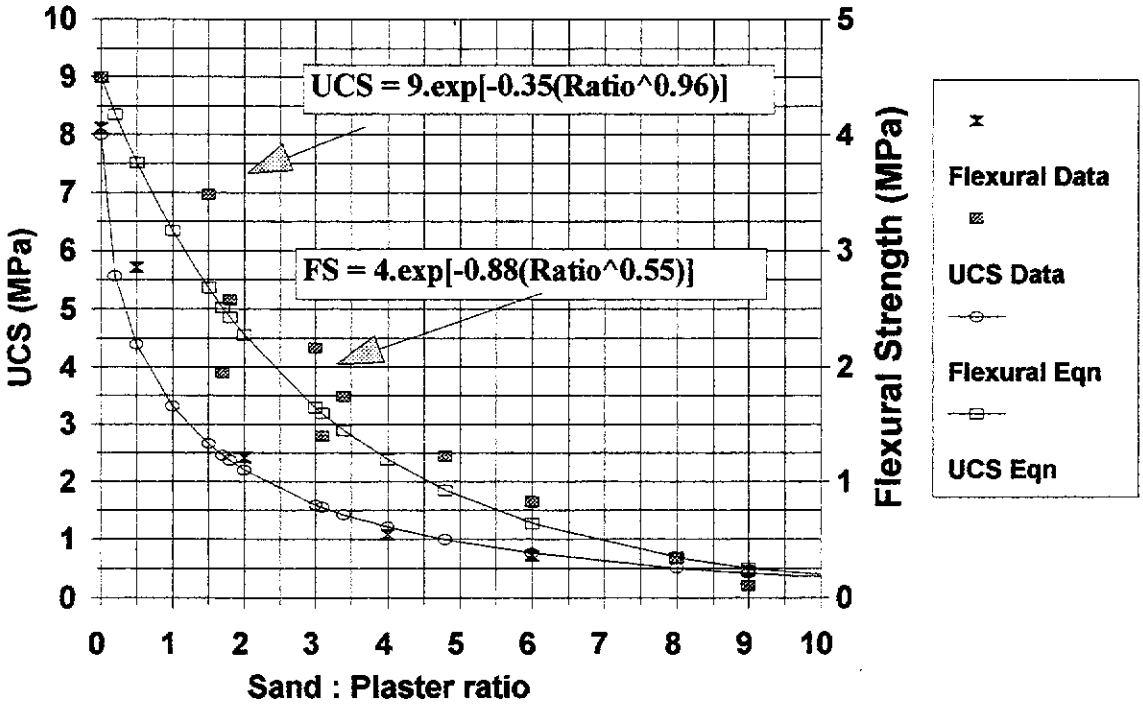

Figure III.5

FLEXURAL STRENGTH TEST RIG AND DEFINITION OF CALCULATION

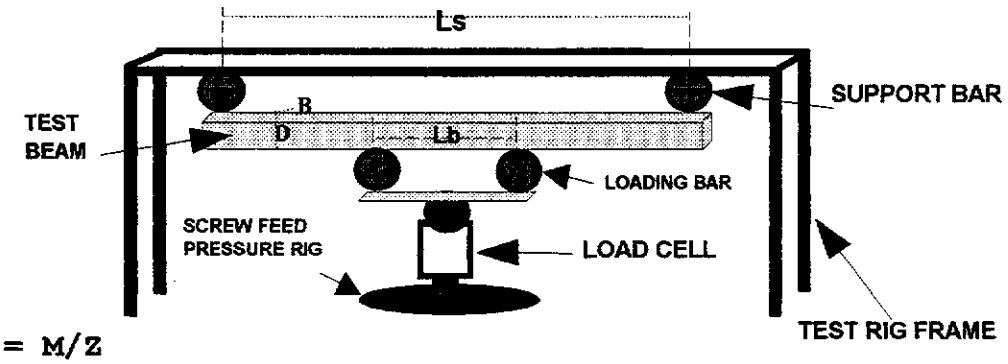

$Fs = M/Z$

Where ;

Fs = Flexural Strength (MPa)

M = Bending Moment at Failure (Nmm) $W/4\ (Ls - Lb)$

Z = Section modulus of test beam specimen (cu.mm) $\frac{BD^2}{6}$

Where ;

W = Yield load (N)

Ls = Distance between support bars (mm)

Lb = Distance between loading bars (mm)

B = Average width of each specimen (mm)

D = Average depth of each specimen (mm)

Figure III.6

TYPICAL LOADING CYCLE FOR FLEXURAL STRENGTH TESTS

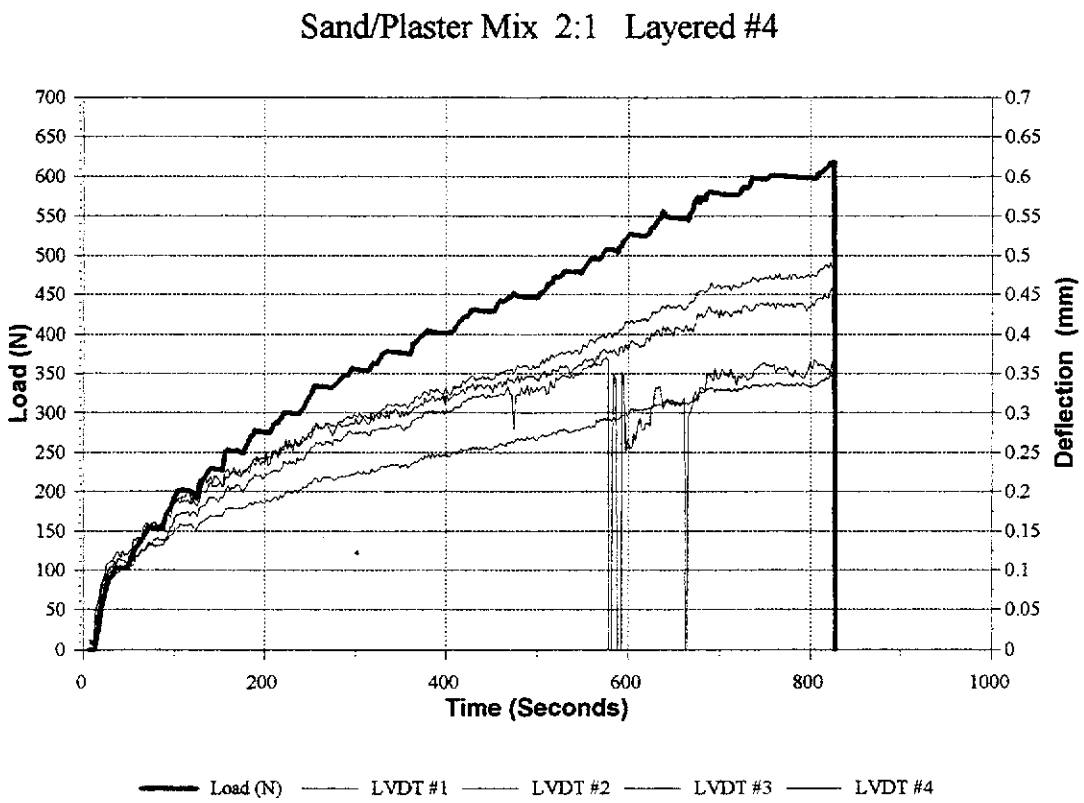

Figure III.7

BEAM DEFLECTION MONITORING SET-UP

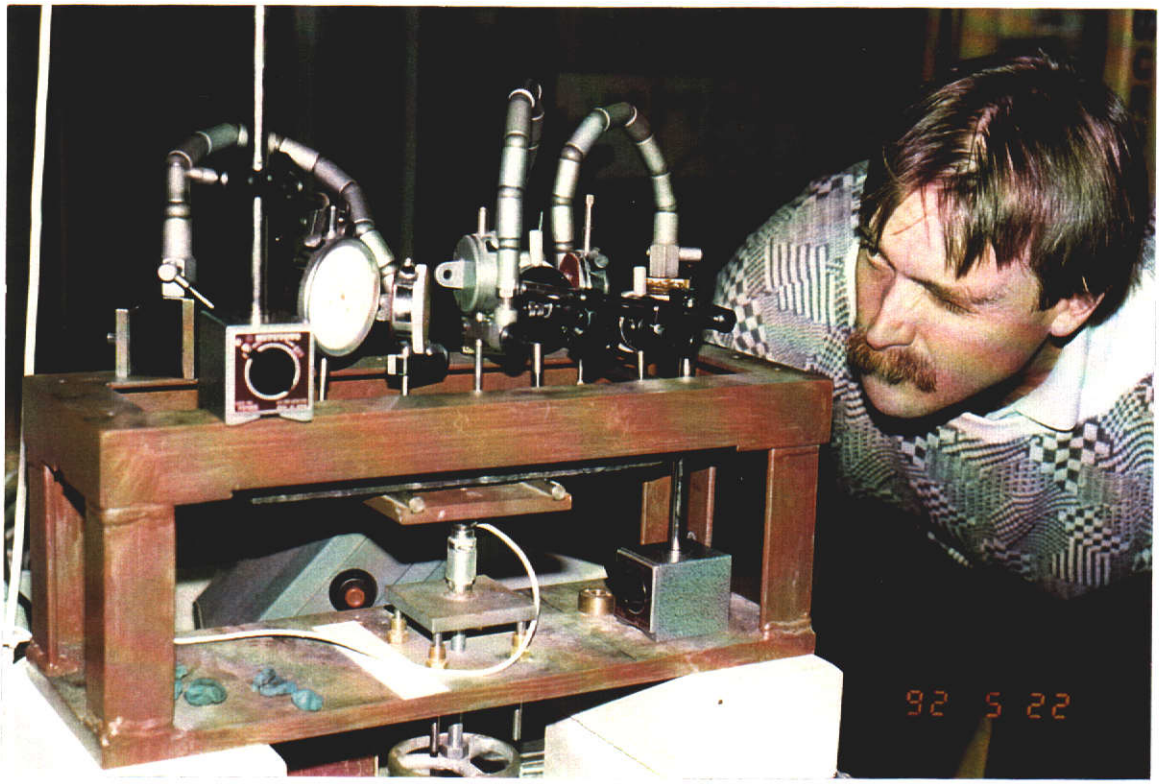

a) Dial gauge set-up

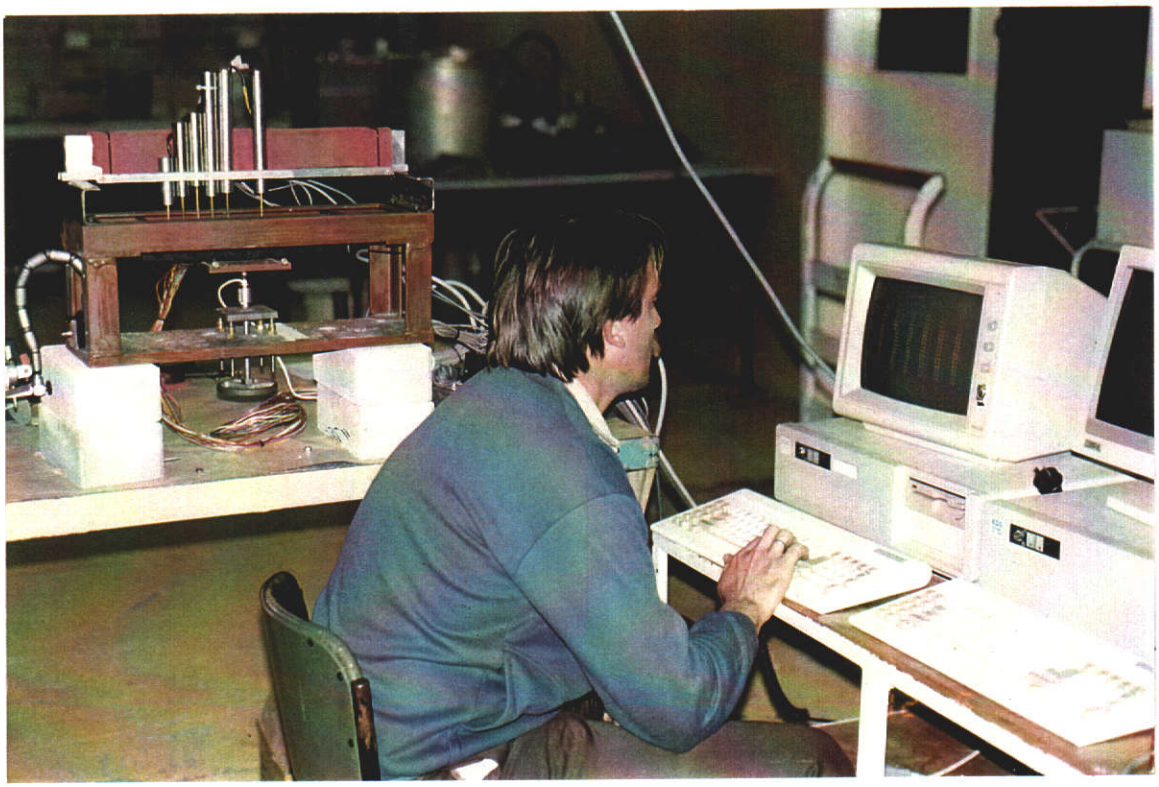

b) LVDT set-up

Figure III.8

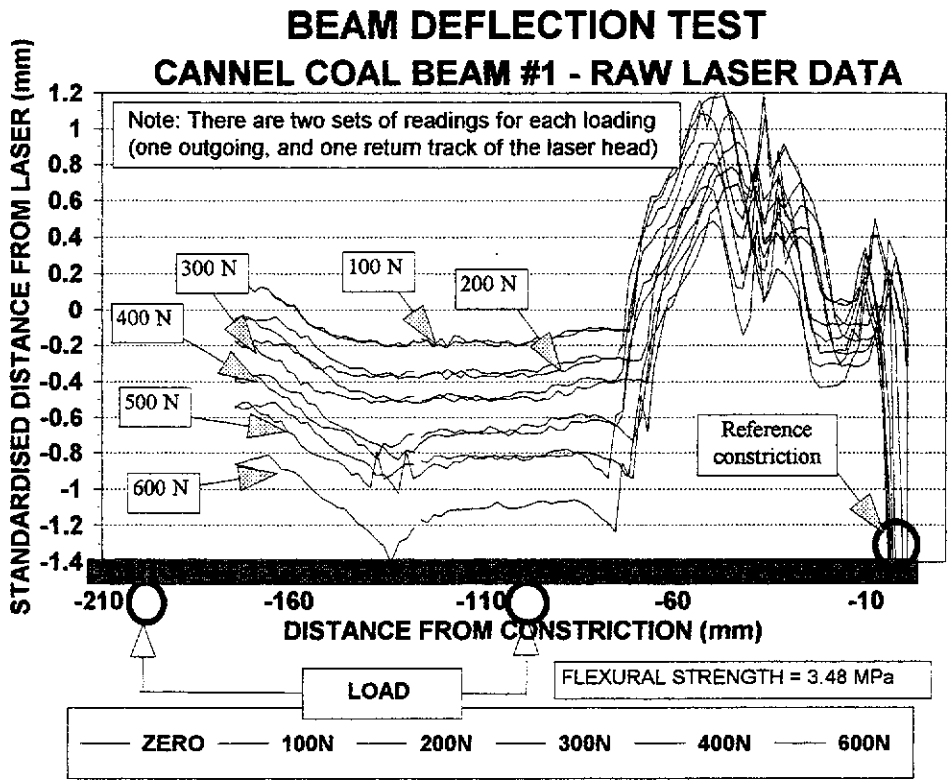

Figure III.9 a

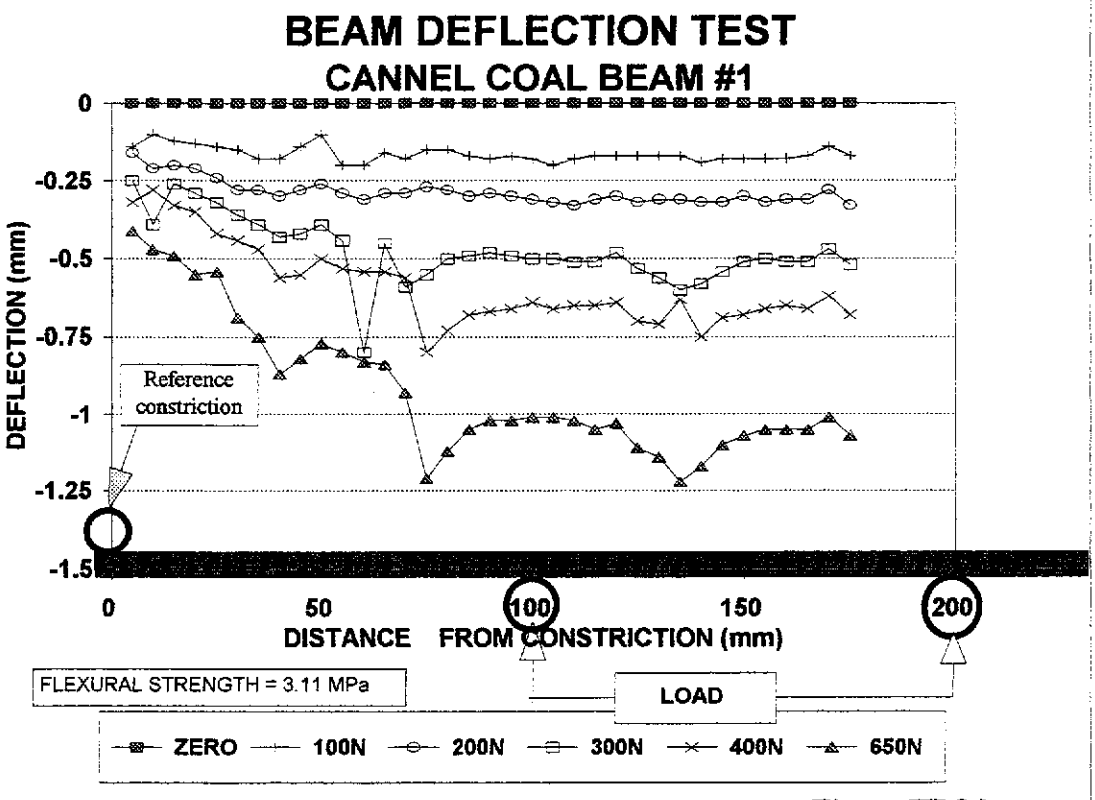

Figure III.9 b

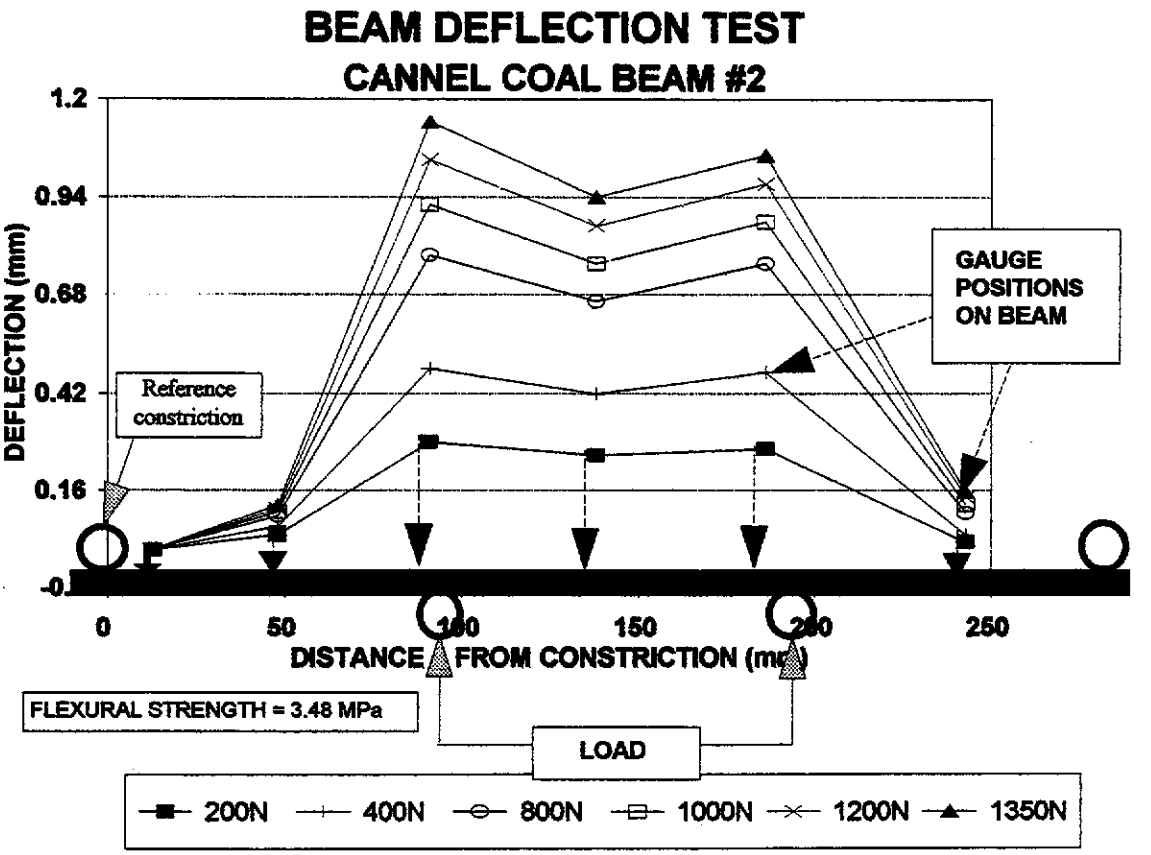

Figure III.10

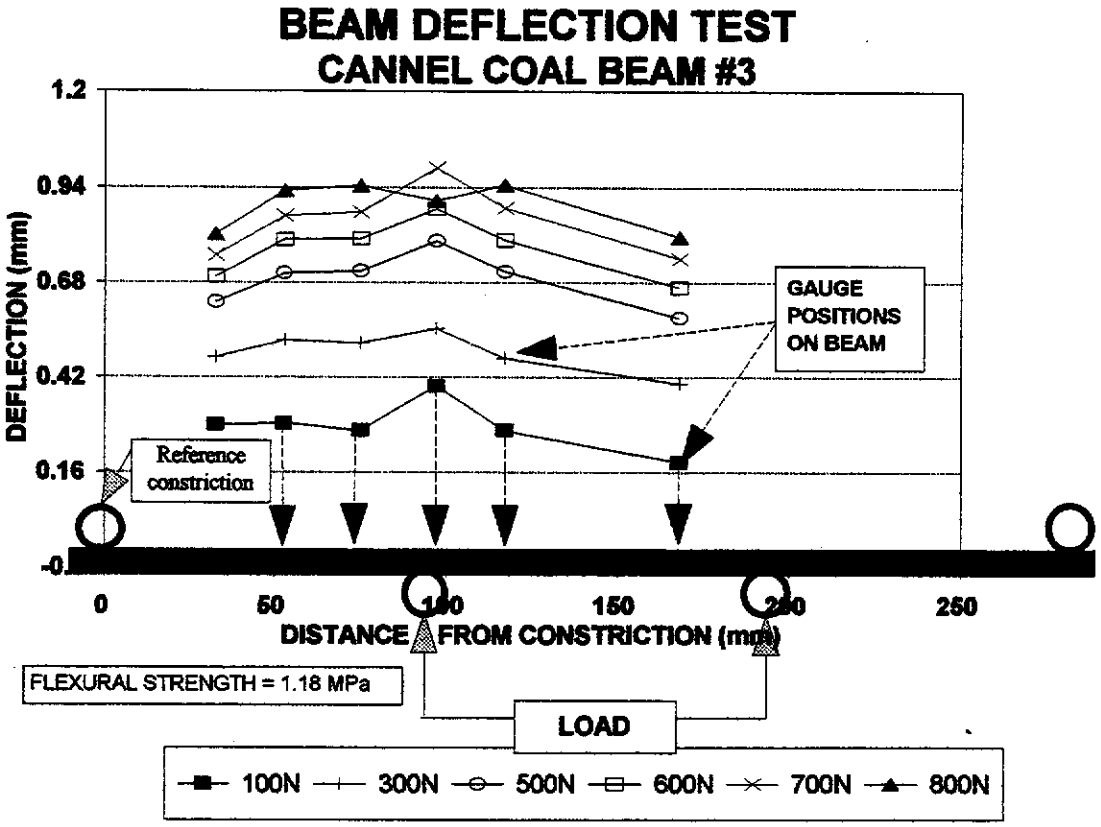

Figure III.11

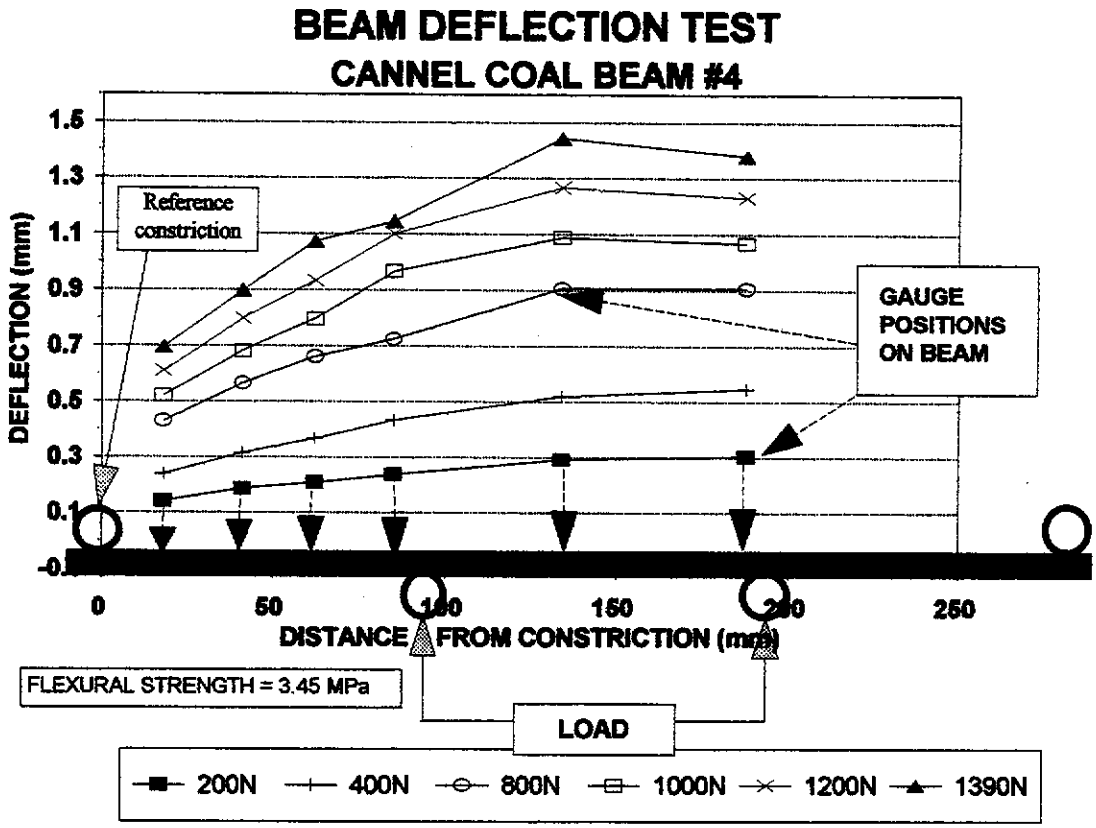

Figure III.12

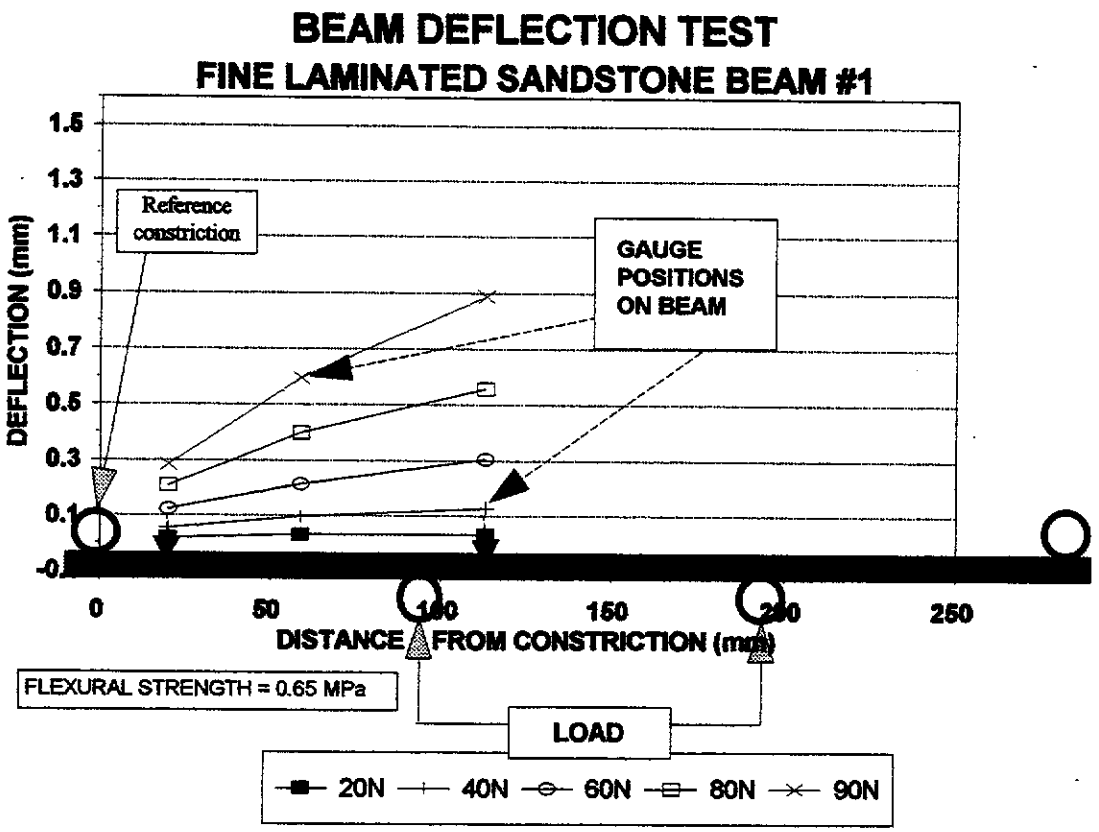

Figure III.13

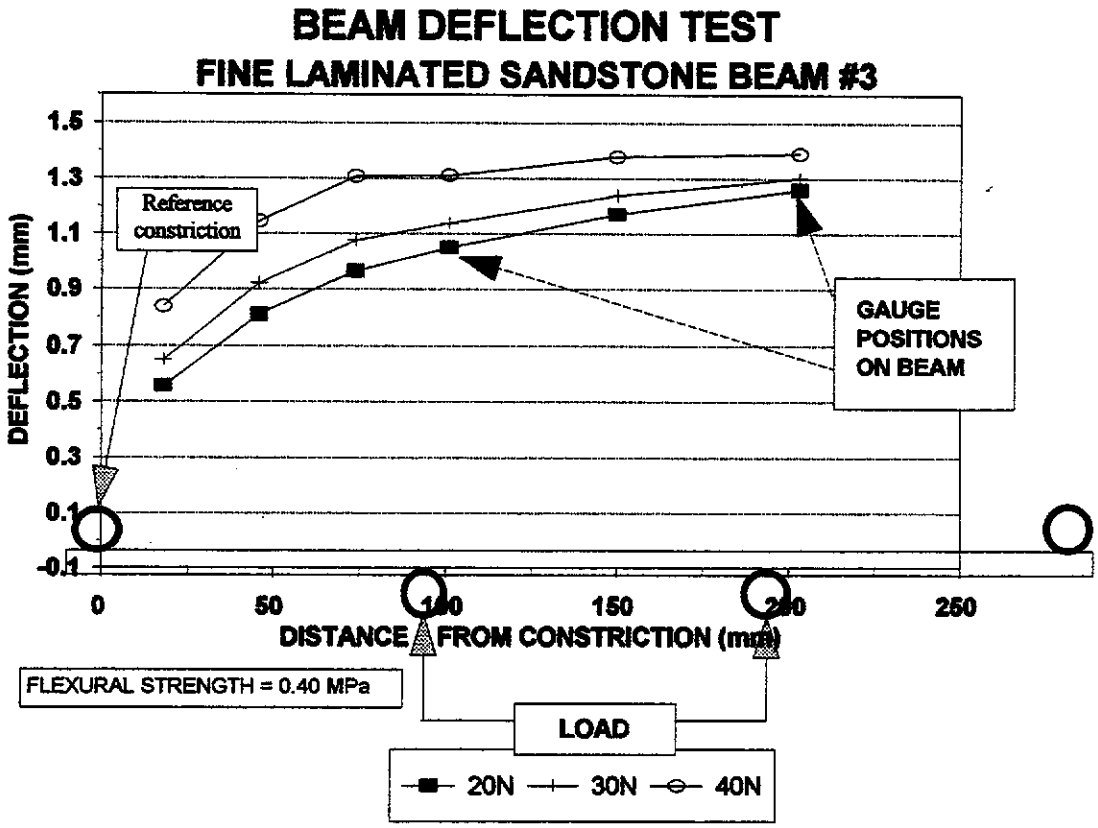

Figure III.14

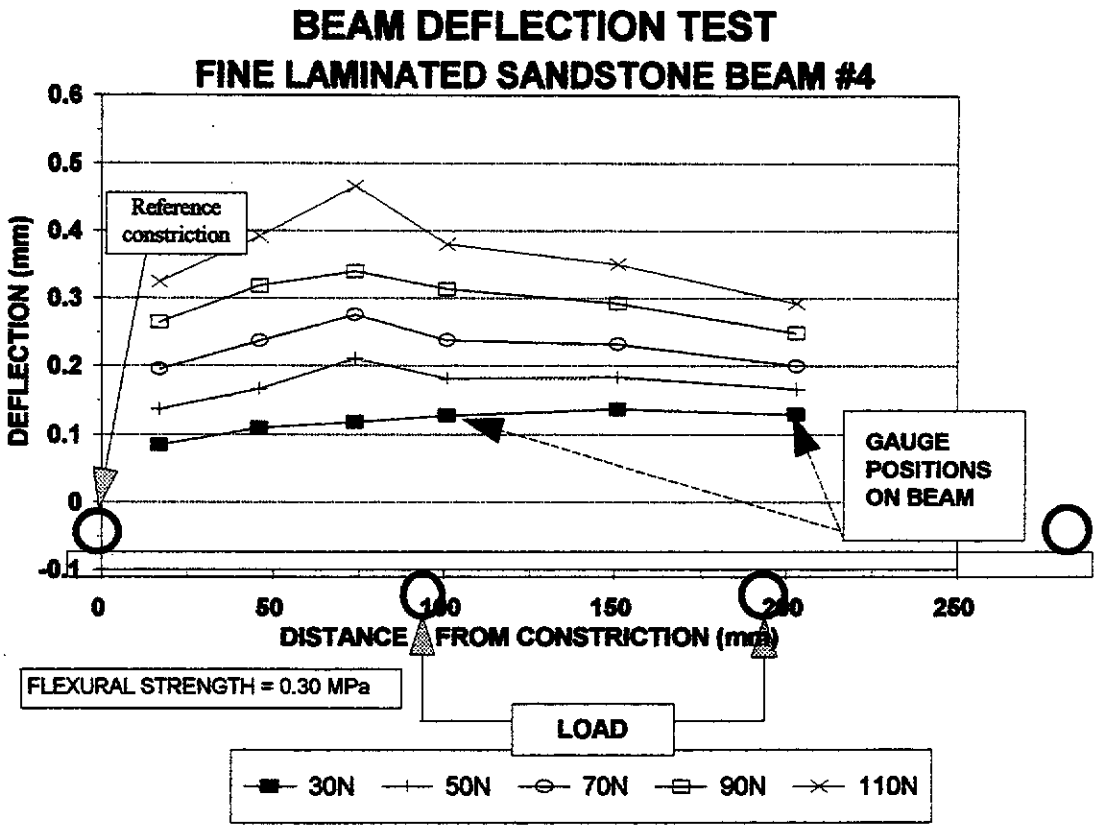

Figure III.15

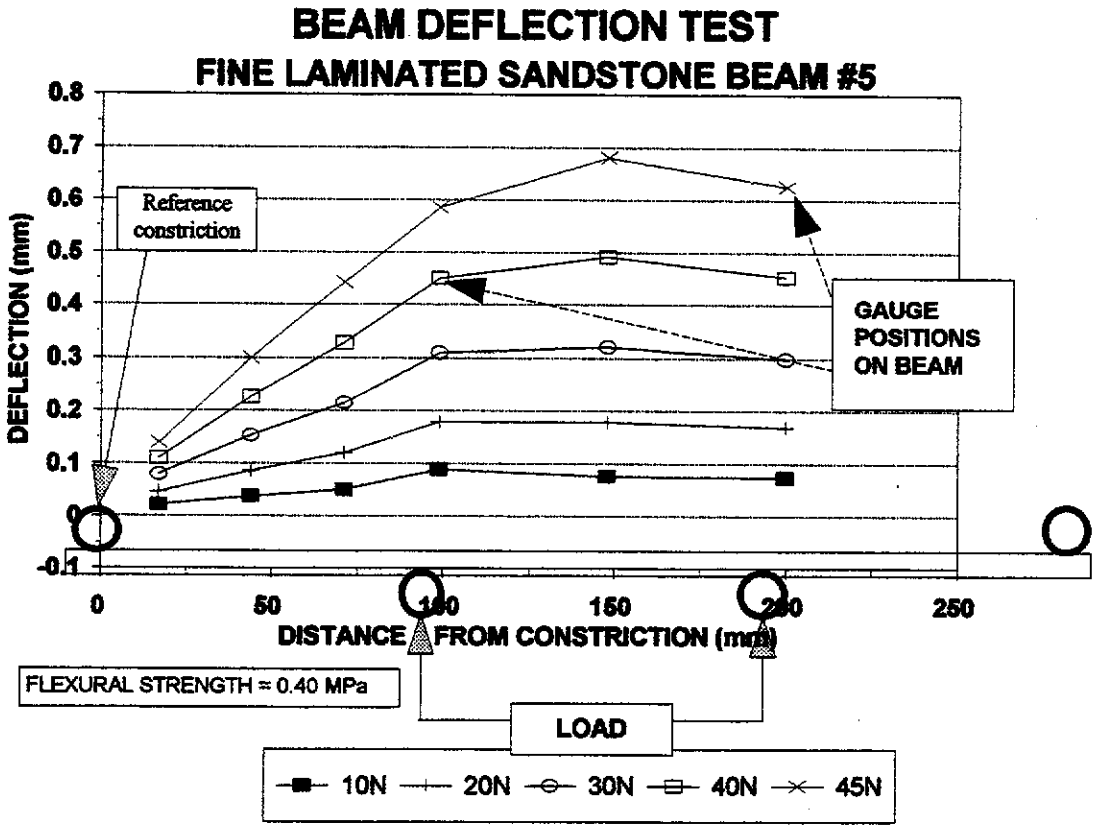

Figure III.16

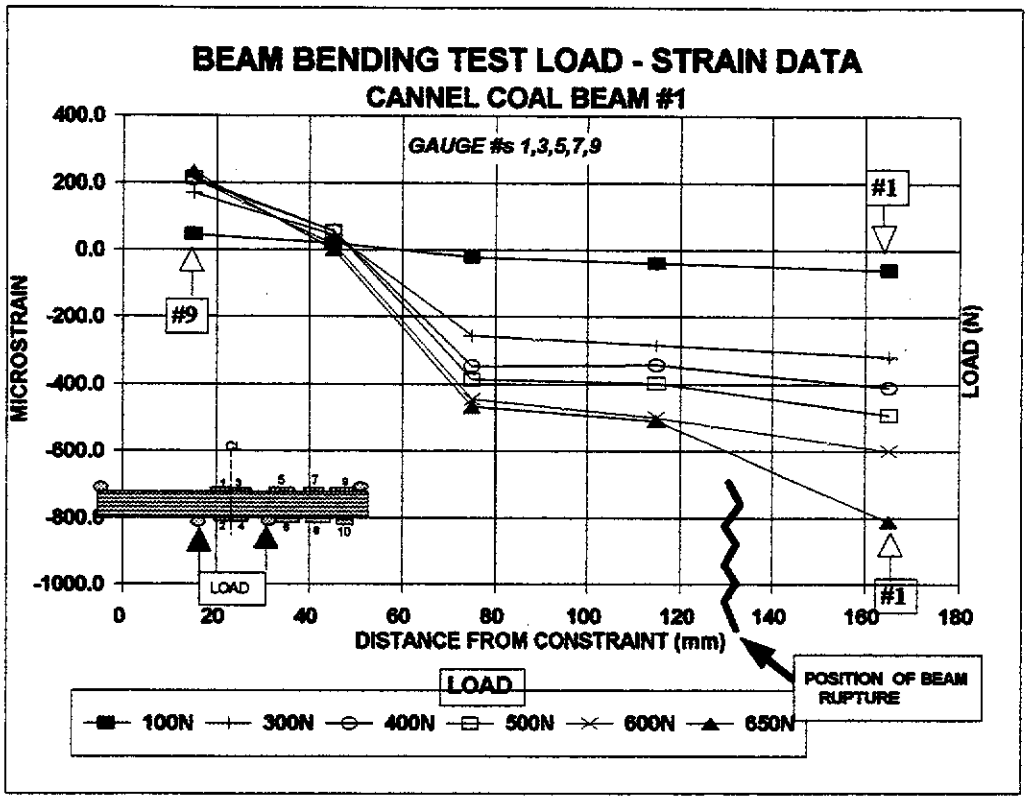

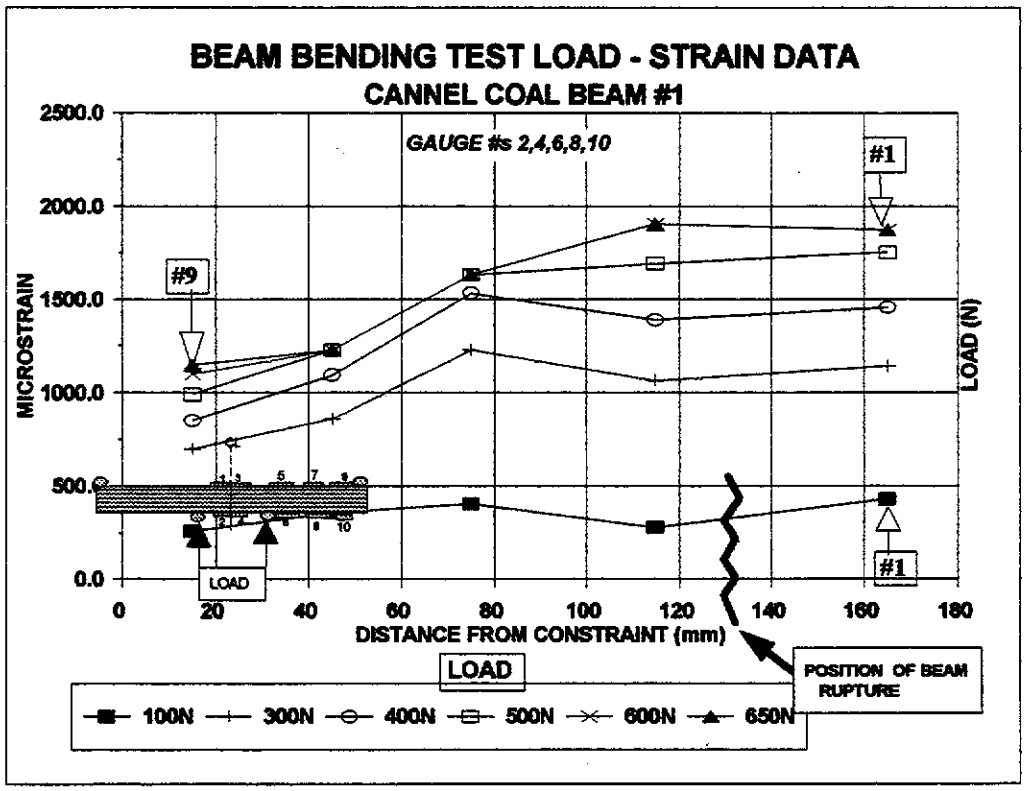

Figure III.17

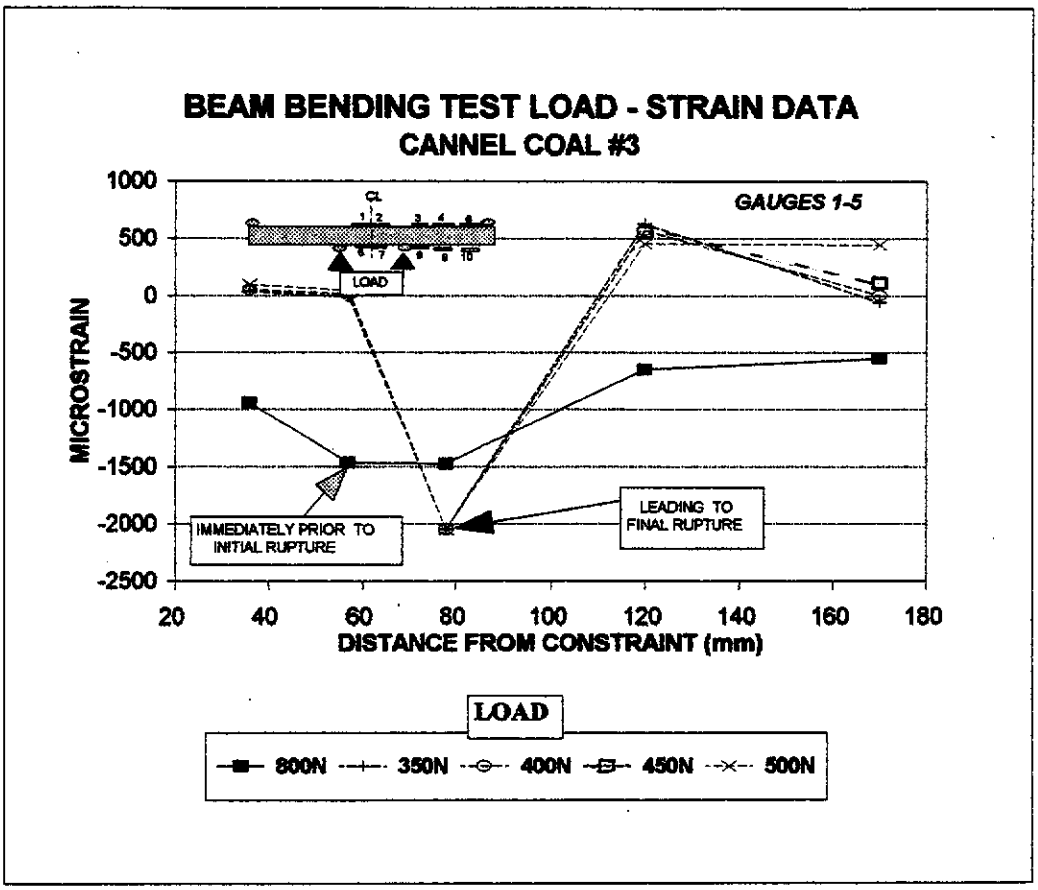

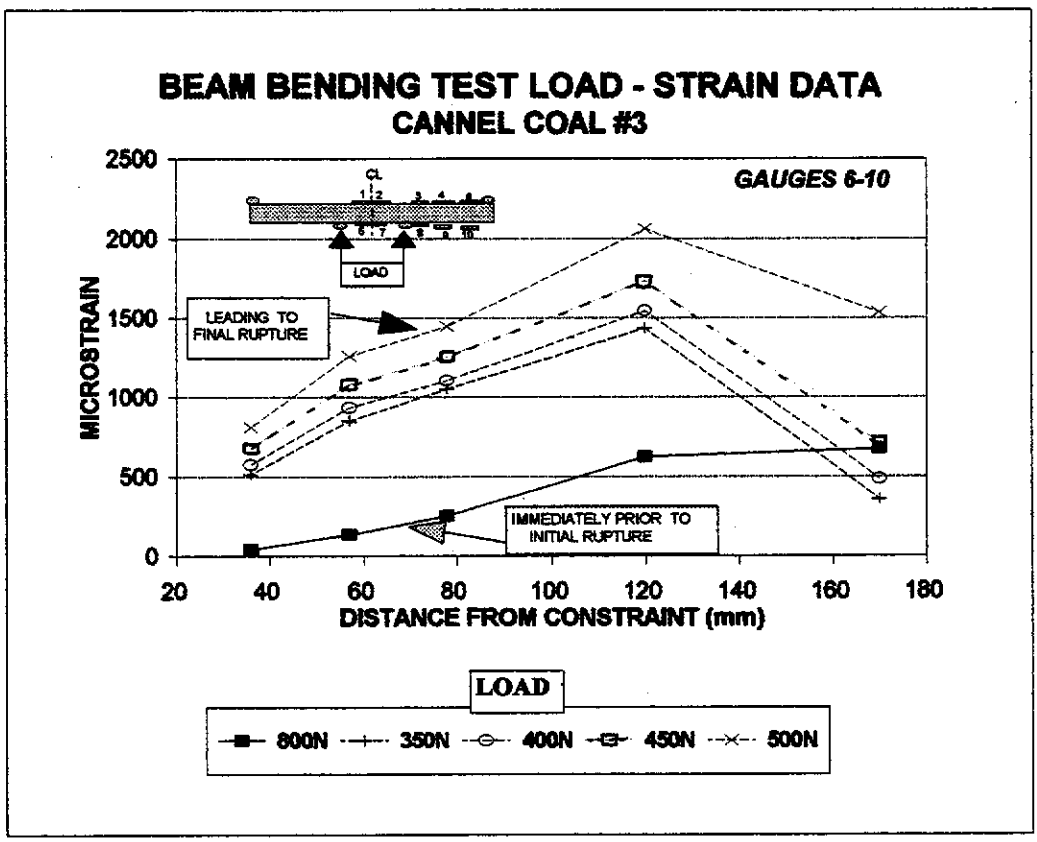

Figure III.18

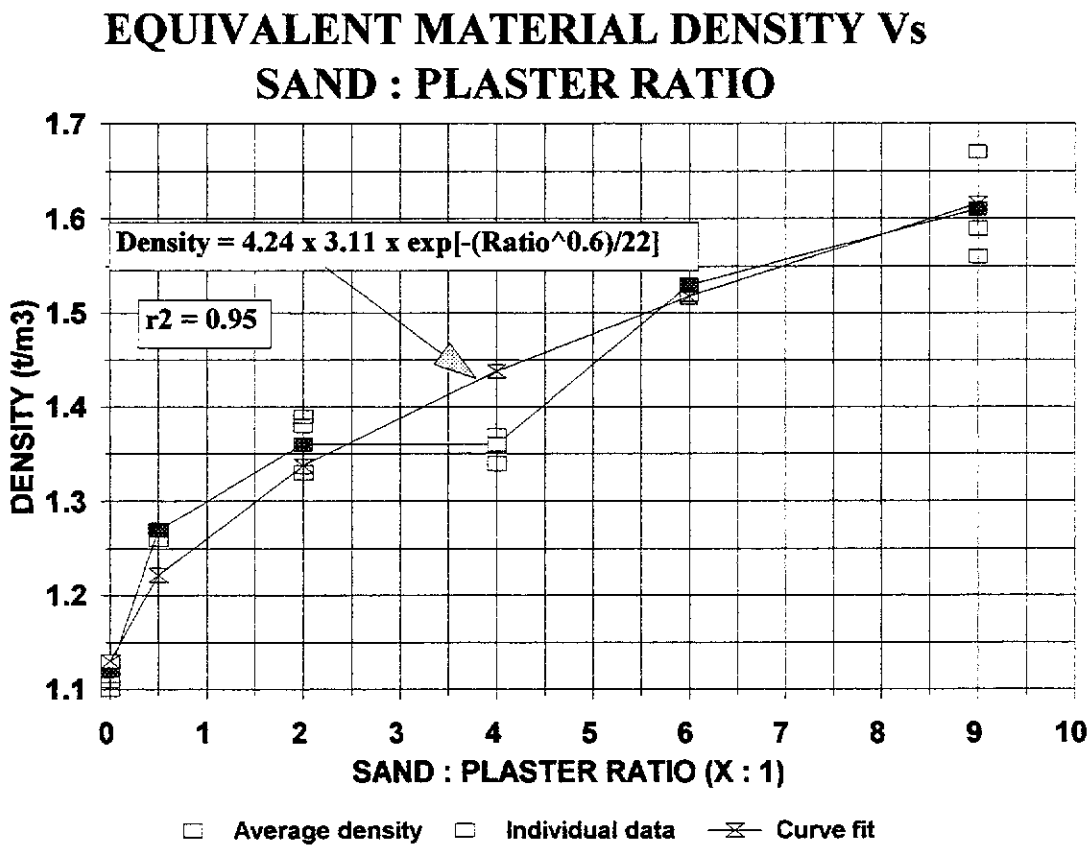

Figure III.19

TABLE III.2

INSITU MATERIAL MECHANICAL PROPERTY TESTING

	BEAM BENDING TESTS						UCS TESTS			
SAMPLE LITHOLOGY	LENGTH (Ls) (mm)	LENGTH (Ll) (mm)	WIDTH (mm)	DEPTH (mm)	YIELD LOAD (N)	FLEXURAL STRENGTH (MPa)	UCS (MPa)	E (MPa)	v	BULK DENSITY (t/m3)
CANNEL COAL #1	282	100	38.0	38.0	651.1	3.24				
CANNEL COAL #2	290	100	48.0	48.0	1350.0	3.48				
CANNEL COAL #3 **	288	100	50.0	49.0	503.6	1.18				
CANNEL COAL #4	290	100	49.0	48.5	1395.6	3.45				
					AV.=	3.39				
COARSE SSTONE #1	287	100	38.0	40.0	95.0	0.44	12.2	143	0.03	1.92
COARSE SSTONE #2	285	100	50.0	49.5	250.0	0.57	7.6	233	0.08	1.92
					AV.=	0.51	9.9	188	0.06	1.92
FINE LAM. SSTONE #1	300	100	34.0	33.0	80.0	0.65	1	74	0.29	1.82
FINE LAM. SSTONE #2	300	100	34.5	35.0	49.7	0.35	1.93			2.06
FINE LAM. SSTONE #3	298	100	31.0	32.0	42.3	0.40	0.32			
FINE LAM. SSTONE #4	300	100	51.5	49.0	123.6	0.30	0.32			
FINE LAM. SSTONE #5	300	100	32.5	35.0	47.4	0.36	0.4			
					AV.=	0.41	0.43			
							0.73			1.94

** = BROKE ALONG BEDDING PLANE WEAKNESS
SSTONE = SANDSTONE, LAM. = LAMINATED

TABLE III.3

EQUIVALENT MATERIAL MECHANICAL PROPERTY TESTING

BEAM BENDING TESTS

SAND:PLASTER MIX RATIO	LENGTH (Ls) (mm)	LENGTH (Ll) (mm)	WIDTH (mm)	DEPTH (mm)	YIELD LOAD (N)	FLEXURAL STRENGTH (MPa)	Maximum Deflection (mm)	DENSITY (t/m3)	CURING TIME	COMMENTS
0:1 #1 (laminated)	290	100	50	50	1947	4.44	0.6	1.13		
0:1 #2 (laminated)	290	100	50	50	1181	2.69	0.8	1.11		broke on laminations
0:1 #3 (laminated)	290	100	50	50	1100	2.51	0.8	1.13		broke on laminations
0:1 #4 (laminated)	290	100	50	50	1611	3.67	0.5	1.1		broke on laminations
					AV.=	4.06	0.68	1.12		
.5:1 #1 (homogenous)	290	100	50	50	1039	2.37		1.27	48hrs	
.5:1 #2 (homogenous)	290	100	50	50	1350	3.08	0.3	1.26		
.5:1 #3 (homogenous)	290	100	50	50	1368	3.12				
					AV.=	2.86	0.3	1.27		
2:1 #1 (homogenous)	290	100	50	50	475	1.08	0.4		<12hrs	
2:1 #2 (homogenous)	290	100	50	50	532	1.21	0.6	1.33	48hrs	
2:1 #3 (homogenous)	290	100	50	50	521	1.19	0.4		<12hrs	
2:1 #4 (homogenous)	290	100	50	50	545	1.24		1.33	7 DAYS	
2:1 #5 (homogenous)	290	100	50	50	631	1.44	0.38		<12hrs	
2:1 #5a (homogenous)	290	100	50	50	222	0.51			<12hrs	not fully cured
					AV.=	1.23	0.44	1.33		
2:1 #1 (laminated)	290	100	50	50	458	1.04	0.45	1.39	48hrs	
2:1 #2 (laminated)	290	100	50	50	374	0.85	0.42	1.38	48hrs	
2:1 #3 (laminated)	290	100	50	50	600	1.37	0.52	1.38	<12hrs	
2:1 #4 (laminated)	290	100	50	50	617	1.41	0.49	1.36	<12hrs	
2:1 #5 (laminated)	290	100	50	50				1.38		
2:1 #6 (laminated)	290	100	50	50				1.38		
					AV.=	1.17	0.46	1.38		
4:1 #1 (laminated)	290	100	50	50	322	0.73	1	1.37	<12hrs	
4:1 #2 (laminated)	290	100	50	50	211	0.48	0.35	1.34	48hrs	broke on laminations
4:1 #3 (laminated)	290	100	50	50	220	0.50	0.48	1.36	7 DAYS	broke on laminations
4:1 #4 (laminated)	290	100	50	50				1.36		
					AV.=	0.54	0.41	1.36		
6:1 #1 (homogenous)	290	100	50	50	192	0.44		1.53	48hrs	
6:1 #2 (homogenous)	290	100	50	50	123	0.28	0.27	1.52		
6:1 #3 (homogenous)	290	100	50	50						
6:1 #4 (homogenous)	290	100	50	50						
					AV.=	0.36	0.27	1.53		
9:1 #1 (homogenous)	290	100	50	50	92	0.21		1.56	48hrs	
9:1 #2 (homogenous)	290	100	50	50	83	0.19		1.59		
9:1 #3 (homogenous)	290	100	50	50	123	0.28		1.67	7 DAYS	
9:1 #4 (homogenous)	290	100	50	50						
					AV.=	0.23		1.61		

NOTE : LOW STRENGTH VALUES RESULTING FROM BEDDING FAILURES WERE NOT INCLUDED IN AVERAGED VALUES

UCS TESTS

SAND: PLASTER MIX RATIO	UCS (MPa)	E (MPa)	CURING TIME (days)
24:1	BROKE UP DURING HANDLING		
12:1	0.35	96	13
12:1	0.37	70	17
12:1	0.23		22
AV. =	0.32	83	
8:1	0.85	300	13
8:1	0.66	80	16
8:1	0.49	55	
AV. =	0.67	145	
6:1	0.95	350	8
6:1	2.60	766	14
6:1	1.40	440	28
AV. =	1.65	519	
4.8:1	1.39	343	
4.8:1	3.27	881	8
4.8:1	2.70	1001	14
AV. =	2.45	742	21
3:4	2.53	840	7
3:4	3.70	1100	14
3:4	4.23	1300	21
AV. =	3.49	1080	7
3:1	2.34	747	14
3:1	4.47	1440	21
3:1	4.17	1070	
AV. =	4.32	1255	7
1.6:1	3.60	1170	13
1.6:1	5.57	2010	20
1.6:1	6.32	2350	
AV. =	5.16	1843	
1.5:1	8.80	2307	7
1.5:1	5.70	1530	7
1.5:1	6.40	1920	
AV. =	6.97	1919	
0:1	9.00		
1.7:1	3.90		
3:1	2.80		
9:1	0.20		
6:1	1.15		

TABLE III.4

UCS TESTS ON IN SITU MATERIAL USED IN CENTRIFUGE MODELS PS01 - PS03

SRC Laboratories
A division of Aust-Amec Pty Ltd

Correspondence: P.O. 184 Doubleview W.A. 6018
34 Walters Drive, Herdsman Business Park
Osborne Park W.A. 6017
Phone (09) 244 1199 Telex: AA197099
Facsimile (09) 244 1457

REF: S8835/DW:ld

28 July 1992

WESTERN COLLIERIES LTD
PO Box 21
COLLIE WA 6225

ATTENTION: Mr I Misich

Dear Sir

RE: CENTRIFUGE TEST INSITU MATERIAL NO.3 - ORDER NO: 63902

Attached are the following documents of report for work required by you on the above project:

1	PLATE	Unconfined Compressive Strength Of Intact Rock Specimens Summary
1	PLATE	Photographic Summary

If we can assist further, please advise.

Yours faithfully
DAWN WIMPERIS

Branch Manager WA
for SRC Laboratories

CLIENT:	WESTERN COLLIERIES LTD	**SHEET No.:** 2	**OF:** 3
PROJECT:	CENTRIFUGE TEST INSITU MATERIAL 3	**JOB No.:**	S8835
		DATE TESTED:	27/7/92

UNCONFINED COMPRESSIVE STRENGTH OF INTACT ROCK SPECIMENS SUMMARY

Tested in accordance with ASTM D2938-71a

SAMPLE IDENTIFICATION:

Rectangular Prism with Height to Width Ratio: 2.2:1

PHYSICAL DESCRIPTION:

Name Of Rock: Fine - Medium Sandstone

SPECIMEN DATA:

HEIGHT:	130.7	mm
WIDTH:	60.5	mm
DEPTH:	57.7	mm
MASS:	826.9	g
DRY DENSITY:	1.81	t/m^3
HEIGHT/WIDTH RATIO:	2.2:1	
MOISTURE CONTENT:	12.3	%
RATE OF LOADING:	1	kN/minute
UNCONFINED COMPRESSIVE STRENGTH:	1930	kPa
REMARKS:	Nil	

TESTED BY: KM CHECKED BY: AG DATE: 28/7/92

* Denotes use of Rock Colour Chart

CLIENT:	WESTERN COLLIERIES LTD	**SHEET No.:** 3	**OF:** 3
PROJECT:	CENTRIFUGE TEST INSITU MATERIAL 3	**JOB No.:**	S8835
		DATE TESTED:	27/7/92

PHOTOGRAPHIC SUMMARY

SAMPLE IDENTIFICATION:

Rectangular Prism with Height to Width Ratio: 2.2:1

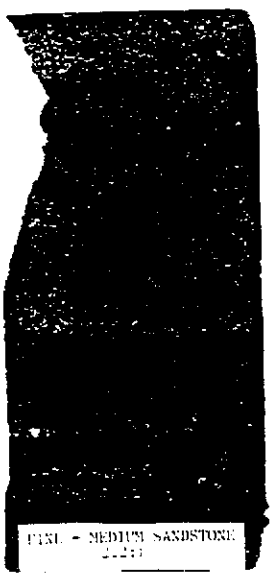

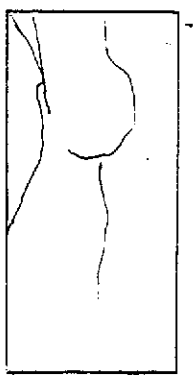

Sketch not to scale

TESTED BY: KM CHECKED BY: DW DATE: 28/7/92

* Denotes use of Rock Colour Chart

SRC Laboratories
A division of Aust-Amec Pty Ltd A.C.N. 003 066 715

Correspondence: P.O. 184, Doubleview W.A. 6018
34 Walters Drive, Herdsman Business Park
Osborne Park W.A. 6017
Phone: (09) 244 1199. Telex: AA197099
Facsimile: (09) 244 1457

REF: S8467/DW:jp SHEET NO: 1 OF 10

29 May 1992

WESTERN COLLIERIES LIMITED
PO Box 2
COLLIE WA 6225

ATTENTION: Mr I Misich

Dear Sir

RE: CENTRIFUGE TEST 1 - ORDER NO: 60667

Attached are the following documents of report for work required by you on the above project:

9 PLATES Elastic Moduli of Intact Rock Core Specimens in Uniaxial Compression Summary

If we can assist further, please advise.

Yours faithfully
DAWN WIMPERIS

Branch Manager WA
for SRC Laboratories

enc

CLIENT: WESTERN COLLIERIES LTD

PROJECT: CENTRIFUGE TEST 1

SHEET No.: 2 **OF:** 10

JOB No.: S8467

DATE TESTED: 12/5/92

ELASTIC MODULI OF INTACT ROCK CORE SPECIMENS IN UNIAXIAL COMPRESSION SUMMARY

SAMPLE IDENTIFICATION:

Rectangular Prism with Height to Width Ratio: 2:1

PHYSICAL DESCRIPTION:

Name of Rock: Fine Medium Sandstone

SPECIMEN DATA:

Height:	121.7	mm
Width:	61.2	mm
Depth:	62.2	mm
Wet Mass:	843.2	g
Wet Density:	1.82	t/m^3
Dry Density:	1.68	t/m^3
Moisture Content:	8.1	%
DEFORMATION RATE:	0.2	mm / minute
UNCONFINED COMPRESSIVE STRENGTH:	1000	kPa

REMARKS: Axial strain was determined using the change in distance between the platens.

TESTED BY: KM CHECKED BY: DW DATE: 30/5/92

* Denotes use of Rock Colour Chart

CLIENT: WESTERN COLLIERIES LTD

PROJECT: CENTRIFUGE TEST 1

SHEET No.: 3 **OF:** 10

JOB No.: S8467

DATE TESTED: 12/5/92

SAMPLE IDENTIFICATION:

Rectangular Prism with Height to Width Ratio: 2:1

STRESS VERSUS AXIAL & DIAMETRIC STRAIN SUMMARY

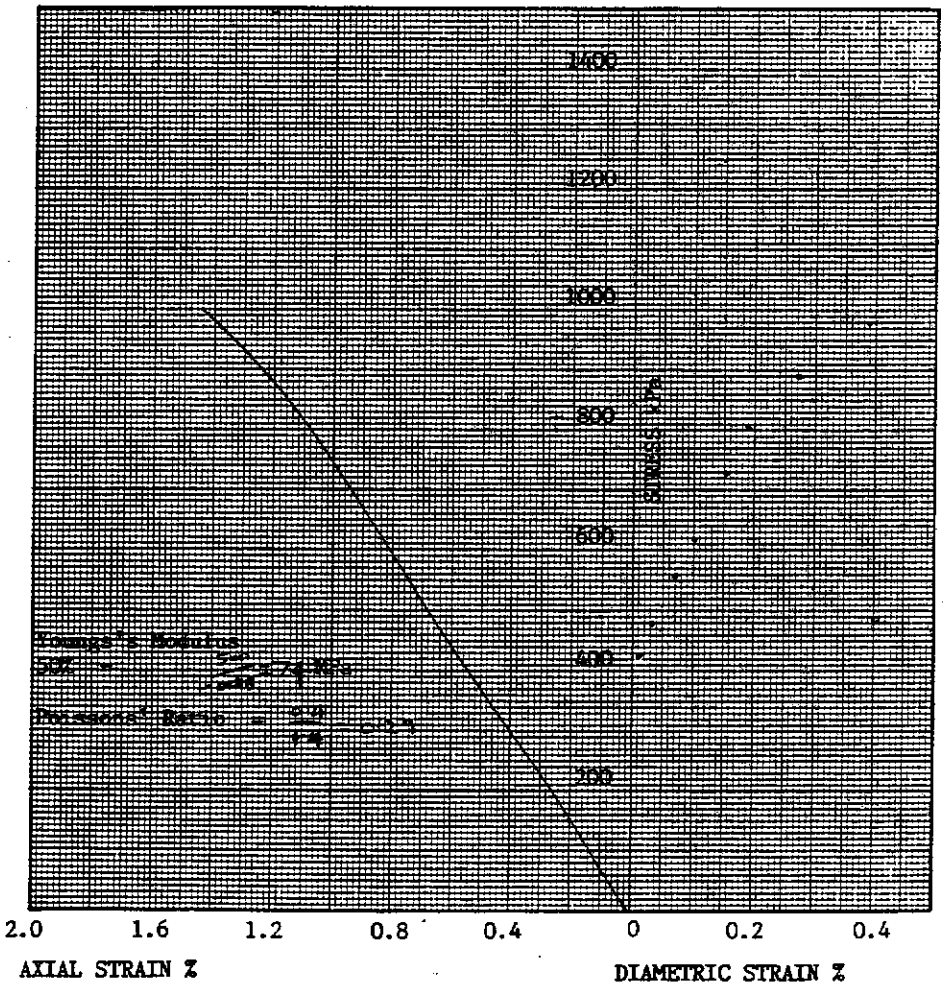

TESTED BY: KM CHECKED BY: DW DATE: 29/5/92

* Denotes use of Rock Colour Chart

CLIENT:	WESTERN COLLIERIES LTD	**SHEET No.:** 4	**OF:** 10
PROJECT:	CENTRIFUGE TEST 1	**JOB No.:**	SS467
		DATE TESTED:	12/5/92

PHOTOGRAPHIC SUMMARY

SAMPLE IDENTIFICATION:

Rectangular Prism with Height to Width Ratio: 2:1

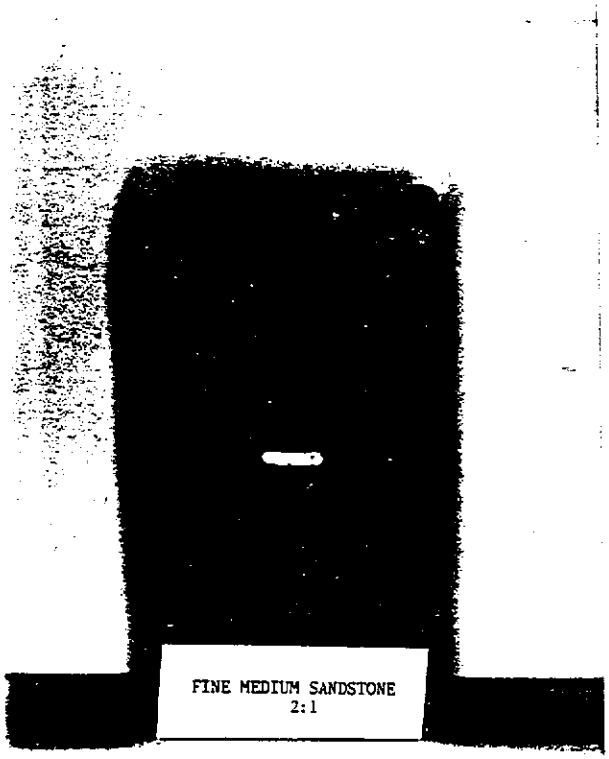

TESTED BY: KM CHECKED BY: DW DATE: 29/5/92

*Denotes use of Rock Colour Chart

CLIENT:	WESTERN COLLIERIES LTD	**SHEET No.:** 5	**OF:** 10
PROJECT:	CENTRIFUGE TEST 1	**JOB No.:**	S8467
		DATE TESTED:	12/5/92

ELASTIC MODULI OF INTACT ROCK CORE SPECIMENS IN UNIAXIAL COMPRESSION SUMMARY

SAMPLE IDENTIFICATION:

Rectangular Prism with Height to Width Ratio: 2:1

PHYSICAL DESCRIPTION:

Name of Rock: Medium Coarse Sandstone

SPECIMEN DATA:

Height:	122.0	mm
Width:	60.5	mm
Depth:	58.5	mm
Wet Mass:	829.0	g
Wet Density:	1.92	t/m^3
Dry Density:	1.78	t/m^3
Moisture Content:	7.6	%
DEFORMATION RATE:	0.2	mm / minute
UNCONFINED COMPRESSIVE STRENGTH:	1380	kPa

REMARKS: Axial strain was determined using the change in distance between the platens.

TESTED BY: KM CHECKED BY: DW DATE: 30/4/92

* Denotes use of Rock Colour Chart

CLIENT: WESTERN COLLIERIES LTD

PROJECT: CENTRIFUGE TEST 1

SHEET No.: 6 **OF:** 10

JOB No.: S8467

DATE TESTED: 12/5/92

SAMPLE IDENTIFICATION:

Rectangular Prism with Height to Width Ratio: 2:1

STRESS VERSUS AXIAL & DIAMETRIC STRAIN SUMMARY

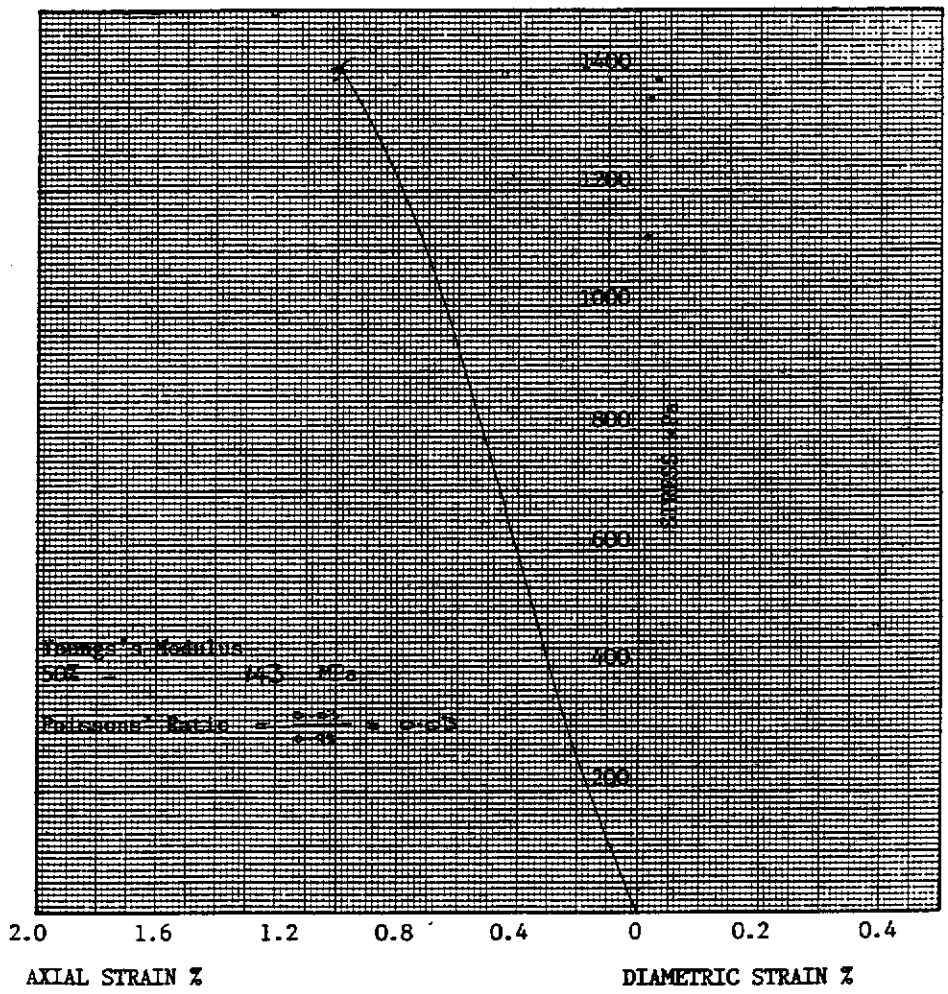

TESTED BY: KM CHECKED BY: DW DATE: 12/5/92

* Denotes use of Rock Colour Chart

CLIENT: WESTERN COLLIERIES LTD

PROJECT: CENTRIFUGE TEST 1

SHEET No.: 7 **OF:** 10

JOB No.: S8467

DATE TESTED: 12/5/92

PHOTOGRAPHIC SUMMARY

SAMPLE IDENTIFICATION:

Rectangular Prism with Height to Width Ratio: 2:1

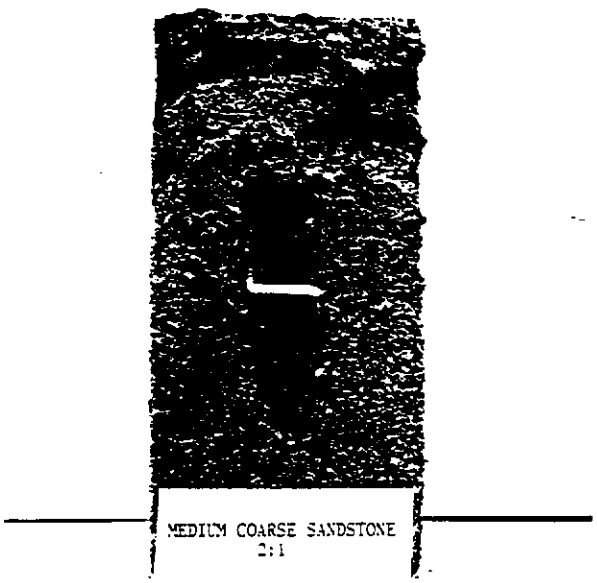

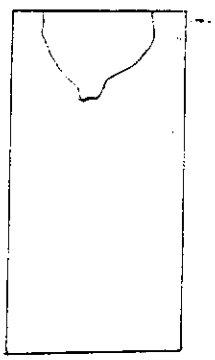

TESTED BY: KM CHECKED BY: DW DATE: 29/5/92

*Denotes use of Rock Colour Chart

CLIENT:	WESTERN COLLIERIES LTD	**SHEET No.:** 8	**OF:** 10
PROJECT:	CENTRIFUGE TEST 1	**JOB No.:**	S8467
		DATE TESTED:	12/5/92

ELASTIC MODULI OF INTACT ROCK CORE SPECIMENS IN UNIAXIAL COMPRESSION SUMMARY

SAMPLE IDENTIFICATION:

Rectangular Prism with Height to Width Ratio: 2.4:1

PHYSICAL DESCRIPTION:

Name of Rock: Medium Coarse Sandstone

SPECIMEN DATA:

Height:	149.7	mm
Width:	62.5	mm
Depth:	60.5	mm
Wet Mass:	1086.6	g
Wet Density:	1.92	t/m^3
Dry Density:	1.78	t/m^3
Moisture Content:	7.6	%
DEFORMATION RATE:	0.2	mm / minute
UNCONFINED COMPRESSIVE STRENGTH:	1530	kPa

REMARKS: Axial strain was determined using the change in distance between the platens.

TESTED BY: KM CHECKED BY: DW DATE: 30/4/92

* Denotes use of Rock Colour Chart

CLIENT: WESTERN COLLIERIES LTD

PROJECT: CENTRIFUGE TEST 1

SHEET No.: 9 **OF:** 10

JOB No.: S8467

DATE TESTED: 12/5/92

SAMPLE IDENTIFICATION:

Rectangular Prism with Height to Width Ratio: 2.4:1

STRESS VERSUS AXIAL & DIAMETRIC STRAIN SUMMARY

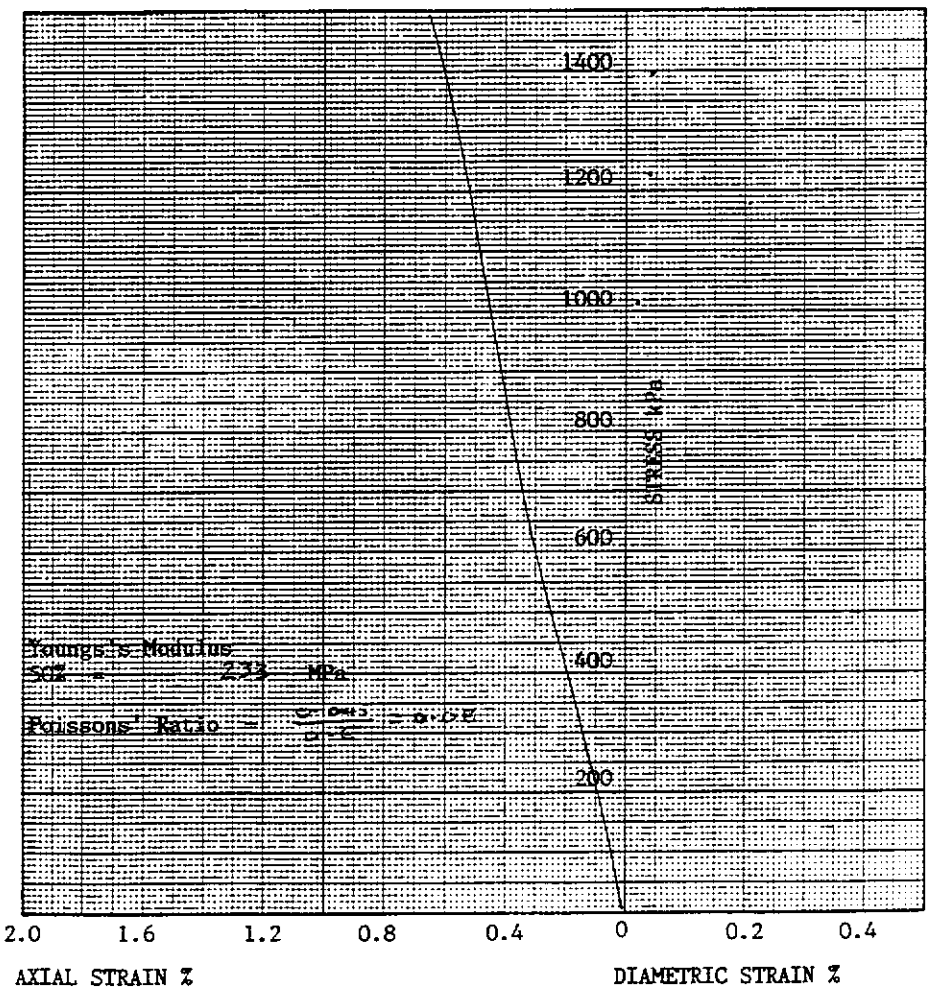

TESTED BY: KM CHECKED BY: DW DATE: 29/5/92

* Denotes use of Rock Colour Chart

CLIENT: WESTERN COLLIERIES LTD

PROJECT: CENTRIFUGE TEST 1

SHEET No.: 10 **OF:** 10

JOB No.: S8467

DATE TESTED: 12/5/92

PHOTOGRAPHIC SUMMARY

SAMPLE IDENTIFICATION:

Rectangular Prism with Height to Width Ratio: 2.4:1

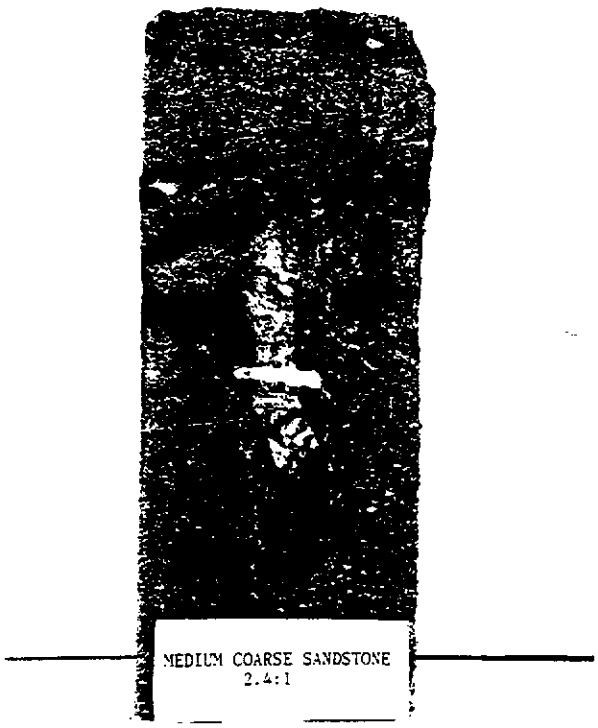

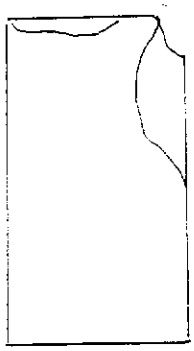

TESTED BY: KM CHECKED BY: DW DATE: 29/5/92

* Denotes use of Rock Colour Chart

UNCONFINED COMPRESSION TEST DATA
INSITU MATERIAL

TEST PS02
ROOF BLOCK

SAMPLE	DIMENSIONS			ASPECT	LOAD	STRESS	WATER
	H	W	B	RATIO	(N)	MPa	CONT %
1	57.5	55.5	57.5	1.02	13425	4.21	
2	56.8	52	57.4	1.04	12875	4.31	
3	100	50.8	49	2	12200	4.9	
4	121.8	60	60.4	2.02	9100	2.51	
5	120.6	60.6	61.4	1.98	8325	2.24	12.2

UPPER BLOCK

1	51.5	49.8	50.5	1.02	875	0.35	
2	54	60	60.5	0.9	1925	0.53	
3	125.5	60.4	59.1	2.1	1135	0.32	18.64
4	114	46	42.3	2.58	620	0.32	15.91
5	113.3	46	45	2.49	825	0.4	14.93
6	113.5	43	45.1	2.58	345	0.18	16.31
7	113	45.3	43.1	2.56	845	0.43	17.92

TABLE III.5

BEAM BENDING TEST - CANNEL COAL BEAM #1
LASER DEFLECTION DATA

Laser travel (mm)	zero load	100N	200N	300N	400N	650N
			DEFLECTION (mm)			
0.00						
5.00	0.17	0.03	0.01	-0.08	-0.15	-0.24
10.00	0.30	0.20	0.09	-0.09	0.02	-0.17
15.00	0.04	-0.08	-0.16	-0.22	-0.29	-0.45
20.00	0.05	-0.08	-0.16	-0.24	-0.30	-0.50
25.00	0.34	0.20	0.10	0.02	-0.08	-0.20
30.00	0.81	0.66	0.53	0.45	0.37	0.12
35.00	0.78	0.60	0.50	0.39	0.31	0.03
40.00	0.73	0.55	0.43	0.30	0.17	-0.14
45.00	0.94	0.80	0.66	0.52	0.39	0.12
50.00	1.18	1.08	0.92	0.79	0.68	0.41
55.00	1.07	0.87	0.78	0.63	0.54	0.27
60.00	0.80	0.60	0.49	0.00	0.26	-0.03
65.00	0.62	0.46	0.33	0.17	0.08	-0.22
70.00	0.24	0.06	-0.05	-0.35	-0.32	-0.69
75.00	-0.12	-0.27	-0.39	-0.67	-0.92	-1.33
80.00	-0.11	-0.26	-0.39	-0.61	-0.84	-1.23
85.00	-0.12	-0.29	-0.42	-0.61	-0.80	-1.17
90.00	-0.14	-0.32	-0.43	-0.62	-0.81	-1.16
95.00	-0.16	-0.33	-0.46	-0.65	-0.82	-1.18
100.00	-0.18	-0.36	-0.49	-0.68	-0.82	-1.19
105.00	-0.17	-0.37	-0.49	-0.67	-0.83	-1.18
110.00	-0.17	-0.35	-0.50	-0.68	-0.82	-1.19
115.00	-0.17	-0.34	-0.48	-0.68	-0.82	-1.22
120.00	-0.20	-0.37	-0.50	-0.68	-0.84	-1.23
125.00	-0.17	-0.34	-0.49	-0.70	-0.87	-1.28
130.00	-0.20	-0.37	-0.51	-0.76	-0.91	-1.34
135.00	-0.20	-0.37	-0.51	-0.80	-0.83	-1.42
140.00	-0.17	-0.36	-0.49	-0.75	-0.92	-1.34
145.00	-0.15	-0.33	-0.47	-0.69	-0.84	-1.25
150.00	-0.14	-0.32	-0.44	-0.65	-0.82	-1.21
155.00	-0.08	-0.26	-0.40	-0.58	-0.74	-1.13
160.00	0.03	-0.15	-0.28	-0.48	-0.62	-1.02
165.00	0.08	-0.09	-0.23	-0.43	-0.58	-0.97
170.00	0.10	-0.04	-0.18	-0.37	-0.52	-0.91
175.00	0.13	-0.04	-0.20	-0.39	-0.55	-0.94

TABLE III.6

BEAM BENDING TEST - CANNEL COAL BEAM#2
DIAL GAUGE DEFLECTION DATA

	DISTANCE FROM CONSTRICTION (mm)					
	13	48	91	138	186	243
LOAD (N)	DEFLECTION (mm)					
0	0.000	0.000	0.000	0.000	0.000	0.000
50	0.000	0.001	0.060	0.051	0.025	0.005
100	0.000	0.018	0.120	0.127	0.112	0.010
150	0.000	0.036	0.240	0.203	0.221	0.016
200	0.000	0.041	0.290	0.254	0.272	0.020
250	0.000	0.050	0.354	0.305	0.326	0.024
300	0.000	0.055	0.400	0.356	0.381	0.028
350	0.001	0.058	0.440	0.381	0.424	0.034
400	0.001	0.064	0.485	0.419	0.475	0.039
450	0.001	0.072	0.555	0.483	0.549	0.046
500	0.001	0.077	0.595	0.521	0.585	0.055
600	0.002	0.081	0.630	0.546	0.627	0.067
650	0.002	0.084	0.685	0.584	0.671	0.078
700	0.002	0.086	0.720	0.610	0.701	0.086
800	0.002	0.094	0.785	0.660	0.762	0.100
850	0.002	0.097	0.805	0.686	0.782	0.104
900	0.002	0.099	0.845	0.711	0.810	0.109
950	0.002	0.102	0.880	0.737	0.843	0.116
1000	0.002	0.104	0.920	0.762	0.874	0.123
1050	0.002	0.107	0.960	0.787	0.897	0.129
1100	0.002	0.109	0.980	0.813	0.925	0.132
1150	0.002	0.112	1.010	0.838	0.953	0.138
1200	0.002	0.113	1.040	0.864	0.975	0.142
1250	0.002	0.116	1.070	0.889	0.996	0.148
1300	0.002	0.118	1.105	0.914	1.026	0.152
1350	0.002	0.121	1.140	0.940	1.052	0.157
1400	0.0022					

TABLE III.7

BEAM BENDING TESTS - CANNEL COAL BEAM #3 **LVDT DEFLECTION DATA**						
	DISTANCE FROM CONSTRICTION					
	32.5mm	53mm	75mm	97mm	117mm	168mm
LOAD	DEFLECTION (mm)					
100N	0.29	0.29	0.27	0.39	0.27	0.19
300N	0.47	0.52	0.51	0.55	0.47	0.40
500N	0.63	0.71	0.71	0.79	0.71	0.58
600N	0.70	0.80	0.80	0.88	0.80	0.67
700N	0.76	0.86	0.87	0.99	0.88	0.75
800N	0.81	0.93	0.94	0.90	0.95	0.81

TABLE III.8

BEAM BENDING TEST - CANNEL COAL BEAM #4
LVDT DEFLECTION DATA

	DISTANCE FROM CONSTRICTION (mm)					
	18	41	62	85	134	188
LOAD (N)	DEFLECTION (mm)					
0	0.00	0.00	0.00	0.00	0.00	0.00
41	0.05	0.06	0.07	0.04	0.10	0.11
106	0.09	0.12	0.12	0.08	0.18	0.19
155	0.11	0.15	0.16	0.13	0.23	0.24
201	0.14	0.18	0.20	0.22	0.29	0.30
248	0.16	0.21	0.24	0.23	0.34	0.35
310	0.19	0.26	0.29	0.36	0.41	0.42
359	0.22	0.29	0.33	0.32	0.47	0.48
392	0.24	0.32	0.37	0.38	0.54	0.55
450	0.27	0.36	0.41	0.48	0.58	0.61
510	0.29	0.39	0.45	0.48	0.64	0.65
600	0.34	0.45	0.52	0.49	0.74	0.74
697	0.38	0.51	0.59	0.58	0.82	0.82
800	0.43	0.57	0.66	0.71	0.91	0.90
900	0.47	0.62	0.73	0.78	1.00	0.98
1000	0.52	0.68	0.79	0.87	1.09	1.07
1095	0.56	0.74	0.87	0.91	1.18	1.15
1200	0.61	0.80	0.93	1.06	1.27	1.23
1300	0.66	0.85	1.01	1.17	1.37	1.30
1395	0.70	0.90	1.07	1.13	1.45	1.37

TABLE III.9

BEAM BENDING TEST
LAMINATED SANDSTONE BEAM #1
DIAL GAUGE DEFLECTION DATA

	DISTANCE FROM CONSTRICTION (mm)		
	20	59	113
LOAD (N)	DEFLECTION (mm)		
0	0.00	0.00	0.00
10	0.01	0.02	0.03
20	0.02	0.03	0.03
30	0.04	0.06	0.08
40	0.05	0.10	0.13
45	0.08	0.13	0.19
50	0.09	0.15	0.22
60	0.12	0.21	0.30
70	0.14	0.27	0.40
80	0.21	0.40	0.56
90	0.28	0.60	0.89

TABLE III.10

BEAM BENDING TEST
LAMINATED SANDSTONE BEAM #3
LVDT DEFLECTION DATA

	DISTANCE FROM CONSTRICTION (mm)					
	203	150	101	74	46	18
LOAD (N)	DEFLECTION (mm)					
1.51	0.20	0.17	0.14	0.12	0.09	0.06
2.79	1.10	0.97	0.83	0.72	0.56	0.35
17.23	1.23	1.12	0.99	0.88	0.73	0.49
22.40	1.26	1.18	1.06	0.96	0.82	0.57
27.45	1.28	1.21	1.10	1.02	0.88	0.62
28.81	1.30	1.24	1.14	1.07	0.92	0.65
39.12	1.39	1.38	1.31	1.32	1.14	0.84
41.91	1.42	1.43	1.38	1.38	1.24	0.91

TABLE III.11

BEAM BENDING TEST
LAMINATED SANDSTONE BEAM #4
LVDT DEFLECTION DATA

	DISTANCE FROM CONSTRICTION (mm)					
	203	151	101	74	46	17
LOAD (N)	DEFLECTION (mm)					
0.000	0.00	0.00	0.00	0.00	0.00	0.18
30.06	0.13	0.14	0.13	0.13	0.11	0.09
40.1	0.15	0.16	0.15	0.14	0.14	0.11
45.1	0.16	0.17	0.17	0.17	0.16	0.12
49.33	0.17	0.18	0.18	0.17	0.17	0.14
55.14	0.17	0.20	0.20	0.23	0.19	0.15
59.87	0.18	0.21	0.21	0.25	0.21	0.17
68.54	0.20	0.23	0.24	0.24	0.24	0.20
74.54	0.21	0.25	0.26	0.27	0.26	0.22
79.92	0.23	0.27	0.28	0.35	0.28	0.24
90.25	0.25	0.30	0.31	0.34	0.32	0.27
99.99	0.27	0.33	0.35	0.42	0.36	0.30
119.79	0.32	0.40	0.44	0.55	0.46	0.38
123.57	0.33	0.41	0.45	0.54	0.48	0.39

TABLE III.12

BEAM BENDING TEST
LAMINATED SANDSTONE BEAM #5
LVDT DEFLECTION DATA

	DISTANCE FROM CONSTRICTION (mm)					
	17	44	71	99	148	200
LOAD (N)	DEFLECTION (mm)					
0.00	0.00	0.00	0.00	0.00	0.00	0.00
9.88	0.02	0.04	0.05	0.07	0.08	0.07
19.71	0.05	0.09	0.12	0.18	0.18	0.17
25.54	0.06	0.12	0.17	0.22	0.25	0.23
29.61	0.08	0.15	0.22	0.30	0.32	0.30
35.25	0.10	0.19	0.27	0.37	0.40	0.37
39.57	0.11	0.23	0.33	0.45	0.49	0.45
45.23	0.13	0.27	0.39	0.50	0.59	0.54
47.41	0.14	0.30	0.44	0.59	0.68	0.63

STRAIN GAUGE DATA FOR CANEL COAL BEAM TEST #1										
LOAD (N)	gauge1	gauge2	gauge3	gauge4	gauge5	gauge6	gauge7	gauge8	gauge9	gauge10
				STRAIN (micro_strain)						
0N	0.00	0.00	0.00	0.00	0.00	0.00	0.00	0.00	0.00	0.00
100N	-60.52	-39.87	-21.35	19.19	45.02	429.37	278.37	403.42	360.60	257.51
200N	-169.37	-98.50	-24.47	41.32	101.78	757.44	586.71	807.73	612.92	481.14
300N	-318.33	-284.17	-257.21	44.24	169.44	1139.72	1064.73	1227.23	859.60	697.64
400N	-409.48	-343.07	-345.66	57.01	210.14	1456.19	1388.90	1532.58	1093.39	851.30
500N	-490.00	-395.81	-385.60	55.51	215.98	1752.92	1692.10	1632.72	1227.50	992.59
600N	-599.25	-498.12	-445.08	16.45	210.75	1874.60	1906.04	1632.72	1227.50	1098.93
650N	-810.48	-507.75	-467.53	0.26	233.14	1874.60	1906.04	1632.72	1227.50	1145.90
				constriction distance (mm)						
	165.00	115.00	75.00	45.00	15.00	165.00	115.00	75.00	45.00	15.00

TABLE III.13

TABLE III.14

BEAM BENDING TEST - CANNEL COAL BEAM #3

STRAIN GAUGE DATA INITIAL RUPTURE

	DISTANCE FROM CONSTRICTION									
	170mm	120mm	78mm	57mm	36mm	170mm	120mm	78mm	57mm	36mm
GAUGE # >	1	2	3	4	5	6	7	8	9	10
LOAD	STRAIN (microstrain)									
100N	-74.6	-91.0	-185.0	-175.1	-119.4	105.8	101.3	48.3	40.1	23.8
300N	-211.6	-270.6	-701.9	-632.7	-379.8	276.1	239.2	3.9	14.7	18.0
500N	-339.2	-420.1	-1092.8	-1034.6	-621.1	435.3	388.5	33.7	13.7	13.2
600N	-406.6	-493.8	-1225.9	-1193.1	-728.3	516.5	470.4	100.7	45.5	20.6
700N	-477.6	-577.1	-1363.2	-1351.1	-850.8	597.8	551.2	184.1	94.2	35.4
800N	-544.3	-644.9	-1474.8	-1470.6	-935.0	669.7	621.0	251.4	134.7	38.7

STRAIN GAUGE DATA FINAL RUPTURE

	DISTANCE FROM CONSTRICTION									
	170mm	120mm	78mm	57mm	36mm	170mm	120mm	78mm	57mm	36mm
GAUGE #	1	2	3	4	5	6	7	8	9	10
LOAD	STRAIN (microstrain)									
800N	-550.9	-651.6	-1475.2	-1468.5	-939.8	669.1	620.8	253.3	136.5	42.1
350N	-54.0	625.3	-2050.0	-12.9	33.9	355.8	1434.9	1048.0	846.8	514.9
400N	4.6	573.4	-2050.0	10.7	52.6	482.3	1547.2	1103.2	930.9	574.4
450N	107.6	537.6	-2050.0	29.0	75.0	703.4	1732.3	1255.9	1079.7	674.5
500N	445.4	456.1	-2050.0	45.9	98.8	1534.6	2062.5	1448.3	1261.1	806.8

TABLE III.15

DIRECT SHEAR TESTS ON BEDDING PLANES

SRC Laboratories
A division of Aust Amec Pty Ltd

Correspondence PO 184 Doubleview WA 6018
34 Walters Drive Herdsman Business Park
Osborne Park WA 6017
Phone (09) 244 1199 Telex AA197099
Facsimile (09) 244 1457

REF: S8009/DW:jp

20 February 1992

WESTERN COLLIERIES LIMITED
PO Box 21
COLLIE WA 6225

ATTENTION: Mr I Misich

Dear Sir

RE: GYPSUM INTERFACE STUDY - ORDER NO: 56926 (COLLIE FEDERATED SCHOOL OF MINES)

Attached are the following documents of report for work required by you on the above project:

2	PLATES	Laboratory Determination of Direct Shear Strength Summary
2	PLATES	Direct Shear Test - Multistage Test
2	PLATE	Shear Stress Versus Horizontal Displacement

If we can assist further, please advise.

Yours faithfully
DAWN WIMPERIS

Dwimperis

Branch Manager WA
for SRC Laboratories

enc

Refer Andrew Gradisen

CLIENT: WESTERN COLLIERIES LIMITED
PROJECT: GYPSUM INTERFACE STUDY

SHEET No.: 2 **OF:** 7
JOB No.: S8009
DATE TESTED: 17/2/92

LABORATORY DETERMINATION OF DIRECT SHEAR STRENGTH SUMMARY

Tested in accordance with I.S.R.M Rock Characterisation Testing and Monitoring 1981.

SAMPLE IDENTIFICATION: Carbonaceous Shale/Sandstone without Gypsum Interface Mix

INITIAL SPECIMEN DATA:	CARBONACEOUS SHALE	SANDSTONE
Initial Surface Area (mm^2):	4900	4900
Initial Moisture Content (%):	22.3	17.8
Initial Wet Density (t/m^3):	1.36	1.78
Initial Dry Density (t/m^3):	1.11	1.51

RESULTS:

Friction Ø: °
Cohesion 'c': kPa

NOTE:
1. Order of Confining Stress During Test 0.025, 0.5, 1.0 MPa
2. Rate of Strain 0.02mm/ minute
3. The sample was reversed after each cycle

TESTED BY: KM CHECKED BY: DW DATE: 18/2/92

* Denotes use of Rock Colour Chart

CLIENT: WESTERN COLLIERIES LIMITED **SHEET No.:** 3 **OF:** 7

PROJECT: GYPSUM INTERFACE STUDY **JOB No.:** S8009

DATE TESTED: 17/2/92

SAMPLE IDENTIFICATION: Carbonaceous Shale/Sandstone without Gypsum Interface Mix

DIRECT SHEAR TEST - MULTISTAGE TEST

Shear Stress / Normal Stress Plot

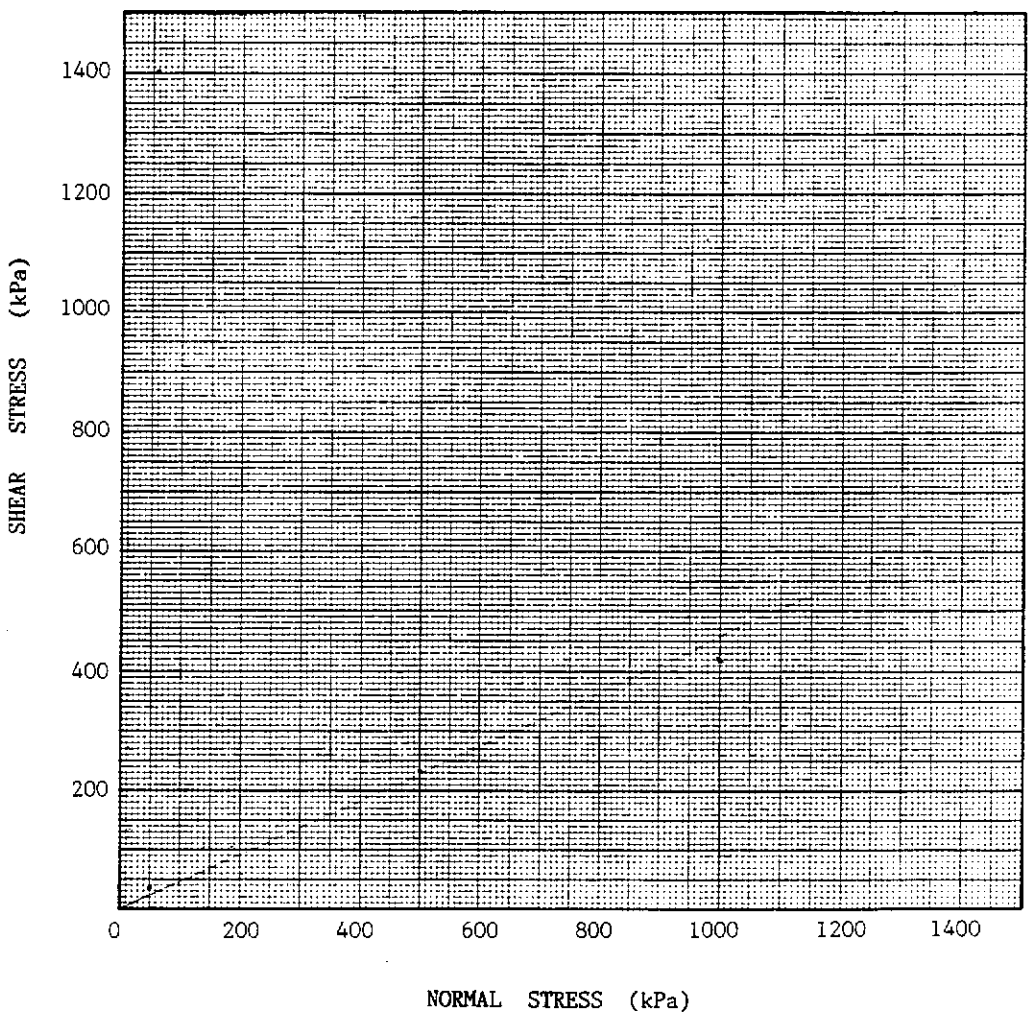

TESTED BY: KM CHECKED BY: DW DATE: 18/2/92

* Denotes use of Rock Colour Chart

CLIENT: WESTERN COLLIERIES LIMITED **SHEET No.:** 4 **OF:** 7

PROJECT: GYPSUM INTERFACE STUDY **JOB No.:** S8009

DATE TESTED: 7/2/92

SAMPLE IDENTIFICATION: Carbonaceous Shale/Sandstone without Gypsum Interface Mix

SHEAR STRESS VERSUS HORIZONTAL DISPLACEMENT

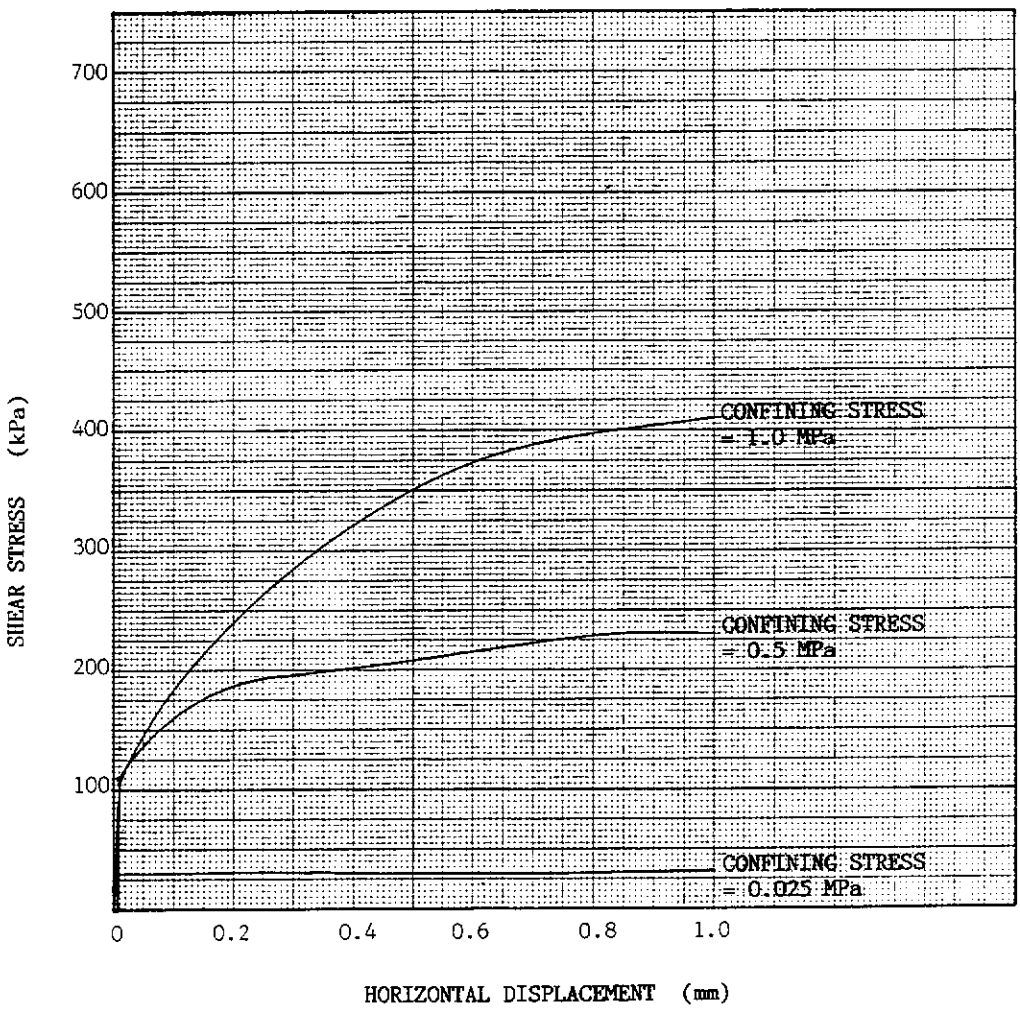

TESTED BY: KM CHECKED BY: DW DATE: 18/2/92

* Denotes use of Rock Colour Chart

CLIENT: WESTERN COLLIERIES LIMITED

PROJECT: GYPSUM INTERFACE STUDY

SHEET No.: 5 **OF:** 7

JOB No.: S8009

DATE TESTED: 17/2/92

LABORATORY DETERMINATION OF DIRECT SHEAR STRENGTH SUMMARY

Tested in accordance with I.S.R.M Rock Characterisation Testing and Monitoring 1981.

SAMPLE IDENTIFICATION: Carbonaceous Shale/Sandstone with Gypsum Interface Mix

INITIAL SPECIMEN DATA:	CARBONACEOUS SHALE	SANDSTONE
Initial Surface Area (mm^2):	4900	4900
Initial Moisture Content (%):	22.3	17.8
Initial Wet Density (t/m^3):	1.36	1.78
Initial Dry Density (t/m^3):	1.11	1.51

RESULTS:

Friction Ø: °

Cohesion 'c': kPa

NOTE:
1. Order of Confining Stress During Test 0.025, 0.5, 1.0 MPa
2. Rate of Strain 0.04, 0.04, 0.03 mm/minute
3. The sample was reversed after each cycle

TESTED BY: KM CHECKED BY: DW DATE: 18/2/92

* Denotes use of Rock Colour Chart

CLIENT: WESTERN COLLIERIES LIMITED **SHEET No.:** 6 **OF:** 7

PROJECT: GYPSUM INTERFACE STUDY **JOB No.:** S8009

DATE TESTED: 17/2/92

SAMPLE IDENTIFICATION: Carbonaceous Shale/Sandstone with Gypsum Interface Mix

DIRECT SHEAR TEST - MULTISTAGE TEST

Shear Stress / Normal Stress Plot

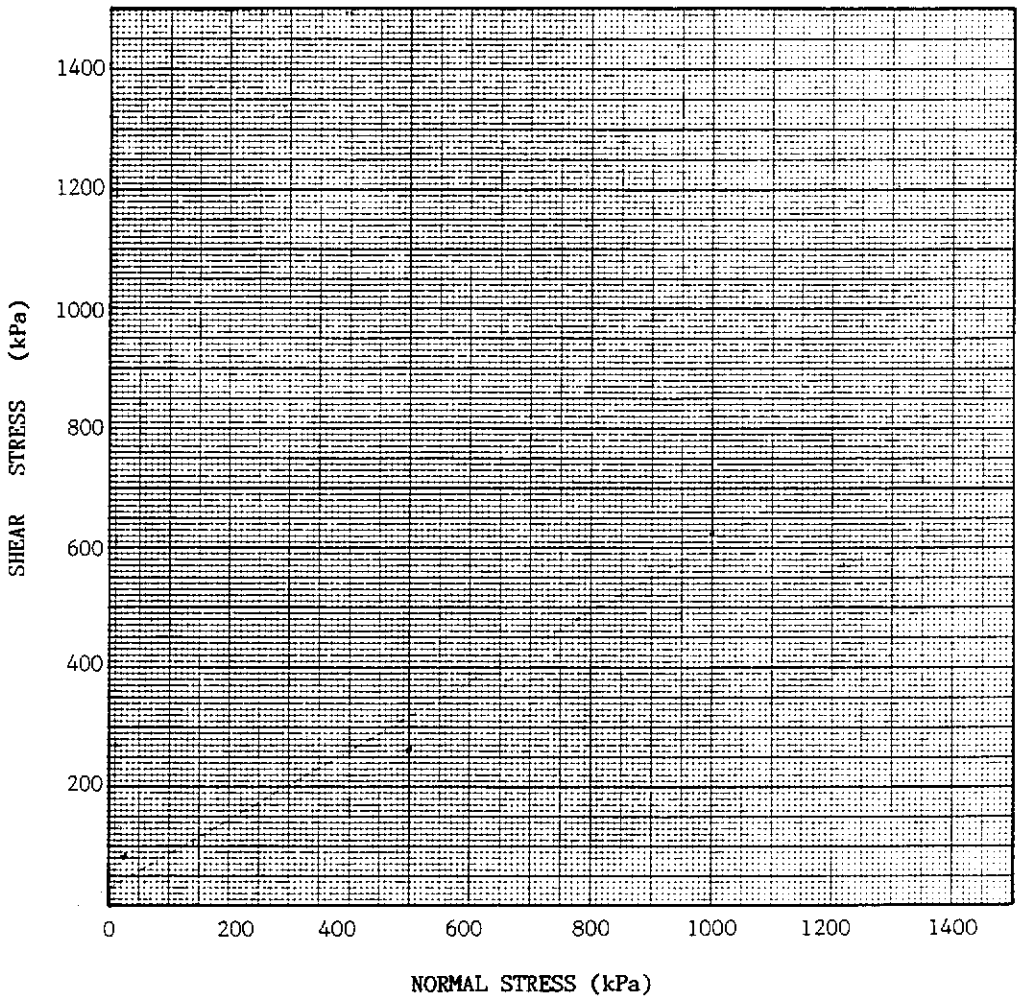

TESTED BY: KM CHECKED BY: DW DATE: 18/2/92

* Denotes use of Rock Colour Chart

CLIENT: WESTERN COLLIERIES LIMITED

PROJECT: GYPSUM INTERFACE STUDY

SHEET No.: 7 **OF:** 7

JOB No.: S8009

DATE TESTED: 17/2/92

SAMPLE IDENTIFICATION: Carbonaceous Shale/Sandstone with Gypsum Interface Mix

SHEAR STRESS VERSUS HORIZONTAL DISPLACEMENT

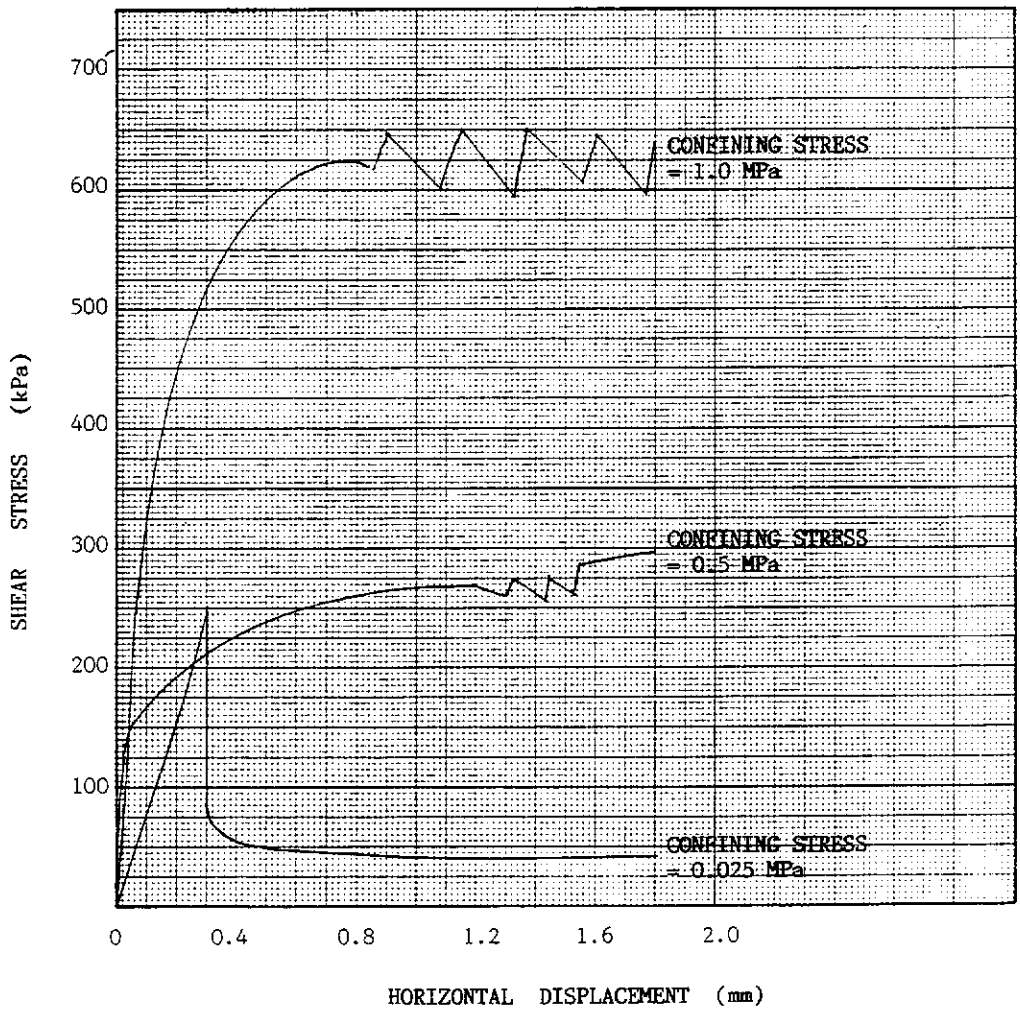

TESTED BY: KM CHECKED BY: DW DATE: 18/2/92

* Denotes use of Rock Colour Chart

TABLE III.16

MECHANICAL PROPERTY TESTING OF BORECORE FROM DIAMOND DRILL HOLES D212 & D213 - 1 NORTH PANEL

SRC Laboratories
A division of Aust-Amec Pty Ltd

Correspondence: P.O. 184, Doubleview W.A. 6018
34 Walters Drive, Herdsman Business Park
Osborne Park W.A. 6017
Phone (09) 244 1199. Telex: AA197099
Facsimile (09) 244 1457

REF: S5937/DW:me

30th November, 1990

COLLIE FEDERATED SCHOOL OF MINES,
P.O. Box 268,
COLLIE W.A. 6225

ATTENTION: Mr. A. Evans

Dear Sir,

RE: 1 NORTH WD6

Attached are the following documents of report for work required by you on the above project:

21 PLATES	Elastic Moduli of Intact Rock Core Specimens in Uniaxial Compression Summary
35 PLATES	Triaxial Compressive Strength of Undrained Rock Core Specimens Summary
12 PLATES	Indirect Tensile Strength by the Brazil Test

If we can assist further, please advise.

Yours faithfully,
DAWN WIMPERIS

Branch Manager W.A.
for SRC LABORATORIES

Encls.

CLIENT: COLLIE SCHOOL OF MINES

PROJECT: 1 NORTH WD6

SHEET No.: 2 **OF:** 69

JOB No.: S5937

DATE TESTED: 27/11/90

TRIAXIAL COMPRESSIVE STRENGTH OF UNDRAINED ROCK CORE SPECIMENS WITHOUT PORE PRESSURE MEASUREMENTS SUMMARY

Tested in accordance with ASTM D 2664 - 80.

SAMPLE IDENTIFICATION:

Bore Hole No :	D212/1 O/B
Depth in Metres :	15.00 - 16.00

PHYSICAL DESCRIPTION:

Name of Rock :	FINE-COARSE CLAYEY SANDSTONE (DISTURBED SAMPLE)

SPECIMEN DATA:

Height :	130.0	mm
Diameter :	60.0	mm
Wet Mass :	750.8	g
Wet Density :	2.04	t/m^3
Dry Density :	1.90	t/m^3
Moisture Content :	7.5	%

DEFORMATION RATE:	0.2	mm / minute

REMARKS: The disturbed sample was remoulded to the specified density and the multi stage triaxial test was carried out on this reconstituted test specimen as instructed.

TESTED BY: KM CHECKED BY: DW DATE: 30/11/90

* Denotes use of Rock Colour Chart

CLIENT: COLLIE SCHOOL OF MINES **SHEET No.:** 3 **OF:** 69

PROJECT: 1 NORTH WD6 **JOB No.:** S5937

DATE TESTED: 27/11/90

TRIAXIAL COMPRESSION TEST SUMMARY

VISUAL CLASSIFICATION (A.S.1726)

SAMPLE IDENTIFICATION/DEPTH	DESCRIPTION	SYMBOL
D212/1 O/B 15.00 - 16.00m	FINE-COARSE CLAYEY SANDSTONE (DISTURBED SAMPLE)	

TEST PARAMETER SUMMARY

CONFINING STRESS (σ_3) kPa	300	600	1200
POREWATER PRESSURE (U) kPa	NR	NR	NR
EFFECTIVE CONFINING STRESS(σ_3-U)	NR	NR	NR
DEVIATOR STRESS (σ_1-σ_3) kPa	617	1187	2033
SHEAR STRESS $\frac{(\sigma_1 - \sigma_3)}{2}$ kPa	308.5	593.5	1016.5
INTERNAL FRICTION (ϕ) Degrees	- 27°		
YOUNG'S/SECANT MODULUS (kPa)	-		
COHESION (c) (kPa)	-		

COMMENTS

MOHR'S CIRCLES

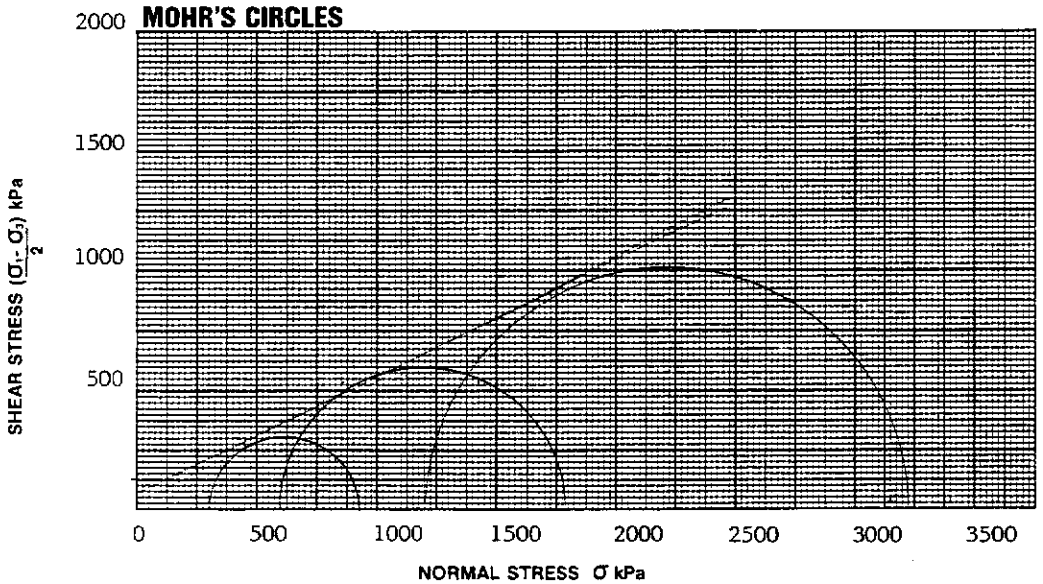

TESTED BY: KM CHECKED BY: DW DATE: 30/11/90

* Denotes use of Rock Colour Chart

SRC 85-3

CLIENT: COLLIE SCHOOL OF MINES

PROJECT: 1 NORTH WD6

SHEET No.: 4 **OF:** 69

JOB No.: S5937

DATE TESTED: 27/11/90

SAMPLE IDENTIFICATION: Bore Hole D212/1
Depth in Metres 15.00 - 16.00

DEVIATOR STRESS/AXIAL STRAIN SUMMARY

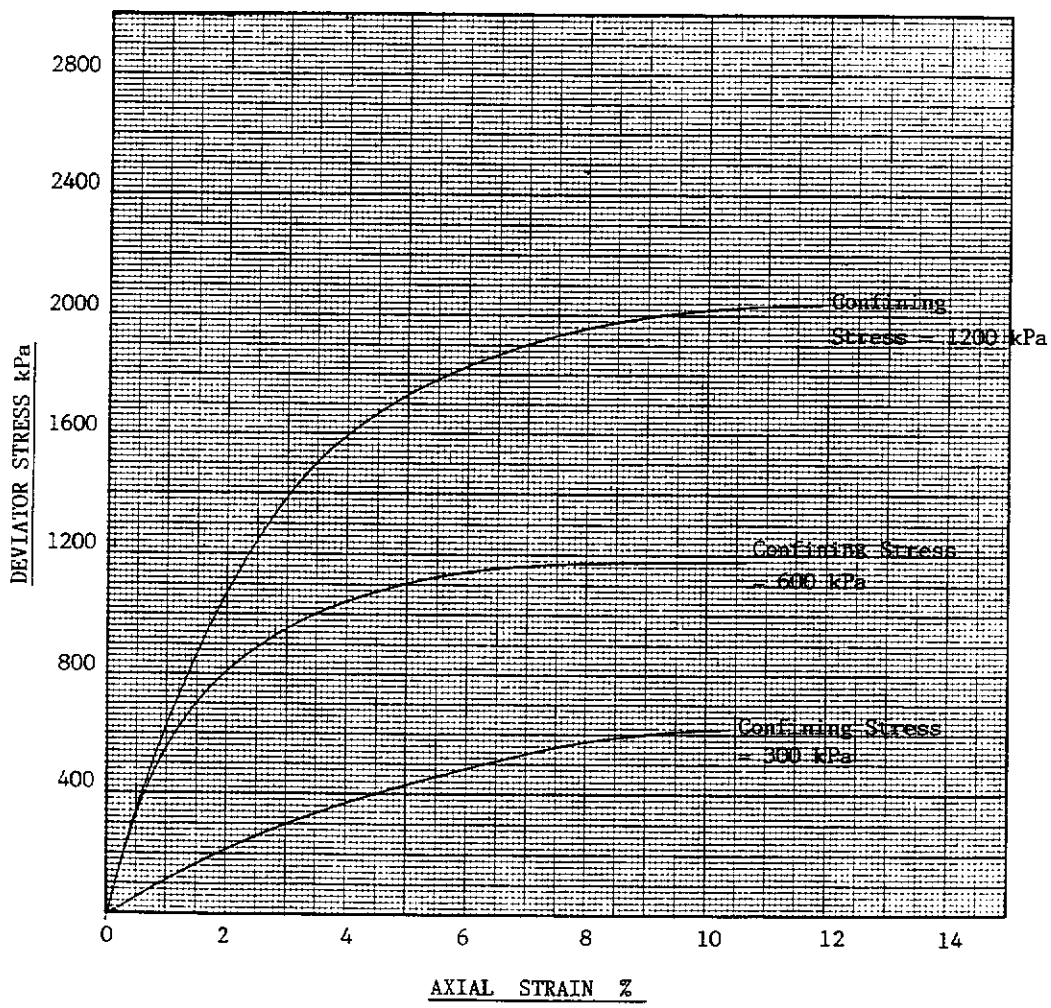

TESTED BY: KM CHECKED BY: DW DATE: 30/11/90

*Denotes use of Rock Colour Chart

CLIENT: COLLIE SCHOOL OF MINES

PROJECT: 1 NORTH WD6

SHEET No.: 5 **OF:** 69

JOB No.: S5937

DATE TESTED: 30/11/90

TRIAXIAL COMPRESSIVE STRENGTH OF UNDRAINED ROCK CORE SPECIMENS WITHOUT PORE PRESSURE MEASUREMENTS SUMMARY

Tested in accordance with ASTM D 2664 - 80.

SAMPLE IDENTIFICATION:

Bore Hole No :	D213/2 O/B
Depth in Metres :	26.00 - 27.00

PHYSICAL DESCRIPTION:

Name of Rock :	FINE-COARSE CLAYEY SANDSTONE (DISTURBED SAMPLE)

SPECIMEN DATA:

Height :	118.0	mm
Diameter :	60.0	mm
Wet Mass :	699.2	g
Wet Density :	2.10	t/m^3
Dry Density :	1.90	t/m^3
Moisture Content :	10.3	%

DEFORMATION RATE: 0.2 mm / minute

REMARKS: The disturbed sample was remoulded to the specified density and the multi stage triaxial test was carried out on this reconstituted test specimen as instructed.

TESTED BY: KM CHECKED BY: DW DATE: 30/11/90

* Denotes use of Rock Colour Chart

CLIENT: COLLIE SCHOOL OF MINES

PROJECT: 1 NORTH WD6

SHEET No.: 6 OF: 69

JOB No.: S5937

DATE TESTED: 30/11/90

TRIAXIAL COMPRESSION TEST SUMMARY

VISUAL CLASSIFICATION (A.S.1726)

SAMPLE IDENTIFICATION/DEPTH	DESCRIPTION	SYMBOL
D213/2 O/B 26.00 - 27.00m	FINE-COARSE CLAYEY SANDSTONE (DISTURBED SAMPLE)	

TEST PARAMETER SUMMARY

CONFINING STRESS (σ_3) kPa	500	1000	2000
POREWATER PRESSURE (U) kPa	NR	NR	NR
EFFECTIVE CONFINING STRESS(σ_3-U)	NR	NR	NR
DEVIATOR STRESS (σ_1-σ_3) kPa	898	1901	4800
SHEAR STRESS $\frac{(\sigma_1 - \sigma_3)}{2}$ kPa	449	950.5	2400
INTERNAL FRICTION (ϕ) Degrees	- 32°		
YOUNG'S/SECANT MODULUS (kPa)	-		
COHESION (c) (kPa)	- 0		

COMMENTS

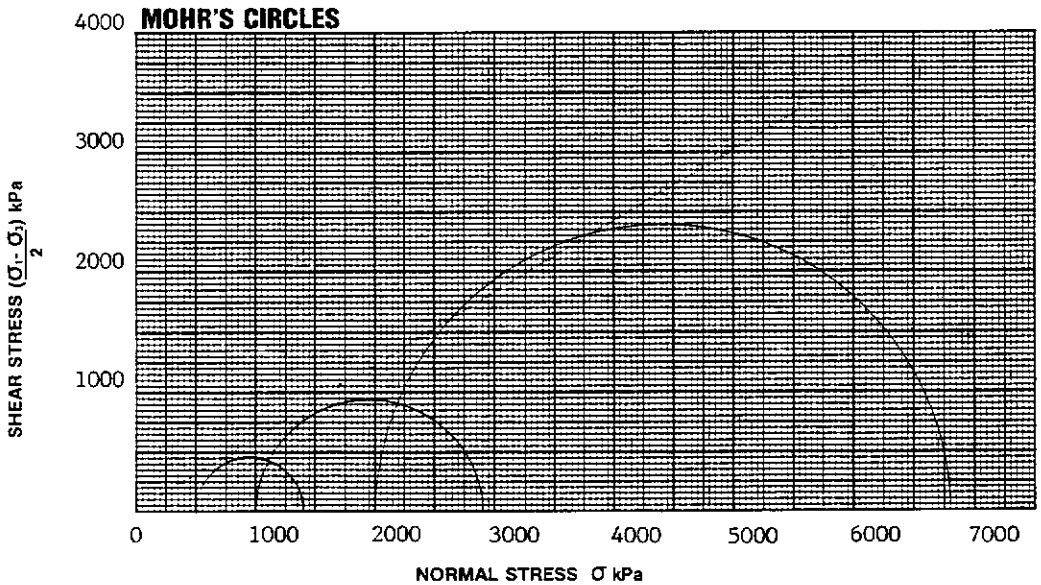

TESTED BY: KM CHECKED BY: DW DATE: 30/11/90

* Denotes use of Rock Colour Chart

SRC 85.9

CLIENT: COLLIE SCHOOL OF MINES

PROJECT: 1 NORTH WD6

SHEET No.: 7 **OF:** 69

JOB No.: S5937

DATE TESTED: 30/11/90

SAMPLE IDENTIFICATION: Bore Hole D213/2
Depth in Metres 26.00 - 27.00

DEVIATOR STRESS/AXIAL STRAIN SUMMARY

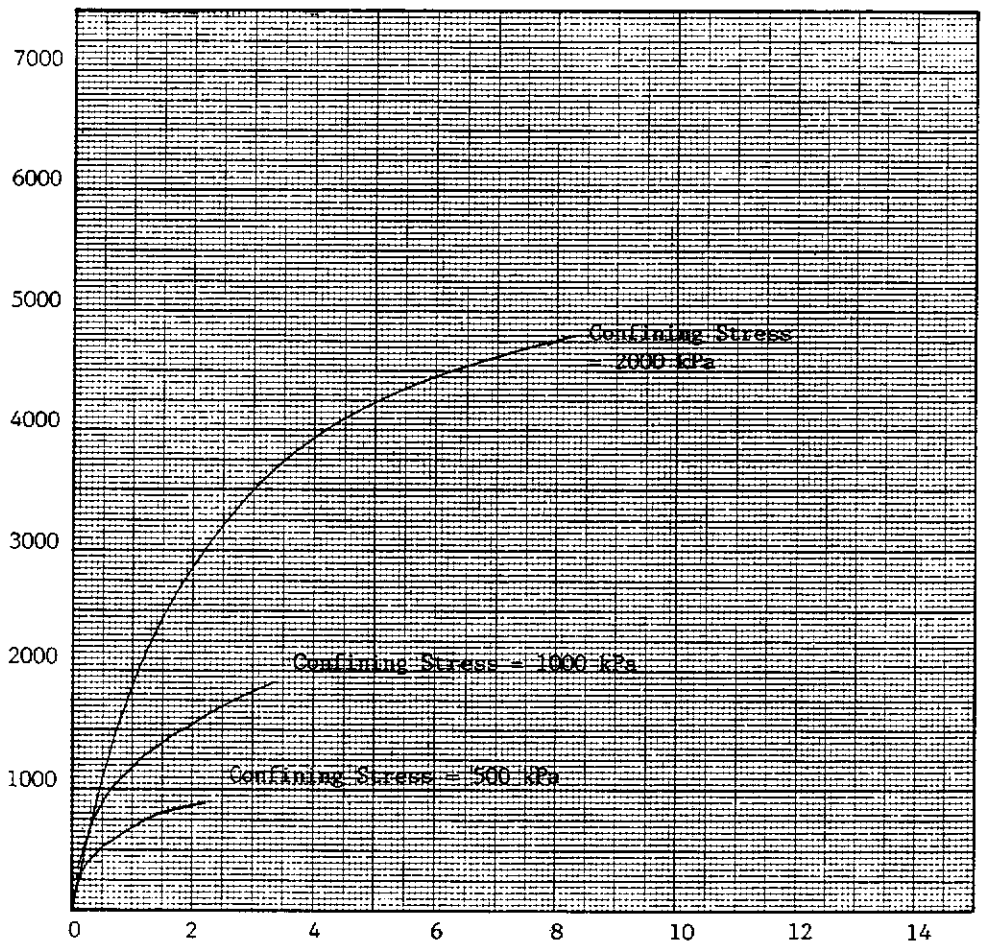

TESTED BY: KM CHECKED BY: DW DATE: 30/11/90

*Denotes use of Rock Colour Chart

CLIENT: COLLIE SCHOOL OF MINES

PROJECT: 1 NORTH WD6

SHEET No.: 8 **OF:** 69

JOB No.: S5937

DATE TESTED: 30/11/90

TRIAXIAL COMPRESSIVE STRENGTH OF UNDRAINED ROCK CORE SPECIMENS WITHOUT PORE PRESSURE MEASUREMENTS SUMMARY

Tested in accordance with ASTM D 2664 - 80.

SAMPLE IDENTIFICATION:

Bore Hole No :	D213/3 UPS - AS I/B
Depth in Metres :	50.00 - 52.00

PHYSICAL DESCRIPTION:

Name of Rock :	LOOSE, CLEAN, MEDIUM-COARSE SANDSTONE (DISTURBED SAMPLE)

SPECIMEN DATA:

Height :	120.0	mm
Diameter :	60.0	mm
Wet Mass :	715.2	g
Wet Density :	2.11	t/m^3
Dry Density :	2.00	t/m^3
Moisture Content :	5.4	%

DEFORMATION RATE:	0.2	mm / minute

REMARKS: The disturbed sample was remoulded to the specified density and the multi stage triaxial test was carried out on this reconstituted test specimen as instructed.

TESTED BY: KM CHECKED BY: DW DATE: 30/11/90

* Denotes use of Rock Colour Chart

CLIENT: COLLIE SCHOOL OF MINES **SHEET No.:** 9 **OF:** 69

PROJECT: 1 NORTH WD6 **JOB No.:** S5937

DATE TESTED: 30/11/90

TRIAXIAL COMPRESSION TEST SUMMARY

VISUAL CLASSIFICATION (A.S.1726)

SAMPLE IDENTIFICATION/DEPTH	DESCRIPTION	SYMBOL
D213/3 UPS - AS I/B 50.00 - 52.00m	LOOSE, CLEAN, DEDIUM-COARSE SANDSTONE (DISTURBED SAMPLE)	

TEST PARAMETER SUMMARY

CONFINING STRESS (σ_3) kPa	1000	1500	2000
POREWATER PRESSURE (U) kPa	NR	NR	NR
EFFECTIVE CONFINING STRESS(σ_3-U)	NR	NR	NR
DEVIATOR STRESS (σ_1-σ_3) kPa	3664	5228	6684
SHEAR STRESS $\frac{(\sigma_1-\sigma_3)}{2}$ kPa	1832	2614	3342
INTERNAL FRICTION (ϕ) Degrees	- 39°		
YOUNG'S/SECANT MODULUS (kPa)	-		
COHESION (c) (kPa)	- 0		

COMMENTS

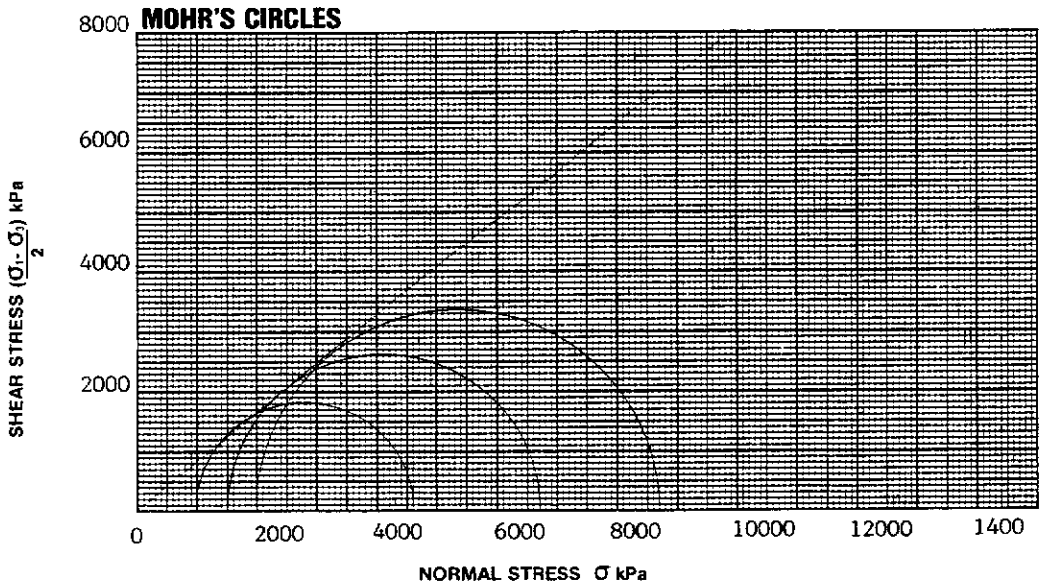

TESTED BY: KM CHECKED BY: DW DATE: 30/11/90

* Denotes use of Rock Colour Chart

SRC 85-9

CLIENT: COLLIE SCHOOL OF MINES

PROJECT: 1 NORTH WD6

SHEET No.: 10 **OF:** 69

JOB No.: S5937

DATE TESTED: 30/11/90

SAMPLE IDENTIFICATION: Bore Hole D213/3 UPS - AS I/B
Depth in Metres 50.00 - 52.00

DEVIATOR STRESS/AXIAL STRAIN SUMMARY

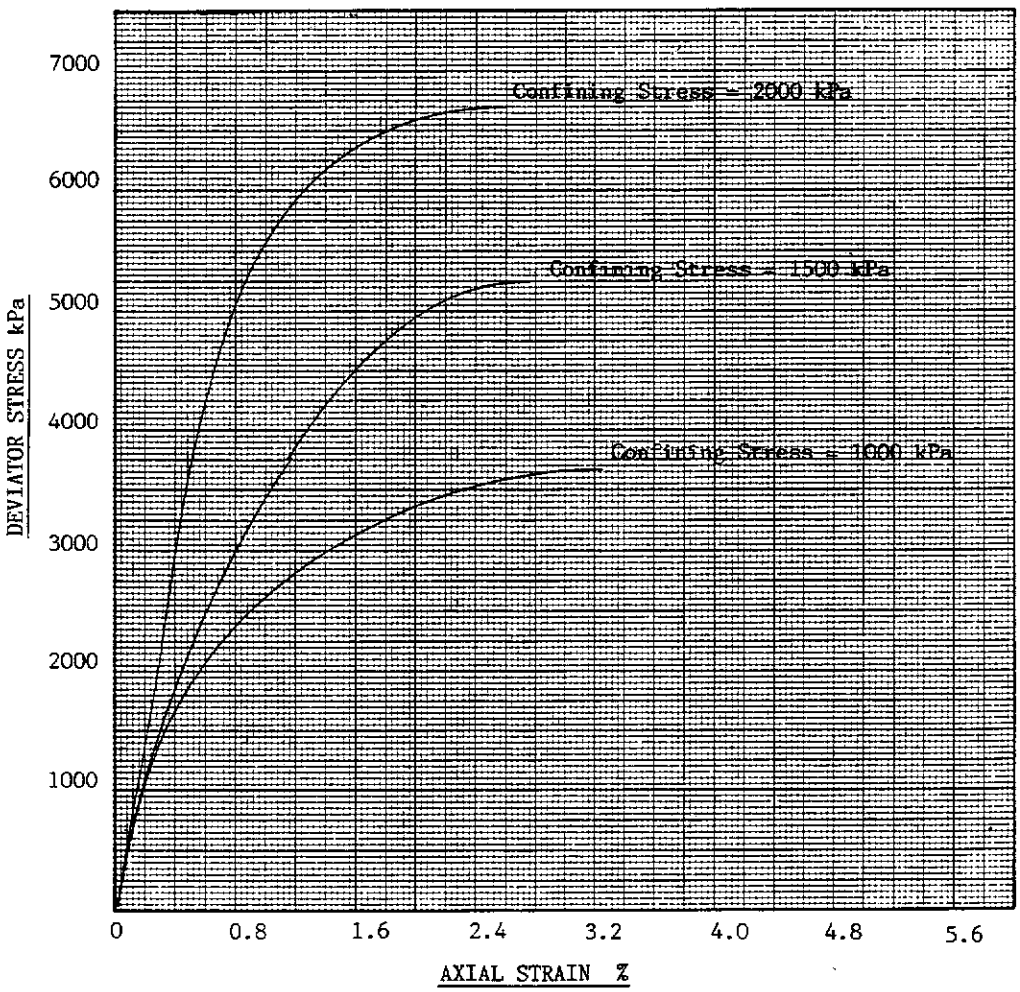

TESTED BY: KM CHECKED BY: DW DATE: 30/11/90

* Denotes use of Rock Colour Chart

CLIENT: COLLIE SCHOOL OF MINES **SHEET No.:** 11 **OF:** 69

PROJECT: 1 NORTH WD6 **JOB No.:** S5937

DATE TESTED: 8/11/90

DETERMINATION OF THE INDIRECT TENSILE STRENGTH BY THE BRAZIL TEST

Tested in accordance with the International Society for Rock Mechanics, Rock Characterisation Testing and Monitoring - 1981

SAMPLE IDENTIFICATION

Bore Hole No: D212/4 UPSILON SEAM

Depth in Metres: 39.17 - 39.32

PHYSICAL DESCRIPTION

Name of Rock: COAL

SPECIMEN DATA

Thickness:	29.2	mm
Diameter:	60.5	mm
Wet Density:	1.28	t/m^3
Dry Density:	0.90	t/m^3
Moisture Content:	41.4	%
DEFORMATION RATE:	0.2	mm/minute

RESULTS

SPECIMEN No	1	2	3	4
TENSILE STRENGTH (MPa)	1.03	0.52	1.80	0.65

AVERAGE TENSILE STRENGTH: 1.00 MPa

REMARKS: NIL

TESTED BY: KM CHECKED BY: DW DATE: 12/11/90

* Denotes use of Rock Colour Chart

SAMPLE IDENTIFICATION:

Bore Hole No.	D212/4 UPSILON SEAM
Depth in Metres:	39.17 - 39.32

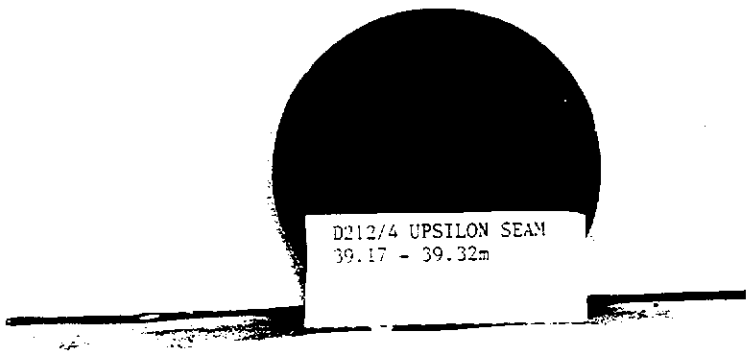

TESTED BY: KM CHECKED BY: DW DATE: 12

* Denotes use of Rock Colour Chart

CLIENT: COLLIE SCHOOL OF MINES

PROJECT: 1 NORTH WD6

SHEET No.: 13 **OF:** 69

JOB No.: S5937

DATE TESTED: 15/11/90

ELASTIC MODULI OF INTACT ROCK CORE SPECIMENS IN UNIAXIAL COMPRESSION SUMMARY

Tested in accordance with ASTM D 3148 - 80.

SAMPLE IDENTIFICATION:

Bore Hole No:	D212/5 UPSILON SEAM
Depth in Metres:	39.32 - 39.47

PHYSICAL DESCRIPTION:

Name of Rock:	COAL

SPECIMEN DATA:

Height:	123.4	mm
Diameter:	60.5	mm
Wet Mass:	357.9	g
Wet Density:	1.01	t/m^3
Dry Density:	0.74	t/m^3
Moisture Content:	37.2	%
DEFORMATION RATE:	0.2	mm / minute
UNCONFINED COMPRESSIVE STRENGTH:	14610	kPa

REMARKS: Axial strain was determined using the change in distance between the platens.

TESTED BY: KM CHECKED BY: DW DATE: 19/11/90

* Denotes use of Rock Colour Chart

CLIENT: COLLIE SCHOOL OF MINES

PROJECT: 1 NORTH WD6

SHEET No.: 14 **OF:** 69

JOB No.: S5937

DATE TESTED: 15/11/90

SAMPLE IDENTIFICATION: Bore Hole D212/5 UPSILON SEAM

Depth in Metres 39.32 - 39.47

STRESS VERSUS AXIAL & DIAMETRIC STRAIN SUMMARY

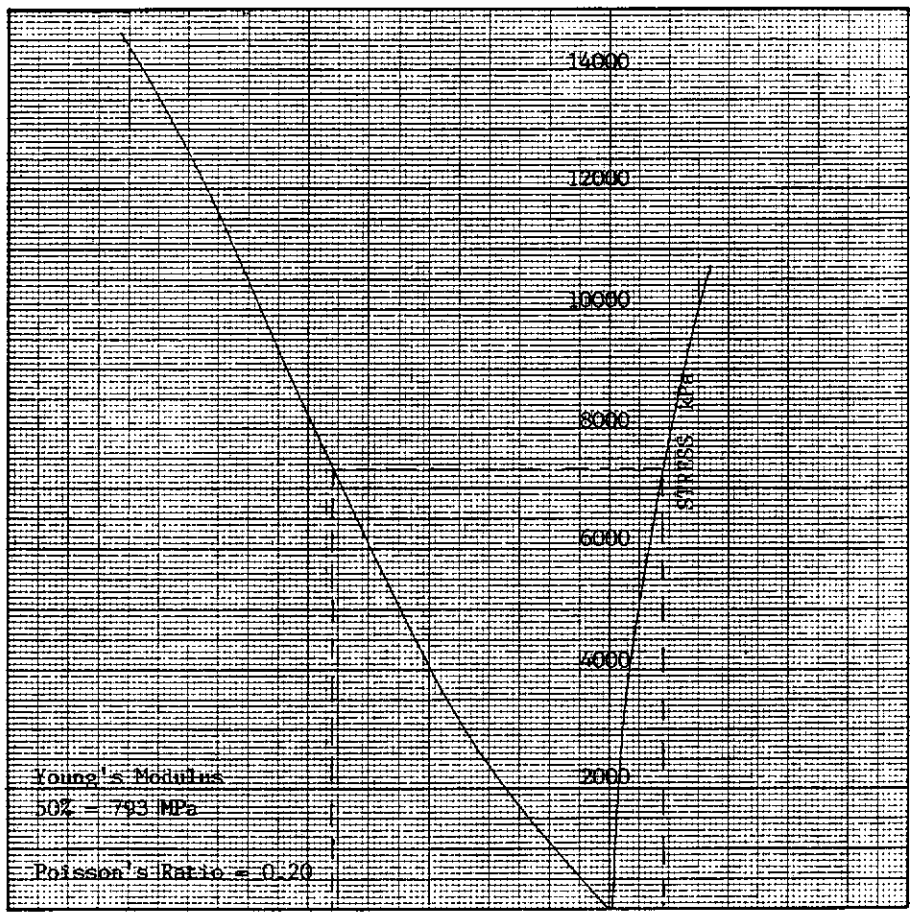

TESTED BY: KM CHECKED BY: DW DATE: 19/11/90

* Denotes use of Rock Colour Chart

PHOTOGRAPHIC SUMMARY

SAMPLE IDENTIFICATION:

Bore Hole No: D212/5 UPSILON SEAM

Depth in Metres: 39.32 - 39.47

TESTED BY: KM CHECKED BY: DW DATE: 19/

* Denotes use of Rock Colour Chart

CLIENT: COLLIE SCHOOL OF MINES

PROJECT: 1 NORTH WD6

SHEET No.: 16 **OF:** 69

JOB No.: S5937

DATE TESTED: 13/11/90

TRIAXIAL COMPRESSIVE STRENGTH OF UNDRAINED ROCK CORE SPECIMENS WITHOUT PORE PRESSURE MEASUREMENTS SUMMARY

Tested in accordance with ASTM D 2664 - 80.

SAMPLE IDENTIFICATION:

Bore Hole No :	D212/6 UPSILON SEAM
Depth in Metres :	39.47 - 39.63

PHYSICAL DESCRIPTION:

Name of Rock :	COAL

SPECIMEN DATA:

Height :	119.8	mm
Diameter :	60.5	mm
Wet Mass :	447.9	g
Wet Density :	1.30	t/m^3
Dry Density :	0.95	t/m^3
Moisture Content :	36.4	%

DEFORMATION RATE:	0.2	mm / minute

REMARKS: Inadvertantly tested at 0.4 MPa

NOTE: Deviation from standard - Pore Pressure measurements were recorded as requested by client. Refer to Sheet No. 19 of 69 .

TESTED BY: KM CHECKED BY: DW DATE: 16/11/90

* Denotes use of Rock Colour Chart

CLIENT: COLLIE SCHOOL OF MINES

PROJECT: 1 NORTH WD6

SHEET No.: 17 OF: 69

JOB No.: S5937

DATE TESTED: 13/11/90

TRIAXIAL COMPRESSION TEST SUMMARY

VISUAL CLASSIFICATION (A.S.1726)

SAMPLE IDENTIFICATION/DEPTH	DESCRIPTION	SYMBOL
D212/6 UPSILON SEAM 39.47 - 39.63	-	-

TEST PARAMETER SUMMARY

CONFINING STRESS (σ_3) kPa	400		
POREWATER PRESSURE (U) kPa	7		
EFFECTIVE CONFINING STRESS(σ_3-U)	393		
DEVIATOR STRESS (σ_1-σ_3) kPa	20836		
SHEAR STRESS $\frac{(\sigma_1 - \sigma_3)}{2}$ kPa	10418		
INTERNAL FRICTION (ϕ) Degrees	-		
YOUNG'S/SECANT MODULUS (kPa)	-		
COHESION (c) (kPa)	- 2000		

COMMENTS

MOHR'S CIRCLES

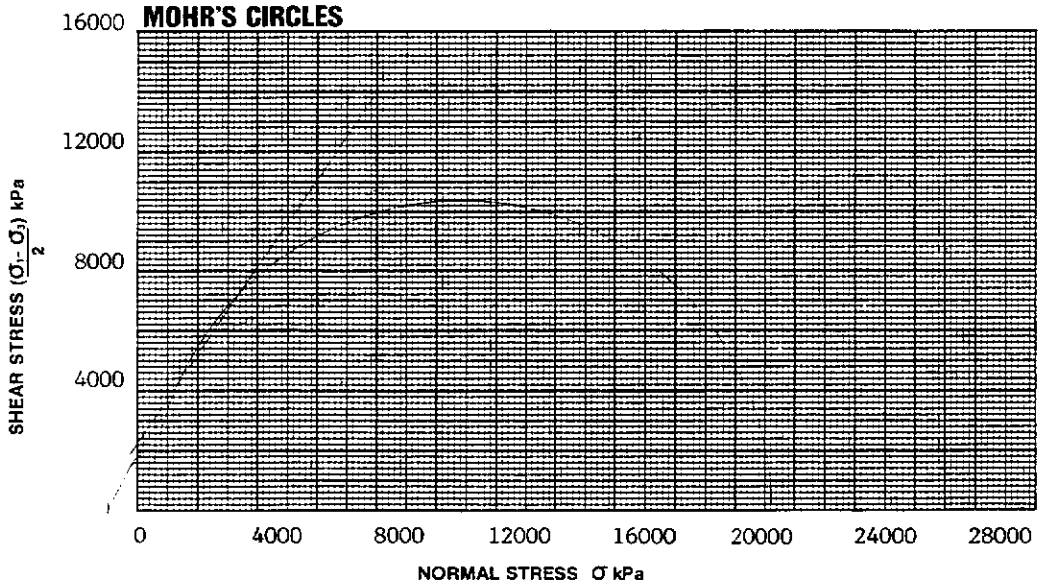

TESTED BY: KM CHECKED BY: DW DATE: 16/11/90

* Denotes use of Rock Colour Chart

SRC 86 5

CLIENT: COLLIE SCHOOL OF MINES

PROJECT: 1 NORTH WD6

SHEET No.: 18 **OF:** 69

JOB No.: S5937

DATE TESTED: 13/11/90

SAMPLE IDENTIFICATION: Bore Hole No. D212/6 UPSILON SEAM

Depth in Metres 39.47 - 39.63

DEVIATOR STRESS/AXIAL STRAIN SUMMARY

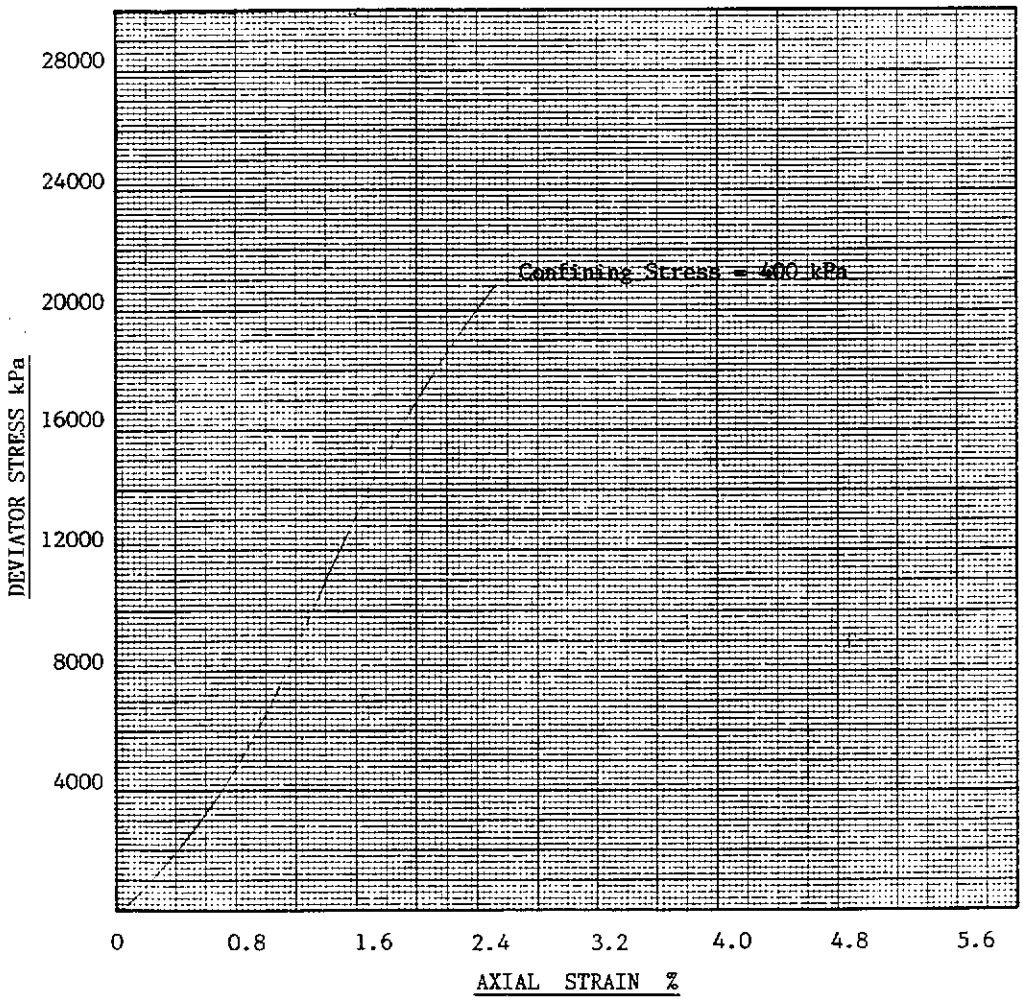

TESTED BY: KM CHECKED BY: DW DATE: 16/11/90

* Denotes use of Rock Colour Chart

CLIENT: COLLIE SCHOOL OF MINES

PROJECT: 1 NORTH WD6

SHEET No.: 19 **OF:** 69

JOB No.: S5937

DATE TESTED: 13/11/90

SAMPLE IDENTIFICATION: Bore Hole No. D212/6 UPSILON SEAM

Depth in Metres 39.47 - 39.63

PORE PRESSURE/AXIAL STRAIN SUMMARY

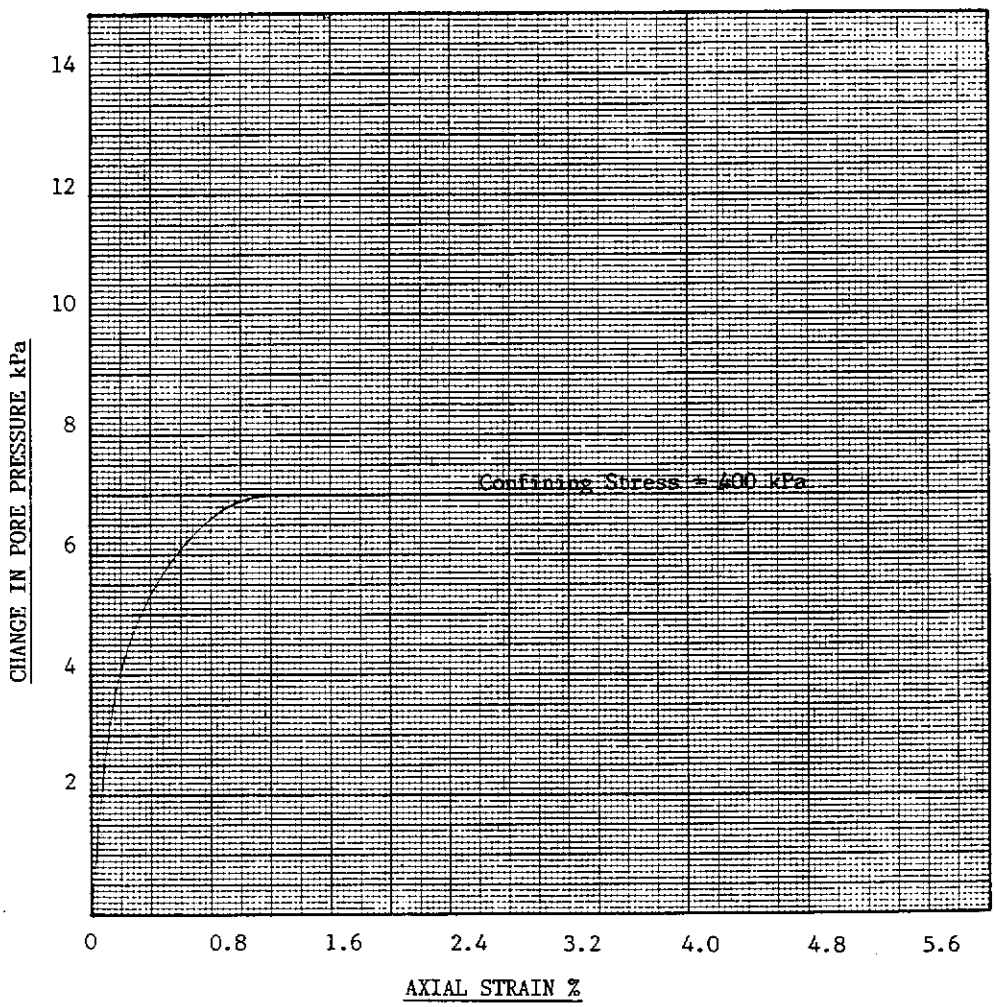

TESTED BY: KM CHECKED BY: DW DATE: 16/11/90

* Denotes use of Rock Colour Chart

CLIENT: COLLIE SCHOOL OF MINES

PROJECT: 1 NORTH WD6

SHEET No.: 20 **OF:** 69

JOB No.: S5937

DATE TESTED: 13/11/90

PHOTOGRAPHIC SUMMARY

SAMPLE IDENTIFICATION:

Bore Hole No: D212/6 UPSILON SEAM

Depth in Metres: 39.47 - 39.63

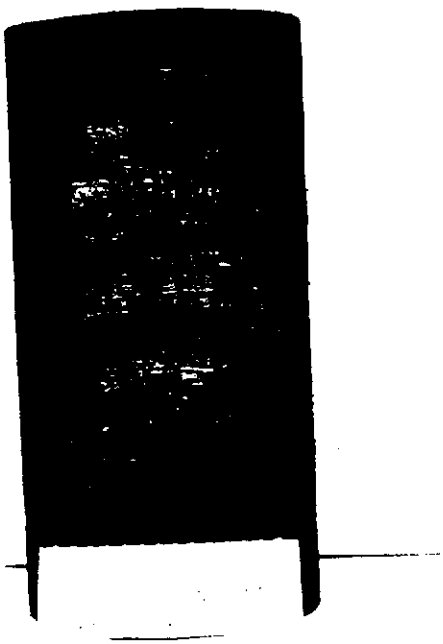

TESTED BY: KM CHECKED BY: DW DATE: 16/11/90

* Denotes use of Rock Colour Chart

CLIENT: COLLIE SCHOOL OF MINES **SHEET No.:** 21 **OF:** 69

PROJECT: 1 NORTH WD6 **JOB No.:** S5937

DATE TESTED: 8/11/90

DETERMINATION OF THE INDIRECT TENSILE STRENGTH BY THE BRAZIL TEST

Tested in accordance with the International Society for Rock Mechanics, Rock Characterisation Testing and Monitoring - 1981

SAMPLE IDENTIFICATION

Bore Hole No: D212/7 ALPHA ROOF

Depth in Metres: 55.70 - 55.90

PHYSICAL DESCRIPTION

Name of Rock: CARBONACEOUS SILTSTONE/FINE SANDSTONE

SPECIMEN DATA

Thickness:	30.5	mm
Diameter:	60.5	mm
Wet Density:	1.87	t/m^3
Dry Density:	1.58	t/m^3
Moisture Content:	18.7	%
DEFORMATION RATE:	0.2	mm/minute

RESULTS

SPECIMEN No	1	2	3	4
TENSILE STRENGTH (MPa)	0.89	0.87	0.65	0.73

AVERAGE TENSILE STRENGTH: 0.78 MPa

REMARKS: NIL

TESTED BY: KM CHECKED BY: DW DATE: 12/11/90

* Denotes use of Rock Colour Chart

CLIENT: COLLIE SCHOOL OF MINES

PROJECT: 1 NORTH WD6

SHEET No.: 22 **OF:** 69

JOB No.: S5937

DATE TESTED: 8/11/90

PHOTOGRAPHIC SUMMARY

SAMPLE IDENTIFICATION:

Bore Hole No. D212/7 ALPHA ROOF

Depth in Metres: 55.70 - 55.90

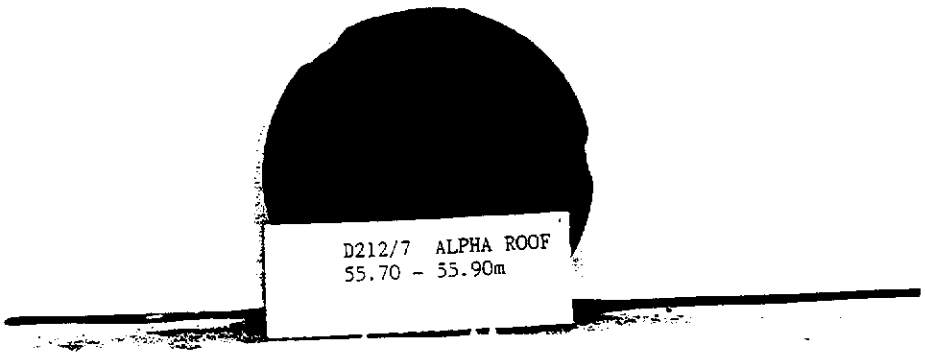

TESTED BY: KM CHECKED BY: DW DATE: 12/11/90

* Denotes use of Rock Colour Chart

CLIENT: COLLIE SCHOOL OF MINES **SHEET No.:** 23 **OF:** 69

PROJECT: 1 NORTH WD6 **JOB No.:** S5937

DATE TESTED: 14/11/90

TRIAXIAL COMPRESSIVE STRENGTH OF UNDRAINED ROCK CORE SPECIMENS WITHOUT PORE PRESSURE MEASUREMENTS SUMMARY

Tested in accordance with ASTM D 2664 - 80.

SAMPLE IDENTIFICATION:

Bore Hole No :	D212/8 ALPHA ROOF
Depth in Metres :	55.90 - 56.05

PHYSICAL DESCRIPTION:

Name of Rock :	CARBONATE SILTSTONE/FINE SANDSTONE

SPECIMEN DATA:

Height :	120.5	mm
Diameter :	60.5	mm
Wet Mass :	655.1	g
Wet Density :	1.89	t/m^3
Dry Density :	1.59	t/m^3
Moisture Content :	18.9	%

DEFORMATION RATE:	0.2	mm / minute

REMARKS: NIL

NOTE: Deviation from standard - Pore Pressure measurements were recorded as requested by client. Refer to Sheet No. 26 of 69 .

TESTED BY: KM CHECKED BY: DW DATE: 16/11/90

* Denotes use of Rock Colour Chart

CLIENT: COLLIE SCHOOL OF MINES

PROJECT: 1 NORTH WD6

SHEET No.: 24 OF: 69

JOB No.: S5937

DATE TESTED: 14/11/90

TRIAXIAL COMPRESSION TEST SUMMARY

VISUAL CLASSIFICATION (A.S.1726)

SAMPLE IDENTIFICATION/DEPTH	DESCRIPTION	SYMBOL
D212/8 ALPHA ROOF 55.90 - 56.05	-	-

TEST PARAMETER SUMMARY

CONFINING STRESS (σ_3) kPa	1000		
POREWATER PRESSURE (U) kPa	6		
EFFECTIVE CONFINING STRESS(σ_3-U)	994		
DEVIATOR STRESS (σ_1-σ_3) kPa	5426		
SHEAR STRESS $\frac{(\sigma_1 - \sigma_3)}{2}$ kPa	2713		
INTERNAL FRICTION (ϕ) Degrees	- 27°		
YOUNG'S/SECANT MODULUS (kPa)	-		
COHESION (c) (kPa)	- ≈250		

COMMENTS

MOHR'S CIRCLES

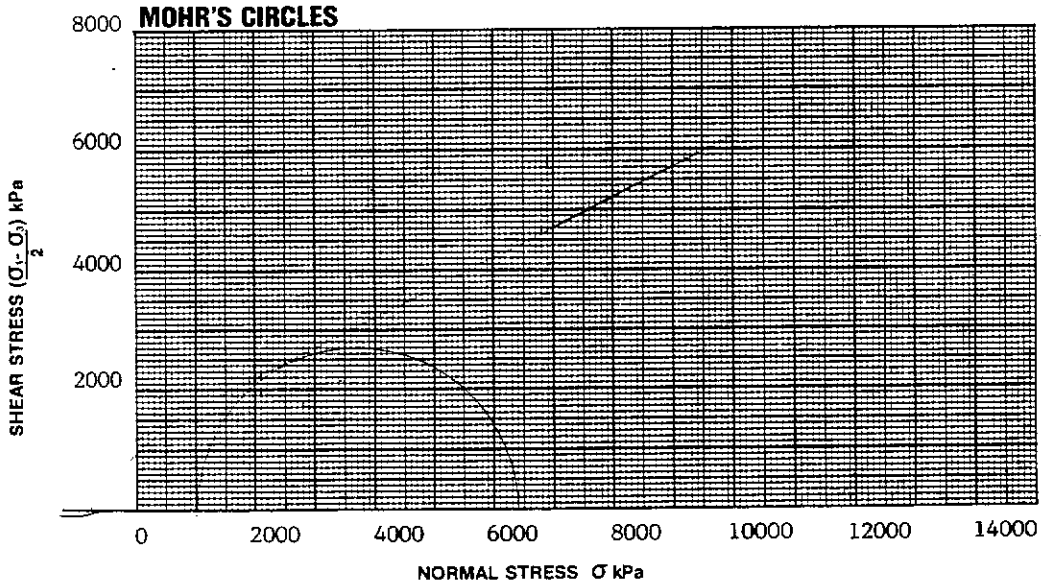

TESTED BY: KM CHECKED BY: DW DATE: 16/11/90

* Denotes use of Rock Colour Chart

SRC 85.9

CLIENT: COLLIE SCHOOL OF MINES

PROJECT: 1 NORTH WD6

SHEET No.: 25 **OF:** 69

JOB No.: S5937

DATE TESTED: 14/11/90

SAMPLE IDENTIFICATION: Bore Hole No. D212/8 ALPHA ROOF

Depth in Metres 55.90 - 56.05

DEVIATOR STRESS/AXIAL STRAIN SUMMARY

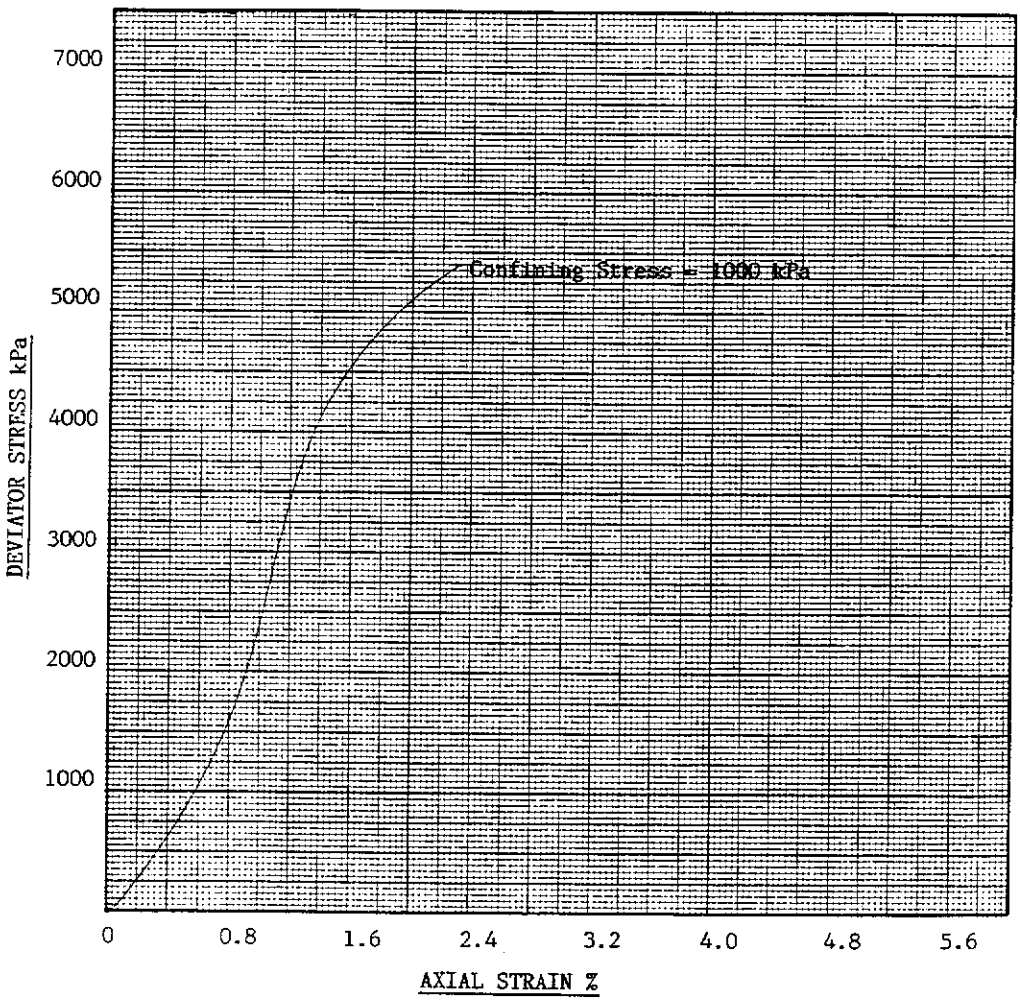

TESTED BY: KM CHECKED BY: DW DATE: 16/11/90

* Denotes use of Rock Colour Chart

CLIENT: COLLIE SCHOOL OF MINES

PROJECT: 1 NORTH WD6

SHEET No.: 26 **OF:** 69

JOB No.: S5937

DATE TESTED: 14/11/90

SAMPLE IDENTIFICATION: Bore Hole No. D212/8 ALPHA ROOF

Depth in Metres 55.90 - 56.05

PORE PRESSURE/AXIAL STRAIN SUMMARY

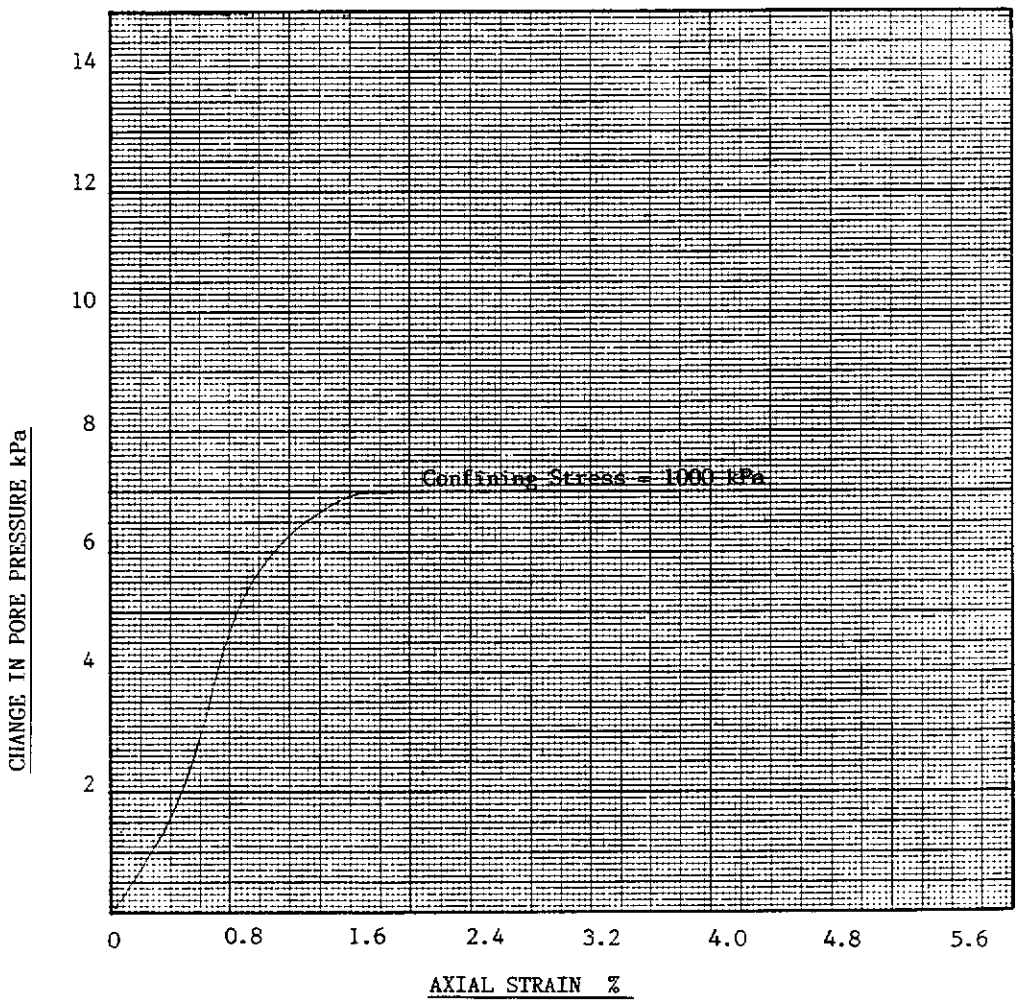

TESTED BY: KM CHECKED BY: DW DATE: 16/11/90

* Denotes use of Rock Colour Chart

CLIENT: COLLIE SCHOOL OF MINES

PROJECT: 1 NORTH WD6

SHEET No.: 27 **OF:** 69

JOB No.: S5937

DATE TESTED: 14/11/90

PHOTOGRAPHIC SUMMARY

SAMPLE IDENTIFICATION:

Bore Hole No: D212/8 ALPHA ROOF

Depth in Metres: 55.90 - 56.05

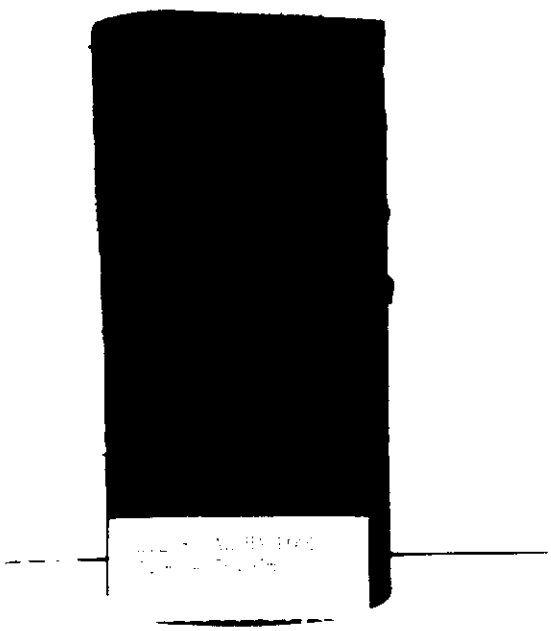

TESTED BY: KM CHECKED BY: DW DATE: 16/11/90

* Denotes use of Rock Colour Chart

CLIENT: COLLIE SCHOOL OF MINES

PROJECT: 1 NORTH WD6

SHEET No.: 28 **OF:** 69

JOB No.: S5937

DATE TESTED: 15/11/90

ELASTIC MODULI OF INTACT ROCK CORE SPECIMENS IN UNIAXIAL COMPRESSION SUMMARY

Tested in accordance with ASTM D 3148 - 80.

SAMPLE IDENTIFICATION:

Bore Hole No:	D212/9 ALPHA ROOF
Depth in Metres:	56.05 - 56.20

PHYSICAL DESCRIPTION:

Name of Rock:	CARBONACEOUS SILTSTONE/FINE SANDSTONE

SPECIMEN DATA:

Height:	119.0	mm
Diameter:	60.4	mm
Wet Mass:	641.4	g
Wet Density:	1.88	t/m^3
Dry Density:	1.59	t/m^3
Moisture Content:	18.2	%
DEFORMATION RATE:	0.2	mm / minute
UNCONFINED COMPRESSIVE STRENGTH:	3870	kPa

REMARKS: Axial strain was determined using the change in distance between the platens.

TESTED BY: KM CHECKED BY: DW DATE: 19/11/90

* Denotes use of Rock Colour Chart

CLIENT: COLLIE SCHOOL OF MINES

PROJECT: 1 NORTH WD6

SHEET No.: 29 **OF:** 69

JOB No.: S5937

DATE TESTED: 15/11/90

SAMPLE IDENTIFICATION: Bore Hole No. D212/9 ALPHA ROOF

Depth in Metres 56.05 - 56.20

STRESS VERSUS AXIAL & DIAMETRIC STRAIN SUMMARY

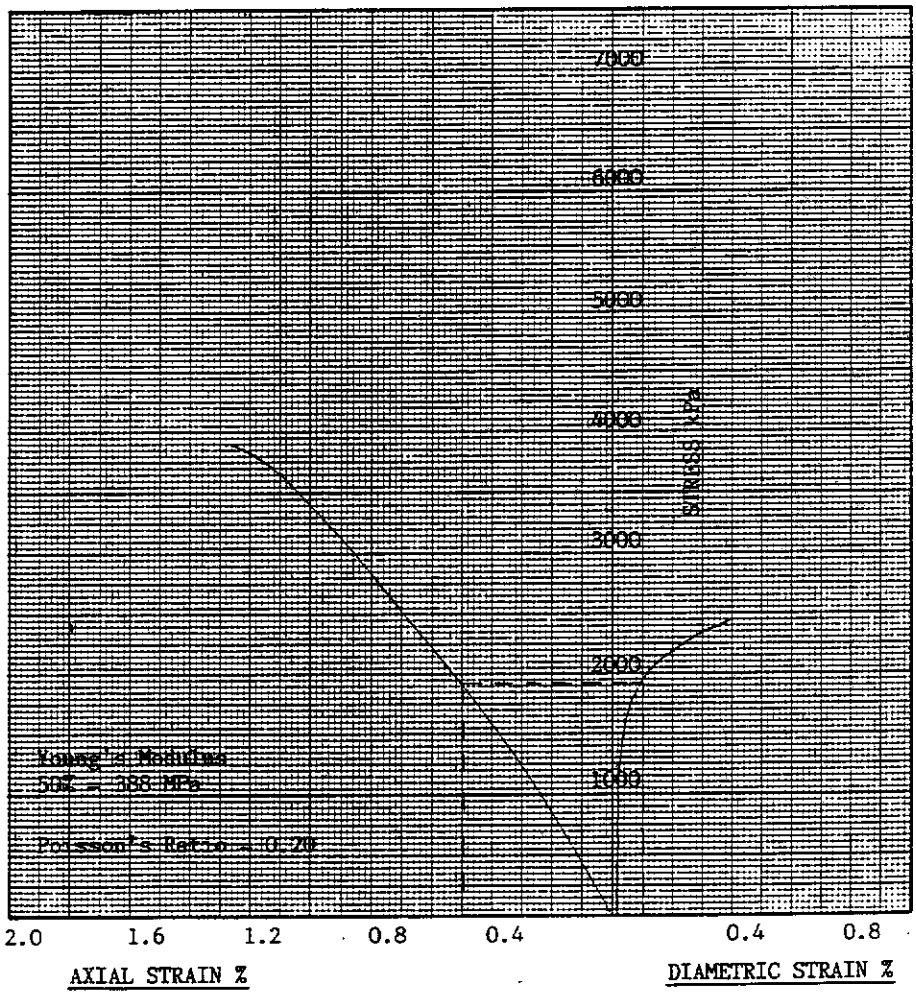

TESTED BY: KM CHECKED BY: DW DATE: 19/11/90

* Denotes use of Rock Colour Chart

CLIENT: COLLIE SCHOOL OF MINES

PROJECT: 1 NORTH WD6

SHEET No.: 30 **OF:** 69

JOB No.: S5937

DATE TESTED: 15/11/90

PHOTOGRAPHIC SUMMARY

SAMPLE IDENTIFICATION:

Bore Hole No: D212/9 ALPHA ROOF

Depth in Metres: 56.05 - 56.20

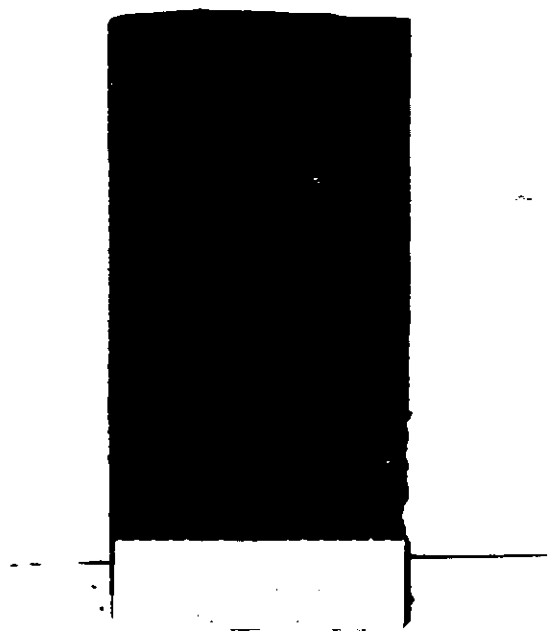

TESTED BY: KM CHECKED BY: DW DATE: 19/11/90

* Denotes use of Rock Colour Chart

CLIENT: COLLIE SCHOOL OF MINES

PROJECT: 1 NORTH WD6

SHEET No.: 31 OF: 69

JOB No.: S5937

DATE TESTED: 8/11/90

DETERMINATION OF THE INDIRECT TENSILE STRENGTH BY THE BRAZIL TEST

Tested in accordance with the International Society for Rock Mechanics, Rock Characterisation Testing and Monitoring - 1981

SAMPLE IDENTIFICATION

Bore Hole No: D212/10 AS-WS I/B

Depth in Metres: 71.13 - 71.31

PHYSICAL DESCRIPTION

Name of Rock: MEDIUM - VERY COARSE SANDSTONE

SPECIMEN DATA

Thickness:	27.0	mm
Diameter:	60.5	mm
Wet Density:	2.02	t/m^3
Dry Density:	1.76	t/m^3
Moisture Content:	14.8	%

DEFORMATION RATE: 0.2 mm/minute

RESULTS

SPECIMEN No	1	2	3	4
TENSILE STRENGTH (MPa)	0.58	0.52	0.77	0.40

AVERAGE TENSILE STRENGTH: 0.57 MPa

REMARKS: NIL

TESTED BY: KM CHECKED BY: DW DATE: 12/11/90

* Denotes use of Rock Colour Chart

CLIENT: COLLIE SCHOOL OF MINES

PROJECT: 1 NORTH WD6

SHEET No.: 32 **OF:** 69

JOB No.: 55937

DATE TESTED: 8/11/90

PHOTOGRAPHIC SUMMARY

SAMPLE DESCRIPTION:

Bore Hole No. D212/10 AS-WS I/B

Depth in Metres: 71.13 - 71.31

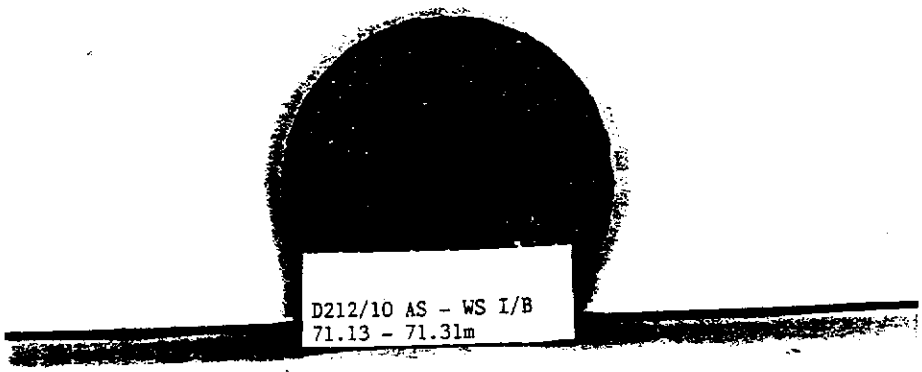

TESTED BY: KM CHECKED BY: DW DATE: 12/11/90

* Denotes use of Rock Colour Chart

CLIENT: COLLIE SCHOOL OF MINES

PROJECT: 1 NORTH WD6

SHEET No.: 33 **OF:** 69

JOB No.: S5937

DATE TESTED: 15/11/90

ELASTIC MODULI OF INTACT ROCK CORE SPECIMENS IN UNIAXIAL COMPRESSION SUMMARY

Tested in accordance with ASTM D 3148 - 80.

SAMPLE IDENTIFICATION:

Bore Hole No:	D212/11 AS - WS I/B
Depth in Metres:	71.31 - 71.48

PHYSICAL DESCRIPTION:

Name of Rock:	MEDIUM - VERY COARSE SANDSTONE

SPECIMEN DATA:

Height:	116.5	mm
Diameter:	60.3	mm
Wet Mass:	683.7	g
Wet Density:	2.06	t/m^3
Dry Density:	1.81	t/m^3
Moisture Content:	13.6	%
DEFORMATION RATE:	0.2	mm / minute
UNCONFINED COMPRESSIVE STRENGTH:	3640	kPa

REMARKS: Axial strain was determined using the change in distance between the platens.

TESTED BY: KM CHECKED BY: DW DATE: 19/11/90

* Denotes use of Rock Colour Chart

CLIENT: COLLIE SCHOOL OF MINES

PROJECT: 1 NORTH WD6

SHEET No.: 34 **OF:** 69

JOB No.: S5937

DATE TESTED: 15/11/90

SAMPLE IDENTIFICATION: Bore Hole No. D212/11 AS - WS I/B

Depth in Metres 71.31 - 71.48

STRESS VERSUS AXIAL & DIAMETRIC SUMMARY

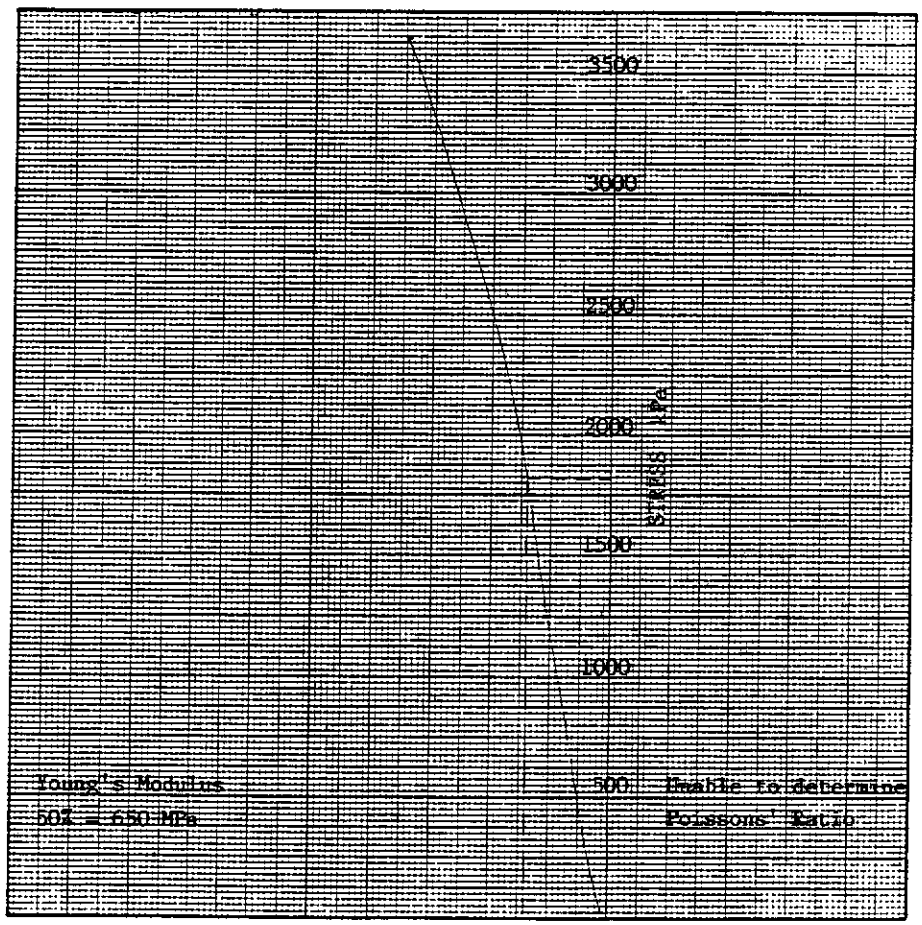

2.0 1.6 1.2 0.8 0.4

AXIAL STRAIN %

DIAMETRIC STRAIN %

TESTED BY: KM CHECKED BY: DW DATE: 19/11/90

* Denotes use of Rock Colour Chart

CLIENT: COLLIE SCHOOL OF MINES

PROJECT: 1 NORTH WD6

SHEET No.: 35 **OF:** 69

JOB No.: S5937

DATE TESTED: 15/11/90

PHOTOGRAPHIC SUMMARY

SAMPLE IDENTIFICATION:

Bore Hole No: D212/11 AS - WS I/B

Depth in Metres: 71.31 - 71.48

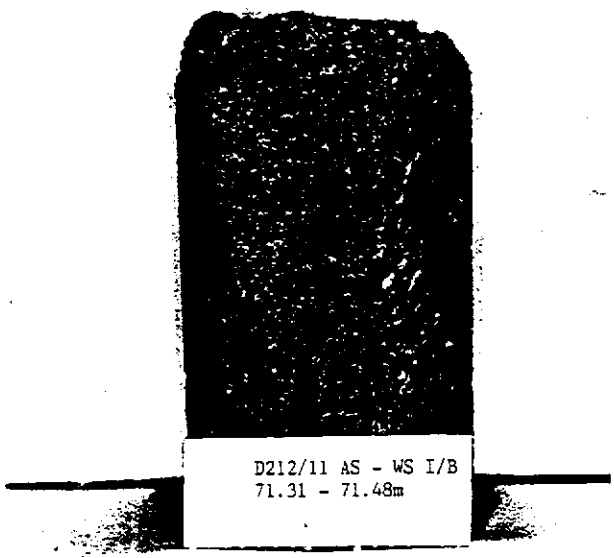

TESTED BY: KM CHECKED BY: DW DATE: 19/11/90

* Denotes use of Rock Colour Chart

CLIENT: COLLIE SCHOOL OF MINES **SHEET No.:** 36 **OF:** 69

PROJECT: 1 NORTH WD6 **JOB No.:** S5937

DATE TESTED: 14/11/90

TRIAXIAL COMPRESSIVE STRENGTH OF UNDRAINED ROCK CORE SPECIMENS WITHOUT PORE PRESSURE MEASUREMENTS SUMMARY

Tested in accordance with ASTM D 2664 - 80.

SAMPLE IDENTIFICATION:

Bore Hole No :	D212/12 AS - WS I/B
Depth in Metres :	71.48 - 71.65

PHYSICAL DESCRIPTION:

Name of Rock :	MEDIUM - VERY COARSE SANDSTONE

SPECIMEN DATA:

Height :	116.4	mm
Diameter :	60.4	mm
Wet Mass :	689.4	g
Wet Density :	2.07	t/m^3
Dry Density :	1.82	t/m^3
Moisture Content :	13.3	%

DEFORMATION RATE:	0.2	mm / minute

REMARKS: NIL

NOTE: Deviation from standard - Pore Pressure measurements were recorded as requested by client. Refer to Sheet No. 39 of 69 .

TESTED BY: KM CHECKED BY: DW DATE: 19/11/90

*Denotes use of Rock Colour Chart

CLIENT: COLLIE SCHOOL OF MINES **SHEET No.:** 37 **OF:** 69

PROJECT: 1 NORTH WD6 **JOB No.:** S5937

DATE TESTED: 14/11/90

TRIAXIAL COMPRESSION TEST SUMMARY

VISUAL CLASSIFICATION (A.S.1726)

SAMPLE IDENTIFICATION/DEPTH	DESCRIPTION	SYMBOL
D212/12 AS - WS I/B 71.48 - 71.65	-	-

TEST PARAMETER SUMMARY

CONFINING STRESS (σ_3) kPa	1000		
POREWATER PRESSURE (U) kPa	4		
EFFECTIVE CONFINING STRESS(σ_3-U)	996		
DEVIATOR STRESS (σ_1-σ_3) kPa	10400		
SHEAR STRESS $\frac{(\sigma_1 - \sigma_3)}{2}$ kPa	5200		
INTERNAL FRICTION (ϕ) Degrees	-		
YOUNG'S/SECANT MODULUS (kPa)	-		
COHESION (c) (kPa)	-		

COMMENTS

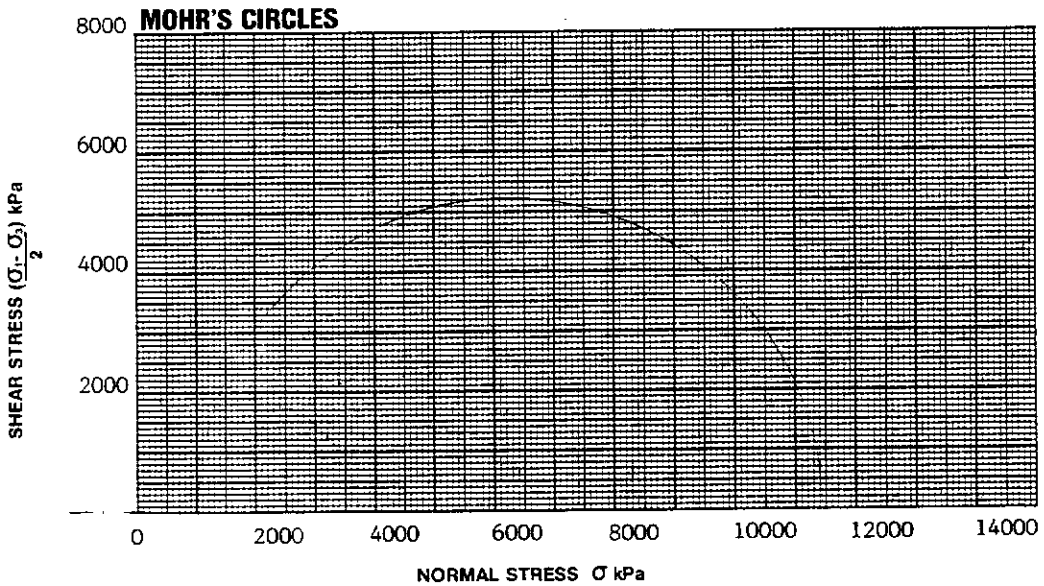

TESTED BY: KM CHECKED BY: DW DATE: 19/11/90

* Denotes use of Rock Colour Chart

SRC 85-9

CLIENT: COLLIE SCHOOL OF MINES

PROJECT: 1 NORTH WD6

SHEET No.: 38 **OF:** 69

JOB No.: S5937

DATE TESTED: 14/11/90

SAMPLE IDENTIFICATION: Bore Hole No. D212/12 AS - WS I/B

Depth in Metres 71.48 - 71.65

DEVIATOR STRESS/AXIAL STRAIN SUMMARY

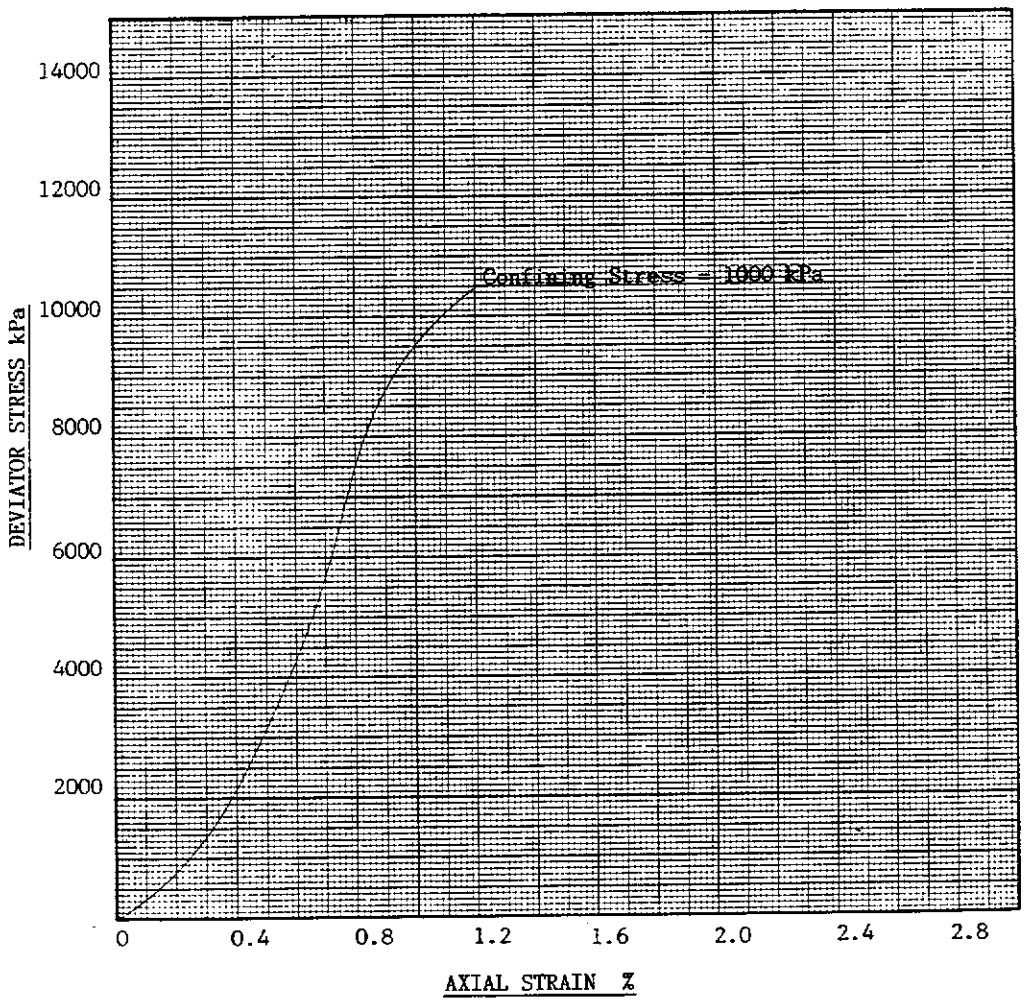

TESTED BY: KM CHECKED BY: DW DATE: 19/11/90

* Denotes use of Rock Colour Chart

CLIENT: COLLIE SCHOOL OF MINES

PROJECT: 1 NORTH WD6

SHEET No.: 39 **OF:** 69

JOB No.: S5937

DATE TESTED: 14/11/90

SAMPLE IDENTIFICATION: Bore Hole No. D212/12 AS - WS I/B

Depth in Metres 71.48 - 71.65

PORE PRESSURE/AXIAL STRAIN SUMMARY

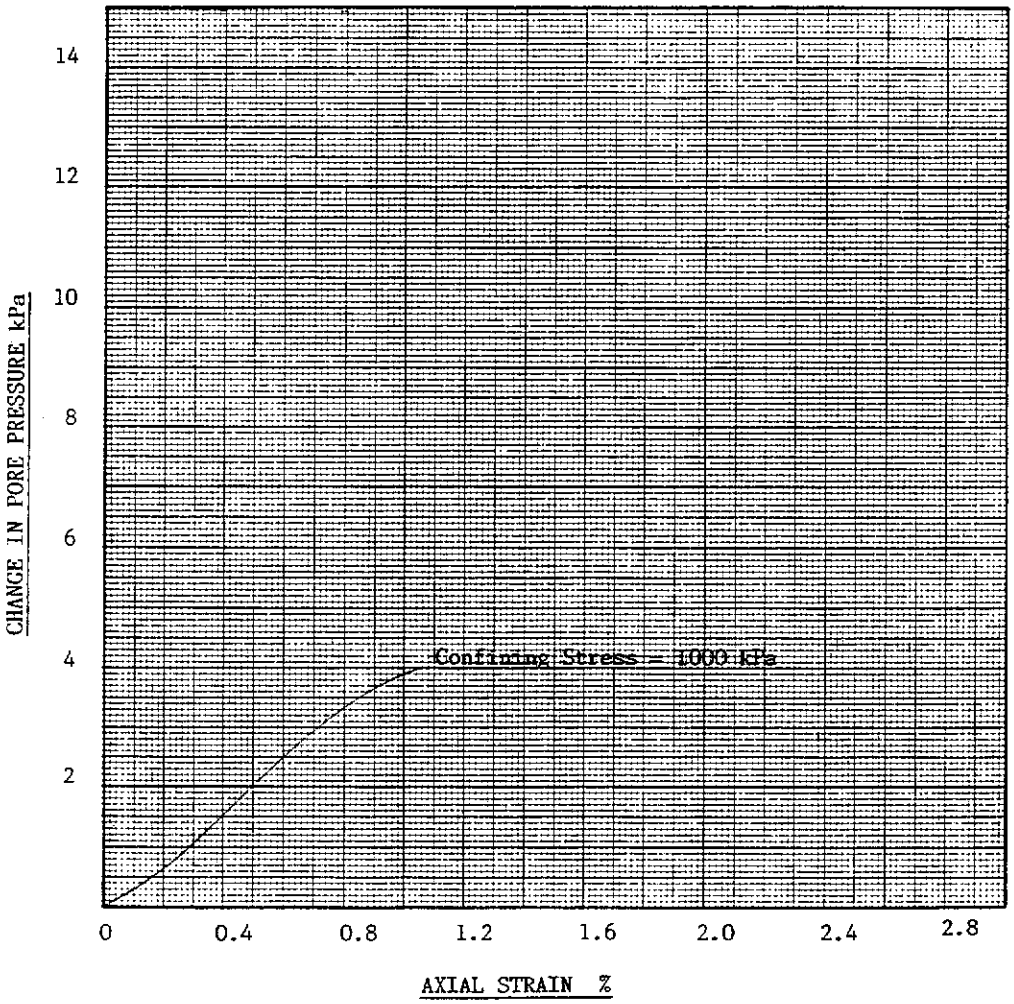

TESTED BY: KM CHECKED BY: DW DATE: 19/11/90

*Denotes use of Rock Colour Chart

CLIENT: COLLIE SCHOOL OF MINES

PROJECT: 1 NORTH WD6

SHEET No.: 40 **OF:** 69

JOB No.: S5937

DATE TESTED: 14/11/90

PHOTOGRAPHIC SUMMARY

SAMPLE IDENTIFICATION:

Bore Hole No: D212/12 AS - WS I/B

Depth in Metres: 71.48 - 71.65

TESTED BY: KM CHECKED BY: DW DATE: 19/11/90

* Denotes use of Rock Colour Chart

CLIENT: COLLIE SCHOOL OF MINES **SHEET No.:** 41 **OF:** 69

PROJECT: 1 NORTH WD6 **JOB No.:** S5937

DATE TESTED: 14/11/90

TRIAXIAL COMPRESSIVE STRENGTH OF UNDRAINED ROCK CORE SPECIMENS WITHOUT PORE PRESSURE MEASUREMENTS SUMMARY

Tested in accordance with ASTM D 2664 - 80.

SAMPLE IDENTIFICATION:

Bore Hole No :	D212/13 AS - WS I/B
Depth in Metres :	71.76 - 71.91

PHYSICAL DESCRIPTION:

Name of Rock :	MEDIUM - VERY COARSE SANDSTONE

SPECIMEN DATA:

Height :	118.4	mm
Diameter :	60.3	mm
Wet Mass :	687.4	g
Wet Density :	2.03	t/m^3
Dry Density :	1.78	t/m^3
Moisture Content :	13.9	%

DEFORMATION RATE:	0.2	mm / minute

REMARKS: NIL

NOTE: Deviation from standard - Pore Pressure measurements were recorded as requested by client. Refer to Sheet No. 44 of 69 .

TESTED BY: KM CHECKED BY: DW DATE: 19/11/90

* Denotes use of Rock Colour Chart

CLIENT: COLLIE SCHOOL OF MINES

PROJECT: 1 NORTH WD6

SHEET No.: 42 OF: 69

JOB No.: S5937

DATE TESTED: 14/11/90

TRIAXIAL COMPRESSION TEST SUMMARY

VISUAL CLASSIFICATION (A.S.1726)

SAMPLE IDENTIFICATION/DEPTH	DESCRIPTION	SYMBOL
D212/13 AS - WS I/B 71.76 - 71.91	-	-

TEST PARAMETER SUMMARY

CONFINING STRESS (σ_3) kPa	2000		
POREWATER PRESSURE (U) kPa	1		
EFFECTIVE CONFINING STRESS(σ_3-U)	1999		
DEVIATOR STRESS (σ_1-σ_3) kPa	12781		
SHEAR STRESS $\frac{(\sigma_1 - \sigma_3)}{2}$ kPa	6390.5		
INTERNAL FRICTION (ϕ) Degrees	-		
YOUNG'S/SECANT MODULUS (kPa)	-		
COHESION (c) (kPa)	-		

COMMENTS

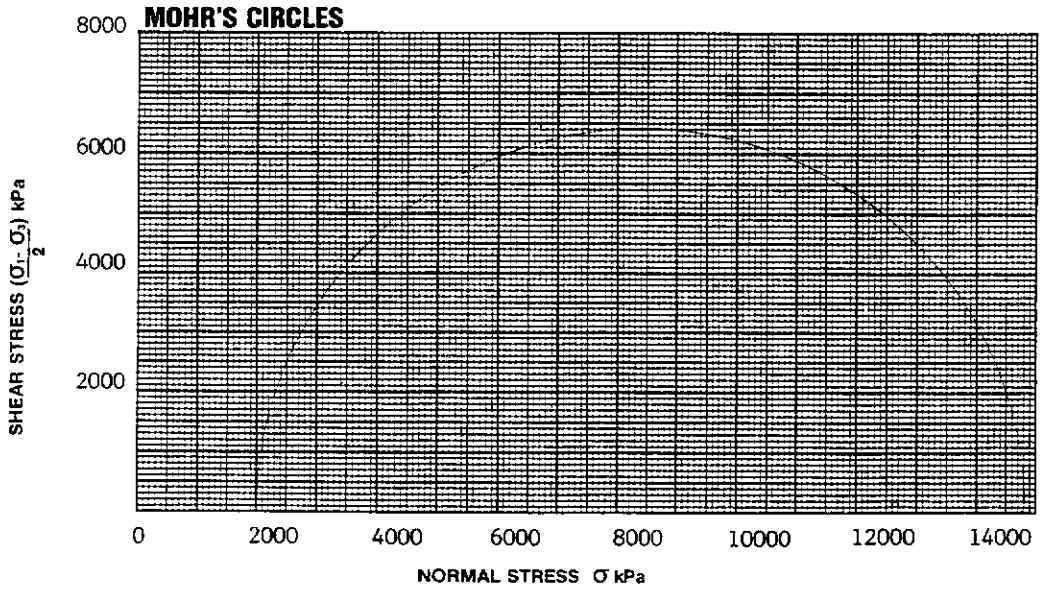

TESTED BY: KM CHECKED BY: DW DATE: 19/11/90

* Denotes use of Rock Colour Chart

CLIENT: COLLIE SCHOOL OF MINES

PROJECT: 1 NORTH WD6

SHEET No.: 43 **OF:** 69

JOB No.: S5937

DATE TESTED: 14/11/90

SAMPLE IDENTIFICATION: Bore Hole No. D212/13 AS - WS I/B

Depth in Metres 71.76 - 71.91

DEVIATOR STRESS/AXIAL STRAIN SUMMARY

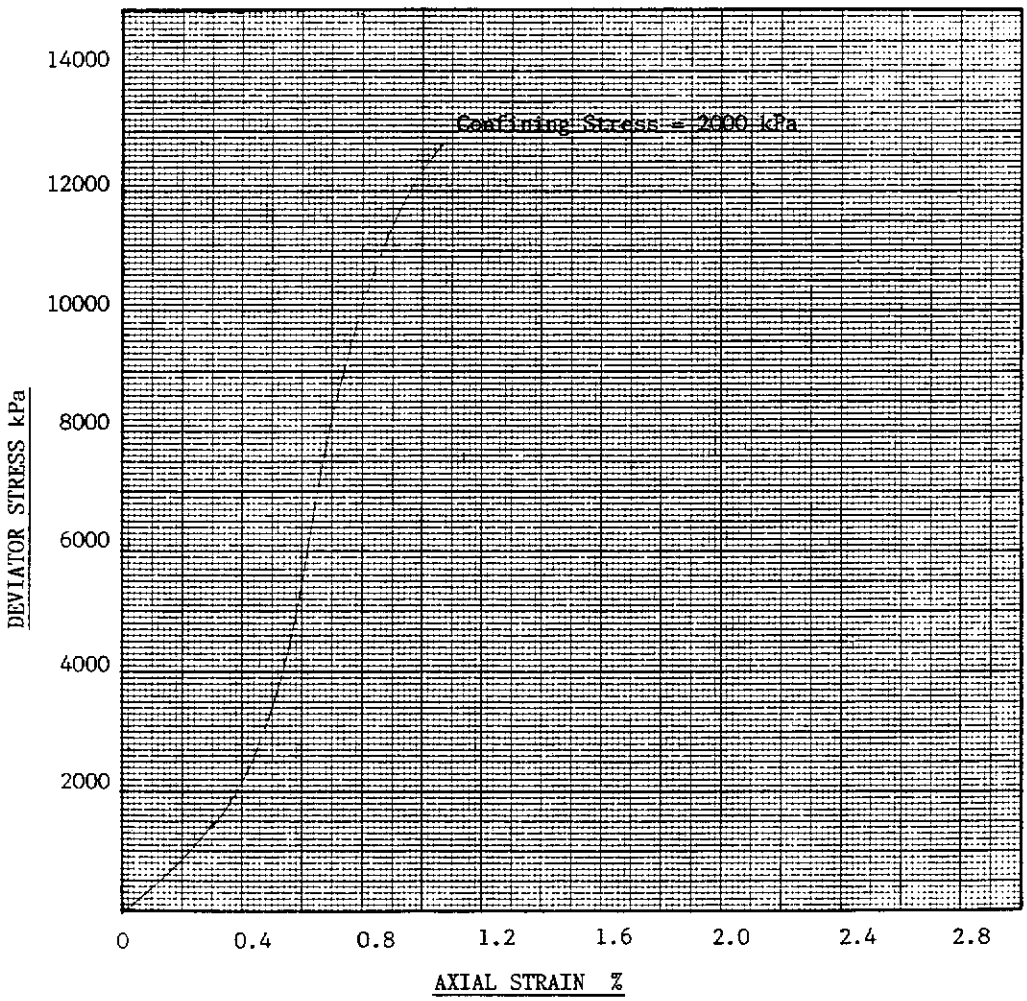

TESTED BY: KM CHECKED BY: DW DATE: 19/11/90

*Denotes use of Rock Colour Chart

CLIENT: COLLIE SCHOOL OF MINES

PROJECT: 1 NORTH WD6

SHEET No.: 44 **OF:** 69

JOB No.: S5937

DATE TESTED: 14/11/90

SAMPLE IDENTIFICATION: Bore Hole No. D212/13 AS - WS I/B

Depth in Metres 71.76 - 71.91

PORE PRESSURE/AXIAL STRAIN SUMMARY

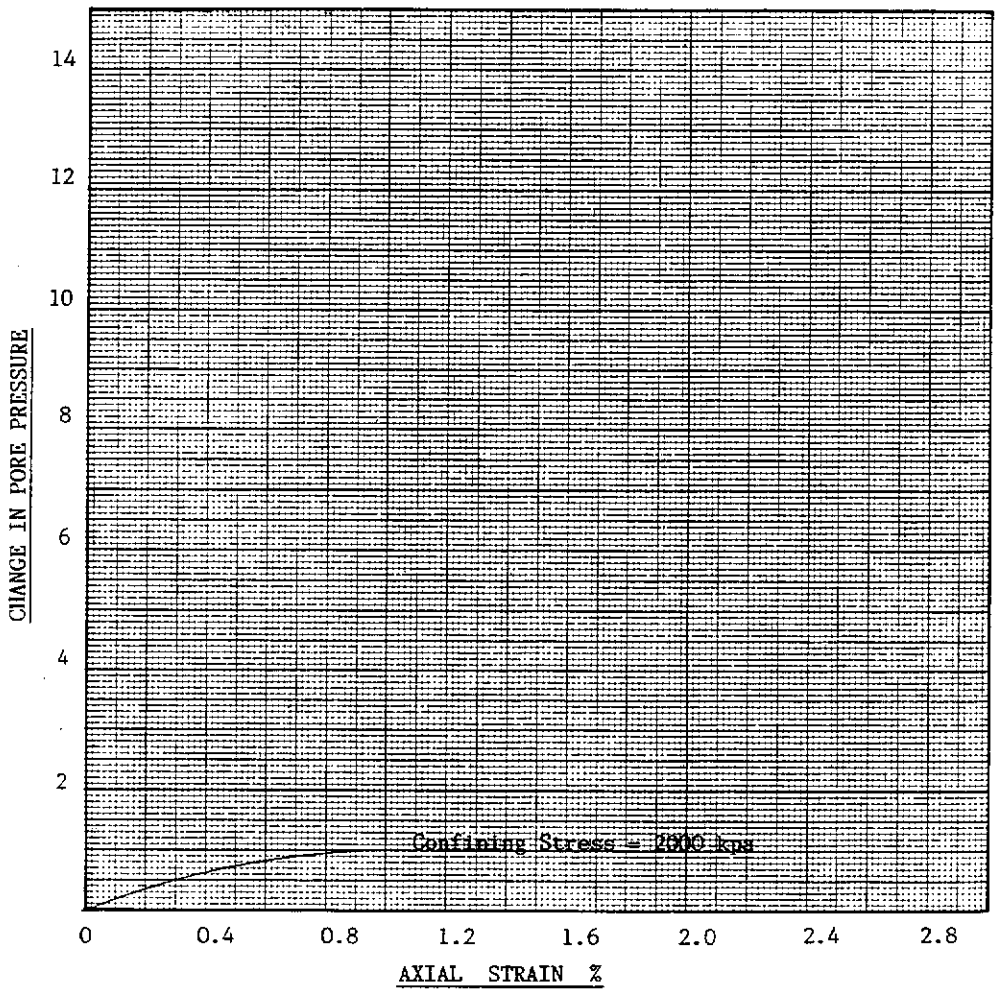

TESTED BY: KM CHECKED BY: DW DATE: 19/11/90

* Denotes use of Rock Colour Chart

CLIENT: COLLIE SCHOOL OF MINES

PROJECT: 1 NORTH WD6

SHEET No.: 45 **OF:** 69

JOB No.: S5937

DATE TESTED: 14/11/90

PHOTOGRAPHIC SUMMARY

SAMPLE IDENTIFICATION:

Bore Hole No: D212/13 AS - WS I/B

Depth in Metres: 71.76 - 71.91

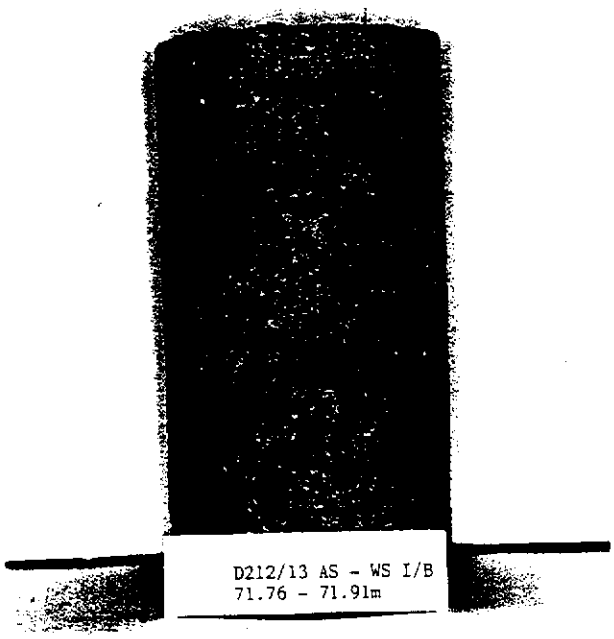

TESTED BY: KM CHECKED BY: DW DATE: 19/11/90

* Denotes use of Rock Colour Chart

CLIENT: COLLIE SCHOOL OF MINES

PROJECT: 1 NORTH WD6

SHEET No.: 46 OF: 69

JOB No.: S5937

DATE TESTED: 14/11/90

TRIAXIAL COMPRESSION TEST SUMMARY

VISUAL CLASSIFICATION (A.S.1726)

SAMPLE IDENTIFICATION/DEPTH	DESCRIPTION	SYMBOL
D212/12 71.48 - 71.65m d212/13 71.76 - 71.91m	MEDIUM - VERY COARSE SANDSTONE	

TEST PARAMETER SUMMARY

CONFINING STRESS (σ_3) kPa	1000	2000	-
POREWATER PRESSURE (U) kPa	4	1	-
EFFECTIVE CONFINING STRESS(σ_3-U)	996	1999	
DEVIATOR STRESS (σ_1-σ_3) kPa	10400	12781	-
SHEAR STRESS $\frac{(\sigma_1 - \sigma_3)}{2}$ kPa	5200	6390.5	-
INTERNAL FRICTION (ϕ) Degrees	-		
YOUNG'S/SECANT MODULUS (kPa)	-		
COHESION (c) (kPa)	-		

COMMENTS The Mohr Circle Plot was derived from two single stage tests carried out on the samples identified above.

MOHR'S CIRCLES

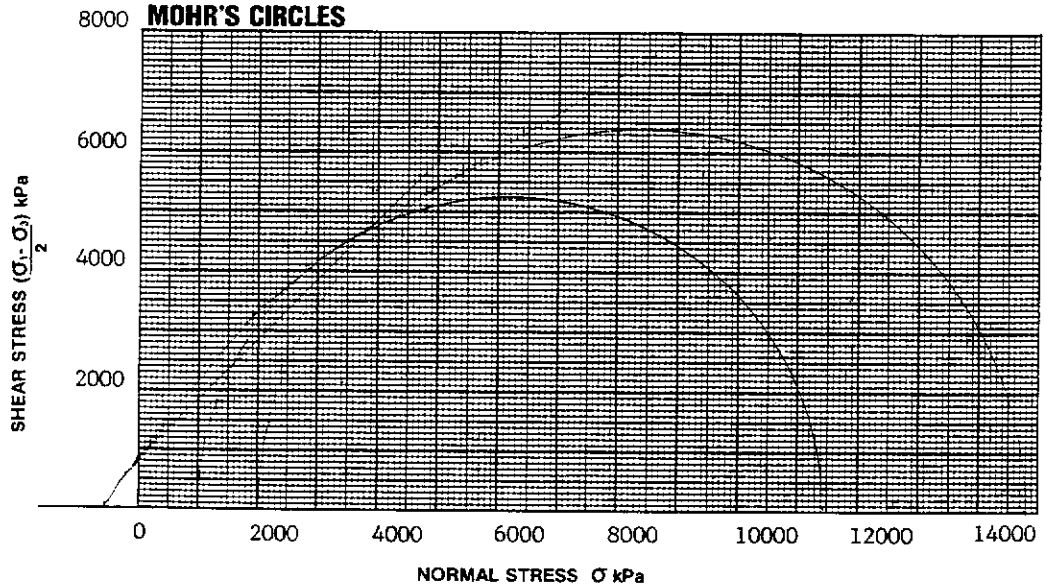

TESTED BY: KM CHECKED BY: DW DATE: 19/11/90

* Denotes use of Rock Colour Chart

SRC 85 9

CLIENT: COLLIE SCHOOL OF MINES

PROJECT: 1 NORTH WD6

SHEET No.: 47 **OF:** 69

JOB No.: S5937

DATE TESTED: 16/11/90

ELASTIC MODULI OF INTACT ROCK CORE SPECIMENS IN UNIAXIAL COMPRESSION SUMMARY

Tested in accordance with ASTM D 3148 - 80.

SAMPLE IDENTIFICATION:

Bore Hole No:	D213/14 WS ROOF
Depth in Metres:	89.46 - 89.64

PHYSICAL DESCRIPTION:

Name of Rock:	LAMINATED FINE SANDSTONE/ CARBONACEOUS SILTSTONE

SPECIMEN DATA:

Height:	110.2	mm
Diameter:	60.5	mm
Wet Mass:	658.7	g
Wet Density:	2.08	t/m^3
Dry Density:	1.76	t/m^3
Moisture Content:	18.2	%
DEFORMATION RATE:	0.2	mm / minute
UNCONFINED COMPRESSIVE STRENGTH:	1560	kPa

REMARKS: Axial strain was determined using the change in distance between the platens.

TESTED BY: KM CHECKED BY: DW DATE: 19/11/90

* Denotes use of Rock Colour Chart

CLIENT: COLLIE SCHOOL OF MINES

PROJECT: 1 NORTH WD6

SHEET No.: 48 **OF:** 69

JOB No.: S5937

DATE TESTED: 16/11/90

SAMPLE IDENTIFICATION: Bore Hole No. D213/14 WS ROOF

Depth in Metres 89.46 - 89.64

STRESS VERSUS AXIAL & DIAMETRIC STRAIN SUMMARY

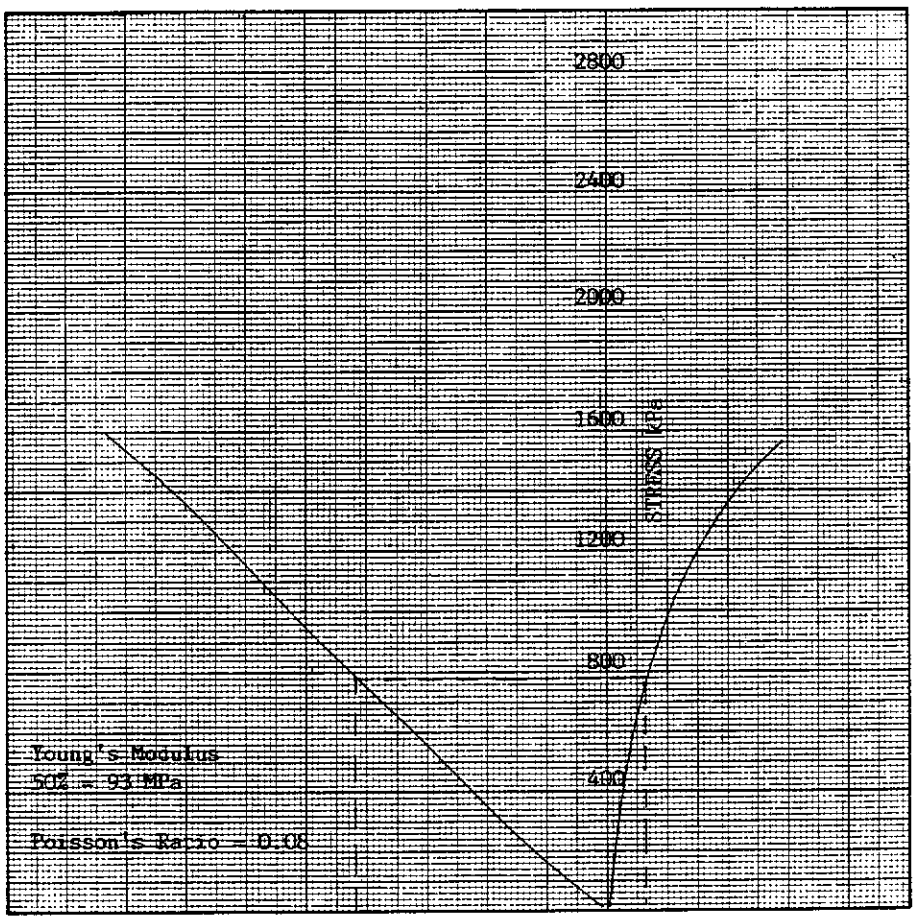

TESTED BY: KM CHECKED BY: DW DATE: 19/11/90

* Denotes use of Rock Colour Chart

CLIENT: COLLIE SCHOOL OF MINES

PROJECT: 1 NORTH WD6

SHEET No.: 49 **OF:** 69

JOB No.: S5937

DATE TESTED: 16/11/90

PHOTOGRAPHIC SUMMARY

SAMPLE IDENTIFICATION:

Bore Hole No: D213/14 WS ROOF

Depth in Metres: 89.46 - 89.64

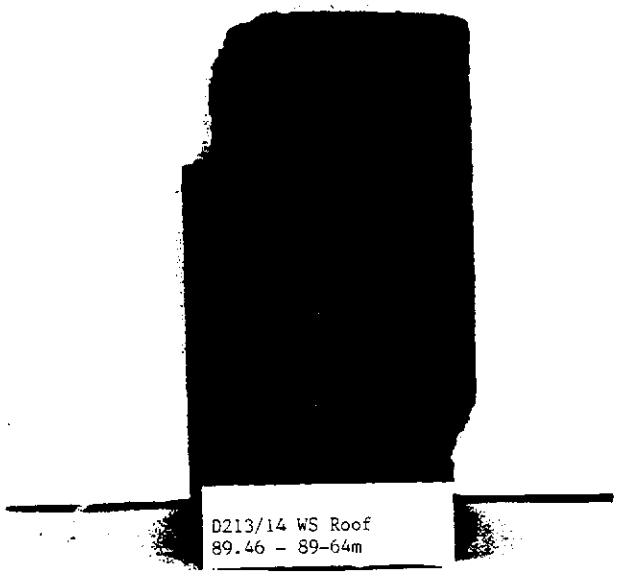

D213/14 WS Roof
89.46 - 89-64m

TESTED BY: KM CHECKED BY: DW DATE: 19/11/90

* Denotes use of Rock Colour Chart

CLIENT: COLLIE SCHOOL OF MINES **SHEET No.:** 50 **OF:** 69

PROJECT: 1 NORTH WD6 **JOB No.:** S5937

DATE TESTED: 9/11/90

DETERMINATION OF THE INDIRECT TENSILE STRENGTH BY THE BRAZIL TEST

Tested in accordance with the International Society for Rock Mechanics, Rock Characterisation Testing and Monitoring - 1981

SAMPLE IDENTIFICATION

Bore Hole No: D213/15 WS ROOF

Depth in Metres: 89.46 - 89.64

PHYSICAL DESCRIPTION

Name of Rock: LAMINATED FINE SANDSTONE/CARBONACEOUS SILTSTONE

SPECIMEN DATA

Thickness:	31.0	mm
Diameter:	60.3	mm
Wet Density:	2.10	t/m^3
Dry Density:	1.81	t/m^3
Moisture Content:	16.0	%
DEFORMATION RATE:	0.2	mm/minute

RESULTS

SPECIMEN No	1	2	3	4
TENSILE STRENGTH (MPa)	0.34	0.33	0.26	-

AVERAGE TENSILE STRENGTH: 0.31 MPa

REMARKS: NIL

TESTED BY: KM CHECKED BY: DW DATE: 12/11/90

* Denotes use of Rock Colour Chart

CLIENT: COLLIE SCHOOL OF MINES

PROJECT: 1 NORTH WD6

SHEET No.: 51 **OF:** 69

JOB No.: S5937

DATE TESTED: 9/11/90

PHOTOGRAPHIC SUMMARY

SAMPLE IDENTIFICATION:

Bore Hole No.	D213/5 WS ROOF
Depth in Metres:	89.46 - 89.64

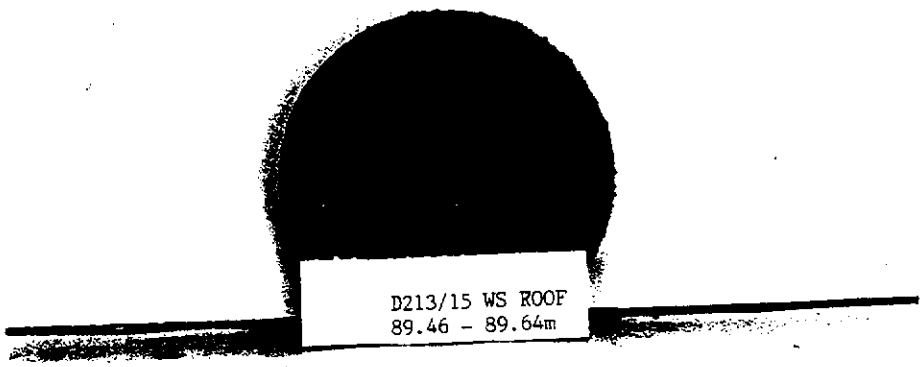

TESTED BY: KM CHECKED BY: DW DATE: 12/11/90

* Denotes use of Rock Colour Chart

CLIENT: COLLIE SCHOOL OF MINES **SHEET No.:** 52 **OF:** 69

PROJECT: 1 NORTH WD6 **JOB No.:** S5937

DATE TESTED: 16/11/90

ELASTIC MODULI OF INTACT ROCK CORE SPECIMENS IN UNIAXIAL COMPRESSION SUMMARY

Tested in accordance with ASTM D 3148 - 80.

SAMPLE IDENTIFICATION:

Bore Hole No:	D213/16 WYV. SEAM	
Depth in Metres:	91.11 - 91.30	

PHYSICAL DESCRIPTION:

Name of Rock:	COAL	

SPECIMEN DATA:

Height:	120.0	mm
Diameter:	60.8	mm
Wet Mass:	451.9	g
Wet Density:	1.30	t/m^3
Dry Density:	1.01	t/m^3
Moisture Content:	28.8	%
DEFORMATION RATE:	0.2	mm / minute
UNCONFINED COMPRESSIVE STRENGTH:	10130	kPa

REMARKS: Axial strain was determined using the change in distance between the platens.

TESTED BY: KM CHECKED BY: DW DATE: 19/11/90

* Denotes use of Rock Colour Chart

CLIENT: COLLIE SCHOOL OF MINES

PROJECT: 1 NORTH WD6

SHEET No.: 53 **OF:** 69

JOB No.: S5937

DATE TESTED: 16/11/90

SAMPLE IDENTIFICATION: Bore Hole No. D213/16 WYV. SEAM

Depth in Metres 91.11 - 91.30

STRESS VERSUS AXIAL & DIAMETRIC STRAIN SUMMARY

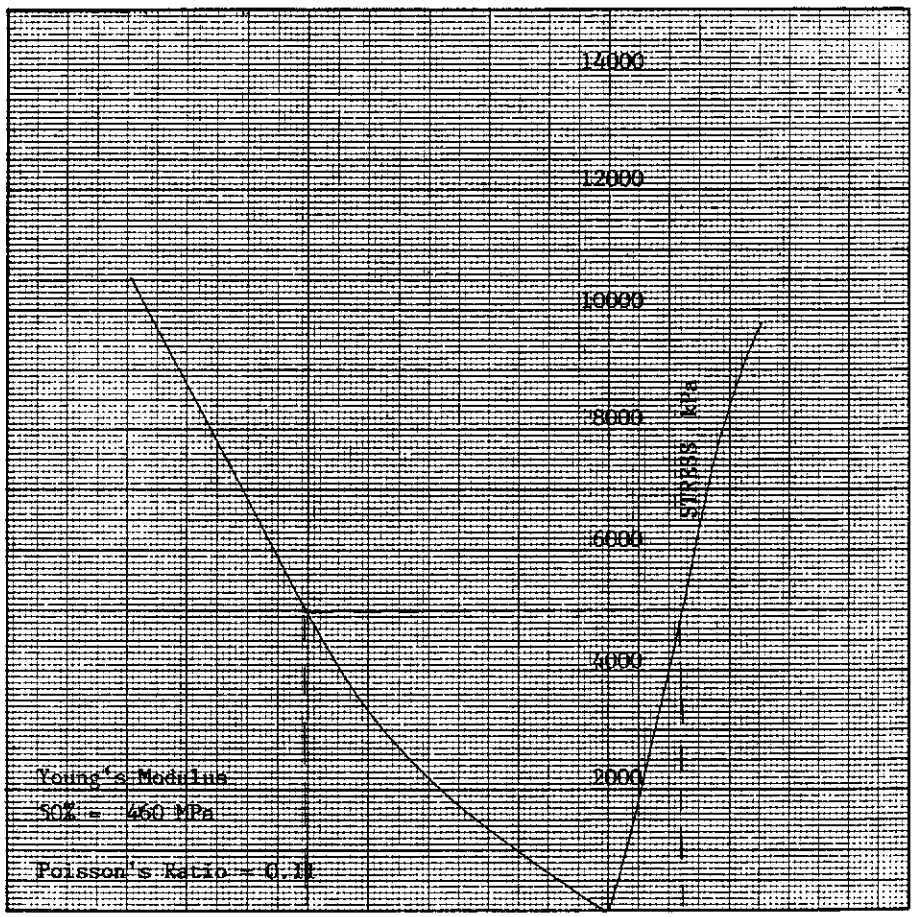

TESTED BY: KM CHECKED BY: DW DATE: 19/11/90

* Denotes use of Rock Colour Chart

CLIENT: COLLIE SCHOOL OF MINES

PROJECT: 1 NORTH WD6

SHEET No.: 54 **OF:** 69

JOB No.: S5937

DATE TESTED: 16/11/90

PHOTOGRAPHIC SUMMARY

SAMPLE IDENTIFICATION:

Bore Hole No: D213/16 WYV. SEAM

Depth in Metres: 91.11 - 91.30

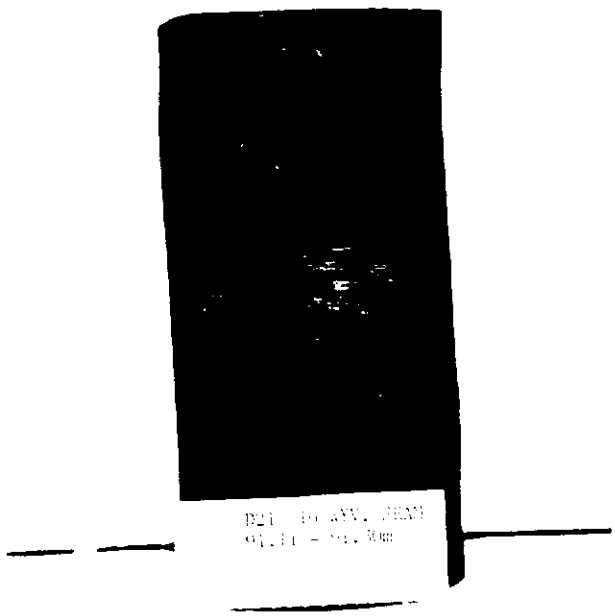

TESTED BY: KM **CHECKED BY:** DW **DATE:** 19/11/90

* Denotes use of Rock Colour Chart

CLIENT: COLLIE SCHOOL OF MINES **SHEET No.:** 55 **OF:** 69

PROJECT: 1 NORTH WD6 **JOB No.:** S5937

DATE TESTED: 9/11/90

DETERMINATION OF THE INDIRECT TENSILE STRENGTH BY THE BRAZIL TEST

Tested in accordance with the International Society for Rock Mechanics, Rock Characterisation Testing and Monitoring - 1981

SAMPLE IDENTIFICATION

Bore Hole No: D213/17 WS FLOOR

Depth in Metres: 94.15 - 94.30

PHYSICAL DESCRIPTION

Name of Rock: LAMINATED FINE SANDSTONE/CARBONEOUS SILTSTONE

SPECIMEN DATA

Thickness:	30.5	mm
Diameter:	60.8	mm
Wet Density:	1.94	t/m^3
Dry Density:	1.68	t/m^3
Moisture Content:	15.4	%
DEFORMATION RATE:	0.2	mm/minute

RESULTS

SPECIMEN No	1	2	3	4
TENSILE STRENGTH (MPa)	0.72	0.89	1.08	0.96

AVERAGE TENSILE STRENGTH: 0.91 MPa

REMARKS: NIL

TESTED BY: KM CHECKED BY: DW DATE: 12/11/90

* Denotes use of Rock Colour Chart

CLIENT: COLLIE SCHOOL OF MINES

PROJECT: 1 NORTH WD6

SHEET No.: 56 **OF:** 69

JOB No.: S5937

DATE TESTED: 9/11/90

PHOTOGRAPHIC SUMMARY

SAMPLE IDENTIFICATION:

Bore Hole No.	D213/17 WS FLOOR
Depth in Metres:	94.15 - 94.30

TESTED BY: KM CHECKED BY: DW DATE: 12/11/90

* Denotes use of Rock Colour Chart

CLIENT: COLLIE SCHOOL OF MINES

PROJECT: 1 NORTH WD6

SHEET No.: 57 **OF:** 69

JOB No.: S5937

DATE TESTED: 16/11/90

ELASTIC MODULI OF INTACT ROCK CORE SPECIMENS IN UNIAXIAL COMPRESSION SUMMARY

Tested in accordance with ASTM D 3148 - 80.

SAMPLE IDENTIFICATION:

Bore Hole No:	D213/18 WS FLOOR
Depth in Metres:	94.30 - 94.46

PHYSICAL DESCRIPTION:

Name of Rock:	LAMINATED FINE SANDSTONE/ CARBONACEOUS SILTSTONE

SPECIMEN DATA:

Height:	113.5	mm
Diameter:	60.5	mm
Wet Mass:	680.2	g
Wet Density:	2.08	t/m^3
Dry Density:	1.84	t/m^3
Moisture Content:	13.5	%
DEFORMATION RATE:	0.2	mm / minute
UNCONFINED COMPRESSIVE STRENGTH:	1460	kPa

REMARKS: Axial strain was determined using the change in distance between the platens.

TESTED BY: KM CHECKED BY: DW DATE: 19/11/90

*Denotes use of Rock Colour Chart

CLIENT: COLLIE SCHOOL OF MINES

PROJECT: 1 NORTH WD6

SHEET No.: 58 **OF:** 69

JOB No.: S5937

DATE TESTED: 16/11/90

SAMPLE IDENTIFICATION: Bore Hole No. D213/18 WS FLOOR

Depth in Metres 94.30 - 94.46

STRESS VERSUS AXIAL & DIAMETRIC STRAIN SUMMARY

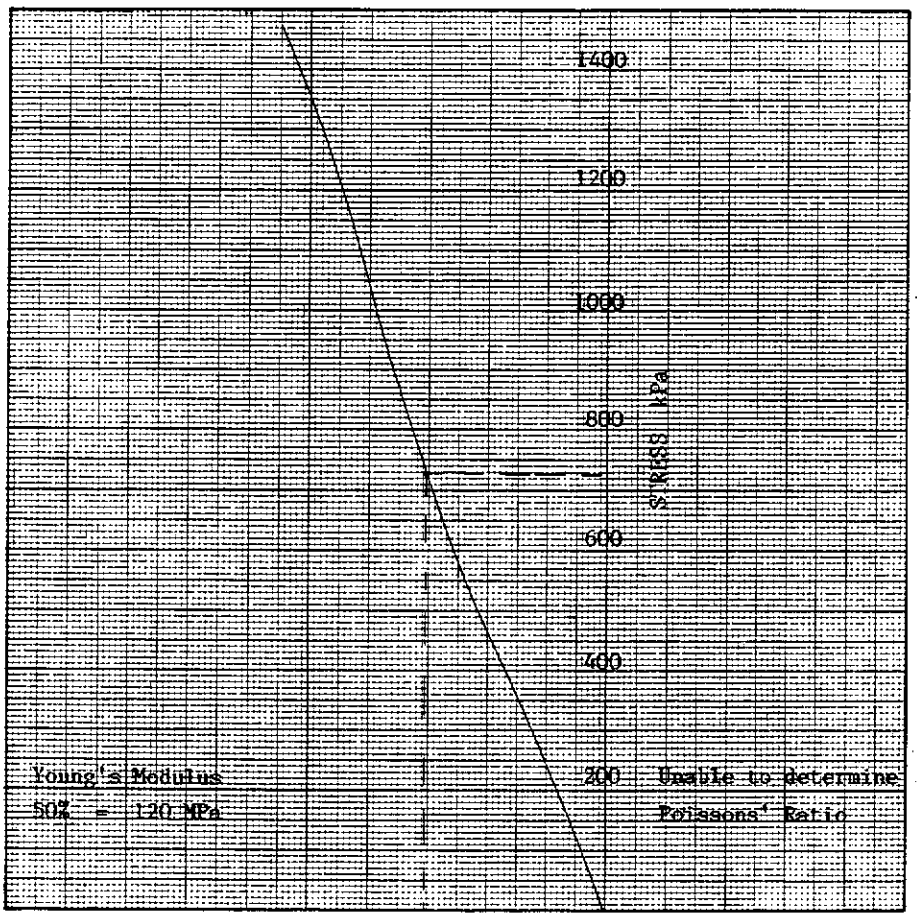

TESTED BY: KM CHECKED BY: DW DATE: 19/11/90

* Denotes use of Rock Colour Chart

CLIENT: COLLIE SCHOOL OF MINES

PROJECT: 1 NORTH WD6

SHEET No.: 59 **OF:** 69

JOB No.: S5937

DATE TESTED: 16/11/90

PHOTOGRAPHIC SUMMARY

SAMPLE IDENTIFICATION:

Bore Hole No: D213/1S WS FLOOR

Depth in Metres: 94.30 - 94.46

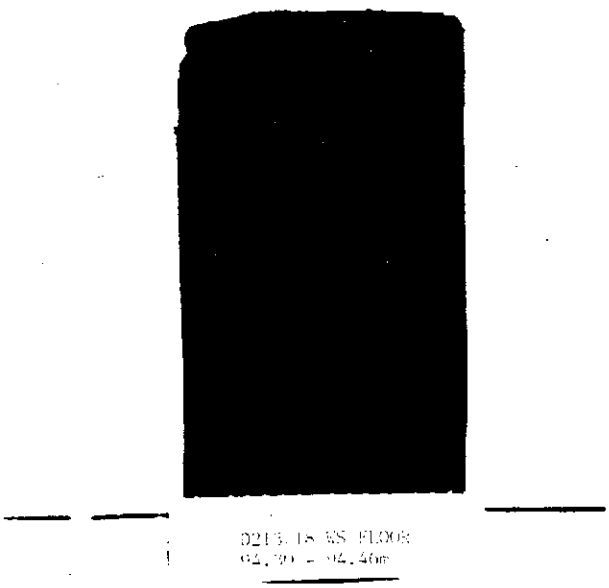

D213/1S WS FLOOR
94.30 - 94.46m

TESTED BY: KM CHECKED BY: DW DATE: 19/11/90

* Denotes use of Rock Colour Chart

CLIENT: COLLIE SCHOOL OF MINES **SHEET No.:** 60 **OF:** 69

PROJECT: 1 NORTH WD6 **JOB No.:** S5937

DATE TESTED: 9/11/90

DETERMINATION OF THE INDIRECT TENSILE STRENGTH BY THE BRAZIL TEST

Tested in accordance with the International Society for Rock Mechanics, Rock Characterisation Testing and Monitoring - 1981

SAMPLE IDENTIFICATION

Bore Hole No: D213/19 BELOW WS FLOOR

Depth in Metres: 94.62 - 94.79

PHYSICAL DESCRIPTION

Name of Rock: FINE-COARSE SANDSTONE

SPECIMEN DATA

Thickness:	28.5	mm
Diameter:	60.4	mm
Wet Density:	2.04	t/m^3
Dry Density:	1.74	t/m^3
Moisture Content:	17.1	%
DEFORMATION RATE:	0.2	mm/minute

RESULTS

SPECIMEN No	1	2	3	4
TENSILE STRENGTH (MPa)	0.26	0.15	0.40	0.25

AVERAGE TENSILE STRENGTH: 0.26 MPa

REMARKS: NIL

TESTED BY: KM CHECKED BY: DW DATE: 12/11/90

* Denotes use of Rock Colour Chart

CLIENT: COLLIE SCHOOL OF MINES

PROJECT: 1 NORTH WD6

SHEET No.: 61 **OF:** 69

JOB No.: S5937

DATE TESTED: 9/11/90

PHOTOGRAPHIC SUMMARY

SAMPLE IDENTIFICATION:

Bore Hole No. D213/19 BELOW WS FLOOR

Depth in Metres: 94.62 - 94.79

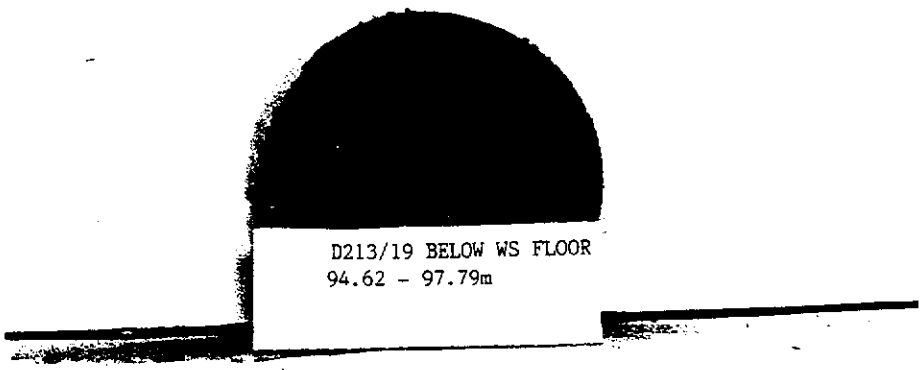

TESTED BY: KM CHECKED BY: DW DATE: 12/11/90

* Denotes use of Rock Colour Chart

CLIENT: COLLIE SCHOOL OF MINES

PROJECT: 1 NORTH WD6

SHEET No.: 62 **OF:** 69

JOB No.: S5937

DATE TESTED: 16/11/90

ELASTIC MODULI OF INTACT ROCK CORE SPECIMENS IN UNIAXIAL COMPRESSION SUMMARY

Tested in accordance with ASTM D 3148 - 80.

SAMPLE IDENTIFICATION:

Bore Hole No:	D213/20 BELOW WS FLOOR
Depth in Metres:	94.79 - 94.99

PHYSICAL DESCRIPTION:

Name of Rock:	FINE - COARSE SANDSTONE

SPECIMEN DATA:

Height:	103.8	mm
Diameter:	60.2	mm
Wet Mass:	617.2	g
Wet Density:	2.09	t/m^3
Dry Density:	1.81	t/m^3
Moisture Content:	15.4	%
DEFORMATION RATE:	0.2	mm / minute
UNCONFINED COMPRESSIVE STRENGTH:	1650	kPa

REMARKS: Axial strain was determined using the change in distance between the platens.

TESTED BY: KM CHECKED BY: DW DATE: 19/11/90

* Denotes use of Rock Colour Chart

CLIENT: COLLIE SCHOOL OF MINES

PROJECT: 1 NORTH WD6

SHEET No.: 63 **OF:** 69

JOB No.: S5937

DATE TESTED: 16/11/90

SAMPLE IDENTIFICATION: Bore Hole No. D213/20 BELOW WS FLOOR

Depth in Metres 94.79 - 94.99

STRESS VERSUS AXIAL & DIAMETRIC STRAIN SUMMARY

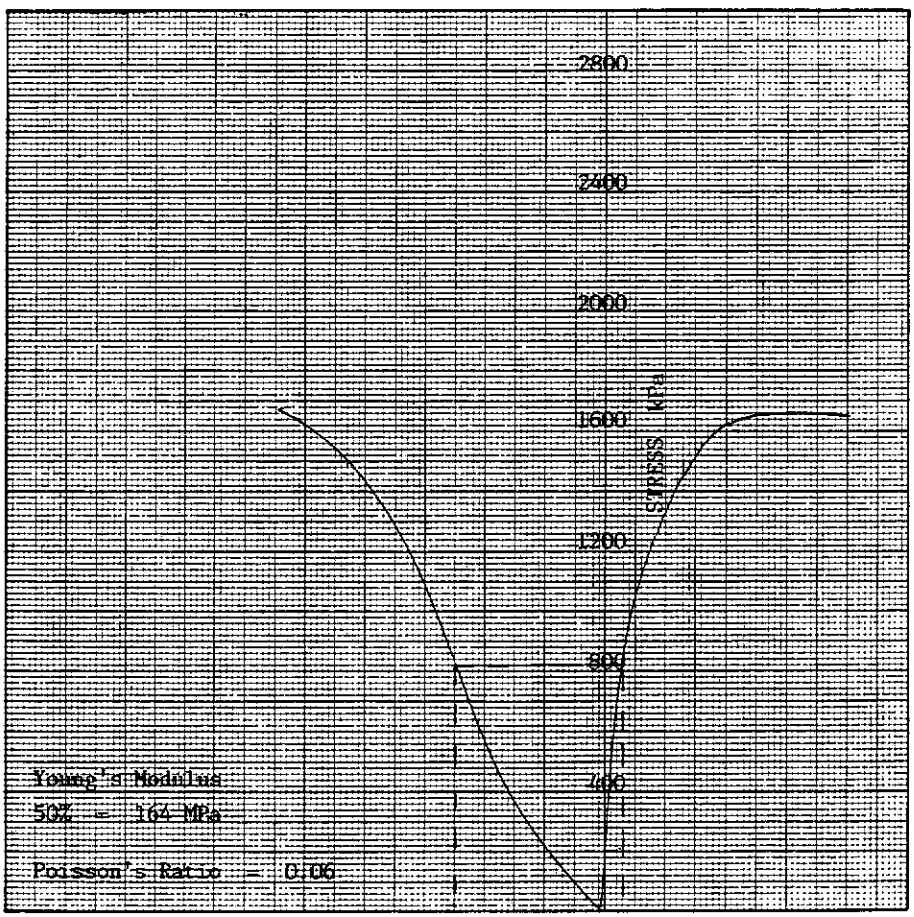

TESTED BY: KM CHECKED BY: DW DATE: 19/11/90

* Denotes use of Rock Colour Chart

CLIENT: COLLIE SCHOOL OF MINES

PROJECT: 1 NORTH WD6

SHEET No.: 64 **OF:** 69

JOB No.: S5937

DATE TESTED: 16/11/90

PHOTOGRAPHIC SUMMARY

SAMPLE IDENTIFICATION:

Bore Hole No: D213/20 BELOW WS FLOOR

Depth in Metres: 94.79 - 94.99

D213/20 BELOW WS FLOOR
94.79 - 94.99m

TESTED BY: KM CHECKED BY: DW DATE: 19/11/90

*Denotes use of Rock Colour Chart

CLIENT: COLLIE SCHOOL OF MINES **SHEET No.:** 65 **OF:** 69

PROJECT: 1 NORTH WD6 **JOB No.:** S5937

DATE TESTED: 14/11/90

TRIAXIAL COMPRESSIVE STRENGTH OF UNDRAINED ROCK CORE SPECIMENS WITHOUT PORE PRESSURE MEASUREMENTS SUMMARY

Tested in accordance with ASTM D 2664 - 80.

SAMPLE IDENTIFICATION:

Bore Hole No :	D213/21 BELOW WS FLOOR
Depth in Metres :	95.07 - 95.25

PHYSICAL DESCRIPTION:

Name of Rock :	FINE - COARSE SANDSTONE

SPECIMEN DATA:

Height :	117.0	mm
Diameter :	60.5	mm
Wet Mass :	723.4	g
Wet Density :	2.15	t/m^3
Dry Density :	1.86	t/m^3
Moisture Content :	15.4	%

DEFORMATION RATE:	0.2	mm / minute

REMARKS: NIL

NOTE: Deviation from standard - Pore Pressure measurements were recorded as requested by client. Refer to Sheet No. 68 of 69 .

TESTED BY: KM CHECKED BY: DW DATE: 19/11/90

* Denotes use of Rock Colour Chart

CLIENT: COLLIE SCHOOL OF MINES SHEET No.: 66 OF: 69

PROJECT: 1 NORTH WD6 JOB No.: S5937

DATE TESTED: 14/11/90

TRIAXIAL COMPRESSION TEST SUMMARY

VISUAL CLASSIFICATION (A.S.1726)

SAMPLE IDENTIFICATION/DEPTH	DESCRIPTION	SYMBOL
D213/21 BELOW WS FLOOR 95.07 - 95.25	-	-

TEST PARAMETER SUMMARY

CONFINING STRESS (σ_3) kPa	2000		
POREWATER PRESSURE (U) kPa	34		
EFFECTIVE CONFINING STRESS(σ_3-U)	1966		
DEVIATOR STRESS (σ_1-σ_3) kPa	7827		
SHEAR STRESS $\frac{(\sigma_1 - \sigma_3)}{2}$ kPa	3913.5		
INTERNAL FRICTION (ϕ) Degrees	-		
YOUNG'S/SECANT MODULUS (kPa)	-		
COHESION (c) (kPa)	-		

COMMENTS

MOHR'S CIRCLES

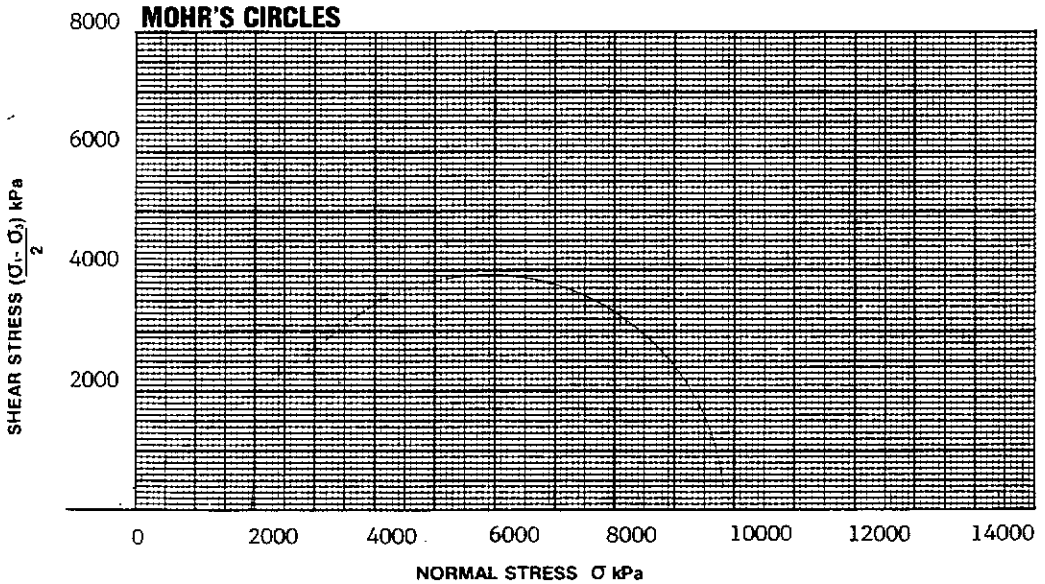

TESTED BY: KM CHECKED BY: DW DATE: 19/11/90

* Denotes use of Rock Colour Chart

CLIENT: COLLIE SCHOOL OF MINES

PROJECT: 1 NORTH WD6

SHEET No.: 67 **OF:** 69

JOB No.: S5937

DATE TESTED: 14/11/90

SAMPLE IDENTIFICATION: Bore Hole No. D213/21 BELOW WS FLOOR

Depth in Metres 95.07 - 95.25

DEVIATOR STRESS/AXIAL STRAIN SUMMARY

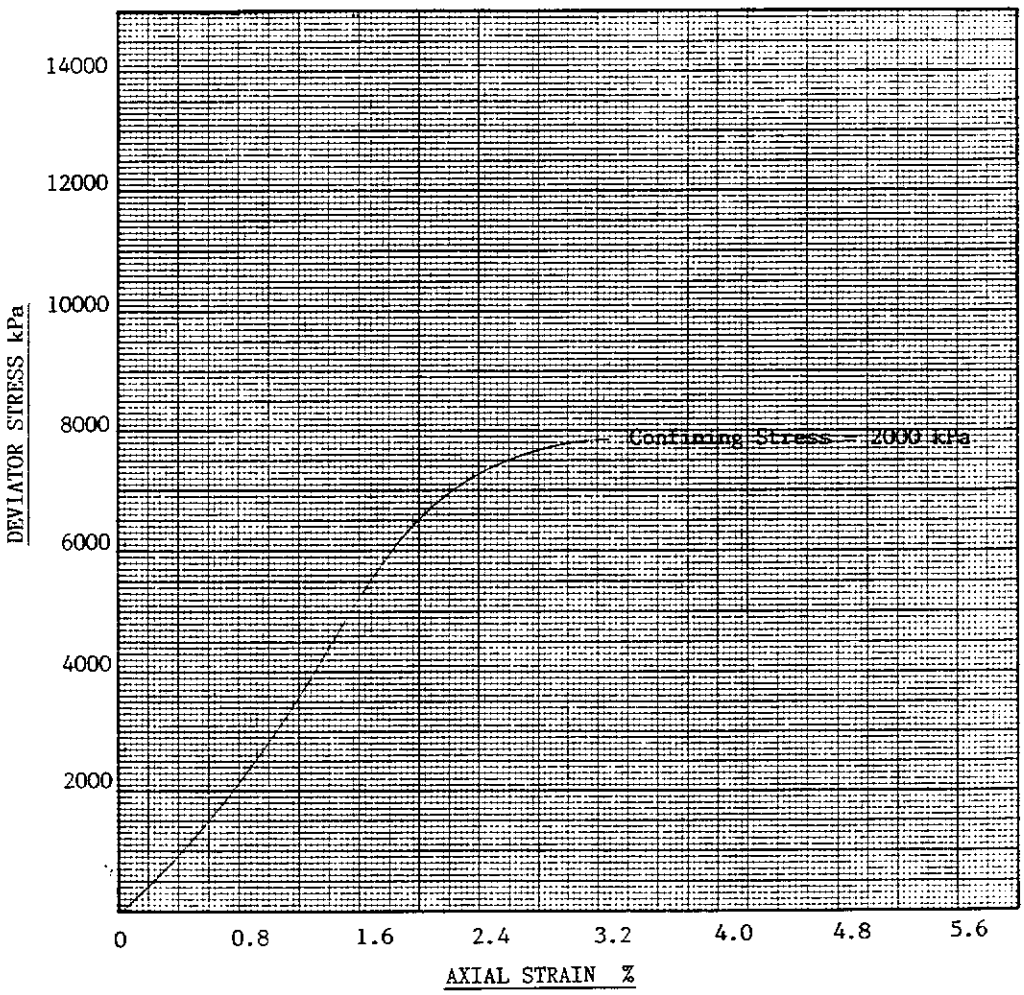

TESTED BY: KM CHECKED BY: DW DATE: 19/11/90

* Denotes use of Rock Colour Chart

CLIENT: COLLIE SCHOOL OF MINES

PROJECT: 1 NORTH WD6

SHEET No.: 68 **OF:** 69

JOB No.: S5937

DATE TESTED: 14/11/90

SAMPLE IDENTIFICATION: Bore Hole No. D213/21 BELOW WS FLOOR

Depth in Metres 95.07 - 95.25

PORE PRESSURE/AXIAL SUMMARY

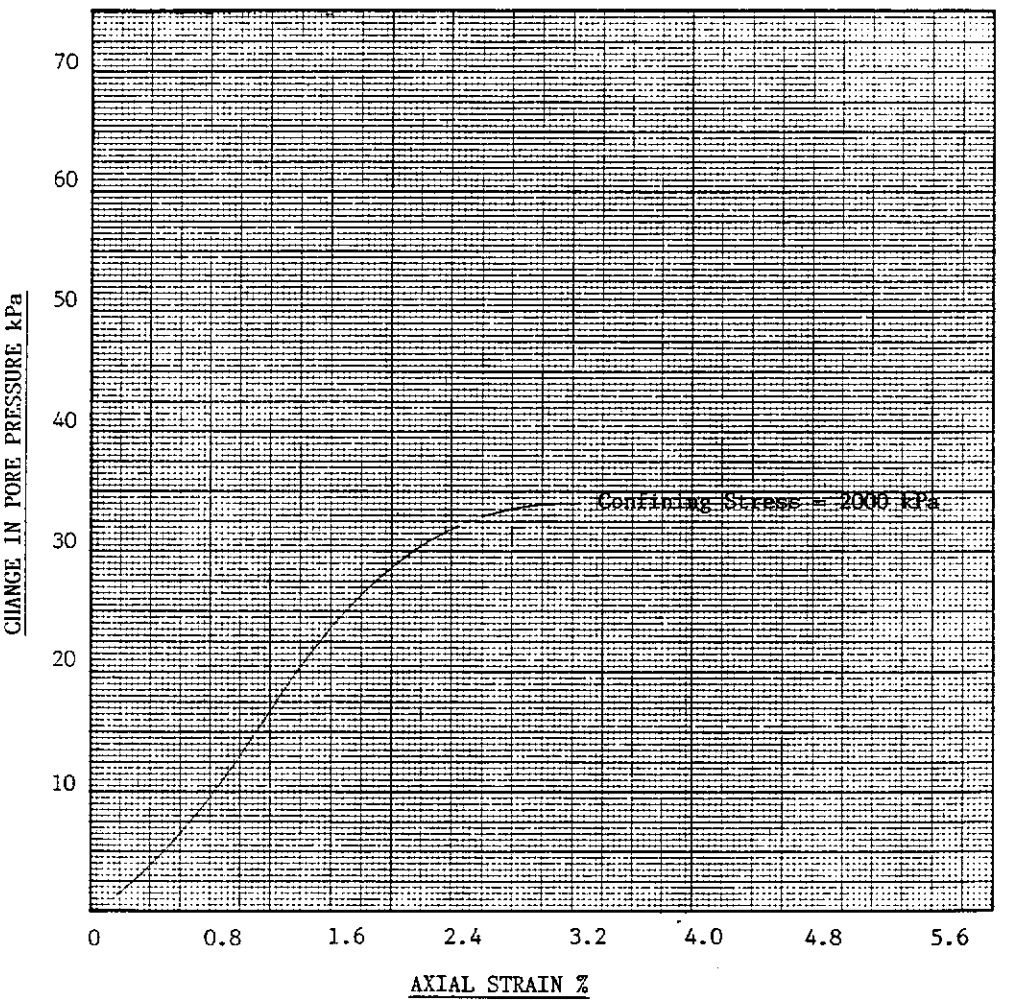

TESTED BY: KM CHECKED BY: DW DATE: 19/11/90

* Denotes use of Rock Colour Chart

CLIENT: COLLIE SCHOOL OF MINES

PROJECT: 1 NORTH WD6

SHEET No.: 69 **OF:** 69

JOB No.: S5937

DATE TESTED: 14/11/90

PHOTOGRAPHIC SUMMARY

SAMPLE IDENTIFICATION:

Bore Hole No: D213/21 BELOW WS FLOOR

Depth in Metres: 95.07 - 95.25

D213/21 BELOW WS FLOOR
95.07 - 95.25m

TESTED BY: KM CHECKED BY: DW DATE: 19/11/90

* Denotes use of Rock Colour Chart

APPENDIX IV

PHASE II CENTRIFUGE-MODELLING DETAILS

In order to stream line the main body of the report, the details of model construction and results gained from each model in the phase II tests have been provided in the Appendix. Some duplication of information is therefore required between the main text and the Appendix to assist with the explanation of the full sequence of events in the Appendices. Furthermore, as the data files created by closely spaced logging of strain gauges and load cells during testing, and frame grabing of video post-testing are too voluminous to include in hard copy in this report, a copy of the raw data has been provided on computer disk. This detailed information is available at the Engineering faculty, Curtin University of Technology, Perth, Western Australia.

IV.1 CENTRIFUGE MODEL PS01

Model type - 2 dimensional "Plane Strain", in situ material.

Scaling factors - Given that the model dimensions which fitted comfortably into the strong-box was 1/200 of the prototype, the required operating force was 200 g, which represents the maximum accelerated gravity achievable by the Accutronic centrifuge. A true scaling of time (as given in Equation 4.2(12) in the main body of the report) was not attempted during this model due to concerns of the UWA's centrifuge manager for a large mass operating at 200g for prolonged periods.

A summary of the general make-up of the model is listed in the text table provided below and illustrated in Figures IV.1a & b :

	Mining Parameters	Model Dimensions	Prototype Dimensions
1.	Cover depth	295 mm	59 m
2.	Individual mining blocks	45 x 68 mm top caps (Representing 70% of the width of "one way lifting")	9 m wide x 13.6 m long

3.	Total extraction panel	270 x 201 mm	54 m wide x 40 m long slice of an infinitely long panel.
4.	Mining height	12.5 mm	2.5 m

The layout of the model stratigraphy is summarised below:

Model lithology	**Layer Thickness**	**Height to base of unit**	**Equivalent Height Above Prototype**
Sandstone aquifer	130 mm	0 mm	0 m
Coal aquitard	35 mm	130 mm	26 m
Sandstone aquifer	130 mm	165 mm	33 m
Surface		295 mm	59 m

Drop sequence - 5 minute spin-up; 30 sec delay after each piston was dropped; 2 min delay between rows; 5 min final spin after all pistons were lowered.

Data collection - Listed below:

1. Laser profiling - surface
2. Visual a) during test - CCD camera/video tape through window
   b) post-test - crack tracing
   - marker dots and line tracing.

   In order to measure subsidence throughout the model during testing, the face of the model was painted with black dots (typically 1-2 mm in diameter) by spraying gloss paint across a 0.6 mm thick tin plate drilled with 1.5 mm diameter holes on a 15 mm grid. The appearance of the model before testing is illustrated in Figure IV.1 a & b.

   Each black dot was "digitised" using the computer software package ACCUware which "grabs" specific images (e.g. dark spots of specific size) from individual video frames recorded by CCD camera during the test. Details of the ACCUware processing package and "frame grabbing" are given in Appendix IV.10. This approach was used for all future tests.
3. Strain gauges on aquitard.

In order to assess the influence of subsidence on the aquitard layer, strain gauges were fixed (by epoxy resin) to the top surface of the aquitard slab. The gauges used were an inexpensive wire in a paper carrier type - see Appendix IV.11. Other forms of gauges, such as etched foil on a polyamide or epoxy backing, were not considered necessary because the nature of testing was quick and destructive. There was no need to use the more precise, expensive gauges for long term "stability" of the gauges.

Positioning of the gauges on the aquitard blocks was assisted by carefully measuring and marking out the precise location of all gauges on the surface of the slab. This sped up the process and reduced the error in location of the gauges. In test PS01, only seven strain gauges were installed, which left some large gaps between strain gauges. (In the in situ material tests only one junction box, connecting the strain gauges to the computer operated recording unit, was available which could only take up to ten channels. In later tests, the number of both the terminals and junction boxes were increased to provide a more continuous representation of the strain across the full length of aquitard above the "extraction panel".)

In test PS01 the gauges were set up for a ± 2000 μ strain tolerance - see Appendix IV.11. The gauges in all other tests were configured to withstand a strain variance of ± 4000 μ strain. This higher strain output tolerance in latter tests allowed for wider ranges of measurement, though slightly less accurate.

Stooks - Yes

Mining direction - Left to Right

Comments - The rock fabric used in this test was selected as being representative of typical strata above extraction panels in the Collie Basin.

The prototype equivalent mining width per row is only 9 m which is atypical (it is normally 13 m for one-way lifting). The complete panel is sub-critical width (54/59 = 0.92); therefore the test could not develop full subsidence.

The model aquitard width of 35 mm represents the thickness of all coal and shales in the Alpha seam aquitard in the field. It was not clear at this stage whether these materials should be included in the model as being part of the aquitard. (No SUBSOL

tests had been received to this stage.) Nonetheless, it was decided that the thicker aquitard in the first test - provided it worked - would give useful information regarding bending and bridging characteristics of the coal in comparison to other tests with correctly scaled aquitard thicknesses. It was also not certain whether a thin plate of cannel coal (5-8 mm thick) could withstand rigorous handling during cutting, strain gauging, and placement in the box and laying another block on top.

Selection of suitable blocks for testing was very difficult. Firstly, the blocks had to be at least 200 x 200 x 650 mm to fit in the strong-box in one piece, but not too large to handle. There could be no jointing, and the shape of the block had to be regular in order to obtain the required cut block dimension in each direction.

Results - Subsidence development during each stage of the PS01 test is illustrated by Figure IV.2 a & b. Figure IV.2 a represents the sequence of subsidence events as captured by the CCD camera through the perspex window fixed to the strong-box as each piston is sequentially lowered. Each of the frames in Figure IV.2 a was created by the ACCUware software package which firstly captures individual video tape frames (when specified) and then converts captured picture frames from binary code to bitmap format for printing - see Appendix IV.10.

Figure IV.2 b represents the subsidence interpreted by the change in alignment of sub-horizontal rows of dots (painted on the model face) after each mining step. Also included in the Figure are crack developments and bed separations as noted through the perspex window during the test. The "control" frame represents the status of the model face prior to the first piston being dropped. The total subsidence frame represents the difference in dot/line positions between the control and the final piston drop. Subsidence is illustrated by heavy shading, bed separation is represented by striped shading. The frames given between the control and total subsidence frames represent the incremental subsidence between individual piston drops. For example the frame marked as 3rd row(2) represents the status of the face of the model after the third row has been dropped. The subscript (2) refers to the particular number of the frame grab within a sequence of frames, usually taken to illustrate the staged development of subsidence after certain pistons were lowered. This approach has been used in all centrifuge tests.

The major observations made during and after testing include:

- A definite sequence of caving has been identified. The caving sequences, given by the lines of fracture are represented in Figure IV.2 b and summarised by Figure IV.2 c. These figures illustrate:
  - > Two types of collapse - firstly, a vertical, "roof beam" type collapse which results in greater subsidence at the trailing edge of the panel, followed by a sequential cantilever, rotational type collapse. This "first collapse" effect has been observed in the field, with higher amounts of surface subsidence being surveyed toward the panel edge,
  - > Bed separation beneath the aquitard (Figures IV.1b and IV.3a & b), also interpreted from field data. The exact magnitude of this bed separation could not be measured whilst the test was being operated. However, it has been estimated from tracings taken after completion of the test that the bed separation is typically between 6 - 7 mm. This equates to a subsidence factor at the top of the goafed material of

    $$6.5/12 = 0.54,$$

    which is slightly less than field observations for surface subsidence (0.64). However, it does not compare with the expected limit of bed separation (to three times the mining height) as would be predicted with a bulking factor, for unconfined goaf material, of 1.34.
  - > An overall caving angle (at the trailing edge abutment) of 23° (Figure IV.3 a).
  - > A lower gradient, curved caving angle on the advancing edge for the first four "lifts" (Figure IV.2 c). This feature was somewhat different to previous tests in the pilot study. This curved line of caving could be explained by a lack of vertical pressure on the strata underlying the thick bridging aquitard when extraction widths are small. During the latter stages of testing, the angle of caving steepened and finally became sub-vertical (see Figure IV.3 b). The sub-vertical caving is not considered to represent prototype observations; it is thought to be a result of greater abutment loads generated when extraction widths are large. These superincumbent loads greatly exceed the shear strength of the sandstone (overhang) at the caving edge resulting in sub-vertical shear.

- Large scale caving (secondary caving) was observed only after five rows of pistons had been lowered. This equates to 54 m in the prototype, which represents the upper range interpreted from field observations. One possible reason why the PS01 model required a greater width of extraction before initiating secondary caving is that the thick spanning aquitard, initially reduced the load transfer to the basal sandstone and thereby reduced both the shear stresses and the propensity for caving.

- Quantitative details of subsurface subsidence could not be obtained using the ACCUware software due to the lack of contrast between the black painted dots and the grey colour of the insitu material, and inadequate lighting across the face of the model. (The ACCUware software was very sensitive to variable contrast across the screen, and although visual inspection of the video image during testing implied there was more than adequate lumination, it was not of sufficient standard for the frame grabbing and digitising package). The poor clarity of Figure IV.2 a is testimony to the lighting problem.

- Strain gauge data suggests that the time delays adopted for this model were sufficient to reach what appeared to be equilibrium before the next piston or row of pistons were dropped. Equilibrium was adjudged to have developed when the strain gauges, glued to the surface of the aquitards, gave reasonably steady readings (allowing for hysteresis). The results of strain gauging are summarised in Figure IV.4 and Table IV.1. The location of each gauge in relation to each row of mining elements (pistons) is depicted by both the background shading and diagrammatical section provided beneath the graph denoted by Figure IV.4.

- Strain measurements also suggest that the integrity of the aquitard remained intact until all pistons had been lowered - representing 54 m extraction. The maximum strain measured (1.6 mm/m) was compressive, and on the opposite side of the tensile crack which developed at the base of the aquitard once the caved overhang material sheared sub-vertically. It can therefore be inferred that the aquitard beam cracked after an unsupported span, represented by the bed separation illustrated in Figure IV.3 a, of 222 mm (44 m in the prototype), had developed.

- It is also interesting to note that the caved material had recompacted and re-knitted to form a cohesive mass during testing. Figure IV.5 illustrates the compact nature of the goaf.

Subsidence - No discernible surface subsidence was noted either during or after the test. Once the test model was dismantled, it appeared that any deflection of the thick aquitard layer and/or upper sandstone block had rebounded elastically under one gravity.

Aquitard cracking	-	Observed face cracks are listed below and illustrated in Figure IV.6:
Aquitard #1	-	crack No.1
Crack Position	-	5 mm to the left of the mid-point of the panel, on the lower side of the aquitard slab.
Crack Type	-	tensile, penetrating only the lower 2/3 of the aquitard (no strain gauge data available for this side - see Figure IV.4).
Timing of Cracking	-	after the sixth row of pistons were dropped (54 m in the prototype).
Interpreted Strain (at time of rupture)	-	Compressive strain - 1.1 mm/m

IV.2 CENTRIFUGE MODEL PS02

Model type - 2 dimensional "plane strain", in situ material.

Scaling factor - 1:200

Effective Mining Dimensions	**Model Dimensions**	**Prototype Dimensions**
1. Cover depth(H)	284 mm	57 m
Individual mining blocks	68 x 68 mm	13.6 m wide x 13.6 m long
Total excavation	402 x 201 mm	79.8 m wide x 40 m SLICE
Mining height	12.5 mm	2.5 m

The layout of the model stratigraphy is summarised below:

Model lithology Height	Layer Thickness	Height to base of unit	Equivalent AbovePrototype
Sandstone aquifer	146 mm	0 mm	0 m
Coal aquitard	8 mm	146 mm	29.2 m
Sandstone aquifer	130 mm	154 mm	30.8 m
Surface		284 mm	57.8 m

Drop sequence - As for PS01

Data collection - As for PS01, except 10 strain gauges were installed on top of the aquitard (discussed later).

Comments - The dimensions of each actuator were increased to 67 x 67 mm. This gave a more representative extraction (row) width of 13.4 m for one-way lifting in the prototype.

The effective panel width of 80.4 m equates to a W/H ratio of 1.4, which makes this test of "critical" width.

No problems were encountered with the thin (8 mm) aquitard layer. Handling was assisted using a flat wooden base so the aquitard could be clamped while moved. Cutting the slab had some problems initially; however, these were solved after several attempts. A 3mm spacer was put in the sawn cut and pressure applied to the free edge. Two operators were required.

Unlike the previous test models, the thickness of the PS02 aquitard block represents only the width of coal and cannel coal within the Alpha seam aquitard; the presence of shale and siltstone units have been ignored. The importance of restricting the aquitard thickness in the model to the thickness of coals was highlighted by initial results from the mathematical modelling which had become available immediately prior to construction of this test. Early SUBSOL investigations indicated that when the full aquitard thickness (including shales and silts) was included in modelling as one stiff layer, the resultant subsidence profiles were reduced significantly. This observation compares well with the results of the first insitu material test - PS01. The SUBSOL results showed that when the model aquitard thickness equated to the coal thickness only, the resultant subsidence profiles more closely matched field results.

This supports earlier assumptions that the non-coals are only passive members in the subsidence process, and the coal seams act as reinforcement within the overall mass and thereby tend to restrict full subsidence development. From this point onwards, the thickness of aquitard in all models approximated only the interpreted thicknesses of coal within the composite aquitards.

Finding the best block of sandstone which met the objectives of this test took several hours. The difficulty was to firstly find a physically manageable lump of rock of sufficient size in all dimensions to adequately fill the plane strain strong-box once it was trimmed to size. The second requirement was to have no obvious bedding planes, and yet not possess large, very coarse-grained particles of silica; the concern with the particle size was that at 200 g, a 5 mm grain of silica would correspond to a 1 m boulder, which would be unacceptable. The resultant block had a maximum particle size of 1 mm which still represents atypical size prototype sandstone grains at 200 g; however, the proportion of these particles was visually low within the overall mass of the block.

Thirdly, the block had to be of similar strength to the previous block, and of similar moisture content. It is obvious that the strength of the specific block is difficult to determine in underground mines. In order to obtain a reasonable idea of the material strength, a point load index tester was taken underground to test irregular lumps of material found adjacent to the blocks. To better assess the strength of the insitu material selected, UCS tests were performed at a NATA registered laboratory. The results of these tests are given in Appendix III.

Comparison of UCS tests on samples of the insitu material blocks for each test suggest that given the natural variation in test samples from each sandstone block, the compressive strengths were reasonably similar; the average UCS of each sandstone block was approximately 1.46 MPa. Importantly, though, it can be seen that even with careful selection processes, the intact strength of the material within the blocks can vary by more than 30%. The possible effects this could have on small-scale centrifuge models is obvious.

Results - Subsidence development during each stage of the PS02 test is illustrated by Figure IV.7 a & b. Figure IV.7 a represents the video frame as

captured from the CCD camera, and Figure IV.7b represents the interpreted subsidence (from dot tracings) between each mining step. The results are discussed in detail below.

- Both the photographical and strain gauging results demonstrate the significant effect of using material with no apparent bedding. During the test, no significant caving occurred until some time after all pistons were lowered - probably after the stooks began to "punch" into the sandstone. The first series of events was localised caving of the immediate roof across the base of the model. Large-scale collapse of the remainder of the block then followed within 30 seconds of the initial collapse. What appeared to be happening was that the flexural strength of the "massive" sandstone block was very high and allowed the sandstone to bridge across from stook to stook. After the model was dismantled, it was evident that the middle piston in the second row did not lower fully. This semi-raised piston could also have been contributing to the support of the overlying strata; however, it would not have significantly affected the flat caving angle (illustrated in Figures IV.8 and IV.9).

  The nature of the caving was totally different to that observed in PS01. The ultimate collapsed mass essentially broke off in one piece, with a very low angle of break at the goaf edges (~40°), and a central tensile fracture from the base of the block to the top of the broken triangular slab (Figure IV.8 a). It is postulated that the angle of caving of massive structures is less than in well-bedded structures - which effectively have, by definition, less flexural strength.

- The height of "secondary caving" did not extend to the top of the basal block, finishing 3 mm below the aquitard. A gap of 6 - 12 mm was maintained between the collapsed goaf and the intact sandstone after all six rows of pistons were lowered. This represents a bulking factor of between 50% and 100% of "mining"/drop height.

- Another significant result of this test was the supportive effect of the uncaved overhang immediately above the edge of the "mine workings" (see Figure IV.9a). Very little flexure of the aquitard and strata immediately above the collapsed ground was noted and very small flexural strains were measured on the top of the

gauged aquitard (Figure IV.10, and Table IV.2). Given the full caving width of the immediate roof, the reason for the small strains on the aquitard must be that the uncaved overhang is of sufficient stiffness and strength to support the aquitard in a similar fashion to a building gable. The supportive influence of this overhang is further discussed by Misich (1996).

- No discernible subsidence was measured above the level of the aquitard.
- No aquitard cracking was noted during the test. The maximum compressive and tensile strains measured were 0.62 mm/m and 0.68 mm/m respectively (Figure IV.10). Both maximum values are well within the yielding strain for cannel coal, and support the fact that no cracks were noted in the aquitard.

IV.3 CENTRIFUGE MODEL PS03

Model type - 2 dimensional "Plane Strain"

Operating force - 200g

Scaling factor - 1:200

The layout of the model stratigraphy is summarised below:

Model lithology	Layer Thickness	Height to base of unit	Equivalent Height Above Prototype
Sandstone aquifer	137 mm	0 mm	0 m
Coal aquitard	5 mm	137 mm	27.4 m
Overburden	135 mm	142 mm	28.4 m
Surface		277 mm	55.4 m

Model type - 2 dimensional "Plane Strain"

Panel dimension - As for PS02

Comments - Due to concern that surface subsidence could be influenced by using a block of lithified material as the upper overburden, it was decided that this test would incorporate more typical, softer, overburden material. As mentioned above, this material was sampled from the WO-5B mine, which at certain

locations, is sited above the WD6 Mine. (This material was therefore thought to be representative of the general overburden in the project area.) The sample was sieved to remove large grains or lumps of material. The remaining grain size was -0.5 mm.

Problems associated with sample selection for the immediate roof block in this test were even more demanding due to the additional selection criteria for continuous bedding across the length of the block.

The stringent selection criteria for strength was not put into practice for selecting this block. Only visual comparison was made to select similar strength materials (based on more than 10 years experience in the Collie area).

The thickness of the cannel coal (aquitard) layer thickness was inadvertently reduced to 5 mm (instead of 8 mm) - due to cutting problems.

Results - The heights of initial caving above the raised level of the piston top-caps varied from 10 mm to 36 mm. The typical height of roof collapse was 20 mm (4 m in the prototype), which is approximately 50% of the height of initial roof collapses observed within the mine. No significant collapse occurred until the fourth row of pistons was lowered (see Figure IV.11 a & b). Under scaling laws this corresponds to 53 m of fully extracted coal (4 x 13.3 m one-way lifts). This effective mining width is in the order of 15 m greater than the field observation for initiation of the first large-scale collapse of overlying strata.

After this secondary caving, the laminated sandstone sheared off in single, rhomboidal blocks for the full thickness of the lower block, as illustrated by Figure IV.12, which represents the post-test crack tracings on the front of the model.

The caving angle on both the trailing and advancing edges approximated 23°; however, the caving angle on the leading edge is somewhat disguised by what appears to be some localised crushing immediately above the "solid coal" abutment. The height of this crushed zone is in the order of 65 mm (13 m in the prototype). This observation appears to match field observations for the shallow extraction panel 2 South A panel in the WD6 mine, on which this model is based.

The strains measured along the aquitard (summarised by Figure IV.13, and Table IV.3) exceeded the adopted yielding strains; this matches the observed

cracking, illustrated in Figure IV.12. The location of each strain gauge in relation to the mining elements (pistons) is depicted by both the background shading and diagrammatical section provided beneath the graph denoted by Figure IV.13. It is interesting to note that the cracking at the surface of the aquitard slab was curved from the front to the rear of the block.

Another interesting feature was the manner in which the coal initially spanned, then fractured across the goaf edge. The cantilever aquitard then dropped/sagged in one piece, remaining somewhat intact (though cracked - see Figure IV.14) By collapsing in this manner, the line of shearing is not continued to the strata immediately above. Therefore, above this coal aquitard, there is no further caving of strata, and the superincumbent ground subsides by sagging only - resulting in a more continuous shaped subsidence tough.

This truncation of the line of shear at the interface of major aquitards is seen to be an important point for surface subsidence development because it prevents the development of pot-holes or stepped subsidence.

The maximum surface subsidence measured in this test was 10 mm, which corresponds to a subsidence factor (Smax/T) of 10/12 = 0.83. This factor is significantly higher than the subsidence factor proven from field observations, i.e. 0.64 (Misich et al., 1990). (Subsidence was measured manually, from tracings of the front of the model after the test was completed).

In order to isolate the effect of consolidation of the top layer of overburden, a horizontal line was drawn from the dots near the extreme edges of the box, outside the influence of the subsidence trough (see Figure IV.11 b). Subsidence due to mining was taken to be representative of the vertical separation between the horizontal line and the subsided row of dots.

This measured vertical subsidence (10 mm) was, within standard error, present throughout the full depth of the model. It was considered that the high subsidence factor was due to minimal small-scale collapse and bulking, particularly near seam level.

The exact shape of the subsidence trough could not be measured accurately and was assumed not to be representative of the prototype subsidence. This was because:

- the advancing edge was too close to the end of the box which led to a sharper subsidence trough on this side.
- the standard error involved with measurement of subsidence (±0.5 mm for frame grabbing and ± 1.0 mm overall for dot tracing) corresponds to prototype-equivalent subsidence of 100 - 200 mm.

The estimated angle of draw on the trailing edge side of the model is 18°. This value represents a somewhat narrow angle of draw; however, it does fit within the range measured in the field (Table 3.2).

Aquitard cracking is illustrated in Figure IV.12, and measured aquitard strains are represented in Figure IV.13. Details of cracking are listed as follows:

Aquitard No.1	-	crack No.1.
Crack Position	-	45 mm inwards from trailing edge toward the middle of the panel.
Crack Type	-	tensile, penetrating the top 4/5 of the aquitard.
Timing of Crack	-	after the 5th row of pistons were dropped (68 m in prototype).
Interpreted Strain (at time of rupture)	-	2.0 mm/m (tensile).

Aquitard No.1	-	crack No.2.
Crack Position	-	100 mm inwards from trailing edge toward the middle of the panel.
Crack Type	-	tensile at lower side leading to compressive on the upper side of the aquitard block. The crack penetrated the full width of the aquitard (though no open cracking was evident).
Timing of Crack	-	after the 6th row of pistons were dropped (80 m in prototype).
Interpreted Strain (at time of rupture)	-	-1.3 mm/m (compressive).

Aquitard No.1 - crack No.3.

Crack Position - 24 mm inwards from leading edge to the middle of the panel.

Crack Type - shear, penetrating the full width of the aquitard. No open cracking was noted. The aquitard was vertically displaced by approximately 1.5 mm (300 mm in the prototype).

Timing of Crack - after the 6th row of pistons were dropped (80 m in prototype).

Interpreted Strain - no strain gauges were installed on this side of the model. (at time of rupture)

Cracking Comments- The sub-vertical shear (crack 3) through the aquitard was interpreted to have developed when the majority of the triangular gable-type caved overhang sheared off and displaced vertically, leaving little support for the aquitard in this location. The difference between the two goaf edges on either side of the extraction panel (one sheared, one not) could be due to natural variation throughout the block of insitu material.

IV.4 CENTRIFUGE MODEL PS04

The procedures required to obtain reasonable similitude between the equivalent material and prototype strata are laborious and time consuming, accounting for approximately 80% of the time required to complete a test run.

For this model, one large base block of "sandstone" was made with the aquitard placed on top. The purpose was to cut the lower section off (to correct thickness) and use this block for the next block above to attempt to speed up the construction and drying stage. This method did not work, however, as the cutting water softened the aquitard layer, and some of the sandstone bedding delaminated. From this point onward, all blocks were cast individually.

The PS04 model (and all remaining models) was then built in stages, within the plane strain box, on top of the hydraulic pistons and support assembly. In this test the model was developed in three stages:

i) Casting of the mine roof sandstone member (122 mm thick) and first aquitard (Alpha seam - 10 mm thick). This block was left to cure for at least 24 hrs; then the sides were removed and the block and base

placed in the oven to dry (see Appendix III). Strain gauges were then glued in place on top of the aquitard layer and water proofed.

ii) The strong-box sides were reinstated around the roof block and the second sandstone block (83 mm thick) was cast; again in 5mm thick layers, on top of the first block. This second block also had an 8 mm thick layer representing the next aquitard layer (Upsilon seam) cast on top. The strong-box sides were then removed and the new mould - inclusive of the first phase block - is placed in the oven to "dry". Once suitably dry, the second aquitard was then strain gauged.

iii) The last sequence involved the placement of the overburden layer. The method used to construct this material is given previously for test PS03. The thickness of this layer was 105 mm (prior to spin-up)

These procedures were maintained for all future equivalent material models, although individual block thicknesses may vary slightly. This model stratigraphy was constructed as being representative of the first test panel 1 North Panel, based on drill information from boreholes D212 and D213 (see Figure 3.44, and stratigraphic plots in Appendix V.). No specific mixes were made to represent the immediate laminated roof, or laminated material immediately adjacent to aquitards.

The stratigraphy of this test was simplified such that laminated semi-stiff shale and silt materials - usually associated with aquitards, and located intermittently throughout the strata sequence - were omitted from the model. It was proposed to introduce these laminated members into later tests to evaluate whether they had any impact on the subsidence process.

Both the thicknesses of successive layers above the mining horizon, and the sand/plaster/water mixing ratios required to maintain similitude between the model and prototype, are listed below:

Model lithology	Layer Thickness (mm)	Sand : Plaster Ratio	Height to base of unit (mm)	Equivalent Height Above Prototype (m)
1) Aquifer 2	122	9:1	0	0
2) Aquitard (Alpha seam)	8	1.7:1	122	36.6
3) Aquifer 3	83	9:1	130	39.0
4) Aquitard (Upsilon Seam)	8	1.7:1	213	63.9
5) Overburden	97	(in situ)	221	66.3
6) Surface			318	95.4

The plaster mixes required were determined from beam bending tests (see Appendix III) and by Buckingham's dimensional scaling laws (Section 4.2.2.1). The equivalent mining parameters represented by the model are summarised below:

	Mining Parameters	Model Dimensions	Prototype Dimensions
1.	Cover depth	318 mm	95 m
2.	Individual mining blocks	67 x 67 mm	20 x 20 m
3.	Total extraction panel	6 x 67 mm wide 3 x 67 mm long	122 m wide x 61m long slice through an infinitely long panel
4.	Mining height	14 mm	4.2 m

Due to continuing problems with lighting across the face of the models and strong-box window of the in situ material tests, the front of the model was painted black with white dots.

Model Type - 2 dimensional plane strain using equivalent material

Scaling Factor - 1:300

Drop sequence - left to right

Data Collation - CCD camera, frame grabbing, crack and dot traces, strain gauge

Comments - Following an investigation into the techniques for fabricating equivalent materials, it was found that the most applicable materials were mixes of sand, water and building plaster. Developing procedures for making equivalent materials was not a simple matter. It was necessary to investigate the best mixing and curing procedures and which strength parameters to employ in the model. This information is provided in Appendix III.

The connecting strain gauge wiring was incorrectly fixed along the long axis of the model, and grouped together, rather than taken back, individually, to the rear of the box as for all other tests. (Figure IV.15 illustrates the strain gauge set-up for tests PS04 and PS05). This change in gauge installation was made by a UWA contract technician who at the time was unsupervised and decided to alter the proven system without consultation.

The fault was detected prior to completion of the model; however, as the model was 90% complete at that point, it was decided to finish construction and run a full test. Concern was held that the longitudinally glued wires would give additional support to the aquitard beams and thus reduce the superincumbent loading on lower aquitards and goafed material.

The thickness of each block varied slightly from that proposed across the model. This variation appeared to be ± 2 mm for aquitard, and ± 5 mm for aquifers.

It was proposed that the drop height be 8 mm (2.4 m in the prototype), however during the test, the piston top-caps actually dropped 14 mm - which represents the maximum stroke of the pistons. This fault was corrected by the next test.

In order to assist with determining the influence of specific parameters on subsidence, the model stratigraphy was simplified to comprise of essentially three components; weak aquifer material, stiff coal aquitard layers and overburden.

Results - Subsidence development during each stage of the PS04 test is illustrated by Figure IV.16 a & b. Figure IV.16 a represents the video frame as captured from the CCD camera, and Figure IV.16 b represents the interpreted subsidence (from dot tracings) between each mining step.

One interesting point to arise from this test was the manner in which the immediate roof caved. It was evident that as the triangular mass of roof material collapsed

above each actuator, the amount of subsidence above the middle of the actuator caps was more than that above the edges of the caps or (fenders). What appears to happen is; as primary caving occurs immediately above the actuator cap, the goafed material bulks slightly and supports the angular shaped intact material above the edge of caving.

When the adjacent actuator cap is lowered, this process is repeated, thus developing an inverted triangular shaped wedge mass between the two caps which does not subside as much as the ground immediately to either side of it.

This phenomenon is illustrated in Figures IV.17 and IV.18 and helps explain the peculiar field measurement in 2SA and Blue panels, where the extensometer anchors closest to the workings actually moved less than those immediately above. This feature was seen in previous models; however, the mechanism of development was not as clear as for this model.

The PS04 model was "spun up" for five minutes prior to running the test to minimise the consolidation of the insitu overburden material during the mining stages of the test. After the test was completed it was found that this approach worked well; however, approximately 1 mm additional consolidation did occur over the complete model during testing. This consolidation throughout centrifuge models has been noted by other, for example Sutherland et al., (1986) noted approximately 13 mm of consolidation.

Maximum surface subsidence, measured was 12 mm which represents 86% of mining height. Subsidence is calculated as the difference in the elevation of lines traced between the dots painted on the face of the model (best illustrated by Figure IV.16 b) from a reference point at the edge of the centrifuge model unaffected by subsidence. It is not warranted to comment further on the subsidence measured because the bridging strain gauge wiring has affected the performance of the model.

The height of first caving immediately after each piston is lowered was far greater than that expected from observations made from the centrifuge tests using insitu material. Figures IV.17 and IV.18, which represent the tracings and photographs respectively of the face of the model after completion of the test, illustrate that the height of primary caving varied from 48 mm to 98 mm (14.4 m to 29.4 m in the prototype). This was significantly greater than that measured in the field and in

earlier tests. The aquitard cracking noted is illustrated in Figure IV.19, the specific details are as follows:

Aquitard No.1	-	crack No.1
Crack Position	-	13 mm (39 m in the prototype) away from the trailing edge toward side of the model
Crack Type	-	tensile, on the top side penetrating the upper 4/5 of the aquitard
Timing of Crack	-	after the 2nd row of pistons was dropped (40 m in prototype)
Interpreted Yielding-Strain		tensile - value not given - an estimation was not plausible
Aquitard No.1	-	crack No.2
Crack Position	-	68 mm inwards from trailing edge toward the middle of the panel
Crack Type	-	tensile at lower side penetrating the bottom 2/3 of the aquitard
Timing of Crack	-	after the 3rd row of pistons was dropped (60 m in prototype)
Interpreted Yielding-Strain		compressive (the major yielding strain was not measured On the under-side) - value not given - an estimation was not plausible
Aquitard No.1	-	crack No.3
Crack Position	-	86 mm inwards from the leading edge toward the middle of the panel
Crack Type	-	tensile at lower side penetrating the bottom ½ of the aquitard, leading to compressive on the upper side
Timing of Crack	-	after the 5th row of pistons was dropped (100 m in prototype)
Interpreted Yielding-Strain		compressive (initially tensile) tensile - value not given - an estimation was not plausible

Aquitard No.1 - crack No.4

Crack Position - 15 mm outwards from trailing edge toward the side of the model

Crack Type - tensile at upper side, penetrating the top 2/3 of the aquitard

Timing of Crack - after the 6th row of pistons was dropped (120 m in prototype)

Interpreted Yielding-Strain - tensile - value not given - an estimation was not plausible

No cracking was noted on the face of the model on the second aquitard above the extraction horizon even though high tensile strains (>1.0 mm/m) were measured above the edges of the panel; however, three very fine cracks were noted above the panel edges on top of the aquitard as the model was dismantled (Figure IV.19).

Aquitard No.2 - crack No.1

Crack Position - 58 mm outwards from trailing edge toward the side of the model

Crack Type - tensile on upper side penetrating the top 1/5 of the aquitard

Timing of Crack - after the 3rd row of pistons was dropped (60 m in prototype)

Interpreted Yielding Strain - tensile - value not given - an estimation was not plausible

[The location of strain gauges and the magnitudes of strain measured during the test are summarised by Figure IV.20c, and Table IV.4.]

Aquitard No.2 - crack No.2

Crack Position - 19 mm (5.7 m in the prototype) away from the trailing edge toward side of the model (Figure IV.19)

Crack Type - tensile, on the top side penetrating the upper 1/5 of the aquitard

Timing of Crack - after the 3rd row of pistons was dropped (60 m in prototype)

Interpreted Yielding-Strain - tensile - value not given - an estimation was not plausible

Aquitard No.2 - crack No.3

Crack Position - 86 mm from the leading edge toward the side of the model

Crack Type - tensile at upper side penetrating the top 1/5 of the aquitard

Timing of Crack - after the 6th row of pistons was dropped (120 m in prototype)

Interpreted Yielding-Strain - <1.0 mm/m (initially tensile)

Crack Comments - The third crack on aquitard 2 appeared to develop in two stages; immediately after the 4th row of pistons was lowered, when the aquitard was deflecting downwards (with convex curvature) across what was the panel edge at that point in time; and when the final row was lowered and the aquitard curvature became concave (developing compressive strain). This crack was much more defined than any of the other cracks to develop.

After lowering the 5th row of pistons, strain gauge #8 on the lower aquitard, and gauge #10 on the upper aquitard, noted 2.1 mm/m and 1.2 mm/m tensile strain which denotes failure of the aquitard. However, no cracking could be detected visually, suggesting closure of cracking with subsequent mining cycles.

The opening and closing of cracks is an important feature of this test and is interpreted as representing the effects of the subsidence "wave" which develops as mining progresses from one point to another. (This "wave" phenomenon is described by many researchers, for example Dunrud, 1984). Figure IV.20 provides a good illustration of the effect of a subsidence wave on aquitard strains. In this figure it is noted that the sequential peak tensile strains for "mining" rows 3, 4, 5, & 6 on aquitard 1 (Alpha seam) migrate from strain gauges 6, 7, 8, to 10 respectively, as the width of "extraction" increases in sequence.

Furthermore, the peak tensile strains associated with any particular row or width of extraction are greatly reduced with the subsequent lowering of the next row of pistons in the given sequence. For example, the peak tensile strain recorded when row #5 was dropped was approximately 2.1 mm/m (by strain gauge #8); however, when the next row (6th and final) was lowered, the tensile strain measured by gauge #8 reduced to only 0.1 mm/m. In fact, at this point, gauges 5, 6, & 7 expressed compressive strain which suggests that between these points, the aquitard was being squeezed together and any cracks developed previously could re-knit.

IV.5 CENTRIFUGE MODEL PS05

Model Construction - Identical, within practical limitations, to PS04 (small variations were noted in layer thickness). Strain gauges were positioned with each individual data transfer cable positioned across the block to the rear of the centrifuge box as done for all tests prior to PS04 (see Figure IV.15).

The front of this model, unlike PS04 was painted grey, with black dots. This was due to the problems with frame grabbing video records for PS04. As the PS04 model subsided, the black paint on the face of the model broke-up (Figure IV.18) and exposed the white plaster which therefore provided no contrast to the white painted dots. The result was that the ACCUware software could not locate a significant proportion of the white dots remaining on the face of the model.

Model Type - 2 dimensional plane strain using equivalent material

Scaling Factors - As for PS04

Panel Dimension - As for PS04, except the drop/mining height was reduced to 12 mm (3.6 m in the prototype)

Drop Sequence - Front to back for each row, sequentially from right to left. Drop 5 sec, wait 30 sec for each actuator with a 14 minute wait between rows

Data collation - As for PS04

Comments - Because the main purpose of this test was to establish whether placing strain gauge wires along the long axis of the model had any effect on th performance of the model, PS05 was constructed in identical fashion to PS04, with the exception of the placement of the strain gauge wiring.

During the initial spin-up of the model, a light bulb "fixed" to the side of the centrifuge box dislodged and shattered against the actuator solenoid valve rack. A piece of broken glass pierced the black polyethylene hose feeding the front actuator on the extreme right hand side (RHS) of the model. This actuator consequently dropped immediately, thus initiating "mining" on the RHS. It was then decided to proceed with the test, mining from right to left, which is the reverse of PS04.

As it turns out, during the uncontrolled collapse of the front RHS actuator, some debris prevented the middle actuator in the same row (hidden from view) from lowering. This severely restricted the development of subsidence, particularly in the

early stages.

Results - Subsidence development during each stage of the PS05 test is illustrated by Figure IV.21 a & b. Figure IV.21 a represents the video frame as captured from the CCD camera, and Figure IV.21 b represents the interpreted subsidence (from dot tracings) between each mining step. The post-test fracturing traced on the front of the model is illustrated by Figure IV.22.

The effect of the middle RHS piston remaining in an upright position on the early caving characteristics of the model was significant. It was not until three rows were dropped that a regular pattern of caving appeared to develop.

In fact, due to the abnormal pressures at the edge of the "extraction" panel at the RHS of the model, the amount of fracturing traceable at this trailing edge was far greater than that observed in previous tests and caused the development of a vertical shear from the level of mining through to the surface of the model (Figure IV.23).

Surface cracking was generally much more developed in PS05 than PS04, indicating a sharper loading/shear edge. This accentuated loading would be expected if the PS04 gauge wires were reinforcing the aquitards and thus more evenly distributing the forces.

Aquitard strains measured during this test were significantly higher than for test PS04 (summarised by Figure IV.24 and Table IV.5). This is readily demonstrated by comparing Figures IV.20 and IV.24 where the maximum tensile strains for test PS05 at aquitard 2 are typically at least twice those measured in test PS04. The compressive strains in the PS05 model are almost an order of magnitude greater.

Strain gauge #2 was not functioning correctly. This is evident by the high compressive strains measured (1.4 mm/m) when rows 1 & 2 were lowered on the opposite side of the model.

It was also evident from the strain measurements that a subsidence wave had developed during the test in a similar manner to that identified in PS04. The effect of the subsidence wave is best recognised in Figure IV.24 b which plots the measured strains on the surface of the upper aquitard against the sequential mining steps.

Aquitard cracking, illustrated in Figure IV.25, was noted as follows (crack nomenclature has been listed from right to left, signifying the direction of mining):

Aquitard No.1 - crack No.1

Crack Position - 25 mm (7.5 m in the prototype) outwards from leading edge toward the side of the mode.

Crack Type - tensile, on the top side penetrating the upper 3/4 of the aquitard

Timing of Crack - after the 3rd row of pistons was dropped (60 m in prototype)

Interpreted Yielding-Strain - -0.6 mm/m (compressive)

Aquitard No.1 - crack No.2

Crack Position - 68 mm from trailing panel edge toward the middle of the panel

Crack Type - tensile at lower side penetrating the bottom 1/4 of the aquitard and delaminated

Timing of Crack - after the 4th row of pistons was dropped (80 m in prototype)

Interpreted Yielding-strain - -0.9 mm/m (compressive) The major yielding strain was not measured on the under-side.

Aquitard No.1 - crack No.3

Crack Position - 17 mm from leading panel edge toward the side of the model

Crack Type - tensile at upper side, penetrating the top ½ of the aquitard

Timing of Crack - after the 5th row of pistons was dropped (100 m in prototype)

Interpreted Yielding-Strain - tensile - value not given - an estimation was not plausible

Aquitard No.2 - crack No.1

Crack Position - 24 mm outwards from leading panel edge to RHS of model.

Crack Type - tensile at upper side, penetrating the top 1/5 of the aquitard.

Timing of Crack - after the 3rd row of pistons was dropped (60 m in prototype).

Interpreted Yielding-Strain - ≈1 mm/m (tensile)

Aquitard No.2 - crack No.2

Crack Position - 35 mm outwards from leading panel edge toward the LHS of the model

Crack Type - tensile at upper side, penetrating the top 2/3 of the aquitard

Timing of Crack - after the 5th row of pistons was dropped (100 m in prototype)

Interpreted Yielding-Strain - tensile - value not given - an estimation was not plausible

It was again evident that large open vertical cracks did not develop through the body of the model during the test, even though large-scale shearing did take place.

In order to illustrate the extent of cracking across the aquitards, traces of the cracks in plan were made whilst the model was being dismantled (Figure IV.25). Separate layers of aquifer and aquitard were carefully prised apart using a wide bladed scraping tool. It is interesting to note that the pattern of cracking on the lower aquitard suggests that this aquitard bridges the line of shear, and cracks in large slabs when critical spans are reached. It is also important to note that the positioning of the aquitard cracking at these critical spans is outside the primary line of shear.

The results of frame-grabbing of the painted dots, though better than previously achieved, still had problems with a number of sources of error (see Appendix IV.10). The best results are achieved in the lower middle section where there is better lighting and no lens distortion effect.

Maximum subsidence measured in this test (as depicted in Figure IV.22) was 12 mm, which represents 100% of the drop height of the pistons. This amount of subsidence is unrepresentative of field data measured in the Collie Basin. This excessive subsidence suggests that bulking (which is a crucial element of the subsidence project) is not occurring near the roof horizon within the model. [Field information (from 1 North Panel - see Figures 3.49 & 3.50) suggests that over time, in supercritical width panels, subsurface subsidence at all horizons gradually assumes very similar magnitudes to surface subsidence. These field results therefore indicate that, apart from the immediate caved area the superincumbent strata can, in the end, be considered to have moved as one mass. Any bulking or lasting dilation which gives rise to a final subsidence factor of 64% must occur in the immediate roof only. (In this case, below the Marker seam - 6 to 8 m above the Wyvern seam.)]

The probable reason for the lack of bulking is twofold:

a) the reasonably large area "mined" at one time (effectively 400 m^2 in the two equivalent material tests when the individual pistons are lowered), which could be allowing for "first caving" type collapse, and

b) the inability of the centrifuge model to represent the time dependent "running" cantilever-type collapse of the immediate roof as observed in the field. This type of collapse in the prototype (which can randomly involve 400 m^2 of roof material), even though it may be over in very few seconds (Hebblewhite & Humphreys, 1988), allows the immediate roof to break up into individual slabs which can then rotate and bulk up or "swell".

Strain gauge results indicate that the scaling factor for time $t.g^{½} / l^{½}_{(m)} = t.g^{½} / l^{½}_{(p)}$, does not apply to these sand-plaster models.

IV.6 CENTRIFUGE MODEL PS06

Model Construction - As this test was based on the then proposed trial extraction panel - North West B3 panel - in the WD6 underground mine (NWB3 panel), the model was generally scaled from the adjacent drill hole W665 (illustrated by stratigraphic column given in Appendix V - Figure V.2) sited above ACIRL Panel. The discrepancy between the model and prototype panel stratigraphy was that the thickness of overburden material did not match the prototype, due to weight limitations of the centrifuge. As seen below, the equivalent depth of cover in the model is approximately 107 m, which compares to the actual depth of cover of 140 m in the field.

The mixing and curing procedures used were identical to those adopted for PS04 and PS05. The thicknesses of successive layers above the mining horizon are listed below:

Model lithology	**Layer Thickness**	**Sand : Plaster Ratio**	**Height to base of unit**	**Equivalent Height Above Prototype**
1) Aquifer 2	82 mm	9:1	0 mm	0 m
2) Aquitard (Alpha seam)	8 mm	1.7:1	83 mm	24.9m
3) Aquifer 3	62 mm	9:1	91 mm	27.3m
4) Aquitard (Upsilon Seam)	7 mm	1.7:1	153 mm	45.9m
5) Aquifer 4	139 mm	10:1	160 mm	48.0m
6) Aquitard (Collieburn 1)	8 mm	1.7:1	299 mm	89.7m
12) Overburden	55 mm	(in situ)	307 mm	92.1m
13) Surface			362 mm	108.6m

As for the previous two equivalent material tests, the stratigraphy was simplified at the roof horizon by not including laminated roof material in the model.

Model type - 2 dimensional plane strain, using equivalent material

Operating force - 200 g

Scaling factor - $1_{(m)}:300_{(p)}$

Mining Parameters		Model Dimensions	Prototype Dimensions
1.	Cover depth	362 mm	108.6 m
2.	Individual mining blocks	67 x 67 mm	20 x 20 m
3.	Total extraction panel	2x67 mm + 3x67 mm	1x40 m & 1x60 m
4.	Mining height	8.4 mm	2.5 m

Drop sequence - To represent the proposed panel/pillar extraction panel design, the "mining" steps were :-

i) Sequentially lower two adjacent rows of pistons on the leading edge side (representing 40 m goaf width),

ii) Leave the third row of pistons fully extended (to represent intra-panel pillars), and

iii) Lower, again in succession, two more rows of pistons.

iv) The centrifuge test was then stopped, the strong-box sides dismantled and the model examined for fracturing characteristics and displacements.

v) Following examination, the sides of the strong-box were reassembled, and the model was again spun up to 200g at which point a fifth row of pistons was lowered.

The time delays between lowering individual actuators and rows of actuators were identical to the previous equivalent material tests (with the obvious exception of the last row).

These mining steps represent two sub-panels, separated by a 20 m wide pillar. The first sub-panel scales to 40 m wide in the prototype; the second sub-panel, initially 40 m wide, was later widened to 60 m to check the impact of mining wider sub-panels.

Data collection - CCD camera, frame grabbing, crack and dot traces, strain gauging.

Comments - It was recognised that the proposed model design was very conservative (considering the expected lack of bulked goaf) and that there was

a risk that the results may have proven unduly negative because of this. However, due to the high level of concern held for minimising groundwater ingress into the mine workings, this approach was considered to be justifiable.

Once the fourth row of pistons was lowered (representing two 40 m wide sub-panels separated by a 20 m wide intra-panel pillar), the middle row of pistons dropped unexpectedly. This undesired event is attributed to the additional loading on the actuator system developed by having fully caved ground on either side. This additional load exceeded the burst pressure of the hydraulic piston's thin HDPV feeder tubes with the result that the tubes perforated, releasing hydraulic pressure and subsequently lowering the row of pistons representing the intra-panel pillar. From video evidence, the timing of this event appeared to be gradual at first, with ultimate collapse occurring suddenly about 25 seconds after the 4th row of pistons was lowered.

Results - Figures IV.26 a & b and IV.27 respectively depict the model's subsidence and crack development during the test. The following comments summarise the most pertinent results noted.

- Subsidence measurements have not been included or discussed due to the unrepresentative collapse of the middle row of pillars.
- Following the ramp-down and re spin-up period (prior to the lowering of the 5th row) when the model was partly dismantled, it was noted that some strain gauge readings did not return to their original values. It appears reasonable to assume that the gauges returning to the same value of micro-strain attained immediately prior to the ramp-down were still behaving elastically and had not gone into yield. Conversely, strain gauges that assumed different values after the re-spin can be assumed to have yielded and altered shape permanently. Assuming this to be true, the plots of the strain readings during the complete test (summarised in Figures IV.28 a, b, & c and IV.29 a, b, c & d, and Table IV.6) suggest that the limiting strain for equivalent materials - when confined within the model - is 800 μ strain in tension and 700 μ strain compression. (These limiting values represent the highest strains observed which rebounded to original strain values.)

- Prior to the ultimate collapse of the middle row of pistons representing the intra-panel pillar (at approximately 4,580 seconds), the results from the centrifuge study largely supported the NWB3 test panel design assumptions for minimal interaction between sub-panels, with relatively small aquitard strains being expressed on all aquitards (see Figures IV.29 a to IV.29 d).
- It appears that one strain gauge did not function correctly (A102).
- Strain gauges A302, A203 and A105, each superimposed above the panel pillar, were unexpectedly in compression (-ve strain) for almost the entire test. This unusual feature has been interpreted to have resulted from a combination of differential consolidation across the model and a gradual lowering of the middle row of pistons before they ultimately collapsed. The decreasing magnitude of compressive strain from the surface to the mining horizon suggests that the major cause for the compressive strain is consolidation.
- Although there was no evidence that interaction between separate goafs would connect the two collapsed areas above each sub-panel it was recognised that it may still have been possible for time-dependent failure of the pillar support system had the middle rows not collapsed unexpectedly.
- Once the middle row of pistons (intra-panel pillars) collapsed, the tensile strain above the panel edges exceeded the yielding strain, indicating that the aquitards would have cracked. Figures IV.29 a, b, c & d illustrate the sequence of strain development on the surface of each aquitard. The location of each gauge in relation to the mining elements (pistons) is depicted by background shading and the diagrammatical section provided beneath the graphs.

No crack data are provided due to the middle row of pillars lowering. This information is misleading.

IV.7 CENTRIFUGE MODEL PS07

Model Construction - The mixing and curing procedures used were identical to those adopted for PS04, PS05, and PS06 with the exception that the model included layers of loose sand above each aquitard. The presence of the loose sand required the back and sides of the model to be left on whilst drying in the oven to keep the sand in place. This slowed the drying process significantly.

This test (PS07) and those remaining also included the semi-lithified silts and shales associated with aquitards and mine roof. The integration of these layers into the model was considered to be important for the proposed modelling of water-filled aquifers in future tests. [It was thought that if water was applied to the sand layer in direct contact with the equivalent material aquitards the effective strength of the stiff aquitard layers would be softened before the end of a test. Consequently these less porous shale/silt equivalent layers (with a higher propotion of plaster) were introduced to minimise the impact of pressurised water in future models]. The thicknesses of successive layers above the mining horizon, and the sand/plaster/water mixing ratios in the model, are listed below:

Model lithology	Layer Thickness	Sand : Plaster Ratio	Height to base of unit	Equivalent Height Above Prototype
1) Immediate roof	20 mm	3.1:1	0 mm	0 m
2) Aquifer 2	103 mm	9:1	20 mm	6.0m
3) Aquitard (Alpha Seam)	8 mm	1.7:1	123 mm	36.9m
4) Aquitard Roof Laminite	17 mm	3.1:1	131 mm	39.3m
5) Loose sand	5 mm	100%	148 mm	44.4m
6) Aquifer 3	82 mm	9:1	153 mm	45.9m
7) Aquitard (Orion Seam)	5 mm	1.7:1	235 mm	70.5m
8) Aquitard Roof Laminite	7 mm	3.1:1	240 mm	72.0m
9) Loose sand	5 mm	100%	247 mm	74.1m
10) Aquifer 4	44 mm	10:1	252 mm	75.6m
11) Aquitard (Collieburn 1)	7 mm	1.7:1	296 mm	88.8m
12) Overburden	45 mm	(insitu)	303 mm	90.9m
13) Surface		348 mm	103.4m	

The sand:plaster mixes representing each of the stratigraphic components in the model were adapted from models PS04 - PS06. This model represents the maximum payload the centrifuge can withstand at 200 g (approximately 200 kg). The aquitard roof material mix was calculated to represent a prototype flexural strength of 1.6 MPa. No rock mass reduction factors were applied for the non-coal "roof" or aquitard material - as explained previously.

PS07 and the remainder of the proposed parametric tests were to be representative of the typical stratigraphy above Wyvern seam, as defined by Figure 3.2. However, after the test was completed, an error in the location of the aquifer 4 aquitard - the Upsilon seam - was noted. This incorrect placement resulted from a typographical error which positioned the Upsilon seam at the Orion seam level. (The Orion seam, located approximately mid-point in aquifer 4, is not a recognised aquitard - Hammond et al., 1983.) It was decided to repeat the modified stratigraphy in the next two tests so that parametric studies (into the effect of water in the aquifers and a narrower intra-panel pillar) could be assessed appropriately.

Model type - 2 dimensional, plane strain

Scaling factor - $1_{(m)}$:$300_{(p)}$ (As for PS04 -PS06.)

Panel Dimension - 1 x 40 m & 1 x 60 m

14.1 mm drop (4.2 m mining height)

Drop sequence - To represent the proposed panel/pillar extraction panel design, the "mining" steps used were essentially identical to PS06:

I) sequentially lowering two rows of three pistons representing 40 m goaf width,

ii) lower, again in succession, the three remaining rows of pistons on the other side of the 20 m wide intra-panel pillar to represent 60 m of extraction. (This test was not stopped in flight, unlike PS06, and the intra-panel pillar was immobilised to remove potential for another failure of the hydraulic system.)

Data collation - CCD camera, frame grabbing, crack and dot traces, strain gauge, and load cells. Following the elevated load rupturing of the PS06 piston feeder tubes, it was decided to modify the piston support columns so that load transfer can be measured throughout future tests. The design of these load cells, based on strain gauging techniques, is described in greater detail in Appendix IV.12.

Comments - This model was the first of a sequence of three tests to assess the effect of:

i) increased mining height (low key investigation),

ii) water pressure in aquifers 3 & 4,

iii) reduced intra-panel pillar width.

Therefore each of these tests was made "identically" so the effect of each variable could be gauged more accurately. Consequently, as the next test (PS08) required 5 mm of loose sand above the aquitard layer to allow water pressure to be incorporated into the model, each of the other tests also included the 5 mm layer of sand in similar positions. The height of extraction (14.2 mm) represents the maximum "play" in the piston system and also approximates the maximum thickness of the Wyvern seam within the WD6 mine lease.

Results - The general appearance of the model before and after testing is illustrated in Figure IV.30 a and b. The sequential development of subsidence throughout the test is illustrated in Figures IV.31 a and IV.31 b. Figure IV.32 represents the cracking identifiable on the face of the model at completion of the test. As for previous tests, the frame representing the "control" - prior to mining - was captured off the video immediately before lowering the first piston. By waiting for this moment, the vast majority of settlement has occurred in the model and therefore any movement of the face dots after this can be interpreted as being almost entirely due to mining subsidence. A list of the more significant observations made from these plots is given below:

- The minimal bulking of both the caved immediate roof and collapsed interburden resulted in a 34 mm wide unsupported span at the first aquitard, equivalent to 10 m in the prototype. The unsupported span also appeared to be widened slightly by some crushing of the overhang supporting the aquitard. This open span could not be sustained and subsequently failed in tension at the mid-point of the lower side of the aquitard (in similar fashion to the PS01 test).
- The timing of the tensile fracture of the aquitard also coincided with a crushing of the triangular wedge of strata overhang (Figure IV.33) which develops during the caving process. This overhang was acting as a form of support to the aquitard (in similar fashion to model PS02) prior to it being crushed.

- This assumption is further investigated in Section 5.1 where the finite element program FESOL was used to assess the impact of an elastic, triangular-shaped support (at the base of the aquitard) on the shape and magnitudes of subsidence of the aquitard beam. This work, along with the practical demonstration in the centrifuge model, probably accounts for the problems previous researchers have had with using beam theory to explain the subsidence process. This matter was not pursued any further as it was outside the scope of the project.
- Maximum subsidence measured above sub-panel 1; the intra-panel pillars; and sub-panel 2 are 8 mm, 9 mm and 10 mm respectively. In terms of mining height, these deflections represent 56%, 63% and 70% of the maximum possible movement. Each of these measured subsidences is far greater than would be expected in the field.
- Figure IV.33 also demonstrates that the surficial painted layer can separate from the model and wrongly imply additional subsidence. (Note the 19 mm subsidence above sub-panel 1 when only 14.2 mm was "mined").
- Figure IV.31 b illustrates how, prior to lowering the third row of pistons in the second sub-panel, there was minimal subsidence noted (as depicted by shading above the traced lines).
- Once again, the column of sandstone immediately above the intra-panel pillar did not fail. However, as illustrated by Figures IV.33 and IV.34 (which represents the X, Y coordinates for dot positions both before mining and after the 4th row of pistons was lowered), some settlement of the weaker interburden above the pillar did occur. The dot co-ordinate data used to develop Figure IV.34 is provided in Table IV.7.

Throughout this test, strain gauge and load cell data was being automatically recorded.

Figures IV.35 a,b & c and Table IV.8 summarise the strain gauge measurements made during testing. The location of each gauge in relation to the mining elements (pistons) is depicted by both the background shading and diagrammatical section depicted by Figure IV.35 d. These plots demonstrate:

- That the tensile strain development at aquitard #1 (the Alpha seam) above the intra-panel pillar and outside the panel edge greatly exceeded the yielding strain for equivalent materials. These results were confirmed by crack tracing of aquitard #1 (see Figure IV.32).
- The development of large compressive strains mid-point above each area of extraction. The type, timing, and magnitude of strain measured was expected.
- In both sub-panels, after the second row of pistons was lowered, the yielding strains on aquitard #1 were exceeded. The strain values noted during this test were at least twice those measured in the comparative test PS06 which had a standard equivalent mining height.
- The maximum strain measured on aquitard #2 during the test was 0.82 mm/m. This value only marginally exceeded the previously acknowledged yielding strain (0.8 mm/m) and suggests that aquitard #2 remained close to and possibly within its elastic limits throughout the test. This assumption is supported by the fact that no cracking was evident on the surface of the second aquitard and further supports the assumed tensile yielding strain of the equivalent materials.
- Aquitard #3 again appears to have been influenced by some settlement, with unusually high compressive strains being measured by gauges 301 & 302 after only two rows of pistons were lowered.
- It is also interesting to note that the aquifer #3 strain gauge, sited immediately above the middle of the intra-panel pillar, expressed compressive strain when all "mining" was completed. This suggests that the subsidence trough has levelled out at this point and is slightly concave. (There is no hump in the subsidence profile above the intra-panel pillar - as illustrated by Figure IV.32 - which was originally expected prior to the completion of the test.) This can be explained by the crushing of weak interburden over the intra-panel pillar above the stiffer immediate roof strata.

As mentioned previously, this test incorporated load cells (strain gauges fixed onto the surface of the actuator pistons - described in detail in Appendix IV.12). In order to minimise costs, load cells were only developed on the middle series of pistons on both the longitudinal and sectional axes. Two sets of load cells were made, the difference between the two sets being a thicker gauge of the supporting cylinder

(where the strain gauges were fixed) on the middle row of three (pillar) pistons which were expected to carry significantly more tributary load once caving had fully developed.

The text figure below illustrates the layout of the load cells within the model. Figure IV.36 presents photographs of the load cells as placed within the strong-box.

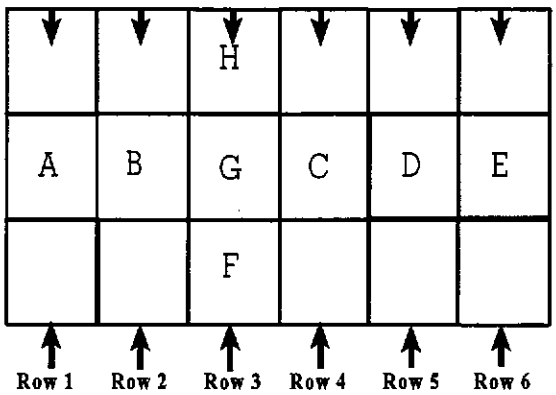

Plan view of load cell arrangement

It should be noted that the load data measured from "mobile" load cells A - E, prior to them being lowered, are misleading and were consequently not used for analyses. The reason for this inaccuracy is due to the manner in which the load is transferred through the rubber O-rings as well as the steel cylinder to the base plate prior to being lowered - see Appendix IV.12.

Figure IV.37 and Table IV.9 summarise the load cell output after each row of pistons were lowered. The results have also been represented diagrammatically by Figures IV.38 and IV.39 to better illustrate the progressive caving, and measured load redistribution.

Figure IV.38 presents loads as both:

- the total load measured by each of the mobile load cells once they have been lowered, and
- the change in load recorded by load cells in an upright position (including the pillar load cells).

The following points summarise the more significant results noted:

- The middle three load cells (representing the intra-panel pillars) were indicating greater loads {6,200 N - 365 N for the actuator cap = 5,835 N} than would be expected prior to mining {$6.7 \times 6.7 \times (18.6 + 16.0) \times 9.8 \times 200 \times 1.61 = 5,185$ N} . This

13% additional load could be a result of settlement during the consolidation spin-up, which increased the effective density of the equivalent material (model dimensions were taken post-test). If this is the case then the densified material would equate to 1.92 t/m^3. Another possibility was the fact that the middle pillars were stiffer than the adjacent actuators and therefore accepted more load. (This latter option is supported by Iglesia et al., 1991.)

- Surprisingly, the middle row of pistons only detected a relatively small increase in load after both rows in sub-panel #1 were lowered. This suggests that a great deal of tributary load is being distributed in the abutment between the two cantilevered goaf edges above the middle of the panel.

- The load measured by the intra-panel pillar load cells (F,G, & H) after three rows of pistons had been dropped was slightly larger than when four rows had been lowered (Figure IV.38). The lower load in the latter case has been interpreted to have occurred as the tributary load is transferred onto the goaf. The timing of the transfer most likely coincides with the localised crushing of the weaker strata above the pillar (mentioned above) after four rows were lowered. Furthermore, the magnitude of vertical load measured at this point (7,691 N - of which 365 N is due to the top-cap) is much less than expected by the tributary load theory.

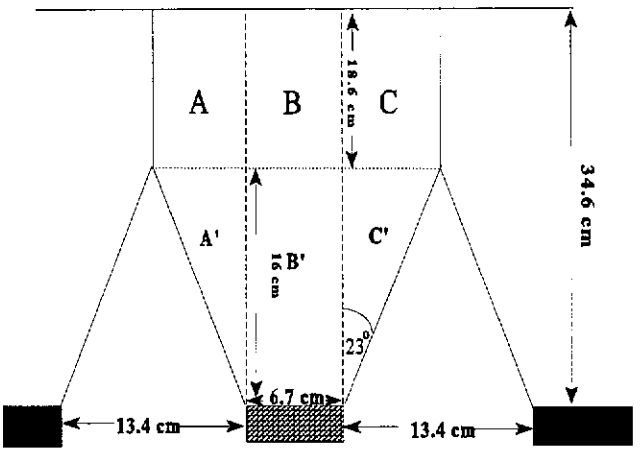

ILLUSTRATION OF TRIBUTARY LOADING

If tributary load theory is assumed, and for simplicity the line of caving assumed to be 23° as determined in Section 3.2.5, the estimated expected loads can be calculated by:

Tributary load = (A + B + C + A' + B' + C') x 6.7

= (3 x 18.6 x 6.7+16.4 x 6.7+2 x 0.5 x 6.7 x 16.4) x 6.7

= 3979 cm^3

= 12,570 N

This represents 70% more than the total measured load (7326 N). Assuming that the total measured load includes the load attributable to the weight of the column of strata vertically above the pillars (4,930 N), the additional measured tributary load is 2396 N. This additional loading represents less than 1/3 of the additional load expected by summing areas A & C illustrated in the text figure above. In fact the inferred additional tributary area approximates to a 5° "loading angle". If it is assumed that the equivalent material has densified, the loading angle approximates 3°.

This suggests that either the tributary loading changes once any crushing occurs at the abutments or again there is a large component of frictional self-support between the two masses of goaf edge overhang. More investigation is required to establish exactly what is causing this loading response.

- After the fifth row of pistons was dropped, the load on both the pillar load cells and sub-panel #2 load cells increased significantly. Minimal change was noted for the load cells in sub-panel #1, indicating that the integrity of ground support members on this side of the pillar have not degenerated further. However, in each case, the measured loads were again significantly lower than expected by the tributary area theory.
- It is interesting to note that the average tributary loads measured on the actuated load cells in each sub-panel after all five rows had been lowered were similar. The average load measured in sub-panel #1 was 2517 N similarly, the load on the sub-panel #2 load cells averaged 2664 N.
- It was also evident that the middle load cell in sub-panel #2 had more tributary load redistributed onto it (3590 N). This would be expected as this load cell is further away from the support abutments on either side of the panel.
- It also appears that load cells at the immediate advancing edge receive less load than trailing cells. This indicates that there is less consolidation at this point and the leading load cells are within a stress shadow. This observation is supported in the field where subsidence profiles on the advancing edge tilt into the panel far less steeply than on the trailing side (see Figure 6.2).

IV.8 CENTRIFUGE MODEL PS08

Model Construction - The thicknesses of successive layers above the mining horizon, and the sand/plaster/water mixing ratios used in the PS08 model, were based on those in test PS07. The actual model details achieved are listed below:-

Model lithology	Layer Thickness	Sand : Plaster Ratio	Height to base of unit	Equivalent Height Above Prototype (m)
1) Immediate roof	20 mm	3.1:1	0 mm	0
2) Aquifer 2	98 mm	9:1	20 mm	6.0
3) Aquitard (Alpha Seam)	8 mm	1.7:1	118 mm	35.4
4) Aquitard Roof Laminite	17 mm	3.1:1	126 mm	37.8
5) Loose sand	5 mm	100%	143 mm	42.9
6) Aquifer 3	94 mm	9:1	148 mm	44.4
7) Aquitard (Orion Seam)	5 mm	1.7:1	242 mm	72.6
8) Aquitard Roof Laminite	7 mm	3.1:1	247 mm	74.1
9) Loose sand	5 mm	100%	254 mm	76.2
10) Aquifer 4	54 mm	10:1	259 mm	77.7
11) Aquitard (Collieburn 1)	6 mm	1.7:1	313 mm	93.9
12) Overburden	32 mm	(in situ)	319 mm	95.7
13) Surface			351 mm	105.3

Due to concern for maintaining an effective seal at the model's edges, to keep water pressures constant throughout the test, the sand layer was enclosed in a thin (0.5 mm) neoprene gasket rubber sheet. The rubber sheeting was cut to size using a sharp blade, and had the central section cut out (so the bending moments of the aquitard beam would not be greatly affected by the rubber membrane). The dimensions of the rubber sheet were determined by the dimensions of the strong-box, and the thickness of the laminated roof, and sand bed.

The rubber was put in place at the top of each aquitard prior to the laminated "roof" material being cast. Once the laminated material was cast on the rubber, a 5 mm thick loose sand bed, followed by 5 mm of aquifer mix material was put in place. The flaps of the rubber sheet were then folded over these three layers. The folds were held in place by rubberised engine gasket sealer. The length of overlap of the rubber on top of the sand bed and beneath the laminated material was approximately 30 mm. The configuration of the rubber aquifer is illustrated by Figure IV.40 b, which was photographed after the model was dismantled. This approach, though looking somewhat crude because of the bulky corners where the rubber was folded over, was seen to be adequate for the model as the bulky corners were sufficiently away from the main area of concern in the model. Water was added to the model via stand-pipes attached to the side of the model (Figure IV.41).

Model type - 2 Dimensional Plane strain, equivalent materials

Scaling factor - $1_{(m)}$:$300_{(p)}$. The scaling for time was not changed even though water was introduced into the model, as the purpose of the test was to observe the effect of water pressure on caving characteristics and not fluid flow. The scaling factor for water pressure is 1:200, as the density of the tap water used is identical to the prototype water.

Panel Dimension - 1 x 40 m & 1 x 60 m

14.1 mm drop (4.2 m mining height)

Drop sequence - To represent the proposed panel/pillar extraction panel design, the "mining" steps used were identical to PS07, whereby two sub-panels are simulated. The first sub-panel represents a 40 m wide prototype sub-panel; the second sub-panel, initially also 40 m wide, is later widened to 60 m to check the impact of mining wider sub-panels. The two sub-panels are separated by an equivalent 20 m wide pillar.

Data collation - CCD camera, frame grabbing, crack and dot traces, strain gauge, load cells, and water pressure transducers.

Results - Post-test photographs portraying the front and back of the model are given in Figures IV.42 a and IV.42 b respectively. Figure IV.42 b also

illustrates the positioning of the two aquifers constructed for the model. The sequence of subsidence development is represented by Figure IV.43. The strain gauge measurements recorded during the test are summarised in Table IV.10 and Figures IV.44. Load cell measurements are summarised by Table IV.11 and Figures IV.45 & IV.46 respectively.

Due to problems with "groundwater" leakage, and the first piston not lowering, no detailed analysis has been undertaken for this test; however, interesting points observed during the test were:

- Figure IV.47 (representing the traced face of the completed PS08 test) illustrates the significant effect the piston that remained in an upright position had on subsidence development; no major caving was noted at all above the first row of pistons. It is essential that all pistons are lowered fully, particularly for plane strain models.
- Immediately following the consolidation test spin-up, it was visibly noted that some settlement had occurred within the body of the model as well as within the compacted insitu overburden material. This supports previous assumptions regarding the anomalous strains measured in the upper aquitards above the intra-panel pillars.
- Figure IV.48, which illustrates the loading data during the initial spin-up/consolidation of the model, further supports the previous conclusions regarding the variability of edge load cells; and the inaccuracy of the mobile load cells prior to being lowered (by not returning to zero load when the model is ramped-down from 200g to 1g).
- Figure IV.48 also demonstrates that the load measured by the middle "pillar" load cells is approximately 17% greater than for PS07. This additional load can be attributed to the extraneous water in the model.

Again, no cracking data have been provided.

IV.9 CENTRIFUGE TEST PS09

Model Construction - Every attempt was made to keep the construction of the equivalent materials identical to PS07. The average model depth was 350 mm, which is 2 mm more than test PS07. Figure IV.49 a represents the overall make-up of the model both before and after testing; the gold coloured face provided ready recognition of each aquitard, aquifer, overburden and laminite component.

The only variation designed into the model was a reduction in width of the middle row of piston top-caps representing intra-panel pillars.

Modification of the top caps was a relatively easy process; the dowelled top-cap extensions - in place since test PS02 - were dismantled. These modifications to the middle row of top-caps necessitated modification to the base plate. Simplistically, the original base plate was machined into three separate pieces and reduced in width on either side of the central row of pistons to match the reduction in width of the top-cap. The three separate sections were then butted together in the original sequence and fixed to a new base plate. Every effort was made to ensure that the new top-caps did not foul against each other or allow debris to collect between the top-caps.

An additional data transfer multiplexing (Mux) box was utilised in this test. This additional Mux box allowed an extra eighteen data points to be recorded during the test, which were used to gain more detailed strain measurements across the length of the aquitards.

The thicknesses of successive layers above the mining horizon and the sand/plaster/water mixing ratios in the model were designed to reproduce those in test PS07. The actual values achieved were:

Model lithology	Layer Thickness	Sand : Plaster Ratio	Height to base of unit	Equivalent Height Above Prototype (m)
1) Immediate roof	20 mm	3.1:1	0 mm	0
2) Aquifer 2	108 mm	9:1	20 mm	6.0
3) Aquitard (Alpha Seam)	8 mm	1.7:1	128 mm	38.4
4) Aquitard Roof laminite	15 mm	3.1:1	137 mm	38.1
5) Loose sand	5 mm	100%	152 mm	45.6

6)	Aquifer 3	80 mm	9:1	157 mm	47.1
7)	Aquitard (Orion Seam)	5 mm	1.7:1	237 mm	68.1
8)	Aquitard Roof laminite	7 mm	3.1:1	242 mm	72.6
9)	Loose sand	5 mm	100%	249 mm	74.7
10)	Aquifer 4	55 mm	10:1	254 mm	76.2
11)	Aquitard (Collieburn 1)	6 mm	1.7:1	309 mm	92.7
12)	Overburden	35 mm	(in situ)	315 mm	94.5
13)	Surface			350 mm	104.4

Model type - Plane Strain using equivalent material.

Scaling factor - $1_{(m)}$:$300_{(p)}$

Panel Dimension - As for PS06, PS07, and PS08.

Drop sequence - As for PS06, PS07, and PS08.

Data collation - As for PS06, PS07, and PS08, incorporating more strain gauges.

Results - The appearance of the final subsided model is portrayed by Figures IV.49 b and Figure IV.50, and the sequential development of subsidence throughout the test is illustrated in Figures IV.51 a & b. The more significant observations made from these plots are given below:

- Unlike test PS07, the caving of interburden above the first sub-panel did not result in a gap between the base of the first aquitard and the top of the goaf pile. This brings into question the level of repeatability attainable using the centrifuge modelling technique.
- Figure IV.51 b illustrates how, prior to lowering the second row of pistons in the first sub-panel, there was minimal subsidence noted (as depicted by shading above the traced lines) above aquitard #1.
- As for test PS07, the first aquitard developed a tensile crack at approximately its mid-point above sub-panel #1. The timing of the tensile fracture of the aquitard also coincided with a crushing of the triangular wedge of strata overhang (Figure IV.52) after the lowering of two rows of pistons (representing completion of sub-panel 1).

- Within seconds of lowering the first row of pistons in the second sub-panel, the sandstone pillar above the aluminium spacers (representing the coal pillars) collapsed. This collapse eventually resulted in a maximum surface subsidence of approximately 12 mm, which represents 85% of the mining height. Table IV.12 and Figure IV.53 present the "blob" analysis using the ACCUware frame grabbing software. Figure IV.53 presents the blob/dot co-ordinate data as displacement vectors to illustrate both the magnitude and direction of subsidence near the collapsed intra-panel pillar.
- This additional subsidence represents more subsidence than noted in PS07 (being 70% mining height), but less than 100% mining height as measured in the PS05 model where all pistons were lowered.
- For the first time in the equivalent material models a displaced shearing crack developed through aquitard #1 above the edge of the second sub-panel. No evidence was noted which suggested that this crack remained open during or after the test. Crack mapping at the surface of each aquitard was not completed due to difficulty in separating the upper plies of sandstone from the aquitard.

Throughout this test, strain gauge and load cell data were being automatically recorded.

Figures IV.54 & IV.55 illustrate the strain measurements against time and mining width respectively. Table IV.13 lists that data used to create Figure IV.55; the data used for Figure IV.54 is too voluminous to present in gard copy form. These plots demonstrate:

- The development of tensile strain on aquitard #1 (the Alpha seam); above the intra-panel pillar, and outside the panel edge greatly exceeds the yielding strain for equivalent materials. The locations of the strain peaks roughly coincide with cracks noted on aquitard #1 (Figure IV.50).
- A greatly reduced level of tensile strain above the intra-panel pillar compared with PS07. This can be attributed to collapse of the superincumbent sandstone column above the pillar which would have levelled the subsidence profile above the pillar.
- That the maximum strain measured on aquitard #2 during the test was 3.5 mm/m and developed after lowering the first row of pistons in the second sub-panel

(immediately after the collapse of the sandstone column). This value greatly exceeds the previously acknowledged yielding strain (0.8 mm/m) - along with the strain noted for gauges 1, 2, 12, 18 & 19 - and suggests that aquitard #2 ruptured during this early stage of the test. This assumption is supported by the cracking evident on the front of the model on the second aquitard (Figure IV.50).

- Strains measured on aquitard #3 are also significantly higher than the base test - PS07. It is interesting to note that, unlike aquitards 1 and 2, a large tensile strain was developed above the intra-panel pillar (although no cracking was detected at the face of the model during dismantling - probably due to the trouble experienced with stripping off the upper layer). This high tensile strain would be expected under normal circumstances. The variation of measured strain between aquitards can possibly be best explained by localised crushing/shearing at aquitards #1 & #2 which masks the tensile strain at these levels. At the aquitard #3 horizon, these compressive pressures are significantly less and therefore allow for the reflection of tensile strain only.
- There is a significant difference between the strain noted on aquitard #3 in this test and tests PS07 and PS06, where compressive strains were experienced by the strain gauges sited vertically above the pillar.

Figures IV.56 and IV.57 represent the load cell output with time and mining width respectively. The data used to create Figure IV.57 is presented in Table IV.14. Again the data in Figure IV.56 is too voluminous to present in hard copy form. The layout of the load cells is identical to that used within model PS07. Figure IV.58 represents a series of diagrammatic sketches of caving and loading sequences during the test.

The more significant observations made from the load cell data include:

- the load data measured from "mobile" load cells, prior to their being lowered, were again misleading and not used for analyses - as for test PS07.
- Following some small improvements to the top-cap configuration, the load measurements between the three middle load cells were reasonably consistent. As a result, the average loads have been used for analyses in this test.
- Prior to "mining", the middle three pillar load cells were indicating higher loads (average 5150 N) than those expected assuming tributary area principles. The middle row of three pistons would be expected to carry a vertical column of

material equivalent to the plan area of the top-cap (A) and the depth of the model (H). In this case the volume (V) of this superincumbent column of material is estimated by:

$$\mathbf{V = A \times H} = 4.5 \times 35.0 \times L \ (cm^3); \quad \text{where L = length of top-cap}$$

$$= 1055 \ cm^3$$

Assuming a bulk density for the equivalent material of 1.61 t/m^3, this equates to a weight of:

$$1055 \times 1.61 = 1.7 \ kg$$

Including the weight of the top-cap (186 g), the calculated total weight supported by each load cell would be:

$$1.7 + 0.186 = 1.9 \ kg.$$

At 200g this weight corresponds to a load of :

$$1.9 \times 9.81 \times 200 = 3{,}728 \ N$$

Therefore, the measured load represents an additional 28% more than the calculated loads. This additional load is twice the proportional additional load noted in test PS07 (13%) prior to mining.

- After the first row of pistons was lowered in sub-panel #1, the load measured by load cell A was 677 N. This equates to a mass of:

$$\frac{677 \times 1000}{9.81 \times 200} \ g = 345 \ g$$

which equates to a weight of 159 g, or 99 cm^3 of caved equivalent material (after subtracting the weight of the top-cap).

If it is assumed that the shape of the caved mass approximates a cubic triangle, the height of initial caving above the "mine roof" (h) is calculated by:

$$0.5 \times 6.7 \times h \times 6.7 = 99$$

i.e.

$$h = 99 \div 22.45$$

$$= 4.4 \ cm$$

If the shape of the initial caving is assumed to be approximately rectangular - as observed during the test (see Figure IV.51) - the caving height is 2.2 cm.

These calculated caving heights greatly exceed the height of initial caving observed during the early stages of the test (see Figure IV.51). The discrepancy can be explained by one of three possibilities:

a) the front window of the model is providing some support to the material above the first piston and thus the visible caving at the front of the model is being slightly retarded;

b) the load cell is not functioning correctly; or

c) there is some additional load being provided by the caved edge abutments where they come in contact with the goaf material.

With the information available it is not possible to determine the exact cause of the variation.

- The additional load measured by load cells F, G & H after three rows of pistons had been dropped was close to half the load measured when two rows had been lowered (Figure IV.58). The lower load in the former case has been interpreted to have occurred as the tributary load (attributable to the caved areas - A & C in the text figure below) is transferred onto the goaf after the collapse of the sandstone column. This assumption is supported by the load cell data plotted against time (Figure IV.56), where immediately after the third row of pistons was lowered, the load measurements peaked to approximately 7100 kN and suddenly dropped to around 5200 kN before settling at 5950 kN. At the same time, the load noted by cells A & B, in particular load cell B, (located in sub-panel #1) increased significantly, suggesting a complete redistribution of stress.

- After row 4 had been lowered (representing 2 x 40 m sub-panels and the subsequent collapse of the sandstone pillar) the pillar support system could not accept loading as depicted by the standard tributary area theory. This assumption is supported by the average load measured by the three central load cells - 6,434 N - of which 365 N is attributable to the top-cap). The actual tributary load thus equates to 1921 cm^3 of superincumbent equivalent material in the model. If the tributary area theory is assumed, the volume of material located vertically above the pillars is:

  4.5 x 35.0 x 6.7 = 1,055 cm^3.

  Therefore the volume of additional superincumbent material is:

  1921 - 1055 = 866 cm^3.

If the tributary area is assumed to approximate the line of caving (23°), the estimated additional volume of material would equate to:

(A + C + A' + C') x L

i.e. 2 x (19.0x6.7+0.5x6.7x16.0) x 6.7

= 2424 cm^3

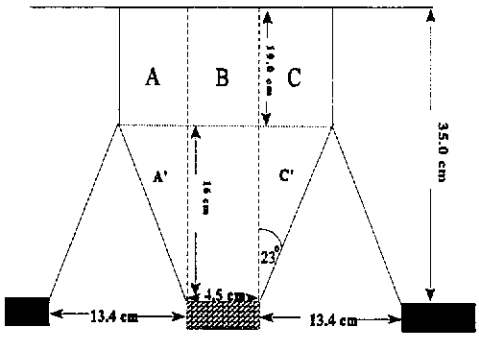

ILLUSTRATION OF TRIBUTARY LOADING

This represents almost three times the additional volume as indicated by the load measurements. In fact the inferred additional tributary area approximates to a 6° loading angle on either side of the pillar, which is very similar to the additional tributary loading angle calculated for PS07 at the corresponding stage in mine extraction. This also matches the tensile cracks noted at the surface of 1 North Panel (located outside the panel edge).

- After row 5 was lowered, the total tributary load on the middle three load cells increased to 7200 N. Only relatively marginal increases in load were monitored for cells A and B in sub-panel 1 at this stage. This indicates that after the collapse of the sandstone column, most of the recompaction had taken place once the 4th row of pistons was lowered.
- The increased tributary load after five rows had been lowered can be attributed to the reduced influence of the self-supporting aquitard "beams" above the second sub-panel. Assuming that the "effective loading angle" above the first sub-panel remains at 6° (providing 433 x 1.61/1000 x 9.81 x 200 N = 1,367N) the additional load measured after the 5th row was lowered is:

  7,200 - 365 - (1,367 + 3,333 N) = 2,135 N

  or 2,135 ÷ 1.61 ÷ 9.81 ÷ 200 cm^3 = 675 cm^3

  and approximates to an effective loading angle of:

  0.5β x 35 x 6.7 = 675 i.e. β = 5.8 cm

  tan(α) = 5.8 ÷ 35

  α = 9°

- Some dilation is evident within the near-surface overburden (see Figure IV.50). The maximum confirmed dilation is 2 mm which represents 0.6 m dilation in the prototype. The location of the greatest amount of dilation appears to be in close proximity to the panel edge. This measured dilation was relatively constant across the model.

IV.10 VIDEO FOOTAGE FRAME GRABBING

After the relative success of the phase I (pilot) centrifuge study, it was decided that it was necessary to be able to monitor and measure subsidence after each mining step. It was proposed that the most suitable method to record information at particular moments in time was to record video output from a miniature CCD camera. Once on permanent record, it is then possible to capture individual frames of this time-in-motion recording using computer software, to create a binary file which can be stored and manipulated at a later date. A similar technique had been used by the University of Nottingham for quantifying staged mining subsidence in their 1g models; however, the original images are obtained from still photography (personal communication, Reddish,1990). These single frame images are then digitally scanned to produce the base binary files.

At the time of the pilot study, an imaging system had been developed for monitoring the real-time motion of up to eighteen discrete points visible through the strong-box window and for back-analysing video footage of the model tests to produce displacement records of visible markers. It was later found that this system was not sufficiently accurate. Problems occurred with identifying all the markers on the face of the model in "one pass" due to variation in:

a) artificial lighting across the perspex window,

b) post-test cracking which altered the dimensions of the markers, and in some cases obliterated some painted dot markers.

It was therefore concluded that the existing frame grabbing package was inadequate for the requirements of the research study and that it was necessary to look at other frame-grabbing software packages which could locate and store any number of dots (or blobs) and identify each one separately, if required. Following investigation into the frame-grabbing software/hardware available, it was established by UWA staff that the most applicable commercially available system was a total frame grabbing

software package - ACCUware®, which was duly purchased.

The ACCUware® software proved to be a much more manageable system; however, small inaccuracies were noted between each frame. A brief summary of the procedure and methodology of this software and problems associated with the software is provided below.

The following paragraphs, modified from a "user's operating manual" written by Mr D Adhikary, post-graduate research student at UWA, explain the methodology involved in capturing individual video frames in binary code. The fine details of the frame grabbing procedures have been included for future reference, as much time was wasted at the start of the investigation in obtaining reproducible and adequate scanned images.

Before this program can be invoked, the OD3 device driver must be installed; this is done simply from the D:\OD300 directory and typing "od3" at the D:> prompt. (The frame grabber hardware cable must be connected to the VCR output port.)

Once the OD300 device driver is installed, the AVI imaging program needs to be initialised by typing "AVI" (from the ACCU directory; this displays the AVI menu on the monitor - from which various options are selected by 'mouse' operation.

Highlight "util" and click the left button. Select "clear screen". Then return to the previous menu by clicking the right button. Select "live". Play the VCR and click the left button in order to grab the video image. To store the image for future reference select Save-Images: .tiff. The screen menu will ask to position the image window. Choose the right position and the size of the image window. The numeric value of the image-window displayed in the main screen should be noted for future reference, as exactly the same window settings are required for all successive image grabbing. Since this program digitises the image data in global co-ordinates (against a fixed origin), any change in position of the image window will result in variations in the digitised co-ordinate data . In this way grab any number of video images and save them in succession for further analysis.

By following these steps, and creating binary tiff files up-front, most of the user-defined settings are saved between image selections. This simplifies the process.

The system is now set-up for digitising particular objects (in this case dots painted on the face of the model) within each tiff file. Any movement of the dots will be detected

and quantified by comparison of subsequent X, Y co-ordinates for each dot.

Once all the images of a test are saved, select "util" and clear the screen. Select "Get-images from menu" then select the image-file name. Position the image window, and make note of the numeric value of the window, as it is necessary to choose the same window for other images. Once the image is displayed, choose 'Count-blobs" Press "F10" to get the Polygon. Click the right button and position the polygon as desired to define the selection area. Press the left button to start counting. By moving the mouse adjust the image contrast and press the left button when satisfied with the product on the screen. The number of blobs in the defined limit will be written on the top of the screen. Then press the left mouse button to go to the menu and select plot blobs. Make sure that the small red cross-mark is placed on top of each of the blobs. If some of the blobs are left unmarked select "undo" and start whole operation once again and try to adjust the threshold (contrast) carefully so that all the blobs look equally dark. If some of the blobs are left unmarked once again, leave it like that. Now select "dump-blobs", and give your output data-file name. The digitised data will be stored in the file. Now return to blob counting and position the polygon on the blobs left unmarked at the previous attempt. Plot blobs and dump them in a separate file. The data from the subsequent files is appended manually to the previous file, once exited from the ACCUware® program. Similarly, choose the other images and get the digitised information one at a time.

It has been noticed that digitisation of data points by ACCUware® occurs quite randomly. Most often, the numbering of the data points at different stages of a test does not follow the same pattern. This was a most frustrating characteristic with the package, as it made visual identification of particular dots very difficult, particularly when "ghosting" dots values were created by the package.

Hence, it is essential that all dots are sorted in some order which allows direct comparison of each dot for mathematical manipulation.

The author firstly attempted to sort the data within the spreadsheet program QUATTRO PRO®, as it was proposed that manipulation of the sets of data could be best accomplished by a spreadsheet analysis. After many attempts, it was found that automatic sorting was not feasible, and manual filtering of extraneous data was required. This was a laborious, time consuming exercise.

In order to logically sort sequential dots, UWA's geomechanical group developed a FORTRAN program (SORT.exe). This program is designed to read directly centrifuge data digitised using ACCUware. The output files from ACCUware provide five columns of data with some text at the top of the data. However, it is necessary to delete the text from the ACCUware output files (using a suitable text editor) before proceeding further. When necessary, a number of separate files can be created for complete video frames which were not able to have all dots located by one contrast setting. In these instances, all the individual files need to be merged to adequately assess dot movements.

This program was very rigid with input requirements, and could not work successfully unless the same number of dots were present in each row and column. This was very difficult to achieve, as some dots were destroyed by large-scale movements, and the software invariably selected "phantom" dots when the painted surface started cracking during the subsidence process. Again manual manipulation of the data was required before this program could be used. (In some cases, it was necessary to create dot co-ordinates by estimation from movements of surrounding dots and insert these "dummy" dots at the correct position in the data file). This obviously is subjective and is a source of error. The author decided to persist with this program because of the useful sub-set deflection and strain vector plotting program associated with it.

The sorting program (SORT.exe) sorts out the data in two stages. Firstly, the data are sorted out and listed in ascending values of x-coordinates. This is further refined by rearranging the band of data in one row according to the ascending values of their respective y-coordinates. In order to run this program the total number of data points, number of data points in a vertical row, and the data-file name must be known beforehand. The program also requires an output data file name for the rearranged data, for use during execution of other programs. Once the data are sorted, it is recommended that the accuracy of the data sorting be checked by running the program DISP.exe Should there be any misplaced data, an abnormal displacement vector will identify the error. In such cases data files must be sorted out and rearranged in order manually.

The displacement vector calculation and plotting program (DISP.exe) is designed to plot the displacement vectors from 2 sets of data of a Centrifuge Test. In order to be

able to run this program, type disp at the D~prompt. Provide the name of the two data files (sorted by using SORT.exe) containing the X-Y Co ordinate information. The "Graph" displayed on the screen may be printed out using "print screen" command. Once the Graph is printed out, press "Esc" to exit to DOS.

After many attempts at obtaining accurate digitisation of all dots on the face of the models between sequential video frames, it was decided that dot analysis should only be attempted for selected, small regions in the centre of the model. (Such as above the intra panel pillar in centrifuge test PS09.) This recommendation was based on two factors:

- because dot analysis was generally open to various sources of error - particularly lighting and edge effects - as discussed below, and
- because the magnitudes of subsidence in the models did not accurately represent field subsidence data. It was therefore a meaningless task considering the time and effort involved.

The afore mentioned inaccuracies were attributed to:

a) variation in artificial lighting across the perspex window,

b) post-test cracking which altered the dimensions of the markers, and in some cases obliterated some painted dot markers,

c) an inherent flicker of the video image,

d) the subjectivity with which individual dots are identified (by optimising the contrast between each dot and the back ground shading). As a result, dot image dimensions could not always be repeated identically and were given slightly different X, Y coordinates.

e) The precise X, Y coordinate of each dot on the face of the model, was masked by lens distortion proportional to the focal point of the CCD camera. This error was more pronounced for the dots nearer the edges of the strong-box window. It was recognised that it could have been possible to apply a correction factor to each dot according to the radial distance from the focal point of the camera, but this action was not seen to be required due to the other variable sources of error.

IV.11 STRAIN GAUGING

The gauges used for monitoring the performance of aquitards were an inexpensive, 10 mm long wire in a paper carrier (Figure IV.59) type. Other forms of gauges such as etched foil on a polyamide or epoxy backing were not seen as necessary because the nature of the test was a once off - quick - test to failure. There was no need to have more precise, expensive gauges for long term "stability" between terminals. The main quality required by the gauges was the ability to measure between the range of strains expected during the centrifuge tests; see below.

Positioning of the gauges on the aquitard blocks was assisted by carefully measuring and marking out the precise location of all gauges on the surface of each block. (Figure IV.59 illustrates the strain gauges fixed into position for centrifuge model PS09.) This sped up the process and reduced the error in location of the gauges.

Once the gauges were glued into place, the wires were soldered to form a full 1/4 bridge configuration with variable resistors, the loose ends of the connecting wires were then soldered in turn onto a 37 pin connector box. Each 1/4 bridge was then balanced within the expected operating range of the gauge. Each gauge was gained by a factor of 1000 to simplify readout, and 2 ½ volt excitation was passed across each bridge.

Voltage (V) emitted from the 1/4 bridge is a function of:

$$V(out) = V(in) \times k \times \epsilon \times N/4$$

where k = the gauge factor (2.13 in this case), and

N = the number of active arms (always = 1 for this study).

In most models (not all gauges used were the same in all tests) this equated to:

$$0.001 = 2.5 \times 2.13 \times \epsilon \times 1/4, \text{ and}$$

$$\epsilon = 0.00075 \text{ m/m, or}$$

ϵ = 750 micro strain ($\mu\epsilon$) for each volt output.

In terms of readout equipment, voltage is given as "bits" of data. By calibrating the readout equipment, it was determined that one volt was equivalent to 409.6 bits. Therefore, each bit measured during testing equated to 750/409.6 = 1.83 $\mu\epsilon$.

The strain gauges were collected in groups of pairs of wires and gathered into a 37 pin "D" Male plug which connects the gauges to the computer driven data logging processes via a 1/4 bridge multiplexing junction box. The number of gauges on any

of the tests in the study were dependent on the number of channels installed on the centrifuge itself. Early tests had only one junction box with up to ten channels. In later tests, the number of both the terminals and junction boxes were increased to provide a more continuous representation of the strain across the full length of aquitard above the "extraction panel". In centrifuge model PS09, a total of 44 strain gauges were able to be measured simultaneously as well as the 8 load cells in three separate junction boxes. The maximum number of gauges that could be measured in this test was 3 x 18 = 54.

The junction box/multiplexing unit can switch from one gauge to the next each 20 millisecond. The multiplexing box is also fitted with a trimmer (potentiometer) which can be used to set each 1/4 bridge to zero gain before the test starts. The action of zeroing in the voltage output makes the change in strain of each gauge easier to recognise during and after testing.

When the gauge wires are soldered, they become very brittle and snap at the base of the gauge with any movement. To counter this problem, the gauges were dipped in epoxy resin and hung over a rack to dry beforehand. By dipping the gauge into epoxy resin, the gauge is also kept water proof and prevents shorting out between terminals on the gauge. Water proofing is further enhanced by putting a layer of epoxy resin on the aquitard block at the position where the gauge is to be fixed.

IV.12 LOAD CELLS

The detailed design of the load cells was provided by Mr J. White, in consultation with the author, from whom the request for the load cell was originated. The basic philosophy of the load cell was to permanently attach an etched-foil type strain gauge (type - 062UT 'C' - with a two element 90° rosette - which has minimal hysteresis) onto the surface of the hollow piston cylinders and calculate the applied loads according to the theoretical stress-strain relationships for materials, in this case stainless steel.

The aim of the load cells was to measure piston loads - prior, during, and after 'mining' - using the existing stainless steel cylinders to minimise costs. Two load cell types were required; one for the stationary row of pistons which represent the base of the intra-panel pillars, and another for the five rows of pistons designed to be lowered to represent the excavation of coal.

All load cells had to be encased in stainless steel sleeves which served as waterproofing for the strain gauges in the event of any future testing which included water in the aquifer systems.

It was also desirable to design the load cell so that the expected loads measured during the test fall within the optimum sensitivity range of the strain gauges used (750 μstrain). This was achieved by designing the respective thicknesses of the load cell cylinder walls to generate required levels of strain, given the known elastic modulus of the cylinders and assumed tributary loads.

The tributary load assumptions and calculations used to design these load cells are listed and illustrated below:

- Equivalent material bulk density (ρ) = 1900 kg/m^3. This value is conservative, to take account for any water in future tests. (The bulk density of 'dry' equivalent material is around 1.6 kg/m^3.)
- Operating gravity force, g(max) = 200
- Modulus of stainless steel load cell (E) = 210 x 10^3
- Model height 375 mm
- Maximum strain (ε) = 750 x10^{-6}
- Loading/shearing angle (conservative) = 27°

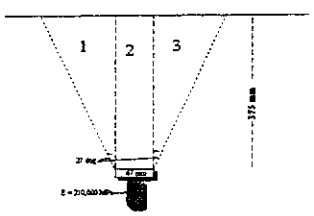

SIMPLIFIED TRIBUTARY LOADING

Using standard trigonometric laws, A1 = A3 = 0.0358 m^2, and the corresponding volume of material within A1,A3 (V1,V3) = 0.0358 x 0.067 = 2.4 x 10^{-3} m^3.

It follows that A2 = 0.0251 m^2, and the volume of material above the load cell (V2) = 1.683 10^{-3} m^3.

Therefore the total volume of material above any one of the central load cells is assumed to be:

$$V1 + V2 + V3 = 6.48 \times 10^{-3}\ m^3.$$

At 200 g (max), this volume of material would correspond to a downward force of:

$$(1900).\ (200).(9.8).(\ 6.48 \times 10^{-3})\ kN \quad = 24.1\ kN$$

However, the total load on the load cells must include the weight of the piston top-cap which represents the area of extraction of each piston. This additional load is

calculated in the same way as the previous step. Thus, assuming the density of the aluminium is 2.77 x 10^3 kg/m^3, this additional force of the 28.1 mm thick top-cap at 200 g is:

$$= (0.0281).(0.067).(0.067).(2770).(200).(9.8) \qquad = 0.7 \text{ kN}$$

and the total force (F) acting on each of the central load cells is 24.8 kN.

Therefore, assuming that the tributary load acting on each of the central pistons is 24.8 kN, the required dimension of the hollow cylinder to generate the preferred operating strain for the gauges selected can be estimated using the following approach:

If the vertical pressure (σ_1) can be defined as:

$$\sigma_1 = F/A(req) = E.\epsilon, \quad \text{where:}$$

A(req) = cross-sectional area of the hollow cylinder (required),

E = the elastic modulus of stainless steel, and

ϵ = the preferred active strain level for the strain gauges

it follows that the required cross-sectional area of the cylinder is calculated as :

$$A(req) = \frac{F}{E.\epsilon} = \frac{24.8 \times 10^3}{(210\times10^3)\,(750\times10^{-6})}$$

$$= 157 \text{ mm}^2$$

If it is assumed that the internal dimensions of the proposed load cell cylinder are to approximate those of the existing bronze cylinder casing (R2 = 15.875 mm) for neatness of fit and simplicity of operation, the required wall thickness to give a cross-sectional area of 157 mm^2 across the cylinder (as illustrated in the figure below) is :

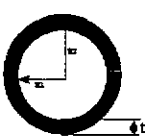

PLAN VIEW OF LOAD CELL

$A_1 - A_2 = 160 \text{ mm}^2$

i.e. $A_1 = 160 + A_2$

$= 952 \text{ mm}^2$

and $R1 = \sqrt{952/\pi} = 17.4$ mm

$\therefore \quad t = 17.4 - 15.9 = 1.5$ mm

Therefore, the preferred dimensions for the stainless steel cylinder were: 15.88 mm ID, and 17.4 mm OD with a machined wall thickness of 1.5 mm. The actual design

for the load cell and peripherals is illustrated in the text figure below

Note: the existing bronze cylinders had an external radius of 20.0 mm.

Similar calculations for the design of the load cell cylinders to be attached to the central longitudinal row of pistons which are to be lowered during the tests define a preferred wall thickness of 0.45 mm. The resultant load cell design is illustrated in the text figure below.

The main variation between the two sets of load cell calculations was the assumption of a vertical rectangular column as the shape of the tributary mass of material supported by the "mining" piston load cells (which gives a much less load than the intra-panel pillar load cells).

Because of concern that this thickness (0.445 mm) would allow too much deflection which could foul the system or distort the load cell, a cross-check calculation was done. This check is listed below:

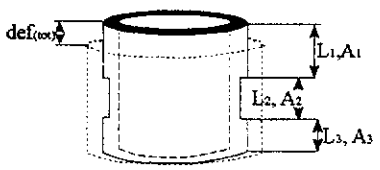

SECTION THROUGH LOAD CELL

As illustrated, there are essentially three different cross-sectional areas within the proposed design for the load cell. Therefore in order to estimate the total closure, deflection must be calculated for each component and summed, as represented by:

$$\mathbf{def_{(tot)}} = \frac{P.L_1}{E.A_1} + \frac{PL_2}{E.A_2} + \frac{PL_3}{E.A_3}$$

$$= \frac{24.800\ .\ (0.012 + 0.020 + 0.015)}{210000.(2.32\times10^{-4}+1.64\times10^{-4}+1.91\times10^{-4})}$$

$$= 3.1\times10^{-5}$$

$$= 0.031 \text{ mm}$$

It is realised that some error will arise where a small slot is cut into the region A_3; however, as the tributary loading is largely conservative, particularly for the pistons adjacent to the caved edge, and considering the very small total deflection as calculated, this error is not of concern.

IV.12.1 Calibration of Load Cells

Due to the very thin nature of the load cell walls, and the possible error associated with machining, and strain gauging, it was decided that each load cell be calibrated to check the validity of manufacture with the design. Calibration was achieved in two ways:

a) by applying sequentially increasing loads via a proving ring and measuring the gauge output, and

b) by attaching known weights to the top of the piston top-caps and spinning the piston arrangement on the centrifuge apparatus. This test was considered to be more appropriate as it incorporates all the characteristics of the actuator system under high gravities.

The results of the proving ring calibration tests are summarised by Figures IV.60 to IV.67. It can be seen that in each case, a statistically acceptable linear calibration factor was able to be fitted between the number of Newtons per "bit" read by the instrumentation and the applied load.

As the load cell readout is automatically zeroed before the start of any testing, the term representing the intercept can be ignored, only the multiplier term in the linear calibrations need be considered in each case. The load cell results for cells A to G, obtained from spin-up tests with known weights attached (as illustrated by Figure IV.36), are plotted in Figures IV.68 to IV.74. The mass of the loads strapped to each cell is provided in Table IV.1. The results indicate that the system in general works well, with reasonable correlation between static loading calibration and centrifuge loading measurements. It should be noted that these graphs represent as-monitored data using the automated logging system at the UWA and that the readout for the gravity force has an inherent error of approximately 8%; the maximum gravity force reached is 200 g, not 185 g as depicted. Figure IV.75 illustrates the variation between expected loads as calculated by dimensional processes and measured loads operating at 200 g. The calibration correction factor depicted in Figure IV.75 represents the calibration constant of each load cell. This constant when multiplied by the load cell readout equates the load to the expected dimensional equivalent load (at 200g for each of the standard masses strapped to the load cells):

Expected dimensional load = load reading x constant.

A correction factor of 1.0 signifies that both the expected loads and the measured loads are identical and therefore the load cell is 100% accurate. It can be seen that load cell H underestimates load by slightly more than 25%.

Figures IV.68 to IV.74 also demonstrate that the "mobile" load cells (load cells A to E) do not accurately portray loads during the spin-up; prior to being lowered. This inaccuracy is thought to be due to the manner in which the load is transferred via the rubber O-ring to the strain gauged basal cylinder.

IV.13 LASER PROFILING

The laser unit emits an infra-red laser beam from its source onto the surface of the model and captures reflected beam signals. The time delay between emitting and receiving the signal pulses relates to a vertical distance from the source. The output from the laser detection unit is directly connected via a RS-232 plug to a computer which runs the data recording and storage software.

The laser unit is mounted on an aluminium frame approximately 400 mm long which rests on the top of the strong-box and can be moved at a controlled, constant rate either vertically or laterally as required. Movement is initiated by a screw-fed, motor-driven, actuator. The typical rate of advance of the laser head is 0.3 mm/sec. The general set-up of the laser unit on the centrifuge model strong-box is illustrated in Figure IV.76.

In order to obtain accurate distance measurements from the laser, it is first required to set up the laser above a sample surface of known distance from the laser source. The recorded output is then calibrated against this known distance. It is important, during calibration, to use the same or very similar materials as the base/reference datum.

During the course of testing, it was found that the laser profiling was difficult and was susceptible to poor repeatability. These problems were attributed to:

a) remnant plaster from the superimposed strata being left on the surface of the aquitard once the model was dismantled,

b) an inherent error in laser profile calibration with granular, uneven surfaces, or

c) an inability of the laser to give accurate readings on granular, angular material.

In this case, it was probably a combination of all three. Subsurface profiling was disregarded and not attempted after the first trials in Westcoll 3 & 4. After centrifuge test PS03, laser scanning was not used other than as a retrial for test PS09 which reaffirmed these concerns for the method.

PRE-TEST PHOTOGRAPH OF CENTRIFUGE MODEL PS01

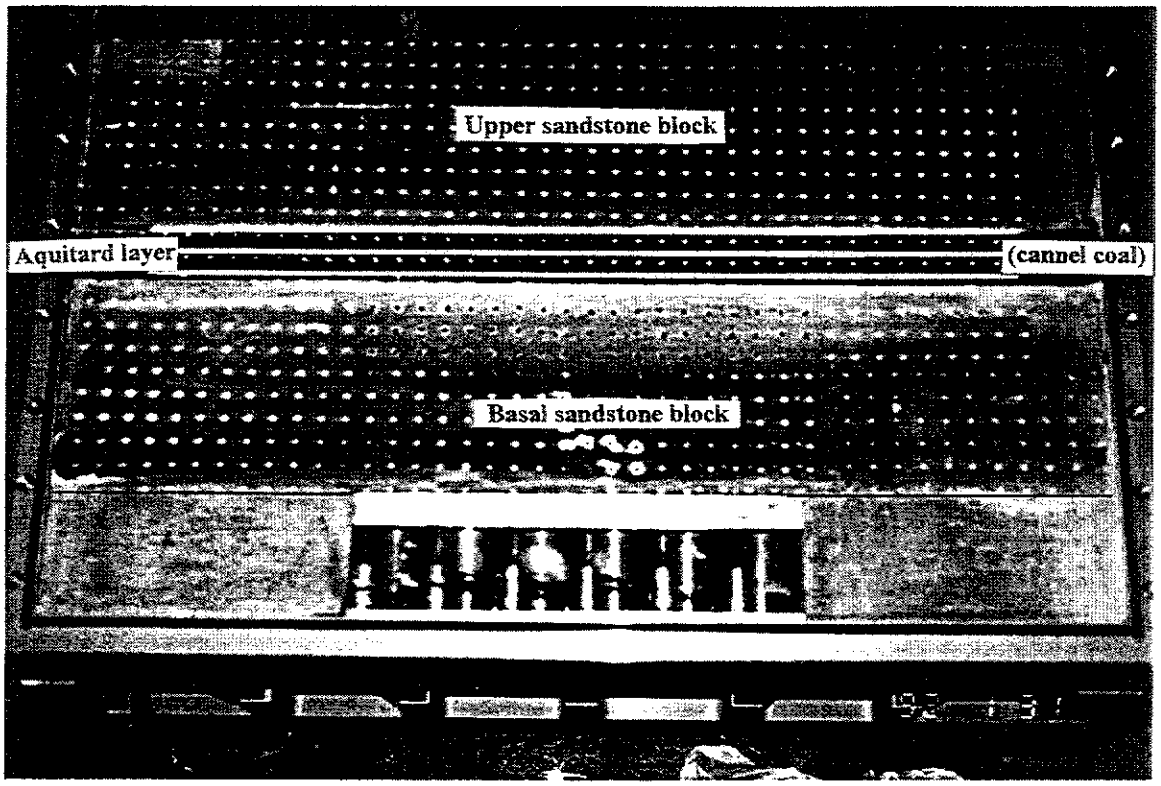

Figure IV.1 a

POST-TEST PHOTOGRAPH OF CENTRIFUGE MODEL PS01

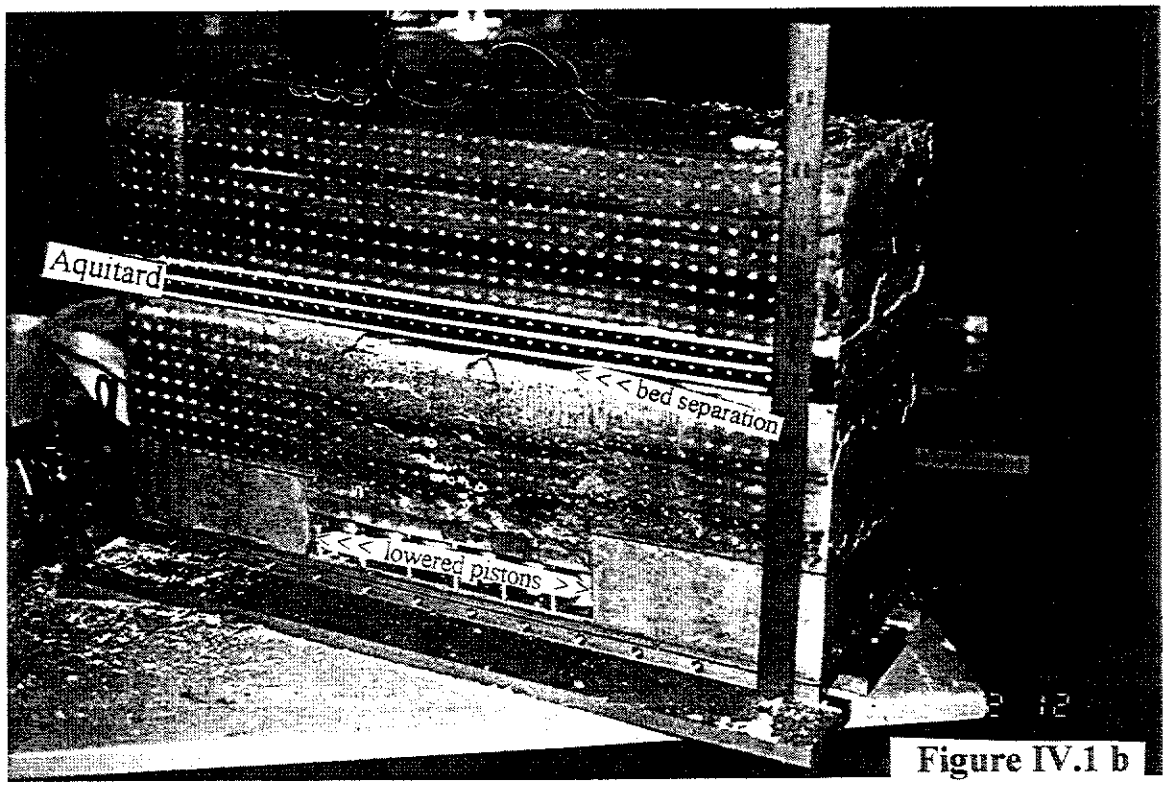

Figure IV.1 b

GEOTECHNICAL CENTRIFUGE TEST PS01

SUBSIDENCE DEVELOPMENT

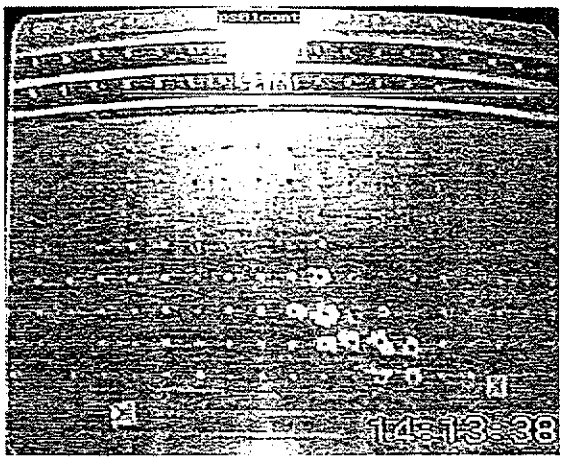

Control

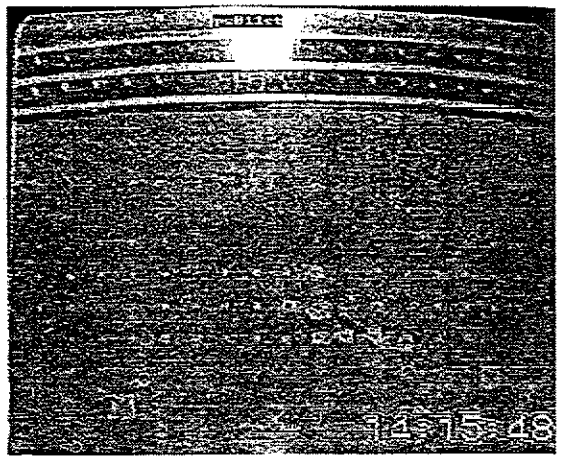

1st Row

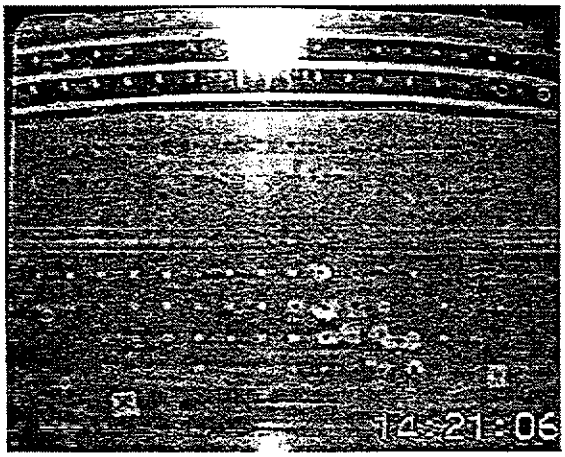

2nd Row

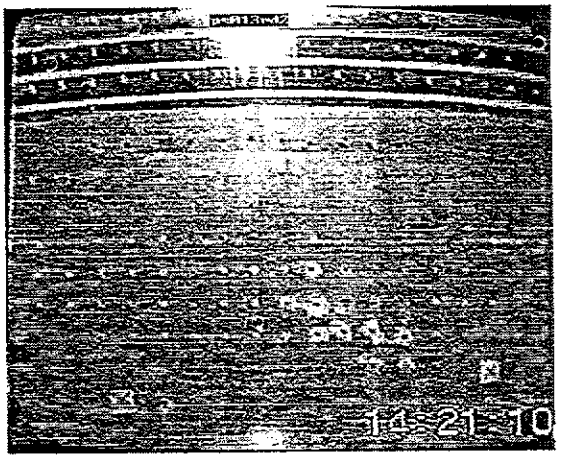

3rd Row (2)

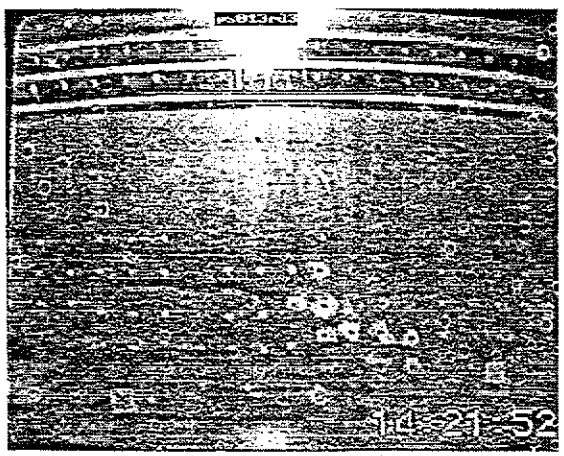

3rd Row (3)

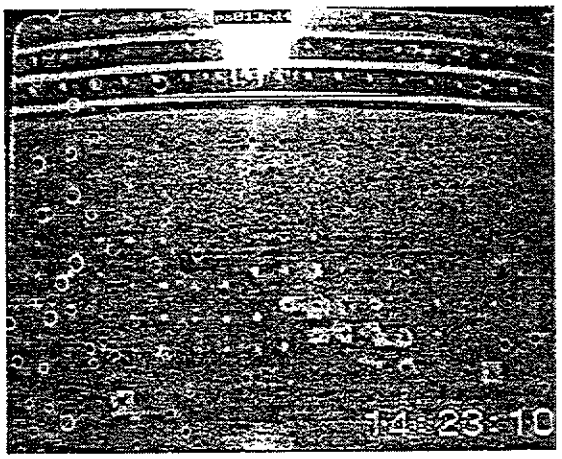

3rd Row (4)

Figure IV.2 a

GEOTECHNICAL CENTRIFUGE TEST PS01

SUBSIDENCE DEVELOPMENT

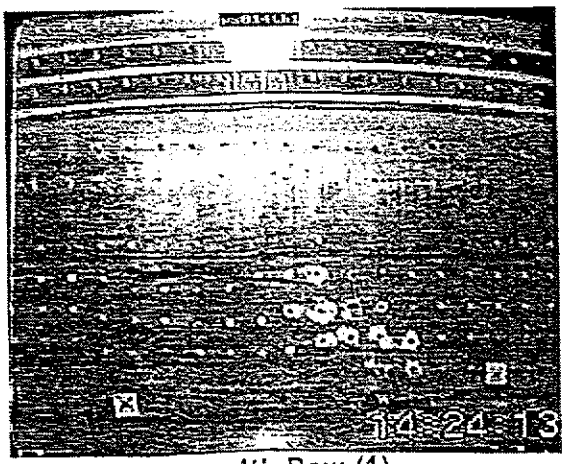

4th Row (1)

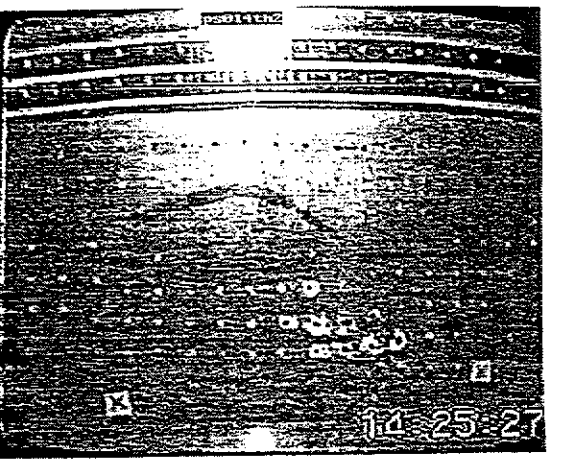

4th Row (2)

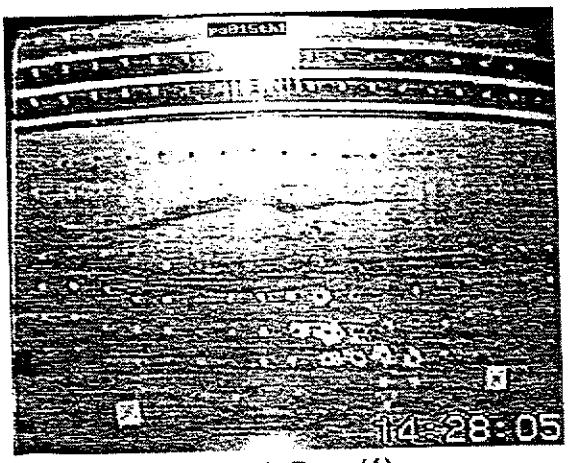

5th Row (1)

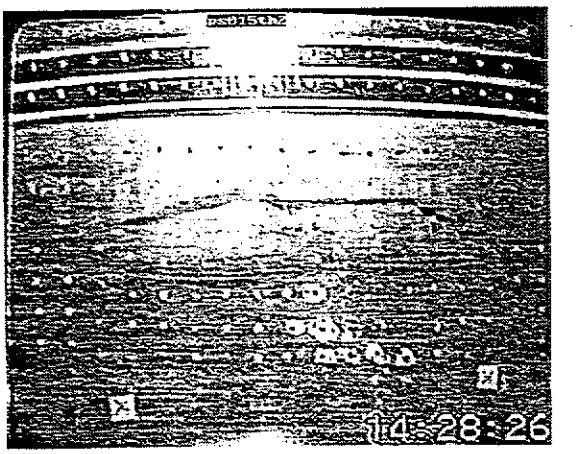

5th Row (2)

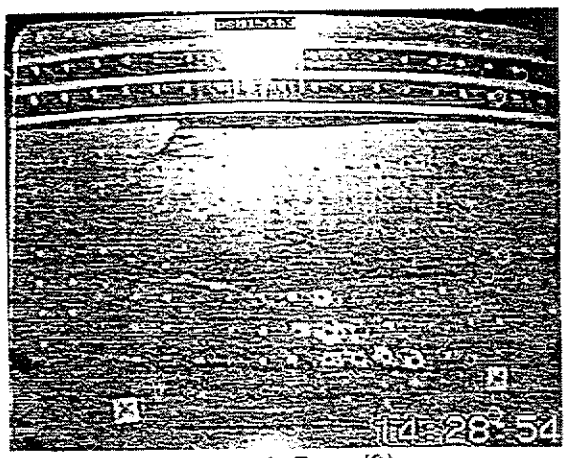

5th Row (3)

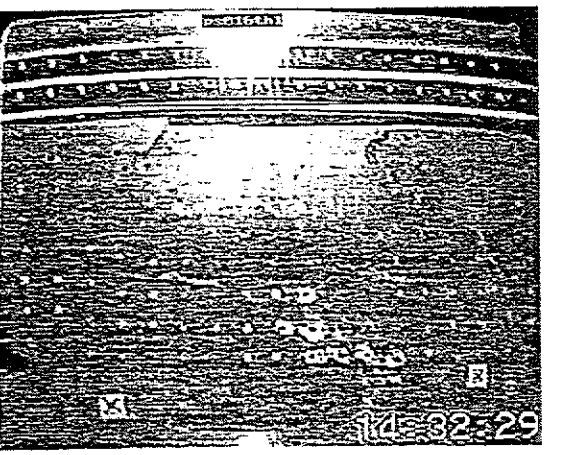

6th Row (1)

Figure IV.2 a

GEOTECHNICAL CENTRIFUGE TEST PS01

SUBSIDENCE DEVELOPMENT

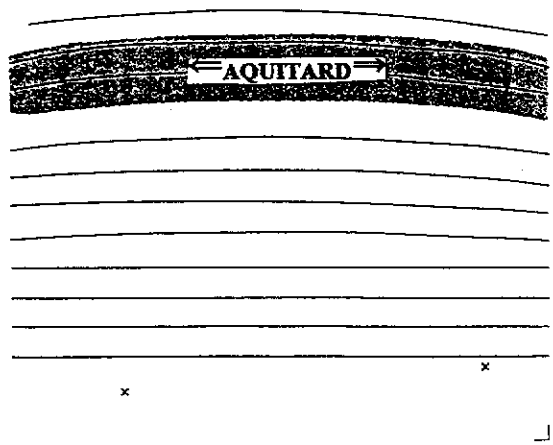

Control

1st Row

2nd Row

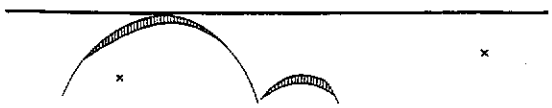

3rd Row (2)

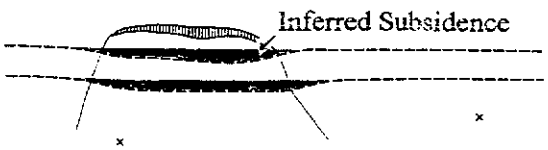

3rd Row (3)

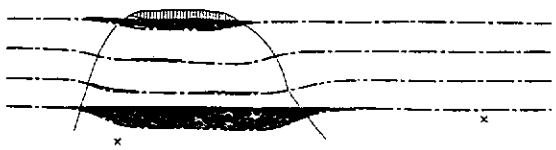

3rd Row (4)

Figure IV.2 b

GEOTECHNICAL CENTRIFUGE TEST PS01

SUBSIDENCE DEVELOPMENT

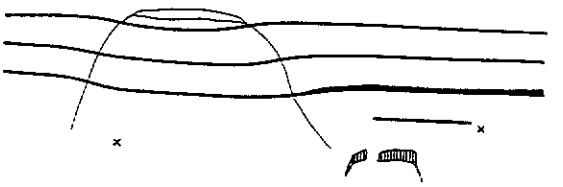

4th Row (1)

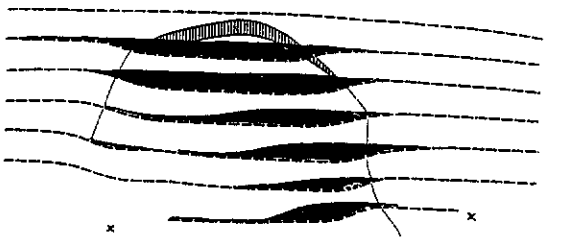

4th Row (2)

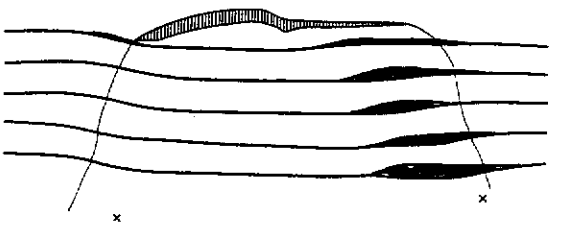

5th Row (1)

5th Row (2)

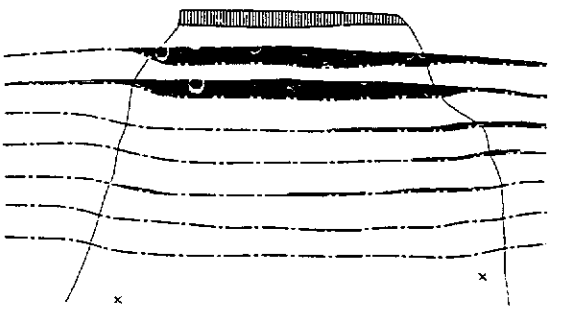

5th Row (3)

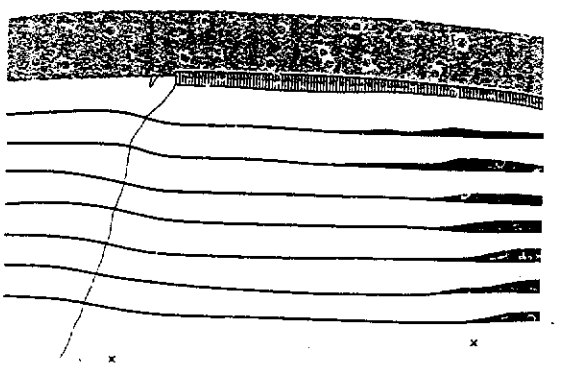

6th Row (1)

Figure IV.2 b

GEOTECHNICAL CENTRIFUGE TEST PS01

SUBSIDENCE DEVELOPMENT

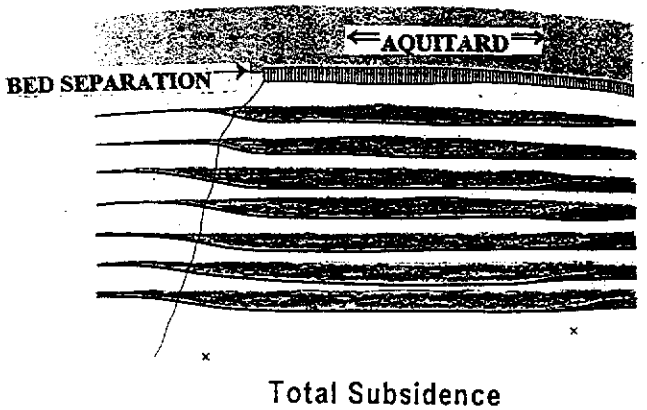

Figure IV.2 b

SUMMARY OF THE CAVING SEQUENCES OF CENTRIFUGE TEST PS01

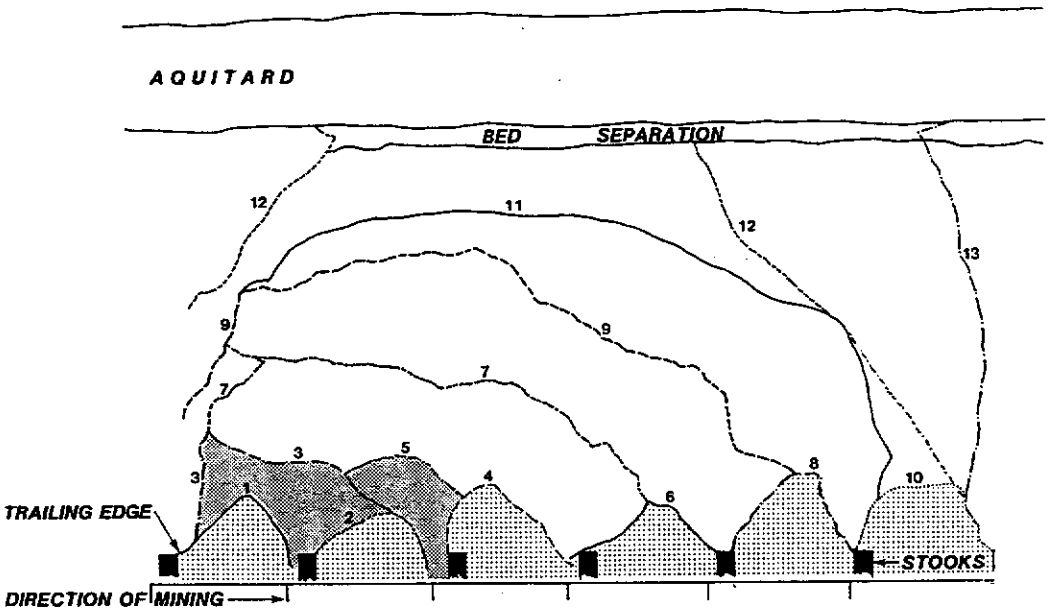

Figure IV.2c

POST-TEST BED SEPARATION BENEATH AQUITARD - CENTRIFUGE MODEL PS01

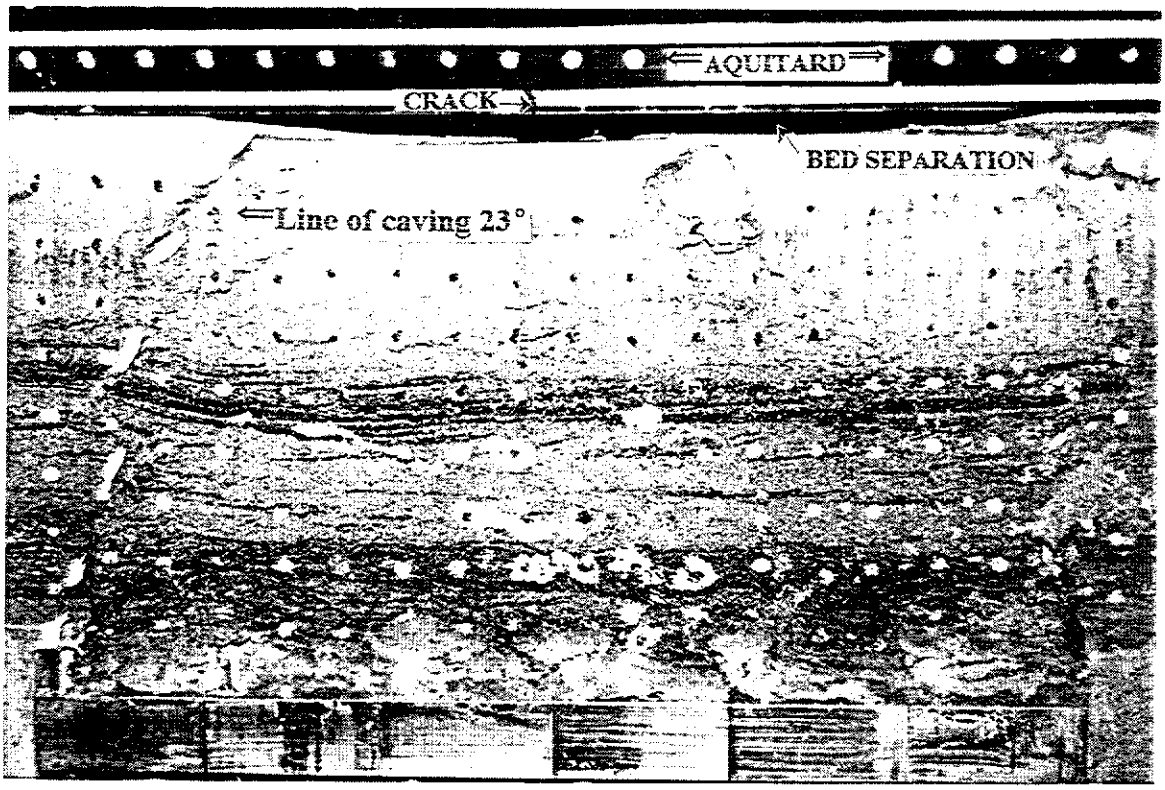

Figure IV.3 a

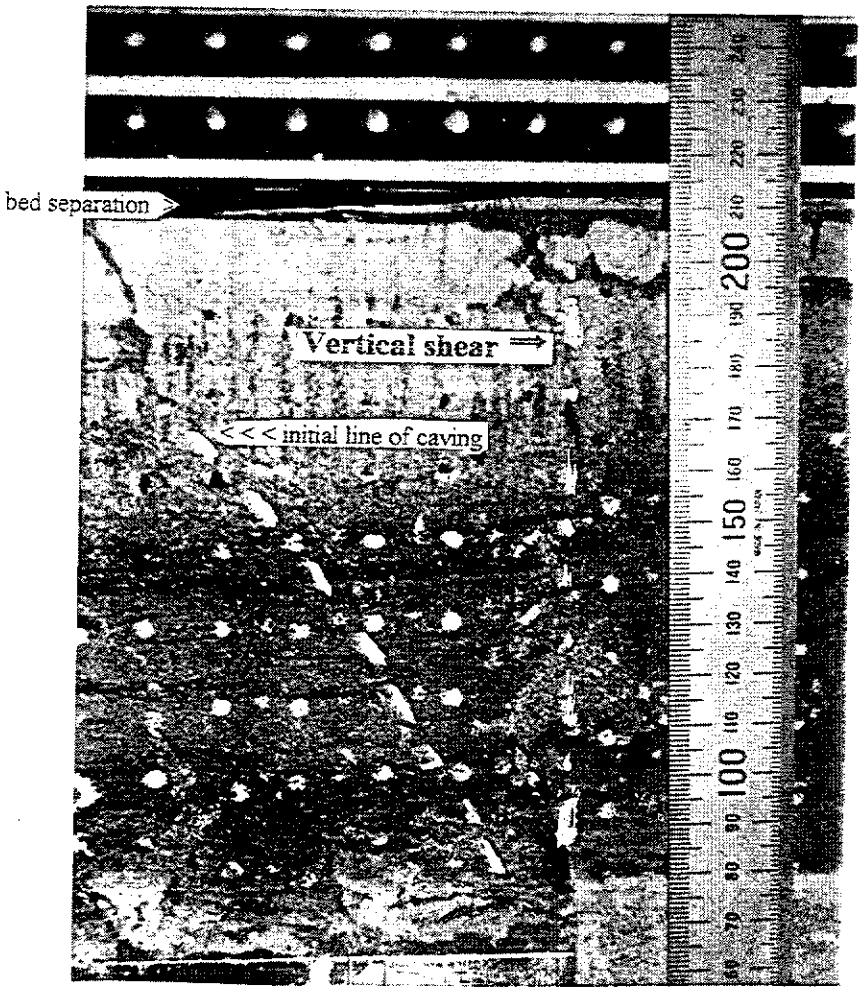

CAVING AT THE LEADING EDGE OF CENTRIFUGE MODEL PS01

Figure IV.3 b

STRAIN GAUGE DATA - CENTRIFUGE MODEL PS01

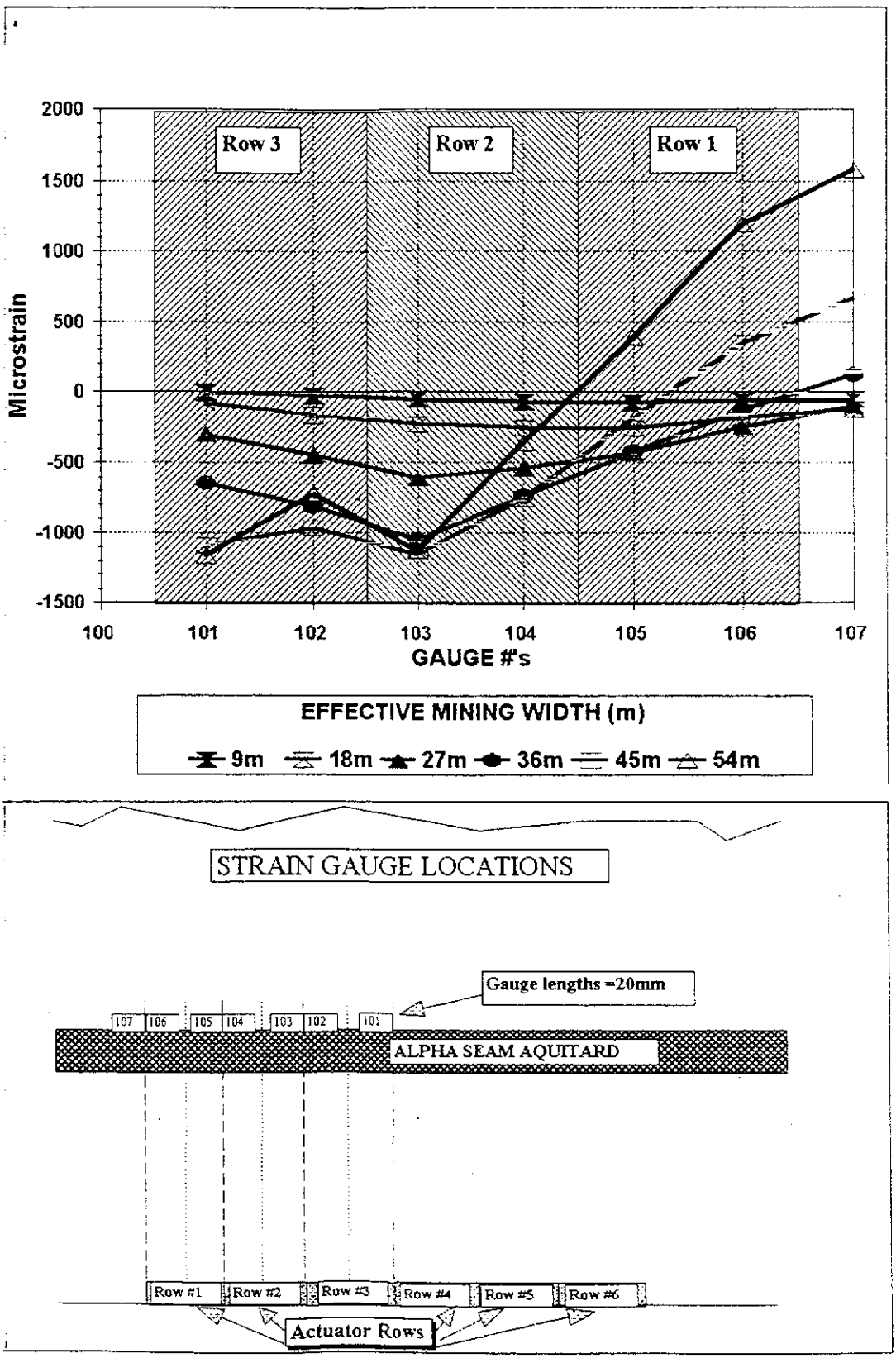

Figure IV.4

TABLE IV.1 SUMMARY OF CENTRIFUGE TEST PS01 STRAIN GAUGE DATA RAW DATA

ROW #	EFFECTIVE MINING WIDTH (m)	STRAIN GAUGE #'s 1 mstrain	2 mstrain	3 mstrain	4 mstrain	5 mstrain	6 mstrain	7 mstrain
0	0	-218	-141	-160	-202	-164	-171	-154
1	13	-214	-117	-86	-134	-87	-108	-103
2	26	-135	21	92	50	92	12	-35
3	39	79	305	269	337	268	81	-52
4	52	425	671	262	540	261	-43	-276
5	65	875	826	16	553	14	-513	-824
6	78	945	580	-547	155	-550	-1116	-1556

COMPACTED GOAF MATERIAL
CENTRIFUGE MODEL PS01

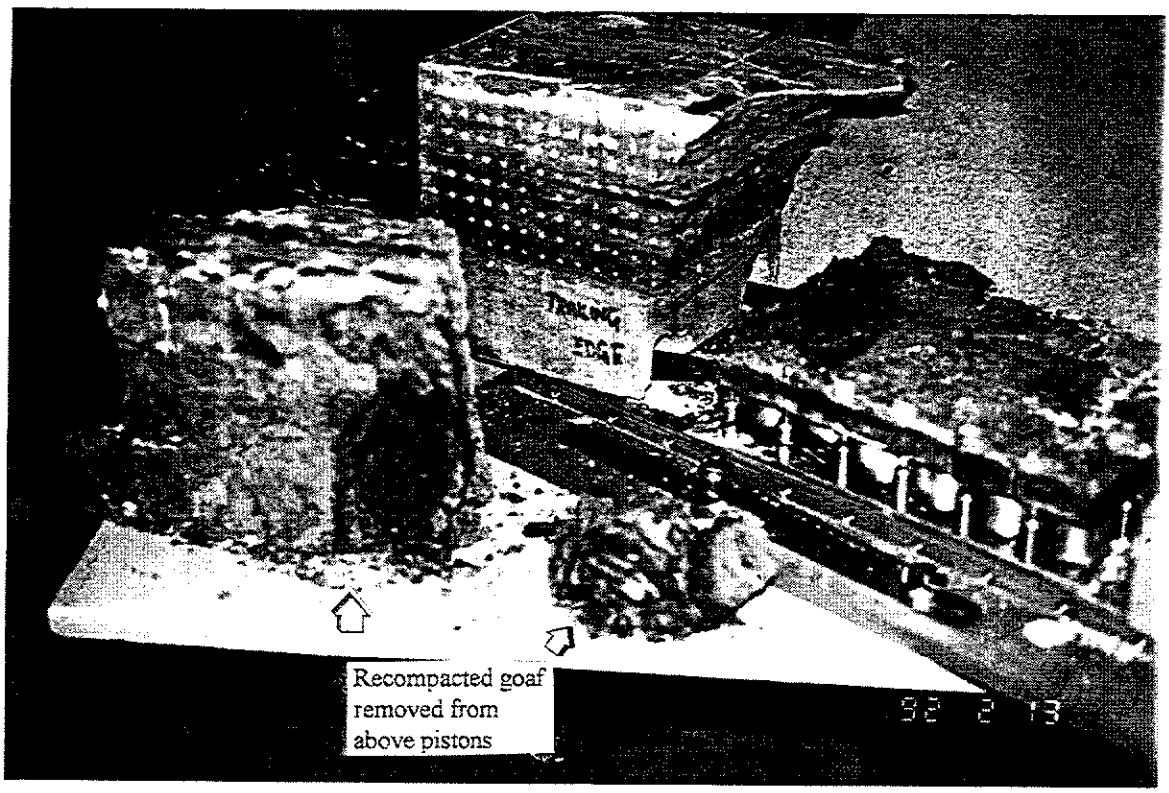

Figure IV.5

CRACK TRACING ON AQUITARD & FRONT OF CENTRIFUGE MODEL PS01

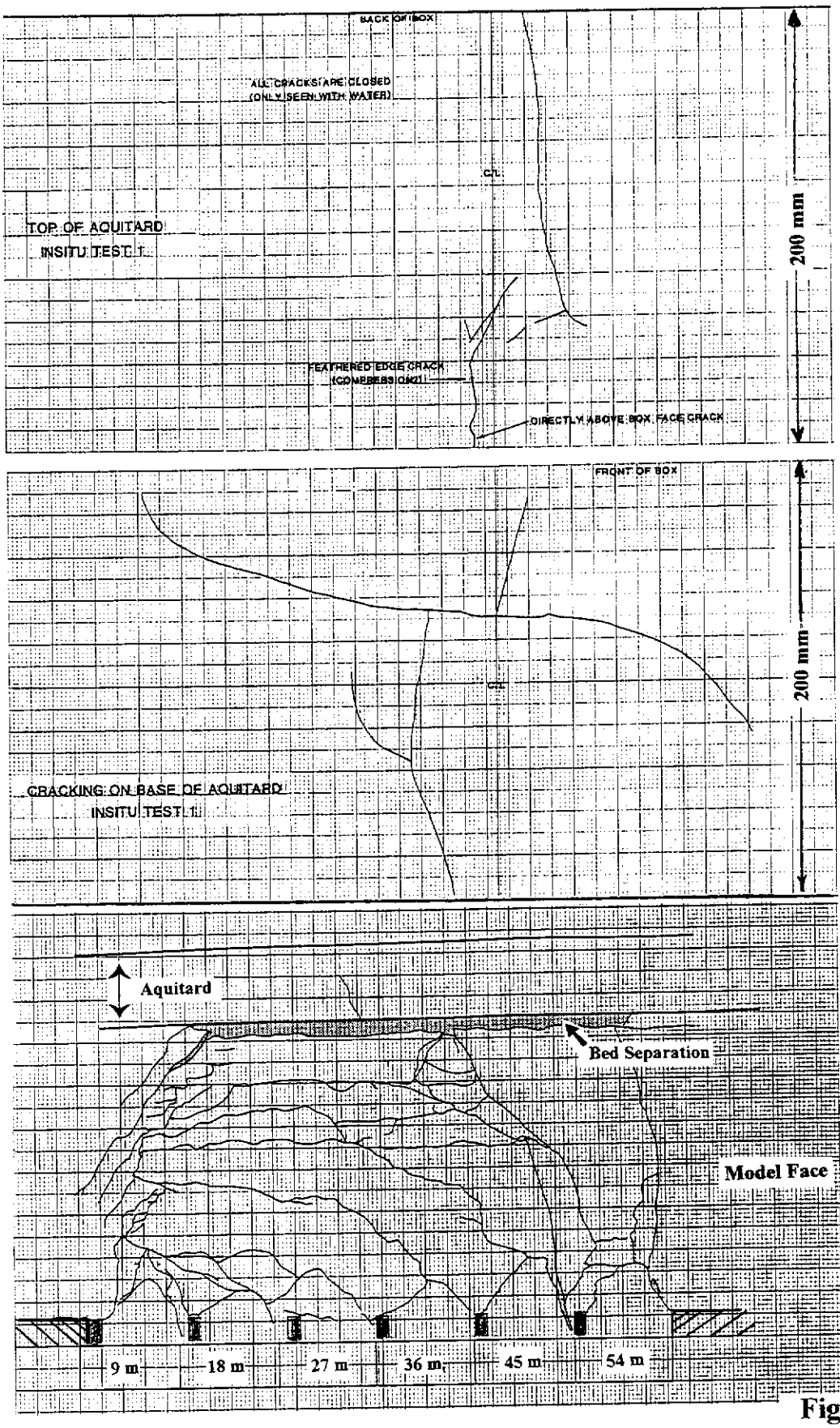

Figure IV.6

GEOTECHNICAL CENTRIFUGE TEST PS02

SUBSIDENCE DEVELOPMENT

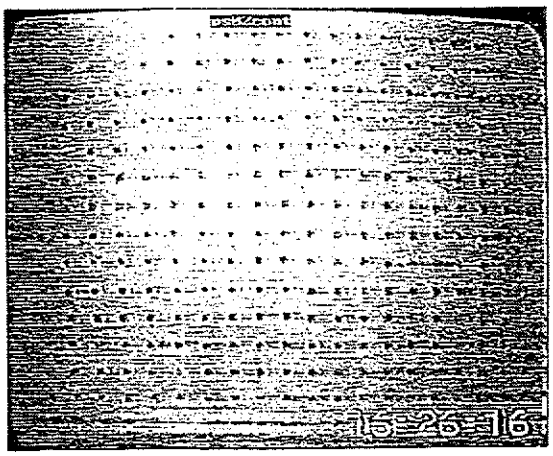

Control

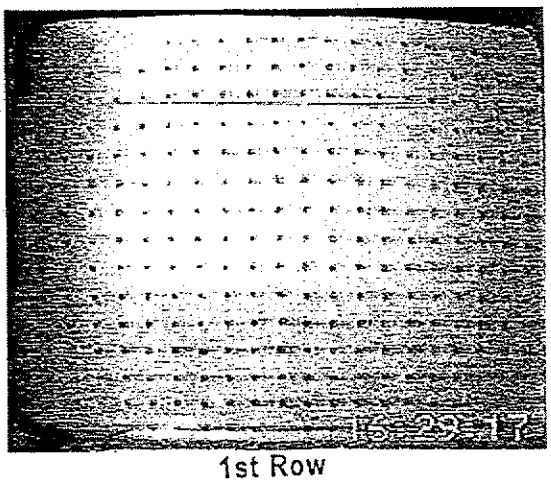

1st Row

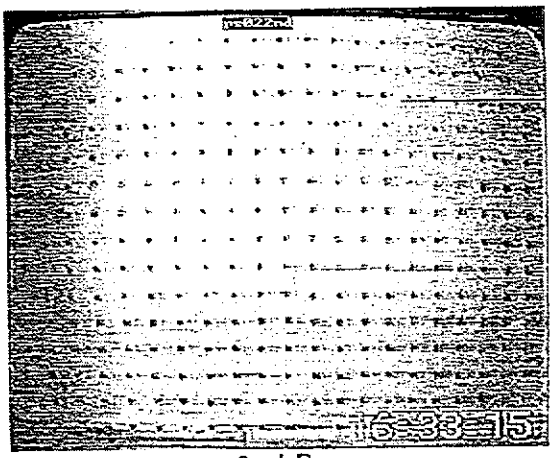

2nd Row

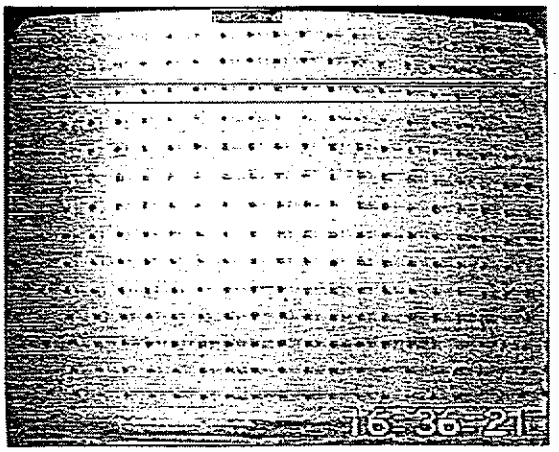

3rd Row

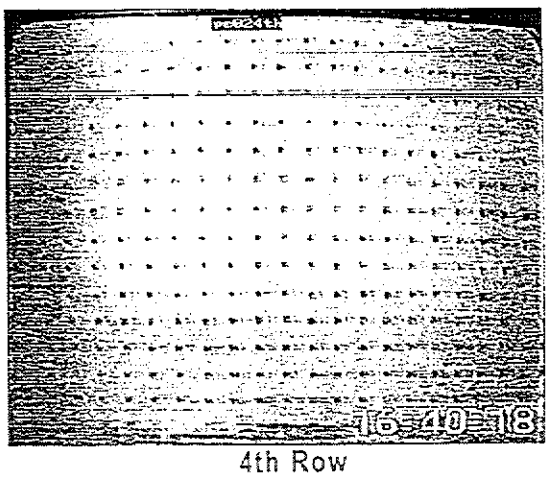

4th Row

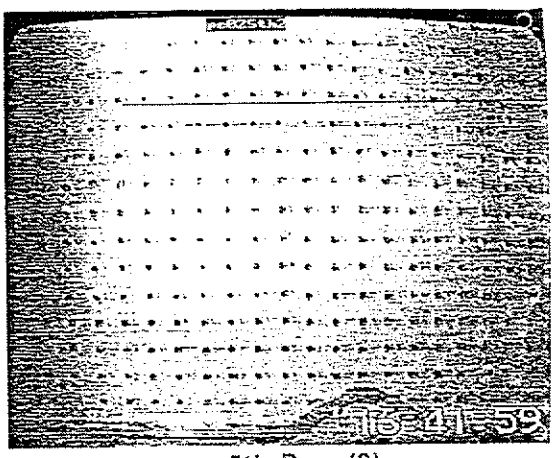

5th Row (2)

Figure IV.7 a

GEOTECHNICAL CENTRIFUGE TEST PS02

SUBSIDENCE DEVELOPMENT

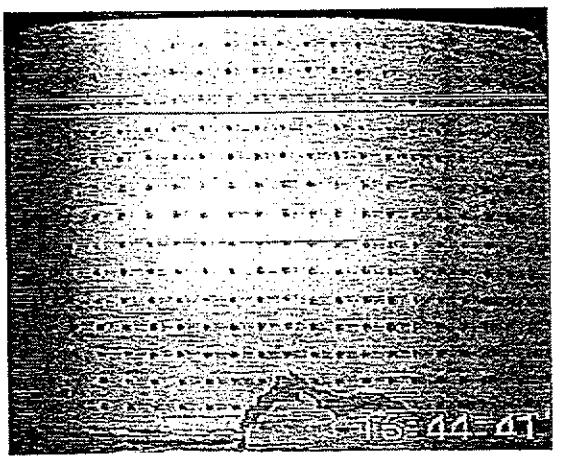

5th Row (4)

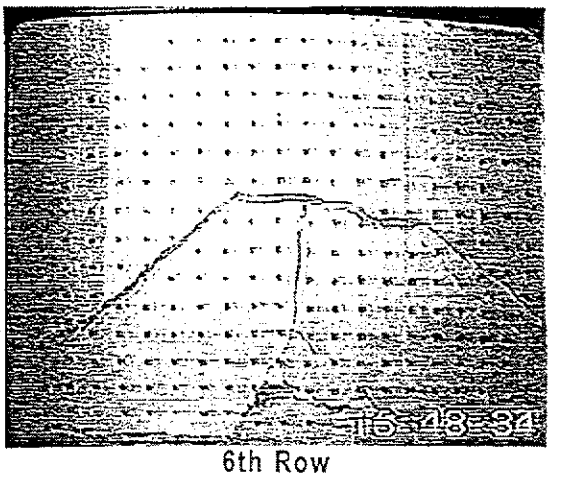

6th Row

Figure IV.7 a

GEOTECHNICAL CENTRIFUGE TEST PS02

SUBSIDENCE DEVELOPMENT

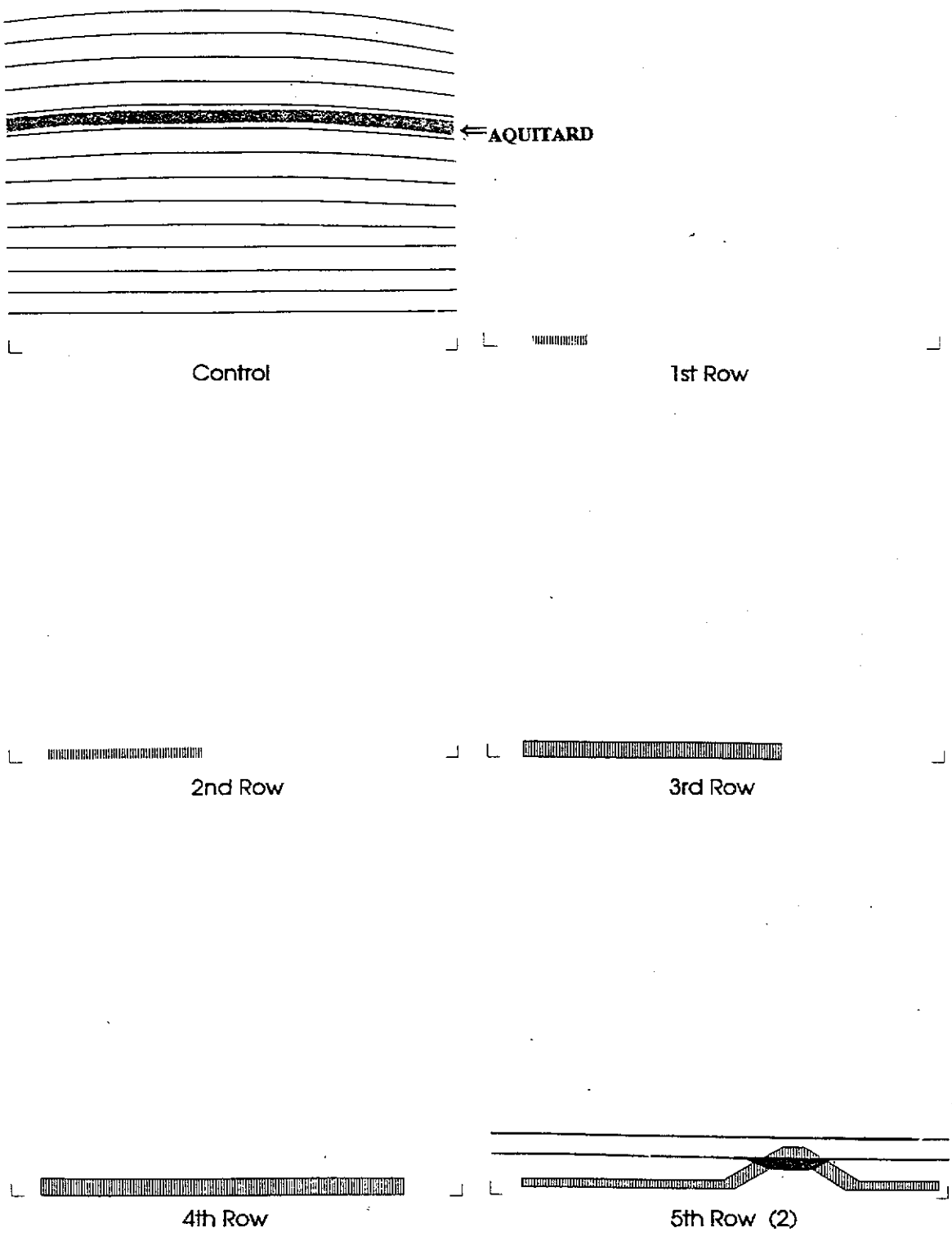

Figure IV.7 b

GEOTECHNICAL CENTRIFUGE TEST PS02
SUBSIDENCE DEVELOPMENT

5th Row (4)

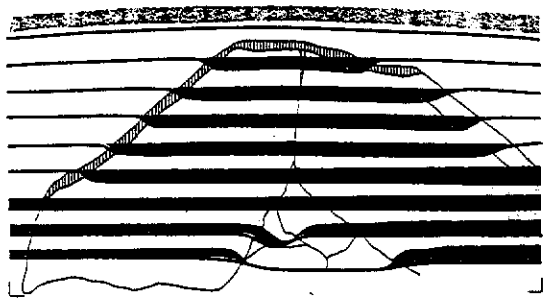

6th Row

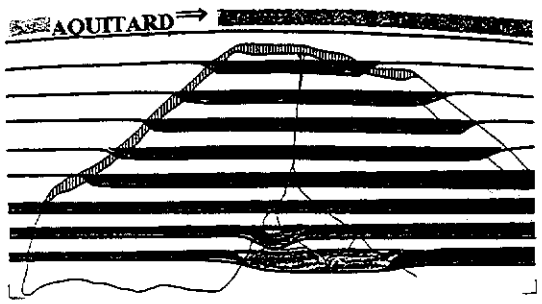

Total Subsidence

Figure IV.7 b

POST-TEST PHOTOGRAPH OF THE REAR OF CENTRIFUGE MODEL PS02

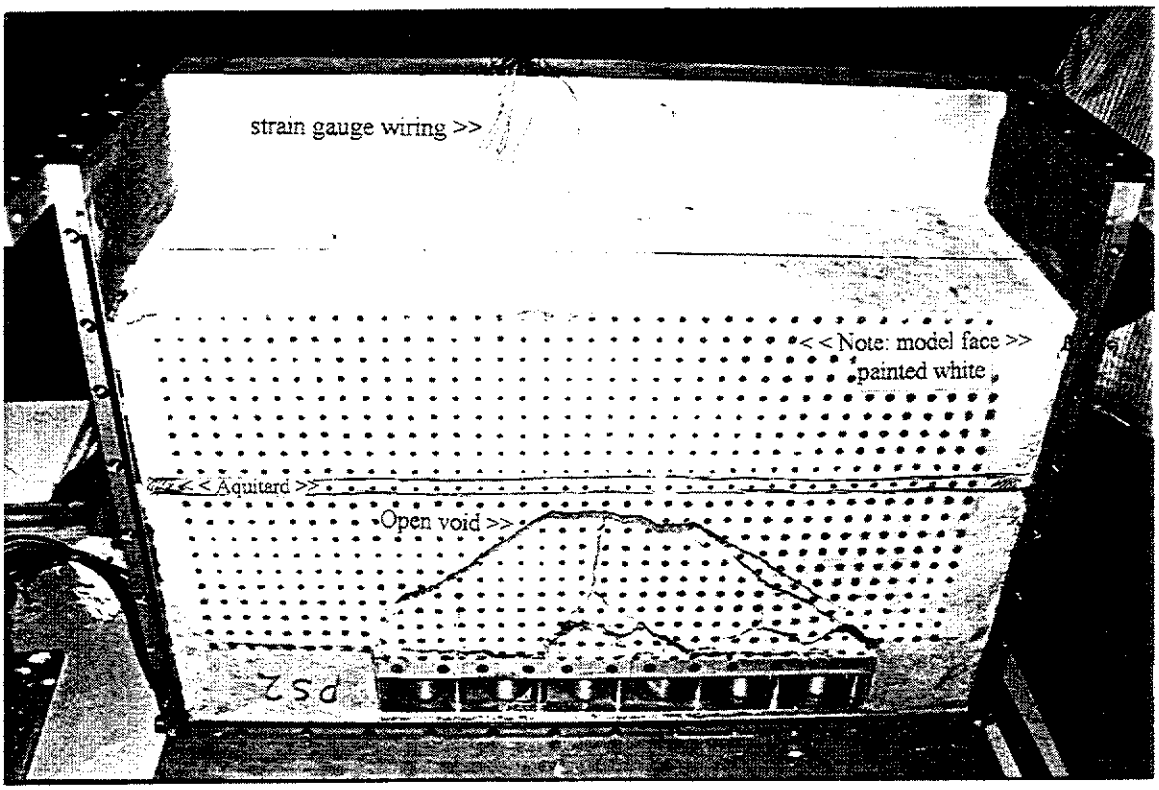

Figure IV.8 a

POST-TEST PHOTOGRAPH OF THE FRONT OF CENTRIFUGE MODEL PS02

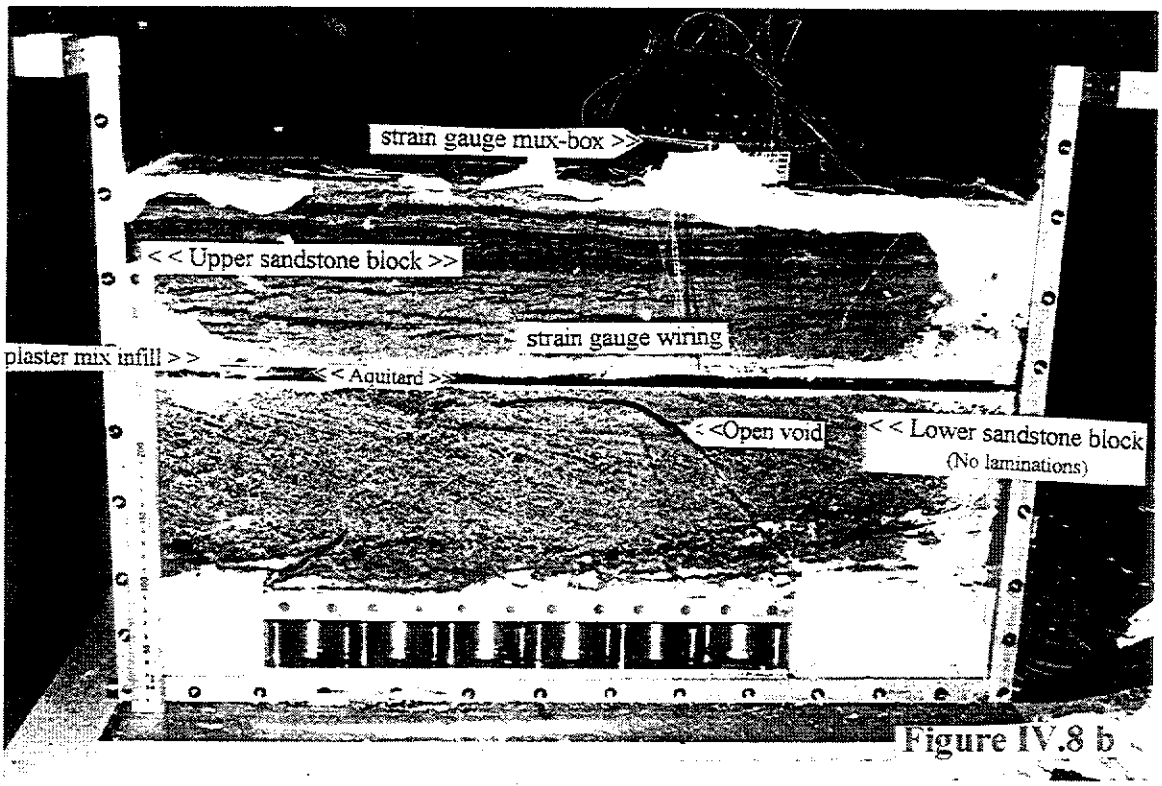

Figure IV.8 b

POST-TEST PHOTOGRAPHS OF THE LOW CAVING ANGLE & SUPPORTIVE OVERHANG - PS02

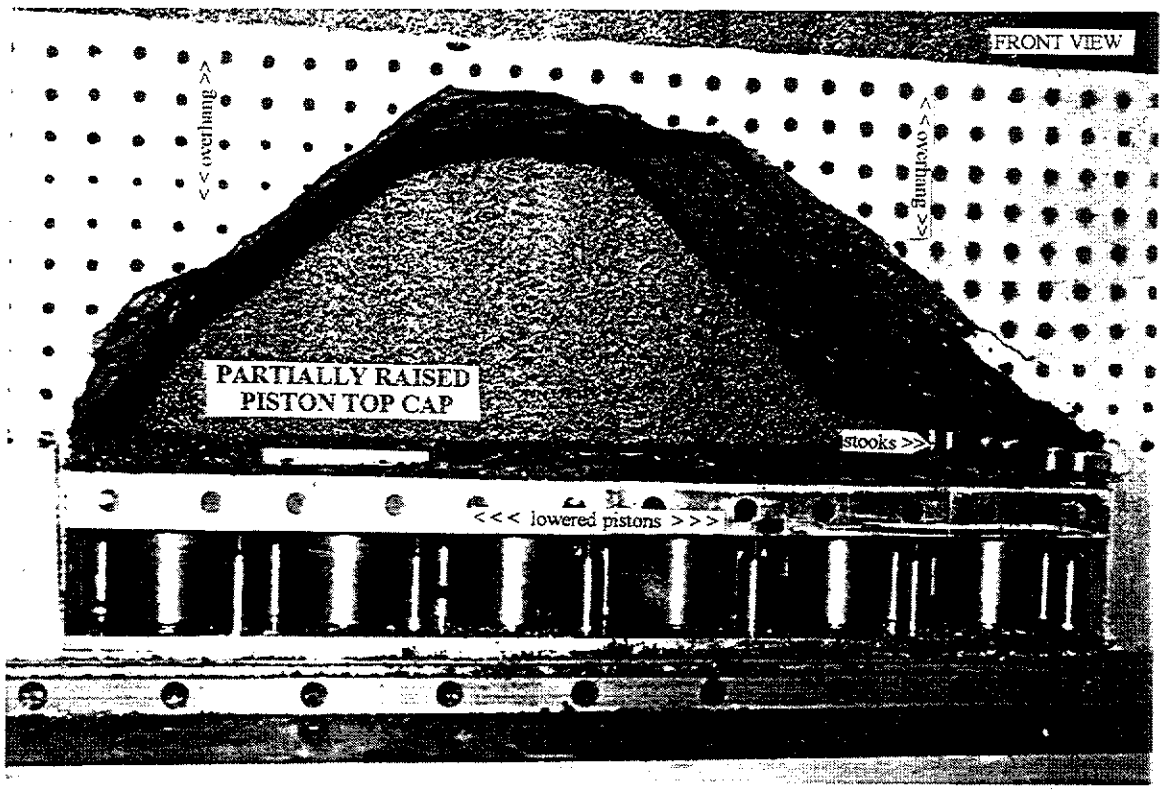

Figure IV.9 a

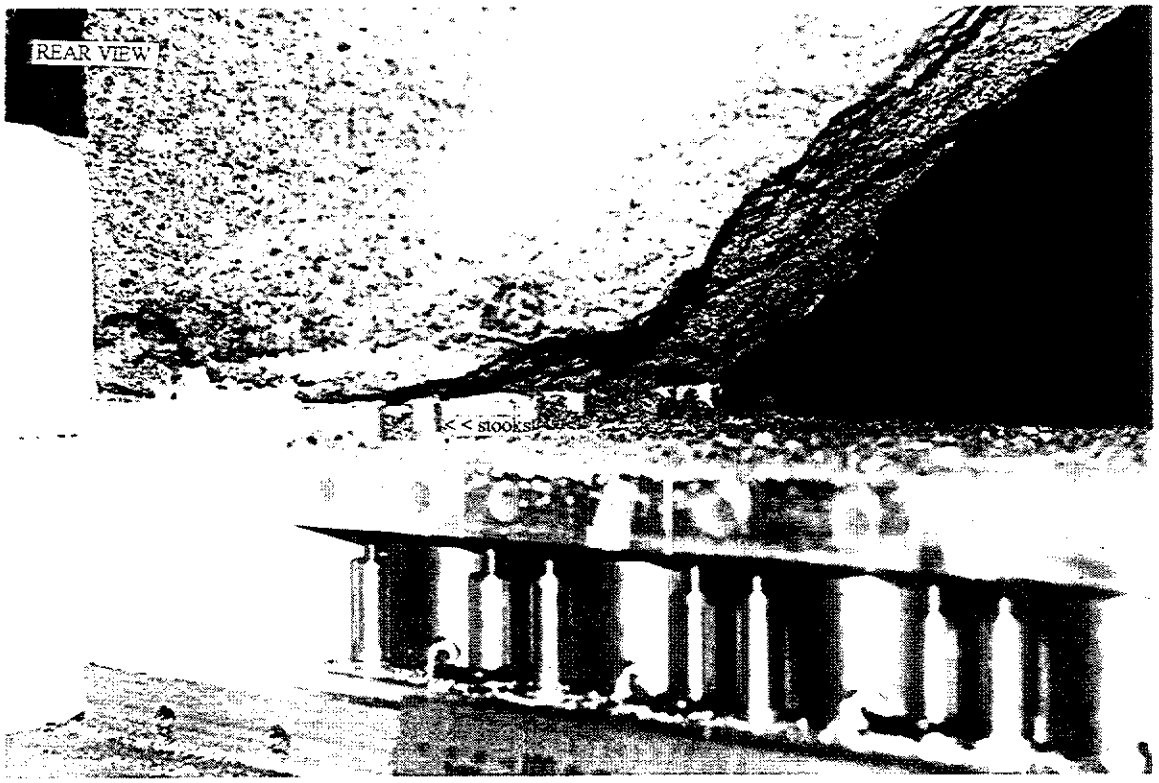

Figure IV.9 b

STRAIN GAUGE DATA - CENTRIFUGE MODEL PS02

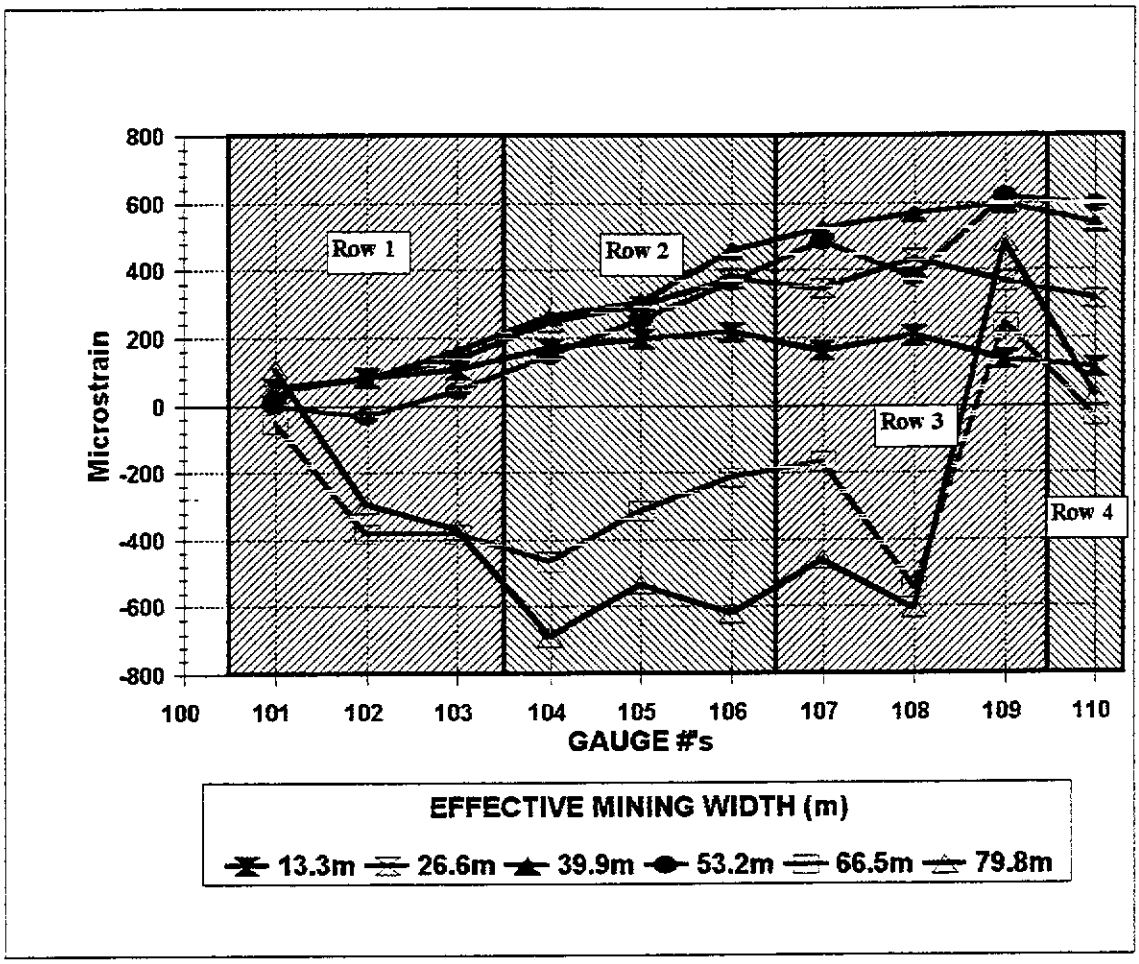

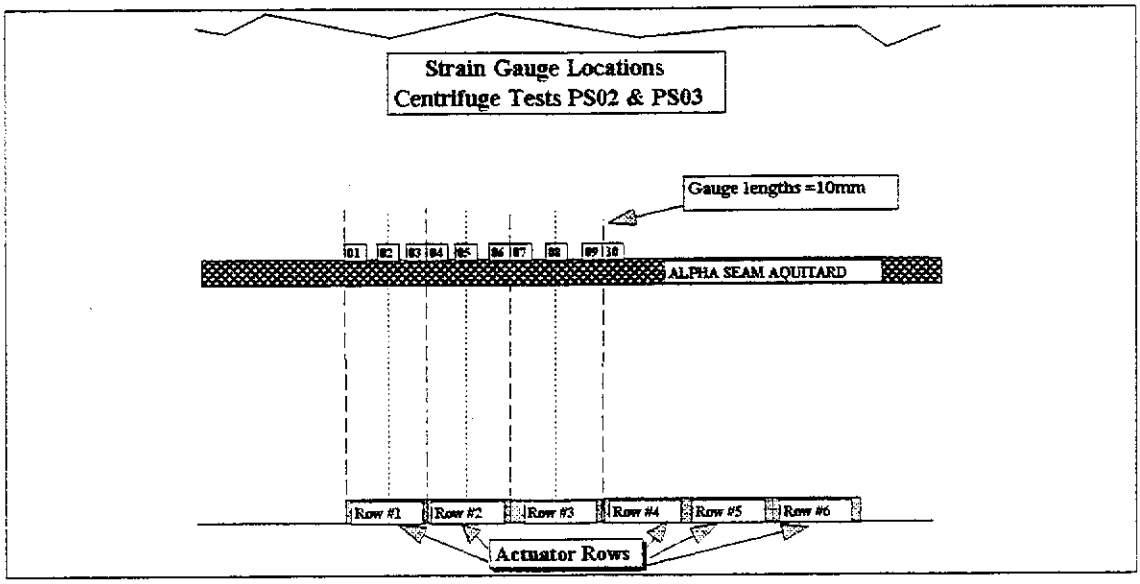

Figure IV.10

TABLE IV.2

SUMMARY OF CENTRIFUGE TEST PS02 STRAIN GAUGE DATA RAW DATA

ROW #	EFFECTIVE MINING WIDTH (m)	STRAIN GAUGE #'s									
		1	2	3	4	5	6	7	8	9	10
		mstrain	mstrain	mstrain	mstrain	mstrain	mstrain	mstrain	mstrain	mstrain	mstrain
0	0	37	54	56	34	82	47	17	52	24	32
1	20	92	136	163	204	280	265	179	260	163	146
2	40	73	140	194	282	378	422	363	486	391	346
3	60	82	135	217	299	387	505	540	621	621	570
4	80	37	22	101	181	336	411	503	428	643	626
5	100	-15	-327	-325	-430	-232	-166	-150	-492	267	0
6	120	146	-239	-312	-654	-450	-574	-443	-555	508	62

GEOTECHNICAL CENTRIFUGE TEST PS03

SUBSIDENCE DEVELOPMENT

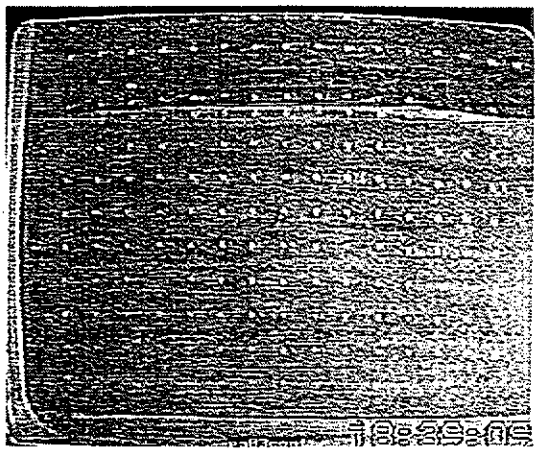

Control

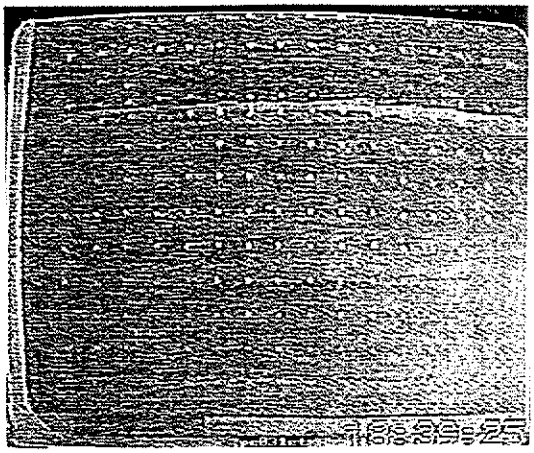

1st Row

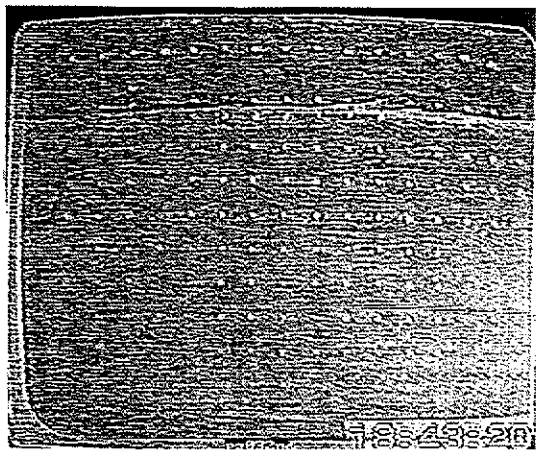

2nd Row

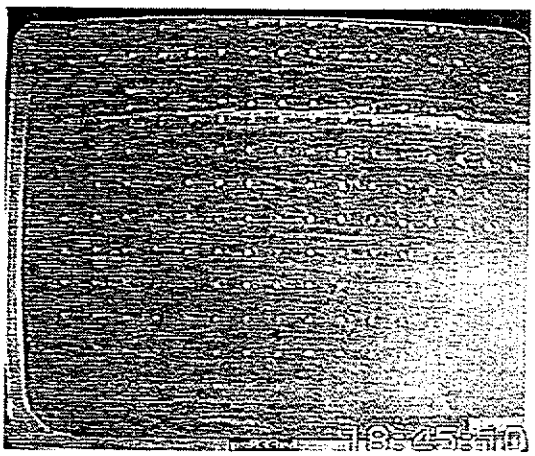

3rd Row

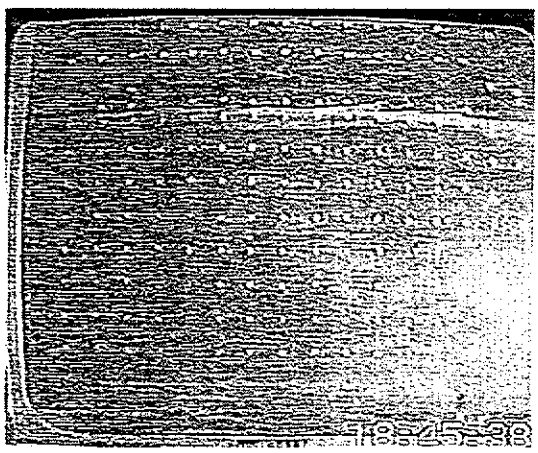

4th Row (1)

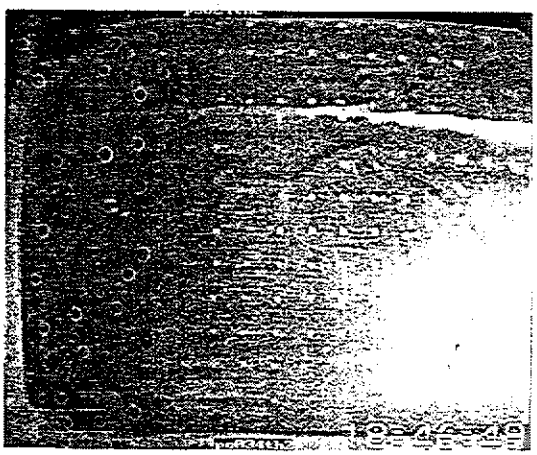

4th Row (2)

Figure IV.11 a

GEOTECHNICAL CENTRIFUGE TEST PS03

SUBSIDENCE DEVELOPMENT

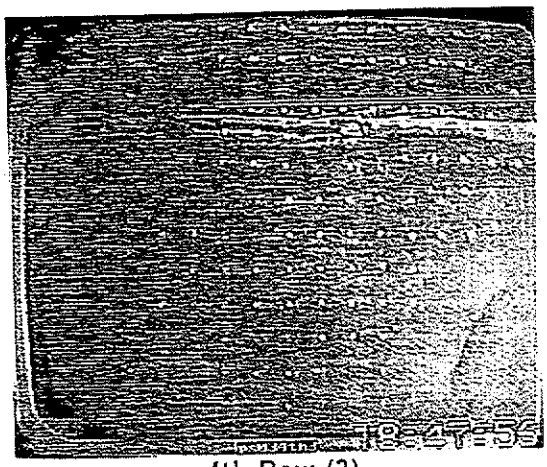

4th Row (3)

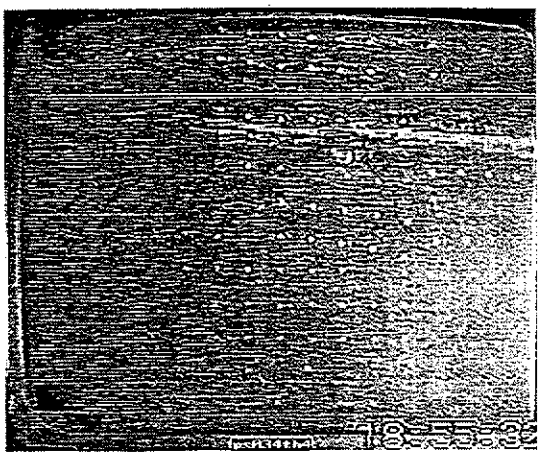

4th Row (4)

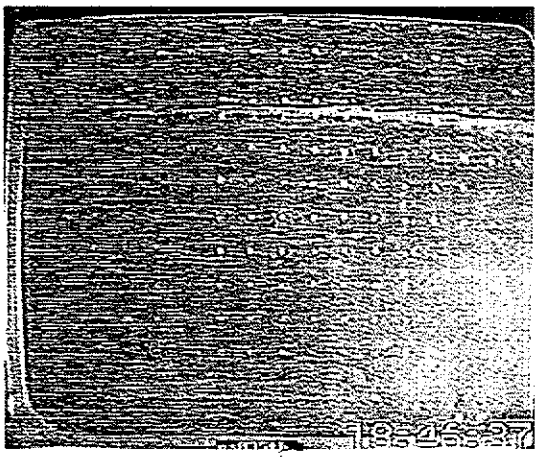

5th Row

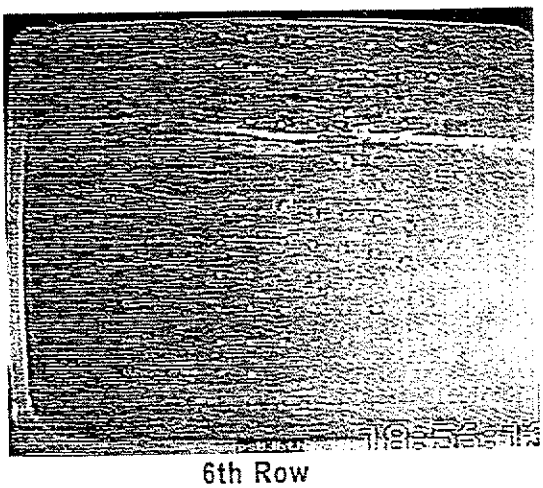

6th Row

Figure IV.11 a

GEOTECHNICAL CENTRIFUGE TEST PS03

SUBSIDENCE DEVELOPMENT

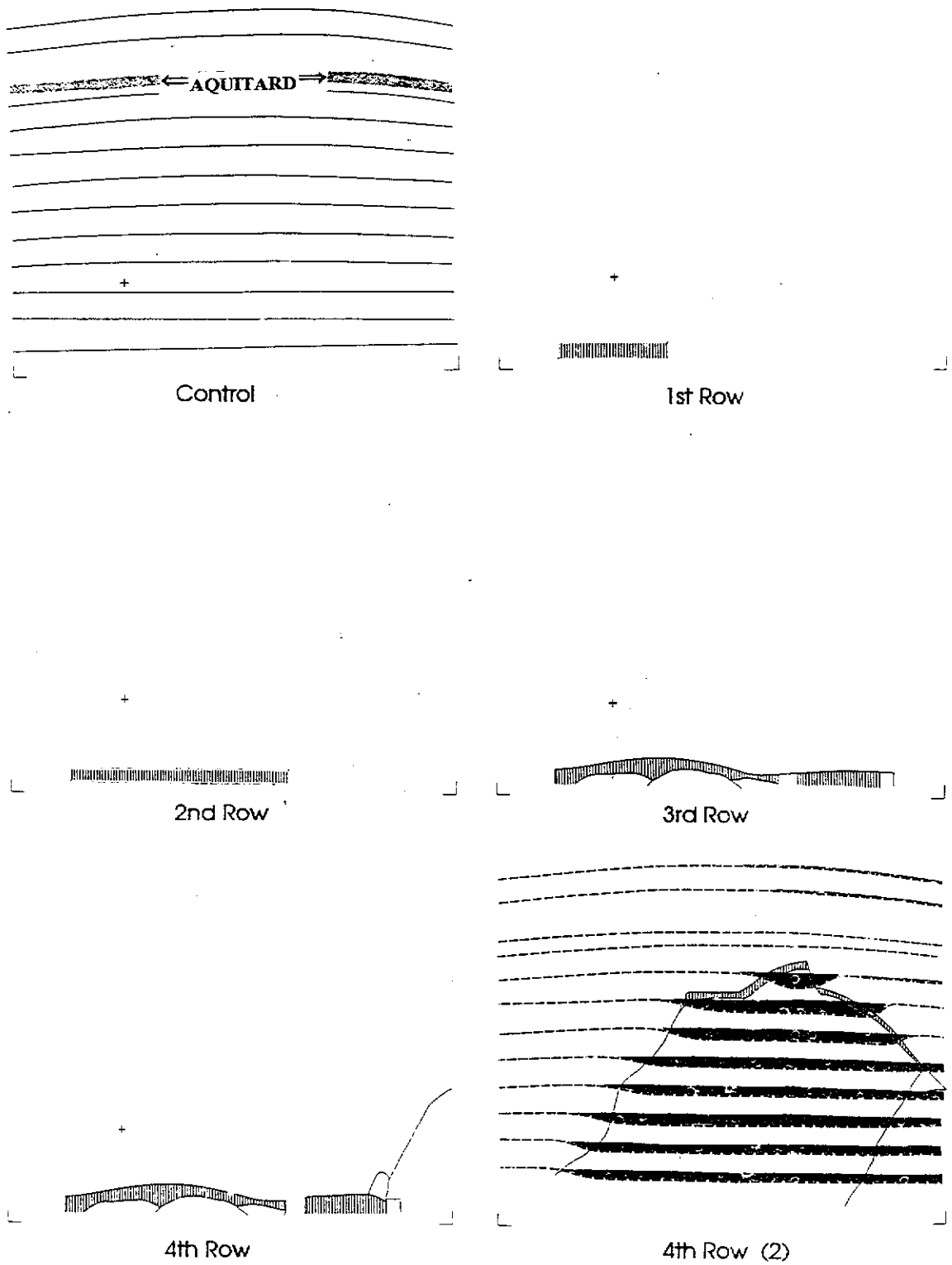

Figure IV.11 b

GEOTECHNICAL CENTRIFUGE TEST PS03

SUBSIDENCE DEVELOPMENT

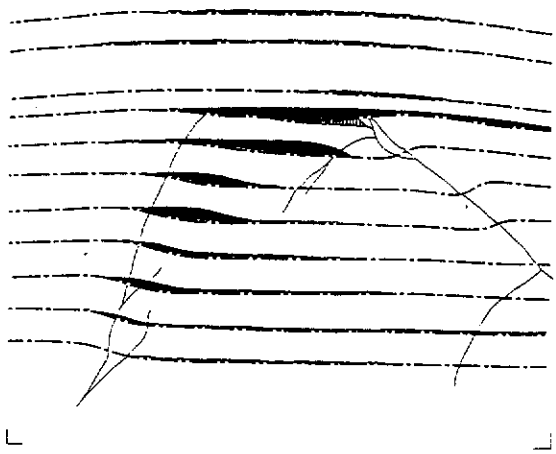

4th Row (3)

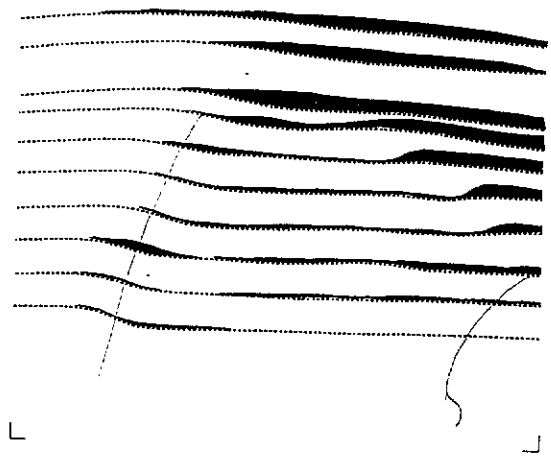

4th Row (4)

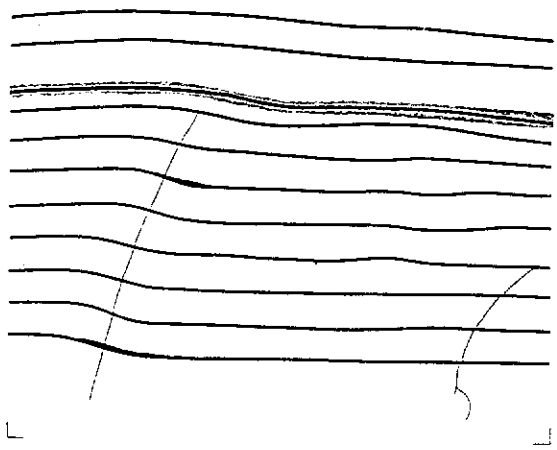

5th Row

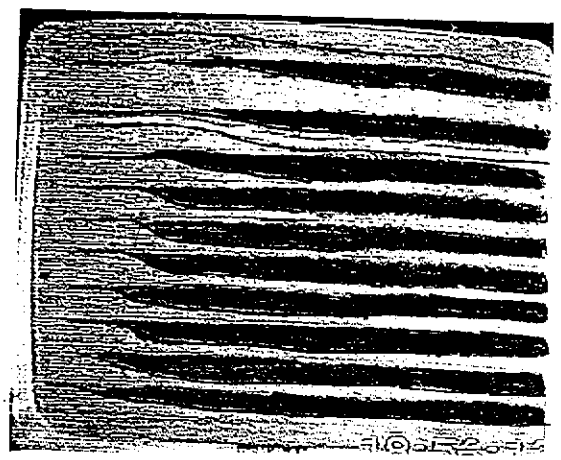

Total Subsidence

Figure IV.11 b

CRACK TRACING ON FRONT OF CENTRIFUGE MODEL PS03

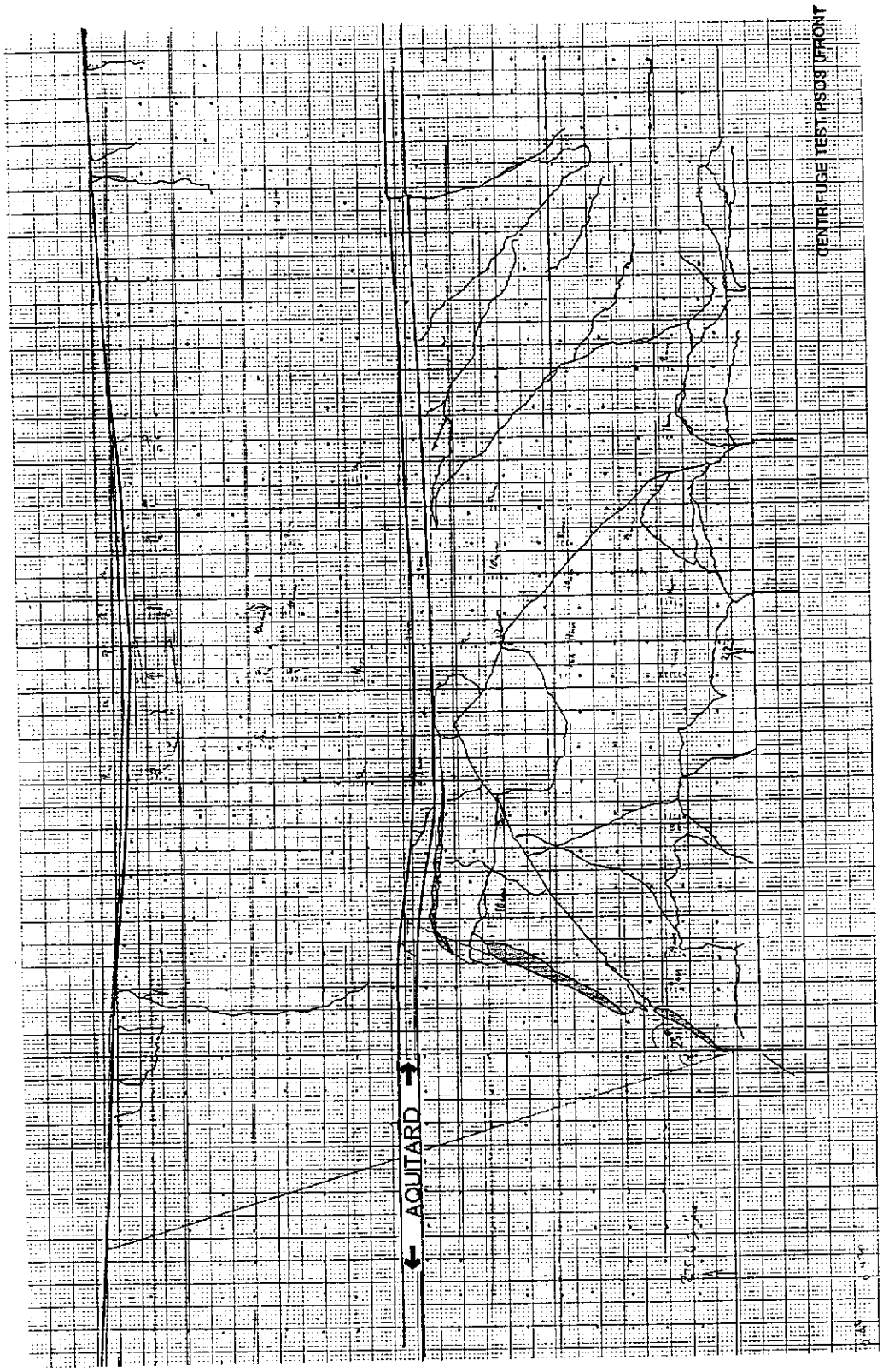

Figure IV.12

STRAIN GAUGE DATA - CENTRIFUGE MODEL PS03

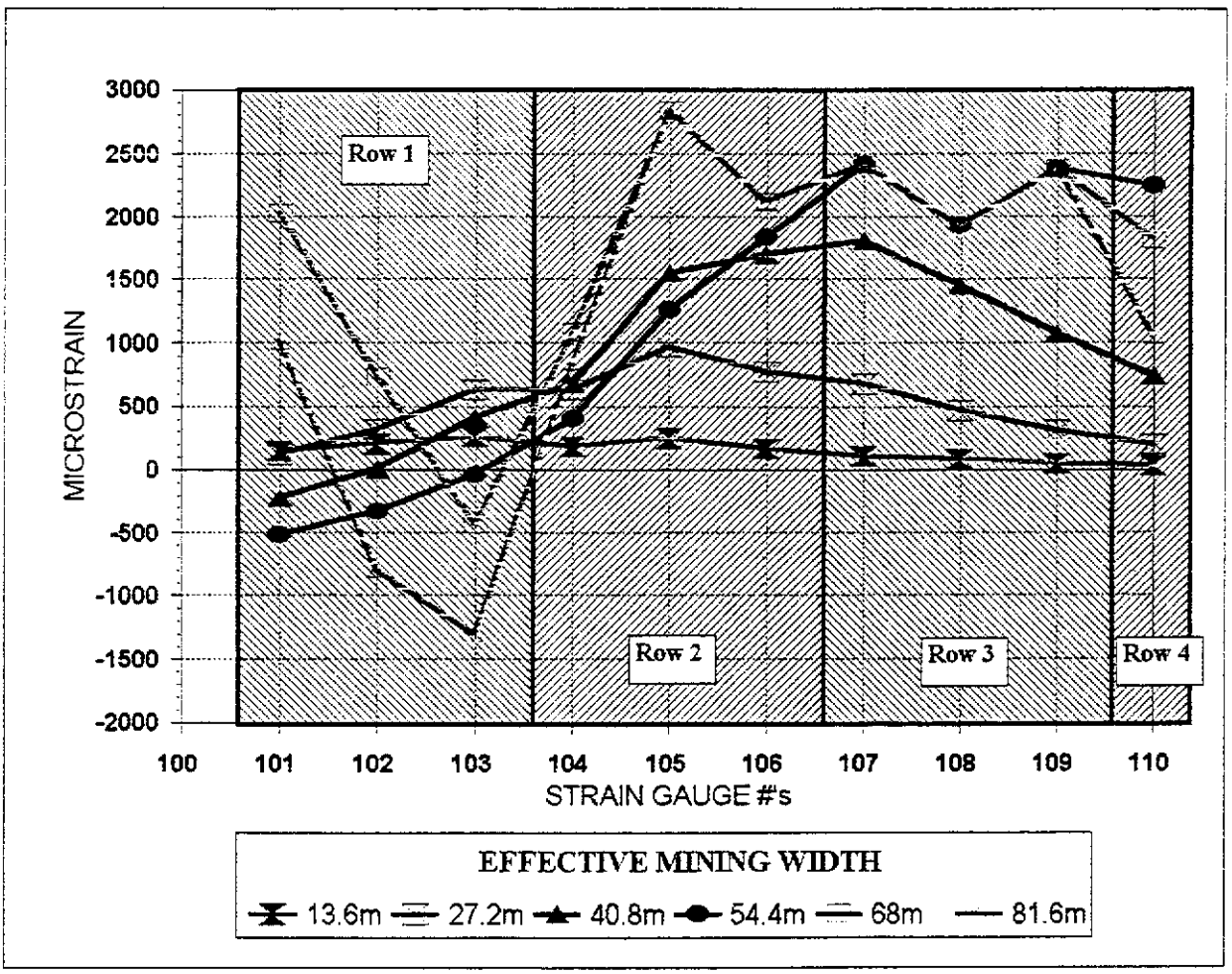

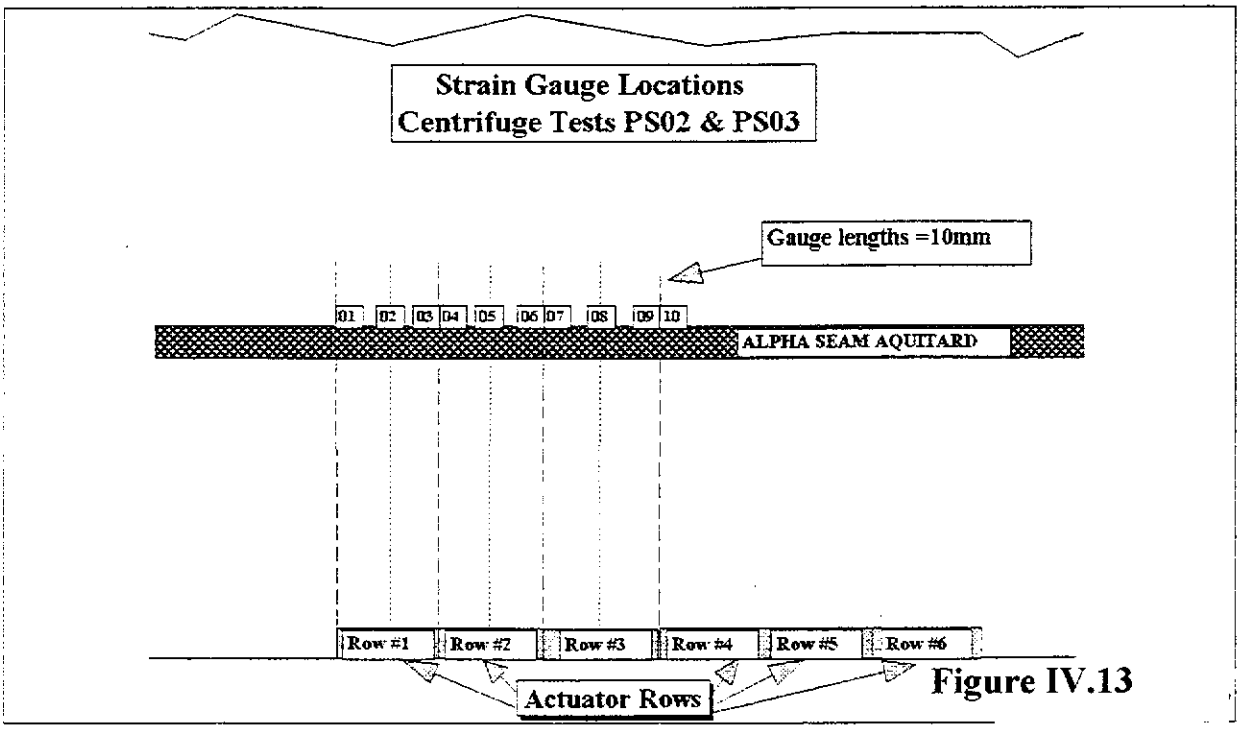

Figure IV.13

TABLE IV.3

SUMMARY OF CENTRIFUGE TEST PS03 STRAIN GAUGE DATA RAW DATA

ROW #	EFFECTIVE MINING WIDTH (m)	STRAIN GAUGE #'s 1	2	3	4	5	6	7	8	9	10
		mstrain	mstrain	mstrain	mstrain	mstrain	mstrain	mstrain	mstrain	mstrain	mstrain
0	0	-4	-9	-2	-17	7	4	7	24	13	47
1	13	299	396	508	350	478	333	224	185	112	121
2	26	237	617	1224	1206	1828	1510	1327	938	626	445
3	39	-428	7	804	1303	2904	3282	3499	2820	2091	1491
4	52	-989	-645	-71	768	2362	3536	4665	3747	4605	4381
5	65	3912	1420	-824	2088	5321	4095	4667	3747	4605	3560
6	78	1951	-1548	-2499	1634	5321	4095	4667	3747	4605	2086

POST-TEST PHOTOGRAPH OF THE LEADING EDGE AT THE REAR OF CENTRIFUGE MODEL PS03

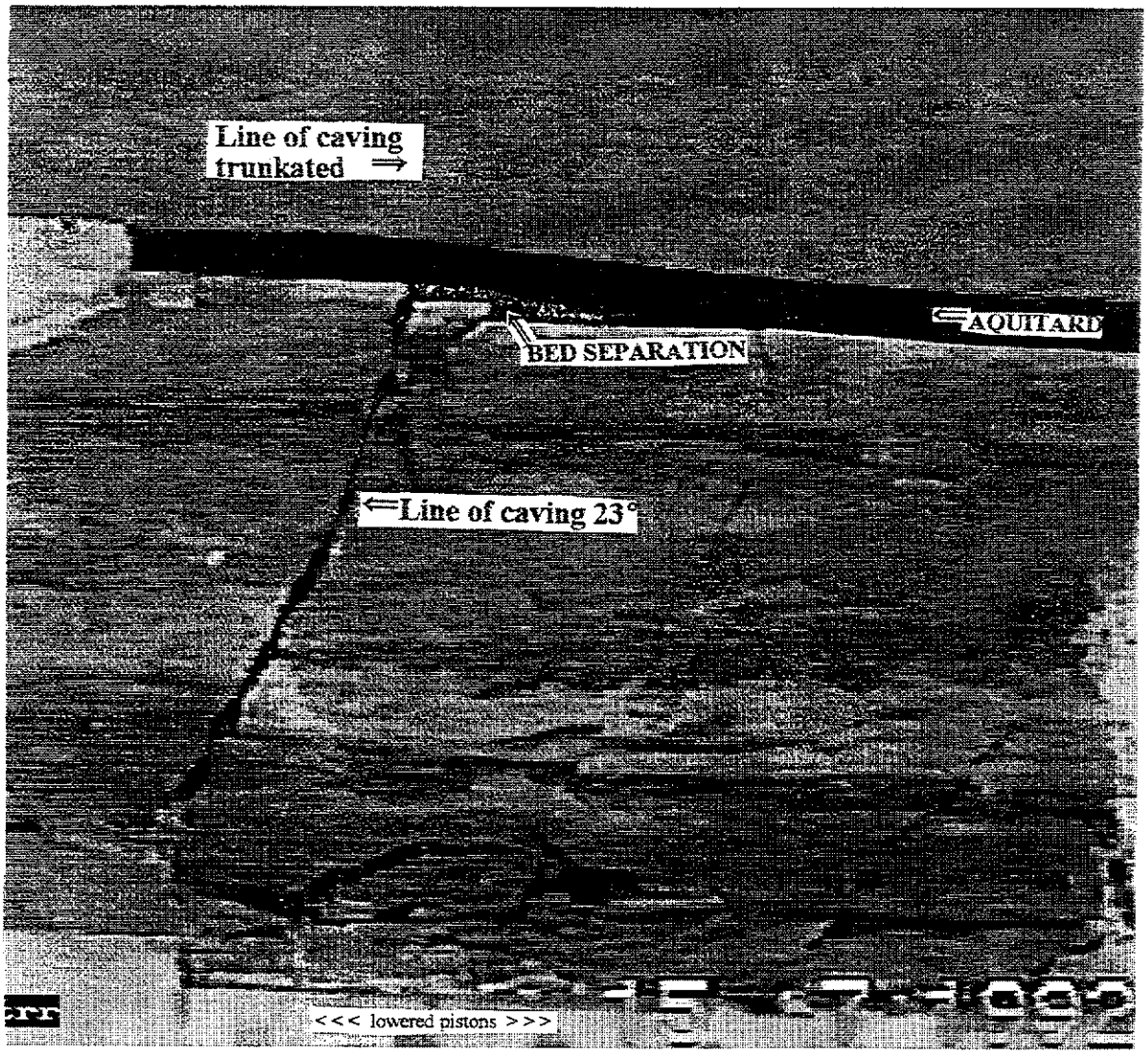

Figure IV.14

STRAIN GAUGE LAYOUT FOR CENTRIFUGE MODELS PS04 & PS05

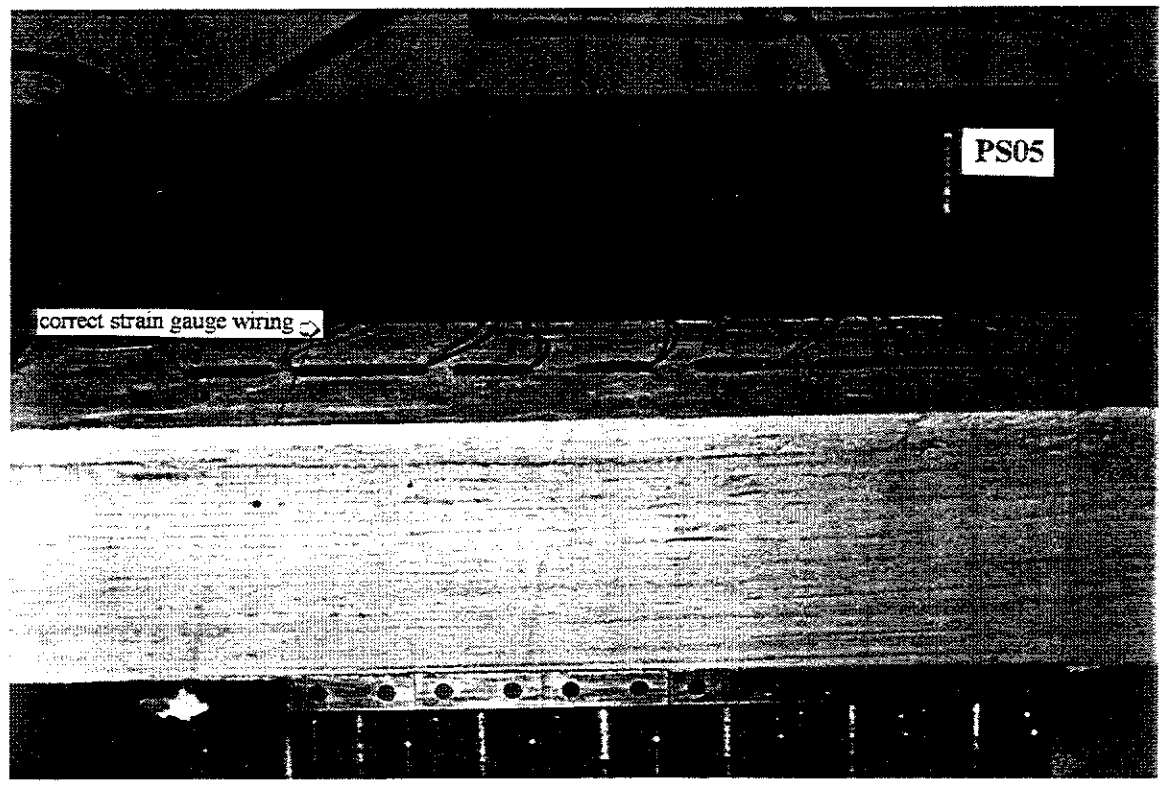

Figure IV.15

GEOTECHNICAL CENTRIFUGE TEST PS04

SUBSIDENCE DEVELOPMENT

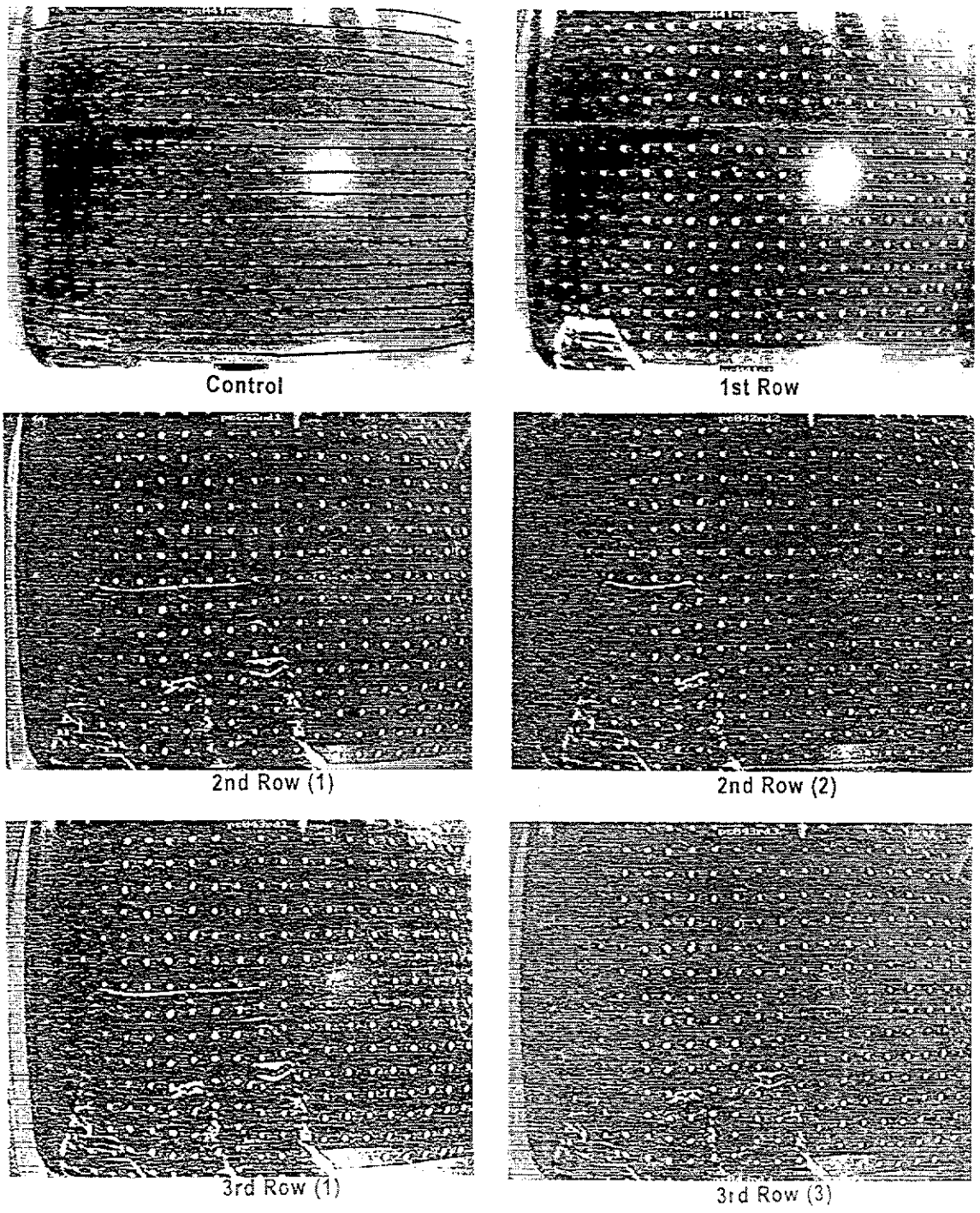

Figure IV.16 a

GEOTECHNICAL CENTRIFUGE TEST PS04

SUBSIDENCE DEVELOPMENT

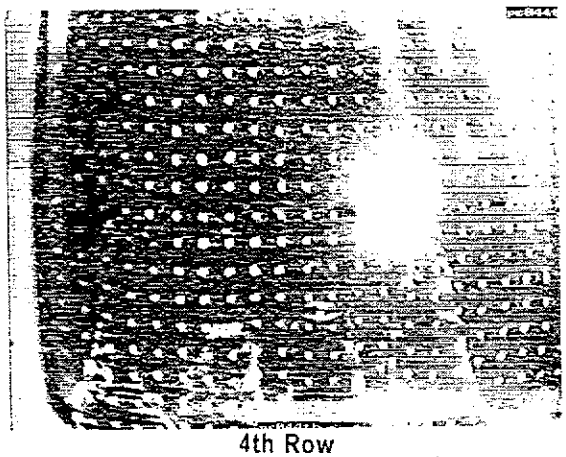

4th Row

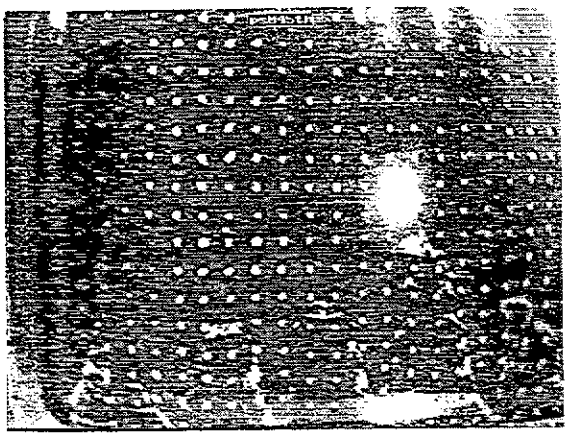

5th Row

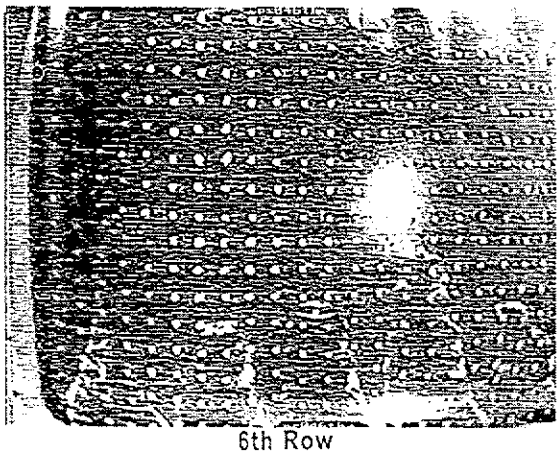

6th Row

Figure IV.16 a

GEOTECHNICAL CENTRIFUGE TEST PS04

SUBSIDENCE DEVELOPMENT

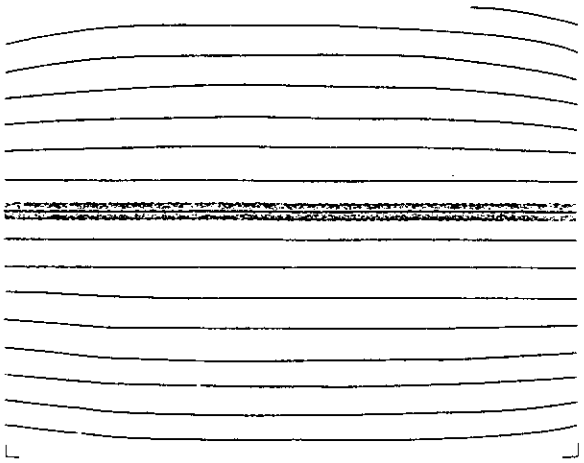

Control

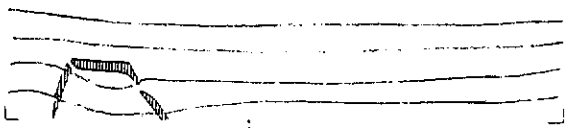

1st Row

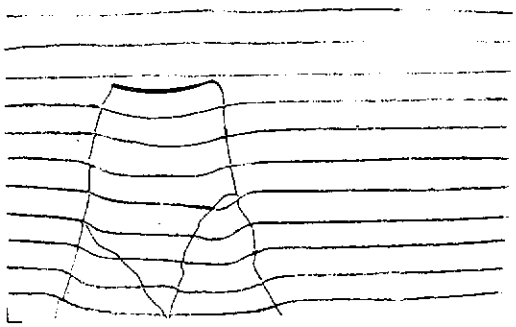

2nd Row (1)

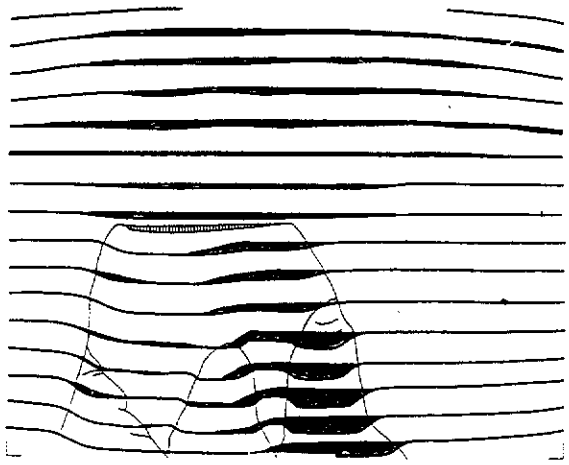

3rd Row (1)

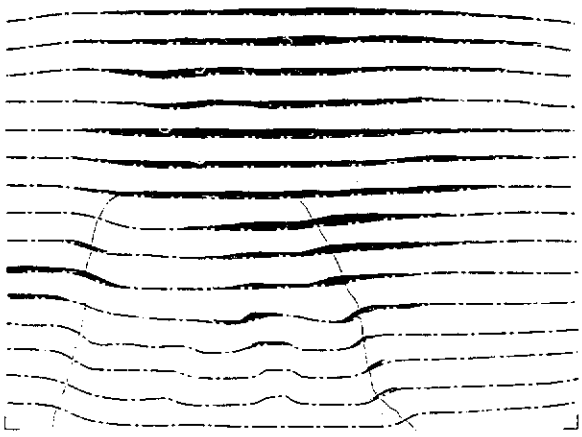

3rd Row (3)

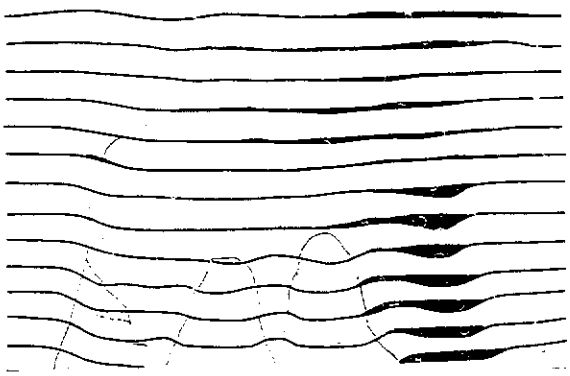

4th Row (1)

Figure IV.16 b

GEOTECHNICAL CENTRIFUGE TEST PS04

SUBSIDENCE DEVELOPMENT

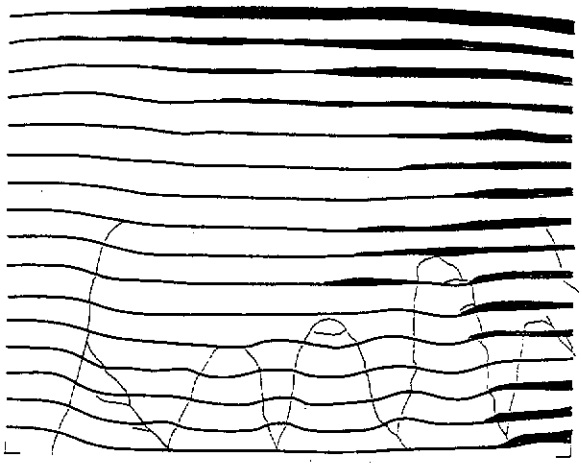

5th (Row)

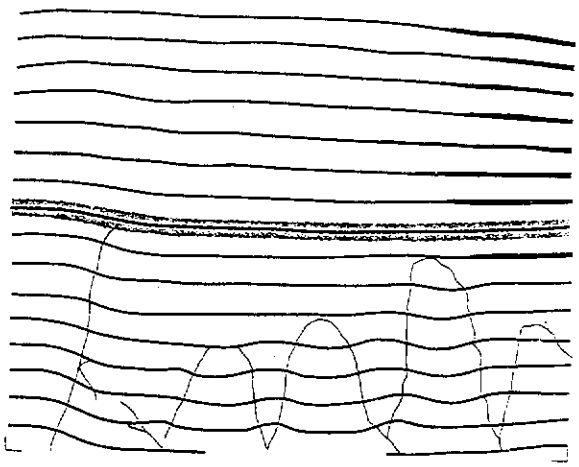

6th Row

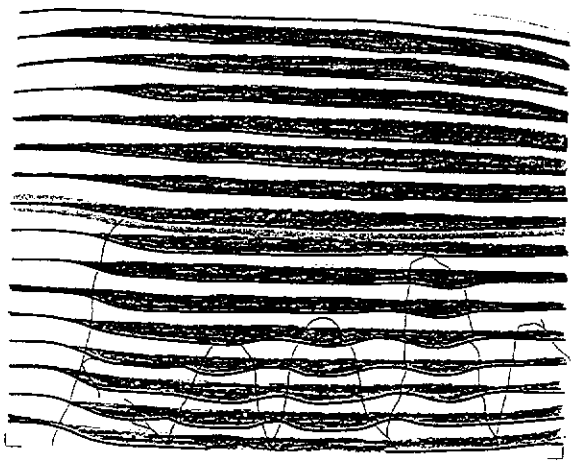

Total Subsidence

Figure IV.16 b

CRACK TRACING ON FRONT OF CRENTRIFUGE MODEL PS04

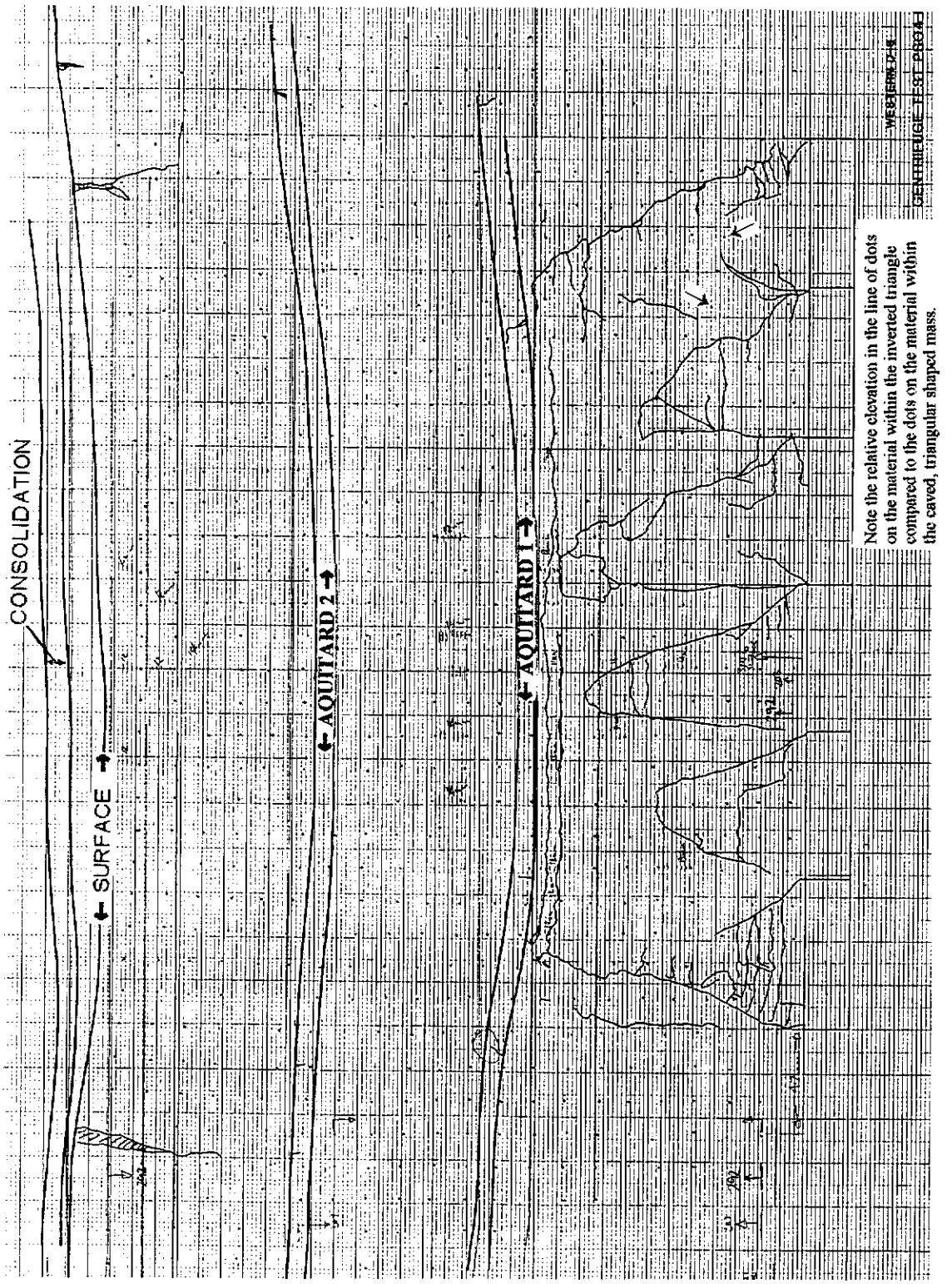

Figure IV.17

POST-TEST PHOTOGRAPHS OF CENTRIFUGE MODEL PS04

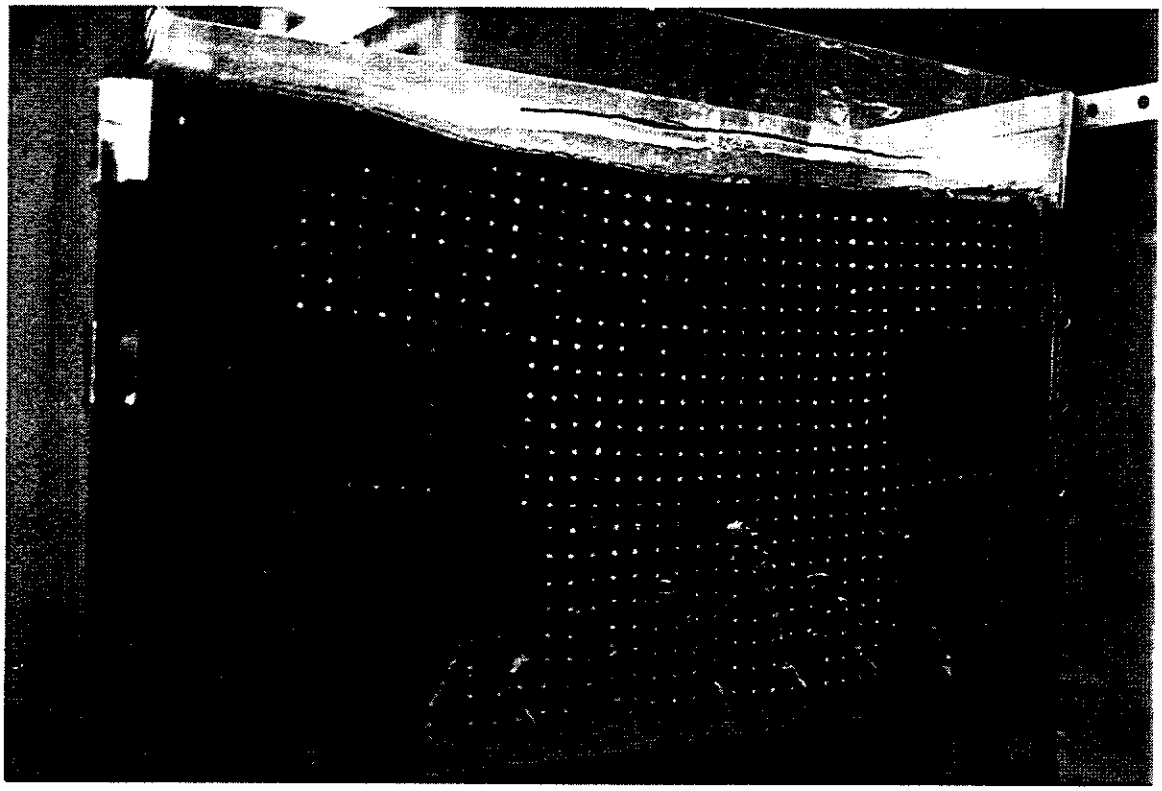

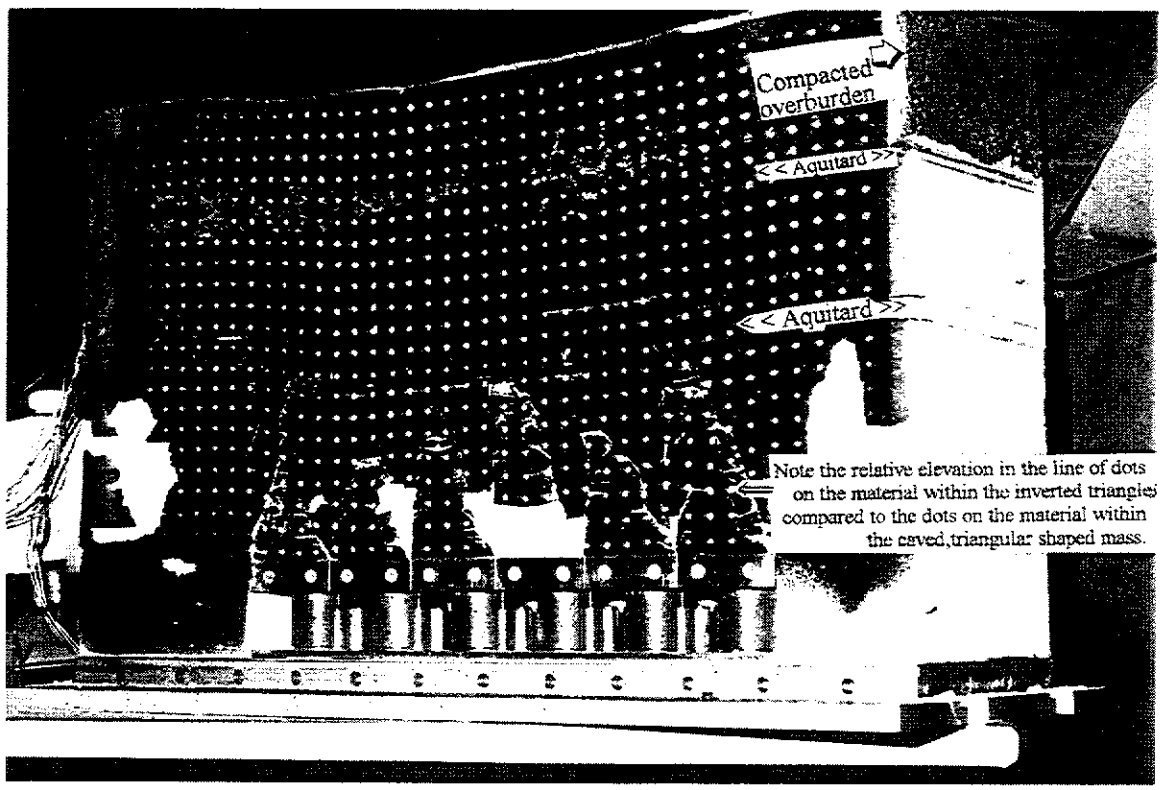

Figure IV.18

CRACK TRACING ON AQUITARDS IN CENTRIFUGE MODEL PS04

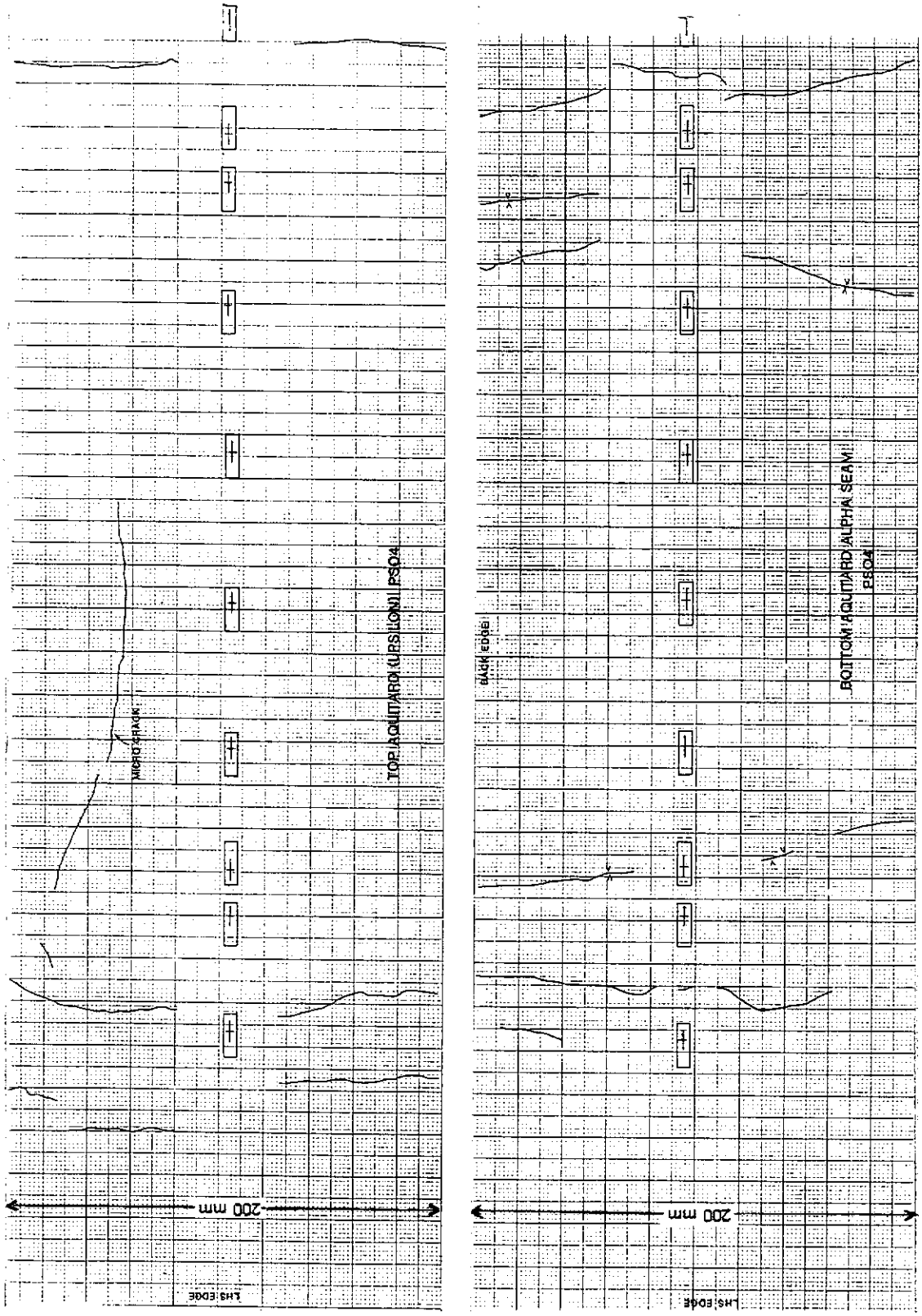

Figure IV.19

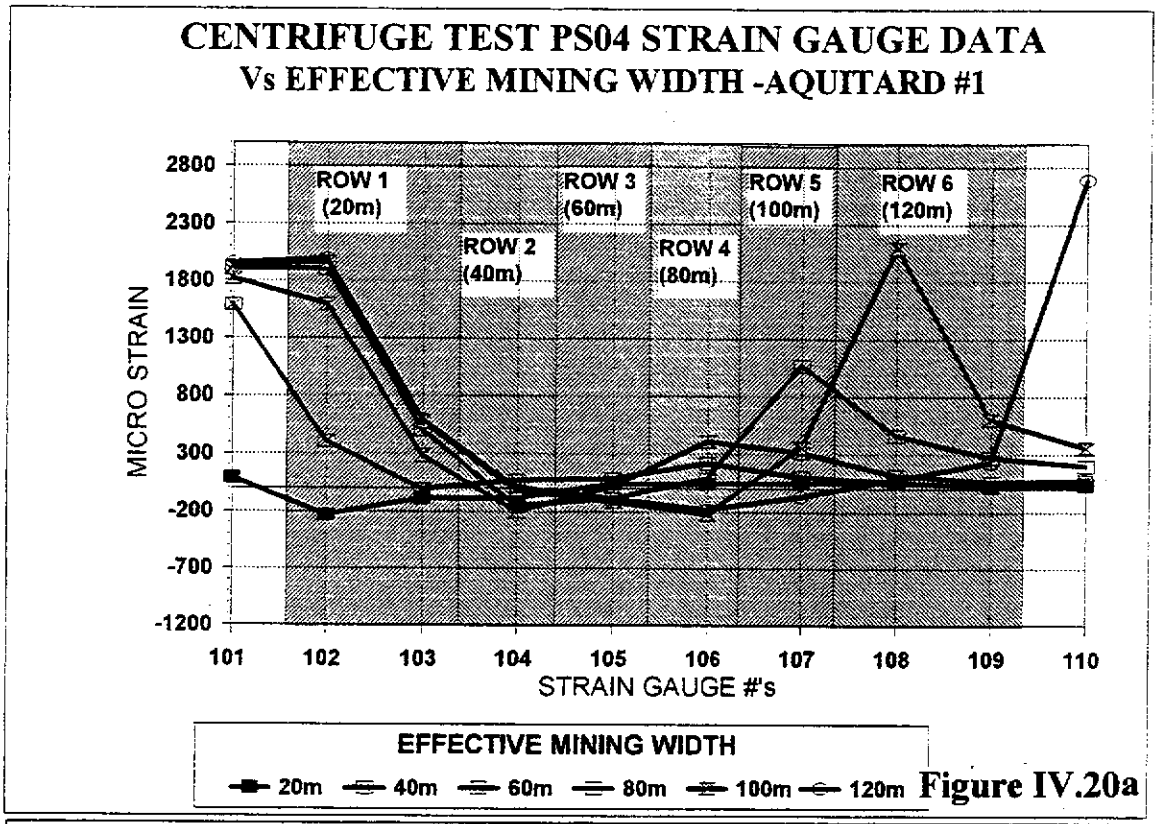

Figure IV.20a

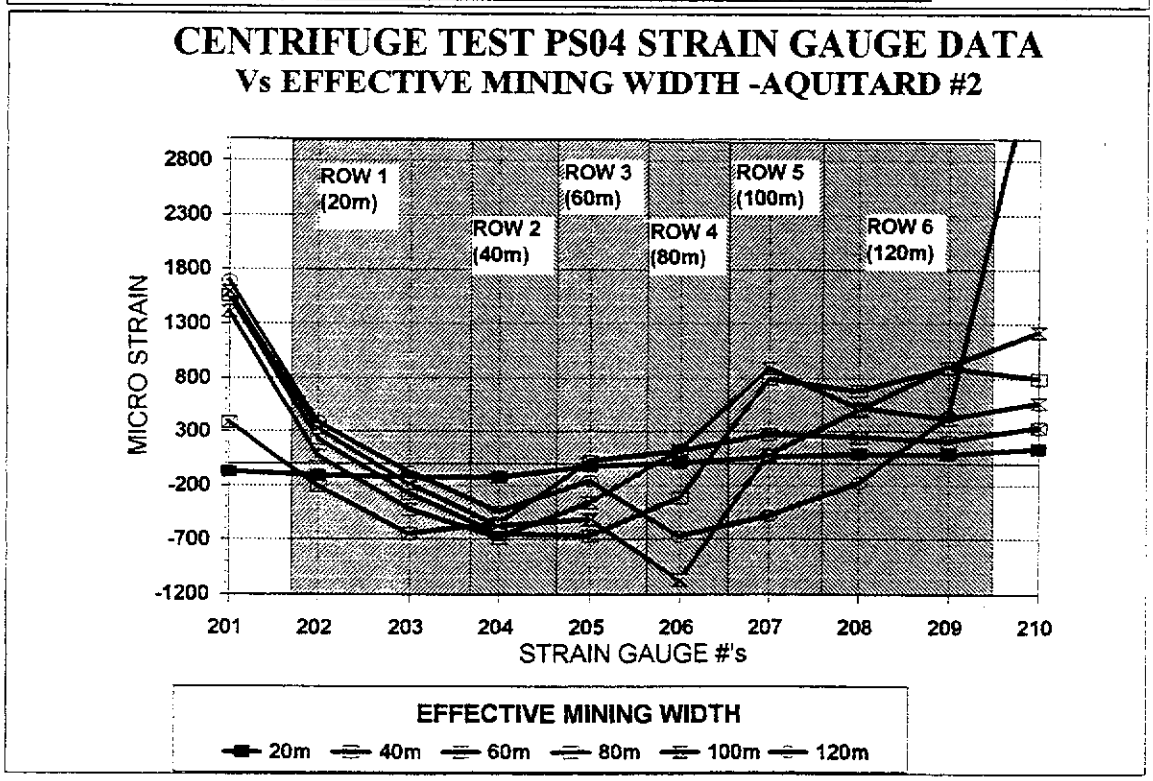

Figure IV.20 b

STRAIN GAUGE LAYOUT - CENTRIFUGE MODEL PS04

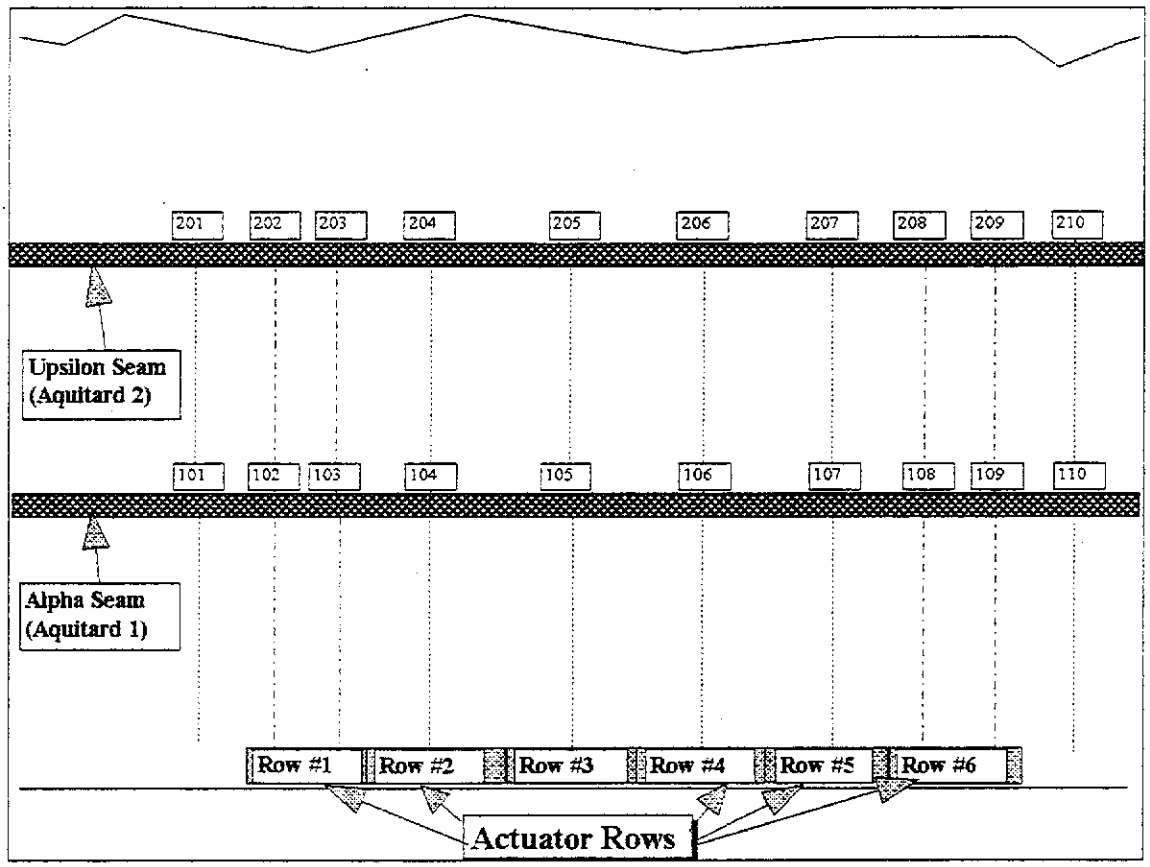

Figure IV.20 c

TABLE IV.4

SUMMARY OF CENTRIFUGE TEST PS04 STRAIN GAUGE DATA
RAW DATA

ROW #	EFFECTIVE MINING WIDTH(m)	STRAIN GAUGE #'s 101	102	103	104	105	106	107	108	109	110
		mstrain	mstrain	mstrain	mstrain	mstrain	mstrain	mstrain	mstrain	mstrain	mstrain
0	0	-5	16	-9	-7	-77	-53	-49	-7	-46	-41
1	13	91	-216	-94	-90	-39	-8	-1	42	-20	-8
2	26	1586	424	-19	62	9	170	57	50	-24	10
3	39	1816	1611	279	-211	-61	356	269	112	13	34
4	52	1903	1925	497	-159	-169	31	1019	457	227	161
5	65	1919	1985	568	-20	-195	-280	305	2092	562	315
6	78	1952	2011	592	4	-163	-242	-117	76	183	2650
		201	**202**	**203**	**204**	**205**	**206**	**207**	**208**	**209**	**210**
0	0	-20	-135	-87	-101	-70	-89	-62	-58	-77	-6
1	13	-93	-245	-213	-226	-90	-82	-4	34	12	136
2	26	367	-341	-732	-652	-44	30	213	189	131	332
3	39	1393	-59	-506	-786	-426	43	834	462	343	561
4	52	1535	99	-362	-750	-737	-402	730	625	815	789
5	65	1574	194	-271	-671	-581	-1161	23	436	829	1220
6	78	1679	256	-159	-547	-226	-763	-544	-240	366	3974

GEOTECHNICAL CENTRIFUGE TEST PS05

SUBSIDENCE DEVELOPMENT

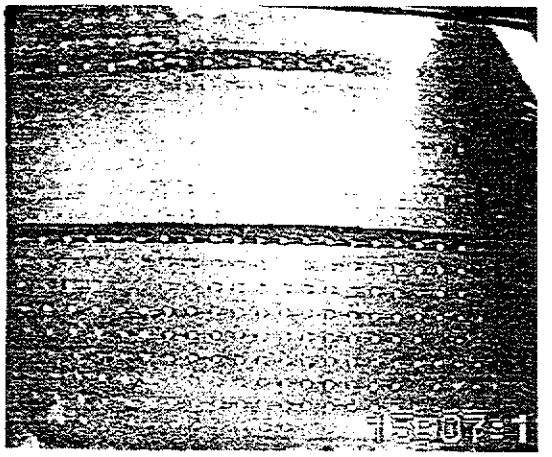

Control

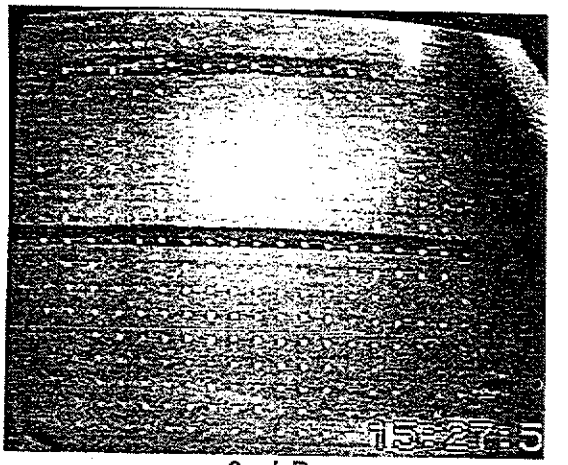

2nd Row

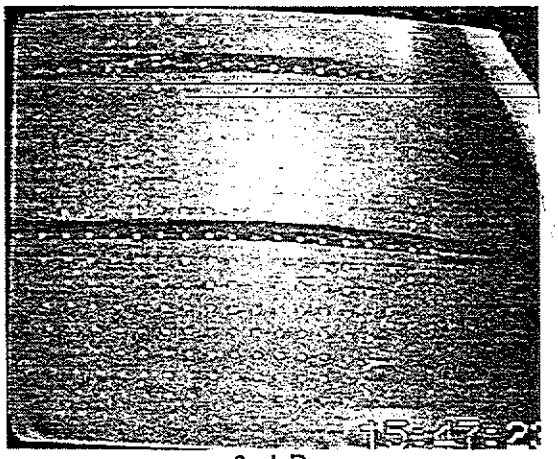

3rd Row

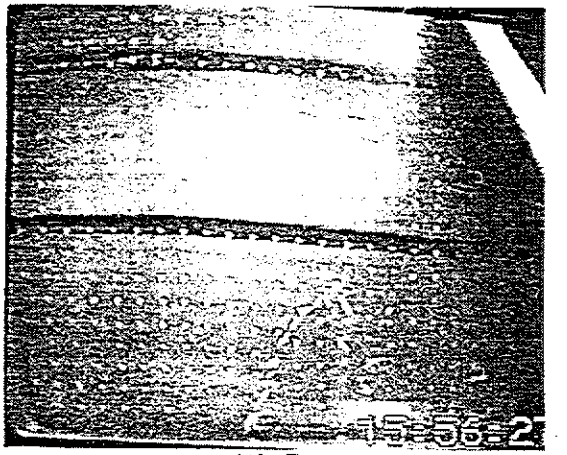

4th Row

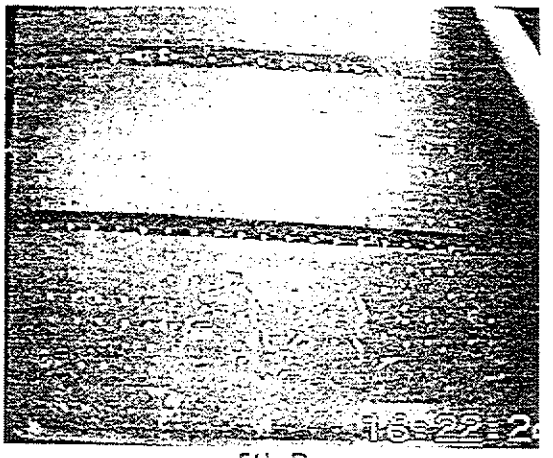

5th Row

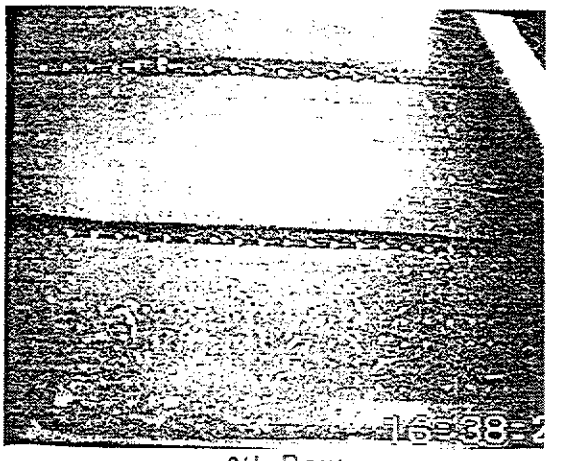

6th Row

Figure IV.21 a

GEOTECHNICAL CENTRIFUGE TEST PS05

SUBSIDENCE DEVELOPMENT

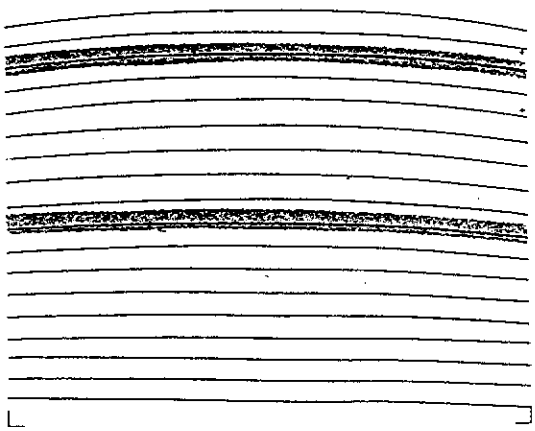

Control

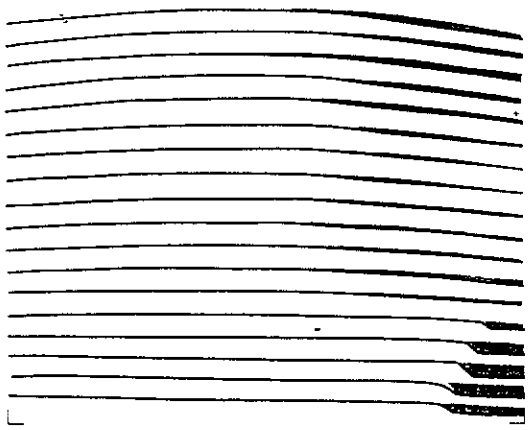

2nd Row

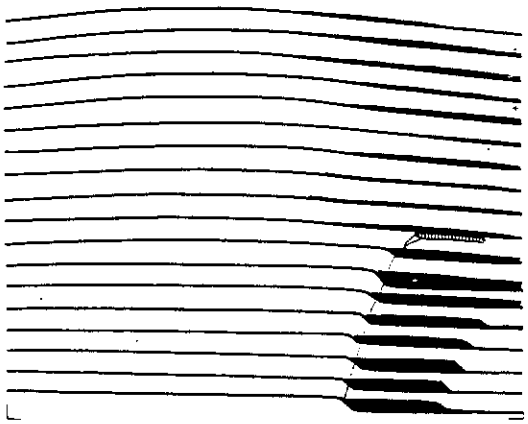

3rd Row

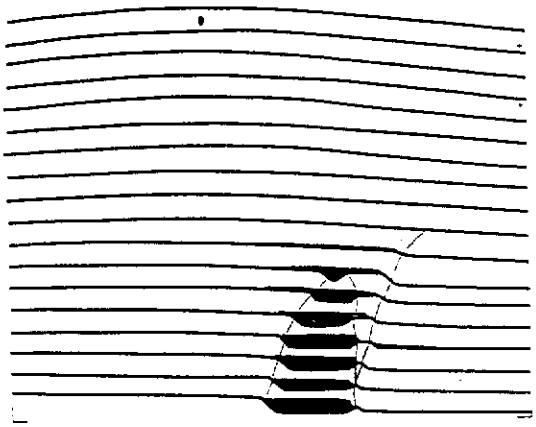

4th Row

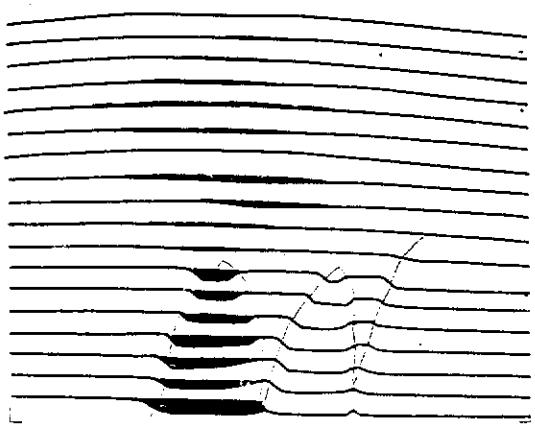

5th Row

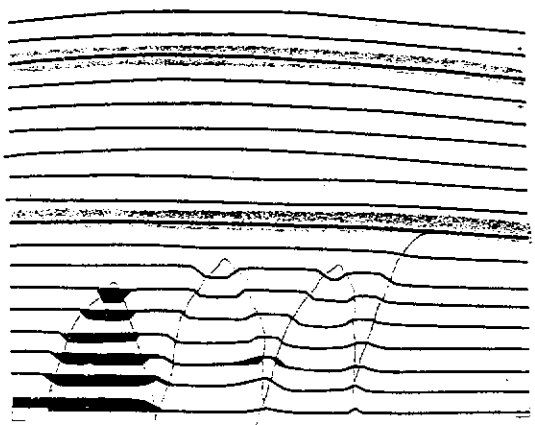

6th Row

Figure IV.21 b

GEOTECHNICAL CENTRIFUGE TEST PS05

SUBSIDENCE DEVELOPMENT

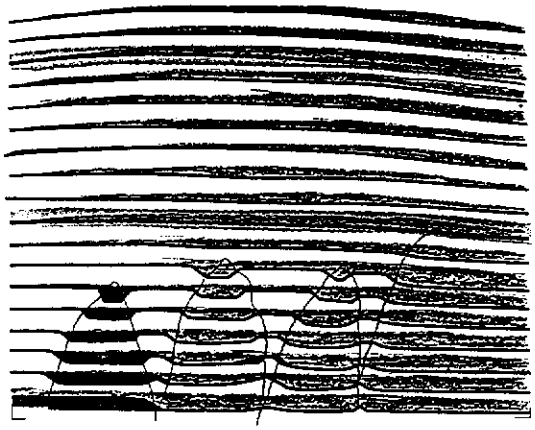

Figure IV.21 b

CRACK TRACING ON FRONT OF CENTRIFUGE MODEL PS05

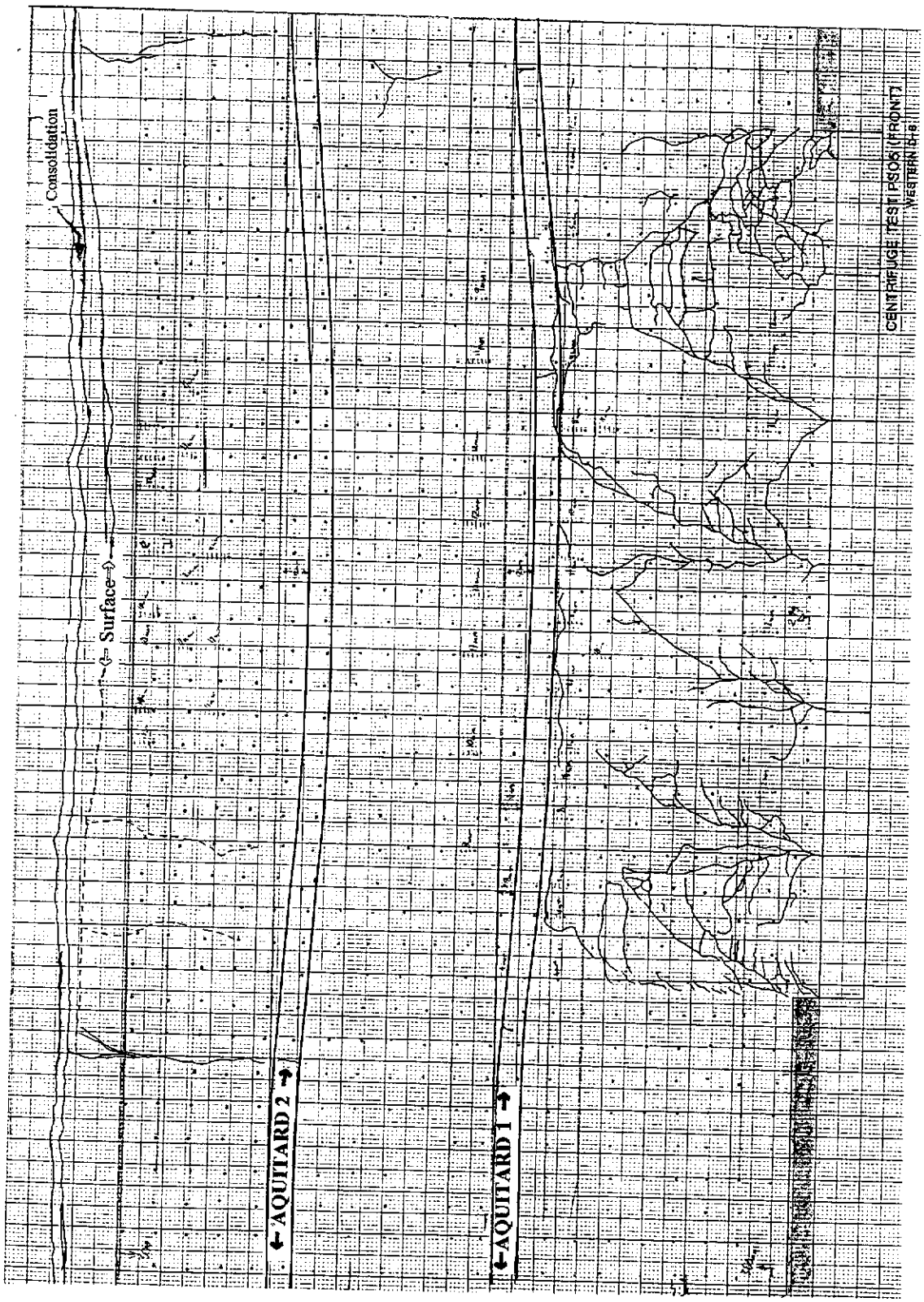

Figure IV.22

POST-TEST PHOTOGRAPHS OF CAVING/SHEARING IN LOWER AQUIFER - CENTRIFUGE MODEL PS05

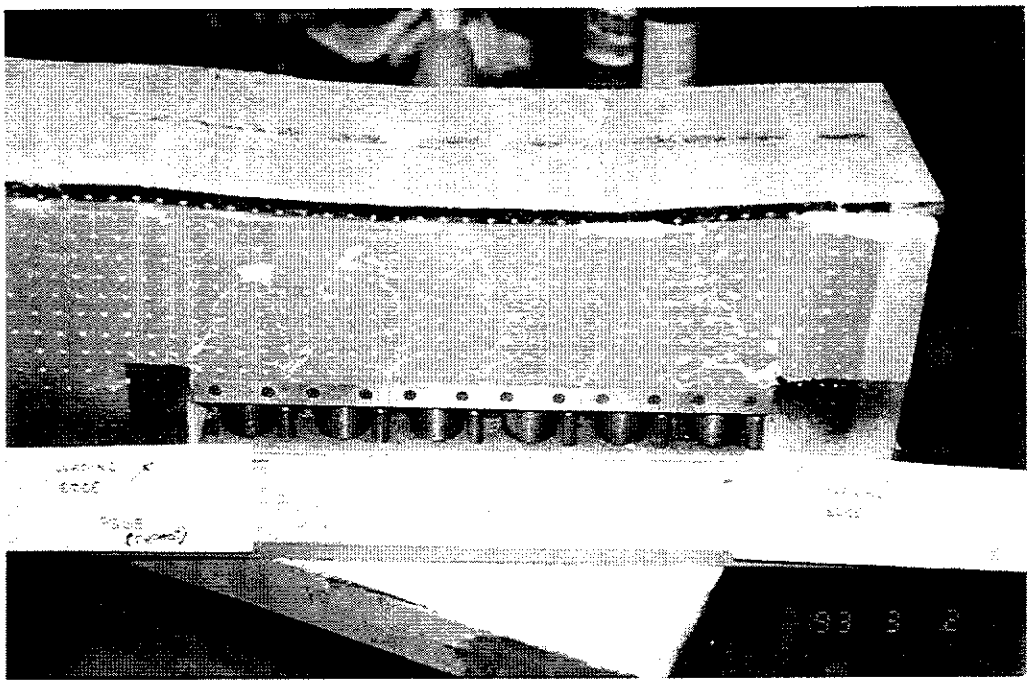

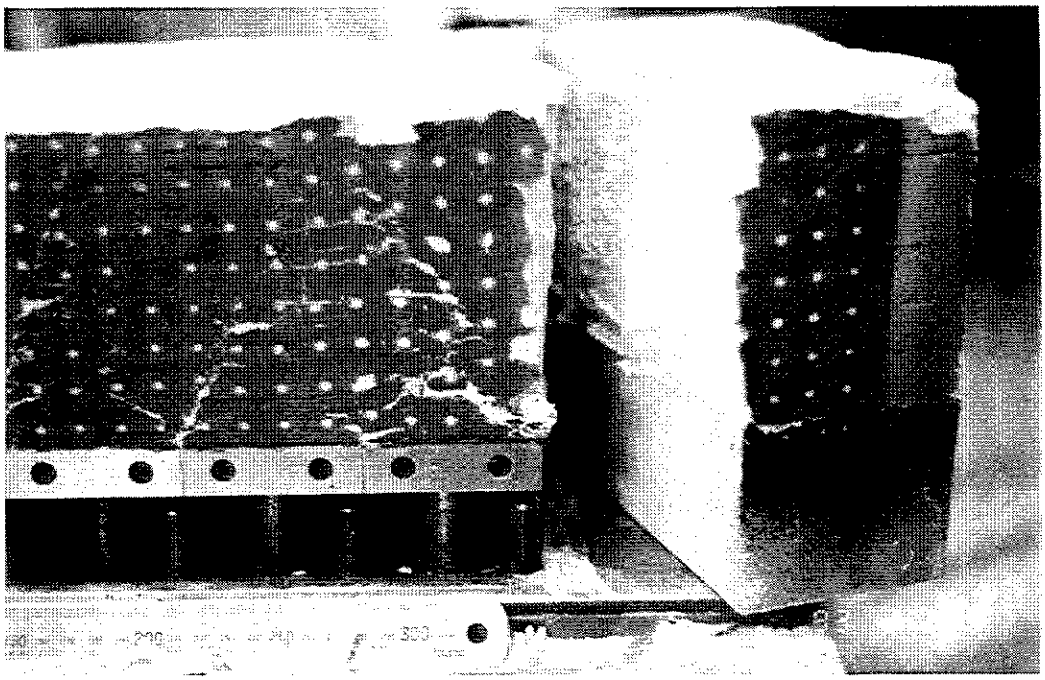

Figure IV.23

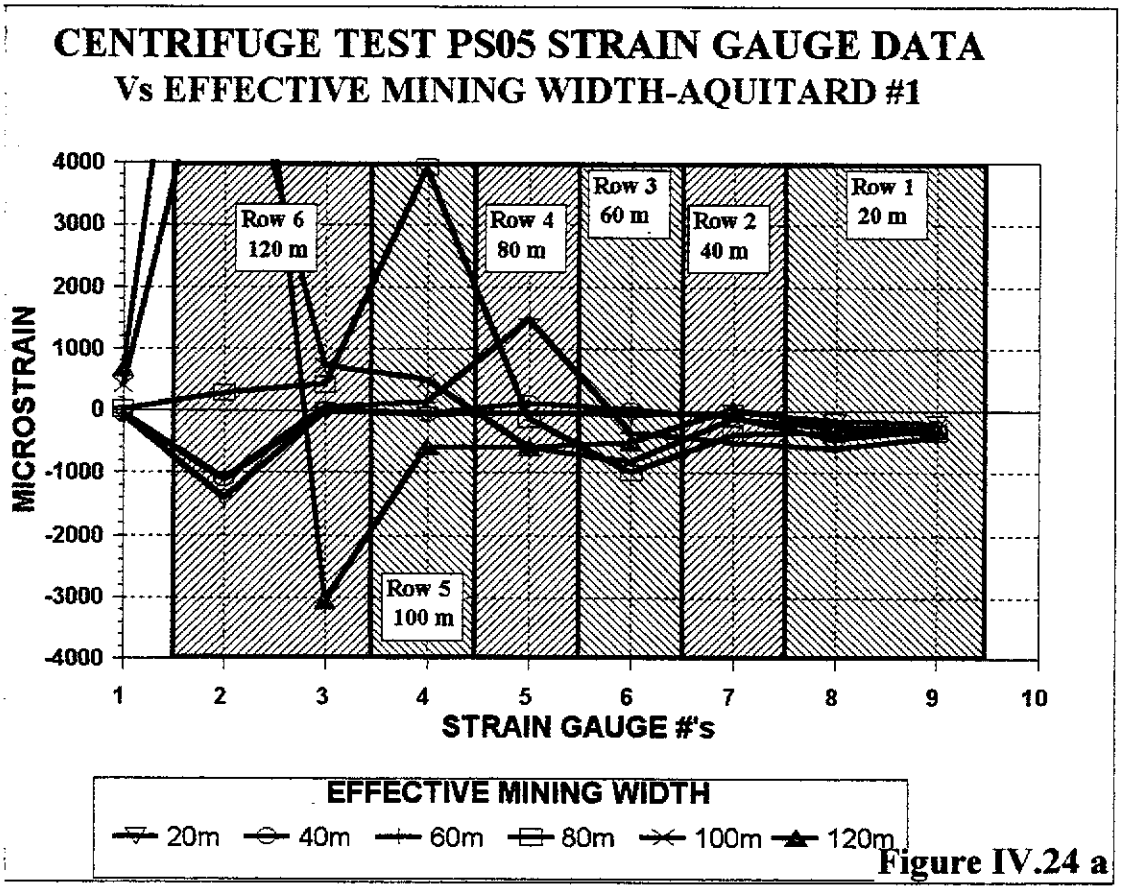

Figure IV.24 a

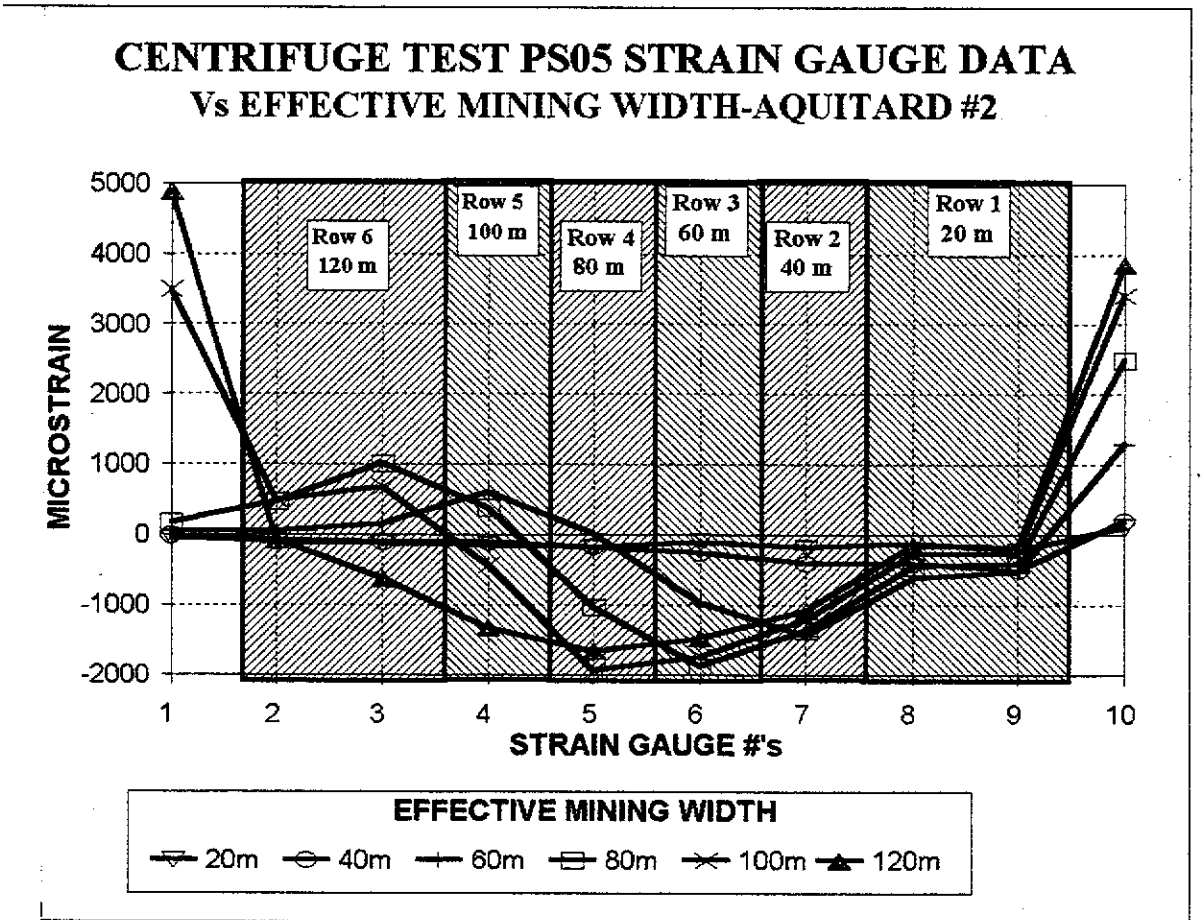

Figure IV.24 b

STRAIN GAUGE LAYOUT - CENTRIFUGE MODEL PS05

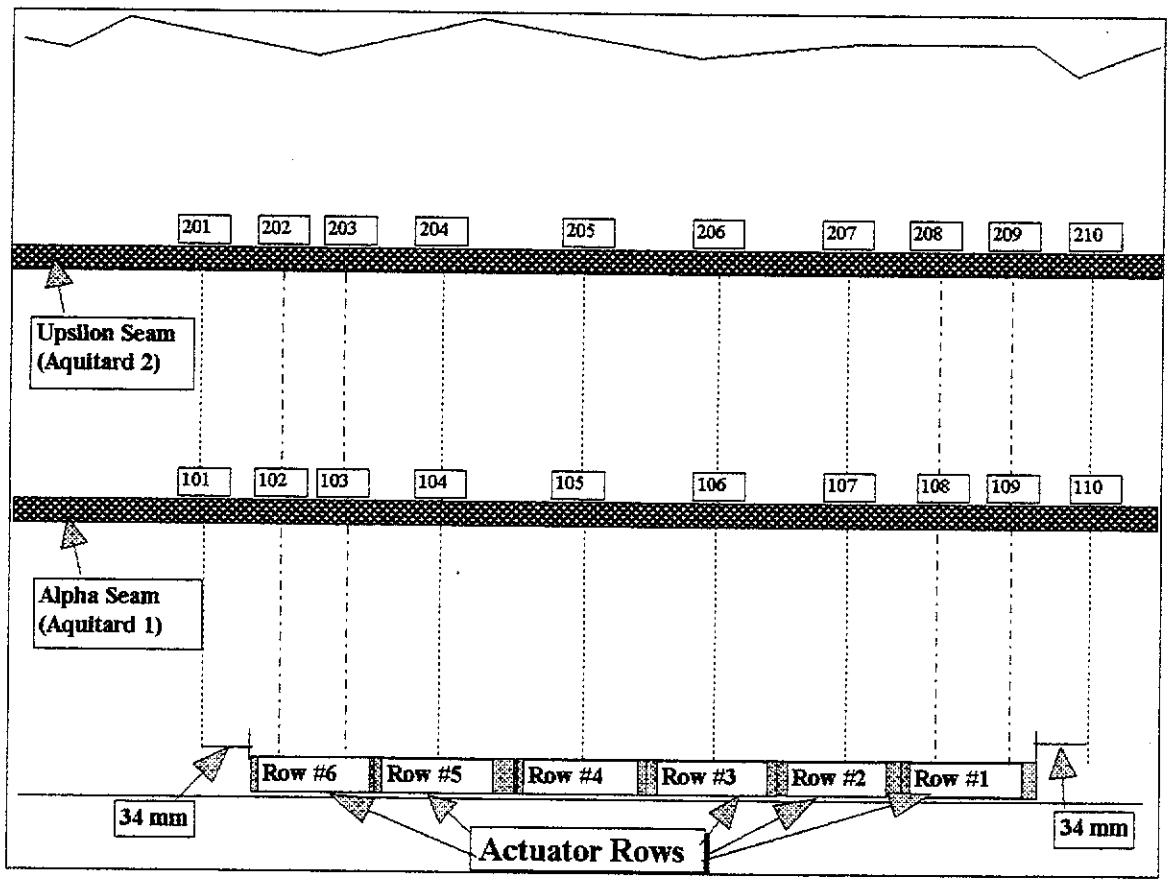

Figure IV.24 c

TABLE IV.5

SUMMARY OF CENTRIFUGE TEST PS05 STRAIN GAUGE DATA

RAW DATA

ROW #	EFFECTIVE MINING WIDTH(m)	STRAIN GAUGE #'s 101	102	103	104	105	106	107	108	109	110
		mstrain	mstrain	mstrain	mstrain	mstrain	mstrain	mstrain	mstrain	mstrain	mstrain
0	0	7	111	-15	-1	-9	-72	-141	0	2	
1	13	86	1521	3	74	36	-4	-120	161	207	
2	26	69	1219	-29	57	-120	-82	-37	450	296	
3	39	68	1198	-66	-130	-1482	287	367	618	417	
4	52	-10	-170	-432	-3919	122	919	236	344	352	
5	65	-388	-6835	-732	-486	584	739	-21	275	304	
6	78	-666	-11746	3042	573	576	429	-167	252	291	
		201	**202**	**203**	**204**	**205**	**206**	**207**	**208**	**209**	**210**
0	0	3	-1	2	-9	-1	-12	-11	-46	6	1
1	13	54	107	128	132	188	87	169	74	237	-109
2	26	14	75	98	100	172	246	403	365	517	-195
3	39	-41	-46	-153	-623	-14	961	1428	580	540	-1287
4	52	-172	-476	-1014	-397	1035	1875	1349	406	409	-2486
5	65	-3500	-494	-687	427	1944	1725	1198	228	262	-3415
6	78	-4894	77	622	1320	1661	1468	1074	102	188	-3857

CRACK TRACING ON AQUITARDS IN CENTRIFUGE MODEL PS05

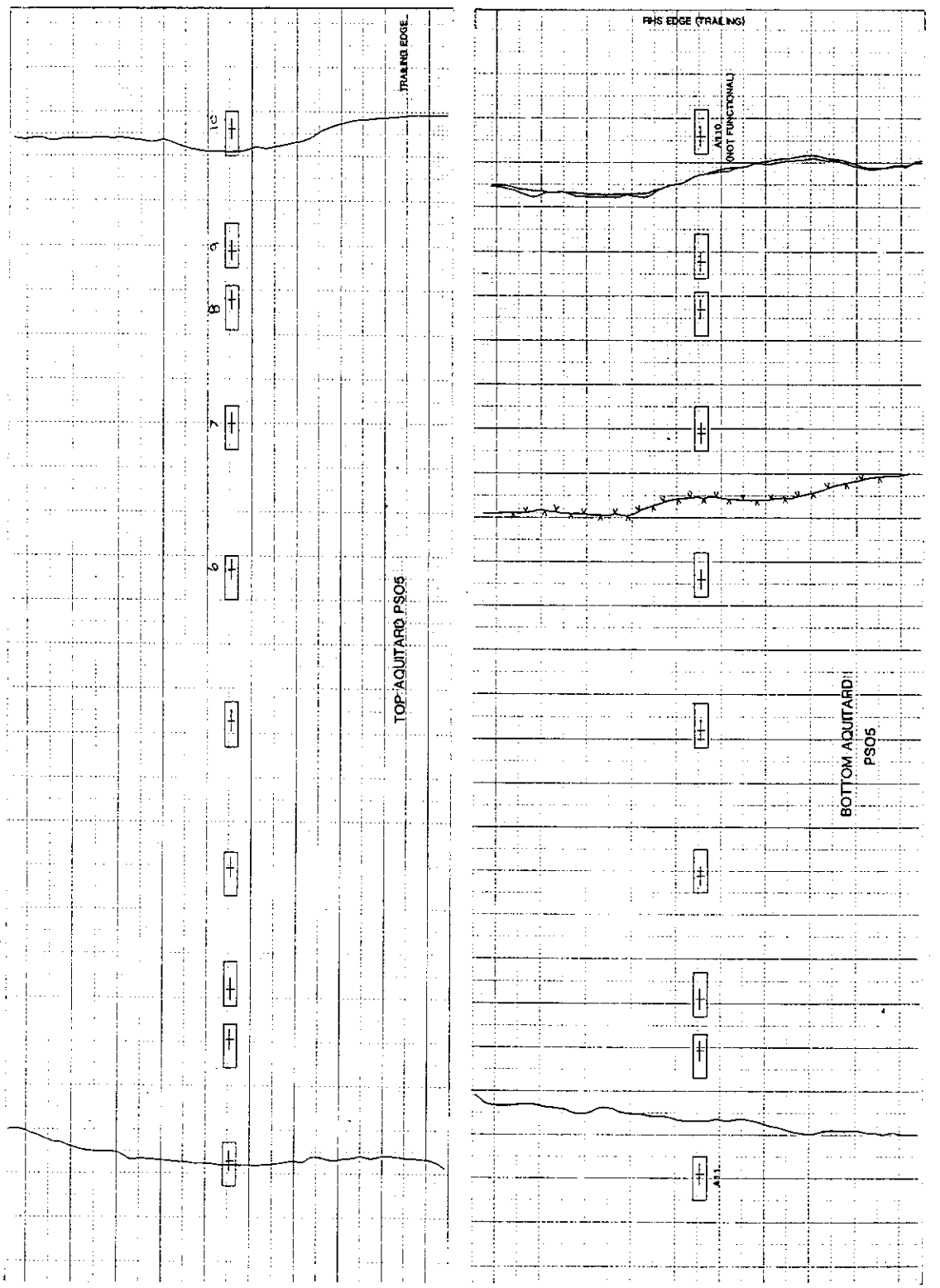

Figure IV.25

GEOTECHNICAL CENTRIFUGE TEST PS06

SUBSIDENCE DEVELOPMENT

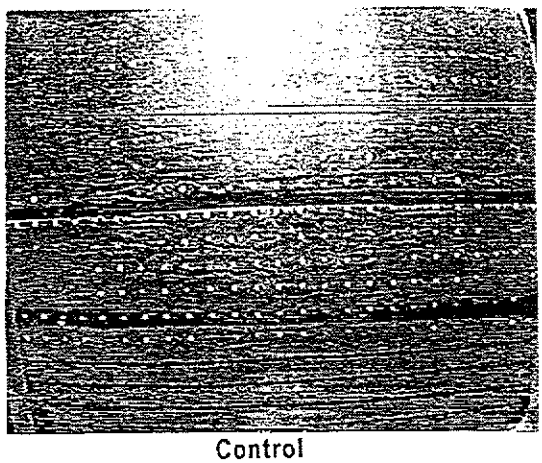

Control

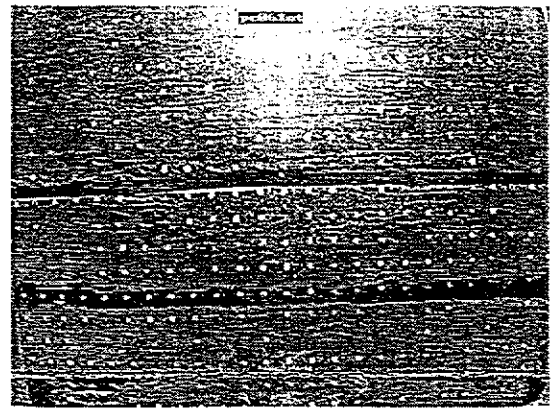

1st Row

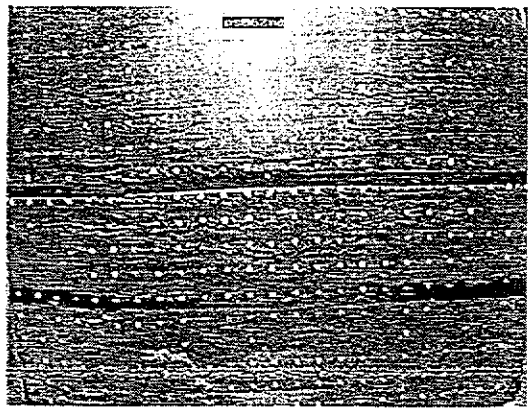

2nd Row

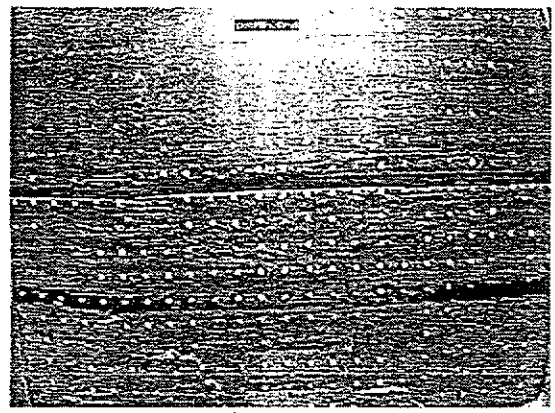

3rd Row

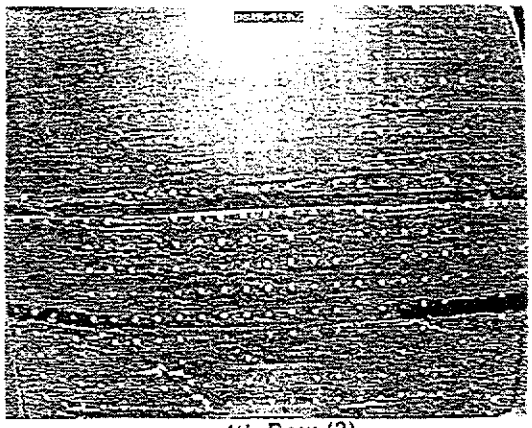

4th Row (2)

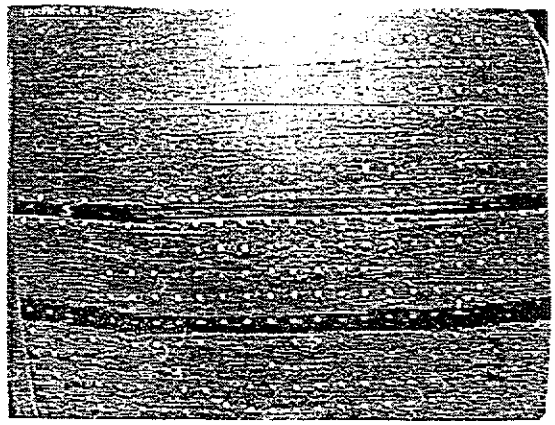

5th Row (1)

Figure IV.26 a

GEOTECHNICAL CENTRIFUGE TEST PS06

SUBSIDENCE DEVELOPMENT

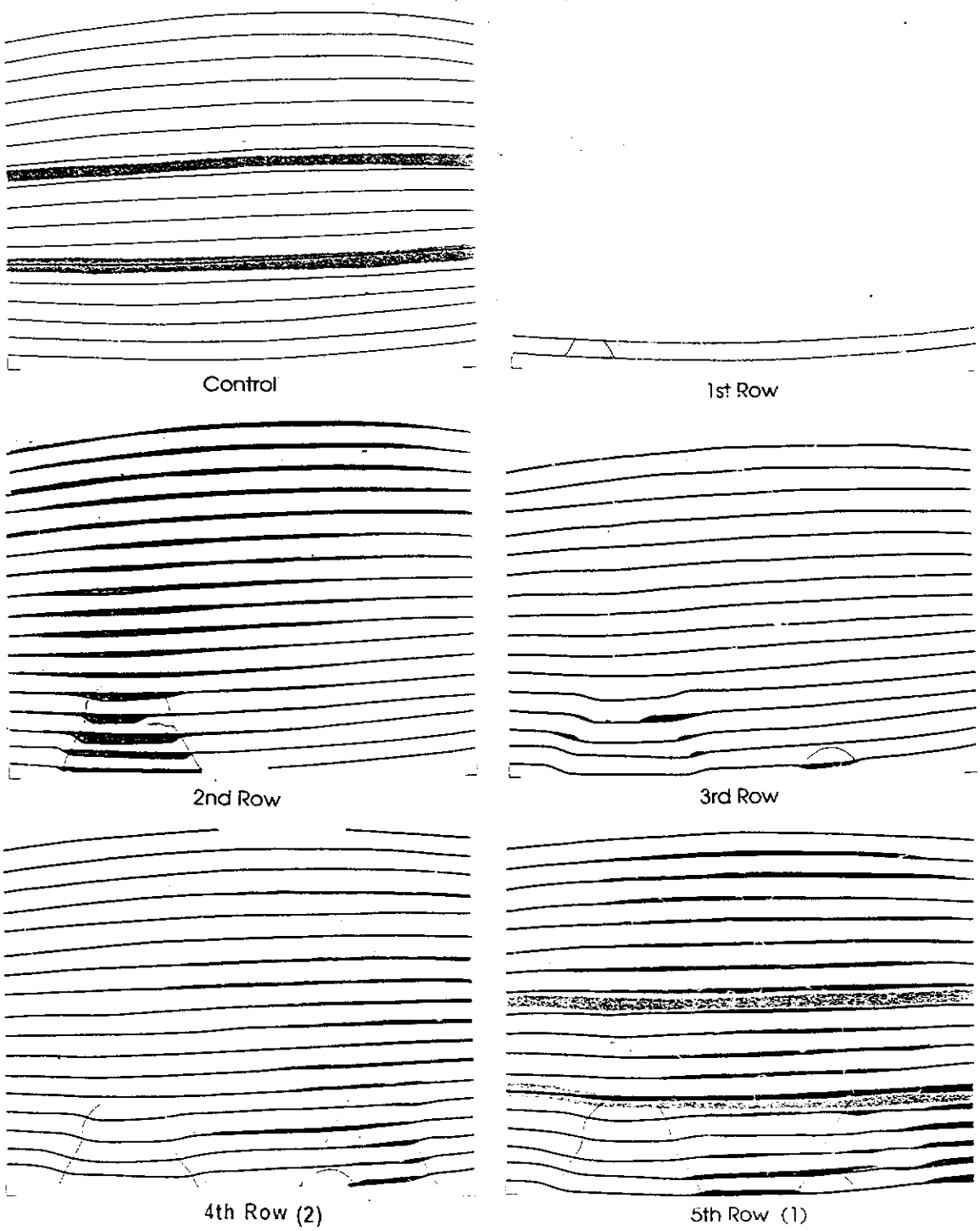

Figure IV.26 b

GEOTECHNICAL CENTRIFUGE TEST PS06

SUBSIDENCE DEVELOPMENT

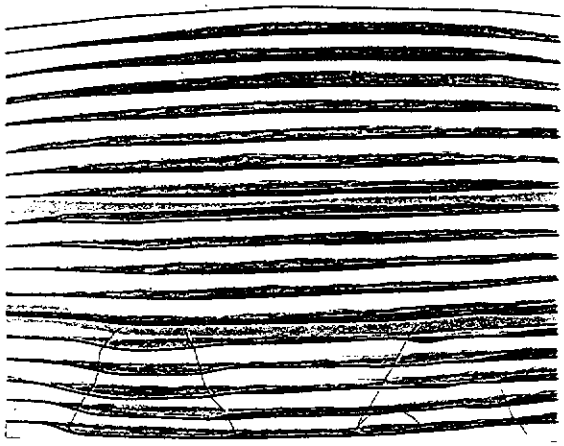

Total Subsidence

Figure IV.26 b

CRACK TRACING ON FRONT OF CENTRIFUGE MODEL PS06

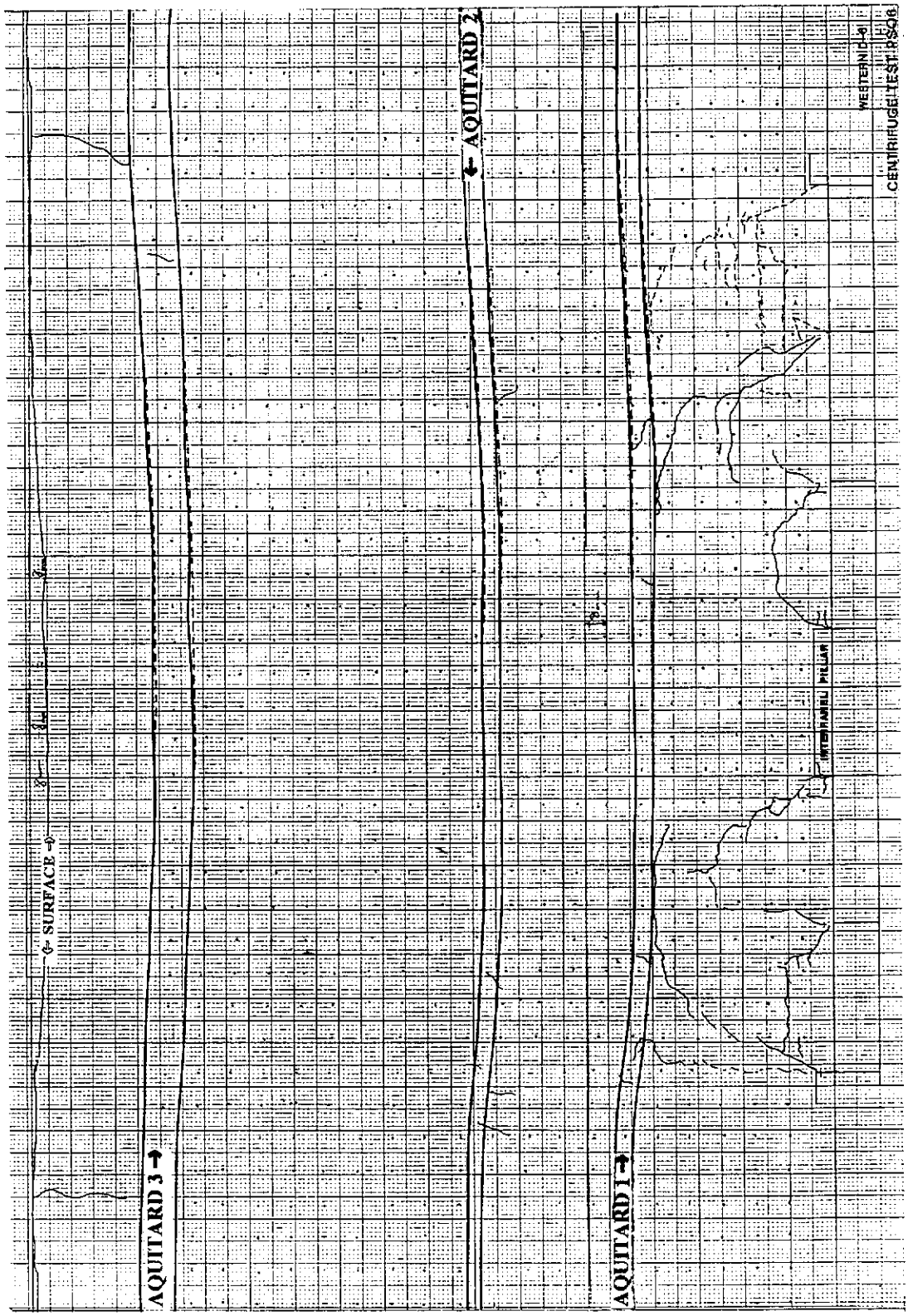

Figure IV.27

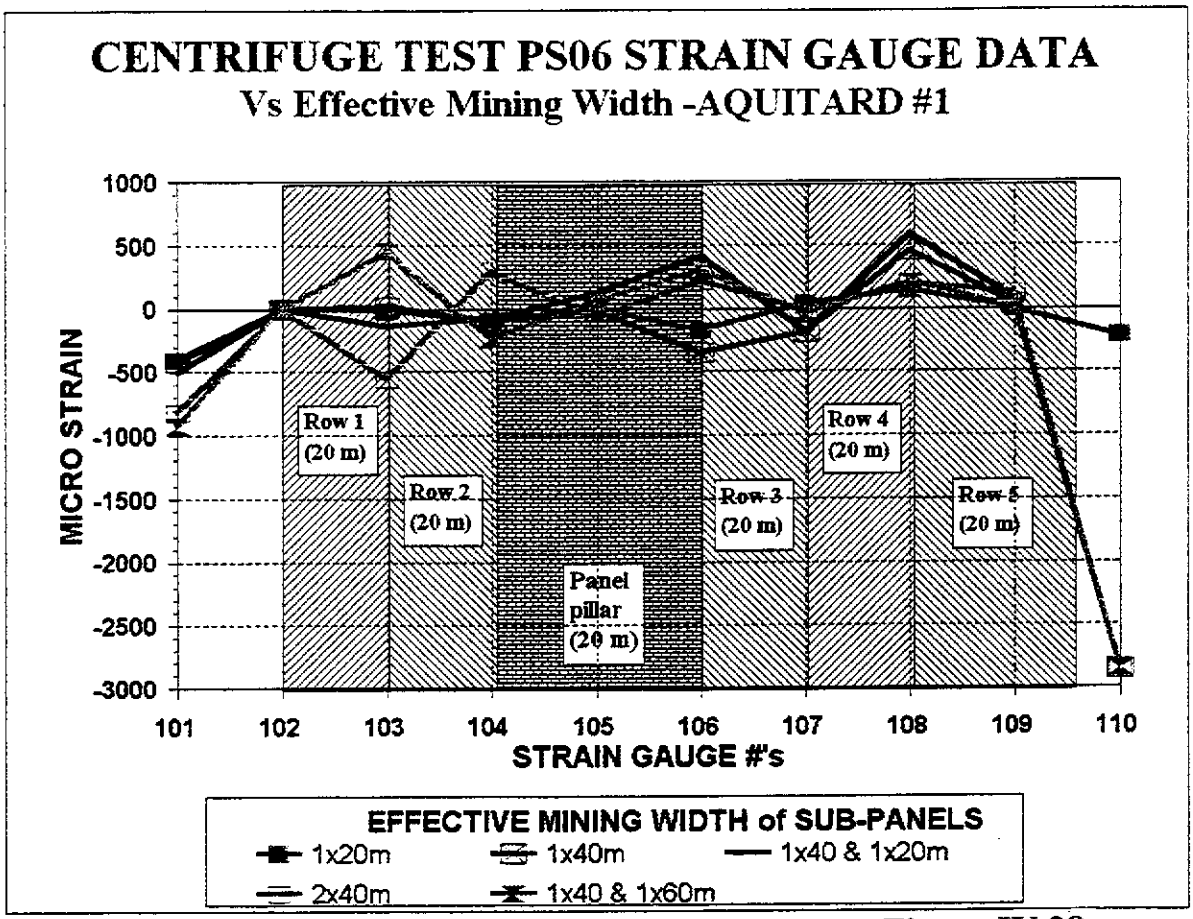

Figure IV.28 a

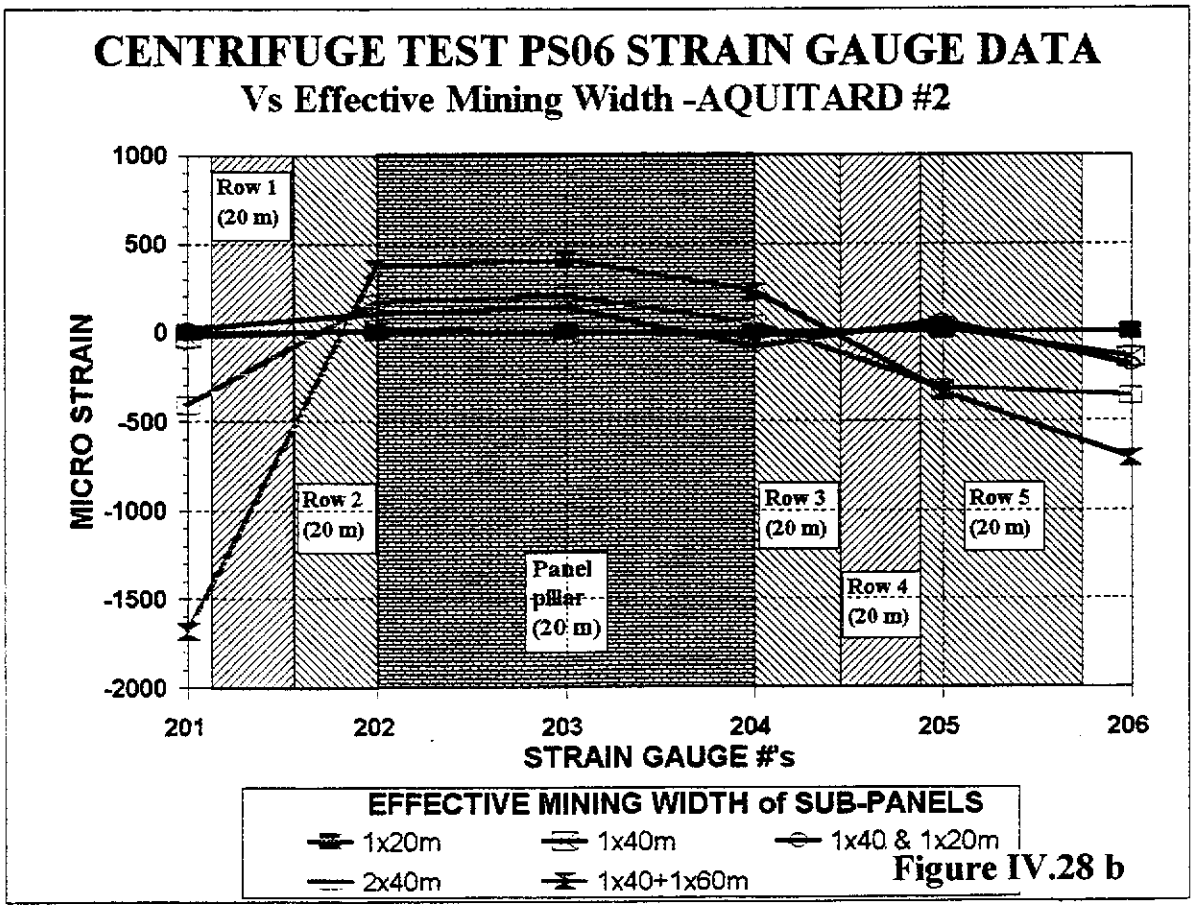

Figure IV.28 b

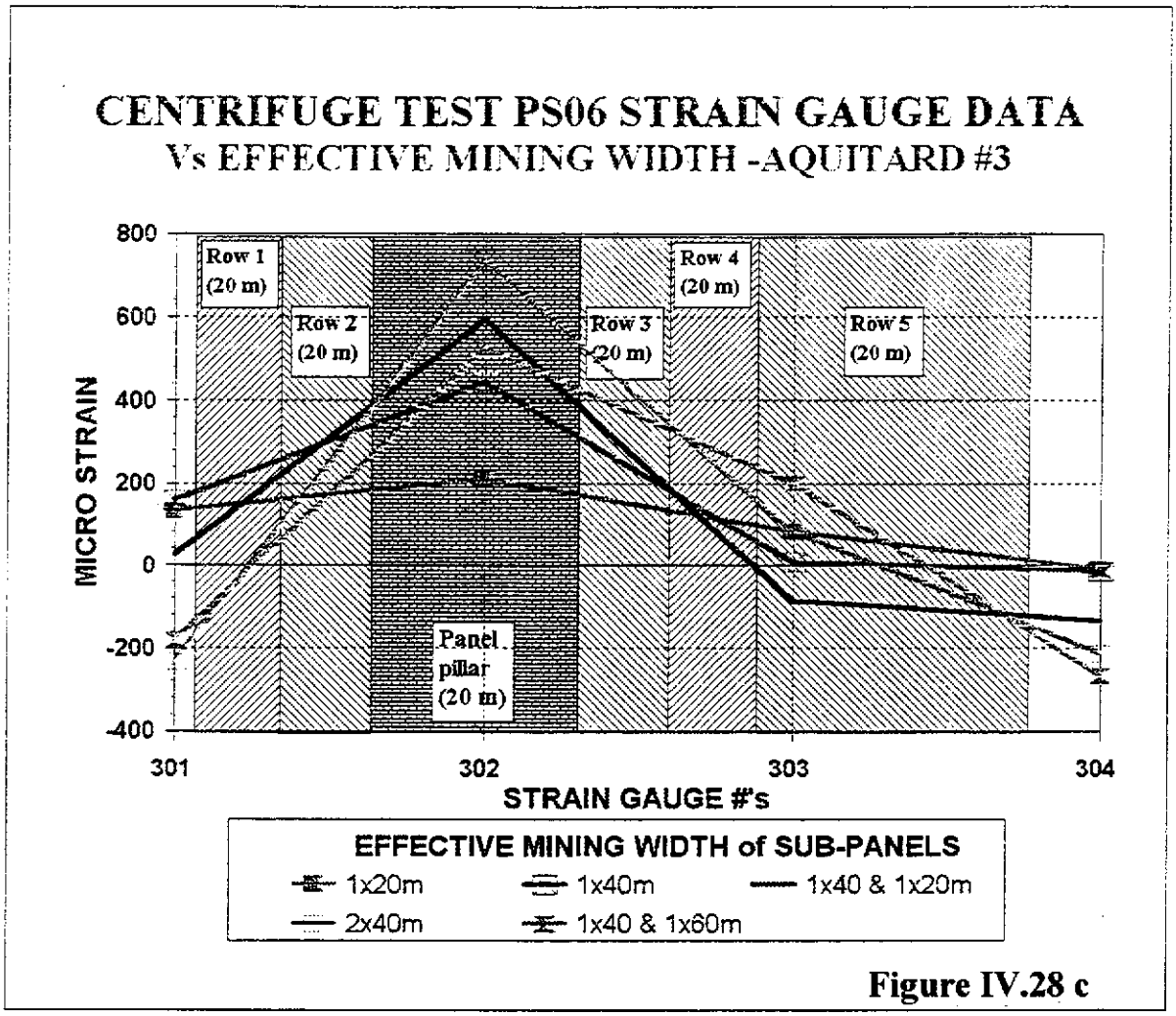

Figure IV.28 c

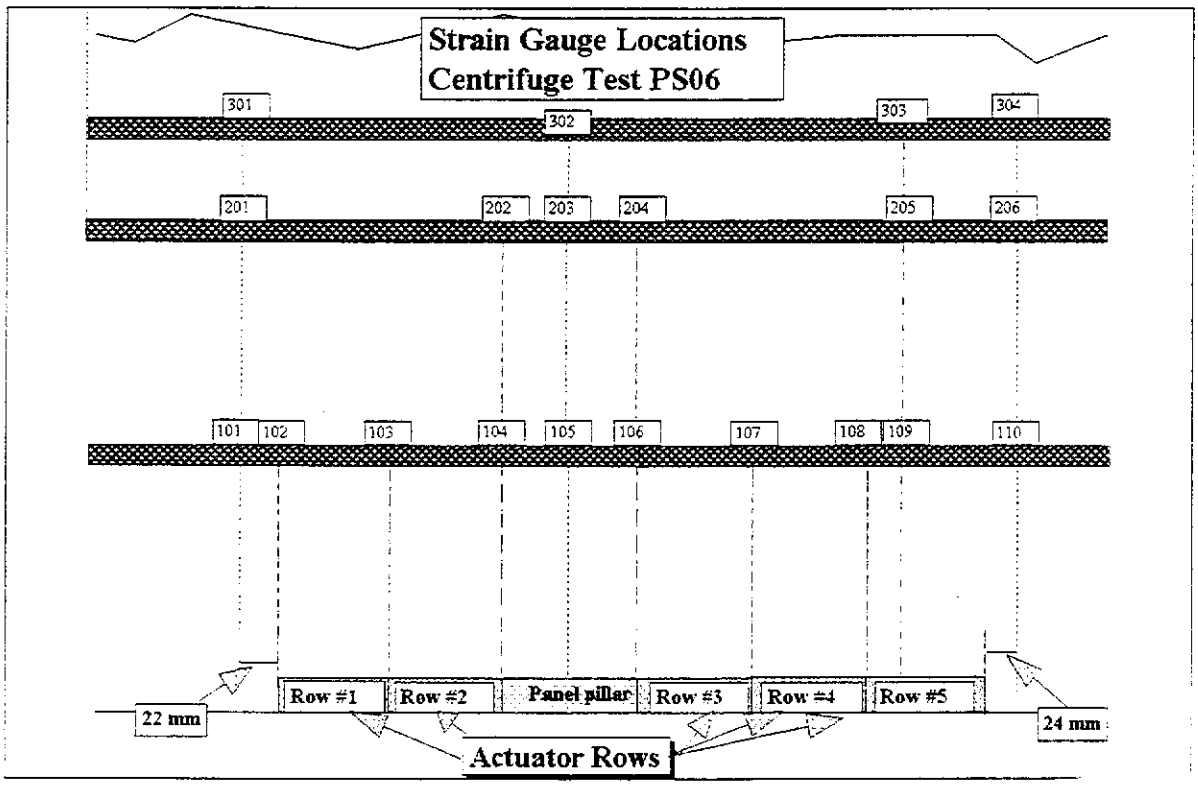

Figure IV.28 d

TABLE IV.6

SUMMARY OF
CENTRIFUGE TEST PS06 STRAIN GAUGE DATA
RAW DATA

ROW #	EFFECTIVE MINING WIDTH(m)	STRAIN GAUGE #'s 101	102	103	104	105	106	107	108	109	110
		mstrain	mstrain	mstrain	mstrain	mstrain	mstrain	mstrain	mstrain	mstrain	mstrain
0	0	-23	0	4	5	17	33	9	30	1	-41
1	20	384	0	23	93	7	207	-34	-113	4	180
2	40	397	0	-16	112	26	383	196	-426	-35	2809
3	20	478	0	146	88	-111	-386	192	-560	-77	2809
4	40	797	0	559	-292	87	-184	24	-164	-123	2809
5	60	902	0	-448	233	-49	-272	45	-180	-13	2809

		201	202	203	204	205	206
0	0	2	9	7	7	-5	-13
1	20	34	0	19	29	-29	133
2	40	-15	-93	-126	93	-62	174
3	20	406	-158	-198	-38	311	347
4	40	1684	-353	-403	-225	326	694
5	60	1172	-402	-407	-206	75	626

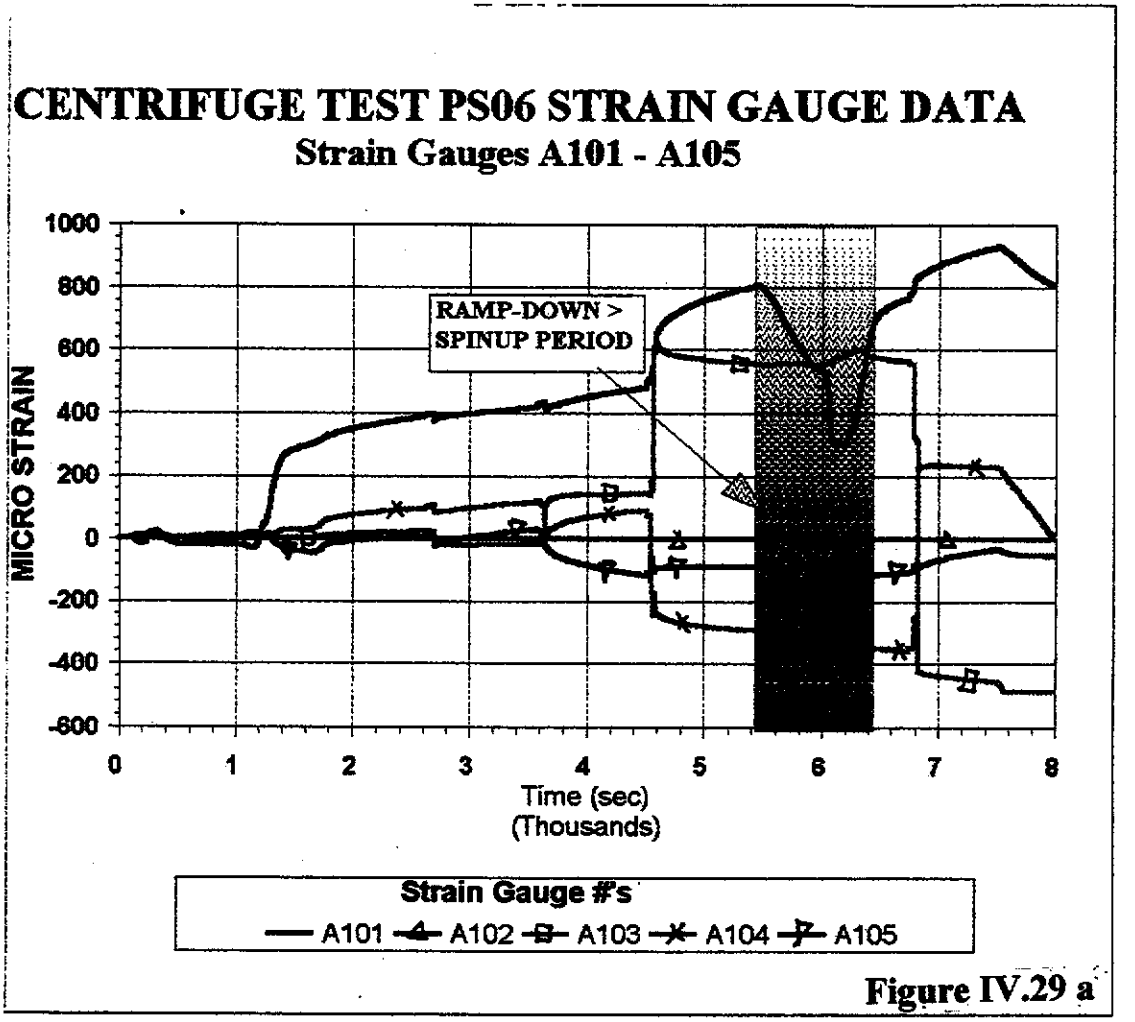

Figure IV.29 a

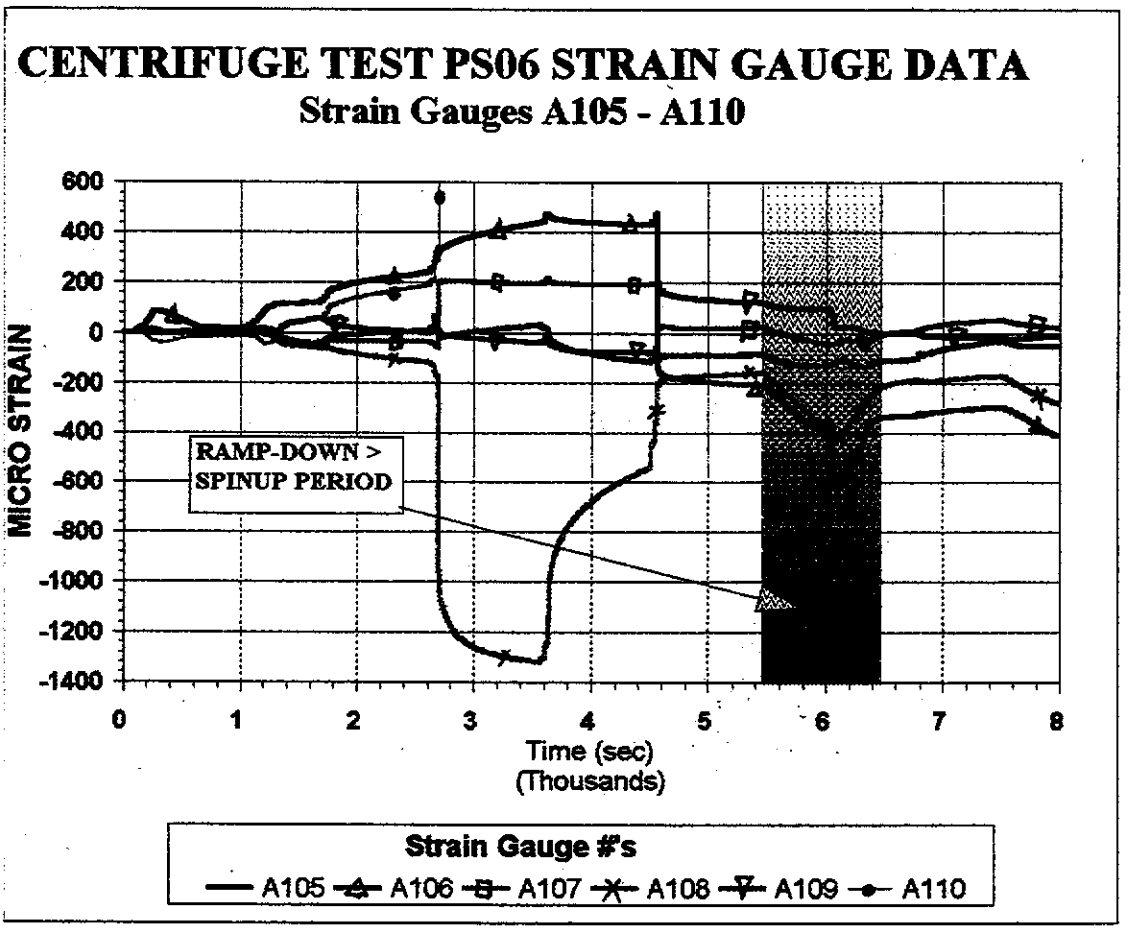

Figure IV.29 b

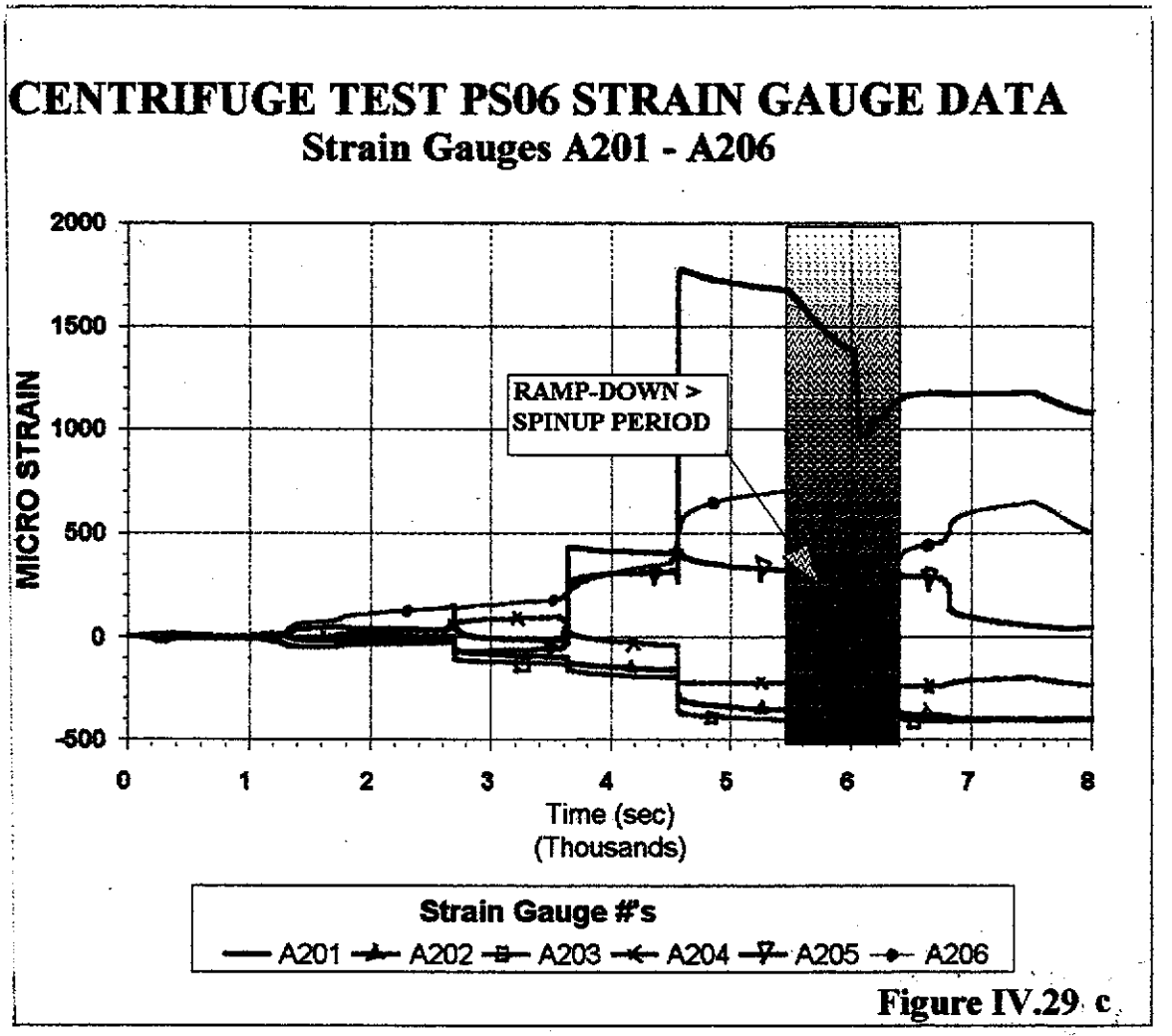

Figure IV.29 c

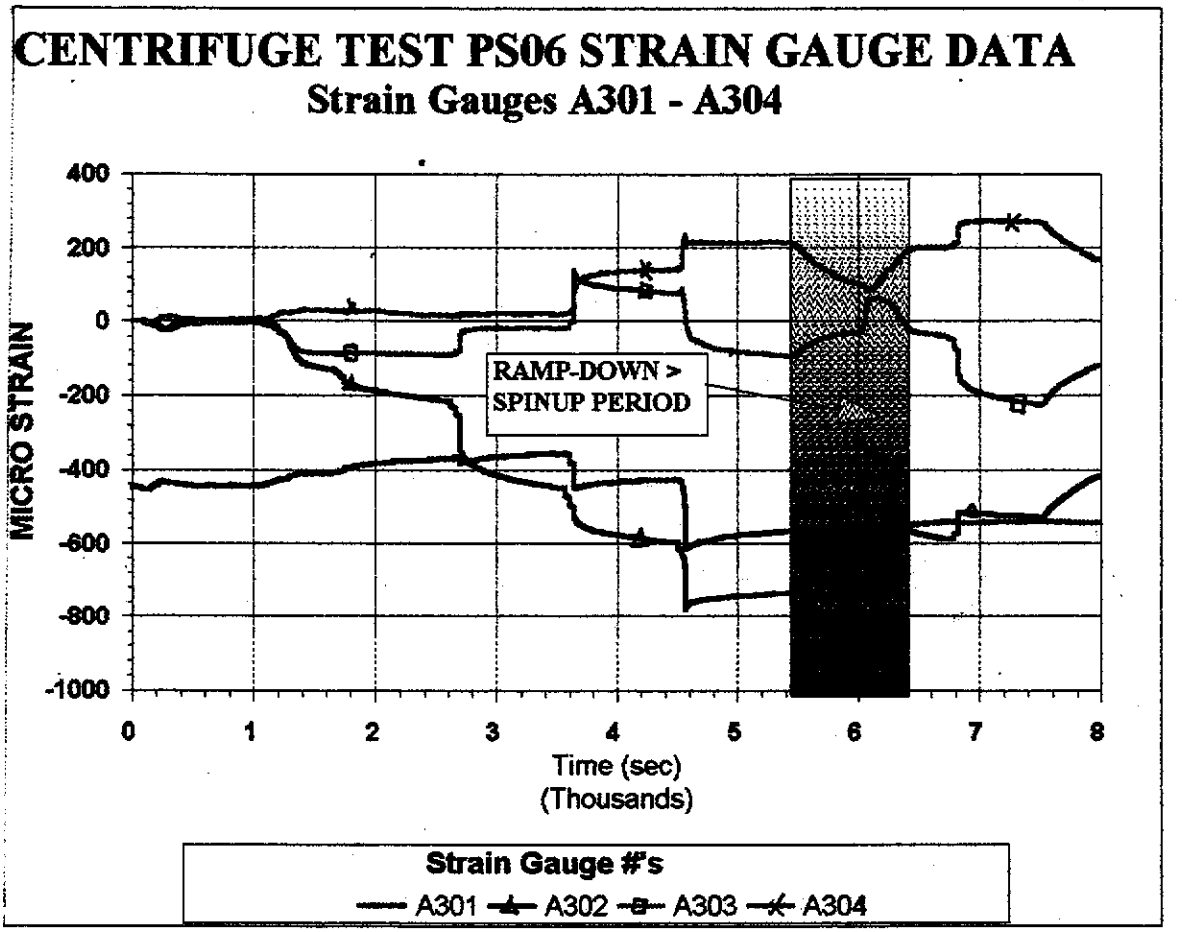

Figure IV.29 d

PRE-TEST PHOTOGRAPH OF CENTRIFUGE MODEL PS07

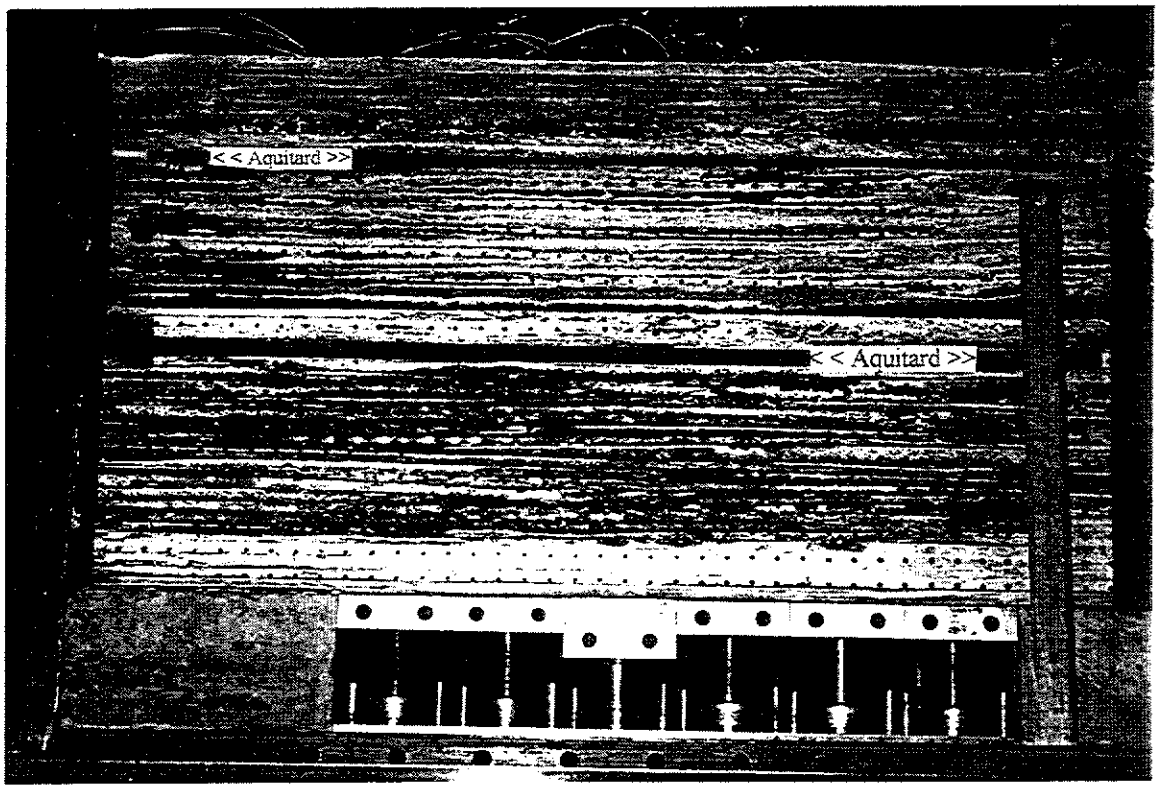

Figure IV.30 a

POST-TEST PHOTOGRAPGH OF CENTRIFUGE MODEL PS07

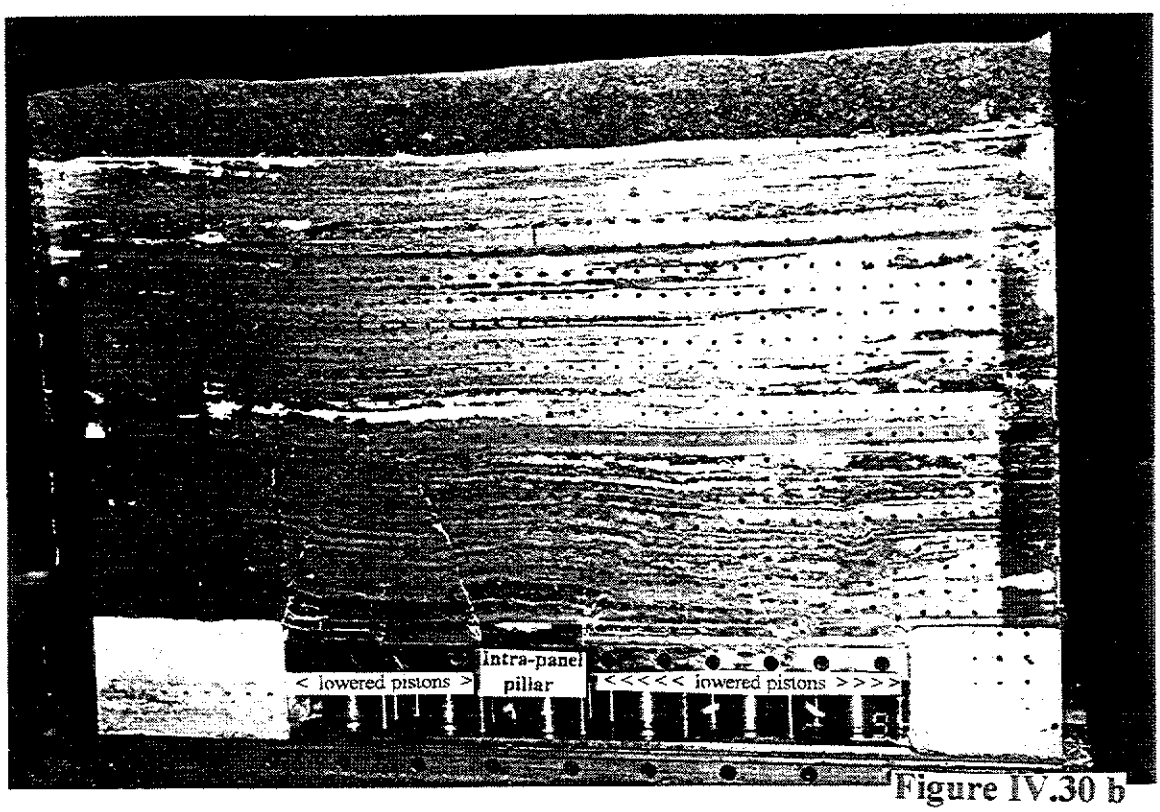

Figure IV.30 b

GEOTECHNICAL CENTRIFUGE TEST PS07

SUBSIDENCE DEVELOPMENT

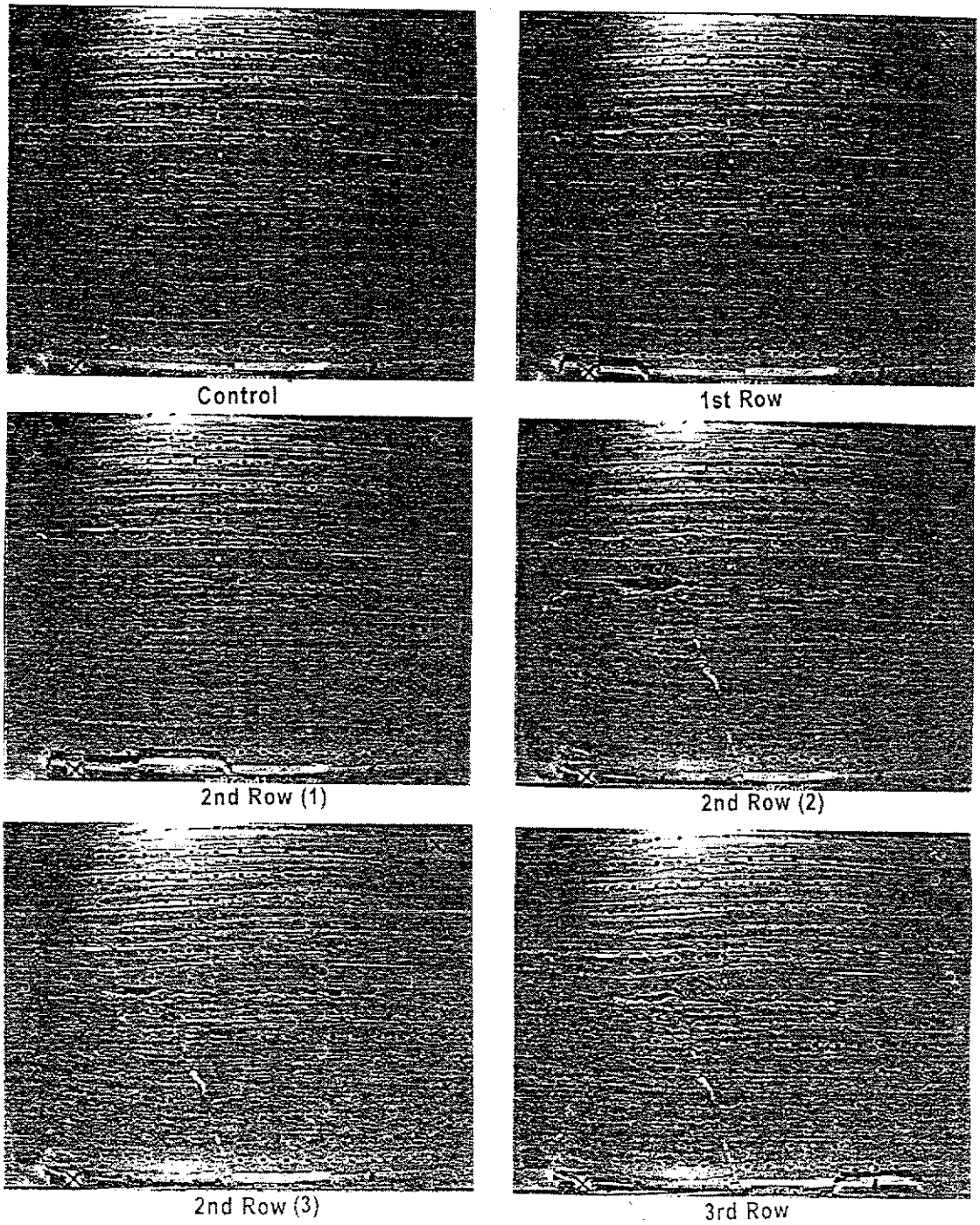

Figure IV.31 a

GEOTECHNICAL CENTRIFUGE TEST PS07

SUBSIDENCE DEVELOPMENT

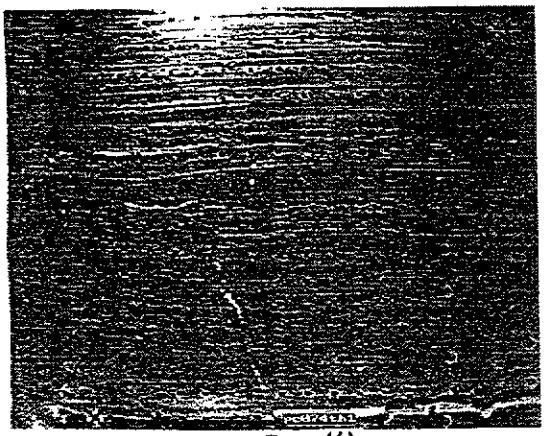

4th Row (1)

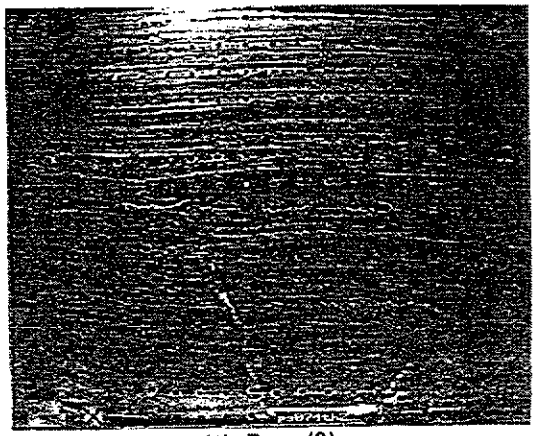

4th Row (2)

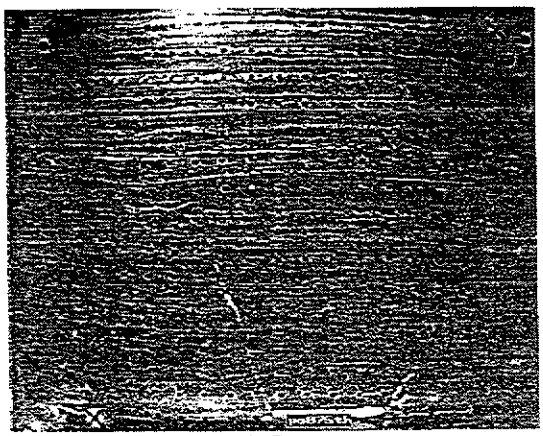

5th Row

Figure IV.31 a

GEOTECHNICAL CENTRIFUGE TEST PS07

SUBSIDENCE DEVELOPMENT

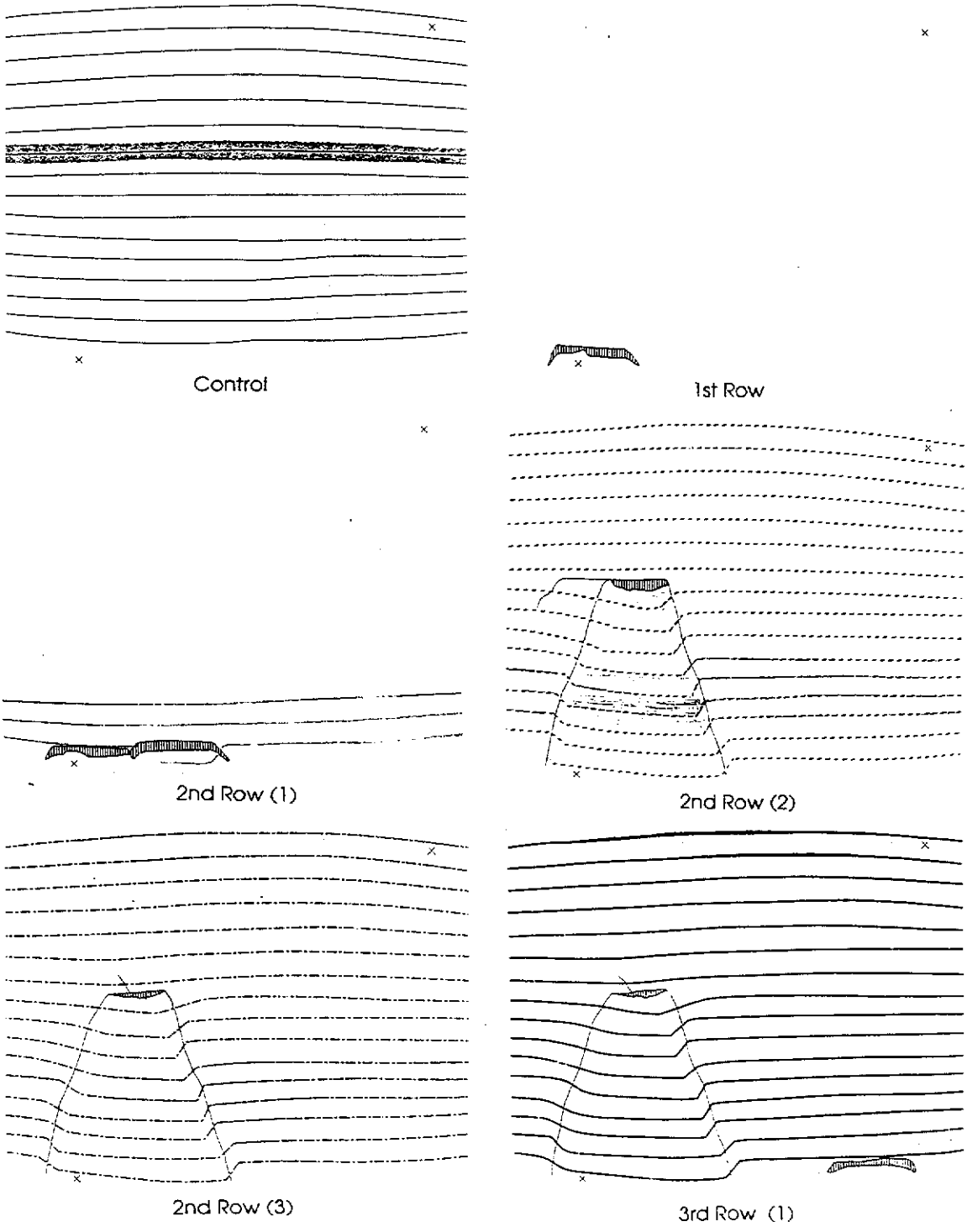

Figure IV.31 b

GEOTECHNICAL CENTRIFUGE TEST PS07

SUBSIDENCE DEVELOPMENT

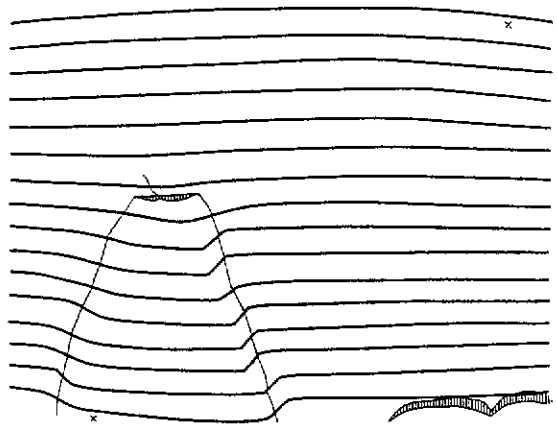

4th Row (1)

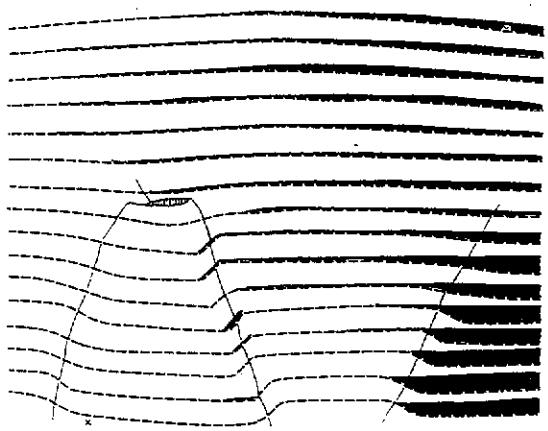

4th Row (2)

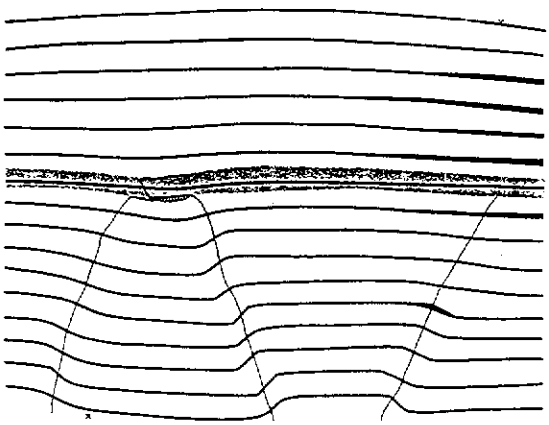

5th Row

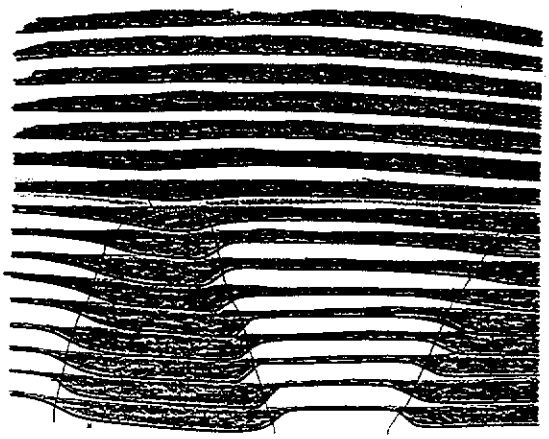

Total Subsidence

Figure IV.31 b

CRACK TRACING ON FRONT OF CENTRIFUGE MODEL PS07

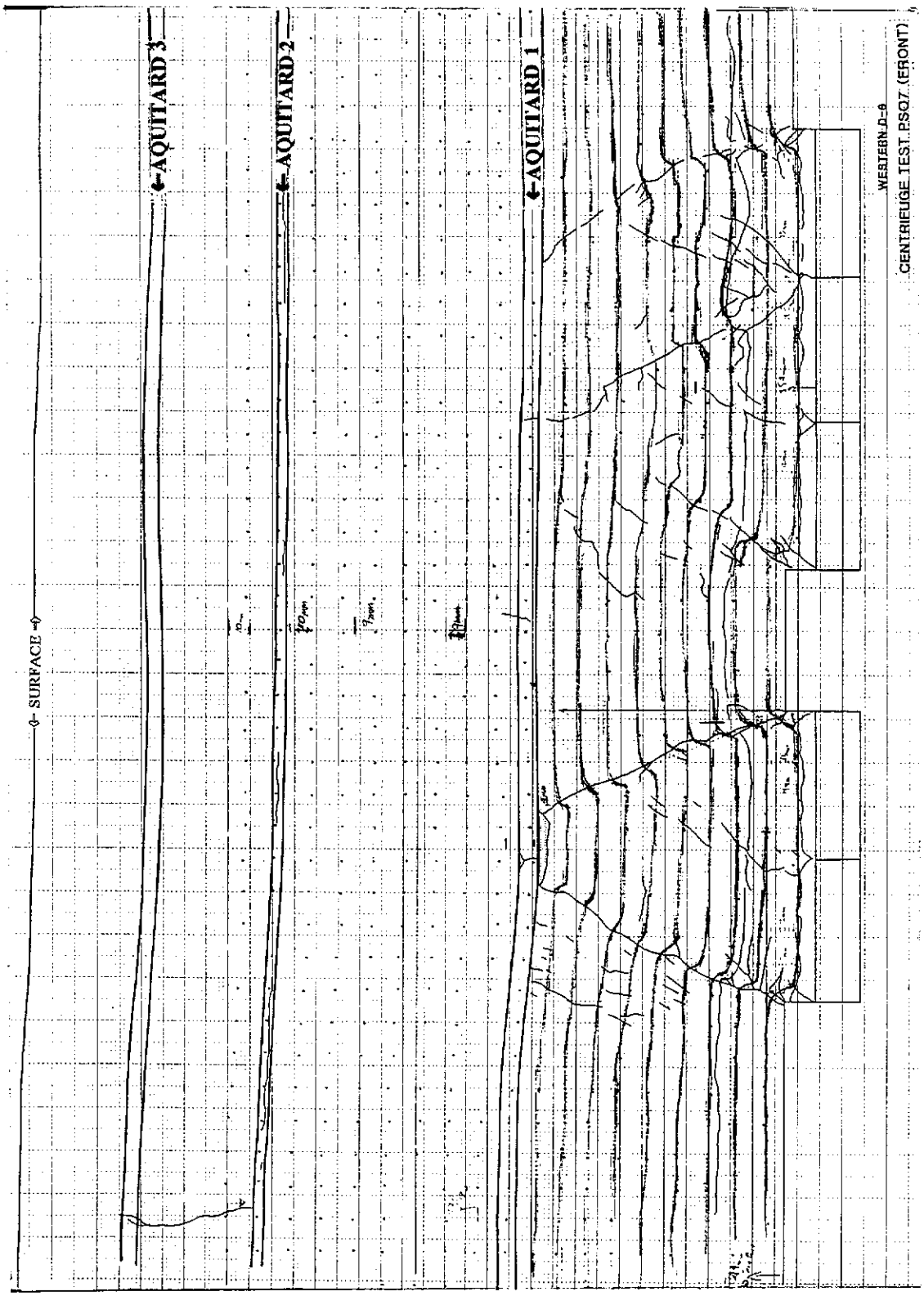

Figure IV.32

ILLUSTRATION OF CRUSHED OVERHANG BELOW THE FIRST AQUITARD - CENTRUFUGE MODEL PS07

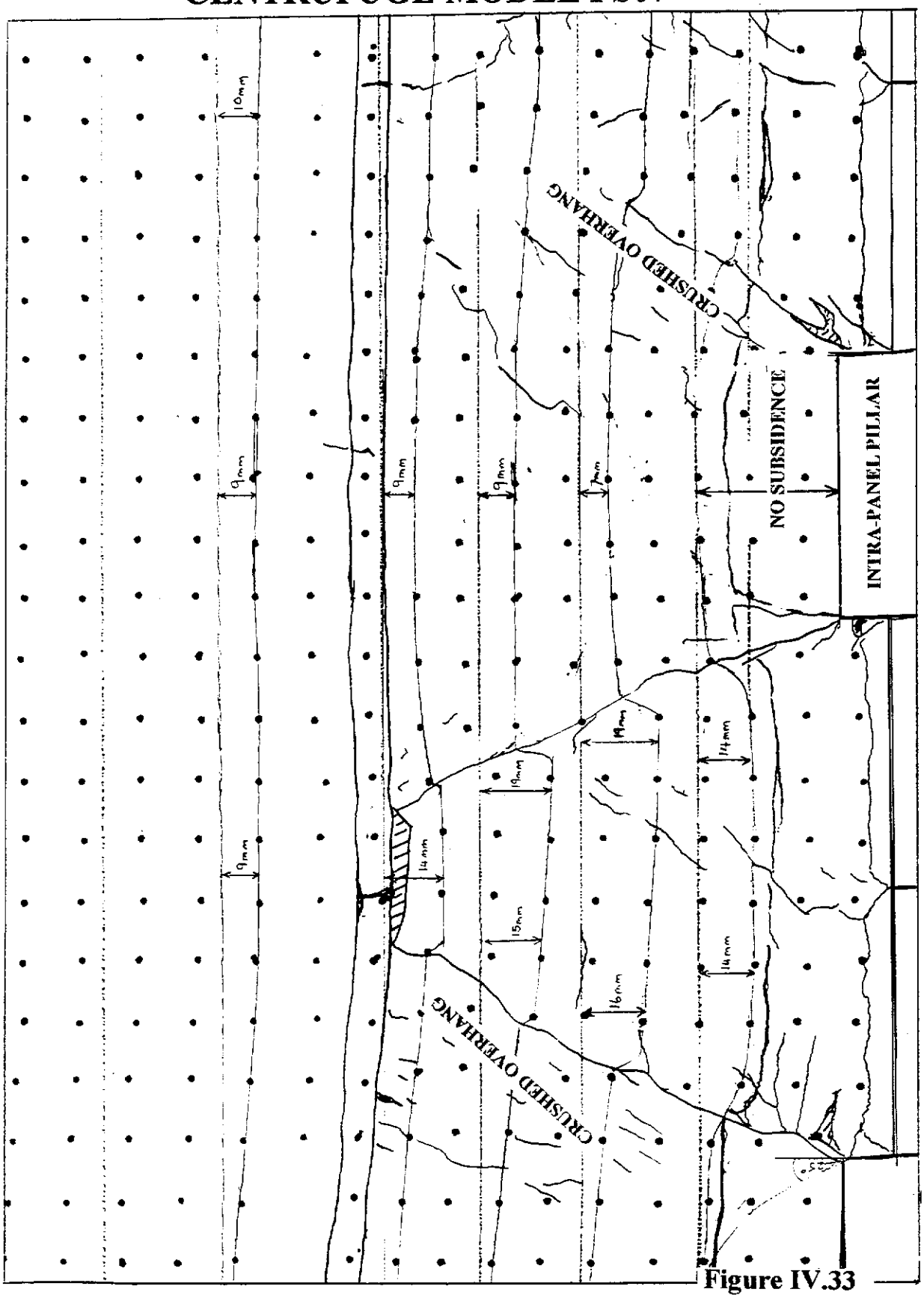

Figure IV.33

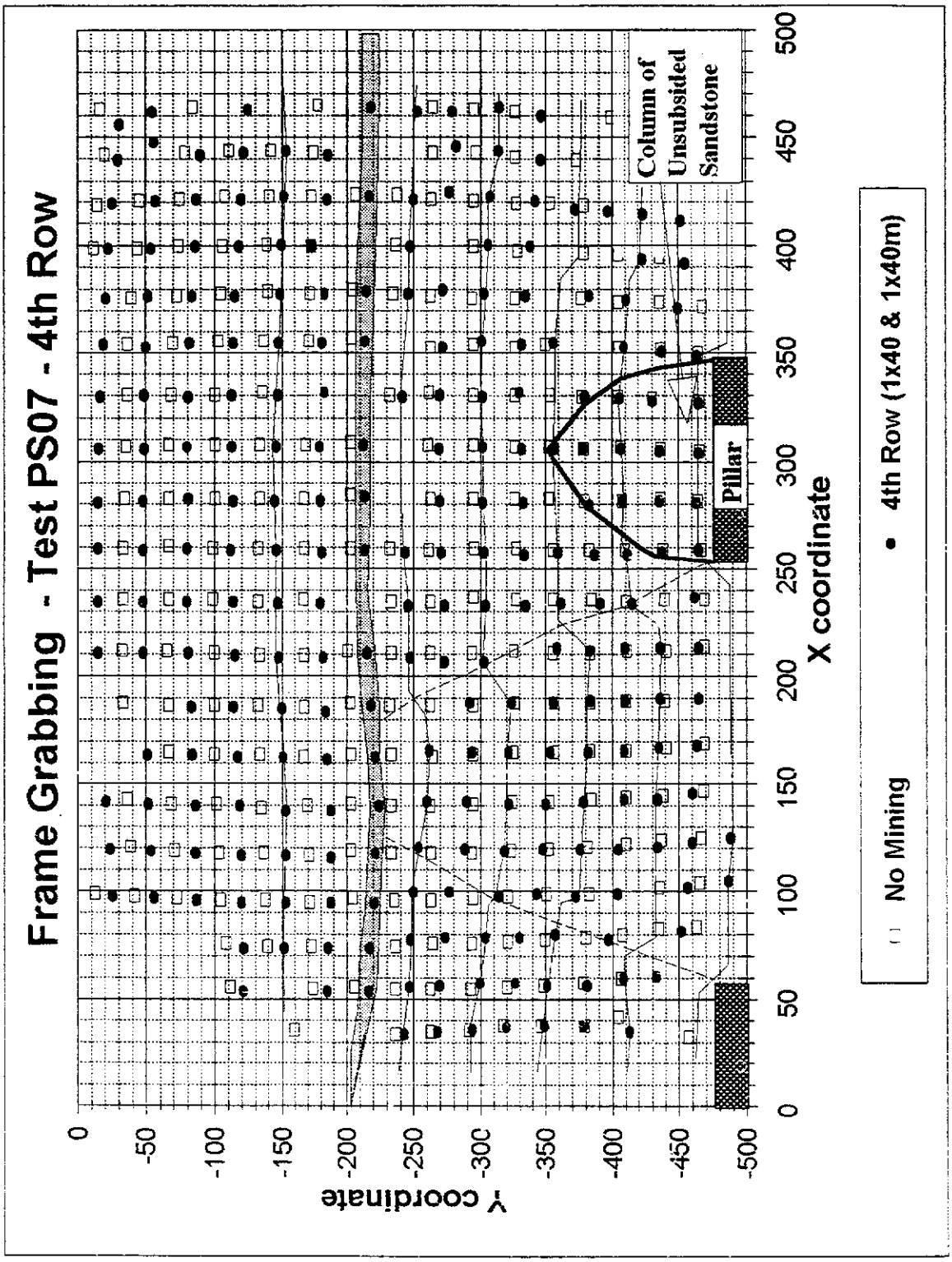
Frame Grabbing - Test PS07 - 4th Row
Column of Unsubsided Sandstone
Pillar
No Mining
4th Row (1x40 & 1x40m)
Y coordinate
X coordinate
0
-50
-100
-150
-200
-250
-300
-350
-400
-450
-500
0
50
100
150
200
250
300
350
400
450
500

Figure IV.34

TABLE IV.7 FRAME GRABBING OF PS07 FACE DOTS DURING TESTING

NO "MINING"			2ND ROW DROP			4TH ROW DROP			5TH ROW DROP			NO "MINING"			2ND ROW DROP			4TH ROW DROP			5TH ROW DROP		
cont			2nd			4th			5th			cont			2nd			4th			5th		
dot #	X	Y	dot #	X	Y	dot #	X	Y	dot #	X	Y	dot #	X	Y	dot #	X	Y	dot #	X	Y	dot #	X	Y
	coordinate "mm"			coordinate "mm"			coordinate "mm"			coordinate "mm"			coordinate "mm"			coordinate "mm"			coordinate "mm"			coordinate "mm"	
280	33	-457	134	32	-241	149	34	-243	139	34	-243	97	236	-166	195	257	-328	25	235	-46	94	234	-149
138	34	-236	257	33	-435	165	35	-268	156	35	-268	200	236	-327	228	257	-382	56	235	-80	110	234	-182
157	35	-263	154	34	-267	268	35	-413	176	36	-295	220	236	-355	245	257	-409	76	235	-114	230	234	-383
95	36	-159	183	34	-293	184	36	-284	192	37	-320	241	236	-384	264	257	-437	289	237	-462	244	234	-391
163	38	-291	180	36	-319	201	37	-320	212	37	-349	278	236	-439	279	257	-465	212	257	-334	6	235	-17
183	38	-317	201	36	-347	222	38	-349	233	38	-380	294	236	-469	5	258	-9	248	257	-387	47	235	-82
205	38	-346	223	37	-378	238	38	-379	45	40	-78	173	237	-294	19	258	-40	265	257	-412	22	236	-50
229	38	-379	110	53	-182	89	54	-121	46	52	-78	144	259	-261	59	258	-105	121	258	-181	295	236	-491
247	42	-404	137	54	-245	126	54	-185	114	54	-188	216	259	-355	77	258	-138	151	258	-244	281	237	-462
112	55	-173	156	56	-269	140	54	-217	130	54	-218	237	259	-382	120	258	-207	170	258	-271	160	257	-271
139	55	-236	205	56	-361	152	56	-247	142	56	-247	253	259	-409	129	258	-237	192	258	-303	181	257	-304
146	55	-262	226	56	-381	167	57	-270	159	57	-272	274	259	-438	213	258	-356	232	258	-360	205	257	-334
184	55	-292	174	57	-298	224	57	-351	177	57	-300	287	259	-466	40	259	-73	279	258	-438	243	257	-387
70	56	-111	184	58	-326	239	57	-381	217	57	-351	11	260	-33	37	275	-66	26	259	-46	258	257	-412
126	56	-206	242	58	-407	185	58	-300	236	57	-382	52	260	-98	99	260	-171	72	258	-112	111	256	-182
184	56	-320	254	60	-433	206	58	-327	197	58	-327	76	280	-132	224	280	-380	95	259	-146	229	258	-361
208	57	-348	111	73	-182	257	60	-408	250	59	-408	101	260	-167	259	280	-436	137	259	-214	271	258	-438
226	58	-378	123	73	-215	271	61	-433	264	61	-433	118	280	-202	275	280	-464	294	259	-465	283	258	-464
248	60	-406	72	74	-118	90	74	-122	105	74	-154	128	260	-232	20	281	-41	6	280	-15	68	259	-115
88	75	-139	138	77	-246	107	74	-152	115	74	-186	181	260	-295	41	281	-72	57	260	-80	92	259	-148
108	75	-172	177	77	-302	128	74	-186	131	74	-219	201	260	-327	60	281	-108	247	280	-383	125	259	-218
141	75	-236	231	77	-396	141	74	-218	84	75	-122	37	281	-66	78	281	-138	8	281	-15	141	258	-245
67	76	-108	157	78	-273	155	78	-248	57	76	-89	233	282	-379	148	281	-264	188	281	-302	4	260	-17
158	78	-264	184	78	-329	250	78	-397	144	78	-249	251	282	-407	171	281	-296	211	281	-333	23	260	-50
165	76	-293	212	79	-366	175	79	-274	245	78	-397	263	282	-464	192	281	-328	291	281	-464	48	260	-82
185	77	-321	266	81	-452	187	79	-304	163	79	-274	12	283	-34	209	281	-352	27	282	-48	241	280	-383
207	78	-349	71	94	-115	206	79	-330	183	79	-304	38	283	-66	241	281	-407	77	282	-114	7	281	-18
232	79	-380	94	94	-149	229	80	-357	198	79	-330	56	283	-100	117	283	-206	96	282	-145	158	281	-271
252	80	-407	114	94	-184	282	82	-452	221	80	-358	79	283	-133	280	305	-465	117	282	-180	178	281	-303
265	83	-434	125	94	-218	66	95	-120	274	82	-453	102	283	-167	221	304	-378	166	282	-270	201	281	-334
282	84	-463	59	95	-84	106	95	-153	101	95	-154	153	283	-262	280	304	-436	260	282	-406	228	281	-359
109	95	-171	34	96	-52	131	96	-186	119	95	-189	174	283	-294	6	305	-9	275	282	-436	254	281	-408
83	96	-104	15	97	-23	145	96	-221	133	95	-222	192	283	-326	21	305	-40	80	283	-81	284	281	-463
66	96	-137	178	97	-313	68	98	-87	58	96	-88	214	283	-362	38	305	-71	134	284	-214	24	282	-51
137	96	-236	200	97	-343	42	97	-56	79	96	-121	267	283	-436	185	305	-327	295	304	-466	71	282	-116
147	96	-263	216	96	-372	16	98	-26	34	97	-57	119	285	-202	207	305	-353	276	305	-436	93	282	-148
44	97	-72	233	96	-403	197	98	-314	17	98	-28	288	305	-465	239	305	-408	9	306	-16	109	282	-181
124	97	-204	138	99	-248	234	98	-373	189	98	-315	230	306	-378	56	306	-104	28	306	-49	267	282	-436
169	97	-294	156	99	-276	219	99	-343	231	98	-373	268	306	-436	79	306	-137	166	306	-268	50	283	-83
19	98	-41	267	101	-457	252	99	-404	210	99	-344	13	307	-35	97	306	-171	209	306	-332	126	284	-215
186	98	-321	70	116	-114	156	100	-250	247	99	-404	193	307	-326	144	306	-261	230	306	-357	267	304	-465
2	99	-12	91	116	-146	176	100	-277	147	100	-252	211	307	-352	164	306	-295	241	306	-379	268	305	-436
208	99	-350	113	116	-183	286	102	-457	168	100	-278	249	307	-406	118	307	-205	255	306	-407	157	306	-270
234	99	-382	52	117	-82	288	105	-487	278	102	-457	39	308	-66	281	326	-466	56	307	-80	179	306	-302
266	102	-435	126	117	-218	132	116	-188	292	105	-487	57	308	-100	250	327	-430	73	307	-113	200	306	-333
285	104	-465	13	118	-19	87	117	-120	120	116	-189	81	308	-133	208	328	-353	97	307	-146	222	306	-367
105	117	-170	33	118	-49	109	117	-153	83	117	-121	103	308	-168	237	328	-405	116	307	-179	235	306	-380
61	118	-103	179	118	-318	65	118	-86	102	117	-154	143	308	-260	22	329	-40	189	307	-302	251	306	-407
84	118	-136	159	119	-286	147	118	-222	56	118	-88	167	308	-294	39	329	-72	135	308	-213	8	307	-19
131	118	-233	202	119	-347	39	119	-54	136	118	-224	120	309	-202	57	329	-104	296	327	-465	27	307	-51
148	118	-263	217	119	-376	200	119	-319	32	119	-55	289	328	-465	128	329	-234	270	328	-431	49	307	-82
166	118	-293	140	120	-252	17	120	-24	193	119	-320	261	329	-430	185	329	-294	254	329	-406	72	307	-115
43	119	-70	238	120	-405	180	120	-259	232	119	-378	231	330	-377	166	329	-328	11	330	-17	95	307	-149
121	119	-203	269	122	-459	223	120	-348	15	120	-25	243	330	-404	76	330	-138	59	330	-81	124	308	-215
187	119	-323	92	137	-147	237	120	-376	172	120	-289	15	331	-36	145	330	-262	150	330	-242	288	327	-465
210	120	-352	112	137	-182	253	120	-405	213	120	-347	41	331	-68	100	331	-173	190	330	-302	263	328	-431
18	121	-38	50	139	-80	180	121	-254	248	120	-406	58	331	-100	276	348	-464	242	330	-360	249	329	-406
235	121	-381	69	139	-113	272	121	-434	149	121	-254	129	331	-232	281	350	-436	29	331	-49	140	330	-244
254	122	-410	127	139	-220	287	123	-460	265	121	-434	175	331	-294	147	351	-263	74	331	-113	182	330	-303
272	124	-437	10	140	-15	299	125	-489	280	123	-460	194	331	-326	187	351	-328	100	331	-147	237	330	-360
286	125	-466	28	140	-46	110	138	-153	293	125	-488	213	331	-353	240	351	-405	169	331	-270	10	331	-20
82	139	-134	219	140	-378	133	138	-188	103	138	-153	83	332	-135	7	352	-10	122	332	-183	28	331	-52
100	140	-169	160	141	-290	66	140	-86	121	138	-189	145	332	-261	23	352	-40	207	332	-330	52	331	-84
134	140	-233	181	141	-320	85	140	-119	59	140	-88	284	350	-484	186	352	-294	292	349	-484	73	331	-116
149	140	-262	203	141	-350	148	140	-225	80	140	-120	269	352	-436	204	352	-351	280	351	-436	96	331	-149
40	141	-66	142	142	-258	33	141	-52	138	140	-227	154	353	-262	42	353	-72	31	353	-50	161	331	-272
60	141	-101	243	142	-408	202	141	-322	30	141	-54	195	353	-326	58	354	-104	174	353	-272	224	331	-356
122	141	-203	268	145	-459	225	141	-350	194	141	-322	250	353	-405	80	354	-138	261	353	-409	199	332	-331
170	141	-284	89	161	-145	14	142	-21	216	141	-351	18	354	-36	96	354	-171	13	354	-19	285	349	-463
188	142	-324	109	161	-179	162	142	-260	234	141	-380	176	354	-294	115	355	-204	210	354	-332	272	351	-438
212	142	-353	68	162	-111	181	142	-290	13	142	-23	209	354	-349	282	370	-466	61	355	-82	167	352	-274
14	143	-36	124	162	-216	240	142	-379	154	142	-260	42	355	-69	282	372	-435	78	355	-114	256	353	-409
239	143	-384	49	163	-78	258	143	-409	173	142	-291	59	356	-102	238	373	-405	101	355	-148	12	354	-23
255	144	-410	162	164	-262	273	143	-434	252	143	-409	85	356	-136	8	374	-11	119	355	-181	29	354	-53
273	145	-438	182	164	-321	288	148	-460	279	148	-460	106	356	-170	167	374	-294	228	355	-358	55	355	-85
291	147	-468	206	164	-353	127	152	-185	294	147	-468	125	357	-203	188	374	-328	136	356	-214	74	355	-117
96	163	-156	225	164	-382	64	163	-117	118	162	-187	290	372	-467	218	374	-378	166	356	-301	113	355	-184
158	163	-264	143	165	-261	105	163	-151	77	163	-118	244	374	-404	28	375	-41	201	371	-450	180	356	-302
53	164	-99	244	165	-408	146	163	-222	100	163	-153	270	374	-435	148	375	-263	264	375	-411	202	355	-334
80	164	-133	255	166	-434	34	164	-51	134	163	-224	20	376	-39	43	376	-73	15	376	-21	223	355	-357
116	164	-203	273	167	-463	62	164	-94	53	164	-86	168	376	-293	61	376	-105	35	377	-52	98	356	-150
135	164	-233	108	183	-178	183	165	-294	195	164	-323	196	376	-328	82	376	-140	64	377	-84	127	356	-216
171	164	-294	48	185	-77	203	165	-322	31	165	-53	225	376	-378	130	376	-235	79	377	-115	273	371	-451
35	165	-66	64	185	-108	228	165	-354	174	165	-294	45	377	-72	103	377	-173	214	377	-335	14	376	-25
190	165	-325	88	185	-143	243	165	-382	218	165	-354	155	377	-262	116	378	-205	244	377	-383	259	376	-413
217	165	-356	122	186	-213	164	166	-262	238	165	-383	64	378	-104	277	392	-464	103	378	-149	33	377	-56
236	166	-383	161	187	-290	259	166	-409	155	166	-263	107	378	-171	256	393	-434	123	378	-183	206	377	-336
256	166	-410	183	188	-323	274	167	-435	253	166	-409	136	378	-234	222	395	-378	154	378	-246	242	377	-384
275	167	-440	211	188	-354	290	168	-464	266	167	-435	59	379	-139	234	395	-404	191	378	-303	60	378	-88
292	169	-469	229	189	-383	124	184	-184	299	169	-493	123	380	-204	9	397	-12	138	379	-215	78	378	-119
98	186	-167	246	189	-410	102	185	-150	116	184	-185	271	385	-435	27	397	-43	171	380	-272	104	378	-154
36	187	-66	263	189	-436	63	186	-83	150	185	-256	245	386	-404	193	397	-328	285	392	-455	117	378	-186
54	187	-99	274	189	-484	75	186	-114	54	186	-85	227	387	-376	48	398	-75	268	394	-423	146	378	-249
77	187	-132	155	206	-288	143	187	-219	89	186	-116	202	388	-328	83	398	-106	16	399	-23	185	378	-305
130	187	-232	175	207	-299	182	188	-282	99	186	-151	3	389	-11	131	398	-237	37	398	-54	128	379	-218
150	187	-262	85	208	-142	204	188	-324	26	187	-51	22	389	-43	166	398	-295	87	400	-86	166	381	-274
180	187	-294	105	208	-178	227	188	-356	132	187	-221	46	400	-73	83	399	-139	62	400	-118	277	392	-456
9	188	-33	136	208	-241	245	189	-384	9	188	-19	65	400	-105	272	413	-462	114	400	-174	282	394	-425
117	188	-202	44	209	-74	262	189	-410	175	188	-293	110	400	-172	252	414	-432	158	400	-248	18	399	-27
191	188	-326	66	209	-108	277	190	-437	196	188	-325	177	400	-294	235	416	-404	215	400	-338	36	399	-59
218	188	-356	3	210	-9	293	190	-465	220	189	-356	87	401	-138	220	417	-377	104	401	-150	148	399	-251
240	188	-383	25	210	-42	172	207	-273	239	189	-385	140	401	-238	11	418	-16	195	401	-306	81	400	-90
257	188	-410	199	210	-338	193	207	-303	256	189	-411	281	416	-462	210	418	-354	283	412	-452	81	400	-122
276	189	-439	121	211	-211	56	209	-148	289	190	-437	262	416	-432	169	419	-295	269	415	-424	207	400	-340
78	210	-133	268	211	-436	120	209	-182	286	190	-464	246	417	-404	191	419	-327	251	416	-397	106	401	-154
98	210	-167	227	212	-382	157	209	-248	164	207	-274	4	419	-14	29	420	-46	236	417	-373	137	401	-223
55	211	-89	247	212	-409	80	210	-115	184	207	-304	228	419	-376	47	421	-78	19	420	-26	167	402	-308
132	211	-233	214	213	-357	7	211	-15	112	208	-184	199	420	-327	65	421	-109	44	421	-57	280	411	-483
151	211	-262	275	213	-464	24	211	-48	97	209	-150	215	420	-353	84	421	-142	218	421	-342	276	413	-453
172	211	-293	133	232	-239	55	211	-81	145	209	-249	25	421	-45	104	421	-174	89	422	-87	261	415	-425
219	211	-355	153	232	-267	139	211	-216	78	210	-157	178	421	-294	132	421	-238	88	422	-120	246	417	-399
238	211	-383	176	232	-299	248	212	-383	5	211	-18	47	422	-74	149	421	-264	129	422	-155	18	421	-31
8	212	-32	81	233	-139	231	213	-359	21	211	-50	159	422	-263	119	422	-207	169	422	-250	39	421	-60
33	212	-65	196	233	-331	263	213	-410	51	211	-83	69	423	-107	271	432	-461	108	423	-152	211	421	-344
115	212	-200	215	233	-359	278	213	-437	128	211	-218	90	423	-140	253	435	-432	142	423	-218	88	422	-125
189	212	-325	249	233	-412	297	213	-466	240	212	-364	111	423	-172	232	437	-401	186	423	-306	151	422	-254
259	212	-411	4	234	-9	153	233	-246	257	213	-410	127	424	-206	14	439	-19	177	425	-277	62	423	-92
277	212	-440	24	234	-41	173	233	-273	270	213	-438	142	424	-237	32	439	-48	21	440	-30	107	423	-157
293	214	-469	45	234	-74	194	233	-304	289	213	-465	263	437	-432	189	440	-327	220	440	-345	122	423	-189
75	235	-132	62	234	-106	213	233	-335	227	214	-359	224	440	-373	51	441	-79	70	442	-90	135	423	-223
133	235	-233	102	234	-174	99	234	-147	204	232	-336	197	441	-326	152	441	-265	130	442	-168	188	423	-311
152	235	-262	230	234	-386	118	234	-180	143	233	-247	7	442	-19	172	441	-296	91	443	-122	169	428	-280
258	235	-410	270	236	-461	233	234	-362	165	233	-274	48	443	-78	67	442	-110	111	444	-154	275	433	-453
10	236	-33	101	257	-173	249	234	-391	188	233	-304	113	443	-174	86	442	-143	198	444	-314	19	440	-35
34	236	-66	151	257	-264	267	234	-415	260	233	-415	160	443	-264	106	442	-175	179	446	-282	214	440	-348
51	236	-98	173	257	-297	5	235	-15	70	234	-116	182	443	-296	251	455	-430	48	448	-56	64	443	-95
97	236	-166	195	257	-328	25	235	-48	94	234	-149	71	444	-110	190	460	-329	22	456	-31	87	443	-127
200	236	-327	228	257	-382	56	235	-80	110	234	-182	91	444	-141	170	461	-296	221	460	-347	123	443	-191
220	236	-355	245	257	-408	76	235	-114	230	234	-363	242	459	-399	135	462	-241	41	462	-55	108	444	-159
241	236	-384	264	257	-437	289	237	-462	244	234	-391	198	462	-326	150	462	-265	161	462	-263	190	444	-315
278	236	-439	279	257	-465	212	257	-334	8	235	-17	6	463	-16	54	463	-88	178	462	-279	171	446	-285
294	236	-469	5	258	-9	248	257	-387	47	235	-82	179	463	-295	90	463	-145	92	463	-125	215	460	-349
173	237	-294	19	258	-40	265	257	-412	22	236	-50	49	464	-83	12	464	-15	144	464	-219	152	462	-258
144	259	-261	59	258	-105	121	258	-181	295	236	-491	161	464	-264	107	464	-177	189	464	-315	170	462	-283
216	259	-355	77	258	-138	151	258	-244	281	237	-462	114	465	-177	35	479	-50				191	464	-318

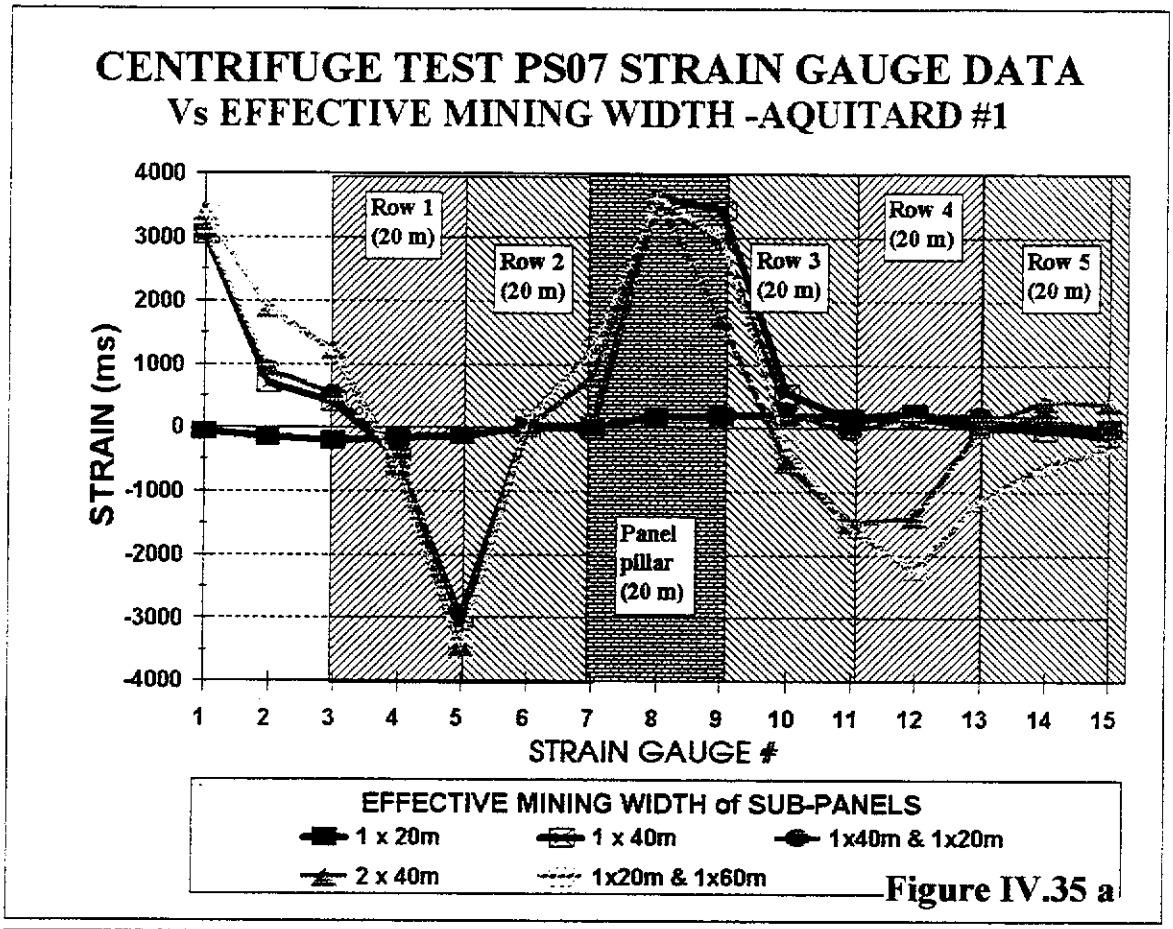

Figure IV.35 a

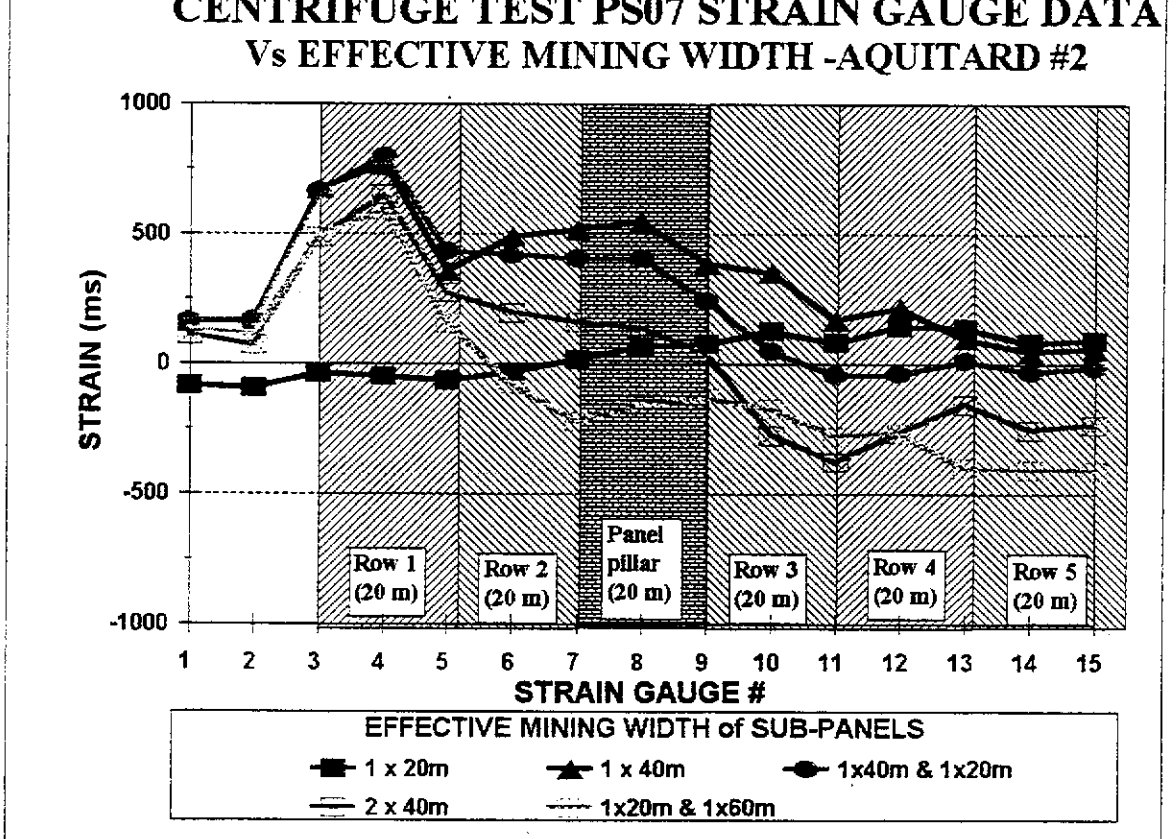

Figure IV.35 b

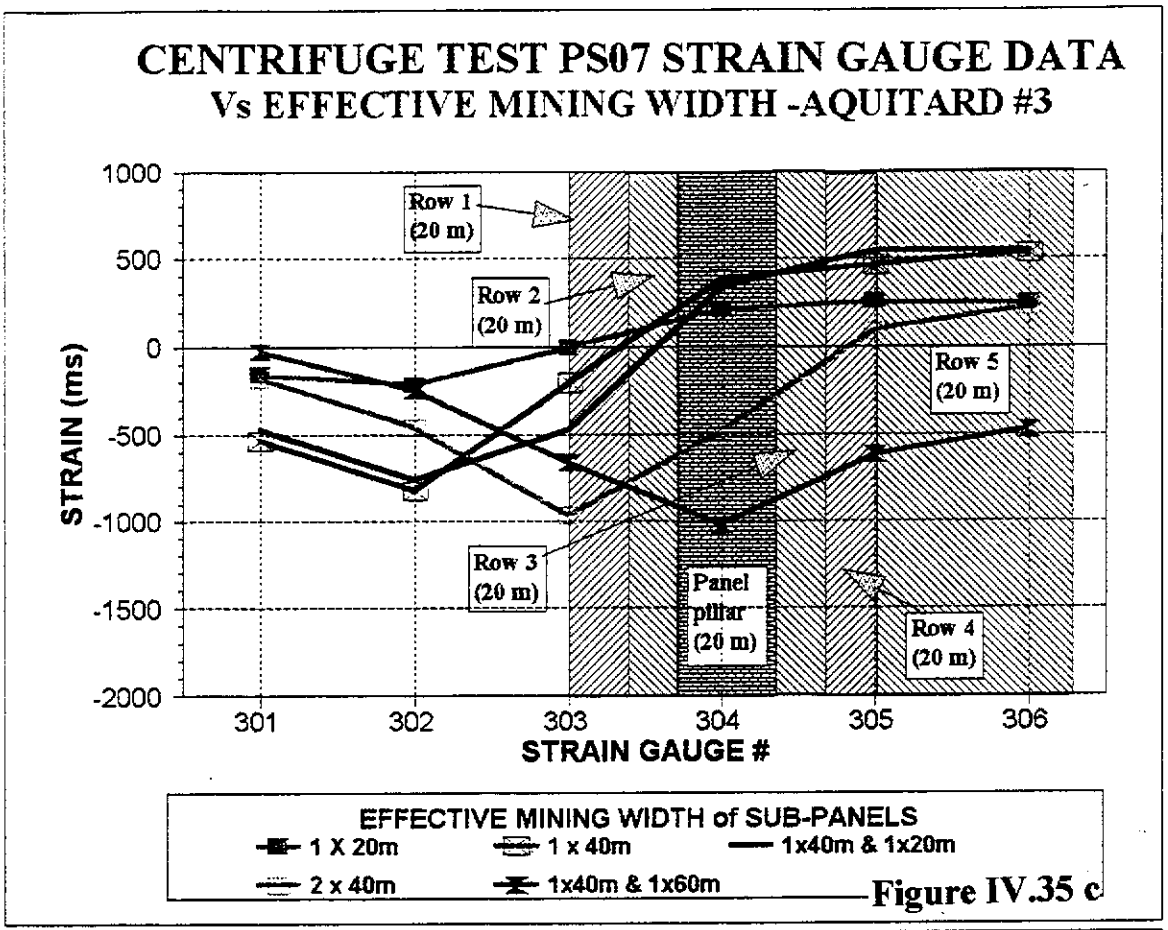

Figure IV.35 c

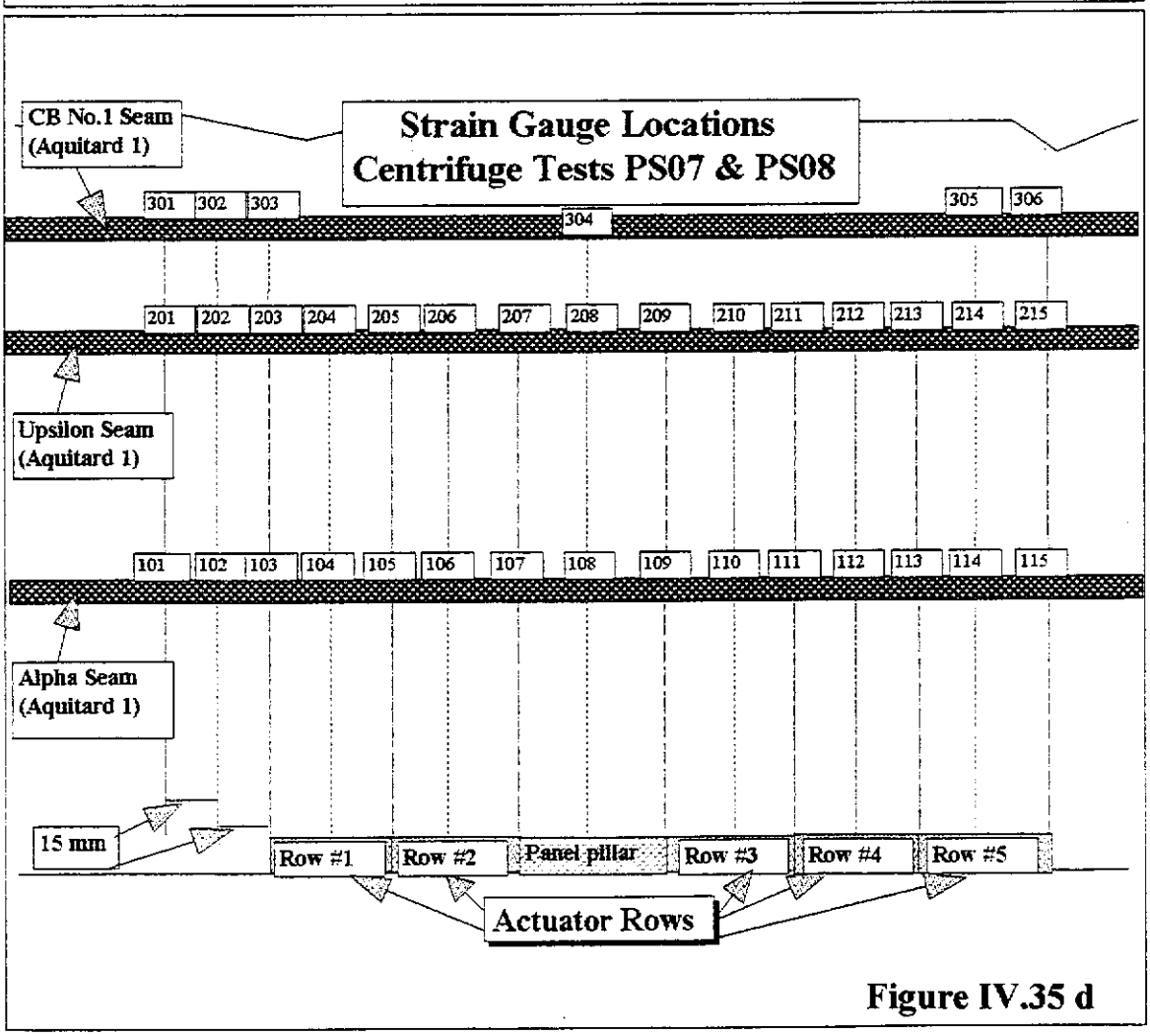

Figure IV.35 d

TABLE IV.8

SUMMARY OF CENTRIFUGE TEST PS07 STRAIN GAUGE DATA RAW DATA

GAUGE #	ROW # 0 mstrain	1 mstrain	2 mstrain	3 mstrain	4 mstrain	5 mstrain
101	-307	-247	-3347	-3369	-3702	-3702
102	-285	-133	-984	-1199	-2160	-2150
103	-184	28	-589	-714	-1396	-1365
104	-7	163	474	444	595	650
105	-88	43	2908	2924	3362	3416
106	10	22	1	-20	10	-118
107	22	14	42	-32	-763	-1227
108	-51	-222	-3707	-3595	-3707	-3707
109	-42	-235	-3477	-2987	-1756	-3044
110	-20	-205	-569	-287	538	312
111	-19	-177	-159	37	1483	1541
112	-74	-308	-254	-262	1332	2160
113	-66	-142	-78	-262	-70	1069
114	-100	-146	-66	-223	-528	484
115	-5	0	116	8	-386	348
201	-186	-101	-344	-350	-295	-320
202	-135	-40	-298	-301	-205	-247
203	-10	29	-683	-673	-498	-503
204	-1	50	-765	-797	-651	-594
205	-26	39	-382	-458	-296	-178
206	-25	9	-515	-441	-220	53
207	14	0	-503	-390	-144	235
208	63	1	-485	-342	-72	222
209	72	-2	-312	-167	33	204
210	138	14	-211	92	412	312
211	86	7	-80	131	464	364
212	152	10	-63	192	418	417
213	178	44	82	171	333	578
214	89	10	47	124	343	496
215	66	-23	11	84	299	477
301	138	295	671	611	319	162
302	97	314	922	861	554	344
303	397	402	600	865	1364	1056
304	376	163	-5	39	862	1396
305	465	209	1	-82	372	1083
306	539	295	11	-6	313	1009

TABLE IV.9

LOAD CELL DATA Vs ACTUATOR ROW

LOAD CELL #	ACTUATOR ROW # 0	1	2	3	4	5
	LOAD (N)					
1	4640	308	1643	1892	2200	2339
2	4184	4591	1182	1550	2504	2695
3	4484	4486	4561	796	2216	2817
4	3731	3630	3510	3014	1590	3590
5	3267	3181	3122	2942	1887	1584
6	6174	6641	6509	7297	7228	7787
7	6270	6840	6595	7397	7276	8231
8	7679	8246	7684	8635	8569	9648

LOAD CELL ARRANGEMENT FOR CENTRIFUGE TESTS PS07 - PS09
(TOP CAPS REMOVED)

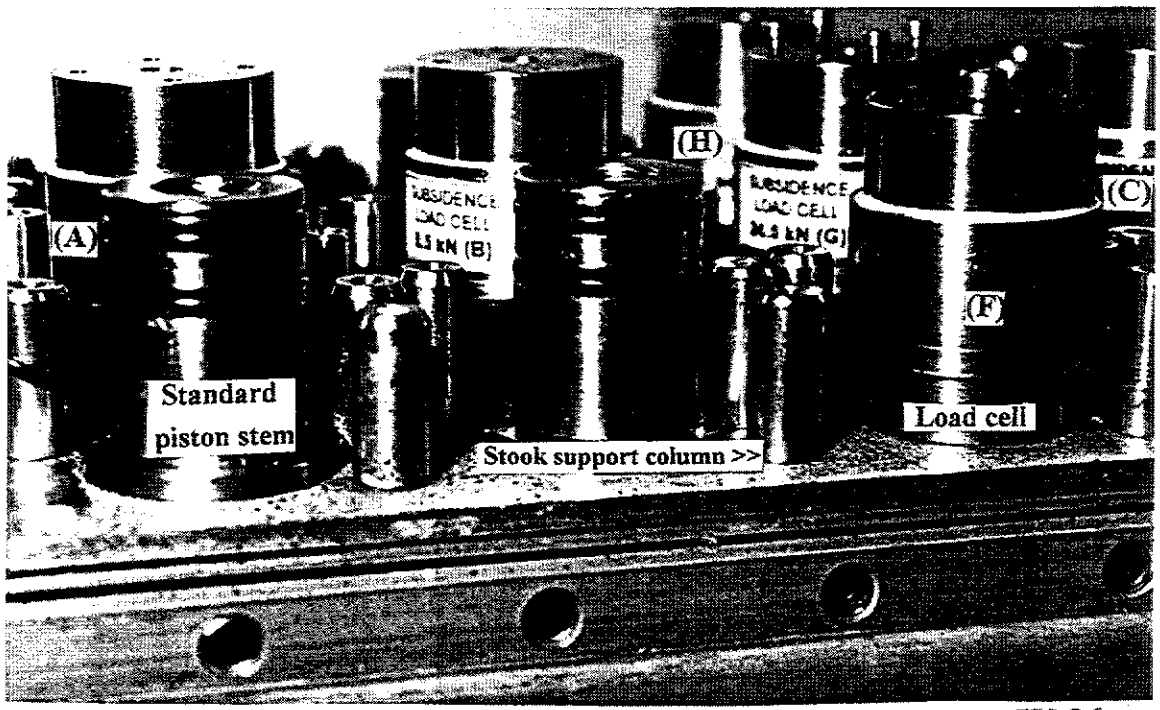

(Only load cells A, B, C, F, G, H are displayed) **Figure IV.36 a**

LOAD CELL CALIBRATION WEIGHTS

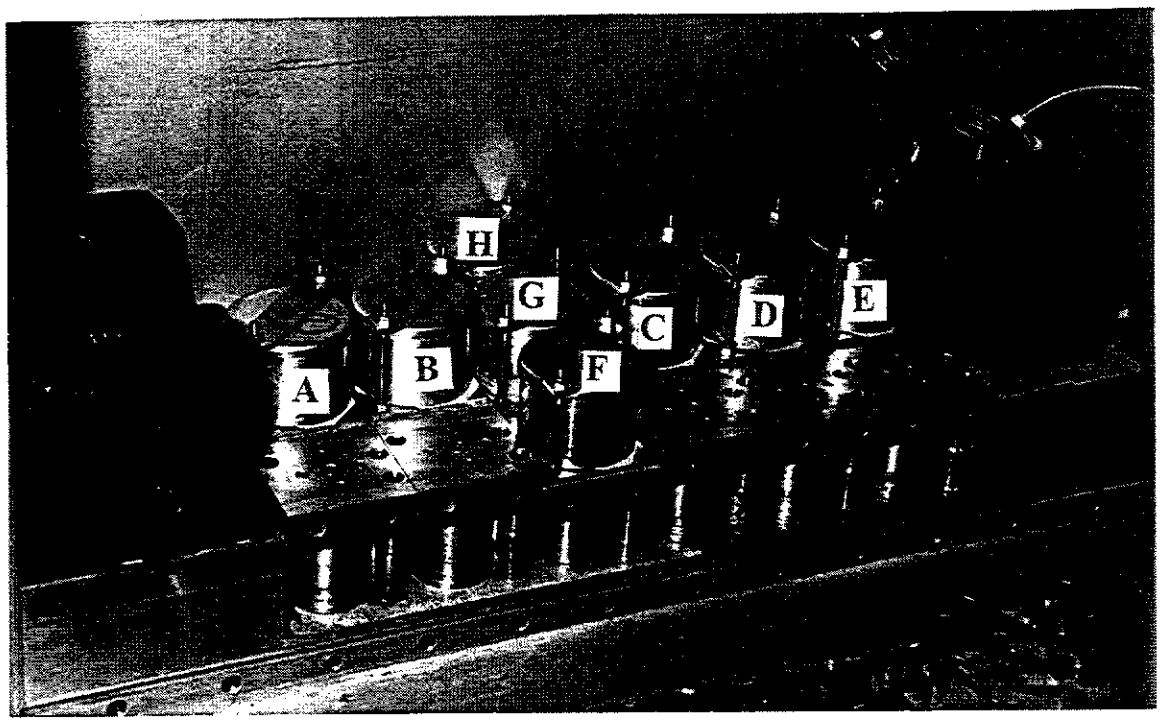

Calibration weights clamped at corresponding load cell positions.

Figure IV.36 b

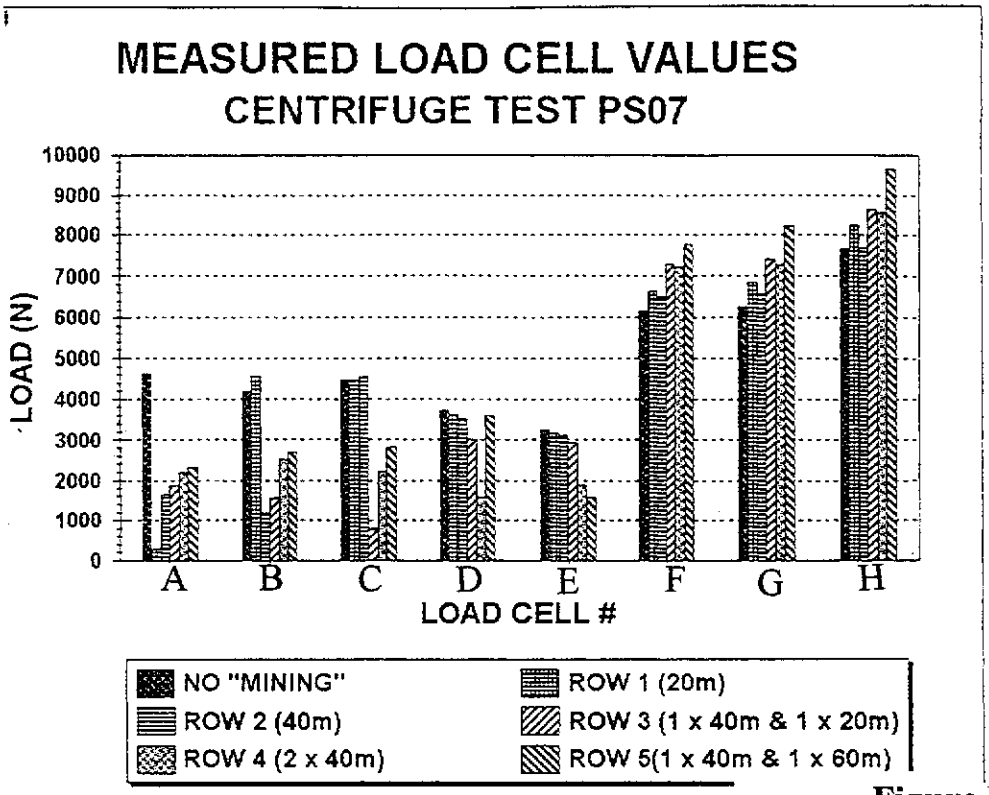

Figure IV.37 a

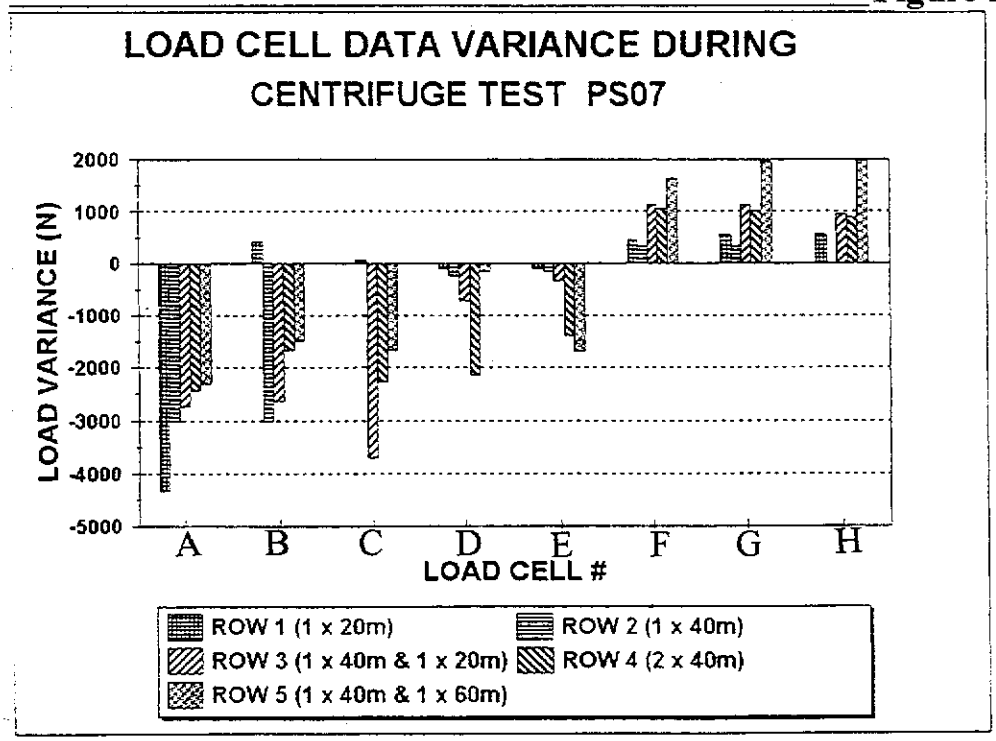

Figure IV.37 b

DIAGRAMMATICAL VIEW OF LOAD CELL VALUES CENTRIFUGE TEST PS07

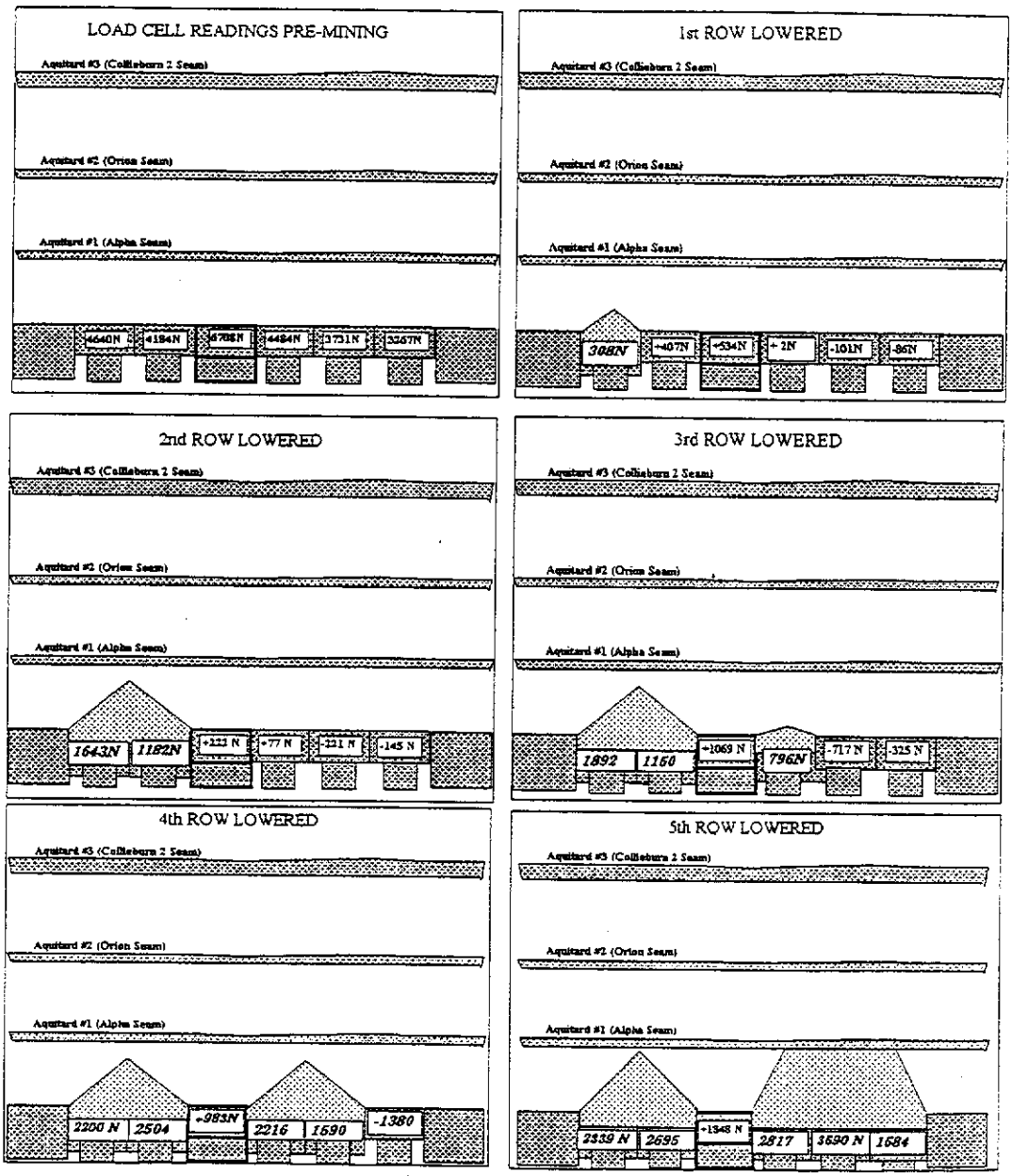

Note :- Loads are given as : a) total loads for lowered actuators, and
b) load variance from pre-mining loads
for unlowered actuators

Figure IV.38

3 DIMENSIONAL SCHEMATIC VIEW OF LOAD CELL DATA PS07

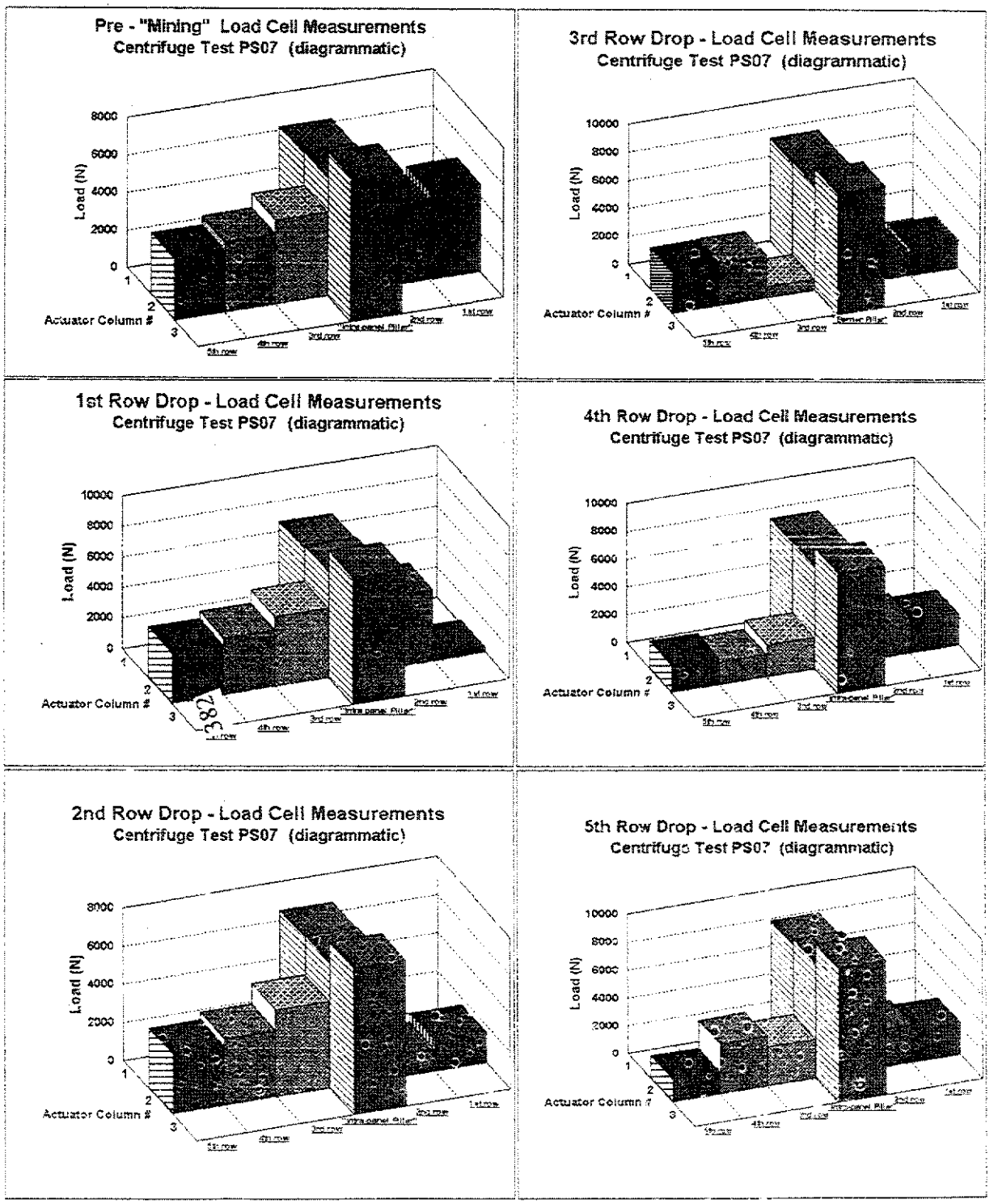

Figure IV.39

WATER FILLED AQUIFER CONSTRUCTION
CENTRIFUGE MODEL PS08

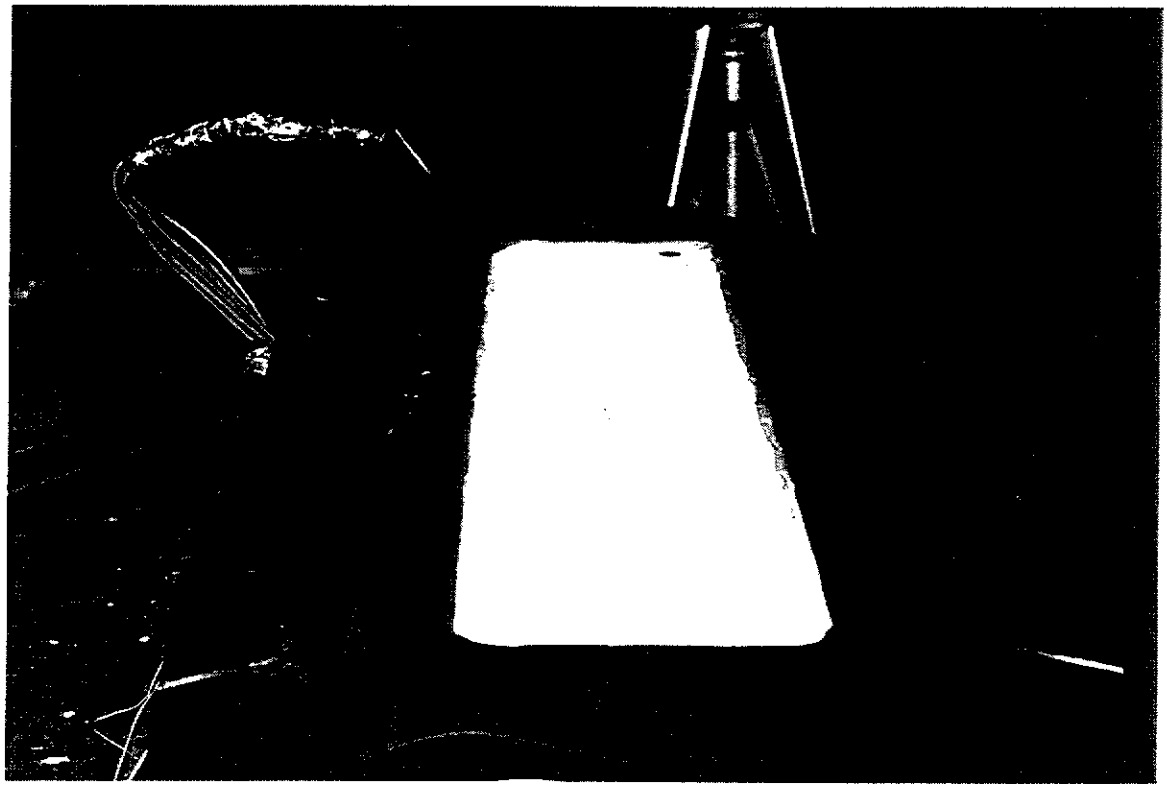

a) Neoprene Rubber Gasket Cut to Shape

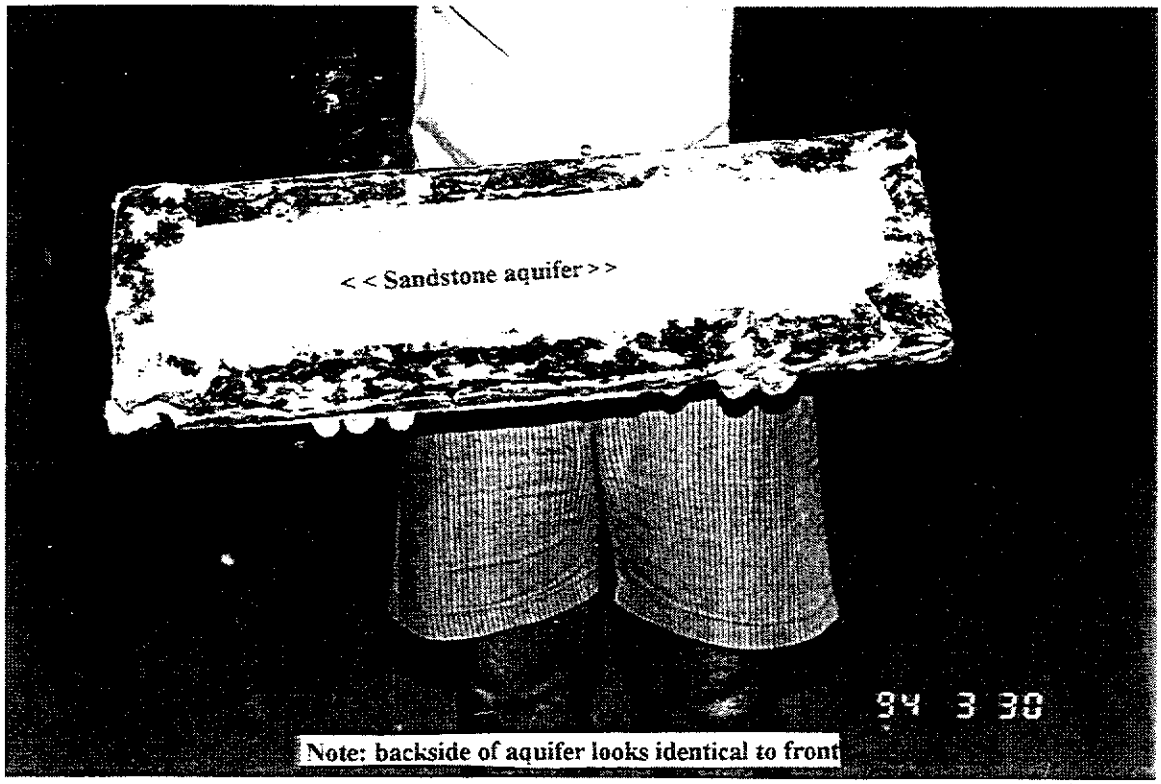

b) Isolated Aquifer after Dismantling

Figure IV.40

STAND-PIPE CONFIGURATION
CENTRIFUGE MODEL PS08

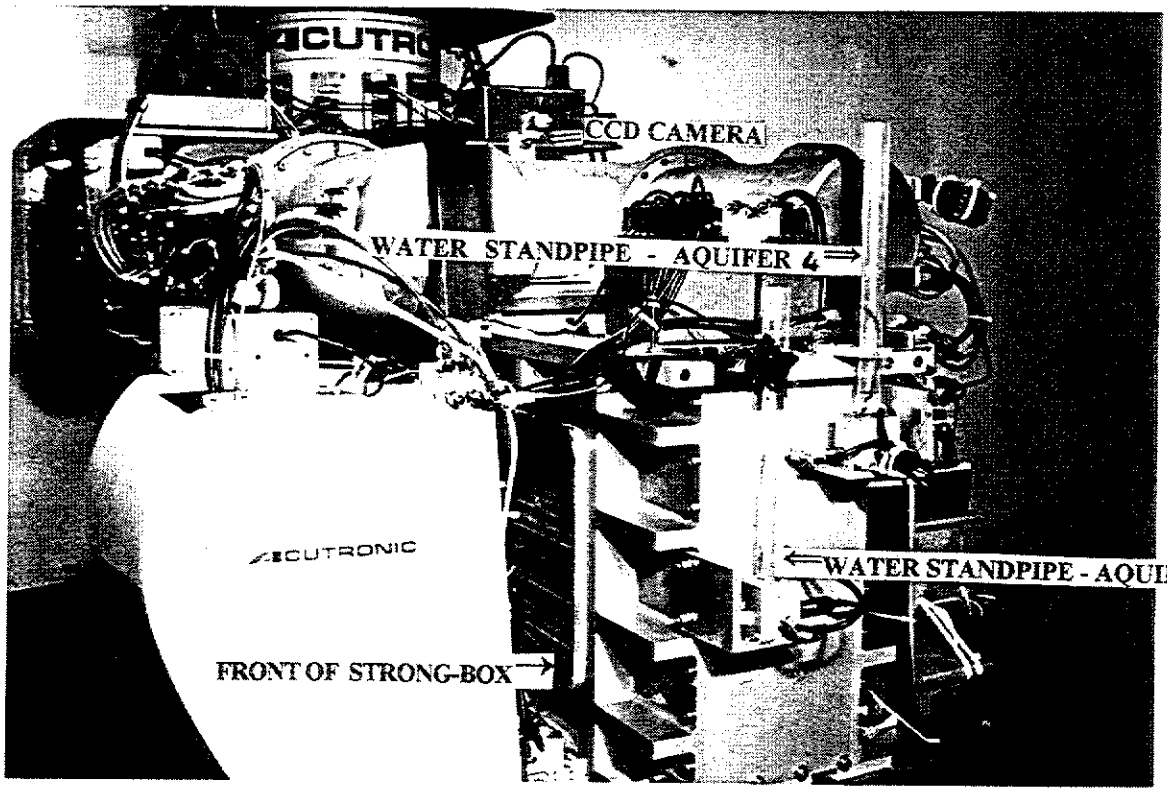

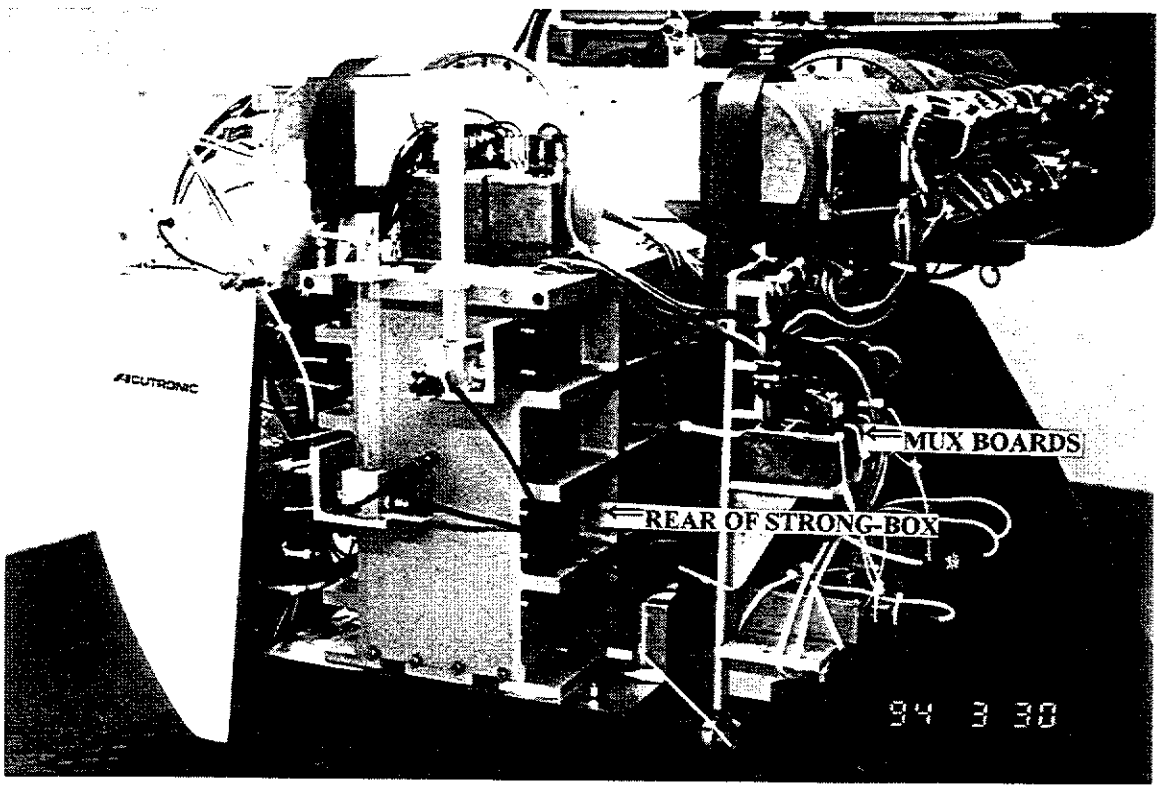

Figure IV.41

POST-TEST PHOTOGRAPHS OF CENTRIFUGE MODEL PS08

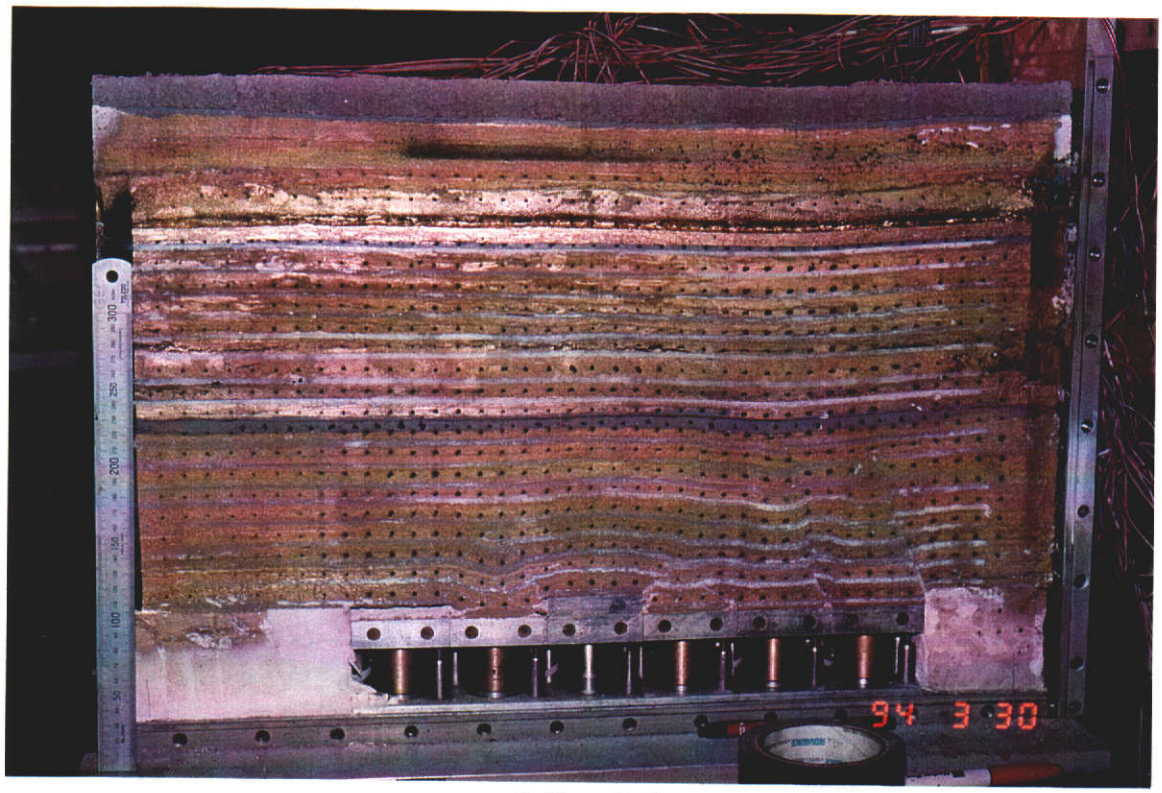

a) Front view

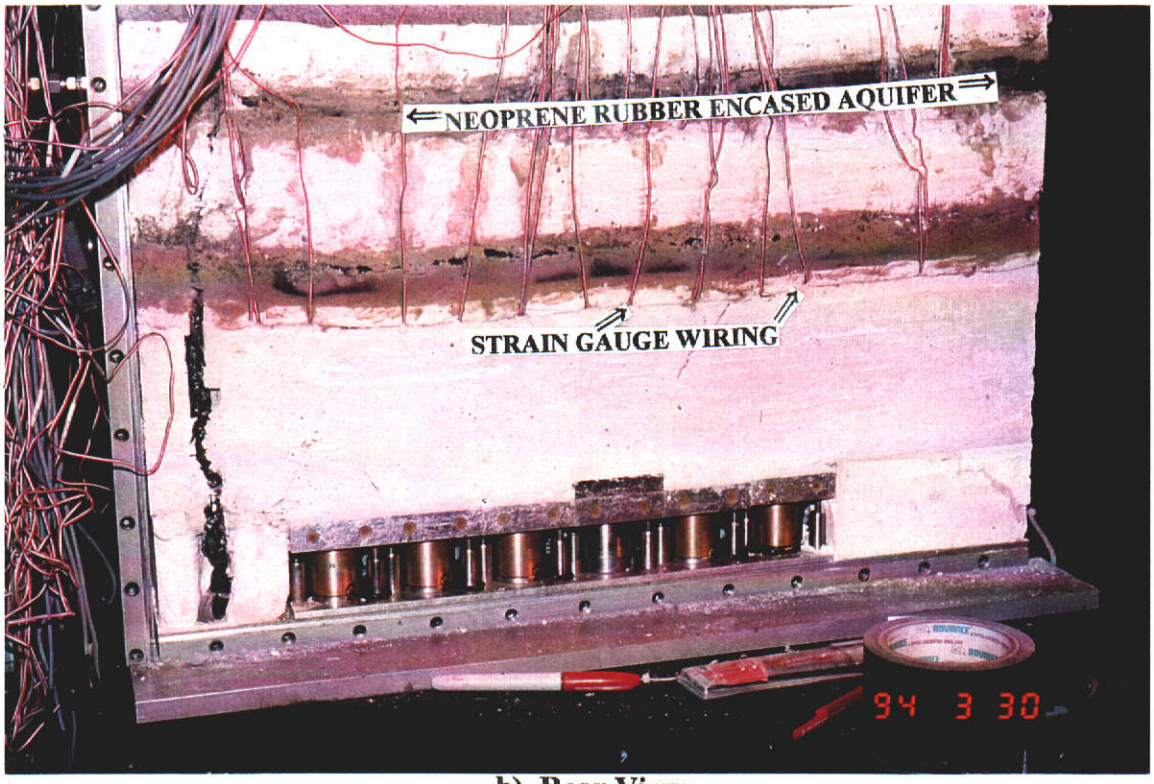

b) Rear View

Figure IV.42

GEOTECHNICAL CENTRIFUGE TEST PS08

SUBSIDENCE DEVELOPMENT

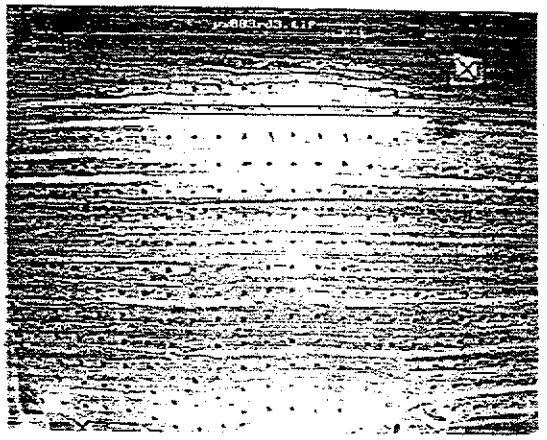

3rd Row (3)

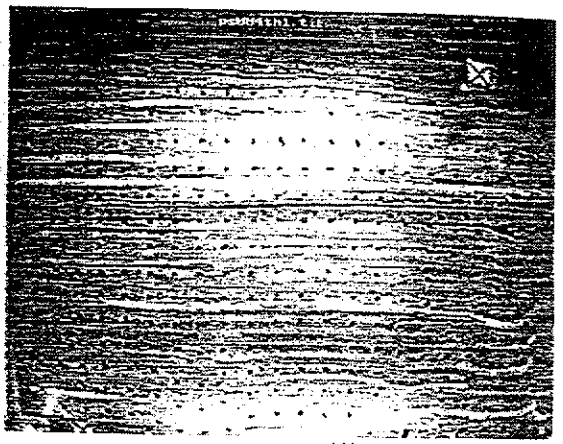

4th Row (1)

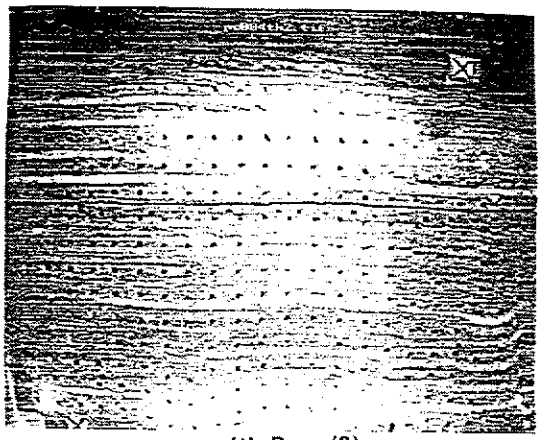

4th Row (2)

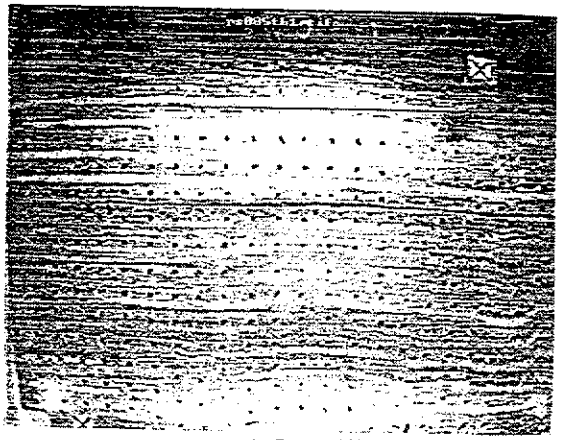

5th Row (1)

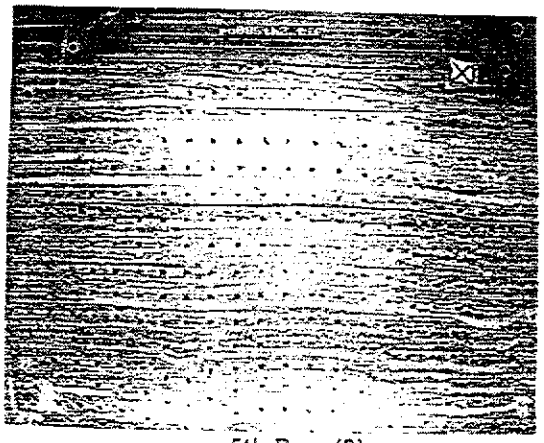

5th Row (2)

Figure IV.43 a

GEOTECHNICAL CENTRIFUGE TEST PS08

SUBSIDENCE DEVELOPMENT

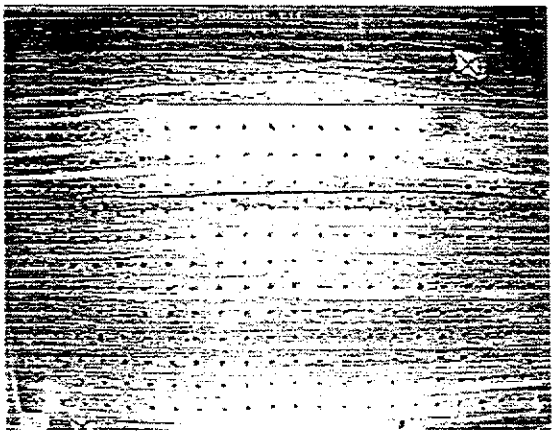

Control

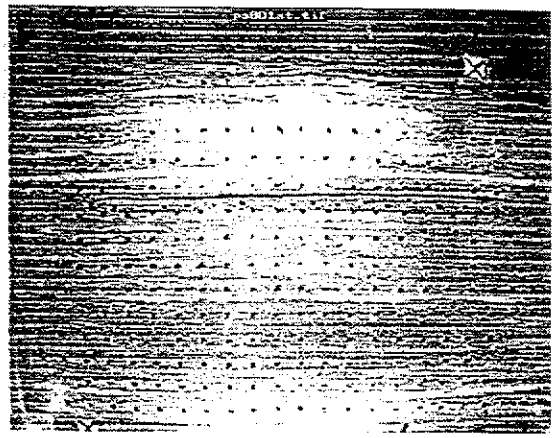

1st Row

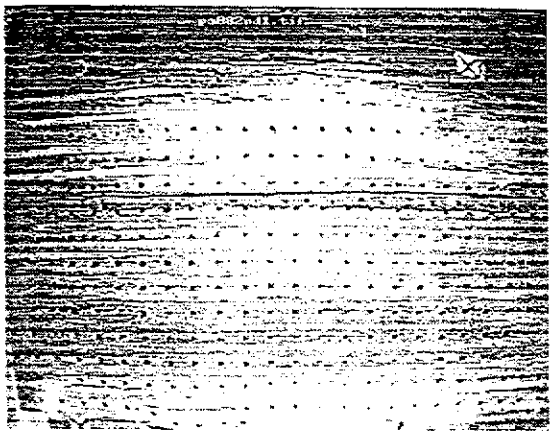

2nd Row (1)

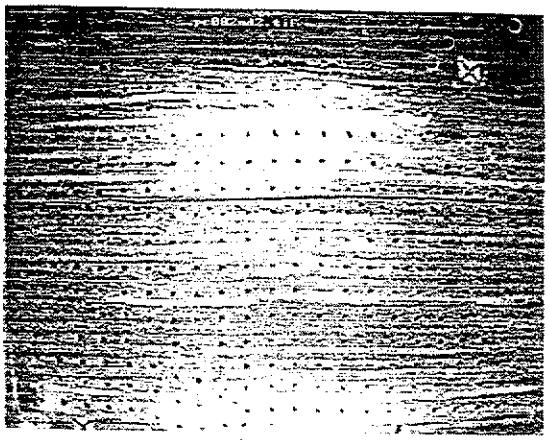

2nd Row (2)

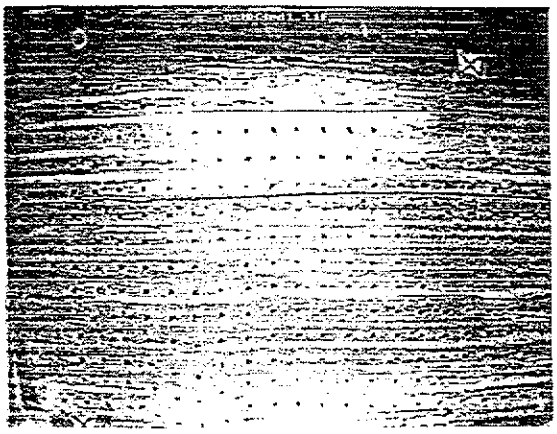

3rd Row (1)

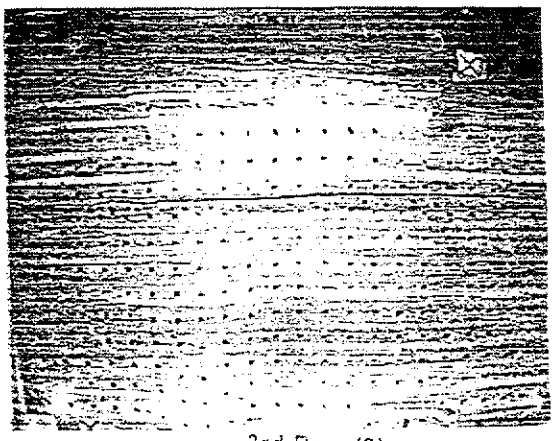

3rd Row (2)

Figure IV.43 a

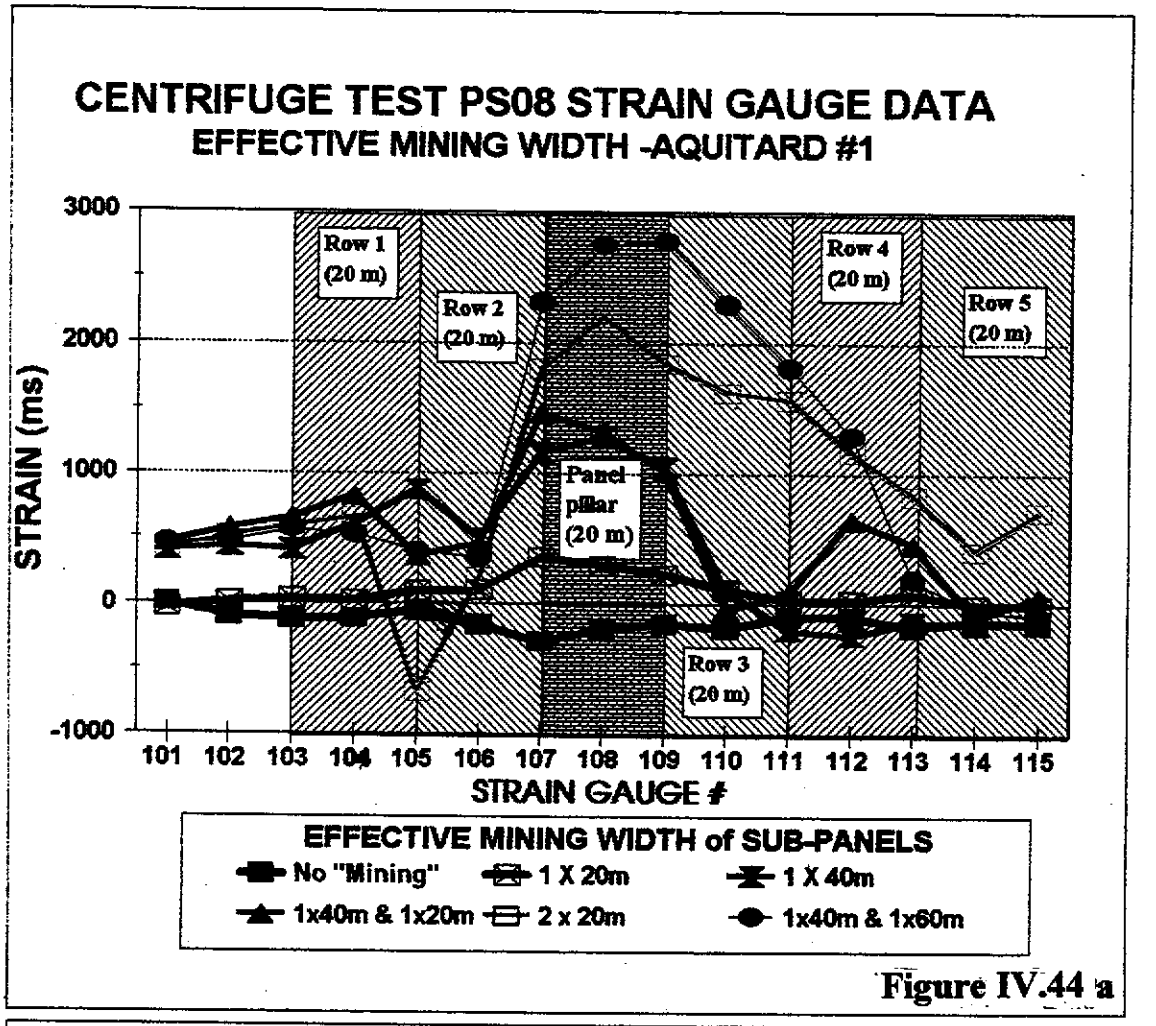

Figure IV.44 a

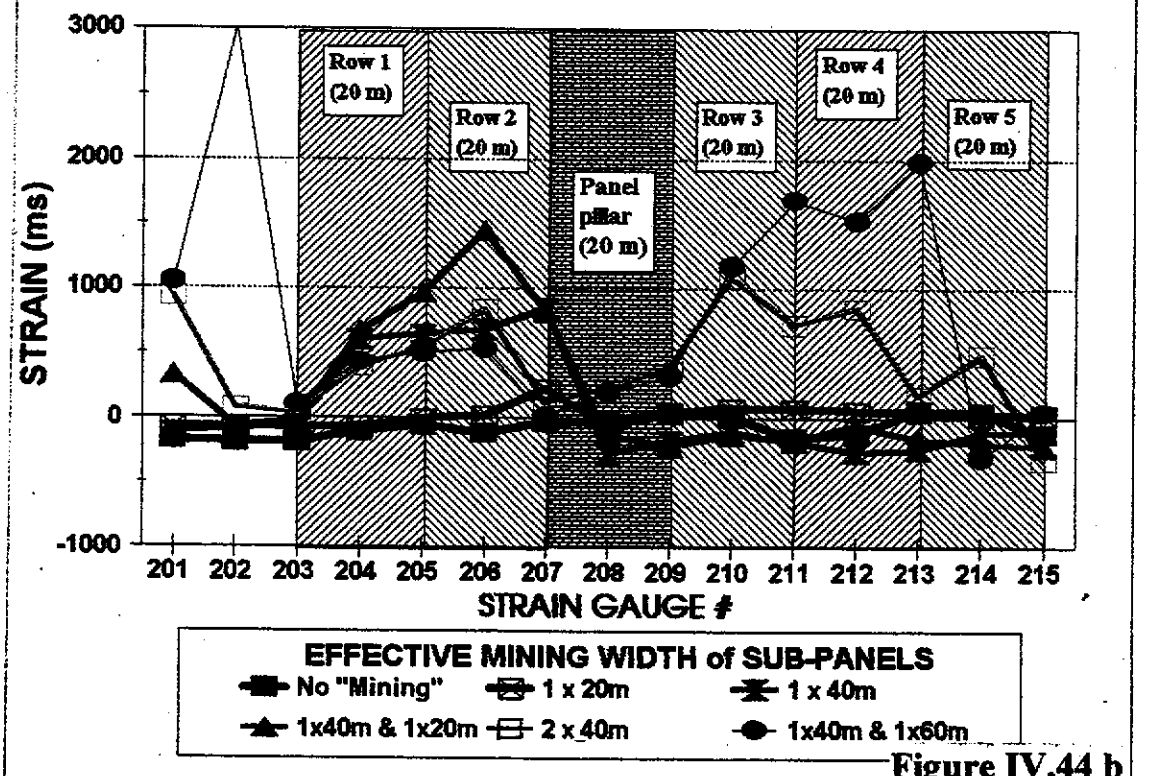

Figure IV.44 b

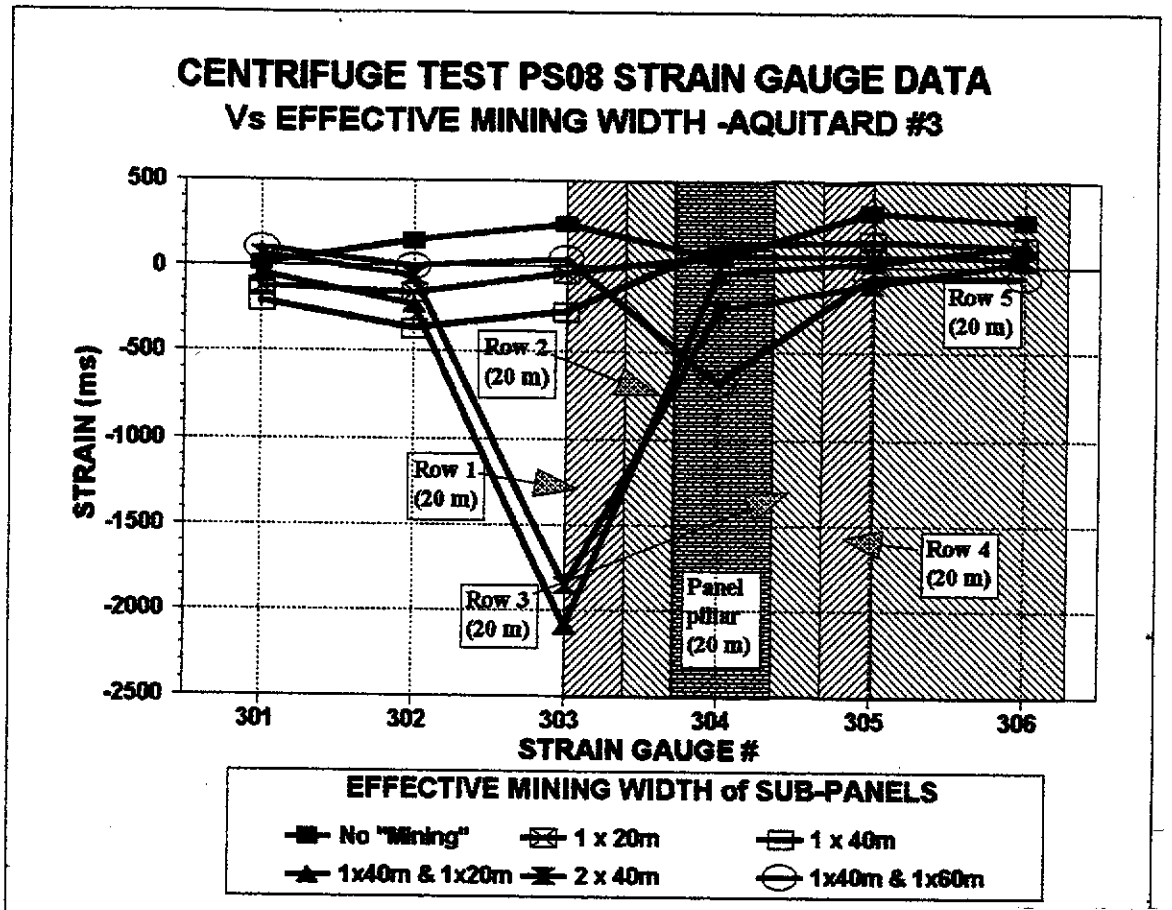

Figure IV.44c

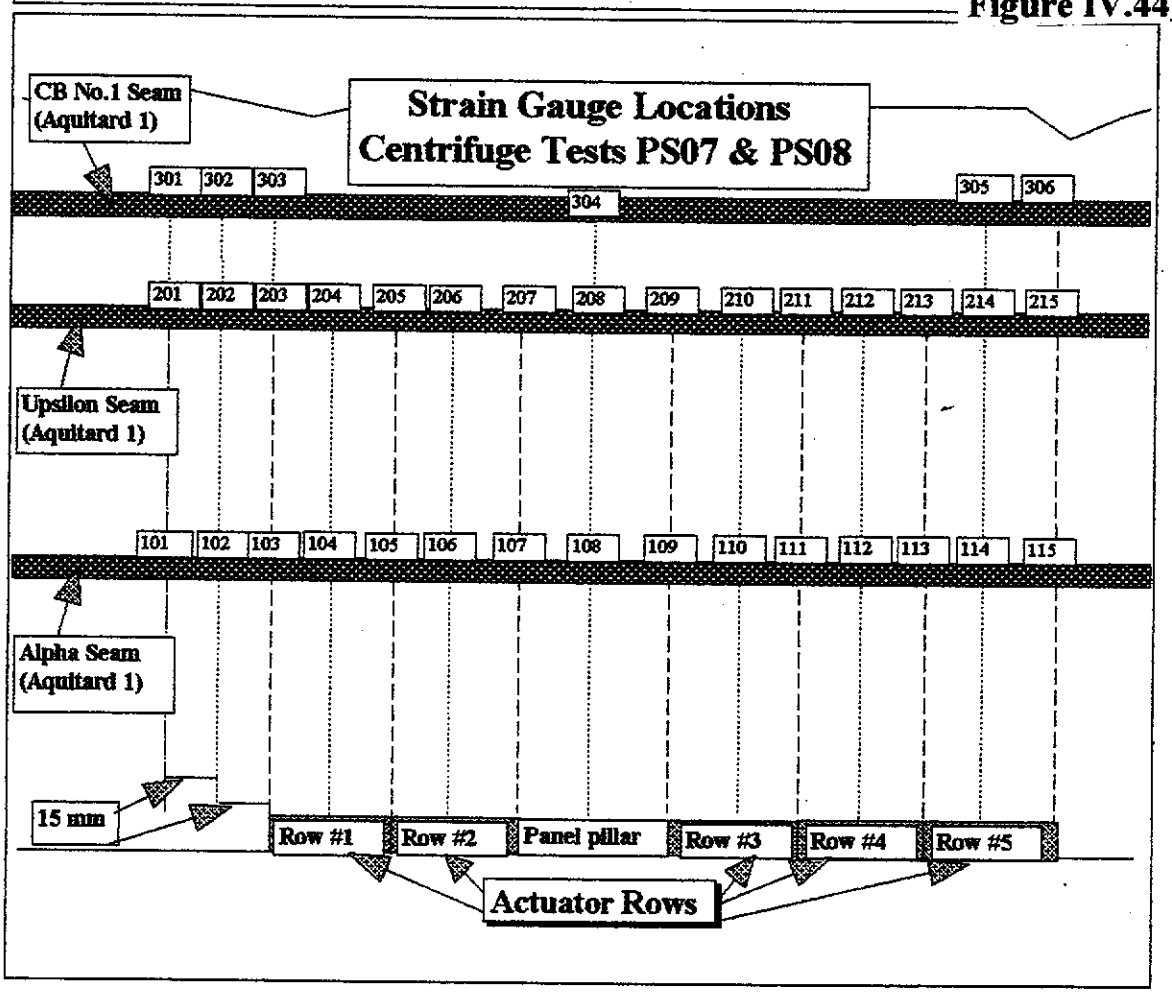

Figure IV.44 d

TABLE IV.10

SUMMARY OF CENTRIFUGE TEST PS08 STRAIN GAUGE DATA RAW DATA						
GAUGE #	ACTUATOR ROW #					
	0	1	2	3	4	5
	mstrain	mstrain	mstrain	mstrain	mstrain	mstrain
101	4	36	-391	-454	-411	-454
102	-97	-105	-526	-663	-607	-569
103	-123	-159	-528	-773	-711	-685
104	-115	-134	-711	-935	-769	-642
105	-56	-151	-923	-415	626	-446
106	-163	-266	-659	-618	-351	-508
107	-289	-639	-1447	-1749	-2089	-2605
108	-193	-478	-1469	-1506	-2385	-2931
109	-154	-374	-1199	-1162	-1989	-2928
110	-186	-292	-295	-141	-1800	-2476
111	-100	-125	102	-183	-1661	-1906
112	-96	-121	147	-734	-1256	-1382
113	-182	-255	-42	-631	-1005	-369
114	-130	-125	29	-29	-530	-87
115	-158	-151	-24	-216	-862	-70
201	-169	-103	-52	-498	-1100	-1211
202	-191	-113	-101	-125	-270	-3210
203	-191	-125	-141	-165	-220	-295
204	-110	-38	-710	-779	-505	-542
205	-53	-44	-692	-1011	-591	-553
206	-118	-133	-795	-1556	-947	-651
207	-32	-252	-868	-845	-150	-48
208	-25	42	252	100	-252	-225
209	42	8	224	264	-355	-282
210	9	-69	118	138	-1064	-1157
211	-155	-228	28	19	-868	-1836
212	-122	-179	136	-69	-965	-1641
213	61	17	305	225	-105	-1922
214	42	16	159	237	-447	345
215	-126	-153	-10	97	205	-173
301	8	130	221	57	-55	-94
302	143	300	511	370	202	150
303	246	288	513	2340	2101	204
304	45	-15	-77	87	303	721
305	317	254	164	295	423	380
306	267	219	146	139	234	328

TABLE IV.11

LOAD CELL #	SUMMARY OF PS08 LOAD CELL DATA Vs ACTUATOR ROW #					
	ACTUATOR #					
	0	1	2	3	4	5
	LOAD (N)					
1	4079	-1820	-1783	-1668	-1509	-1414
2	4382	5181	-812	-807	-813	-812
3	4378	4735	4717	1349	2179	2673
4	3669	3789	3645	3874	1171	2755
5	2638	2589	2283	2457	2157	1105
6	8364	8757	8250	7995	8024	8558
7	7453	8673	8281	7970	8503	9743
8	5886	7157	6418	6248	6859	7777

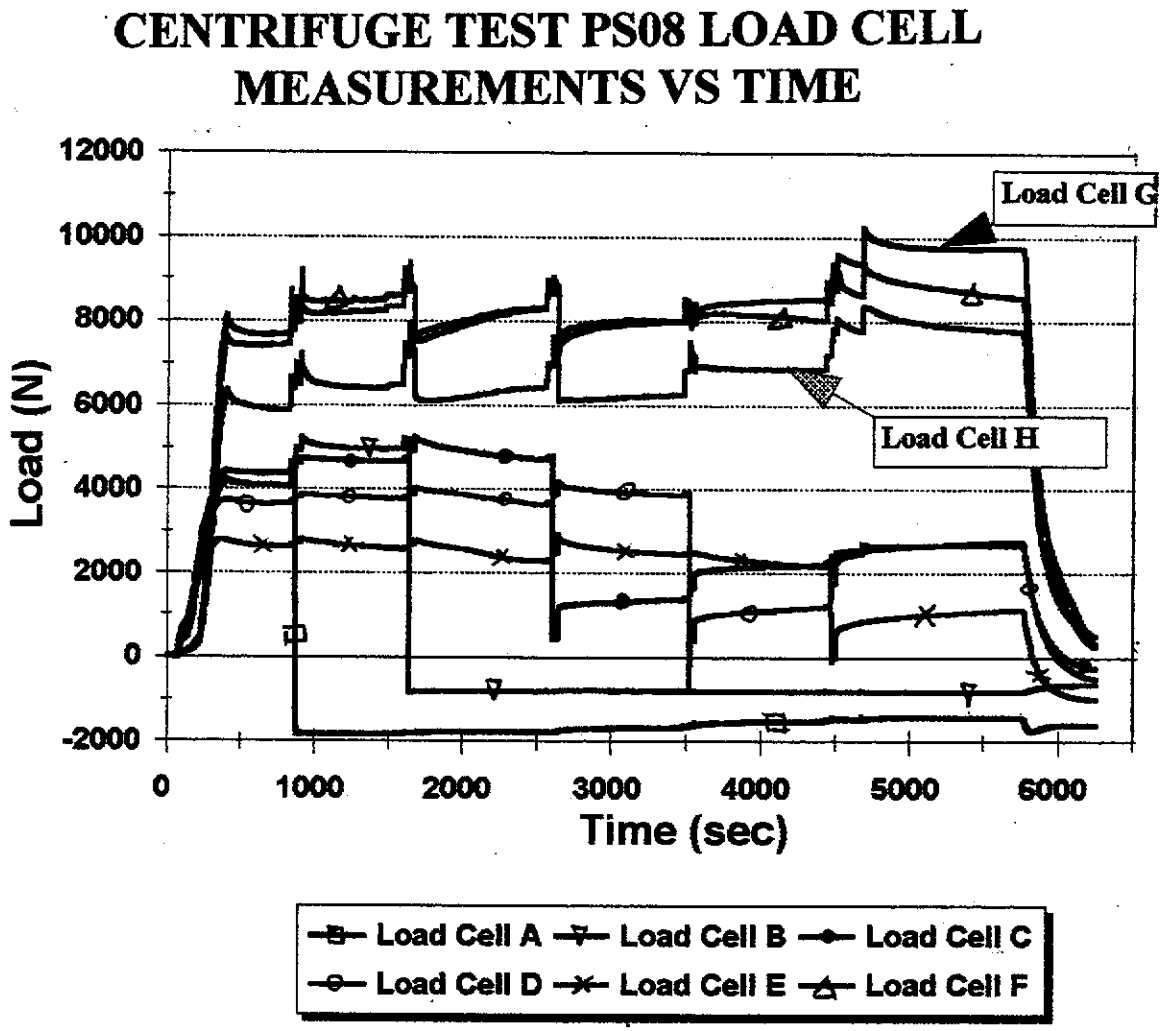
CENTRIFUGE TEST PS08 LOAD CELL MEASUREMENTS VS TIME
Load (N)
12000
10000
8000
6000
4000
2000
0
-2000
0
1000
2000
3000
4000
5000
6000
Time (sec)
Load Cell G
Load Cell H
Load Cell A
Load Cell B
Load Cell C
Load Cell D
Load Cell E
Load Cell F

Figure IV.45

DIAGRAMMATICAL VIEW OF LOAD CELL VALUES CENTRIFUGE TEST PS08

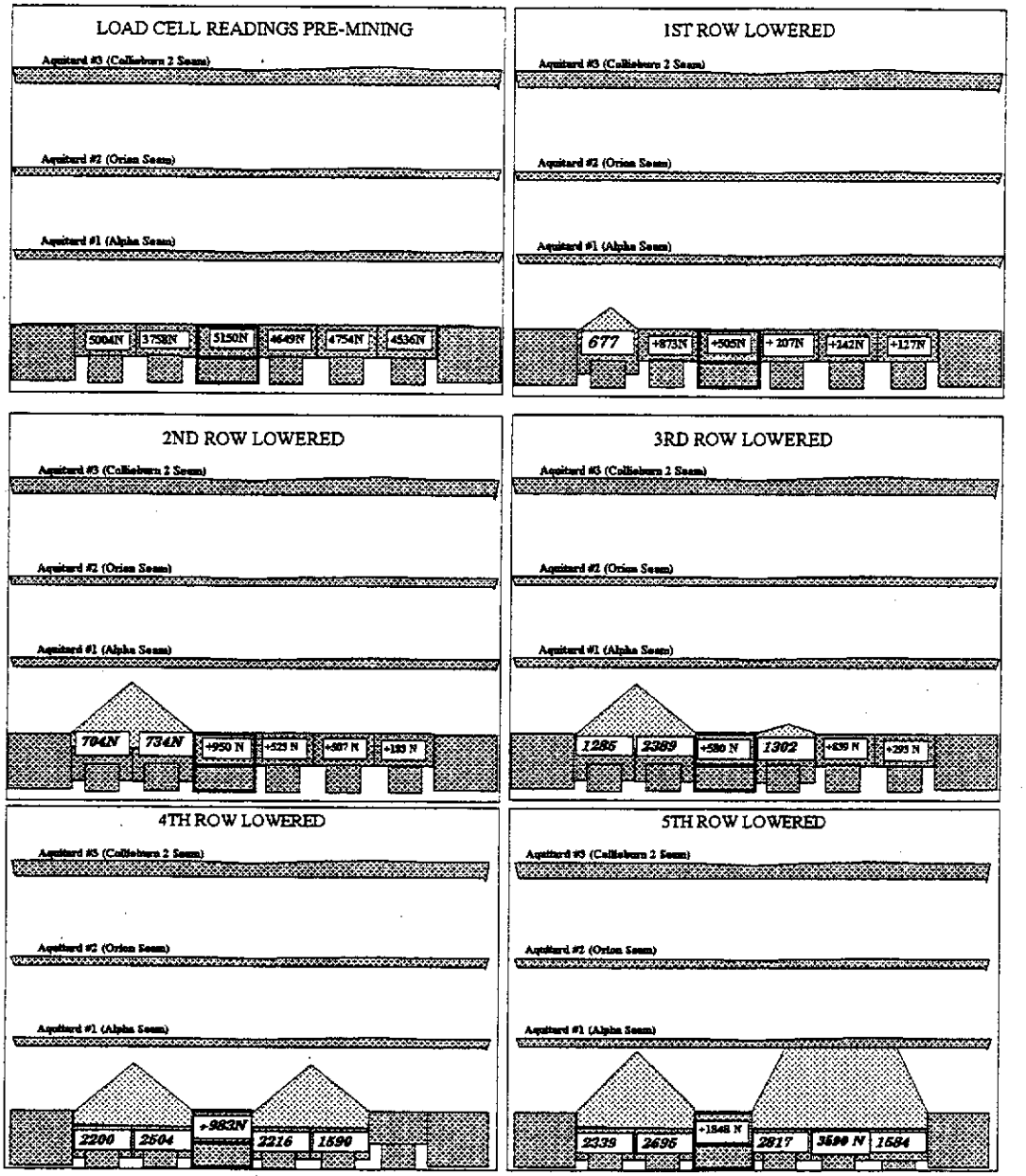

Note :- Loads are given as : a) total loads for lowered actuators, and
b) load variance from pre-mining loads for unlowered actuators

Figure IV.46

CRACK TRACING ON FRONT OF CENTRIFUGE MODEL PS08

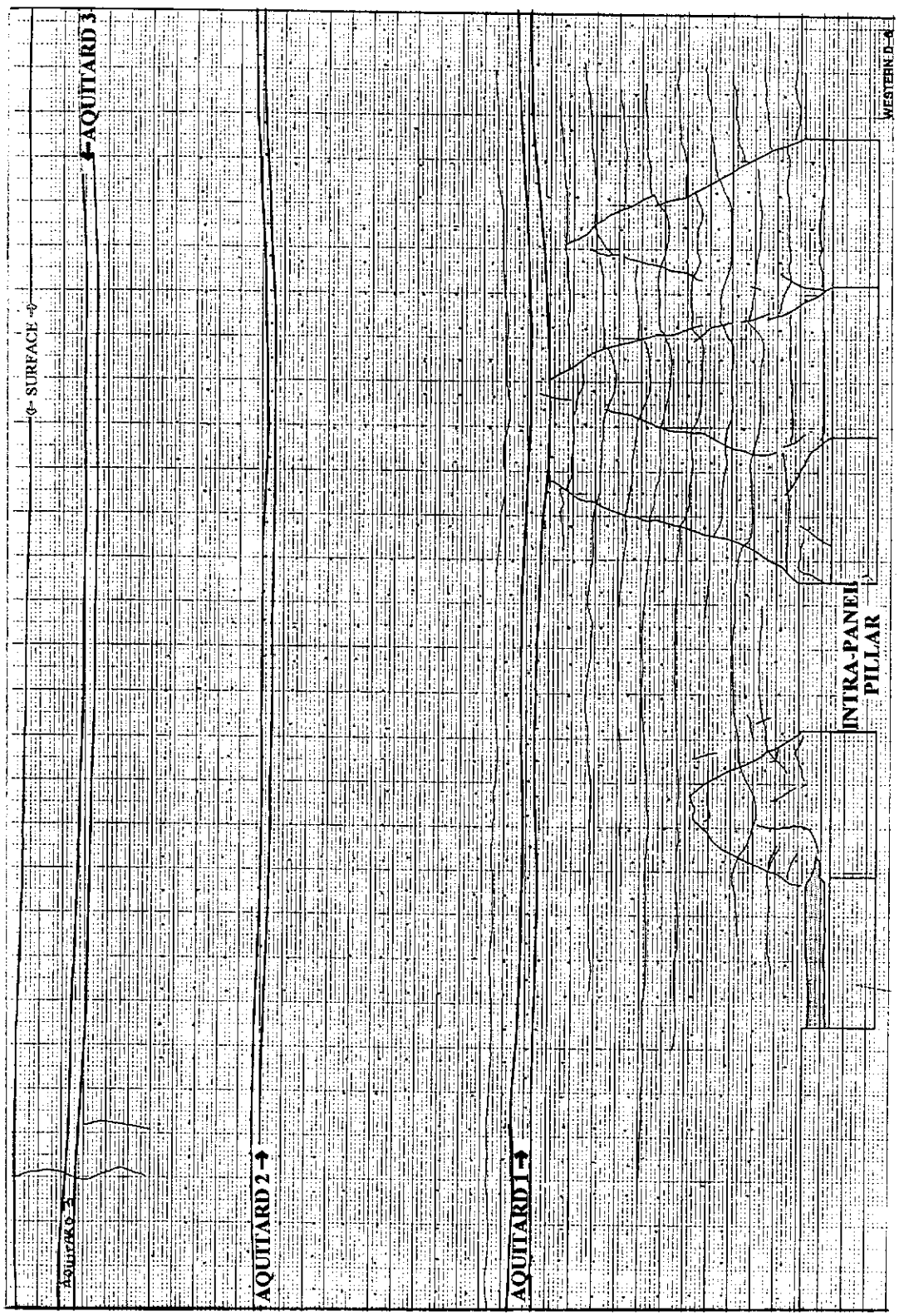

Figure IV.47

PS08 LOAD CELL RESULTS DURING CONSOLIDATION

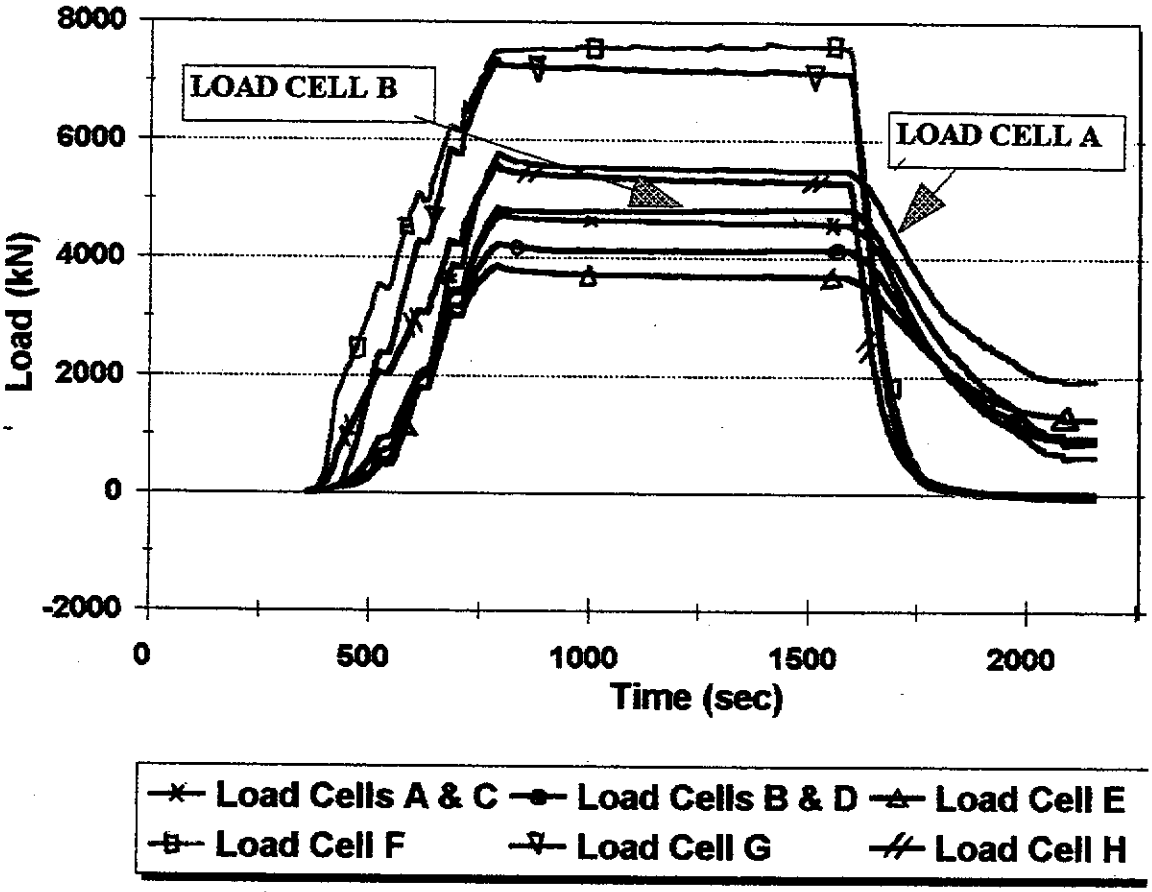

Figure IV.48

PRE-TEST PHOTOGRAPH OF CENTRIFUGE MODEL PS09

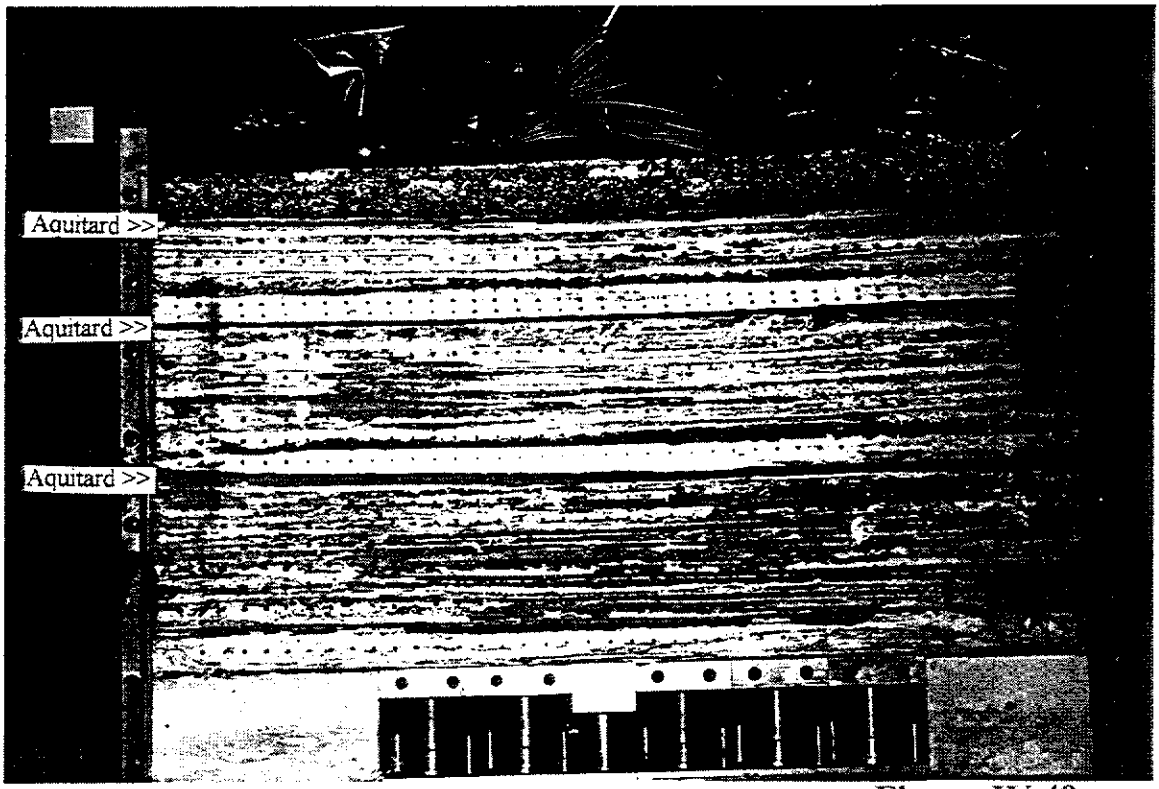

Figure IV.49 a

POST-TEST PHOTOGRAPH OF CENTRIFUGE MODEL PS09

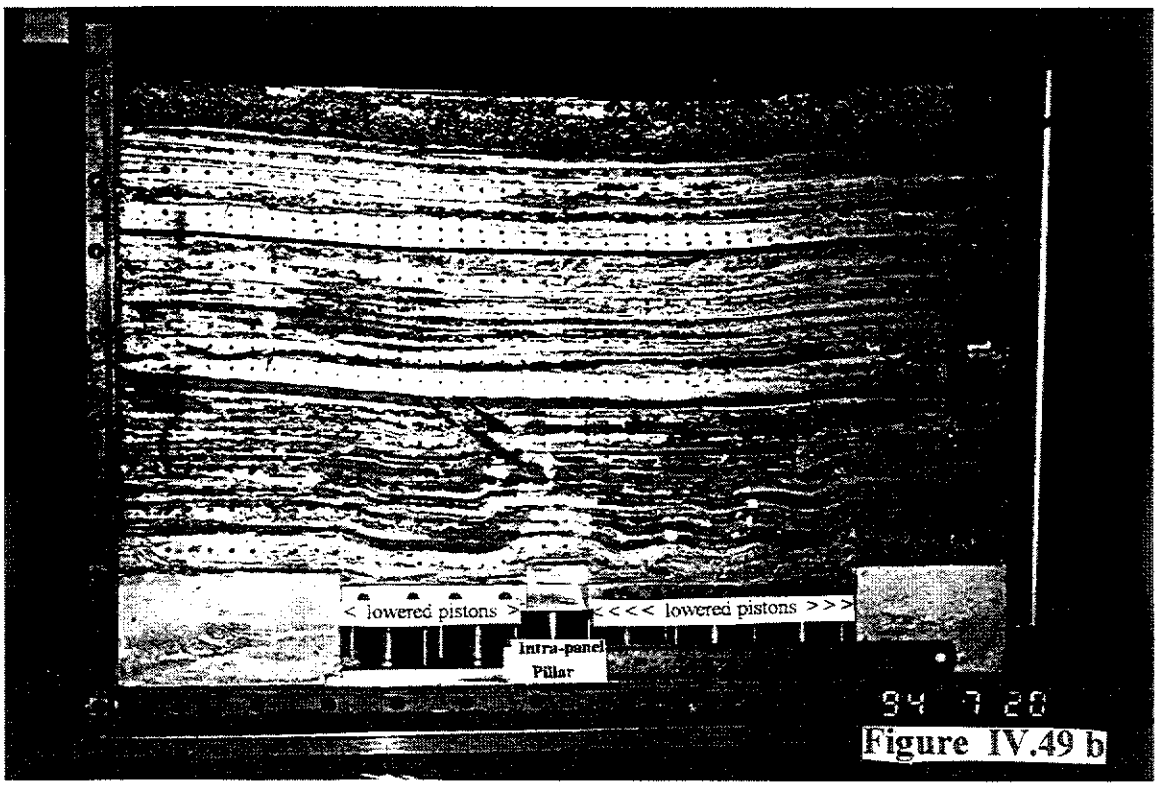

Figure IV.49 b

CRACK TRACING ON FRONT OF CENTRIFUGE MODEL PS09

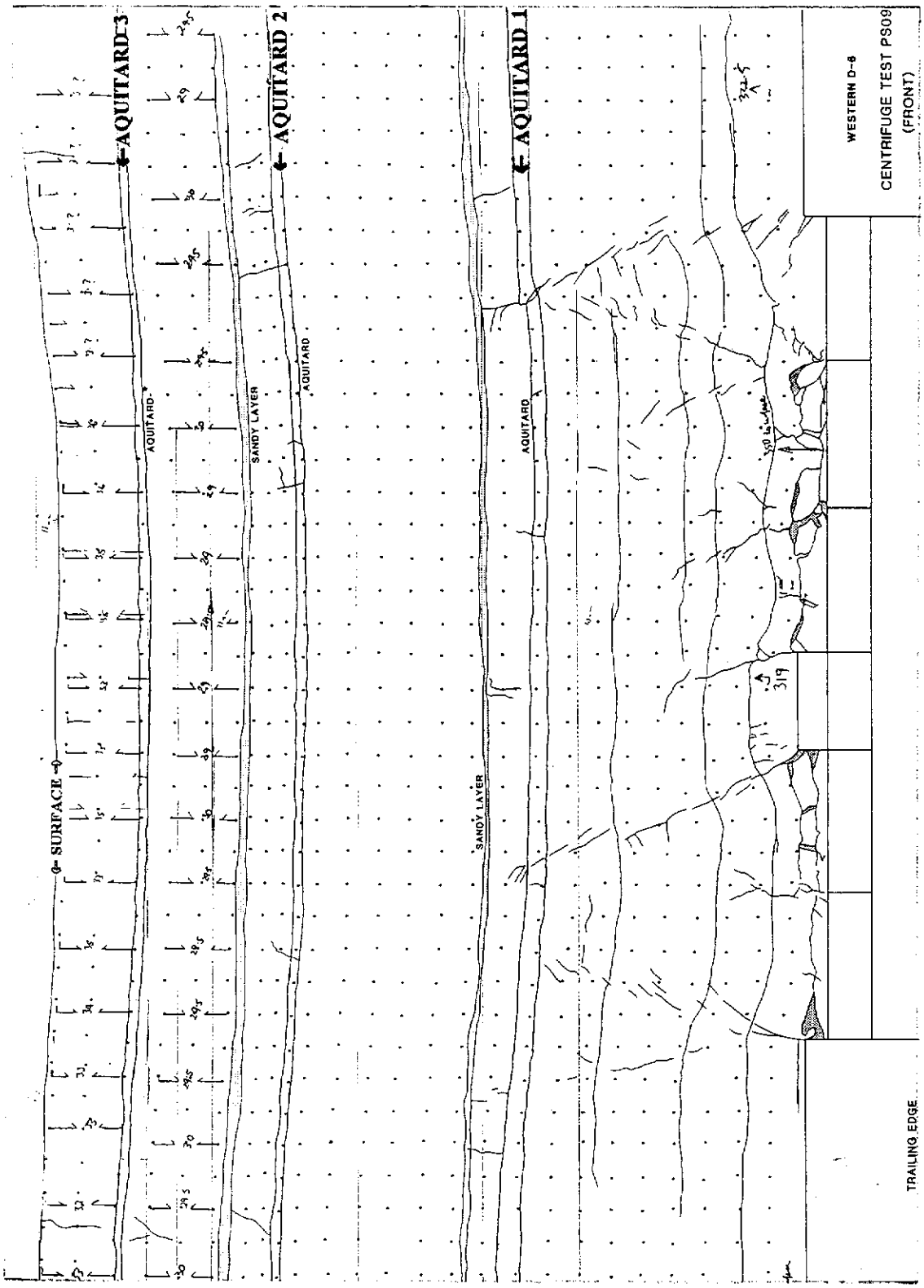

Figure IV.50

GEOTECHNICAL CENTRIFUGE TEST PS09

SUBSIDENCE DEVELOPMENT

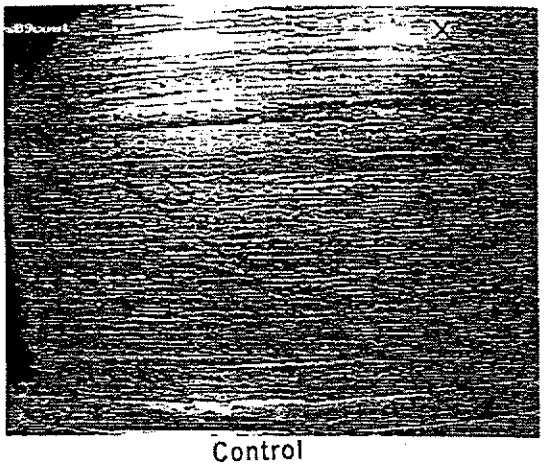

Control

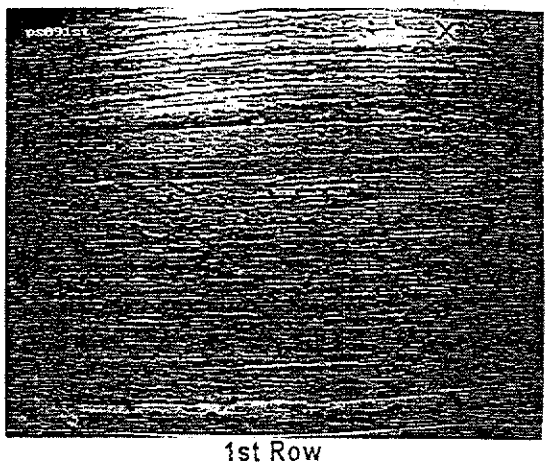

1st Row

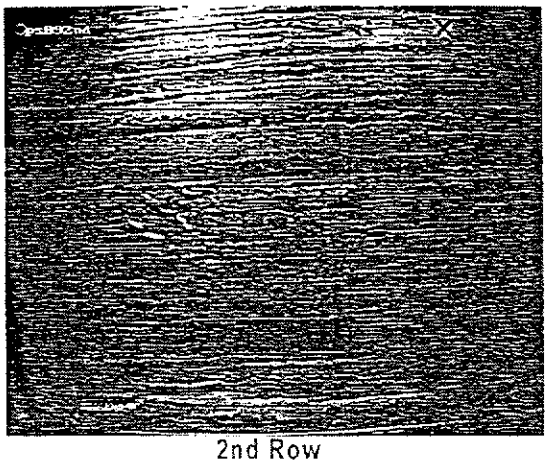

2nd Row

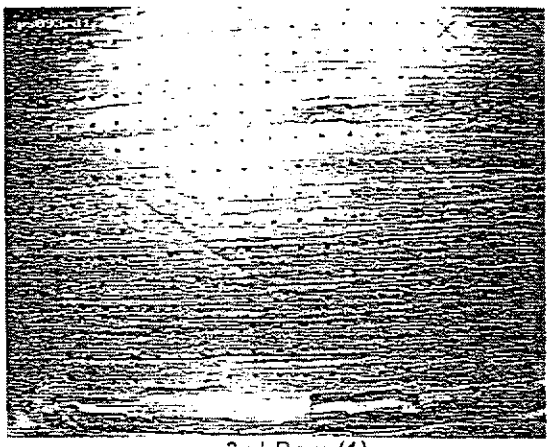

3rd Row (1)

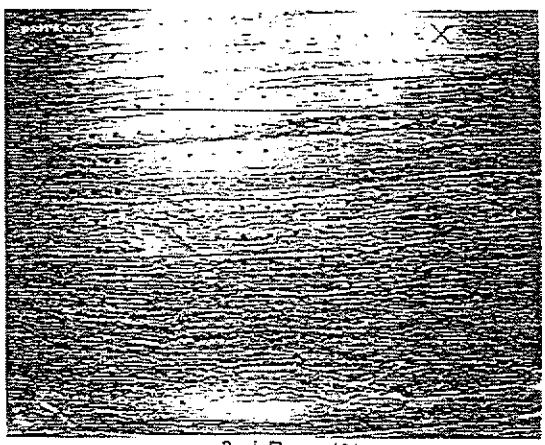

3rd Row (3)

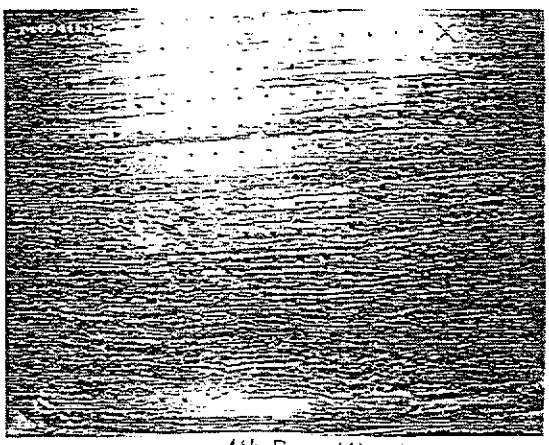

4th Row (1)

Figure IV.51 a

GEOTECHNICAL CENTRIFUGE TEST PS09

SUBSIDENCE DEVELOPMENT

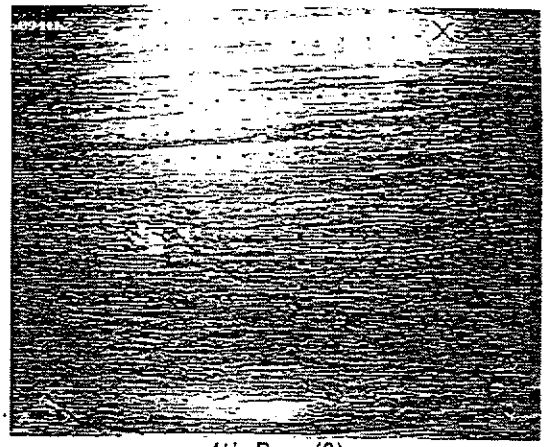

4th Row (2)

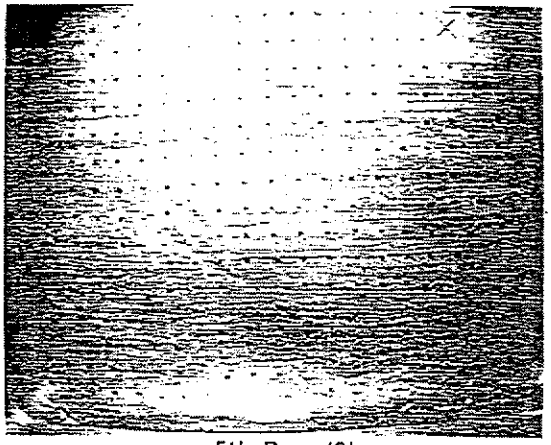

5th Row (2)

Figure IV.51 a

GEOTECHNICAL CENTRIFUGE TEST PS09

SUBSIDENCE DEVELOPMENT

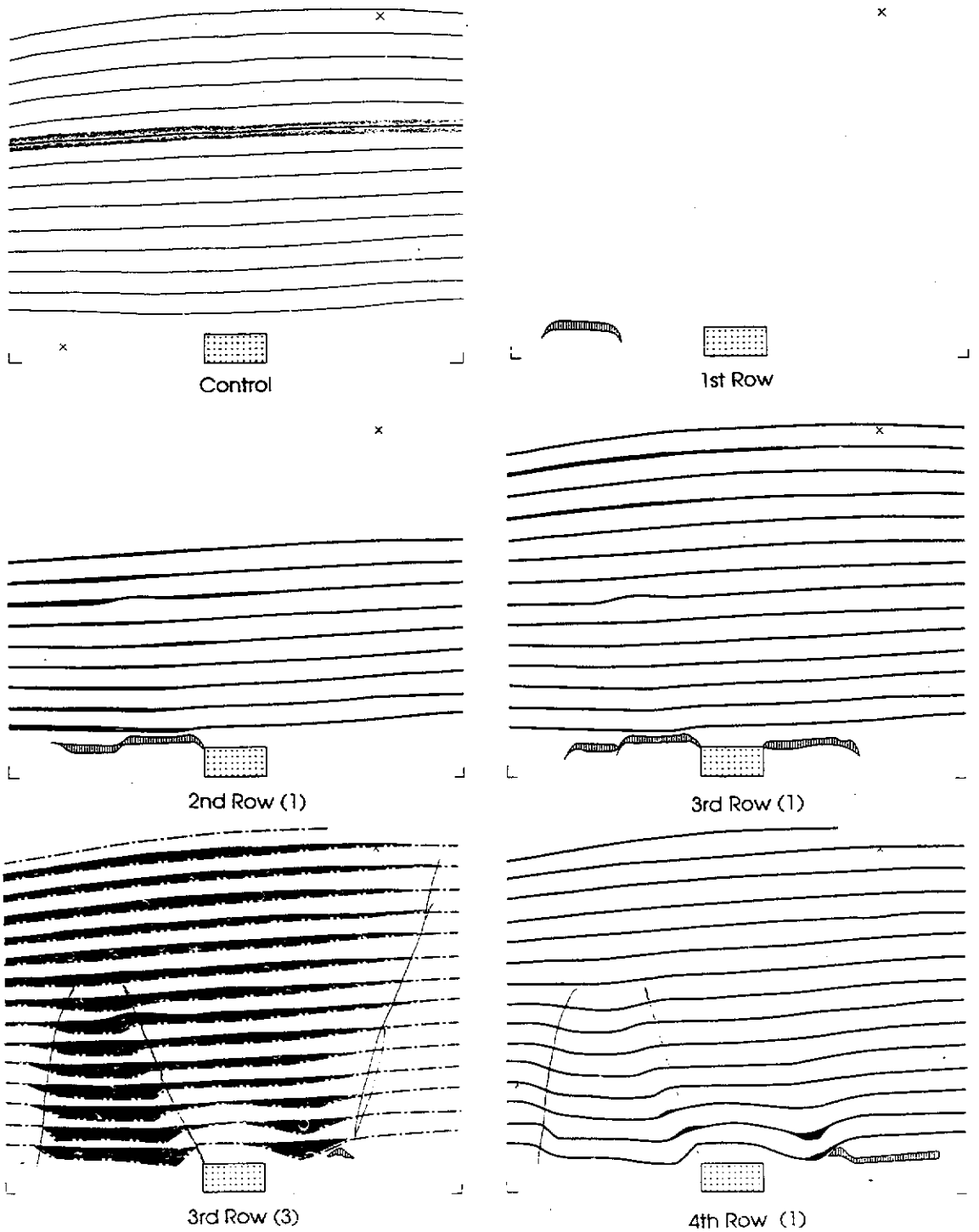

Figure IV.51 b

GEOTECHNICAL CENTRIFUGE TEST PS09

SUBSIDENCE DEVELOPMENT

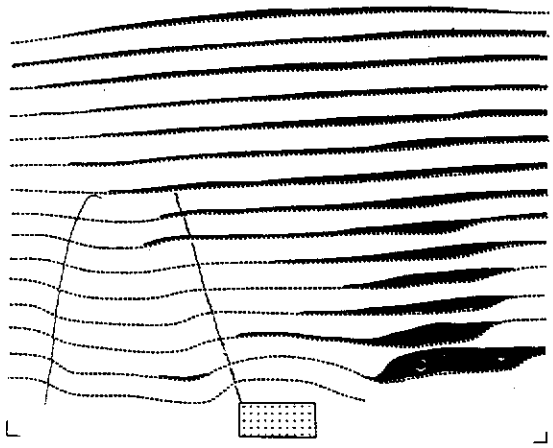

4th Row (2)

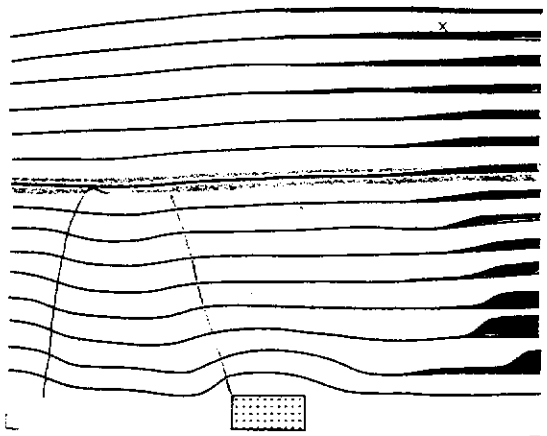

5th Row (2)

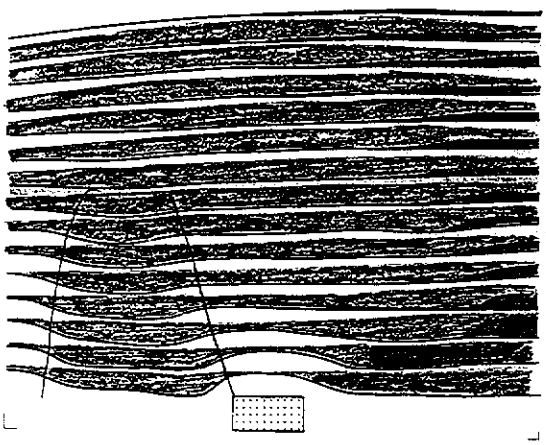

Total Subsidence

Figure IV.51 b

ILLUSTRATION OF CRUSHED OVERHANG BELOW THE FIRST AQUITARD - CENTRIFUGE MODEL PS09

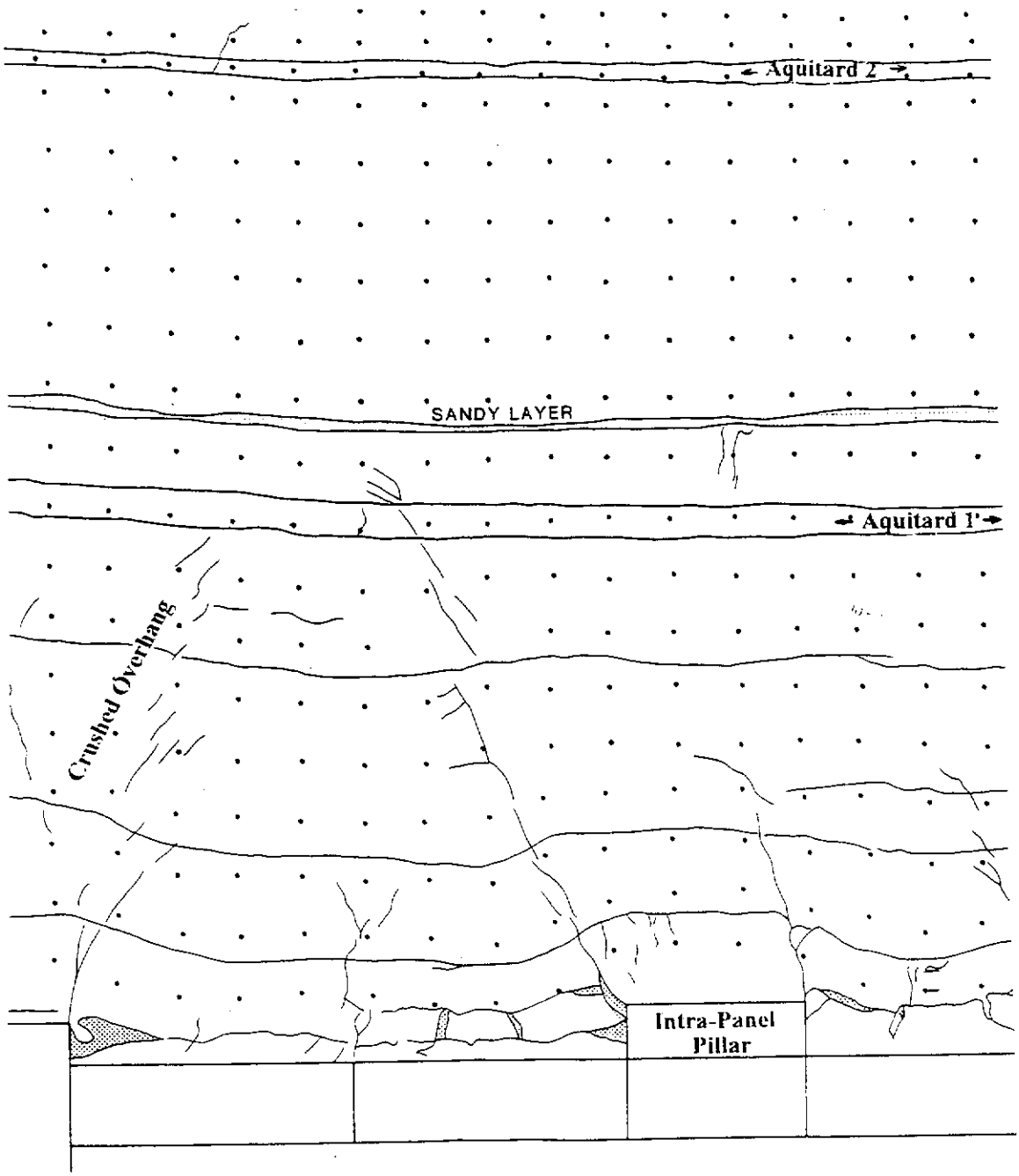

Figure IV.52

DISPLACEMENT ABOVE THE INTRA-PANEL PILLAR - CENTRIFUGE MODEL PSO9

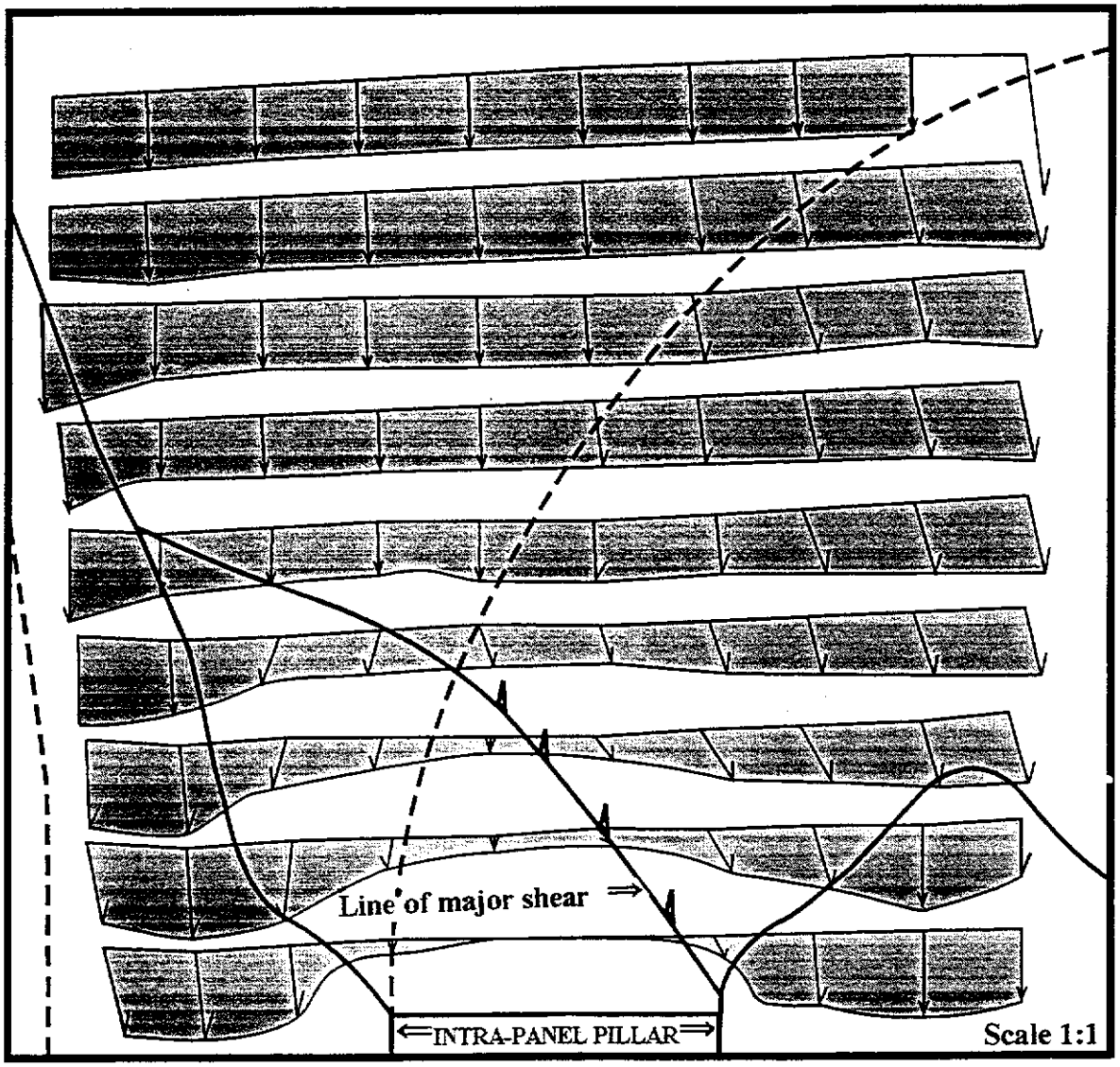

Note that the displacement vectors are divided into zones of directional movement

vertical movement - ↓ movement to the left - ↙ movement to the right - ↘

Figure IV.53

TABLE IV.12

FRAME GRABBING OF DOTS ON PS09 MODEL FACE BEFORE AND AFTER PILLAR FAILURE

X-COORD BEFORE FAILURE (mm)	Y-COORD BEFORE FAILURE (mm)	X-COORD AFTER FAILURE (mm)	Y-COORD AFTER FAILURE (mm)	X-COORD BEFORE FAILURE (mm)	Y-COORD BEFORE FAILURE (mm)	X-COORD AFTER FAILURE (mm)	Y-COORD AFTER FAILURE (mm)
138	-197	139	-218	250	-188	251	-209
137	-225	139	-254	251	-221	252	-241
137	-252	138	-286	251	-253	253	-272
141	-289	142	-316	254	-283	256	-301
143	-320	143	-347	254	-318	255	-334
145	-351	145	-376	256	-347	258	-357
147	-380	148	-405	256	-379	259	-385
147	-411	151	-434	257	-407	259	-410
151	-441	155	-465	258	-437	258	-437
159	-195	160	-218	273	-187	274	-209
159	-226	160	-247	274	-219	276	-240
161	-257	161	-277	275	-252	277	-271
163	-289	162	-305	276	-283	278	-301
163	-322	162	-339	280	-315	281	-331
165	-352	166	-373	279	-346	282	-361
167	-382	169	-408	278	-377	284	-390
169	-412	170	-438	279	-406	284	-418
171	-441	173	-466	280	-436	283	-443
182	-192	182	-214	295	-185	297	-207
183	-224	183	-245	296	-218	298	-239
183	-255	184	-274	297	-251	301	-270
184	-289	185	-306	299	-282	302	-300
186	-320	186	-335	298	-314	303	-331
188	-351	185	-363	300	-344	303	-360
189	-379	187	-393	300	-378	305	-390
191	-410	189	-433	301	-405	305	-422
191	-440	192	-460	302	-436	303	-455
203	-191	204	-212	320	-184	321	-206
205	-224	206	-244	319	-217	322	-238
205	-254	206	-274	321	-247	324	-266
208	-286	209	-303	322	-279	325	-299
208	-318	209	-332	322	-311	326	-331
209	-350	207	-361	322	-343	326	-361
210	-380	208	-389	324	-374	328	-392
212	-409	211	-418	324	-405	325	-429
212	-438	213	-441	325	-434	324	-459
226	-190	227	-211	344	-184	348	-225
228	-222	229	-242	344	-216	348	-238
228	-254	229	-273	344	-246	347	-268
229	-282	231	-303	344	-278	347	-299
230	-319	230	-334	346	-310	349	-331
231	-348	233	-359	345	-342	348	-361
233	-380	233	-383	342	-372	346	-392
234	-409	234	-412	345	-403	345	-418
235	-438	235	-438	345	-434	346	-454

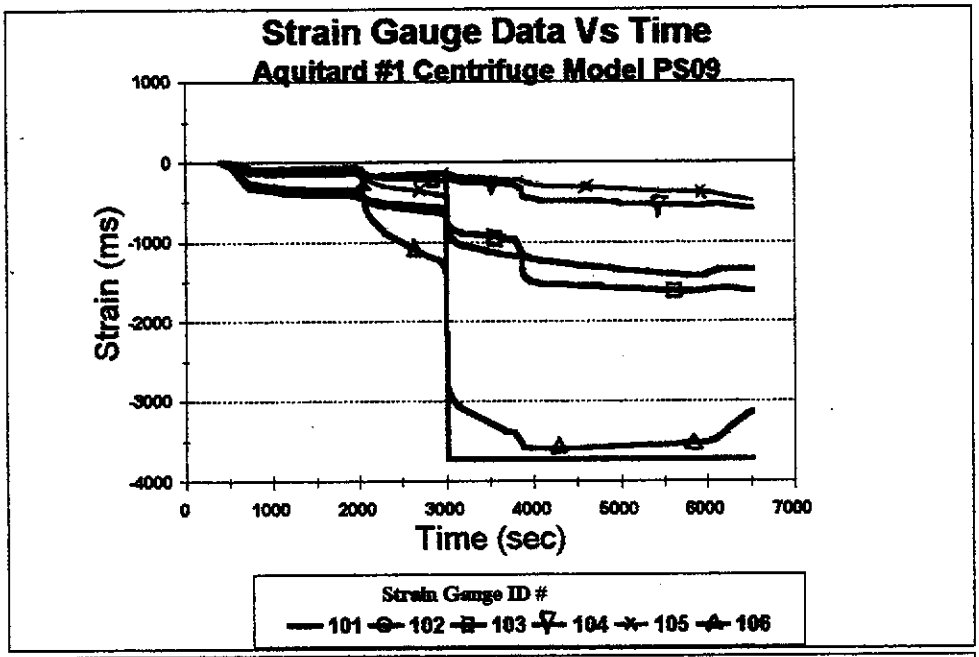

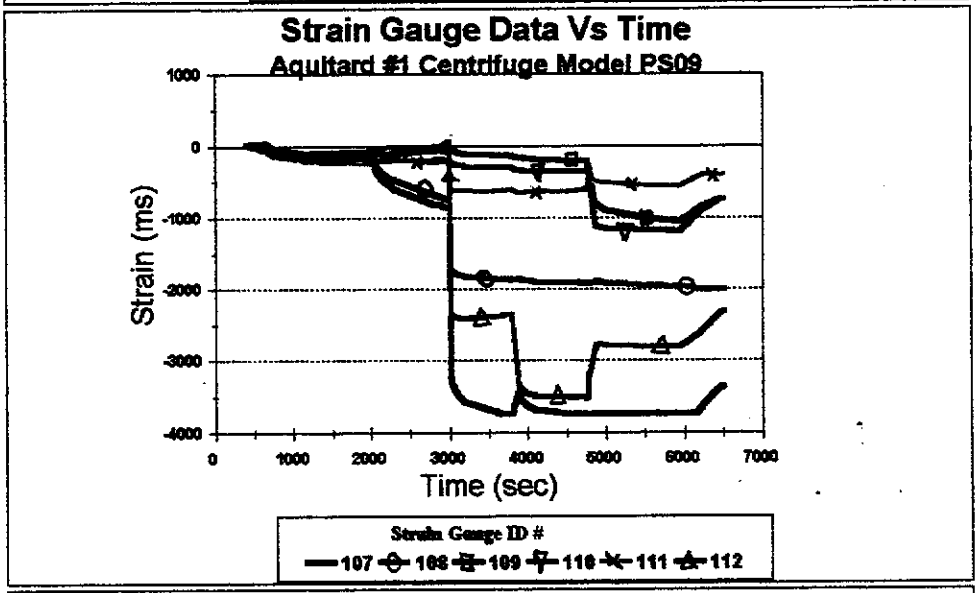

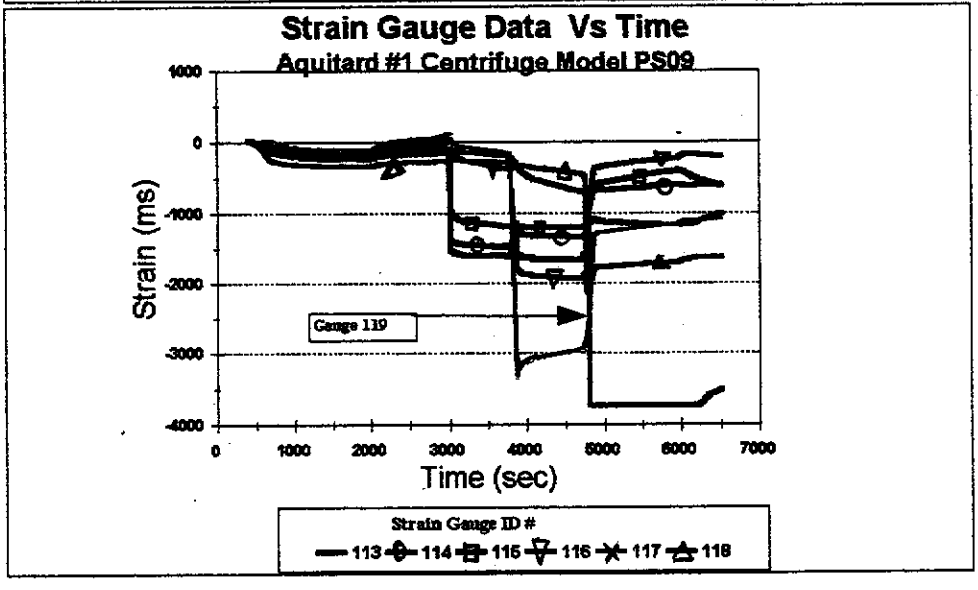

Figure IV.54 a

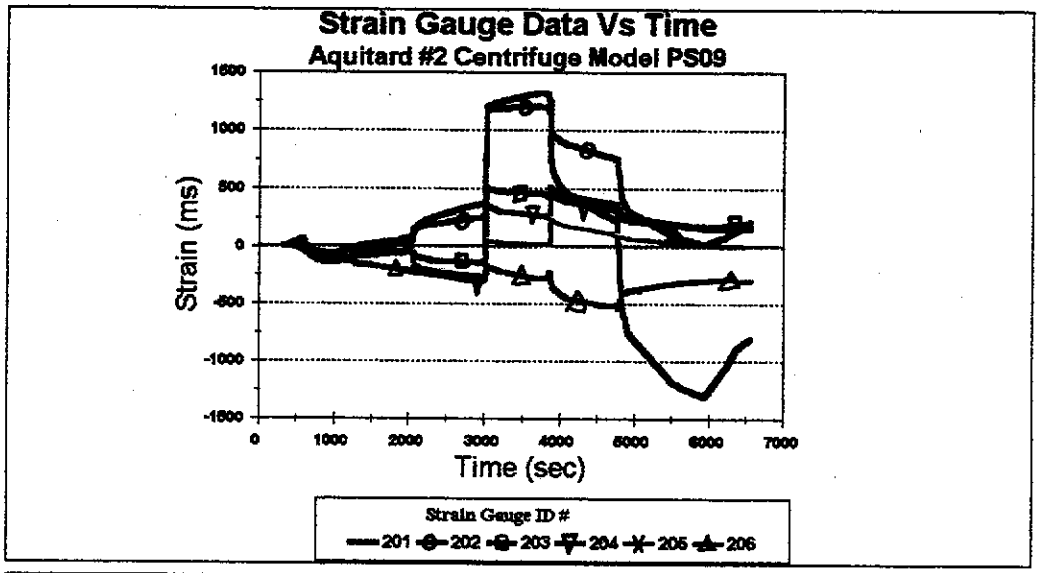

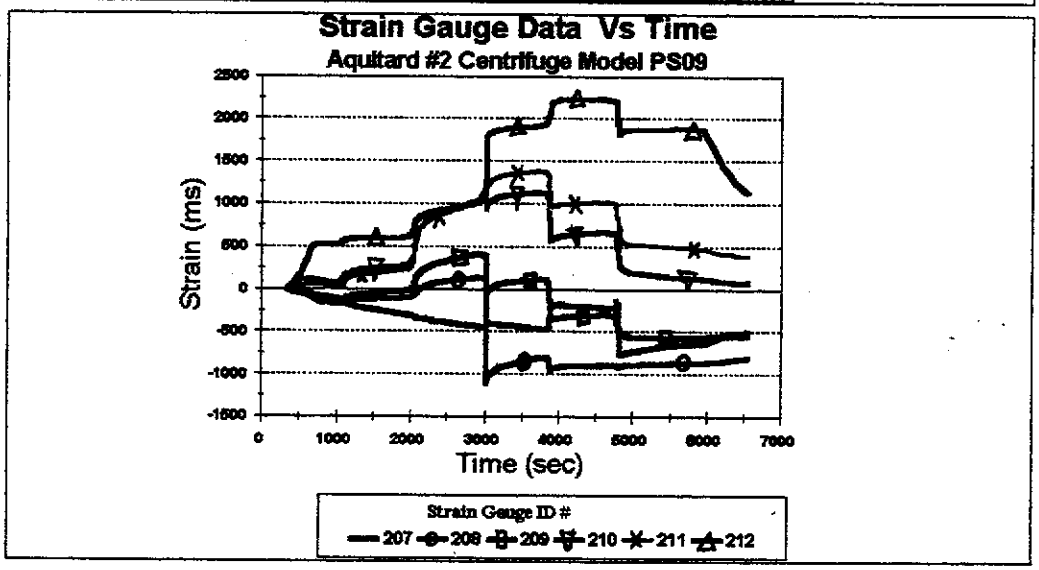

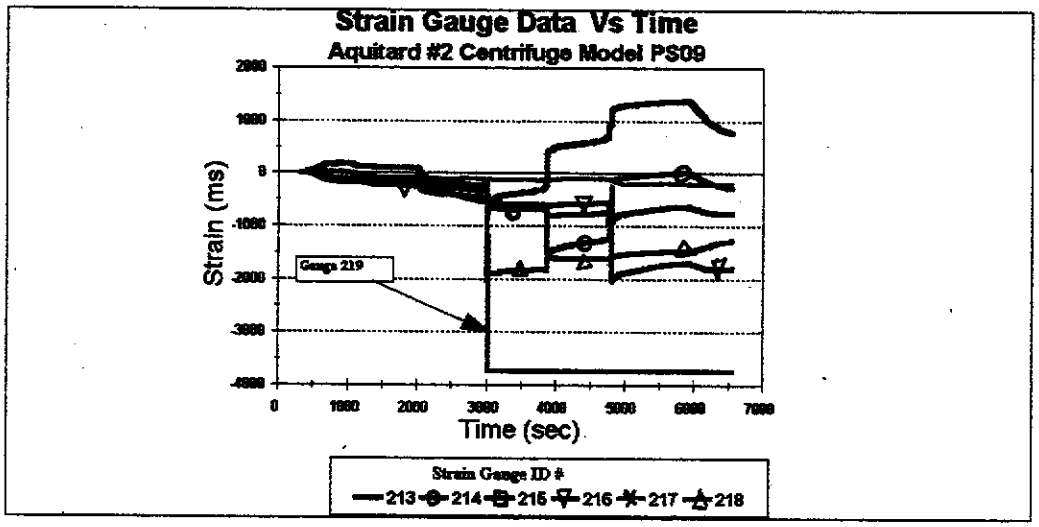

Figure IV.54 b

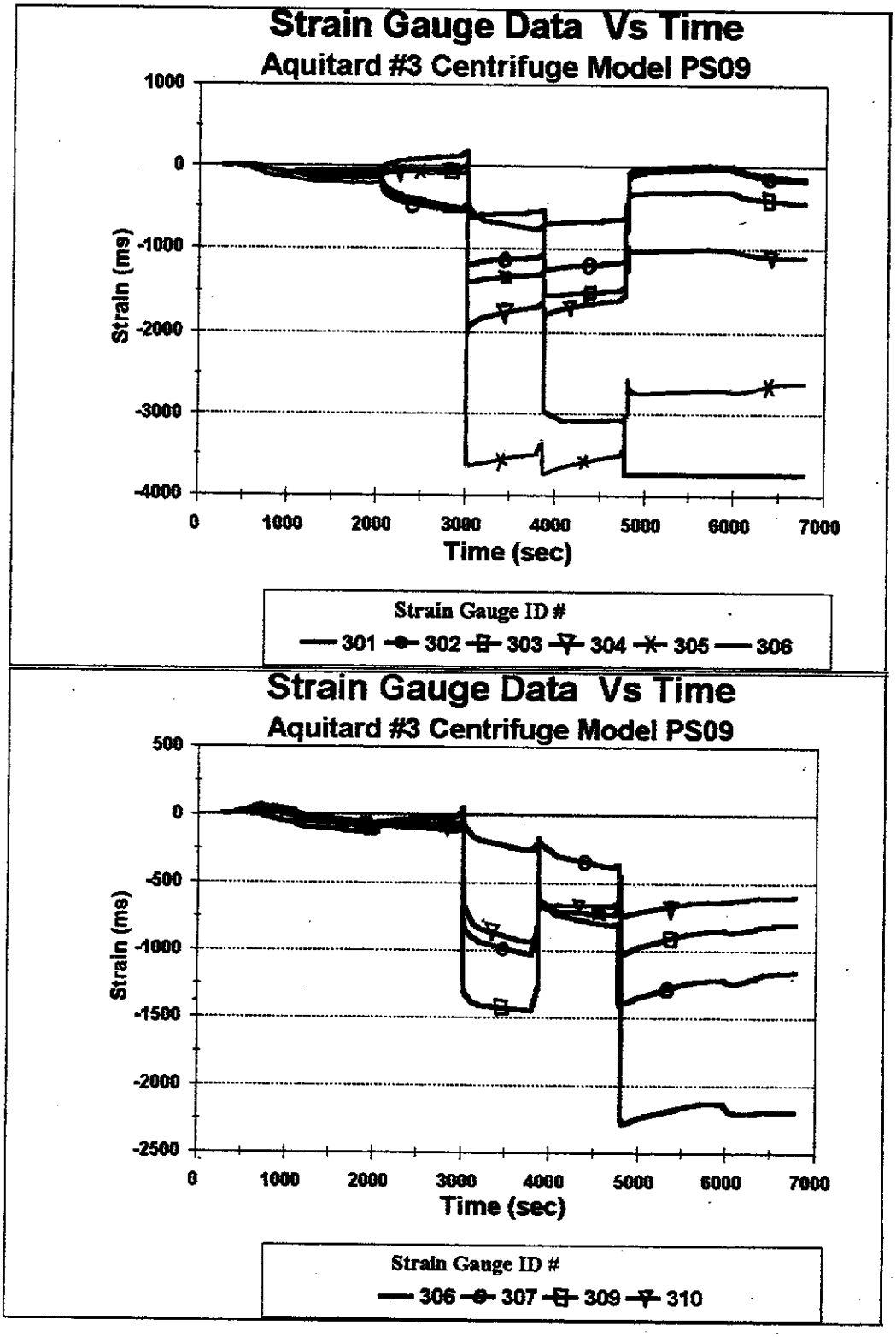

Figure IV.54 c

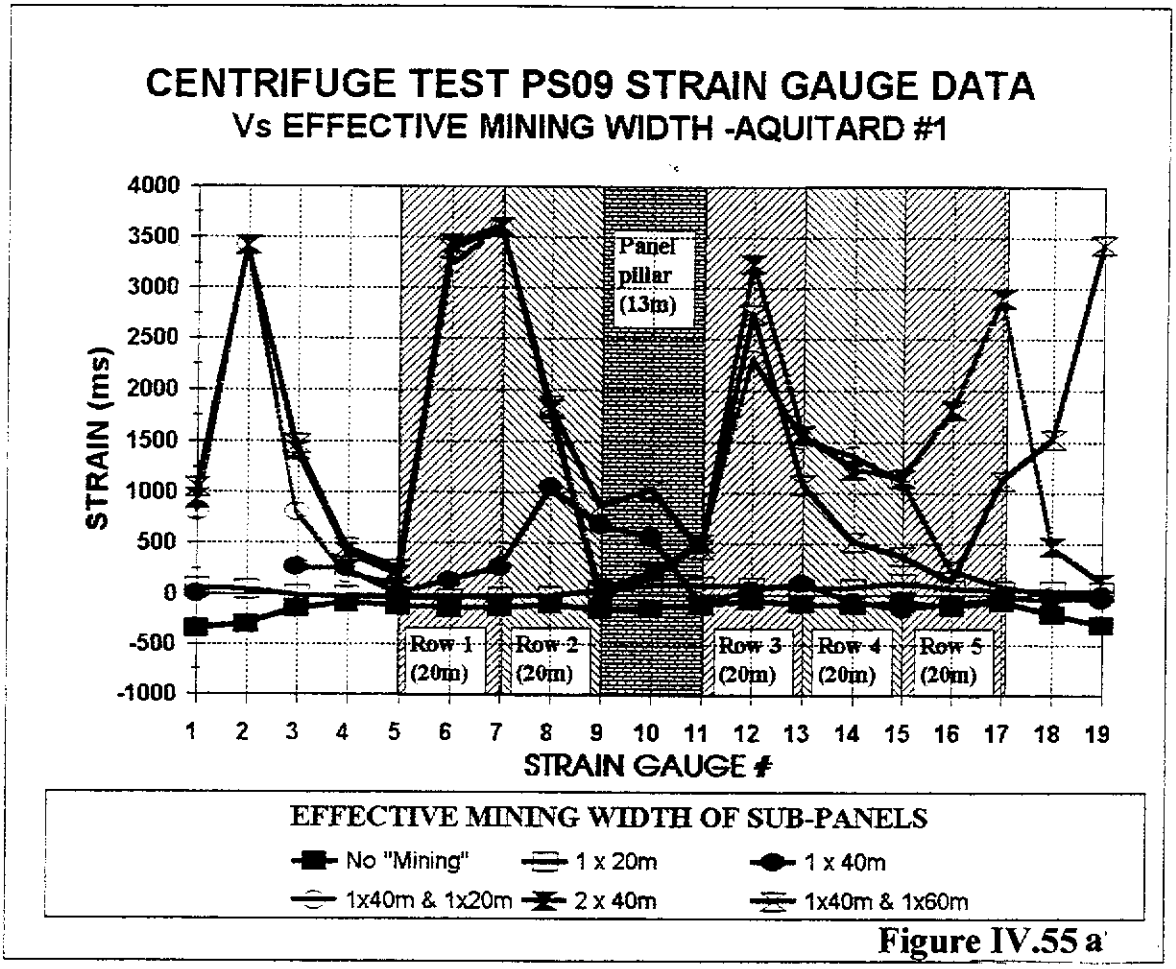

Figure IV.55 a

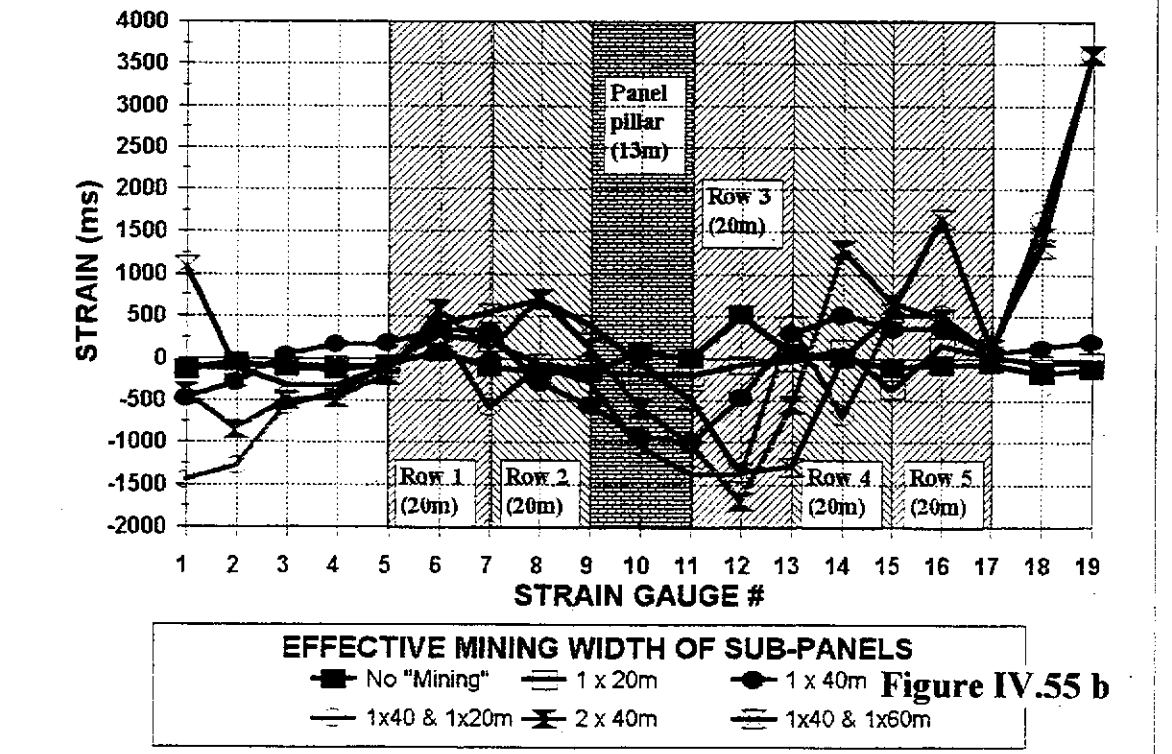

Figure IV.55 b

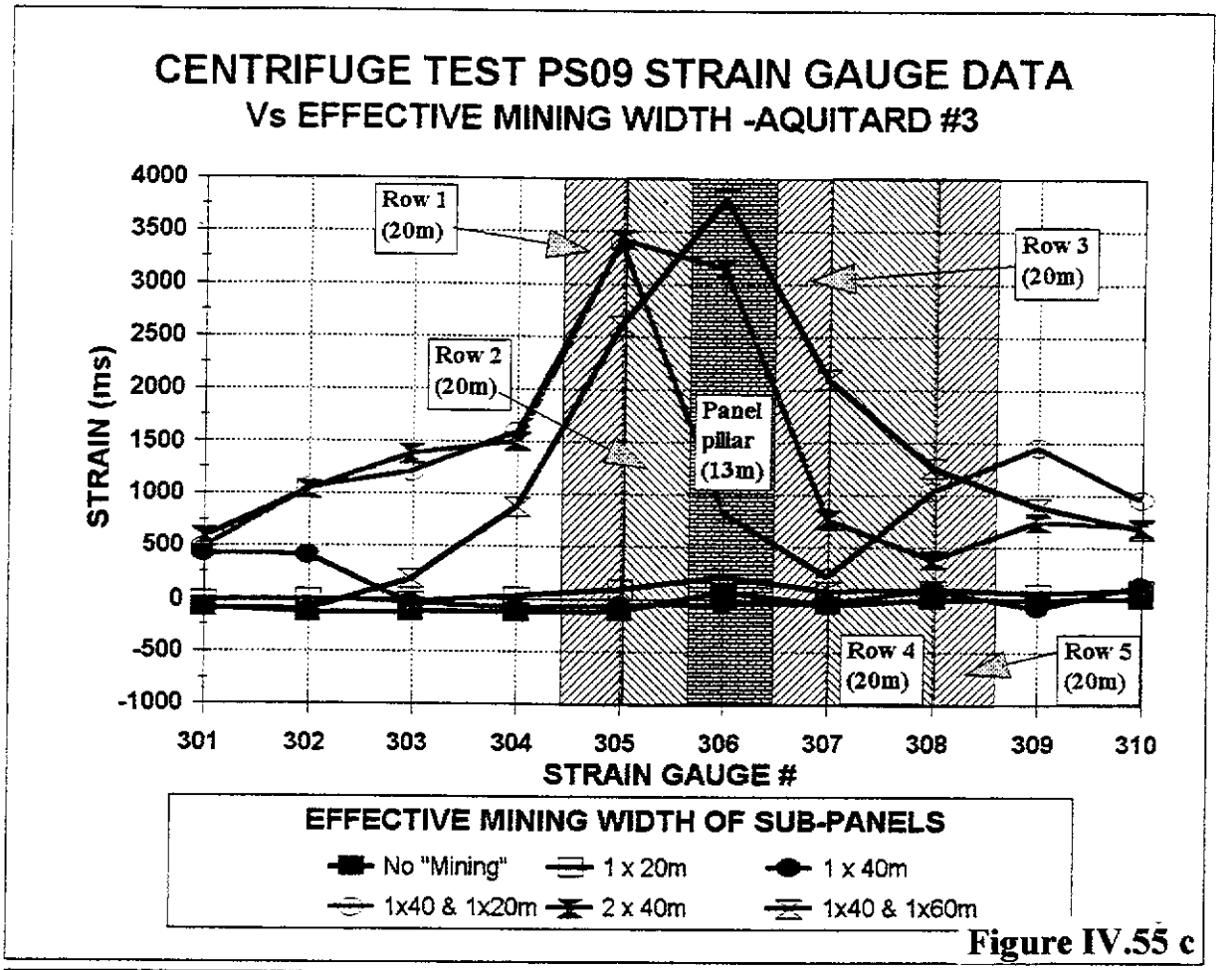

Figure IV.55 c

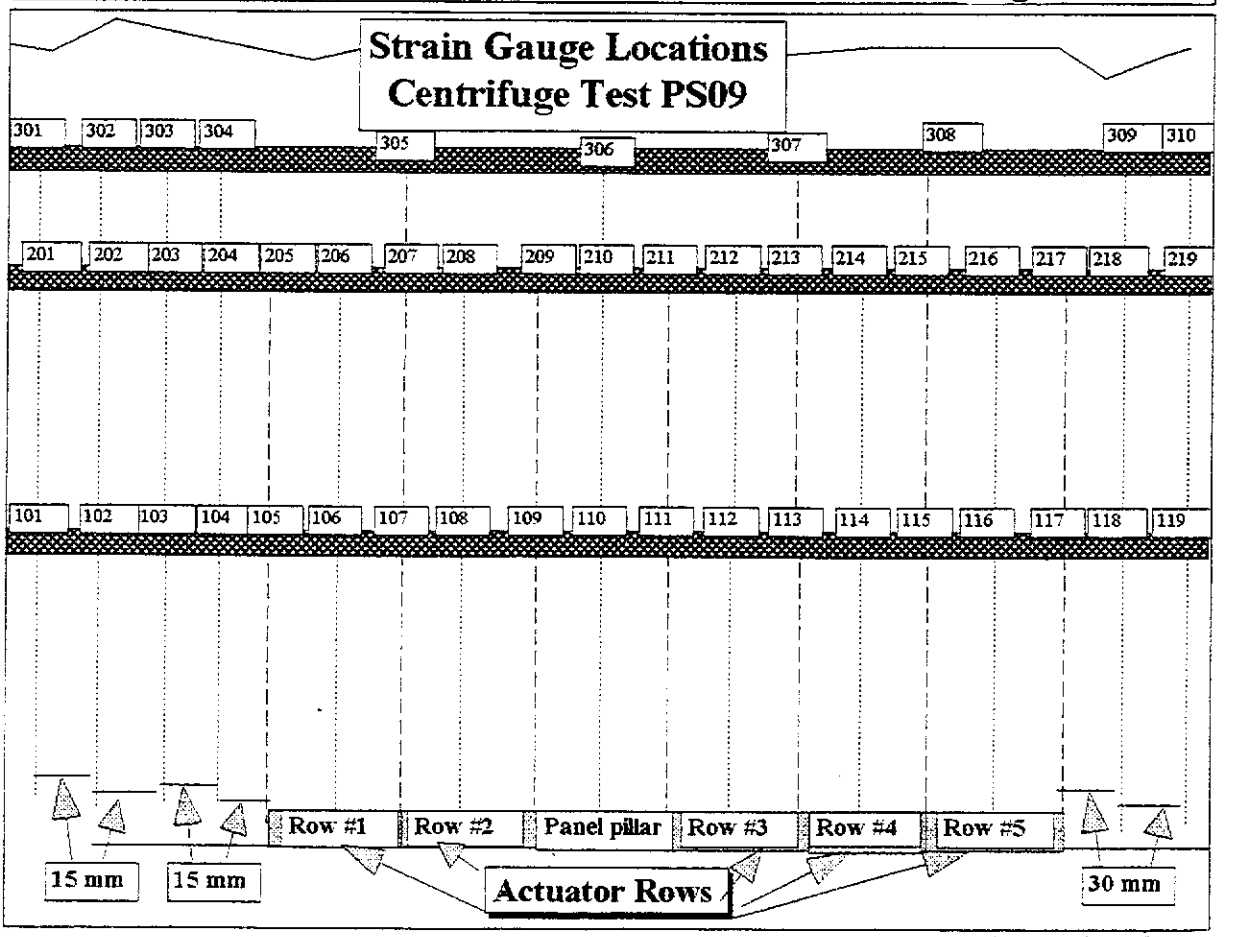

Figure IV.55 d

TABLE IV.13

SUMMARY OF CENTRIFUGE TEST PS09 STRAIN GAUGE DATA RAW DATA

GAUGE #	ACTUATOR ROW # 0	1	2	3	4	5
	mstrain	mstrain	mstrain	mstrain	mstrain	mstrain
101	-353	-418	-621	-1164	-1302	-1408
102	-303	-344	-557	-3724	-3724	-3724
103	-151	-137	-150	-961	-1560	-1623
104	-88	-65	-221	-283	-494	-547
105	-124	-79	-386	-220	-314	-375
106	-144	-91	-1191	-3370	-3583	-3532
107	-135	-108	-811	-3737	-3737	-3737
108	-108	-89	-674	-1865	-1917	-1952
109	-156	-194	-61	-130	-200	-1020
110	-147	-232	-188	-296	-364	-1180
111	-111	-200	-219	-613	-627	-553
112	-65	-144	3	-2365	-3311	-2813
113	-92	-147	57	-1609	-1663	-1175
114	-107	-176	-20	-1476	-1343	-628
115	-71	-187	-20	-1190	-1219	-452
116	-124	-182	-81	-366	-1938	-261
117	-70	-112	-19	-153	-2977	-1198
118	-195	-240	-152	-186	-669	-1724
119	-310	-341	-267	-280	-429	-3742
201	-131	3	345	1321	277	-1222
202	-55	56	237	1230	789	68
203	-116	-43	-148	455	380	188
204	-142	-54	-302	268	328	174
205	-74	0	-253	16	125	32
206	68	-208	-276	-279	-518	-318
207	-113	-306	-432	468	-228	-656
208	-167	-102	117	-81	-884	-865
209	-170	-28	388	114	-296	-572
210	74	268	1002	1125	668	136
211	2	209	1008	1377	1015	487
212	524	604	993	1909	2224	1882
213	63	96	-230	-345	612	1358
214	4	-112	-506	708	-1290	-8
215	-116	251	-463	-614	-772	-668
216	-83	-232	-448	-604	-570	-1742
217	-65	-85	-111	-134	-115	-191
218	-180	-112	-300	-1825	-1629	-1491
219	-125	-88	-325	-3737	-3737	-3737
301	-76	-60	-503	-560	-654	0
302	-132	-137	-544	-1188	-1169	-31
303	-121	-97	-83	-1319	-1501	-310
304	-122	-148	-35	-1717	-1628	-1002
305	-115	-204	-52	-3510	-3532	-2715
306	71	-141	114	-754	-3075	-3740
307	-45	-132	-21	-256	-807	-2150
308	5	-96	-89	-1022	-377	-1250
309	2	-62	78	-1448	-738	-881
310	20	-83	-118	-934	-670	-651

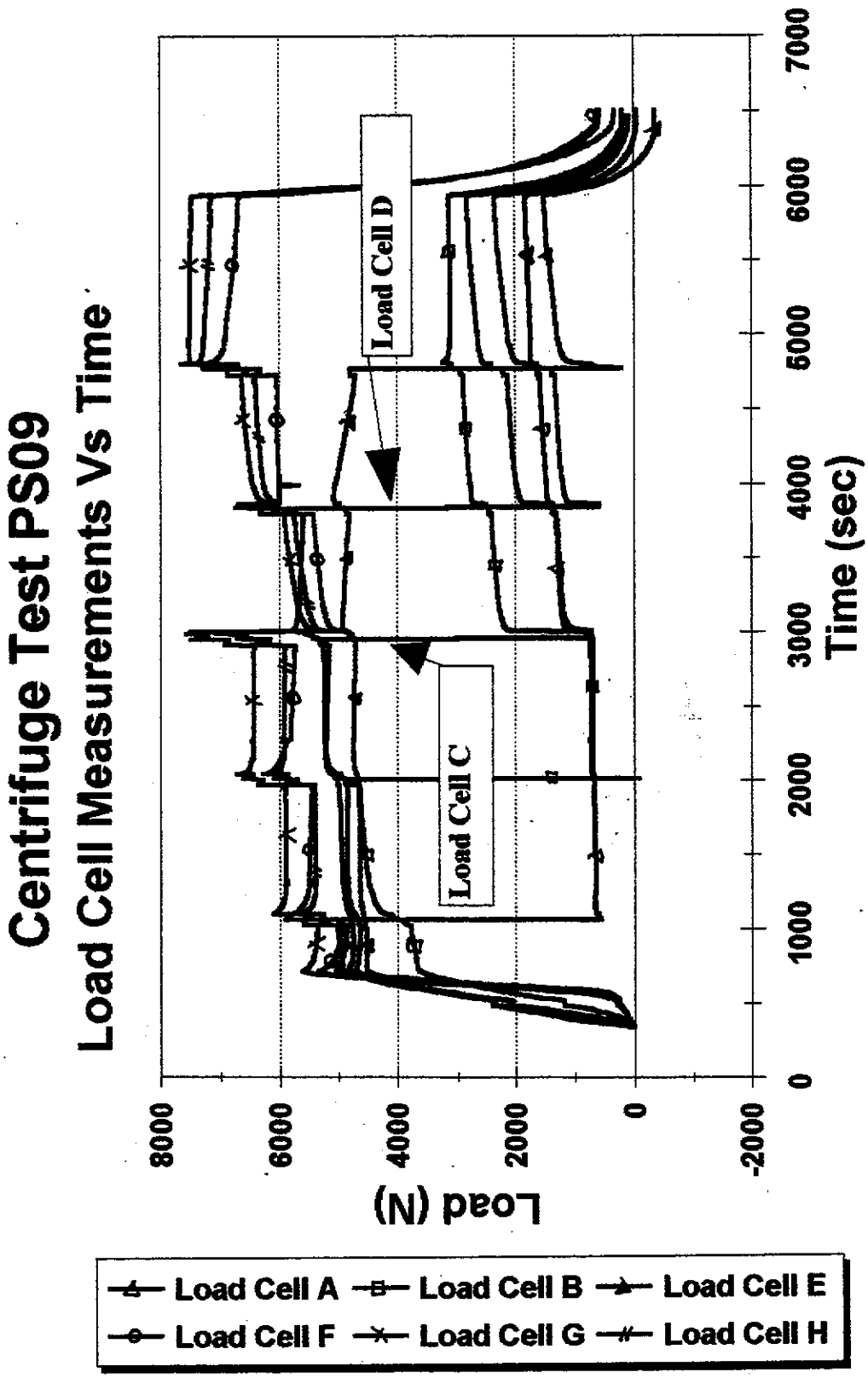
Centrifuge Test PS09
Load Cell Measurements Vs Time
Load Cell D
Load Cell C
Load (N)
8000
6000
4000
2000
0
-2000
Time (sec)
0
1000
2000
3000
4000
5000
6000
7000
Load Cell A
Load Cell B
Load Cell E
Load Cell F
Load Cell G
Load Cell H

Figure IV.56

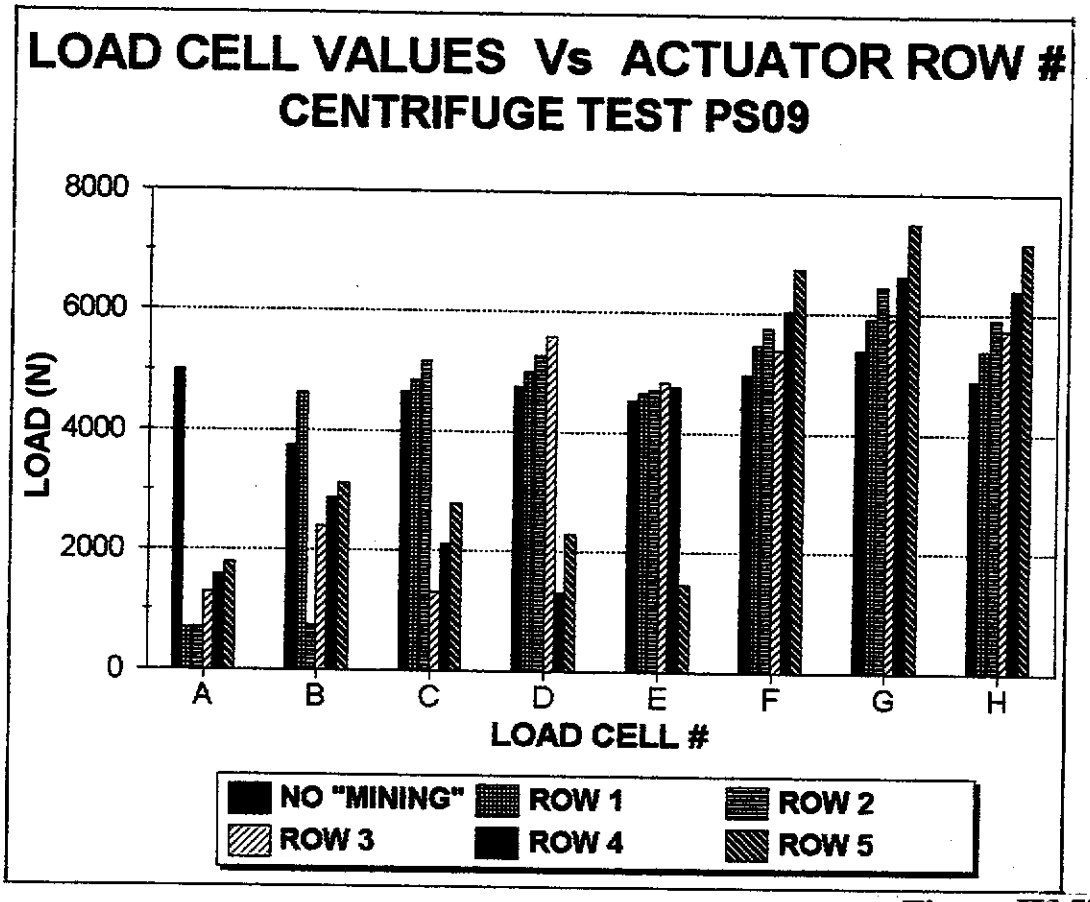

Figure IV.57 a

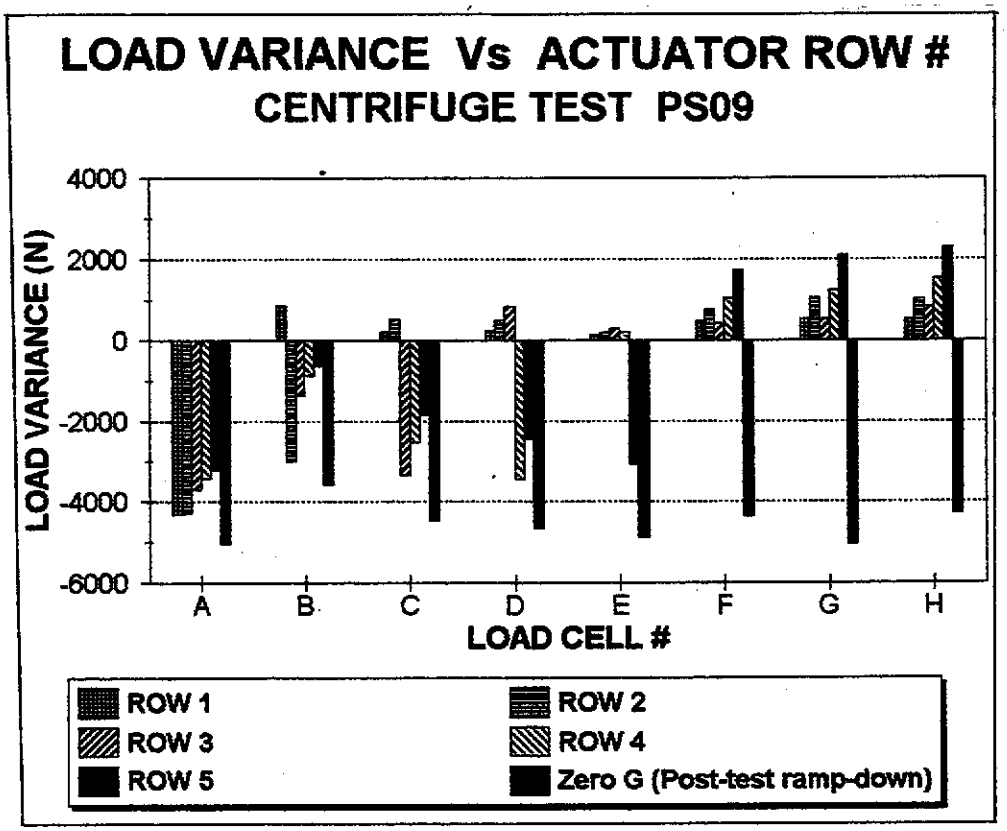

Figure IV.57 b

TABLE IV.14

LOAD CELL #	SUMMARY OF PS09 LOAD CELL DATA Vs ACTUATOR ROW #					
	ACTUATOR ROW #					
	0	1	2	3	4	5
	LOAD (N)					
1	5004	677	704	1285	1568	1793
2	3758	4631	734	2389	2880	3114
3	4649	4856	5172	1302	2114	2785
4	4754	4996	5261	5593	1300	2294
5	4536	4663	4719	4829	4756	1456
6	4986	5455	5747	5396	6036	6729
7	5382	5902	6441	5899	6625	7496
8	4881	5400	5909	5733	6396	7175

DIAGRAMMATICAL VIEW OF LOAD CELL VALUES CENTRIFUGE TEST PS09

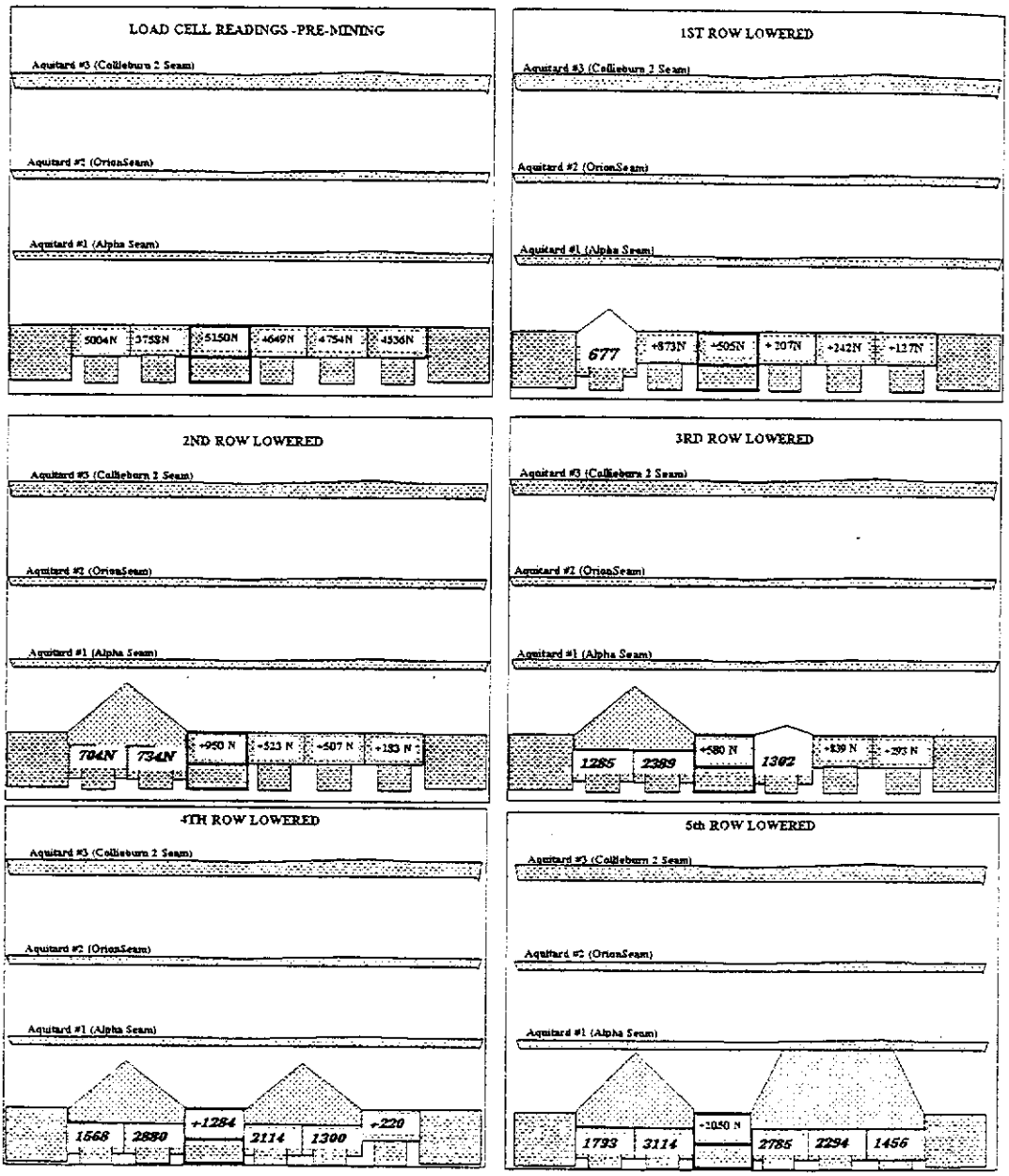

Note : Loads are Given as :-
a) Total loads for lowered actuators, and
b) Load variance from pre-mining loads for unlowered actuators

Figure IV.58

MODEL STRAIN GAUGE UNITS

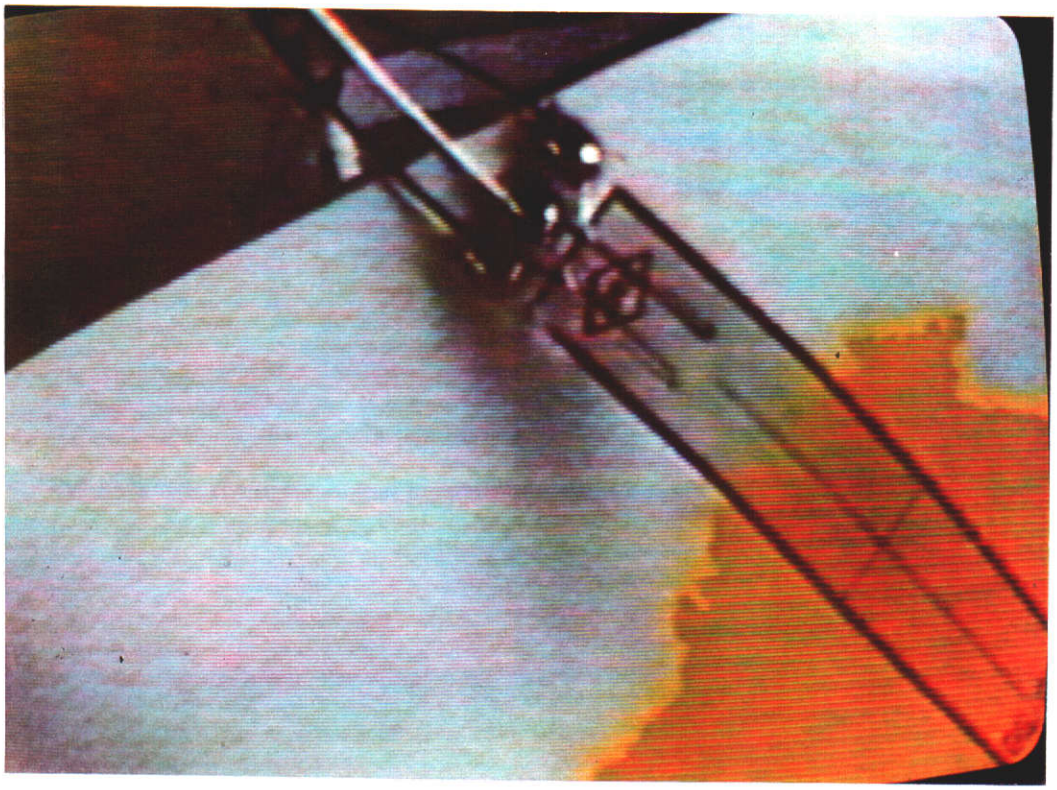

a) Individual Strain Gauge

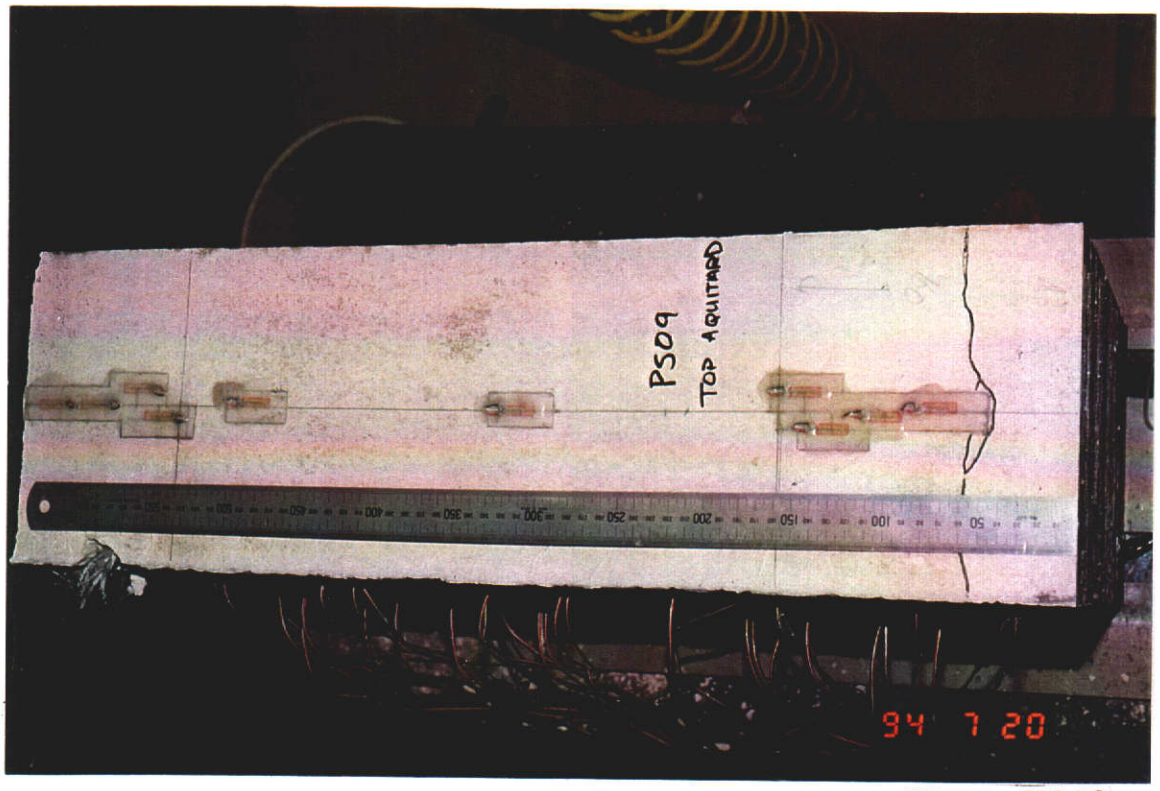

b) Strain gauge layout - top aquitard - PS09

Figure IV.59

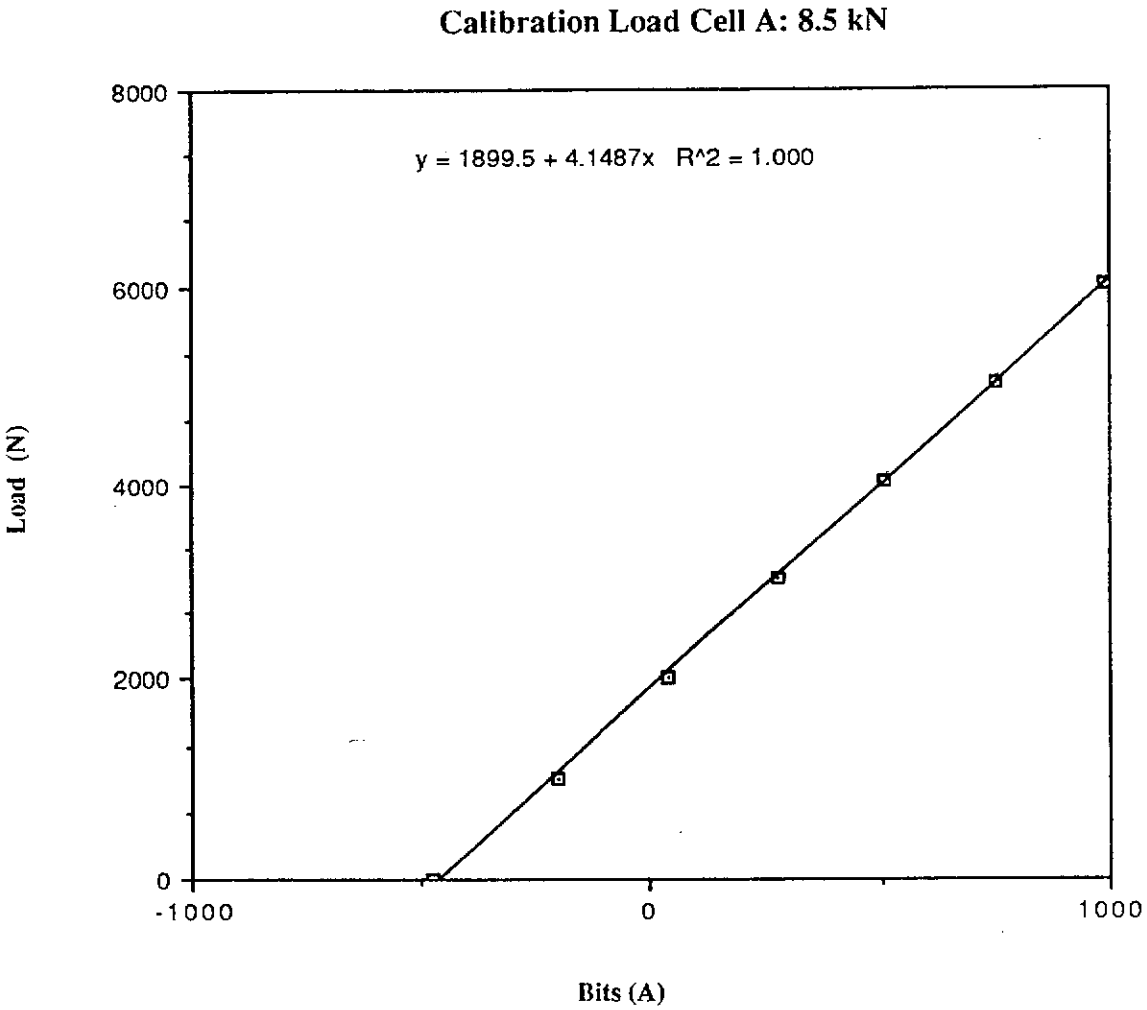
Calibration Load Cell A: 8.5 kN
y = 1899.5 + 4.1487x R^2 = 1.000
8000
6000
4000
2000
0
-1000
0
1000
Load (N)
Bits (A)

Figure IV.60

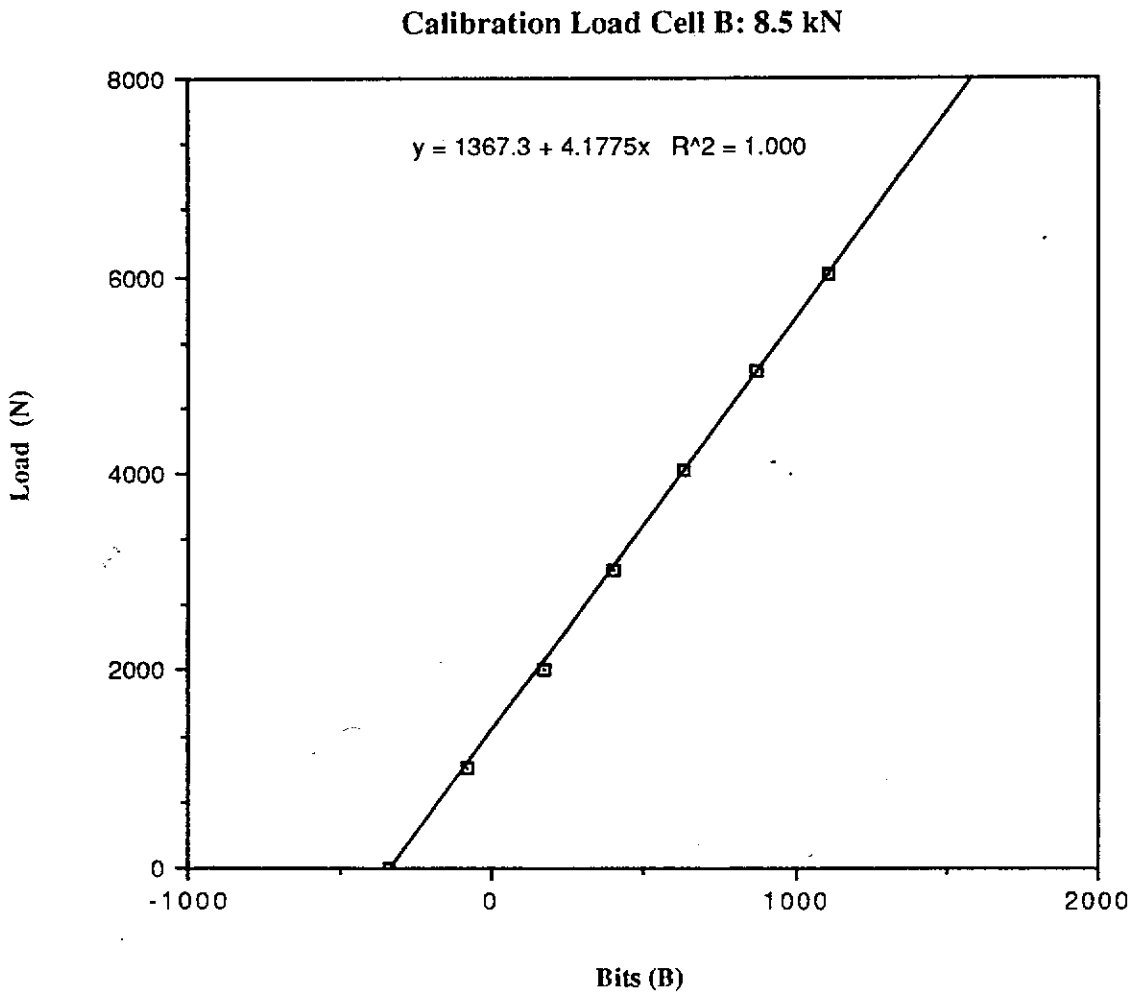
Calibration Load Cell B: 8.5 kN
y = 1367.3 + 4.1775x R^2 = 1.000
8000
6000
4000
2000
0
-1000
0
1000
2000
Load (N)
Bits (B)

Figure IV.61

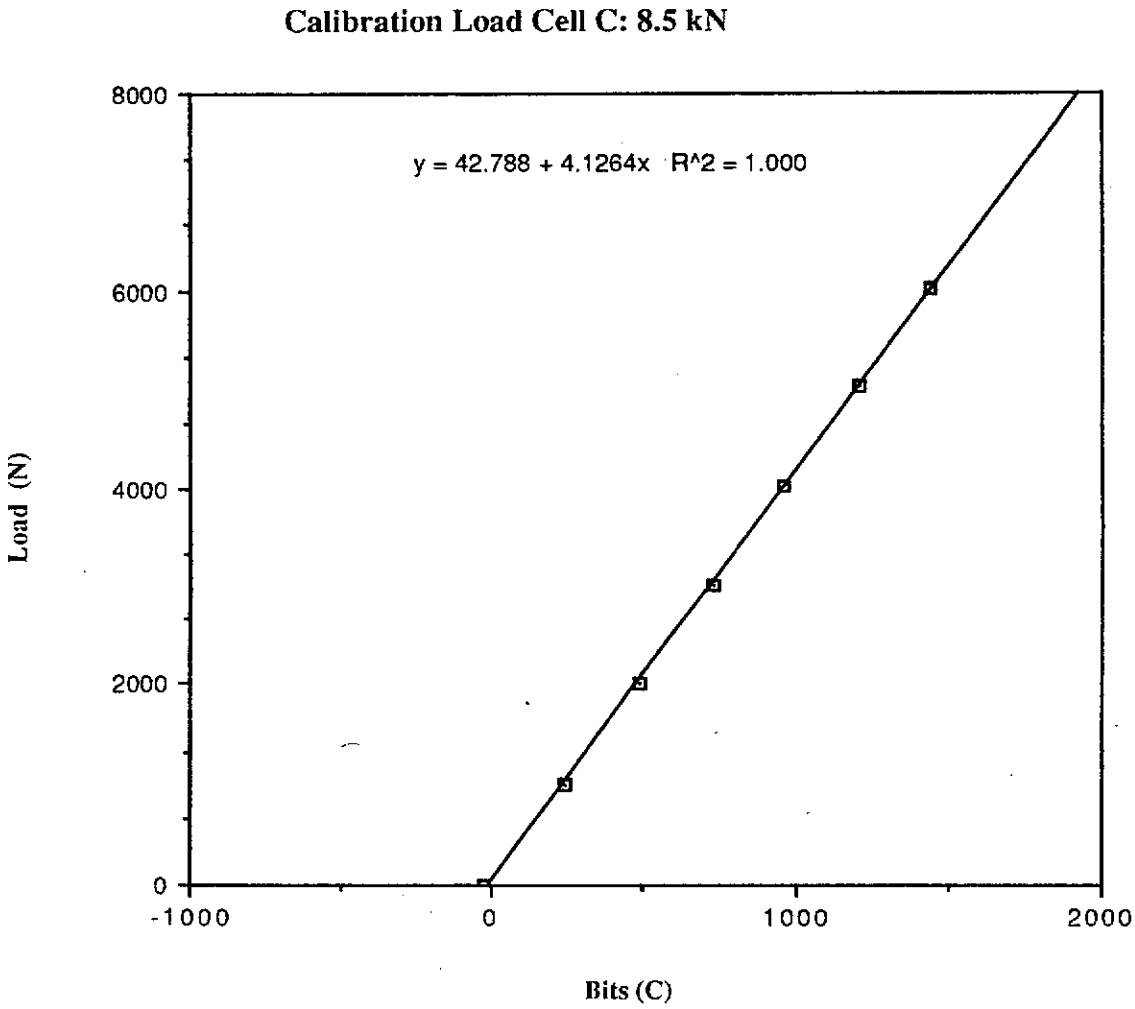
Calibration Load Cell C: 8.5 kN
y = 42.788 + 4.1264x R^2 = 1.000
Load (N)
8000
6000
4000
2000
0
-1000
0
1000
2000
Bits (C)

Figure IV.62

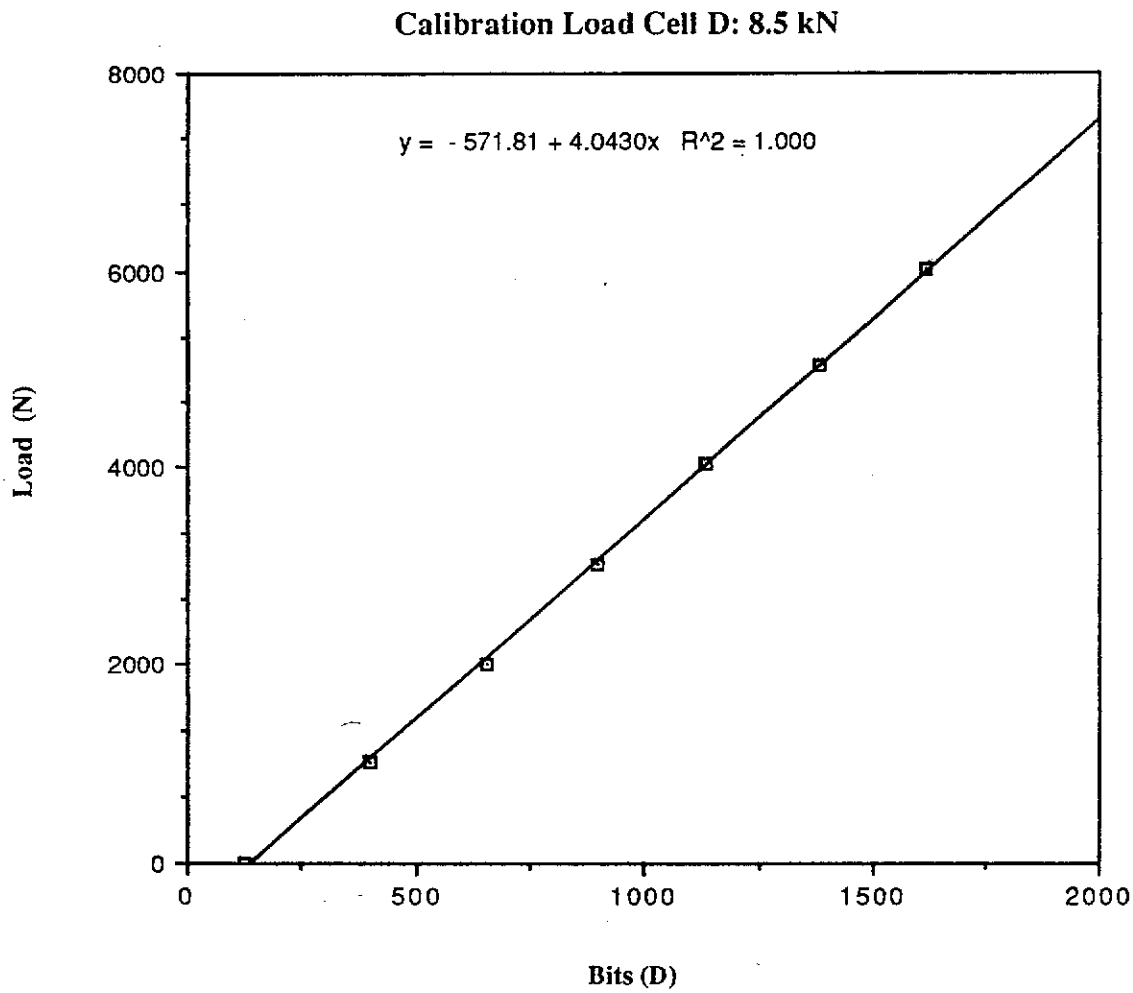
Calibration Load Cell D: 8.5 kN
y = - 571.81 + 4.0430x R^2 = 1.000
Load (N)
Bits (D)
8000
6000
4000
2000
0
0
500
1000
1500
2000

Figure IV.63

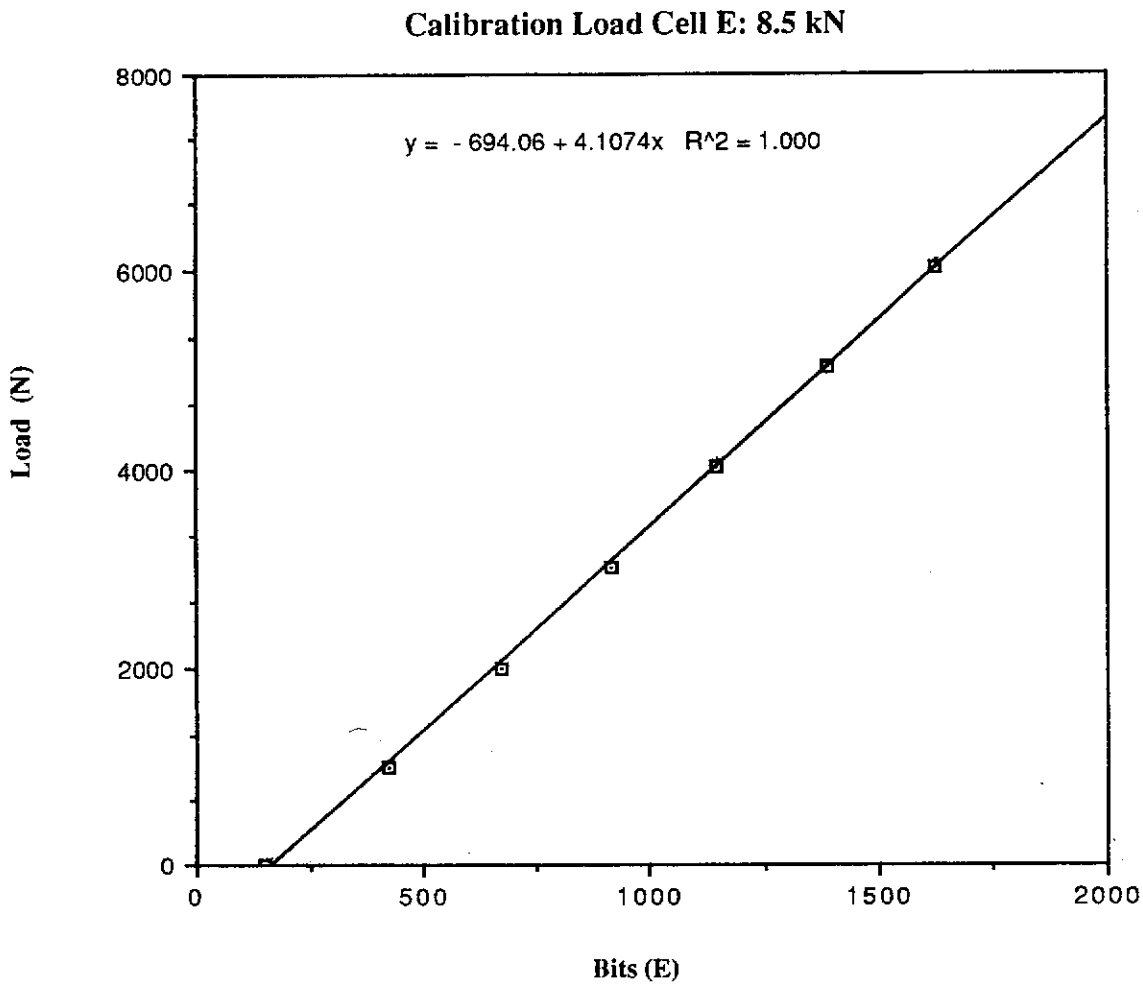
Calibration Load Cell E: 8.5 kN
y = - 694.06 + 4.1074x R^2 = 1.000
Load (N)
Bits (E)
8000
6000
4000
2000
0
0
500
1000
1500
2000

Figure IV.64

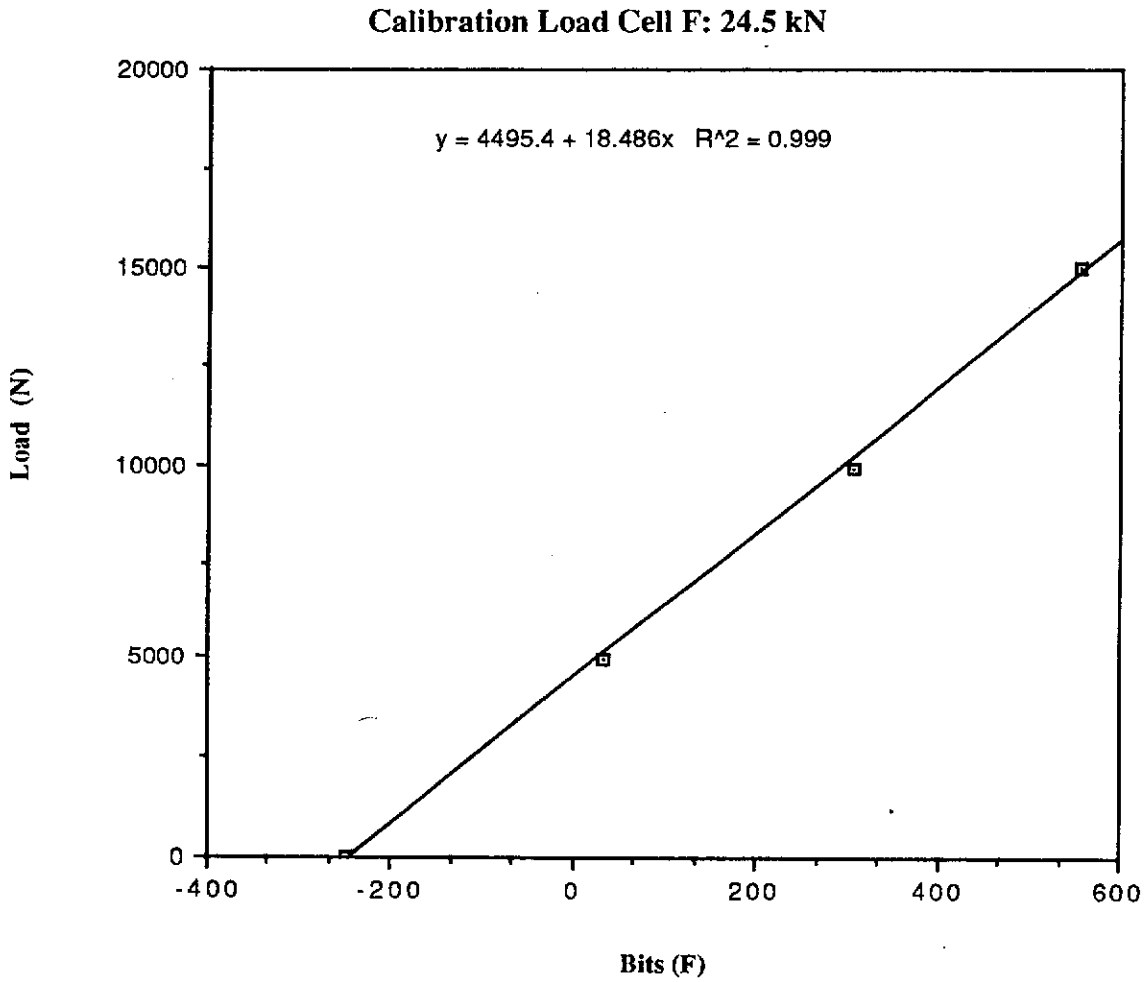
Calibration Load Cell F: 24.5 kN
y = 4495.4 + 18.486x R^2 = 0.999
Load (N)
20000
15000
10000
5000
0
-400
-200
0
200
400
600
Bits (F)

Figure IV.65

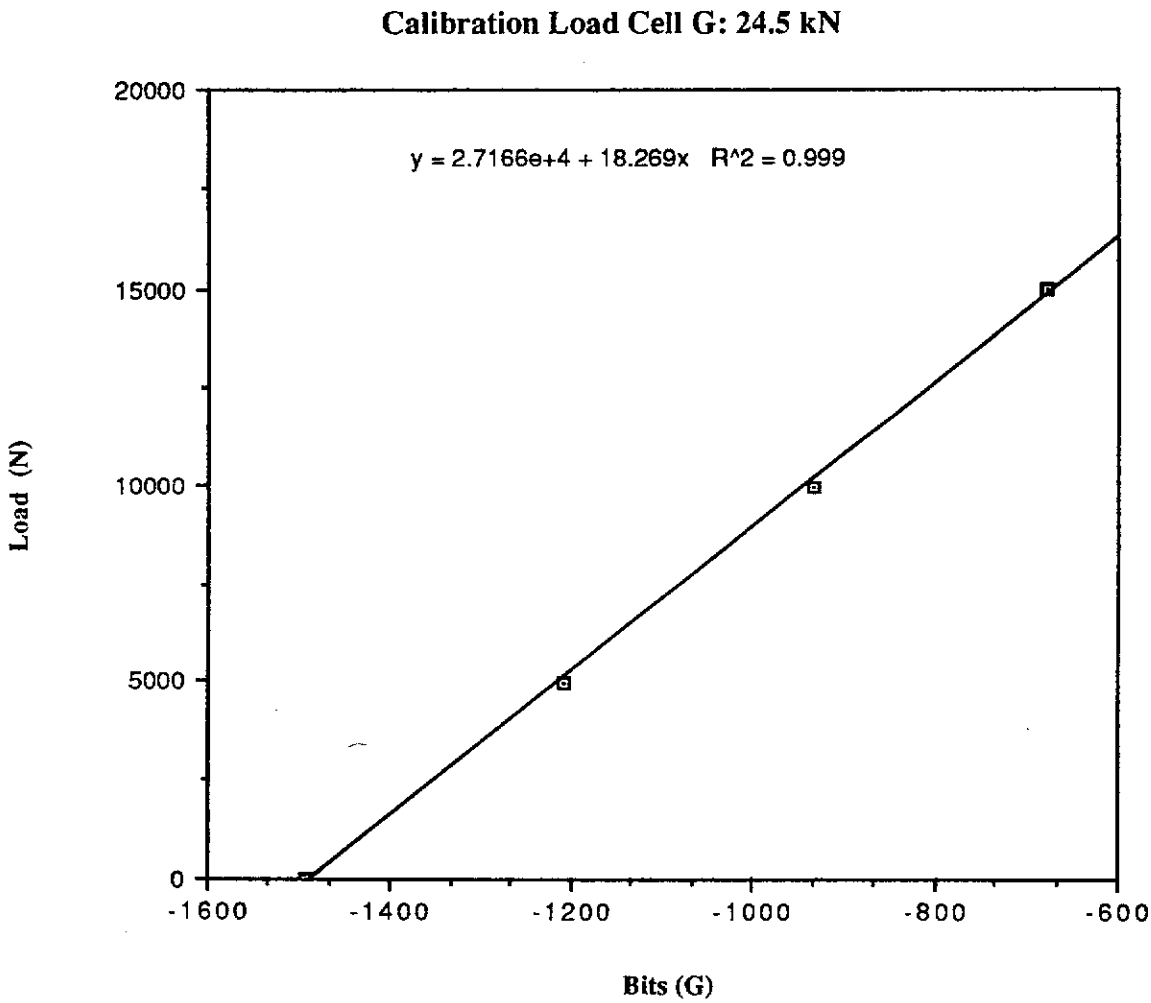
Calibration Load Cell G: 24.5 kN
y = 2.7166e+4 + 18.269x R^2 = 0.999
20000
15000
10000
5000
0
Load (N)
-1600
-1400
-1200
-1000
-800
-600
Bits (G)

Figure IV.66

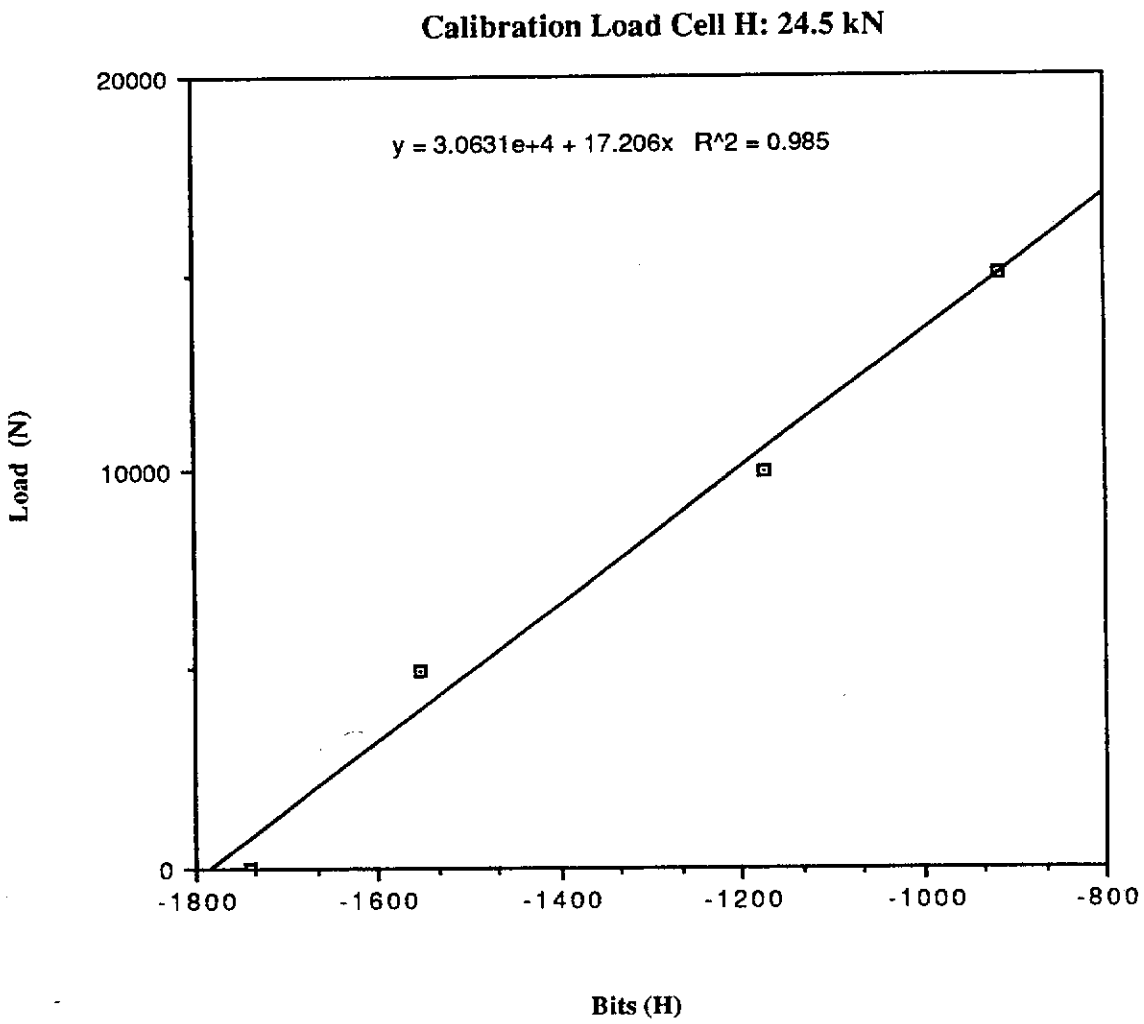
Calibration Load Cell H: 24.5 kN
y = 3.0631e+4 + 17.206x R^2 = 0.985
20000
10000
0
Load (N)
-1800
-1600
-1400
-1200
-1000
-800
Bits (H)

Figure IV.67

LOAD CELL DATA DURING TEST SPIN-UP Vs TIME & ACCELERATION

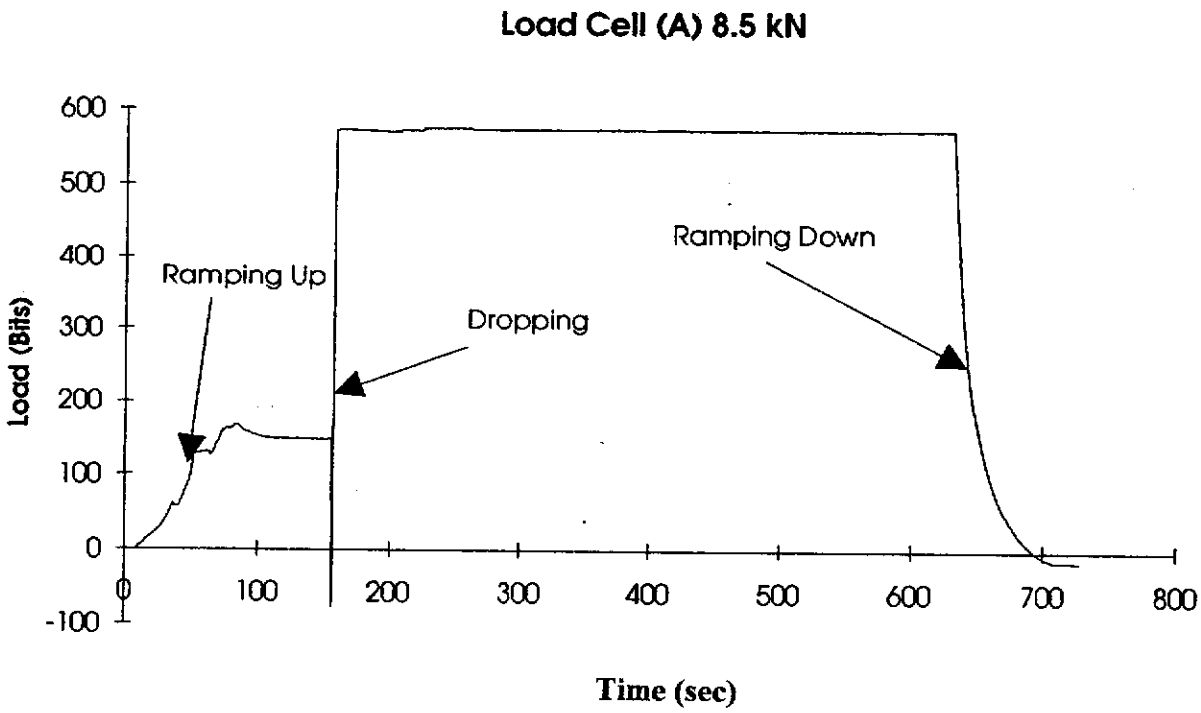

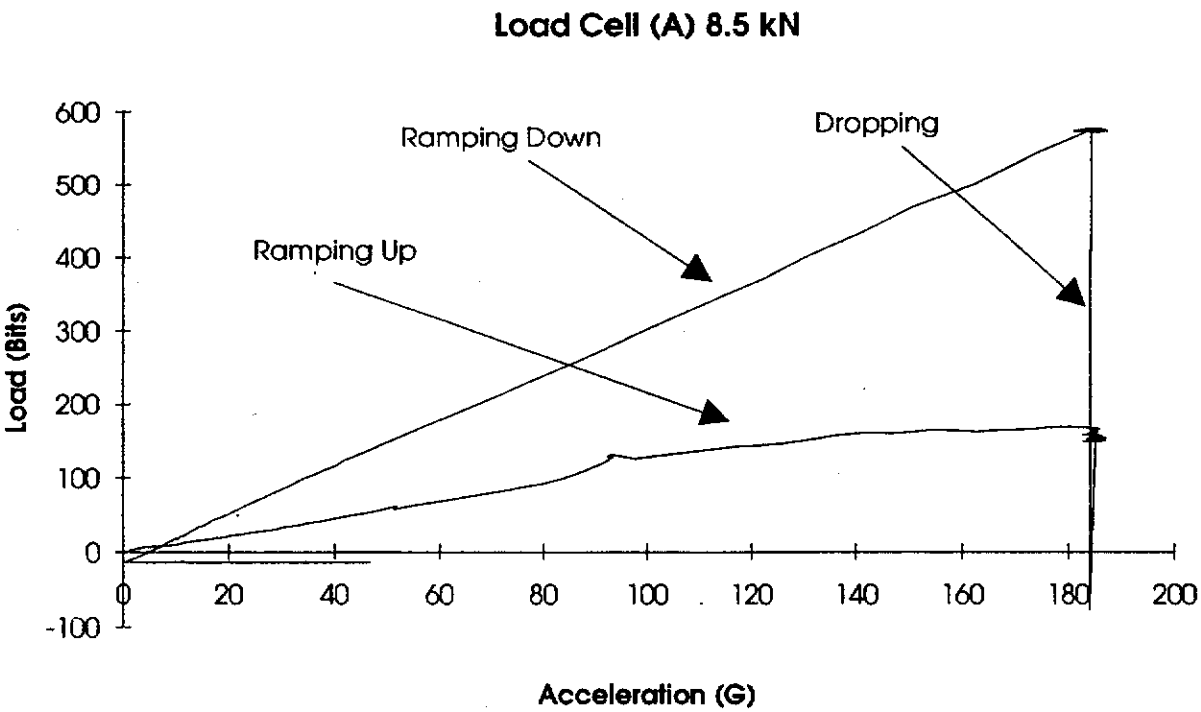

Figure IV.68

LOAD CELL DATA DURING TEST SPIN-UP Vs TIME & ACCELERATION

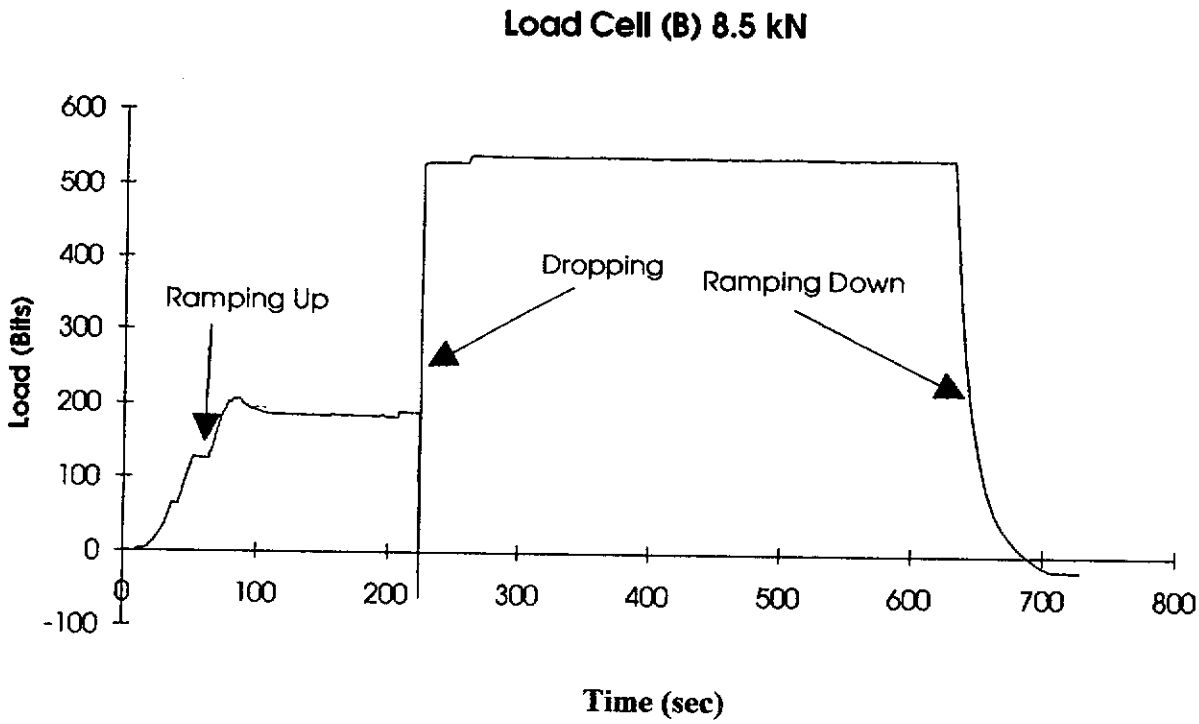

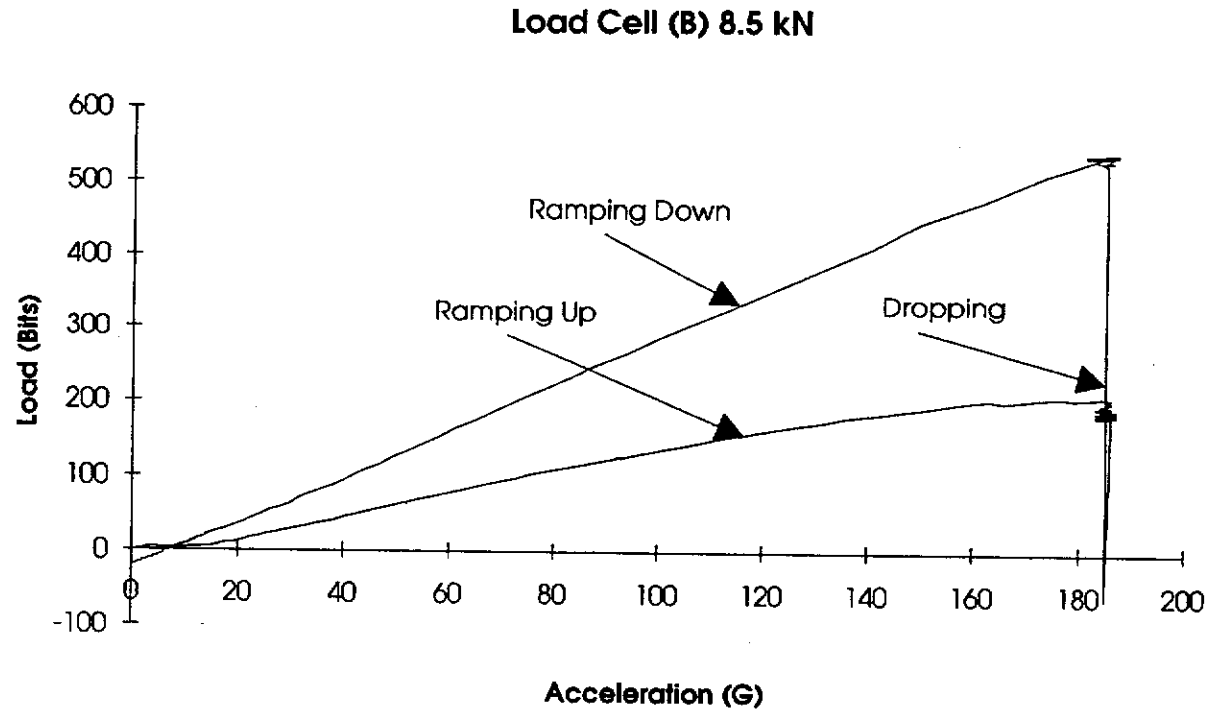

Figure IV.69

LOAD CELL DATA DURING TEST SPIN-UP Vs TIME & ACCELERATION

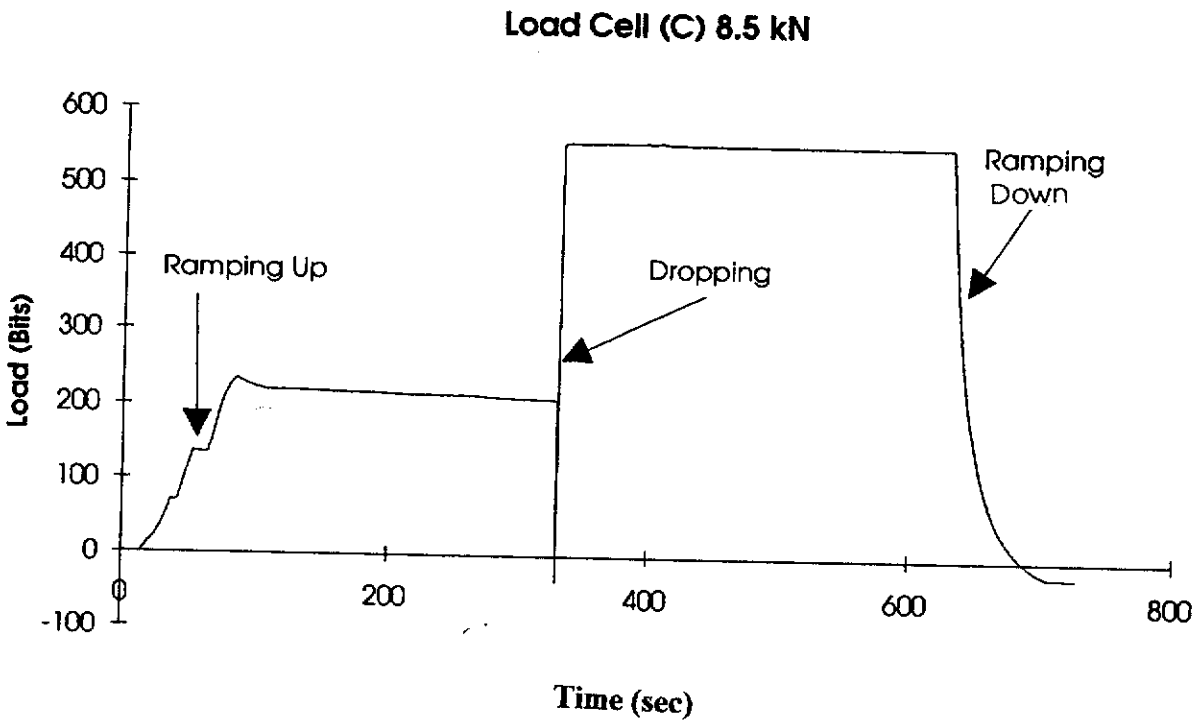

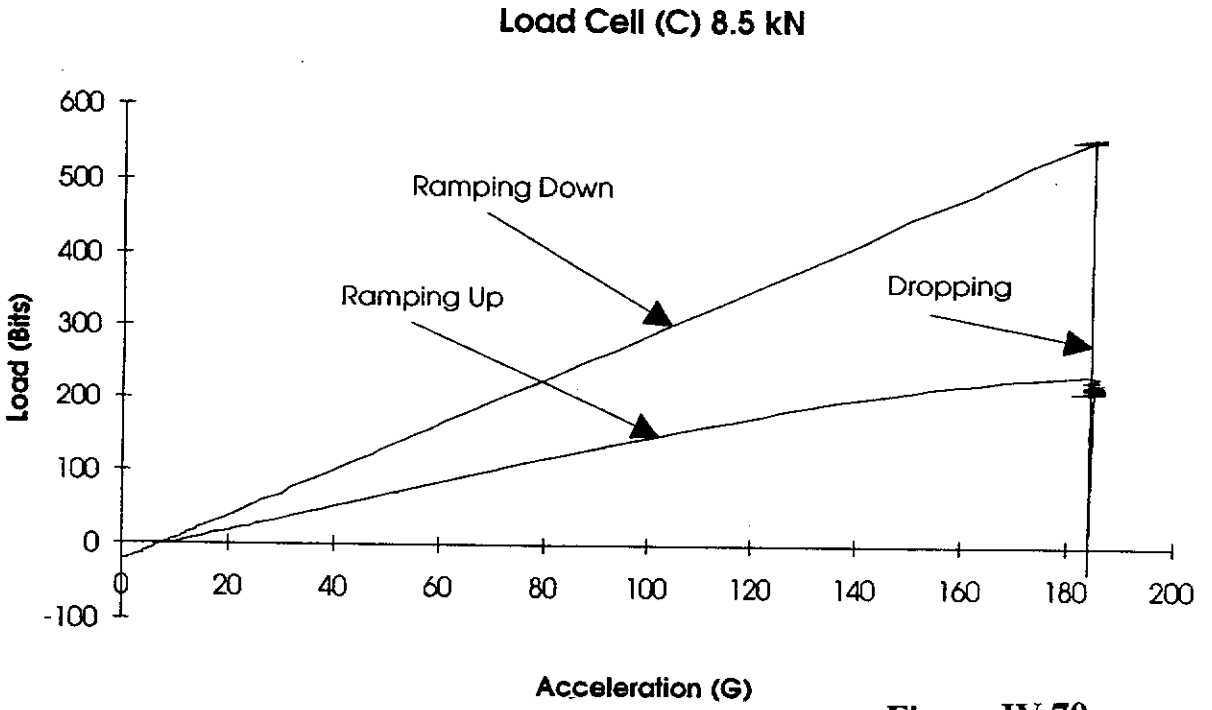

Figure IV.70

LOAD CELL DATA DURING TEST SPIN-UP Vs TIME & ACCELERATION

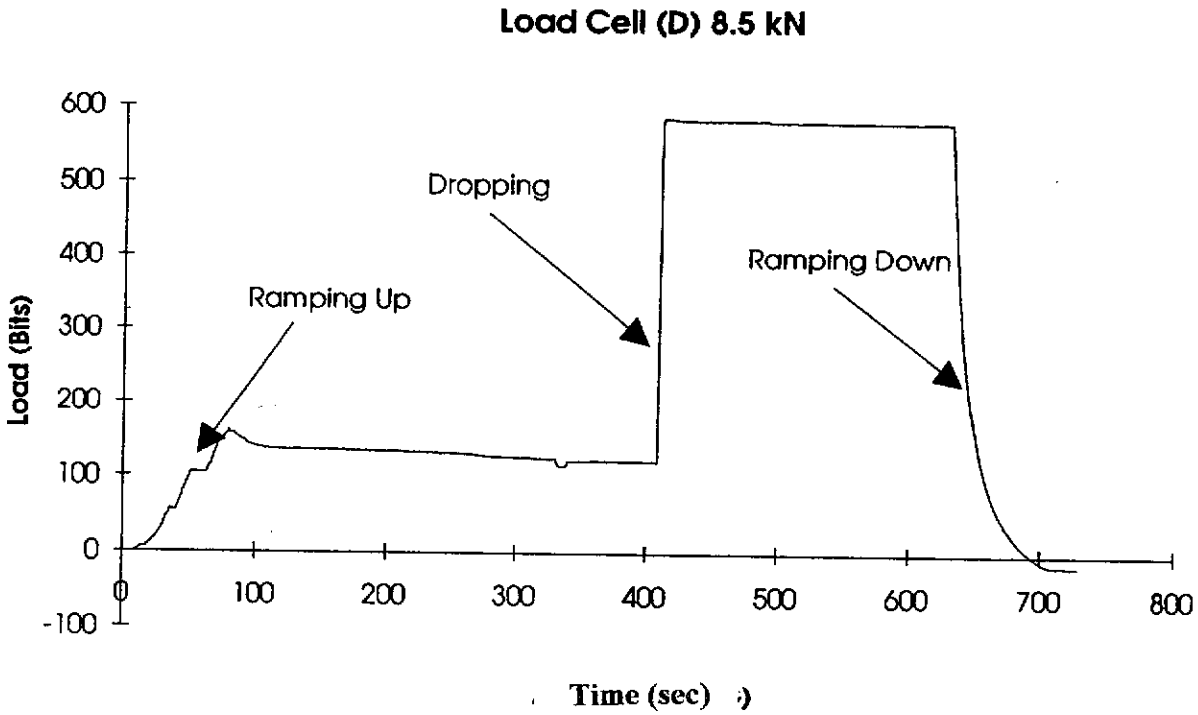

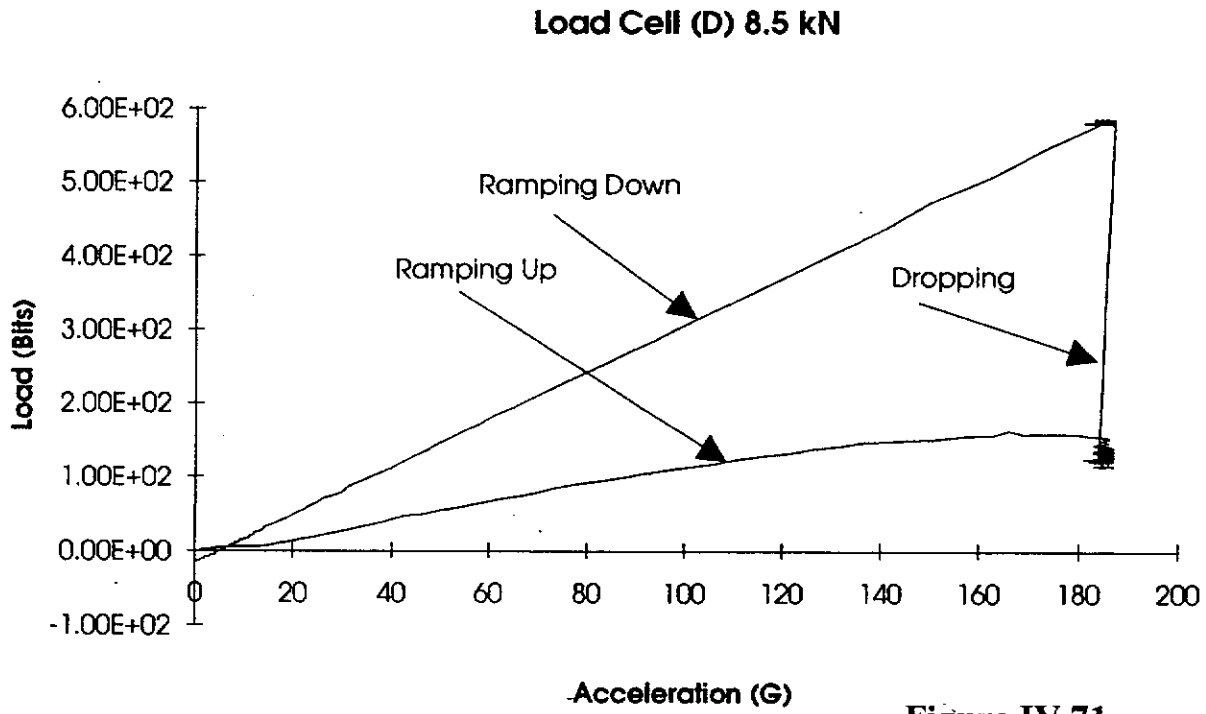

Figure IV.71

LOAD CELL DATA DURING TEST SPIN-UP Vs TIME & ACCELERATION

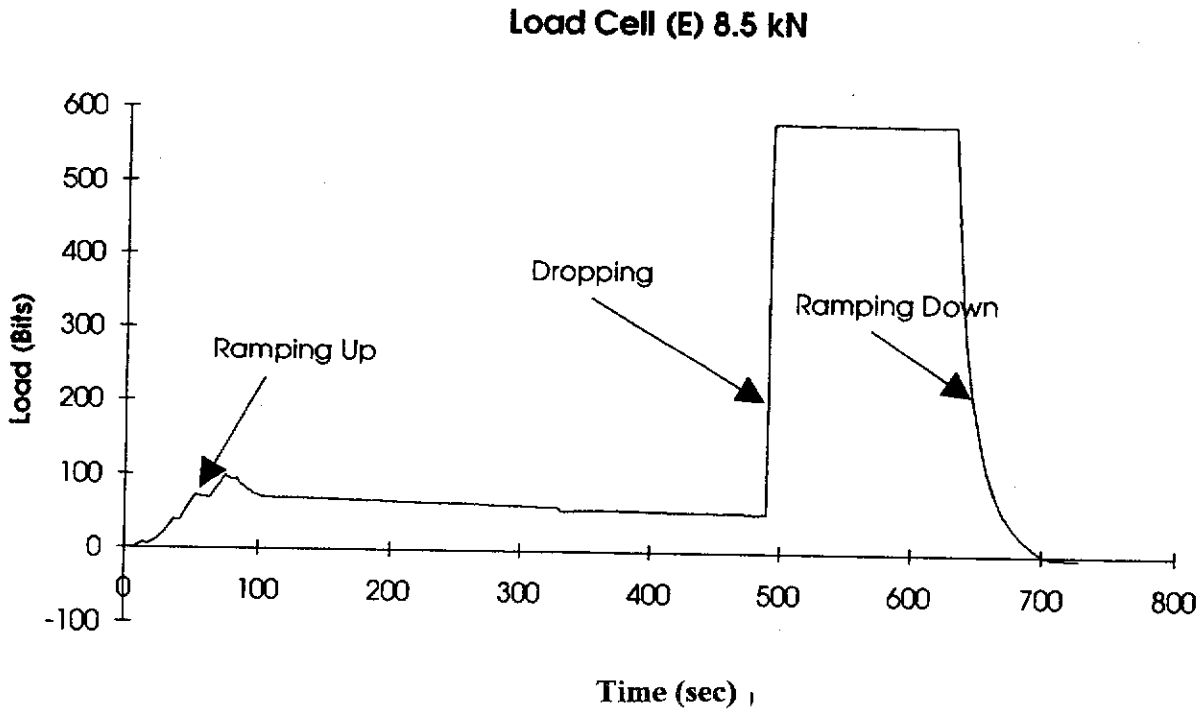

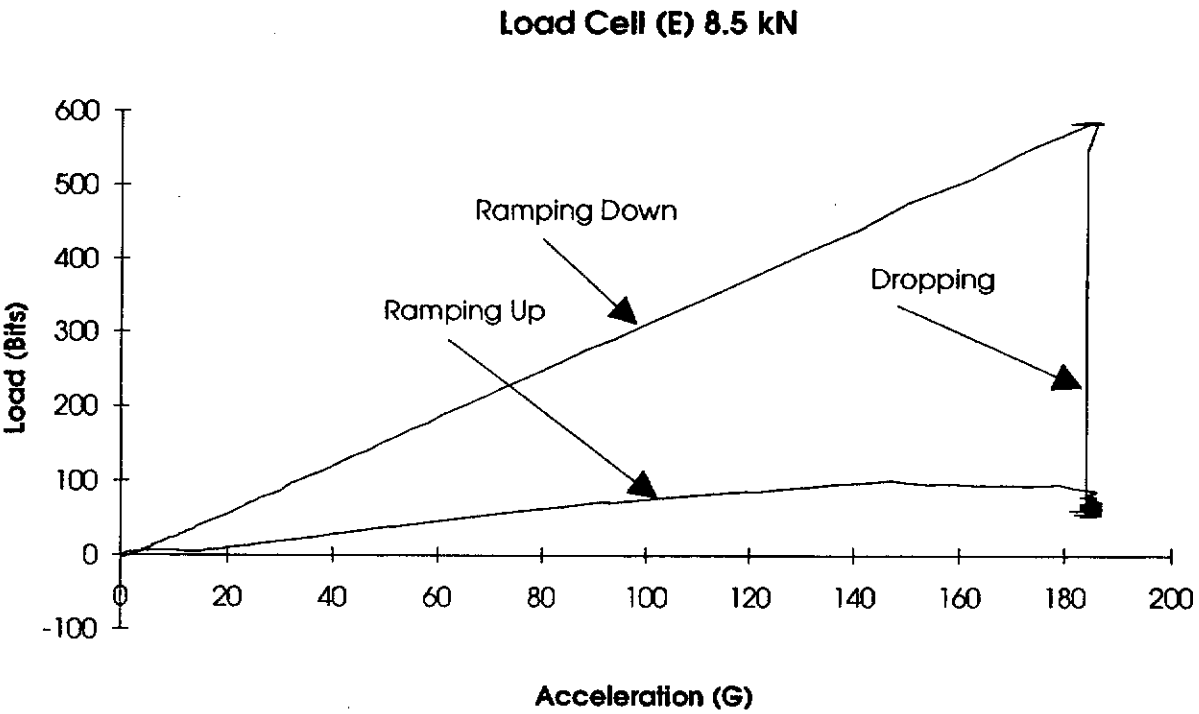

Figure IV.72

LOAD CELL DATA DURING TEST SPIN-UP Vs TIME & ACCELERATION

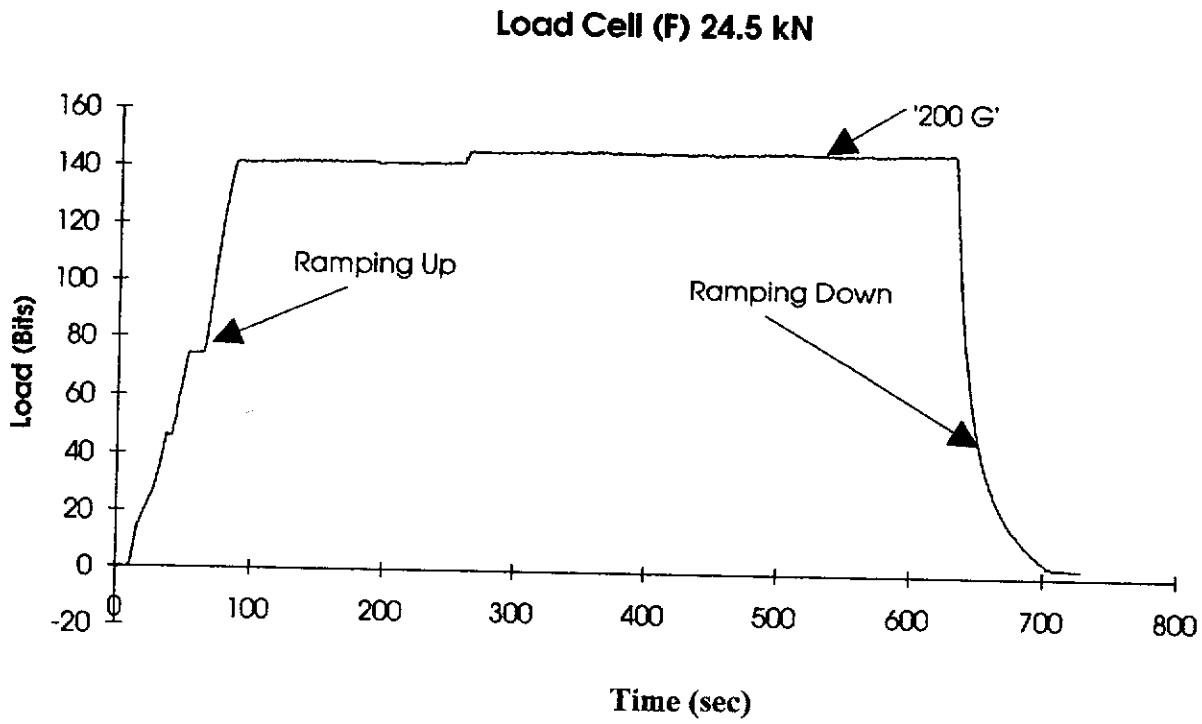

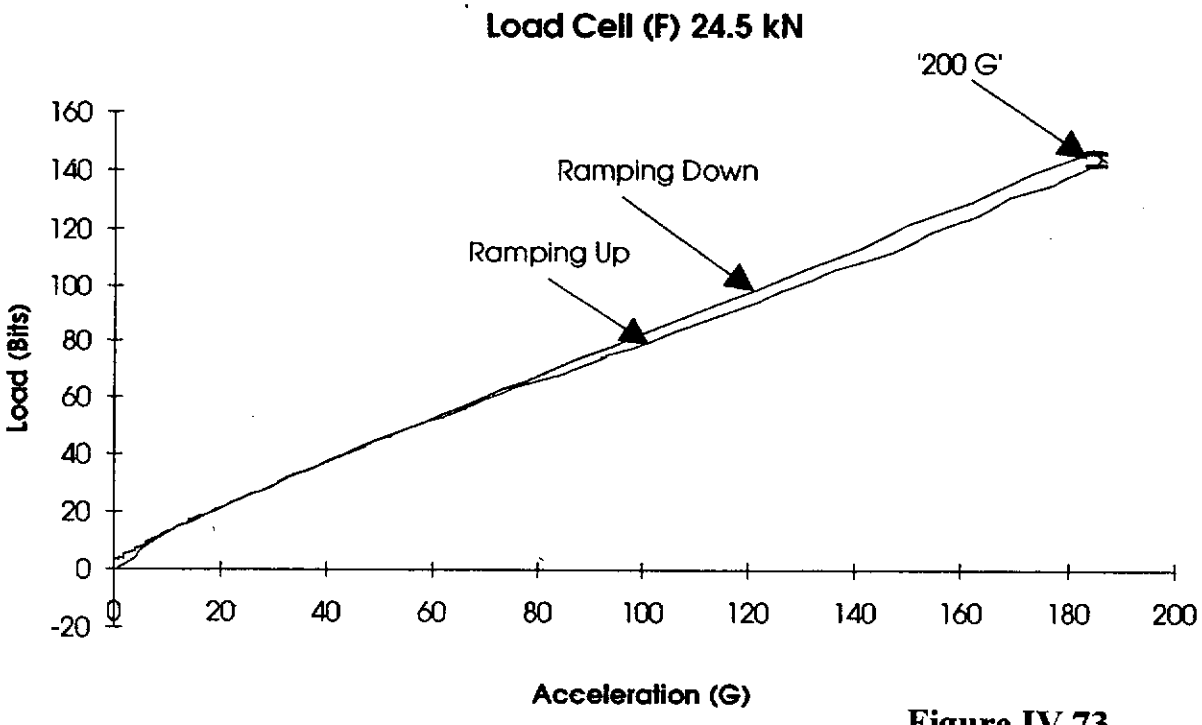

Figure IV.73

LOAD CELL DATA DURING TEST SPIN-UP Vs ACCELERATION

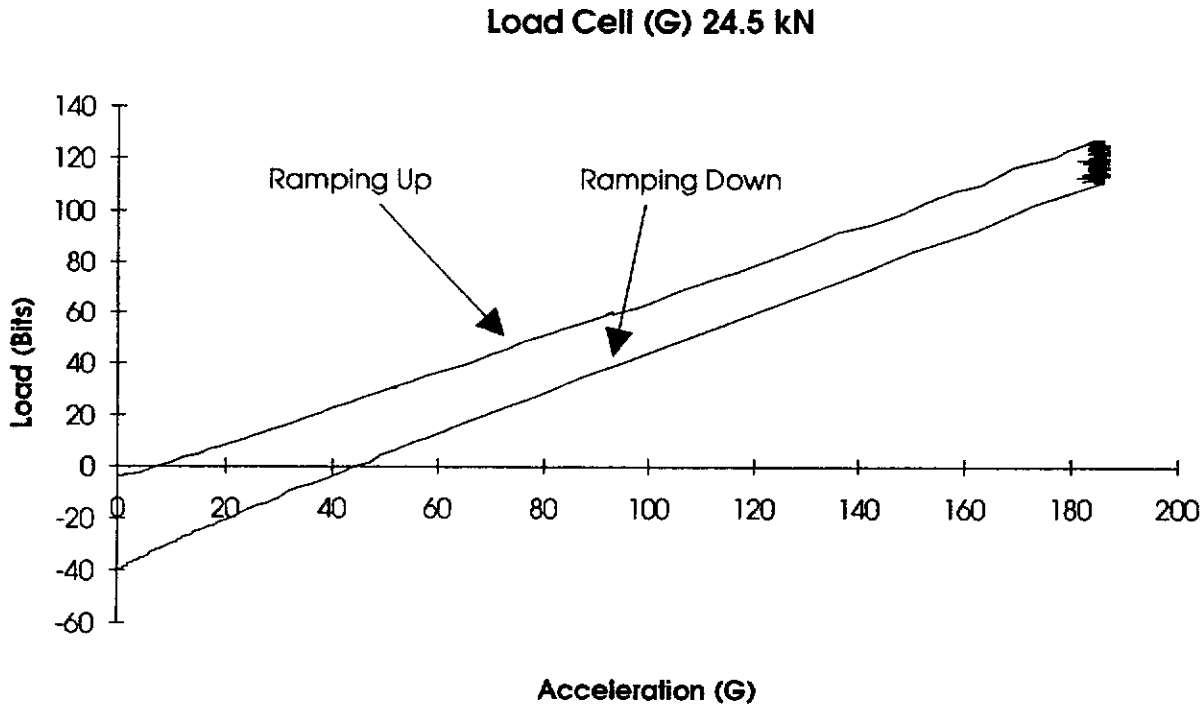

Figure IV.74

LOAD CELL CALIBRATION CHECK

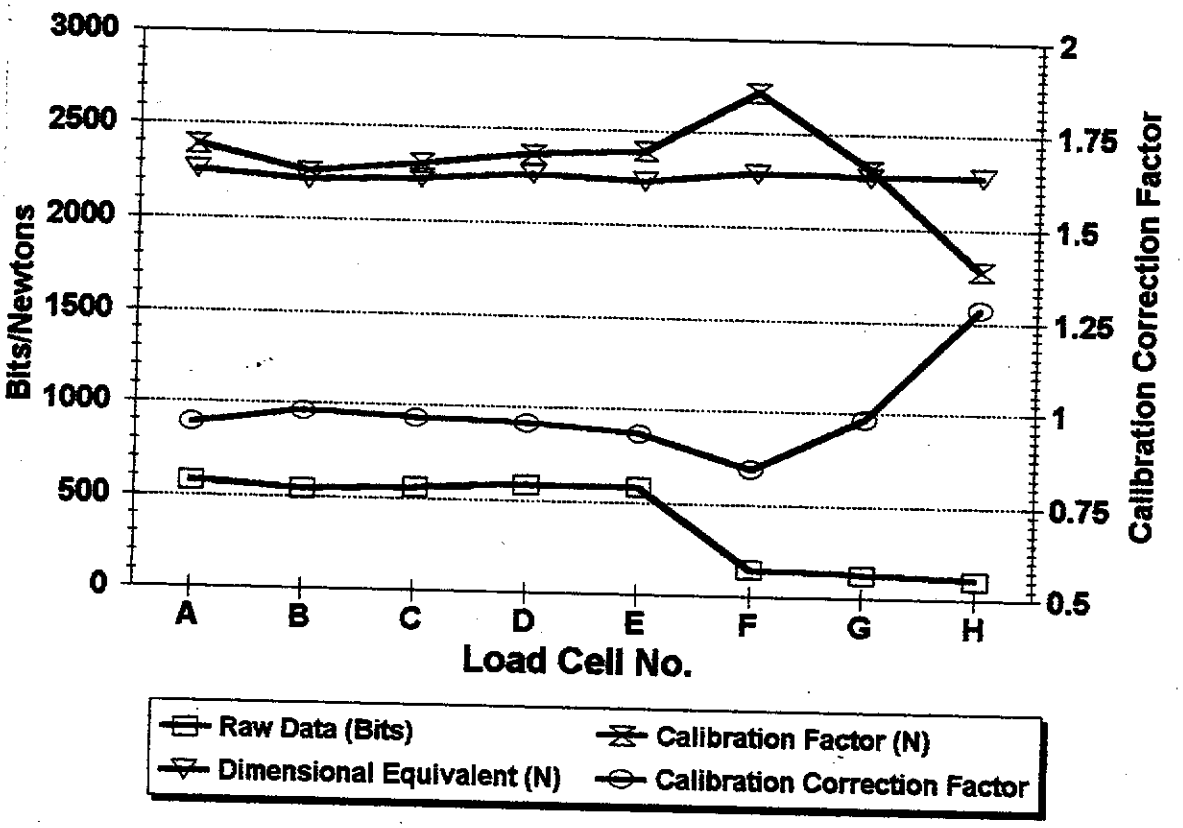

Figure IV.75

TABLE IV.15 LOAD CELL CALIBRATION MASSES

LOAD CELL 8.5 kN	MASS (g)
A	962.1
B	938.1
C	946.4
D	965.5
E	951.3
LOAD CELL 24.5 kN	MASS (g)
F	978.4
G	971.6
H	973.7

TYPICAL SET-UP OF LASER SYSTEM ON TOP OF CENTRIFGUGE STRONG BOX

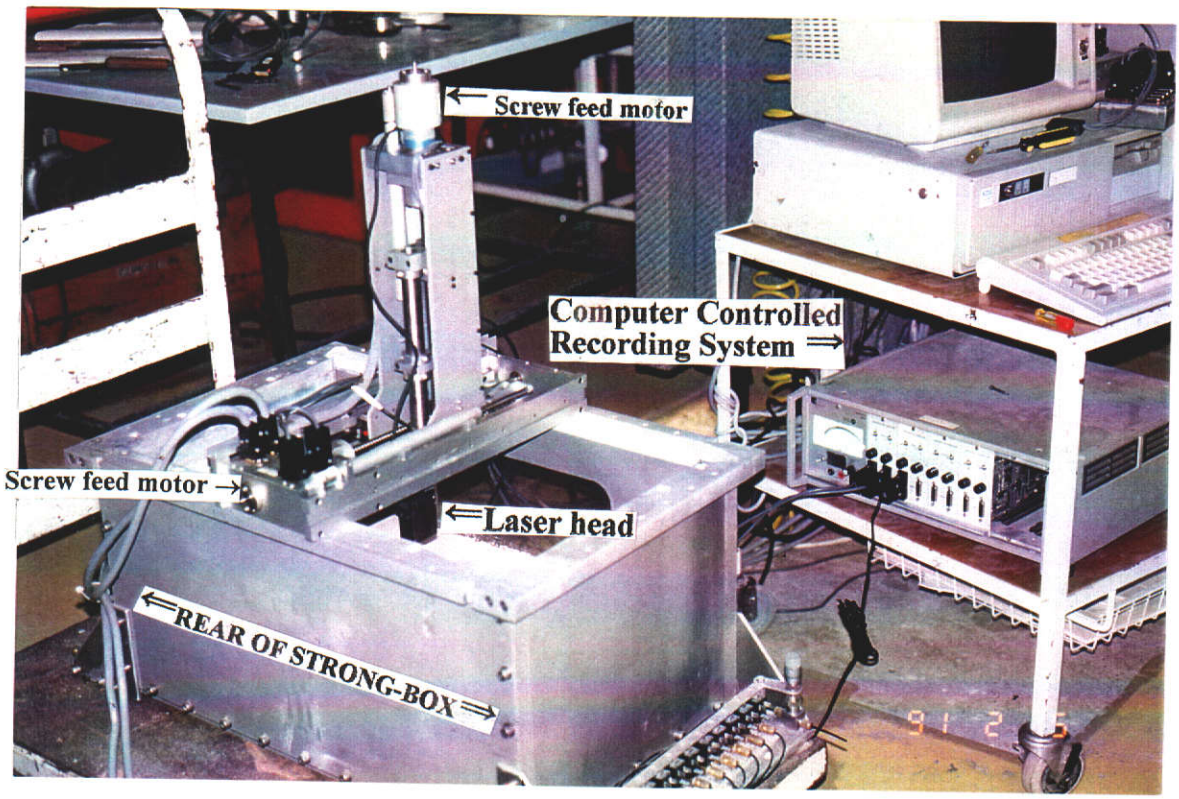

Figure IV.76

APPENDIX V

SUBSOL CALIBRATION PHASE

V.1 SUBSOL DEVELOPMENT AND MODEL SET-UP

The SUBSOL investigation was operated in two stages. The first stage involved the calibration of the model to reproduce the subsidence measured above two completed extraction panels (ACIRL and 2SA panels). The second was to verify the "calibrated" model by comparing model predictions against field surface and subsurface subsidence measured from a panel in the process of being mined (1 North panel). The general development of SUBSOL and model set-up process and parameters used for each model are described below.

Comparison of the initial model's output with measured subsidence revealed a number of shortcomings in the model. Of particular concern was the application of a suitable goafing "element" and process to define failure of subsequent aquifer and aquitard layers as mining progresses. Other factors requiring better definition included establishing the optimal number of variables within the model such as seam partings, stratigraphic layers and number of elements so that subsequent run times would be minimised without significantly impacting on the results. [When early models, which included the complete range of subsidence-related variables with a large number of elements (more than 200,000 elements) were run, the model run-time was taking up to five days to reach the prescribed iterative state of equilibrium. This made it difficult to calibrate the model effectively.]

The goaf model used was based on a variation of a hyperbolic curve developed by MINCAD from previous analyses of Eastern States mine sites (Wardle and Enever, 1983) and was calibrated to the results of a consolidation test undertaken on a "typical" sandstone specimen at ACIRL's Belambi laboratories for Western Collieries Ltd (see Figure V.1). This test indicated that the rate of consolidation from an unloaded bulked goaf density of 1.32 t/m^3 is rapid; and there is little change in the bulk density beyond a vertical stress of 2.0 MPa (>100 m cover), when a residual bulk density of 1.83 t/m^3 is achieved. This residual density represents a final bulking factor of 1.04. These results compare well with Peng and Chiang (1984), who defined the range of original (unloaded) and residual (consolidated) bulking factors for sand to be

between 1.06 to 1.15 and 1.01 to 1.03 respectively. The process of the application of the goaf element involves encoding restriction of the displacements of "roof and floor" discontinuity elements to according to the goaf consolidation model. The limiting displacement of the upper roof movement is approximately 50% mining height.

The number of parting planes required was found to not have such a large impact on the surface subsidence, however, subsurface subsidence was affected by the location and number of parting/discontinuity planes. With fewer parting planes, the separation at each parting horizon was greater. It was therefore necessary to establish an acceptable compromise. MINCAD found that parting planes, other than those at the aquitard horizons, had most effect on the results in the aquifer material below the first aquitard.

It was found that the stratigraphic horizons requiring definition in the model were only the aquitard layers. Furthermore, it was established that the thickness of aquitard layers in the models should be restricted to the thickness of coal (and not inclusive of shales and silts) in each aquitard. It was found that only the stiff coal layers were impacting on subsidence development. Model stratigraphy and material values were derived from nearby boreholes (eg W669 and W665, in ACIRL panel - Figure V.2), previous investigation by Lawrence (1986), and additional data provided by the author as required. The bulk density of materials used in the model was 2.15 for non-coals and 1.3 t/m^3 for coals.

The shear resistance of the layer interfaces is expressed in terms of an effective friction angle and cohesion. Variable regions of normal and shear stiffness are included in the material input data. The measurement of strata interface shear strength in the field is impractical; these parameters are estimated from small-scale tests on selected samples of material (Appendix III) and MINCAD's past experience. These estimates were further refined as the model was calibrated against the field subsidence data. The key defect parting material parameters used were a residual cohesion of 0 MPa and pre- and post-failure friction angles of 30 and 10 degrees respectively. A residual shear stiffness of 100 MPa per metre was also used by the model for all partings.

One of SUBSOL's pertinent features to the subsidence process is the manner in which the program continually updates the moduli of the various stratigraphic layers (aquitards and aquifers), depending on the state of stress and the material strength of the strata. This effectively takes into account the varying distortions and fracturing of the layers during mining extraction. The stress state and loading history at any

location in the rock mass determines the current layer material properties.

The criteria used for updating of pre-mining input parameters to post-failure parameters were limited to a specified "free" span/opening width of a displacement discontinuity joint. This mechanism represents the observed sequence of failure of bridging coal beams once reaching a critical span. Once this critical width was reached in a model, the spanning model layer was deemed to have failed, and this material subsequently assumes post-failure shear strength properties. In the case of the ACIRL panel the allowable span was 2 x 3 m wide elements, which effectively allowed for limiting spans between 6 and 8 m to develop in the model before "failure" occurred. For 1North and 2SA panels, the allowable limit was a single 5 m wide element; which represented a limiting span between 5 and 9 m width. The variation between element dimensions occurred because it was found that the smaller elements in the ACIRL model took too much processing time. Personal communication with MINCAD suggests that there is insignificant variation in model performance with either element dimension.

A hydrostatic stress field, based on average material densities, was used in all analyses. There were no field stress measurements to support this assumption, however this assumption had been used previously by Lawrence (1986) with reported success. Furthermore the observed ground conditions in WCL's underground mines did not indicate that there was an elevated horizontal stress.

The model input parameters are therefore:

* **Rockmass young's modulus.**
* **Rockmass Poisson's ratio.**
* **Rockmass bulk density.**
* **Rockmass shear modulus.**
* **Geometry of excavation and stratigrapghy.**
* **Location of displacement discontinuity planes and size/numbers of elements along these planes of discontinuity.**
* **Shear strength and stiffness of the discontinuity (pre- and post-failure) partings.**
* **Failure mode definition and goaf model definition.**

V.2 ACIRL TEST PANEL

The initial series of test runs revealed a number of limitations in the SUBSOL program. These primarily involved the existing treatment of the failure criterion for the parting planes. A cycle of program modification, rerunning and testing of the model was subsequently undertaken. This process allowed an initial working model to be produced that could be further refined with subsequent analyses.

The final model consisted of nine stratigraphic layers (illustrated by Figure 4.1 a which represents a perspective view of the discretised model). These layers (reducing in area nearer the seam to minimise the number of elements) represent each of the major aquitard and aquifer units above the ACIRL panel. The stratigraphic layers were assumed to be parallel and horizontal. The excavation seam plane (at the base of Figure 4.1a and presented in plan in Figure 4.1 b) was modelled with 10,000 x 3 metre square elements; more detailed information on the excavation plane grid is presented later.

The format of individual elements forming the development roadways, pillars and areas of extraction for Sub-Panel A and Sub-Panel B are presented in Figures 4.2 a and 4.2 b respectively. The mine roadways were modelled as two 6 m wide elements. The extraction height modelled was 2.7 m. The average cover depth for this panel was 140 m. A hydrostatic stress field, based on average material densities, was used in all analyses. This equated to a vertical stress of about 3.5 MPa at the excavation plane.

The interfaces located between the base of the aquitards and the top of the aquifers were modelled by a further 30,000 three metre square non-linear Mohr-Coulomb joint elements. SUBSOL allows these elements to shear and crack open and alter their stiffness as required by the stress and displacement changes induced by the sequential panel extraction. The model was constructed with sufficient elements on the parting planes to allow the propagation of any shear forces to re-establish a state of equilibrium state away from the excavation boundaries.

Table V.1 shows the initial material values used for Young's Modulus, Poisson's ratio and shear modulus for the stratigraphic layers used in the ACIRL model.

Table V.1: SUBSOL'S INITIAL MODEL PROPERTIES - ACIRL TEST PANEL.

Lithology, layer # from surface	Coal Seam Depth (m)	Modulus E (MPa)	Poisson's Ratio	Shear Modulus (MPa)
# 1 -Aquifer (clayey/sandstone)		300.0	0.33	113.0
#2 - Aquitard Collieburn 1 Seam	55.6	2000.0	0.25	800.0
# 3 - Aquifer (sandstone)		600.0	0.30	230.0
Layer 4 - Aquitard Upsilon Seam	92.0	2000.0	0.25	800.0
Layer 5 - Aquifer (sandstone)		600.0	0.30	230.0
Layer 6 - Aquitard Alpha seam	114.0	2000.0	0.25	800.0
Layer 7 - Aquifer (sandstone)		800.0	0.28	312.5
Layer 8 - mine Wyvern seam	140.0	2000.0	0.25	800.0
Layer 9 - Floor strata (sandstone)		800.0	0.28	312.5

V.3 2SA PANEL

The development roadways and surrounding bord and pillar workings (Figure 4.9) were not included in the model for simplicity. Their effect at this shallow depth of cover on the overall subsidence profile was seen to be negligible (other than the collapsed roadways to the east of the panel). The final model consisted of six stratigraphic layers based on the geological log of extensometer borehole W 668 (Figure V.2). Material property data from the ACIRL Test Panel calibration was modified for the geological log of extensometer borehole W 668 as shown in Table V.2.

The excavation seam plane was modelled with 6,000 five metre square elements. The final extracted panel dimensions were 350 m wide by 140 m long. The cover depth modelled was 56 m which represents the average depth. The depth of cover in situ varies from 70 m at the western edge to 50 m at the eastern edge. The mining height was taken as 2.5 m.

The interfaces between the aquifers and aquitards were modelled by a further 18,000 Mohr-Coulomb non-linear joint elements. As mentioned earlier, SUBSOL allows these elements to shear, open, and alter their stiffness as required by the stress and displacement changes induced by sequential extraction. The initial material properties applied to each member is modified automatically by the program according to the amount of displacement predicted.

The material properties shown in Table V.2 are for the starting (prescaled) values. The parting material properties were based on the earlier ACIRL Test Panel analyses as described earlier.

TABLE V.2 SUBSOL'S INITIAL MODEL PROPERTIES - 2 SOUTH A PANEL

Lithology (layer number from surface)	Coal Seam Cover Depth (m)	Young's Modulus E (MPa)	Poisson's Ratio	Shear Modulus Gv (MPa)
Layer 1 - Aquifer		300.0	0.31	115.0
Layer 2 - Aquitard (coal) Alpha seam	24.5	1500.0	0.25	600.0
Layer 3 - Aquifer		600.0	0.26	238.0
Layer 4 - Aquitard (coal)Wyvern seam		1000.0	0.25	400.0
Layer 5 - mine	56.0	2000.0	0.25	800.0
Layer 6 - Floor sandstone		800.0	0.28	312.5

V.4 1 NORTH PANEL

The development roadways (as illustrated in Figure 3.43 in the main body of the thesis) were not included in the model, as for 2SA panel, for simplicity. The final model consisted of nine stratigraphic layers. The excavation plane was modelled with 6,000 elements, each 5 metres square. The interfaces between the overlying aquifers and aquitards were modelled by a further 18,000 Mohr-Coulomb non-linear joint elements. The cover depth modelled was 92 m, representing the cover depth at the position of the extensometers. A plan view of the panel layout and the range of cover depth is provided in Figure 3.43; extraction details are provided in Table I.20 - Appendix I. This panel, unlike the other two test case panels, used two-way split/fender lifting methods (see Figure 1.3 in Section 1.0).

Table V.3 shows the initial material values used in the model. These were based on the previous models and the geological log of boreholes D212 and D213 (Figure V.2). Parting material properties were again based on ACIRL Panel analyses.

For this model 'run', MINCAD were requested to provide subsidence data at significant levels above the mine horizon so that a better assessment could be made of the model's capability to represent the development of subsurface subsidence. Of particular interest was the ability to model the curvature and strain of the aquitards across the panel edge.

The provision of this additional data required additional time steps, and modification to the model set-up and resulted in the model run-time being extended significantly. In order to speed up the run-time of this model, the partings were not allowed to stay open along the sides of the panel (but not at the face). This was achieved by greatly reducing the stiffness of the edge elements. This resulted in an accelerated convergence, as these edge elements did not require repetitive checking during iteration stages. This approach was not seen to have a significant effect on the convergence of the aquitards near the middle of the panel as the panel width was more than twice the panel depth and any edge effects would not extend for such a large distance.

TABLE V.3: SUBSOL'S INITIAL MODEL PROPERTIES - 1 NORTH PANEL.

Lithology (layer number from surface	Cover Depth (m)	Young's Modulus E (MPa)	Poisson's Ratio	Shear Modulus Gv (MPa)
Layer 1 - Aquifer (clayey/ sandstone)		300.0	0.33	113.0
Layer 2 - Aquitard (coal) Collieburn 1 Seam	29.0	2000.0	0.25	800.0
Layer 3 - Aquifer (sandstone)		600.0	0.30	230.0
Layer 4 - Aquitard (coal) Upsilon Seam	40.0	2000.0	0.25	800.0
Layer 5 - Aquifer (sandstone)		600.0	0.30	230.0
Layer 6 - Aquitard (coal) Alpha seam	57.0	2000.0	0.25	800.0
Layer 7 - Aquifer (sandstone)		800.0	0.28	312.5
Layer 8 - mine level (coal)Wyvern seam	92.0	2000.0	0.25	800.0
Layer 9 - Floor (sandstone)		800.0	0.28	312.5

CONSOLIDATION TEST ON WEAK SANDY MATERIAL From the Premier Deposit

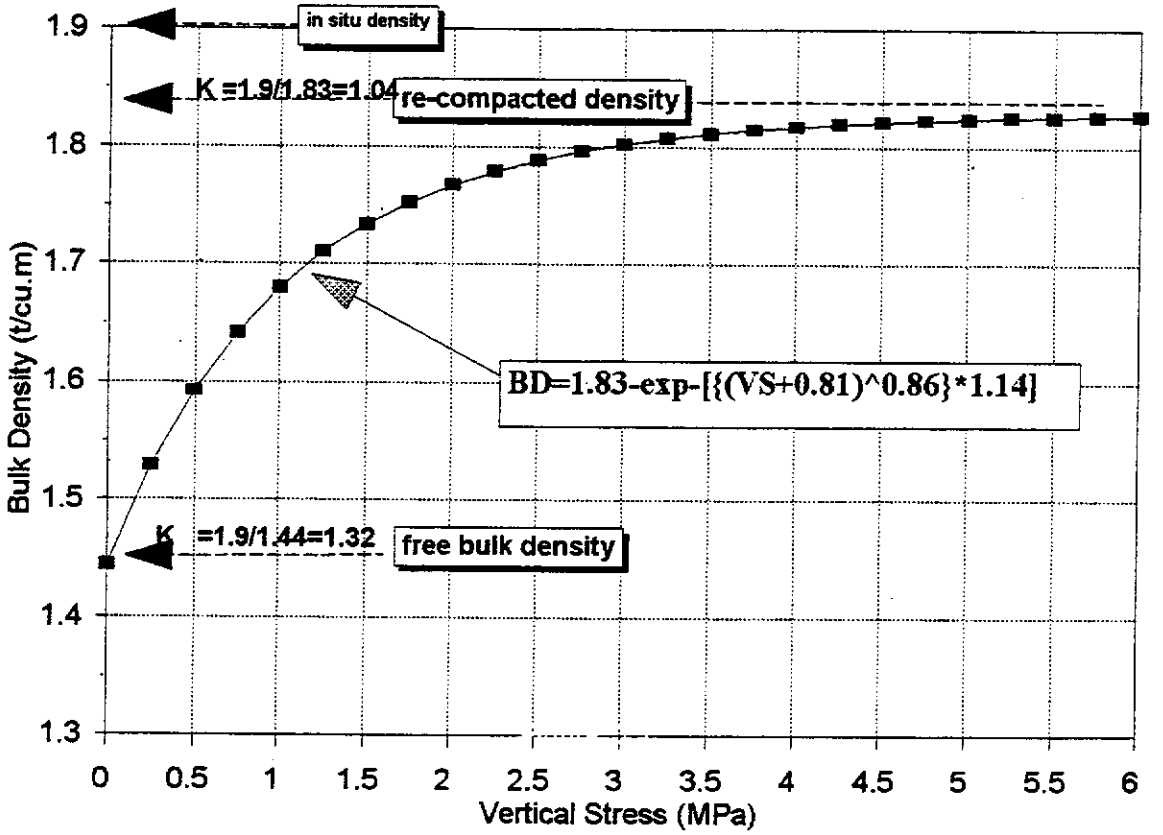

Figure V.1

DETAILED STRATIGRAPHY ABOVE EXTRACTION PANELS USED IN THE MODELLING PHASE

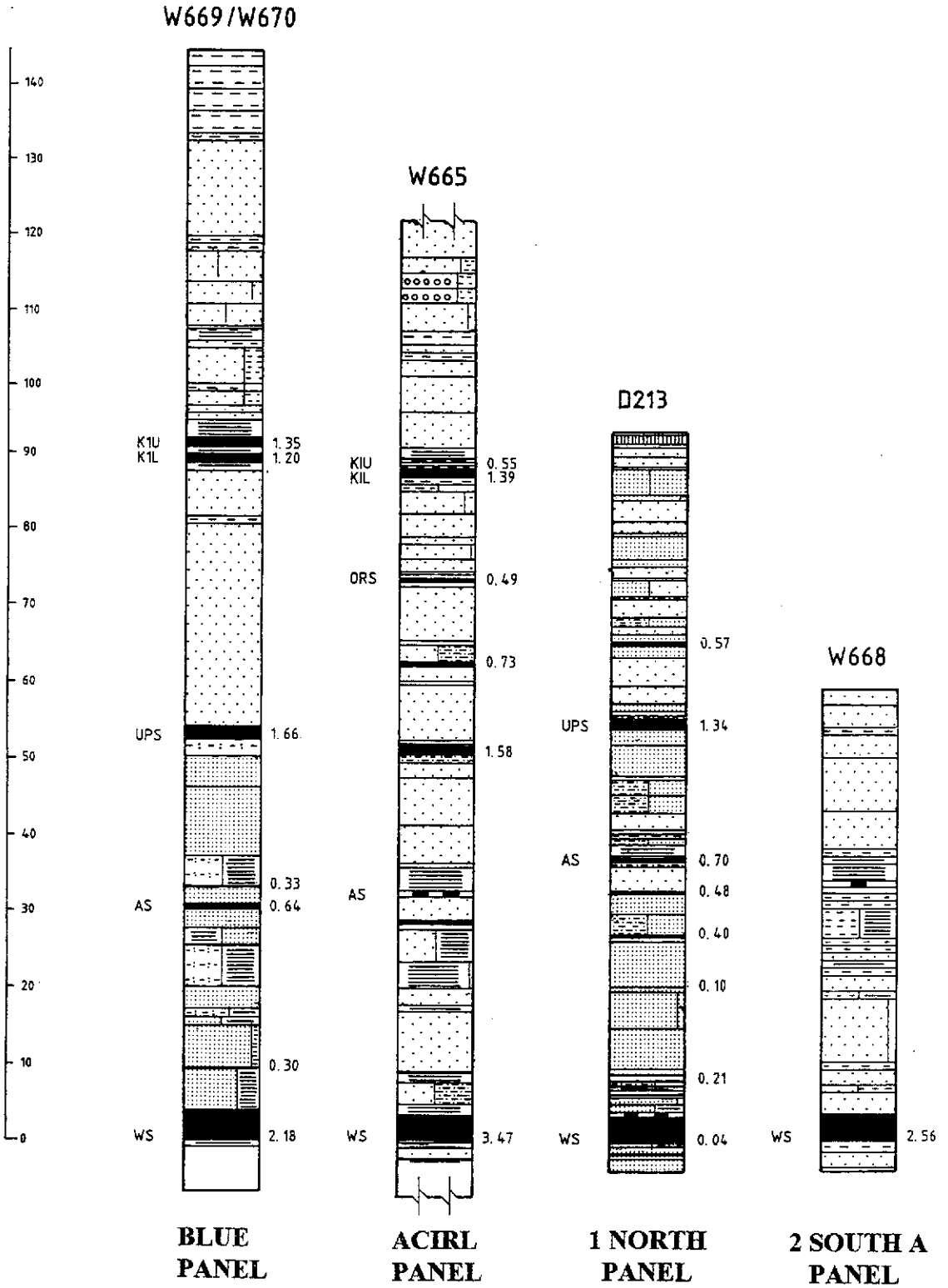

Figure V.2